NATURE ENVIRONMENT & POLLUTION TECHNOLOGY

*A Multidisciplinary, International Journal
on Diverse Aspects of Environment*

INSTRUCTIONS TO AUTHORS

Scope of the Journal

The Journal publishes original research/review papers covering almost all aspects of environment like monitoring, control and management of air, water, soil and noise pollution; solid waste management; industrial hygiene and occupational health hazards; biomedical aspects of pollution; conservation and management of resources; environmental laws and legal aspects of pollution; toxicology; radiation and recycling etc. Reports of important events, environmental news, environmental highlights and book reviews are also published in the journal.

Format of Manuscript

- The manuscript (*mss*) should be typed in double space leaving wide margins on both the sides.
- First page of mss should contain only the title of the paper, name(s) of author(s) and name and address of Organization(s) where the work has been carried out along with the affiliation of the authors.

Nature Environment and Pollution Technology
Vol. 19, No. (3), September, 2020

CONTENTS

The Journal is Currently Abstracted and Indexed in:

International Scientific Indexing (UAE) with Impact Factor 2.236 (2018)

NAAS Rating of the Journal (2019) = 3.85

Scopus®, SJR (0.127) 2019

Index Copernicus (2018) = 135.97

EI Compendex of Elsevier

Indian Science Abstracts, New Delhi, India

Chemical Abstracts, U.S.A.

Elsevier Bibliographic Databases

Pollution Abstracts, U.S.A.

Paryavaran Abstract, New Delhi, India

Zoological Records

Electronic Social and Science Citation Index (ESSCI)

Indian Citation Index (ICI)

EBSCO: Environment Index™

CrossRef (DOI)

DOAJ

Google Scholar

ProQuest, U.K.

Environment Abstract, U.S.A.

British Library

WorldCat (OCLC)

JournalSeek

CSA: Environmental Sciences and Pollution Management

Indian Science

Geobase

SHERPA/RoMEO

Directory of Science

Access to Global Online Research in Agriculture (AGORA)

Full papers are available on the Journal's Website: www.neptjournal.com

Scopus CiteScore (2019) = 0.5

Ulrich's (Refereed) database

Zetoc

J-Gate

Centre for Research Libraries

Connect Journals (India)

Research Bible (Japan)

Elektronische Zeitschriftenbibliothek (EZB)

CNKI Scholar (China National Knowledge Infrastructure)

AGRIS (UN-FAO)

UDL-EDGE (Malaysia) Products like *i*-Journals, *i*-Focus and *i*-Future

www.neptjournal.com

Nature Environment and Pollution Technology

Original Research Paper https://doi.org/10.46488/NEPT.2020.v19i03.001 **Open Access Journal**

Kinetics, Isotherm and Thermodynamic Properties of the Basement Complex of Clay Deposit in Ire-Ekiti Southwestern Nigeria for Heavy Metals Removal

S. S. Asaolu, S. O. Adefemi, O.A. Ibigbami†, D.K. Adekeye and S. A. Olagboye

Department of Chemistry, Ekiti State University, Ado-Ekiti, Nigeria
†Corresponding author: Ibigbami O.A.; olayinkaibigbami@yahoo.co.uk

ABSTRACT

Raw kaolinite clay collected from Ire-Ekiti, Ekiti State, Nigeria, was used to adsorb some heavy metals (Pb, Cr, Ni and Cu) from their aqueous solution through batch experiments. Adsorption studies were performed at the different temperatures, concentration and time to determine the kinetics, isotherm and thermodynamic properties of the adsorption processes. The adsorption thermodynamic properties showed that sorption of Cu, Cr and Ni on the raw clay was exothermic, while adsorption of Pb was endothermic. The negative values of ΔG for Pb adsorption revealed the feasibility and spontaneity of the adsorption process while the positive ΔG values for Cu, Cr and Ni sorption showed non-spontaneity of the adsorption process. Langmuir, Freundlich and Elovich isotherms were applied to explicate the nature of adsorption process, while Pseudo-first-order (PFO), Pseudo-second-order and Elovich kinetics were applied to literarily determine the adsorbate-adsorbent interaction. Pseudo-second-order kinetics was the best fitting kinetics for adsorption of the metals on the raw clay.

INTRODUCTION

The presence of heavy metals like chromium, copper, lead, nickel, arsenic, etc. in water bodies, has become a growing environmental problem. Water bodies are mostly contaminated with these heavy metals through anthropogenic activities. These heavy metals enter into water bodies through various industrial processes, including metal plating, fertilizer production, mining, metallurgy, battery manufacturing and textile dyeing, and others (Barhoumi et al. 2009, Eloussaief & Benzina 2010). Their potential toxicity, persistence and bio-accumulation problems pose a great threat to both man and other forms of life. High concentrations of them in the environment may constitute long-term health risks to ecosystems and humans.

A wide range of various treatment techniques such as ion exchange, photodegradation, biosorption, oxidation, electrochemical treatment, precipitation, and adsorption have been reportedly used for removal of heavy metal ions from industrial effluents (Bailey et al. 1999, Ku & Jung 2001, Babel & Kurniawan 2003, Bradl 2004, Fu & Wang 2011, Shim et al. 2014). However, adsorption has been universally accepted as one of the most effective pollutant removal processes, with low cost, ease in handling, low consumption of reagents, as well as scope for recovery of value-added components through desorption and regeneration of adsorbent (Olivella et al. 2011, Dawodu et al. 2012). Materials that have been used as an adsorbent for heavy metals include rubber seed coat pecan shells, jute fibre (Senthilkumaar et al. 2005), Indian rosewood sawdust, olive stones, pinewood and clay (Rengaraj et al. 2002, Shawabke et al. 2002, Tsenga et al. 2003, El-Sheikh et al. 2004, Garg et al. 2004).

Clay plays an important role in the environment by acting as a natural pollutant remover, taking up cations and anions either through ion exchange, surface complexation, pore diffusion, precipitation or direct bonding (Arnamwong et al. 2016, Emam et al. 2016). Natural clays have been known to possess a reasonable ability to remove heavy metal contaminants from their contaminated medium. Clays from Africa have been reportedly used for the removal of heavy metals and they have been found to possess great removal efficiency for the metals (Eloussaief et al. 2009, Mbaye et al. 2014, Olu-owolabi et al. 2016, Adekeye et al. 2019). A recent study by Adekeye et al. (2019) has reported the adsorption properties of Cu, Ni, Pb and Cr of the basement complex of clay deposit from the present study area. The present work is aimed at elucidating the kinetics, isotherm and thermodynamics properties of the adsorption processes of the metals on the clay adsorbent.

MATERIALS AND METHODS

Sample Collection and Preparation

The clay soil was collected from Ire-Ekiti, Southwestern Nigeria. Both topsoil (at the depth of 5 cm away from the

surface) and subsurface soil (at the depth of 15 cm away from the surface) were taken at four cardinal points with equidistance of 0.5 km away from one another. The soil samples were homogeneously mixed to obtain a representative sample for use. An adequate amount of the sample for use was taken, dried at room temperature, crushed and dispersed in deionized water. Floating debris from plants was removed by handpicking and also by decantation. The suspension was thoroughly stirred to separate non-clay materials from the clay. The clay soil was recovered from the water by centrifuging the suspension at 3000 rpm. The recovered clay soil was oven-dried at 110°C for 12 hours and cooled in a desiccator. After cooling, the dried clay sample was crushed in a ceramic mortar and sieved through sieves of different sizes ranging from 200-500 μm. The sieved clay soil was stored in a black polyethylene bags prior to subsequent analysis.

Preparation of Metal Solution

The reagents used to prepare solutions of metal ions were of analytical grades. The stock solutions (1000 mg.L^{-1}) of the metal ions (Ni, Pb, Cu and Cr) were prepared by dissolving weighed quantities of metal salts (potassium chromate, lead nitrate, copper nitrate and hydrated nickel sulphate) in deionised water and serially diluted to prepare solutions of varying initial concentration for as required for the experimental works. Both the initial and equilibrium concentrations of metal ions were determined using an Atomic Absorption Spectrophotometer (Agilent AAS 55AA).

Characterization

The functional group determination of the clay soil was carried out by Fourier Transformed Infrared Spectrophotometer (FTIR). Scanning Electron Microscope (SEM) was used to show surface morphology of the clay soil while the elemental composition was determined by Energy Dispersive X-ray Emission technique.

Batch Adsorption Experiments

Adsorption experiments were carried out in batch by adding 50 mL of 10 mg/L adsorbate solution into conical flasks containing 0.50 g of the adsorbent. The adsorbent and adsorbate mixtures were then equilibrated at pH value of 5.0 by shaking at 200 rpm in temperature (298 K) using a rotary orbital shaker until equilibrium. After equilibration, the mixtures were centrifuged for 10min at 3000 rpm after which the supernatants were collected and analysed for equilibrium concentrations of the Cu, Ni, Pb and Cr using AAS. To study the adsorption isotherm, adsorption of Cu, Ni, Pb and Cr unto the clay soil was optimized at different concentrations of 20, 40, 60, 80 and 100 ppm with an equilibration time of 90 min at pH value of 5. Agitation time was varied from 10 to 80 min also at pH 5 to study the adsorption kinetics. The adsorption temperatures of 300, 315, 330, 340 and 350 K were implored to understand the thermodynamic properties of the adsorption process.

RESULTS AND DISCUSSION

Morphology of the Raw Clay Soil

The SEM image (Fig. 1) of the raw clay soil showed a dense arrangement of the particles. This arrangement results from the stacking of the particles upon one another. Inter-aggregate pores which could allow permeation of adsorbates on the clay soil are also present in small size.

Elemental Composition of the Raw Clay Soil

The result from Energy Dispersive X-ray Emission technique (Fig. 2) showed that oxygen, aluminium and silicon are the major elemental constituents and possessing the highest percentage by weight (20.70, 15.10 and 50.00 respectively) of the raw clay soil. The presence of oxygen and the absence of hydrogen showed that the elements were present in the form of oxide rather hydroxide. The elemental composition
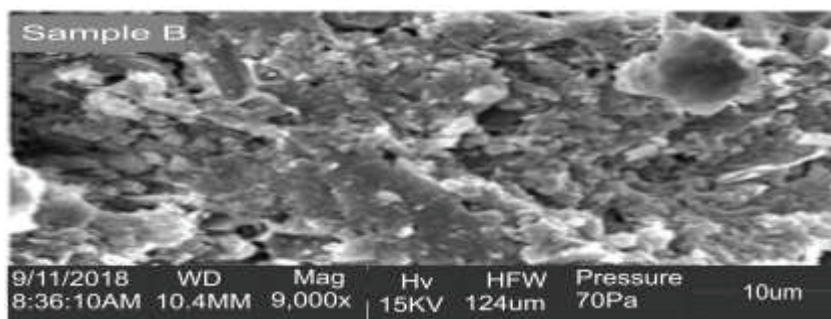
Fig. 1: SEM image of the raw clay soil.
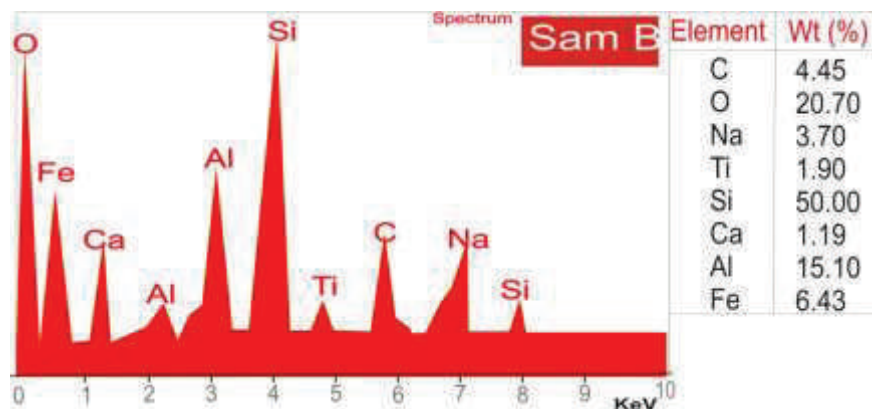
Fig. 2: EDX spectra of the raw clay soil

of the raw clay soil also showed that the clay soils contained some important exchangeable cations such as Na (3.70 %), Ca (1.19 %) and Fe (6.43 %). The presence of these exchangeable cations in the soil could bring about the ion-exchange mechanism for the removal of the adsorbates from their respective solution. The percentage abundance by weight of Si and Al compared to other elements showed that the clay soil is kaolinite.

Fourier Transform Infrared Spectra of the Raw Clay Soil

The bands at 1633 and 1402 cm^{-1} (Table 1) are due to the presence of C=O and C=C which indicate the presence of organic matter in the clay soil. The band at 536 cm^{-1} is due to the presence of Si-O-Al group. The absorption bands at 3671 and 3620 cm^{-1} showed the presence of OH group of bonded water while the bands at 3421 and 3263 cm^{-1} showed the OH group of organic matter and also confirming the presence of organic matter in the clay soil.

The presence of metallic oxide in the clay soil is shown by the intensity bands at 468 and 432 cm^{-1}. The FTIR result (Fig. 3) of this study is consistent to the results of Van der-Marel & Beutelspacher (1976), Petit et al. (1995), Wilson (1994) and Saikia et al. (2003) on the characterization of clay minerals.
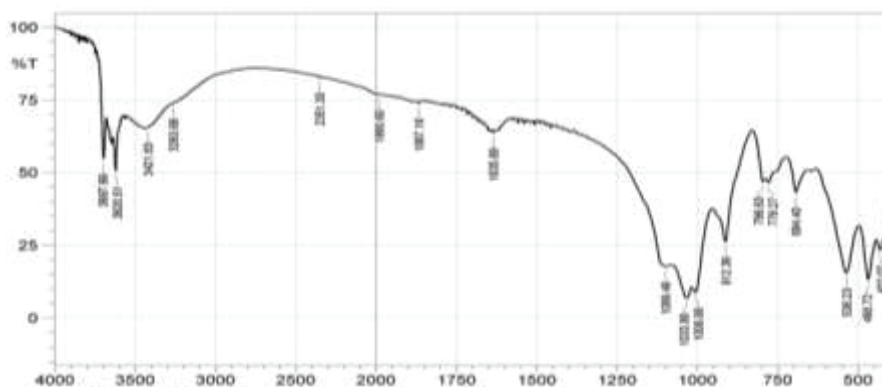
Fig. 3: Fourier Transform Infrared Spectra of the raw clay soil.

Table 1: Fourier Transform Infrared spectra of the raw clay soil

M-O	OH	C=C	C=O	Si-O-Si	Si-O-Al
468, 432	3671, 3620	1420	1633	1099-1006	536
	3421, 3263				

Effect of Adsorption Parameters

Effect of agitation time: The effect of agitation time on the removal of Ni, Pb, Cu and Cr is shown in Fig. 4. The removal of Pb by the raw clay was optimized (98.75%) within a short period (40 min) and tended to be stable for 80 min. The optimum removal of copper was observed to be at 60 min then tended to be stable after 60 min while Cr and Ni adsorption increased with increase in time until equilibration was achieved at 60 and 70 min for the metals respectively. The increased adsorption during the initial stages might be due to the presence of abundant active sites on the surface of the clay soil, which became saturated with time until equilibrium was attained.

A good adsorbent does not only have high adsorption efficiency but also a fast rate of adsorption (Akpomie et al. 2017). It could also be seen that the equilibrium adsorption time for all the metals was attained within 30-70 min. This showed that the clay soil is good enough to be applied for both domestic and industrial purposes for the removal of heavy metals from contaminated aqueous medium.

Effect of Adsorbate Concentrations

The concentration of adsorbates is also an important parameter in an effective adsorption study. The effect of adsorbate concentration on adsorption process on the raw clay soil is shown in Fig. 5. Results from this study showed that the adsorption capacity of raw clay soil increased with increase in metal ion concentration from 20 mg/L to 100 mg/L.

This trend was attributed to the fact that when the transport of metals between the adsorbent's external surface film and internal pores are equal, the trans-boundary movement of metals will not be significantly permissible; however, increasing concentration could re-initiate the trans-boundary movement (depending on the nature of the adsorbate and adsorbent) and hence, the adsorption process would be concentration dependent. Similar results were also reported by Eba (2010), Mbaye et al. (2014) and Zouraibi (2016).

Effect of Temperature

The temperature has been shown to possess significant effects on adsorption phenomenon (Zouraibi et al. 2016,
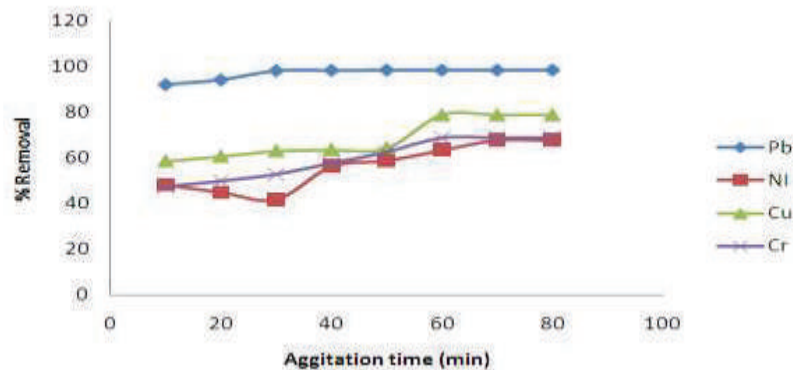
Fig. 4: Adsorption trend with increase agitation time.
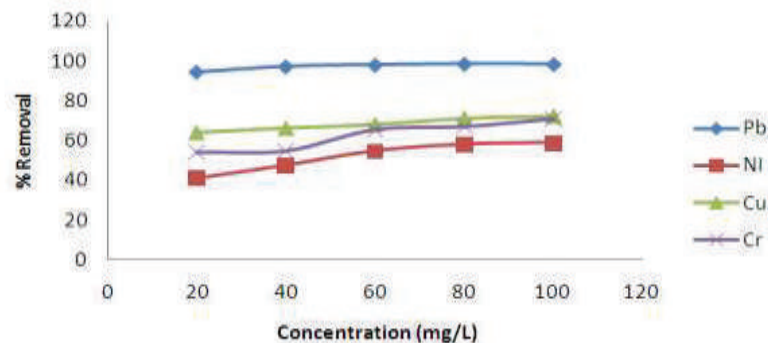
Fig. 5: Adsorption trend with increase in concentration.

Akpomie et al. 2017). Temperature affects two major aspects of adsorption *viz* the equilibrium position in relation with the exothermicity and endothermicity of the process and the swelling capacity of the adsorbent (Rattanaphani et al. 2007, Natalia et al. 2015). Thus, adjustment of temperature may be required in the adsorption process. As observed in the raw clay soil (Fig. 6), the uptake capacity of Pb decreased with increasing temperature.

This is due to the endothermic effect of the surroundings during the adsorption process while the adsorption of Ni, Cu and Cr by the raw clay oil increased with temperature increase. This showed the potential of copper, chromium and nickel to overcome resistance to mass transfer with increase kinetic energy to undergo an interaction with the active sites of the adsorbents. Similar results to this study have been reported by Gonzalez et al. (2005), Rattanaphani et al. (2007), El-Sayed et al. (2011) and Zouraibi et al. (2016).

Adsorption Kinetics

Pseudo-first-order kinetics: The adsorption data were modelled using the Lagergren pseudo-first-order model given by:

$$\log (q_e - q_t) = -\frac{k_1}{2.303} t + \log q_e \qquad \ldots(1)$$

This model was used to predict physical adsorption mechanism for the metals' adsorption processes on the raw clay. Where q_t (mg/g.min) is the amount of metal adsorbed on the surface of the sorbent at time t (min), q_e is the amount of metal adsorbed at equilibrium and K_1 (min^{-1}) is the equilibrium rate constant of pseudo-first-order adsorption (Lagergren 1908). The rate constant K_1, was calculated from the slope of $\log (q_e - q_t)$ versus time t for plots in which straight lines were obtained. If a straight line is obtained and q_{eCal} values are close to q_{eExp}, it suggests the applicability of the model.

Results of this research showed that straight line graphs were obtained for metals adsorption on the raw clay soil as shown in Fig. 7.

But the values of q_{eCal} did not correlate to those of q_{eExp} as given in Table 2 which suggests that the adsorption processes cannot be represented by pseudo-first-order kinetics model.

Pseudo-second-order kinetics: The linearized pseudo-second-order kinetics was also applied to evaluate its applicability.
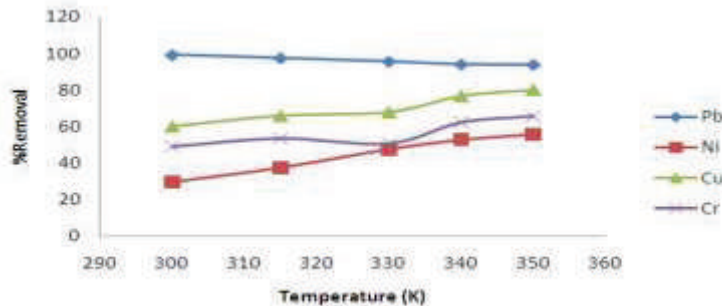
Fig. 6: Adsorption trend with increase in temperature for the metals.
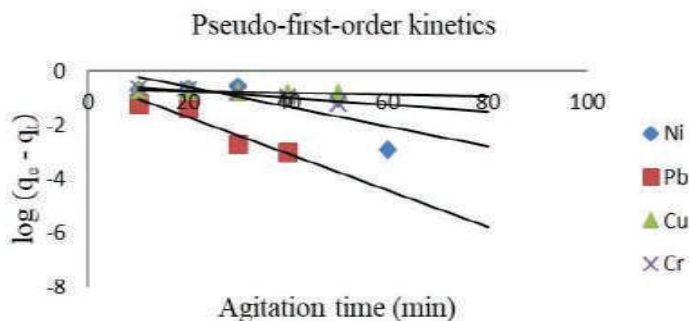
Fig. 7: Plot of log $(q_e - q_t)$ vs agitation time (min) for raw clay.

Table 2: Pseudo first-order kinetics for raw clay

	Pb	Ni	Cu	Cr
R^2	0.9033	0.5736	0.9330	0.9078
K_1	1.566	0.0836	0.0083	0.0299
q_{eExp}	0.4193	1.3424	0.2125	0.3334
q_{eCal}	0.988	0.680	0.790	0.699

Table 3: Pseudo-second-order kinetics for raw clay

	Pb	Ni	Cu	Cr
R^2	0.9999	0.9463	0.9712	0.9837
K	1.242	0.1117	0.1478	0.1467
q_{eExp}	1.009	0.7968	0.866	0.7833
q_{eCal}	0.988	0.680	0.790	0.699

It is given by equation (2):

$$\frac{t}{q_t} = \frac{1}{h} + \frac{t}{q_e} \qquad \ldots(2)$$

Where, $h = k_2 q_e^2$ [mg/(g.min)].

Hence, the pseudo-second-order equation can be written as:

$$\frac{t}{q_t} = \frac{1}{k_2 q_e^2} + \frac{t}{q_e} \qquad \ldots(3)$$

Where, qt (mg/g.min) is the amount of metal adsorbed on the surface of the sorbent at time t, k (g/(mg.min)) is the pseudo-second-order rate constant, while q_e (mg/g) is the amount of metal adsorbed at equilibrium. The values of q_e, k and h were determined experimentally by plotting $^t/q_t$ against t.

Pseudo-second-order plots for the raw clay are shown in Fig. 8, the values of q_{eCal} for the sorption process of all the metal adsorbates onto the raw clay correlate to those of q_{eExp} as given in Table 3. This shows that the adsorption process can be represented by pseudo-second-order kinetics. The R^2 values of the pseudo-second-order for all the metals' adsorption processes are closer to unity than the pseudo-first-order plot. This showed that the sorption processes best fit the pseudo-second-order kinetics.

The fitting of the adsorption processes to pseudo-second-order kinetics implies that there is a possible chemical interaction between the adsorbates and adsorbent during sorption processes. It could also be assumed that the rate-limiting step may be chemical sorption involving valence forces, through exchange or sharing of electrons between sorbate and sorbent. Similar results of this study were observed in studies conducted by Ho & Mckay (1999) and Nethaji et al. (2013).

Elovich kinetics: The Elovich kinetics was modelled us-

ing the linear form of the equation as represented in equation (4) (Kumara et al. 2011).

$$q_t = \frac{1}{\beta} \ln(\alpha\beta) + \frac{1}{\beta} \ln(t) \qquad \ldots(4)$$

The constants α and β could be obtained from the slope and intercept of the linear plot of qt versus $\ln T$. Table 4 gives the Elovich kinetic parameters and Fig. 9 shows Elovich kinetic plots.

The correlation coefficient values (Fig. 9) for all the metals adsorption processes are less close to unity than the pseudo-first-order and pseudo-second-order kinetics. This suggests that the adsorption processes cannot be represented by the Elovich model.

Adsorption Isotherms

The adsorption isotherms were used to show the sorption processes of the metals on the raw clay. This was achieved through the imploration of Langmuir, Freundlich, and Elovich plots.

Langmuir adsorption isotherm: The linearized Langmuir equation was used to show the surface binding properties of Cr. This was done using equation (5) (Kinnburgh 1986):

$$\frac{1}{q_e} = \frac{1}{Q_0} + \frac{1}{Q_0 K_L C_e} \qquad \ldots(5)$$

Where, C_e (mg/L) is the equilibrium concentration, q_e (mg/g) is the amount of ion adsorbed, Q_o (q_{max}) maximum monolayer coverage capacity (mg/g) and K_L (L/mg) is Langmuir adsorption equilibrium constant. The values of q_{max} and K_L were computed from the slope and intercept of the Langmuir plot of $^1/q_e$ versus $^1/C_e$ (Langmuir 1918). The essential features of the Langmuir isotherm were also expressed in terms of equilibrium parameter R_L, which is a

dimensionless constant, referred to as separation factor or equilibrium parameter.

$$R_L = \frac{1}{1+(1+K_L C_o)} \quad \text{...(6)}$$

Where, C_o is the initial concentration and K_L is the constant related to the energy of adsorption. If K_L is less than (<) 0 the adsorption process does not correlate to Langmuir isotherm. Separation factor R_L value indicates the adsorption nature to be either unfavourable if R_L greater than (>) 1, linear if $R_L = 1$, favourable if $0 < R_L < 1$ and irreversible if $R_L = 0$. A negative R_L value indicates that the adsorption process does not fit Langmuir isotherm, hence, cannot be explained using the Langmuir isotherm.

From the data calculated in Table 5, the K_L and R_L values for Ni, Pb and Cu adsorption on the raw clay are < 0 which showed that the adsorption processes could not be explained by Langmuir isotherm. On the other, the K_L value for Cr on the raw clay was 54.34 L/mg. Also, R_L values in the range of 1.84×10^{-5} and 9.2×10^{-4} were also obtained for the raw clay. The R_L values for chromium adsorption on the raw clay is greater than 0 but less than 1, thus, Langmuir isotherm is favourable; the positive K_L values are indicative that the adsorption processes correlate to the Langmuir isotherm. The R^2 values for Cr, Pb, Cu and Ni adsorption onto the raw clay are 0.9837, 0.7531, 0.9705 and 0.9937 respectively. Even though Ni has the highest R^2 value (0.9937), but its negative K_L value (-56.81) showed that its adsorption does
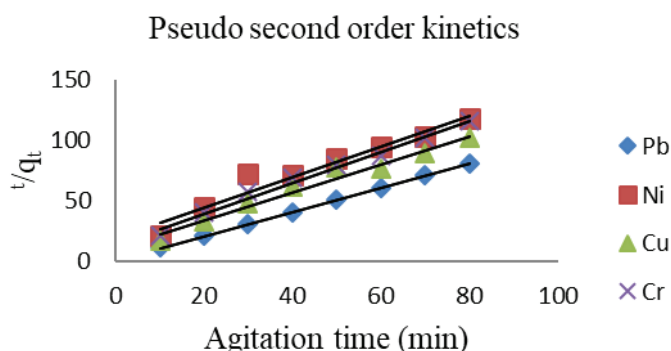
Fig. 8: Plot of $^t/q_t$ vs agitation time (min) for the raw clay.
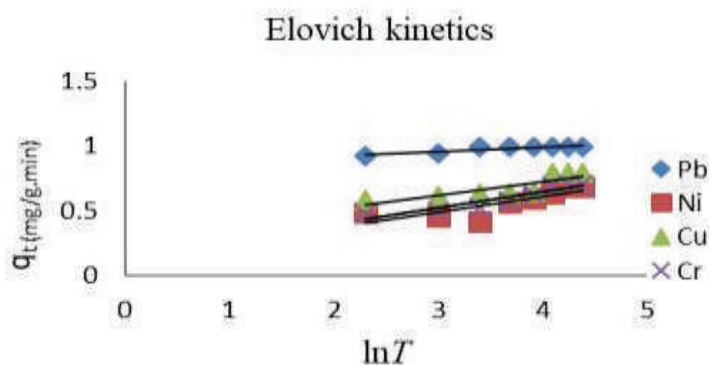
Fig. 9: Plot of q_t(mg/g.min) vs ln$T$ for the raw clay.

Table 4: Elovich kinetics parameters for the raw clay

	Pb	Ni	Cu	Cr
R^2	0.8565	0.6696	0.7159	0.8929

Table 5: Langmuir isotherm parameters for raw clay

	Ni	Pb	Cu	Cr
R^2	0.9937	0.7531	0.9705	0.9837
q_{max}	0.0578	0.1800	0.162	-0.0978
K_L	-56.81	-11.90	-59.88	54.34
R_L	$-(2\times10^{-4} - 9\times10^{-4})$	$-(8\times10^{-4} - 4.2\times10^{-3})$	$-(1.7\times10^{-4} - 8.4\times10^{-4})$	$(1.84\times10^{-5} - 9.2\times10^{-4})$

not correlate to the Langmuir isotherm.

This shows that R^2 value is not sufficient to show the fitness of an adsorption process to Langmuir isotherm. The data obtained from the isotherms showed that chromium adsorption on the raw clay is in best compliance with the Langmuir isotherm. This implies monolayer adsorption of Cr on the clay's flat surfaces. The correlation was not only judged by the linear regression coefficient but also other parameters of the tested isotherms as the R^2 value is not enough to describe the fitness and correlation of an adsorption process to Langmuir isotherm.

Freundlich isotherm: Freundlich isotherm was used to show possible multilayer adsorption process of Ni and Cu on the clay's rough surfaces. The Freundlich isotherm was elucidated using equation (7) and (8) (Freundlich 1906).

$$q_e = K_F C_e^{1/n} \qquad …(7)$$

Where K_F is Freundlich isotherm constant (mg/g), n is adsorption intensity, and C_e is the equilibrium concentration of adsorbate (mg/L). Hence,

$$\log q_e = \log K_F + \frac{1}{n} \log C_e \qquad …(8)$$

K_F and $^1/n$ are empirical constants, indicating the adsorption capacity and the strength of adsorption in the adsorption process respectively. K_F and $^1/n$ were obtained by plotting $\log q_e$ against $\log C_e$ (Voudrias et al. 2002). If the value of $^1/n$ is below one it indicates normal adsorption. On the other hand, if $^1/n$ is above one, it indicates cooperative adsorption (Mohan & Karthikeyan 1997). Linear regression is generally used to determine the parameters for the Freundlich isotherm model (Guadalupe et al. 2008).

From the data in Table 6, the values of $^1/n$ are greater than 1 for Cr, Pb and Cu sorption processes onto the raw clay soil. This showed that the adsorption processes were cooperative while the sorption of Ni on the raw clay was favourable. From all the isotherms, the highest R^2 values for Cu (0.9663) and Ni (0.9287) were obtained from the Freundlich isotherm. This shows that the adsorption processes of the Cu and Ni on the raw clay fit best to the Freundlich isotherm than other adsorption isotherms.

Thus, the adsorption process of Ni and Cu describes a heterogeneous system characterized by multilayer adsorption on the rough surfaces of the clay. A similar result in this study was also reported by Olu-owolabi et al. (2016).

Elovich isotherm: Elovich isotherm was used to show the multilayer adsorption of Pb on the raw clay.

The isotherm was modelled using equation (9), as expressed by Achmed et al. (2012):

$$\frac{qe}{qm} = K_e C_e e^{-\frac{qe}{qm}} = \qquad …(9)$$

The linear regression coefficient was used to judge the correlation. The regression coefficient for Pb sorption on the raw clay is 0.9344 which is higher than that for Langmuir and Freundlich isotherms as given in Table 7.

Therefore, the adsorption of Pb on the raw clay does fit the Elovich isotherm better than others. This implies that Pb adsorption on the raw clay is based on a kinetic principle which assumes that adsorption sites increase exponentially with adsorption; thus, Pb sorption is multilayer adsorption.

Table 6: Freundlich isotherm parameters for the raw clay

	Cu	Ni	Cr	Pb
R^2	0.9963	0.9287	0.9502	0.8375
K_f	1.20	0.787	0.029	1.27
n	0.817	6.211	0.625	0.080
$^1/n$	1.228	0.161	1.599	12.39

Adsorption Thermodynamics

The adsorption thermodynamics was used to elucidate the nature of adsorption. Thermodynamic parameters associated with adsorption which include equilibrium constant K, that depends on temperature, the change in free energy ΔG (KJ/mol), enthalpy ΔH(KJ/mol) and entropy ΔS (J/mole.K) associated to the adsorption process were calculated by following equations (Ramesh et al. 2005).

The free energy (ΔG) of the adsorption process is given by equation (10)

$$\Delta G = \Delta H - T\Delta S \qquad \qquad …(10)$$

By considering the adsorption equilibrium constant K, the equation could be written as:

$$\Delta G = -RT \ln K \qquad \qquad …(11)$$

T is the temperature in Kelvin and R is gas constant (8.314 $J\ mol^{-1}K^{-1}$).

$$K = \frac{q_e}{C_o} \qquad \qquad …(12)$$

$$\ln K = \ln \frac{q_e}{C_o} \qquad \qquad …(13)$$

Hence, ΔH and ΔS were calculated from the slope and intercept of the plot of $\ln K$ vs $^1/_T$ (Fig. 10).

The sorption of Pb on the raw clay decreased with increase in temperature as given Table 8. This is because an increase in temperature results to increase in entropy of the system.

The positive values of ΔS for Pb sorption on the raw clay reflects an increased degree of disorderliness at the solid-liquid interface during the adsorption of Pb on the raw clay. On the other hand, the values of ΔS for sorption of Cu, Cr and

Table 7: Elovich isotherm parameters for the raw clay

	Pb	Ni	Cu	Cr
R^2	0.9344	0.6186	0.2548	0.7093

Table 8: Thermodynamic parameters for the raw clay.

	Temp.	$^1/_T$	C_e	q_e	$\dfrac{q_e}{C_o}$	$\ln \dfrac{q_e}{C_o}$	ΔG	ΔH	ΔS
Pb	300	0.00333	0.068	0.993	14.60	2.618	-6686.95		
	315	0.00317	0.245	0.976	3.984	1.382	-3477		
	330	0.00303	0.514	0.949	1.846	0.613	-1681.84	11.93	7898.14
	340	0.00294	0.586	0.941	1.606	0.474	-1339.88		
	350	0.00286	0.614	0.939	1.529	0.425	-1236.71		
Ni	300	0.00333	6.999	0.300	0.043	-3.147	7849.25		
	315	0.00317	6.216	0.378	0.061	-2.797	7325.09		
	330	0.00303	5.223	0.478	0.092	-2.386	6546.28	-129.40	-57402.71
	340	0.00294	4.711	0.529	0.112	-2.189	6187.78		
	350	0.00286	3.416	0.558	0.192	-1.650	4801.34		
Cu	300	0.00333	3.993	0.601	0.151	-1.890	4714.04		
	315	0.00317	3.411	0.659	0.193	-1.645	4308.11		
	330	0.00303	3.214	0.679	0.211	-1.556	4269.07	-92.23	-38973.72
	340	0.00294	2.330	0.767	0.329	-1.112	3143.36		
	350	0.00286	1.998	0.800	0.400	-0.916	2665.47		
Cr	300	0.00333	5.080	0.492	0.097	-2.333	5818.97		
	315	0.00317	4.627	0.537	0.116	-2.154	5641.13		
	330	0.00303	4.220	0.509	0.137	-1.988	5454.32	-48.75	-28250.36
	340	0.00294	3.732	0.627	0.168	-1.784	5042.74		
	350	0.00286	3.393	0.661	0.195	-1.635	4757.69		
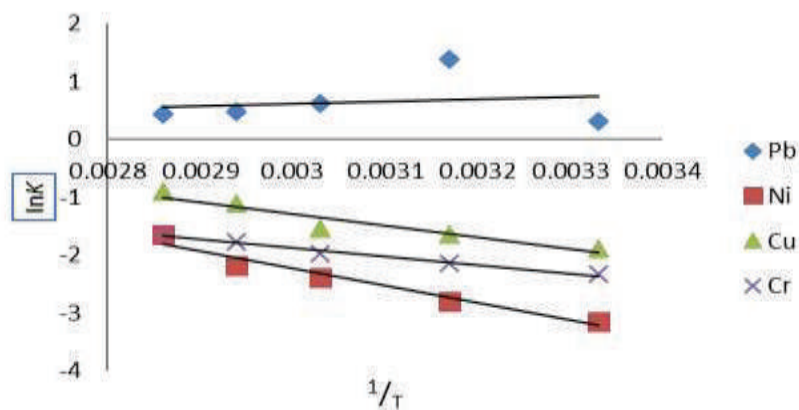
Fig. 10: plot of ln$K$ against $^1/_T$ for the raw clay.

Ni were negative, which implies a decrease in randomness at the solid-solution interface during sorption of the metals on the raw clay adsorption; hence, the adsorption was favoured with the increase in temperature. The endothermic nature of Pb sorption by the raw clay was confirmed by the positive values of ΔH, while the negative ΔH values for Cu, Cr and Ni sorption showed exothermicity of the adsorption processes.

The negative values of ΔG for Pb sorption showed that the adsorption process was feasible and spontaneous while the positive ΔG values for Cu, Cr and Ni sorption is an indication that the adsorption process was not spontaneous. It has been suggested that positive values for ΔG are quite common with ion-exchange mechanism of adsorption of metal ions because of the activated complex of the metal ion formed with the adsorbent in the excited state (Unuabonah et al. 2007). The negative values of ΔG for Pb could be associated to the fact that the Pb may have been covalently bound to the surfaces of the adsorbent by complexation mechanisms. Thus, adsorption of Cu, Ni and Cr could also be by ion-exchange mechanism while Pb adsorption could be surface complexation.

CONCLUSION

This study has investigated the kinetics, isotherm and thermodynamic properties of raw kaolinite clay for the adsorption of heavy metals (Cu, Cr, Ni and Pb) from their aqueous medium. Findings from this study showed that there is a possible chemical reaction between the adsorbates and adsorbent during the sorption processes as the adsorption equilibrium kinetics correlated reasonably well with the pseudo-second-order model. Freundlich, Langmuir and Elovich isotherms showed the processes to which the metals were adsorbed on the raw clay. Nature of the adsorption processes

as shown by the thermodynamic properties showed that Pb adsorption on the raw clay was endothermic, while Cu, Cr and Ni sorption was exothermic. Also, the adsorption of Pb on the raw clay was spontaneous, while Cu, Cr and Ni sorption on the raw clay was not spontaneous. The result is further supported by the fitness of the Pb, Cr, Ni and Cu to the pseudo-second-order kinetics.

REFERENCES

Achmed, A., Kassim J., Suan, T.K., Amat, C. and Seey, T.L. 2012. Equilibrium, kinetic and thermodynamic studies on the adsorption of direct dye unto a novel green adsorbent developed from Ucariagambir extract. J. Physical Sci., 23(1): 1-13.

Adekeye, D.K., Asaolu, S.S., Adefemi, S.O. and Ibigbami O.A. 2019. Heavy metal adsorption properties of the basement complex of clay deposit in Ire-Ekiti Southwestern Nigeria. IOSR J. Environ. Sci. Toxicol. Food Tech., 13(2):1-8.

Akpomie, K.G., Odewole, O.A., Ibeji, C.U., Okagu, O.D. and Agboola., I.I. 2017. Enhanced sorption of trivalent chromium unto novel cassava peel modified kaolinite clay. Der. Pharma. Chemica., 9(5): 48-55.

Arnamwong, S., Suksabye, P. and Thiravetyan, P. 2016. Using Kaolin in reduction of arsenic in rice grains: Effect of different types of Kaolin, pH and arsenic complex. Bull. Environ. Contam. Toxicol., 96: 556-561.

Babel, S. and Kurniawan, T.A. 2003. Low-cost adsorbents for heavy metals uptake from contaminated water: a review. J. Hazard. Materials, 97(1): 219-243.

Bailey, S. E., Olin, T. J., Bricka, R. M. and Adrian, D. D. 1999. A review of potentially low-cost sorbents for heavy metals. Water Research, 33(11): 2469-2479.

Barhoumi, S., Messaoudi, I., Deli, T., Said, K. and Kerkeni, A. 2009. Cadmium bioaccumulation in three benthic fish species, *Salaria basilisca*, *Zosterisessor ophiocephalus* and *Solea vulgaris* collected from the Gulf of Gabes in Tunisia. J. Environ. Sci., 21(7): 980-984.

Bradl, H. B. 2004. Adsorption of heavy metal ions on soils and soils constituents. J. Colloid Interface Sci., 277(1): 1-18.

Dawodu, F. A., Akpomie G. K. and Ejikeme P. C. N. 2012. Equilibrium, thermodynamic and kinetic studies on the adsorption of lead (II) from solution by "Agbani Clay. Research J. Engine. Sci., 1(6): 9-17.

Eba, F., Gueu, S., Eya'A-Mvongbote A., Ondo J. A., Yao B. K., Ndong N. J., and Kouya, B.R. 2010. Evaluation of the absorption capacity of the natural clay from Bikougou (Gabon) to remove Mn (II) from aqueous solution. Inter. J. Engine. Sci. Tech., 10: 5001-5016.

El-Sayed G.O., Aly H.M. and Hussien S.H.M. 2011. Removal of acrylic dye blue-5G from aqueous solution by adsorption on activated carbon prepared from maize crops. Int. J. Res. Chem. Environ., 1: 132-140

El-Sheikh, A.H., Newman, A.P., Al-Daffaee, H.K., Phull, S. and Cresswell, N. 2004. Characterization of activated carbon prepared from a single cultivar of Jordanian Olive stones by chemical and physicochemical techniques. J. Anal. Appl. Pyrolysis, 71: 151-164.

Eloussaief, M., Jarraya, I. and Benzina, M. 2009. Adsorption of copper ions on two clays from Tunisia: pH and temperature effects. Appl. Clay Sci., 46(4): 409-413.

Eloussaief, M. and Benzina, M. 2010. Efficiency of natural and acid activated clays in the removal of Pb(II) from aqueous solutions. J. Hazard. Mater., 178(1-3): 753-757.

Emam, A.A., Ismail, L.F.M., AbdelKhalek, M.A. and Azza, R. 2016. Adsorption study of some heavy metal ions on modified kaolinite clay. Interna. J. Advance. Enginee. Tech. Manag. Appl. Sci., 3(7): 152-163.

Freundlich, H.M.F. 1906. Over the adsorption in solution. J. Phys. Chem., 57: 385-471.

Fu, F. and Wang, Q. 2011. Removal of heavy metal ions from wastewaters: A review. J. Environ. Manag., 92(3): 407-418.

Garg, K.V., Amita, M., Kumar, R. and Gupta, R. 2004. Basic dye (methylene blue) removal from simulated wastewater by adsorption using Indian Rosewood sawdust: A timber industry waste. Dyes Pigments, 63: 243-250.

Gonzalez, R.J., Videa, P.J.R. Rodriguez, E., Ramirez, S.L., and Gardeaorresdey J.L. 2005. Determination of thermodynamics parameters of Cr(VI) adsorption from aqueous solution onto *Agave lechuguilla* biomass. J. Chem. Thermodynamics, 37: 343-347.

Guadalupe, R., Reynel-Avila, H.E., Bonilla-Petriciolet, A. Cano-Rodríguez, I., Velasco-Santos, C. and Martínez-Hernández, A.L. 2008. Recycling poultry feathers for Pb removal from wastewater: Kinetic and equilibrium studies. Proceedings of World Academy of Science, Engineering and Technology, 30.

Ho, Y.S. and Mckay, G. 1999. Pseudo-second order model for sorption process. Process Biochem., 34(5): 451-465.

Kinnburgh, D.G. 1986. General purpose adsorption isotherms. Environ. Sci. Tech., 20(9): 895-904.

Ku, Y. and Jung, I.L. 2001. Photocatalytic reduction of Cr(VI) in aqueous solutions by UV irradiation with the presence of titanium dioxide. Water Research, 35(1): 135-142.

Kumara, P. S., Ramalingamb, S., Kiruphac, S. D., Murugesanc, A. Vidhyadevic, T. and Sivanesan, S. 2011. Adsorption behavior of nickel(II) onto cashew nut shell: Equilibrium, thermodynamics, kinetics, mechanism and process design. Chemical Engine. J., 167: 122-131.

Lagergren, S. 1908. Zurtheorie der sogenannten adsorption gelösterstoffe (About the theory of so-called adsorption of soluble substances). Kungliga Svenska Vetenskapsakademiens. Handlingar, 24(4): 1-39.

Langmuir, I. 1918. The adsorption of gases on plane surfaces of glass, mica and platinum. J. American Chem. Soc., 40: 1362-1403.

Mbaye, A., Diop, C. A., MieheBrendle, K., Jocelyne, S. F and Maury. T. 2014. Characterization of natural and chemically modified kaolinite from Mako (Senegal) to remove lead from aqueous solutions. Clay Minerals, 49: 527-539.

Mohan, S. and Karthikeyan. J. 1997. Removal of lignin and tannin color from aqueous solution by adsorption on to activated carbon solution by adsorption on to activated charcoal. Environ. Pollu., 97: 183-187.

Mohan, S.V., Kisa, T., Ohkuma, T., Kanaly, R.A. and Shimizy, Y. 2006. Bioremediation technologies for treatment of PAH-contaminated soil and strategies to enhance process efficiency. Rev. Environ. Sci. Biotech., 5: 347-374.

Natalia, C. D., Patrícia, A.S. and Maria-Cristina, B. B. 2015. Characterization and modification of a clay mineral used in adsorption tests. J. Mineral Mater. Characteriz. Engine. 3: 277-288.

Nethaji, A., Sivasamy, A. and Mandal, B. 2013. Adsorption isotherms, kinetics and mechanism for the adsorption of cationic and anionic dyes onto carbonaceous particles prepared from Juglansregia shell biomass. Int. J. Environ. Sci. Technol., 10: 231-242.

Olivella, M.A., Jove, P. and Oliveras, A. 2011. The use of cork waste as a biosorbent for persistent organic pollutants–study of adsorption/desorption of polycyclic aromatic hydrocarbons. J. Environ. Sci. Health A Tox. Hazard. Subst. Environ. Eng., 46: 824-832.

Olu-Owolabi, B.I., Alabi, A.H., Unuabonah, E.I., Diagboya, P.N., Böhmd, L. and During, R. 2016. Calcined biomass-modified bentonite clay for removal of aqueous metal ions. J. Environ. Chem. Enginee., 4: 1376-1382.

Petit, S., Decarreau, A., Mosser, C., Ehret, G. and Grauby, O. 1995. Hydrothermal synthesis (250ºC) of copper substituted kaolinites. Clay Minerals, 43: 482-494.

Ramesh, A., Lee, D.J. and Wong, J.W.C. 2005. Thermodynamic parameters for adsorption equilibrium of heavy metals and dyes from wastewater with low-cost adsorbents. J. Colloid Interface Sci., 291: 588-592.

Rattanaphani, S., Chairat, M., Bremner, J. and Rattanaphani, V. 2007. An adsorption and thermodynamics study of lac dyeing on cotton pretreated with chitosan. Dyes and Pigment, 72: 88-96.

Rengaraj, S., Moona, S.H., Sivabalan, R., Arabindoo, B. and Murugesan, V. 2002. Removal of phenol from aqueous solution and resin manufacturing industry wastewater using an agricultural waste: Rubber seed coat. J. Hazard Mater., 89: 185-196.

Saikia, N.J., Bharali, D.J., Sengupta, P., Bordoloi D., Goswamee, R.L., Saskia, P.C. and Borthakur, P.C. 2003. Characterization, beneficiation and utilization of a kaolinite clay from Assam, India. Applied Clay Science, 24: 93-103.

Senthilkumaar, S., Varadarajan, P.R., Porkodi, P.K. and Subbhuraam, C.V. 2005. Adsorption of methylene blue onto jute fiber carbon: kinetics and equilibrium studies. J. Colloid Interface Sci., 284: 78-82.

Shawabke, R.A., Rockstraw, D.A. and Bhada, R.K. 2002. Copper and strontium adsorption by a novel carbon material manufactured from pecan shells. Carbon, 40: 781-786.

Shim, H.Y., Lee, K.S., Lee, D.S and Jeon, D.S. 2014. Application of electrocoagulation and electrolysis on the precipitation of heavy metals and particulate solids in washwater from the soil washing. J. Agric. Chem. Environ., 3(4): 130-138.

Tsenga, R.L., Wub, F.C. and Juang, R.S. 2003. Liquid-phase adsorption of dyes and phenols using pinewood-based activated carbons. Carbon, 41: 487-495.

Unuabonah, E.I., Adebowale, K.O. and Olu-Owolabi, B.I. 2007. Kinetic and thermodynamic studies of the adsorption of lead (II) ions onto phosphate modified kaolinite clay. J. Hazard. Mater., 144: 386-395.

Voudrias, E., Fytianos, F. and Bozani, E. 2002. Sorption description isotherms of Dyes from aqueous solutions and wastewaters with different sorbent materials, Global Nest. Int. J. 4(1): 75-83.

Pham, T.D., Nguyen, H.H., Nguyen, N.V., Vu, T.T., Pham, T.N.M., Doan, T.H.Y., Nguyen, M.H. and Ngo, T.M.V. 2017. Adsorptive removal of copper by using surfactant modified laterite soil. Journal of Chemistry, Article ID 1986071, 1-11.

Van der-Marel, H.W. and Beutelspacher, S. 1976. Atlas of Infrared Spectroscopy of Clay Minerals and Their Mixtures. Elsevier, Amsterdam, pp. 397.

Wilson, M.J. 1994. Clay Mineralogy: Spectroscopic and Chemical Determinative Methods, Chapman and Hall, London, UK18-60.

Zouraibi, M., Ammuri, A. K. Z. and Saidi, M. 2016. Adsorption of Cu(II) onto natural clay: Equilibrium and thermodynamic studies. J. Mater. Environ. Sci., 7(2): 566-570.

Accumulation Characteristics and Risk Assessment of Potentially Toxic Elements for Major Crops and Farmland Around A High-arsenic Coal Mine in Xingren, Guizhou, Southwest China

F.X. Qin*(**)†, Y. Yi**, J.Y. Gong**, Y.B. Zhang*, K. Hong* and Y.K. Li**

* School of Life sciences, Guizhou Normal University, Guiyang 550001, P.R. China
**Key Laboratory of State Forestry Administration on Biodiversity Conservation in Karst Mountainous Areas of South-western China, Guizhou Normal University, Guiyang 550001, P.R. China
†Corresponding author: Fanxin Qin; fanxq0822@163.com

ABSTRACT

This study assessed the contamination by toxic elements (TEs), including lead (Pb), cadmium (Cd), chromium (Cr), zinc (Zn), copper (Cu) and arsenic (As), and their accumulation characteristics in soil-crop systems in Xingren, Guizhou, southwest China, by using the target hazard quotient (THQ) to evaluate the possible health risk in the target area. The mean value of the geo-accumulation index (I_{geo}; 1.95, 1.89 and 1.96 for rice, maize and *Coix lacryma-jobi L.*, respectively) shows As in partial contamination level. The potential ecological risk index (RI) values show that 90% of samples exceed in considerable ecology risk level (120 < RI 240). The concentration of investigated TEs (except Zn) in the edible part of the three crops tended to be lower than in other tissues: root > stalk > leaf > husk >edible part. Maize showed a major restriction in TE intake compared to rice and *Coix lacryma-jobi* L. The THQ of As was from 0 to 6.33 in all the plant samples, which indicates that the THQ exceeded the safe limit (THQ=1) in some samples. The total THQs (TTHQ) had a similar trend as RI, further indicating the potential health risk of the elements in combination. These data indicate that local people experience significant health risks if they ingest crops from the investigated area.

INTRODUCTION

Toxic elements (TEs) are ubiquitously distributed in the pedosphere and the geosphere. Soil TE contamination is an environmental issue in China and worldwide (Sun et al. 2010) because of its adverse impacts, such as contamination of water and soil, phytotoxicity, biotoxicity, accumulative behaviour and potential human health risk (Yu et al. 2008). Eating plants from the contaminated area or inhalation of polluted particles are the principal factors contributing to TE exposure for the human population (Loutfy et al. 2006).

For instance, it has been recognised that the food chain can serve as an important pathway of TE exposure for humans and animals (Dudka & Miller 1999). TEs are likely to transfer and accumulate through the soil-crop system and thus may affect the quality of agricultural products and cause health risks to humans (Mico et al. 2006). Total TE content in soils is directly related to the background level, but anthropogenic activities seem to have the far-reaching impact (Singani & Ahmadi 2012). Anthropogenic activities, including mining, sewage irrigation and vehicular exhaust, are the major sources of TE pollution of farmland (Li et al.

2014). TE contamination in the vicinity of mining areas is mainly from smelting and refining, wastewater discharge and tailings disposal. Levels of TE pollution of air, water, sediments, soil and crops in the mine-affected areas are reported to be greatly higher than areas without mining activities (Balabanova et al. 2010, Razo et al. 2004, Liu et al. 2005, Liu et al. 2010, Bi et al. 2006).

Researchers worldwide have carried out studies of the distribution of TEs in different tissues of crops (Funtua et al. 2014, Hu et al. 2014, Rahman et al. 2014). TE accumulation in plants depends on plant species, plant tissues, TE species, the efficiency of different plants to take up metals and soil-to-plant bioaccumulation factors (Rattan et al. 2005, Liao et al. 2016). Wang et al. (2017) indicated that wheat was more likely to accumulate TEs than maize. Similarly, the TE contents in wheat and barley were higher than those in maize (Pruvot et al. 2006) and the mean value of TEs in rice was higher than maize in the edible part (Zarcinas et al. 2004). Chen et al. (2016) indicated that the transferability of Cu, Pb, Zn and Cd in a soil-rice system was stronger than those in soil-wheat and soil-canola systems. Cadmium had

a stronger transfer capacity from soil to crops and the root acted as a barrier for Pb uptake. The heavy metal uptake by plants shows the greatest accumulation of Cu, Cr and Pb in the roots, Cd in the leaves, and Zn in the seeds of rice (Fazeli et al. 1998). A large proportion of TEs easy accumulates in the metabolic organ, but a small amount accumulates in the vegetative organs. Nan et al. (2002) found that the order of translocation ratios of Cd and Zn in different tissues of maize and wheat were root > stem > grain. Therefore, the accumulative situation in crops was dissimilar among the investigated TEs.

A series of studies have been carried out in the Xingren coalmine area in southwest Guizhou province, China. Most studies have focused on the occurrence and enrichment of toxic elements in coals (Ding et al. 1999, Yang et al. 2006, Zhao et al. 1998, Yang et al. 2006), environmental geochemical characteristics (Yang & Liu, 1997, Qu et al. 2016), soil pollution and risk assessment in the vicinity of the mine (Qin et al. 2016) and water environment chemistry (Wu et al. 2009, Sun et al. 2013, Tang et al. 2009). Due to the exposure and accumulation of TEs, the health risk to local people is associated with crops grown in the polluted area. A study focused on the potential health risks of the TEs in soil and brown rice from Hunan province of China indicated that Cd had greater transferability from soil to the plant than other elements (Zeng et al. 2015). Meanwhile, the research shows that long-term exposure to TEs through brown rice consumption poses both potential non-carcinogenic and carcinogenic health risks to the local residents (Zeng et al. 2015). Nevertheless, due to the limited assessments of metal pollution and health risks in Xingren, research gaps remain between the TE levels and accumulation characteristics in soil-crop systems.

The objective of this study was to analyse the content of TEs in soil and crop tissues, to evaluate the soil toxic element pollution and to comprehensively understand the pollution of toxic elements in the study area. The representative farmland soil-crop (rice, maize and *Coix lacryma-jobi* L.) systems of Xingren were selected since they are the daily diet for the local people. The risk of crop intake was evaluated by the target risk coefficient, which provides a reference for the food safety of the residents in the mining area.

MATERIALS AND METHODS

Study Area

Xingren county (104°54′-105°34′E; 25°16′-25°48′N) is located in the southwest of Guizhou Province, China. This area has a subtropical humid climate with an annual average rainfall of 1300~1450 mm and monthly rainfall from May to October greater than 100 mm. The coal resource from the Xingren coalfield is plentiful and thus Xingren is listed as being one of 200 major coal-producing counties in China. The large numbers of high-coal mining operations caused environmental deterioration during the 1980s and 1990s. Although the mining activities in the high-arsenic coal area have been prohibited in 1994, there are still abandoned coalmines and coal gangue across the county. In particular, the acid wastewaters, which come into being through the migration of dust and rain leaching, are the main source of TE pollution for farmland. The major source of income for local residents is growing crops, which include rice, maize and *Coix lacryma-jobi* L., in the study area.

Sampling and Preparation

Sampling was carried out in October 2015. There were 67 sample sites and 8~10 soil and 3~5 plant samples were collected from each (Fig. 1). The soil was prepared by first randomly collected samples from a depth of 0-20 cm. All the samples were stored in clean polyethylene plastic bags to avoid further contamination and transported to the laboratory immediately. All soil samples were air-dried at room temperature (20-25°C). Stones, plant roots and other debris were removed and then the soil was sieved through a nylon sieve (pore size 2 mm). Crop samples were washed with purified deionised water (18.2 MΩ·cm) and dried overnight at 105°C for 2 h, then at 75°C to a constant weight. After drying, the samples were crushed with a porcelain mortar and pestle and then sieved through a 2-mm nylon sieve. Portions of all samples were ground in an agate grinder and passed through a 0.149-mm sieve to further remove impurities. The prepared samples were stored in airtight Ziploc bags at 20°C for laboratory analysis.

Sample Testing and Quality Assurance

Soil samples (200 mg) were digested with 10 mL of concentrated HNO_3-$HClO_4$ in a 9:4 ratio at 160°C and then the levels of TEs (Pb, Cd, Cr, Zn and Cu) were determined. Additionally, As was extracted using 50 vol% aqua-regia [HNO_3 (68 mass%): HCl (37 mass%) = 1:3]. Plant samples were put in an airtight polytetrafluoroethylene tube and acidic mixture (HNO_3-H_2O_2 in a 3:1 ratio) was added for digestion on a fully automatic digestion instrument (Mars 6, CEM, USA). The total TE (Pb, Cd, Cr, Zn, Cu and As) concentrations were determined by an atomic absorption spectrometer (ZEEnit700P®, Analytikjena, Germany). The instrumental parameters of the atomic absorption spectrometer for determination of Pb, Cd, Cr, Zn and Cu are given in Table 1 and the atomisation program is presented in Table 2.

Arsenic was analysed using an atomic fluorescence
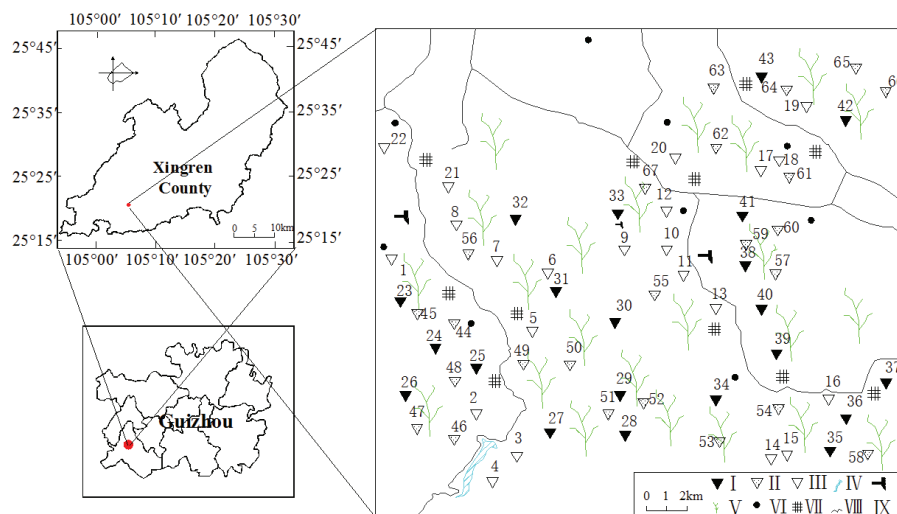
Fig. 1: Sampling location and the study area site (I Soil/maize, II Soil/*Coix lacryma-jobi* L., III Soil/rice, IV Water, V Crops, VI Country, VII Tailings, VIII Road, IX coal mine).

spectrometer (AFS-933, Beijing Titan, China). The test conditions for As were: wavelength 197.3 nm; negative high voltage 270 V; total current 60 mA; complement cathodes 30 mA; atomiser height 8 mm. The digesting reagents were of analytical grade and purified deionised water (18.2 MΩ·cm) was used for dilution.

The accuracy of the measurements was verified using the national standard reference materials from the National Research Centre (Beijing, China): GBW07405 and GBW07454 for soil samples; GBW07603 for plant samples. Addition one duplicate of five samples were used for quality control.

Blanks were used for background correction and control deviation of two blanks under 20%. The deviation of duplicate measurement results was within the tolerance range (<5%).

Evaluation Methods

Geo-accumulation index: The geo-accumulation index (I_{geo}) was used to evaluate the degree of anthropogenic- or geogenic-induced accumulated pollution (Bhutiani et al. 2017). The index reflects the natural variation of the TE distribution and can estimate the impact of human activities on the environment. I_{geo} is widely used to investigate quantitative

Table 1: Instrumental parameters for atomic absorption spectrophotometry analysis for determination of TEs elements.

Parameter	Element				
	Pb	Cd	Cr	Zn	Cu
Wavelength (nm)	283.3	228.8	357.9	213.9	324.8
Slit width (nm)	0.5	0.5	0.8	0.5	0.8
Lamp type	HCl	HCl	HCl	HCl	HCl
Lamp current (mA)	2	2	4	2	2

Table 2: Temperature programme for atomic absorption spectrophotometry for the determination of TEs elements.

Step	Pb			Cd			Cr			Zn			Cu		
	Temp °C	Ramp (S)	Hold (S)	Temp °C	Ramp (S)	Hold (S)	Temp °C	Ramp (S)	Hold (S)	Temp °C	Ramp (S)	Hold (S)	Temp °C	Ramp (S)	Hold (S)
Drying	110	5	10	110	6	20	110	5	10	110	5	10	110	5	10
Pyrolysis	800	300	10	500	300	10	1300	300	10	650	50	20	1100	300	10
Atomization	2000	1600	4	1500	1500	3	2300	1500	5	2150	1500	3	2100	1500	4
Clean-out	2450	500	4	2450	500	4	2450	500	4	2450	500	4	2450	500	4

indicators of TEs pollution in sediments and soil (Förstner et al. 1993). The formula is:

$$I_{geo} = \log_2(\frac{C_n}{1.5B_n}) \qquad \ldots(1)$$

Where, I_{geo} is the index of geo-accumulation for an element in soil samples; and are the determined concentration of the metals in the target and reference areas, respectively. The values used were the average background values of TEs in Guizhou soil: As = 20.00 mg/kg, Cr = 95.90 mg/kg, Pb = 35.20 mg/kg, Zn = 99.50 mg/kg, Cd = 0.66 mg/kg and Cu = 32.00 mg/kg (MEPPRC 1990). I_{geo} and the classification of pollution level (Müller 1969) are given in Table 3.

Potential Ecological Risk: The Potential Ecological Risk Index (RI) evaluates the ecological degree for toxins and toxic elements in soils (Häkanson 1980) that could be toxic for biological species (Yisa et al. 2012). As one of the most common risk assessment methods of toxic element pollution for soil, it not only reflects the impact of a single pollutant in a particular environment but also reflects the comprehensive impact of a variety of pollutants. The formulas are shown as follows:

$$E_r^i = T_r^i \cdot \frac{C_i}{C_n^i} \qquad \ldots(2)$$

$$RI = \sum E_r^i = \sum T_r^i \cdot C_f^i \qquad \ldots(3)$$

Where, is the pollution coefficient for a certain element, which reflects the pollution level of a single TE (Zhuang & Gao 2014). is the concentration of the ith toxic metal in soil, and indicates the reference background concentration of toxic elements in the soils of Guizhou Province (MEPPRC 1990). is the potential ecological risk coefficient of the particular TE. is the toxic-response factor for element i. According to Häkanson (1980), is set as follows: Pb = 5, Cd = 30, Cr = 2, Zn = 1, Cu = 5 and As = 10. The potential ecological risk index was classified into five categories (Table 4) (Häkanson 1980, Zhuang & Gao 2014).

There were some differences with the classical Häkanson potential ecological hazard index method (Häkanson 1980). In the studies of Häkanson (1980) and Zhuang & Gao (2014), the first-stage upper limit of the is obtained by the non-polluted pollution coefficient (= 1) multiplied by the maximum toxicity coefficient in the reference pollutant. In this paper, the value of Cd is the largest one among the six of TEs, as = 30. From this, the first grading criterion of is 30, and the other criterion is multiplied by 2 on the previous stage (Li et al. 2015).

From Formula (3), RI is related to the type and quantity of pollutants. Specifically, the pollutants constituted more complex have stronger toxicity (the larger), the greater the RI value. Thus, it must be considered that appropriate adjustment the type and quantity of pollutants when using the RI ecological risk assessment.

Using Häkanson's first-level classification limit (150) and the total toxicity factor of eight pollutants (133) to get the unit toxicity coefficient (1.13). Taken unit toxicity coefficient (1.13) to multiply total toxicity coefficient (53) of six TE, and round the decimal to get the first limit of RI (about 60), the other criterion was multiplied by 2 on the previous stage. The classification criteria for the assessment of the potential ecological risk of TEs in soils are given in Table 4. It is different from the Häkanson's classification.

Plant enrichment is closely related to plant species, soil substrate, and TEs' categories. The bioaccumulation factor or transfer factor (BAF/TF) is usually used to characterise plant TE accumulation (Khan et al. 2010), which reflects the plant ability for metal storage in roots and/or translocation to aerial organs. The BAF was calculated as follows:

$$BAF = \frac{C_r}{C_s} \qquad \ldots(4)$$

Table 3: Index of Geo-accumulation (I_{geo}) and classification of pollution level (Müller 1969).

Degree of pollution	Clean	Light Pollution	Partial contamination	Contamination	Emphasis on pollution	Heavy pollution	Serious pollution
I_{geo}	$I_{geo} \leq 0$	$0 < I_{geo} \leq 1$	$1 < I_{geo} \leq 2$	$2 < I_{geo} \leq 3$	$3 < I_{geo} \leq 4$	$4 < I_{geo} \leq 5$	$I_{geo} > 5$
Grade	0	1	2	3	4	5	6

Table 4: Grading standards of potential ecological risk of TEs in soils.

Degree	Low	Moderate	Considerable	High	Very hight
E_r^i	≤ 30	30~60	60~120	120~240	≥ 240
RI	60	60~120	120~240	≥ 240	

$$TF = \frac{C_t}{C_r} \qquad \ldots(5)$$

Where, C_t represents the TE concentration in tissues (stalk, leaf, husk or edible parts) of crops; C_r represents the concentration in the root; C_s represent concentration in soils on a dry-weight basis.

The target hazard quotient (THQ) is a health risk assessment model recommended by the US Environmental Protection Agency (US EPA 1997). The health risks from consumption of crops depend on the level of exposure and the amount of absorption by local inhabitants. The estimated risk using the THQ is based on the equation below (US EPA 1997, Bhatti et al. 2017).

Where, C_C is the metal concentration in crops (mg/kg); D_F is food ingestion (g/person/d); B_W is the average adult body weight (60 kg); RfD is the oral reference dose (mg/kg/d).

$$THQ = \frac{C_{crop} \times D_{foodintake} \times EF \times ED}{B_W \times AT \times RfD} \qquad \ldots(6)$$

Where, C_{crop} is the metal concentration in food (mg/kg); $D_{food\,intake}$ is food ingestion (g/person/d); BW is the average body weight, adult (60 kg); EF is exposure frequency (365 days/year)；ED is exposure duration (70 years); AT is averaging time for noncarcinogens (365 days/year × number of exposure years, assuming 70 years in this study); RfD is the oral reference dose (mg/kg/d). Oral reference doses were 3.5×10^{-3}, 1.0×10^{-2}, 1.5, 0.3, 4.0×10^{-2} and 3.0×10^{-4} mg/kg/d for Pb, Cd, Cr, Zn, Cu and As respectively (US EPA 1997).

Considering the literature (US EPA 1997, Bhatti et al. 2017, Fang et al. 2015, Du et al. 2013, Zeng et al. 2015, Wang et al. 2016) and the US EPA exposure factors handbook, it was determined that the adult intake in this area was 0.25, 0.15 and 0.20 kg/person/d for rice, maize and *Coix lacryma-jobi* L., respectively. If the THQ is ≥ 1, the exposed population is likely to experience serious health risks and if the level of the THQ is < 1, the risk associated with exposure to the metal is negligible.

The potential impact of TEs on human health is generally a combined effect of a variety of elements (Bhatti et al. 2017).

To assess the combined effect of more than one element, Total THQ (TTHQ) is calculated by the following modified equation (US EPA 1997):

$$TTHQ(crop) = \sum THQ_M = THQ_{M1} + THQ_{M2} + \cdots + THQ_{Mn} \quad \ldots(7)$$

When TTHQ ≤ 1, it means there is no significant negative impact; when 1 ≤ TTHQ <10, the TEs may be potential non-carcinogenic health risks, and when TTHQ > 10, the presence of TEs will cause chronic toxic effects.

The data were processed in Excel 2007 for preliminary data processing. Statistical analyses were performed with the Statistical Package for the Social Sciences (SPSS 18.0). Charts and graphs were created using Origin (Origin 8.5, OriginLab) and The R Programming Language (R i386 3.4.1).

RESULT AND DISCUSSION

Concentration of TEs in Crop Soils

The soil pH varied between 3.95 and 6.37. The rice soil had lower pH compared to the two other crops. Table 5 summarises the pH and variation coefficient (VC, SD/mean) of Pb, Cd, Cr, Zn, Cu and As in soils from the target area. According to the soil background value of Guizhou (MEPPRC 1990), all elements in the soil were higher than the background value, especially Pb and As. The mean concentrations of Pb (183.11 mg/kg) and As (119.03 mg/kg) in rice soil were 5.2 and 5.95 times higher than the background value (Pb = 35.20 mg/kg, As = 20.00 mg/kg), respectively. Similar results were found for maize and *Coix lacryma-jobi* L. The Cd and As minimum concentrations in soils exceeded the grade II of environmental quality standard values (Cd = 0.30 mg/kg, As =30 mg/kg in paddy field or 40 mg/kg in dry land) for soils of China (MEPPRC 1990); in particular, the As in paddy soil was 2.45 times above the standard value.

The mean value of Pb, Cd, Cr, Zn, Cu and As in soil exceeded the maximum permitted levels (Fig. 2). The concentrations of Pb, Cd and As were found to be far more than the reported levels (Shen et al. 2011) in the target area, while Zn and Cu showed less difference. One reason is that the investigated area suffered sewage irrigation, as well as spraying of pesticides, manure and fertiliser, which possibly increase

Table 5: pH and variation coefficient (VC) of TEs in soil samples.

Soil usage type	pH	Statistics	Pb	Cd	Cr	Zn	Cu	As
Rice soil (n=22)	3.95~6.19	VC/%	29.74	20.95	16.41	9.63	30.72	23.13
Maize soil (n=22)	4.28~6.22	VC/%	22.37	22.82	17.28	11.77	38.90	22.20
Coix lacryma-jobi L. soil (n=24)	4.35~6.37	VC/%	18.80	21.34	17.39	13.48	42.89	25.80

the TE contamination compared to that of agricultural land. Another possible reason is the mining activities and factories around the study area (Li et al. 2014), which may also contribute to the TE exposure. The mean levels of Pb, Cd, Cr, Zn and Cu in the three crops were in this order: upland (207.89, 0.89, 194.00, 102.52 and 131.43 mg/kg for maize; 212.18, 0.88, 197.31, 106.40 and 128.01 mg/kg for *Coix lacryma-jobi* L.) > paddy soil (183.11, 0.78, 188.73, 97.22 and 147.10 mg/kg). These five elements had similar trends in the maize soil and the *Coix lacryma-jobi* L. soil.

Assessment of TE Pollution by the Index of Geo-accumulation:

The geo-accumulation indexes calculated for the soil of the target areas are shown in Fig. 3. The mean I_{geo} for toxic elements had a trend of As and Pb > Cu > Cr > Cd > Zn. A similar study by Qin et al. (2016) indicated that As and Pb had relatively higher contamination levels ($I_{geo} \geq 3$). The result from Fig. 3. showed that Zn from all the soil samples was similar to the unpolluted level, Cd (86.36% soil samples for rice, 76.19% soil samples for maize, 79.17% soil samples for *Coix lacryma-jobi* L.) was at the clean level and Cr (90.91%, 90.48% and 95.83% for rice, maize and *Coix lacryma-jobi* L.) indicated light pollution, while Pb, Cu and As indicated moderate contamination. According to the mean I_{geo}, the elemental concentration in the studied soil samples could be categorised as: (1) As, Pb and Cu in the moderately polluted category; the source could be coal gangue, which contains Cu and Pb, and uncontrolled discarded wastewater (Qishlaqi et al. 2008); (2) Cr was in the lightly polluted category and might be mainly related to atmospheric deposition (Shi et al. 2014, Zeng & Wu 2013); and (3) Cd and Zn were in the unpolluted category. The results are similar to those reported by Qin et al (2016) in which the contamination levels were in the order: As, Pb and Cu > Cr > Cd.

Assessment of TE Pollution by Potential Ecological Risk

According to the formulas (2-3), the ecological risk (ER) value and potential ecological risk values (RI) for each of
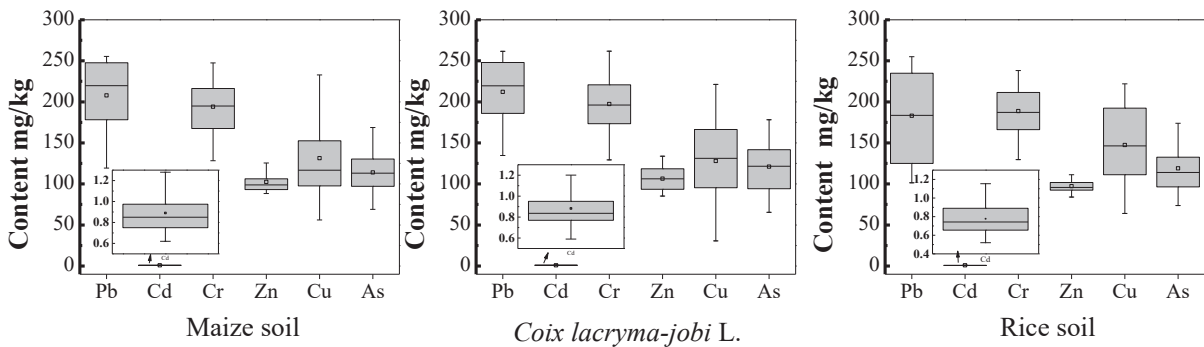
Fig. 2: Box plots for content of TEs in different type soils. (n=67) Guizhou soil background: As=20.00mg/kg, Cr=95.90mg/kg, Pb=35.20mg/kg, Zn=99.50mg/kg, Cd=0.66mg/kg, Cu=32.00mg/kg. Standards values (pH <6.5) were 250, 0.30, 200, 50 mg/kg for Pb, Cd, Zn and Cu; 250, 30 mg/kg for Cr and As in paddy field, 130, 40 mg/kg for Cr and As in dry land. (Grade II of environmental quality standards values for soils of China, GB 15618-1995).
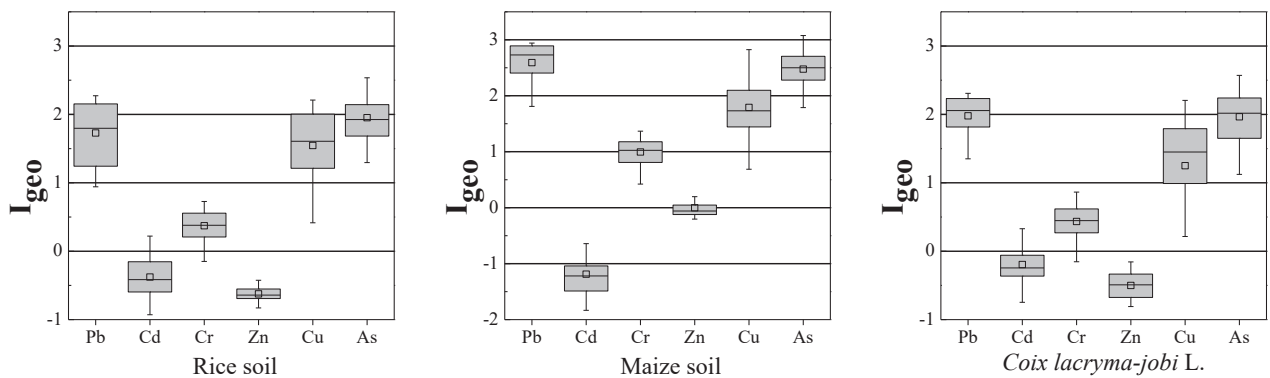
Fig. 3: Box plots for I_{geo} of TEs in different type soils, the horizontal lines represent I_{geo} values of -1, 0, 1, 2 and 3. (n=67).

the studied metals are shown (individually and in total) in Fig. 4 and 5. The risk indices of the metals are in the order: As > Cd > Pb > Cu > Cr > Zn.

The ER values for Cr and Zn were mostly at low levels, while these values were high for the other examined elements. The results indicate that the contribution of Cr and Zn to the potential ecological risk is relatively low. The sample of ER_{Pb} in low ecological risk level (50% of samples) and moderate ecological risk level (50% of samples) is in equal possibility. Almost every sample of ER_{Cu} was of low potential ecological risk. From Fig. 3, almost all the ER_{As} and ER_{Cd} values from the study area reached the level of moderate potential ecological risk (30 < ER < 60).

The I_{geo} result indicates that Pb and As are in a similar pollution situation. The reason why $ER_{As} > ER_{Pb}$ is that the toxic-response factor of As is double that of Pb. Cadmium posed a moderate potential ecological risk, which differs from the I_{geo} level because the toxic-response coefficient is

relatively high (= 30). The rank of the ER average of each element in the three types of land-use was similar to the results of I_{geo}, indicating that the soil pollution impacts its ER.

Fig. 5 shows that nearly 94% of the study area reached the level of considerable potential ecological risk (120 < RI < 240). The variation decreased in the order: maize (100-205) > rice (97-196) > *Coix lacryma-jobi* L. (117-195). Average RI was highest in *Coix lacryma-jobi* L. followed by maize and rice. The mean and individual values showed considerable potential ecological risk due to a high level of TEs in the study area. The interaction of the six elements increases the risk of the study area and the high degree of potential ecological risk may lead to crop contamination.

It is crucial to integrate these methods to obtain more knowledge of the TEs risk in the target area due to the limitation of the current models (Zhang et al. 2012). Long-term mining activities (> 10 years) resulted in high arsenic levels in coalmining areas (Chen et al. 2002), which polluted the
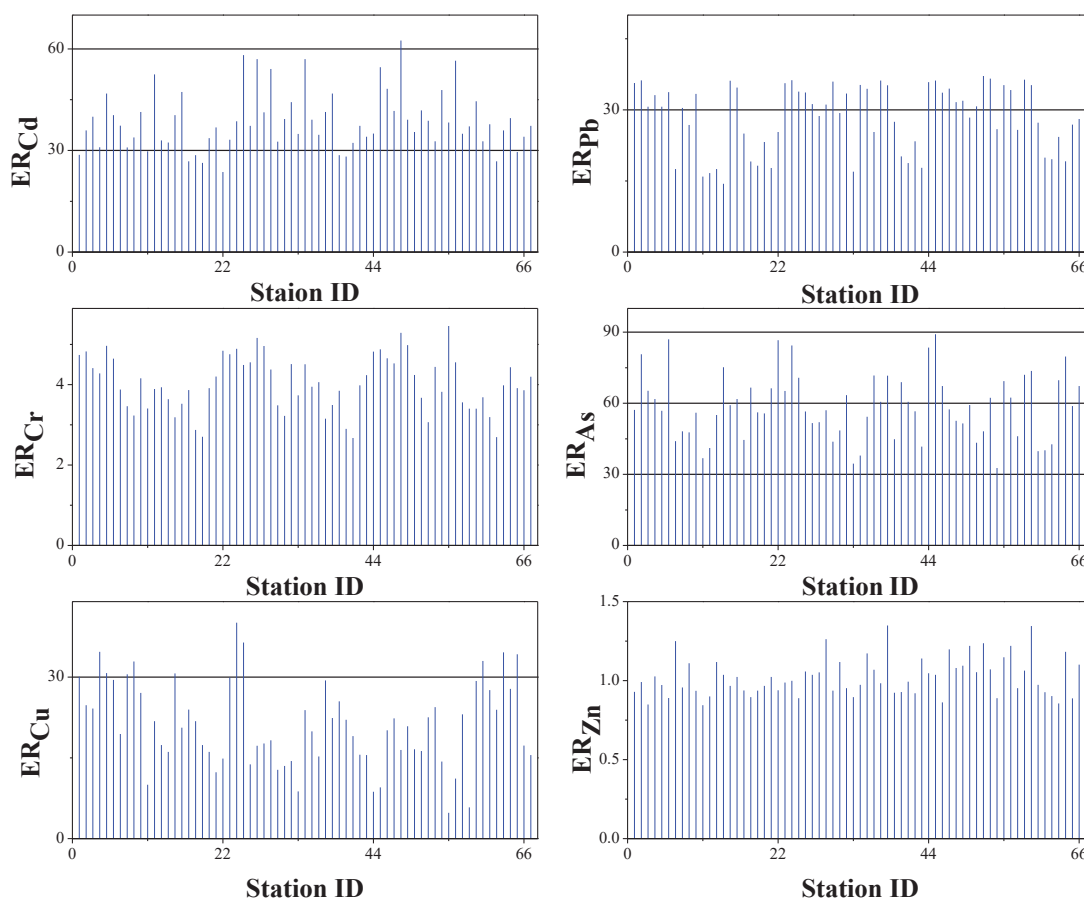
Fig. 4: The ecological risk (ER) of HMs in soil samples, the horizontal lines represent ER values of 30, 60 and 90. (n=67 soil, rice is range 1 to 22, maize is 23 to 43, *Coix lacryma-jobi* L. is 44 to 67).

nearby water and affected ecological functions. There was moderate contamination by As and the considerable potential ecological risk is shown by merging the results of I$_{geo}$ and the potential ecological risk.

Assessment of TE Concentration in Crops

The concentration of TEs in each plant portion is presented in Fig. 6. TEs were widely distributed in different parts of the plant and the TEs in root were significantly higher than in other parts (Bose & Bhattacharyya 2008). It is important to focus on the TE content of the edible part because it is the main source of dietary exposure (Khan et al. 2015). The mean concentration of Pb (0.12 mg/kg), Cd (0.07 mg/kg), Cr (0.64 mg/kg), Cu (1.58 mg/kg) and As (0.17 mg/kg) in the edible part of rice were less than other organisation (the minimum of other organisation: 0.75, 0.08, 1.44, 1.80, 0.65 mg/kg). Similar results were found in maize and *Coix lacryma-jobi* L.

Analysis of the levels of the elements in three crops (rice, maize and *Coix lacryma-jobi* L.) showed that TEs (except Zn) were highest in the root and lowest in the edible part. However, Zn showed a different trend. Zn was higher in the stalk and leaf for rice, in the leaf and husk for maize, and the leaf and edible parts for *Coix lacryma-jobi* L. Compared with rice and maize, the edible part of *Coix lacryma-jobi* L. has a relatively strong capacity for Zn storage. According to the maximum permitted level of contaminants in food set by the Ministry of Heath of the People's Republic of China (MHPRC 2012), the mean value of the edible portions of the three crops was below the threshold of safety value for Pb, Cd, Cr, Zn, Cu and As (0.20, 0.10, 1.00, 50.00, 10.00 and 0.20 mg/kg). The concentrations of Pb in the edible part were highest in *Coix lacryma-jobi* L. (0.14 mg/kg) and lowest in maize (0.10 mg/kg), which was similar to

Cr and As. Zinc was highest in *Coix lacryma-jobi* L. (10.91 mg/kg) and lowest in rice (6.24 mg/kg), which was the same as Cd and Cu.

Compared TEs content of three crops show that As and Cd were highest (lowest) in rice (maize) and maize (rice), respectively; Cu was higher in *Coix lacryma-jobi* L. There was an interspecific difference among crops. As and Pb content was high and matched the geo-accumulation index evaluation result. Compared to the concentration of Cd in soil, the concentration in crops was at a higher level.

The TF and BAF of the Crops

To assess the transfer of TEs from soil to crops, the transfer factor (TF) and bioaccumulation factor (BAF) were calculated (Fig. 7). The BAF and TF of different TEs in crops were dissimilar. The capacity of plants to uptake toxic elements is different and the same toxic element can be accumulated in different ratios in various plant species (Singh et al. 2010). The transport and enrichment ability of TEs was higher in the aerial parts than the underground parts of the crops. The reason is that aerial parts of plants mainly consist of metabolic organs and biomass is higher than underground.

Transfer factors of the edible parts (leaf, stalk and husk) for TEs decreased in the order Cd > Zn > Cu > Cr > As > Pb. The TF$_{Pb}$ values (except above total) was lower than 0.01 for the three cultivation systems. The possible reason was that the root hinders uptake of Pb (Cui et al. 2014). The BAF$_{root}$ (except As of maize and Pd of *Coix lacryma-jobi* L) decreased in the order Cd > Cu > Zn > As > Cr > Pb, which is similar to the study by Chen et al. (2016) in rice of the Yangtze River Delta region. The TF$_{Zn}$ and TF$_{As}$ of the aerial part (except As of rice) were in contrast to those of the root (Zn > Cu and Cr > As). This result shows that the aerial parts
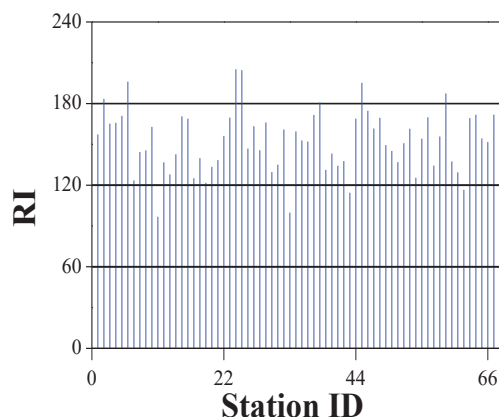
Fig. 5: The potential ecological risk index (RI) of TEs in soil samples, the horizontal lines represent RI values of 60, 120 and 180. (n=67 soil, rice is range 1to 22, maize is 23 to 43, *Coix lacryma-jobi* L. is 44 to 67.)

could absorb the Zn by the root and hinder the migration of As. BAF (TF) of Cd was significantly higher than other elements. Cd performed a higher capacity of transportation inside the plant and the soil-crop system, which may explain that why soil evaluated in clean level has a potential risk. These results indicate that despite Cd in soil was not polluted (I_{geo} <0), but the ability of three crops for the absorption of Cd was relatively strong. BAFs of Zn were slightly lower than those of Cd. The synergism between Cd and Zn enhances the efficiency of each other's transfer (Nan et al. 2002). In the rice-soil system, BAF_{Zn} and BAF_{As} showed the highest values, which were different depending on the soil type (dry land > paddy field). These data indicate that the accumulation of TEs in crops is not only influenced by soil concentration, but also by physical and chemical properties of the soil or other factors. For instance, the equilibrium pH value (<4) could affect toxic elements sorption and desorption on soil components thus affecting the migration of metals (Najafi & Jalali 2015). Most soils of the target area are acidic, which may promote the migration of toxic elements from soil to crop (Chen et al. 2016). Possible reasons include (1)

rice having a strong transferability for Zn and As; (2) water evaporates out cause the pH to decrease during the maturation period (Shamshuddin et al. 2014), which may lead to metal desorption and metal ions being released into the soil solution (Chen et al. 2016).

The BAF and TF of each metal were dependent on the crop type and species. The bioaccumulation of toxic elements is different for different plant species, which is reflected by differences in their growth, reproduction, occurrence and survival in the metal-contaminated soil (Khan et al. 2015). Notably, different plant species possess different tolerance to the same pollutant under the same conditions. This difference may be explained by the different mechanisms and efficiency in the elemental uptake of plant species (Garty 2001). The BAF (TF) of TEs (except for Zn) in the three crops can be divided into three levels: root > stalk and leaf > husk and edible parts, while the Zn is disordered. Fig. 6 shows that the accumulation ability of edible part is highest in *Coix lacryma-jobi* L (except Cr) compared to other crops. The TF of As in each part of rice is higher than other crops in this study, which represent that As was easily absorbed by
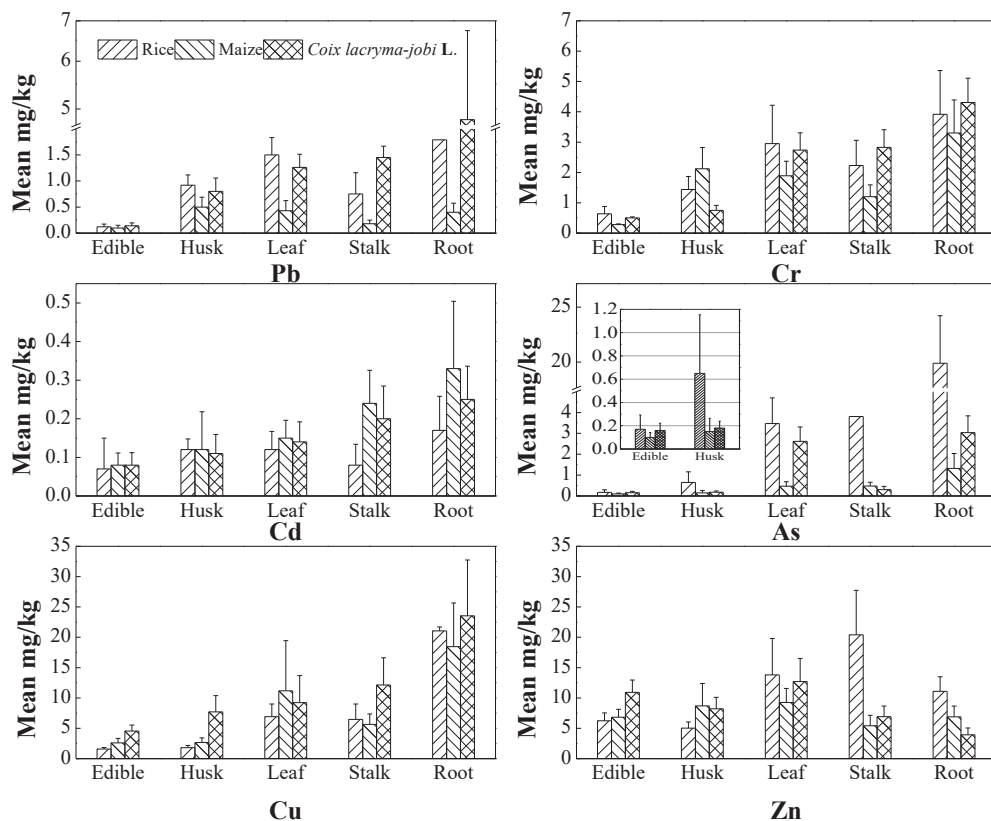
Fig. 6: The concentrations of TEs in each part of crop samples (mg/kg).

the rice. Maize had relatively lower enrichment and transport capacity compared to rice and *Coix lacryma-jobi* L, except for Cd. Combining the BAF and TF$_{above\ total}$ it was found that the absorption of Cu (Zn) of *Coix lacryma-jobi* L. (rice) was higher than other plants.

Correlation Coefficient Between TEs in Soil and Crop Tissue

As shown in Fig. 8, the *r*-values were found to be significant ($p<0.05$). Thus, all the observed correlations were not high. The *r*-value depicted the strongest positive correlation as being between root and soil. The most significant positive correlation was observed for As of rice, Cu of maize and Zn of *Coix lacryma-jobi* L. (*r*-values of 0.415, 0.437 and 0.413, respectively). TEs in root were positively correlated with soils, showing an increase in the concentration of one metal with a decrease in the concentration of other metals. No significant positive or negative correlation was observed
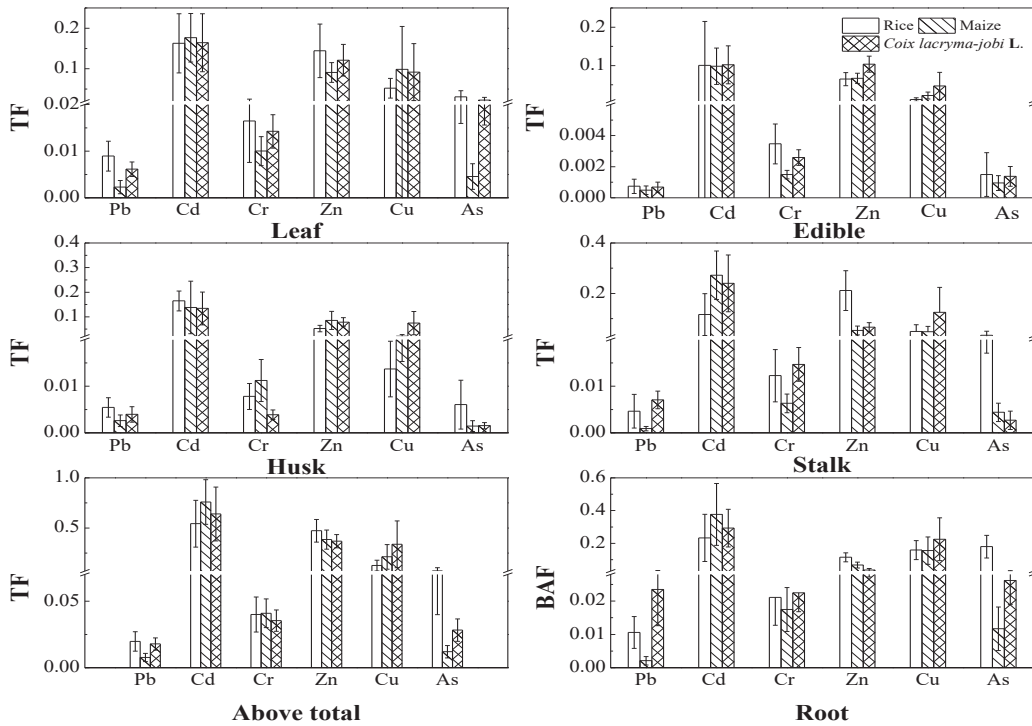
Fig. 7: Transfer factor and bioaccumulation factor of TEs in the three soil-crop systems.
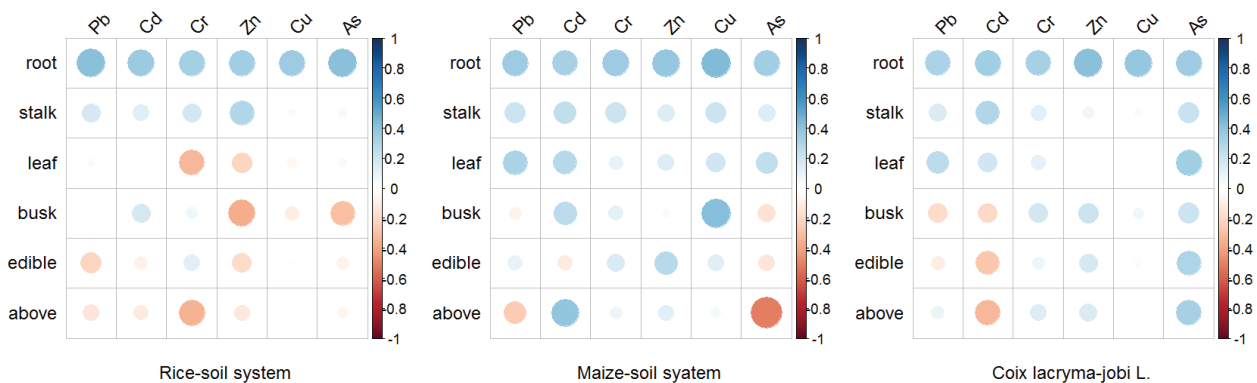
Fig. 8: r-values distribution between TEs contents in soil and different tissues of plants.

in other parts of the plants, which indicates that the sources of the elements in the soil were not the same.

Health Risk Assessment of TEs through the Food Chain

Target hazard quotient through the food chain quantification health risk, and the assessment process main determined by exposure to various virulence factor (Bhatti et al. 2017). The THQ is a tool to assess the level of risk associated with a particular pollutant. The estimation of the hazard quotient of metals in different crops from various sites is given in Table 6.

In the entire study area, the THQs for TEs through food (crops) consumption were found to be in the order: As > Cd > Cu > Pb > Zn > Cr (except *Coix lacryma-jobi* L.). The THQ values in this study were <1 for all TEs expect As. The THQ_{As} in rice, maize and *Coix lacryma-jobi* L. was 0~6.33, 0~1.22 and 0.56~3.03, respectively, which indicates that some samples' THQ was >1 and above the safe limits. The mean value of THQ_{As} for maize was <1 (Table 6), while those of rice and *Coix lacryma-jobi* L. were >1. The results display similar trends with the BAF and TF (rice > *Coix lacryma-jobi* L. > maize). It is critical to reduce BAF and TF to ensure food safety.

The ranking orders of TTHQ for each plant were rice > *Coix lacryma-jobi* L. > maize. The potential risk of consumption of rice in the target area is higher than the others. The TTHQ of crop species was ≥ 1, indicating potential non-carcinogenic risks from ingestion of local crops (rice, maize and *Coix lacryma-jobi* L.). Since the THQ was <1 for TEs in maize, the health risk could be negligible to the inhabitants of the studied area by individual TE, but the combined effect of the metals may pose a health risk. The estimated TTHQ was mainly due to As. The THQ accounted for 76.77% (rice), 62.86% (maize) and 66.14% (*Coix lacryma-jobi* L.) of the TTHQ.

CONCLUSIONS

TE content in the investigated agricultural soils were in the order As > Pb > Cu > Cr > Cd > Zn. The average TE values were greater than the respective background values of the local area, while the soil contamination content exceeded the national standard.

The results of I_{geo} signify that As was at the highest contamination level compared to other TEs, while Pb and Cu were at the moderately polluted level, Cr was in the lightly polluted level, and Cd and Zn were not pollutants. The results of RI showed that exceeding 90% soil sample point is in the considerable potential ecological risk level, especially soil growing *Coix lacryma-jobi* L., and the highest contributing element was As. Therefore, urgent measures must be taken to control contamination with As in this area.

The TF_{Cd} value was significantly higher than other elements, while Pb was second highest. There was competition in transport and absorption between Pb and Cd. Comparing the three plants, As was easily absorbed by the rice, while Cd was easily absorbed by maize and Cu was easily absorbed by *Coix lacryma-jobi* L. Pb, Cd, Cr and As are accumulated in rice, indicating that rice (compared maize and *Coix lacryma-jobi* L.) has a strong capability to transfer these metals from root to grain. Maize shows lower intake of TEs compared to rice and *Coix lacryma-jobi* L., while rice enriched the toxic elements.

The TTHQs values for the target area were ≥ 1, which indicates potential health risks. Therefore, measures must be taken to cut down the contents of TEs in the grain and soil and to use new technology to remove or reduce pollution due to anthropogenic activities.

ACKNOWLEDGEMENT

Table 6: THQ and TTHQ values for TEs caused by the consumption of crops.

Stem	Statistics	THQ						TTHQ
		Pb	Cd	Cr	Zn	Cu	As	
Rice	Minimum	0.03	0.02	1.03×10^{-3}	0.07	0.11	0.00	0.23
	Maximum	0.27	0.92	3.39×10^{-3}	0.15	0.20	6.33	7.88
	Mean	0.15	0.30	1.78×10^{-3}	0.09	0.16	2.30	3.00
Maize	Minimum	0.03	0.00	4.10×10^{-4}	0.04	0.08	0.00	0.14
	Maximum	0.16	0.33	5.33×10^{-4}	0.07	0.25	1.22	2.02
	Mean	0.07	0.21	4.69×10^{-4}	0.06	0.16	0.84	1.33
Coix lacryma-jobi L.	Minimum	0.06	0.02	1.04×10^{-3}	0.09	0.24	0.56	0.97
	Maximum	0.32	0.45	1.39×10^{-3}	0.17	0.50	3.03	4.47
	Mean	0.13	0.28	1.11×10^{-3}	0.12	0.38	1.79	2.70

REFERENCES

Balabanova, B., Stafilov, T., Ba eva, K. and Šajn. 2010. R Biomonitoring of atmospheric pollution with heavy metals in the copper mine vicinity located near Radoviš, Republic of Macedonia. J. Environ. Sci. Health, Part A, 45: 1504-1518.

Bhatti, S.S., Sambyal, V., Singh, J. and Nagpal, A.K. 2017. Analysis of soil characteristics of different land uses and metal bioaccumulation in wheat grown around rivers: Possible human health risk assessment. Environ. Dev. Sustain., 19: 571-588.

Bhutiani, R., Kulkarni, D.B., Khanna, D.R. and Gautam, A. 2017. Geochemical distribution and environmental risk assessment of heavy metals in groundwater of an industrial area and its surroundings, Haridwar, India. Energy. Ecol. Environ., 2: 155-167.

Bi, X.Y., Feng, X.B., Yang, Y.G., Qiu, G.L., Li, G.H., Li, F.L., Liu, T.Z., Fu, Z.Y. and Jin, Z.S. 2006. Environmental contamination of heavy metals from zinc smelting areas in Hezhang County, western Guizhou, China. Environ. Int., 32: 883-890.

Bose, S. and Bhattacharyya, A.K. 2008. Heavy metal accumulation in wheat plant grown in soil amended with industrial sludge. Chemosphere, 70: 1264-1272.

Chen, H.Y., Yuan, X.Y., Li, T.Y., Hu, S., Ji, J.F. and Wang, C. 2016. Characteristics of heavy metal transfer and their influencing factors in different soil-crop systems of the industrialization region, China. Ecotox. Environ. Safe, 126: 193-201.

Chen, P., Huang, W.H. and Tang, X.Y. 2002. Features of arsenic content, occurrence in coal and its effect on environment in China. Coal. Geol. Explor., 30: 1-4.

Cui, L.W., Feng, X.B., Lin, C.J., Wang, X.M., Meng, B., Wang, X. and Wang, H. 2014. Accumulation and translocation of ^{198}Hg in four crop species. Environ. Toxicol. Chem, 33: 334-340.

Ding, Z.H., Zheng, B.S., Zhang, J., Belkin, H.E., Finkelman, R.B., Zhao, F.H., Zhou, D.X., Zhou, Y.S. and Chen, C.G. 1999. Preliminary study on the mode of occurrence of arsenic in high arsenic coals from southwest Guizhou Province. Sci. China. Ser. D, 42: 655-661.

Du, Y., Hu, X.F., Wu, X.H., Shu, Y., Jiang, Y. and Yan, X.J. 2013. Effects of mining activities on Cd pollution to the paddy soils and rice grain in Hunan province, Central South China. Environ. Monit. Assess., 185: 9843-9856.

Dudka, S. and Miller, W.P. 1999. Accumulation of potentially toxic elements in plants and their transfer to human food chain. J. Environ. Sci. Health, Part B, 34: 681-708.

Fang, T., Liu, G.J., Zhou, C.C. and Lu, L.L. 2015. Lead in soil and agricultural products in the Huainan Coal Mining Area, Anhui, China: levels, distribution, and health implications. Environ. Monit. Asse., 187(3): 152.

Fazeli, M.S., Khosravan, F., Hossini, M., Sathyanarayan, S. and Satish, P.N. 1998. Enrichment of heavy metals in paddy crops irrigated by paper mill effluents near Nanjangud, Mysore District, Karnataka, India. Environ. Geol., 34: 297-302.

Förstner, U., Ahlf, W. and Calmano, W. 1993. Sediment quality objectives and criteria development in Germany. Water. Sci. Technol., 28: 307-316.

Funtua, M., Agbaji, E. and Pam, A. 2014. Heavy metals contents in soils and some crops irrigated along the Bindare Stream Zaria-Kaduna State, Nigeria. American. Chemical. Science. Journal, 4: 855-864.

Garty, J. 2001. Biomonitoring atmospheric heavy metals with lichens: theory and application. Crit. Rev. Plant. Sci., 20: 309-371.

Häkanson, L. 1980. An ecological risk index for aquatic pollution control: A sediment to logical approach. Water. Res., 14: 975-1001.

Hu, W.Y., Chen, Y., Huang, B. and Niedermann, S. 2014. Health risk assessment of heavy metals in soils and vegetables from a typical greenhouse vegetable production system in China. Hun. Ecol. Risk. Asse., 20: 1264-1280.

Khan, A., Kha, S., Khan, M.A., Qamar, Z. and Waqas, M. 2015. The uptake and bioaccumulation of heavy metals by food plants, their effects on plants nutrients, and associated health risk: A review. Environ. Sci. Pollut., 22: 13772-13799.

Khan, S., Rehman, S., Khan, A.Z., Khan, M.A. and Shah, M.T. 2010. Soil and vegetables enrichment with heavy metals from geological sources in Gilgit, northern Pakistan. Ecotox. Environ. Safe., 73: 1820-1827.

Li, Y.M., Ma J.H., Liu D.X., Sun Y.L. and Chen Y.F. 2015. Assessment of heavy metal pollution and potential ecological risks of urban soils in Kaifeng city, China. Environ. Sci, 36: 1034-1044.

Li, Z.Y., Ma, Z.W., Van der Kuijp, T.J., Yuan, Z.W. and Huang, L. 2014. A review of soil heavy metal pollution from mines in China: pollution and health risk assessment. Sci. Total. Environ, 468: 843-853.

Liao, J.B., Wen, Z.W., Ru, X., Chen, J.D., Wu, H.Z. and Wei, C.H. 2016. Distribution and migration of heavy metals in soil and crops affected by acid mine drainage: Public health implications in Guangdong Province, China. Ecotox. Environ. Safe., 124: 460-469.

Liu, C.P., Luo, C.L., Gao, Y., Li, F.B., Lin, L.W., Wu, C.A. and Li, X.D. 2010. Arsenic contamination and potential health risk implications at an abandoned tungsten mine, southern China. Environ. Pollut., 158: 820-826.

Liu, H.Y., Probst, A. and Liao, B.H. 2005. Metal contamination of soils and crops affected by the Chenzhou lead/zinc mine spill (Hunan, China). Sci. Total. Environ., 339: 153-166.

Loutfy, N., Fuerhacker, M., Tundo, P., Raccanelli, S., EL Dien, A. and Ahmed, M.T. 2006. Dietary intake of dioxins and dioxin-like PCBs, due to the consumption of dairy products, fish/seafood and meat from Ismailia city, Egypt. Sci. Total. Environ., 370: 1-8.

MEPPRC 1990. Background Concentrations of Elements in Soils of China. Ministry of Environmental Protection of the People's Republic of China, China Environmental Science Press, Beijing.

MHPRC 2012. Maximum Levels of Contaminants in Food (GB 2762-2012). Ministry of Health of the People's Republic of China, Chinese Standard Press, Beijing.

Mico, C., Recatala, L., Peris, M. and Sánchez, J. 2006. Assessing heavy metal sources in agricultural soils of a Europea Mediterranean area by multivariate analysis. Chemosphere, 65: 863-872.

Müller, G. 1969. Index of geo-accumulation in sediments of the Rhine river. Geo. Journal, 2: 108-118.

Najafi, S. and Jalali, M. 2015. Effects of organic acids on cadmium and copper sorption and desorption by two calcareous soils. Environ. Monit. Assess., 187: 585.

Nan, Z.G., Li, J.J., Zhang, J.M. and Cheng, G.D. 2002. Cadmium and zinc interactions and their transfer in soil-crop system under actual field conditions. Sci. Total. Environ., 285: 187-195.

Pruvot, C., Douay, F., Hervé, F. and Waterlot, C. 2006. Heavy metals in soil, crops and grass as a source of human exposure in the former mining areas. J. Soil. Sediment, 6: 215-220.

Qin, F.X., Wei, C.F., Zhong, S.Q., Huang, X.F., Pang, W.P. and Jiang, X. 2016. Soil heavy metal (loid)s and risk assessment in vicinity of a coal mining area from southwest Guizhou, China. J. Cent. South. Univ., 23: 2205-2213.

Qishlaqi, A., Moore, F. and Forghani, G. 2008. Impact of untreated wastewater irrigation on soils and crops in Shiraz suburban area, SW Iran. Environ. Monit. Assess., 141: 257-273.

Qu, Q.Y., Liu, G.J., Sun, R.Y. and Kang, Y. 2016. Geochemistry of tin (Sn) in Chinese coals. Environ. Geochem. Hlth., 38: 1-23.

Rahman, M.A., Rahman, M.M., Reichman, S.M., Lim, R.P. and Naidu, R. 2014. Heavy metals in Australian grown and imported rice and vegetables on sale in Australia: Health hazard. Ecotox. Environ. Safe., 100(1): 53-60.

Rattan, R.K., Datta, S.P., Chhonkar, P.K., Suribabu, K. and Singh, A.K. 2005. Long-term impact of irrigation with sewage effluents on heavy metal content in soils, crops and groundwater-a case study. Agr. Ecosyst. Enviro., 109(3): 310-322.

Razo, I., Carrizales, L., Castro, J., Díaz-Barriga, F. and Monroy, M. 2004. Arsenic and heavy metal pollution of soil, water and sediments in a semi-arid climate mining area in Mexico. Water. Air. Soil. Poll., 152: 129-152.

Shamshuddin, J., Elisa Azura, A., Shazana, M.A.R.S., Fauziah, C.I., Panhwar, Q.A. and Naher, U.A. 2014. Properties and management of acid sulfate soils in Southeast Asia for sustainable cultivation of rice, oil palm and cocoa. Adv. Agron., 124: 91-142.

Shen, W.T., Wu, Y.G., Huang, B.P., Wang, L.T., Liao, F. and Chen, C. 2011. Heavy metal contamination and enzyme activity of topsoil in abandoned coal mining area in Xingren County of Guizhou Province. Guizhou. Agr. Sci., 39: 111-115.

Shi, P., Xiao J., Wang, Y. and Chen, L. 2014. Assessment of ecological and human health risks of heavy metal contamination in agriculture soils disturbed by pipeline construction. Int. J. Environ. Res. Public Health, 11: 2504-2520.

Singani, A.A.S. and Ahmadi, P. 2012. Manure application and cannabis cultivation influence on speciation of lead and cadmium by selective sequential extraction. Soil. Sediment. Contam., 21: 305-321.

Singh, R., Singh, D.P., Kumar, N., Bhargava, S.K. and Barman, S.C. 2010. Accumulation and translocation of heavy metals in soil and plants from fly ash contaminated area. J. Environ. Biol., 31: 421-430.

Sun, J., Tang, C.Y., Wu, P., Liu, C.Q. and Zhang, R.X. 2013. Migration of Cu, Zn, Cd and As in epikarst water affected by acid mine drainage at a coalfield basin, Xingren, Southwest China. Environ. Earth. Sci., 69: 2623-2632.

Sun, Y.B., Zhou, Q.X., Xie, X.K and Liu, R. 2010. Spatial, sources and risk assessment of heavy metal contamination of urban soils in typical regions of Shenyang, China. J. Hazard. Mater., 174, 455-462.

Tang, C.Y., Wu, P., Tao, X.Z., Zhang, C.P. and Han, Z.W. 2009. The basin acidification affected by AMD: A case study in Xingren county, Guizhou, China. Carsologica Sinica, 28: 135-143.

US EPA.1997. Integrated Risk Information System Database. United States Environmental Protection Agency, Washington, DC. http://www2.epa.gov/iris/iris-recent-additions-2013-1997.

Wang, S.Y., Wu, W.Y., Liu, F., Liao, R.K. and Hu, Y.Q. 2017. Accumulation of heavy metals in soil-crop systems: a review for wheat and corn. Environ. Sci. Pollut. R, 24: 15209-15225.

Wang, X.Q., Zeng, X.D., Liu, C.Q., Li, F.B., Xu, X.H. and Lv, Y.H. 2016. Heavy metal contaminations in soil-rice system: source identification in relation to a sulfur-rich coal burning power plant in Northern Guangdong Province, China. Environ. Monit. Assess., 188: 1-12.

Wu, P., Tang CY., Liu CQ., Zhu LJ., Pei TQ. and Feng LJ. 2009. Geochemical distribution and removal of As, Fe, Mn and Al in a surface water system affected by acid mine drainage at a coalfield in Southwestern China. Environ. Geol., 57: 1457-1467.

Yang, J.Y. 2006. Concentrations and modes of occurrence of trace elements in the Late Permian coals from the Puan Coalfield, southwestern Guizhou, China. Environ. Geochem. Hlth., 28: 567-576.

Yang, W.H. and Liu, Y.M. 1997. Sediment-hosted gold deposits in China-geochemistry and prospecting. Chin. J. Geochem., 16: 202-212.

Yang, Z.J., Tang, Y.G., Zheng, X., Li, J.J., Han, W.L. and Yang, S.T. 2006. Enrichment of arsenic, antimony, thallium and selenium in high-arsenic coal from Xingren County, Guizhou Province. Chin. J. Geochem., 25: 50.

Yisa, N.J., John, J.O. and Onoyima, C.C. 2012. Assessment of toxic levels of some heavy metals in road deposited sediments in Suleja, Nigeria. Am. J. Chem., 2: 34-37.

Yu, R.L., Yuan, X., Zhao, Y.H., Hu, G.R. and Tu, X.L. 2008. Heavy metal pollution in intertidal sediments from Quanzhou Bay. J. Environ. Sci. China, 20: 664-669.

Zarcinas, B.A., Pongsakul, P., McLaughlin, M.J. and Cozens, G. 2004. Heavy metals in soils and crops in Southeast Asia 2. Thailand. Environ. Geochem. Hlth., 26: 359-371.

Zeng, F.F., Wei, W., Li, M.S., Huang, R.X., Yang, F. and Duan, Y.Y. 2015. Heavy metal contamination in rice-producing soils of Hunan province, China and potential health risks. Int. J. Environ. Res. Public. Health, 12: 15584-15593.

Zeng, H.A. and Wu, J.L. 2013. Heavy metal pollution of lakes along the mid-lower reaches of the Yangtze river in China: intensity, sources and spatial patterns. Int. J. Environ. Res. Public Health, 10: 793-807.

Zeng, X.F., Wang, Z.W., Wang, J., Guo, J.T., Chen, X.J. and Zhuang, J. 2015. Health risk assessment of heavy metals via dietary intake of wheat grown in Tianjin sewage irrigation area. Ecotoxicology, 24: 2115-2124.

Zhang, Y., Hu, X.N. and Tao, Y. 2012. Distribution and risk assessment of metals in sediments from Taihu Lake, China using multivariate statistics and multiple tools. B. Environ. Contam. Tox., 89: 1009-1015.

Zhao, F.H., Ren, D.Y., Zheng, B.S., Hu, T.D. and Liu, T. 1998. Modes of occurrence of arsenic in high-arsenic coal by extended X-ray absorption fine structure spectroscopy. Chinese Sci. Bull., 43: 1660-1663.

Zhuang, W. and Gao, X.L. 2014. Integrated assessment of heavy metal pollution in the surface sediments of the Laizhou Bay and the coastal waters of the Zhangzi Island, China: Comparison among typical marine sediment quality indices. Plos. One, 9: e94145.

Original Research Paper https://doi.org/10.46488/NEPT.2020.v19i03.003 **Open Access Journal**

Comparative Analyses of the Inhibitive Influence of *Cascabela thevetia* and *Jatropha curcas Leaves* Extracts on Mild Steel

A. S. Adekunle*, A. A. Adeleke*, P. P. Ikubanni **† and O. A. Adewuyi*

*Department of Mechanical Engineering, University of Ilorin, Nigeria
**Department of Mechanical Engineering, Landmark University, Omu-Aran, Nigeria
†Corresponding author: P. P. Ikubanni; ikubanni.peter@lmu.edu.ng

ABSTRACT

The inhibitive properties of the extracts of *Cascabela thevetia* and *Jatropha curcas* were comparatively studied on corrosion of mild steel in H_2SO_4 acid. The extracts of both plants contained active phytochemical constituents such as tannins, saponins, alkaloids, flavonoids, terpenes and phenols which made them useful as good corrosion inhibitors. The extract concentrations were varied from 0.3 to 1.5 g/L during both the gravimetric and gasometric analyses for an exposure time of 7-28 days. The weight loss of the coupon, corrosion rate, surface coverage and inhibitive efficiency was evaluated for both the extracts. The results of the gravimetric and gasometric analyses indicated that inhibitive efficiency increased with an increase in the concentration of inhibitors and the highest was 55.77% for *Jatrophas curcas* at the concentration of 1.5 g/L. The weight loss was a little lower for *Cascabela thevetia* (4.36 g) compared to *Jatrophas curcas* (4.66 g) at the highest exposure time used (28 days). *Cascabela thevetia* has a better surface coverage (0.68) than *Jatropha curcas* (0.61), hence, *Cascabela thevetia* inhibits better for a 7-day exposure time. However, when the mild steel was further exposed for more than 7 days, *Jatropha curcas* exhibited a better inhibitive property. The highest and least hydrogen gas evolution was obtained at 0.3 g/L concentration (7 minutes) and 1.5 g/L concentration (1 minute) for both *Cascabela thevetia* and *Jatropha curcas* leaves extracts, respectively. Based on the results, the utilization of extracts of *Cascabela thevetia* and *Jatropha curcas* leaves as replacements for toxic organic inhibitors in industries are recommended.

INTRODUCTION

The deterioration of materials as a result of its reaction with the environment is termed corrosion. It is a natural phenomenon that results in the destructive attack of any metal through chemical or electrochemical reaction with the environment (Bradford 1993, Perez 2004). It is described as the propensity of metallic materials to return to its organic state in a steadier mineral form (Mshelia et al. 2017). Apart from gold and platinum, nearly all metals will disintegrate in the environment that is oxidized thereby leading to the formation of compounds either in their oxides, sulphides or hydroxides state. Although metals tend to corrode naturally, the environment that metal is exposed to has great strength on the speed at which it will disintegrate (Syed 2006).

Corrosion is said to be a societal menace that causes numerous damages, destruction and degradation especially in industries as well as in automobiles, aeroplanes, highway bridges, household gadgets and many more (Odusote & Ajayi 2013). Corrosion is a constant and continuous problem which cannot be eliminated. Prevention is one of the best methods

to combat corrosion. Therefore, engineering materials are required to be protected against corrosion. One of such engineering materials is the mild steel which has found usefulness in automobile, construction, petrochemical industries and many more. It is a choice material due to its availability, low cost and excellent mechanical properties (Al-Otaibi et al. 2012). These materials are very susceptible to corrode in harsh and hostile aggressive environment. To mitigate the effect of corrosion on metal, the metallic corrosion rate can be avoided, prevented or lowered with the addition of corrosion inhibitor, which is one of the best-known methods of corrosion protection that is mostly used in the industry (Al-Otaibi et al. 2012).

Corrosion inhibitors are materials or substances which are introduced into a corrosion system in a little amount to lower or avert the metal reaction of the corrosive media (Singh et al. 2012). Various methods that have been used to control corrosion include coatings, inhibitors, designs, material selection and cathodic protection. However, inhibitors utilization has been one of the most practicable technique for corrosion protection in harsh environment (Ansari et al.

2012). Fundamentally, the various forms of corrosion inhibitors include anodic, cathodic, mixed and volatile corrosion inhibitors (Taghavikish et al. 2017, Asmara et al. 2017). Moreover, synthetic (organic), metallic (inorganic) and green inhibitors (natural products) are the variously classified corrosion inhibitors (Ajayi et al. 2012, Rani & Basu 2012). Researches have revealed that the toxicity of some of the synthetic and inorganic inhibitors is instigating mutation of genes as well as the failure of kidney and liver, to mention but a few (Singh et al. 2012). Green corrosion inhibitors have been prompted due to the environmental toxicity of organic corrosion inhibitors (Rani & Basu 2012). The advantages of green corrosion inhibitors over organic inhibitors are their biodegradability, environmental friendliness, ecological acceptance and they do not possess heavy metal or other toxic compounds. They are also not expensive, readily available and renewable (Odusote & Ajayi 2013, Rani & Basu 2012).

Green corrosion inhibitors have been seen to be effective in reducing the rate of corrosion of metals that are exposed to a hostile environment. Various studies have reported that these inhibitors (extract from leaves, barks, seeds, roots, and so on) have good inhibition efficiencies both in acidic and other aggressive media (Odusote & Ajayi 2013, Umoren et al. 2006). Corrosion inhibiting abilities of these green inhibitors have been attributed to the existence of organic compounds. These compounds are mainly tannins, saponins, alkaloids, steroids, flavonoids, amino acids, etc. in the plants (Rani & Basu 2012, Martinez 2003, Chowdhary et al. 2004, El-Etre et al. 2005). More so, numerous extracts from different parts of plants have been examined as metal corrosion inhibitors and have been reported to have inhibitive effects through the formation of a passivating layer (protective film) on the surface of the metal by adsorption of phytochemical molecules that are present in the plants on the surface of the metal (Oguzie & Ebenso 2006, El-Etre & El-Tantawy 2006). The plant parts, as well as their location, is a great determinant in the compound yields and the corrosion inhibitor abilities (Okafor et al. 2008). A few of plants extracts are *Delonix regia* extract (Abiola et al. 2007), natural onion juice (El-Etre 2006), *Carica papaya* leaf extract (Oki et al. 2015), *Punica granatum* extract (Rani & Selvaraj 2010), *Hibiscus sabdariffa* extract (Oguzie 2008), *Rhizophora racemose* extract (Oki et al. 2011), *Azadirachta indica* extract (Okafor et al. 2010), *Lawsonia* extract (El-Etre et al. 2005) and others.

Based on the current focus on green inhibitors, this study aims at exploring the utilization of plant extracts as green corrosion inhibitors for metallic materials. The study investigates the corrosion inhibitive properties of *Cascabela thevetia* and *Jatropha carcus* leaves extracts on mild steel corrosion by employing gravimetric and gasometric methods. Furthermore, comparison of the inhibitive effects was made between these two green inhibitors to ascertain the one which has higher inhibitive properties.

MATERIALS AND METHODS

Materials and equipment: The materials used for the experiment were mild steel (coupon) with its composition given in Table 1, sulphuric acid (H_2SO_4) solution, *Cascabela thevetia* leaves, *Jatropha curcas* leaves, methanol, ethanol and acetone.

A mild steel rectangular specimen was mechanically cut into coupons of $35 \times 20 \times 1$ mm with a 3 mm hole drilled in each of the coupons for suspension purpose. The exposed area of each coupon was mechanically abraded with emery paper of different grades, polished and degreased in ethanol, cleaned with acetone and then kept inside the desiccator.

Preparation of the inhibitors (*Cascabela thevetia* and *Jatropha curcas* leaf extracts): The leaves were plucked from a farm in Ilorin, Nigeria and washed and sliced into pieces. The sliced leaves were dried at room temperature and pulverized into powdery form. The pulverized form of the leaves was soaked with methanol for 48 hours. To obtain the needed extract, solution filtration was carried out while methanol was evaporated from the filtrate. A digital electronic weighing balance was used to weigh the extract. Fig. 1(a & b) show how the extracts were filtered while Fig. 1c represents the experimental set up for gasometric analysis.

***Cascabela thevetia* and *Jatropha curcas* leaves phytochemical analysis:** The phytochemical analysis of both the leaves disclosed the existence of tannins, saponins, flavonoids, alkaloids, phenol and terpenoids. It has been reported that the most active green inhibitor constituents in plants are tannins, saponins and alkaloids (Rani & Basu 2012, Martinez 2003, Chowdhary et al. 2004, El-Etre et al. 2005).

Key: + means present, - means absent

Gravimetric analysis: Extract ranging from 0.3 to 1.5 g were dissolved in separate beakers that contain 1 litre of sulphuric acid solution each, as the inhibited environments. The pre-treated coupons were removed from the desiccator. The weights of these coupons (w_1) were determined using a

Table 1: Compositional analysis of mild steel sample.

Element	C	Si	Mn	P	S	Cr	Ni	Mo	Fe
Composition (%wt.)	0.242	0.119	0.304	0.012	0.007	0.175	0.154	0.094	98.7
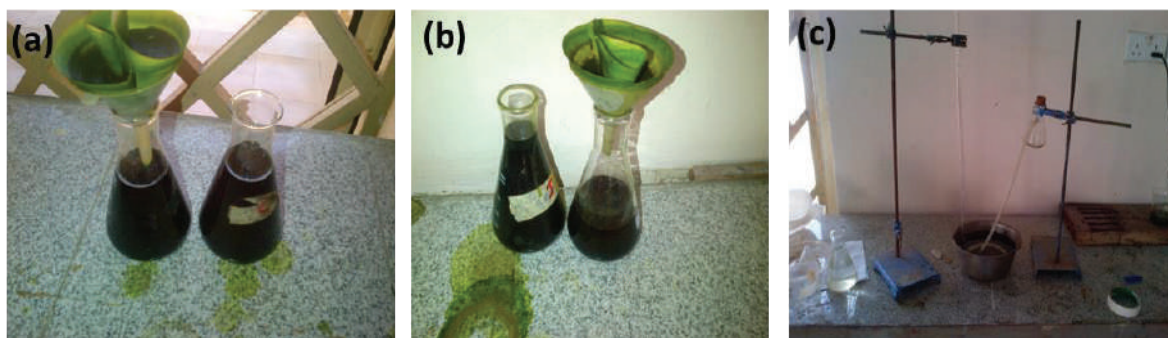
Fig. 1: (a) Filtration of *Cascabela thevetia* extract, (b) Filtration of *Jatropha curcas* extract, (c) Apparatus setup for gasometric analysis

digital electronic weighing balance of ±0.01g accuracy and the corresponding weight (w_1) was recorded. The prepared coupons were suspended into the prepared environment. The coupons were taken away from the different environments (either uninhibited or inhibited environments) at the end of 7 days. The coupons were then removed and rinsed with ethanol and with acetone at the end of each interval. The coupon samples were weighed again and the obtained weights (w_2) noted for each coupon. The experimentation for the study was carried out for 14, 21 and 28 days.

To obtain the weight loss for both the uninhibited and inhibited samples for each immersion period and the concentration of the inhibitors, Eq. (1) was used. Equations (2-4) were utilized to determine the corrosion rate, surface coverage and inhibitive efficiency of each inhibitor concentration (Ebenso et al. 2008, Eddy 2009):

$$\Delta w = w_1 - w_2 \qquad \ldots(1)$$

Where, Δw = weight loss, w_1 = initial coupon weight before immersion (g) and w_2 = final coupon weight after immersion (g).

$$Corrosion\ Rate\ (CR) = \frac{\Delta W}{AT} \qquad \ldots(2)$$

Where, A = Coupon area (mm^2) and T = Time spent in both media (h).

$$Surface\ Coverage\ (\Theta) = \frac{(CR_1 - CR_2)}{CR_1} \qquad \ldots(3)$$

$$Inhibitive\ Efficiency\ (I.\ E.) = \theta \times 100\% \qquad \ldots(4)$$

Where, CR_1 = Uninhibited environment corrosion rate and CR_2 = Inhibited environment corrosion rate, at the same interval.

Gasometric analysis: This experiment was carried out using $15 \times 10 \times 1$ mm mild steel coupons. With regards to the evolution of gas at the interphase of corrosion, the gasometric (gas-volumetric) method offers a quick and dependable way of determining any perturbation by the inhibitor. Each coupon was released into the Buckner flask which contains 4M H_2SO_4 solutions in the presence of both leaves' inhibition extracts at various concentrations (0.3-1.5 g/L) as well as the blank one at room temperature. The initial hydrogen gas volume was recorded as v_1. The experimental arrangement was permitted to stay for seven minutes and hydrogen gas volume evolved was recorded per minute interval as v_2. The gasometric experiment was done within 24 hours.

Equations (5-8) were used to determine the volume change (Δv), gas evolution rate (RV_H), surface coverage (θ) and inhibitive efficiencies (I.E %).

$$\Delta v = v_1 - v_2 \qquad \ldots(5)$$

Where, v_1 = initial hydrogen gas volume and v_2 = final hydrogen gas volume

$$Rate\ of\ gas\ evolved\ (RV_H) = \frac{\Delta V}{AT} \qquad \ldots(6)$$

Where, A = Area of the coupon (mm^2) and T = Time spent in both media (min)

$$Surface\ Coverage\ (\theta) = \frac{(RV_1 - RV_2)}{RV_1} \qquad \ldots(7)$$

$$Inhibitive\ Efficiency\ (I.\ E.) = \theta \times 100\% \qquad \ldots(8)$$

Where, RV_1 = initial rate of gas evolved and RV_2 = final rate of gas evolved

RESULTS AND DISCUSSION

Gravimetric studies: Figs. 2 and 3 show the obtained results from the weight loss, corrosion rate and inhibitive efficiency of *Cascabela thevetia* and *Jatropha curcas* inhibitors at the varied concentrations of the inhibitor with exposure time, respectively for the coupons suspended in H_2SO_4.

With the use of *Cascabela thevetia* and *Jatropha curcas*, the weight loss increases with time of exposure for both the uninhibited (blank) and inhibited environments (Figs. 2 &

3). It was also discovered that in both cases, as the concentrations of the inhibitors increase, the weight loss reduce. In both cases, it was observed that a very high amount of weight was lost for the blank (un-inhibited) samples when compared with the inhibited samples between day 7 and day 14 when subjected into H_2SO_4 environment. This implies that uninhibited steel will easily corrode when exposed to a corrosive environment. The weight loss at day 14 for the blank sample in H_2SO_4 environment was 5.18 g. However, within 21 days, the weight losses were observed to increase for both inhibitors in the inhibited environment. For the inhibited samples at various concentrations of *Cascabela thevetia*, same weight loss patterns were observed as the days increase from 7 to 21 days. However, between days 21 and 28, the weight loss increases for 0.3 g/L concentration between 5.43 and 5.88 g/L while for other concentrations, the weight losses reduce (Fig. 2). Moreover, from Fig. 3, the weight losses of the inhibited samples follow the same
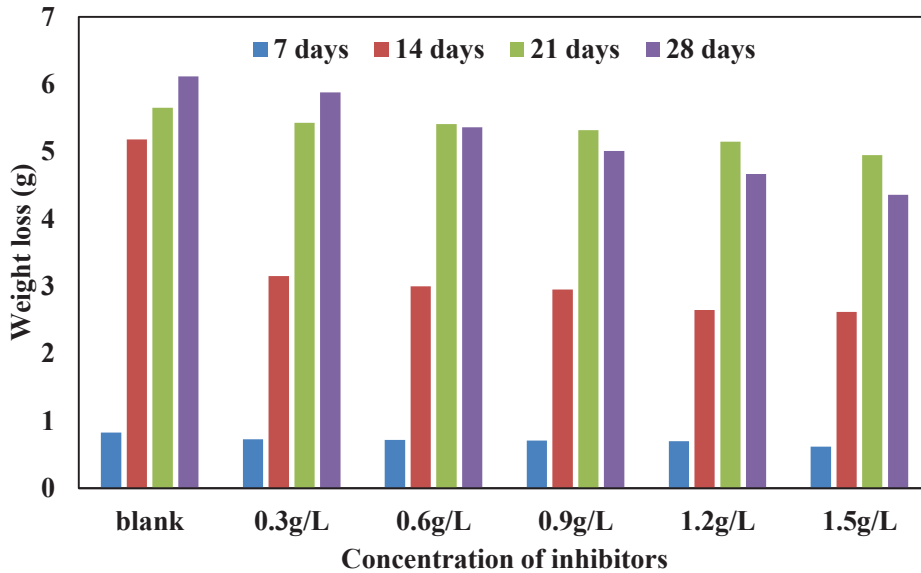
Fig. 2: Weight loss of mild steel in H_2SO_4 with different concentration of *Cascabela thevetia* inhibitor.
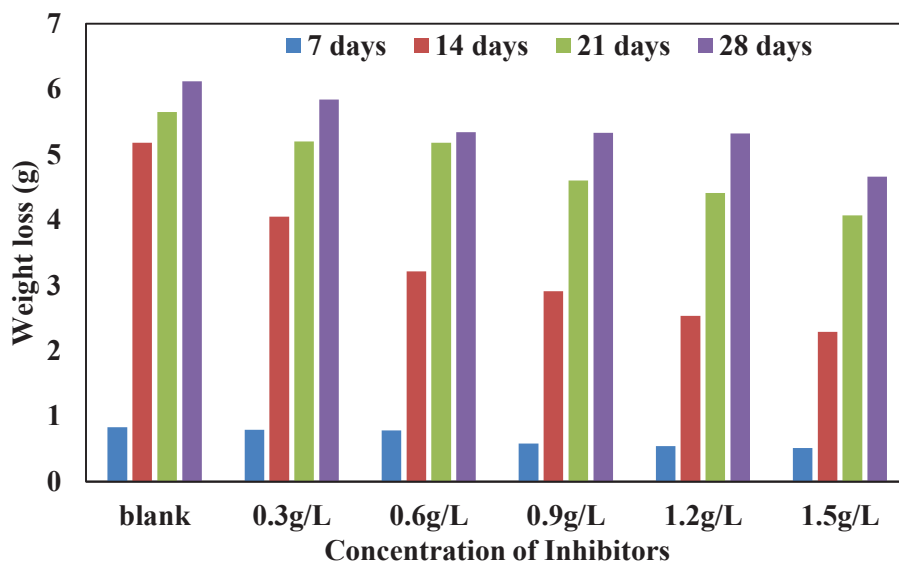
Fig. 3: Weight loss of mild steel in H_2SO_4 with different concentration of *Jatropha curcas* inhibitor.

pattern at 0.6, 0.9, 1.2 and 1.5 g/L concentrations of *Jatropha curcas* between days 7 and 21. Only at 0.6 g/L concentration of *Jatropha curcas* was the weight loss slightly increased while other concentrations show distinct weight losses between 21 and 28 days.

The weight loss reduction can be attributed to shielding film layer formation on the mild steel surface in the inhibited system (Oguzie & Ebenso 2006, El-Etre & El-Tamtawy 2006). The weight loss of the coupon in both inhibitors indicates that within 7-14 days at high concentration of 0.9-

1.5 g/L, *Cascabela thevetia* proves to be a superior inhibitor when compared to *Jatropha curcas*. However, *Jatropha curcas* displays the minimum weight loss within 14-21 days regardless of the inhibitor concentration. Therefore, *Jatropha curcas* demonstrates to be a superior inhibitor within 21 to 28 days than *Cascabela thevetia*.

Additionally, the rate of corrosion for the blank sample increases and reaches a peak at day 14. A declining nature in the corrosion rate was observed between 14 and 28 days (Figs. 4 & 5). The *Cascabela thevetia* has the highest cor-
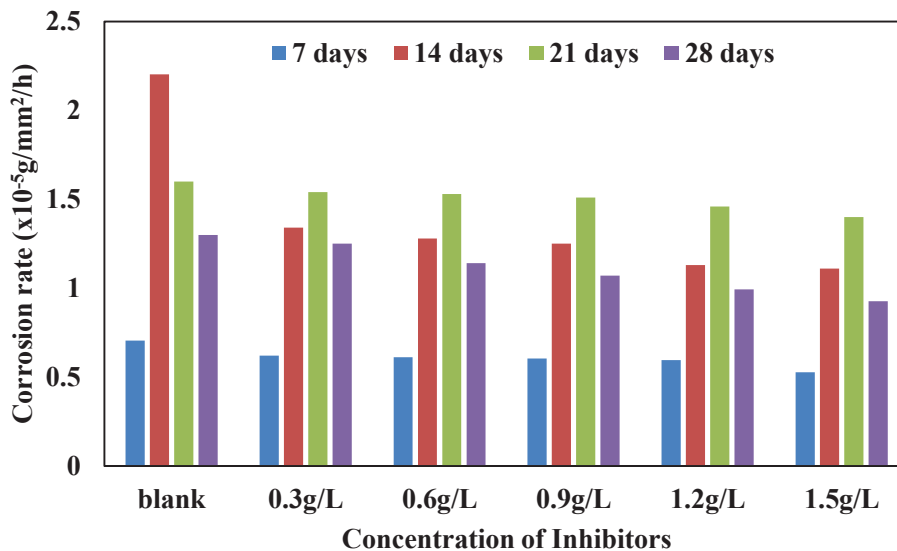
Fig. 4: Corrosion rate of mild steel in H_2SO_4 with varied concentrations of *Cascabela thevetia* inhibitor.
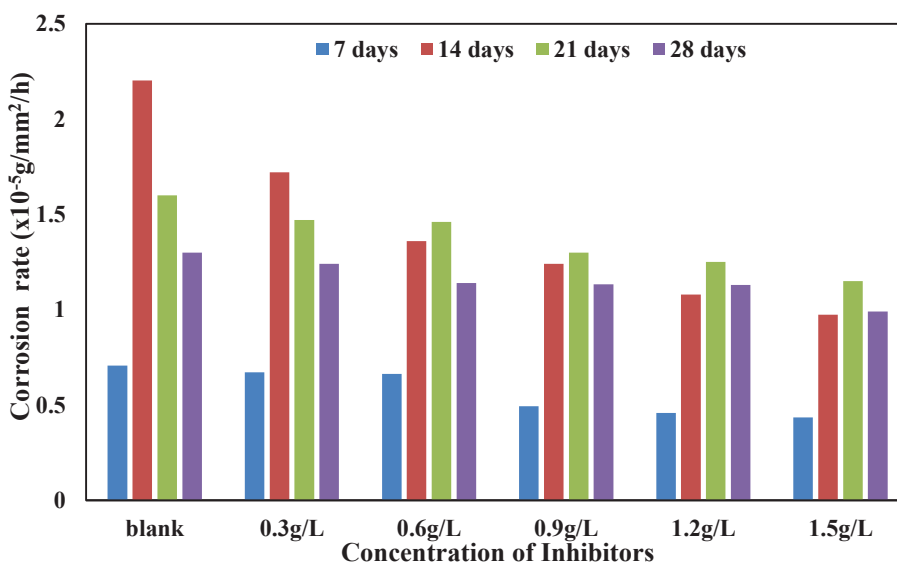
Fig. 5: Corrosion rate of mild steel in H_2SO_4 with varied concentrations of *Jatropha curcas* inhibitor.

rosion rate of 1.54×10^{-5} g/mm^2/h (in 0.3 g/L) and 1.4×10^{-5} g/mm^2/h (in 1.5 g/L) as the least. However, *Jatropha curcas* has the highest corrosion rate of 1.72×10^{-5} g/mm^2/h (in 0.3 g/L) and the least to be 0.974×10^{-5} g/mm^2/h (in 1.5/L). Generally, for both corrosion inhibitors at different concentrations, the rate of corrosion without regards to the level of inhibitor concentration is lower than the blank. From Fig. 4, it was observed that as the exposure time increases from days 7 to 21, the corrosion rates increase for all the inhibited samples at various concentrations of *Cascabela thevetia* while the corrosion rates decline from days 21 to 28. At 0.3 g/L concentration of *Jatropha curcas*, the corrosion rate increases between days 7 and 14 where a peak was reached and declined until the end of day 28. However, other concentrations of *Jatropha curcas* increase from days 7 to 21 and a slight decline was observed until day 2 (Fig. 5). It can be said that the higher the concentration of the inhibitors in the environment, the lower the corrosion rate. This implies that the extracts from the leaves are good enough to protect or reduce the steel materials from corrosion. Higher concentrations of the extracts lower the rate of disintegration for a long time.

The decline in the rate of corrosion when the coupons are in the inhibited environments could be as a result of the inhibitor concentration increment which invariably suggests the adsorption of organic compounds present in the leaf extracts which could have formed the passive protecting film layer that has lowered the penetrability of the sulphuric acid onto the surface of the coupons mild steel. The corrosion rates could mean that the inhibitive effect of the inhibitor does not affect regardless of the inhibitor concentration after 21 and 14 days for *Cascabela thevetia* and *Jatropha curcas*, respectively. This might be as a result of the suspension of H_2SO_4 into H_2 gas and SO_4^{2-}, that is, the H_2 gas evolving and the media becomes less corrosive since SO_4 is a base. Thus, *Jatropha curcas* is more effective as a corrosion inhibitor than *Cascabela thevetia* due to the number of days obtained from the experiment.

Figs. 6 and 7 show the inhibitors' inhibitive efficiency on mild steel coupon at different concentrations in H_2SO_4. The results show that for both *Cascabela thevetia* and *Jatropha curcas* inhibitors during the initial 14 days, the inhibitor concentration is proportional to the inhibitive efficiency, that is, increase in the inhibitor concentration is an increase in the inhibitive efficiency in an acidic environment. Considering Figs. 6 and 7, the highest inhibitive efficiencies of the *Cascabela thevetia* and *Jatropha curcas* inhibitors at 1.5 g/L were obtained to be 49.6% and 55.8%, respectively. At the same concentration, it can be said that *Jatropha curcas* gives better inhibitive efficiency than *Cascabela thevetia*. The maximum inhibitive efficiencies obtained at 1.5 g/L concentration of the inhibitors in H_2SO_4 environment could be as a result of increased thickness of the shielding film layer formation which could be attributed to increase in the
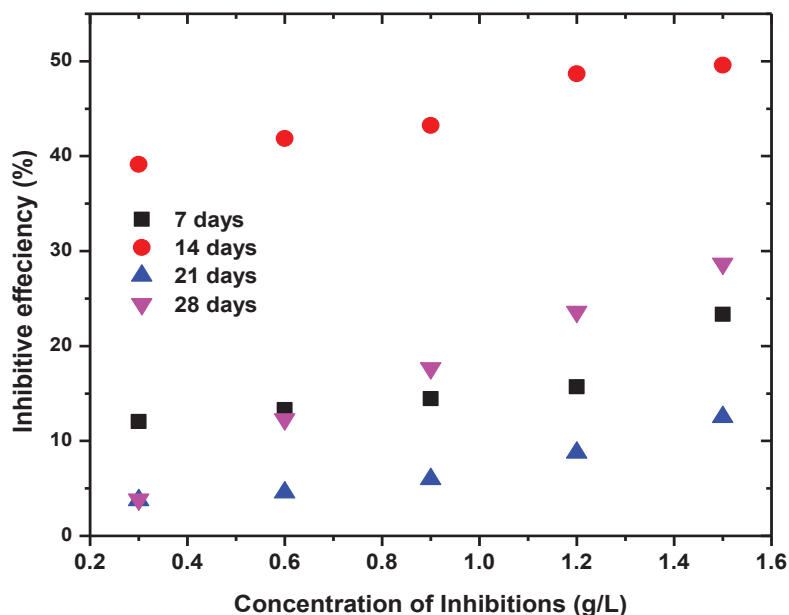
Fig. 6: Inhibitive efficiency under various concentrations of the *Cascabela thevetia* inhibitor.
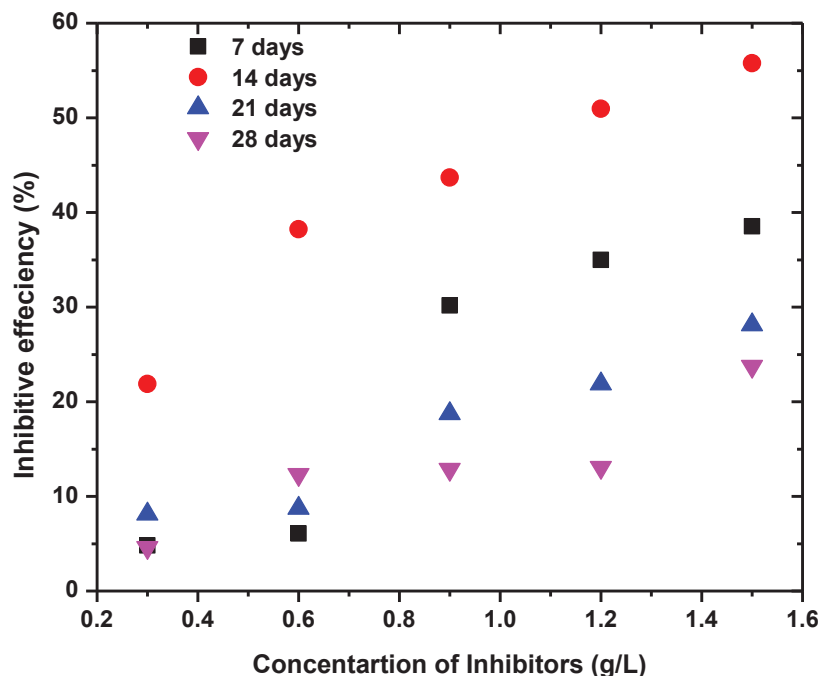
Fig. 7: Inhibitive efficiency under various concentrations of the *Jatropha curcas* inhibitor.

inhibitor concentration in the system. This could be instigated by phytochemical constituents' adsorption which is existing in the inhibitors (Table 2) that consequently cause a reduction in the penetrability of H_2SO_4 onto the surface of the metal. The least inhibitor inhibitive efficiency at 0.3 g/L was found to be 21.9 and 39.2% for *Jatropha curcas* and *Cascabela thevetia,* respectively. After 14 days, without regard to the inhibitor concentration, the inhibitive efficiencies decline for both green inhibitors used. This study finds agreement with previous studies on corrosion inhibition as it was reported that mild steel corrosion rate in the corrosion system of nitric acid/*Carica papaya* decreased with increment in the concentration of the inhibiting leaf extracts while corrosion efficiency and surface coverage increased as inhibitors'

concentration increase (Oki et al. 2015). More so, as the concentration of corrosion inhibitor increases, there is always a decrease in the weight loss of the metal in the corrosion system (Odusote & Ajayi 2013, Oki et al. 2015, Salami et al. 2012). This was obtained from this study and such should be expected as stated by Oki et al. (2015) that the inhibiting species number will rise in proportion to the leaf extracts concentration in the system (Oki et al. 2015).

Gasometric studies: For both inhibitors, there was a linear decline in the hydrogen gas evolution rate as a result of time increment. This was, however, not as rapid as that of the blank (uninhibited) samples (Figs. 8 & 9). Also, it was observed that the presence of the green inhibitors (*Cascabela thevetia* and *Jatropha curcas*) rapidly lowers the rate at which

Table 2: Phytochemical constituents of the inhibitors.

Phytochemical constituent	*Cascabela thevetia*	*Jatropha curcas*
Tanins	+	+
Saponins	+	+
Phenols	-	+
Flavonoids	+	+
Alkaloids	+	+
Terpenoids	+	+
Nicotine	-	-
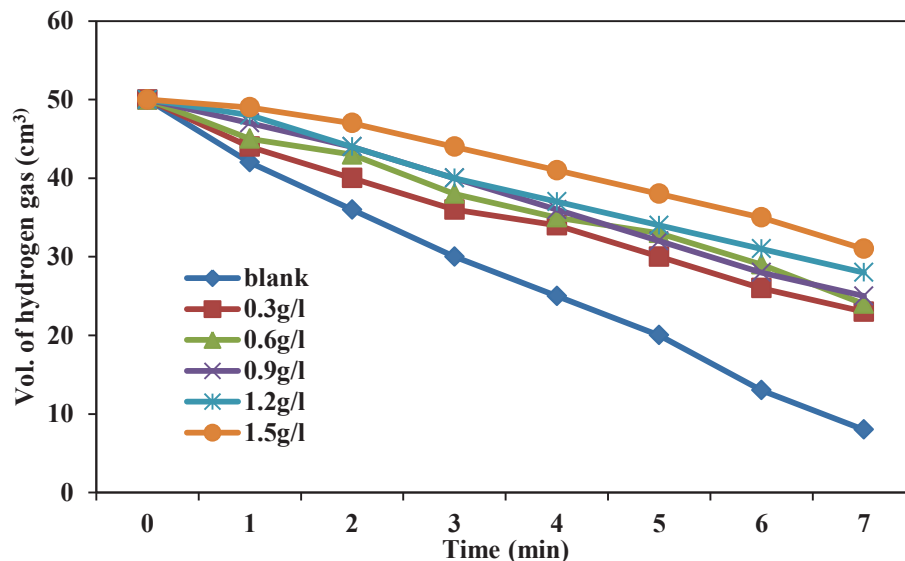
Fig. 8: Volume of hydrogen gas evolved against time (*Cascabela thevetia).*
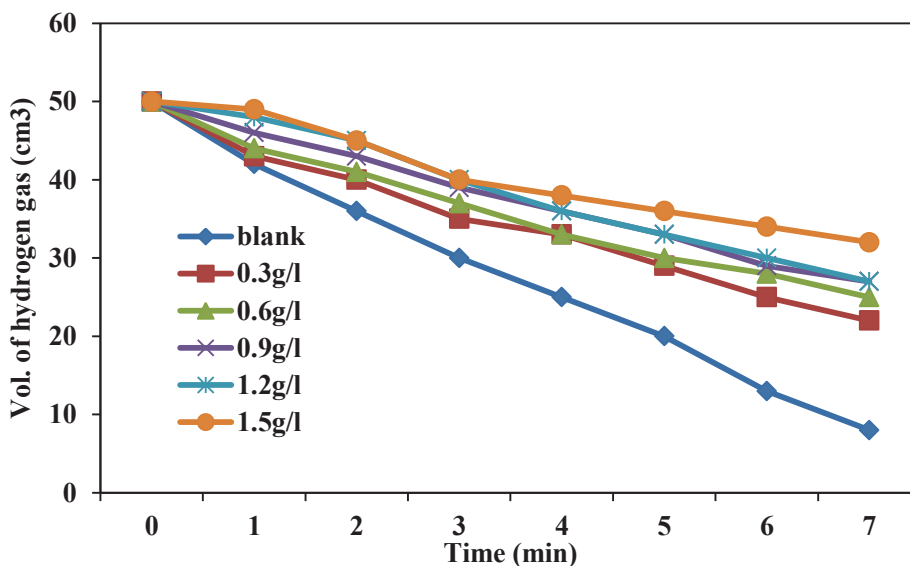
Fig. 9: Volume of hydrogen gas evolved against time (*Jatropha curcas).*

the hydrogen gas volume evolves. Also, it is observed that the gas evolution of the gas is inversely proportional to the inhibitors' concentration. This implies that the increment in the inhibitors' concentration results in a decrease in the evolution of the gas for both inhibitors. The same observation was reported by Oki et al. (2015) in which corrosion activities reduced with increment in leaf extract concentration of *Carica papaya* extracts in the corrosion system. The highest gas of evolution volumes at 0.3 g/L concentration were 24

and 22 cm^3 while the least gas evolution volumes at 1.5 g/L concentration were 31 and 32 cm^3 for both *Cascabela thevetia* and *Jathropha curcas* inhibitors, respectively at 7 minutes.

It was observed that there is an increment in the surface coverage for both green inhibitors as the concentration increases (Fig. 10). This could be the aftermath effect of the interactive reaction between the phytochemical constituents and H_2SO_4 which results in the declining nature of the acidic reaction rate on the mild steel coupons. This consequently
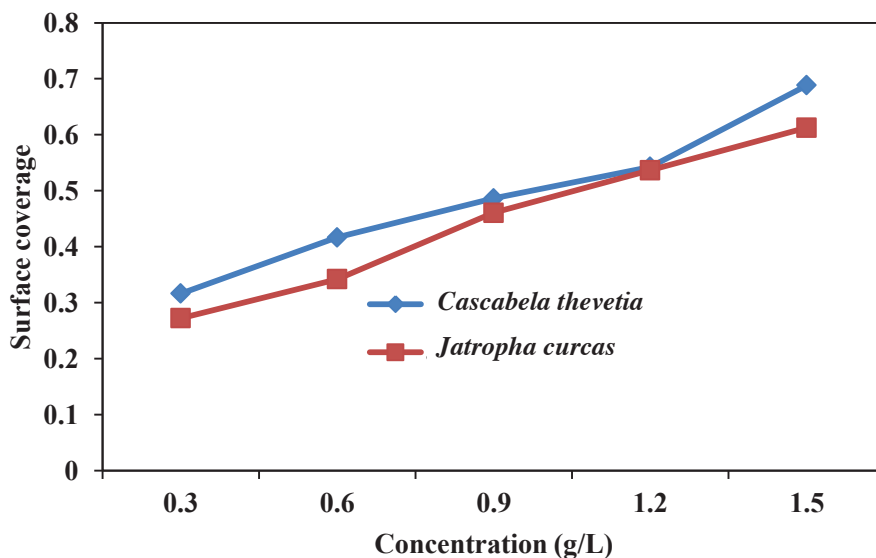
Fig. 10: Surface coverage against concentration for both inhibitors.

lowers the metal corrosion rate. The maximum surface coverage for the green inhibitors, *Cascabela thevetia* and *Jatropha curcas,* at 1.5 g/L concentration were 0.68 and 0.61, respectively and the lowest surface coverage at 0.3 g/L concentration were 0.31 and 0.27, respectively. This is an indication that *Cascabela thevetia* has a superior surface coverage for a short period of time compared to *Jatropha curcas*. The increment in time of surface coverage makes *Jatropha curcas* inhibit better and superiorly effective than *Cascabela thevetia*.

With increase in inhibitors' concentration, there is an increment in the inhibitive efficiency of both green inhibitors (Fig. 11). The highest inhibitive efficiency was at 1.5 g/L concentration for both inhibitors and the values were 68.9% and 61.3% for *Cascabela thevetia* and *Jatropha curcas,* respectively. The lowest inhibitive efficiency was at 0.3 g/L for both inhibitors and the values were 31.6 and 27.2% for *Cascabela thevetia* and *Jatropha curcas,* respectively.

This trend in corrosion inhibition efficiencies at various inhibitors concentrations indicate the phytochemical
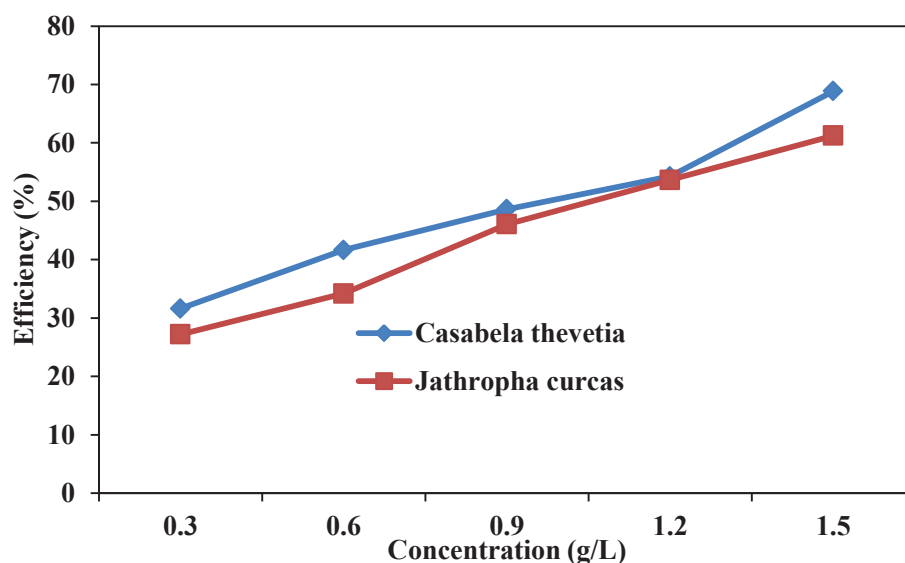
Fig. 11: Inhibitive efficiency against concentration for both inhibitors.

constituents' chemisorption of the inhibitors on the metal surface. The mild steel coupon corrosion in H_2SO_4 solutions increase inhibitors' concentration which was attributed to the adsorption of the inhibitors' components on the metal surface.

Consequentially, during corrosion reactions, the anodic reaction rate is always equal to the cathodic reaction rate. This is so as a result of the utilization of all electrons released in the anodic half reaction by the cathodic half. Therefore, the gas evolution rate is a function and measure of the corrosion rate of the metallic specimen in the corrosion system (Oki et al. 2015).

CONCLUSION

Comparative examination of the influence of *Cascabela thevetia* and *Jatropha curcas* leaves extracts on mild steel was carried out in this study and the following were deduced.

1. The extracts have inhibitive efficiencies at 1.5 g/L concentration (after 28 days) in H_2SO_4 to be 49.59 and 55.77% for *Cascabela thevetia* leaves and *Jatropha curcas* leaves, respectively.

2. As the concentration of the inhibitors (*Cascabela thevetia* and *Jatropha curcas)* increased in the H_2SO_4 medium, the weight loss, the corrosion rate and the hydrogen gas evolved decreased.

3. *Cascabela thevetia* had better surface coverage for a shorter period while *Jatropha curcas* had superior coverage with prolonged time. The inhibition property is best with *Jatropha curcas*.

4. The gas evolution is dependent on the inhibitors' concentration, therefore, increment in the inhibitors' concentration reduces gas evolution.

REFERENCES

Abiola, O.K., Oforka, N.C., Ebenso, E.E. and Nwinuka, N.M. 2007. Eco-friendly corrosion inhibitors: The inhibitive action of *Delonix regia* extract for the corrosion of aluminium in acidic media. Anti-Corros. Meth. Mat., 54(4): 219-224.

Ajayi, O.O., Joseph, O.O., Omotosho, O.A. and Olabowale, T.O. 2012. *Rauvolfia vormitoria* effect on the degradation of aluminium alloy in 2.5M hydrochloric acid solution, In: Proceeding of ICCEM: 21-29.

Al-Otaibi, M.S., Al-Mayouf, A.M., Khan M., Mousa, A.A., Al-Mazroa, S.A. and Alkhathlan, H.Z. 2012. Corrosion inhibitory action of some plant extracts on the corrosion of mild steel in acidic media. Arab. J. Chem., 7(3): 340-346

Ansari K.R., Yadav, D.K., Ebenso, E.E. and Quraishi, M.A. 2012. Novel and effective pyridyl substituted 1,2,4-triazole as corrosion inhibitor for mild steel in acidic solution. Int. J. Electrochem. Sci., 7: 4780 - 4799

Asmara, Y.P., Suraj, V., Sire6gar, J.P., Kurniawan, T., Bachtiar, D. and Mohamed, N.M.Z.N. 2017. Development of green vapour corrosion inhibitor. 4th International Conference on Mechanical Engineering research. In: IOP Conference Series: Materials Science and Engineering, 257 (012089): 1-7.

Bradford, S. A. 1993. Corrosion Control, Van Nostrand Reinhold, New York: 1

Chowdhary, R., Jain, T., Rathoria, M. K. and Mathur, S. P. 2004. Corrosion inhibition of mild steel by acid extracts of *Prosopis juliflora*. Bullet. Electrochem., 20(2): 67-75.

Ebenso, E. E., Eddy, N. O. and Odiongeyi, A. O. 2008. Corrosion inhibitive properties and adsorption behaviour of ethanol extract for *Piper guinensis* as a green corrosion inhibitor for mild steel in H_2SO_4. Afr. J. Pure App. Chem., 2(11): 107-115.

Eddy, N. O. 2009. Ethanol extract of Phyllanthus amarus as a green inhibitor for the corrosion of mild steel in H_2SO_4. Portug. Electrochem. Acta, 29(5): 579-589.

El-Etre, A. Y. and El-Tantawy, Z. 2006. Inhibition of metallic corrosion using *Ficus* extract. Portug. Electrochim. Acta, 24(3): 347- 356.

El-Etre, A. Y., Abdallah, M. and El-Tantawy, Z. E. 2005. Corrosion inhibition of some metals using *Lawsonia* extract. Corros. Sci., 47(2): 385-395.

El-Etre, A. Y., Abdallah, M. and Z. E. El-Tantany. 2005. Corrosion inhibition of some metals using *Lawsonia* extract. Corrosion Science, 47: 385-395.

El-Etre, A.Y. 2006. Natural onion juice as inhibitor for zinc corrosion. Bullet. Electrochem., 22(2): 75-80.

Martinez, S. 2003. Inhibitory mechanism of *Mimosa* tannin using molecular modeling and substitutional adsorption isotherms. Mat. Chem. Phys., 77: 97-102.

Mshelia, A.D., Aji, I.S. and Yawas, D.S. 2017. Comparative analysis of *Jatropha curcas* and Neem leaves extracts as corrosion inhibitors on mild steel. Faculty of Engineering Seminar Series, 8: 106-113.

Odusote, J.K. and Ajayi, O.M. 2013. Corrosion inhibition of mild steel in acidic medium by *Jatropha curcas* leaves extract. J. Electrochem. Sci. Technol., 4(2): 81-87.

Oguzie, E. E. and Ebenso, E. E. 2006. Studies on the corrosion inhibiting effect of Congo red dye halide mixtures. Pigment & Resin Technol., 35(1): 30-35.

Oguzie, E. E. 2008. Corrosion inhibitive e ect and adsorption behaviour of *Hibiscus sabdari a* extract on mild steel in acidic media. Portug. Electrochim. Acta, 26: 303-314.

Okafor P.C., Ikpi, M.E., Uwah, I. E., Eneso, E.E., Ekpe, U.J. and Umoren, S.A. 2008. Inhibitory action of *Phyllanthus amarus* extracts on the corrosion of mild steel in acidic media. Corrosion Science, 50(8): 2310-2317.

Okafor, P. C., Ebenso, E. E. and Ekpe, U. J. 2010. *Azadirachta indica* extracts as corrosion inhibitor for mild steel in acid medium. Int. J. Electrochem. Sci., 5: 978-993.

Oki, M., Anawe, P. A. L. and Fasakin, J. 2015. Performance of mild steel in nitric acid/*Carica papaya* leaf extracts corrosion system. Asian J. Appl. Sci., 3(1): 110-116

Oki, M., Charles, E., Alaka, C. and Oki, T. K. 2011. Corrosion inhibition of mild steel in HCl by tannins from *Rhizophora racemose*. Mat. Sci. App., 2: 592-595.

Perez, N. 2004. Electrochemistry and Corrosion Science. Kluwer Academic Publishers, New York: 1.

Rani B.E.A. and Basu, B. B. J. 2012. Green inhibitors for corrosion protection of metals and alloys: An overview. Int. J. Corros., 2012: 1-15.

Rani, P. D. and Selvaraj, S. 2010. Inhibitive and adsorption properties of *Punica granatum* extract on brass in acid media. J. Phytology, 2(11): 58-64.

Salami, L., Wewe, T. O. Y., Akinyemi, O. P. and Patinvoh, R. J. 2012. A study of the corrosion inhibitor of mild steel in sulphuric acid using *Musa sapientium* peels extract. Glob. Eng. Technol. Rev., 2(12): 1- 6.

Singh A., Ebenso, E.E. and Quraishi, M. A. 2012. Corrosion inhibition of carbon steel in HCl solution by some plant extracts. Int. J. Corros., 2012: 1-20.

Syed, S. 2006. Atmospheric corrosion of materials. Emir. J. Eng. Res., 11(1): 1-24.

Taghavikish, M., Dutta, N.K, and Choudhury, N.R. 2017. Emerging corrosion inhibitors for interfacial coating. Coatings, 7(12): 217-244.

Umoren S.A., Obot, I.B., Ebenso, E.E., Okafor, P.C., Ogbobe, O. and Ogusie, E.E. 2006. Gum Arabic as a potential corrosion inhibitor for aluminium in alkaline medium and its adsorption characteristics, anti-corros. Methods and Materials, 53(5): 277-282.

Assessment of Health of River Ganga at Varanasi, India

Sonali Saxena† and Prabhat Kumar Singh

Department of Civil Engineering, Indian Institute of Technology (Banaras Hindu University), Varanasi, India
†Corresponding author: Sonali Saxena; sonali16d@gmail.com

ABSTRACT

World across, there is an increasing concern about river health. In India, Ganga River Basin Management Plan (GRBMP) 2015 considered River Ganga as an ecological entity. This paper attempts to present a framework for river health assessment in India and discusses its applicability for River Ganga near Varanasi. In the proposed framework, the River Health Condition (RHC) is assessed through the calculation of River Health Index (RHI) on a 0-100 scale and categorized as Acceptable or Poor. RHI is calculated by using selected parameters/indices normalized on the 0-5 scale based on their critical and target values. River Health is presented through a coloured circumscribed pentagon each of whose side represents one of five indicator groups: i. Organo-electrolytic-bacterial qualities. ii. Nutrients, iii. Algae, iv. Macroinvertebrates, and v. Fish. Application of the proposed framework has been tested and explained using observed data for four seasons per year for two years from five locations of River Ganga near Varanasi. The colour of circumscribing pentagon reflects overall river health condition at a given location and each side of pentagon reflects health score concerningto one indicator group. The analyses indicate that the health of River Ganga near Varanasi is improving with time. The river health is found at its best level during Spring season and unstable during Post Monsoon period at most of the locations. The severely reduced RHI indicate "Overstressed" condition of River Ganga at the confluence points of River Assi and Varuna, which are evidenced by the presence of pollution tolerant biotic species. There are clear stretches of the river near outfall points which are nutrients rich and organically polluted causing poor health of river showing a disturbed balance of biotic species. Indicator group score based RHI gives a clear identification of critical parameters which may be used in strategic planning for river health restoration.

INTRODUCTION

Since ages, rivers have been taken as a source of water. Seeing its importance, the Government of India declared River Ganga as the National River in the year 2008 (MoWR 2014)**.** However**,** the river is getting polluted from many sources, including domestic sewage, industrial wastewaters and surface run off from fields. Different types of pollutants enter the river system which affects the water quality in turn affecting the aquatic organisms present in the riverine environment. For most of the times, water resource managers understand water quality by measuring a few physico-chemical and biological characteristics and suggest its suitability for various beneficial uses. Ganga River Basin Management Plan (GRBMP) 2015 prepared by Government of India has considered River Ganga as 'ecological entity'. From this perspective, researchers and experts in the field have been feeling the need to define river health and parameters for its assessment. It has been realized that in addition to physico-chemical and bacteriological water quality parameters, it is necessary to include aquatic organisms, such as algae, macroinvertebrates and fishes present in the riverine environment as indicators

to define river health. These aquatic organisms convey the integrated and continuous characteristics of water quality. Therefore, many experts (Hawkes 1979, Sladecek 1979, Tittizer & Koth 1979, Hellawell 1986, Rosenberg & Resh, 1993, Allan 1995) are of the view that algae, macroinvertebrates and fish should be considered as suitable indicators for assessing the health of rivers. The Australia-China Environment Development Partnership (ACEDP) Report 2011, under the title 'Assessment of River Health in Liao River Basin, Taizi Sub-catchment', China is a good example in this line of thinking. In the study, from the whole spectrum of water quality characteristics, 15 parameters have been selected and divided into five categories: i. Physical and Chemical parameters (P&C), ii. Nutrients (NT), iii. Algae (A), iv. Macroinvertebrates (MI), and v. Fish (F). Five P&C parameters included Electrical Conductivity (EC), Dissolved Oxygen (DO), Biochemical Oxygen Demand (BOD), Chemical Oxygen Demand (COD) and Phenols. Two NT parameters include Ammonia-N (NH_4-N) and Total Phosphorus (TP). Two algal indices include a multi-metric Index of Biotic Integrity (A_BI2) and Berger-Parker dominance index (A_BP). Three macroinvertebrate indices include family-level rich-

ness (M_S), BMWP score (M_BMWP) and family-level EPT richness (M_EPT_S). Three fish indices include family-level richness (F_S), fish index of biotic integrity (F_BI) and Berger Parker index (F_BP). River health assessment has been made using these 15 parameters. River Health Report Card (2012) has been presented in pictorial form in the shape of a pentagon, each side of pentagon depicting river health in terms of one category of characteristics, i.e. P&C, nutrients, algae, macroinvertebrates and fish. Under Indian conditions, it has been observed that organic pollution is predominant in rivers and almost all the surface water sources have the presence of Coliform group of bacteria to some extent (Bhardwaj 2005). Accordingly, Singh & Saxena (2018) proposed calculation of River Health Index (RHI) based on suitably selected indicators and parameters. In this framework, Faecal Coliform (FC) was included (replacing Phenol taken in Australia-China Study) among five P&C category characteristics, NT parameters were increased from 2 to 3 by including Total Nitrogen (TN) as this is more readily available data. Among biotic indicators, identification and counting based simple indices for algae, macroinvertebrate and fish which could be performed by non-experts also, were selected and used. This included Algal Palmer Genus Pollution Index (APPI), (index for algae), Macroinvertebrate Shannon Weiner Diversity Index (M_SW), Macroinvertebrate BMWP score (M-BMWP) (two indices-for macroinvertebrates), and Fish Family level Richness Index (F_S), Shannon Weiner Diversity index (FSW) (two indices for fishes).

The present work is an attempt to interpret and understand the above framework of river health assessment for Ganga at Varanasi taking water quality and biotic indicators together into consideration. The framework calculates River Health Index (RHI) based on five indicator group scores, using a total of 13 parameters/indices. Organo-Electrolytic-Bacterial (OEB) group has five parameters (BOD, COD, DO, Electrical Conductivity and Fecal Coliform values), Nutrients (NT) group consists of 3 monitoring characteristics: NH_3-N, Total-Nitrogen and Total Phosphorus measurements. In addition, algae, macroinvertebrates and fishes are represented

using five indices suitable for their groups. River Health Condition (RHC) has been classified as Acceptable (Excellent, Very Good, Good) and Poor (Stressed, Overstressed, Critical and Sick/Dead) based on RHI.

MATERIALS AND METHODS

Study Area

The Varanasi district lies in Uttar Pradesh (UP) province of India between 82°56'E-83°03'E and 25°14'N-25°23.5'N. The city of Varanasi is situated in the middle stretch of Ganges basin in the eastern part of Uttar Pradesh. The crescent-shape Ganges banks are all through the left side of the city (Fig. 1). The samples of the river water were collected for two years from September 2016 to May 2018 during four seasons: Post Monsoon (16 Sep-15 Nov), Winter (16 Nov-15 Jan), Spring (16 Jan-15 Mar) and Summer (16 Mar-15 May) from 5 locations along the Ghats, starting from Saamne Ghat (upstream of confluence point of river Assi with Ganga) to the confluence point of River Varuna with Ganga in the downstream side of the city. The samples were collected from Saamne Ghat (L1), the confluence of (C/O) Assi Nala with Ganga (L2), Dashashwamedh Ghat (L3), Raaj Ghat (L4) and C/O Varuna with Ganga (L5) stretched in a length of around 7 km.

The Framework of River Health Index (RHI) Calculation

In this study, the framework of River Health Index (RHI) calculation is based on scores of aquatic environment parameters divided into five indicator groups: i. Organo-Electrolytic-Bacterial (OEB) group (comprising of EC, DO, BOD, COD and FC, Total 5 parameters), ii. Nutrients (NT) group (consisting of NH_3-N, TN and TP, Total= 3 parameters), iii. Algae (Genus level Algal Palmer Pollution Index (APPI) One index), iv. Macroinvertebrate (Shannon Weiner Diversity index (MSW) and Macroinvertebrate BMWP score (MBMWP), Two Indices), and v. Fishes (Family level Fish

Fig.1: River Ganga near Varanasi and sampling locations.

Species richness index (FS) and Shannon Weiner Diversity index (FSW), Two indices).

The group scores of Organo-Electrolytic-Bacterial (OEB), Nutrient (NT), Algae (A), Macroinvertebrate (MI) and Fish (F) indicators were used to calculate the River Health Index (RHI) by the following formula:

River Health Index (RHI)

$$= [(OEB \times w_1) + (NT \times w_2) + (A \times w_3) + (MI \times w_4) + (F \times w_5)] \qquad …(1)$$

Where, OEB = Organo-Electrolytic-Bacterial indicator group score, NT = Nutrient indicator group score, A= Algal indicator group score, MI = Macroinvertebrate indicator group score, and F= Fish indicator group score and w_1, w_2, w_3, w_4 and w_5 are weightages given to different groups (Table 1). The OEB and NT group indicators are normally affected by short term fluctuations, whereas biotic indicators such as algae, macroinvertebrates and fish are long term integrators of river health. Therefore, the biotic indicators should contribute more heavily towards an overall RHI. With similar reasoning, macroinvertebrates and fish indicators are weighted more heavily than algal indicators as they are longer lived than algae (Leigh et al. 2012).

River Health Condition (RHC) is defined based on indicator group score andRiver Health Index (RHI) and colour code is given for visual representation, as shown in Table 2.

The river health is considered Acceptable or Poor if RHI is greater than or less than 60. Acceptable river health may be of three categories: Good (RHI 60-70), Very Good (RHI 70-80) or Excellent (RHI>80). With poor river health, rivers may be categorized as Stressed (RHI 50-60), Overstressed (RHI 40-50), Critical (RHI 20-40) or Sick/Dead (RHI ≤ 20). The river health is pictorially represented by a circumscribed pentagon in which colour of each side represents one indicator group score of water quality in the river environment and the colour of the circumscribing pentagon represents the river health condition (RHC) based on overall River Health Index (RHI) for the site (Fig. 2).

Sample Collection and Analyses

Samples for organo-electrolytic-bacterial, nutrient, algae and macroinvertebrate analyses were collected from 5 locations along the Ghats of Varanasi during post-monsoon (16Sep-15Nov), winter (16Nov-15Jan), spring (16Jan-15Mar) and summer (16Mar-15May) for two years 2016-2017 and 2017-2018. Three grab samples were collected during morning hours between 8.00 a.m. and 11.00 a.m. from each location and mixed to form a compound sample for that location once every month and grouped in seasons. The total number of samples for which analyses have been performed is 360 (120 each for Organo-Electrolytic-Bacterial, Nutrient, Algae and Macroinvertebrate). Some parameters such as electrical conductivity (EC), dissolved oxygen (DO) (includ-

Table 1: Weightage of different indicator groups.

	Indicator Group	Parameters/Indices	No. of Parameters/Indices	Weight factor	Weight factor given in the present study
1	Organo-Electrolytic-Bacterial (OEB)	EC,DO,BOD,COD,FC	5	w_1	0.15
2	Nutrient Score (NT)	NH_3-N, TN, TP	3	w_2	0.15
3	Algae Score (A)	APPI	1	w_3	0.20
4	Macroinvertebrate Score (MI)	MSW, MBMWP	2	w_4	0.25
5	Fish Score (F)	FS, FSW	2	w_5	0.25
	Total		13		1.00

Table 2: River Health Condition (RHC) based on Indicator Group Score and River Health Index (RHI).

River Health	Indicator Group Score/ RHI Score	RHC	Colour Code
Acceptable	>80	Excellent	Blue
	70-80	Very Good	Green
	60-70	Good	Yellow
Poor	50-60	Stressed	Orange
	40-50	Over Stressed	Grey
	20-40	Critical	Red
	≤20	Sick/Dead	Black

Fig. 2: Circumscribed pentagon for the river health condition and river health index.

ing temperature, and pH) were recorded on the site using a multi-parameter analyser. Others including biochemical oxygen demand (BOD) by 5-day BOD test, chemical oxygen demand (COD) by closed reflux titrimetric method (Hanna Instrument), faecal coliforms (FC) by multiple tube fermentation technique and nutrient parameters, such as ammonia-nitrogen (NH_3-N) by titrimetric method, total nitrogen (TN) and total phosphorous (TP) by stannous chloride method were tested in the laboratory as per the standard methods (APHA 2005).

The samples for algal analyses were collected in bottles and preserved in 4% formalin solution and transported to the laboratory for identification using the microscope.

The Genus based Algal Palmer Pollution Index (APPI) was calculated using Table 3 (Palmer 1969, Nandan & Patel 1986). Pollution classification of Palmer (1969) suggests that APPI =0-10 represents lack of organic pollution, 10-15 indicates moderate pollution, 15-20 marks probable high organic pollution, and 20 or more confirms high organic pollution.

The macroinvertebrate samples were collected using standard D-frame dip net having 500-micron opening. Benthic macroinvertebrates were collected systematically from all available instream habitats by kicking the substrate and jabbing with a D-frame dip net. The samples were preserved in 4% formalin solution and transported to the laboratory for further examination. In the laboratory, the samples were rinsed thoroughly with pure water to remove the preservative. Collected samples were examined and counted using the hand lens and microscope. The macroinvertebrates were identified to the lowest possible taxonomic level using standard taxonomic literature APHA (2005), Gerber & Gabriel (2002), Barbour et al. (1999), Merritt & Cummins (1996), William & Feltmate (1992), Pennak (1989), Durrand & Leveque (1981), Tonapi (1980), Pennak (1978) and Needham & Needham (1969). The Macroinvertebrate Shannon Weiner Diversity Index (MSW) was calculated as follow:

$$MSW = -\Sigma pi.\ln pi$$

Where, pi = S/N, S = Number of individual of particular specie, N = Total number of individuals of all species in the sample.

Macroinvertebrate Biological Monitoring Working Party (MBMWP) score was calculated based on the presence of

Table 3: Genus based Algal Palmer Pollution Index (APPI) (Palmer 1969, Nandan & Patel 1986).

Genus	Pollution Index	Genus	Pollution Index
Anacystis	1	Micractinium	1
Ankistrodesmus	2	Navicula	3
Chlamydomonas	4	Nitzschia	3
Chlorella	3	Oscillatoria	5
Closterium	1	Pandorina	1
Cyclotella	1	Phacus	2
Euglena	5	Phormidium	1
Gomphonema	1	Scenedesmus	4
Lepocinclis	1	Stigeoclonium	2
Melosira	1	Synedra	2
Anabaena	1		

Note: Pollution classification of Palmer (1969) suggest that APPI = 0-10 represents lack of organic pollution, 10-15 indicates moderate pollution, 15-20 marks probable high organic pollution, and 20 or more confirms high organic pollution.

taxonomical class and families using Table 4 (De Zwart &Trivedi 1994).

The two fish indices, i.e. Fish Species Index (FS) and Shannon Weiner Diversity Index (FSW) were calculated based on species count and process suggested in the available literature (Das et al. 2013, Dwivedi et al. 2016).

The 'Target Value' and 'Critical Value' for the indicators were obtained from available literature as given in Table 5.

The values of individual parameter/indices obtained from sample analysis are used to calculate the score of the parameter/index at a particular location. For making the score calculation more precise, the full range between 'Target value' and 'Critical value' has been divided into five zones on a 0-5 scale, as given in Table 6. According to this, if at a particular site, the observed value of an indicator is better than or equal to the target value, the site would have an indicator score 5 and if the observed value is less than the critical value, the indicator score would be 0.

The group indicator score is calculated by aggregating the parameters/indices score of each group.

Indicator Group Score

= [Σ scores of parameters or indices/(5×No. of parameters or indices in the group)]×100   …(2)

Table 4: Biological Monitoring Working Party (BMWP) Score (De Zwart & Trivedi 1994).

Taxonomical Class	Taxonomical Families	BMWP Score
Ephemeroptera	Heptogeniidae, Leptophlebiidae, Ephemerellidae, Ephemeridae, Potoaminthidae, Siphonuridae	10
Plecoptera	Leuctridae, Capniidae, Perlodidae, Perlidae, Taeniopterygidae	
Hemiptera	Aphelocheiridae	
Trichoptera	Leptoceridae, Goeridae, Lepidostomatidae, Brachycentridae, Sericostomatidae	
Odonata	Lestidae, Gomphidae, Cordulegasteridae, Aeschnidae, Corduliidae, Libellulidae, Plathycnemididae	8
Trichoptera	Psychomyiidae, Philopotomidae	
Ephemeroptera	Caenidae	7
Plecoptera	Nemouridae	
Trichoptera	Rhyacophilidae, Polycentropodidae, Limnephilidae	
Mollusca	Ancylidae, Hydrobiidae, Neritidae, Viviparidae, Thiaridae, Bithynidae, Unionidae	6
Trichoptera	Hydroptilidae	
Crustacea	Palaemonidae, Atydae, Gammaridae	
Polychaeta	Nereidae, Nephthyidae	
Odonata	Coenagriidae, Agriidae	
Hemiptera	Mesovelidae, Hydrometridae, Gerridae, Nepidae, Naucoridae, Notonectidae, Pleidae, Corixidae, Veliidae, Hebridae, Belestomatidae	5
Coleoptera	Haliplidae, Hygrobidae, Dytiscidae, Gyrinidae, Hydrophilidae, Noteridae, Helodidae, Dryopidae, Elminthidae, Psephenidae	
Trichoptera	Hydropsychidae	
Diptera	Tipulidae, Culicidae, Blepharoceridae, Simulidae	
Planaria	Planariidae, Dendroceolidae	
Ephemeroptera	Baetidae	4
Megaloptera	Sialidae	
Hirudinea	Piscicodidae	
Mollusca	Lymnaeidae, Planorbidae, Sphaeridae	3
Hirudinea	Glossiphonidae, Hirudidae, Erpobdellidae	
Planaria	Dugesiidae	
Crustacea	Asselidae	
Diptera	Chironomidae, Syrphidae	2
Oligochaeta	All families	1

Table 5: Target and Critical values for parameters/indices in a river environment.

S.N.	Indicator Group	Parameter/ Indices	Target value	Critical value	Source
1	Organo-Electrolytic-Bacterial (OEB)	i. EC (µmhos/cm)	≤400	>1500	EHMP (2010); (Anon 2000)
		ii. DO (mg/L)	≥7	<3	UNECE (1994)
		iii. BOD (mg/L)	≤3	>8	CPCB (2015)(Existing); CPCB (2002)
		iv. COD (mg/L)	≤30	>80	Assumed (Currently no limit is available).
		v. FC (MPN/100mL)	≤500	>2500	CPCB (2015) (Existing)
2	Nutrients (NT)	i. NH_3-N (mg/L)	≤0.3	>1.5	CPCB (2002); MEP (2008)
		ii. TN (mg/L)	≤0.5	>2	Anon (2000); MEP (2008)
		iii. TP (mg/L)	≤0.1	>0.3	CPCB (2002)
3	Algae (A)	i. Genus APPI	≤10	>20	Palmer (1969)
4	Macroinvertebrate (MI)	i. MSW	>3.5	0	Kerkhoff (2010)
		ii. MBMWP (Saprobic)	>7	0	CPCB (2015)
5	Fish (F)	i. Family Level Fish Species Richness Index (FS)	≥75	0	Das et al. (2013)
		ii. FSW	>3.5	0	Das et al. (2013)

Table 6: Score of parameters/indices on a 0-5 scale.

	Indicator Group	Parameter/Indices	Score					
			0	1	2	3	4	5
1	Organo-Electrolytic-Bacterial (OEB)	i. EC (µmhos/cm)	>1500	1250-1500	1000-1250	750-1000	400-750	≤400
		ii. DO (mg/L)	<3	3-4	4-5	5-6	6-7	≥7
		iii. BOD (mg/L)	>8	6.5-8	5.0-6.5	4.0-5.0	3.0-4.0	≤3
		iv. COD (mg/L)	>80	65-80	50-65	40-50	30-40	≤30
		v. FC (MPN/100 mL)	>2500	2000-2500	1500-2000	1000-1500	500-1000	≤500
2	Nutrients (NT)	i. NH_3-N (mg/L)	>1.5	1.2-1.5	0.9-1.2	0.6-0.9	0.3-0.6	≤0.3
		ii. TN (mg/L)	>2	1.6-2.0	1.2-1.6	0.8-1.2	0.5-0.8	≤0.5
		iii. TP (mg/L)	>0.3	0.25-0.3	0.2-0.25	0.15-0.2	0.1-0.15	≤0.1
3	Algae (A)	i. APPI (Genus)	>20	18-20	15-17	13-14	11-12	≤10
4	Macroinvertebrate (MI)	i. MSW	0	0-1.0	1.0-2.0	2.0-3.0	3.0-3.5	>3.5
		ii. MBMWP (Saprobic)	0	0-2.0	2.0-4.0	4.0-5.5	5.5-7.0	>7
5	Fish (F)	i. FS (Species)	0	1-15	15-35	35-55	55-75	≥75
		ii. FSW	0	0-0.75	0.75-1.5	1.5-2.5	2.5-3.5	>3.5

RESULTS AND DISCUSSION

The list of algae and different macroinvertebrate families found at all five locations of sampling in Varanasi during the study period is listed in Tables 7 and 8.

The range of values observed for different parameters/indices at all 5 locations of Varanasi during four seasons of two years period is given in Table 9.

The observed value of parameter/index is assigned a score between 0-5 using Table 6. The value of the indicator group score is calculated using Eqn. (2). Based on the indicator group score, the River Health Index (RHI) is calculated from Eqn. (1)and the River Health Condition (RHC) is categorized. The parameter/index score of the individual parameter/index, indicator group score, RHI and RHC at a particular location for two years (Sep 2016-May 2017 and Sep 2017- May 2018) is given in Table 10.

From Table 10, it is observed that, based on RHI calculated through the proposed framework, health condition of River Ganga at Varanasi is acceptable and under 'Good' category

Table 7: Algal groups and genera found at different locations of River Ganga near Varanasi (Sept 2016-May 2018).

Group	Genus	Group	Genus
Bacillariophyceae	*Achnanthes*	Chlorophyceae	*Mougeotia*
	Asterionella		*Oedogonium*
	Cocconeis		Oocystis
	Cyclotella		*Palmella*
	Cymbella		*Pediastrum*
	Fragilaria		*Scenedesmus*
	Gomphonema		*Sphaerocystis*
	Melosira		*Spirogyra*
	Navicula		*Staurastrum*
	Nitzschia		*Stigeoclonium*
	Stauroneis		*Tetraspora*
	Surirella		*Tribonema*
	Synedra		*Ulothrix*
	Tabellaria		*Volvox*
			Zygnema
Chlorophyceae	*Actinastrum*		
	Ankistrodesmus		*Anabaena*
	Chlorella		*Anacystis*
	Chlorococcum	Cyanophyceae	*Cylindrospermum*
	Cladophora		*Lyngbya*
	Clostridium		*Merismopedia*
	Coelastrum		*Oscillatoria*
	Crucigenia		*Phormidium*
	Draparnaldia		*Spirulina*
	Hydrodictyon		
	Microspora	Xanthophyceae	*Vaucheria*

Table 8: Macroinvertebrate Groups and Families found at different locations in River Ganga near Varanasi (Sept 2016-May 2018).

	Taxonomical Group	Taxonomical Families	Common names
1	Coleoptera	Dytiscidae	Diving Beetles
		Elmidae	Riffle Beetles
		Hydrophilidae	Water scavenger Beetles
2	Diptera	Chironomidae	Non biting Midges
		Culicidae	Mosquito larvae
		Psychodidae	Moth fly
		Simuliidae	Black fly
		Syrphidae	Rat-tailed maggot
		Tabanidae	Horse fly
		Tipulidae	Crane fly
		Muscidae	Muscid fly
3	Ephemeroptera	Baetidae	May fly
4	Mollusca	Lymnaeidae	Pond Snails
		Physidae	Pouch Snails
		Pilidae	Apple Snail
		Viviparidae	Snails
5	Oligochaeta	Tubifex	Worms
		Tubificidae	Worms

Table 9: Range of values of parameters/indices observed in River Ganga near Varanasi in four seasons during Sept 2016-May 2018.

Parameter/ Indices	Unit	2016-2017				2017-2018			
		Post Monsoon (16Sep-15Nov)	Winter (16Nov-15Jan)	Spring (16Jan-15Mar)	Summer (16Mar-15May)	Post Monsoon (16Sep-15Nov)	Winter (16Nov-15Jan)	Spring (16Jan-15Mar)	Summer (16Mar-15May)
Temperature	°C	23.0-24.5	17.0-18.0	22.1-23.5	27.2-28.2	23.4-24.9	17.1-18.0	22.3-23.8	27.3-28.2
pH		7.8-8.4	8.2-8.8	8.0-8.6	7.5-7.9	7.8-8.3	8.1-8.6	7.9-8.6	7.5-8.0
EC	μmhos/cm	600-700	265-300	300-400	420-900	572-650	293-372	332-390	420-1100
DO	mg/L	3.9-6.5	4.0-6.3	4.1-6.3	2.9-5.8	4.2-6.7	4.6-6.5	4.2-6.3	2.9-5.9
BOD	mg/L	4.3-7.0	4.2-6.2	4.0-6.0	4.3-6.8	4.7-6.8	3.9-6.0	4.0-6.4	4.4-6.9
COD	mg/L	34-72	38-68	55-82	60-100	40-68	42-78	52-80	52-110
FC	MPN/100 mL	1100-4200	1500-3200	1300-2200	1800-3600	1200-3100	1200-2200	1200-1900	1600-3300
NH3-N	mg/L	0.40-1.48	0.50-1.50	0.45-1.04	0.90-2.01	0.60-1.18	0.38-0.60	0.19-0.56	0.90-1.50
TN	mg/L	0.91-2.34	1.35-2.50	1.08-1.68	1.37-2.40	1.35-1.65	0.68-1.38	0.52-1.32	1.35-2.00
TP	mg/L	0.160-0.359	0.195-0.378	0.145-0.410	0.210-0.320	0.202-0.280	0.195-0.298	0.125-0.220	0.160-0.290
APPI(Genus)		13-16	13-18	13-17	15-18	13-16	13-16	13-15	15-21
MSW		0.70-1.09	1.18-1.59	1.33-1.58	0.64-1.27	0.99-1.20	0.88-1.64	1.41-1.65	1.11-1.33
MBMWP		3.00-4.50	3.83-4.40	3.83-4.80	3.00-5.20	4.25-4.33	3.60-4.80	4.20-5.00	3.00-5.00
FS		70	70	70	70	70	70	70	70
FSW		2.23	2.23	2.23	2.23	2.23	2.23	2.23	2.23

Table 10: The Parameter/Index Score, Indicator Group Scores, RHI and RHC (Sep 2016-May 2018).

		EC	DO	BOD	COD	FC	OEB	NH3-N	TN	TP	NT	APPI	A	MSW	MBMWP	MI	FS	FSW	F	RHI	RHC
		Parameter/Index Score (0-5)					Indicator Group Score (0-100)	Parameter/Index Score (0-5)			Indicator Group Score (0-100)	Parameter/Index Score (0-5)	Indicator Group Score (0-100)	Parameter/Index Score (0-5)		Indicator Group Score (0-100)	Parameter/Index Score (0-5)		Indicator Group Score (0-100)	River Health Index (0-100)	River Health Condition
2016-2017																					
Post Monsoon (16Sep-15Nov)	L1	4	4	3	4	3	72	4	3	3	67	3	60	1	3	40	4	3	70	60.3	Good
	L2	4	1	1	1	0	28	1	0	0	7	2	40	1	2	30	4	3	70	38.2	Critical
	L3	4	4	3	2	1	56	3	1	2	40	3	60	2	3	50	4	3	70	56.4	Stressed
	L4	4	4	2	2	1	52	2	1	1	27	3	60	1	3	40	4	3	70	51.3	Stressed
	L5	4	3	2	1	0	40	1	1	0	13	2	40	2	2	40	4	3	70	43.5	Over Stressed
Winter (16Nov-15Jan)	L1	5	4	3	4	3	76	4	2	3	60	3	60	2	3	50	4	3	70	62.4	Good
	L2	5	2	2	1	0	40	2	0	0	13	1	20	2	2	40	4	3	70	39.5	Critical
	L3	5	3	3	3	2	64	3	1	1	33	3	60	2	3	50	4	3	70	56.6	Stressed
	L4	5	3	3	3	1	60	2	1	0	20	3	60	2	2	40	4	3	70	51.5	Stressed
	L5	5	2	3	2	1	52	1	1	0	13	3	60	2	2	40	4	3	70	49.3	Over Stressed

Table Cont....

Cont. Table...

Season	Loc																			Score	Category
Spring (16Jan-15Mar)	L1	5	4	4	2	3	72	4	3	4	73	3	60	2	3	50	4	3	70	63.8	Good
	L2	5	2	2	0	1	40	2	1	0	20	2	40	2	3	50	4	3	70	47.0	Over Stressed
	L3	5	4	3	2	2	64	4	3	1	53	3	60	2	3	50	4	3	70	59.6	Stressed
	L4	5	3	3	2	2	60	4	2	1	47	3	60	2	3	50	4	3	70	58.0	Stressed
	L5	5	3	2	1	1	48	4	2	0	40	3	60	2	2	40	4	3	70	52.7	Stressed
Summer (16Mar-15May)	L1	4	3	3	2	2	56	3	2	2	47	2	40	2	3	50	4	3	70	53.4	Stressed
	L2	3	0	1	0	0	16	0	0	0	0	1	20	1	2	30	4	3	70	31.4	Critical
	L3	4	3	2	2	2	52	2	2	1	33	2	40	2	3	50	4	3	70	50.8	Stressed
	L4	3	2	2	0	1	32	2	1	2	33	2	40	1	3	40	4	3	70	45.3	Over Stressed
	L5	3	1	1	0	0	20	1	1	1	20	1	20	2	2	40	4	3	70	37.5	Critical
2017-2018																					
Post Monsoon (16Sep-15Nov)	L1	4	4	3	4	3	72	4	2	2	53	3	60	2	3	50	4	3	70	60.8	Good
	L2	4	2	1	2	0	36	2	2	1	33	2	40	1	3	40	4	3	70	45.9	Over Stressed
	L3	4	4	3	3	2	64	3	2	2	47	3	60	2	3	50	4	3	70	58.6	Stressed
	L4	4	4	3	2	1	56	2	2	2	40	3	60	2	3	50	4	3	70	56.4	Stressed
	L5	4	3	2	1	1	44	2	1	1	27	2	40	2	3	50	4	3	70	48.6	Over Stressed
Winter (16Nov-15Jan)	L1	5	4	4	3	2	72	4	3	3	67	3	60	2	3	50	4	3	70	62.9	Good
	L2	5	2	2	1	1	44	4	2	1	47	2	40	2	2	40	4	3	70	49.1	Over Stressed
	L3	5	4	3	3	3	72	4	4	2	67	3	60	2	3	50	4	3	70	62.8	Good
	L4	5	3	3	3	2	64	4	3	1	53	3	60	1	3	40	4	3	70	57.1	Stressed
	L5	5	3	3	1	1	52	4	2	2	53	2	40	2	3	50	4	3	70	53.8	Stressed
Spring (16Jan-15Mar)	L1	5	4	4	2	3	72	4	4	4	80	3	60	2	3	50	4	3	70	64.8	Good
	L2	5	2	2	1	2	48	5	4	2	73	2	40	2	3	50	4	3	70	56.2	Stressed
	L3	5	4	3	2	3	68	5	4	3	80	3	60	2	3	50	4	3	70	64.2	Good
	L4	5	3	3	2	3	64	5	4	3	80	3	60	2	3	50	4	3	70	63.6	Good
	L5	5	3	3	1	2	56	4	2	2	53	2	40	2	3	50	4	3	70	54.4	Stressed
Summer (16Mar-15May)	L1	4	3	3	2	2	56	3	2	3	53	2	40	2	3	50	4	3	70	54.4	Stressed
	L2	3	0	1	0	0	16	1	1	1	20	0	0	2	2	40	4	3	70	32.9	Critical
	L3	4	3	2	2	2	52	2	2	2	40	2	40	2	3	50	4	3	70	51.8	Stressed
	L4	4	2	2	1	1	40	2	1	1	27	2	40	2	2	40	4	3	70	45.5	Over Stressed
	L5	2	1	1	0	1	20	2	1	1	27	1	20	2	2	40	4	3	70	38.5	Critical

only at upstream location (L1) and this location also becomes stressed during the summer season. All other locations are under poor river health category, varying from 'Stressed' to 'Critical' levels. Fig. 3 shows the variation of RHIas graphs and Fig.4 gives the coloured pictorial representation of River Health Condition (RHC) as quality pentagon and scores under various categories for four seasons during 2016-17 and 2017-18 at different locations.

From Fig. 3, based on River Health Index (RHI), it appears that river health is at its lowest levels during the summer season, which improves during post-monsoon months. During winter, the river health improves further and attains its best levels during the spring season (16Jan-15Mar). It is also observed that near Varanasi, the river health at most of the Ghats has improved in 2017-2018 with respect to the year 2016-2017. Better river health during the spring season (16Jan-15Mar) could be due to increasing temperature and other environmental factors. Among OEB parameters, BOD and faecal coliforms in the riverine environment are at lowest levels in the spring in comparison to other seasons. The OEB group score at L1 and L3 is Very Good and Good respectively during the spring season. All the nutrient parameters decreased during the spring season which increases the NT score and all locations except L5 are in 'Very Good' category. As water quality improves for these parameters, there is an increase in the population and diversity of biotic indicators. The population of pollution sensitive species increase, which increases the scores of biotic indices. The algal group scores at L1, L3 and L4 are in 'Stressed' range and L2 & L5 are in 'Critical' condition during the spring season. It is noted that locations L1, L3 and L4 show presence of the genera *Flagilaria*, *Spirogyra*,
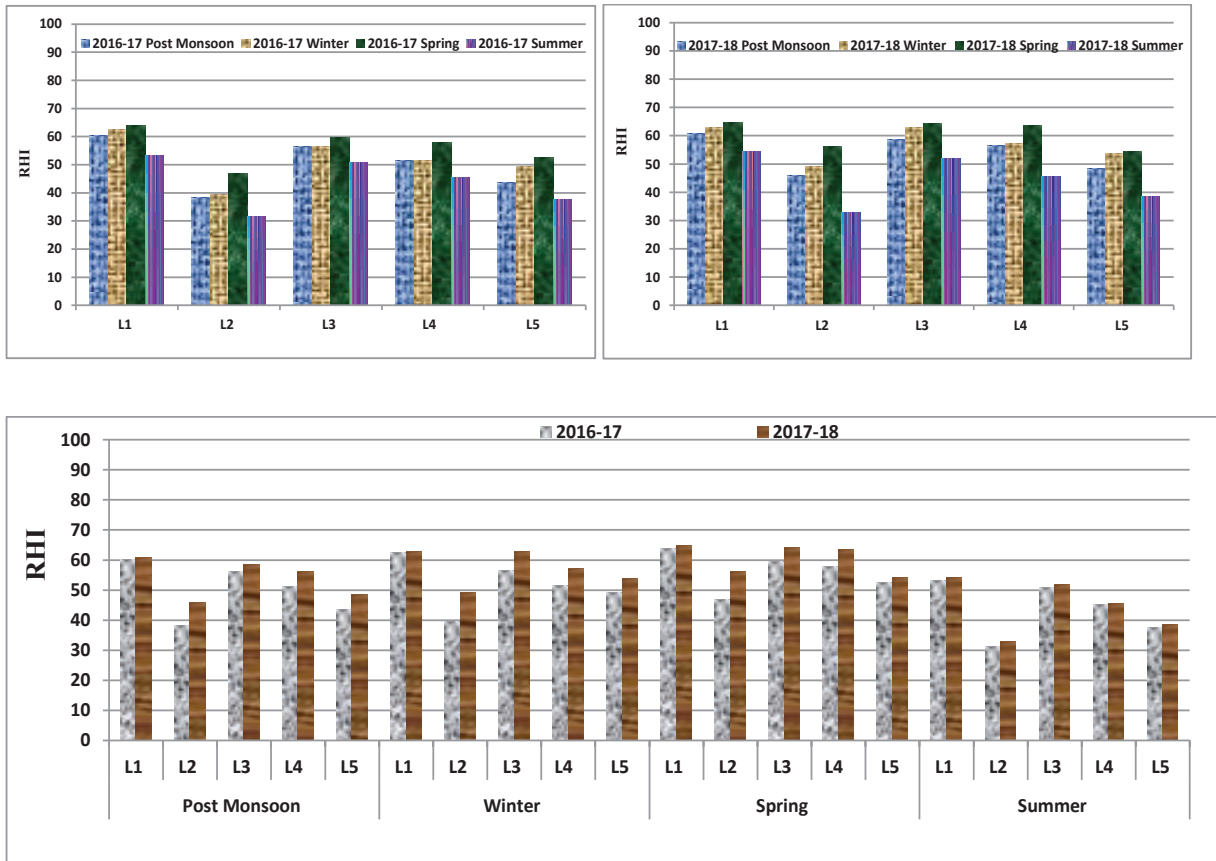
Fig. 3: Variation of River Health Index (RHI) for River Ganga at different locations near Varanasi during 2016-2017 and 2017-2018.

Staurastrum, etc. of algae. Venkateswarlu & Reddy (1985) reported that the abundance of green algal flora like *Zygnema*, *Spirogyra*, *Mougeotia*, *Euastrum*, *Staurastrum*, etc. indicate less polluted water. Among macroinvertebrates, presence of moderately sensitive species such as Baetidae, Culicidae, Dytiscidae, Elmidae, Hydrophilidae, Psychodidae families at locations L1, L3 and L4 indicate good quality of water at these locations. Adakole (2001) also noted that the presence of Mayflies and Caddisflies reflects clean water. This increase in biotic scores improves the River Health Index (RHI). A higher RHI indicated a better River Health Condition (RHC).

The water quality and river health are found at its lowest levels during summer (16Mar-15May), possibly because with the onset of summer, the temperature starts rising and the DO starts decreasing due to high microbial activities involved in organic matter decomposition. The decrease in DO and an increase in BOD and faecal coliforms reduce the OEB group score. Due to low dilution and increased pollution, nutrient concentration also increases. The decrease in water quality affects the aquatic biota present. Due to low level of DO, reduced discharge and increased concentration of

pollutants, sensitive biotic species decreases and there is an increase in the number of pollution resistant species (Genter & Lehman 2000, Biosson & Perrodin 2006). This increase in pollution resistant species decreases the biotic indices score which lowers the RHI value, indicating deteriorating river health condition. At L2 (the confluence of Assi Nala with Ganga) and L5 (the confluence of Varuna with Ganga), large amounts of sewage are added to River Ganga. The presence of algal genera such as *Ankistrodesmus*, *Euglena*, *Navicula*, *Nitzschia*, *Oscillatoria*, *Scenedesmus*, etc. at these locations during the period is indicative of polluted water, as noted by Patrick (1965) and Palmer (1969) who concluded that *Ankistrodesmus*, *Euglena*, *Navicula*, *Scenedesmus*, *Stigeoclonium*, *Oscillatoria*, *Chlamydomonas* and *Nitzschia* are highly pollution tolerant genera and found in organically polluted waters. Pearsall (1932) was the first to establish a correlation between blue-green algae and organic pollution tolerant species of diatoms such as *Anabaena*, *Chlorella*, *Closterium*, *Cosmarium*, *Eudorina*, *Melosira*, *Navicula*, *Pandorina*, *Scenedesmus* and *Spirulina*. Rai et al. (2008), Das et al. (2007), Sanap (2007), Jafari & Gunale (2006), Goel et al.
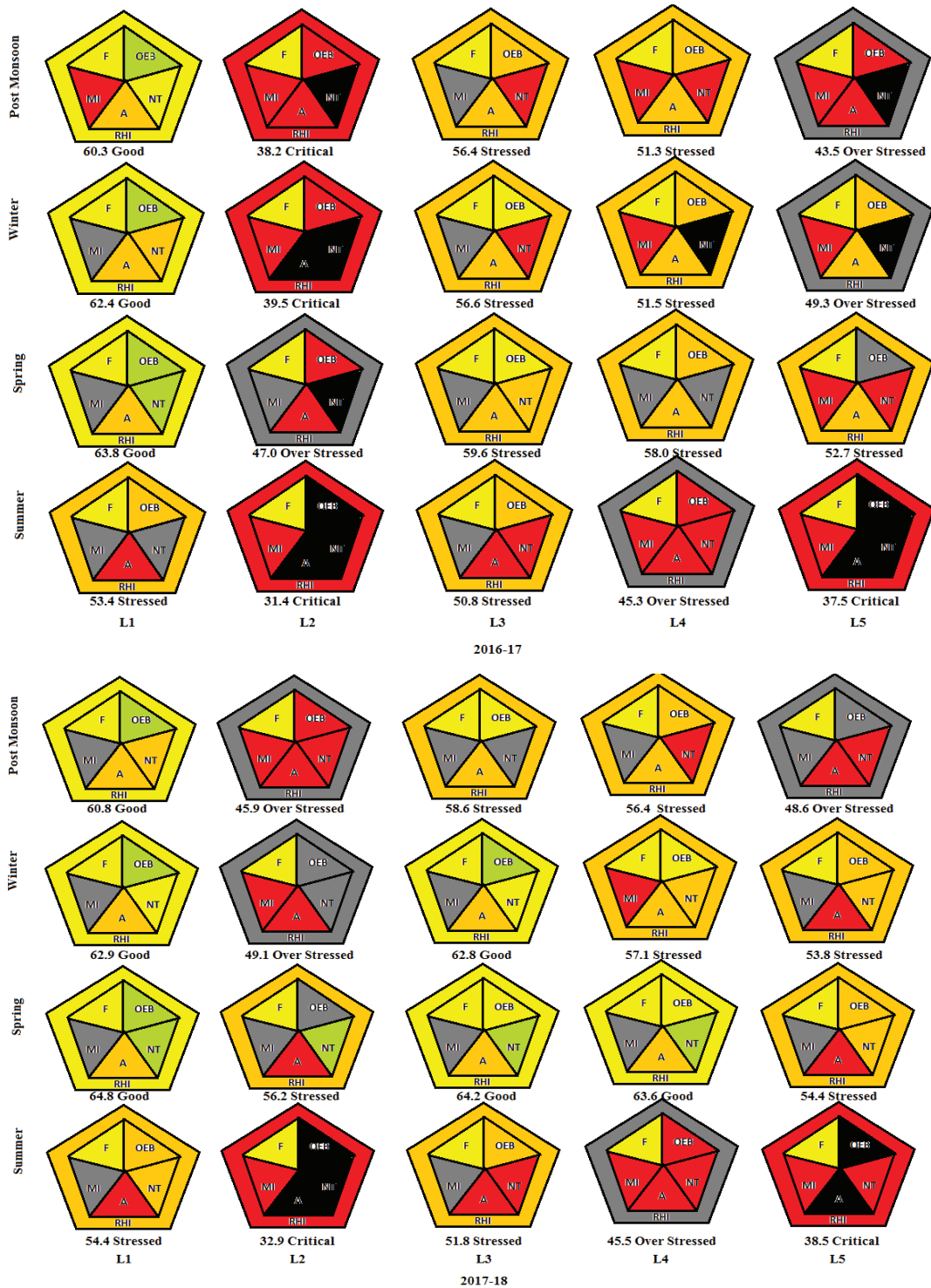
Fig. 4: Pictorial representation for River Ganga at different locations near Varanasi during 2016-2017 and 2017-2018.

(1986), Gunale & Balakrishnan (1981)and Ratnasabapathy (1975) also suggested that the presence of these pollution tolerant species indicate polluted waters. At locations, L2, L4 and L5 the repeated presence of macroinvertebrates Oligochaeta (Tubificids, Tubifex) Chironomids (midge larvae), Physidae and Muscidae indicate polluted water which is in accordance with the findings of Adakole (2001) who reported that certain tubificids (especially *Tubifex tubifex* and *Lumnodrilus hoffmeisteri)* or midge larva of the genus *Chironomus* or *Eristalis* larvae or class Oligochaeta can reflect low DO levels and high organic concentration in an area. The macroinvertebrate species which are pollution tolerant are expected to be more dominant in polluted waters (Sallenave 2015). Sharma et al. (2014) gave the order of disappearance of organisms due to continuous increase in pollution as Plecoptera (stoneflies): Ephemeroptera (mayflies, damselflies etc): Trichoptera (caddisflies): *Gammarus* (freshwater shrimp): *Asellus* (water hog louse): Chironomidae (blood worms): Oligochaeta (tubificid worms).

It is evident from Fig 4. that at upstream of Varanasi (L1), the health of River Ganga is in 'Good' condition. As it enters the city, the first point is C/O of Assi Nala (L2) where a large quantity of sewage is being added to the river and the health condition varies at this point between 'Over Stressed' and 'Critical' during various seasons of the year. In OEB group category, DO decreases and there is an increase in the BOD, COD and faecal coliforms. In Nutrient group, there is an increase in NH_3-N, TN and TP concentration.

At Dashashwamedh Ghat (L3), both OEB and NT group parameters seem to have improved possibly due to self-purification, or some physico-chemical reactions, and the health comes in the 'Good' category during winter and spring and 'Stressed' condition during summer. However, as it moves downstream to Raaj Ghat (L4) and C/O Varuna with Ganga (L5), the concentration of COD and faecal coliform parameters of OEB group and TN and TP parameters of NT group increase. Consequently, the river health again comes under 'Stressed' to 'Critical' condition at these points.

CPCB (2018) reported the biological water quality of River Ganga at Varanasi in moderate pollution range in May 2017 and March 2018. The results of these analyses are also reflective of similar conclusions, although with a deeper diagnostic approach.

Using the observational data for two years (Sept 2016-May 2018), the river health condition of Ganga near Varanasi may be categorized as 'Good' to 'Stressed' at upstream of Varanasi (L1), and near Dashaswamedhghat (L3), 'Stressed' to 'Overstressed' near Rajghat (L4), and 'Overstressed' to 'Critical' near the confluence of river Assi with Ganga (L2) and Varuna with Ganga (L5). For comparison, the river health condition of Ganga as categorized from the framework presented in this study, based on RHI calculation at Rishikesh (near Laxman Jhoola) in winter and spring 2019 is 'Very Good' and 'Excellent' respectively, as shown in Fig. 5.

Thus, the framework for an understanding of river health condition, based on river health index (RHI) calculation, as discussed in the present study appears to give good results capable of describing the riverine condition in a simple but scientifically sound manner. Its coloured representation of scores for five indicators groups of river water quality and overall river health condition makes it simpler to the scientific community for diagnostic and corrective step purposes.

CONCLUSIONS

In the present study, a framework for a scientific assess-
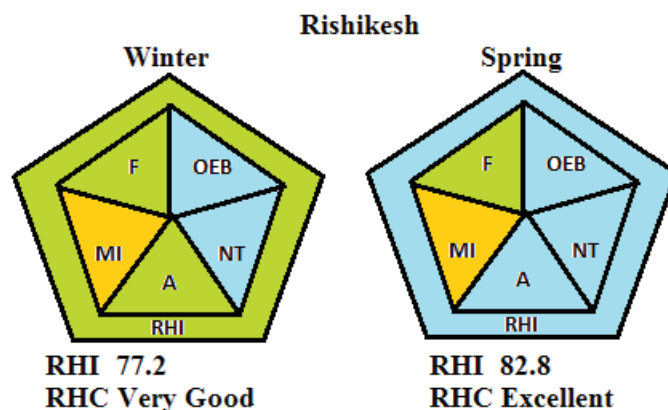
Fig. 5: RHI and RHC of Laxman Jhoola, Rishikesh during winter and spring.

ment of river health condition involving eight water quality parameters and five biotic indices, have been proposed and tested. Water quality parameters have been divided into two groups: i. Organo-Electrolytic-Bacterial (OEB) and ii. Nutrients (NT). Also, one algal (A), two macroinvertebrates(MI) and two fish (F) indices have been used to calculate River Health Index (RHI) on a 0-100 scale. Based on RHI value, River Health Condition (RHC) has been classified from Sick/Dead to Excellent and represented through a coloured circumscribed pentagon, each side depicting the condition of river health for one category of riverine water quality. This framework has been used to assess the health of River Ganga near Varanasi through measurement of relevant water quality parameters and evaluation of biotic indices for four seasons (post-monsoon, winter, spring and summer) continued for two years. Based on RHI calculation, the health of River Ganga near Varanasi was found to be slightly improving in the year 2017-2018 for 2016-2017. River health is observed unstable during the post-monsoon period and found its best levels during the spring season (16Jan-15March). At polluted locations of the river, pollution resistant and at clean/less polluted locations sensitive or moderately sensitive algae and macroinvertebrate community are present. Pollution resistant species of algae and macroinvertebrate were observed near the confluence of river Assi (L2) and Varuna with Ganga (L5), and clean locations such as SaamneGhat (L1) and DashashwamedhGhat (L3) and moderately polluted location near RaajGhat (L4) showed the presence of sensitive or moderately sensitive species. The confluence of river Assi (L2) and the confluence of Varuna with Ganga (L5) were found to be organically polluted. In spatial terms, the river health is generally acceptable and found as 'Good' near Saamne Ghat, followed by Dashashwamedh Ghat and Raaj Ghat in Varanasi stretch. Overall, it varied between 'Good' to 'Overstressed'conditions during the full year, except near Assi and Varunariver confluence points, where it is found to be 'Critical'. The Indicator Group Score based approach of River Health Index (RHI) calculation gives insights for identification of critical parameters and strategic plan preparation for restoration. The analyses indicate that RHI can be used as a tool to understand river health conditions.

To improve the River Health Condition, the restoration plan should focus on parameters whose group score are below acceptable (less than 3 on the 0-5 scale). Nutrients (NT) group of parameters appear the most critical and algal score seems the worst affected for river health near Assi and Varuna confluence points. Highly polluted waters coming from these rivers need to be checked and controlled. Instream treatment such as ponding and active algal harvesting to reduce organic pollutants and nutrients load, use of boulders to create roughness in the bed, fountains for aeration, and floating algal mats in the streams can be used to improve the water quality of Assi and Varunarivers before they meet River Ganga. With these initiatives, the river health condition of Ganga near Varanasi may be improved substantially and maintain it at acceptable levels all around the year.

REFERENCES

ACEDP 2011. Australia-China Environment Development Partnership River Health and Environmental Flow in China. Assessment of River Health in the Liao River Basin (Taizi Sub-Catchment) Project Report: Prepared by the International Water Centre and the Chinese Research.

Adakole, J.A. 2001. The effect of domestic agricultural and industrial effluents on the water quality and biota of Bindare Stream, Zaria-Nigeria.Ph.D. Thesis, Deptt. of Biological Sciences, Ahmadu Bello University, Zaria.

Allan, J.D. 1995. Stream Ecology: Structure and Function of Running Waters, 2nd Edition. Kluwer Academic Publishers. The Netherlands.

Anon 2000. Australian and New Zealand Guidelines for Fresh and Marine Water Quality. Volume 1, The Guidelines, Australian and New Zealand Environment and Conservation Council, Agriculture and Resource Management Council of Australia and New Zealand.

APHA 2005. Standard Methods for the Examination of Water and Wastewater. 21st Edition, American Public Health Association/American Water Works Association/Water Environment Federation, Washington DC.

Barbour, M.T., Gerritsen, J., Snyder, B.D. and Stribling, J.B. 1999. Rapid Bioassessment Protocols for Use in Streams and Wadeable Rivers: Periphyton, Benthic Macroinvertebrates andFish, Second Edition. EPA 841-B-99-002. U.S. Environmental Protection Agency, Office of Water, Washington, D.C.

Bhardwaj, R.M. 2005. Water Quality Monitoring in India- Achievements And Constraints. IWG-Env, International Work Session on Water Statistics, Vienna.

Biosson, J. C. and Perrodin, Y. 2006. Effects of road runoff on biomass and metabolic activity of periphyton in experimental streams. Journal of Hazardous Materials, 132(2-3): 148-154.

Leigh, C., Qu, X., Zhang, Y., Kong, W., Meng, W., Hanington, P., Speed, R., Gippel, C., Bond, N., Catford, J., Bunn, S. and Close, P. 2012. Assessment of River Health in the Liao River Basin (Taizi Subcatchment) International Water Centre, Brisbane, Australia.

CPCB 2002. Water Quality Criteria and Goals. Feb 2002, Central Pollution Control Board, Delhi.

CPCB 2015. A Concept and Plan Conservation of Water Quality of Ganga: A Segmental Approach Proposed Primary Water Criteria For Bathing Water. Dec 2015, Central Pollution Control Board, Delhi.

CPCB 2018. Biological Water Quality Assessment of the River Ganga (2017-18). Bio-Science Division, Central Pollution Control Board, Ministry of Environment, Forest & Climate Change, Govt. of India, Delhi, June 2018.

Das, S.K., Biswas, D. and Roy, S. 2007. Phytoplanktonic community of organically polluted tropical reservoirs in Eastern India. Chinese Journal of Applied Environmental Biology, 13(4): 449-453.

Das, M.K., Sharma, A.P., Vass, K.K., Tyagi, R.K., Suresh, V.R., Naskar, M. and Akolkar, A.B. 2013. Fish diversity, community structure and ecological integrity of the tropical RiverGanges, India, Aquatic Ecosystem Health & Management, 16(4): 395-407.

De Zwart, D. and Trivedi, R. C. 1994. Manual on Integrated Water Quality Evaluation (Report 802023003). National Institute of Public Health and Environmental Protection (RIVM), Bilthoven, The Netherlands.

Durrand, J. R. and Leveque, C. 1981. Flore et fauna Aqua tyries De l' AfrqueSaholo-Soudamienne edition de l' office de la Recherche Scientific et Technique actre-marcollectioninitiatins. Documentations Technique No. 45 Paris.

Dwivedi, A.C., Mishra, A. S., Mayank, P. and Tiwari, A. 2016. Persistence and structure of the fish assemblage from the Ganga River (Kanpur to Varanasi section), India. Journal of Geography & Natural Disasters, 6: 159.

EHMP 2010. Ecosystem Health Monitoring Program 2008-09, Annual Technical Report, South East Queensland Healthy Waterways Partnership, Brisbane.

Genter, R.B. and Lehman, R.M. 2000. Metal toxicity inferred from algal population density, heterotrophic substrate use, and fatty acid profile in a small stream. Environmental Toxicology and Chemistry, 19(4): 869-878.

Gerber, A. and Gabriel, M.J.M. 2002. Aquatic Invertebrates of South African Rivers. Field Guide. Volume 1 and II, Institute for Water Quality Studies, Department of Water Affairs and Forestry.

Goel, P.K., Khatavkar, S.D., Kulkarni, A.Y. and Trivedy, R. K. 1986. Limnological studies of a few freshwater bodies in southwestern Maharasthra with special reference to their chemistry and pollution. Poll. Res., 5(2): 79-84.

GRBMP 2015. Ganga River Basin Management Plan. Main Plan Document. Consortium of seven Indian Institute of Technologies (IITs), India.

Gunale, V. R. and Balakrishnan, M.S. 1981. Biomonitoring of eutrophication in the Pavana, Mula and Mutha rivers flowing through Poona. Indian Journal of Environmental Health, 23: 316-322.

Hawkes, H.A. 1979. Invertebrates as indicators of river water quality. In: Biological Indicators of Water Quality, James, A. and Evison L. (Eds.), pp. 2.1-2.45, Chichester, New York, John Wiley and Sons, UK.

Hellawell, J.M. 1986. Biological Indicators of Freshwater Pollution and Environmental Management. Elsevier, London, p. 546.

Jafari, N.G. and Gunale, V. R. 2006. Hydrobiological study of algae of an urban freshwater river. Journal of Applied Science and Environment Management, 10(2): 153-158.

Kerkhoff, 2010. Measuring biodiversity of ecological communities. Ecology lab, Biology, 229. http://biology.kenyon.edu/courses/biol229/diversity.pdf

MEP 2008. Report on the State of the Environment in China 2006, Ministry of Environmental Protection, People's Republic of China.

Merritt, R.W. and Cummins, K.W. 1996. An Introduction to the Aquatic Insects of North America, 3rd edition. Dubuque, J. O, Kendall-Hunt, Iowa.

MoWR 2014. Ganga Basin-Version 2.0. Ministry of Water Resources, Govt. of India.

Nandan, S.N. and Patel, R. J. 1986. Assessment of water quality of Vishwamitra river by algal analysis. Indian J. Environ. Health, 29(2): 160-161.

Needham, J. G. and Needham, P. R. 1969. A Guide to the Study of Freshwater Biology. Holden-Day Inc., San Francisco, 108.

Palmer, C.M. 1969. Composite rating of algae tolerating organic pollution. Journal of Phycology. 5: 78-82.

Patrick, R. 1965. Algae as indicator of pollution. In: Biological Problems in Water Pollution. 3rd Seminar, Bot. A. Tuft. Sanitary Engg. Centre, Cincinnati, Ohio. https://www.researchgate.net/publication/268375252_ALGAE_AS_AN_INDICATOR_OF_RIVER_WATER_POLLUTION_-_A_REVIEW

Pearsall, W. H. 1932. Phytoplankton in the English lakes II. Ecol., 22: 241-262.

Pennak, W. P. 1978. Freshwater Invertebrates of the United State. Oxford, Ronald.

Pennak, R. W. 1989. Fresh-water Invertebrates of the United States: Protozoa to Mollusca. 3rd. ed. John Wiley and Sons, New York.

Rai, U.N., Dubey, S., Shukla, O.P., Dwivedi, S. and Tripathi, R.D. 2008. Screening and identification of early warning algal species for metal contamination in freshwater bodies polluted from point and non-point sources. Environmental Monitoring Assessment, 144: 469-481.

Ratnasabapathy, M. 1975. Biological aspects of Wardieburn sewage oxidation pond. Malaysian Science, 3(a): 75-87.

Rosenberg, D.M. and Resh, V.H. 1993. Freshwater Biomonitoring and Benthic Macroinvertebrates. Chapman & Hall, London, p. 488.

Sallenave, R. 2015. Stream biomonitoring using benthic invertebrates. Circular 677. http://aces.nmsu.edu/pubs/_circulars/CR677.pdf, New Mexico State University 4 Cooperative Extension Service. College of Agricultural, Consumer and Environmental Sciences.

Sanap, R.R. 2007. Hydrobiological studies of Godavari River up to Nandur-Madhmeshwar dam, Dist Nashik, Maharashtra. Ph. D. Thesis, University of Pune, Pune, India.

Sharma, Shailendra, Dawar, Bhavna and Barkale, Shitika 2014. Biomonitoring a biological approach to water quality management. Elixir Bio Diver., 66: 20635-20638.

Singh, P. K. and Saxena, S. 2018.Towards developing a river health index. Ecological Indicators, 85: 999-1011.

Sladecek, V. 1979. Continental systems for the assessment of river water quality. In: Biological Indicators of Water Quality. James, A. and Evison L. (Eds.), John Wiley & Sons, Chichester.

Tittizer, T.T. and Koth, P. 1979. Possibilities and limitations of biological methods of water analysis. In: James A. and Evison L. (Eds.), Biological Indicators of Water Quality, John Wiley and Sons, Chichester.

Tonapi, G. T. 1980. Freshwater Animals of India- An Ecological Approach. Oxford and IBH Publishing Co., New Delhi, 341.

UNECE 1994. ECE Standard Statistical Classification of Surface Freshwater Quality for The Maintenance of Aquatic Life. The United Nations Economic Commission for Europe.

Venkateswarlu, V. and Reddy, P.M., 1985. Algae as biomonitors in river ecology. In: Symposium on Biomonitoring, State of Environment, New Delhi, India, pp. 183-189.

William, D.P. and Feltmate, B. W. 1992. Aquatic Insects. C.A.B. International, Wallingford Oxon, UK.

Hazards of Environmental Disruption in Mine Goafs and Stability Evaluation in Gaofeng Mining Area

Chun Bai*, Meng Xian Yun** and Jun Mei Wang*†

*College of Civil Engineering, Xuchang University, Xuchang, 461000, China
**Zhumadian Cigarette Factory of China Tobacco Henna Industrial. CO, LTD
†Corresponding author: Jun Mei Wang; ansysbc@163.com

ABSTRACT

China is rich in mineral resources with many points and broad faces in metal and nonmetal mines. However, numerous goafs are formed due to backward mining technology, low intensification degree, incomplete safety precautions, and the excessive exploitation of mineral resources, thus leading to severe environmental disruption. Accidents, like goaf collapse, are major geological disasters in mine production, and goaf stability evaluation is of great importance for reducing natural disasters in goafs and implementing environmental protection. The hazard types of environmental disruption caused by mine goafs were first analyzed in this study. Then, an influence factor index system of goaf stability was established, and a case study of a mine goaf in Henan Province was conducted using an analytic hierarchy process (AHP)-based fuzzy comprehensive evaluation model. Results show that the hazards of environmental disruption in mine goafs are manifested in the structural failure of surrounding buildings, massive water and soil loss, the exhaustion of water resources, the degradation of soil quality, and the remarkable reduction of overlying animals and plants. Technical factors exert the maximum influence on underground goaf stability with the total weight value reaching 72.42%, and the influence weight of goaf span on goaf stability reaches 21.43%, followed by goaf area and pillar distribution with influence weights of 18.58% and 11.17%, respectively. Through fuzzy AHP-based comprehensive evaluation and calculation, the goaf stability of the Henan Sandaozhuang open-pit mine in the case study belongs to grade (ordinary), that is, the goaf stability is in the ordinary state, and the evaluation result reflects the reality. The study results have improved the reasonable stability and safety management scheme for complex multi-layer goaf and solved complex goaf hazards faced by Gaofeng mining area, so they will be of general significance for the environmental governance of other underground mine goafs.

INTRODUCTION

With the sustainable and rapid development of the national economy of China, the demand for and utilization of various mineral resources are continuously increasing. Meanwhile, Fig. 1 shows that the exploitation of mineral resources is increasing in quantity annually in China, though large reserves exist. Metal and nonmetal mines have many points and broad faces, but many underground goafs are formed due to backward mining technology, low intensification degree, incomplete safety precautions, and the excessive exploitation of mineral resources. In view of the complex underground goaf distribution and the difficulty in predicting goaf roof caving (collapse), the stability analysis of underground goafs has become a major limiting factor of the development of mines, and accidents, like goaf collapse, have become major geological disasters in mine production. Goafs are cavity areas left after underground mineral products are excavated. Natural rock masses are originally in a natural balanced

state. All kinds of spaces, like roadways and stopes, must be excavated from rock masses to exploit mineral deposits, disrupting the natural balance state of rock masses. Furthermore, the exploited space changes the original stress field of the rock mass and thus generates a secondary stress field. Under the action of the secondary stress field, the rock mass around the exploited space undergoes deformation and even failure and movement until a new balance is reached. A mining area can be divided into old, present, and future mining areas according to the mining time.

However, as the open-stope method is adopted in most small- and medium-sized mines in China, the scale of the goaf left is extremely large. Meanwhile, some goafs have already become major risks to the safe production of mine enterprises due to the poor hydrogeological conditions in goafs and the harsh geological environmental conditions around them. Mining activities lead to surface subsidence, slope instability, ground fracture, and other geological

disasters. The development of mineral resources will result in soil resource loss, the pollutant discharge in the development process of mineral resources will cause environmental pollution, and the whole mining activity will lead to the imbalance of the underground water system and aggravate the water and soil loss and land desertification in the mining area. These problems exist in the coal mining process and have a huge environmental impact on the entire mining area in the form of geological disasters, like goaf collapse, and a severe effect on the economic development, people's lives, and property safety in the mining area. With the exhaustion of mineral resources, most mine enterprises are in the residual ore recovery phase, and some are guilty of excessive exploitation so that the exposure areas of goafs are further enlarged. Moreover, the surrounding rock stability in goafs is degraded and the recovery safety is threatened under the impacts of water flow erosion and blast vibration.

PAST STUDIES

Environmental pollution and governance problems in mine goafs have always been among the main difficulties of mine enterprises. Domestic and foreign experts and scholars have carried out many theoretical research works and scientific practices. The main foreign mining countries have turned their attention to the goaf stability problem very early. Regarding the environmental disruption caused by goafs, Ma et al. (2012) deemed that the large-area continuous solid shallow-buried goaf group generated by the open-stope method would collapse completely because the partial instability of upright and roof led to the collapse of the whole mine, displaying the domino effect, that is, causing severe environmental disruption. Youhong et al. (2015) investigated the collapse mechanism of the third mining area in Gongchangling District, Liaoyang City and related influence factors and distribution laws through a geological survey.

Their results show that mining is the primary factor of surface subsidence, while underground water infiltration accelerates this process. Huang et al. (2017) deemed that the exploitation of China's coal resources would cause permanent fracture and the movement of the stratigraphic texture and thus cause the fracture and collapse of the overlying strata; furthermore, surface subsidence and water leakage at aquifers around the coal seam would occur. These phenomena would not only result in loss of land and water resources but would also lead to serious threats to and accidents in underground mining and further cause the destruction and degradation of the ecosystem. Zhao et al. (2018) introduced the coal stone backfill and banding mining method to perform case analysis of the Tangshan coal mine in Hebei Province, China, and their study suggests that the surface subsidence and coal stone caused by mining activity might seriously impact the nearby environment. Hengjie et al. (2018) believed that the coal mining processes in the whole world have left many goafs. If pillars fail to maintain permanent stability, sudden large-area goaf collapse might occur, which would cause serious environmental pollution. Ma et al. (2019) believe that the coal stones generated during the coal mining and dressing process are a severe threat to the ground environment and proposed a new governance method. The main researches on goaf stability are as follows. Whittles et al. (2006) developed an analysis method for predicting the possible influence of the shear strain generated in rock mass on the subsequent shaft stability and then provided a derivation method. Gao et al. (2016) deemed that underground coal mining would have a major adverse effect on road stability and proposed a numerical method combing SRM-UDEC (Synthetic Rock Mass-Universal Distinct Element Code) Trigon to investigate the roadway failure mechanism along unstable goafs. Chuanqu et al. (2006) thought that goaf stability is comprehensively influenced by multiple factors, such as the strength of surrounding rock, coal strength, mining depth, gaps in sur-
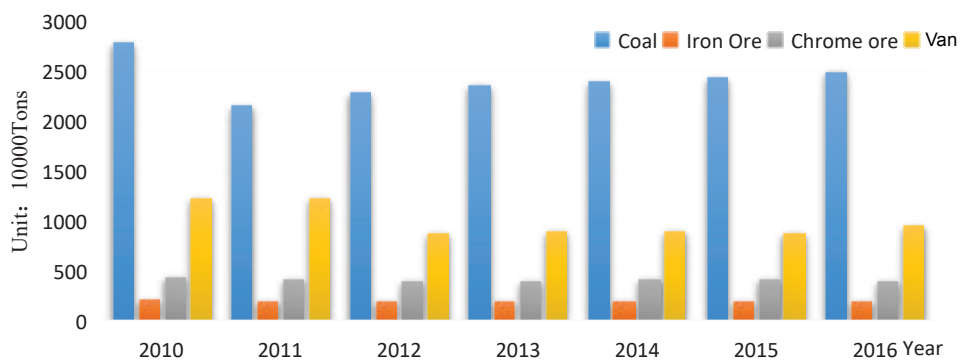
Fig. 1: Reserves of main mineral resource types in China during 2010-2016.

rounding rock, mining operation, top coal thickness, and coal seam width, and thus constructed a subordinate function for the influence factors of gob-side roadway stability on a fully mechanized working face and built a grey fuzzy classification model to carry out an empirical study. Chen et al. (2010) included the microcosmic goaf governance problem into the innovative design of the mining method and probed the synergistic effect between the two problems. The catalyzed fission mining area of the 105# ore body in Gaofeng Mining Area, Guangxi was taken as an example. Some typical goafs were selected, and their stability was calculated through the discrete element method according to their differences in scale, environmental conditions, and geo-stress field. The research results indicate that collaborative research on goafs in fission ore segments and goaf management can improve the safety of ore deposits. Li et al. (2016) evaluated the long-term stability of the rock strata above an old goaf and its possible influence on the buildings above the rock strata, analyzed the releasable space in the rock strata, proposed a stability evaluation method for the building foundation above the goaf under the abovementioned circumstance, and applied the proposed method to engineering practice. Feng (2018) explored the influences of the strength of backfill materials on the deformation of coal and the rock strata constituted by multiple goafs during the excavation process through the backfill method. The numerical results show that the supporting ability of the backfill materials in the goaf was enhanced with the increase of BMS (the strength of backfilling materials). Wu et al. (2018) believed that the mining process is accompanied by the gradual accumulation of disasters and selected 10 influence factors to evaluate the ground stability of goafs. According to level of each evaluation factor, the surveyed area was divided into four regions-the unstable, basic unstable, basic stable, and stable regions-based on the fuzzy comprehensive evaluation, and the study results would contribute to predicting and controlling the surface subsidence disaster caused by underground mining in similar areas. Yang et al. (2019) investigated the gob-side roadway stability under the disturbance of the underground coal face and raised concrete control measures. The existing literature indicates that studying the overall mine stability during the underground exploitation process helps mines take necessary measures to eliminate or reduce their potential safety hazards, like surface subsidence or collapse, effectively control ground pressure disasters, protect the surface environment, and realize green mining. On this basis, the hazard types of environmental disruption caused by mine goafs were analyzed first in this study. A mine in Henan Province was taken as an example, an influencing factor index system of goaf stability was established, and an analytic hierarchy process (AHP)-based fuzzy comprehensive evaluation method was used to evaluate the goaf stability of this mine. Qualitative and quantitative safety evaluations of the underground goaf stability were conducted, and goaf management measures were proposed according to the evaluation results for the mine to eliminate and control some unstable goafs. This will not only contribute to safe underground mining but also bring economic benefits to the mine.

HAZARDS OF ENVIRONMENTAL DISRUPTION IN MINE GOAF

Structural Failure of Buildings

Geological disasters related to goaf ground fracture present slow development. Geological disasters gradually emerge and escalate with the increasing number and scale of ground fracture activities. For instance, high tensile stress is generated inside buildings on ground fracture due to ground fracture activity. As the ground fracture activity continues to increase, cracks will generate after the tensile stress generated by buildings reaches the limit value and continuously propagate with the ground fracture activity, thus leading to the structural failure of buildings and finally influencing their overall stability. This process is generally a long-term process and not a sudden disaster.

Massive Water and Soil Loss

Under a shallow surface water table, a swamp area or water collection pool will form on the earth's surface when the underground water level at a sedimented low-lying place is approximate to or higher than the surface level, leading to certain water and soil loss. For land resources in goafs, the ground fracture will dewater the shallow groundwater and cause large-area damage to land and water resources. With the continuous coal mining activities, the surface water is influenced by "three zones," the surface runoffs leak and runoff along the fissure zone and then gradually decrease, the motion state of the underground water body is transformed from the original transverse motion into longitudinal motion, which reduces the surface water capacity and the underground water level by a large margin, and then a series of problems, such as the flow cutoff of surface spring water, emerges. When goafs are under the joint action of ground fracture, land erosion can be divided into rill, gully, and gravitational erosions. Rill erosion enlarges soil gaps with reduced capillary water content and increased gravitational water along with the formation of fine soil particles and the reduction of water content. Gully erosion cuts the land and causes land slope. Gravitational erosion leads to direct soil displacement under the action of gravity and water and can easily cause the direct occurrence of geological disasters, like collapse and landslide.

Exhaustion of Water Resources

Continuous coal mining activities also influence the underground water circulating supply system and change the hydraulic connection between underground aquifers. Within the scope of a coal mining area, pit water infiltrates underground via the diversion fissure zone and replenishes the underground water, polluting the underground water, and the utilizable quantity of nearby underground water resources is reduced or even exhausted. Coal mining activities lead to underground water pollution. Given the existence of cracks at the upper strata in a goaf, the water recharge acquired by the lower aquifer in the vertical direction and the water content at the underlying aquifer increase. The degree of mineralization and hardness of underground water gradually increases during the long-term oxidation-reduction process, and the pollution also escalates every year.

Degradation of Soil Quality

The change in soil quality in the overlying region caused by mining-out is mainly reflected in the change in soil moisture content, pH, rapidly available phosphorus, rapidly available potassium, and so on. Soil moisture content, porosity, and the contents of rapidly available phosphorus and potassium in the overlying region decrease due to mining-out. The comparative changes in moisture content and porosity directly indicate that ground fracture changes the soil water containing, holding and retaining capacities, and the soil pH value has a bearing on the effectiveness of soil nutrients. The comparative changes in the rapidly available phosphorus and potassium contents directly reflect the effect of ground fracture on soil fertility.

Marked Reduction of Overlying Animals and Plants

Given the influences of water and soil loss caused by the ground fracture in the goaf on water and soil environments, the growth of the overlying vegetations is degraded. Influenced by ground fracture, the damaged caused by the ground fracture to plant root systems influences the moisture and nutrient absorption of plant root systems and inhibits plant growth. Coal mining reduces the number of wild plant species, and the richness of wild species in the goaf is evidently lower than that in non-mined out area.

GOAF STABILITY EVALUATION

Profile of AHP-Based Fuzzy Comprehensive Evaluation Model

As a general rule, many factors should be considered in measuring and calculating complicated problems, like goaf stability, and these factors are located at different levels. Thus, the evaluation factors must be divided into several types according to one property. First, each type is comprehensively evaluated, and then high-level comprehensive evaluation is performed between different types based on the evaluation results of each type. In this way, the multilevel fuzzy comprehensive evaluation problem is generated. The multilevel fuzzy comprehensive evaluation model can be established through the following steps.

The evaluation factor set (U) is divided into m subsets according to one property, satisfying Formula (1):

$$\begin{cases} \sum_{i=1}^{m} U_i = U \\ U_i \bigcap U_j = \Phi \ (i \neq j) \end{cases} \quad \ldots(1)$$

Then, the second-level evaluation factor set is obtained using Formula (2):

$$U = \{u_1, u_2, ..., u_m\} \quad \ldots(2)$$

In Formula (2), $U_i = \{U_{ik}\}(i = 1,2,..., n)$, and the evaluation factors in each subset (U_i) are evaluated through a single-level fuzzy comprehensive evaluation model. If the weight allocation of the factors in U_i is A_i, then the evaluation decision matrix is R_i. Then, the comprehensive evaluation result of the ith subset (U_i) is obtained as follows:

$$B_i = A_i \times B_i = [bi_1, b_{i2}, ...b_{in}] \quad \ldots(3)$$

m evaluation factor subsets (i.e., $U_i (i = 1,2, ..., m)$ in U_i are comprehensively evaluated, and the evaluation decision matrix is:

$$R = \begin{bmatrix} B_1 \\ B_2 \\ \vdots \\ B_m \end{bmatrix} = \begin{bmatrix} b_{11} & b_{12} & \cdots & b_{1n} \\ b_{21} & b_{22} & \cdots & b_{2n} \\ \vdots & \vdots & \ddots & \vdots \\ b_{m1} & b_{m2} & \cdots & b_{mn} \end{bmatrix} \quad \ldots(4)$$

If the weight allocation of the factor subsets in U is A, then the comprehensive evaluation result can be obtained as follows:

$$B^* = A \times R \quad \ldots(5)$$

B^* in Formula (5) is not only the comprehensive evaluation result of U but also that of all the evaluation factors in U.

Index System and Study Object

According to the existing research results of scholars, the important influence factors of goaf stability mainly depend on the three following aspects: the factors of the goaf itself, geological factors, and mining disturbance. The mutually independent influence factors for goaf stability, which consist of three first-level indexes and 14 second-level indexes, are finally formed as given in Table 1.

Table 1: Influence Factors of Goaf Stability.

First-level index	Second-level index
Technical factors	Area
	Span
	Pillar distribution
	Burial depth of goaf
	Thickness of overlying strata
	Span–depth ratio of goaf
Geological factors	Rock mass structure
	Geological structure
	Rock mass quality
	Geographic orientation
	Underground water activity
Other factors	Conditions of adjacent goaf
	Mining disturbance
	Protective measures

The study object is the Sandaozhuang mining area, which is located in Lengshui Town, Luanchuan County, Luoyang City, Henan Province and a subordinate of China Molybdenum Co., Ltd. The mining area is approximately 20 miles from Luanchuan County. The Sandaozhuang Lingyucheng Ridge in the mining area is a watershed for two major water systems, the Yangtze and Yellow rivers. The northern water system flows into the Yellow River through the Yihe River, while the southern water system flows into the Yangtze River via the Xiaohe River and the Laoguan River. This mining area has a high-mountain climate that is cool in summer and severe cold in winter. Located in the Funiu Mountain area, this mining area has a large population with a relatively small land and focuses on agriculture with auxiliary industry, forestry, and mining industry. The present production capacity of the Sandaozhuang open-pit mine is 30,000 t/day. The mine started as small-scale underground mining in the 1960s, employing the open-stope method. Owing to excessive and unplanned excavations and mining in the entire mining area, severe destruction and waste of national resources have been experienced. Meanwhile, many irregular goafs are formed in the mining area.

EMPIRICAL STUDY

Weight Determination

The AHP was used in this study to determine the weights of influence factors. The AHP judgment matrix is given in Tables 2-5.

The final calculated weight results are provided in Table 6.

According to Table 6, technical factors have the most influence on underground goaf stability, with their total weight value reaching 72.42%, while the total weight of the other factors is the minimum, that is, 8.25%. Therefore, importance should be attached to subfactors in technical factors in the goaf stability analysis. Among the subfactors, the influence weight of goaf span on goaf stability reaches 21.43%, and thus the most important influence factor, followed by goaf area and pillar distribution, with respective influence weights of 18.58% and 11.17%, respectively. Hence, these main influence factors should be highlighted in the goaf stability evaluation and calculation process.

Table 2: Judgment matrix of First-level factors.

	Technical factor	Geological factor	Other factors
Technical factor	1.00	5.00	7.00
Geological factor	0.20	1.00	3.00
Other factors	0.14	0.33	1.00

Table 3: Judgment matrix of technical factors.

	Area	Span	Pillar distribution	Burial depth of goaf	Thickness of overlying strata	Span-depth ratio of goaf
Area	1.00	1.00	3.00	4.00	1.00	3.00
Span	1.00	1.00	2.00	4.00	5.00	3.00
Pillar distribution	0.33	0.50	1.00	5.00	3.00	0.50
Burial depth of goaf	0.25	0.25	0.20	1.00	0.33	0.33
Thickness of overlying strata	1.00	0.20	0.33	3.00	1.00	1.00
Span-depth ratio of goaf	0.33	0.33	2.00	3.00	1.00	1.00

Table 4: Judgment matrix of geological factors.

	Rock mass structure	Geological structure	Rock mass quality	Geographic orientation	Underground water activity
Rock mass structure	1.00	3.00	0.20	0.33	7.00
Geological structure	0.33	1.00	3.00	1.00	5.00
Rock mass quality	5.00	0.33	1.00	0.33	3.00
Geographic orientation	3.00	1.00	3.00	1.00	5.00
Underground water activity	0.14	0.20	0.33	0.20	1.00

Table 5: Judgment matrix of other factors.

	Conditions of adjacent goaf	Mining disturbance	Protective measures
Conditions of adjacent goaf	1.00	3.00	7.00
Mining disturbance	0.33	1.00	3.00
Protective measures	0.14	0.33	1.00

Table 6: Index weights determined via AHP.

First-level index	First-level weight	Second-level index	Second-level index weight	Combined weight
Technical factor	0.7242	Goaf area	0.2566	0.1858
		Goaf span	0.2959	0.2143
		Pillar distribution	0.1542	0.1117
		Burial depth of goaf	0.0468	0.0339
		Thickness of overlying strata	0.1178	0.0853
		Span-depth ratio of goaf	0.1286	0.0931
		Rock mass structure	0.2246	0.0434
		Geological structure	0.2403	0.0464
Geological factor	0.1933	Rock mass quality	0.1960	0.0379
		Geographic orientation	0.2966	0.0573
		Underground water activity	0.0426	0.0082
		Conditions of adjacent goaf	0.6698	0.0553
Other factors	0.0825	Mining disturbance	0.2427	0.0200
		Protective measures	0.0875	0.0072

Table 7: Membership evaluation grade sets of second-level indexes.

Second-level index	Evaluation grade				
	Very good	Relatively good	Ordinary	Relatively poor	Poor
Goaf area	0.2	0.3	0.3	0.2	0
Goaf span	0.3	0.1	0.5	0.1	0
Pillar distribution	0.2	0.2	0.1	0.4	0.1
Burial depth of goaf	0.3	0.2	0.2	0.1	0.2
Thickness of overlying strata	0.1	0.2	0.2	0.3	0.2
Span-depth ratio of goaf	0.4	0.1	0	0.3	0.2
Rock mass structure	0.3	0.1	0.3	0.3	0
Geological structure	0.2	0.4	0.1	0.1	0.2
Rock mass quality	0.3	0.2	0.2	0.1	0.2
Geographic orientation	0.4	0	0.1	0.2	0.3
Underground water activity	0.1	0.4	0.1	0	0.4
Conditions of adjacent goaf	0.3	0.2	0.1	0.3	0.1
Mining disturbance	0.5	0	0	0.3	0.2
Protective measures	0.4	0.3	0.2	0.1	0

Membership Analysis

A total of 18 mine safety experts were invited to evaluate the quantitative indexes, the evaluation grade set of each second-level index was obtained, and their memberships were obtained through fuzzy statistics as shown in Table 7.

Fuzzy Synthetic Calculation

According to Formulas (2)-(5), a fuzzy calculation of the second-level indexes is carried out one by one to obtain the following matrix.

$$B_i = \begin{bmatrix} 0.2342 & 0.1832 & 0.3108 & 0.1839 & 0.0879 \\ 0.2379 & 0.3043 & 0.1240 & 0.1875 & 0.1465 \\ 0.1816 & 0.1485 & 0.2670 & 0.2515 & 0.1515 \end{bmatrix}$$

According to Formula (5), the following is finally obtained:

$$B^* = A \times R = \begin{bmatrix} 0.7242 \\ 0.1933 \\ 0.0825 \end{bmatrix}^T * \begin{bmatrix} 0.2342 & 0.1832 & 0.3108 & 0.1839 & 0.0879 \\ 0.2379 & 0.3043 & 0.1240 & 0.1875 & 0.1465 \\ 0.1816 & 0.1485 & 0.2670 & 0.2515 & 0.1515 \end{bmatrix}$$
$$= [0.2305 \quad 0.2037 \quad 0.2711 \quad 0.1901 \quad 0.1045]$$

According to the actual situation in the goaf site and considering the maximum membership principle, the goaf stability belongs to grade (ordinary) through the fuzzy AHP, that is, the goaf stability is in an ordinary state, and the evaluation result is consistent with the reality. The study results indicate that most goafs within the Sandaozhuang open-pit mine are of unstable and extremely unstable goaf grades, and large-scale goaf disaster can easily occur any time.

CONCLUSION

Low goaf stability is one of the geological disasters that trigger mine accidents and can lead to surface subsidence, surface cracks, wall caving, earthquake, and so on, resulting in immeasurable losses to the production of mine enterprises and endangering employees. To prevent and reduce the severe hazards brought by goafs and guarantee safe and normal mine production, a comprehensive evaluation study of goaf stability must be conducted. First, an influence factor index system of goaf stability was built, and an AHP-based fuzzy comprehensive evaluation model was used in a case study of a mine goaf in Henan Province. The study results indicate that the mine goaf will result in the structural failure of surrounding buildings, massive water and soil loss, the exhaustion of water resources, the degradation of soil quality, and an evident reduction of overlying animals and plants. Technical factors have the maximum influence on underground goaf stability, with the total weight value reaching 72.42%, while those of the goaf span, the goaf area, and the pillar distribution are 21.43%, 18.58%, and 11.17%, respectively. The stability of the Sandaozhuang open-pit mine goaf in Henan Province belongs to grade (ordinary), that is, the goaf stability is under ordinary state, and the evaluation result is consistent with the reality. Thus, in-depth research regarding

enriching the factor system of goaf stability is suggested to establish a more accurate and complicated evaluation model and acquire related mechanical parameters needed for the reliability analysis of goaf stability, such as the compressive strength, tensile stress, elasticity modulus, and density of the ore-bearing rocks in the goaf.

REFERENCES

Chen, Q.F., Zhou, K.P., Hu, J.H. and Zhang, S.C. 2010. Synergism study of mining and goaf treatment in cataclastic ore section. Zhongnan Daxue Xuebao (Ziran Kexue Ban)/Journal of Central South University (Science and Technology), 41(2): 728-735.

Gao Fu qiang, Stead Doug, Kang Hong Pu and Wu Yong Zheng, 2014. Discrete element modelling of deformation and damage of a roadway driven along an unstable goaf - A case study. International Journal of Coal Geology,127: 100-110.

Huang Jiu, Tian Chuyuan, Xing Longfei, Bian Zhengfu and Miao Xiexing 2017. Green and sustainable mining: Underground coal mine fully mechanized solid dense stowing-mining method. Sustainability, 9(8): 1-18.

Luan, Hengjie, Lin Huili, Jiang Yu jing and Wang Yahua, 2018. Risks induced by room mining goaf and their assessment: A case study in the Shenfu-Dongsheng mining area. Sustainability, 10(3): 631.

Li, Liang, Wu, K. and Zhou, D.W. 2016. Evaluation theory and application of foundation stability of new buildings over an old goaf using longwall mining technology. Environmental Earth Sciences, 75(9): 763.

Ma, Dan, Liu Hong, Li Jiang, Zhou Xi and Long Zi 2019. The role of gangue on the mitigation of mining-induced hazards and environmental pollution: An experimental investigation. Science of the Total Environment, 10: 436-448.

Ma, Haitao, Wang, J. and Wang, Y. 2012. Study on mechanics and domino effect of large-scale goaf cave-in. Safety Science, 50(4): 689-694.

Whittles, D.N., Lowndes, L.S., Kingman, S.W., Yates, C. and Jobling, S. 2006. Geomechanical factors affecting the installation and stability of a surface goaf well at a deep UK coal mine. Archives of Mining Sciences, 51(2): 197-230.

Wu, Zhiyong, Niu Qinghe, Li Wenping, Lin Naing Htun and Liu Shiliang 2018. Ground stability evaluation of a coal-mining area: a case study of Yingshouyingzi mining area, China. Journal of Geophysics and Engineering, 15(5): 2252-2265.

Xiaojun Feng and Qiming Zhang, 2018. The effect of backfilling materials on the deformation of coal and rock strata containing multiple Goaf: A Numerical Study. Minerals, 8(6): 224.

Yang, Houqiang, Han Changliang, Nong Zhang, Sun Changlun, Pan Dongjiang and Dong Minghui, 2019. Stability control of a goaf-side roadway under the mining disturbance of an adjacent coal working face in an underground mine. Sustainability, 11(22): 6398.

Youhong, Xiangding and Wenfei, Lina, 2015. Mechanism and stability evaluation of goaf ground subsidence in the third mining area in Gong Changling District, China. Arabian Journal of Geosciences, 8: 639-646.

Zhu, Chuanqu, Weijun, W. and Shiliang, S. 2006. Classification model and its application of stability of roadway driving along next goaf for fully-mechanized caving face. Engineering Science, 8(3): 35-38.

Zhao, Tongbin, Shuqi Ma and Zhenyu Zhang 2018. Ground control monitoring in backfilled strip mining under the metropolitan district: Case Study. International Journal of Geomechanics, 18(7): 05018003.

Heavy Metal Accumulation in Soil-Wheat System of Coal Mining Area and Health Risk Assessment: A Case Study in Northern Anhui Province, China

Q. Li*(**)† and S. B. Zhou*
*College of Life Sciences, Anhui Normal University, Wuhu 241000, China
**College of Environment and Surveying Engineering, Suzhou University, Suzhou 234000, China
†Corresponding author: Q. Li; liqi821113@163.com

ABSTRACT

An investigation of 43 soil samples and their corresponding wheat samples collected from Qinan (QN) and Luling (LL) coal mining areas in Suzhou, China, was conducted to study the accumulation of heavy metals (Cu, Pb, Zn, Cd, Cr and Ni) in the soil-wheat system, and to evaluate the potential human health risk posed by heavy metals from long-term ingestion of local wheat. Results showed that Cu, Zn, Cd and Ni were accumulated in the soils from the two mining areas, higher proportions of all the investigated metals in residual fraction were recorded, while large amounts of Cd, Cu, Zn, Pb were also observed in the bioavailable or potential bioavailable fractions. Metal contents in the different parts of wheat mainly followed the order of Root>Stem>Grain. The trends of Bioaccumulation factor (BF) and Translocation factor (TF) values were Zn>Cd>Cu>Ni>Pb>Cr and Cu>Cd>Zn>Cr>Pb>Ni, respectively. Correlation analysis suggested that the accumulated metals in the grain were mainly supplied from exchangeable and carbonate bound fractions in soil. Since the health risk posed by heavy metals ingestion was very close to the maximum allowable limit, the safety of wheat consumption in the coal mining areas should be continually concerned.

INTRODUCTION

Heavy metals are widespread pollutants in the environment and well-known for their high toxicity, non-degradable properties and bioaccumulation. Excessive heavy metals in agricultural soil are the result of vehicular exhaust, fertilization and sewage irrigation, as well as industrial and mining activities (Yan et al. 2007). Mining of coal is an important source of heavy metal pollution in soil. It produces a large quantity of coal wastes with different composition. These materials are often deposited near coal mines and exposed to atmospheric conditions. Gradual weathering of the wastes causes the release of toxic metals into the surrounding environment. Some previous studies regarding environmental pollution in coal mining area have found significant accumulation of heavy metals in soils, dusts, sediments and vegetables (Rout et al. 2015, Zhang et al. 2016, Brandelero et al. 2017, Rai et al. 2015).

In soil-crop systems, heavy metal ions can be gradually absorbed by crop roots and then migrate upward to stems, leaves and grains, which not only represent a threat to the growth and yield of crops but also probably lead to the problem of agricultural product safety (Dong et al. 2012, Wang et al. 2017). Mobility and bioavailability of heavy metal in soil mainly depend on their specific chemical fractions rather than

the total elemental contents (Baeyens et al. 2003). Based on the Tessier sequential extraction, heavy metals in soils can be classified into exchangeable (EXC), carbonate bound (CAB), Fe-Mn oxides bound (Fe-Mn), organic matter/sulphide bound (OMS) and residual (RES) fractions (Tessier et al. 1979). EXC fraction is considered to be bioavailable, CAB, Fe-Mn and OMS fractions are potentially bioavailable, while RES fraction is unavailable to plants. The occurrence and relative distribution of metals among these various fractions have been used as an important reference for understanding a metal's bioavailability in soil (Zhu et al. 2015). Besides, several studies were conducted to explore the other factors affecting heavy metals absorption by crops, including soil types, crop species and growth conditions (Wang et al. 2013, Yang et al. 2014, Khan et al. 2017).

Consumption of crop is the major route of human exposure to heavy metals (Zeng et al. 2015). Contaminated crop contains excessive essential and toxic metals, which can cause serious harmful diseases to inhabitants through the food chains. Thus, it is very essential to estimate the potential health risk posed by heavy metals from long-term ingestion of the crops grown in the contaminated areas. Research on monitoring heavy metal concentrations in wheat collected from a market in Bangladesh showed the health risk associated with wheat consumption was negligible (Ahmed et

al. 2015). However, another study found significant heavy metal exposure risk for residents from the consumption of wheat grown in Huaibei, and the inhabitants in the rural area experienced higher health risk than those in the urban area (Shi et al. 2013).

Suzhou, which is located in northern Anhui province, is an important production base of agricultural grain in China and known as "Barn of Central Plains". It had a population of 1.72 million in 2017. Wheat flour is the staple food of most local residents in Suzhou, especially in rural areas. Since the 1970s, coal mining activities in Suzhou gradually increased, which also caused serious ecological environmental problems in the mining areas. The main purpose of this work was: (i) to investigate the accumulation of the selected heavy metals (Cu, Pb, Zn, Cd, Cr and Ni) in the soil-wheat system from the coal mining areas, including metal contents in soil, in chemical fractions of soil and in different parts of wheat, (ii) to examine whether metal content in wheat grain relates to metal concentration in soil or any of the chemical fractions of soil, and (iii) to estimate the potential human health risk posed by heavy metal from long-term ingestion of wheat grown in the coal mining areas.

MATERIALS AND METHODS

Study Areas and Samples Collection

The areas of field sampling in the present study are located around Qinan (QN) and Luling (LL) coal mine in the south east of Suzhou City. The region has a sub-humid monsoon climate, which is characterized by a wide seasonal variation in temperature ranging from 32°C in summer to -2°C in winter. The average annual rainfall and temperature are 890 mm and 14.4°C. The soils in these areas are mainly Yellow fluvo-aquic soil and lime concretion black soil. Suzhou is abundant in coal resources and has a long history of mining. The exploitation of QN and LL coal mine began in 2000 and 1969, respectively. At present, more than 1.5 million tons of coal can be produced annually from QN mine. Owing to the long-term exploitation, LL mine has inevitably faced the threat of resource exhaustion and is planned to be closed down in 2019.

Forty-three sampling sites of farmland were selected for the present study, twenty-one of them are located in QN coal mining area and the others are located in LL coal mining area (Fig. 1). Sampling was carried out at wheat maturity.
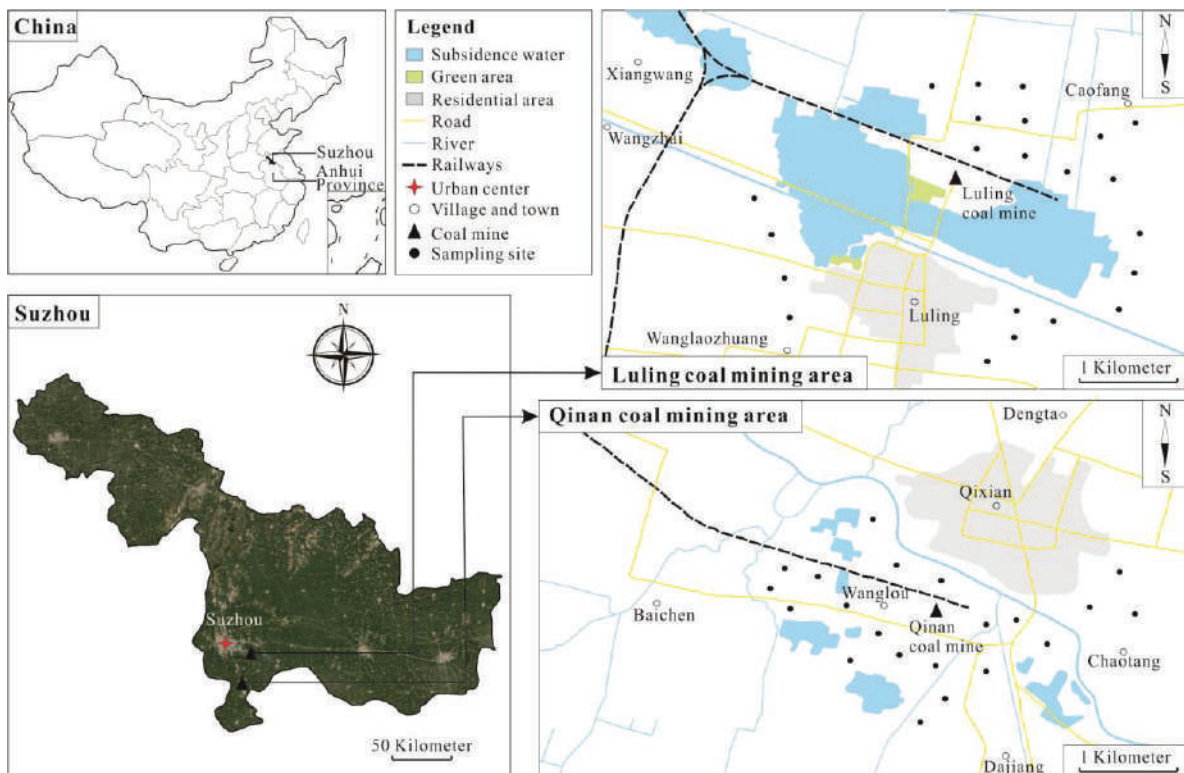
Fig. 1: Location of sampling sites in the investigated areas.

At each site, one soil sample (approximately 0.5 kg) from the 0-20 cm depth of the A horizon and its corresponding wheat sample were collected, while coordinate of sampling station was recorded with the aid of a handheld Global Positioning System (GPS). The collected samples were put into a plastic self-sealing bag and labelled before the laboratory processing.

Sample Preparation

After being transported to the laboratory, each soil sample was air-dried and then divided into two parts. One part was ground and passed through a 2-mm sieve for pH analysis, and the other part was ground with an agate mortar to pass a 0.149 mm nylon sieve for acid digestion and soil organic matter analysis. Each wheat sample was carefully cut into four parts of root, stem, leaf and grain with scissors. All the parts were thoroughly washed with running tap water to remove dirt and rinsed with deionized water three times. The cleaned roots, stems, leaves and grains were oven-dried at 80 to constant weight, then ground to powder for acid digestion.

Sample digestion: 0.2 g of each soil sample was digested with a mixture of 8 mL acids (aqua regia, $HClO_4$ and HF, 4:1:1, v/v) in a Teflon beaker and 0.50 g of each wheat sample (root, stem, leaf and grain) was also digested with a mixture of 5 mL acids (HNO_3, HCl and $HClO_4$, 5:1:1, v/v) in a glass beaker. The beakers were placed on an electric hot plate and heated at 110 for thermal decomposition of samples. After the samples were completely digested, the remaining liquid in the beakers was carefully transferred to

glass volumetric flasks and diluted with MilliQ water to a final volume of 50 mL.

Chemical fraction extraction of heavy metal for soil: A five-step sequential extraction procedure (Tessier et al. 1979) was performed in this study for quantifying the contents of heavy metals in different chemical fractions in soil samples. Fraction of metal, defined by the Tessier sequential extraction method, includes five forms of exchangeable (EXC), carbonate bound (CAB), Fe-Mn oxides bound (Fe-Mn), organic matter/sulphide bound (OMS) and residual (RES). The extraction sequence, the reagents used, the extraction conditions and the extraction processes are presented in Table 1.

Analysis Methods and Quality Control

Soil pH was measured in soil-deionized water (2.5:1, v/w) suspension using a pH meter, and the content of soil organic matter was tested using the acid dichromate oxidation method (Bao 2000). The contents of heavy metals in all of the solution prepared in the above digestion and extraction procedures were determined by atomic absorption spectrophotometer (Model TAS-990FG, Purkinje General Instrument, Beijing, China).

All chemicals used in this study were of analytical grade. All the glassware, Teflon beakers and centrifuge tubes were treated with the proper cleaning procedure, including a 24 h immersion in 10% HNO_3 and thorough rinses with deionized water twice, before being used. Standard reference materials GSS-16 (GBW07430) for soil and GSB-2 (GBW10011) for

Table 1: Sequential extraction procedure of Tessier.

Extraction sequence	Extraction fraction	Reagenths	Extraction conditions	Extraction processes	Collection processes of extracts
Step 1	Exchangeable (EXC)	Solution A: 1 M $MgCl_2$	pH 7.0, 25°C	1.0 g soil sample + 8 mL solution A, shaking for 1 h continuously	**Step 1-4:** After extraction of each step, the solution was centrifuged at 3000 rpm for 20 min, the supernatant liquid was collected for analysis. **Step 5:** After the solid residue was completely digested, the remaining liquid in Teflon beaker was carefully transferred to glass volumetric flasks and diluted with MilliQ water to a final volume of 50 ml for analysis.
Step 2	Carbonate bound (CAB)	Solution B: 1 M NaOAc	pH 5.0, 25°C	Solid residue from step 1 + 8 mL solution B, shaking for 5 h continuously	
Step 3	Fe-Mn oxides bound (Fe-Mn)	Solution C: 0.04 M $NH_2OH \cdot HCl$ in 25% (v/v) HOAc	96±3°C	Solid residue from step 2 + 20 mL solution C, heating for 6 h with occasional agitation	
Step 4	Organic matter / sulphide (OMS)	(1) Solution D: 30% H_2O_2+0.02 M HNO_3 (5:3, v/v) (2) Solution E: 30% H_2O_2 (3) Solution F: 3.2 M NH_4OAc in 20% (v/v) HNO_3	(1) pH 2.0, 85±3°C (2) pH 2.0, 85±3°C (3) 25°C	(1) Solid residue from step 3 + 8 mL solution D, heating for 2 h. (2) Then add 3 mL solution E, heating for 3 h with intermittent agitation. (3) Adding 5 mL solution F, shaking for 30 min continuously	
Step 5	Residual (RES)	Solution G: Aqua regia+ $HClO_4$+HF (4:1:1, v/v)	110°C	Solid residue from step 4 was transferred to Teflon beaker and digested with 8 ml solution G	

wheat were used to check the analytical accuracy of metal concentration in the experimental procedure. The recoveries of Cu, Pb, Zn, Cd, Cr and Ni in the reference materials were in the range of 84-112%. Additionally, the standard was tested repeatedly after every ten samples to check the reproducibility.

Bioaccumulation Factor and Translocation Factor

To evaluate the uptake efficiency of heavy metal by wheat, Bioaccumulation factor (BF) index of the root was adopted. It is defined as the ratio of the heavy metal concentration of wheat root to the corresponding soil. The following equation was used for the calculation.

$$BF = \frac{C_{root}}{C_{soil}} \qquad …(1)$$

Where C_{root} (mg·kg^{-1}) and C_{soil} (mg·kg^{-1}) are the concentrations of heavy metal in wheat root and in soil on the basis of dry weight, respectively.

Translocation factor (TF) index reflects the ability that transports the metal ion from plant root upward to other parts. In this study, the wheat root-to-grain TF was adopted and calculated as follows:

$$TF = \frac{C_{grain}}{C_{soil}} \qquad …(2)$$

Where C_{grain} (mg·kg^{-1}) is the concentration of heavy metal in wheat grain based on the dry weight.

Health Risk Assessment Model

To estimate the potential health risk posed by heavy metals from long-term ingestion of wheat grown in the coal mining areas, chronic daily intake (CDI) and hazard quotients (HQ) were calculated for quantifying the adverse health effects. Chronic daily intake (CDI) is the exposure to the population expressed as the mass of a substance per unit body weight per unit time averaged over a long period (a lifetime) (Garg et al. 2014). It can be calculated by the following equation:

$$CDI = \frac{C_{grain} \times IR \times EF \times ED}{BW \times AT} \qquad …(3)$$

Where IR (kg·person·d^{-1}) is the daily wheat flour intake rate. According to the data provided by the Statistical Bureau of China, IR values in this study are 0.143 and 0.052 kg·person·d^{-1} for adults and children, respectively. EF is the exposure frequency (350 d·year^{-1}), ED (year) is the exposure duration, in this study of 30 years for adults and 6 years for children. BW (kg) is the average weight of residents, in this

study, of 61.6 kg for adults and 18.6 kg for children. AT is the average exposure time for non-carcinogens ($E_D \times 365$ days)

Hazard quotients (HQ) is defined as the ratio of the estimated daily intake of metals and the oral reference dose (Rfd). It is calculated following the formula established by the US Environmental Protection Agency (US EPA 2011).

$$HQ = \frac{CDI}{RfD} \qquad …(4)$$

Where RfD represents the maximum oral dose level without any appreciable risk, and its values for Cu, Pb, Zn, Cd, Cr and Ni are 4.0×10^{-2}, 3.5×10^{-3}, 3.0×10^{-1}, 1.0×10^{-3}, 1.50 and 2.0×10^{-2} mg·kg^{-1}·day^{-1}, respectively (US EPA 2009).

To assess the overall potential health risks posed by more than one metal, hazard index (HI) was calculated as the sum of the HQs due to individual metal in wheat grain (Garg et al. 2014), as described in the following equation:

$$HI = HQ_1 + HQ_2 + \cdots + HQ_n \qquad …(5)$$

If HI≤1.0, there will be no obvious adverse effects through wheat ingestion, whereas a HI>1.0 indicates that potential risk for wheat ingestion is possible (Xue et al. 2012).

Data Statistics

Data statistics were performed by SPSS 13.0 software package, and all figures in this article were produced by CorelDRAW 12.0. Pearson correlation coefficients were calculated to identify the relationships between metal content in wheat grain and total metal concentration in soil, as well as between metal content in wheat grain and metal content in any of the chemical fractions.

RESULTS AND DISCUSSION

Physico-Chemical Properties and Heavy Metal Contents in Soil

The statistical characteristics of physico-chemical properties and metal concentrations in soils collected from QN and LL mining areas are given in Table 2. Soils in the investigated areas were slightly acidic and had mean pH values of 6.87 in QN and 6.58 in LL. Compared with "the classification criterion of soil nutrients based on the second soil survey of China", the organic matter content was in the lacking level. In the two mining areas, higher Cd contamination than the other metals in soil was observed. The mean Cd concentrations in QN (0.381 mg·kg^{-1}) and LL (0.421 mg·kg^{-1}) were 1.27 and 1.40 times higher than the environmental quality standard for agricultural soil in China (GB15618-2018), while mean concentrations of the other metals were all lower than the

Table 2: Descriptive statistics of physico-chemical properties and heavy metal concentrations in soil.

		pH	Organic matter (g·kg^{-1})	Cu (mg·kg^{-1})	Pb (mg·kg^{-1})	Zn (mg·kg^{-1})	Cd (mg·kg^{-1})	Cr (mg·kg^{-1})	Ni (mg·kg^{-1})
QN (n=21)	Max.	8.19	18.06	50.51	59.73	106.44	0.813	108.75	100.14
	Min.	5.53	3.27	12.63	16.81	48.68	0.159	43.42	28.62
	Mean	6.87	11.42	26.60	26.88	73.39	0.381	70.73	39.81
	Stdev.	1.05	5.14	10.15	9.57	17.43	0.174	16.89	16.89
	C.V.(%)	15.30	45.01	38.15	35.59	23.75	45.89	23.88	37.24
LL (n=22)	Max.	8.13	19.22	49.66	39.25	113.04	0.775	80.80	79.84
	Min.	5.17	3.10	13.36	14.73	43.35	0.126	49.11	26.03
	Mean	6.58	10.77	31.71	27.83	72.47	0.421	65.24	42.26
	Stdev.	0.98	5.55	8.23	5.42	16.94	0.120	10.02	10.42
	C.V.(%)	14.92	51.48	25.96	19.49	23.37	28.44	15.36	24.65
Environmental Standard for Agricultural soils in China (GB15618-2018)		-	-	100	120	250	0.3	200	100
Anhui Background		-	-	20.4	26.6	62.0	0.097	67.5	29.8

standard. But when compared to the background values of Anhui province in China, mean concentrations of Cu (26.60 mg·kg^{-1} in QN and 31.71 mg·kg^{-1} in LL), Zn (73.39 mg·kg^{-1} in QN and 72.47 mg·kg^{-1} in LL), Cd and Ni (39.81 mg·kg^{-1} in QN and 42.26 mg·kg^{-1} in LL) were higher, while Pb (26.88 mg·kg^{-1} in QN and 27.83 mg·kg^{-1} in LL) was slightly higher, indicating that noticeable metal accumulations in soils had emerged and were very likely to be caused by the intensive mining activities in the investigated areas.

Compared with QN area, the mean concentrations of Cu, Pb, Cd and Ni in soils from LL area were higher, while the mean concentrations of Zn and Cr were slightly lower. Additionally, Coefficients of Variation (C.V.) of the six heavy metals in LL area were all lower than that in QN area, proving that the spatial distribution of heavy metal contents in soils around LL mine was more uniform. The difference between the two mining areas might be due to their different mining duration. LL mine is an old coal mine with a mining history of nearly 50 years, the long-term anthropogenic disturbance and impacts of natural factors in this mining area have not just resulted in the accumulative effect of toxic metals in the soil environment, but intensified the migration and diffusion
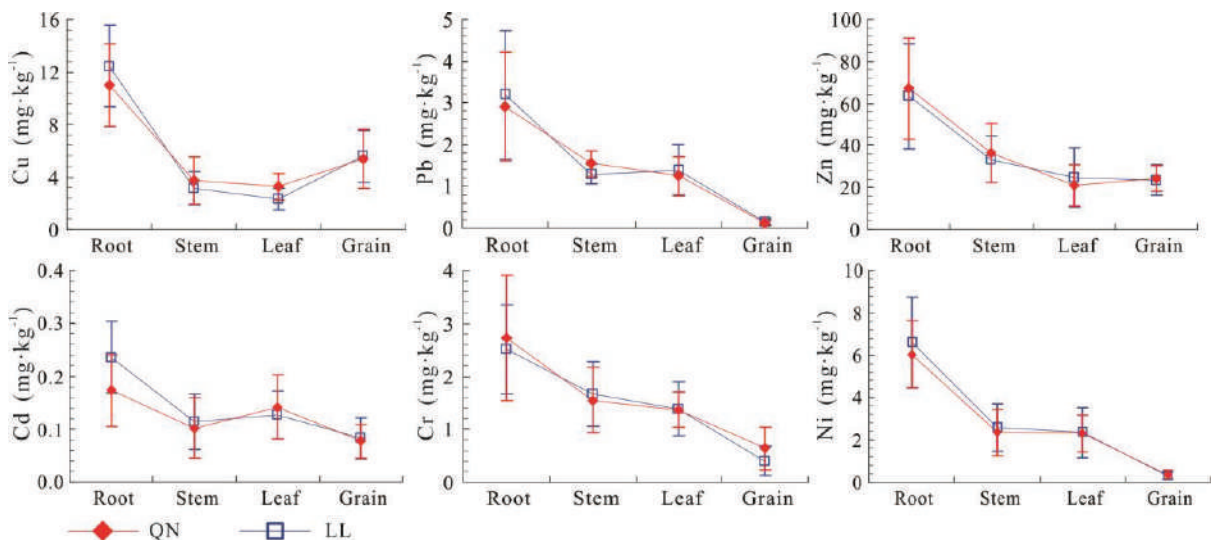
Fig. 2: Concentrations of heavy metals in different parts of wheat samples.

of pollutants as well, thus leading to the more uniform spatial distribution of soil contamination in the mining area.

Chemical Fraction of Heavy Metals in Soil

The concentrations and percentage of heavy metals present in the various fractions are given in Table 3. For further examining the accuracy of analytical results obtained from sequential extraction procedure in this study, an internal check was carried out by comparing the sums of metal concentrations in all the five fractions with the total metal concentrations in soils obtained from acid digestion. Metal recoveries were calculated by the following equation and the results are also presented in Table 3.

$$Recovery = \frac{EXC + CAB + Fe\text{-}Mn + OMS + RES}{C_{soil}} \times 100\%$$

$$\ldots(6)$$

As given in Table 3, the values of metal recoveries in the two mining areas ranged from 89.9-108.1%, so it can be concluded that the results obtained from sequential extraction were in good agreement with those by digestion.

The bioavailability and ecotoxicity of heavy metals are mainly related to their chemical fractions. Metals in EXC fraction are weakly sorbed on the soil surface by electrostatic interaction and could be easily released by ion exchange processes (Kumar & Ramanathan 2015, Barać et al. 2016).

Table 3: Concentrations and percentages of heavy metals in the five fractions.

		EXC	CAB	Fe-Mn	OMS	RES	Sum	Recovery (%)
QN area								
Cu	Content (mg·kg⁻¹)	0.97±0.36	4.19±1.95	3.24±2.66	6.12±2.73	10.23±3.91	24.75	93.1
	Percentage (%)	3.92±1.45	16.93±7.88	13.09±10.75	24.73±11.03	41.33±15.8		
Pb	Content (mg·kg⁻¹)	2.57±1.08	3.44±1.54	10.24±3.55	3.53±1.62	8.65±7.04	28.43	105.8
	Percentage (%)	9.04±3.8	12.13±5.45	36.01±12.45	12.41±5.7	30.41±24.75		
Zn	Content (mg·kg⁻¹)	5.42±1.50	15.29±4.68	11.35±3.42	7.94±2.16	30.71±9.53	70.71	96.3
	Percentage (%)	7.67±2.12	21.62±6.62	16.05±4.84	11.23±3.05	43.43±13.48		
Cd	Content (mg·kg⁻¹)	0.070±0.031	0.083±0.038	0.061±0.040	0.019±0.014	0.156±0.130	0.389	102.0
	Percentage (%)	18.12±8.03	21.32±9.71	15.57±10.32	4.88±3.61	40.10±33.51		
Cr	Content (mg·kg⁻¹)	1.09±0.33	2.01±0.76	2.37±0.49	4.07±1.92	64.17±17.37	73.70	104.2
	Percentage (%)	1.48±0.45	2.73±1.03	3.22±0.66	5.52±2.6	87.06±23.57		
Ni	Content (mg·kg⁻¹)	3.59±1.14	4.42±1.95	3.53±1.40	5.10±2.38	26.41±9.56	43.05	108.1
	Percentage (%)	8.34±2.65	10.27±4.53	8.2±3.25	11.85±5.53	61.35±22.21		
LL area								
Cu	Content (mg·kg⁻¹)	1.14±0.44	4.87±8.52	3.56±1.81	7.36±2.30	13.96±5.45	30.89	97.4
	Percentage (%)	3.69±1.42	15.77±27.58	11.52±5.86	23.83±7.45	45.19±17.64		
Pb	Content (mg·kg⁻¹)	2.91±1.03	4.06±1.48	9.64±3.28	4.35±1.77	8.90±4.73	29.86	107.3
	Percentage (%)	9.74±3.41	13.59±4.95	32.27±10.98	14.6±5.93	29.8±15.84		
Zn	Content (mg·kg⁻¹)	4.90±1.24	16.26±6.28	11.88±4.62	7.37±1.78	24.73±7.59	65.14	89.9
	Percentage (%)	7.52±1.92	24.96±9.64	18.24±7.09	11.31±2.75	37.96±11.65		
Cd	Content (mg·kg⁻¹)	0.087±0.030	0.099±0.031	0.067±0.022	0.014±0.004	0.127±0.106	0.394	93.6
	Percentage (%)	22.01±7.51	25.12±7.89	17.00±5.50	3.56±0.98	32.31±26.97		
Cr	Content (mg·kg⁻¹)	1.01±0.28	1.64±0.80	2.01±0.57	3.70±1.55	57.25±9.47	65.61	100.6
	Percentage (%)	1.54±0.43	2.5±1.22	3.06±0.87	5.64±2.36	87.26±14.43		
Ni	Content (mg·kg⁻¹)	3.25±1.09	3.72±1.62	2.96±0.50	5.14±1.97	26.30±7.45	41.37	97.9
	Percentage (%)	7.86±2.63	8.99±3.92	7.15±1.21	12.42±4.76	63.57±18.01		

Sum = EXC+CAB+Fe-Mn+OMS+RES

Among the six metals in this study, Cd showed the highest percentage (18.12% in QN and 22.01% in LL) in EXC fraction, while Cr occupied the lowest EXC fraction as only 1.48% in QN and 1.54% in LL. The percentages of Pb, Zn and Ni in EXC fraction seemed to have a slight difference (7-10%).

In CAB fraction, the proportional distribution was in the order of Cd≈Zn>Cu>Pb>Ni>Cr. Over 20% of Cd and Zn were found in CAB fraction, implied that Cd and Zn are more inclined to be associated with carbonate minerals. This finding is consistent with the result of the previous research (Barać et al. 2016). A possible explanation for this is that Cd and Zn have an ionic radius similar to that of Ca, so they could easily substitute the Ca ions in calcium carbonate in the soils and co-precipitate with the carbonates.

Metals bounded by Fe-Mn oxides in soil have potential activity and can be released in reducible conditions. In the Fe-Mn fraction, the largest percentage was observed for Pb, in comparison with the other metals. Pb also dominantly existed in the third fraction, with the mean percentage values of 36.01% in QN and 32.27% in LL, while a considerable amount of Zn (16.05% in QN and 18.24% in LL) and Cd (15.57% in QN and 17.00% in LL) were also found in this fraction. Previous studies concerned with soil have observed high proportions of Pb and Zn in Fe-Mn fraction (Jalali & Hemati 2013, Li et al. 2015). However, the high proportion of Cd in this fraction is rarely reported. The strong associations between Cd and the Fe-Mn oxides may be related to the redox condition in the soil. Under the influence of mining activities, a large number of SO_4^{2-}, originating from colliery wastewater and leaching solution of coal gangue, were discharged into the soils in the mining area. SO_4^{2-} is an important oxidant in soil, and its massive accumulation will result in the raising of oxidation-reduction potential (ORP) values, which are highly favourable for the association between the Fe-Mn oxides and some metal ions, such as Pb, Cd and Zn. A previous study also found that Cd contents in Fe-Mn fraction increased when a certain amount of Na_2SO_4 was added into the soil (Li et al. 2017).

Heavy metals associated with OMS fraction are ordinarily considered to be relatively stable under normal soil conditions, but the degradation of organic matter under oxidizing conditions can lead to the release of soluble metals bound to those materials (Bakircioglu et al. 2011). In this fraction, the proportional distribution was in the order of Cu>Pb>Ni>Zn>Cd>Cr. A relatively large amount (more than 20%) of Cu associated with OMS fraction was observed in this study. This suggested that quite a few Cu ions in soil probably exist in the form of organically complexed metal species, and may be because Cu has a high affinity to some natural organic matters, such as humic substances (Pempkowiak et al. 1999).

Generally, RES fraction is considered to be unavailable and metals in this fraction are securely fixed in the crystal of minerals (Ashraf et al. 2012). In this study, almost all the investigated metals, except Pb, were dominantly associated with RES fraction in soil. Cr occupied the largest RES fraction in both QN (87.06%) and LL (87.26%) areas, followed by Ni (61.35% in QN and 63.57% in LL), indicating that the two metals in soils from the investigated areas could hardly be released under natural condition.

Heavy Metal Concentrations in Different Parts of Wheat

Heavy metal concentrations in different parts of wheat samples are illustrated in Fig. 2. The distribution of most metals in wheat occurred in the following order: Root>Stem>Grain, only with an exception of Cu, of which concentration in grain was higher than those in the stem. Mean concentrations of Cu, Pb, Zn, Cd, Cr and Ni in the roots, of 11.01, 2.92, 67.17, 0.17, 2.73 and 6.04 mg·kg^{-1} in QN area and of 12.43, 3.19, 63.33, 0.24, 2.52 and 6.61 mg·kg^{-1} in LL area, were much higher than those in the aboveground organs, showing that these metals are mainly trapped by roots after being assimilated, and only a few of them can be transported to other organs of wheat. This is also considered to be an adaptive strategy of wheat under the adverse conditions for avoiding toxic
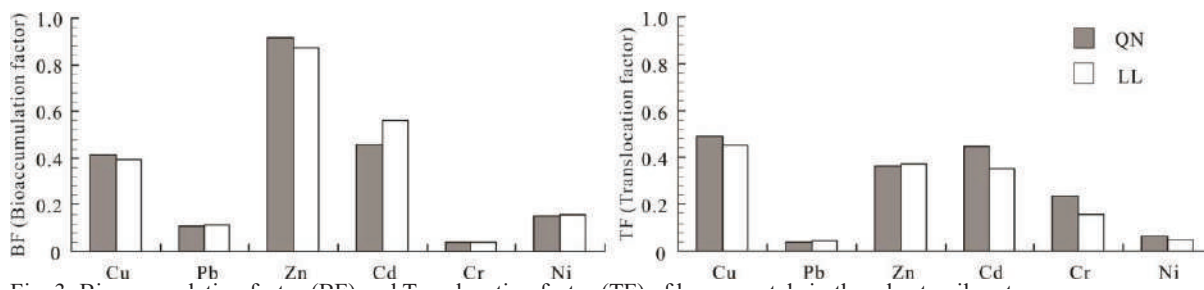
Fig. 3: Bioaccumulation factor (BF) and Translocation factor (TF) of heavy metals in the wheat-soil system.

hazards of heavy metals to photosynthesis and metabolism (Khan et al. 2015). Cd in leaves in the two mining areas and Pb in leaves in LL area were slightly higher than those in stems, the other metals in leaves showed the approximately equal concentrations or slightly lower concentrations to than those in stems. Compared with the existing standards applied to food safety in China (Table 4), the mean concentrations of all six metals in grains were below the tolerance limits. Nevertheless, not all the samples were in the safe range. The numbers of sample exceeding the tolerance limits of Pb, Cd and Cr accounted for 14.3%, 33.3% and 19.0% in QN area, and 18.2%, 22.7% and 4.5% in LL area, respectively. It can be seen from the above data that Cd pollution in wheat grains was relatively more common in the investigated areas, which coincides with the high total Cd content in the soils.

As wheat absorbs heavy metals in soils mainly through the roots and then migrate to other parts of the plant (Dong et al. 2012), it is necessary to evaluate the absorbing capacity of roots and transporting capacity from root to grain. The mean values of BF and TF for Cu, Pb, Zn, Cd, Cr and Ni in the soil-wheat system are shown in Fig. 3. The trend of mean BF values of heavy metals was Zn>Cd>Cu>Ni>Pb>Cr, while mean TF values followed the order of Cu>Cd>Zn>Cr>Pb>Ni. These trends are consistent with the result obtained from the laboratory pot experiments of wheat (Skiba & Wolf 2017), and similar to the data obtained from a case study of wheat grown on sewage irrigated soils (Meng et al. 2016). Higher BF and TF values for Cu, Zn and Cd observed in this study indicated that wheat plants from the investigated areas are more efficient uptakers of these metals, and this might be related to the active absorption and transport of the three trace elements by wheat. As the essential nutrient elements for plant growth and for synthesizing of some important enzymes, Cu and Zn are widely involved in various physiological activities of the plant. Therefore, the two metals can be actively absorbed and transferred by the plant during the metabolic processes. Though Cd is the non-essential element of plant, the similarities of ionic radius and valence between Cd^{2+} and Ca^{2+}, as well as Zn^{2+}, enable Cd^{2+} ions to combine with enzymes in place of Ca^{2+} and Zn^{2+}, and also to be transferred to plant cells through the channels of Ca^{2+} and Zn^{2+} (Gu et al. 2005, Wang et al. 2017).

Table 4: Tolerance limits (Chinese standard) of heavy metals in wheat grain, as well as the numbers and percentages of wheat sample exceeding the standards in this study.

	Tolerance limits (mg·kg^{-1})	QN (n=21)			LL (n=22)		
		Metal contents in grain (mg·kg^{-1})	Sample numbers exceeded standards	Percent exceeded standards(%)	Metal contents in grain (mg·kg^{-1})	Sample numbers exceeded standards	Percent exceeded standards(%)
Cu	10[a]	5.38±2.23	0	0	5.60±1.97	0	0
Pb	0.2[b]	0.12±0.06	3	14.3	0.15±0.07	4	18.2
Zn	50[a]	24.23±6.08	0	0	23.45±7.31	0	0
Cd	0.1[b]	0.077±0.032	7	33.3	0.083±0.039	5	22.7
Cr	1.0[b]	0.64±0.41	4	19.0	0.40±0.28	1	4.5
Ni	1.0[b]	0.37±0.20	0	0	0.31±0.16	0	0

a: Chinese Agricultural Standard for wheat (NY861-2004). b: Chinese Hygiene Standard for wheat (GB2762-2012).

Table 5: Pearson correlation coefficients between the metal contents in wheat grains and those in any of the chemical fractions of soils, as well as total metal contents of in soils (n=43).

Element	Metal fraction					Total concentration in soil
	EXC	CAB	Fe-Mn	OMS	RES	
Cu	0.464[*]*	-0.173	0.035	0.374[*]	0.055	0.166
Pb	0.330*	0.508[**]	0.057	-0.056	0.125	0.321[*]
Zn	0.034	-0.034	-0.123	0.161	0.095	0.056
Cd	0.540[**]	0.559[**]	0.318[*]	0.126	0.008	0.459[**]
Cr	0.434[**]	0.365[*]	-0.337[*]	-0.029	-0.053	-0.046
Ni	0.709[**]	0.475[**]	-0.120	0.373[*]	0.053	-0.002

[*]Correlation is significant at 95% confidence level (n=43, $r_{critical}$=0.301); [**]Correlation is significant at 99% confidence level (n=43, $r_{critical}$=0.389).

Correlation Analysis

To investigate whether the metal content in wheat grain relates with that in soil or any of the chemical fractions, correlation analysis was performed based on testing data of the 43 soil and wheat samples collected from the two mining areas, and the results are given in Table 5. The correlation between grain metals and total soil metals for Cd was very significant (R=0.459), and for Pb was significant (R=0.321), whereas for Cu, Zn, Cr and Ni were insignificant, suggesting that total contents of heavy metals in soil, except Cd and Pb, could hardly be the adequate indicators for metal uptake by wheat.

Most of the metals in wheat grains had the strongest correlations with those in EXC fraction or CAB fraction, which showed that the accumulated metals in grain were mainly supplied from the two fractions, or one of the two fractions in soil. For example, grain-Cu correlated with EXC-Cu very significantly (R=0.464), grain-Cd correlated with EXC-Cd (R=0.540) as well as CAB-Cd (R=0.559) very significantly. An exception of the relationship was for grain-Zn, which had a very low correlation with any of the fractions extracted by Tessier procedure, and it might be associated with the disturbance to Zn contents in various chemical fractions in soils caused by frequent and repeated applications of Zn fertilizer in the investigated areas. The correlations between metals in wheat grain and those in RES fraction were all insignificant, reconfirming the view that metals in RES fraction are unlikely to be absorbed by the plant (Bakircioglu et al. 2011). Furthermore, significant positive correlations were also observed between grain-Cd and Fe-Mn-Cd (R=0.318), grain-Cu and OMS-Cu (R=0.374), and grain-Ni and OMS-Ni (R=0.373), revealing that Cu and Ni in OMS fraction and Cd in Fe-Mn fraction were important sources of the accumulated metals in wheat grain.

Risk Assessment

Based on the mean concentrations of Cu, Pb, Zn, Cd, Cr and Ni in wheat grains from the investigated mining areas, chronic daily intake (CDI), hazard quotient (HQ) and hazard index (HI) of heavy metals by consumption of wheat were calculated and listed in Table 6. In the two mining areas, the CDI values of heavy metals for adult and children followed the identical order of Zn>Cu>Cr>Ni>Pb>Cd, which was similar to the result of a previous study in Tianjin sewage irrigation area (Zeng et al. 2015). Children had higher CDI values of each metal than adults.

HQ values of the studied metals for both adults and children showed the following decreasing order of Cu>Zn>Cd>Pb>Ni>Cr in QN area, and of Cu>Cd>Zn>Pb>Ni>Cr in LL area. All the metals in this study had the HQ values far below 1.0, and Cu reached the highest value of 0.377 for children in LL area. Therefore, it can be deduced that intake of a single metal through wheat consumption in mining areas could not cause an obvious adverse effect on human health. The data in the present study were higher than the HQ values of wheat in the irrigated area of Jinghui in China (Lei et al. 2015) and those of wheat from the markets of Bangladesh (Ahmed et al. 2015), but lower than the results obtained from metal mining areas, where several studies showed the HQ values far above 1.0 (Lim et al. 2008, Du et al. 2018).

As given in Table 6, the HI values for adults and children in QN area were 0.771 and 0.931, slightly lower than those (0.801 and 0.968) in LL area. It seemed that children were more susceptible to heavy metal exposure through local wheat consumption than adults, and the consistent results were reported by other scholars (Si et al. 2014, Zota et al. 2011). In both the mining areas, Cu, Zn and Cd made important contributions to the calculated HI values, which

Table 6: Chronic daily intake (CDI), hazard quotient (HQ) and hazard index (HI) for heavy metals by consumption of wheat grain around the two coal mining areas.

	QN				LL			
	Adult		Children		Adult		Children	
	CDI (mg·kg^{-1}·d^{-1})	HQ	CDI (mg·kg^{-1}·d^{-1})	HQ	CDI (mg·kg^{-1}·d^{-1})	HQ	CDI (mg·kg^{-1}·d^{-1})	HQ
Cu	1.20×10^{-2}	0.300	1.45×10^{-2}	0.363	1.25×10^{-2}	0.312	1.51×10^{-2}	0.377
Pb	2.64×10^{-4}	0.075	3.19×10^{-4}	0.091	3.26×10^{-4}	0.093	3.94×10^{-4}	0.112
Zn	5.41×10^{-2}	0.180	6.53×10^{-2}	0.218	5.23×10^{-2}	0.174	6.32×10^{-2}	0.211
Cd	1.72×10^{-4}	0.172	2.08×10^{-4}	0.208	1.86×10^{-4}	0.186	2.24×10^{-4}	0.224
Cr	1.42×10^{-3}	0.001	1.72×10^{-3}	0.001	8.90×10^{-4}	0.001	1.07×10^{-3}	0.001
Ni	8.36×10^{-4}	0.042	1.01×10^{-3}	0.051	6.97×10^{-4}	0.035	8.42×10^{-4}	0.042
HI		0.771		0.931		0.801		0.968

coincides with the high BF and TF values of the three metals in soil-wheat system mentioned before (Fig. 3). Although there was insignificant health risk through ingestion of wheat grown in the mining areas because all the HI values calculated in this study were below 1.0, it should be also noticed that the HI values for local residents, especially for children, were very close to 1.0, which suggested that more attention should be continually paid to the safety of wheat consumption in the coal mining areas.

CONCLUSIONS

The mean concentrations of Cu, Zn, Cd and Ni in soil from the investigated areas were higher than the background values of Anhui province. In particular, Cd concentration was higher than the environmental quality standard for agricultural soil in China (GB15618-2018). Compared with QN mine, LL mine had a longer mining duration, which caused relativity more uniform spatial distribution of heavy metals in soils around this mine. Chemical fraction analysis reflected that Cu, Zn, Cd, Cr and Ni dominantly existed in RES fraction, while Pb mainly existed in both Fe-Mn and RES fractions. Considerable amounts of Cd were observed in EXC, CAB and Fe-Mn fractions, a high percentage of Zn were also found in CAB and Fe-Mn fractions, while over 20% of Cu was detected in OMS fraction. Cr and Ni were most stable in soil because over 60% of them were associated with RES fraction. Heavy metals, except Cu, in the different parts of wheat, followed the order of root>stem>grain, and mean concentration of all the six metals in grains were below tolerance limits of the existing standards in China. Higher BF and TF values for Cu, Zn and Cd were observed in this study, showing that the wheat plants from the investigated areas are more efficient uptakers of these metals. Correlation analysis suggested that EXC and CAB fractions were the dominant sources of the metals accumulated in grain, followed by Fe-Mn and OMS fractions. Furthermore, although high health risk posed by heavy metals from ingestion of wheat grown in the mining areas was not observed, all the HI values calculated in this study were very close to the maximum allowable limit of risk (1.0), which suggested that the safety of wheat consumption in the coal mining areas should be still continually concerned.

ACKNOWLEDGEMENTS

REFERENCES

Ahmed, M. K., Shaheen, N., Islam, M. S., Habibullah-Al-Mamun, M., Islam, S. and Banu, C. P. 2015. Trace elements in two staple cereals (rice and wheat) and associated health risk implications in Bangladesh. Environmental Monitoring and Assessment, 187(6): 326.

Ashraf, M. A., Maah, M. J. and Yusoff, I. 2012. Study of chemical forms of heavy metals collected from the sediments of tin mining catchment. Chemical Speciation & Bioavailability, 24(3): 183-196.

Baeyens, W., Monteny, F., Leermaakers, M. and Boullion, S. 2003. Evaluation of sequential extractions on dry and wet sediments. Analytical and Bioanalytical Chemistry, 376(6): 890-901.

Bakircioglu, D., Kurtulus, Y. B. and Ibar, H. 2011. Investigation of trace elements in agricultural soils by BCR sequential extraction method and its transfer to wheat plants. Environmental Monitoring and Assessment, 175(1-4): 303-314.

Bao, S. D. (ed.) 2000. Soil Agrochemical Analysis. Agricultural Press., pp.30.

Barać, N., Škrivanj, S., Mutić, J., Manojlović, D., Bukumirić, Z., Živojinović, D., Petrović, R. and Ćorac, A. 2016. Heavy metals fractionation in agricultural soils of Pb/Zn mining region and their transfer to selected vegetables. Water Air and Soil Pollution, 227(12): 481.

Brandelero, S. M., Miquelluti, D. J., Campos, M. L. and Dors, P. 2017. Water and sediment monitoring in a coal mining area of the Palmeiras River, Tubarao Watershed (SC), Brazil. Engenharia Sanitaria E Ambiental, 22(1): 203-212.

Dong, J. H., Yu, M., Bian, Z. F., Zhao, Y. D. and Cheng, W. 2012. The safety study of heavy metal pollution in wheat planted in reclaimed soil of mining areas in Xuzhou, China. Environmental Earth Sciences, 66(2): 673-682.

Du, F., Yang, Z. G., Liu, P. and Wang, L. 2018. Accumulation, translocation, and assessment of heavy metals in the soil-rice systems near a mine-impacted region. Environmental Science and Pollution Research, Published online, https://doi.org/10.1007/s11356-018-3184-7.

Garg, V. K., Yadav, P., Mor, S., Singh, B. and Pulhani, V. 2014. Heavy metals bioconcentration from soil to vegetables and assessment of health risk caused by their ingestion. Biological Trace Element Research, 157(3): 256-265.

Gu, J. G., Lin, Q. Q., Hu, R., Ping, Z. Y. and Zhou, Q. X. 2005. Translocation behavior of heavy metals in soil-plant system: a case study from Qingchengzi lead-zinc mine in Liaoning Province. Journal of Agroenvironmental Science, 24(4): 634-637.

Jalali, M. and Hemati, N. 2013. Chemical fractionation of seven heavy metals (Cd, Cu, Fe, Mn, Ni, Pb, and Zn) in selected paddy soils of Iran. Paddy & Water Environment, 11(1-4): 299-309.

Khan, A., Khan, S., Khan, M. A., Qamar, Z. and Waqas, M. 2015. The uptake and bioaccumulation of heavy metals by food plants, their effects on plants nutrients, and associated health risk: A review. Environmental Science and Pollution Research, 22(18): 13772-13799.

Khan, Z.I., Ahmad, K., Rehman, S., Siddique, S., Bashir, H., Zafar, A., Sohail, M., Ali, S. A., Cazzato, E. and De Mastro, G. 2017. Health risk assessment of heavy metals in wheat using different water qualities: Implication for human health. Environmental Science and Pollution Research, 24(1): 947-955.

Kumar, A. and Ramanathan, A. 2015. Speciation of selected trace metals (Fe, Mn, Cu and Zn) with depth in the sediments of Sundarban mangroves: India and Bangladesh. Journal of Soils and Sediments, 15(12): 2476-2486.

Lei, L. M., Liang, D. L., Yu, D. S., Chen, Y. P., Song, W. W. and Li, J. 2015. Human health risk assessment of heavy metals in the irrigated area of Jinghui, Shaanxi, China, in terms of wheat flour consumption. Environmental Monitoring and Assessment, 187(10): 647.

Li, J., Li, K., Cave, M., Li, H. B. and Ma, L. Q. 2015. Lead bioaccessibility in 12 contaminated soils from China: Correlation to lead relative

bioavailability and lead in different fractions. Journal of Hazardous Materials, 295: 55-62.

Li, X. Q., Zheng, X. Q. and Zheng, S. A. 2017. Soil heavy metal Cd in sewage-irrigated saline soil: chemical forms and influencing factors. Chinese Agricultural Science Bulletin, 33(12): 43-47. (In Chinese)

Lim, H. S., Lee, J. S., Chon, H. T. and Sager, M. 2008. Heavy metal contamination and health risk assessment in the vicinity of the abandoned Songcheon Au-Ag mine in Korea. Journal of Geochemical Exploration, 96(2-3): 223-230.

Meng, W. Q., Wang, Z. W., Hua, B. B., Wang, Z. L., Li, H. Y. and Robbin, C. G. 2016. Heavy metals in soil and plants after long-term sewage irrigation at Tianjin China: A case study assessment. Agricultural Water Management, 171: 153-161.

Pempkowiak, J., Sikora, A. and Biernacka, E. 1999. Speciation of heavy metals in marine sediments vs their bioaccumulation by mussels. Chemosphere, 39(2): 313.

Rai, S., Gupta, S. and Mittal, P. C. 2015. Dietary intakes and health risk of toxic and essential heavy metals through the food chain in agricultural, industrial, and coal mining areas of northern India. Human and Ecological Risk Assessment, 21(4): 913-933.

Rout, T. K., Masto, R. E., Padhy, P. K., Ram, L. C., George, J. and Joshi, G. 2015. Heavy metals in dusts from commercial and residential areas of Jharia coal mining town. Environmental Earth Sciences, 73(1): 347-359.

Shi, G.L., Lou, L.Q., Zhang, S., Xia, X.W. and Cai, Q.S. 2013. Arsenic, copper, and zinc contamination in soil and wheat during coal mining, with assessment of health risks for the inhabitants of Huaibei, China. Environmental Science and Pollution Research, 20(12): 8435-8445.

Si, W. T., Liu, J. M., Cai, L., Jiang, H. M., Zheng, C. L., He, X. Y., Wang, J. Y. and Zhang, X. F. 2015. Health risks of metals in contaminated farmland soils and spring wheat irrigated with yellow river water in Baotou, China. Bulletin of Environmental Contamination and Toxicology, 94(2): 214-219.

Skiba, E. and Wolf, W. M. 2017. Commercial phenoxyacetic herbicides control heavy metal uptake by wheat in a divergent way than pure active substances alone. Environmental Sciences Europe, 29(1): 26.

Tessier, A., Campell, P. G. C. and Bisson, M. 1979. Sequential extraction procedure for the speciation of particulate trace metals. Analytical Chemistry, 51(7): 844-850.

USEPA 2009. Risk-Based Concentration Table. United States Environmental Protection Agency, Washington D.C.

USEPA 2011. Risk Assessment Guidance for Superfund. United States Environmental Protection Agency, Washington D.C.

Wang, C., Yang, Z.F., Yuan, X.Y., Browne, P. and Chen, L.X. 2013. The influences of soil properties on Cu and Zn availability in soil and their transfer to wheat (Triticum aestivum L.) in the Yangtze River Delta region, China. Geoderma, 193(2):131-139.

Wang, S. Y., Wu, W. Y., Liu, F., Liao, R. K. and Hu, Y. Q. 2017. Accumulation of heavy metals in soil-crop systems: A review for wheat and corn. Environmental Science and Pollution Research, 24(18): 15209-15225.

Xue, Z. J., Liu, S. Q., Liu, Y. L. and Yan, Y. L. 2012. Health risk assessment of heavy metals for edible parts of vegetables grown in sewage-irrigated soils in suburbs of Baoding City, China. Environmental Monitoring and Assessment, 184(6): 3503-3513.

Yan, S., Ling, Q. C. and Bao, Z. Y. 2007. Metals contamination in soils and vegetables in metal smelter contaminated sites in Huangshi, China. Bulletin of Environmental Contamination and Toxicology, 79(4): 361-366.

Yang, S.Q., Cheng, H.K., Zhang, B., Jing, X.X., Sun, X.X. and Zhao, P. 2014. Differences in Pb accumulation between wheat varieties. Journal of Ecology and Rural Environment, 30(5): 646-651. (In Chinese)

Zeng, X.F., Wang, Z.W., Wang, J., Guo, J.T., Chen, X.J. and Zhuang, J. 2015. Health risk assessment of heavy metals via dietary intake of wheat grown in Tianjin sewage irrigation area. Ecotoxicology, 24(10): 2115-2124.

Zhang, W. T., You, M. and Hu, Y. H. 2016. The distribution and accumulation characteristics of heavy metals in soil and plant from Huainan coalfield, China. Environmental Progress & Sustainable Energy, 35(4): 1098-1104.

Zhu, X. D., Yang, F. and Wei, C. Y. 2015. Factors influencing the heavy metal bio-accessibility in soils were site dependent from different geographical locations. Environmental Science and Pollution Research, 22(8): 13939-13949.

Zota, A.R. and Morello-Frosch, R. 2011. Maternal and Child Health Disparities: Environmental Contribution. Encyclopedia of Environmental Health, 12(1): 630-634.

Potency of Mancozeb Conjugated Silver Nanoparticles Synthesized from Goat, Cow and Buffalo Urine Against *Colletotrichum gloeosporioides* Causing Anthracnose Disease

S. N. Raghavendra, H. S. Raghu†, C. Chaithra and A. N. Rajeshwara
Department of Biochemistry, Kuvempu University, Shankarghatta-577451, Karnataka, India
†Corresponding author: H. S. Raghu; hsr1983@gmail.com

ABSTRACT

Silver nanoparticles of 22-40 nm size were synthesized using goat, cow and buffalo urine. These nanoparticles are conjugated with a fungicide (Mancozeb). The antifungal activity of these conjugated nanoparticles (Mc-AgNPs) was tested against *Colletotrichum gloeosporioides* which causes anthracnose disease in various fruits and vegetables. This fungus infects during pre and post-harvesting seasons causing a significant decrease in the quantity and quality of the product. The fungicide conjugated AgNPs were characterized by UV-Visible, FTIR, SEM and XRD analysis. The synthesis of AgNPs was confirmed by the UV-visible spectroscopy. The shape of AgNPs was found to be spherical. The Mc-AgNPs from goat, cow and buffalo urine exhibited 146.15%, 133.33% and 114.28% more antifungal activity than the fungicides alone respectively. The results indicate that the Mc-AgNPs from goat urine showed more efficacy than cow and buffalo urine. The fungicide-conjugated AgNPs drastically reduce the amount of fungicide to be applied against *Colletotrichum gloeosporioides*, which in turn reduce the hazardous effect caused by fungicides. Further, these can be tested to control other pathogenic fungi also.

INTRODUCTION

In every facet of nanotechnology, the buzzing of nanotechnology has been flourishing at a remarkable rate in recent decades (Jain et al. 2011). The bionanoparticles can work efficiently as fertilizer, pesticide and fungicide in the field of agriculture and horticulture. The biological products can reduce metal ions to metal nanoparticles. The biological products are ecofriendly, less toxic, cost-effective and also have sacred molecules which enhance the quality and quantity of products in agriculture and horticulture (Govarthanan et al. 2014). The biomaterials like plant extracts, animal secretions and microorganisms can be used to synthesize the AgNPs (Kumar et al. 2009, Ahmad et al. 2003, Shahverdi et al. 2007, Jha et al. 2009, Atul et al. 2008, Lee et al. 2013). The proteins are involved in the reduction and stabilization of nanoparticles (Velmurugan et al. 2011).

The world has a very rich heritage in the domestication of a wide range of livestock. The cow, buffalo and goat are common livestock which are widely reared all over the world. According to 19th livestock census-2012 from Department of Animal Husbandry, Dairying and Fisheries following Ministry of Agriculture, India, the distribution of livestock population was found to be 37.28% cattle, 21.23% buffaloes,

12.17% sheep, 26.04% goats and 2.01% pigs. The population of buffalo is 108.7 million, cow 122.9 million, goat 135.17 million and sheep 65.06 million. The secretions from these livestock have great importance in Ayurveda, Unani and Siddha medicine, which are rich in proteins, lipids, carbohydrates, micronutrients and antioxidants. The cattle like cow and buffalo are treated as sacred in world heritage and the use of the secretions like milk, dung, urine, ghee, buttermilk and curd are widely used.

Goat urine (Ajamutra) is an astringent, sweet with wholesome many beneficial properties as per Ayurveda (Vaibhav et al. 2018). The goat urine has antibacterial and antifungal properties against various pathogens. The Ajamutra has nitrogenous constituents like nitrogen, uric acid, allantoin, hippuric acid, creatine, creatinine and ammonia, and the non-nitrogenous contents like carbonates, bicarbonates, phosphates, sulphates, chlorides, calcium and magnesium (Ferichani 2013). The cow urine (Gomutra) and Ajamutra have great future in modern pharmacology because of their universal availability, cost-effective and many beneficial uses (Hazarika et al. 2018).

Cow urine is nectar with many beneficial potentialities which is capable of removing several ill effects and imbalances in the body during infection. It consists of 95% water,

2.5% urea, and other 2.5% is the combination of 24 types of salts, hormones, enzymes, vitamins, minerals and antioxidants (Edwin et al. 2008). It is used as biofertilizer to enrich nutrient contents in soil and biopesticides to kill bacteria, viruses and fungi (Jandaik et al. 2015). Cow urine has a pool of sources like nitrogen, phosphorus, potassium, calcium, magnesium, sulfur, chlorite, iron, silicon, lactose, carbolic acid, urea, aromatic acids, aurum hydroxide, hippuric acid, protein and creatinine. The urea vitamins in urine are A, B, C, D and E and gold acids (Pathak & Kumar 2003). It also works as a plant hormone to enhance the growth of the plant and correct micronutrient deficiency in plants (Pradhan et al. 2018, Sahu et al. 2016).

Buffalo urine (Mahishamutra) has been in use in Ayurveda and traditional medicines. The contents of Mahishamutra are like that of cow urine but the exception is reduced level of nitrogen and phosphorus content and increased level of solids, urea and uric acid (Gianluca et al. 2014, Shourbagy & Abdel 1953). The cattle urine also contains the microelements like barium, strontium, copper, lead, zinc, nickel and copper (Raghu 2015). The urine composition of buffaloes varies in their oestrous cycle and gestation period (Barman et al. 2013). The Mahishamutra is used as a medicine in the treatment of oedema, piles, abdominal diseases and also alleviate the loss of appetite (Thakur 2004).

Mango (*Magnifera indica* L.) belongs to Anacardiaceae family and is the eighth most produced fruit in the world. The global demand for mango is fast-paced because it is a cardinal component of the diet and rich in vitamins and minerals. India produces over 18.7 million tons of mango where it stands number one in production (Felipe 2000). The mango is very eminent due to its wide range of adaptability, high nutritive value, richness in variety and delicious taste.

Anthracnose is a prominent pre and post-harvest disease of many plants including fruits and vegetables. The disease appears in flowers, young fruits, leaves, twigs and stored mature fruits as slightly, black, sunken, irregular shape lesions (Prakash et al. 1997, Fitzell & Peak 1984, Jefferies et al. 1990). The quiescent infection on immature fruits leads to a reduction of yield to 25-30% in mango (Abd-Alla & Wafaa 2010). The disease spreads with rain splash, insects, wind and garden tools. Anthracnose is caused by fungi of genus *Colletotrichum*. It is commonly called as brown blight (coffee and tea), dieback (citrus), stem canker and anthracnose tear stain (mango) (Sayiprathap et al. 2018, Kamle et al. 2013).

Colletotrichum gloeosporioides is most common disease plant pathogenic fungus in many host plants like citrus, yam, papaya, tomato, mango, coffee and sweet pepper. The life cycle encountered by fungi involves the production of spores on a susceptible host, dispersal of spores, penetration of host tissue, the start of infection process inside the cell, the emergence of lesions, the formation of bristly spores and spreads in various ways. The pathogen has high graving dimension at high humidity and temperature of 20-30°C (Davis et al. 1987). The Penzig reported the pathogenic *Colletotrichum gloeosporioides*. The *C. gloeosporioides* (Penz.) is ubiquitous species belonging to Ascomycetes family and order Melanovoniales, with cosmopolitan distribution (Kamle & Pradeep 2016, Ajay Kumar 2014). The pathogen infects either as a parasite (primary disease-causing organism), saprophyte (infect deteriorated plant parts) or endophytic fungi (live inside plant tissue). The optimal growth conditions for *C. gloeosporioides* are high humidity, the temperature of 25-30°C and pH 6-7.

Mancozeb is a non-systemic broad-spectrum protectant fungicide for control of a wide range of disease in agriculture, horticulture and ornamental crops. It is a member of ethylene-bis (dithiocarbamate) (EBDC). In I962, Rohm and Haas signified mancozeb as zinc ion complex of maneb. The most versatile group of an organic fungicide is EBDC fungicide among which mancozeb is most significant in commercial use. The empirical formula is $[SCSNHCH_2CH_2NHCSSMN-]_x(Zn)_y$ (Venugopal & Sainadh 2016). It is grey to yellow coloured powder with multisite action. Mancozeb is a profungicide and breaks down to release ethylene bis-isothiocyanate sulphide (EBIS) on exposure to water, and converted to ethylene bis-isothiocyanate (EBI) on the action of UV light. For control of diseases, mancozeb is sprayed with an interval of 14 days between panicle emergence and fruit set (Gullino et al. 2010, Jigneshkumar et al. 2014).

MATERIALS AND METHODS

Pathogen Culture

The spores of fungus *Colletotrichum gloeosporioides* were cultured using potato dextrose agar (PDA) medium and mango fruit extract agar (MFEA) (Abera et al. 2016) for 6-8 days at 30°C. The cultural isolate was obtained from infected fruits and vegetables such as mango, papaya and chilly. The spores were harvested in 7-10 mL of sterile double distilled water using inoculation loop in aseptic condition. The cyclomixer was used for spore suspension unification and the spore concentration was found to be 10^6 spores per mL with the aid of haemocytometer (Abd-Alla & Wafaa 2010).

Urine Sample Collection

Urine samples of goat, cow and buffalo were collected from the domestic yard of Santhekadur village, Shimoga district, Karnataka, India. During dawn, around 50-80mL of urine sample was collected from healthy livestock in sterile wide-

X-Ray Diffraction Analysis

The Scherrer formula was used to calculate the crystallite domain size from the width of XRD peaks, assuming that they are free from non-uniform strains.

$$D = 0.94\,\lambda\,/\,\beta\,\text{Cos}\,\theta$$

Where, D is the average crystallite domain size perpendicular to the reflecting planes, λ is the X-ray wavelength, θ is the full width at half maximum (FWHM), and β is the diffraction angle. To eliminate additional instrumental broadening the FWHM was corrected, using the FWHM from a large-grained Si sample. B corrected = (FWHM^{2}sample - FWHM^{2}si)$^{1/2}$.

The lyophilized Mancozeb, AgNPs and Mc-AgNPs of different urine samples (goat, cow and buffalo) were coated on the grid and subjected to X-ray diffraction (XRD) measurements (Rigaku Miniflex 600). The analysis was carried out using X-ray diffractometer with an operating voltage of 40 kV and a current of 15mA.

Fourier Transform Infrared Spectroscopy

The Mancozeb, AgNPs and Mc-AgNPs of different urine samples (goat, cow and buffalo) were subjected to Fourier transform infrared (FT-IR) spectroscopy (Bruker, USA) to analyze their spectra. The analysis was carried out with potassium bromide (KBr) pellets, recorded in the range of 500-4000 cm^{-1}.

In Vitro Antifungal Activity of AgNPs and Mc-AgNPs

The antifungal activity of AgNPs and Mc-AgNPs of different urine samples (goat, cow and buffalo) was investigated by well plate method, *in vitro* along with fungicide Mancozeb as control. The synthesized fungicides Mancozeb, AgNPs and Mc-AgNPs were added to wells made in the solidified potato dextrose agar media or mango fruit extract agar (MFEA) spread with the sporal culture of *Colletotrichum gloeosporioides* uniformly. The plates were incubated at 30°C for 48-72 hours for the visualization of inhibition zones. The inhibition by fungicide Mancozeb was considered as control.

RESULTS AND DISCUSSION

UV-Visible Spectroscopy

The UV-Visible spectroscopy is one of the most widely used techniques for the structural characterization of AgNPs. The absorption band in 350 to 550 nm region is typical for the AgNPs. The UV-visible spectra showed absorption bands in 350 to 550 nm region which confirms the formation of AgNPs (Sastry et al. 1997, Henglein 1993, Sastry 1998). In the present study, we found that the biological synthesis

mouth containers. After the collection of samples, they were immediately transferred to the laboratory and stored at 4°C for further use. The urine samples were confirmed for normal biochemicals parameters (glucose, pH, specific gravity, bilirubin, urobilinogen, ketones) with the aid of reagent dip strips urinanalysis (URS-10 T strips, Mumbai, India). The debris and bacterial contamination in samples were filtered through 0.1 μ membrane filter.

Synthesis of Silver Nanoparticles

Silver nanoparticles (AgNPs) were synthesized by the biological method using urine samples from goat, cow and buffalo. Double distilled deionized water was used to prepare silver nitrate (AgNO$_3$). Different volumes (5, 10, 15 mL of 0.001M) of silver nitrate were added dropwise to 50 mL of pre-chilled urine samples with constant stirring for 4-6 hours. The solution turned to light yellow after the addition of 10 mL of silver nitrate and to brown when all of the silver nitrate has been added. The stirring was continued even after all the silver nitrate was added. Finally, the colloid breaks down to settled out the particles (Geoprincy et al. 2013).

Synthesis of Mancozeb Conjugated Silver Nanoparticles (Mc-AgNPs)

The fungicide, Mancozeb (0.1%) was mixed with urine samples of goat, cow and buffalo. The mixture was pre-chilled for 20 minutes. Silver nitrate (0.001M) solution was added dropwise to this mixture with vigorous stirring for about 3 to 5 hours. The solution turned to brown after the addition of 20-25 mL of silver nitrate (Raghavendra et al. 2019).

UV-Visible Spectroscopy

The optical properties of synthesized silver nanoparticles were determined by UV-Visible spectrometry (Thermoscientific). The UV-Visible absorption spectra of AgNPs and Mc-AgNPs of goat, cow and buffalo were observed in the range 350 nm to 450nm.

Scanning Electron Microscopy (SEM) Analysis

The surface topography and 3D view of the synthesized nanoparticles were analysed in SEM (EVO MA18 with Oxford EDS). The morphological characteristics of AgNPs and Mc-AgNPs from different cattle urine samples (goat, cow and buffalo) were established by SEM. The thin films of the samples were prepared on a carbon-coated copper grid by dropping a very small amount of the sample on the SEM grid and the film was allowed to dry by keeping it under a mercury lamp for 5-7 min and then subjected for SEM analysis with a magnification of 1,00,000x.

of AgNPs and Mc-AgNPs using goat urine sample showed the characteristic absorption peak at 403 nm and 432 nm respectively (Fig. 1a and b). The AgNPs and Mc-AgNPs synthesized using Cow urine sample showed the characteristic peak at 377 nm and 405 nm respectively (Fig. 1c and d). And the AgNPs and Mc-AgNPs synthesized using Buffalo urine sample showed the characteristic peak at 392 nm and 433 nm respectively (Fig. 1e and f).

Scanning Electron Microscopy (SEM) Analysis

Microscopic surface features including morphology and particle size of synthesized AgNPs and fungicide conjugated AgNPs were assessed by SEM analysis. The AgNPs and Mc-AgNPs synthesized using goat urine sample were found
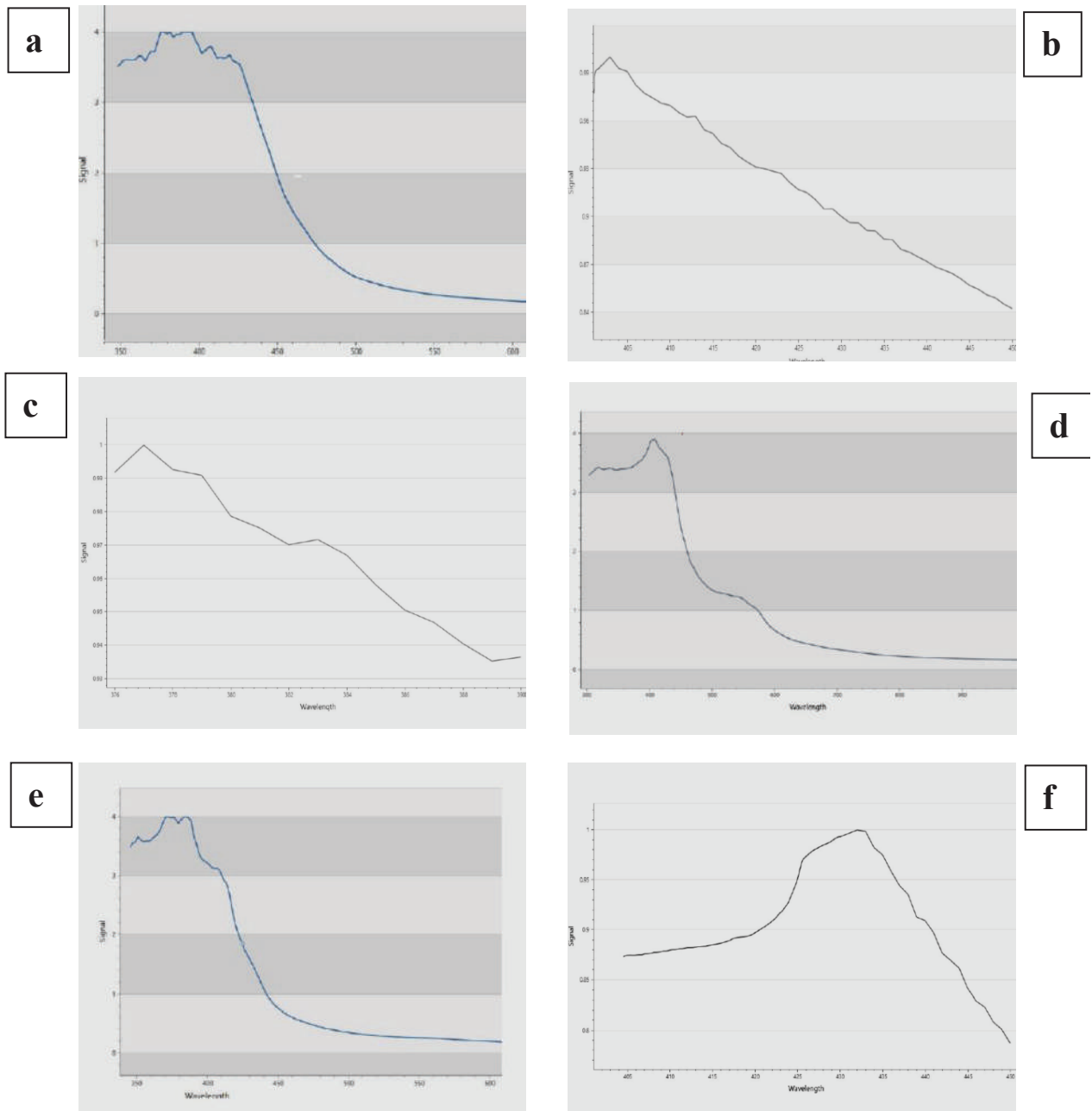
Fig. 1: UV-Vis absorption spectra of (a) AgNPs and (b) Mancozeb conjugated AgNPs synthesized from goat urine sample; (c) AgNPs and (d) Mancozeb conjugated AgNPs synthesized from cow urine sample; (e) AgNPs and (f) Mancozeb conjugated AgNPs synthesized from buffalo urine sample.

to be spherical with a diameter ranging from 22 to 28 nm and 26 to 32 nm respectively (Fig. 2a and b). The AgNPs and Mc-AgNPs synthesized from cow urine sample were found to be spherical with a diameter ranging from 26 to 34 nm and 30 to 36 nm respectively (Fig. 2c and d). The AgNPs and Mc-AgNPs synthesized using buffalo urine sample were found to be spherical with a diameter ranging from 28 to

36 nm and 32 to 40 nm respectively (Fig. 2e and f). SEM image also confirms that the synthesized nanoparticles are well separated with no aggregation.

X-ray Diffraction Analysis

The Mancozeb and synthesized AgNPs and Mc-AgNPs from different cattle urine samples were subjected to X-ray diffrac-
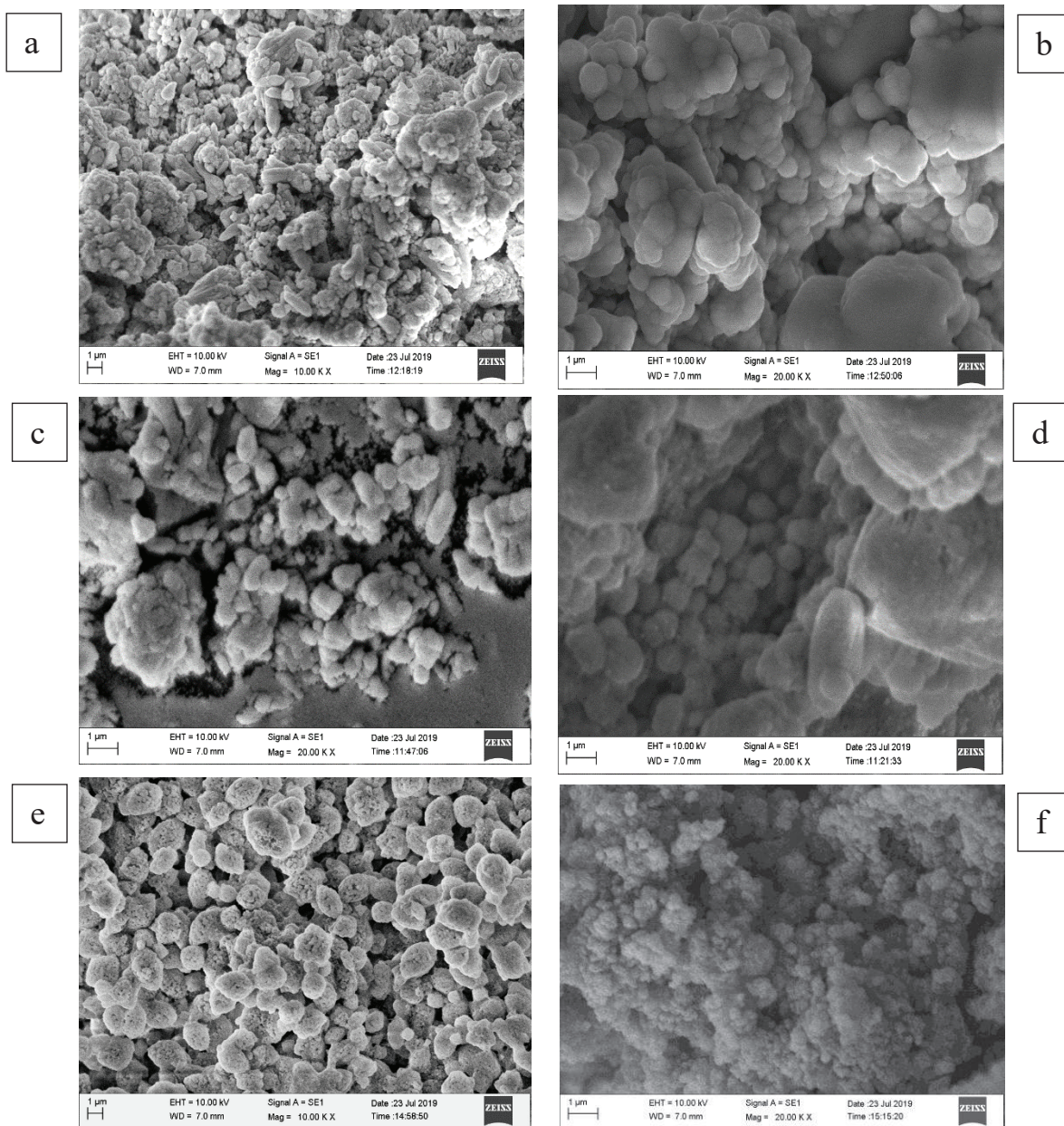
Fig. 2: SEM Images of (a) AgNPs and (b) Mancozeb conjugated AgNPs synthesized from goat urine sample; (c) AgNPs and (d) Mancozeb conjugated AgNPs synthesized from cow urine sample; (e) AgNPs and (f) Mancozeb conjugated AgNPs synthesized from buffalo urine sample.

tion studies to understand the crystallinity and to establish the average particle size. As shown in Fig. 3a, the XRD pattern of Mancozeb alone showed prominent characteristic peaks of 2θ at 20.15°, 29.64° and 39.75° which confirms the presence of Mancozeb (Liang et al. 2010).

The XRD pattern of AgNPs synthesized from goat urine sample (Fig. 3b) has prominent diffraction peaks of the 2θ values of 30.34°, 39.16°, 46.82° and 65.59° which can be assigned to (111), (200), (220) and (311) planes, respectively, with some minor peaks (Jamdagni et al. 2018). The XRD pattern of Mc-AgNPs synthesized from goat urine sample (Fig. 3c) showed characteristic peaks of 2θ at 20.65°and 29.89° corresponding to Mancozeb and the peaks of 2θ at 39.56° and 47.68° corresponding to AgNPs.

The XRD pattern of AgNPs synthesized from cow urine sample (Fig. 3d) has prominent diffraction peaks of the 2θ
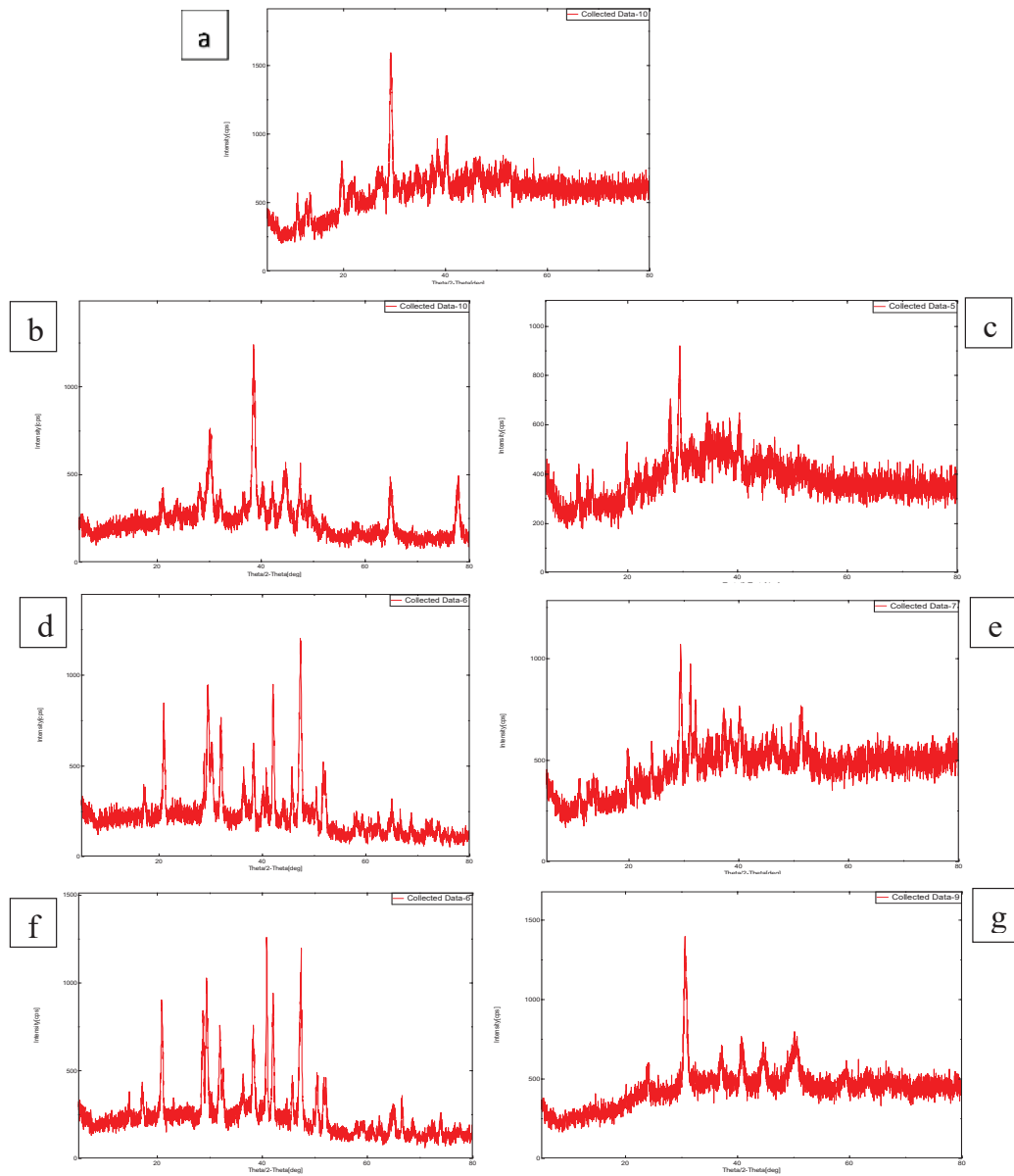
Fig. 3: XRD pattern of (a) Mancozeb; (b) AgNPs synthesized from goat urine sample; (c) Mancozeb conjugated AgNPs synthesized from goat urine sample; (d) AgNPs synthesized from cow urine sample; (e) Mancozeb conjugated AgNPs synthesized from cow urine sample; (f) AgNPs synthesized from buffalo urine sample; (g) Mancozeb conjugated AgNPs synthesized from buffalo urine sample.

values of 21.22°, 30.89°, 38.73°, 48.59° and 53.32° which can be assigned to (111), (200), (220) and (311) planes, respectively, with some minor peaks. The XRD pattern of Mc-AgNPs synthesized from cow urine sample (Fig. 3e) showed characteristic peaks of 2θ at 20.17° and 39.86° corresponding to Mancozeb and the peaks of 2θ at 30.69° and 53.62° corresponding to AgNPs.

The XRD pattern of AgNPs synthesized from buffalo urine sample (Fig. 3f) has prominent diffraction peaks of the 2θ values of 21.08°, 28.86°, 32.52°, 42.79° and 47.96° which can be assigned to (111), (200), (220) and (311) planes, respectively, with some minor peaks. The XRD pattern of Mc-AgNPs synthesized from buffalo urine sample (Fig. 3g) showed characteristic peaks of 2θ at 39.29° corresponding to Mancozeb and the peaks of 2θ at 32.04°, 42.09° and 47.91° corresponding to AgNPs.

The data confirm that Mancozeb has been successfully adsorbed on the surface of AgNPs.

Fourier Transform Infrared Spectroscopy

The Mancozeb and synthesized AgNPs and Mc-AgNPs from different cattle urine samples were subjected to Fourier transform infrared spectroscopy studies. The FTIR spectrum of Mancozeb (Fig. 4a) shows characteristic peaks at 3313.46 cm^{-1} showed the stretching vibrations of -N-H group, 2978.95 cm^{-1} corresponds to -C-H groups and 1286.51 cm^{-1} Corresponds to -C-N group which confirms the presence of Mancozeb as shown earlier (Bahram et al. 2017).

The FTIR spectra of synthesized AgNPs synthesized from goat urine sample showed various absorption bands for different chemical groups (Fig. 4b) at 3319.62 cm^{-1}, 1627.57 cm^{-1}, 1108.46 cm^{-1} and 874.21 cm^{-1} (Arment et al. 2005). The FTIR spectrum of Mc-AgNPs synthesized from goat urine sample (Fig. 4c) shows distinct peaks at 3295.13 cm^{-1} illustrating the stretching vibrations confirms the AgNPs. The peaks at 2976.05 cm^{-1} and 1282.61 cm^{-1} establish the adhesion of Mancozeb on the AgNPs.

The FTIR spectra of synthesized AgNPs synthesized from cow urine sample showed various absorption bands for different chemical groups (Fig. 4d) at 3429.14 cm^{-1}, 1626.96 cm^{-1}, 1119.04 cm^{-1} and 714.88 cm^{-1}. The FTIR spectrum of Mc-AgNPs synthesized from cow urine sample (Fig. 4e) shows distinct peaks at 3424.62 cm^{-1} and 719.99 cm^{-1} illustrating the stretching vibrations confirms the AgNPs. The peaks at 3302.62 cm^{-1} and 2970.67 cm^{-1} establish the adhesion of Mancozeb on the AgNPs.

The FTIR spectra of synthesized AgNPs synthesized from buffalo urine sample showed various absorption bands for different chemical groups (Fig. 4f) at 3438.81cm^{-1}, 1641.78

cm^{-1}, 875.56 cm^{-1} and 476.34cm^{-1}. The FTIR spectrum of Mc-AgNPs synthesized from goat buffalo sample (Fig. 4g) shows distinct peaks at 3440.03 cm^{-1}, 1640.98 cm^{-1}, 871.42 cm^{-1} illustrating the stretching vibrations confirms the Ag-NPs. The peaks at 2968.74 cm^{-1} establish the adhesion of Mancozeb on the AgNPs.

Antifungal Activity of AgNPs, Mancozeb and Mc-AgNPs

The antifungal potential of AgNPs, Mancozeb and Mc-Ag-NPs was assessed against *Colletotrichum gloeosporioides* which causes anthracnose disease. The results showed that the inhibition of fungal growth was observed with Mancozeb, AgNPs and Mc-AgNPs of goat urine (Fig. 5). The Mancozeb (1%) significantly inhibited with an inhibition zone of diameter 1.3 cm which is 85.71% more than the AgNPs which showed the inhibition zone of diameter 0.7cm. Further, the Mc-AgNPs exhibited the highest growth inhibition of *Colletotrichum gloeosporioides* (~146.15%) more as compared to fungicide Mancozeb alone with an inhibition zone of 3.2 cm.

The inhibition of fungal growth was observed with Mancozeb, AgNPs and Mc-AgNPs of cow urine sample (Fig. 6). The Mancozeb (1%) significantly inhibited with an inhibition zone of diameter 0.9 cm which is 80.0% more than the AgNPs which showed the inhibition zone of diameter 0.5 cm. Further, the Mc-AgNPs exhibited the highest growth inhibition of *Colletotrichum gloeosporioides* (~133.33%) more as compared to fungicide Mancozeb alone with an inhibition zone of 2.1 cm.

The inhibition of fungal growth was observed with Mancozeb, AgNPs and Mc-AgNPs of buffalo urine sample (Fig. 7). The Mancozeb (1%) significantly inhibited with an inhibition zone of diameter 0.7 cm which is 75.0% more than the AgNPs which showed the inhibition zone of diameter 0.4 cm. Further, the Mc-AgNPs exhibited the highest growth inhibition of *Colletotrichum gloeosporioides* (~114.28%) more as compared to fungicide Mancozeb alone with an inhibition zone of 1.5 cm.

These results illustrate that Mc-AgNPs synthesized from goat urine sample have shown 52.38% more potency against C. *gloeosporioides* compared to Mc-AgNPs synthesized from cow urine sample and 113.33% more effective than the Mc-AgNPs synthesized from buffalo urine sample.

CONCLUSIONS

Currently, there are many chemical fungicides to control plant pathogens which are being used at very high concentrations thus causing environmental pollution. Hence, there is a great need to reduce the use of high concentra-
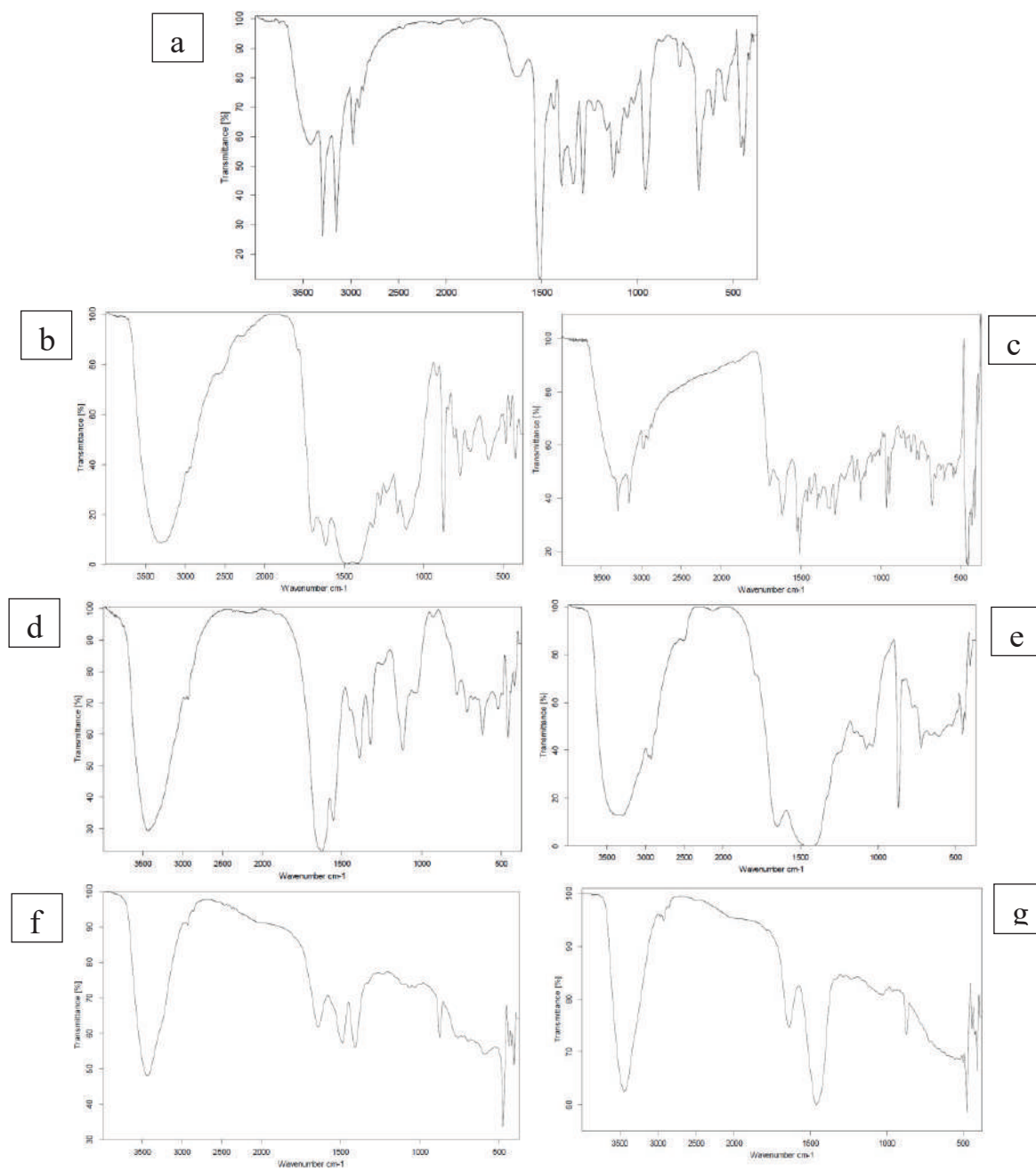
Fig. 4: Fourier transform infrared spectroscopy of (a) Mancozeb. (b) AgNPs synthesized from goat urine sample. (c) Mancozeb conjugated AgNPs synthesized from goat urine sample. (d) AgNPs synthesized from cow urine sample. (e) Mancozeb conjugated AgNPs synthesized from cow urine sample. (f) AgNPs synthesized from buffalo urine sample. (g) Mancozeb conjugated AgNPs synthesized from buffalo urine sample.
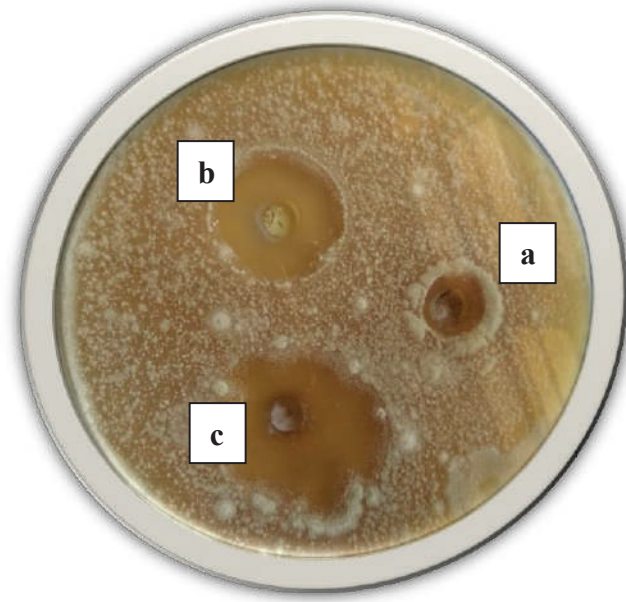
Fig. 5: Antifungal activity of a) AgNPs synthesized from goat urine sample, b) Mancozeb and c) Mancozeb conjugated AgNPs.

tion of fungicides to control plant pathogens which affect several crops worldwide. It has been very well established that AgNPs alone can be an effective means of controlling plant pathogens. However, in the present study, we have synthesized Mc-AgNPs from goat, cow and buffalo urine which greatly enhanced the antifungal potency against *Colletotrichum gloeosporioides* at very low concentrations. These can be applied as an economical and environmentally friendly method to control *Colletotrichum gloeosporioides* which causes anthracnose disease. These Mc-AgNPs could potentially be used in the field to control anthracnose disease caused by *C. gloeosporioides* affecting various plants.
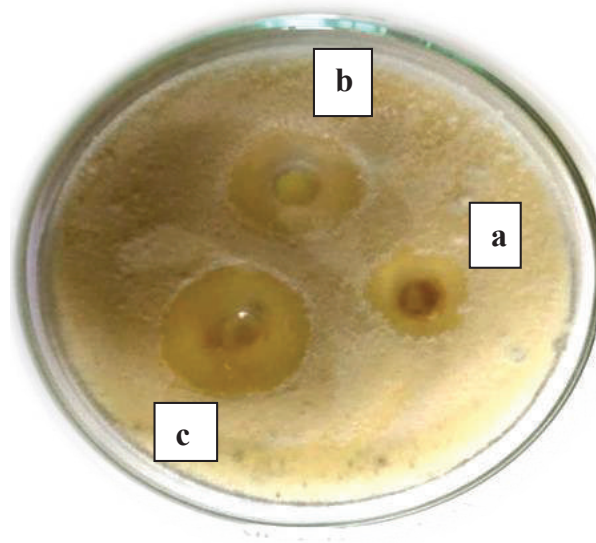
Fig. 6: Antifungal activity of a) AgNPs synthesized from cow urine sample, b) Mancozeb and c) Mancozeb conjugated AgNPs.
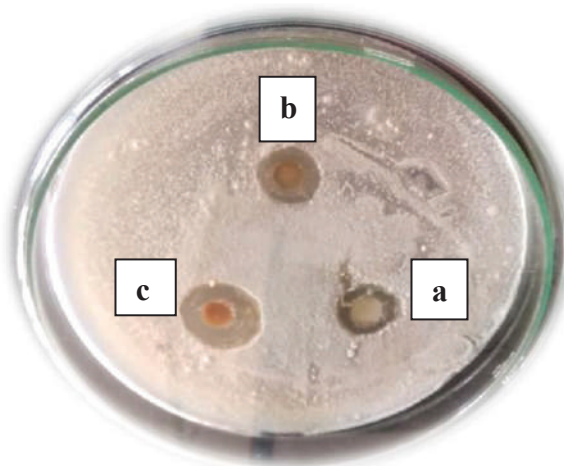
Fig. 7: Antifungal activity of (a) AgNPs synthesized from buffalo urine sample, (b) Mancozeb and (c) Mancozeb conjugated AgNPs.

REFERENCES

Abd-Alla, M. A. and Wafaa, M. H. 2010. New safe methods for controlling anthracnose disease of mango (*Mangifera indica* L.) fruits caused by *Colletotrichum gloeosporioides* (Penz.). Journal of American Science, 8(8): 361-367.

Abera, A., Lemessa, F. and Adunga, G. 2016. Phenotypic characteristics of colletotrichum species associated with mango (*Mangifera indica* L.) in Southwest Ethiopia. Food Science and Quality Management, 48: 106-115.

Ahmad, A., Senapati, S., Khan, M. I., Kumar R. and Sastry, M. 2003. Extracellular biosynthesis of monodisperse gold nanoparticles by a novel extremophilic actinomycete, Thermomonospora sp. Langmuir, 19: 3550-3553.

Ajay Kumar, G. 2014. *Colletotrichum gloeosporioides*: Biology, Pathogenicity and Management in India. J. Plant Physiol. Pathol., 2(2): 2-11.

Arment, S., Garrigues, S. and Guardia, M. 2005. Solid sampling Fourier transform infrared determination of Mancozeb in pesticide formulations. Journal of Talanta, 65: 971-979.

Atul, A. Bharde, Rasesh, Y. Parikh, Maria Baidakova, Samuel Jouen, Baetrice Hannoyer, Toshiaki Enoki, Prasad, B. L. V., Yogesh, S. Shouche, Satish Ogale and Murali Sastry, 2008. Bacteria-mediated precursor-dependent biosynthesis of superparamagnetic iron oxide and iron sulfide nanoparticles. Langmuir, 24: 5787-5794.

Bahram, B. Teimoori, Nikparast, Y., Hojatianfar, M., Akhlaghi, M., Ghorbani, R. and Pourianfar, H. R. 2017. Characterization and antifungal activity of silver nanoparticles biologically synthesised by *Amaranthus retroflexus* leaf extract. Journal of Experimental Nanoscience, 12: 129-139.

Barman, P., Yadav, M. C., Kumar, H., Meur, S. K. and Ghosh, S. K. 2013. Gas chromatographic-mass spectrometric analysis of chemical volatiles in buffalo (*Bubalus bubalis*) urine. Theriogenology, 80: 654-658.

Davis, R. D., Irwin, J. A. G., Cameron, D. F. and. Shepherd, R. K. 1987. Epidemiological studies on the anthracnose diseases of *Stylosanthes* caused by *C. gloeosporioides* in North Queensland and pathogenic specialization within the natural fungal populations. Australian Journal of Agriculture Research, 38: 1019-1032.

Felipe, L. Arauz, 2000. Mango anthracnose: Economic impact and current options for integrated management. Plant Disease, 84(6): 600-611.

Ferichani, M. 2013. The potential Ettawa goat manure and urine management to support the productive and sustainable farming. Journal of Crop and Weed, 9(2): 76-80.

Fitzell, R.D. and Peak, C.M. 1984. The epidemiology of anthracnose disease of mango: Inoculum sources, spore production and dispersal. Ann Appl Biol., 104: 53-59.

Geoprincy, G., Vidhya Sri, B. N., Poonguzhali, U., Nagendra, N. Gandhi and Renganathan, S. 2013. A review on green synthesis of silver nanoparticles. Asian J. Pharm. Clin. Res., 6 (1): 8-12.

Govarthanan, M., Selvankumar, T., Manoharan, K., Rathika, R., Shanthi, K., Lee, K.J., Cho, M., Kamala-Kannan, S. and Oh, B.T. 2014. Biosynthesis and characterization of silver nanoparticles using panchakavya, an Indian traditional farming formulating agent. International Journal of Nanomedicine, 9: 1593-1599.

Gullino, M.L., Tinivella, F., Garibaldi, A., Kemmitt, G.M., Bacci, L. and Sheppard, B. 2010. Mancozeb past, present, and future. Plant Disease, 94(9): 1076-1087.

Hazarika, S., Das, S., Sarma, H. and Sharma, H.K. 2018. Application of cow and goat urine in traditional systems of medicines: A brief review. International Journal of Pharmaceutical and Biological Archives, 9(4): 197-203.

Henglein, A. 1993. Physicochemical properties of small metal particles in solution: Microelectrode reactions, chemisorption, composite metal nanoparticles, and the atom-to- metal transition. Phys. Chem. B, 97: 5457-5471.

Jain, S., Uchegbu, I.F., Betageri, G. and Pastorin, G. 2011. Nanotechnology in advanced drug delivery. Journal of Drug Delivery, 2011: 2.

Jamdagni, P., Rana, J.S. and Khatri, P. 2018. Comparative study of antifungal effect of green and chemically synthesized silver nanoparticles in combination with carbendazim, Mancozeb, and thiram. Advances in Animal Biotechnology and its Applications, 12(8): 1102-1107.

Jandaik, S., Thakur, P. and Kumar, V. 2015. Efficacy of cow urine as plant growth enhancer and antifungal agent. Advances in Agriculture, 2015: 1-7.

Jarald, E., Edwin, S., Tiwari, V., Garg, R. and Toppo, E. 2008. Antioxidant and antimicrobial activities of cow urine. Global Journal of Pharma-

cology, 2 (2): 20-22.

Jefferies, P., Dodd, J. C., Jeger, M. J. and Plumbley, R. A. 1990. The biology and control of Colletotrichum species on tropical fruit crops. Plant Pathol., 39: 343-366.

Jha, A. K. and Prasad, K. 2009. A green low-cost biosynthesis of Sb_2O_3 nanoparticles. Biochem. Eng. J., 43: 303-306.

Jigneshkumar, V. Rohit, Jignasa, N. Solanki and Suresh Kumar, Kailasa, 2014. Surface modification of silver nanoparticles with dopamine dithiocarbamate for selective colorimetric sensing of mancozeb in environmental samples. Sensors and Actuators B: Chemical, 200: 219-226.

Kamle, M., Kumar, P., Gupta, V. K., Tiwari, A. K., Misra, A. K. and Pandey, B. K. 2013. Identification and phylogenetic correlation among *Colletotrichum gloeosporioides* pathogen of anthracnose for mango. Biocat. Agric. Biotechnol., 2(3): 285-287.

Kamle, Madhu and Pradeep Kumar 2016. *Colletotrichum gloeosporioides*: Pathogen of anthracnose disease in mango (*Mangifera indica* L.). In: Kumar, P., Gupta, V., Tiwari, A. and Kamle, M. (eds.) Current Trends in Plant Disease Diagnostics and Management Practices, Fungal Biology, Springer, Cham, pp. 207-219.

Kumar, V. and Yadav, S. K. 2009. Plant-mediated synthesis of silver and gold nano-particles and their applications. J. Chem. Technol. Biotechnol., 84: 151-157.

Lee, K.J., Park, S.H., Govarthanan, M., Hwang, P.H., Seo, Y.S., Cho, M., Lee, W.H., Lee, J.Y., Kamala-Kannan, S. and Oh, B.T. 2013. Synthesis of silver nanoparticles using cow milk and their antifungal activity against phytopathogens. Mater Lett., 105: 128-131.

Liang, F. H., Yong, G. X., Yuan Z. Z., and Min, M. A. 2010. Study on the crystalline structure and thermal stability of silver oxide films deposited by direct-current reactive magnetron sputtering methods. J. Korean Phys. Soc., 56: 1176-1179.

Neglia, G., Balestrieri, A., Gasparrini, B., Cutrignelli, M.I., Bifulco, G., Salzano, A., Cimmino, R., Varricchio, E., D'Occhio, M.J. and Campanile, G. 2014. Nitrogen and phosphorus utilization and excretion in dairy buffalo intensive breeding. Italian Journal of Animal Science, 13(4): 3362.

Pathak, M. L. and Kumar, A. 2003. Cow praising and importance of Panchyagavya as medicine. Sachitra Ayurveda, 5: 569.

Pradhan, S.S., Verma, S., Kumari, S. and Singh, Y. 2018. Bio-efficacy of cow urine on crop production: A review. International Journal of Chemical Studies, 6(3): 298-301.

Prakash, O., Misra, A. K. and Kishun, R. 1997. Some threatening diseases of mango and their management. In: Agnihotri, V. P., Sarbhoy, A. K., and Singh, D. V. (eds.), Management of Threatening Plant Diseases, (1st edn). Malhotra Publishing House, New Delhi, pp.179 -205.

Raghavendra, S. N., Raghu, H. S., Divyashree, K. and Rajeshwara, A. N. 2019. Antifungal efficiency of copper oxychloride (coc) conjugated silver nanoparticles against *Colletotrichum gloeosporioides* which causes anthracnose disease. Asian J. Pharm. Clin. Res., 12(8): 230-233.

Raghu, V. 2015. Study of dung, urine and milk of selected grazing animals as bioindicators in environmental geoscience - A case study from Mangampeta barite mining area, Kadapa District, Andhra Pradesh, India. Environ. Monit. Assess., 187: 4080.

Sahu, R. K., Krishnaiah, N., Ramya, P. and Anusha, P. 2016. Cow urine- therapeutic value. International Journal of Livestock Research, 6(11): 93-99.

Sastry, M., Mayya, K. S. and Bandyopadhyay, K. 1997. pH dependent changes in the optical properties of carboxylic acid derivatized silver colloidal particles. Colloids Surf A, 127: 221-228.

Sastry, M., Patil, V. and Sainkar, S. R. 1998. Electrostatically controlled diffusion of carboxylic acid derivatized silver colloidal particles in thermally evaporated fatty amine films. Phys. Chem. B, 102: 1404-1410.

Sayiprathap, B. R., Ekabote, S. D., Nagarajappa Adivappar, Narayanaswamy, H. and Ravindra, H. 2018. Screening of fungicides against anthracnose disease of mango on nursery seedlings. International Journal of Chemical Studies, 6(4): 1494-1497.

Shahverdi, A. R., Minaeian, S., Shahverdi, H. R., Jamalifar, H. and Nohi A. 2007. Rapid synthesis of silver nanoparticles using culture supernatants of Enterobacteria: A novel biological approach. Process Biochem., 42: 919-923.

Shourbagy, M. R. and Abdel Monem Ahmed 1953. A study of bovine urine in health and disease. The British Veterinary Journal, 109(7): 296-298.

Thakur, A. N. 2004. Therapeutic use of urine in early Indian medicine. Indian Journal of History of Science, 39(4): 415-427.

Vaibhav, T., Rajesh, N., Vijay, P., Ajay, P. S., Debashis, R., Ambika, S., Pawanjit, S. and Abhishek, P. 2018. Evaluation of *in vitro* anti-microbial activity of goat urine peptides. Journal of Animal Research, 8: 33-37.

Velmurugan, P., Shim, J., Kamala Kannan, S., Lee, K.J., Oh, B.T., Balachandar, V. and Oh, B.T. 2011. Crystallization of silver through reduction process using *Elaeis guineensis* biosolid extract. Biotechnol Prog., 27(1): 273-279.

Venugopal, N. V. S. and Sainadh, N. V. S. 2016. Novel polymeric nanoformulation of Mancozeb – An eco-friendly nanomaterial. International Journal of Nanoscience, 15(3): 1650016.

Spectroscopic Characterization of Palm Stearin Biodiesel Derived Through Base Catalysed Transesterification Process

V. Hariram†*, N. Bala Karthikeyan*, S. Seralathan**, T. Micha Premkumar* and J. Godwin John***

*Deptt. of Mechanical Engineering, Hindustan Institute of Technology & Science, Hindustan University, Chennai, India
**Deptt. of Aeronautical Engg., Hindustan Institute of Technology & Science, Hindustan University, Chennai, India
***Deptt. of Automobile Engg., Hindustan Institute of Technology & Science, Hindustan University, Chennai, India
†Corresponding author: V. Hariram; connect2hariram@gmail.com

ABSTRACT

In this research work, the characterization of the palm stearin biodiesel was made using Nuclear Magnetic resonance (NMR), Fourier transform infrared spectroscopy (FITR) and GC/MS methods. Analysis of the composition of fatty acids was done using the GCMS apparatus based on the retention time. Fourier transform infrared spectrometer was used for the spectrum analysis of the various functional groups and bands located in it. The properties of the palm stearin biodiesel were predicted adopting the American Society for Testing and Materials (ASTM) standards. Measured values of the properties were the density at 18°C as 0.88 g/m^3, kinematic viscosity at 35°C as 3.4 mm^2/s, the calorific value of the palm stearin as 37121 kJ/kg and the flash and fire points of the biodiesel as 130°C and 160°C respectively. The rapid and correct characterization of the palm stearin biodiesel was made by the NMR.

INTRODUCTION

The upsurge in the increase in the use of fuel and environmental awareness of pollution has created the urge in many researchers to take up the perfect biodiesel from feedstocks (Sun et al. 1999). Biodiesel was extracted from the feedstocks of waxes, and classified into two namely, animal waxes and plant waxes. Palm stearin wax was classified as plant wax as it was extracted from palm trees. Naturally, waxes have long chain esters of fatty acids, which were converted from long chain esters to fatty acid methyl esters with the transesterification reaction (Hariram et al. 2017, Gelbard et al. 1995).

Gas chromatography coupled with mass spectrometry is a versatile tool for the separation, quantification and identification of unknown organic components and permanent gases. Analysis of complex mixtures can be done by combining sensitivity and high resolving power (Hariram & Vasanthaseelan 2015). The information obtained can be used for the detection of impurities, contamination control and improvement, for example, of semiconductor management. Various fatty acids concentrations were determined from the GCMS graph and ion concentration (Pereira et al. 2002). They depict many components that include ketones, hydrocarbons, ions, fatty acids and esters. FTIR was absorbed in bands that identified the various functional groups of molecules such as OH stretch, C-O and OH bending, C-C stretching, C-O

stretch, C-H stretching and C-C and C-O bending which was located based on the wavelength. FTIR stands for Fourier Transform Infrared Spectroscopy, the preferred method for Infrared spectroscopy.

Nuclear magnetic resonance (NMR) spectroscopy is a powerful analytical technique used in the characterization of organic molecules through the identification of carbon-hydrogen frameworks within the molecules. It determines the physical and chemical properties of atoms or the molecules in which they are contained. NMR has two classifications of variations such as C-NMR and H-NMR used in the characterization of organic structures (Hariram et al. 2017). H-NMR is used in the determination of the number of hydrogen atoms present in the molecules and C-NMR represented in the determination of the number of carbon atoms present in the molecules. NMR is used in the identification of the blending levels in biodiesel blends. This paper gives the hydrogen and carbon atoms present in the palm stearin biodiesel using the NMR spectroscopy method. The focus of the paper is on optimization of various properties of palm stearin biodiesel such as flash point, fire point kinematic viscosity, calorific value, density and iodine value determined and compared with the properties of diesel. The various properties of palm stearin biodiesel are seen in ASTM standards of ASTM D6751-07b and European standards (EN 14214).

Bharathwaaj et al. (2018) have carried out extraction of biodiesel from the species of mellifera waxes. Long chain fatty alcohols are present in the bee wax. Biodiesel determines the properties that include: density of 880 kJ/m³ and calorific value of 35.5 MJ/kg and the cetane number of 48. Arun Shankar et al. (2017) have indicated cottonseed biodiesel as produced from cottonseed oil using the transesterification process. Cottonseed biodiesel was characterized using the GC-MS and FTIR to find out the functional groups present in the biodiesel. The properties of biodiesel such as calorific value (36.18 MJ/kg, 33.78 MJ/kg), flash point (160°C) and kinematic viscosity and density have been predicted. Ng & Yung (2019) have characterized palm oil biodiesel and its blends. NMR was employed for accurate characterization of the oil and its blends. Folayan & Anawe (2019) have done extraction of the argan oil from its kernel. Fatty acid content was employed using the GCMS results. The measured properties of the argan biodiesel were in accordance with the American Society for Testing Methods standards. Eman et al. (2015) have carried out extraction of green algae (*Spirogyra longata*) which was characterized using GC-MS. In GC-MS apparatus, helium gas was employed as a carrier gas with the employment of impact ionization mode. GC graphs show the presence of valuable components such as ketones, phenolic, hydrocarbons. Fatty acids were defined using FTIR spectrum. Naureen et al. (2015) have done biodiesel extraction from sunflower oil used in the prediction of the characteristics of biodiesel using the GC-MS, FTIR and NMR. GCMS results indicated, the presence of seven saturated, one polyunsaturated and three monounsaturated fatty acid methyl esters in the biodiesel.

Monteiro et al. (2009) saw the NMR results of soybean and castor oils biodiesel which had a complex chemical composition, NMR helped prediction of the chemical components in biodiesel mentioned above. Knothe (2001a) reported numerous studies on biodiesel formation and its characterization such as GC/MS, NMR and HPLC methodology which showcased a non-linear behaviour in their corresponding FTIR spectra. Knothe (2001b) have used NMR spectroscopy to predict the vegetable oils and miscible oil with convenient diesel fuel. H-NMR was employed for the determination of the biodiesel fuel quality. Knothe (1999) did the exploration of the chemical structures predicted by the dominant technique that employed the nuclear magnetic resonance spectrometry. Shimamoto et al. (2017) have done characterization of soybean and castor oil. Monterio et al. (2009) have used H-NMR spectroscopy for the characterization of the quality of the biodiesel-diesel blend. H-NMR was used in the making of a higher concentration not exceeding 2% of biodiesel concentration. Portela et al. (2016) evaluated biodiesel content in the diesel fluid using the H-NMR spec-troscopy method. In this process, the multivariable regression model was generated by the use of partial least square (PLS).

In the current work, palm stearin biodiesel produced from palm stearin wax was characterized using NMR, FTIR and GC-MS. The molecular structure was predicted using GC-MS and compared with the NIST library. Characterization of the palm stearin biodiesel was done using FTIR for optimization of the functional groups present in biodiesel. NMR spectroscopy was used in the characterization of the biodiesel, it depicted the carbon and hydrogen groups presented in the biodiesel. In the present study, the properties of palm stearin biodiesel such as density, kinematic viscosity, flash point, fire point, calorific value were investigated through different experiments.

MATERIALS AND METHODS

Palm stearin biodiesel was produced in the laboratory using the palm stearin wax from the transesterification process. Techniques such as NMR, FTIR and GCMS were used for the characterization of palm stearin biodiesel.

Transesterification Process

Palm stearin bio-oil was produced by heating the palm stearin wax to 60°C. In the single-stage transesterification process, the FFA content was below 2%. The FFA content of the bio-oil was 0.3% which was satisfactory, the single-stage transesterification process was employed in this process. The main factors were methanol to oil molar ratio, catalyst concentration and reaction duration which had a significant role in the process. A three-necked 100 mL flask containing palm stearin with reflux container was used in this process. The temperature and speed of the magnetic stirrer were set at 60°C and 600rpm respectively. Initially, bio-oil was heated to 90°C for removing the moisture content in the bio-oil. An appropriate amount of methanol and a catalyst were taken for 100 mL bio-oil. Sodium methoxide solution was produced by mixing NaOH and methanol at 60°C at the speed of 600 rpm, it was mixed with the bio-oil to initiate the process. A magnetic stirrer was employed in this process for around 60 min for steering at a constant speed as shown in Fig. 1. The process took 60 minutes for the layer separation of glycerol and biodiesel. A clear separation was taken 12 hours. Biodiesel was cleaned using distilled water several times to remove the moisture content. After the transesterification process, the biodiesel was heated to 100°C to remove the water content and the excess methanol was present in the biodiesel.

Gas Chromatography and Mass Spectrometry (GC-MS)

GC-MS was used for the characterization of the organic components. This technique was performed using the gas
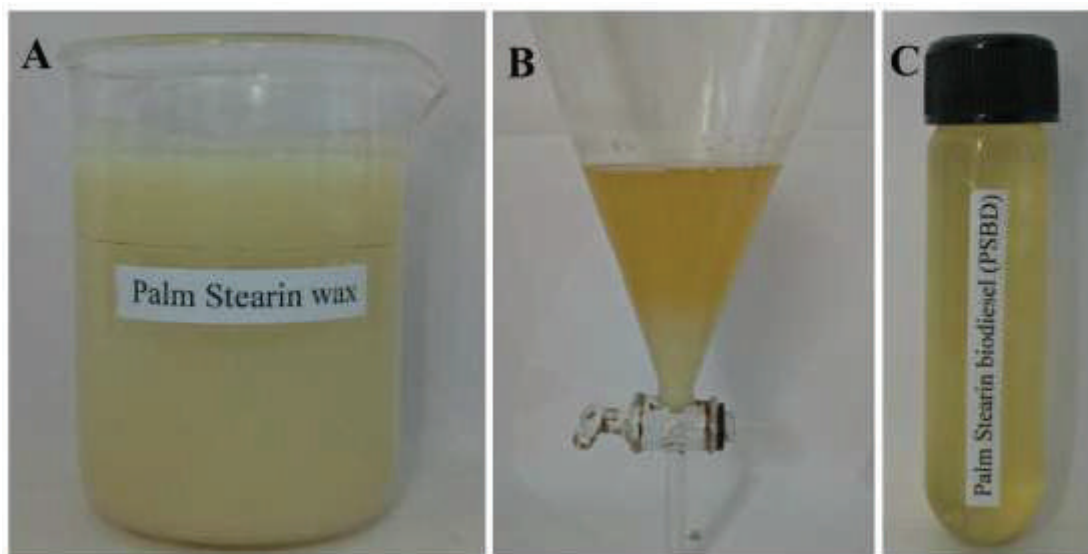
Fig.1: Transesterification process of palm stearin bio-wax.

chromatography and mass spectrometry to identify the samples. With the help of GC-MS, samples were distinguished into the individual compound by the temperature controlled capillary column. Associating and measuring the fragmentation of the unique mass spectrum (m/z) with NIST library, mass spectrum delivered the structural formula and molecular weight. GC-MS was used for the measurement of the molar mass and structural analysis of small biomolecules. In the present work, the JEOL GCMATE 2 GCMS with data system with the maximum resolution of 6000 Daltons with the sources of electron impact (EI), Chemical Ionization (CI) and fast atom bombardment (FAB) were employed. GCMS was employed for finding out the saturated and unsaturated fatty acids determined from retention time and ions.

Fourier Transform Infra-Red Spectrometry (FTIR)

With the help of the infra-red spectrometry, the fragmentation of samples in the infra-red region of the electromagnetic spectrum was absorbed. FTIR was used for the evaluation of the vibrations of organic components such as starching vibrations and bending vibrations of C-H, C-O, C=O component existing in the molecules. The type of the bond was determined by wavelengths of the radiation. FTIR spectrum was used in the estimation of some cases such as chemicals, pharmaceuticals, petroleum products, resins, etc. The Perkin Elmer system one FTIR/ATR instrument was used in this study. It has a scan range of 450-4000 cm^{-1} and resolution of 1.0 cm^{-1} and 50 mg sample was required to find out the results.

Nuclear Magnetic Resonance Spectroscopy (NMR)

Nuclear Magnetic Resonance spectroscopy is a very powerful non-invasive technique that provides detailed structural information relating to various molecular systems. Avance 3500 MHz NMR was employed in this study. NMR is a spectroscopy technique based on the absorption of electromagnetic radiation in the radio frequency regions 4 to 900 MHz by nuclei of the atom. But in the present work, the field strength of the NMR was 500 MHz. The CDCl$_3$ solvent dissolved in the samples in 1:1 ratio.

RESULTS AND DISCUSSION

Gas Chromatography and Mass Spectrometry

GCMS was used for carrying out the experiments to find out the various methyl esters present in the palm stearin biodiesel (Fig. 2). Methyl esters were predicted based on the retention time compound with the NIST library. There are ten various fragmentation patterns developed from the GCMS apparatus which helped determination of the methyl esters structure as tabulated in Table 1. The various retention times were predicted from RT 13.18 min to RT 26.68 min of gas chromatogram operation. Fig. 3A depicts the presence of dodecanoic acid, methyl esters with the highest peak mass ions 214 Daltons at a retention time of 13.18 min. Molecular structure was found to be methyl esters of lauric acid, with a concentration of 0.1%.

Fig. 3B presents the retention time of 15.75 min which had ester of methyl tetradecanoate. The highest mass to

change ratio was predicted at 242 Daltons, myristic acid was adopted as a fatty acid methyl ester with a concentration of 22.90%. Fig. 3C shows the pentadecanoic acid, 14, methyl esters fragmentation pattern at the reaction time of 18.43 with the highest value of peak mass ions of 270 Daltons which was present at the scan of 695 Daltons. Pentadecylic acid was shown as FAME which had a percentage of 25.8%. Fig. 3D portrays the retention time of 19.87 min with the fragmentation pattern of hexadecanoic acid, methyl esters. Palmitic acid was found to be a methyl ester. Methyl esters had a peak mass value of 270 Daltons located at scan 752. The presence of stearic acid is shown in Figs. 3E and 3F at

Table 1: Composition of FAME's in palm stearin biodiesel.

S. No	Retention time (min)	Name of the esters	Fatty acid methyl esters	% Conc.
1	13.18	Dodecanoic acid, methyl ester	Lauric acid	0.19
2	15.78	Methyl tetra deaconate	Myristic acid	22.09
3	18.43	Pentadecanoic acid, 14 -methyl, methyl ester	Penta-de-cyclic acid	23.71
4	19.87	Hexadecanoic acid, methyl ester	Palmitic acid	28.36
5	20.33	9 - Octadecanoic acid (2) - Methyl ester	Stearic acid	0.34
6	21.93	13,16 -Octadecadienoic acid, methyl ester	Stearic acid	0.15
7	22.53	11 - Eicosanoic acid, methyl ester	Arachidic acid	22.04
8	22.77	Eicosanoic acid, methyl ester	Arachidic acid	1.40
9	24.3	Decosanoic acid Methyl ester	Behenic acid	0.62
10	26.68	Octanoic acid, heptadecylic ester	Caprylic acid	1.10
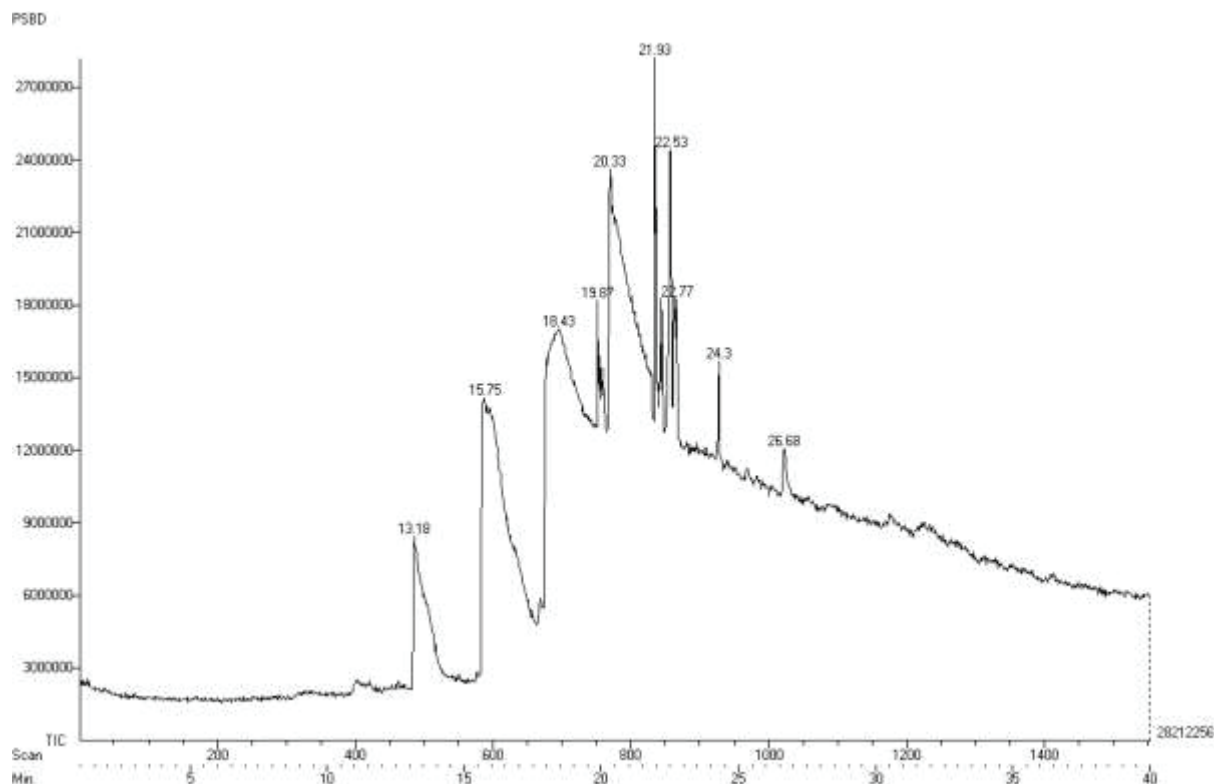
Fig. 2: GCMS chromatogram of palm stearin biodiesel.

the retention time of 20.33 min and 21.93 min which had a 9-octadecanoic acid and 13, 16 octadecadienoic acid, methyl ester. 300 Daltons of highest peak mass value was predicted from the fragmentation patterns of fatty acids.

Fig. 3G depicts the 11, eicosanoic acid and eiosanoic acid esters at the retention times of 22.53 min and 22.77 min which had the highest peak value such as 324 Daltons and 326 Daltons respectively. Molecular structure of arachidic
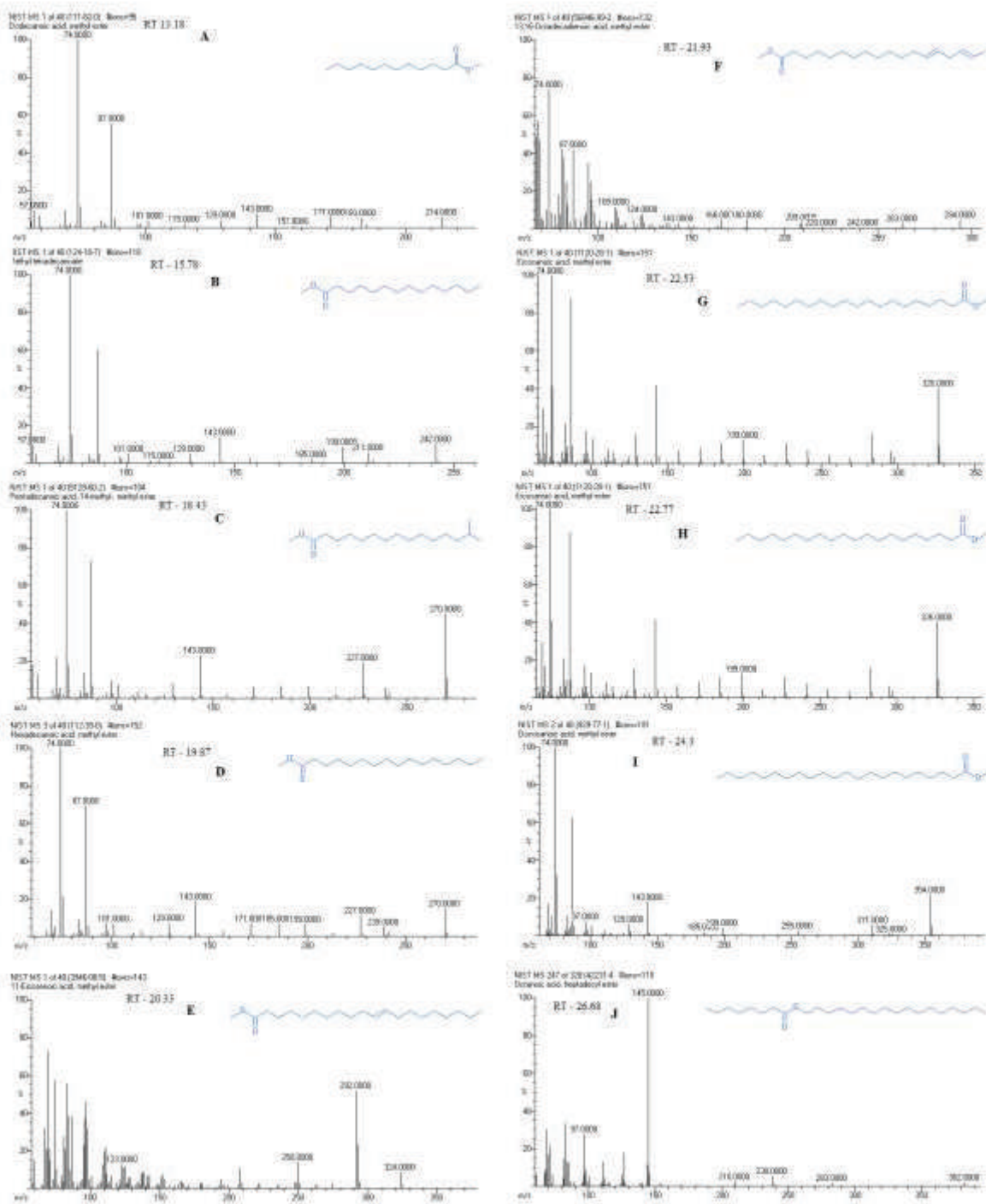
Fig. 3: Fragmentation pattern of palm stearin biodiesel.

acid was predicted from the fragmentation pattern (Hariram & Bharathwaaj 2015).

Fig. 3 presents the fragmentation pattern of the decosanoic acid, methyl esters at the retention time of 24.3 min with a structure of methyl esters to be behenic acid with the concentration of 0.6%, the highest peak value was predicted from the fragmentation pattern as 354 Daltons. Fig. 3J shows the octanoic acid, heptadecyl esters, which was present in the fragmentation pattern at the retention time of 26.68 min with the scan of 1023. Caprylic acid is a general fatty acid methyl ester of these esters which have a low value in concentration. 382 Daltons was predicted as the peak mass value of methyl esters. Finally, the palmitic acid and arachidic acid had a higher concentration in palm stearin biodiesel. Palmitic acid had a high value in the palm stearin biodiesel at the retention time of 19.87 min and 20.33 min.

Fourier Transform Infrared Spectroscopy (FTIR)

Fourier transform Infrared spectroscopy (FTIR) was used for the prediction of the alkyl groups, ester ketones and alcohol group from the wavelengths. Fig. 4 shows the organic and inorganic compounds present in the palm stearin biodiesel. FTIR braced the bonds and steeling such as C-O stretch, OH stretch and C=0, C-H bonds. In the present work, FTIR was

adopted for carrying out the experiments of palm stearin biodiesel. The Perkin ELMER system one FTIR spectroscopy was employed for finding the stretching and vibrations of various natural materials. FTIR was used in the determination of the organic and inorganic stretching vibrations and bonds present in palm stearin biodiesel. A graph has been generated by an instrument of FTIR which indicated the bonds according to wavelength in units of cm^{-1} and the transmittance as percentage placed in Y-axis.

Many vibrations have been created from the FTIR, practiced from 584.82 cm^{-1} to 2922.02 cm^{-1}. Fig. 4 depicts the presence of carboxylic acid and derivatives in O-H stretch present in the peak of 2922.02 cm^{-1} and another peak value of 1741.78 cm^{-1} which was present in the C=0 (saturated aldehyde) that was in aldehydes and ketone groups. The peak value of 1438 cm^{-1} revealed the presence of (α-CH_2 bending) aldehydes and ketones. α-CH_2 bending was present in the graph which shows in the peak value of 1260.66 cm^{-1} that is also in aldehydes and ketones. Some peak value was present in the same functional group which was in carboxylic acids and derivatives such as 1195.53 cm^{-1} which was indicated in the (0-C) (2 bands).

The peak value of 1242.33 cm^{-1} indicated the 0-C bands (sometimes 2 peaks) in carboxylic acids and derivatives. The
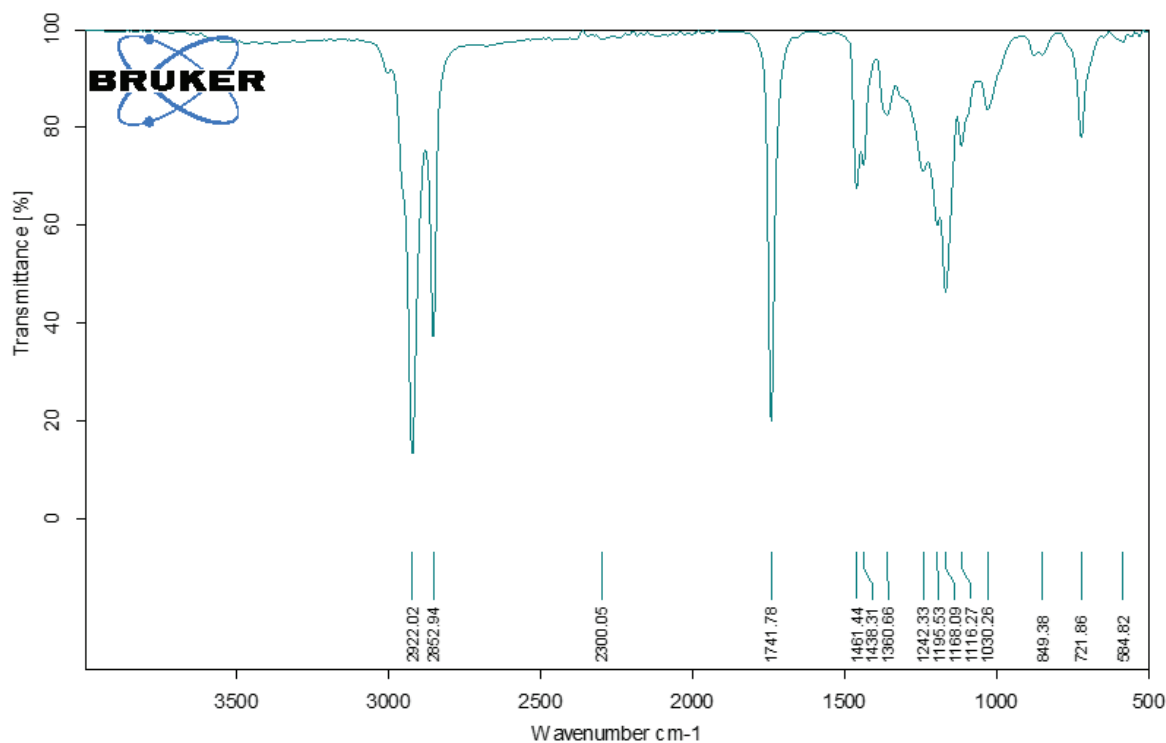
Fig. 4: FTIR spectrum of palm stearin biodiesel.

alkenes group was predicted from the peak value of 849.38 cm^{-1} and 721.86 cm^{-1} influenced in the process which had a functional group of alkenes indicating the CIS-RCH+CHR. The detailed groups of organic compounds and then stretchings and vibrations located in the FTIR spectrum as shown in Fig. 4.

Nuclear Magnetic Resonance (NMR)

Palm stearin wax is the feedstock for producing palm stearin biodiesel (PSBD). PABD mainly consists of stearin and oleins. The ^{13}C and ^{1}H NMR spectrum of PSBD have resemblance as shown in Fig. 5 and Fig. 6 respectively. The NMR spectrum (^{13}C and ^{1}H) of palm stearin wax and its biodiesel were compared. The prominent proton signal at 4.1-4.5 ppm with multiplets, multiplet peaks between 5.2 and 5.5 ppm and singlet peaks at 7.0 and 7.3 ppm of the palm stearin wax were no longer visible in the ^{1}H NMR. Similarly, singlet and multiplet peaks between 65 and 80 ppm of the palm stearin wax were no longer seen in the palm stearin biodiesel. These shifting of peaks indicate the efficiency of transesterification in the formation of fatty acid methyl esters. The palm stearin biodiesel which is the resultant product of transesterification, the palm stearin wax along with methanol reveals the presence of olefinic hydrogen atoms and methoxyl hydrogen atoms as singlet and multiplets peaks (Simpson 2012).

OCH$_3$, singlet peaks at 3.67 ppm and 3.49 ppm confirm the presence of methoxyl hydrogens, whereas multiplet peaks between 5.25 and 5.36 ppm confirm the presets of olefinic hydrogen. The singlet peak was seen at 7.25 ppm of H-NMR indicating the presence of multiple multiplet peaks between 0.8 and 2.4 ppm indicating the presence of aliphatic hydrogens. The absence of the peak between 4.5 and 5 ppm in the ^{1}H NMR along with the existence of olefinic hydrogens indicate the feedstock used in the transesterification process as having a vegetable based origin. The olefinic and methoxyl hydrogen signals of palm stearin wax and its biodiesel were integrated and calibrated. The existence of a linear relationship between the methoxyl and olefinic hydrogen atoms was observed. This relationship was also confirmed by the FTIR studies (Hariram 2019).

Intrinsic Characteristics of Properties of Palm Stearin Biodiesel

The properties of palm stearin biodiesel such as kinematic viscosity, flash point, fire point, calorific value and iodine
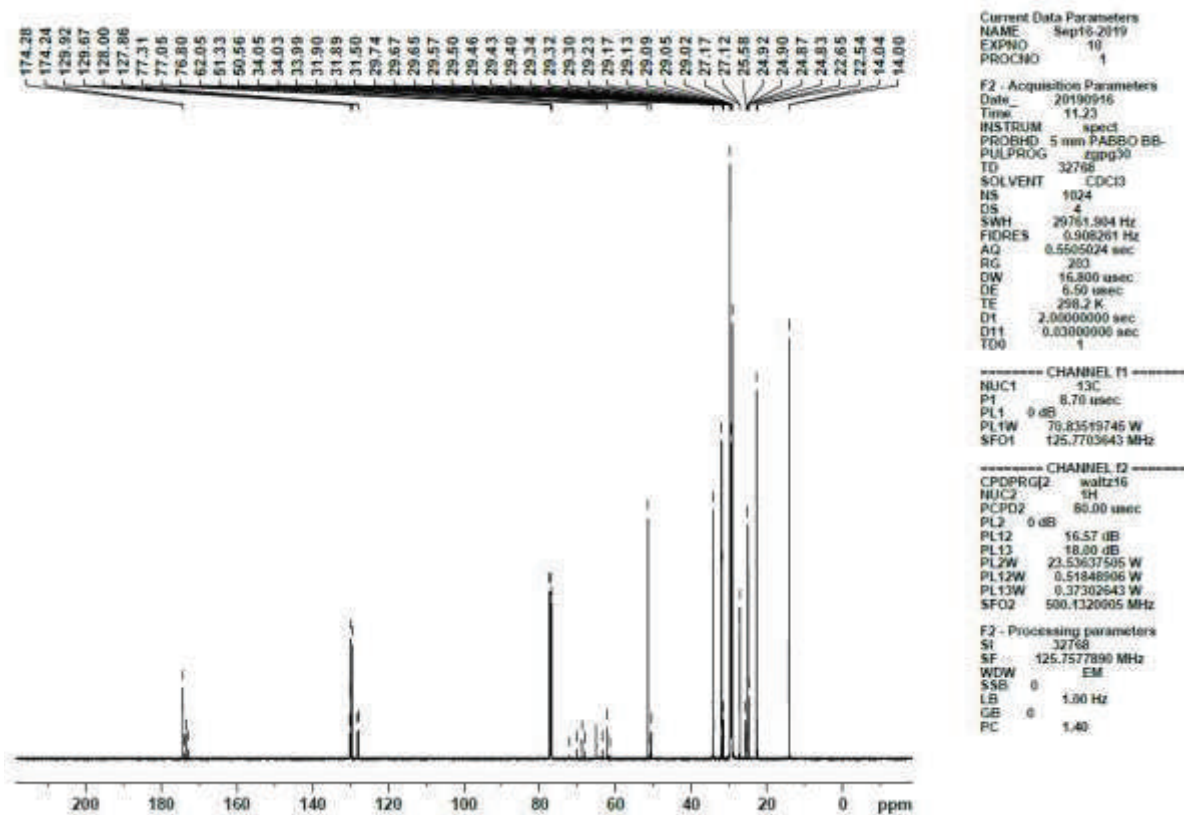
Fig. 5: ^{13}C NMR spectrum of palm stearin biodiesel.
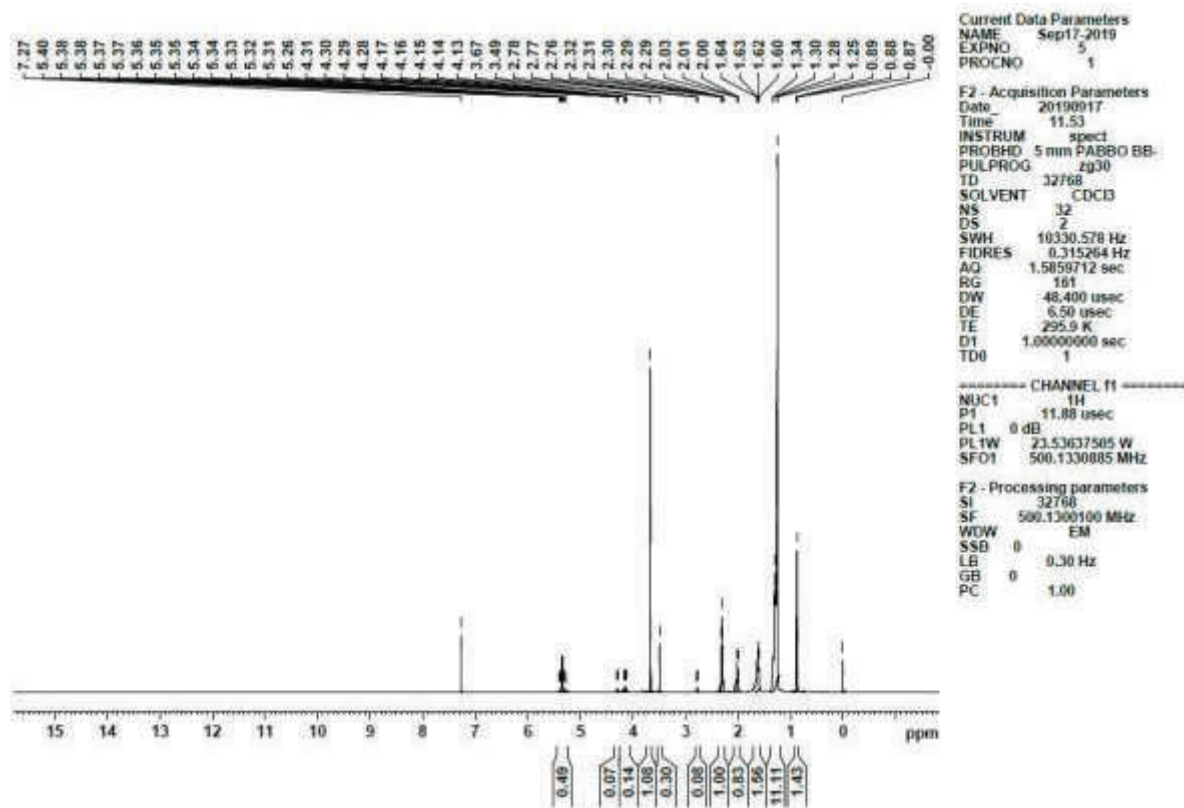
Fig. 6: ^{1}H NMR spectrum of palm stearin biodiesel.

value were characterized using ASTM standard methods as indicated in Table 2.

Kinematic viscosity is the main factor which influences the compression process. It has old and hot kinematic viscosities that affect the engine. Palm stearin bio-oil has a high kinematic viscosity ranges which do not fit the combustion process, that affect the entire engine setup. Palm stearin biodiesel, which had a significant kinematic range fitted for ASTM standards and European standards was produced following the transesterification process. Palm stearin biodiesel has a kinematic viscosity at 35°C of 2.4mm^2/s, which is in ASTM standards among 1.9-6.0 mm^2/s ASTM D6751 and EN14214 were placed in the fuel properties. Flashpoint is the lowest temperature at which the fuel is flashable in the presence of air. Generally, diesel has a flashpoint of 47°C. Palm stearin biodiesel has a flashpoint of 244°C which is in correct proportion compared with the ASTM standard limits. In comparison, the flashpoint of the diesel and palm stearin biodiesel, diesel has a low flashpoint temperature which fluids use in easy combustion. Palm stearin has a high flashpoint temperature and takes a long time to ignition leading to ignition delay. Minimum

Table 2: Physio-chemical properties of PSBD and mineral diesel.

Properties	PSBD	Diesel
Density @ 18°C (g/m^3)	0.88	0.8200
Kinetic viscosity @ 35°C (mm^2/s)	2.4	2.5
Calorific value (kJ/kg)	37121	42957
Flashpoint	244	47
Fire point	166	140

flashpoint regions are used for easy combustion and proper safety (Hariram 2016).

The fire point is one of the factors of characterization of the fuels. Fire points of the palm stearin biodiesel are predicted using the fire point apparatus which has a value of 166°C temperature compared to the value of 140°C related to diesel. They had similar values of fire point. Calorific value is defined by the amount of energy released from the fuels with the help of the combustion. Palm stearin biodiesel has a calorific value of 37121 kJ/kg related to the value of diesel as 42957 kJ/kg. The physio-chemical properties of the palm stearin biodiesel were found to be within ASTM standards. Ignition delay is identified when the calorific value is low. High calorific value improves engine efficiency. Calorific value is employed as the main factor in the process of combustion. Density was predicted from the experiments made in the laboratory. Palm stearin has a density of 0.88 g/m^3 at 18°C which is in line with ASTM standards. Diesel has a density value of 0.8200 g/m^3. Density is also a main factor in the combustion process which influences engine performance (Pimental et al. 2006, Demirbas 1997).

CONCLUSION

This article has discussed the characterization of the palm stearin biodiesel. GC-MS and FTIR spectrometer have proved the ten fatty acids in the palm stearin biodiesel and the C-H stretch, C-O stretch and organic components present in biodiesel. Gas chromatography and mass spectrometry results indicate the palmitic acid and myristic acid having the main role in palm stearin biodiesel. The GC-MS, FTIR and NMR results show the proof of the palm stearin biodiesel of the appropriate biodiesel. Kinematic viscosity of the palm stearin biodiesel to be 3.4 mm^2/s at 35°C and the density at 18°C be 0.88 g/m^3 were seen as the properties of biodiesel. The calorific value of the palm stearin biodiesel was 37,121 kJ/kg. The flash and fire points predicted using the apparatus were 130°C and 166°C. All the physio-chemical properties of palm stearin biodiesel satisfied and were in accordance with the ASTM standard limits. So, the palm stearin biodiesel is suitable for normal compression ignition engines as an alternative fuel without any major modifications.

REFERENCES

Arun Shankar, A., Prudhvi Raj Pentapati and Krishna Prasad, R. 2016. Biodiesel synthesis from cottonseed oil using homogeneous alkali catalyst and using heterogeneous multi walled carbon nanotubes characterization and blending studies. Egyptian Journal of Petroleum, 26:125-133.

Bharathwaaj, R., Nagarajan, P. K., Kabeel, A. E., Madhu, B., Magesh Babu, D. and Ravishankar Sathyamurthy 2018. Formation, characterization and theoretical evaluation of combustion of biodiesel obtained from wax esters of *A. mellifera*. Alexandria Engineering Journal, 57: 1205-1215.

Demirbas, A. 1997. Calibration of higher heating values of biomass fuels. Fuel, 76(5): 431-434.

Eman, I. Abdel-Aal and Amany, M. Haroon Jelan Mofeed 2015. Successive solvent extraction and GC-MS analysis for the evaluation of the phytochemical constituents of the filamentous green alga *Spirogyra longata*. Egypt. J. Aquatic Res., 41(3): 233-246.

Folayan, A.J. and Anawe, P.A.L. 2019. Synthesis and characterization of *Argania spinosa* (Argan oil) biodiesel by sodium hydroxide catalysed transesterification reaction as alternative for petro-diesel in direct injection, compression ignition engines. Heliyon, 5(9): e02427.

Gelbard, G., Brès, O., Vargas, R.M., Vielfaure, F. and Schuchardt, U.F. 1995. ^{1}H nuclear magnetic resonance determination of the yield of the transesterification of rapeseed oil with methanol. J. Am. Oil Chem. Soc., 72(10): 1239-1241.

Hariram, V. and Bharathwaaj, R. 2015. Extraction and optimization of biodiesel yield from wax esters of *Apis melifera* (Honey bee). Int. J. Chem. Tech., 8(9): 433-437.

Hariram, V. and Vasanthaseelan, S. 2015. Optimization of base catalysed transesterification and characterization of *Brassica napus* (Canola seed) for the production of biodiesel. International Journal of Chem. Tech. Research, 8(9): 418-423.

Hariram, V., Godwin John, J. and Seralathan, S. 2017. Cotton seed biodiesel as alternative fuel: Production and its characterization analysis using spectroscopic studies. International Journal of Renewable Energy Research, 7(3): 1333-1339.

Hariram, V., Godwin John, J. and Seralathan, S. 2019. Spectrometric analysis of algal biodiesel as a fuel derived through base-catalysed transesterification. International Journal of Ambient Energy, 40(2): 195-202.

Hariram, V., Seralathan, S., Dinesh, K. M., Vasanthaseelan, S. and Sabareesh. 2016. Analyzing the fatty acid methyl esters profile of palm kernel biodiesel using GC/MS, NMR and FTIR techniques. Journal of Chemical and Pharmaceutical Sciences, 9(4): 3122-3128.

Hariram, V., Seralathan, S., Micha Premkumar, T. and Penchala Tharun 2017. Reduction of exhaust emission using a nano-metallic enriched lemongrass biodiesel blend. Energy Sources, Part A: Recovery, Utilization and Environmental Effects, 39(21): 2065-2071.

Knothe, G. 1999. Rapid monitoring of transesterification and assessing biodiesel fuel quality by near-infrared spectroscopy using a fiber-optic probe. J. Am. Oil. Chem. Soc., 76(7): 795-800.

Knothe, G. 2001a. Analytical methods used in the production and fuel quality assessment of biodiesel. Trans. ASAE, 44(2): 193-200.

Knothe, G. 2001b. Determining the blend level of mixtures of biodiesel with conventional diesel fuel by fiber-optic near-infrared spectroscopy and ^{1}H nuclear magnetic resonance spectroscopy. J. Am. Oil Chem. Soc., 78(10): 1025-1028.

Monteiro, M.R., Ambrozin, A.R.P., da Silva Santos, M., Boffo, E.F., Pereira-Filho, E.R., Lião, L.M. and Ferreira, A.G. 2009. Evaluation of biodiesel-diesel blends quality using ^{1}H NMR and chemo metrics. Talanta, 78(3): 660-664.

Monterio, M.R., Ambrozin, A.R.P., Lião, L.M. and Ferreira, A.G. 2009. Determination of biodiesel blend levels in different diesel samples by ^{1}H NMR. Fuel, 88(4): 691-696.

Naureen, R., Tariq, M., Yusoff, L., Chowdhury, A.J.K. and Ashraf, M.A. 2015. Spectroscopic and chromatographic studies of sunflower oil biodiesel using optimized base catalysed methanolysis. Saudi J. Biol. Sci., 22(3): 332-339.

Ng, M.H. and Yung, C.L. 2019. Nuclear magnetic resonance spectroscopic characterisation of palm biodiesel and its blends. Fuel, 257: 116008.

Pereira, J. A., Casal, S., Bento. A. and Oliveira, M. 2002. Influence of olive storage period on oil quality of three Portuguese cultivars of *Olea europaea*, Cobrancosa, Madural and Verdeal Transmontana. J. Agric. Food Chem., 50(1): 6335-6340.

Pimental, M.F., Ribeiro, G.M., Da Cruz., Pacheco Filho, J.G.A. and Teix-

eira, L.S. 2006. Determination of biodiesel content when blended with mineral diesel fuel using infrared spectroscopy and multivariate calibration. Microchem. Journal, 82(2): 201-206.

Portela, N.A., Oliveira, E.C.S., Neto, A.C., Rodrigues, R.R.T., Silva, S.R.C. and Castro, E.V.R. 2016. Quantification of biodiesel in petroleum diesel by ^{1}HNMR: Evaluation of univariate and multivariate approaches. Fuel, 166(15):12-18.

Shimamoto, G.G., Bianchessi, L. F. and Tubino, M. 2017. Alternative method to quantify biodiesel and vegetable oil in diesel-biodiesel blends through ^{1}H NMR spectroscopy. Talanta, 168: 121-125.

Simpson, J.H. 2012. Organic Structure Determination Using 2-D Nmr Spectroscopy: A Problem-Based Approach. Academic Press. DOI:10.1016/C2010-0-65520-9.

Sun, R. C. Fang, J. M. and Tomkinson, J. 1999. Fractional isolation and structural characterization of lignins from oil palm trunk and empty fruit bunch fibers. J. Wood. Chem. Technol., 19(4): 335-356.

Original Research Paper   https://doi.org/10.46488/NEPT.2020.v19i03.009   Open Access Journal

An Improved InVEST Ecological Service Evaluation Model Based on BP Neural Network Optimization

Feng Wang†, Wenlong Chen and Lei Niu

School of Computer and Information Engineering, Fuyang Normal University, Fu Yang 236037, PR China
†Corresponding author: Feng Wang; wf111625@163.com

ABSTRACT

The land is the material basis for human survival, and the contradiction between people and land has become increasingly prominent. The land ecological problem has gradually become a hot spot of concern. It is imperative to make a scientific evaluation of the land ecological quality and propose reasonable and feasible improvement measures and recommendations. At present, domestic research on environmental cost and environmental cost degradation mostly focuses on theoretical discussion, and there are few applications and practical research on enterprise environmental cost management. Based on the principle of protecting the ecological environment, this paper creates an ecological service assessment model to assess the real economic cost of land use development projects. From small community projects to large-scale national projects, because environmental costs are difficult to estimate, this paper uses the recovery cost method and the preventive expenditure method to quantify environmental costs. The cost of environmental degradation mainly comes from water pollution and air pollution. This paper uses the pollution function method to quantify the cost of environmental degradation. The InVEST model is used to evaluate the value of ecosystem services, and the BP neural network method is used to optimize the ecosystem service model, and the sensitivity analysis of the data is used to feedback the impact of the project on ecosystem services. The ecosystem service model based on neural network optimization makes the accuracy of data measurement results reaching 99.7%, which makes the model having a good generalization. Taking a paper mill as an example, this paper evaluates environmental costs by resource consumption cost, environmental degradation value and environmental governance cost, and estimates environmental degradation costs by major environmental governance costs. Finally, the environmental cost and environmental degradation cost are integrated, and the ecosystem service model is established. The neural network model was established in the Matlab environment based on the InVEST model, and the model simulation results of the ecosystem service system were obtained. Compared with the InVEST results, the results of this paper have better authenticity and market utilization value. Although a paper mill was used as an example, the system was evaluated and the evaluation results were analysed. Compared with the actual situation, there is a certain reliability. However, due to the limited data, the number of verifications is insufficient for the system. It is hoped that more data can be verified later to ensure its reliability.

INTRODUCTION

Ecosystem services are the biosphere that provides many natural processes to maintain a healthy and sustainable human living environment. Accelerate the reform of the ecological civilization system, adhere to the harmonious coexistence between man and nature, and coordinate the management of the landscape system. The improvement of people's living standards is inseparable from the construction of various engineering projects, but the construction of these projects will bring economic benefits and directly affect biodiversity and lead to environmental degradation. At this stage, most land development projects do not take into account the economic costs of changes in the ecosystem services: river pollution, air pollution, solid waste pollution. Therefore, the environmental cost of research projects is necessary for the development

of enterprises. This paper takes a paper mill as an example to investigate the actual data of project development and construct an evaluation model for the environmental cost control of the project.

Traditionally, most land development projects only consider the project investment cost in the cost calculation and do not take into account the environmental costs caused by environmental degradation in production. Environmental degradation restricts ecosystem services. Therefore, the study of ecological service assessment models requires an assessment of environmental costs. Environmental costs include polluted rivers, poor air quality, hazardous waste sites, improperly treated wastewater, and climate change.

This paper presents the following four questions:

(1) Assess the environmental costs of development projects;

(2) Assessing the environmental degradation costs of development projects;
(3) Establish ecological service assessment model;
(4) Using a paper mill as an example to evaluate the effectiveness of the model.

HYPOTHESES AND SYMBOLIC DESCRIPTIONS

Assumptions

- Assume that exhaust gas pollution caused during mining and transportation is not considered.
- Assume that only the influencing factors mentioned in the text are considered.
- Assume that the data in the text are correct.
- Suppose the parameters used in the text are correct.

Symbol Description

Symbol	Definition
w_i	The weight of the input signal corresponding
x_i	The input signal
θ	The threshold
f	The activation function
net_i	The neurons
P_r	The cost of repairing natural resources
C_i	Repair and compensation for the unit cost of i resources
Q_i	The number of fixing i resources

ASSESSMENT OF ENVIRONMENTAL COSTS

The Significance of Studying Environmental Costs

The production and management activities of humans and enterprises will bring some negative impacts to the environment. Some industrial enterprises have high pollution characteristics and have a very bad impact on the ecological environment. The survival and development of an enterprise will affect the environment, but the survival and development of the enterprise depend to a large extent on the gift of the ecological environment. Starting from the micro-level, the environmental problems caused by the enterprise itself will not only generate expenditures other than production costs, but also affect itself, the surrounding environment and the social environment, damage its own social image, and cause the consequences of lowering the economic interests of the enterprise. From a macro perspective, if a country does not carry out environmental protection and prevention when building a business, it will violate the international environmental protection rules and affect the country's overall national strength and international influence. In summary,

enterprises must pay attention to their environmental problems, so environmental cost accounting is a necessary measure. Through environmental cost accounting, we can find the environmental pollution problems generated by enterprises, to clarify the environmental costs of enterprises and to find environmental pollution problems of enterprises to curb environmental pollution and protect ecological environment resources (Li et al. 2011).

Concept and Classification of Environmental Costs

Since enterprises rarely calculate environmental costs into cost expenditures, there is currently no uniform standard for classification and calculation of environmental costs. Different enterprises have different footholds when accounting for environmental costs. For environmental costs, there is no precise definition for the time being. By analysing the cost of expenditure on environmental impacts, environmental costs can be divided into costs incurred in restoring a damaged environment, reducing the costs of pollution in the production process, and preventing the costs of environmental pollution.

Assessment of Environmental Costs

According to the cost source, it can be divided into recovery cost method, preventive expenditure method and pollution function method (Pan et al. 2019). The recovery cost method is generally difficult to accurately measure the cost of environmental damage directly, but it can be replaced with the idea that the expenditure required to restore the damaged natural resources to the previous state is used to measure the value of the damaged environmental resources. In general, natural resources are self-recovering, but if humans over-exploit and destroy natural resources, the natural world cannot be restored to the former state, and it is necessary to use human power to recover the environment. It is called "recovery compensation fee". For example, planting and maintaining the felled forest to restore it to its original state.

Its accounting model is: $P_r = \sum C_i Q_i$

Where, P_r is the cost of repairing natural resources, C_i is for repair and compensation, i is the unit cost of the resource, Q_i is the amount of resources for repair and pollution.

Preventive expenditure method refers to taking preventive measures to avoid or reduce environmental pollution. For example, in a polluted environment, people buy an air purifier to purify the air. The cost of purchasing an air purifier is to prevent expenditure. Pollution function method refers to the use of the correlation function method to measure the environmental costs of pollutants (wastewater, waste gas, solid waste) emitted by the enterprise during the production and operation process.

Environmental costs of certain liquid/gas pollutants: $Cl_i = V \times l \times t \times C_0$

Where, Cl_i is to prevent environmental costs of a liquid/gas pollutant; V is the volume of a liquid/gas contaminant; l is the concentration of a liquid/gas pollutant; t is the pollution equivalent value of a liquid/gas pollutant; C_0 is the environmental pollution cost per unit volume of a liquid/gas pollutant.

Total liquid/gas pollutant cost: $CL = \sum_{i=1}^{n} Cl_i$

Environmental costs of certain types of solid contaminants: $C = V \times f$

Among them, V is the volume of solid waste; f is the environmental cost per unit volume of solid contaminants.

ASSESSMENT OF ENVIRONMENTAL DEGRADATION COSTS

The Significance of Assessing the Cost of Environmental Degradation

The development and utilization of land projects will bring environmental pollution. In particular, some highly polluting projects can exacerbate environmental degradation (Zhao 2016). Environmental degradation affects the image of the company and inhibits its efficiency. Therefore, the survival and development of an enterprise cannot be separated from a good ecological environment.

Concept of Environmental Degradation Costs

Environmental degradation refers to the unreasonable development and utilization of natural resources by human beings, causing changes in the structure of ecosystems, leading to a decline in the self-regulation of ecosystems and a decline in function, which is not conducive to the survival and development of humans and living beings. The cost of environmental degradation is also called environmental pollution loss, including the degradation of natural degradation caused by environmental degradation, and the loss of human health.

Assessment of Environmental Costs

The cost of environmental degradation is difficult to estimate and is generally translated into other losses due to environmental degradation (Yang 2017). For example, the cost of environmental degradation of air pollution is studied, and human health loss and crop yield loss, which account for a large proportion of pollution losses, are evaluated (State Forestry Administration 2014). The main cause of environmental degradation costs is water pollution and air pollution. Therefore, environmental costs are assessed by the

cost of water and air pollution (Wang 2014). According to the pollution function method mentioned above:

Environmental costs of certain liquid/gas pollutants: $Cl_i = V \times l \times t \times C_0$

Total liquid/gas pollutant cost: $CL = \sum_{i=1}^{n} Cl_i$

Therefore, the estimated environmental degradation costs are: $CL = \sum_{i=1}^{n} Cl_i$

ECO-SERVICE ASSESSMENT MODEL

InVEST Model

The InVEST model (Yang et al. 2012) consists of three modules: Freshwater ecosystem assessment, marine ecosystem assessment and terrestrial ecosystem assessment, each of which contains specific assessment projects. Freshwater ecosystem assessments include water production, flood regulation, water quality and soil erosion; marine ecosystem assessments include shoreline formation, coastal protection, aesthetic assessment, aquaculture, habitat risk assessment, overlay analysis, wave energy assessment. terrestrial ecosystem assessments include biodiversity, carbon stocks, pollination and wood production. The InVEST model is hierarchically designed as shown in Table 1.

The level 0 model assesses the relative level of ecosystem services or significant areas of special service demand. For example, coastline mapping in InVEST draws only coastlines that are particularly prone to erosion and flooding, without assessing ecosystem functioning, Grab the simplest model of the nature of the problem.

The Level 1 model is suitable for obtaining more data than level 0, but still meets relatively few data requirements. The first level model can be used to determine the differential biodiversity of the ecosystem service function area, and the ecosystem function under current or future conditions. Regional differences and biodiversity, all primary models can output absolute value and provide users with an economic valuation option.

The Level 2 model can more accurately describe the service value and function of the ecosystem. The results of the assessment are important for environmental protection measures and environmental compensation. The level 3 model is suitable for special areas such as fisheries.

Our model will use a 2-level model to more accurately describe the ecological environment. The BP neural network will also be used to optimize the 2-level model. The results of the evaluation will be adjusted by project planners and managers to reach to expected indicator.

Table 1: Grading design of InVEST model.

Level 0 model	Level 1 model	Level 2 model	Level 0 model
Relative value	Absolute value	Absolute value	Absolute value
No evaluation	Evaluate through a range of methods	Evaluate through a range of methods	Evaluate through a range of methods
Generally no strict time, No annual average	Average time step, no time series	Time step from day to month, have a wide time series	Time series are associated with feedback and value domains
From the basin to the appropriate spatial range of the world	From the basin to the appropriate spatial range of the world	From a small area to the world	From a small area to the world
Suitable for determining important areas(high risk or specialized ecological service area)	Suitable for strategic decision (make a strategic decision based on criteria)	Suitable for the tactical decision, making with absolute value	More accurate assessment of ecosystem services
No interaction between ecosystem services	Interaction between individual ecosystem services	Interaction between individual ecosystem services	Complex ecosystem interactions with feedback and thresholds

InVest Model Applied to Ecological Service Assessment

Ecosystem services mean that the biosphere provides many natural processes to maintain a healthy and sustainable human living environment.

An ecological service evaluation model that the InVest model applies to ecological services is shown in Table 2.

Model Optimization

We used the BP neural network to optimize the ecological environment assessment method of a paper mill. After obtaining the environmental data of a paper mill, data cleaning and fitting methods are used to obtain more reliable data, and the data can meet the requirements of training neural networks. And using a part of the actual data as the test data reached a good expectation, making the accuracy of the BP neural network model reach 99.7%. The use of our trained BP neural network in the national area has also yielded good results.

EXAMPLE APPLICATION

Assessment of Environmental Costs of A Papermaking Enterprise

According to the life cycle idea, the environmental cost that a paper mill may cause during the production and operation process is divided into four parts: raw material mining, product production, product sales and disposal according to the whole process of paper products from raw materials to production to waste stage [Yu 2018.]. Considering that paper products are a kind of material that can be degraded by nature, the environmental impact in the circulation and disposal stages is relatively small. Therefore, this paper mainly accounts for the environmental costs of the two stages of mining raw materials and product production.

Stage of mining raw materials: The cost of the raw material extraction phase includes the following two parts: Part of it is the loss of forest resources caused by the mining of wood and coal; the other part is the cost of the exhaust gas emitted by the vehicles that transport the raw materials (Zheng 2013], but this part of the cost cannot be calculated because the relevant data cannot be obtained.

In 2018, from Table 3, we can get the following conclusion: The pulp consumption of the paper-making enterprise was 10,999.75 tons. The raw materials of pulp were mainly wood pulp and waste paper pulp, of which wood pulp accounted for 34.5%, and waste paper pulp accounted for

Table 2: InVEST Model Module Evaluation Project.

Freshwater ecosystem module	Marine ecosystem module	Terrestrial ecosystem module
Hydroelectric power	Expand check, create GS	Biodiversity
The water quality	Coastal protection	Carbon storage
Water rate	The Marine water quality	Crop pollination
Soil and water conservation	Ecological risk assessment	Wood production
	The aesthetic evaluation	
	Aquaculture	
	Superimposed analysis	

65.5%. The wood converted from paper pulp can be used to calculate the wood consumed.

Wood pulp consumption of wood: $10999.75 \times 34.5\% \times 4.75 = 18025.84 m^3$

Waste wood pulp consumption: $10999.75 \times 65.5\% \times 3 = 21614.51 m^3$

Total amount of wood consumed: $18025.84 + 21614.51 = 39640.35 m^3$

The amount of wood per hectare in the forest is 89.79 m3; forest cost per hectare is about 3,700\$. (7 in the following formula refers to the exchange rate of RMB against the US dollar.)

The resulting forest loss costs: $P_1 = (39640.35/89.79) \times 2.49/7 = 169$ (\$)

In 2018, it consumed 183,100 tons of coal, and the cost of forest loss was calculated according to the recovery cost method.

Mining one ton of coal will disturb 1.1 tons of topsoil, with an average bulk density of 1.7 tons per cubic meter of soil; a soil thickness of 0.3 meters; and a forest value of 24,900 per hectare.

The resulting forest loss costs: $P_2 = [183100 \times 1.1 /(1.7 \ 0.3)] \times 2.49 / 104 \times 10000 / 7 \ 140486$ (\$)

Total forest loss costs:

$P = (1099.28 + 98.34) \times 10000 / 7 = 1710886$ (\$)

Production product stage: The environmental costs incurred during the production phase were calculated based on the pollution generated by the production process of the product. The production process of the product includes pulping section, papermaking section, coating section and processing section. The pollutants produced during the production process mainly include wastewater, waste gas, waste residue and noise. The environmental cost at this stage is mainly reflected in the environmental damage cost caused by pollutant discharge and the environmental governance, prevention and management costs invested by the enterprise.

Environmental Damage Costs

Calculation of wastewater discharge fee: After the wastewater discharged from a paper mill is treated by the company's wastewater treatment system, most of the wastewater is recycled and reused. From Table 4, we can get the following conclusion: The reuse rate of wastewater is 88.79%, and the amount of wastewater to be treated is 88.3 m^3/a.

According to the environmental cost measurement method mentioned above,

Processing CODcr costs: $Q_1 = 191680 \div 1 \times 0.7 / 7 = 134176$ (\$)

Handling nh3-n costs: $Q_2 = 250 \div 0.8 \times 0.7 / 7 = 31.25$ (\$)

Total cost of wastewater treatment: $Q = (134176 + 218.75)/ 7 = 1919.25$ (\$)

Calculation of exhaust gas discharge fee: In 2018, the total amount of exhaust gas produced by a paper mill was 1,446,600 standard cubic meters. The content of the exhaust gas components is shown in Table 5.

Dealing with sulfur dioxide costs: $R_1 = 564160 \div 0.95 \times 0.6 / 7 = 50901.65$ (\$)

Dealing with nitrogen oxides costs: $R_2 = 324760 \div 0.95 \times 0.6 / 7 = 29301.65$ (\$)

Dealing with soot costs: $R_3 = 62780 \div 2.18 \times 0.6 / 7 = 2468.41$ (\$)

Dealing with the total cost of atmospheric pollutants: $R = (356311.58 + 205111.58 + 17278.90)/ 7 = 87671.71$ (\$)

Calculation of carbon emission costs: In 2018, a paper-making enterprise emitted 338,100 tons of carbon dioxide. Although carbon dioxide is not an air pollutant, carbon

Table 3: Wood conversion amount of paper pulp in the paper industry.

Product	Direct consumption of raw materials	Wood folding amount/m^3×t
Wood pulp	Logs, logs, residues	4.75
Waste pulp	Waste paper	3

Table 4: Disposal of wastewater from the Paper Mill in 2015 (Li & Ren 2011).

Amount of wastewater (Ten thousandm^3/a)	Contaminant		Average missions
88.3	CODcr	Concentration (mg/L)	217
		Production amount (t/a)	161.68
	NH3-N	Concentration (mg/L)	0.28
		Production amount (t/a)	0.25

Table 5: Disposal of atmospheric pollutants by a paper mill in 2018 (Li & Ren 2011).

Exhaust gas volume (Ten thousandm3/a)	Contaminant		Average emissions
	SO$_2$	Concentration (mg/Nm^3)	390.50
		Production amount (t/a)	564.16
144.66	NOx	Concentration (mg/Nm^3)	224.5
		Production amount (t/a)	324.76
	Smoke	Concentration (mg/Nm^3)	43.4
		Production amount (t/a)	62.78

dioxide is the most important greenhouse gas, causing global warming and the melting of glaciers. Therefore, carbon dioxide emissions should be treated. The average price of carbon dioxide in 2018 is 6$ per ton.

Carbon emission costs: $338100 \times 6 = 2028600$ ($)

Calculation of sewage charges for solid waste: In 2018, the total amount of solid waste generated by a papermaking enterprise was 72,885.49 tons. The company's solid waste safe disposal rate reached 100%, and the comprehensive utilization rate reached 99.2%. Since the solid waste generated by a paper mill can be safely disposed of 100%, the comprehensive utilization rate reaches 99.2%, and the zero discharge to the external environment is basically realized. The damage caused to the environment can be neglected.

Calculation of noise discharge fee: To reduce the harm of production noise to the personnel in the plant and surrounding neighbourhoods, the company makes reasonable arrangements for the noise-generating equipment in the factory, installs noise-proof walls around the plant, installs silencers at the noise source of the equipment, and constructs green belts for the plant area. As well as avoiding night time transportation and other means, noise reduction will reduce the noise pollution below the national environmental standards, and will not adversely affect the environment and surrounding people. Therefore, it can be determined that the noise emission fee of the plant is zero.

In summary, the environmental costs of pollutant emissions: $W = Q + R = 89590.6$ ($)

Corporate Environmental Governance Costs

Table 6 shows the cost of a paper mill's environmental governance costs divided into seven projects.

Depreciation costs for environmental protection facilities: 720.92 (ten thousand dollars)

Environmental Prevention Costs

Environmental prevention cost refers to the environmental protection costs invested by enterprises to avoid environmental pollution, such as pollution source discharge monitoring systems installed by enterprises, testing fees, and environmental education training for relevant personnel. In 2018, the depreciation expense of the pollution source discharge monitoring system was about 9429$, and the entrusted inspection department commissioned the inspection fee of 1572$, and the environmental protection education and training fee for the relevant personnel was about 5714$.

Through the above calculations, the environmental costs of a paper mill are shown in Table 7.

Assessment of Environmental Costs of A Papermaking Enterprise

The main cause of environmental degradation costs is water pollution and air pollution. Therefore, environmental costs are assessed by the cost of water and air pollution (Zhao 2016).

The environmental degradation cost of a papermaking

Table 6: Environmental protection facilities costs and annual depreciation.

Project	Total/ten thousand	Annual depreciation/ten thousand
Eastern district wastewater recovery facility	297.55	14.13
Western district wastewater recovery facility	28.3	1.35
Incoming wastewater treatment facility	18.88	0.9
Paper machine white water recycling facility	119	5.65
Flue gas treatment facility	203.16	9.65
Noise control	1.48	0.07
Pollution source online monitoring	19.86	0.94

Table 7: Environmental cost report of a paper mill in 2018.

Stage	Cost type	Accounting object	Result/ten thousand
Production phase	Damage cost	Sewage charges	13.44
		Disposal cost	57.87
		Carbon cost	1174.90
		Solid waste cost	0
		Noise cost	0
	Governance cost	Governance	243617
	Prevention cost	Prevention	11.7

enterprise is the sum of the cost of treating water pollution and air pollution.

The environmental degradation costs of paper companies: 101.87 (ten thousand dollars)

Assessment of Ecological Services in The Paper Mill

Using BP neural network to optimize the evaluation method in InVEST, because there is less data disclosure for a paper mill, we will use the fitting method to generate more data and then adjust the data reasonably, including data cleaning and normalization. In the process of fitting, we mainly use the NumPy library in Python to fit (Fig. 1), and get the fitted equation:

$$f = 1.009x^2 - 37.64x + 3.78e + 04$$

To get the final cost of a paper mill in treating wastewater, treating waste gas, treating solid waste, and treating noise, we input the known data as input neurons into our BP neural network model and then train through the NEWFF function in MATLAB. For neural network objects, we have 10 neurons in the hidden layer, 3 neurons in the output layer, and 500 steps in the maximum number of training steps. The training data has 75 different data in the factory over the years. Set the learning rate to 0.05 and the minimum error of the training target to 0.001 (Fig. 2).

Finally, our BP neural network model converges after 495 iterations (Fig. 3).

The gradient size is 0.042 (Fig. 4):

Then carry out regression analysis (Fig. 5):

The final accuracy rate reached 97.33%.

ADVANTAGES AND DISADVANTAGES OF THE MODEL

Model Advantage

(1) In the process of establishing the InVEST model, the second-level model was used, which enabled the eco-environment administrator to have a certain impact on
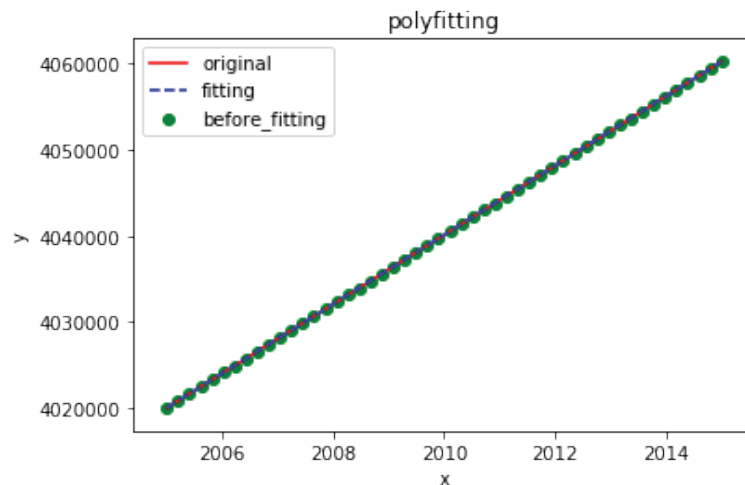
Fig. 1: Fitted function image.
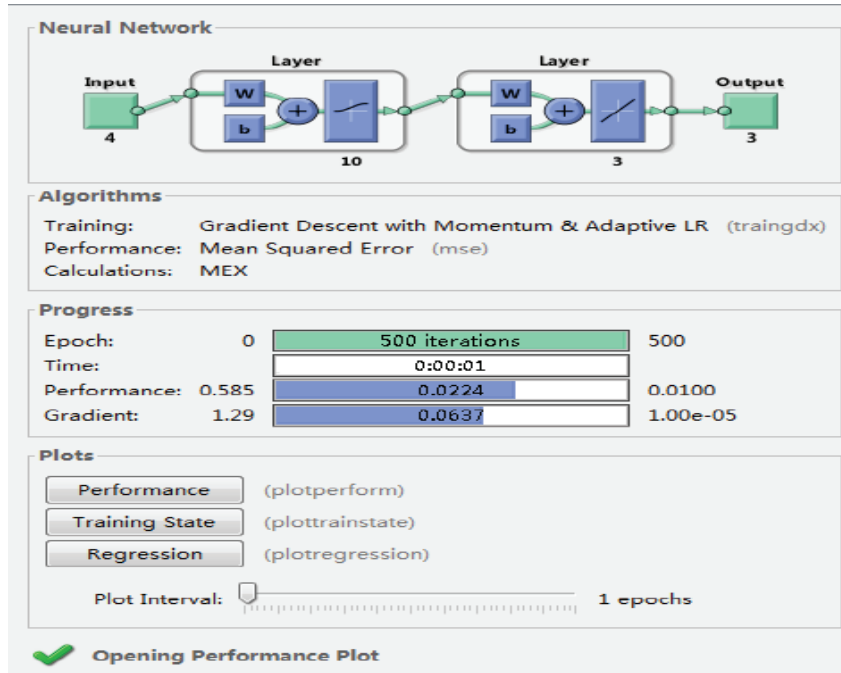
Fig. 2: Results of BP neuron training.

the environmental change, enabling the environmental administrator to participate in the prediction model. We use BP neural network to optimize the weight of each factor in the ecological environment in the InVEST model, and we get better results by example.

(2) Using the specific data to verify the InVEST model, so that the robustness of the model is improved.

Model Defect

The system establishes a system model of natural environment assessment, but the model is not perfect at the regional criteria level. I hope to consider adding more regional indicator factors in future work to meet the natural environment assessment model.
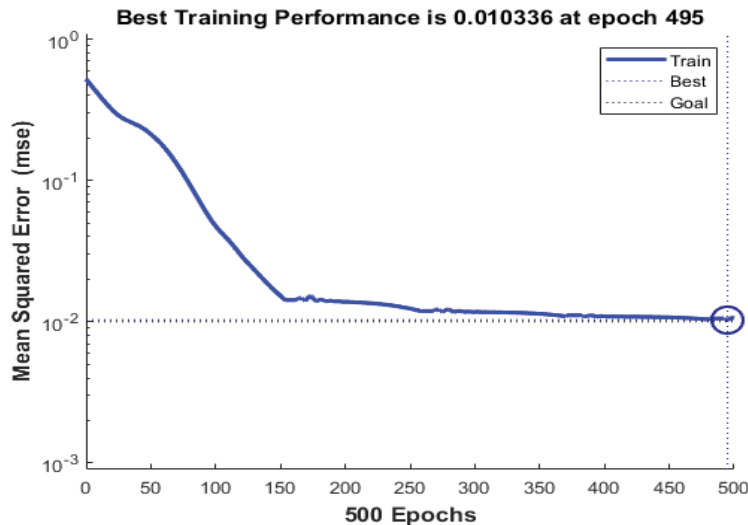
Fig. 3: Image of gradual convergence of neurons.
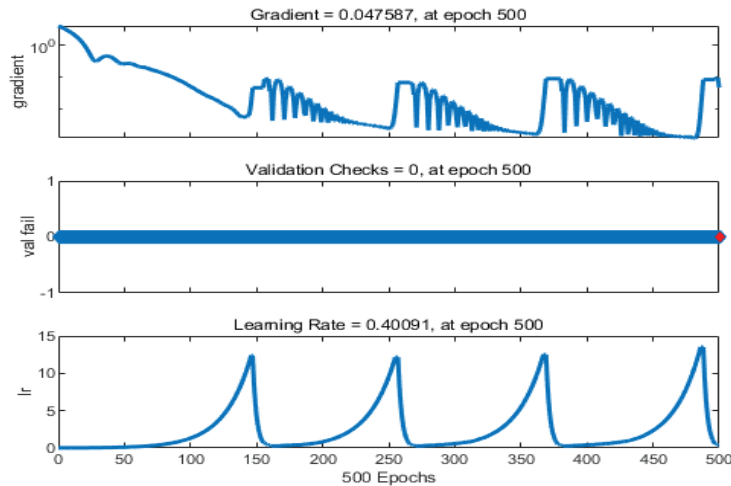
Fig. 4: Neural network training process diagram.
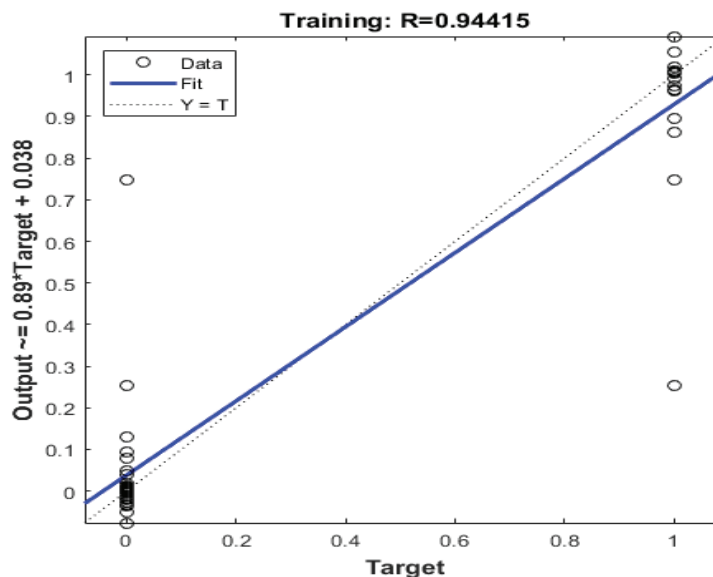
Fig. 5: Image of neurons for regression analysis.

(1) In the survey and data acquisition, a lot of data comes from statistical yearbooks and papers. Some data are missing. In our model, the fitting method is used, which has certain inaccuracy.

(2) Some parameters are based on common sense because very little data can be used.

CONCLUSIONS

Mathematical formulas are established through specific mathematical meanings, and the recovery cost method, preventive expenditure method and pollution function method are defined to quantify the environmental cost and environmental degradation cost, and the true economic cost of the project is clearly expressed in the form of data. The InVEST model is used to evaluate the value of ecosystem services, and the BP neural network method is used to optimize the ecosystem service model. Through the sensitivity analysis of the data, the model simulation results of the ecosystem service system were obtained. Taking a paper mill as an example, based on data generated in previous years, the value of ecosystem services in paper mills was assessed. It can be concluded that the paper mill's management of pollutants has reached an excellent state, and its management method can

be improved and promoted. This research has guiding significance and practical enlightenment for the environmental management of heavy polluting enterprises and has a good market utilization value.

This paper takes a paper mill as an example to evaluate the ecology of the paper mill's location using the ecological service assessment model and the evaluation results were analysed. Compared with the actual situation, the model has a certain reliability. However, the relevant data of this paper mill are insufficient, and the model of this paper cannot be applied to the assessment of ecological services in other places. I hope that there will be more data in the later stage, and I will continue to improve through verification to get a more reliable model.

ACKNOWLEDGEMENT

REFERENCES

Li, J.W. and Ren, B.P. 2011. Research on the path of coordinating China's environmental pollution and economic growth conflict. China Population, Resources and Environment, 21(5): 132-139.

Pan, W.X. and Liu, S.D. 2019. Optimization research and application of BP neural network. Computer Technology and Development, 5: 1-3.

State Forestry Administration 2014. Results of the 8th National Forest Resources Inventory. Forestry Resources Management, 2: 1-2.

Wang. C.M. 2014. Cost Calculation Model and Application Research of Environmental Degradation Based on Air Pollution Intensity. Nanjing: Nanjing University of Information Science and Technology.

Yang, Y.Q. 2017. Research on Enterprise Environmental Cost Accounting System. Zhengzhou: Zhongyuan Institute of Technology.

Yang, Y. Y., Dai, E.F. and Fu, H. 2012. Research framework of value evaluation of ecosystem service function based on InVEST Model. Journal of Capital Normal University, 33(3): 41-47.

Yu, H.F. 2018. Research on Environmental Cost Accounting of X Steel Company. Xi'an: Xi'an Petroleum University.

Zhao, L.M. 2016. Research on Air Quality Prediction and Spatial-Temporal Distribution in Guangzhou Based on Genetic Algorithm and BP Neural Network. Jiangxi University of Technology.

Zhao, Q.X. 2016. Research and Implementation of Land Ecological Assessment System. School of Environment and Surveying.

Zheng, Q.H. 2013. Material flow analysis of timber resources in China's paper industry supply chain. China Paper, 6: 21-27.

Evaluation Index System Construction for Geological Environmental Bearing Capacity and Its Application in Henan Province, China

He Ziguang*†, Zhang Yujiao*, Huang Lei**, Duan Zhao*** and Lin Jianhao*

*Institute of Architecture Engineering, Huanghuai University, Zhumadian 463000, China
**Water Conservancy and Civil Engineering College, Inner Mongolia Agricultural University, Hohhot 010018, China
***College of Geology and Environment, Xi'an University of Science and Technology, Xi'an 710054, China
†Corresponding author: He Ziguang; hzg198762@163.com

ABSTRACT

Geological environment is a resource base, environmental base, and engineering base for human socioeconomic activities. The main function of the geological environment is to provide stable and safe living space and essential resources for the existence and development of human society. However, geological environmental problems become increasingly prominent in some provinces in China due to fragility of the geological environment, uneven population distribution, backward economic development, and massive construction projects. The function of geological environments in some provinces to support sustainable economic and social development is evidently insufficient, and the threshold values of their geological environmental bearing capacity nearly reach the upper limit. For example, Henan Province, China, an evaluation index system for geological environmental bearing capacity, was established from three aspects, as follows: natural hazard, geological disaster, and disaster control. The weights of evaluation indexes were calculated using the variation coefficient method. Finally, the geological environmental bearing capacity of Henan Province during 2010-2018 was measured through the comprehensive evaluation method. Results showed that the constructed evaluation index system for geological environmental bearing capacity, which consisted of 34 indexes, was scientific and reasonable. During 2010-2018, the geological environmental bearing capacity of Henan Province was superior or excellent. Geological environmental bearing capacity can be improved by reinforcing the construction of legal rules and laws for geological environmental protection, carrying out research work regarding geological environmental bearing capacity, launching geological environmental monitoring and early warning system construction, and implementing feasibility demonstration for the geological environment of major construction projects. The study results can provide practical guidance and reference to realize the predictive analysis of geological environmental bearing capacity and coordinate human socioeconomic activities and geological environment.

INTRODUCTION

Geological environment refers to the surface space of lithosphere, which interacts with hydrosphere, atmosphere, and biosphere and is closely related to human activities. It is also a material base and prerequisite for sustainable social development of human beings. Human activities are also based on the natural environment, most of which are closely associated with the geological environment. Geological environmental bearing capacity is the maximum ability of the geological environment to bear the influences and changes brought by human activities. It is an important environmental constituent part in studies on resource environmental bearing capacity. As an important factor used to measure sustainable human development, it can reflect the coordination degree between human activities and geological environmental system. Effective resource distribution and utilization, efficient utilization of land resources, and preventive treatment of geological

environment are urgent problems faced by China in the eco-environmental construction and new-type urbanization process under the major background of capacity utilization reform, supply-side structural adjustment, and socioeconomic updating and upgrading. Especially because of enormous environmental pollution, various geological environmental problems emerge, such as surface subsidence, sand liquefaction, soil salinization, water and soil corrosion, and a partially high degree of mineralization of shallow underground water. Scientific understanding and handling of these geological environmental problems are greatly important to infrastructure construction and resource development and utilization.

Featured by complicated natural geological conditions and fragile ecological environment, Henan Province in China is distributed with special unfavourable geological environmental conditions and severe geological disasters. Moreover, numerous geological environmental problems

are triggered by human activities in Henan Province. Special unfavourable geological environmental conditions mainly include special unfavourable rock and earth mass (collapsible loess and swell-shrinking soil), primary geochemical anomaly (high fluorine water, low iodine water, and saline water), and secondary geochemical anomaly (soil salinization). Geological disasters include collapse, landslide, debris flow, water and soil loss, surface collapse, water inrush of the pit, and gas explosion. Geological environmental problems include exhaustion of water resources, water contamination, and stacking of solid wastes. These factors have become important in restricting the improvement of people's living standards and socioeconomic development in Henan Province. Regional environmental features in Henan Province indicate that its economic development is mainly restricted by geological environmental problems. Thus, studying the geological environmental bearing capacity for economic activities in this region is especially important. Therefore, on the research basis of regional geological environmental background in Henan Province, investigating the influence factors of the regional geological environment on economic activities and evaluating its geological environmental bearing capacity have great theoretical and realistic significance for regulating socioeconomic activities and realizing coordinated development between geological environment and social economy.

PAST STUDIES

Geological environmental bearing capacity is the extension of the environmental bearing capacity theory. It lays particular emphasis on sustainable development and protection of the geological environment. Geological environment is the environmental base for human society. With the emergence of numerous environmental problems and elevated requirements for geological environmental development and protection, studies on the geological environment have gradually developed, initially from susceptibility and danger grading of geological disasters and then to geological environmental quality evaluation until the present studies on geological environmental bearing capacity. Rees (1992) proposed ecological footprint method to evaluate geological environmental bearing capacity by comparing ecological footprints at supply level and ecological bearing capacity at demand level for geological environmental bearing capacity. Fuchu et al. (1994) investigated topography, geology, soil types, and properties and their distribution range in Tongchuan City, as well as main geotechnical engineering and geological environmental problems induced by human engineering activities. Lew (2001) evaluated some developable areas in California, and the results showed that the existence of active

earthquake fault, young loose alluvial deposit, and shallow groundwater was a factor possibly resulting in geological liquefaction in many areas in California. Youquan (2004) analyzed water resource bearing capacity of Wei River basin based on the introduced water resource distribution features of Gansu segment of Wei River basin as well as the existing effective output and bearing capacity. The results showed that the optimal bearing capacity of water resources in this area was 3,550,000 people. Wackernagel et al. (2004) deemed that the damage of rock slope on the Himalayas was a common feature and proposed concrete measures of improving rock stability on the Himalayas. Dill et al. (2005) built a lithofacies relief model for African savannah in the south of Malawi, acquired the evaluation results of rock bearing capacity, and put forward measures of reinforcing geological disaster prediction. Chuan-Ming et al. (2007) expounded the concept of geological environmental bearing capacity, highlighted the geological environmental bearing capacity features based on sustainable development and environmental bearing capacity, and introduced the evaluation process of geological environmental bearing capacity. Chang-Fei et al. (2011) combined actual pile foundation of the marine drilling platform, considering geological drilling of Shuangtaizi estuary engineering, to analyze and discuss the bearing capacity characteristics of mucky strata at Shuangtaizi estuary. Wagner et al. (2013) deemed that the increasing urbanization and construction of high-rise buildings in Meshed of Iran affected the geological environmental bearing capacity. They used sequential indicator simulation and sequential Gaussian simulation methods to establish a 3D geological engineering model for standard penetration test results of Meshed sedimentary deposits. The results showed that civil engineering causes fierce change to the geological environment of Meshed sedimentary basin. Qi-Shan et al. (2015) believed that the geological environmental bearing capacity was poor in covered karst area, and the groundwater development and utilization led to karst collapse. Then, they proposed measures of improving geological environmental bearing capacity in karst areas. Jiang-Ping et al. (2015) explored into soil layer stability and bearing capacity in this area with geophysical interpretation data of offshore areas in the North Sea in Guangxi Province. The results showed that this area is a complicated and diversified marine engineering geological environment, and the overall stability of clayey soil was evaluated. Wang et al. (2017) studied geological environmental bearing capacity in Guizhou karst area, used AHP to perform a numerical simulation of limestone solubility in different areas in Guizhou, and constructed a quantitative method combining these factors. Existing studies have shown to lay particular emphasis on

quantitative evaluation of bearing capacity. The study areas vary in natural, social, and economic conditions, evaluation factors are diverse, and different evaluation methods are applied among studies on bearing capacity. Thus, no mature, complete, and acknowledged research system has been formed in the quantitative measurement process, few studies have involved spatial distribution pattern of regional bearing capacity and identifying the associations among quality, scale, and spatial distribution of bearing capacity is difficult. Geological environmental bearing capacity and its quantitative research are keys to accurately and quantitatively master regional geological environmental bearing capacity. Theoretical studies on bearing capacity have contributed to comprehensive and in-depth studies on bearing capacity. The introduction and development of various mathematical models have greatly improved quantitative level and accuracy of bearing capacity studies. The bearing capacity research methods have developed from single-index static analysis into multiobjective, dynamic, and comprehensive system analysis. Therefore, in Henan Province, China, for example, the changing trend of geological environmental bearing capacity was analyzed from time dimension by comprehensively combing index systems of geological environmental bearing capacity established in the existing studies to enrich the connotations of geological environmental bearing capacity and propose reference suggestions for adjustment of geological environmental bearing capacity.

MODEL PROFILE AND INDEX SYSTEM

Model Profile

(1) Dimensionless processing of indexes: Evaluation indexes vary in dimension; thus, if they are directly calculated, then the results are impacted. Therefore, performing dimensionless processing of the evaluation indexes is necessary. Positive indexes are processed in formula (1), as follows:

$$Y_{ij} = \frac{X_{ij} - X_{i\min}}{X_{i\max} - X_{i\min}} \qquad \ldots(1)$$

For negative indexes, the processing method in formula (2) is used, as follows:

$$Y_{ij} = \frac{X_{i\max} - X_{ij}}{X_{i\max} - X_{i\min}} \qquad \ldots(2)$$

In formulas (1) and (2), Y_{ij} denotes the value of the jth evaluation index of class i after standardization; X_{ij} represents the actual value of the jth evaluation index of class i; $X_{i\max}$ is the maximum value of evaluation indexes of class i; $X_{i\min}$ is the minimum value of evaluation indexes of class i.

(2) Variation coefficient method: Variation coefficient method is used to calculate the weight of each evaluation index. As an objective calculation method, the variation

coefficient method can avoid the influence brought by subjective factors. This method can directly use the information contained in the indexes and calculate their weights. The calculation process is as follows. First, the mean value and standard deviation of each index are calculated in formulas (3) and (4), as follows:

$$\overline{X_i} = \frac{1}{n} \sum_{j=1}^{n} X_{ij} \qquad \ldots(3)$$

$$S_i = \sqrt{\frac{1}{n-1} \sum_{j=1}^{n} (X_{ij} - \overline{X_i})^2} \qquad \ldots(4)$$

Then, the variation coefficient is calculated in formula (5), as follows:

$$Z_i = \frac{S_i}{\overline{X_i}} \qquad \ldots(5)$$

The weight of each index is calculated in formula (6), as follows:

$$W_i = \frac{Z_i}{\sum_{i=1}^{n} Z_i} \qquad \ldots(6)$$

In formulas (3)-(6), i is the class of evaluation index; j is the concrete index under each class of evaluation index. The present foreign evaluation methods of geological environmental bearing capacity mainly include ecological footprint method, state-space method, and comprehensive evaluation method. A comprehensive evaluation model is established on the basis of the comprehensive evaluation method. This method, which is also called multivariable comprehensive evaluation method, uses multiple indexes to evaluate multiple objects participating in the evaluation. The comprehensive evaluation model is feasible and effective with the advantages of strong pertinence, comprehensive analysis contents, easy data acquisition, convenient calculation, and comprehensible evaluation results. It can realize accurate evaluation of geological environmental bearing capacity, which is complex, fuzzy, and variable. The comprehensive evaluation model can be expressed using formula (7), as follows:

$$P = \sum_{i=1}^{n} Y_i \bullet W_i \qquad \ldots(7)$$

In formula (7), P is the geological environmental bearing capacity of the evaluation object; Y_i is the value of the i (th) evaluation index of the evaluation object after nondimensionalization; W_i is the weight of the ith evaluation index of the evaluation object. The classification standard proposed in most studies on geological environmental bearing capacity is divided into four grades, namely, superior, good, medium, and poor using interval method, and the grading standard is given in Table 1.

Index System

Geological environmental bearing capacity is a description of the regional man-land systematic relationship. Thus, indexes are selected mainly from two aspects, namely, "land" and "man." "Land" mainly contains resource subsystem, environmental subsystem, and regulating subsystem; "man" usually includes subsystems, such as population, society, and economy. Variables directly related to the geological environment are mainly considered in the selection of concrete indexes. In addition, indexes, which are incorporated and organized or could be acquired through simple calculation, are selected from national, local, and industrial statistical data. Then, attention is focused on the coordination with the statistical method and various standards in industries such as geology and environmental protection. The established index system for geological environmental bearing capacity in Henan Province is given in Table 2. The investigation period is 2010-2018, and data are derived from the China National Statistical Database.

RESULT ANALYSIS

The collected data are calculated according to the above formula, and the standard deviation, mean value, and variation coefficient of all indexes are calculated, as given in Table 3.

According to formula (7), the geological environmental bearing capacities of Henan Province during 2010-2018 are calculated, as shown in Fig. 1.

Fig. 1 shows that during 2010-2018, the geological environmental bearing capacity in Henan Province is superior or excellent in most of the times. Henan Province is a flat terrain with few faults and geological disasters and good engineering geological conditions. Moreover, it is a developed industry and commerce with convenient transportation and complete infrastructure. However, human engineering activities in Henan Province include dispersive small-scale mining in addition to farming activities in recent years. The quantity of geological disasters is large, but the scale is small. Abundant geological tourism resources are available, but the degree of development and utilization is relatively low; the vegetation cover index is large. Henan Province shall take the lead in establishing exit and access system to measure and evaluate standards following the influence of engineering projects on the geological environment. Meanwhile, depending on various advantages in abundant geological relics, folk custom, and other tourism resources, Henan Province should cultivate and strengthen its green industries, such as tourism, culture, and characteristic agricultural products. Especially in 2011, the geological environmental bearing capacity was only 0.36 in Henan Province, fully indicating that geological
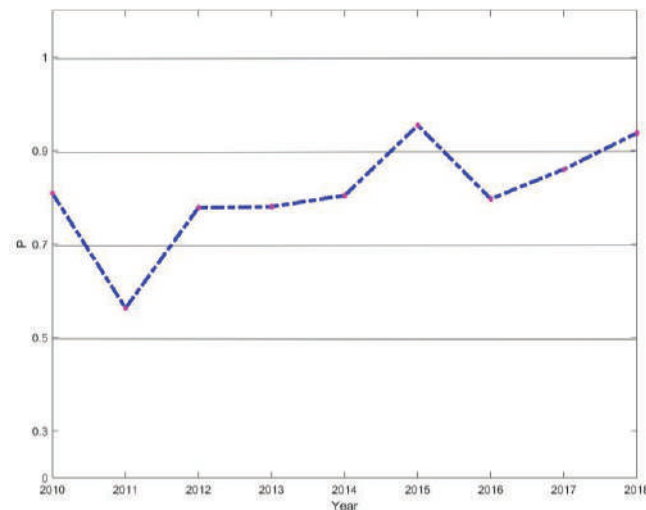

Fig. 1: Geological environmental bearing capacities of Henan Province during 2010-2018.

Table 1: Grading standard of geological environmental bearing capacity.

State	Superior	Good	Medium	Poor
Grading interval	≥0.9	(0.7, 0.9)	(0.5, 0.7)	(0, 0.5)

Table 2: Index system of geological environmental bearing capacity.

First-level index	Second-level index	Unit
Natural disaster	Crop damage area	One thousand hectares
	Crop failure area	One thousand hectares
	Drought-stricken area	One thousand hectares
	Drought-induced crop failure area	One thousand hectares
	Flood, landslide, debris flow, and typhoon-stricken area	One thousand hectares
	Flood, landslide, debris flow, and typhoon-induced crop failure area	One thousand hectares
	Hailstorm-stricken area	One thousand hectares
	Hailstorm-induced crop failure area	One thousand hectares
	Natural disaster-hit population	Ten thousand people
	Natural disaster-induced death population	People
	Direct economic loss of natural disaster	One hundred million yuan
Geological disaster	Number of geological disasters	Number of times
	Number of landslide disasters	Number of times
	Number of collapse disasters	Number of times
	Number of debris flow disasters	Number of times
	Number of surface subsidence disasters	Number of times
	Geological disaster-induced direct economic loss	10 thousand yuan
	Number of geological disaster prevention and control projects	Ea
	Investments on geological disaster prevention and control	10 thousand yuan
Disaster control	Total afforestation area	One thousand hectares
	Artificial afforestation area in the year	One thousand hectares
	Hillsides closed to facilitate afforestation on nonforest land and open-forest land	One thousand hectares
	Land use area in forestry	10 thousand hectares
	Forest area	10 thousand hectares
	Man-made forest area	10 thousand hectares
	Forest coverage rate	%
	Total standing forest stock	One hundred million cubic meters
	Forest growing stock	One hundred million cubic meters
	Investments completed for industrial pollution control	10 thousand yuan
	Investments completed for wastewater management projects	10 thousand yuan
	Investments completed for waste gas management projects	10 thousand yuan
	Investments completed for solid waste management projects	10 thousand yuan
	Investments completed for noise control projects	10 thousand yuan
	Investments completed for other governance projects	10 thousand yuan

environmental protection started late in Henan Province with inefficient measures, insufficient funds, dispersive management, and low consciousness, which were the primary causes for the weak foundation. Moreover, many departments are involved in geological environmental protection problems, along with common problems of barriers between high and low levels; each department attends to its own duties and disunity. With insufficient funds, implementing exploration and governance of geological disasters is difficult. Villages cannot realize required relocation, and consequently, some people are stricken in the threats imposed by geological disasters. The geological disaster information system in

Table 3: Standard deviation, mean value, and variation coefficient of indexes.

Index	Unit	Standard Deviation	Mean value	Variation Coefficient
Crop damage area	One thousand hectares	519.77	1119.85	0.46
Crop failure area	One thousand hectares	60.49	78.07	0.77
Drought-stricken area	One thousand hectares	636.13	640.28	0.99
Drought-induced crop failure area	One thousand hectares	72.08	53.36	1.35
Flood, landslide, debris flow, and typhoon-stricken area	One thousand hectares	418.51	433.52	0.97
Flood, landslide, debris flow, and typhoon-induced crop failure area	One thousand hectares	29.96	30.41	0.99
Hailstorm-stricken area	One thousand hectares	56.58	104.43	0.54
Hailstorm-induced crop failure area	One thousand hectares	6.22	6.71	0.93
Natural disaster-hit population	10 thousand people	770.06	1549.23	0.50
Natural disaster-induced death population	People	43.41	37.14	1.17
Direct economic loss of natural disaster	One hundred million yuan	52.53	85.51	0.61
Number of geological disasters	Number of times	182.79	106.18	1.72
Number of landslide disasters	Number of times	168.95	77.89	2.17
Number of collapse disasters	Number of times	9.84	8.65	1.14
Number of debris flow disasters	Number of times	5.62	3.36	1.67
Number of surface subsidence disasters	Number of times	7.94	17.59	0.45
Geological disaster-induced direct economic loss	10 thousand yuan	5315.15	3550.01	1.50
Number of geological disaster prevention and control projects	Ea	20.04	15.40	1.30
Investments on geological disaster prevention and control	10 thousand yuan	3996.30	4858.23	0.82
Total afforestation area	One thousand hectares	38.32	197.03	0.19
Artificial afforestation area in the year	One thousand hectares	39.05	153.58	0.25
Hillsides closed to facilitate afforestation on non-forest land and open-forest land	One thousand hectares	14.33	32.49	0.44
Land use area in forestry	10 thousand hectares	5.25	456.58	0.01
Forest area	10 thousand hectares	14.70	329.04	0.04
Man-made forest area	10 thousand hectares	6.22	206.90	0.03
Forest coverage rate	%	0.87	19.70	0.04
Total standing forest stock	One hundred million cubic meters	0.12	2.11	0.06
Forest growing stock	One hundred million cubic meters	0.12	1.59	0.08
Investments completed for industrial pollution control	10 thousand yuan	197849.23	331983.82	0.60
Investments completed for wastewater management projects	10 thousand yuan	17432.72	40201.27	0.43
Investments completed for waste gas management projects	10 thousand yuan	178454.04	242109.90	0.74
Investments completed for solid waste management projects	10 thousand yuan	6813.72	5471.57	1.25
Investments completed for noise control projects	10 thousand yuan	347.17	395.22	0.88
Investments completed for other governance projects	10 thousand yuan	64781.49	50803.85	1.28

the entire Henan Province has not been established. Thus, sharing of geological disaster information resources between relevant departments to provide information services for government decision and the public is difficult to realize. Geological disasters in Henan Province have a wide range and high strength. Various hidden dangers, such as the easy and extensive occurrence of geological disasters, exist in its economic pattern and geological environment. Prevention and control measures are far from containing the deteriorated spreading situation of geological disasters, and the preven-

tion and governance works still catch interests of multiple aspects. Therefore, a number of complicated works remain to be completed, namely, construction of guarantee system, elimination of threats from numerous points with hidden hazards, and implementation of prevention scheme.

POLICY RECOMMENDATIONS

Construction of Legal Rules and Laws for Reinforcing Geological Environmental Protection

Henan Regulations on Geological Environmental Protection have played an important role in protecting the Henan geological environment since it was enacted and implemented in 2012. During the implementation process, relevant departments bear clear responsibilities and duties, exert concerted efforts, strictly enforce laws, and strengthen supervision, effectively promoting the comprehensive and in-depth implementation of geological environmental protection. However, concrete scale in the implementation process is limited. To further conduct geological environmental protection work, Henan Province should launch related legislation and investigation works, further define and standardize administration authority and law enforcement status of the Ministry of Land and Resources in the aspect of geological environmental protection, and clarify responsibilities and obligations of different departments. Geological environmental protection should have laws to abide by and standards to quote with clear rights and liabilities and concrete scale.

Carry Out Investigation Work on Geological Environmental Bearing Capacity

In accordance with relevant research results on land bearing capacity, environmental bearing capacity, and resource bearing capacity during the urbanization progress, Henan Province should formulate unified technical standard and establish a scientific and effective research system for geological environmental bearing capacity. The investigation, appraisal, and zoning works should be implemented for geological environmental bearing capacity under different measuring scales within the entire Henan Province. A clear picture of the current status of geological environmental bearing capacity in Henan Province should be obtained, and the main factors influencing and restricting geological environmental bearing capacity should be determined. Key areas to carry out monitoring and early warning demonstration work for geological environmental bearing capacity should be selected, and technical support should be provided to the government to reasonably guide industrial distribution and population mobility. Research work on restoration technology of geological environmental bearing capacity should be

reinforced, restoration studies on all types of impacted and destructed geological environments should be conducted, destructed or saturated bearing capacity should be restored as much as possible, and local socioeconomic development and ecological civilization construction should be performed.

Construction of Geological Environmental Monitoring and Early Warning System

At present, the basic means of geological environmental investigation is the traditional field geological investigation. This approach lacks remote and real-time early modernized and automated warning and monitoring networks with small monitoring scope and backward means and technologies. It fails to provide dynamic real-time early warning information for the prevention and control of geological environmental problems, and it cannot easily prevent the occurrence of geological environmental problems. An ideal approach is suggested to launch geological environmental monitoring and early warning system construction as soon as possible, conduct long-term monitoring of main geological environmental problems of mines, hidden danger points of geological disasters, groundwater level, and groundwater pollution, master change process, and predict future development direction to provide a scientific basis for sustainable socioeconomic development.

Implement Geological Environmental Feasibility Demonstration for Major Construction Projects

With the view of long-term efficiency of geological environmental protection, Henan Province should conduct geological environmental feasibility demonstration for major construction projects and limit human engineering activities within bearable scope. It should focus on supervision and monitoring of construction projects exerting major influences on the geological environment. It should comb and analyze major projects to protect the geological environment, list the directories, perform irregular supervision and inspection, and urge responsible units to practice geological environmental protection. It should synchronously carry out suitability research on geological environmental bearing capacity during the urbanization progress. Henan Province should carry out urban geological environmental quality evaluation and studies on urban geological environmental bearing capacity in full consideration of natural and social properties of cities and towns. Regions suitable for urban development, their development scale, and their development level should be analyzed from the aspect of the geological environment. Also, countermeasures for improving urban geological environmental bearing capacity should be proposed to provide a scientific basis for urban territorial planning and management.

CONCLUSION

With continuous enhancement of human activities and elevation of the scale, strength, and speed of geological environmental development, utilization, and transformation, geological environments in many provinces in China face unprecedented pressure. To effectively control or adjust human activities to adapt to geological environmental conditions and reasonably develop and utilize the geological environment, we must determine current geological environmental bearing capacities in different provinces. In Henan Province, China, for example, the evaluation index system of geological environmental bearing capacity was established, the variation coefficient method was used to calculate the weight of each evaluation index, and the geological environmental bearing capacities of Henan Province during 2010-2018 were calculated through the comprehensive evaluation method. The results showed that during 2010-2018, the geological environmental bearing capacity of Henan Province was superior or excellent. The proposed measures to improve geological environmental bearing capacity include strengthening the implementation of legal rules and laws for geological environmental protection, carrying out investigation works of geological environmental bearing capacity, launching geological environmental monitoring and early warning system construction, and implementing geological environmental feasibility demonstration for major construction projects. An in-depth study is suggested to form systematic and scientific theories and evaluation technology system for resource environmental bearing capacity, establish bearing capacity evaluation model by combining practical situations of different regions, and probe into diversity of territorial resource diversity and fragility of ecological geological environment.

ACKNOWLEDGMENT

REFERENCES

Chang-Fei, T., Fa-Qing, Q. I., Yan-Ping, L., Chun-yu, J.U., Wei, Q.U., Bing-du A.N. and Fang-qi Wang 2011. Bearing capacity of neritic facies silt from Shuangtaizi river estuary. Coastal Engineering, 30(2): 38-42.

Chuan-Ming, M.A. and Yi-Hui, M.A. 2007. Tentative Investigation of Bearing Capacity of Geological Environment for Sustainable Development. Environmental Science & Technology, 30(8): 64-73.

Dill, H.G., Ludwig, R.R., Kathewera, A. and Mwenelupembe, J. 2005. A lithofacies terrain model for the Blantyre Region: Implications for the interpretation of Palaeosavanna depositional systems and for environmental geology and economic geology in southern Malawi. Journal of African Earth Sciences, 41(5): 341-393.

Fuchu, D., Yuhai, L. and Sijing, W. 1994. Urban geology: A case study of Tongchuan city, Shaanxi Province, China. Engineering Geology, 38(1-2): 165-175.

Jiang-Ping, Y., Yao-Hong, S., Ning-Feng, Z., Sheng-Zhong, M. and Tai-hao, C. 2015. Analysis of engineering geological characteristics and specific problems of the offshore area in Beihai, Guangxi. Journal of Geology, 39(4): 633-640.

Lew, M. 2001. Liquefaction evaluation guidelines for practicing engineering and geological professionals and regulators. Environmental & Engineering Geoscience, 7(4): 301-320.

Qi-Shan, D., Zhen-Dong, C., Fan-Tao, M. and Xiao-Qing, S. 2015. Analysis of causes of karst collapse and the corresponding countermeasures during the running of ground source heat pump in the covered karst areas. Groundwater, 37(5): 11-13.

Sastry, R.G.S. and Viladkar, M.N. 2004. Role of integrated geophysical studies in defining the rock profile below steep hill slope at the base of an endangered multi-storeyed building in Himachal Pradesh. Journal of the Geological Society of India, 63(3): 282-290.

Rees, W. E. 1992. Ecological footprints and appropriated carrying capacity: What urban economics leaves out. Environment & Urbanization, 4(2): 121-130.

Wagner, Marian 2013. The geological aspects of meta-lignite and sub-bituminous coal occurrences in Poland within the context of deposits and uneconomic occurrences in Europe. Gospodarka Surowcami Mineralnymi - Mineral Resources Management, 29(4): 25-45.

Wackernagel, M., Monfreda, C., Schulz, N. B., Erb K., Haberl, H. and Krausmann, F. 2004. Calculating national and global ecological footprint time series: resolving conceptual challenges. Land Use Policy, 21(3): 271-278.

Youquan, W. 2004. Analysis on the bearing capacity of water resources in Gansu reaches of Weihe river valley. Groundwater, 26(2)137-139.

Wang, Z.M., Yang, G.L., Yang, R.D., Rawal, K. and Hu, L.B. 2017. Evaluating the factors influencing limestone-dissolution characteristics in the karst regions of Guizhou, China. Journal of Testing and Evaluation, 45(1): 220-229.

Original Research Paper   **Open Access Journal**

Study on Sewage Purification Effect in Surface Flow Constructed Wetland

Xiuli Li†

School of Water Conservancy, North China University of Water Resources and Electric Power, Zhengzhou 450045, China
†Corresponding author: lixiuli96@163.com

ABSTRACT

The status quo that the shortage of water resources in North China and the arbitrary discharge of sewage in rural areas have led to the deterioration of water environment, which not only aggravates the contradiction between supply and demand of regional water resources but also brings harm to people's life and health. How to properly discharge sewage according to the actual situation in rural areas is a question that needs to be answered urgently. The method adopted in this paper is to build a constructed wetland with low cost and simple operation and maintenance in the study area, and purify the water quality through parallel + multi-stage cascade surface flow constructed wetland system. The results show that the purification effect of the wetland system is acceptable, and the removal rate of each index shows a decreasing trend with time. The larger the area is, and the more plant species there are, the better the removal effect will be. The trend of concentration change along the water flow path of each index is also gradually decreasing, and the decline in the early stage is larger. The method of standard index evaluation is adopted to evaluate water quality purification effect of the wetland system, and all indexes reach the standard. In accordance with the Surface Water Environment Quality Standard (GB3838-2002), after wetland purification, the water quality indexes of COD, TP, NH_3-N and DO all reach Class IV water quality standard, and BOD_5 reaches Class II water quality standard. The wetland system effectively reduces the impact of arbitrary sewage discharge on the water environment in rural areas and achieved water quality purification and ecological restoration. The quality of the living environment of local residents is improved. The beautiful environment also promotes people's awareness of protecting wetland ecological environment.

INTRODUCTION

With the development of economy and the improvement of people's living standard, the demands for water resources is increasing, and accordingly, the amount of wastewater and sewage generated is also increasing. Particularly in the economically underdeveloped rural areas, there is no sewage treatment plant, and the domestic sewage generated is discharged directly in the environment. The problem that the water environment is polluted and destroyed by the discharged wastewater and sewage is becoming more and more serious (Zhong et al. 2012, Wan et al. 2016). The pollution of the water environment not only aggravates the crisis of water source shortage but also damages the water ecological environment seriously, which brings challenges to economic development, people's living environment and health. The problem of how to govern the polluted water environment, alleviate the shortage of water resources and return a good living environment to people shall be solved urgently (Zhong et al. 2012). The factors causing water environment damage are more, and governance difficulty is large. To solve those problems, this paper focuses on how to purify polluted water resources, protect and improve the environment, improve

people's health level and build an environment-friendly society by constructing constructed wetland system with low cost and simple operation and maintenance.

Constructed wetland is a kind of process to purify sewage through the triple synergy of physical, chemical and biological effects of substrate, plants and microorganisms. When sewage enters into the constructed wetland, its pollutants are adsorbed, filtered and decomposed by beds to purify water quality (Haberl et al. 2003, Vymazal 2007, Zhang 2011). The constructed wetland combines sewage treatment with the ecological environment, which not only purifies water quality effectively but also beautifies the ecological environment and enhances the appreciation of regional ecological landscape (Wu et al. 2010, Zhang et al. 2012, Shi et al. 2017). The constructed wetland has gained more attention and concern of people by its unique multiple-advantages and now is extensively applied to river sewage treatment. The types of constructed wetlands are divided into surface flow, horizontal subsurface flow, vertical subsurface flow and combined flow (Zhang 2011, Chen et al. 2008).

In the surface flow constructed wetland, the sewage flows horizontally from the inlet end of the pool to the outlet end

without fillers and is purified by wetland plant absorption, rhizome interception and microbial degradation (Tong et al. 2014, Zhao et al. 2018). Surface-flow constructed wetlands have relatively low construction and operational costs but occupy a larger area. In the horizontal subsurface flow constructed wetland, the sewage flows from below the surface of the packing layer and horizontally from the inlet end of the pool to the outlet end. The water quality can be purified by the adsorption and interception of the packing, plant absorption and microbial degradation, which can withstand greater hydraulic load and pollution load (Kato et al. 2010, Czudar 2011). In the vertical subsurface flow constructed wetland, the sewage flows vertically through the filter material layer in the pool. The direction of flow can be from top to bottom or from bottom to top of the packing. It can withstand high pollution load and improve the removal rate of pollutants. The combined flow constructed wetland is generally composed of two or more constructed wetland pools of the same or different types through cascade or parallel mode, etc. The combination mode is usually confirmed according to the actual situation.

The study area is located in the countryside, and the sewage produced by farmers is usually discharged directly and not concentrated. In combination with local actual situation, the surface flow constructed wetland was selected and then constructed to purify the sewage according to the topography, landform and vegetation of the study area. In the long run, surface flow constructed wetland has relatively simple operation and maintenance, long service life, and can create a beautiful natural landscape, providing a good place for people's leisure. In this study, parallel + multi-stage cascade surface flow constructed wetland was selected to treat rural sewage.

MATERIALS AND METHODS

Overview of the study area: The experimental site of this study is located in the south of Yongnian Wa Flood Storage and Detention Area, Handan City, Hebei Province. The constructed surface flow wetland has an area of 5.33ha. The study area belongs to the warm temperate continental monsoon climate, with four distinct seasons during the year. The annual average temperature is 12.9°C, the precipitation is about 550 mm, the water surface evaporation is 1240 mm, and the relative humidity is 67%. The spatial and temporal distribution of annual precipitation is extremely uneven. The precipitation from June to September accounts for about 80% of the annual precipitation, and the characteristics of rainfall are characterized by large and concentrated rainfall. There are many villages and towns in the region. The rural daily domestic sewage, wastewater and sewage from small

food enterprises, farmland irrigation recession water and rainwater are all directly discharged to local rivers, forming the sewage source of constructed wetland.

Trial design: The polluted river water was introduced into constructed wetland through diversion canals, and the wetlands are divided into two parts, i.e. No. I and No. II, with diversion canals as the dividing line. The wetland system is comprised of retention wall, guide wall and drop weir. (1) Wetland is separated from the surrounding environment by using water retaining wall to avoid the influence of the surrounding environment on water purification in the test area. (2) The guide wall is built in the wetland to change water flow direction, make full use of wetland area, increase hydraulic retention time, make sewage react fully with wetland, and improve pollutant removal rate. The guide wall guides the water flow to flow forward along the S-shaped way. Respectively, 15-grade and 13-grade (pool) wetland in series connection are arranged in Wetland I and Wetland II. (3) The drop weir is used to add the content of dissolved oxygen in water, and speed up pollutant decomposition by aerobic microorganisms. Totally 9 drop weirs are set in the wetland, respectively four in Wetland I and 5 in Wetland II. (4) Since sewage entering the wetland is mixed with a large amount of household waste, to avoid long-term pollution caused by the waste entered and retained in the test area, the trash rack shall be built on upstream of the diversion canal. (5) According to plant communities of the wetland, the local advantageous plants with the developed root system, favourable purification effect and good stain, freezing and pesticide prevention ability, which are of high economic value and easy to manage shall be selected: reed and lotus flower.

Lotus flowers were planted in 1-4 and 11-12 (Fig.1) in Wetland I, and reeds were planted in the other area; reeds were planted in all areas of Wetland II.

Testing indexes and method: Water quality sampling in the wetlands was conducted from May to November 2018. To reduce errors, the water samples were collected at the same place in the process of sample collection, and collection cycle was as consistent as possible. Moreover, several groups of data were acquired and calculated to get the mean value. One sampling point was set each on inlet and outlet of the wetland, and outlet of Wetland I and Wetland II, and three in Wetland I and Wetland II respectively, totally nine sampling points (Fig. 1). The sampling frequency was twice averagely every month, and totally 14 times were done.

Indicators for testing water samples include COD, BOD_5, TP, TN, NH_3-N and DO. The water quality testing methods can be seen in Table 1.

RESULTS AND ANALYSIS

Continuous monitoring is applied to the purification system of the constructed wetland in nearly 7 months from May 10 to November 5, 2018. During this period, samples are taken twice from the same place every month averagely, and various indexes are detected.

Hydraulic load analysis: The intelligent flow meter was used to monitor daily average flow rate and daily total water flow in the wetland. To guarantee accurate data, the portable flow rate meter is used for verification. The water flow change scope was $10500m^3/d \sim 13100m^3/d$, and average water inlet volume was $11844m^3/d$ in the wetland during the study period from May to November 2018.

The calculation formula for the hydraulic load is:

$$q_{hs} = Q/A \qquad \ldots(1)$$

In the formula: q_{hs} - Surface hydraulic load, $m^3/(m^2 \cdot d)$;

Q - Wetland water flow, m^3/d; A - Wetland area, m^2

According to calculation formula (1), the wetland hydraulic load change range was $0.15 \sim 0.19m^3/(m^2 \cdot d)$, and the average hydraulic load was $0.17m^3/(m^2 \cdot d)$.

Removal rate analysis: During the study period from May to November 2018, water samples were taken approximately twice a month at a fixed location; totally 14 samples were taken, and each index was tested separately. In accordance with pollutant concentration at the inlet and outlet, the removal rate of each index was calculated. The calculation formula of the removal rate is as follows:

$$\eta = \frac{C_0 - C_e}{C_0} \times 100\% \qquad \ldots(2)$$

In the formula, η: pollutant removal rate; C_0: inlet pollutant concentration, mg/L;

C_e: outlet pollutant concentration, mg/L; The pollutant concentration at the inlet and outlet, and the removal rate of each index can be seen in the Figs. 2-6.

According to Figs. 2-6:

(1) The effluent concentration in Wetland I is lower than that of Wetland II when influent concentrations of various indexes are the same. Thus, the purification effect in Wetland I was superior to that in Wetland II. This is because the water area of Wetland I is larger than that of Wetland II; the plants planted in wetland I are lotus
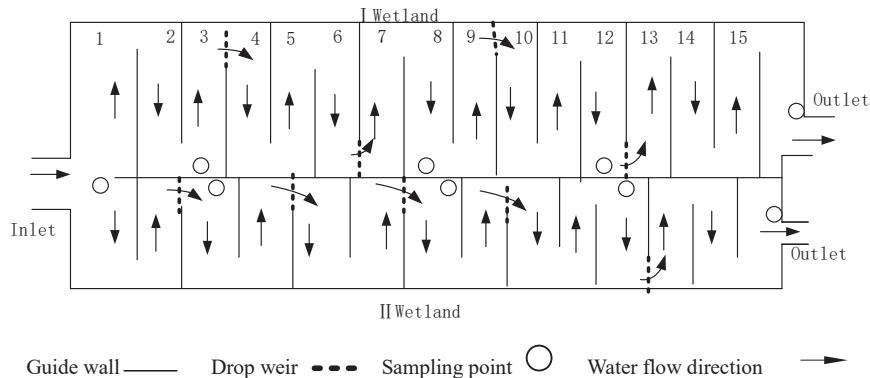
Fig. 1: Layout plan of surface flow constructed wetland.

Table 1: Water quality testing items and methods.

Testing item	Testing method
Chemical oxygen demand (COD)	Dichromate method
Five-day biochemical oxygen demand (BOD$_5$)	Dilution and inoculation test
Total phosphorus (TP)	Ammonium molybdate spectrophotometric method
Total nitrogen (TN)	Alkaline potassium persulfate digestion-UV spectrophotometric method
Ammonia-nitrogen (NH$_3$-N)	Nessler's reagent spectrophotometry
Dissolved oxygen (DO)	Iodometry
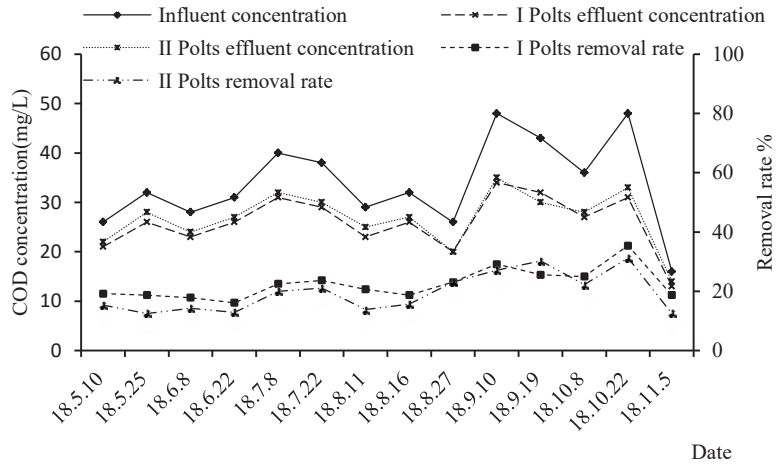
Fig. 2: Inlet and outlet pollutant concentration, and average removal rate of COD on different dates.
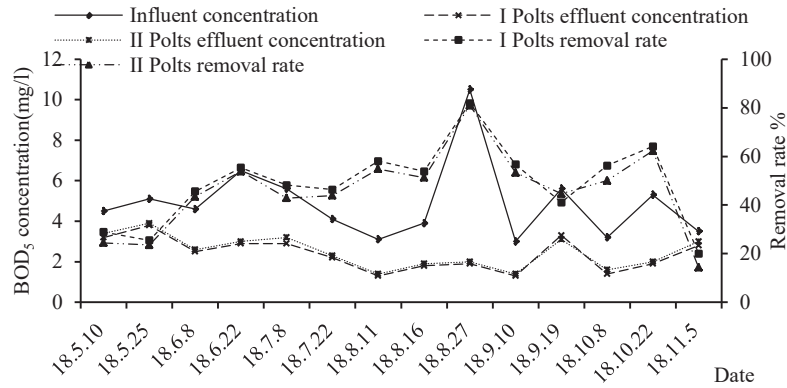
Fig. 3: Inlet and outlet pollutant concentration, and average removal rate of BOD5 on different dates.

dates.
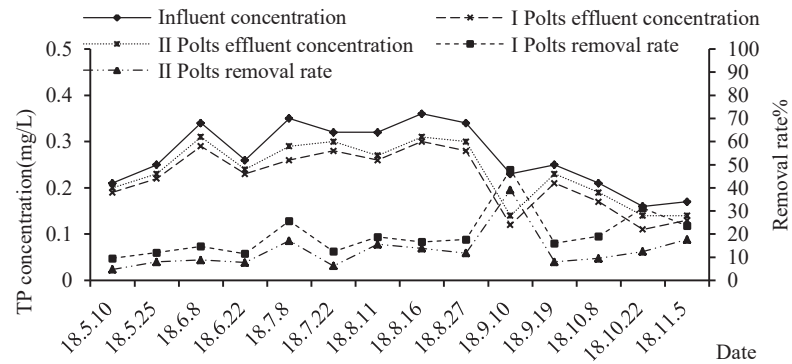
Fig. 4: Inlet and outlet pollutant concentration, and average removal rate of TP on different dates.
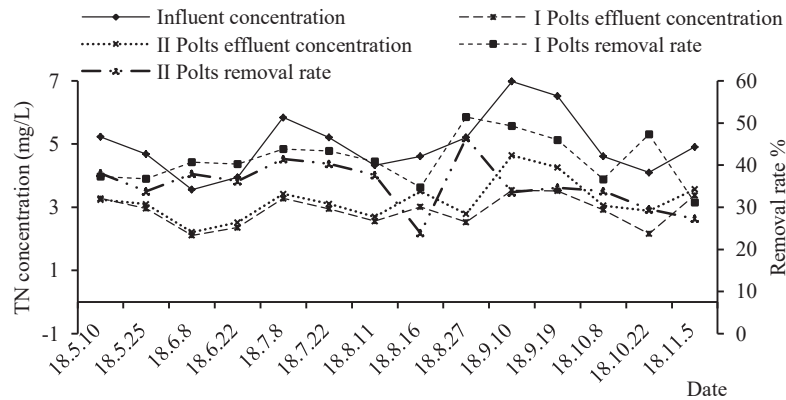
Fig. 5: Inlet and outlet pollutant concentration, and average removal rate of TN on different dates.
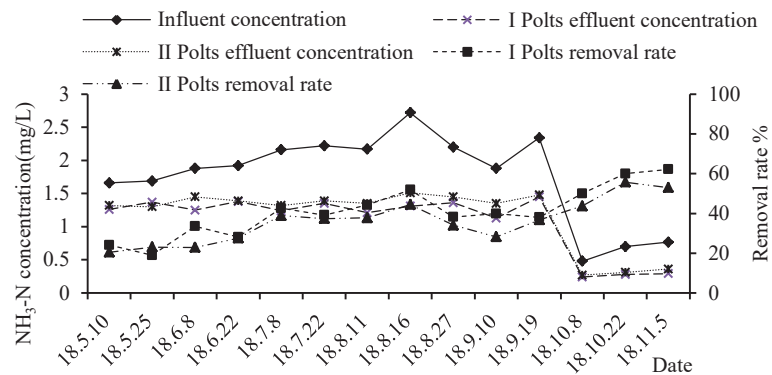
Fig. 6: Inlet and outlet pollutant concentration, and average removal rate of NH$_3$-N on different dates.

flower and reeds, and the plants planted in wetland II are reeds. It can be concluded that the size of water area affects the purification effect, and in large area, the sewage stays a longer time and the purification effect is better; different plants have different purification effects on sewage; the mixed plantation of lotus and reeds has better than plantation of reeds.

(2) Due to different areas and different aquatic plants in Wetland I and Wetland II, the removal rates of various testing indexes in the two areas are different. The mean removal rates of COD, BOD$_5$, TP, TN and NH$_3$-N are respectively 22.5%, 48.7%, 19.8%, 41.5% and 40.8% in Wetland I, and 19.4%, 46%, 12.9%, 35.3% and 36% in Wetland II. In general, the relationship between influent concentration and removal rate is consistent; when the influent concentration is high, the removal rate is higher accordingly.

(3) TP is removed through plant absorption in surface flow constructed wetland. Results show although the removal

rate in Wetland I is slightly higher than that in Wetland II, the removal rate of TP in both Wetland I and Wetland II is not favourable. The higher removal rate in Wetland I is because Wetland I plants lotus flowers while Wetland II does not. The plants may absorb a certain amount of TP during growth and metabolic process, and absorb small molecular phosphate-contained substances in sewage through roots and synthesize to plant structure. However, the phosphate absorption function of plants does not contribute much to TP removal in constructed wetland, and the main approach is substrate's absorption of TP in the wetland. It is not effective for surface low constructed wetland to remove TP relying on plants.

(4) The removal rate of TN reaches the highest in August, and the removal rate is higher in Wetland I than Wetland II. It probably relates to DO concentration in the wetland system. The constructed wetland mainly removes nitrogen in the water body through nitrification and denitrification of microorganism, and the anabolism of

plants (Zhu et al. 2010, Yu et al. 2013). The main content in TN is NO_3-N. When DO concentration is reduced, it will help the denitrification of nitrate nitrogen. The area of Wetland I is large, and higher biomass requires more DO than that of Wetland II, leading to possible internal oxygen deficiency in the system; more NO_3-N is converted and TN removal rate is rising.

(5) The removal trends of NH_3-N in Wetland I and Wetland II are largely consistent. Before August, the removal rate of NH_3-N is increasing; in September, due to impact of water conditions and microorganism activities, the removal rate is reduced; the removal rate of NH_3-N in October and November is increased continuously, probably because of smaller NH_3-N concentration in the water flowing in.

(6) The COD removal situations in Wetland I and Wetland II can be seen in the figure. From May to November, COD is removed to certain degree, and the removal rate in September and October is higher. It is related to COD concentration of water flowing in. When in-flow water COD concentration is high, the removal rate is rising accordingly.

(7) The purification effect of BOD_5 in Wetland I and Wetland II is better, and BOD_5 removal rate is higher from May to October, and in November is low. The removal rate of BOD_5 is related to in-flow water concentration and wetland temperature. According to BOD_5 removal rate changes, in the study stage, there are no obvious rules for BOD_5 removal rate.

Analysis of the change of water quality indicators along the water flow path: In order to analyse the variation of indexes along the water flow path in the wetland, sampling points were set respectively along Wetland I and II. The sampling points in Wetland I are the inlet point, 1#, 2#, 3#, and outlet point; sampling points in Wetland II are the inlet point, 1#, 2#, 3#, and outlet point; the inlet sampling point of Wetland I and Wetland II is the same. Samples were made totally 7 times on the sampling points set along the two wetlands in the beginning of every month from May to November. After water sample testing and analysis, the changes in various indexes along the water flow path were basically consistent in Wetland I and II. Thus, due to space limitation, this paper only analyses rules of indexes changes along Wetland I. The index changes along the water flow path can be seen in the Figs. 7-11.

According to Figs. 7-11.

(1) *The change of COD along the water flow path*: Since the in-flow water quality in the wetland is affected by agricultural or domestic pollution, the change in in-flow water concentration every month is large. COD concentration turns smaller along the water flow path. When in-flow water concentration is high, the corresponding concentration downtrend will be more obvious.

(2) *The change of BOD_5 along the water flow path*: The concentration of BOD_5 decrease gradually except in September and November. Since the in-flow water BOD_5 concentration is smaller in September, there is no removal effect in the wetland; while BOD_5 concentration in November is increased other than decreased probably due to impact of temperature.

(3) *The change of TP along the water flow path*: The concentration of TP show a downward trend along the water flow path, indicating that wetland has a good removal effect on TP. Particularly in August and September, the prosperous plants in the wetland have more obvious absorption effect for phosphate, so that TP concentration along the water flow path is more obvious in August and September than that in other months.

(4) *The change of TN along the water flow path*: The concentration of TP is decreasing along the water flowing direction in the wetland, particularly obvious in the front end of the wetland. Probably due to larger organic content in the front end, and suitable C/N proportion is good for the growth of denitrifying bacteria to improve TN removal effect.

(5) **The change of NH_3-N along the water flow path:** NH_3-N concentration shows a downtrend along the water flowing direction of the wetland. Moreover, when the NH_3-N concentration in in-flow water is high, the decreasing trend is more obvious. The decrease of NH_3-N concentration is caused by microorganism ammonization, and also absorption effect of wetland plants. Higher NH_3-N concentration makes their effects more remarkable.

Evaluation and analysis: According to monitoring data in the study area, the standard index evaluation method was adopted to evaluate water quality purification effect in the wetland system. The results could distinctly and visually show purification situations along the water flow path and main pollution factors.

The calculation formula for standard index S_{ij} of water quality parameter i on j point is:

$$S_{ij} = \frac{C_{ij}}{C_{si}} \qquad \ldots(3)$$

In the formula, S_{ij} - Standard index of water quality parameter i on j point
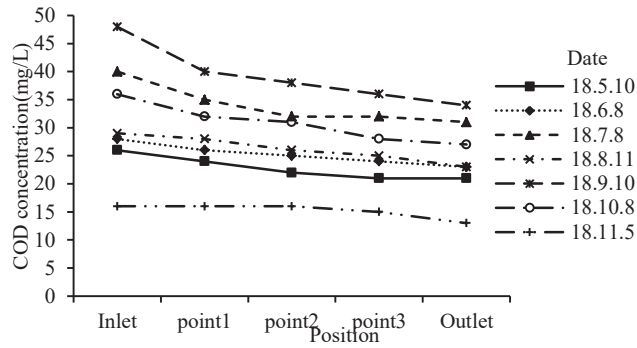
Fig. 7: The change of COD along the water flow path.
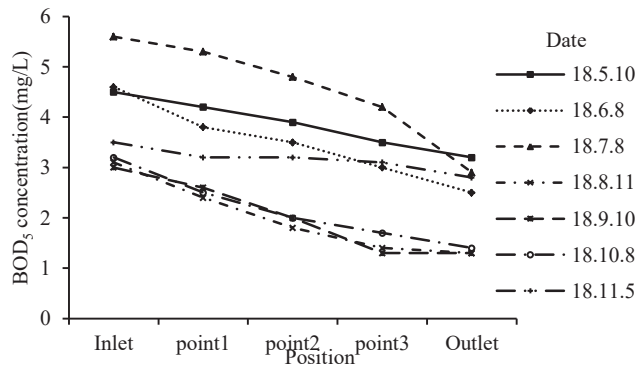
Fig. 8: The change of BOD$_5$ along the water flow path.
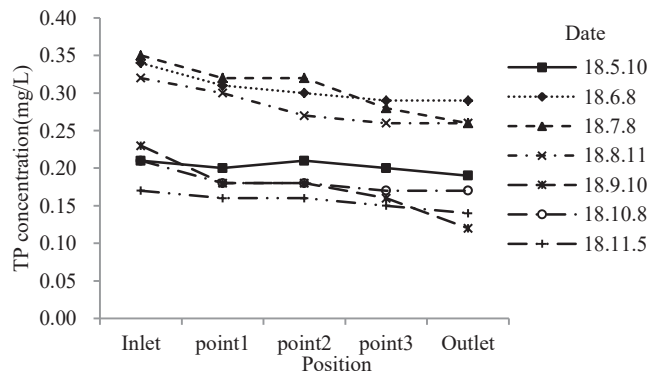
Fig. 9: The change of TP along the water flow path.
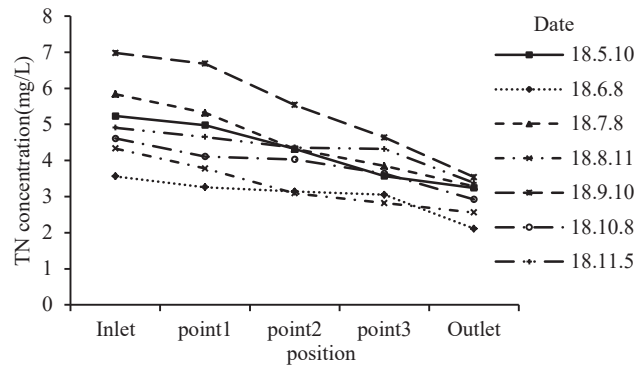
Fig.10: The change of TN along the water flow path.
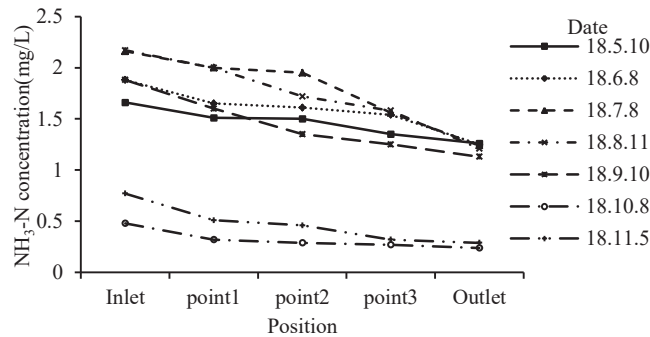
Fig.11: The change of NH$_3$-N along the water flow path.

C_{ij} - Concentration of water quality parameter i on j point, mg/L

C_{si} - Standard value of water quality parameter i point, mg/L

The single factor evaluation index of each index along the water flow path can be acquired, referring to Table 2. The calculation results of single factor evaluation indexes in the table were analysed. If the result is smaller than 1, the water quality reaches the standard, while if the result is larger than 1, the water quality is out of limit.

The table shows the single factor index of DO, TP, NH$_3$-N, COD and BOD$_5$ in out-flow water of Wetland I and Wetland II is largely smaller than 1, reaching the water quality standard; single factory index of TN is larger than 1, and water quality is out of limit. As a whole, each single factor evaluation index shows a downtrend with the movement of purified water flow during wetland purification. It means pollutants are effectively removed along the water flow path, and water quality becomes better gradually.

In line with *Surface Water Environment Quality Standard*

Table 2: Single factor evaluation index of each index along the water flow path.

Evaluation index	Water inlet	Water outlet in Wetland I	Water outlet in Wetland II
DO	0.78	0.77	0.86
TP	0.9	0.73	0.8
TN	3.32	2.04	2.11
NH$_3$-N	1.18	0.72	0.81
COD	1.13	0.87	0.93
BOD$_5$	0.78	0.4	0.35

Table 3: Water quality classification of inlet and outlet water of main indexes from May to Nov 2018.

Water quality Index	Inlet		Wetland I		Wetland II	
	Mean value (mg/L)	Water quality Class	Outlet mean value (mg/L)	Water quality Class	Outlet mean value (mg/L)	Water quality Class
COD	33.8	V	26	IV	27.8	IV
BOD$_5$	4.7	IV	2.4	II	2.4	II
TP	0.27	IV	0.22	IV	0.24	IV
NH$_3$-N	1.77	V	1.08	IV	1.22	IV
DO	5	III	5.1	III	4.3	IV

(GB3838-2002), the water quality class of DO, TP, NH$_3$-N, COD and BOD$_5$ at inlet and outlet can be seen in Table 3. According to the table, after wetland purification, the outlet water quality index COD, TP, NH$_3$-N and DO all reach Class IV water quality standard, and BOD$_5$ reaches Class II water quality standard.

CONCLUSION

In accordance with the observation data of the wetland in nearly one year, the purification effect, concentration changes along the constructed wetland and purification indexes were evaluated and analysed. Results show that the sewage purification effect in parallel + multi-stage cascade surface constructed wetland is favourable. According to aforesaid results:

(1) The mean removal rates of COD, BOD$_5$, TP, TN and NH$_3$-N in the wetland are respectively 22.5%, 48.7%, 19.8%, 41.5% and 40.8% in Wetland I, and 19.4%, 46%, 12.9%, 35.3% and 36% in Wetland II, effectively reducing and eliminating hazards of domestic sewage discharge to the external water body. The size of wetland area and plants varieties affect sewage purification to a certain degree because different types of plants have different absorption functions for various pollutants; the area sizes cause different courses of sewage along the water flow path. Therefore, to improve wetland purification effect, further tests shall try to add sewage course area along the wetland when the wetland area is fixed, and select plants with strong absorption effect to improve the removal rate.

(2) The factors affecting concentration changes of indexes along the water flow path are more; for instance, the in-flow water concentration, temperature and plants and microorganisms in the wetland affect concentration along the water flow path to a certain degree. The concentration of all indexes is decreasing along the water flow path, and the decrease is fast in the front end of the wetland system.

(3) The analysis on water quality after purification according to standard index evaluation method shows that DO, TP, NH$_3$-N, COD and BOD$_5$ all reach the water quality standards; single factory index of TN is larger than 1, and water quality is out of limit.

Wetland treatment effect: NH$_3$-N>TN>BOD$_5$ >COD>TP. In line with *Surface Water Environment Quality Standard* (GB3838-2002), the outlet water quality index of COD, TP, NH$_3$-N and DO, all reach Class IV water quality standard, and BOD$_5$ reaches Class II water quality standard. Although TN outflow water does not reach Class IV class quality standard for lakes and reservoirs, the average removal rate is high, and the removal effect is obvious.

Surface flow constructed wetland has relatively simple operation and maintenance and long service life. Moreover, the plants such as lotus flowers and reeds planted in the wetland not only have ornamental value but also have certain economic value. They could improve the water environment while creating a beautiful natural landscape. Therefore, the surface flow constructed wetland built in rural area with a relatively backward economy can not only achieve water quality purification and ecological restoration but also improve the quality of local residents' living environment. The beautiful environment also promotes people's awareness of wetland ecological environment protection.

REFERENCES

Chen, Jinjun, Zheng, Chong and Zheng, Shaokui 2008. Pollutant purification performance of a surface flow constructed wetland planted with different aquatic macrophytes and their combination. Acta Scientiae Circumstantiae, 28(10): 2029-2035.

Czudar, A., Gyulai, I., Keresztúri, P., Csatári, I., Serra-Páka, S. and Lakatos, G. 2011. Removal of organic material and plant nutrients in a constructed wetland for petrochemical wastewater treatment. Studia Universitatis Vasile Goldis. Seria Stiintele Vietii, (21): 109-114.

Haberl, R., Grego, S., Langergraber, G., Kadlec, R.H., Cicalini, A.R., Dias, S.M., Novais, J.M., Aubert, S., Gerth, A., Thomas, H. and Hebner, A. 2003. Constructed wetlands for the treatment of organic pollutants. Soils Sediments, 3: 109-124.

Kato, K., Inoue, T., Ietsugu, H., Koba, T., Sasaki, H., Miyaji, N., Yokota, T., Sharma, P.K., Kitagawa, K. and Nagasawa, T. 2010. Design and performance of hybrid reed bed systems for treating high content wastewater in the cold climate. In: Masi, F., Nivala, J. (Eds), Proceeding of the 12th International Conference Wetland Systems for Water Pollution Control, IWA, IRIDRA Srl and Pan Srl Padova, Italy, 511-517.

Shi, Xinhui, Shuxia Xu, Yanshuo Pan, Youjing Wang, Jiran Zhang, Kun Wu and Shimin Zhang 2017. Effects of urban constructed wetland on water purification efficacy for artificial lake. Journal of Henan Agricultural University, 51(6): 855-859.

Tong, X., Wang, X., He, X. and Kong, H. 2014. Ammonia nitrogen removal and analysis of the ammonia-oxidizing bacterial community in horizontal subsurface flow constructed wetlands. Research of Environmental Sciences, 27(2): 218-224.

Vymazal, J. 2007. Removal of nutrients in various types of constructed wetlands. Science of the Total Environment, 380(1-3SI): 48-65.

Wan, Yun-wen, Gou, Chang-qiang, Mao, Zhi, Li, Xin-jian, Cui, Yuan-lai and Zhao, Shu-jun. 2016. Sewage purification effect of multi-series surface flow constructed wetland. Transactions of Chinese Society of Agricultural Engineering, 32(3): 220-227.

Wu, C.Y., Liu, J.K., Cheng, S.H., Surampalli, D.E., Chen, C.W. and Kao, C.M. 2010. Constructed wetland for water quality improvement: a case study from Taiwan. Water Science & Technology, 62(10): 2408.

Yu, Junbao, Hou, Xiaokai and Han, Guangxuan 2013. Removal efficiency of multi-medium constructed wetlands on nitrogen and phosphorus in domestic sewage. Wetland Science, 11(2): 233-239.

Zhang, Qing 2011. Construction and application of constructed wetlands. Wetland Science, 9(4): 373-379.

Zhang, Y.R., Wang, R.Q., Zhang, J. and Liu, J. 2012. Evaluation of ecosystem sustainability for large-scale constructed wetlands. Acta Ecologica Sinica, 32(15): 4803-4810.

Zhao, Zhichao and Zhang, Weitang 2018. BCO-constructed wetland treatment of domestic sewage under normal and low temperatures. Journal of Water Resources & Water Engineering. 29(5): 28-34.

Zhong, Lin, Zheng, lei, Ding, Ai-zhong and Chen, De-sheng. 2012. Reconstructed wetlands to treat polluted river-pollutant removal efficiency in China. Journal of Beijing Normal University (Natural Science), 48(1): 66-72.

Zhu, G., Jetten, M.S., Kuschk, P., Ettwig, K.F. and Yin, C. 2010. Potential roles of anaerobic ammonium and methane oxidation in the nitrogen cycle of wetland ecosystems. Applied Microbiology and Biotechnology. 86(4): 1043-1055.

Analysis of Soil Characteristics Near the Solid Waste Landfill Site

P. Vijayalakshmi†, P. K. Raji, P. Eshanthini, R. Rahul Vijay Bennet and Rajesh Ravi

Department of Civil Engineering, Sathyabama Institute of Science and Technology, Chennai, Tamilnadu, India
†Corresponding author: P. Vijayalakshmi; vijayalakshmipanneerselvam@yahoo.co.in

ABSTRACT

In this project, the study of soil characteristics due to the municipal solid waste was carried out in a selected location around the recently closed Municipal Solid Waste (MSW) dumpsite located opposite to Periya Eri in Chromepet, Chennai. Soil samples were collected from the selected location, i.e. 2 sites within 1500m from the dumpsite and another 2 sites beyond 1500m from the dump yard. Total 12 soil samples from 4 sites were collected from a ground depth of 0-30cm, 30-60cm and 60-90cm below the surface. The collected soil samples have been analyzed for pH, moisture, total organic matter, ash content, total organic carbon, specific gravity, conductivity and bulk density and the result were compared with the standards. The study suggested, providing Permeable Reactive Barriers (PRBs) around the solid waste dump site/landfill for reducing the leachate concentration before entering to the soil and thus soil contamination can be minimized to some extent and this technology is cost-effective and eco-friendly since the materials used in the barriers are locally available and low-cost which is sustainable and protect human health, nature and the environment. This study indicated that soil properties did not reach high pollution levels, and therefore posed a low eco-risk potential in surface soil near the landfill.

INTRODUCTION

Soil plays a central role in food safety as it determines the possible composition of food and feed at the root of the food chain. Maintenance or enhancement of soil quality is a more important criterion for analysis and sustainability of soil ecosystems (Schoenholtz 2000)

The soil quality analysis includes an analysis of parameters and processes which affect soil to operate efficiently as a component of a sound ecosystem (Tale & Ingole 2015). Soil is one of the important natural resources which provides the main mineral elements for plant growth and crop production. Formation of 1 cm topsoil layer requires 100-400 years (Deshmukh 2012). Systematic depletion of public health and general living conditions of a given populace is largely traceable to the adaptation of man to his less than the wholesome environment. In the past, waste disposal was not taken too seriously in the developing countries, but in recent years with increasing awareness of the environmental hazards caused by wastes, much concern has been directed to its management (Igwe et al. 2002). The increase in population coupled with rural-urban drift has increased the quantity of wastes generated in the urban areas and the developing countries are faced with not only the challenges of collecting the wastes but how and where to dispose of it without causing further environmental hazards (Oguneleka 2009, Oguche 2013). When pollutants or contaminants find their way into the soil, they interact with the soil and thereby change the chemical and physical properties of the soil.

Study Area

The study area is located around the existing MSW dumpsite (latitude: 12°57′21.1134″ N and longitude: 80°09'0.9678" E) at an altitude of 55 feet above the mean sea level (Fig. 1). The area is having low humidity and high temperature. During winter, the temperature is around 20°C which increases up to a maximum of 44°C in summer. The average annual rainfall of this region is about 1200 mm and forty per cent of the annual rainfall is contributed by the southwest monsoon from June to September. More than 60% of the annual rainfall from October to December is due to northeast monsoon (Vijayalakshmi & Marykutty Abraham 2017). The topography of this region gently slopes towards west and east.

Sample Collection and Analysis

Two sites within 1500m around the dumpsite (namely site L1 and site L2) and another 2 sites between 1500m and 3000m away from the dumpsite (namely site L3 and site L4) have been selected (Fig. 2A). From each site, the soil samples were collected from 0-30cm, 30-60cm and 60-90cm depth below the ground surface (Fig. 2B). Fig. 3 shows photographs of the collected soil samples. The soil samples were analyzed for physical properties by the methods given in Table 1.

A stainless steel trowel was used to collect samples and the soil samples were preserved in polythene bags for further analysis. Soil samples were air-dried for 72 h, crushed, passed through a 2-mm-mesh sieve, and stored at ambient temperature before the soil properties were analyzed (Sharma et al. 2007).

RESULTS AND DISCUSSION

pH

The most significant property of soil is its pH level, which affects all other parameters of soil. If the pH is less than 6 then it is said to be acidic soil, when the pH range from 6-8.5 it is a normal soil and when it is greater than 8.5 the soil is said to be alkaline. pH has been reported as a simple and direct measure of the overall chemical condition of the soil and at pH 6.5, nutrient availability to plants from the soil is at its highest (Praveena & Rao 2016).

The pH of the collected soil sample at site 2 (L2) is higher than site 1 (L1), which has been collected within 1500m from the dumpsite (Table 2). The value of pH of collected soil samples reduces with increase in distance from the dumping site. The values of pH in the soil samples are within the Indian standards.

Fig. 4 clearly shows the variation in pH at all the site locations and for each layer. The pH at L2 is higher than other site locations. From Fig. 4(b), the level of pH at L1 is lower than the L2, and then the level of pH decreases at L3 and L4 as the distance from the dumpsite increases.

Moisture

Water content or moisture content is the quantity of water contained in a material, such as soil called soil moisture. Absorption of the nutrients by soil largely depends on the moisture content of the soil, which also shows its effect on the texture of the soil.

Fig. 1: Location map of the study area.

Table 1: Methods used for the testing of the collected soil sample.

Parameters	Testing Methods
pH	EPA Method-9045 D rev 4,2004
Moisture, %	FAO Method(Pg: NO:23) 2007 (AIR OVEN METHOD)
Total Organic Matter, %	IS 10158-1968 (RA 2003)
Ash Content, %	IS 1155:1968 (RA 2005)
Total Organic Carbon %	FAO Method (PG NO. 61) 2007 (Walkley Black Wet Combustion Method)
Specific Gravity	TNTH/SOP/SOIL/021
Conductivity (µS/cm)	IS 14767:2000
Bulk Density (g/cm^3)	FAO Method (PG NO: 35) 2007
Chloride as Cl (mg/kg)	FAO Method (PG NO: 48) 2007 (Titrimetric Method)

Fig. 2(A): Site selected for collection of samples.

Fig. 2(B): Collection of the samples.

The maximum allowable concentration of moisture in the soil sample should be in a range between 11% to 17% and the moisture content in the collected soil samples are within the Indian standards.

Fig. 5 and Table 3 show the variation in moisture at all the site locations and for each layer. The moisture at L1 and L2 is higher than other site locations (L3 and L4). From Fig. 5(a), the value of moisture at L1 is lower than L2 for 1st and 3rd layer and higher in 2nd layer, then the level of moisture

lowers at L3 and L4 the value decrease for 1st layer and increases for 2nd and 3rd layer.

Total Organic Matter

The high rate of organic matter decomposition under high temperature leads to extremely high oxidizing condition (Uma et al. 2016). Total organic matter (TOM) or soil organic matter (SOM) is the organic matter component of soil, consisting of plant and animal residues at various stages of

Fig. 3: Collected soil samples.
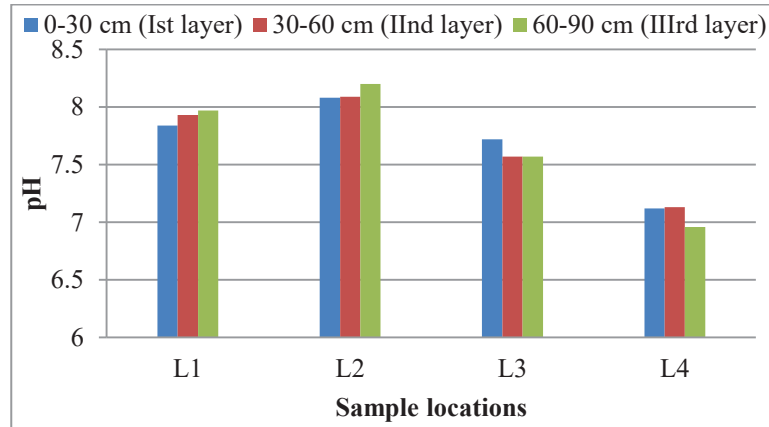
Fig. 4: Variation of pH of collected soil samples.
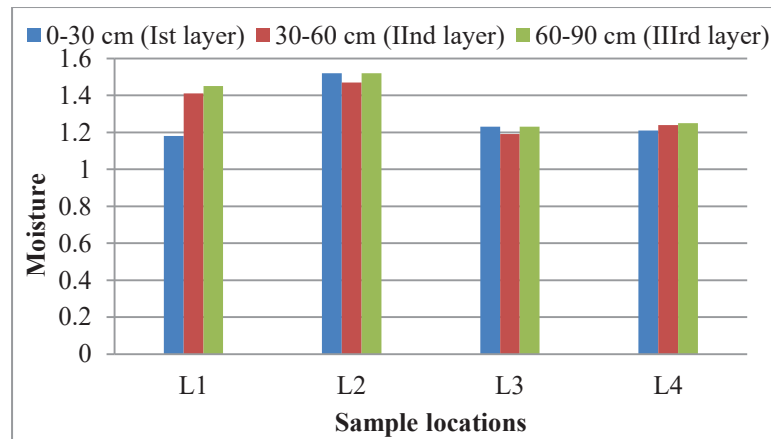
Fig. 5: Variation of moisture content of the collected soil samples.

decomposition, cells and tissues of soil organisms, and substances synthesized by soil organisms. SOM exerts numerous positive effects on soil physical and chemical properties, as well as the soil's capacity to provide regulatory ecosystem services. Particularly, the presence of SOM is regarded as being critical for soil function and soil quality.

Fig. 6 and Table 4 show the variation in total organic matter at all the site locations and for each layer. The total organic matter at L1 and L2 is higher than other site locations.

From Fig. 6(a), 1st layer total organic matter at L1 is higher than L2, the level of total organic matter increases for L3 and then decreases for L4. From Fig. 6(b) and 6(c), 2nd and 3rd layer total organic matter at L1 is equal to L2, then the level of total organic matter decrease at L3 and increases L4 for the 2nd layer.

Ash Content

The substance remaining after ignition is the ash. The ash

Table 2: Value of pH at various depths of soil below the ground surface.

Soil Sample Location	Ist layer 0-30 cm	IInd layer 30-60 cm	IIIrd layer 60-90 cm	Maximum Allowable value
L1	7.84	7.93	7.97	
L2	8.08	8.09	8.2	5.5-8.5*
L3	7.72	7.57	7.57	
L4	7.12	7.13	6.96	

*Source: MSW Management and Handling Rules, 2000, Compost - Consulting development, 2004 and Soil quality standard from England.
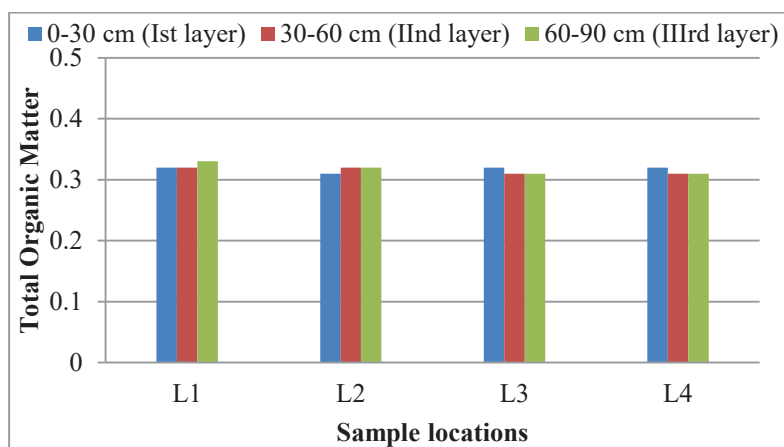
Fig. 6: Variations of total organic matter of the collected soil samples.
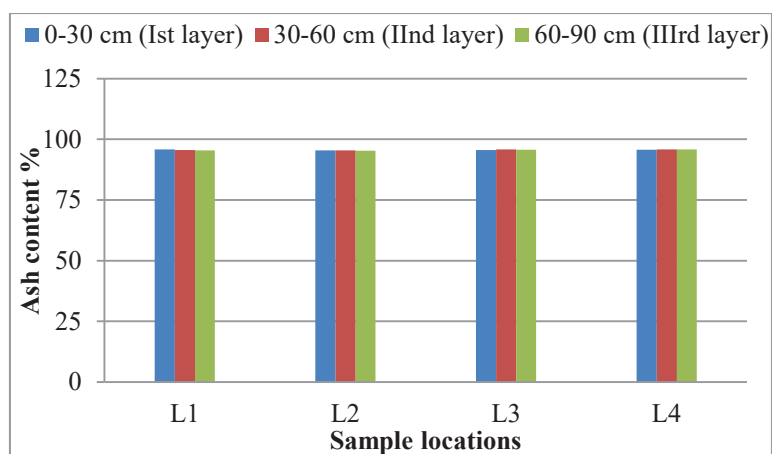
Fig. 7: Variations of ash content of the collected soil samples.

content is expressed as a percentage of the mass of the oven-dried sample.

Fig. 7 and Table 5 show the variation in ash content at all the site locations and for each layer. The total organic matter at the 1st layer of the L1 is higher than that at other site locations. From Fig. 7, ash content in 1st, 2nd and 3rd layers at L1 is higher than L2. The level of ash content increases for L3 and then increases for L4 but 2nd layer L4 value decreases.

Total Organic Carbon

The organic carbon content of a soil is the net result of the rates of carbon input (the rate of net photosynthesis) and organic decay (Isirimah & Dickson 2008). And it contributes significantly to acidity through contributions from organic acids and biological activities (Yun 2003). Flooded soils, due to their low mineralization rate under reduced conditions tend to accumulate fairly substantial organic carbon contents and

Table 3: Moisture content at various depths in the soil.

Soil Sample Location	Ist layer 0-30 cm (%)	IInd layer 30-60 cm (%)	IIIrd layer 60-90 cm (%)	Maximum Allowable Concentration (%)
L1	1.18	1.51	1.45	
L2	1.52	1.47	1.52	
L3	1.23	1.19	1.23	11-17
L4	1.21	1.24	1.25	

Table 4: Concentration of total organic matters at various depths in the soil.

Soil Sample Location	Ist layer 0-30 cm (%)	IInd layer 30-60 cm (%)	IIIrd layer 60-90 cm (%)
L1	0.32	0.32	0.33
L2	0.31	0.32	0.33
L3	0.32	0.31	0.31
L4	0.31	0.32	0.31

Table 5: Variation of ash content at various depths in the soil.

Soil Sample Location	Ist layer 0-30 cm (%)	IInd layer 30-60 cm (%)	IIIrd layer 60-90 cm (%)
L1	95.78	95.53	95.49
L2	95.44	95.39	95.37
L3	95.61	95.8	95.75
L4	95.71	95.77	95.79

these have some influence on soil structural behaviour (To-boada 2004). The total organic carbon content is suggestive of microbial activity leading to the release of organic carbon and acidic substances (Morgan et al. 1989).

Fig. 8 and Table 6 clearly show the variation in total organic carbon at all the site locations and for each layer. The total organic carbon at L1 and L2 is higher than the other site locations. The value of total organic carbon is in the range of 0.18 to 0.19 for all the layers of the collected soil samples (Table 8).

Specific Gravity

Specific gravity (G) is defined as the ratio of mass per volume or ratio of the weight of an equal volume of distilled water at that temperature; both weights are taken in air. The knowledge of specific gravity is needed in the calculation of soil properties like void ratio; the degree of saturation, etc. Soil specific gravity varies with the depth of the ground whereby we can know the conditions of soil structures below the crust.

Fig. 9 and Table 7 show the variation in specific gravity at all the site locations and for each layer. The specific gravity at L2 is higher than other site locations. From Fig. 9, the value of specific gravity at L1 is lower than L2, and then the value of specific gravity is equal for L3 and L4 and for 3rd layer L4 value decreases.

Conductivity

Electrical conductivity is also a very important property of
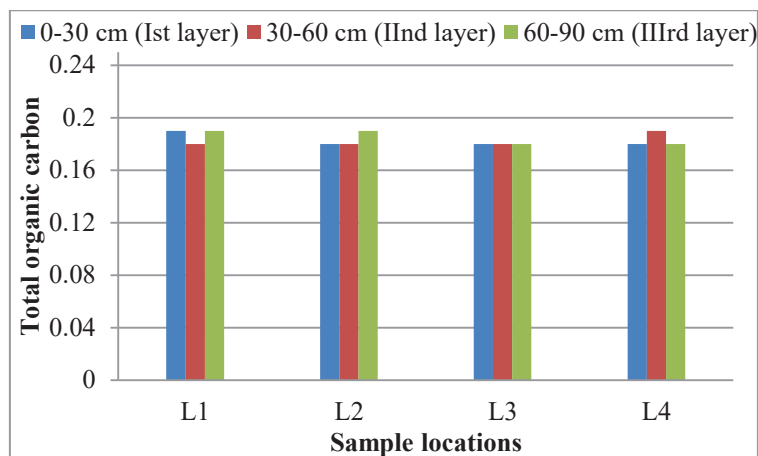
Fig. 8: Variations of total organic carbon of collected soil samples.

Table 6: Total organic carbon at various depths in the soil.

Soil Sample Location	Ist layer 0-30 cm (%)	IInd layer 30-60 cm (%)	IIIrd layer 60-90 cm (%)
L1	0.19	0.18	0.19
L2	0.18	0.18	0.19
L3	0.18	0.18	0.18
L4	0.18	0.19	0.18

the soil, which is used to check the quality of the soil. It is a measure of ions present in the solution (Tale & Ingole 2015). When the soil is more acidic, it shows very high electric conductivity value (Chik 2011). The electrical conductivity of a soil solution increases with the increased concentration of ions. Electrical conductivity is a very quick, simple and inexpensive method to check the health of soils. It is a measure of ions present in the solution. The electrical conductivity of a soil solution increases with the increased concentration of salts.

Fig. 10 and Table 8 show the variation in conductivity at all the site locations for each layer. The conductivity at L2 is higher than other site locations. From the Fig.10, the value of conductivity at L1 is lower than L2, and the value of conductivity decreases for L3 and L4.

If the soil EC is too high, it can be an indication of a high level of exchangeable sodium. Soils with an accumulation of exchangeable sodium are often characterized as low permeability. The soil EC is also related to the specific soil properties that affect the pH, salt concentrations and water holding capacity. It is difficult to say the ideal EC levels, as there are so many variables affecting the EC level.

Bulk Density

Bulk density is defined as the mass of many particles of the material divided by the total volume they occupy. Bulk density is a property of powders, granules, and other masses of particulate matter. Bulk density can change depending on how the material is handled. Bulk density of soil samples is within the Indian standards. It is noted that the bulk density
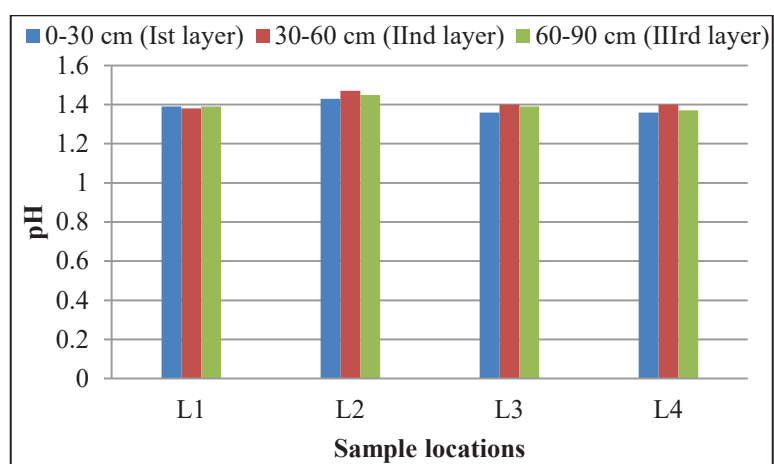
Fig. 9: Variations of specific gravity of the collected soil samples.

Table 7: Specific gravity at various depths in the soil.

Soil Sample Location	Ist layer 0-30 cm	IInd layer 30-60 cm	IIIrd layer 60-90 cm
L1	1.39	1.38	1.39
L2	1.43	1.47	1.45
L3	1.36	1.4	1.39
L4	1.36	1.4	1.37

Table 8: Conductivity at various depths in the soil.

Soil Sample Location	Ist layer–0-30 cm (µS/cm)	IInd layer–30-60 cm (µS/cm)	IIIrd layer–60-90 cm (µS/cm)	Maximum Allowable Concentration (µS/cm)
L1	304	256	219	
L2	323	274	336	200 µS/cm and 1200 µS/cm (General guidelines for good soil)
L3	255	192	211	
L4	148	155	200	
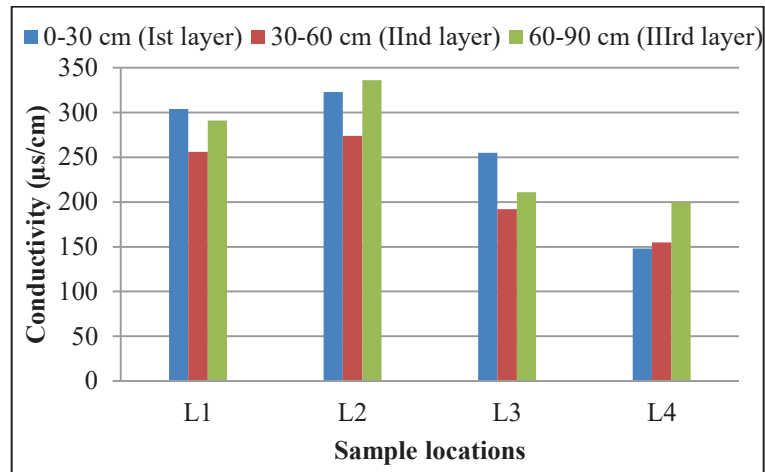
Fig. 10: Variations of conductivity of the collected soil samples.

Table 9: Bulk density at various depths in the soil.

Soil Sample Location	Ist layer–0-30 cm (g/cm^3)	IInd layer–30-60 cm (g/cm^3)	IIIrd layer–60-90 cm (g/cm^3)	Maximum Allowable Concentration (g/cm^3)
L1	1.53	1.39	1.34	
L2	1.6	1.46	1.35	1-1.6
L3	1.46	1.42	1.36	
L4	1.52	1.41	1.43	

of soil sample collected from L2 of the Ist layer is the highest among all the collected soil samples, which is 1.6 (g/cm^3).

Fig.11 and Table 9 show the variation in bulk density at all the site locations for each layer. The bulk density at L2 of the 1st layer is higher than other site locations. From the Fig.11, the value of bulk density at L1 is lower than L2, the value of bulk density decreases for L3 (1st and 2nd layer) and increases for L3 of the 3rd layer and L4 of the 1st layer and 3rd layer increases and then decreases for L4 of the 2nd layer.

CONCLUSION

The pH of the study area, i.e., near the dumpsite within 1.5
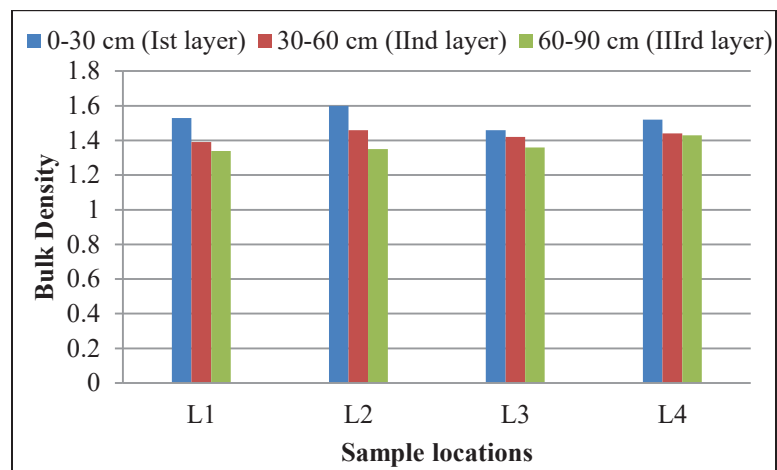
Fig. 11: Variations of bulk density of collected soil samples.

km varies from 7.84 to 8.2, and away from the dumpsite, i.e. beyond 1.5 km, varies from 6.9 to 7.72, the values are below the standard value specified by the MoEF. It indicates that the pH of the soil varies from slightly neutral to highly alkaline. The percentage of moisture content in the soil samples varies from 1.18 % to 1.52% and 1.19% to 1.25% near and away from the dumpsite respectively, which are below the standard value range of 11 to 17%. EC level of the sampling locations ranges from 219 μS/cm to 336 μS/cm and 148 μS/cm to 255 μS/cm near and away from the dumpsite respectively, which are between 200 μS/cm and 1200 μS/cm (general guideline level). Soils having EC levels below 200 μS/cm are sterile soil with little microbial activity. And EC above 1200 μS/cm may indicate a salinity problem due to lack of drainage. The bulk density of the soil samples varies from 1.34 g/cm^3 to 1.60 g/cm^3 and 1.36 g/cm^3 to 1.52 g/cm^3 at near and away from the dumpsite respectively, which are with the standard value range of 1 .0 g/cm^3 to 1.6 g/cm^3. The TOC of the soil samples varies from 0.18% to 0.19% both near and away from the dumpsite which is with the value range of 0.1% to 0.62%. As the organic content is low it allows the contaminant from the solid waste to enter the groundwater. If the organic matter content of the subsoil is high it prevents the pollutants from reaching the groundwater sources as it plays an important role in the adsorption in the soil.

Therefore proper solid waste management practice should be implemented to minimize the adverse impact on the soil. Further *in situ* bioaccumulation studies can also be performed to avoid soil contamination due to open dumping of solid waste. Since the study area is near the non engineered recently closed dumpsite/landfill implementing the new technology providing permeable reactive barriers (PRBs) using low-cost materials available locally will enhance the prevention of soil pollution, otherwise, these pollutants constantly migrate and permeate into soil strata and after a certain period, the entire groundwater system is polluted.

# REFERENCES

Chik, Z. 2011. Study of chemical effects on soil compaction characterizations through electrical conductivity. Int. J. Electrochemical. Sci., 6: 6733-6740.

Deshmukh, K.K. 2012. Studies on chemical characteristics and classification of soils from Sangamner area, Ahmednagar District, Maharashtra, India. Rasayan Journal of Chemistry, 5(1): 74-85.

Igwe, C., Isirimah, N. O. and Teme, S. C. 2002. Distribution and characteristics of solid wastes and waste disposal sites in Port Harcourt municipality, Rivers State, Nigeria. African Journal of Environmental Pollution and Health, 1(2): 51-60.

Isirimah, N. O. and Dickson, A. 2003. Soil chemistry. In: Introductory Soil Chemistry and Biology for Agriculture and Biotechnology. OSIA International Publishers Ltd., Port Harcourt.

Isirimah, N. O. and Yun, O. 2003. Simulating dynamic load of naturally occurring total organic carbon (TOC) from watershed. Water Research, 37: 823-832.

Morgan, P. and Watkinson, R.J. 1989. Hydrocarbon degradation in soils and methods for soil biotreatment. CRC Critical Reviews. Biolechnol, 8(4): 305-330.

Oguche, J.A. 2013. Spatial location of solid waste dumpsites and collection scheduling using the geographic information systems in Bauchi Metropolis Nigeria. European Scientific Journal, 9(11): 374-382.

Oguneleka, T. C. H. 2009. Municipal solid waste characteristics and management in Nigeria. Iranian Journal of Environmental Health Science and Engineering, 6(3): 173-180.

Praveena, S. G. and Rao, P.V. 2016. Impact of leachate on soil properties in the dumpsite. International Journal of Engineering Research and General Science, 4(11): 235-241.

Schoenholtz, S. H. 2000. A review of chemical and physical properties as indicators of forest soil quality: Challenges and opportunities. Forest Ecology and Management, 138: 335-356.

Sharma, R. K., Agrawal, M. and Marshall, F. 2007. Heavy metal contamination of soil and vegetables in suburban areas of Varanasi, India. Ecotoxicol Environ. Safety, 66(2): 258-266.

Tale, Smita and Ingole, Sangita 2015. A review on role of physico-chemical properties in soil quality, Chem. Sci. Rev. Lett., 4(13): 57-66.

Toboada, M.A. 2004. Soil Structural Behaviour of Flooded Soils. No. INIS-XA-989. 2004.

Uma, R. N., Prem Sudha, R. and Murali, K. 2016. Analysis of physico-chemical characteristics of soil and SQI around municipal solid waste dump yard in Vellalore-Coimbatore, Tamilnadu. India. Int. J. Chem. Sci., 14(4): 3265-3276.

Enhanced Enrichment Characteristics and Inhibition Kinetics Characteristics of the Anammox Granular Sludge

Z.Z. Wang*, Y. Ji*, H. Zhang*, L.N. Yan**†, D. Zhao* and P. Gao*

*College of Energy and Environmental Engineering, Hebei University of Engineering, Handan 056038, China
**College of Environmental and Energy Engineering, Beijing University of Technology, Beijing, 100124, China
†Corresponding author: L.N. Yan; w-z-z@163.com

ABSTRACT

The anammox granular sludge was enriched by shortening the hydraulic retention time (HRT) (from 27 h to 6.67 h) in the UASB reactor, which was fed with ammonium chloride and nitrite as the substrates, and the effect of different HRTs on the nitrogen removal performance of anammox granule sludge was studied. After 159 d of operation, the total nitrogen loading rate (NLR_{TN}) reached 1.72 Kg/(m^3·d), the total nitrogen removal rate (NRR_{TN}) reached 1.33 Kg/(m^3·d), and the removal efficiencies of NH_4^+-N (NRE_{NH4-N}) and NO_2-N (NRE_{NO2-N}) were over 95%. The ratio of ΔNO_2-N/ΔNH_4^+-N was 1.31 and ΔNO_3-N/ΔNH_4^+-N was 0.24, which complied with the chemical reaction stoichiometry of anammox. The colour of anammox granular sludge changed from light red to deep red; the percentage of granular sludge larger than 1.5 mm was the highest, which proportionately accounted for 62.32%; and the surface of the granular sludge was found, via Fourier transform infrared spectroscopy (FTIR), to contain abundant functional groups. The inhibitory effect of substrates (NH_4^+-N and NO_2-N) on anammox was studied via an inhibition kinetics batch test using anammox granular sludge (Day 159) in the UASB reactor, and the test results were fitted in the Haldane inhibition model with correlation coefficients (R^2) of 0.9912 and 0.9949.

INTRODUCTION

The development of petrochemical, food and pharmaceutical industries, as well as the improvement of people's living standards, has sharply driven up the nitrogen content in urban sewage, industrial sewage, and landfill leachate, which has caused the severe nitrogen pollution problem in China's bodies of water. Anammox is a novel biological nitrogen removal technology. In the anaerobic condition, NO_2-N is used as an electron acceptor, NH_4^+-N is used as an electron donor, and the reaction product is N_2 (Van de Graaf et al. 1996). The reaction formula is shown as Eq. (1), in which NH_4^+-N:NO_2-N:NO_3^- is 1:1.32:0.26. When compared with the traditional biological nitrogen removal technology, the anammox process has the advantages of low energy consumption, high efficiency, no addition of organic carbon sources, and low operating costs (Mulder et al. 1995).

$$NH_4^+ + 1.32NO_2^- + 0.066HCO_3^- + 0.13H^+ \rightarrow 1.02N_2 + 0.26NO_3^- + 0.066CH_2O_{2.5}N_{0.15} + 2.03H_2O \qquad \ldots(1)$$
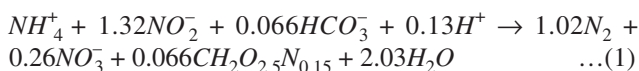
Currently, more than 200 full-scale anammox reactors have been applied in wastewater treatment plants around the world, and anammox has broad application prospects as a new biological nitrogen removal technology (Kang et al. 2019, Cao et al. 2017). The granulation of anammox bacteria have excellent sedimentation, can retain high biomass, and can improve the impact load resistance and the exchange of substances and information between anammox bacteria. However, anammox growth is slow, the doubling time is 11 d (Strous et al. 1998), and anammox bacteria are extremely sensitive to environmental conditions, including the environmental temperature (30-40°C), pH (7.5-8.0), and loading (Tang et al. 2017). Investigating how anammox granular sludge can be enriched has become a research hotspot (Lin & Wang 2017).

Although ammonia and nitrite were used as substrates for anammox bacteria, more than a certain concentration will inhibit the growth of anammox bacteria. Chen et al. (2011) used EGSB as a reactor and anammox granular sludge with the MLVSS of 31.31 g/L as inoculated sludge. The Haldane model was used to describe the degradation kinetics of inhibition by the test. When the concentration of ammonia reached 707.9 mg/L and nitrite reached 768.1 mg/L, their degradation rates were at maximum with ammonia reaching 381.2 mg/gVSS·d and nitrite reaching 304.7 mg/gVSS·d. Therefore, studying the inhibition kinetics of anammox has significance for guiding microbial growing.

Consequently, this paper will combine the continuous flow and sequencing batch test to study (1) the effects of

HRT on the enrichment characteristics of anammox granular sludge and its nitrogen removal performance; (2) granular sludge morphology and its functional group composition; and (3) the inhibition kinetics of substrate concentration on anammox granular sludge, to provide a theoretical basis and technical support for the practical engineering application of the anammox process.

MATERIALS AND METHODS

Anammox UASB reactor: Fig. 1 shows the UASB reactor, which was composed of Plexiglass with a diameter of 11 cm and a height of 110 cm. The reactor's upper part was equipped with a three-phase separator for the separation of sludge, water and gas. The reactor was enwrapped with soft black material for heat preservation and protection from light, a water bath cycle was arranged outside the main reactor, two heating rods were arranged in the water bath's circulation tank for controlling the temperature inside the reactor, and the reactor had external reflux for controlling its rising velocity.

Test water and inoculated sludge: In this experiment, a continuous culture was carried out, and the anammox granule sludge was further enriched with anammox flocculating sludge and anaerobic granule sludge, both of which were cultured for 160 days under inorganic environmental conditions as inoculated sludge.

Synthetic wastewater was used in the test. The concentration of ammonia nitrogen and nitrite nitrogen was 1:1.32, the concentration of KH_2PO_4 was 27.2 mg/L, the concentration of $CaCl_2 \cdot 2H_2O$ was 180 mg/L, and the concentration of $MgSO_4 \cdot 7H_2O$ was 300 mg/L. The concentrations of trace elements I and II were both 1 mL/L. Trace element I (g/L) consisted of 5 EDTA and 5 $FeSO_4$ and trace element II (g/L) consisted of 15 EDTA, 0.43 $ZnSO_4 \cdot 7H_2O$, 0.24 $CoCl_2 \cdot 6H_2O$, 0.99 $MnCl_2 \cdot 4H_2O$, 0.25 $CuSO_4 \cdot 5H_2O$, 0.22 $NaMoO_4 \cdot 2H_2O$, 0.19 $NiCl_2 \cdot 6H_2O$, 0.21 $NaSeO_4 \cdot 10H_2O$ and 0.014 H_3BO_3.

Analysis methods and calculation formulas: Measurements were made every other day, and the water samples were filtered through 0.45 μm filter paper. Test methods were determined via standard methods (APHA 1998), with NH_4^+-N, NO_2^--N, and NO_3^--N determined by a spectrophotometry determination of Nessler's Reagent, N-(1-naphthyl)-ethylenediamine spectrophotometric determination, and ultraviolet spectrophotometry. DO and pH were determined by German Multi3630, and MLSS and MLVSS were determined by the gravimetric method.

Fourier infrared spectroscopy analysis method: The dried anammox granular sludge and KBr were tableted at a dose of 1:100, then analysed by Fourier transform infrared spectroscopy. The collected data were analysed by origin 8.0.

Granular sludge particle size determination method: The particle size distribution of the granular sludge was determined by wet sieving (Laguna et al. 1999) with stainless steel meshes with mesh aperture diameters of 3.0, 2.5, 2.0, 1.5, 1.0 and 0.5 mm. The sludge mixture was taken out of
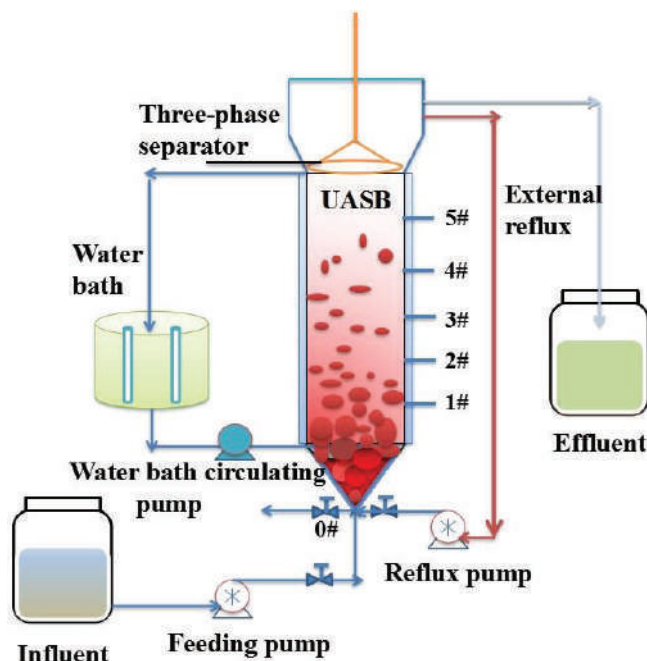

Fig. 1: Schematic diagram of the anammox granular sludge-based UASB reactor.

the reactor, and the steel sieve was positioned vertically from top to bottom according to pore size. A container was placed under the bottom 0.5 mm sieve to hold the fine particles, and the sludge sample was slowly poured into the sieve. After screening, the granular sludge of different particle size ranges was collected into different containers, and the MLSS of each screen that intercepted the granular sludge was measured.

Inhibition kinetic sequencing batch test: The anammox granular sludge (159 d) was taken from the UASB reactor, rinsed three times with clean water to remove the surface matrix, and filtered with filter paper. About 12 g of wet sludge were weighed with an electronic balance, then placed into a 250 mL serum bottle, as shown in Fig. 2. The water bath temperature was controlled to about 33°C, the pH value was controlled at 7.3-7.6, a 10 mL syringe was used for sampling, and the solution was fully mixed with a magnetic stirrer. In the single factor inhibition experiment with NH_4^+-N, other conditions must be controlled. The NH_4^+-N gradients were about 70, 100, 200, 320, 500, and 600 mg/L. In the single factor inhibition experiment with NO_2^--N and other conditions must also be controlled. The NO_2^--N gradients were about 80, 110, 210, 270, 300, and 400 mg/L. Five mL was taken with a 10 mL syringe every 1 h, and the mixture was centrifuged to determine the NH_4^+-N, NO_2^--N and NO_3^--N of the supernatant, while the degradation rate of NH_4^+-N and NO_2^--N were calculated.

RESULTS AND DISCUSSION

Effect of different HRTs on the nitrogen removal performance of anammox granular sludge: The UASB reactor temperature was maintained at 32~34°C, the influent pH value was controlled at 7.3~7.8, and the return flow was kept constant. The test was run under different HRT conditions, and when NRE_{NH+4-N} and $NRE_{NO_2^--N}$ reached 97% or more, HRT conditions were adjusted, along with the concentrations of ammonia and nitrite as given in Table 1.

Removal efficiency of NH_4^+-N and NO_2^--N by HRTs: The removal efficiency of NH_4^+-N and NO_2^--N under different HRT conditions are shown in Fig. 3(a) and (b). In phase I (HRT was 27 h), the anammox granular sludge was adapted to the environment because the inoculated sludge HRT was 27h. After 19 d of operation, $NRE_{NH_4^+-N}$ was 99.03%, and $NRE_{NO_2^--N}$ was 99.18%, while the anammox granular sludge was not inhibited. The removal loading of NH_4^+-N ($NRR_{NH_4^+-N}$) was 0.17 kg/m^3·d and NO_2^--N ($NRR_{NO_2^--N}$) was 0.22 kg/m^3·d. In stage II, the other conditions were essentially unchanged. When HRT was shortened to 20.86 h, the substrate loading suddenly increased. The $NRE_{NH_4^+-N}$ decreased to 93.42% and

Table 1: Operating parameters of anammox granular sludge reactor at different stages.

Stage	Time (d)	HRT (h)	Velocity (m/h)	Reflux ratio	NH_4^+-N concentration (mg/L)	NO_2^--N concentration (mg/L)	NLR (kg/m^3·d)	NRR (kg/m^3·d)
I	1~19	27.00	4.78	121	187.29	242.48	0.40	0.34
II	20~47	20.86	4.79	90	198.24	253.60	0.54	0.45
III	48~81	15.50	4.80	70	177.96	233.70	0.70	0.55
IV	82~119	8.63	4.86	40	175.56	234.39	1.16	0.95
V	120~159	6.67	4.89	30	173.19	234.17	1.72	1.33
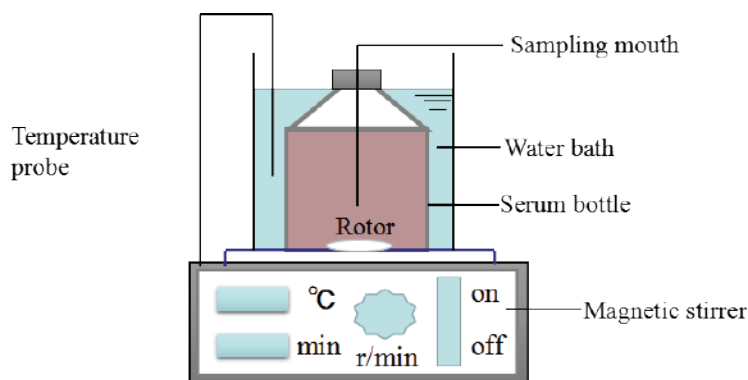
Fig. 2: Schematic diagram of the batching test.

$NRE_{NO_2^--N}$ to 95.31%, while $NRR_{NH_4^+-N}$ rose to 0.21kg/m^3·d and $NRR_{NO_2^--N}$ rose to 0.29kg/m^3·d. After 27 d, $NRE_{NH_4^+-N}$ reached 98.15% and $NRE_{NO_2^--N}$ reached 98.72%.

When HRT was shortened to 15.50 h, in Phase III, the $NRE_{NH_4^+-N}$ began to decrease due to the sudden shortening of HRT and fluctuated around 90%. However, the decrease of NO$_2^-$-N was large, and $NRE_{NO_2^--N}$ decreased from 98.72% in the previous phase to 87.74%, indicating that the inhibition of nitrite nitrogen was more obvious. After 33 d of operation, the activity of anammox bacteria was restored, $NRE_{NH_4^+-N}$ was 97.54% and $NRE_{NO_2^--N}$ was 97.37%, and $NRR_{NH_4^+-N}$ reached 0.27 kg/m^3·d and $NRR_{NO_2^--N}$ reached 0.36 kg/m^3·d. In phase IV (HRT was 8.63 h), the anammox granular sludge activity was better, and at the end of phase IV, $NRE_{NH_4^+-N}$ was 98.27% and $NRE_{NO_2^--N}$ was 98.68%.

In phase V, the HRT was shortened to 6.67 h, $NRE_{NH_4^+-N}$ was significantly reduced to 86.05%, and $NRE_{NO_2^--N}$ was decreased to 79.95%. The reasons for analysis are as follows: (1) The shorter the HRT, the higher the loading of the ammonia nitrogen and nitrite nitrogen, and the anammox activity was inhibited, resulting in a decrease of the treatment effect; (2) The HRT was short and part of the ammonia and the nitrite were discharged outside of the reactor without reaction, increasing the effluent concentration, and a decrease of the removal loading of the ammonia and nitrite. After 39 days, $NRE_{NH_4^+-N}$ was 97.05% and $NRE_{NO_2^--N}$ was 98.21%, and the anammox activity was further improved.

Removal efficiency of TN by HRT: The removal efficiency of TN (NRE_{TN}) under different HRT conditions is shown in Fig. 3(c) and (d). HRT was 27h in phase I. On the first day

(a)

(b)

(c)

(d)
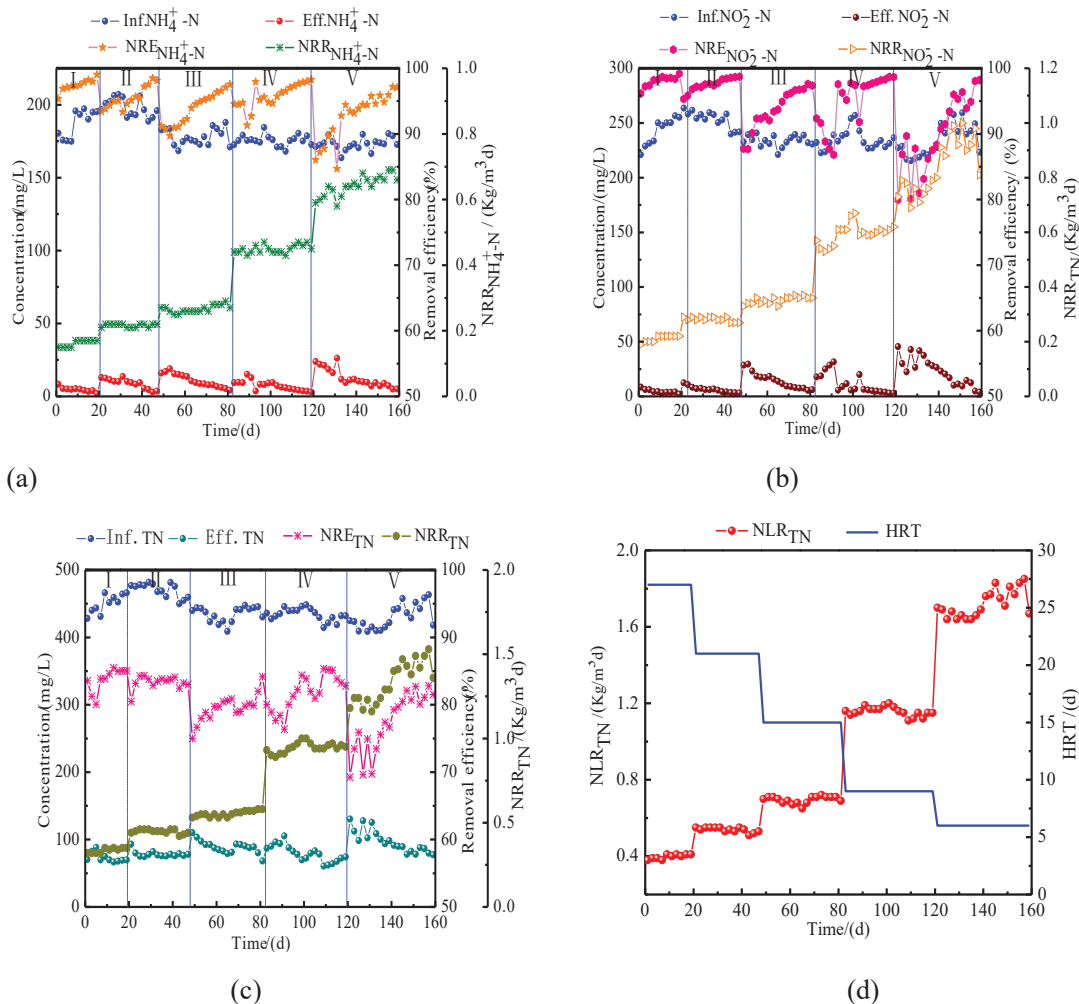
Fig. 3. Under different HRTs (a) NH$_4^+$-N, (b) NO$_2^-$-N, (c) TN nitrogen removal performance, and (d) the variation of NLR.

of operation, TN concentration was 428.04mg/L, total nitrogen output was 70.33 mg/L, NRR_{TN} was 0.32 kg/m^3·d, and NRE_{TN} was 83.57%. After 19 d of operation, NRE_{TN} reached 85.02%, and NRR_{TN} was increased to 0.35 kg/m^3·d. Other conditions remained unchanged. When HRT was shortened to 20.86 h, on the first day of operation NRE_{TN} decreased to 83.77%, and NRE_{TN} continued to drop to 80.47% on the second day. The anammox activity was slightly inhibited due to the shortening of HRT, however, after 27 d of operation, NRE_{TN} reached 83.01%, NRR_{TN} reached 0.44 kg/m^3·d, and NLR_{TN} reached 0.53 kg/m^3·d. The anammox activity was also improved. Then HRT was shortened to 15.50 h, and NRE_{TN} was reduced to 75.01%. After 33 d, NRE_{TN} was increased to 84.16%, NRR_{TN} reached 0.58 kg/m^3·d, and NLR_{TN} was 0.69 kg/m^3·d. In phase IV, HRT was 8.63 h, anammox activity was high, NRR_{TN} was reduced by about 2%, and NRE_{TN} was maintained at about 80%. When HRT was shortened to 6.67 h, NRE_{TN} was decreased by 69.27%, and activity was severely inhibited, resulting in a significant decrease in the removal efficiency. After 39 d, anammox activity was essentially restored, NRE_{TN} reached 81.53%, NRR_{TN} was 1.33kg/m^3·d and NLR_{TN} was 1.72 kg/m^3·d. This showed that anammox activity was further improved and the ability to withstand the loading of nitrogen was strengthened. Yu et al. (2014) studied the effect of nitrogen performance on different HRTs, with HRTs of 72 h, 48 h, 24 h, 12 h and 6 h, NLR_{TN} was increased from 0.28 kg/m^3·d to 1.28 kg/m^3·d and the anammox activity was further improved with the shorting of HRT.

Changes in stoichiometry under different HRT conditions: Fig. 4 shows the changes of $\Delta NO_2^--N/NH_4^+-N$ and $\Delta NO_3^--N/NH_4^+-N$ under different HRT conditions. Table 2 shows the average NO_2^--N/NH_4^+-N values and $\Delta NO_3^--N/NH_4^+-N$ values in different phases. Formula (1) shows the chemical reaction equation of anammox, the ratio of $\Delta NO_2^--N/\Delta NH_4^+-N$ is 1.32 and $\Delta NO_3^--N/\Delta NH_4^+-N$ is 0.26. These ratios can determine the basis of the anammox reaction. Fig. 4 shows that the ratio of $\Delta NO_2^--N/\Delta NH_4^+-N$ fluctuated around 1.32 and $\Delta NO_3^--N/\Delta NH_4^+-N$ fluctuated around 0.26, which complied with the chemical reaction stoichiometry of anammox. Kang et al. (2019) concluded that the ratio of $\Delta NO_2^--N/\Delta NH_4^+-N$ was 1.22 and $\Delta NO_3^--N/\Delta NH_4^+-N$ was 0.22, and the results of this experiment were similar to Kang et al. (2019).

The Morphology of Anammox Granular Sludge

Apparent characteristics: Fig. 5 shows the apparent characteristics of anammox granular sludge at the initial phase of inoculation and operation for 159 d. The colour of anammox granular sludge was light red, and the average particle size was small at the initial phase of inoculation; when the reactor was operated for 159 d, the colour of anammox granular sludge turned dark red. Tang et al. (2011) concluded that the contents of heme C increased with the increase of NRR_{TN}, which lead to the deepening of colour in a similar result to this experiment. Anammox bacteria exhibit the flocculation effect; under the shearing force of a large rising flow rate, the
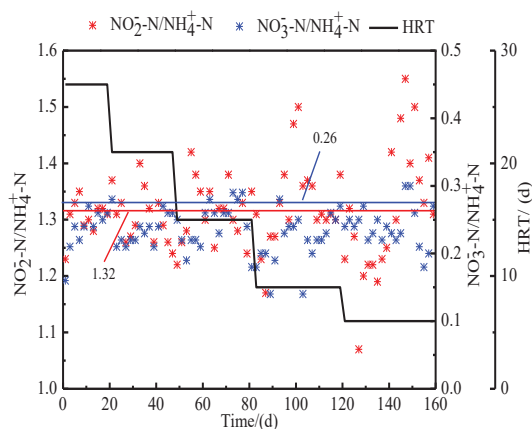
Fig. 4: $\Delta NO_2^--N/NH_4^+N$ and $\Delta NO_3^--N/NH_4^+N$ under different HRT conditions.

Table 2: Average values of $\Delta NO_2^--N/NH_4^+N$ and $\Delta NO_3^--N/NH_4^+N$ under different HRT conditions.

HRT/h	27.00	20.86	15.50	8.63	6.67
$\Delta NO_2^--N/\Delta NH_4^+-N$	1.30	1.31	1.31	1.33	1.31
$\Delta NO_3^--N/\Delta NH_4^+-N$	0.23	0.24	0.24	0.22	0.24

cells gather together and are tired, and anammox granular sludge continues to increase (Lin et al. 2019).

Change in particle size distribution: Fig. 6 shows the particle size distribution of the granular sludge at the bottom of the UASB reactor. The particle size distribution of the granular sludge was characterized by the percentage of the total MLSS of the measured sludge in the range of the particle size gradient. In the initial inoculation, the particle size was 0.50-1.00 mm of granular sludge which accounted for the highest percentage (specific gravity of 27.42%), followed by 1.00-1.50 mm of granular sludge (specific gravity of 25.84%), and the percentage of sludge with a particle size less than 0.50 mm was as high as 13.89%. However, granular sludge with a particle size greater than 3.00 mm has the lowest proportion with only 1.09%. Shortening HRTs increase the rising flow rate, and granular sludge growth was promoted. Cong et al. (2014) showed that the particle diam-

eter was in the range of 0.5-2.0 mm by adjusting the rising flow rate to 9.0 m·h⁻¹ in the EGSB reactor, where granular sludge accounted for more than 65%. After 159 d operating, the particle size of the granular sludge in the reactor showed an increasing trend. Granular sludge with a particle size larger than 1.5mm accounted for 62.32%, with the particle size of 1.50-2.00 mm accounting for the highest proportion of the test (27.53%). The specific gravity of 2.00-2.50 mm was 18.47%, the proportion of 2.50-3.00 mm was 11.03%, particle size greater than 3 mm increased by 4.1 percentage points from the initial inoculation, and the specific gravity of granular sludge with the particle size of 1.00-1.5 mm was 14.04%. The specific gravity of granular sludge with particle size less than 0.50 mm was only 8%, which was 5.89 percentage points lower than the initial inoculation. An et al. (2013) obtained the physical properties of anammox granules with different sizes. 1.0~1.5 mm granular sludge

(a)   (b)
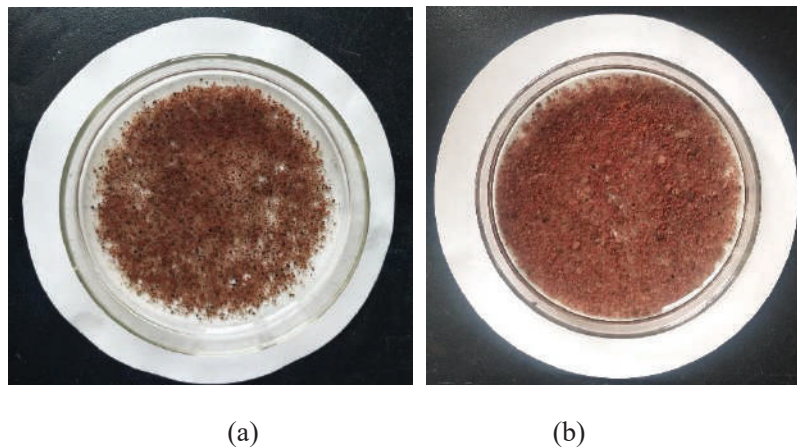
Fig. 5: The variation of anammox granular sludge in (a) 0 d and (b) 159 d.
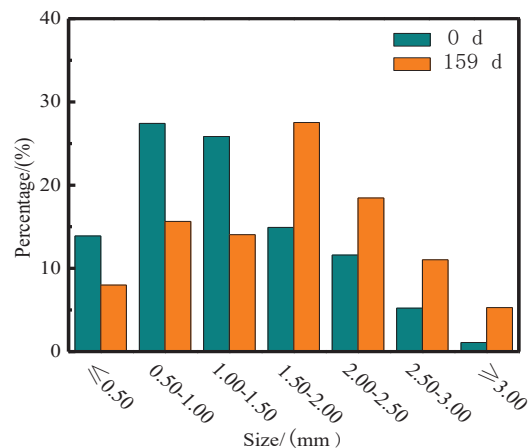
Fig. 6: The changes in the size distribution of anammox granules at different phases.

has the highest activity, and larger granular sludge was more resistant to temperature and nitrogen load shock. However, larger particles also showed larger gas passages and internal voids, reducing the stability of the granular sludge. It can be seen that on the 159 d of the reactor operation, the particle size of the anammox granular sludge gradually changed from small to large. In this experiment, the anammox granular sludge was mainly concentrated in the range of less than 1.00 mm, and the domesticated granular sludge was obtained. The diameter was concentrated in the range of more than 1.50 mm, which was essentially in the particle size range with the highest activity of anammox granular sludge.

FT-IR analysis of granular sludge: Secretions during the cell grew, the shedding of the cell surface, cell lysis and the adsorption of substances from the external environment can carry a large number of functional groups on the surface of the sludge. There are currently many studies on the compositions of EPS and the characteristics of anammox granular sludge (Lotti et al. 2019, Feng et al. 2019, Chen et al. 2016, Fang et al. 2018), but few scholars have reported on the surface functional group properties of anammox granular sludge.

Fig. 7 shows that the characteristics of the functional groups' composition of anammox granular sludge by infrared spectroscopy. In the beginning, the vibration near 3393 cm^{-1} mainly represented O-H stretching vibration and represented the alkane organic matter and C-H in the polysaccharide molecule near 2930 cm^{-1}. O-H stretching vibration in the carboxyl functional group was represented at around 2525 cm^{-1}, C=O stretching vibration in protein amide I was represented at 1600-1700 cm^{-1}, and the peak near 1040 cm^{-1} represented C-O-C stretching of polysaccharide or similar polysaccharide substance vibration. In addition, an obvious absorption peak was also found near the wavelengths of 880 cm^{-1}, 710 cm^{-1}, and 600-900 cm^{-1} which were the fingerprint areas (Yan et al. 2015, Badireddy et al. 2010). Infrared spectroscopy revealed sugar and protein in the surface of anammox granular sludge. As the reaction progressed, a more obvious peak appeared near 3290 cm^{-1}, which was mainly caused by N-H stretching

vibration in amides. The peak intensities of 2930 cm^{-1} and 1788 cm^{-1} increased, indicating C-H stretching in the alkane organic matter and polysaccharide molecules. C=O stretching vibration in the vibration and protein amide I were enhanced, and the sugar and protein contents were further enhanced.

Substrates Inhibition of Anammox and Its Kinetic Analysis

Anammox bacteria used ammonia and nitrite as substrates. At low concentrations, anammox bacteria used the substrates to react. However, at high concentrations, the activity of anammox bacteria is inhibited.

Substrates inhibition kinetics can be described using the Haldane model, which was:

$$v = \frac{v_{max}}{1 + \dfrac{Ks}{S} + \dfrac{S}{K_h}} \qquad \ldots(1)$$

Where v is the removal rate of substrates, mg/(mg·d); v_{max} is the maximum conversion rate, mg/(mg·d); S is the substrate concentration, mg/L; k_S is a half-saturation constant, mg/L; and K_h is the inhibition kinetic constant of Haldane, mg/L.

Since the Haldane model was a kinetic simulation of a single substrate reaction, for anammox reactions under dual substrates conditions, it was first necessary to control a substrate concentration to examine the effect of another substrate concentration. Firstly, the NO_2^--N concentration was controlled to 100 mg/L, and the effect of NH_4^+-N concentration on anammox activity was studied. Table 3 shows that in the range of experimental concentration with the increase of NH_4^+-N concentration, the degradation rate increased at first and then decreased.

Fig. 8 shows the kinetic characteristics of ammonium nitrogen inhibition. The correlation kinetic data of the measured ammonium was fitted to the Haldane model using Origin 8.0 software. The correlation coefficient (R^2) of the fitted curve was 0.9912, and the correlation was good. When the NH_4^+-N concentration reached 303.03 mg/L, the anammox

Table 3: Effect of NH_4^+-N concentrations on Anammox bacterial activity.

NO_2^--N concentration (mg/L)	NH_4^+-N concentration (mg/L)	The degradation rate of NH_4^+-N [mg/(mg.d)]	The degradation of NO_2^--N [mg/(mg.d)]
100	70	0.075	0.130
100	100	0.105	0.098
100	200	0.126	0.109
100	320	0.139	0.113
100	500	0.127	0.108
100	600	0.121	0.084
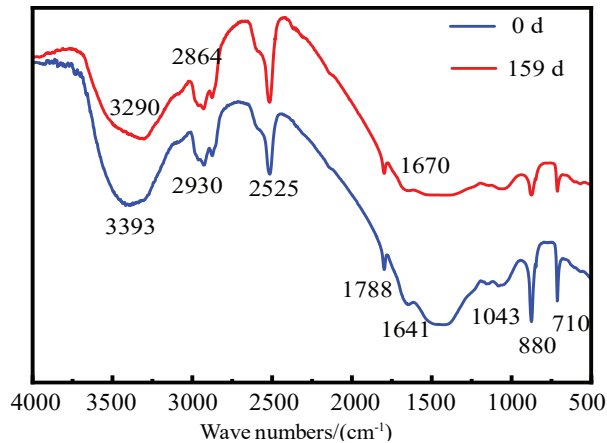
Fig. 7: The FT-IR spectra of granular sludge.
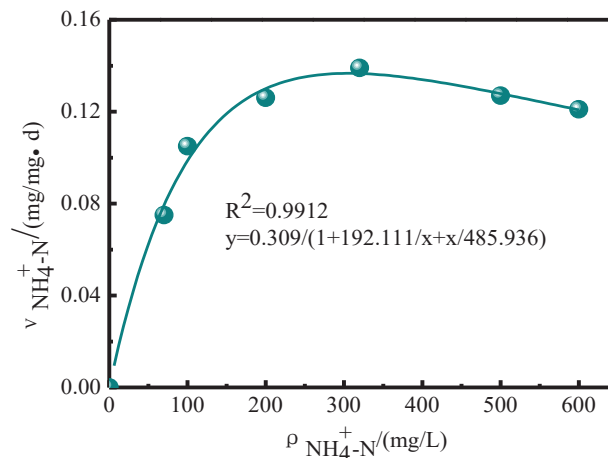
Fig. 8: Inhibition kinetic characteristics of NH_4^+-N concentration on anammox granular sludge.

activity was the highest, and the NH_4^+-N degradation rate was 0.137 mg/(mg.d). When the NH_4^+-N concentration was 600 mg/L, the degradation rate of NH_4^+-N decreased to 0.121 mg/(mg.d), whereas the maximum reaction rate (v_{max}) was 0.309 mg/(mg.d), the half-saturation constant (Ks) was 192.111 mg/L, and the inhibition kinetic constant was 485.936 mg/L.

NH_4^+-N concentration was controlled to be 70 mg/L, and the effect of NO_2^--N concentration on anammox activity was studied. Table 3 shows that in the range of experimental concentration with the increase of NO_2^--N concentration, the degradation rate increased at first and then decreased.

Fig. 9 shows the kinetic characteristics of nitrite inhibition. The correlation inhibition kinetic data of the measured nitrite was fitted to the Haldane model using Origin 8.0

software. The correlation curve (R^2) of the fitted curve was 0.9949 and the result was high. When the concentration of NO_2^--N reached 169.70 mg/L, anammox activity was highest, and the degradation rate of NO_2^--N was 0.115 mg/(mg.d). When the concentration of NO_2^--N reached 400 mg/L, the degradation rate of NO_2^--N decreased to 0.068 mg/(mg.d). The maximum reaction rate (v_{max}) was 0.737 mg/(mg.d), the half-saturation constant (Ks) was 456.739 mg/L, and the inhibition kinetic constant was 61.968 mg/L.

Results showed that when the inhibitor was ammonium, the maximum inhibitory concentration was 303.03 mg/L, the NH_4^+-N degradation rate was 0.137 mg/(mg.d), and the maximum reaction rate was 0.309 mg/(mg·d). When nitrite was an inhibitor, the maximum inhibitory concentration was 169.70 mg/L, the degradation rate of NO_2^--N was 0.115 mg/

Table 4: Effect of NO_2-N concentrations on Anammox bacteria activity.

NH_4^+-N concentration (mg/L)	NO_2^--N concentration (mg/L)	The degradation rate of NH_4^+-N [mg/(mg.d)]	The degradation of NO_2^--N [mg/(mg.d)]
70	80	0.086	0.092
70	110	0.958	0.104
70	210	0.114	0.111
70	270	0.097	0.108
70	300	0.088	0.101
70	400	0.068	0.083
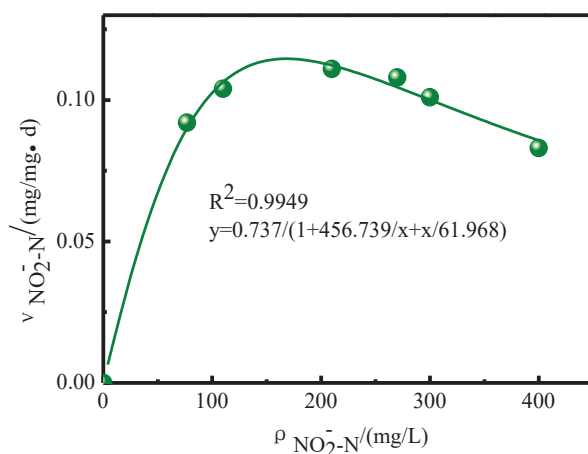
Fig. 9: Inhibition kinetic characteristics of NO_2-N concentration on anammox granular sludge.

(mg.d), and the maximum reaction rate was 0.737 mg/(mg·d). In contrast, the inhibitory effect of nitrate was more significant in both substrates. Similarly, Li et al. (2016) showed that the removal rate of ammonia and nitrite by inhibition kinetic sequencing batch tests increased at first and then decreased. The ammonia nitrogen concentration was 295.62 mg/L, anammox activity was the highest, and the ammonia nitrogen degradation rate was 0.1540 mg/(mg·d). The nitrite degradation rate was 0.1649 mg/(mg·d) at the concentration of 151.10 mg/L, and anammox activity was the highest.

CONCLUSIONS

(1) Anammox granular sludge that was used UASB as the reactor by shorting hydraulic retention time (HRT shortened from 27 h to 6.67 h) was enriched. After 159 d of operation, the $NRE_{NH+ 4-N}$ and NRE_{NO_2-N} reached more than 95%, the NRE_{TN} was 81.53%, and the NRR_{TN} reached 1.33 kg/(m³.d).

(2) In the initial phase of inoculation, the percentage of granular sludge with the particle size of 0.50-1.00 mm was the highest (specific gravity was 27.42%), and the

proportion of granular sludge with particle size greater than 3.00 mm was the lowest, only 1.09%. At 159 d, the average particle size of the granular sludge in the reactor showed an increasing trend, with the highest percentage of 1.50-2.00 mm (specific gravity 27.73%), and the particle size larger than 3 mm accounted for 5.29%, which was 4.1 percentage points higher than the initial inoculation.

(3) Analysing the anammox granular sludge via the Fourier transform infrared spectroscopy revealed that mainly sugar and protein were on the surface of anammox granular sludge. After 159 d of reactor operation, the sugar and protein content further increased.

(4) By inhibition of the kinetic sequencing batch test, the maximum reaction rate was 0.309 mg/(mg·d), the half-saturation constant (Ks) was 192.111 mg/L, and the inhibition kinetic constant was 485.936mg/L. The nitrite maximum reaction rate was 0.737 mg/(mg·d), the semi-saturation constant (Ks) was 456.739 mg/L, and the inhibition kinetic constant was 61.968 mg/L. In contrast, the anammox bacteria in the two substrates were more significantly inhibited by nitrate.

ACKNOWLEDGEMENTS

REFERENCES

APHA 1998. Standard Methods for the Examination of Water and Wastewater. 20th Edn., Edited by American Public Health Association, Washington, DC.

An, P., Xu, X.C., Yang, F.L. and Li, Z.Y. 2013. Comparison of the characteristics of anammox granules of different sizes. Biotechnology and Bioprocess Engineering, 18(3): 446-454.

Badireddy, A.R., Chellam, S., Gassman, P.L., Engelhard, M.H., Lea, A.S. and Rosso, K.M. 2010. Role of extracellular polymeric substances in bioflocculation of activated sludge microorganisms under glucose-controlled conditions. Water Research, 44: 4505-4516.

Chen, T.T., Zheng, P., Shen, L.D., Ding, S. and Mahmood, Q. 2011. Kinetic characteristics and microbial community of Anammox-EGSB reactor. Journal of Hazardous Materials, 190(1-3): 28-35.

Cong, Y., Huang, X. L., Wand, X.L. and Gao, D.W. 2014. Faster formation of anammox granular sludge. Ciesc Journal, 65(2): 664-671.

Cao, Y.S., Van Loosdrecht, M.C.M. and Daiggerr, G.T. 2017. Mainstream partial nitration - anammox in municipal wastewater treatment: status, bottlenecks, and further studies. Applied Microbiology and Biotechnology, 101(4): 1365-1383.

Chen, H., Hu, H.Y., Chen, Q.Q., Shi, M.L. and Jin, R.C. 2016. Successful start-up of the anammox process: Influence of the seeding strategy on performance and granule properties. Bioresource Technology, 211: 594-602.

Feng, C.J., Lotti, T., Lin, Y.M. and Malpei, F. 2019. Extracellular polymeric substances extraction and recovery from anammox granules: Evaluation of methods and protocol development. Chemical Engineering Journal, 374: 112-122.

Fang, F., Yang, M.M., Wang, H., Yan, P., Chen, Y.P. and Guo,J.S. 2018. Effect of high salinity in wastewater on surface properties of anammox granular sludge. Chemosphere, 210: 366-375.

Kang, D., Yu, T., Xu, D.D., Zeng, Z., Ding, Q., Zhang, M., Shan, S.D., Zhang, W.D. and Zheng, P. 2019. The anammox process at typical feast-famine states: Reactor performance, sludge activity and microbial community. Chemical Engineering Journal, 370(15): 110-119.

Kang, D., Xu, D.D., Yu, T., Feng, C.D., Li, Y.Y., Zhang, M. and Zheng, P. 2019. Texture of anammox sludge bed: Composition feature, visual characterization and formation mechanism. Water Research, 154(1): 180-188.

Li, Y., Li, J., Cai, H., Chen, G., Hou A.Y., Hu, X., Bian, W., Guo, R.F. and Liu, Y.F. 2016. Nitrogen removal and inhibition kinetics of ANAMMOX reactor fed with the mature landfill leachate. China Environmental Science, 36(5): 1409-1416.

Laguna, A., Ouattara, A., Gonzalez, R.O., Baron, O., Fama, R., Mamouni, E., Guiot, S., Monroy, O. and Macarie, H. 1999. A simple and low cost technique for determining the granulometry of upflow anaerobic sludge blanket reactor sludge. Water Science Technology, 40(8): 1-8.

Lin, Q.J, Kang, D., Zhang, M., Yu, T., Xu, D.D., Zeng, Z. and Zheng, P. 2019. The performance of anammox reactor during start-up: Enzymes tell the story. Process Safety and Environmental Protection, 121: 247-253.

Lotti, T., Carretti, E., Berti, D., Martina, M.R., Lubello, C. and Malpei, F. 2019. Extraction, recovery and characterization of structural extracellular polymeric substances from anammox granular sludge. Journal of Environmental Management, 236: 649-656.

Lin, X.M. and Wang, Y.Y. 2017. Microstructure of anammox granules and mechanisms endowing their intensity revealed by microscopic inspection and rheometry. Water Research, 120(1): 22-31.

Mulder, A., Van De Graaf, A.A., Robertson, L.A. and Kuenen, J.G. 1995. Anaerobic ammonium oxidation discovered in a denitrifying fluidized bed reactor. FEMS Microbiol. Ecol, 16(3): 177-183.

Strous, M., Heijnen, J. J., Kuenen, J. G. and Jetten, M. S. M. 1998. The sequencing batch reactor as a powerful tool for the study of slowly growing anaerobic ammonium - oxidizing microorganisms. Applied Microbiology and Biotechnology, 50: 589-596.

Tang, C.J., Duan, C.S., Yu, C., Song, Y.X., Chai, L.Y., Xiao, R.Y., Wei, Z.S. and Min, X.B. 2017. Removal of nitrogen from wastewaters by anaerobic ammonium oxidation (ANAMMOX) using granules in upflow reactors. Environmental Chemistry Letters, 15: 311-328.

Tang, C.J., Zheng, P. and Wang, C.H. 2011. Performance of high-loaded ANAMMOX UASB reactors containing granular sludge. Water Research, 45: 135-144.

Van de Graaf, A.A., de Bruijn, P., Robertson, L.A., Jetten, M.S.M. and Kuenen, J.G. 1996. Autotrophic growth of anaerobic ammonium-oxidizing microorganisms in a fluidized bed reactor. Microbiology, 142(8): 2187-2196.

Yan, L.L., Liu, Y., Wen, Y., Ren, Y., Hao, G.X. and Zhang, Y. 2015. Role and significance of extracellular polymeric substances from granular sludge for simultaneous removal of organic matter and ammonia nitrogen. Bioresource Technology, 179: 460-466.

Yu, Y.C., Tao, Y. and Gao, D.W. 2014. Effects of HRT and nitrite/ammonia ratio on anammox discovered in a sequencing batch biofilm reactor. RSC Advances, 4: 54798-54804.

Interaction Between the Tourism Industry and Ecological Environment Based on the Complicated Adaptation System (CAS) Theory: A Case Study on Henan Province, China

Zhong Wei Wang†

Yellow River Conservancy Technical Institute, Kaifeng 475004, China
†Corresponding author: Zhong Wei Wang; 94381557@qq.com

ABSTRACT

Pressure over the destruction of the ecological environment by the tourism industry from the blind development of tourism areas, tourism projects that destroy the ecological environment, tourist overloading during holidays, and poor environmental protection awareness among tourists is increasing. Seeking a balance point between ecological environmental protection and tourism industrial development is key in the sustainable development of the tourism industry. The Complicated Adaptation System (CAS) theory is an important theory in the current system, which focuses on the interaction of the internal elements of a system. Analyzing the interactive development between the tourism industry and the ecological environment based on CAS theory is one way to achieve the harmonious coexistence of the tourism industry and the ecological environment. A case study on Henan Province, China, is conducted, the literature on the interaction between the tourism industry and ecological environment is reviewed, and the environmental pollution status of Henan Province caused by the tourism industry is summarized. Moreover, the complex adaptation of the tourism industry and ecological environment is analyzed. Research results show that most studies support the belief that the tourism industry generates substantial environmental pollution. Environmental pollution from the tourism industry in Henan Province is reflected in tourist overloading, the direct effects of pollution from tourism consumption, damage to cultural relics in star-level tourism areas, and in dwindling habitats for plant and animal survival. Analyzing the interactive relationship between the tourism industry and ecological environment has scientific value and is worth promoting. This relationship is established based on CAS theory from four characteristics, namely, clustering, nonlinearity, flow, and diversity, and three mechanisms, that is, labelling, an internal model, and building blocks. The research conclusions can serve as a reference to better facilitate tourism industry development, estimate the relationship between the tourism economy and ecological environment, and combine ecological tourism and green technological innovation effectively.

INTRODUCTION

The tourism industry is an important component of the modern service industry, which can promote the development of new industries, including ecological tourism, rural tourism, and leisure agriculture. Moreover, the sustainable development of natural ecological environments in tourism destinations can be realized by improving tourism ecological efficiency and promoting ecological protection, thereby achieving interaction between economic development and environmental protection in China. As a "smoke-free industry," the tourism industry is an important direction for local industrial transformation. However, problems in practical development, construction, and tourism activities have emerged, such as the blind development of tourism areas, tourism projects that destroy ecological environments, and tourist overloading during holidays, which can lessen

the environmental carrying capacity of tourism areas. Specifically, the most adverse impact of tourism product consumption on local ecology is reflected in ecological environmental pollution and ecosystem damage. Tourists generate pollution during tourism activities. Faeces and the arbitrary disposal of waste, bottles, papers, and tin cans in domestic wastewater can cause ecological environmental pollution. Driven by economic benefits, numerous tourism areas receive tourist volumes beyond their carrying capacity or develop tourism measures without permission from relevant authorities. Such activities can damage historical relics with substantial historical cultural value or unique and coordinated natural and human landscapes. Tourism suppliers may generate environmental pollution owing to "waste gas, wastewater and waste residues" and the improper layout of tourism service facilities during development, construction, and operation. The surge in population facilitates crowding

and chaos, and tourist destructive behaviour can generate environmental pollution and cause damage. Soil properties deteriorate from being trampled on by numerous people, and lingering tourist populations consume products, natural resources, and energy reserves. Moreover, population concentrations can lead to atmospheric, noise, and visual pollution.

Henan Province is an agricultural province in China with a relatively small population. The province expands its tourism industrial scale continuously by taking advantage of its agricultural industry and tourism resources. After continuous development for nearly 30 years, the tourism industry in Henan Province, especially the rural industry, has formed a preliminary scale. Moreover, Henan Province is an important tourism area owing to its 5,000-year history, cultural artefacts, and unique resources. Nevertheless, the development of the tourism industry in Henan Province has experienced serious challenges in recent years. The development of cultural tourism, which is a subject of tourism products, has slowed down significantly and even halted. Tourism products generate serious environmental pollution and lack the integration of tourism resources. Moreover, the public demonstrates low enthusiasm and environmental protection awareness and lack of responsibility toward tourism environmental resources, thereby influencing environmental pollution in the tourism process. Tourists are direct contributors to environmental pollution in tourism areas during holidays owing to experienced difficulties in parking, eating, defecting, and resting. Selecting a balance point between tourism industry development and environmental protection involves the entire tourism industry development process. Thus, how to address the conflict between industry development and environmental protection in tourism development and realize the sustainable development of the tourism industry and effective protection of the ecological environment should be investigated further.

PAST STUDIES

The tourism industry is an important component of the modern service industry. Tourism ecological efficiency can be improved by new industries, including ecological tourism, rural tourism, and leisure agriculture. However, problems exist in tourism industry development, such as the blind development of tourism areas, tourism projects that destroy ecological environments, and the reduction of ecological environmental capacity owing to tourist overloading during holidays. As a result, studies focus mainly on the interactive relationship between tourism and the environment. With respect to the interactive relationship between the tourism industry and ecological environment, Butler (1991) believed that the tourism industry and relevant developments impact

the environment of "tourism destinations." Owing to a general lack of knowledge, responsibility, and long-term environmental protection planning, the development of numerous tourism areas conforms neither to the environment nor culture of host countries and communities. He et al. (2003) investigated wetland resources in south Dongting Lake and its tourism value and established an evaluation system for the ecological landscape. Moreover, the authors conducted qualitative and quantitative assessments on the value of the wetland landscape to ecological tourism and proposed a principle and framework for the sustainable development of the wetland landscape. Mclennan et al. (2012) discussed the relationship between the economy, society, and environmental indices from three major transformation stages of the tourism industry. Based on a survey of 303 residents in three regions, the authors found that the residents are in different stages of economic development and tourism dependence and thus formulated different tourism, economic, social, and environmental indices. Jinhe et al. (2012) believed that tourism wastes are by-products of resource consumption and environmental digestion and exert environmental and ecological impacts. For example, for the Huangshan National Park in China, the environmental Kuznets curve fit of tourism wastes was tested based on time series data from 1979 to 2010. The results showed that solid-liquid waste emissions from tourists have an environmental Kuznets inverted U-shaped relation with tourism industrial development. Tang et al. (2014) discussed the influence of tourism traffic, accommodations, and activities on total CO_2 emissions from the tourism industry in China from 1990 to 2012 using the top-down method. Cao et al. (2016) investigated large invertebrate communities in nine lakes at the Jiuzhaigou Natural Reserve and found that with the increase of populations and acceleration of urbanization, tourism activities in natural protection zones and other natural reserves exert serious impacts on the ecological environment of animals. Based on the statistical data of 11 provinces (cities) in China's Yangtze River, Zhou. Cheng et al. (2016) established an assessment system for the regional economy, ecological environment, and tourism industry and evaluated the development levels of the three systems using the weighted TOPSIS method. The authors concluded that the regional economy is highly associated with the tourism industry of provinces (cities), but no evident contradiction exists between environmental protection and economic development. Fan et al. (2017) pointed out inadequate tourism resources or poor tourism resource development in different regions, which fail to promote the development of the tourism industry and cause serious damage to local natural ecological environments, thereby resulting in blind and excessive development. Moreover, based on the environmental bearing capacity of tourism landscapes, the authors analyzed the

impact of tourism resource development on the ecological environment and proposed a strategy for sustainable development. Chenyu et al. (2018) constructed a measurement model to assess coordinated development levels and analyze the relevant spatiotemporal evolution model for the period of 2000-2016 based on 14 cities in Gansu Province, China. The authors concluded that ecological environmental development generally lagged behind the tourism industry and economic growth from 2000 to 2016, and the three systems failed to realize synchronous coordinated development. Lopez (2018) believed that the tourism industry is one of the biggest contributors to the gross domestic product of Thailand and suggested the design of a sustainable tourism policy framework with considerations on the sustainable ecological environment. Coordination between public and private sectors may also facilitate the sustainable development of the tourism industry. Schmitz et al. (2018) analyzed the interaction between the environment and coastal tourism industry from the perspective of social-ecological networks and found that social ecosystems in coastal regions are weakened substantially owing to tourism industry development. Liu et al. (2019) analyzed spatiotemporal coupling features between the tourism industry, urbanization, and ecological environment of cities in Shanxi Province for the period of 2000-2017. The research results showed that before 2010, ecological environmental factors dominated the coupling of the urban tourism industry, urbanization, and ecological environment in Shaanxi Province. However, urbanization and the tourism industry became the dominant factors in the coupling development of the three systems after 2010. Zhao et al. (2019) designed an index system for tourism environmental capacity for Pingdingshan City and calculated and examined the tourism environmental capacity of the city. According to the research results, the ecological tourism resource development in Pingdingshan City has advantages of natural conditions, convenient traffic, and perfect infrastructures. However, several problems, such as inadequate resource protection, an unscientific management system, and so on, remain. Yuxi et al. (2020) proposed an international conflict trend predictor (ICTP) between nature-based tourism development and ecological protection and analyzed the spatial distribution features of the ICTP in the study area in China. The results showed that the ICTP level is relatively low or moderate in most regions in China, thereby indicating that most regions suffer from ecological problems caused by natural tourism activities. Based on the above literature review, though the tourism industry drives economic development, it also generates heavy environmental pollution owing to excessive tourism resource development, tourism product consumption relative to environmental carrying capacity, and the coarse commercialization of tourism products. Existing studies on the interaction between tourism industry development and ecological environment protection mainly discuss the linear relationship between tourism industry development and ecological environmental changes by designing a single index system. Besides, such studies do not assess the integral relationship between tourism and the environment from the perspective of comprehensive system theory. Moreover, studies on the interactive development of tourism and the environment as well as evolution mechanisms are inadequate. Hence, an analytical framework for the interactive development of the tourism industry and ecological environment is constructed based on the complicated adaptation system (CAS) theory. Furthermore, a case study on Henan Province, China, is conducted to interpret the evolutionary path of the interactive development of the tourism industry and the ecological environment from a new research perspective.

ENVIRONMENTAL POLLUTION STATUS OF HENAN PROVINCE FROM THE TOURISM INDUSTRY

Tourist Overloading

A good environment is a basis for the creation and development of the tourism industry. Moreover, such an environment is the most fundamental condition for the existence and development of the tourism industry in a country or region. However, tourism environments are vulnerable, and tourism development causes environmental damage and impact. Tourism development is viewed as an economic activity, and the pursuit of economic benefits is emphasized, whereas the universal impact of tourism on the environment is neglect. Tourism areas in Henan Province are operating under overloaded capacities, which can destroy the natural ecosystem equilibrium in tourism regions significantly. Fig. 1 shows that from 2010 to 2017, the total number of tourists in tourism areas in Henan Province increased continuously and reached 235 million in 2017. Overcrowding in tourism areas in Henan Province also increased local infrastructure burden, causing water and electricity supply shortages and traffic owing to the sudden rise in demand. Also, high concentrations of tourists in tourism areas in Henan Province during the peak tourist seasons destroyed local habitats and environments for wild animals and plants owing to poor control. Such overloading operations caused serious damage to vegetation and generated heavy environmental pollution in tourism areas, thereby lowering tourism area attraction and shortening service life significantly.

Tourism Consumption Leading to Direct Environmental Pollution

Tourism activities are consumption-based dynamic behav-
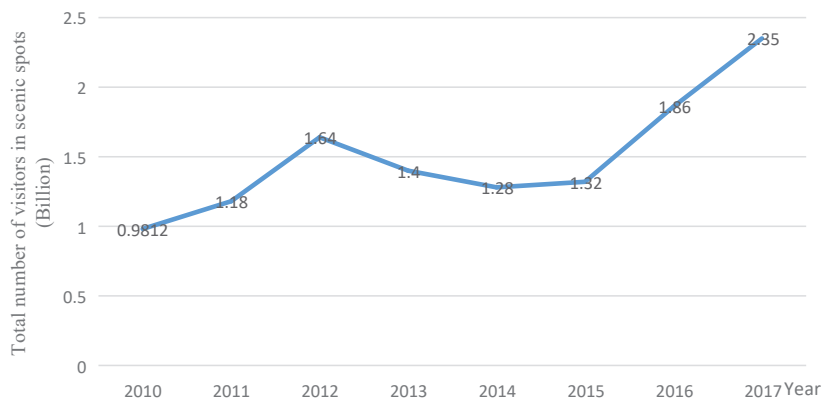
Fig. 1: Number of tourists in tourism areas in Henan Province during the period of 2010-2017 (100 million).
(Data source: EPS dataset: http://olap.epsnet.com.cn/)

iours. The number of foreign tourists staying overnight at Henan Province has increased continuously in recent years. Figure 2 shows the per capita daily cost for foreign tourists and that the number of received foreign tourist staying overnight increased rapidly every year. Tourism activities directly generate environmental pollution. Although administrative departments install garbage bins in tourism areas, many tourists with low personal qualities dispose of their garbage, such as drink bottles and food packages, arbitrarily, which can destroy natural landscapes and pollute scenic spots. As the number of tourists increases, the number of restaurants and hotels near scenic spots likewise increases. This development increases pressure on the tourism environment because tourists' daily activities intensify water pollution. Heavy traffic is a fundamental consequence of tourism. In addition, abundant wastes from traffic, excessive use of air conditioners, and emissions from heating sources can cause air pollution. Moreover, noise generated by vehicles and tourist activities is also a type of environmental pollution.

Damage to Cultural Relics in Star-Level Tourism Areas

Henan Province has a long history, valuable cultural artefacts, and rich tourism resources. According to Table 1, the number of star-level tourism areas and operating revenue of tourism areas in Henan Province increased continuously from 2011 to 2017. However, some tourists with low cultural qualities fail to recognize the value and uniqueness of cultural relics in star-level scenic areas and engage in various uncivilized behaviours, such as carving characters and pictures on cultural relics, sitting or lying on cultural relics to take pictures, removing cultural relics, and so on. Such actions can incur losses and damage cultural relics to a certain extent. While sightseeing, tourists trample on cultural relics, thereby

destroying them, and increased CO_2 emissions may erode cultural relics owing to the abundant water content of CO_2.

Dwindling Habitats for Animal and Plant Survival

Certain regions in Henan Province adopt scale development in constructing artificial scenic spots to develop tourism resources, thereby causing excessive deforestation. Such activities cause serious damage to natural landscapes and plant vegetation. Many tourists walk through planted areas or sit on lawns to rest, thereby influencing the normal growth of plants. Thus, the development of tourism areas may destroy the habitats or shelters of wild animals. Tourism activities and noise made by tourists in tourism areas can disturb the life and reproduction of wild animals. In some wildlife parks, tourists often throw their food wastes to animals directly, which can threaten animal survival.

CAS ANALYSIS OF TOURISM INDUSTRY AND ECOLOGICAL ENVIRONMENT

CAS theory is one of the most important theories in the current system. This theory argues that system evolution is a complex phenomenon, in which the microscopic subjects of a system interact and gradually form macroscopic layers. The concept of CAS theory differs from that of traditional system theory because it emphasizes the interaction of internal factors in a system. According to the relevant concept, CAS theory has seven basic features, including four characteristics (i.e., clustering, nonlinearity, flow, and diversity) and three mechanisms (i.e., labelling, an internal model, and building blocks). In the following section, the interactive relationship between the tourism industry and the ecological environment is analyzed based on the aforementioned seven basic features.

Clustering: In the interaction between the tourism industry

Table 1: Number of Star-level tourism areas and operation revenues in Henan Province for 2011-2017.

	2011	2012	2013	2014	2015	2016	2017
Total number of tourism areas (areas)	235	251	257	243	362	385	412
Number of AAAAA tourism areas (areas)	8	8	9	10	11	12	13
Number of AAAA tourism areas (areas)	81	89	84	74	124	134	146
Number of AAA tourism areas (areas)	103	109	110	101	133	141	163
Number of AA tourism areas (areas)	43	45	54	58	94	97	89
Number of A tourism areas (areas)	0	0	0	0	0	1	1
Operation revenue of tourism areas (100 million yuan)	38.4	91.1	104.31	98	82.91	101.06	110.09

(Data source: EPS database: http://olap.epsnet.com.cn/)
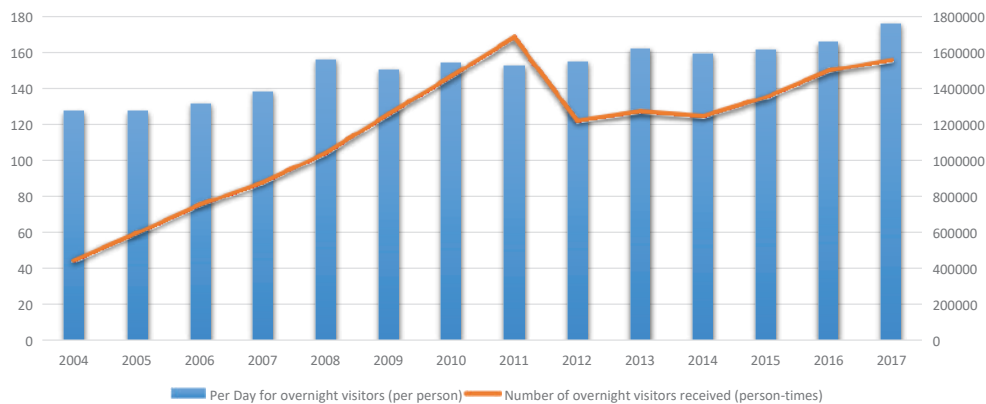
Fig. 2: Per capital daily cost for foreign tourists in Henan Province during the period of 2004-2017. (dollars/people/day), and the total number of received foreign tourists (person) (Data source: EPS dataset: http://olap.epsnet.com.cn/)

and the ecological environment, clustering has two layers of meaning. The first layer is at the primary stage of interaction, in which relevant subjects in different systems cluster and interact actively to realize their development. For example, subjects related to tourism industry development, such as tourism resources, tourism management, tourism hardware facilities, and tourism services, gather in the tourism industry system and coordinate mutually to promote the development of the tourism industry. The influence of ecological tourism subjects on green technological innovation and their benefit pursuits vary to a certain extent. The government mainly influences green technological innovation through policies, and its benefit concerns cover economic benefits, social benefits, and ecological benefits. Meanwhile, the attitude of tourism developers toward green technologies is affected mostly by economic levels, and tourism developers focus on maximizing their economic benefits. Tourism employees focus on their remunerations and social status, whereas communities focus on the improvement of living standards and living environments.

Nonlinearity: A good ecological environment is the foundation of tourism activities and an important impetus that drives the development and progress of the tourism industry. A coupling interactive effect exists between the tourism industry and the ecological environment; however, the internal mechanism of such an effect does not obey a simple linear relationship. According to CAS theory, mutual influences among individuals are complex relations of mutual influences and positive adaption among different interacting systems. In an interaction system, the interactive relationship between the tourism industry system and ecological environment system is formed spontaneously when they seek optimal development. Such an interactive relationship is particularly close in regions with natural resource shortages and vulnerable ecological environments. Diversified subjects are involved in environmental pollution control. The characteristics of the government, social organizations, and ecological tourists are differentiated continuously, and the government has become a subject that provides high-quality public services innovatively. The supervisory function of social organizations

is strengthened, and the awareness of ecological tourists of their ecological responsibility is further solidified.

Flow: In the interaction system, resource flows between the tourist industry and ecological environment mainly include population flow, material flow, cultural flow, information flow, and capital flow. These resource flows follow a circular pattern in the tourism industry system and ecological environment system and between the two systems. Without external disturbances and increased resource input, resource flows may first go to subjects and systems with high utilization. As a result, resource flows that cannot adapt to system interaction and development will weaken and disappear gradually. Owing to continuous material flows, such as energy and information flows, realizing resource sharing and competence augmentation among subjects in an innovation system, the spillover effect of knowledge, the cumulative effect of innovation, and the "crossing priming effect" of technological innovation is possible. In an innovative network comprising the government, communities, and tourism developers, the subjects are nodes, and resource flows, including technological human resources, capital, and information, generate accumulated experiences and adaptation behaviours.

Diversity: The complexity of adaptation generation is the basic principle of CAS theory. Diversity in the CAS is a type of dynamic reflection showing adaptation and apparent complexity. The tourism industry and ecological environment systems possess the characteristic of diversity. Tourism industry development can be promoted by various factors, including macroscopic factors, resource factors, supply-demand factors, enterprise factors, and so on. Moreover, tourism industry development does not involve a mode and pathway owing to such factors. Tourism industry development observes the decisive role of the market in resource allocation and the supervision and guidance of the government.

Labelling: Labelling refers to the mechanism formed to promote clustering. Under the labelling mechanism, subjects with a common value orientation and objective gather spontaneously and gradually form the unique characteristics and boundaries of a system. Labelling is key in forming subsystem categories and layer divisions in the CAS. In the interaction between the tourism industry and ecological environment, the different characteristics, development objects, interest demands, resource use modes, and management mechanisms of subjects are direct sources for labels. Specific subjects involved in tourism pollution control have different objectives, demands, professional advantages, and resources, which are direct sources for labels. For example, the institution and policy labels of the government, the product label of tourism developers, and the knowledge label of tourism employees are guidelines for selecting innovative allies,

sharing knowledge, and reaching innovative consensus and lay a reasonable foundation for specialization and cooperation. Interaction and connection based on the key labels of subjects form the innovative community label.

Internal model: An internal model is a functional model that solidifies gradually when a complex system responds to external input. With the input of abundant resource flows, such as human resources, capital, and information, the inherent form of high-efficiency resource utilization is formed gradually in the tourism industry and ecological environmental systems and between the two systems. The internal model subjects of a system composed of tourism pollution and environmental control are an entire set of rules and programs for adjusting behaviours to adapt to the environment. Based on previous experiences and knowledge, subjects of tourism environmental governance reflect on their conditions, innovative benefits, the strategies of relevant parties, and national ecological regulations and conduct comprehensive evaluations on the innovation of environmental pollution control, thereby making decisions and performing actions. Similarly, the interaction between the tourism industry and ecological environmental systems has a gradually solidified internal model. For example, guided by tourism industry development, the internal model improves ecological environmental quality, increases environmental governance levels, and enhances the environmental education function through tourism development and activities.

Building blocks: Building blocks comprise the CAS. The complexity of a system is determined by the combination mode of building rocks but is unrelated to the number of building blocks. Diversified combinations exist in and among subjects in the tourism industry system. For example, building blocks participate in coordination between enterprises, community residents, and tourists in the subject system; protection in the ecological environmental system; and coordination between environmental pollution control, development, and utilization. In the process of tourism-induced environmental pollution control, the government, communities, tourism developers, tourism employees, social organizations, and ecological tourists are the basic building blocks, and their combination modes in the innovation framework, as well as derived interaction function, play an important role in coordinating economic benefits, social benefits, and ecological benefits and maximizing overall benefits.

CONCLUSIONS

Owing to unscientific tourism resource development, extensive tourism operations, large-scale waste disposal in the tourism process, and abundant exhaust emissions from tourism vehicles, the tourism industry exerts serious pressure

on the ecological environment. With reference to CAS theory, investigating the overall interactive relationship between the tourism industry and the ecological environment from the perspective of comprehensive system theory is beneficial to realize the coordinated development of the two systems. A case study on Henan Province, China, is conducted, which summarizes the province's environmental pollution status caused by the tourism industry and analyzes the CAS of the tourism industry and the ecological environment. The research results demonstrate that currently, the tourism industry in Henan Province generates various problems, such as tourist overloading, direct environmental pollution caused by tourism consumption, damage to cultural relics in star-level tourism areas, and dwindling habitats for animal and plant survival. Constructing the interactive relationship between the tourism industry and ecological environment based on CAS theory from four characteristics, namely, clustering, nonlinearity, flows, and diversity, and three mechanisms, that is, labelling, an internal model, and building blocks, has scientific value and is worth promoting. In-depth research on the development of conceptual models for tourism products optimizing the development mode of tourism products, estimating the comprehensive features of the tourism industry and ecological environment, innovating tourism development and environmental control modes, and strengthening tourist participation in tourism-induced environmental protection is necessary.

REFERENCES

Butler, R.W. 1991. Tourism, environment, and sustainable development. Environmental Conservation, 18(3): 201-209.

Chenyu, L., Wenlei, L., Min, P., Bing, X. and Hong, M. 2018. Quantifying the economy-environment interactions in tourism: Case of Gansu Province, China. Sustainability, 10(3): 711.

Cao, Y., Wang, B., Zhang, J., Wang, L., Pan, Y., Wang, Q., Jian, D. and Deng, G. 2016. Lake macroinvertebrate assemblages and relationship with natural environment and tourism stress in Jiuzhaigou Natural Reserve, China. Ecological Indicators, 62: 182-190.

Fan, S. and Yang, X.Y. 2017. A Study on the impact of tourism resources development on ecological environment. revista de la Facultad de Ingenieria, 32(6): 375-384.

He, P. and Wang, B.Z. 2003. Landscape ecological assessment and eco-tourism development in the South Dongting Lake Wetland, China. Journal of Environmental Sciences, 15(2): 271-278.

Jinhe, Z., Man, L.I., Jing, C., Jing, Z. and Nannan, W. 2012. Analysis of environmental kuznets effect of tourism waste: Case Study of Huangshan National Park. Acta Geographica Sinica, 94(7): 2209-2217.

Lopez, J.C.C. 2018. Sustainable environment and tourism industry: An institutional policy analysis of Northeastern Thailand. Polish Journal of Environmental Studies, 27(1): 31-37.

Liu, J., Li, C., Tao, J., Ma, Y. and Wen, X. 2019. Spatiotemporal coupling factors and mode of tourism industry, urbanization and ecological environment: A Case Study of Shaanxi, China. Sustainability, 11(18): 4923.

Mclennan, C. L., Pham, T., Ritchie, B. and Moyle, B. 2012. Counter-factual scenario planning for long-range sustainable local-level tourism transformation. Journal of Sustainable Tourism, 20(6): 801-822.

Schmitz, M. F., Arnaiz-Schmitz, C., Herrero-Jauregui, C., Díaz Rodríguez P., Gaspar Garcia de Matos, D. and D Pineda F. 2018. People and nature in the fuerteventura biosphere reserve (Canary Islands): socio-ecological relationships under climate change. Environmental Conservation, 45(1): 20-29.

Tang, Z., Shang, J., Shi, C., Liu, Z. and Bi, K. 2014. Decoupling indicators of CO_2 emissions from the tourism industry in China: 1990-2012. Ecological Indicators, 46: 390-397.

Yuxi, Z. and Linsheng, Z. 2020. Identifying conflicts tendency between nature-based tourism development and ecological protection in China. Ecological Indicators, 109: 105791.

Zhou, Cheng, Feng, X. G. and Tang, R. 2016. Analysis and forecast of coupling coordination development among the regional economy-ecological environment-tourism industry- A case study of provinces along the Yangtze economic zone. Economic Geography, 36: 186-193.

Zhao, Y. and Jiao, L. 2019. Resources development and tourism environmental carrying capacity of ecotourism industry in Pingdingshan City, China. Ecological Processes, 8(1): 1-6.

Toxic Trace Metals and Pathological Changes in Organs of Rats Fed with Extract of Polluted Grasses

T. A. Modise*, M. L. Mpholwane**, C. Baker*** and J.O. Olowoyo*†

*Department of Biology, School of Science and Technology, Sefako Makgatho Health Sciences University, Pretoria, South Africa

**Department of Physiology, School of Science and Technology, Sefako Makgatho Health Sciences University, Pretoria, South Africa

***Electron Microscope Unit, Sefako Makgatho Health Sciences University, Pretoria, South Africa

†Corresponding author: J.O. Olowoyo; joshua.olowoyo@smu.ac.za

ABSTRACT

The present study investigated the pathological effects of trace metals in organs of Wistar rats fed with extracts of grasses collected from areas surrounding mining industries. The rats were examined for clinical signs during the experimental period and the concentration of trace metals in organs was examined using ICP-MS. The kidneys were analysed for pathological changes under Transmission Electron Microscopy (TEM). Generally, trace metal concentration in the organs of the rats followed the order Zn > Cu > Mn > As. These trace metals were bio-accumulated more in the spleen than kidneys and livers. Clinical signs such as hair loss, reduced fluid intake, pale ears and feet and skin irritation were observed. TEM investigation of kidney glomeruli showed pathology such as the presence of mesangial deposits, as well as the villous formation and effaced foot processes of the podocytes. Trace metals were bioaccumulated in the organs of the rats and spleen had a higher concentration, which might have negative effects on the organs. It was concluded from the study that plants harvested from polluted sites might be harmful when consumed as they have the potential to induce organ dysfunction.

INTRODUCTION

Developing countries are facing serious issues concerning pollution due to economic growth and various developmental projects, leading to increased concentrations of trace metals in the environment (Jan et al. 2015). The increased level of trace metals in the environment through vehicle exhausts, solid waste disposal, application of sludge, irrigation of wastewater and atmospheric deposition from industries has been experienced by many countries (Qu et al. 2012). China has also shown rapid development, resulting in serious trace metal pollution in their environment (Hu et al. 2014). In South Africa, the studies by Olowoyo et al. (2013) identified different mining activities as a potential source of trace metals in the environment, whereas, Okonkwo et al. (2009) have reported on vehicular activities as a source of trace metals in the urban soils of Pretoria, South Africa. Tshwane (Pretoria) has also been reported as a region in South Africa that has poor air quality due to the trace metal contaminants released by mining industries around the area (Writer 2016). Pollution of the environment by trace metal concentrations is of great concern due to their non-degradable nature and persistent characteristics as this can place risk on the ecosystem (Jan et

al. 2015). These trace metals find their way into human and other mammalian systems through plant uptake from either soil or water, which are then consumed and integrated into their bodies (Durkalec et al. 2014).

Various studies have shown that the human body can become exposed to a significantly elevated concentration of trace metals through different pathways (Stankovic et al. 2014). The most important route into mammalian systems is through inhalation of particulate matters, dermal contact with substances which are likely to cross the skin barrier, as well as ingestion of plants grown in soil contaminated by trace metals or irrigation by water containing trace metals (Moreira et al. 2005, Soewu et al. 2014). The exposure of animals and humans to trace metals can cause progressive and irreversible accumulation in the organs (Baby et al. 2010). Besides, the intake and uptake of trace metals by the body produce numerous interactions because of metabolism and its regulation (Wang et al. 2012). Manganese (Mn) is an essential element that is involved in various metabolic processes such as blood clotting, mineralization of the bones and production of adenosine phosphate (Markiewicz-Gorka et al. 2015). However, in excess Mn affects the optimal functioning of

arteries, heart, nervous system and liver of mammals (WHO 2011, Markiewicz-Gorka et al. 2015). Similarly, zinc (Zn) is known to be responsible for an increase in oxidative stress produced by exposure to lead (Pd) and cadmium (Cd), but in excess, it may cause many side effects in humans such as inadequate diet, irritability, sickle cell disease, tiredness and diarrhoea (Zhai et al. 2015).

The impact of trace metals on mammalian organs has been studied (Mohapatra et al. 2009). Histological exami-nation of albino rats from a busy road site exhibited damage to internal organs such as kidney, liver, heart, and lungs due to the exhaust fumes of cars having a great impact on their physiology (Ajayi et al. 2011). Li et al. (2015) also studied the impact of trace metal bioaccumulation in kidneys and livers of rats and reported that trace metal bioaccumulation causes inflammation in these organs and the occurrence of melanomacrophage centres (aggregates of highly pigmented phagocytes) in the spleen (Arantes et al. 2015). Notably, effects from trace metals in these studies are however ex-aggerated as they were established by acute or sub-chronic exposures that do not reproduce the actual risk to the gen-eral population (Markiewicz et al. 2015). Most of the study carried out on the impact of trace metals on the organs of mammals were carried out using the plants that might seem difficult to consume by the mammals used in the study, as they were not in their natural habitat. The present study used an extract from these polluted grasses to feed the rats used in this study as against the use of the whole grass. Our study therefore in an attempt to duplicate the natural state seeks to establish and examine the levels of toxic trace metals and their pathology in organs of rats fed with an extract of grass collected from areas adjacent to mining sites. The present study also uses TEM (Transmission Electron Microscope) to determine the actual impact on the organs of the rats used in this study.

MATERIALS AND METHODS

Study Design

Approval to conduct the research and experimentation on animals was sought from the Research Ethics Committee and the Animal Ethics Committee of the Sefako Makgatho Health Sciences University before the commencement of the study. The study was conducted during February 2017-Jan-uary 2018 at Sefako Makgatho Health Sciences University, Pretoria, South Africa. All the procedures performed in this study were following the Institutional Animal Care and Use Committee (IACUC) ethical guidelines. A total of thirty three-month old rats (15 adult males and 15 adult females) were obtained from the South African Vaccine Producers, Kempton Park, Gauteng and acclimatized for two weeks,

whereafter they were randomly divided into three groups of 10 (five each males and females). Rats in the experimental group were fed with commercial cubes (mice/rat cubes, Epol™) and 40 mL of water supplemented with 200 mg/kg of the extract obtained from different grasses (*Cynodon dactylon*, *Hyparrhenia hirta* and *Urochloa mosambicensis*) collected from two mining sites. In addition, the third group (control) was fed with only water and commercial rat cubes. This study was conducted for 28 days and clinical signs were observed throughout the experimental period. The rats were kept individually in polycarbonate cages (50 cm × 32 cm) in a well-ventilated animal room (22°C-25°C) kept at a 12 h light/12 h dark cycle. Their beddings were lined with ver-miculite that was regularly replaced, and PVC pipe provided for enrichment purposes.

After the experimental period, the rats were restrained by using the scruff method and euthanized with 0.2 mL of Euthapent solution (pentobarbitone sodium), and thereafter the ventral side of the rat was exposed. A solution of 70% ethanol was used to prepare an area on the ventral side followed by the insertion of a 23G needle at 30°C from the horizontal axis of the sternum to the heart where after 4.5 mL blood was collected. Blood was collected into pre-cooled serum-separating tubes (SST) and yellow-topped containing acid citrate dextrose (ACD). Thereafter, the chests of rats were exposed and organs (kidneys, liver and spleen) were dissected and rinsed with saline to remove excess blood and clots.

Preparation of the Grass Extract

The aerial parts of the grasses were dried in an oven at 40°C for 72 hours and equivalent quantities of the grasses *C. dac-tylon*, *H. hirta* and *U. mosambicensis* (5g: 5g: 5g) was then mixed with 150 mL distilled water. The solution was ultra-sonicated for 60 minutes under ice, followed by the addition of 150 mL warm distilled water (50°C). Stirring commenced for 60 minutes using a magnetic stirrer; left for 24 hours to sediment where after the supernatant was filtered, dried at 40°C and stored at 4°C until further use.

Trace Metal Analysis of Grasses, Grass Extracts and Organs

The grass samples were oven-dried for 48 hrs at 70°C and ground using pestle and mortar. The ground grass samples and extracts were then digested using 2 mL of nitric acid and 3 mL of perchloric acid (Lion et al. 2016), followed by trace metal analysis using ULTIMA Inductively Coupled Plasma Mass Spectrometry (ICP-MS) (Olowoyo et al. 2011).

The organs (liver, spleen and kidneys) were cut into small pieces, and oven-dried at 50°C for five days. The dried organs

were ground using a pestle and mortar and sieved to obtain homogenized particles; thereafter 0.5 g of each of the organs was placed in a pre-washed Erlenmeyer flask. The same volume of extract was transferred to separate conical flasks, and 3 mL nitric acid (55%) was added to fresh samples and left to stand for 10 minutes. The solution was digested at 70°C for approximately 90 min. During digestion, the samples were treated with an additional 2 mL nitric acid and 1 mL distilled water (to prevent the samples from drying out) while heating on a hot plate until all samples were dissolved and a clear solution was obtained. The digested solution was transferred into a 50 mL volumetric flask and filled with distilled water, filtered and stored at 4°C to be analysed for trace metal content ICP-MS. Quality assurance was guaranteed by analysing plant and organ samples in triplicate, followed by the analysis of CRM042 that contain trace metals.

Liver Enzyme Activity

The blood samples were used to determine liver enzyme activity (ALT and AST). Samples were centrifuged at 3000 rpm for 10 minutes at 4°C, and extracted serum was stored at -80°C until required. The frozen serum was left to warm to room temperature, poured into cuvettes and analysed (Human Diagnostics Worldwide, Germany) using system clinical chemical reagents (Indiko™ plus, Thermo Scientific™).

Kidney Pathology Analysis and Antioxidant Activity

The kidneys were cut (1 mm^3), fixed in 2.5% glutaraldehyde, routinely prepared for electron microscopy at the Electron Microscope Unit (Sefako Makgatho Health Sciences University) and viewed using a JEM 1010 Transmission Electron Microscope (JEOL, Japan).

The two antioxidant enzymes, i.e. catalase (CAT) and superoxide dismutase (SOD), as well as glutathione (GSH) were measured to determine kidney antioxidant activity. Tissue samples were prepared by homogenising 300 mg in 2 mL phosphate buffer followed by centrifugation at 15000 rpm for 10 min at 4°C. The supernatant was separated by enzyme-linked Immunosorbent Assay kit (Cloud-Clone Corp, Katy, TX 77494, USA) for CAT, GSH and SOD activity and assessed using a microplate reader (BioTek ELx800, USA).

Statistical Analysis

One way Analysis of Variance (ANOVA) was used to determine differences in kidney antioxidant level, liver enzymes and the concentration of trace metals. Statistical analysis was carried out using SPSS 24.0, where $p < 0.05$ was considered statistically significant. The results are represented as mean± SD.

RESULTS

Concentration of Trace Metals in Pellets and Extract of Grasses Used in the Study

The concentrations of trace metals in rat commercial pellets and grasses harvested from soils around mining areas are given in Table 1. The concentration of Zn ranged from 23.00±0.34 - 67.00±1.08 mg/kg; Cu 4.73±0.16 - 9.50±0.20 mg/kg; and Mn 24.01±0.15 - 342.00±3.50 mg/kg. The highest concentration of trace metals was recorded in *Urochloa mosambicensis*. There was a significant difference ($p < 0.05$) in the concentration of trace metals in the grasses. Furthermore, the concentrations of Zn (152.30±7.54 mg/kg) and Cu (25.67±0.83 mg/kg) in pellets used for this study were higher than the concentration recorded for all grasses.

The mean concentration of trace metals in the extract of grasses from trace metal-polluted areas and tap water are given in Table 2. In extracts, the concentration of copper

Table 1: Trace metals concentration in commercial rat pellets and grasses harvested from the soil around mining areas.

Groups	Grasses	Trace metals (mg/kg)		
		Cu*	Mn*	Zn*
S1	*C. dactylon*	6.20±0.13	223.00±2.20	23.00±0.34
	U. mosambicensis	9.10±0.21	342.00±3.50	67.00±1.08
	H. hirta	4.73±0.16	24.73±0.23	43.60±0.53
S2	*C. dactylon*	7.20±0.11	262.00±3.60	32.00±0.13
	U. mosambicensis	9.50±0.20	295.00±6.20	37.00±0.29
	H. hirta	6.77±0.05	24.01±0.15	42.76±0.51
Commercial rat pellets		25.67±0.83	197.90±3.61	152.30±7.54

Grass from: Site 1 (S1) and Site 2 (S2)
*Significance of comparison means by ANOVA is indicated by (p<0.05)

(Cu) ranged from 8.95±0.15 mg/L to 10.68±0.20 mg/L; zinc (Zn) 71.29±1.03 mg/L to 73.00±1.06 mg/L and manganese (Mn) 93.86±1.18 mg/L to 125.40±1.46 mg/L. The highest concentration of Cu and Zn was recorded from the tap water while Mn was recorded from site S2. It should also be noted that the concentration of Cu (24.86±0.10 mg/L) and Zn (73.00±1.06 mg/L) in tap water was higher than the recorded concentrations from extracts.

Daily Intake of Fluid in the Rats Used for the Study

The results of the experiment for the daily fluid (water or extracts) intake of rats during the study period (Table 3) shows a decrease in the consumption rate when fed with grass extracts collected from sites S1 and S2, in comparison to the more stable intake of tap water by rats in the control group (C) towards the end of week one and week five. During week 1, the intake of grass extracts collected from sites S1 and S2 was higher than the control group. However, intake of the grass extracts collected from S1 and S2 decreased in week five when compared to tap water

(control group).

Clinical Manifestation in Rats During the Study Period

During the second week of the experiment, clinical signs such as pale ears were visible. However, in the third week, wounds around the eyes were also noticeable due to skin irritation. By the fourth week, the rats experienced skin irritation that resulted in wounds around the neck (Fig. 1).

Concentration of Trace Metals in the Organs of Rats

The concentration of toxic trace metals such as Pb, Hg, Cu, Mn, Zn and As in the spleen of the rats is given in Table 4. Concentration for Lead (Pb) ranged from 0.41±0.01 - 0.53±0.02 mg/kg; with Hg 0.18±0.02 - 1.33±0.33 mg/kg and As ranging from 0.69±0.02 - 1.11±0.11 mg/kg. The concentration of trace metals obtained in spleen samples of rats from sites S1 and S2 were significant ($p < 0.05$). The concentration of trace metals in the spleen of the rats from sites S1 and S2 was lower in comparison to the control (C) group.

Table 2: Mean concentration of trace metals in grass extracts and tap water.

Extracts	Trace metals concentrations (mg/L)		
	Cu*	Mn*	Zn*
Extracts of grass from S1	8.95 ±0.15	93.86±1.18	71.29±1.03
Extracts of grass from S2	10.68±0.20	125.40±1.46	71.70±0.94
Plain tap water	24.86±0.10	5.78±0.05	73.00±1.06

Grass extracts from Site 1 (S1) and Site 2 (S2)
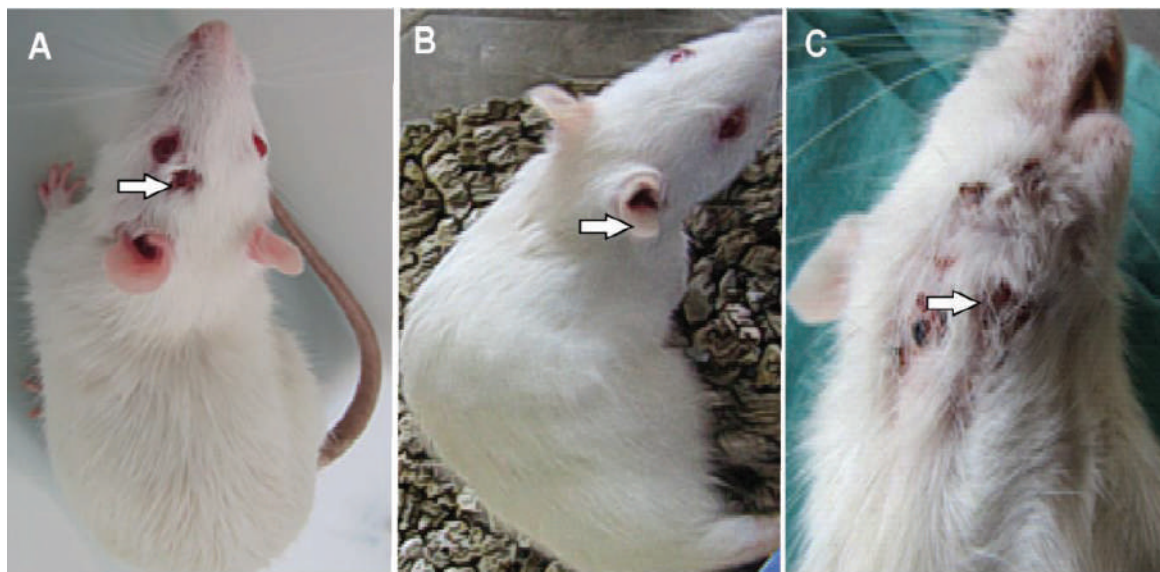*Significance of comparison means by ANOVA is indicated by ($p< 0.05$)

Fig. 1A: Clinical signs observed in rats during the experiment with wounds above the eye. Fig. 1B: Clinical signs observed in rats during the experiment with pale ears. Fig. 1C: Clinical signs observed in rats during the experiment with wounds on the neck.

The results of trace metal concentrations present in livers and kidneys are indicated in Table 5. The kidney concentrations of As ranged from 0.02-9.59 mg/kg; Cu 0.08-12.05 mg/kg; Mn 0.04-0.14 mg/kg and Zn 0.20-0.28 mg/kg. In addition, the concentration of As and Cu in kidneys collected from site S2 was higher compared to rats fed with extracts of grasses collected from site S1 and tap water (C).

Trace metal concentration in kidneys and livers generally followed the order Cu> Zn >Mn> As. The liver concentration of Cu ranged from 3.63-3.86 mg/kg; Mn 0.16-0.29 mg/kg and Zn 1.19-1.33 mg/kg, but the concentration of As in livers of rats' groups were all below the detection limit. The trace metal in the liver was higher than in the kidneys of these rats.

Enzyme Activities in the Organs

Liver enzyme activity is presented in Table 6. The differences in liver enzyme activity from the blood serum of the rats were not significant ($p > 0.05$) as an indicator of liver cell injury. The level of alanine transaminase (ALT) in the blood serum of the rats fed with extracts of grasses from sites S1 and S2 were higher when compared to the control group. The activity of aspartate transaminase (AST) in the blood serum of the rats fed with grass extracts from the mining areas (S1 and S2) were extremely high when compared to the control group.

The antioxidant activity (CAT, SOD and GSH) are presented in Table 7. The superoxide (SOD), catalase (CAT) and glutathione (GSH) activity in kidneys of the rats fed with extracts of grasses collected from sites S1 and S2 was higher compared to the control (C) group. The kidney antioxidant activities between the groups were significant ($p < 0.05$). The values of GSH, SOD and CAT for rats fed with extracts of grasses collected from site S2 and control, followed the sequence GSH> SOD> CAT.

Table 3: Daily intake volumes of rats during the study period

Groups	Volume of grass extract (mL) per day over one week				
	Week 1*	Week 2*	Week 3*	Week 4*	Week 5*
S1	38.13±0.52	37.93±0.51	33.55±1.39	34.09±1.46	31.75±1.46
S2	37.46± 0.85	37.60±1.02	34.86±2.69	34.94±1.59	32.91±3.31
C	36.59 ± 2.00	35.95±2.81	36.06±2.75	36.80±1.07	35.92±1.59

Grass extracts from Site 1 (S1); Site 2 (S2); and control (C)
*Significance of comparison means by ANOVA is indicated by (p< 0.05)

Table 4: Mean concentration of trace metals in the spleen of the rats fed with grasses extract and tap water.

Groups	Trace metals (mg/kg)					
	As*	Cu*	Hg*	Pb*	Mn*	Zn*
S1	0.86±0.11	8.18±0.03	0.41±0.02	0.50±0.0	1.28±0.03	79.43±4.10
S2	1.11±0.11	7.03±0.13	1.33±0.33	0.53±0.02	1.31±0.44	86.37±3.21
C	0.69±0.02	5.93±0.14	0.18±0.02	0.41±0.01	0.68±0.01	63.22±2.11

Grass extracts from Site 1 (S1); Site 2 (S2); and control (C)
*Significance of comparison means by ANOVA is indicated by (p<0.05)

Table 5: Mean concentration of trace metals in the kidney and liver of rats.

Trace metals (mg/kg)	Groups					
	S1		S2		Control	
	Kidney	Liver	Kidney	Liver	Kidney	Liver
As*	0.04	<DL	9.59	<DL	0.02	<DL
Cu**	0.12	3.71	12.05	3.86	0.08	3.63
Mn**	0.14	0.29	<DL	0.17	0.04	0.16
Zn**	0.28	1.32	<DL	1.33	0.20	1.19

Grass extracts from Site 1 (S1); Site 2 (S2); and tap water (C)
*Significance of comparison means by ANOVA is indicated by (p< 0.05)
** No significance of comparison means by ANOVA is indicated by (p> 0.05)
<DL: Detection limit

Transmission electron microscopy (TEM) provided valuable ultrastructural information on the pathological changes observed in the kidney glomerulus (Fig. 2).

DISCUSSION

The concentrations of trace metals such as Zn, Mn and Cu were high in both the grasses and pellets used in this study. Previous studies showed that plants can bioaccumulate trace metals from the soil and may have a high concentration of toxic trace metals (Olowoyo et al. 2013, Lion et al. 2016). The concentration of Zn in *Urochloa mosambicensis* (S1) and rat pellets in this study was higher than the permissible limit set by FAO/WHO (2011) which is 60 mg/kg (Bvenura & Afolayan 2012). However, the high concentration of Zn and Mn in *U. mosambicensis* from site S1 may be due to the translocation factor and bioaccumulation factor of this grass from a polluted area (Lion et al. 2016). The ingestion of food containing a high concentration of Zn and Mn have been reported to cause anaemia, reduced bone formation, kidney stones and pneumonia (USDHH 2012, Yogesh et al. 2013).

The concentration of trace metals such as Mn and Cu in tap water was higher than the acceptable limit set by WHO (2011). The presence of high trace metal concentration in the extracts may thus be due to combining grasses and tap water when preparing the extracts. Moreover, Mn, Zn and Cu affect the blood, kidneys, lungs, urinary tract, stomach and skin (Jarup 2003, USDHHS 2012, Yogesh et al. 2013).

Clinical signs such as fur loss and itching, which are clear indicators of acute pain in the rats, were observed in the experimental groups during the study. Similar results were obtained in the study conducted by Alimba et al. (2012) where rats treated with municipal leachates suffered loss of appetite, hair loss, diarrhoea and signs of ungroomed hair as symptoms of immune dysfunction. The study by Jarup (2003) noted that the changes in skin lesions and presentation of gastrointestinal indicators could be due to high trace metal consumption from the grass extracts thus leading to changes in the immune responses of the rats.

In an earlier study, Rubio et al. (2008) reported on significantly higher concentrations of toxic metals that were bio-accumulated in spleen rather than other organs, although some toxic metals were only detected in the spleen. A related study by Naven et al. (2017) investigated the trace metal content of spleen from rats exposed to chronic fasciolosis and basic zinc-copper, which showed an increase in the concentration of trace metals when the immune system of the animal was compromised similarly to those infected with chronic fascioli, and other infections (Tarantino et al. 2013).

The recorded concentrations of toxic trace metals in the spleen of treated rats during our study were significantly higher than the recommended limit set by National Health and Research Medical Council (NHRMC) and the World Health Organization (WHO). The recommended limit of lead (Pb), mercury (Hg) and arsenic (As) in organs of a healthy body is reported as 0.05 mg/kg, 0.2 mg/kg and 0.5 mg/kg respectively (Norouzi et al. 2017). The studies conducted by Arantes et al. (2015) and Kuang et al. (2016) proposed that the changes observed in the spleen may be due to the toxic level of Pb and Hg accumulation in the visceral organs.

Table 6: Liver enzyme activity

Groups	Liver Enzymes (IU/L)	
	ALT**	AST**
S1	65.67±23.83	166.11±35.83
S2	67.90±18.74	254.40±99.23
Control	64.90±15.50	142.00±26.09

Grass extracts from Site 1 (S1); Site 2 (S2); and tap water (C)
**No significant difference in the values obtained for liver enzymes test in blood serum (p> 0.05)

Table 7: Kidney antioxidant enzyme activities in rats fed with grass extracts and tap water.

Groups	Anti-oxidant Enzymes		
	SOD* (pg/mL)	CAT*(ng/mL)	GSH*(µg/mL)
S1	3.46±0.06	3.46±0.09	3.24±0.16
S2	3.13±0.59	3.06±0.65	3.22±0.17
Control	2.68±1.64	2.60±0.43	3.08±0.15

Grass extracts from Site 1 (S1); Site 2 (S2); and tap water (C)
*Significant difference in the values obtained for kidneys antioxidant activities from different groups (p< 0.05).
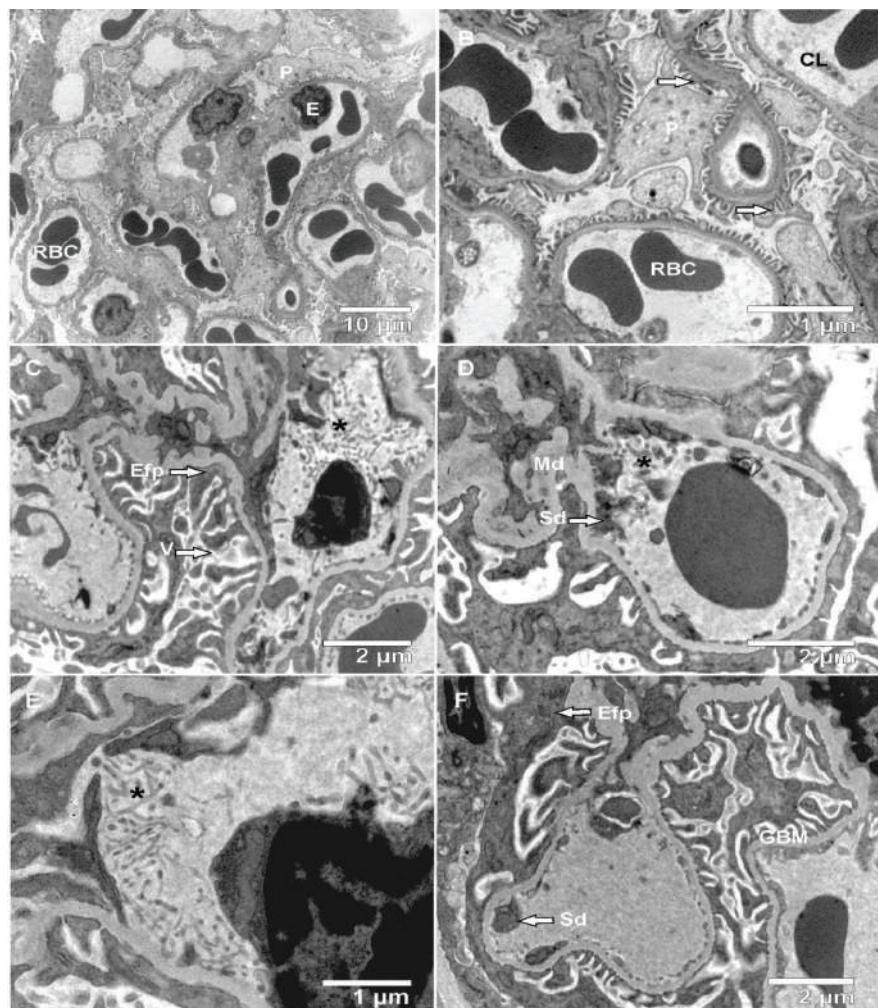
Fig. 2A and B: Electron micrographs of kidney glomeruli control with red blood cells (RBC), capillary lumen (CL) with endothelial cells (E) and podocytes (P) with well-developed fenestrae (arrows); Fig. 2C and D: Rats fed with grass extracts from mining area S1 showing mesangial deposits (Md), villous hypertrophy (V), sub-endothelial deposit (Sd), effaced foot process of podocytes (Efp) and tactoids (*); Fig. 2E and F: The glomerular basement membrane (GBM), tactoids (*), effaced foot process (Efp) and sub-endothelial deposits (Sd).

This study supported the findings of Barbier et al. (2005) which identified kidneys as a secondary bioaccumulator of trace metals, possibly due to their re-absorption potential. The accumulation of As and Cu in kidney tissues of rats fed with grass extracts collected from site S2, is associated with an increase in the level of ALT and AST activities. The recorded trace metal concentrations in the kidneys during this study may affect the metabolic process and transportation of enzymes to the kidney tubules (Pereira et al. 2006) and possibly damage the internal organs (Ajayi et al. 2011). The increased activity of AST in all the groups may be an indication of hepatocellular damage as corroborated by Markiewicz-Gorka et al. (2015) when exposing rats to toxic concentrations of lead, cadmium and manganese. The normal

activity of ALT in all the groups may result from elevated AST since ALT allows the AST level to initially peak due to oxygen starvation (Hall & Cash 2012).

Our study indicates decreased enzymatic activity of CAT and SOD in all the groups, which may be due to apoptosis, proliferation of cells, cell differentiation or maintenance of redox-sensitive signal transduction pathways (Weydert & Cullen 2009). The Markiewicz-Gorka et al. (2015) similarly reports low SOD and CAT activities in rats exposed to trace metals such as lead and manganese. The observed study by the increase of GSH from our study may be due to kidney necrosis as corroborated by Purucker et al. (1995) where an increase of GSH was attributed to renal dysfunction and liver cirrhosis. Our results obtained for GSH corroborate

the work of Scaduto et al. (1988) where increased GSH caused ischemia-induced renal dysfunction and renal failure (Sindhu et al. 2005) resulting in various complications such as anaemia, impaired immunity and abnormalities in haemostasis. It has further been shown that long-term exposure of trace metals in rats can also cause chronic or acute renal dysfunction (Soewu et al. 2014).

Pathology changes in the kidney glomerulus during our investigation may be due to the concentration of trace metals absorbed during experimental exposure. Epithelial cells of the glomerulus also showed the increased villous formation of the podocytes, which caused hypertrophy within the lumen ultimately leading to malfunctioning of these cells (Tobar et al. 2013). The tactoids observed in the capillary lumen signify immunotactoid glomerulopathy also known as a rare glomerular disease (Nasr et al. 2012). This disease is a condition whereby antibodies are deposited abnormally in the kidneys during filtration of blood to produce urine with waste products (UNC Kidney Center 2015).

Acute kidney injury can decrease the rate of glomerular filtration, which fails to eliminate environmental toxins and metabolic waste from the body (Orr & Bridges 2017). Affaced foot processes of podocytes and sub-endothelial deposits (Fig. 2E & 2F) have been reported to be the characteristic of proteinuric renal disease (Degeens et al. 2008), where damaged renal tubular cells present as a sign of acute kidney injury (Lee et al. 2012). Histopathology and electron microscopical examination of tissues can identify the end stages of organ toxicity and lesions caused by xenobiotics such as trace elements (Orr & Bridges 2017).

CONCLUSION

From the present study, the toxicity impact of the trace metals was linked to accelerated weakening of the immune system, causing allergies that negatively affected the normal functioning of the organs of the test animals. It was also noted that the kidney antioxidant activity of the experimental animals was largely impaired as a result of the high level of trace metals found in the kidney. Besides, the mesangial deposits in the kidney of the rats fed with polluted grass resulted in proliferative glomerulonephritis with the visible formation of lesions. High absorption of trace metals in the liver adversely affected the blood serum ALT and AST activities by increasing the serum activity, an indicator of liver damage. Some trace metals found in organs such as the liver, kidney, and spleen of control rats was possibly from the pellets and tap water as recorded in this study. Consumption of polluted grasses as a whole as demonstrated in previous studies or as extracts as demonstrated in the present study have a significant effect on the organs of mammals hence consumption or usage of plant materials harvested from polluted sites should be discouraged as this may pose a serious health risk.

REFERENCES

Ajayi, O.A., Idowu, A.B., Eromosele, C.O., Dedeke G.A. and Ademolu, K.O. 2011. Distribution and effect of some heavy metals in selected organs and tissues of albino rats exposed to vehicular exhaust fumes. Proceedings of the Environmental Management Conference, Federal University of Agriculture, Abeokuta, Nigeria.

Alimba, C.G., Bakare, A.A. and Aina, O.O. 2012. Liver and kidney dysfunction in wistar rats exposed to municipal landfill leachate. Journal of Resources and Environment 2(4): 150-163.

Arantes, F.P., Savassi, L.A., Santos, H.B., Gomes, M.V.T. and Bazzoli, N. 2015. Bioaccumulation of mercury, cadmium, zinc, chromium and lead in muscle, liver and spleen tissues of a large commercially valuable catfish species from Brazil. Annals of the Brazilian Academy of Sciences, 88(1): 137-147.

Baby, J., Raj, J., Biby, E.T., Sankarganesh, P. Jeevitha, M.V., Ajisha, S.U. and Rajanm S.S. 2010. Toxic effect of heavy metals on the aquatic environment. International Journal of Biological and Chemical Sciences, 4(4): 939-952.

Barbier, O., Jacquillet, G., Tauc, M., Cougnom, M. and Poujeol, P. 2005. Effect of heavy metals on and handling by the kidney. Nephron Physiology Journal, 99: 105-110.

Bvenura, C. and Afolayan, A.J. 2012. Heavy metal contamination of vegetables cultivated in home gardens in the Eastern Cape. South African Journal of Science, 108(9/8): 1-6.

Deegens, J.K.J., Dijkman, H.B.P.M., Born, G.F., Steenbergen, E.J., van den Berg, J.G., Weening, J.J. and Wetzels, J.F. 2008. Podocyte foot process effacement as a diagnostic tool in focal segmental glomerulosclerosis. Kidney International Journal, 74(1): 158-1576.

Durkalec, M., Szkoda, J, Kolacz, R., Opalinski, S., Nawrocka, A. and Zmudzki, J. 2014. Bioaccumulation of lead, cadmium, and mercury in roe deer and wild boars from areas with different levels of toxic metal pollution. International Journal of Environmental Research, 9(1): 205-212.

Food and Agricultural Organization/World Health Organization (FAO/WHO). 2011. Joint FAO/WHO food standards programme codex committee on contaminants in foods. http://www.fao.org/tempref/codex/Meetings/CCCF/CCCF5/cf05_INF.pdf. Retrieved on 15/03/2019.

Hall, P. and Cash, J. 2012. What is the real function of the liver 'function' tests? Ulster Medical Society, 81(1): 30-36.

Hu, H., Jin, Q. and Kavan, P. 2014. A study of heavy metal pollution in China: Current status, pollution-control policies and counter measures. Sustainability, 6: 5820-5838.

Jan, A.T., Azam, M., Siddiqui, K., Ali, A., Choi, I. and Haq, Q.M.R. 2015. Heavy metals and human health: mechanistic insight into toxicity and counter defence system of antioxidants. International Journal of Molecular Sciences, 16: 29592-29630.

Jarup, L. 2003. Hazards of heavy metals contamination. British Medical Bulletin, 68: 167-182.

Kuang, P., Deng, H., Cui, H., Chen, L., Fang, J., Zuo, Z., Den, J., Wang, X. and Zhao, L. 2016. Sodium fluoride (NaF) causes toxic effects on splenic development in mice. Oncotarget, 8(3): 4703-4717.

Lee, J.Y., Eom, M., Yang, Y.W., Han, B.G., Choi, S.O. and Kim, J.S. 2012. Acute kidney injury by Arsine poisoning: The ultrastructural pathology of the kidney. Renal Failure, 35(2): 299-301.

Li, Q., Liu, H., Alattar, M., Jiang, S., Ham, J., Ma, Y. and Jiang, C. 2015. The preferential accumulation of heavy metals in different tissues following frequent respiratory exposure to PM2.5 in rats. Scientific Report, 5(16936): 1-8.

Lion, G.N., Olowoyo, J.O. and Modise, T.A. 2016. Trace metals bioaccumulation potentials of three indigenous grasses grown on polluted soils collected around mining areas in Pretoria, South Africa. West African Journal of Applied Ecology, 24(1): 43- 51.

Lusco, M.A., Fogo, A.B., Najafian, B. and Alpers, C.E. 2016. Proliferative glomerulonephritis with monoclonal immunoglobulin deposits. Atlas of Renal Pathology ii, 67(3): e13-e15.

Markiewicz- Gorka, I., Januszewska, L., Michalak, A., Prokopowicz, A., Januszewska, E., Pawlas, N. and Pawlas, K. 2015. Effects of chronic exposure to lead, cadmium, and manganese mixtures on oxidative stress in rat liver and heart. Arh. Hig. Rada Toksikol., 66: 21-62.

Mohapatra, A.K., Kumari, P. and Datta, S. 2009. Cadmium induced histopathological changes in the stomach and small intestine of swiss albino mice, *Mus museulus*. Journal of Applied and Natural Sciences, 1(2): 253-257.

Mohod, C.V. and Dhote, J. 2013. Review of heavy metals in drinking water and their effect on human health. International Journal of Innovative Research in Science, Engineering and Technology, 2(7): 2992-2996.

Moreira, J.C., Silva, A.L.O., Barrocas, P.R.G. and Jacob, S.C. 2005. Dietary intake and health effects of selected toxic elements. Brazil Journal of Plant Physiology, 17(1): 79-93.

Nasr, S.H., Fidler, M.E., Cornell, L.D., Leung, N., Cosio, F.G., Sheikh, S.S., Amir, A.A., Vrana, J.A., Theis, J.D., Dogan, A. and Sethi, S. 2012. Immunotactoid glomerulopathy: Clinicopathologic and proteomic study. Nephrology Dialysis Transplantation, 27(11): 4137-4146.

National Research Council (NRC) 2000. Copper in drinking water. Washington, D.C.: National Academies Press (US).

Naven, V., Vladov, I., Gabrashanka, M., Kandil, O.M, Noha, M.F. and Sedky, H.D. 2017. Rat spleen trace element contents under combined effect of chronic fasciolis and basic zinc-copper compound. Accounts of the Bulgarian Academy of Sciences, 70(8): 1115-1120.

Nazir, R., Khan, M., Masab, M., Rehman, H.U.R., Rauf, N.U.R., Shahab, S., Ameer, N., Sajed, M., Ulah, M., Rafeeq, M. and Shaheen, Z. 2015. Accumulation of heavy metals (Ni, Cu, Cd, Cr, Pb, Zn, Fe) in the soil, water and plants and analysis of physic-chemical parameters of soil and water collected from Tanda Dam Kohat. Journal of Pharmaceutical Sciences and Research, 7(3): 89-97.

Norouzi, M., Bagheri. T.M., Ghodrati, S.H. and Amirjanati, A. 2017. Toxic heavy metal concentration in soft tissues of gray mullet *Liza aurata* (Mugilidae: Perciformes) during the sexual maturity and sexual res. Iran Journal of Fish Sciences, 16(3): 920-934.

Okonkwo, J.O, Moja, S.J. and Forbes, P. 2009. Manganese levels and chemical fraction in street dust in South Africa. International Journal of Environmental Pollution, 36(4): 350-366.

Olowoyo, J.O., Van Heerden, E. and Fischer, J.L. 2011. Trace element concentrations from lichen transplants in Pretoria, South Africa. Environmental Science and Pollution Research, 18(4): 663-668.

Olowoyo, J.O., van Heerden, E. and Fischer, J. 2013. Trace metals concentrations in soil from different sites in Pretoria, South Africa. Sustainable Environment Research, 23(1): 93.

Orr, S.E. and Bridges, C.C. 2017. Chronic kidney disease and exposure to nephrotoxic metal. International Journal of Molecular Sciences, 18: 1-35.

Parveen, P., Abbasi, A.M., Shaheen, N. and Shah, M.H. 2017. Accumulation of selected metals in the fruits of medicinal plants grown in urban environment of Islamabad, Pakistan. Arabian Journal of Chemistry, 13(1): 308-317.

Pereira, R., Pereira, M.L., Ribeira, R. and Goncalves, F. 2006. Tissues, hair residues, histopathology in wild rats (*Rattus rattus* L.), and Algerian mice (*Mus spretus* Lataste) from an abandoned mine area (Southeast Portugal). Environmental Pollution, 139: 561-575.

Purucker, E., Wernze, W. and Krandik, G. 1995. Glutathione in plasma, liver, and kidney in the development of CCl$_4$-induced cirrhosis of the rat. Research in Experimental Medicine, 195(4): 193-199.

Qu, C., Ma, Z., Jin, Y., Liu, Y., Bi, J. and Huang, L. 2012. Human exposure pathways of heavy metals in a lead-zinc mining area, Jiangsu Province China. Plos ONE, 7(11): e46793.

Rubio, J.C., Garcia-Alonso, M.C., Alonso, C., Alobera, M.A., Clemente, C., Munuera, L. and Escudero, M.L. 2008. Determination of metallic traces in kidneys, livers, lungs and spleens of rats with metallic implants after a long implantation time. Journal of Materials Science: Materials in Medicine, 19: 369-375.

Scaduto, R.C., Gattone, V.H., Grotyohann, L.W., Werts, J. and Martin, L.F. 1988. Effect of altered glutathione content on renal ischemic injury. American Journal of Physiology, 255 (5pt2): 911-921.

Sindhu, R.K., Ehdaie, A., Farmand, F., Dhaliwa, K.K., Nguyen, T., Zhan, C.D., Roberts, C.K. and Vaziri, N.D. 2005. Expression of catalase and glutathione peroxidase in renal insufficiency. Biochemica et Biophysica Acta, 1743: 86-92.

Soewu, D.A., Agbolade, O.M., Oladunjoye, R.Y. and Ayodele I.A. 2014. Bioaccumulation of heavy metals in cane rat (*Thryonomys swinderianus*) in Ogun State, Nigeria. Journal of Toxicology and Environmental Health Sciences, 6(8): 154 -160.

Stankovic, S., Kalaba, P. and Stankovic, A.R. 2014. Biota as toxic metal indicators. Environmental Chemistry Letters, 8: 472-481.

Tarantino, G., Scalera, A. and Finelli, C. 2013. Liver-axis: Intersection between immunity, infections and metabolism. World Journal of Gastroenterology, 19(23): 3534-3542.

Tembeni, B., Oyedej, O.O., Ejidike, I.P. and Oyedeji, A.O. 2016. Evaluation of trace metal profile in *Cymbogon validus* and *Hyparrhenia hirta* used as traditional herbs from environmentally diverse region of Komga, South Africa. Journal of Analytical Methods in Chemistry. Article ID 9293165, 8p.

Tobar, A., Ori, Y., Benchetrit, S., Milo, G., Herman-Edelstein, M., Zingerman, B., Lev, N., Gafter, U. and Chagmac, A. 2013. Proximal tubular hypertrophy and enlarged glomerular and proximal tubular urinary space in obese subjects with proteinuria. PLos One, 25: 8(9): e75547.

UNC Kidney Center. 2015. Immunotactoid glomerulopathy. http://www.unckidneycenter.org/. Retrieved on 2/11/2018.

U.S. Department of health and human services (USDHHS). 2012. Toxicological Profile for Manganese. http:// www.atsdr.cdc.gov. Retrieved on 2/11/2018.

Wang, Y., Ou, Y., Liu, Y., Xie, Q., Liu, Q.F., Wu, Q., Fan, T.Q., Yan, L.L. and Wang, J.Y. 2012. Correlations of trace element levels in diet, blood, urine, and feces in the Chinese male. Biological Trace Elements of Research, 145: 127-135.

Weydert, C.J. and Cullen, J.J. 2009. Measurement of superoxide dismutase, catalase and glutathione peroxidase in cultured cells and tissue. National protocol, 5(1): 51-66.

WHO, 2011. Manganese in drinking water. Background document for development of WHO guidelines for drinking water quality. http:// www.who.int/water_sanitation_health/dwq/chemicals/manganese.pdf. Retrieved on 22/11/2016.

Writer, S. 2016. The most polluted city in South Africa is not where you expect. Business Tech. Newsletter. May 12, 2016.

Yogesh, P.P., Sachin, H.P., Sharu, J. and Jitendra, S.K. 2013. Biochemistry of metal absorption in human body: Reference to check impact of nano particles on human being. International Journal of Scientific and Research Publications, 3(4): 1-5.

Zhai, Q., Naarbad A. and Chen, W. 2015. Dietary strategies for the treatment of cadmium and lead toxicity. Nutrients 7: 552-571.

Original Research Paper   https://doi.org/10.46488/NEPT.2020.v19i03.016   Open Access Journal

Assessment of Drinking Water Quality and the Efficiency of the Al-Buradieiah Water Treatment Plant in Basra City

Ahmed Sadiq Al Chalabi†

Department of Environmental and Pollution Eng., Basra Engineering Technical College,
Southern Technical University, Basra, Iraq
†Corresponding author: Ahmed Sadiq Al Chalabi; ahmed.sadiq@stu.edu.iq

ABSTRACT

This study was conducted on the oldest water treatment plant in the city of Basra, which is the Al-Buradieiah Water Treatment Plant (BWTP) during the period from December 2017 to March 2018. The study aimed to evaluate the efficiency of the plant by calculating the efficiency of sedimentation, filtration and sterilization basins, as well as to examine the water quality by examining the physical and chemical characteristics of raw water and treated water in this plant and then compare it with the World Health Organization (WHO) and Iraqi standards. The results of this study showed that the efficiency of sedimentation basins is 54%, while the efficiency of filtration basins is 24% and sterilization efficiency ranging from 37 to 65%. As well as, laboratory results of treated water quality have also shown that the turbidity equal to (7.24 NTU), electrical conductivity (EC) equal to 5040 µS/cm, the total dissolved solids (TDS) equal to 3380 mg/L and the total suspended solids (TSS) equal to 190 mg/L of the water outside from the BWTP. All these water quality results are higher than the WHO and Iraqi standard limitations except the value of pH, which is 6.9 and within the permissible limits.

INTRODUCTION

Water is the single most important substance for the sustenance of life known in the world. It is the elixir of life and without it, life is not possible. It represents a fundamental requirement for all life activities and is essential to humans, animals and plants (Fetter 1988). Its supply is endless as it covers over 80% of the earth's surface; however, only a small fraction of the water in the world is available for the human use (Sundstrom & K1ei 1979). Water is a vital liquid for maintaining life on earth. About 97% of the water that exists in oceans is not suitable for drinking and only 3% is freshwater, whereas 2.97% is comprised of glaciers and ice caps. The remaining 0.3% is available as surface and ground-water for human use (Miller 1997). Safe drinking water is a basic need for good health. Freshwater is already a limited resource in many parts of the world. During the next century, it will become even more limited due to increasing population, urbanisation, and climate change (Jackson et al. 2001).

Basra is the third largest city of the Republic of Iraq and is the administrative and political centre of the province of Basra, located in the far south of Iraq on the West Bank of Shatt al-Arab. It was the first water crossing in Iraq, and Basra is the economic capital with a population of about 2.5 million people, according to estimates in 2014. The Shatt al-Arab river consists of the confluence of the Tigris and Euphrates rivers in the region of Kerma Ali, at the northern entrance to the city of Basra, 375 km south of Baghdad. It is about 190 km long and is located in the Arabian Gulf at the edge of Al Faw city, which is the most extreme point in southern Iraq; in some areas, the width of the Shatt al-Arab river reaches two kilometres.

According to recent estimates, the quantity of available water in the developing regions of South Asia, the Middle East and Africa is decreasing sharply, while the quality of water is deteriorating rapidly due to fast urbanization, deforestation and land degradation. Therefore, many cities in Asia are facing an increase in organic and nutrient materials in drinking water due to the discharge of untreated domestic and industrial wastewater into these resources (Annachhatre 2006). The quality of water is affected by an increase in anthropogenic activities and any pollution, either physical or chemical, causes changes to the quality of the receiving water body (Aremu et al. 2011). The water quality and quantity audit include an analysis of historical water quality and quantity data, an evaluation of treatment system effectiveness, an investigation of customer satisfaction, an evaluation of monitoring and reporting practices, and an assessment of the water supply's future sustainability.

Similarly, during a study conducted in Iraq to evaluate the drinking water quality of the large treatment plant in the

Ramadi city at the Al-Anbar Province, the results indicated that the sedimentation unit has about 36% removal efficiency, which must be 70%-90%, the filtration unit has about 23.4% removal efficiency and the disinfection stage has about 97%-100% disinfection efficiency (Ramel 2010). Another study, conducted in Al-Fallujah, found that Al-Fallujah water treatment plant had an efficiency of 57% in the deposition, and an efficiency of 50% in the nomination phase and efficiency of 40%-90% in the sterilisation stage (Abdul Rahman et al. 2009). Another study conducted to evaluate the efficiency of Gas Al-Shamal water treatment plant showed that the plant was efficient for turbidity and total suspended solids removal. The results indicated that the characteristics of the total dissolved solids (TDS), total hardness (TH), electrical conductivity (EC), chloride (Cl), and sulphate were within the characteristic limits of Iraqi drinking water standards for raw and treated water. The results also showed that the (pH) values were beyond the suitable values of flocculation materials. The fluoride values of raw and treated water were low within the standards (Saleh et al. 2015). Another study assessed physical-chemical drinking water quality in the Logone valley (Chad-Cameroon); the samples were analysed for their physical-chemical and microbiological quality to identify contamination problems and suggest appropriate solutions. Results of the assessment confirmed that in the studied area there were several parameters of health and aesthetic concerns (Sorlini et al. 2013). Another study evaluated the quality of drinking water in urban areas of Pakistan (a case study of Gulshan-e-Iqbal Karachi, Pakistan). The results of the study demonstrated that the physical and chemical quality of water was satisfactory. Some samples (three) were possibly contaminated by leaking water mains and cross-connections between water mains and sewers due to proximity (Syed et al. 2016).

Study Area

The study area is located between Latitude (30°30'9.15"N) and Longitude (47°51'19.95"E), as shown in Fig. 1. Al-Buradieiah city is located in the province of Basra in the city centre, overlooking Shatt al-Arab through a small corniche. The Shatt al-Arab river limits Al-Buradieiah city from the east and Khurha River from the north. The Basra Water Project is big in the region for the distribution of drinking water to the population of the city. The water source of this plant is the Shatt al-Arab river. This station is equipped with all of the Aljaza'ar, Albradheah, Abbaseya, Mishraq, and Amtiha

Fig. 1: Map of the study area (BWTP).

regions; it has a design of 1500 m^3/h and its total capacity is 5000 m^3/hour. This station contains three projects:

1. The first project was in 1957 and had a capacity of 1500 m^3/h.

2. The second project was in 1964 and had a capacity of 1500 m^3/h.

3. The third project, which is called Al-Buradieiah station, was in 2012 and had a capacity of 2000 m^3/h.

The old project is considered better than the modern project due to the highly efficient English Company, while the modern project was conducted by the Turkish Company; its efficiency is lower but its design is better than the old project.

Basic Operational Phases in the Station

The station consists of several stages, as in Fig. 2.

1. **Drag system:** Consists of different capacity pumps; three pumps operate with a capacity of 2000 m^3/h and two pumps of 500 m^3/h capacity with a dive capacity of 1000 m^3/h.

2. **Adding alum:** Alum is added according to the value of turbidity, where alum is not added unless the turbidity value of 25 or above. In addition, there is a special lab

with determines ratios added, according to the supervisor's instructions of the project in terms of the pumping power and the value of turbidity. The process continues for 24 hours.

3. **Sedimentation basins:** The station consists of four sedimentation basins; two basins for each of the first and the second project, in which they are circular and large in size (see Fig. 2), with a diameter of one basin at 24m and a height of 9m.

4. **Filters:** Each project consists of 14 candidates as the third project filters operate as a pressure filter, while filters of the first and the second project acts as a streamline filter.

5. **Placed chlorine system:** Liquid chlorine is added to water by chlorine placed device. The process of adding chlorine continues for 24 hours.

6. **Payment system:** The project consists of many payment pumps. These pump water through the pipes; the first and second projects contain four pumps, while the third project contains three.

7. **Ground reservoir:** Water enters the ground reservoir with a discharge of 2000 m^3/h only in the modern project.
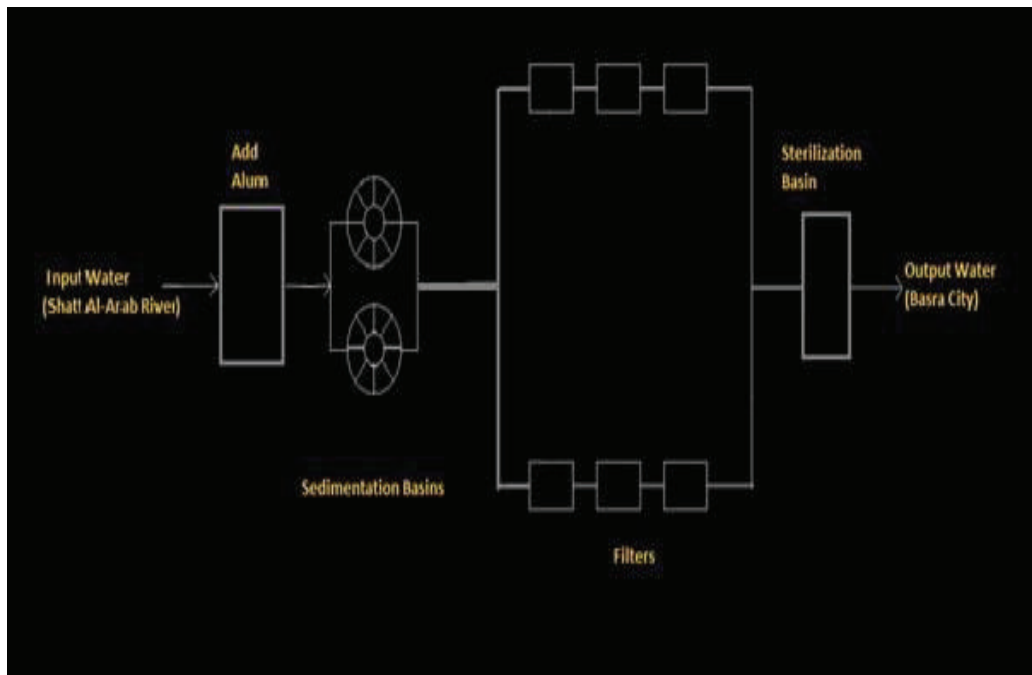

Fig. 2: The diagram showing the parts of BWTP.

MATERIAL AND METHODS

Sample Collection

Water samples were collected in plastic bottles with a capacity of 500 mL from each stage of purification at the station starting from the raw water (river water) to the outside of the station water (tap water). The samples of the sedimentation basin were taken at different depths (1.5, 3, 4.5, 6 and 7.5 metres away from the aquarium) and at a certain time (at 8:00 am). This was assumed to be the zero hour. Then the samples were taken on the same previous depths at different times, i.e. 1, 2 and 3 hours from the virtual zero hour, while the bio-screening water samples were collected in sterile plastic bottles over a period of four months (December, January, February, March) with three samples each month.

The standard methods (APHA 1998) were used for the analysis. The samples were analysed for different characteristic parameters such as pH, turbidity, electric conductivity (EC), total dissolved solids (TDS), total suspended solids (TSS), magnesium, sulphates, and nitrates. Table 1 summarises the water quality parameters, the analytical methods, and the instruments used for the analyses (APHA 1998).

Efficiency of Sedimentation Basins

The ideal sedimentation basin design is based on the fact that when they put grain in a liquid, it is lower than its density, which is accelerated to that of regular speed and then equal to the weight of the submerged body with the power disability friction leading to deposition. When the stuck particles of different density are left to be deposited, there is different deposition speed of each particle from other particles; therefore, the speed of the particles is less dense and inflicted by the particles with faster speed (size or larger weight). This situation is generated by many collisions that lead to the union of the particle and composition of flocculants, especially when adding the adjuvant to form flocculants,

such as alum. Alum is added to the solution at a rate of $4g/m^3$ in the basin with rapid mixing. The calculation and estimation of the efficiency of a sedimentation basin require either the size distribution of the particles suspended or using sedimentation column, in which they draw equal removal curves (isoremoval curves). Samples are taken at different depths and different times for each depth, after knowing the concentration of suspended solids to raw water (C_0) and by taking samples (using a sedimentation column device) during a given time and then calculating the concentration of suspended material (C_1, C_2, ..., C_n) to different depths of the sedimentation basin (H_1, H_2, ..., H_n), which can be seen in Fig. 3. From the results of the sedimentation column experience the proportion of suspended particles can be calculated from equation (1) (Ahmed 1995):

$$S_{ij} = \frac{c_{ij}}{c_o} \qquad (1)$$

Where,

S_{ij}: represent a percentage of solid particles remaining at a certain depth (h_{ij}) and a certain time (t_{ij}).

C_0: the concentration of total suspended solid particles of raw water units (mg/L).

Also, the percentage of particles removed (x_{ij}) for each depth and a certain weight can be found from equation (2):

$$E = 100 - X_0 + \left[\frac{1}{V_{So}}\right] \times \int_0^{X_o} V dx \qquad (2)$$

Where,

X_{ij}: represents the percentage of particles that will be removed at a certain depth (h_{ij}) and a certain time (t_{ij}) and from which total removal can be calculated by the equation (3) (Ahmed 1995, Steel & Mcghee 1979):

$$E = 100 - X_0 + \left[\frac{1}{V_{So}}\right] \times \int_0^{X_o} V dx \qquad ...(3)$$

Table 1: Water quality parameters and analytical methods for water source evaluation.

Parameter	Analytical method	Instrument
pH	Instrumental, analyse on site	EC500 - EXTECH (pH meter)
Turbidity	Instrumental, analyse on site	Turbi Direct - Lovibond
EC	Instrumental, analyse on site	Cond 3110 – WTW
TDS	Instrumental, analyse on site	EC500 - EXTECH (pH meter)
TSS	Gravimetric method	Gravimetric method SMEWW5520D
Magnesium	Photometric method	UV-2601-BIOTECH-Spectrophotometer, Ascorbic Acid Method
Sulphates	Photometric method	UV-2601- BIOTECH-Spectrophotometer, Ascorbic Acid Method
Nitrates	Photometric method	UV-2601-BIOTECH- Spectrophotometer, SMEWW 4500-NO$_3$

$$V_{S0} = \frac{Q}{A} \qquad \dots(4)$$

Where,

V_{S0}: represents the settling velocity (mm/sec)

The integration limit in equation (3) represents the shaded area of the chart in Fig. 4, which can be calculated using the Simpson theory or the Newton-Raphson theorem or by approximation of the graph (Ahmed 1995, Steel & Mcghee 1979).

Efficiency of Filters

The efficiency of the filters account for the disposal of suspended solids by finding the concentration of suspended solids in the water out of the sedimentation basin (Ce) in (mg/L), and then finding the efficiency of filters according to the equation (5) for the following:

$$E_f = 1 - \left(\frac{C_{out}}{C_e}\right) \times 100 \qquad \dots(5)$$

The Efficiency of the Sterilization Process (Disinfection) of Water

It is known that filtration does not work with great efficiency to remove bacteria and viruses, because of their small size, which is less than one micron, so quick sand filter does not produce potable water in the aspects of bacteriology. Chlorine must be added to remove bacteria and germs (Ahmed 1995). It is well known that the filtration does not work efficiently

for the removal of bacteria. The degree of killed germs depends on the number of germs that are already present. The killing of germs depends on many factors that overlap with each other, such as the efficiency of the cleanser to penetrate the cell forces.

CALCULATION AND RESULTS

Sedimentation Efficiency

The samples from the sedimentation basin at different depths and at different times and extracting the concentration of the solids remaining suspended in each sample are given in Table 2. The calculated velocity and percentage of removal suspended materials are presented in Table 3.

Discharge of one basin = Total flow rate / No. of Basins

$$Q = 2000/2 = 1000 \text{ m}^3/\text{h}$$

$$= 0.278 \text{ m}^3/\text{sec}$$

$$\text{Area of Basin} = \frac{\pi}{4} \times (\text{Diameter of Basin})^2$$

$$= \frac{\pi}{4} \times (24)^2 = 452.39 \text{ m}^2$$

$$V_{so} = \frac{Q}{A} = \frac{0.278}{452.39} = 0.000614 \text{ m/sec}$$

$$= 0.614 \text{ mm/sec}$$

From Fig. 5, $X_0 = 58$ %

E = (100 - 58) + (1/0.614) × 7.21 ≈ 54 %

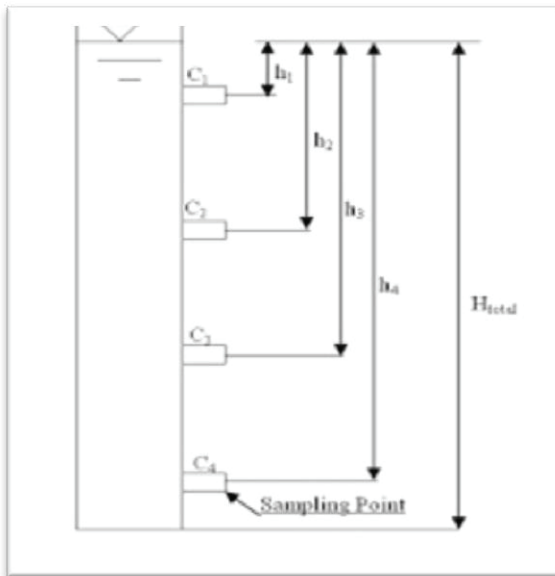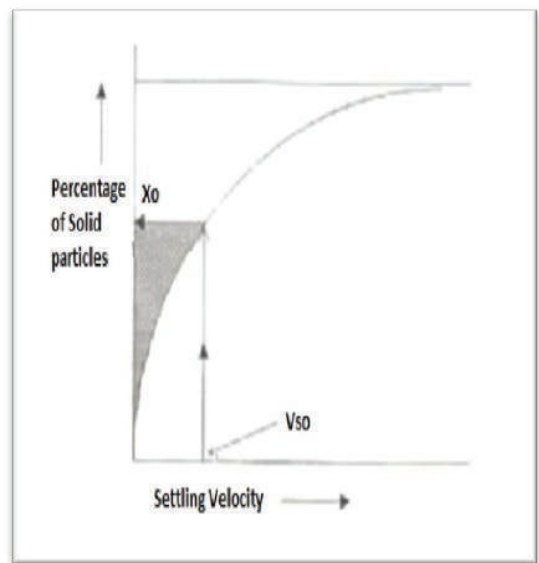
Fig. 3: Sedimentation column

Fig. 4: Curved suspended material.

Table 2: Concentration of TSS for sediment basin samples.

Depth (m)	TSS (mg/L)			
	Settling Time (h)			
	0	1	2	3
1.5	325	100	160	170
3.0	325	60	220	140
4.5	325	30	200	110
6.0	325	20	170	100
7.5	325	10	130	50

Efficiency of Filters

$$E_f = 1 - \left(\frac{C_{out}}{C_e}\right) * 100 = 1\text{-} (190/250) \times 100 = 24\%$$

Efficiency of Sterilisation

Efficiency of Sterilization =

$$1 - \frac{\text{no.of bacteria outside of the station}}{\text{no.of bacteria inside the station}} \times 100$$

December → The efficiency of sterilisation =

$$1 - \left(\frac{44.5}{93}\right) \times 100\% = 52.15\%$$

January → The efficiency of sterilisation =

$$1 \text{-} \left(\frac{30}{86}\right) \times 100\% = 65.12\%$$

February → The efficiency of sterilisation =

$$1 \text{-} \left(\frac{43}{84}\right) \times 100\% = 48.8\%$$

March → The efficiency of sterilisation =

$$1 \text{-} \left(\frac{56}{90}\right) \times 100\% = 37.78\% = 37.78\%$$

Water Quality

The properties of water, pH, turbidity, total dissolved solids, electrical conductivity, total suspended solids were examined. During the liquidation phases in the station, from the moment the water entered into the station and left for citizens, we determined from the test results that the pH of the water inside the station was 6.95 and outside 6.9 with the degree of pH affected by the addition of chlorine and alum to the water. Only the pH values were within the allowable limit in Iraq and WHO (Fig. 7); the water turbidity entering the station was 43.3 NTU but became 7.42 NTU after treatment. The turbidity of the water entering the filters was 15.6 (Fig.

Table 3: Results of velocity and percentage of removal suspended materials.

Depth (mm)	Time (sec)	Velocity (mm/sec)	Removal Solids	Removal per cent (%)
1500	3600	0.417	0.31	69
1500	7200	0.208	0.49	51
1500	10800	0.139	0.52	48
3000	3600	0.833	0.18	82
3000	7200	0.417	0.67	32
3000	10800	0.278	0.43	57
4500	3600	1.25	0.09	91
4500	7200	0.625	0.61	39
4500	10800	0.417	0.33	66
6000	3600	1.667	0.06	94
6000	7200	0.833	0.52	48
6000	10800	0.556	0.3	69
7500	3600	2.083	0.03	97
7500	7200	1.042	0.4	60
7500	10800	0.694	0.153	85

8), which is high as it is supposed to be less than 10 NTU turbidity (Steel & Mcghee 1979). The total concentration of salt values was 8030 mg/L and 3380 mg/L of water inside and outside of the station respectively (Fig. 9), while the electrical conductivity was 5040 µS/ms for the water outside the station (Fig. 10). While the total suspended solids in the water were noted by the results of the tests, the raw water from the Shatt al-Arab river contained a high concentration of suspended solids valued at 325 mg/L (Fig. 11). The purification operations at the station experienced a reduction in this percentage, which significantly reached 190 mg/L of water coming out of the station but remained outside the boundaries of drinking water specifications (Table 4). Figs. 7-11 show these results.

The concentration of magnesium, nitrate and sulphate was also measured for the water entering the station and the water outside it and the calculation of the removal ratio is shown in Fig. 12. It was found that the concentration of magnesium inside the plant was 67mg/L, while the external concentration was 54mg/L, and the concentration of nitrate entering the station was 3.5mg/L and outside was 2.9mg/L. It was found that the concentration of sulphate inside the station was 433mg/L and the outside was 424mg/L. All these values are lower than the limits in Iraq and the WHO, except for the sulphate concentration (Table 4).

DISCUSSION

Through the results of calculations and tests that have been

carried out in this research, the most important findings and their causes have been determined:

1. The efficiency of the sedimentation basin (54%) is not as good as the deposition process, which must rid the water of at least 90% of the particulate matter. The reason for this is that the station is lacking a device to identify the doses of alum, leading to not putting the appropriate amount of alum to get rid of the turbidity of the water.

The alum used in the plant is considered to be outdated because of its old production.

2. The efficiency of the sedimentation tanks leads to the entry of water to the filters with high turbidity, as the specifications define turbidity as 10 units, preferably 5 units of water entering the filters (Steel & Mcghee 1979). However, it is noted that the value is higher than that (Fig. 8), which caused a decline in the efficiency of the filters

Table 4: Drinking water standards, according to the WHO and Iraqi Standard (WHO 2004).

Parameter	WHO in (mg/L)	Iraqi Standard in (mg/L)
pH (No units)	6.5-8.5	6.5-8.6
Total Hardness	100-250	500
Turbidity	5 NTU	5 NTU
TDS	500-1000	1500
EC	1000	1000
TSS	0	0
Iron	0.3-1	0.3
Manganese	0.05-0.1	0.1
Chloride	200-250	250
Magnesium	150	150
Sulphate	200-400	400
Fluoride	0.6-1.2	1
Calcium	150	200
Nitrate	50	50
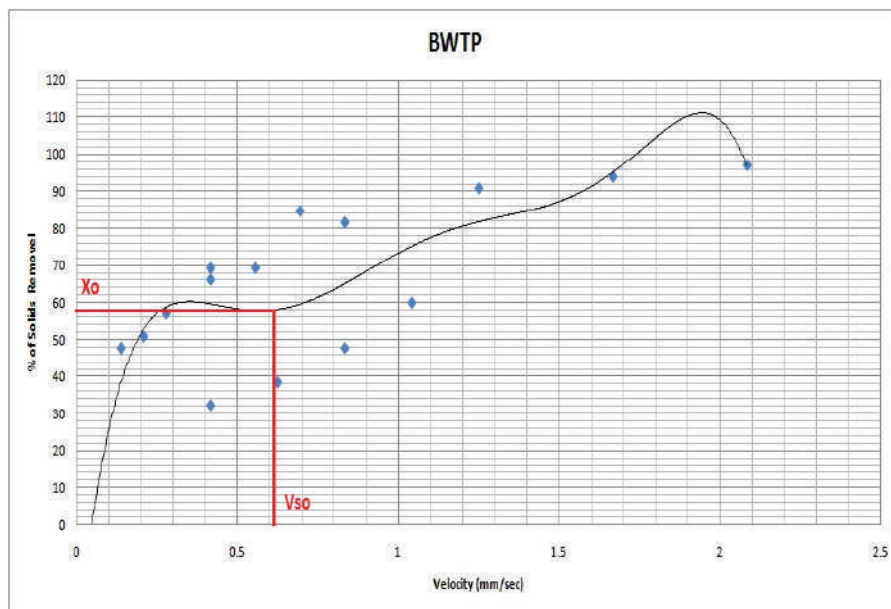
Fig. 5: Curved distribution of remaining suspended material.
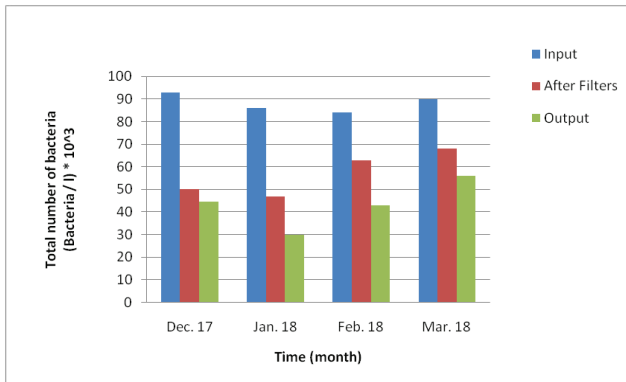
Fig. 6: Diagram showing the total number of bacteria.
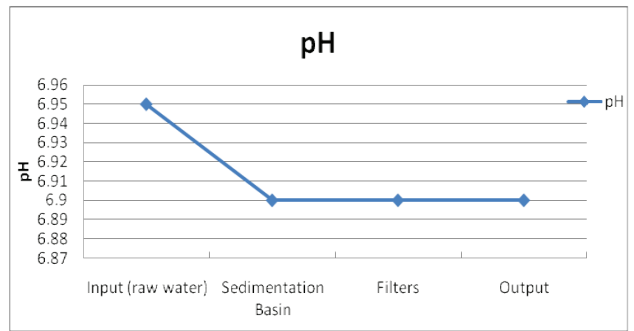
Fig. 7: Change in the value of pH in the stages of treatment in the BWTP.
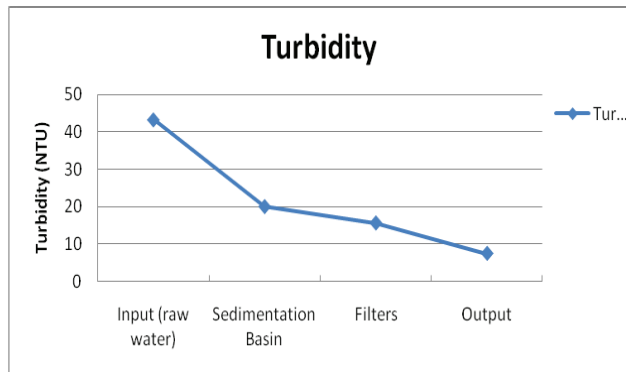
Fig. 8: Change in the value of turbidity in the stages of treatment in the BWTP.
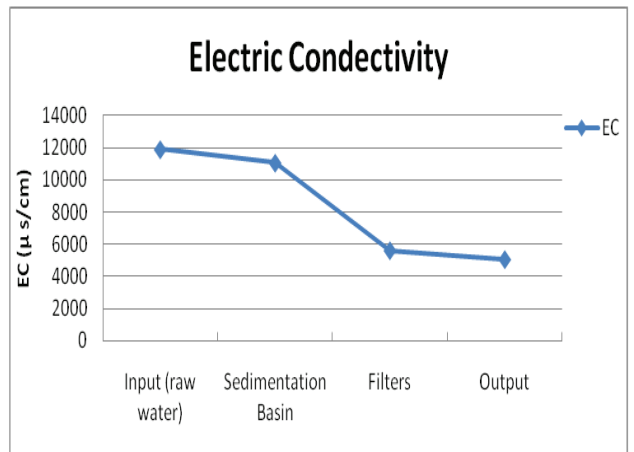
Fig. 9: Change in the value of EC in the stages of treatment in the BWTP.
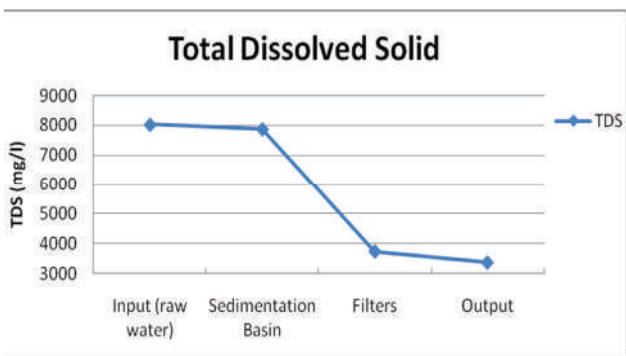
Fig. 10: Change the concentration of TDS in the stages of treatment in the BWTP.
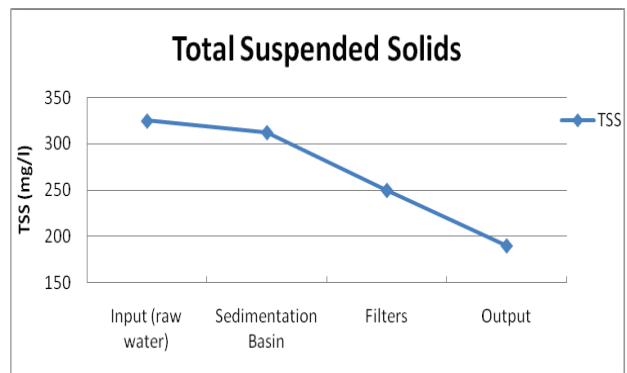
Fig. 11: Change the concentration of TSS in the stages of treatment in the BWTP.
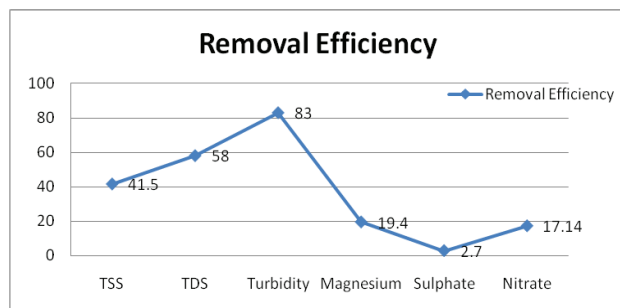
Fig. 12: The removal efficiency of water quality characteristics.

(24%) by a small percentage. Another reason for the low efficiency of the filters was the lack of substitution layers filters when they were needed. The replacement of filter layers was last completed five years ago and the lack of washing filters from time to time led to this result. The increase in the concentration of the suspended material to an allowable limit helps bacteria, viruses, and parasites to grow in the water causing pollution.

3. The results showed the total bacteria decreased in the water that the station was pumping to citizens (Fig. 6). According to US specifications, this water cannot be used for other purposes, e.g. the food industry because the bacteria can cause damage to processed food. Although the station added chlorine to improve the quality, it was unable to kill all the types of bacteria that were abounding in the cold weather. There is a range of factors that affect the reaction of chlorine to germs, with regard to cholera and other germs. Factors are related to chlorine (temperature, pH and the presence of organic matter) as chlorine reacts with the organic matter first and the rest reacts with germs.

CONCLUSIONS

1. Lack of efficiency of the station in terms of the efficiency of sedimentation, filtration and sterilization is desired for the removal of suspended solids in the water.

2. The station's different units do not perform well, especially when the plant is dealing with bad quality water.

RECOMMENDATIONS

1. Conduct similar studies on water treatment projects in the province.

2. The development of the water treatment process in the project by monitoring the quality of raw water per day and processed to suit the specifications of drinking water, by selecting the accurate dose of alum and coagulants in the laboratory, to control the amount of water in the processing units and periodic maintenance of processing units.

3. Perform general technical maintenance of the station stages and clean sedimentation basins.

REFERENCES

Abdul-Rahman, E.A., Mulood, A.A. and Whran, M.S. 2009. Assessment of the quality of drinking water and the efficiency of the water purification plant in Falluja. Iraqi Journal of Civil Engineering, 6(1): 27-38.

Ahmed, E.A. 1995. Environmental Engineering (5 ed.). Engineering College, Sultan Qaboos University, Al-Mustakbal Company, Oman, pp. 261-289.

Annachhatre, P. A. 2006. Water Quality and Wastewater Management. School of Environment Resources and Development & Asian Institute of Technology, Thailand, pp. 125-129.

APHA 1998. Standard Methods for the Examination of Water and Wastewater (20 ed.). American Public Health Association, Washington, D. C., USA.

Aremu, M.O., Olaofe, O., Ikokoh, P.P. and Yakubu, M.M. 2011. Physico-chemical characteristics of stream, well and borehole water sources in Eggon, Nasarawa state. Chemical Society of Nigeria, 36 (1): 131-136.

Fetter, C. W. 1988. Applied Hydrogeology (2 ed.). Macmillan, New York, U. S. A., pp. 367-369.

Jackson, R.B., Carpenter, S.R., Dahm, C.N., Mcknight, D.M., Naiman, R.J., Postel, S.L. and Running S.W. 2001. Water in a changing world. Ecological Society of America, 9(1): 1-16.

Miller, G. T. 1997. Environmental Science: Working with the Earth (6 ed.). Wadsworth Publishing Company, California, U.S.A., pp. 423-481.

Ramel, M. M. 2010. Evaluating the drinking water quality supplied by the large treatment plant in Ramadi city. Al-Qadisiyah Journal for Engineering Sciences, 3(2): 33-56.

Saleh, R.A., Edaan, I.G. and Abdul Wahed, A.K. 2015. Evaluation of the efficiency of gas Al-Shamal water treatment plant. Diyala Journal of Engineering Sciences, 8(1): 1-12.

Sorlini, S., Palazzini, D., Sieliechi, J.M. and Ngassoum, M.B. 2013. Assessment of physical-chemical drinking water quality in the Logone valley (Chad-Cameroon). Sustainability, 5(1): 3060-3076.

Steel, E.W. and Mcghee, T.J. 1979. Water Supply and Sewerage. McGraw Hill Education Europe, New York, U.S.A., pp. 234-267.

Sundstrom, D.W. and Klei, H.E. 1979. Waste Water Treatment. Prentice Hall, Englewood Cliffs, U S A, pp. 3-6.

Syed, A.H., Alamdar, H., Urooj, F., Wajid, A., Amjad, H. and Nasir, H. 2016. Evaluation of drinking water quality in urban areas of Pakistan: A case study of Gulshane-Iqbal Karachi, Pakistan. Journal of Biodiversity and Environmental Science, 8(3): 64-76.

WHO 2004. Guidelines for Drinking Water Quality (3 ed., Vol. 1). World Health Organization, Geneva.

Legislative Norms from the Perspective of Water Resources Management in Zhejiang Province of China

Chencan Liu†

School of Public Administration, North China University of Water Resources and Electric Power, Zhengzhou 450046, China

†Corresponding author: Chencan Liu; acan71@msn.com

ABSTRACT

As an important material resource of human being, water resource is of great significance to promote sustainable development of economy and society, and it must be managed and utilized reasonably. Water resources management in Zhejiang Province has always been at the forefront of China, but the lagging development of the local legal system has seriously hindered the construction of water ecological civilization. To meet the actual work demand of water resource management in Zhejiang Province of China, its social development and water resource management situation in 2019 was probed by using comparative analysis. Results show that water resource management and local legal system construction has a logic relationship and that their hidden dangers and shortcomings in the practice of water resources legal system in Zhejiang Province of China. Legislation standard path and countermeasures are put forward for water resources management in Zhejiang Province of China.

INTRODUCTION

At present, water security in China presents a severe situation, in which new and old problems are intertwined, especially new problems, including water resources shortage, water ecological damage, water environment pollution and so on. Water resources have become a serious shortage of products, the main factors restricting environmental quality, and the serious security problems faced by economic and social development in China. Xi Jinping, President of the People's Republic of China, pointed out that the spatial and temporal distribution of water resources was extremely uneven, and floods and droughts were frequent. To further promote the reform of water conservancy and construction of water conservancy legal system, Zhejiang Province of China carried out the project of basic research on water resource management reform and legislation according to the actual work demand of water resource management. China's current water resource management system and basin management institutions have not been effectively established which is extremely incompatible with the requirements of the situation.

Zhejiang Province of China is one of the provinces with the smallest difference in economic development. According to the sample survey of 5‰ population change in 2019, the province's permanent population at the end of the year was 58.5 million, with an increase of 1.1 million over the end of the previous year. According to Water Resources Bulletin of Zhejiang Province of China issued by the water resources department in 2019, the total amount of water resources is 86.65 billion cubic meters (including underground water), which is 9.3% less than the average annual total amount of water resources, ranking the third in China after Guangdong Province and Fujian Province. Water resources protection is of great political and economic significance to the sustainable development of China's national economy. In view of the serious absence of water resources management legislation, current water resources management system and basin management institutions in Zhejiang of China have not been effectively established which is extremely incompatible with the requirements of the situation. There are problems in the legislation of water resources protection.

According to requirements of the strictest water resource management system, by using comparative analysis, this study carries out research on social development and water resource management situation in Zhejiang Province of China, and legislative study on its practice of water administration and the relevant laws and policies issued at the national level in recent years. Finally, the standard path and countermeasures are put forward.

STATE OF ART

At present, China still adopts the dual legislation mode of resource legislation and pollution prevention legislation, and

the understanding of water resources protection is biased and comprehensive legislation is missing (Yuan et al. 2012). Moreover, laws and regulations of ecological protection of water resources are not perfect, and legislation cannot clarify the responsibilities and rights of the administrative subject, which will be a major mistake (Nie 2009). In terms of water saving management, China had established basic water saving system, but it was mainly provided in principle, and there was still a lack of special water saving laws and regulations, which was not conducive to changing the extensive use of water resources (Zhang et al. 2018). It could be seen that China's water resource management legislation was still lagging behind, and a complete set of laws and regulations system for basin water resources management had not been formed, and the expected objectives of water resources management could not be achieved (Liang 2014).

Then, it was the natural identification value of water resources legislation. Water resources management legislation should choose non-rights-based legislative model, and apply a duty-based legislative model (Smarzynska et al. 2005, Chen 2006). For the legislation of river basin water resources, the objects to be protected should be clearly specified in the legislation, and the basin water resources and ecological environment should be taken as the purpose of legislative protection (Zhou 2008).

Some scholars also carried out research on legislative countermeasures of water resources protection. Water resources legislation was not static, but dynamic, open and developing. The reform of water rights and the legal system of river basin ecological compensation should actively be promoted (Xiong et al. 2020). Comprehensive, coordinated and sustainable development as the content should be carried out, with the legislation of the scientific development con-

cept, and the coordinated development of social economy and environmental protection should be achieved, to maintaining a new balance in the development (Wu 2007). A comprehensive management system and management organization should be established for the water environment and water resources basin (Du et al. 2020).

WATER RESOURCE MANAGEMENT OF ZHEJIANG

Zhejiang's GDP in 2019 was 6,235.2 billion RMB, with an increase of 6.8% over the previous year (as shown in Figure 1). Among them, the added value of the primary industry was 209.7 billion RMB, and the added value of the secondary industry is 2,656.7 billion RMB, and the added value of the tertiary industry was 3,368.8 billion RMB, increasing by 2.0%, 5.9% and 7.8% respectively. The contribution rate of the tertiary industry to GDP growth was 58.9%, and the added value structure of these three industries was 3.4:42.6:54.0 (as shown in Fig. 2), and the per capita GDP was 107,624 RMB (converted to 15,601 dollars at the annual average exchange rate), increasing by 5.0%. In 2019, the per capita disposable income of residents in the province was 49,899 RMB, with an increase of 8.9% over the previous year, and an increase of 5.8% after deducting the price factor. The per capita disposable income of urban and rural residents was 60,182 RMB and 29,876 RMB respectively, with an increase of 8.3% and 9.4%, and an increase of 5.4% and 6.0% after deducting the price factor. The income ratio of urban and rural residents decreased from 2.04 last year to 2.01. The per capita disposable income of Zhejiang residents was 1.6 times the national average level (30,733 RMB), ranking the third in China. The per capita disposable income of urban residents is 1.4 times the national average level (42,359
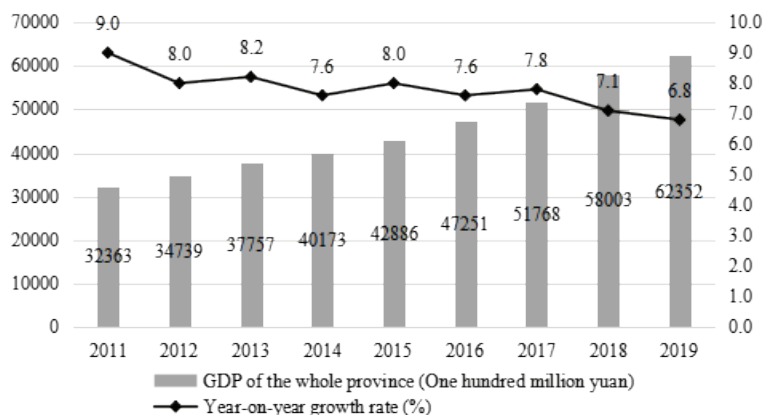
Fig. 1: GDP and growth rate of Zhejiang Province of China in 2011-2019.
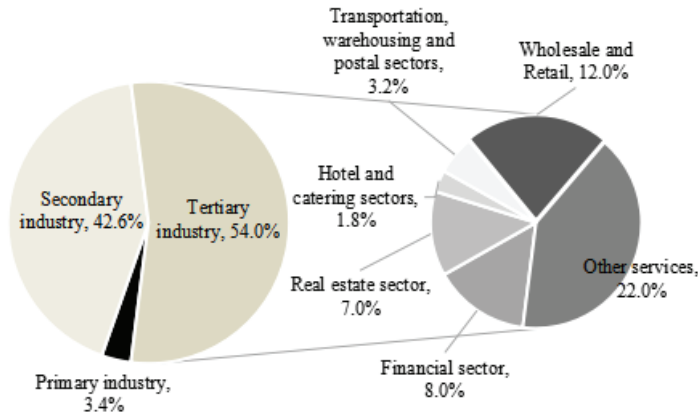
Fig. 2: Proportion of added value of various industries in regional GDP of Zhejiang Province of China in 2019.

RMB), ranking the third in China. The per capita disposable income of rural residents is 1.9 times the national average level (16,021 RMB), ranking the second in the country. On the whole, the economy in Zhejiang is running steadily and making progress instability, and the trend of major economic indicators is better than that of the whole country.

The average precipitation of the whole province is 1,640.3 mm, which is 2.3% more than the average annual precipitation. The total annual water consumption of the whole province is 17.4 billion cubic meters. Domestic water consumption of residents is 2.856 billion cubic meters, accounting for 16.4%. Water consumption of ecological environment is 550 million cubic meters, accounting for 3.2% (as shown in Fig. 3). There are 194 large and medium-sized reservoirs in the province, with a total storage capacity of 24.3 billion cubic meters at the end of the year, including 34 large reservoirs, with a total storage capacity of 21.9 billion cubic meters. It has an increase of 1.8 billion cubic meters compared with the end of the previous year. In addition,

there are 160 medium-sized reservoirs, with a total storage capacity of 2.4 billion cubic meters at the end of the year, an increase of 299 million cubic meters compared with the end of the previous year. There are 1,112 water function areas in the whole province, with 16,923 kilometres of river length. There are 717 key water function areas assessed by the province during the 13th five-year plan, with a total river length of 12,114 kilometres. The annual compliance rate is 89.1% (as shown in Figure 4).

In the aspect of water resource management system construction, Zhejiang Province of China has made remarkable achievements depending on the long-term economic foundation. Water Resources Management Regulations of Zhejiang Province was the first local regulation regulating water resources management in China since Water Law of the People's Republic of China. The purpose was to reasonably develop, utilize, save and protect water resources, and to provide a legal basis for strengthening the unified management of water resources quality and quantity. It tried to explore the
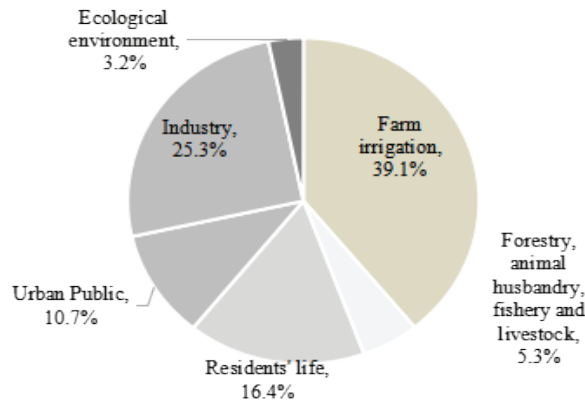
Fig. 3: Schematic diagram of water structure proportion of the whole province in China.
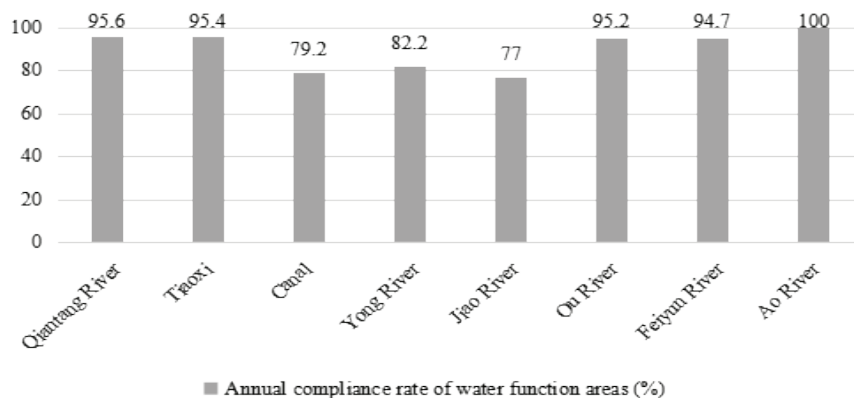
Fig. 4: Water quality compliance rates of eight water system water function areas.

initial water right distribution scheme. Zhejiang Province was one of the earliest provinces to carry out the administrative legislation of water conservation management. Water Conservation Measures of Zhejiang Province was implemented. In addition, Zhejiang Province had organized and compiled a series of water resource management plans, including Master plan for water resources protection, development and utilization, water-saving society construction plan, water-saving irrigation plan, and water resources protection. It also issued a series of normative documents, including opinions on promoting the construction of water ecological civilization, the implementation plan for accelerating the construction of water-saving society in Zhejiang Province of China. For further improving water-saving management system and water resource protection system of Zhejiang Province of China, it provided a strong legal basis and system guarantee for the provincial water administration, and also provided a "Zhejiang Model" of China for the national water resource management.

Although Zhejiang Province is rich in total water resources in China, the per capita water volume is only about 1800 m³, about 8 percentage points lower than the national per capita level, which is less than 1/4 of the world per capita level. In recent years, with the rapid growth of urban and industrial water consumption, the contradiction between water supply and demand in Zhejiang Province is very prominent, especially the general shortage of water resources in most islands in the province, and the serious shortage of production and domestic water supply. In addition, deterioration of water environment, degradation of water ecology and overdraft of groundwater lead to the water crisis are imminent. At present, there are new problems in water resource management of Zhejiang Province of China. Water administration is decentralized, involving multiple management departments, and it is difficult to adapt to the complex

relationship of the water system. What's worse, economic leverage of water resource management is limited, which may mains that the water price system is unreasonable, and that the market-oriented policy is not mature. It is urgent to promote water price reform and to improve the water price system. Supporting system of water resource management is insufficient, especially the auxiliary information system of water resource management, and the illegal disposal is lack of force. Official publicity and education of water conservation and water resource protection are not enough, and the public awareness of water conservation and participation is not generally formed. It can be seen that the current water law and regulation system in Zhejiang Province of China has seriously lagged behind economic development and that local legislation should be adopted to strengthen the administrative management of water resources.

LEGISLATIVE AND FEASIBILITY ANALYSIS

Because of the actual work demand of water resources management in Zhejiang Province of China, this study puts forward the legislative amendment proposal of organic integration of Water Resources Management Regulations of Zhejiang Province and Water Conservation Measures of Zhejiang Province. Based on the previous legislative research, Water Resources Management Regulations of Zhejiang Province and Water Conservation Measures of Zhejiang Province will be merged, and Regulations on Water Conservation and Water Resource Management of Zhejiang Province of China with legality, rationality, coordination, operability and standardization will be promulgated and implemented through legislative channels (Bravo-Macias et al. 2019). Raising "water conservation" to the same legal level as "water resource management" can effectively regulate current water administration behaviour. It also can improve public awareness of water conservation and environmental

protection, which has the significance of the rule of law and practical feasibility of the times.

Firstly, it should meet the needs of the practice of the new concept of water control. Water-saving has been mentioned at an unprecedented height, and it can be made a conscious action for individuals and social organizations. It is required to vigorously publicize the behaviour of water-saving and water cleaning. It is necessary for Zhejiang Province of China to comprehensively summarize the experience, to find out weak links of water-saving work, and to put forward targeted system and mechanism guarantee. The effective integration of Water Resources Management Regulations of Zhejiang Province and Water Conservation Measures of Zhejiang Province will also enhance the legal status of water-saving management. The new idea of water control in the new era should be put into practice. The management system should be further improved, and the management ability should be improved to better realize the purpose of water resource conservation and protection in Zhejiang Province of China.

Secondly, it should adapt to the needs of ecological civilization system reform. With the national attention to the construction of water ecological civilization year by year, a series of important water administration measures have been announced in succession. Methods include implementing the strictest water resource management system, promoting the implementation of water pollution prevention and controlling action plan, strongly promoting the river lake system and "five water co-governance", etc., which have a profound impact on water resource management reform and legal system construction in Zhejiang Province. It has made beneficial explorations and accumulated practical experience in aspects of the strictest assessment of water resource management system, construction of water-saving society, reform of water licensing, demonstration of planned water resources, compensation of basin ecological protection, and reform of water right system. In the future, promulgation and implementation of Regulations on Water Conservation and Water Resources Management of Zhejiang Province will consolidate practical experience and reform achievements by means of the rule of law and will continue to guide and promote reform and development of the water ecological civilization system in Zhejiang Province.

Thirdly, it should ensure sustainable development of economy and society. Water resources are a basic guarantee for sustainable development of economy and society and construction of ecological civilization. Rapid economic and social development has brought deep structural changes in water supply and demand. As an economically developed region in China, Zhejiang Province is facing with severe challenges in the new era, which needs to further promote

reform of water resources supply, to adhere to the water resources management principle of "Water determines the city, the land, the people and the production", to take actions by measuring the number of water resources, and measures according to the situation of water resources, and to strengthen rigid restriction of water resources. Both Water Resources Management Regulations of Zhejiang Province and Water Conservation Measures of Zhejiang Province are not in line with current water resources development situation in Zhejiang Province of China, so it is urgent to comprehensively revise and integrate them, and to provide effective legal support for water resources management reform through the way of national coercive force.

Finally, it should meet the needs of water conservation and management according to law. China has promulgated a series of basic water laws, including Water Law, Law on Prevention and Control of Water Pollution, Law on Soil and Water Conservation and Flood Control Law. However, there are some problems in judicial practice, such as the weakness of water laws and regulations, and the lack of initiative and legitimacy of local water administrative departments to manage water according to law, which may lead to the phenomenon of weak operation of the local legal system and lax law enforcement, and the result of the reduced force of water laws. Through the implementation of the new Regulations on Water Conservation and Water Resource Management of Zhejiang Province of China, a series of basic systems for water conservation and water resource management will be established from perspective of the rule of law to ensure legalization and standardization, to clarify legal obligations and responsibilities of water conservation and protection of water resources in the whole society, and to form a good social water resource environment for the whole people to manage and protect water according to law.

PATH OF LOCAL LAWS AND REGULATIONS OF WATER RESOURCES MANAGEMENT

The Path of Legislative Norms Based on Water Resources Management Regulations of Zhejiang Province Perspective

As the first local law of water resource management in China, Water Resources Management Regulations of Zhejiang Province has played an important role in strengthening water resource utilization planning, reducing water pollution, improving water resource utilization efficiency and promoting social sustainable development since its implementation in 2002 (Copeland et al. 2003). Attention should be paid to the implementation of local system guarantee in the strictest water resource management work in the country, which can

be further modified and improved in the following aspects.

Firstly, the rules of the water efficiency control system need to be detailed. The efficiency of water use is not high and the shortage of water resources has become an important restricting factor for the sustainable development of economy and society. The provisions set up the basic framework of water use efficiency control in the Water Resources Management Regulations of Zhejiang Province. From the perspective of relationship with Water Law, it stipulates obligations of the state and the government, obligations of units and individuals to save water, improvement of agricultural water use efficiency, and improvement of industrial water use efficiency, water-saving facilities and water-saving instruments. There is no problem with their legality. However, compared with the lower law, the provisions of Water Resources Management Regulations of Zhejiang Province are still rough. Regulations on Water Conservation and Water Resource Management of Zhejiang Province should be incorporated to some extent.

Secondly, the content of water function zone pollution control system needs to be expanded. The core content of the system is to strengthen supervision and monitoring and to carry out protection and repair. The provisions of Water Resources Management Regulations of Zhejiang Province on the total emission are relatively simple, only stipulating that the government puts forward opinions on the total emission to competent environmental authorities and that provisions of the upper law should be appropriately absorbed. It is necessary to refer to the relevant provisions of "restoration of water ecological system" in Environmental protection law, and at the same time set up the main responsibility for violating the protection of water ecological system.

Thirdly, water resource management assessment system needs to be established. Water resource management responsibility and assessment system is the fundamental guarantee to implement the strictest water resource management system, which is easy to be ignored in practice. The overall system arrangement can be made by referring to provisions of opinions on implementing the strictest water resource management system of the State Council, and its principle, subject, content, method, period, plan and report shall be specified.

The Path of Legislative Norms Based on Water Conservation Measures of Zhejiang Province Perspective

Water Conservation Measures of Zhejiang Province is a special government regulation of Zhejiang Province in China, which can more comprehensively and systematically regulate series of water conservation management systems or penalties, further clarify and refine the important systems in Water Resources Management Regulations of Zhejiang Province, and can make up for the shortcomings of Water Resources Management Regulations of Zhejiang Province in-depth and breadth. To sum up, the revision of Water Conservation Measures of Zhejiang Province can be divided into two parts. Firstly, it revises the water conservation clause in Water Resources Management Regulations of Zhejiang Province. Then, it merges with Water Resources Management Regulations of Zhejiang Province to form Regulations on Water Conservation and Water Resource Management of Zhejiang Province (Draft) of China and improves the refinement and overall planning of the system. The specific revision suggestions are as follows.

Firstly, it's what needs to be improved. For the problems of unclear and repeated responsibilities in Water Conservation Measures of Zhejiang Province, it is necessary to clarify the responsibilities of water-saving management, and effectively to connect the water-saving management work of each link in combination with the "three definite plans" of the water-related management department. The provincial water administrative department is responsible for formulating water-saving policies, preparing water-saving plans, standardizing water-saving standards, guiding the construction and management of water-saving irrigation projects, and assessing with relevant departments to promote the construction of a water-saving society in the province (Kolkis 2019). It is necessary to improve the water-saving planning system and clarify corresponding formulation, implementation and revision departments. Water Conservation Measures of Zhejiang Province shall specify the system to be implemented for water fee collection, and shall implement the system of over plan and over quota progressive price increase. It is stipulated that water users shall use water according to the approved plan index or water quota. If water consumption exceeds the plan and over quota, water fee exceeding the plan shall be increased according to the method of the progressive price increase. The provisions of Water Conservation Measures of Zhejiang Province that lack water-saving reward and punishment is too light should be modified. The people's government at or above the county level shall establish a special fund for the reward of water-saving technology research, development, promotion of water-saving facilities construction and water-saving management. For violations of water-saving regulations, bad information shall be included in the credit file following the provisions of Zhejiang credit rules.

Secondly, it's what needs to be added. "Contract water-saving" provisions shall be added to encourage the development of water-saving service institutions, and to support water-saving service institutions to carry out con-

tract water-saving, water-saving consultation, water balance test and other services. It shall recover investment and obtain reasonable profits in the way of water conservation benefit-sharing, and shall carry out contract water-saving management in public institutions, high water consumption industry, high water consumption service industry, efficient water-saving irrigation and other fields. The quality supervision department shall conduct supervision, spot check, special inspection and verification management for the products listed in the list of water efficiency identification products according to law. Products and equipment that have obtained water-saving product certification in accordance with relevant regulations should be listed in the list of government procurement with priority. In addition, it shall implement the "water efficiency leader" system, establish a water efficiency leader system, develop indicators for water efficiency leaders, and shall carry out leading actions for water efficiency leaders in the fields of industry, agriculture, public institutions and domestic water use.

Thirdly, in view of the need for a large number of technical personnel and complete technical support, the administrative cost of the water-saving audit is too high, which is not suitable for water resources and environment of Zhejiang Province of China, and it should be abolished. Due to the lack of sufficient technical force, it is difficult for rural water management institutions to undertake the responsibility of managing and maintaining agricultural irrigation water-saving facilities, which is not suitable to name the water management organization established by the rural collective economic organization. Since water quotas are usually set by industry authorities in practice, the intervention of local governments should be deleted due to the lack of operational procedures.

CONCLUSIONS

Water Resources Management Regulations of Zhejiang Province belongs to local laws and regulations in the nature of law. Local laws and regulations occupy an important legal position in the socialist legal system of our country. In order to build a legal society, attention should not only be paid to the formulation of local laws and regulations but also should be paid to actual operation state, together with results and existing problems after the formulation of laws and regulations. Although Water Resources Management Regulations of Zhejiang Province had been revised three times in 2009, 2011 and 2017, so far, it was difficult to meet new ideas and requirements for water conservancy work and was also hard to cope with new problems and situations in water administration of Zhejiang Province of China. Its legal norms and legal objectives are not compatible with the

current water-saving management work. Meanwhile, Water Conservation Measures of Zhejiang Province has not taken the protection and improvement of ecological environment as the basic purpose of the legislation, seriously lagging behind the water administration work of Zhejiang Province of China, with poor timeliness. The revised Water Law in 2016 marked a new stage in the construction of the rule of law for water control and protection according to law. Zhejiang Province is one of the first provinces to make local legislation on water resources management, and evaluation of water resources has been at the forefront of China.

ACKNOWLEDGEMENT

REFERENCES

Bravo-Macias, C., Sarmentero-Bon, I., Rodriguez-Sanchez, Y. and Gomez-Figueroa, O. 2019. Evaluation of organizational competencies through performance indicators. Dyna, 94(5): 490.

Chen, X.J. 2006. A new exploration of watershed legislation. Journal of Zhengzhou University (Philosophy and Social Science Edition), 47(5): 61-65.

Copeland, B. and Taylor, S. 2003. Trade and the Environment: Theory and Evidence. Princeton University Press, Princeton.

Du, Y. C. and Wang, R. X. 2020. Impact of corporate governance ability on capital gains in mixed ownership enterprises. Transformations in Business & Economics, 19(2): 92-113.

Kolkis, S. 2019. Benchmarking the sustainability of urban energy, water and environment systems and envisioning a cross-sectoral scenario for the future. Renewable and Sustainable Energy Reviews, 103: 529-545.

Liang, J.Y. 2014. A Study on the legislation of water resources management in river basins in China. Environmental Science and Management, 40(2): 178-181.

Nie, A.P. 2009. Discussion on legislation of water resources ecological protection in China. Jiangxi Social Sciences, 9(11): 141-144.

Smarzynska, B.K. and Wei, S.J. 2005. Pollution havens and foreign direct investment: Dirty secret or popular myth. Economic Analysis & Policy, 3(2): 8-38.

Wu, Y. P. 2007. Research on integrated management system of water environment and water resources basin. Hebei Law, 28(7): 119-123.

Xiong, Z., Wang, P.J. and Zhao, Y. 2020. Re-innovation from failure, institutional environmental differences, and firm performance: Evidence from China. Amfiteatru Economic, 22(53): 197-219.

Yuan, J.W. and Tu, J.F. 2012. Legislative status and improvement of water resources protection in China. Journal of Hubei University of Economics (Humanities and Social Sciences), 9(11): 74-75.

Zhang, R.M., Wang, Y.J. and Chen, X. 2018. Current situation of water resources management legislation and new requirements of supply side reform. Water Economics, 38(1): 27-31.

Original Research Paper \quad https://doi.org/10.46488/NEPT.2020.v19i03.018 \quad **Open Access Journal**

Valorisation of Natural Waste: Dam Sludge for Road Construction

A. Larouci*, Y. Senhadji*, L. Laoufi *† and A. Benazzouk**

*University of Mascara, Faculty of Science and Technology, Department of Civil Engineering, Mascara, Algeria
** Department of Civil Engineering, University of Picardie Jules Verne, Amiens, France
†Corresponding author: L. Laoufi; laoufifr@yahoo.fr; l.laoufi@univ-mascara.dz

ABSTRACT

The Algerian dams are in a more or less silted state. Fergoug dam is the most silted dam since it records a rate of siltation of 95%. The siltation of the dam is undoubtedly the most dramatic consequence of the problem of erosion in Algeria. The investigations are at two levels: either prevent the solids to arrive in the dam (that is to put obstacles to break the forces of the runoff water, but we can only hope partial results) or the evacuation of sediments by appropriate management of bottom. But in our opinion, their valorisation in the field of construction is the most appropriate solution. This valorisation helps protect the environment and natural materials. Many mud treatment methods are often used to improve the insufficient geotechnical properties before reuse for a certain function in the structure. Lime treatment is one of the most common methods of converting soils to new materials that provide the desired performances. The objective of this work is to study the mud behaviour of the Fergoug dam (Algeria) for its use in the application of road engineering. The study consists of reconstituting samples of the Fergoug dam mud with various proportions of lime in the laboratory and subjecting them to various tests (Proctor, VBS, CBR index, DRX, etc.). The results obtained are encouraging and therefore allow the valorisation of sediments of the Fergoug dam which are a cumbersome waste for the environment.

INTRODUCTION

The management of the dredged material generated by this activity is confronted with legal, financial, environmental, technical and scientific difficulties. The solidification/stabilization technique based on hydraulic binders and/or aerial is used to valorise and reuse the treated dredging sediments. This technique will make it possible to find economic and environmental solutions to dredged sediments from dams, based on scientific and technical work. The treatment with hydraulic binders is preferential for valorisation in road techniques (underlayment or embankments).

The results of the sediment recovery study thus treated show that the mechanical performances (threshold of 1 MPa required for the simple compressive strength at 28 days) associated with an environmental and economic approach are achieved with several combinations of pre-treatment and treatment (Sannier et al. 2009, Levacher et al. 2011).

The methodology of valorisation of sediments as road material (more particularly in the form layer) is based on the recommendations of the LCPC-SETRA technical guides for road earthworks and soil treatment with lime and hydraulic binders (GTR 2000).

The results analysed here are related to sediment treatment of dam Fergoug (Algeria) and they will be studied in terms of processability. The dam of Fergoug offers a distressing view due to its sedimentation rate, estimated at 95%. The initial storage capacity of this dam was 17 million m³. In 2005, it underwent a dredging operation which allowed recovering 10 million cubic meters of sediments. Therefore, because of these huge quantities, the valorisation of these dredged sediments remains a real challenge (Laoufi et al. 2016, Larouci et al. 2018). The dredging operation is an important phase in the recovery and preservation of useful storage volumes of dams. But the fate of the large quantities of sediment recovered is a major environmental and economic challenge (Levacher et al. 2006).

The mechanical behaviour will be analysed to identify trends and correlations between the geotechnical properties of a side and treat the ability of binders and thus enhance the value of sediment of another side.

The tests include measurements of unconfined compressive strengths (UCS). The results obtained show that the sediments of Fergoug dam do not reach the mechanical performance required by the geotechnical and safety works (GTS).

MATERIALS AND METHODS

Sediment Sampling

Sediment samples were collected at the Fergoug dam. This dam is located 20 km upstream from Mohamadia on the road

to Mascara city (RN17) in the north-west of Algeria Fig.1. It was built upon the installation of the first settlers in Oran city, during the last century. Fergoug dam is a dam in the earth having in 1963 a capacity of 18 million m^3. The filling rate of the Fergoug dam was 95% in 2019 (ANBT 2014). To ensure an acceptable level of service, the dam authorities regularly dredged it during the period from 1986 to 1989 generating very large volumes of material (10 million m^3 of silt were extracted) (Semcha 2006).

Deposited downstream in grossly developed areas, the dredged mud is again eroded to the mouth of the Macta wadi. Sediment samples were collected from three different sites downstream of the Fergoug Dam. All sampled sediments were transported to the laboratory and homogenized to obtain raw sediments; these were stored in airtight containers.

Granular Corrector Sampling

In this study, an aerial binder was used to formulate road materials containing quantities of dredged sediment. This aerial binder was mainly composed of lime. It is a natural tuff which was extracted from a quarry located in Douar Sidi Ali Cherif (Mascara, Algeria). The characteristics of this Sidi Ali Cherif tuff (SCT) are given in Table 1. According to this table, we can say that the tuff is loamy soil, weakly plastic and rich in fine elements. It is therefore finally a sandy and gravelly soil rich in fine elements.

Organic matter has some undesirable characteristics in road construction because of its swelling structure. The Fergoug dam sediments (FDS) have a significant organic matter content of 3.15% versus a value of 0.31% for Sidi Ali Cherif Tuff (SCT). These values can have a significant impact on the geotechnical and mechanical behaviour of sediments.

Organic materials can also have an impact on binder hydration. For our study, the rate of silt used was incorporated which neglects the risk of the negative effect of organic matter. The organic material test was carried out on a fraction by weight of 0/2 mm at 450°C during 3 hours. In addition, it will be possible to use these values to classify different sediments according to the French Guide to Road earthworks (GTR 2000).

RESULTS AND DISCUSSION

The Limits of Atterberg

The Figs. 2, 3 and 4 show LL, PL, PI as a function of lime added (0, 2, 4, 6 and 8%) for 10, 20 and 30% of FDS. As we see for these three figures, more the percentage of lime increases more LL and PI decrease. As for PL, it increases with the increase in the percentage of lime.

The addition of lime leads to an improvement in the consistency because of a significant reduction of the plasticity index which results in an increase in the limit of plasticity accompanied by a decrease of the limit of liquidity. Thus, the specific surface is reduced immediately after the incorporation of the lime at the end of the clays flocculation. These results have been confirmed by many researchers. Guney et

Fig. 1: Fergoug dam (Algeria).

Table 1: Geotechnico-physical characteristics of SCT and FDS.

Characteristics	Designation	FDS	SCT
Natural water content	Wn (%)	58,10	8,34
Liquid limit	LL (%)	62,54	25,19
Plastic Limit	PL(%)	29,29	15,87
Plasticity index	PI(%)	33,26	9,32
Dry density	γ_{max} (g/cm^3)	1,779	1,985
Optimum water content	W_{opt} (%)	19,30	10,97
Methylene blue value	MBV (%)	3,42	0,66
Carbonates	$CaCO_3$ (%)	27,94	88,70
Organic material	OM (%)	3,15	0,31
Fine elements <80 μm	FE (%)	17.77	-
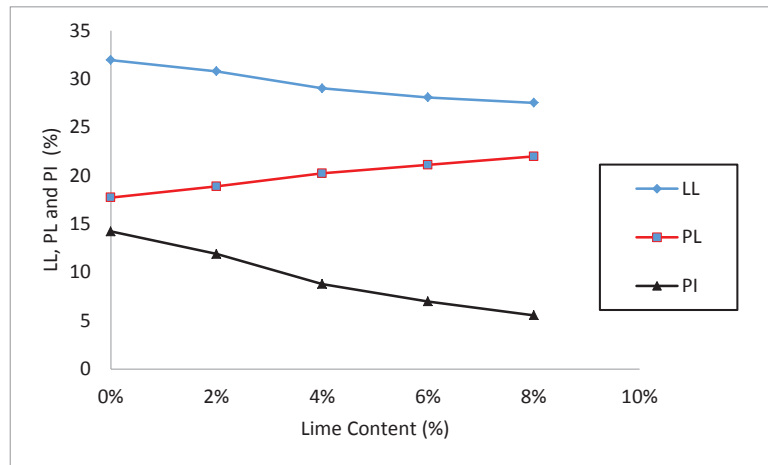
Fig. 2: 10% FDS treated with 0, 2, 4, 6 and 8% lime.
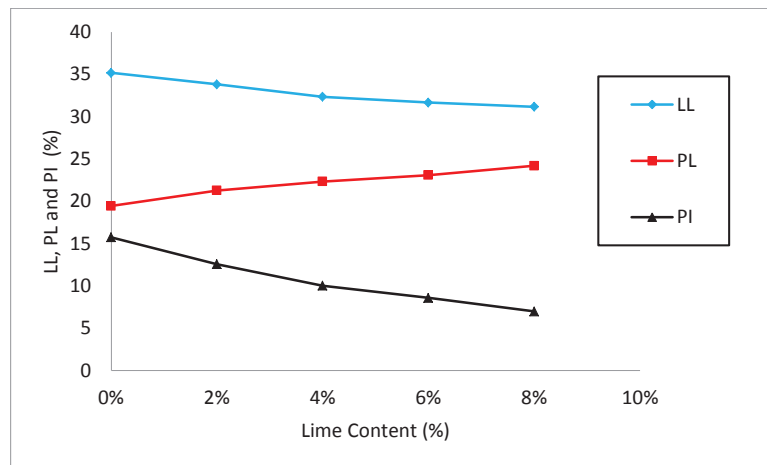
Fig. 3: 20% FDS treated with 0, 2, 4, 6 and 8% lime.

al. (2007), Manassah & Olufemi (2008) who have worked on similar themes demonstrated in their investigations that the liquid limit (LL) varies according to the lime mix and the nature of the clay soil treated, with respect to the plastic limit (PL) large increase was still observed. George et al. (1992) concluded in their study that the soil plasticity index decreased with the addition of lime and this decrease was related with the increase of the plasticity limit rather than the decrease of the liquidity limit.

Methylene Blue Value (MBV)

For each sediment and lime content, we measured the methylene blue value (Fig. 5). The results of the blends are illustrated in the graph of Fig. 5. The increase of the lime content caused a decrease of the MBV and consequently the specific surface area of the mixture treated (SCT + % FDS) decreased. This decrease was remarkable for an addition of 2% lime content for all mixtures, then it was less accented for the other percentages (4, 6 and 8%). Hydrates resulting from the pozzolanic reaction have coated the surface of the soil particles and have acted as binders between the particles. This has reduced the surface area of the clay particles and hence the methylene blue value.

Compaction Tests (Modified Proctor)

The compaction characteristics depend on three parameters, the grain size distribution, the soil specific gravity and stabilizing mineral additions. These stabilizers initially
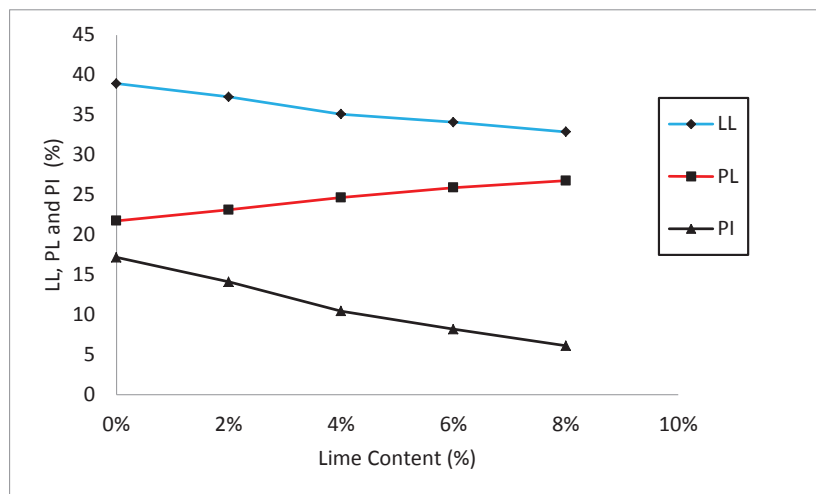
Fig. 4: 30% FDS treated with 0, 2, 4, 6 and 8% lime.
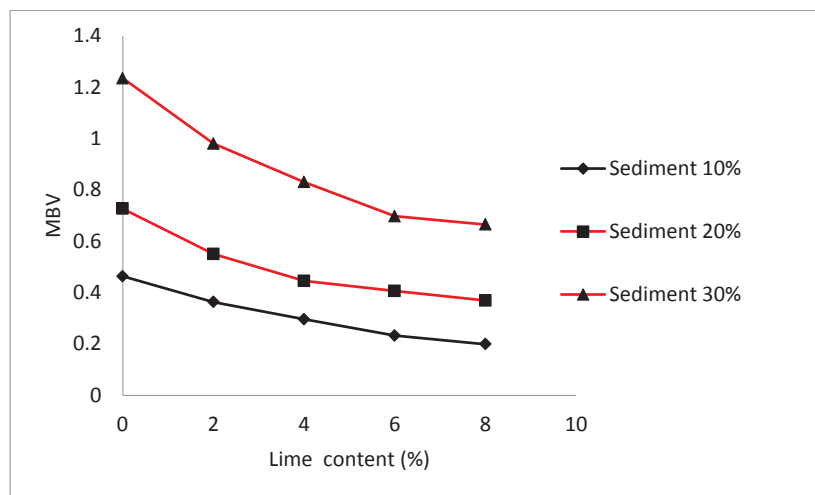
Fig. 5: The evolution of the methylene blue value as a function of the lime content.

react with the soil to form large aggregates and so occupy a large space. However, soil fine particles tend to decrease dry density and the stabilizers (which tend to increase dry density) offset larger.

The lime treatment of the mixtures, as we see in Figs. 6, 7 and 8, reduces the maximum value of the dry density more and more and increases the value of the optimal moisture content (GTS 2000). The increase in the optimum water content was due to the increase of the total particle surface of the mixtures treated by the fine grains of the added lime. The reason for the decrease in the maximum dry density was the low density of the lime contained in the mixture. These results confirm the results of the researchers Kavak &

Akyarh (2007) and Hossain et al. (2007) who explained that the reduction in maximum dry density was due firstly to the formation of aggregate particles so that they will occupy a large space and therefore to the graduation of soils. Second, the specific density of lime was lower than the specific gravity of the lateral soil, which has been confirmed by Ola (1977). Third, increasing the optimal water content with increasing the lime was due to the additional water required for pozzolanic reactions, the result confirmed by the researchers Manassah & Olufmi (2008). Another remark is the shape of compaction curves treated with lime compared to others, they take a flattened shape, which explains the insensitivity to the water of these mixtures. These results have been confirmed by the researchers (Mellal 2010).
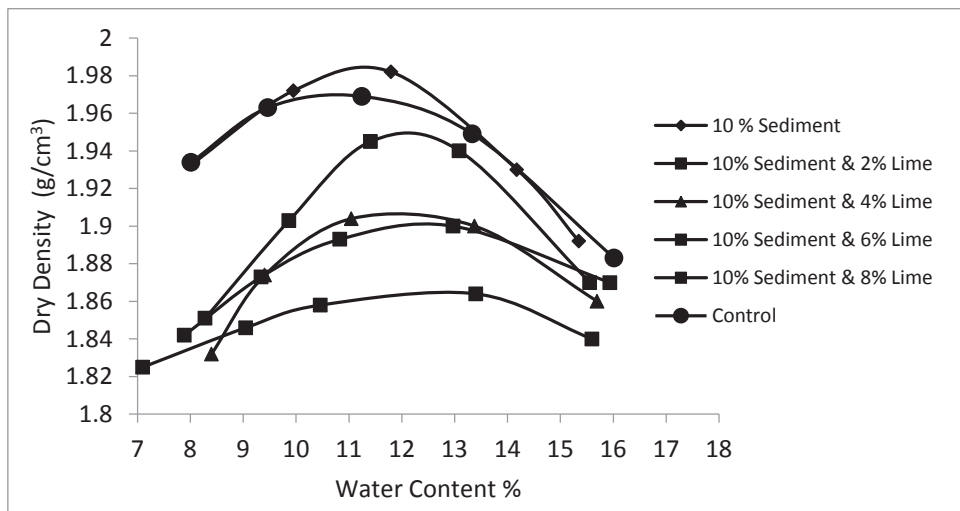
Fig. 6: Evolution of the maximum dry density of (SCT + 10% FDS) + 2, 4, 6 and 8% of the lime as a function of the water content.
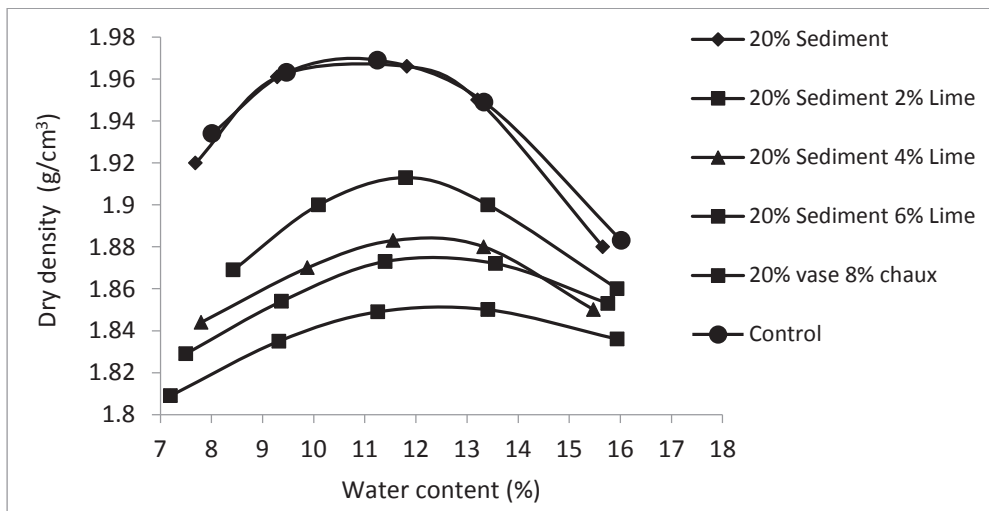
Fig. 7: Evolution of the maximum dry density of (SCT + 20% FDS) + 2, 4, 6 and 8% of the lime according to the water content.

Lift Tests (CBR After Immersion)

As we see in Fig. 9, the addition of sediment significantly reduced the CBR index of the mixture (SCT + FDS), it was 68.9, 66.6 and 32.9% for road aggregates and the additions of 10 and 30 % of sediments respectively. Vat in the wet state (immersion) even in small proportion can affect the lift of the mixtures (Larouci et al. 2018). Indeed, the wet sediment has a very low punching resistance. The grains surrounded by sediment easily avoid the pressures generated by the cylinder of the punching apparatus moving towards the points of low pressures; these displacements are more and more favoured by the addition of sediment.

This action occurs between the lime and the clay minerals present in the added sediment when their proportion is significant (Larouci et al. 2017). The principle of pozzolanic reaction is based on the possibility, in high pH medium (greater than
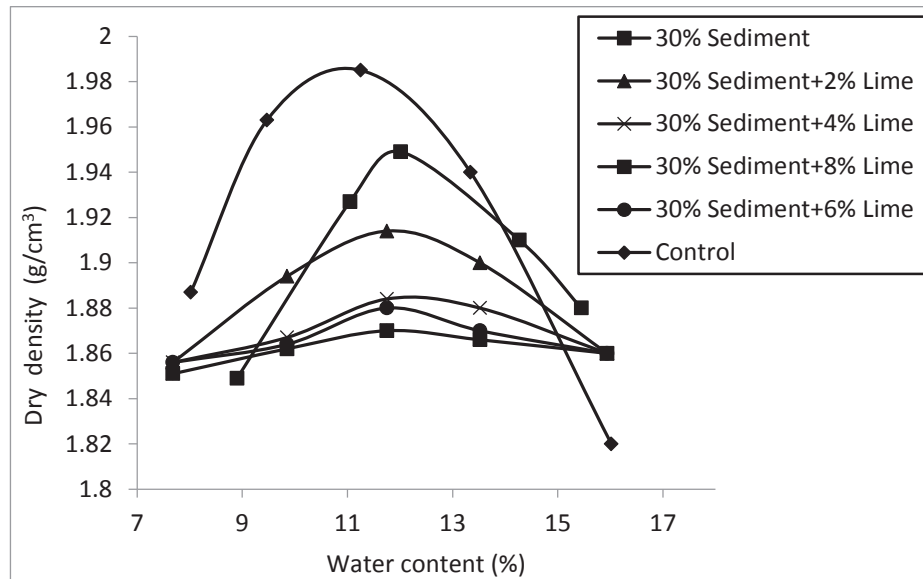
Fig. 8: Evolution of the maximum dry density of (SCT + 30% FDS) + 2, 4, 6 and 8% of the lime as a function of the water content.
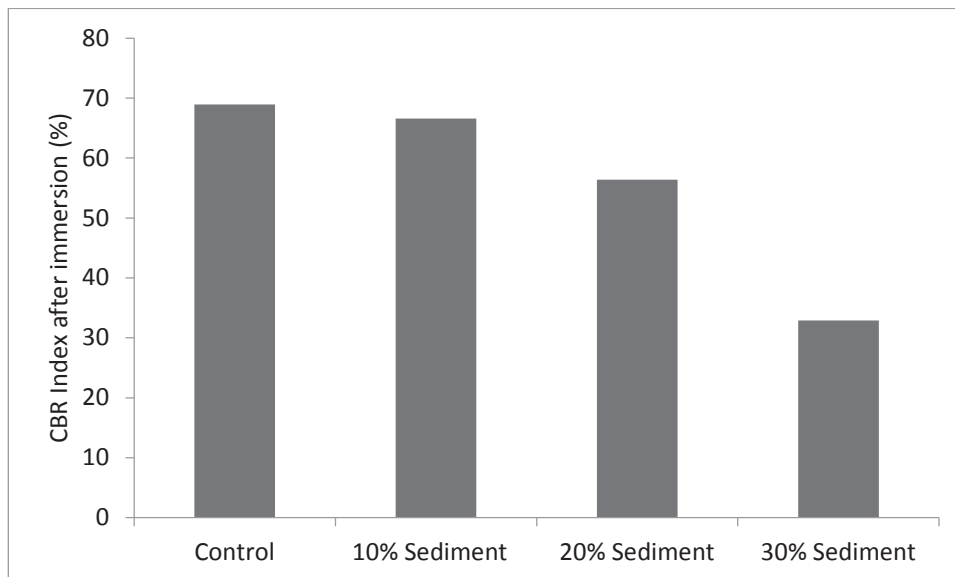
Fig. 9: Evolution of the CBR index after immersion as a function of the sediment content (before treatment).

12), of dissolution of silica, alumina, iron oxides present in clay minerals under crystallized forms more or less altered.

These elements in solution then react with lime to form insoluble lime ferro-silicoaluminates which precipitate and crystallize in the presence of water thus creating bonds of the same nature as those produced with hydraulic binders according to GTS (2000).

The manifestation of this action is shown in Fig. 10 by the increase of the CBR index after 4 days of immersion. In this case, after the lime treatment, we notice a strong increase of CBR index for all the mixtures (sediment + lime).

The decrease in the CBR index for the proportion of 30% of sediment treated with 2% of the lime is due to the proportion of clay minerals exaggerated in relation to the lime content.

Unconfined Compressive Strength (UCS)

Fig. 11 shows the results of the mechanical strength of the tested samples. The UCS was measured at the age of 28 days. The UCS decreased from the first addition of FDS despite the addition of 10 % DFS at a higher dry density than the other additions. This decreased the low lift of FDS, the grains of FDS present between the grains of SCT undergo low friction generated by the pressure of the device.
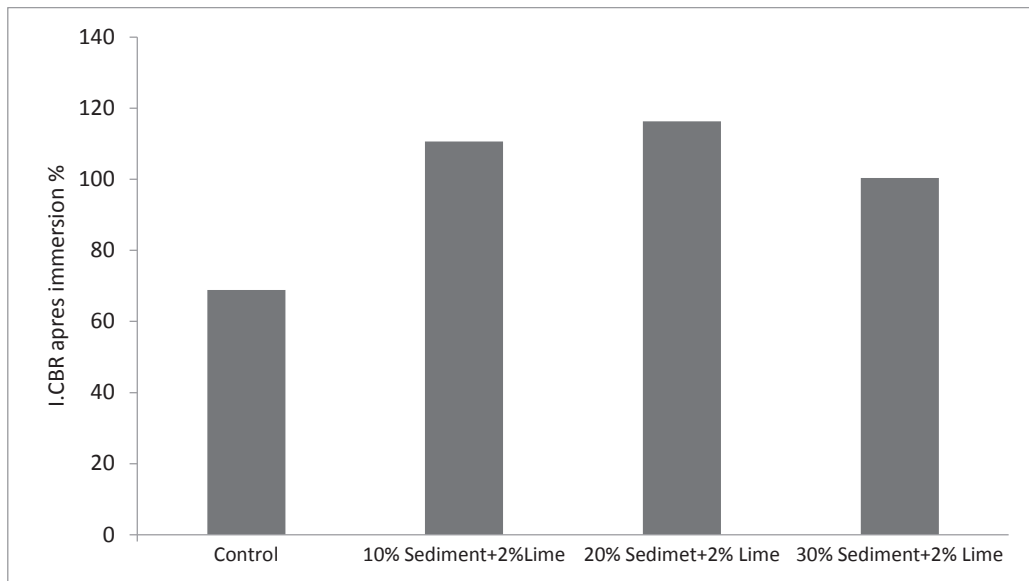
Fig. 10: Evolution of the CBR index after immersion as a function of the sediment content (after treatment).
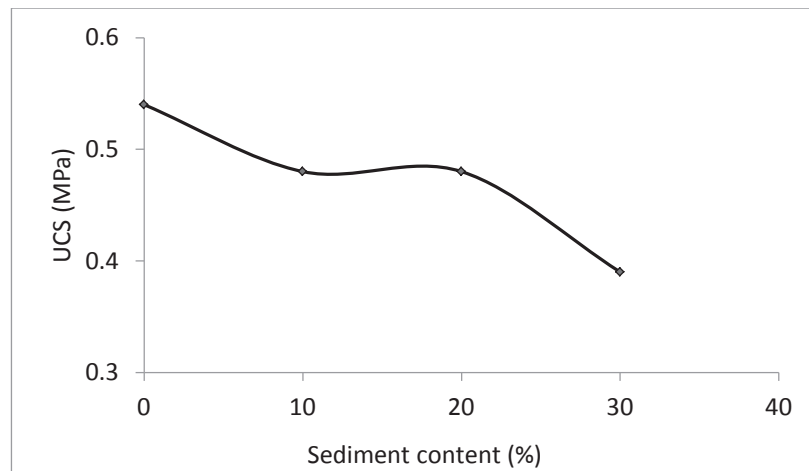
Fig. 11: Evolution of the UCS as a function of the sediment content (before treatment).

Fig. 12 shows the results of the mechanical strength of the test samples. The UCS of lime samples is higher than samples containing SCT + % FDS alone. Compression resistance increased from 0.48 to 1.11 MPa for a treatment of 10% FDS + 2% lime and from 0.48 to 1.67 for a 10% addition of FDS + 2% lime. It can be seen that the proportion of 20% FDS + 2% lime in a mixture can improve the strength to 150% of the mixture.

The immediate reaction of clay soil with mineral additions caused modifications in the rheological behaviour of the treated soils due to the phenomenon of flocculation causing a change in particle size by aggregation (Sakr et al. 2008, Okagbue & Ochulor 2007, Ansary et al. 2006) and inducing an improvement in the properties of treated soils. Even if the optimum of compaction is shifted to higher water contents and if compacting density is lower, the mechanical properties improve with the treatment of mineral additions (Osinubi 2006, Guney et al. 2007). According to Bell (1996), the mechanical strength of clay soils increases with the lime addition which is consistent with the results of Attoh-Okine (1995).

Bell (1996) noted that compressive resistance depends on the presence of pozzolan. When the pozzolan is available, it reacts with lime and this improves the compressive resistance. It would prove than the absolute amount of silica and alumina required to support the pozzolanic reaction in clay soils is relatively low.

CONCLUSION

The study was undertaken to study the physical and mechanical behaviour of silt dredged from the Fergoug dam treated with lime as a substitute for tuff to use in road earthworks.

The parameters studied are multiple and varied, including the percentages of constituents (sediment + lime), the method of samples preparation as well as the characteristics of each test. At the end of this study, we can draw the following main results:

- The addition of lime leads to an improvement in consistency because of a significant reduction in the plasticity index. The specific surface is reduced immediately after the incorporation of lime at the end of the clay's flocculation.

- The value of methylene blue index decreases with the addition of lime.

- The addition of lime to mixtures increases their optimal water content and reduces their maximum dry density.

- The lift of the mixture of (2% lime + (20% FDS + 80% SCT)) is more to that (20% FDS + 80% SCT) for about 68%, which explains the positive effect of the addition of lime

- The combination (2% lime + (20% FDS + 80% SCT)) is ideal to significantly improve the geotechnical properties of the studied silt; always for this same combination the compressive strength at 28 days is 3 times more than the untreated mixture value;

- The addition of lime improves compressive and punching resistance. This improvement is even more significant with the cure and it can be attributed to the filler

Fig. 12: Evolution of the UCS as a function of the sediment content (after treatment).

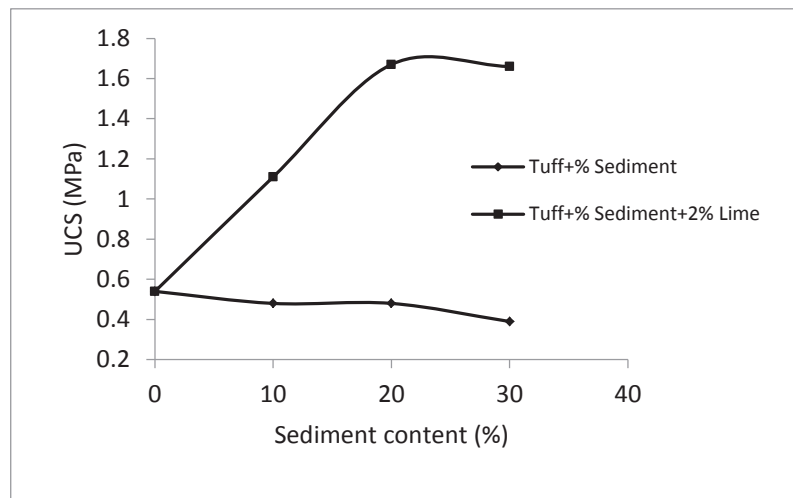effect due to its specific surface and the formation of the C-S-H gels due to the pozzolanic reaction. So, there is a creation of cementation of the soil particles which allows the increase of the resistance.

- The effectiveness of natural silt in the stabilization of soil/lime is thus acquired and we can use it in the field of roads construction.

REFERENCES

ANBT (Agence Nationale des Barrages et Transferts) 2014. Rapport annuel d'activité sur l'état des barrages Algériens. Kouba, Algeria,

Ansary, M.A., Noor, M.A. and Islam, M. 2006. Effect of fly ash stabilization on geotechnical properties of Chittagong coastal soil. In: Soil Stress-strain Behavior: Measurement, Modeling and Analysis, pp. 443-454. Springer, Dordrecht.

Attoh-Okine, N.O. 1995. Lime treatment of laterite soils and gravels-revisited. Construction and Building Materials, 9: 283-287.

Bell, F.G. 1996. Lime stabilization of clay minerals and soils. Engineering Geology, 42: 223-237.

George, S.Z., Ponniah, D.A. and Little, J.A. 1992. Effect of temperature on lime-soil stabilization. Construction and Building Materials, 6(4): 247-252.

GTR 2000. Guide technique pour la réalisation des remblais et des couches de forme. Fascicule I, principes généraux, LCPC-SETRA 100 pages.

GTS 2000. Traitement des sols à la chaux et aux liants hydrauliques-Guide technique. LCPC-SETRA, 240 pages.

Guney, Y., Sari, D., Cetin, M. and Tuncan, M. 2007. Impact of cyclic wetting–drying on swelling behavior of lime-stabilized soil. Building and Environment, 42: 681-688.

Hossain, K.M.A., Lachemi, M. and Easa, S. 2007. Stabilized soils for construction applications incorporating natural resources of Papua New Guinea. Resources, Conservation and Recycling, 51: 711-731.

Kavak, A. and Akyarh, A. 2007. A field application for lime stabilization. Environment Geology.51: 987-997.

Laoufi, L., Senhadji, Y. and Benazzouk, A. 2016. Valorisation of mud from Fergoug dam in manufacturing mortars. Case Studies in Construction Materials. 5: 26–38. http://dx.doi.org/10.1016/j.cscm.2016.06.002 2.

Larouci, A., Senhadji, Y., Laoufi, L. and Benazzouk, A. 2017. Valorisation de la vase du barrage de Fergoug pour une construction routière. 3rd International Symposium on Materials and Sustainable Development (ISMSD2017). Boumerdès, Algérie.

Larouci. A., Senhadji, Y., Laoufi, L. and Benazzouk, A. 2018. Improvement of the mechanical performance of Fergoug dam sediments treated for reuse in road engineering. MATEC Web of Conferences 149, 01031, https://doi.org/10.1051/matecconf/201814901031.

Levacher, D., Colin, D., Perroni, A.C., Duan, Z. and Sun L. 2006. Recyclage et valorisation de sédiments fins de dragage à usage de matériaux routiers. IXème Journées Nationales Génie Civil- Génie Côtier, Brest, France, pp. 603-612.

Levacher, D., Sanchez, M., Duan, Z. and Liang, Y. 2011. Valorisation en unité pilote de sédiments méditerranéens: étude des caractéristiques géotechniques et de la perméabilité. Revue Paralia, 4 : 4.1-4.20, doi: 10.5150/revue-paralia.2011.004.

Manassah, J. and Olufemi, A.T. 2008. Effect of lime on some geotechnical properties of Igumale Shale. EJGE, 13.

Mellal, F. 2010. Etude du comportement physicochimique et mécanique d'un remblai routier marneux amélioré par la chaux éteinte, cas de l'autoroute Est-Ouest tronçon Oued Fodda /Khemis Miliana. Chlef : Thèse, Université Hassiba Benbouali de Chlef, Algérie.

Okagbue, C. O. and Ochulor, O. H. 2007. The potential of cement-stabilized coal-reject as a construction material. Bulletin of Engineering Geology and Environment, 66: 143-151.

Ola, S. A. 1977. The potentials of lime stabilization of lateritic soils. Eng. Geol., 11(4): 305–317.

Osinubi, K.J. 2006. Influence of compactive efforts on lime-slag treated tropical black clay. Journal of Materials in Civil Engineering, 18(2): 175-181.

Sakr, M.A., Shahin, M.A. and Metwally, Y.M. 2008. Utilization of lime for stabilizing soft clay soil of high organic content. Geotechnical Geology Engineering, 27(1): 105.

Sannier, L., Levacher, D. and Jourdan, M. 2009. Approche économique et validation de méthodes de traitements aux liants hydrauliques de sédiments marins contaminés. Revue Paralia, 2: s2.1-s2.15. doi:10.5150/revue-paralia.2009.s02.

Semcha, A. 2006. Etude des propriétés géomécaniques des sédiments d'envasement de barrage et leur valorisation. Thèse de doctorat à l'université des sciences et de la technologie d'Oran, Algérie.

Adsorption of Dye Reactive Brilliant Red X-3B by Rice Wine Lees from Aqueous Solutions

Q. Wang*, F. F. Xi*, L. P. Liang*†, Y. T. Zhang*, Y. Y. Xue*, Q. Wu*, L. B. Cheng* and X. Meng**

*School of Civil Engineering, College of Life Science, College of Textile and Garment, Shaoxing University, Shaoxing, 312000, P.R.China

**Key Laboratory of Clean Dyeing and Finishing Technology of Zhejiang Province, Shaoxing University, Shaoxing, 312000, P. R. China

†Corresponding author: L. P. Liang; liangliping0702@163.com

ABSTRACT

In this study, the adsorption performance of rice wine lees on reactive brilliant red (X-3B) was studied. Five aspects of SEM, FTIR characterization of rice wine lees, initial X-3B pH, rice wine lees dosage and initial dye concentration were studied. The characterization of rice wine lees indicated that it was a good adsorbent due to its larger specific surface area. And the experiment results showed that pH had a great influence on the adsorption effect of rice wine lees, and the adsorption performance decreased with the increase of pH. At the same time, the removal rate of reactive brilliant red X-3B increased with the increase of the dosage of rice wine lees and decreased with the increase of initial concentration of dyes. In the meanwhile, the experimental data were fitted to find that the adsorption of Reactive Brilliant Red X-3B by rice wine lees followed the Langmuir isotherm model. The adsorption kinetics was consistent with the intraparticle diffusion model and the maximum adsorption capacity was 12.376 mg/g.

INTRODUCTION

In the textile industry, various textile chemicals, such as dyes, surfactants, fixing agents, softeners and many other additives, are used in the production process (Sundrarajan et al. 2007). Therefore, the textile wastewater discharged during the production process is extremely loaded, in which dye sewage is the main component of the wastewater. Reactive Brilliant Red (X-3B) is a kind of azo dye which is widely used in the textile industry due to its unique colour. However, this kind of brilliant red dye wastewater is subject to the change of water quality, water quantity and water temperature, and its chromaticity and COD value are extremely high (Yong et al. 2008). Besides, due to the -N=N- double bond in their molecular structure, dye wastewater is very stable in water and is not easily biodegraded, toxic degradation is really slow, causing damage to aquatic organisms and some terrestrial organisms. Therefore, these dyes are classified as environmentally harmful materials (Lu et al. 2009). To avoid polluting the river channel, it must be treated to discharge emission standards before discharging the dye wastewater.

At present, the methods for treating dye wastewater mainly include adsorption method (Annadurai et al. 2002), biological treatment method (Tantak & Chaudhari 2006), chemical oxidation method (Arslan et al. 2000), electrolysis method (Bechtold et al. 2010) and photocatalytic degradation method (Konstantinou & Albanis 2004). However, these methods have some disadvantages such as the high adsorbent price, generation of large amounts of sludge, difficulty in the regeneration of adsorbents, and membrane fouling. Among them, the adsorption method is one of the economical and efficient methods for treating dye wastewater. To solve the problem of expensive industrial adsorbents, in recent years, researchers have used non-living biomass to adsorb dyes in wastewater and achieved remarkable results. Wang et al. (2008) successfully removed methylene blue from aqueous solution by using the nonliving-biomass of seaweed and freshwater plants. And another researcher modified the peanut shell with citric acid and successfully adsorbed methylene blue in aqueous solution (Peng et al. 2015). Some researchers have also discovered that orange peel is a good adsorbent to adsorb the acid dyes in aqueous solution (such as Acid Violet 17) (Sivaraj et al. 2001). In addition to using agricultural waste to treat dye wastewater, researchers have found that distiller's grains may also be a good adsorbent.

Rice wine lees are the main by-products of southern yellow wine enterprises. The annual output of 10 kt rice wine produces about 727 t of rice wine lees every year. As a by-product of the rice wine brewing process, the rice wine grains are rich in a large amount of protein, amino acid

and other nutrients and contain a large number of microorganisms including mould, yeast, etc. (Zheng & He 2007), which may be a good adsorbent. It has been reported by many researchers about the adsorption of dyes in wastewater by rice wine lees. For example, Xiaolian et al. (2016) used white distiller's grains to degrade Congo red and malachite green in aqueous solution. However, a large amount of rice distiller's grains is mainly used for feed, and some of them are directly discarded, which pollutes the environment. If a large amount of rice wine grains can be treated with dye wastewater, the effect of 'disused waste' can be achieved, which not only saves energy but also provides a new idea for the degradation of dye wastewater.

In this study, rice wine lees was used as non-living biosorbent, and X-3B was used as the adsorption target. The effects of initial pH, initial concentration and adsorbent dosage on the adsorption performance of rice wine lees adsorbed X-3B were studied. Through the adsorption of isothermal adsorption equation and the kinetic fitting analysis, the adsorption and removal mechanism of rice wine lees on X-3B in wastewater was discussed.

MATERIALS AND METHODS

Materials

All the chemicals were of analytical grade including X-3B, HCl and NaOH. During the experiment, the corresponding dye was dissolved in ultra-pure water produced by the Milli-Q water purification system.

Advanced Treatment by the Adsorbent Rice Wine Lees

The lees used in this experiment was produced during the brewing process of rice wine. A certain amount of rice wine lees was washed with tap water repeatedly until the water flow was excellent and nearly colourless followed by rinsing again 3-4 times with distilled water. It was then wrapped with gauze and squeezed to flush out the water, and later put on a clean tin foil in a tray and spread evenly and loosely. The tray was later placed in an oven for drying. The rice wine lees was turned over for every 5-6 hours to make it properly drier.

SEM Characterization

The original rice wine lees was characterized by SEM and the
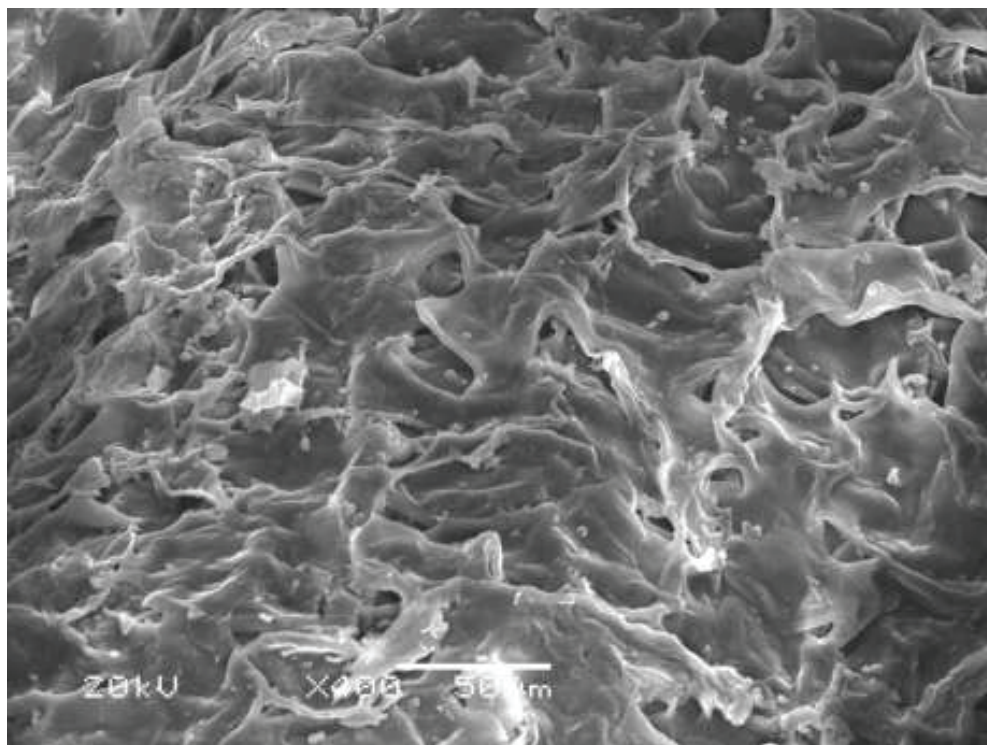
Fig. 1: SEM characterization of original rice wine lees.

results are shown in Fig. 1. It could be seen that the surface of the rice wine lees has many pores, larger pore size, rougher surface and larger specific surface area, which increased the contact area between the rice wine lees and the reactive brilliant red dye molecules. The increase in active sites provided further possibilities for the successful adsorption of reactive brilliant red by the rice wine lees.

Adsorption Experiment

0.500 g X-3B was accurately obtained and dissolved into the 500 mL bottle with deionized water to prepare the standard storage solution of 1 g/L, which was diluted to the corresponding concentrations according to the proportion used during the experiment. 1.25 g rice wine lees was added to a certain concentration of 500 mL containing X-3B solution, placed in a constant temperature shock water bath at 25°C, and stirred in an agitator with rotating speed of 400 r/min. The sample was filtered at a specific time, and the concentration of the remaining X-3B in the solution was measured by ultraviolet-visible spectrophotometry at a wavelength of 536 nm.

Experimental Data Analysis

A standard curve of the absorbance of X-3B concentration was plotted based on the measured absorbance of X-3B, and the equation obtained was y = 0.0178x-0.0028 with R^2 = 0.9997. Due to the high correlation coefficient (R^2 = 0.9997), it was seen that there was a good linear relationship between concentration and absorbance, which indicated that the equilibrium concentration of X-3B was more accurate. The adsorption could be calculated by equation 1.

$$q_e = \frac{(C_0 - C_e)V}{W} \qquad \ldots(1)$$

Where, q_e is the equilibrium concentration of X-3B (mg/L), C_0 and C_e are the initial and equilibrium concentration of X-3B (mg/L), respectively. V is the volume of X-3B solution (L) and W is the weight of used rice wine lees (g).

RESULTS AND DISCUSSION

The FTIR Analysis of Rice Wine Lees

The FTIR spectra of the rice wine lees before and after the reaction are shown in Fig. 2. It can be seen from the figure that the FTIR spectrum of the rice wine lees ranged from 500 cm⁻¹ - 4000 cm⁻¹ and had a series of adsorption peaks, showing the complex characteristics of the rice wine lees. There was a distinct O-H vibration absorption peak near 3300 cm⁻¹, the characteristic region of the -COOH group near at 2500 ± 300cm⁻¹, C-H stretching vibration of saturated hydrocarbon at 1450 cm⁻¹, and C-O stretching vibration near 1720-1715 cm⁻¹, indicating that there were a lot of hydroxyl and carboxyl groups in the rice wine lees. The absorption peaks of the hydroxyl and carboxyl groups of rice wine lees after the reaction were significantly weakened.
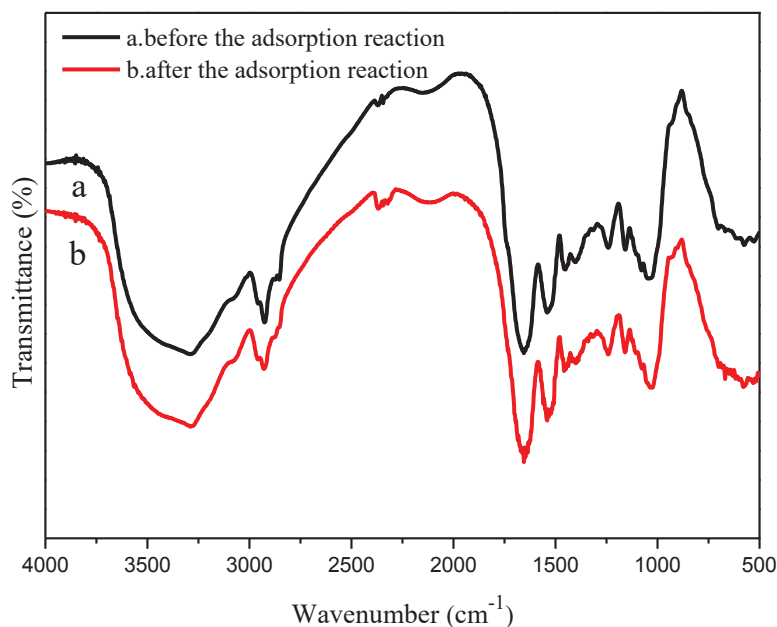
Fig. 2: The FTIR study of rice wine lees.

Effect of Initial pH on Adsorption of X-3B by Rice Wine Lees

The influence of initial pH on the removal efficiency of X-3B by rice wine lees was investigated and the results are shown in Fig. 3. It could be seen that the removal efficiency of X-3B decreased with the increase of pH value. When the pH values were 3.00, 5.00, 7.00 and 9.00, the removal rates of X-3B were 100%, 56.6%, 18.8% and 6.6%, respectively. It could be seen obviously that the pH value of the solution affected the removal efficiency of Reactive Brilliant Red X-3B by the rice wine lees, and the lower the pH value, the higher the removal efficiency of Reactive Brilliant Red X-3B. Since rice wine lees is a by-product of rice wine fermentation, it is rich in protein, amino acids and various amino groups ($-NH_2$, $-NH$, $-N$) on biological protein molecules, which are easily protonated under acidic conditions and existed as the forms of $-NH_3^+$, $-NH_2^+$ and $-NH^+$ (Won et al. 2004). These positively charged amino groups combined with negatively charged dye molecules, allowing the rice wine lees to adsorb X-3B successfully. The amount of protonated amine groups increased as the pH decreased, which provided more binding sites. This was consistent with the experimental results. A similar phenomenon was also reported by Wong et al. (2004), who considered that the removal of anionic dyes by Chitosan was mainly due to the combination with protonated amines.

Effect of Different Initial Concentrations on Adsorption of X-3B by Rice Wine Lees

Under the same pH value and the dosage of rice wine lees (5 g/L), the effects of different initial concentrations of dyes on dye removal efficiency by rice wine lees were investigated and the results are shown in Fig. 4. As the figure depicted, the removal efficiency of Reactive Brilliant Red X-3B gradually decreased as the initial concentration of X-3B increased. When the initial concentration of X-3B was 20 mg/L, the removal rate of X-3B was 96.9% after 24 h of reaction. And when the initial concentration of X-3B was increased to 40 mg/L and 60 mg/L, the degradation rate of X-3B was reduced to 92.5% and 90.3%. As the initial concentration of Reactive Brilliant Red X-3B continued to increase to 80 mg/L, the removal rate of Reactive Brilliant Red X-3B was only 73.6%. This may be due to the increasing number of anion sulfonate groups in reactive brilliant red molecules binding to a limited binding site, resulting in the saturation of binding sites and then leading to the degradation efficiency of X-3B.

Effect of Rice Wine Lees Dosage on X-3B Adsorption

Different dosages of rice wine lees were selected to explore the effect of dosage of adsorbent on the adsorption efficiency and the results are shown in Fig. 5. Obviously, in the condition of the same initial concentration of X-3B (10 mg/L) and pH, the removal efficiency of X-3B increased with the increase of rice wine lees dosage. When the dosage of rice wine lees was 5 g/L, the removal rate of X-3B was 29.9% after 120 min of reaction. And when it was 10 g/L, the removal rate of X-3B was 42.7% after 60 minutes of reaction. After 90 minutes of reaction, the removal rates of rice wine lees were 60.4% and 67.7%, respectively, as the dosage were 14
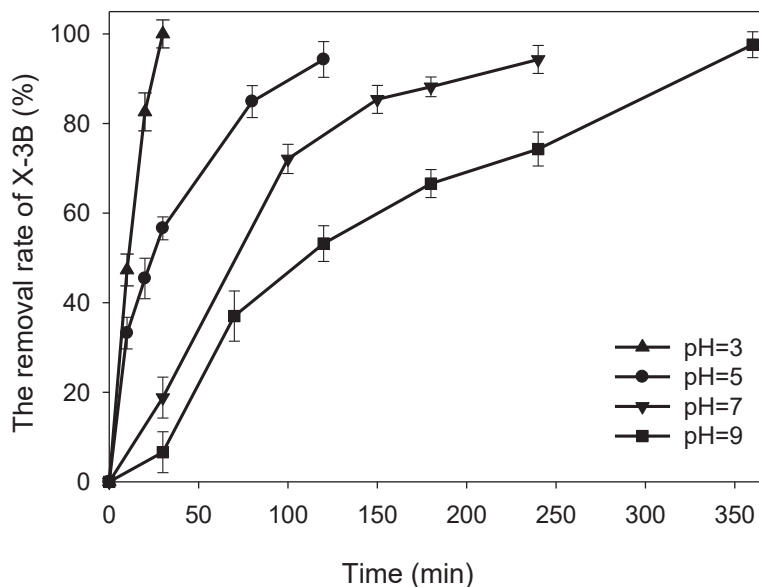
Fig. 3: Effect of different initial pH on the removal of X-3B.
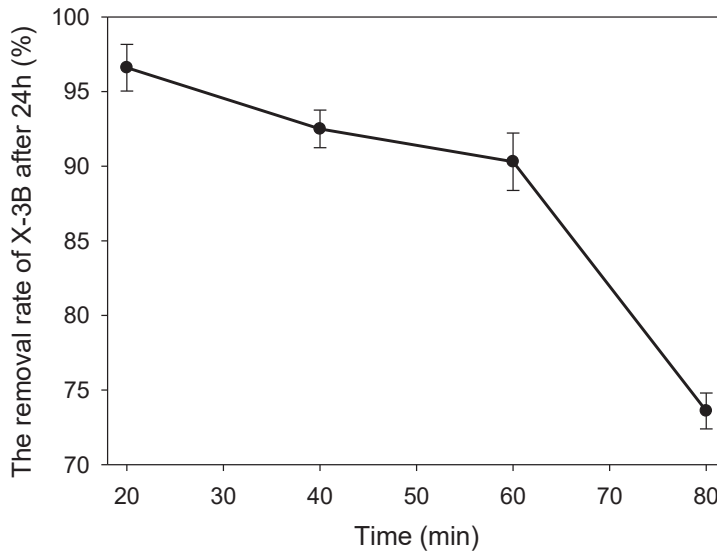
Fig. 4: Removal rate of X-3B at different initial concentrations after 24 hours.

g/L and 18 g/L. It could be seen that increasing the dosage of rice wine lees could increase the removal efficiency of X-3B, and the greater the dosage of rice wine lees, the higher the removal rate of Reactive Brilliant Red X-3B. This was due to the increase of adsorption dose, which led to the increase of adsorption surface area, the increase of functional groups and the increase of the number of qualitative amino groups, thus improving the adsorption efficiency.

Adsorption Isotherms

The adsorption isotherm results of the rice wine lees on reactive brilliant red X-3B are shown in Fig. 6. When the pH was 5, the adsorbent dosage was 5 g/L, and the dye concentration was 10 mg/L. The adsorption isothermal data were linearly fitted by the Langmuir equation, the Freundlich equation and the Temkin equation (equations 2-4), respectively, the fitting results are shown in Fig. 6 and Table 1.

$$\frac{q_e}{C_e} = \frac{C_e}{q_m} + \frac{1}{k_L q_m} \qquad \ldots (2)$$

$$Ln q_e = Ln K_F + \frac{1}{n} Ln C_e \qquad \ldots (3)$$

$$q_e = \frac{RT}{b_T} Ln A_T + (\frac{RT}{b_T}) Ln C_e \qquad \ldots (4)$$

Where, q_e is the adsorption capacity of X-3B at equilibrium (mg/g), C_e is dye concentration at equilibrium (mg/L), q_m is saturated adsorption capacity (mg/g), and k_L is the equilibrium constant of Langmuir adsorption isotherm, K_F is Freundlich constant, and R, A, T and b are Temkin constants.

It can be seen from Table 1 that the Langmuir isothermal model has the highest correlation coefficient (R^2=0.9821) compared with the Freundlich and Temkin isotherm models, indicating that the adsorption of reactive brilliant red X-3B by the rice wine lees was more suitable for description by the Langmuir isotherm model. It was further illustrated that the adsorption was mainly the adsorption of the monolayer. The Langmuir equation obtained by fitting was y = 0.1095x+0.0838 (R^2=0.9821) and the maximum adsorption capacity of the residue was 12.38 mg/g. It could be seen that the adsorption performance of the rice wine lees was high.

Adsorption Kinetics

Under the condition of pH 5, the dosage of 5 g/L, the temperature of 298 k and initial dye concentration of 10 mg/L,

Table 1: Adsorption results of X-3B by rice wine lees.

Langmuir isotherm equation			Freundlich isotherm equation			Temkin isotherm equation		
R^2	q_m	k	R^2	k	n	R^2	A	B
0.9821	12.38	0.716	0.9414	4.951	3.026	0.9570	9.2627	2.3628
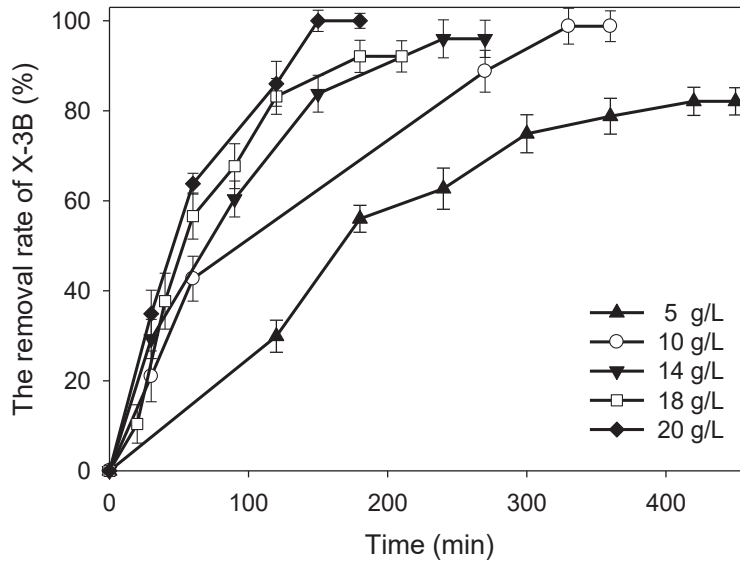
Fig. 5: Effect of different dosage of rice wine lees on the removal of X-3B.

the adsorption kinetics of rice wine lees adsorbed X-3B was investigated. The pseudo-first-order kinetic equation, the pseudo-second-order kinetic equation and the intraparticle diffusion models were used to fit the adsorption data, which are represented by equations 5, 6 and 7, respectively.

$$Ln(q_e - q_t) = Lnq_e - k_1t \qquad \ldots(5)$$

$$\frac{t}{q_t} = \frac{1}{k_2q_e^2} + \frac{t}{q_e} \qquad \ldots(6)$$

$$q_t = k_{id}t^{1/2} + C \qquad \ldots(7)$$

Where q_e and q_t (mg/g) are the amounts of X-3B at equilibrium and at any time t and k_1 and k_2 are the rate constants of pseudo-first-order and pseudo-second-order adsorption. k_{id} is the rate constant of the intraparticle diffusion model and C is truncation. The specific fitting results are shown in Fig. 7 and Table 2. It could be seen from Table 2 that the correlation coefficients (R^2) of the intraparticle diffusion model were
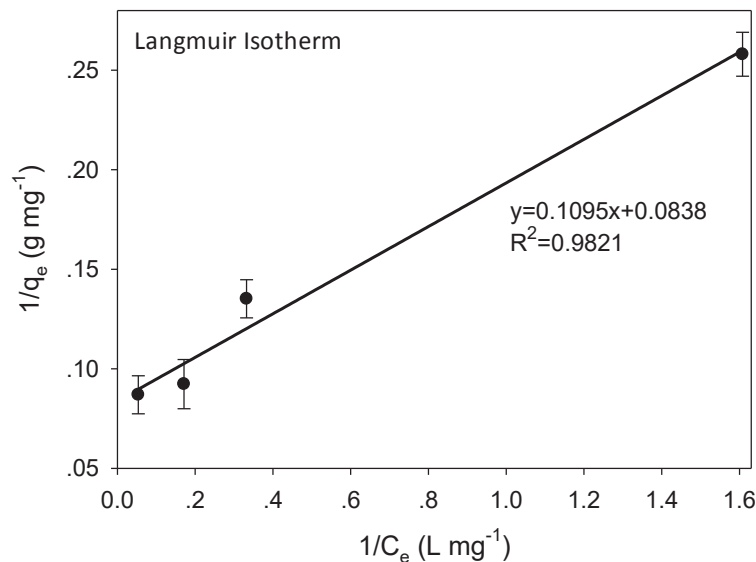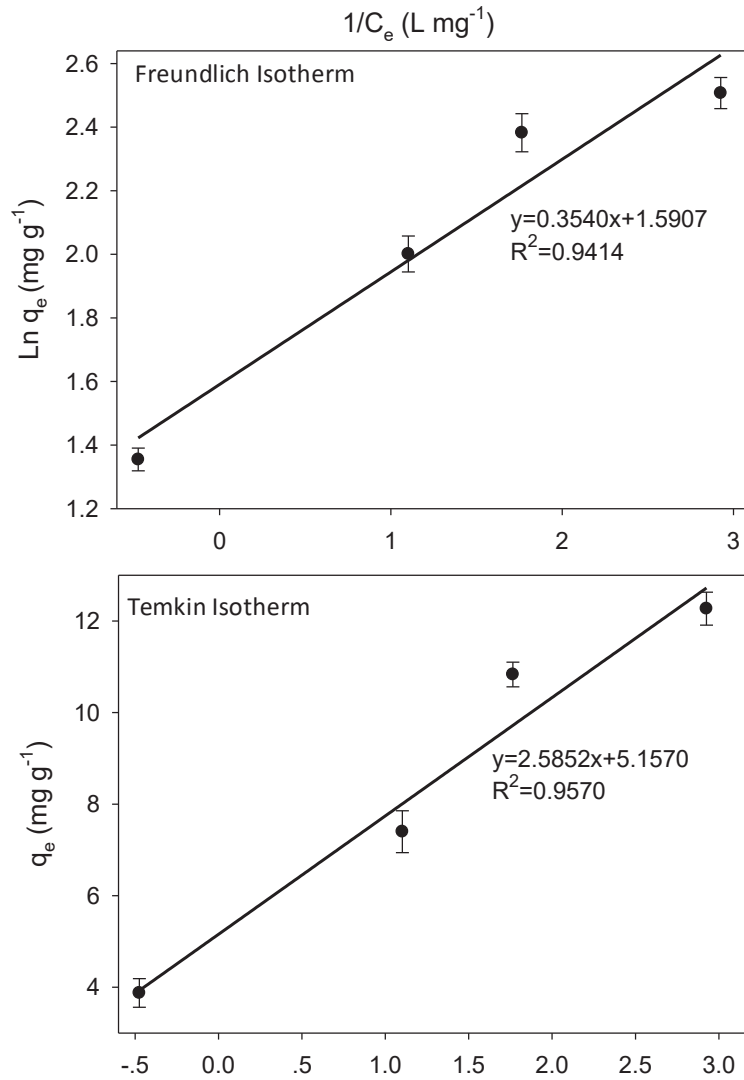
Fig. 6: Three adsorption isotherms for adsorption of X-3B by rice wine lees.

Table 2: Adsorption kinetics and intra-particle diffusion model constant and correlation of X-3B by rice wine lees

Rice wine lees (g/L)	q_e	pseudo-first-order kinetic model		pseudo-second-order kinetic model		intraparticle diffusion model	
		R^2	K_1	R^2	K_2	R^2	K_{id}
5	1.876	0.9975	-0.0023	0.9409	0.5687	0.9998	0.0832
10	1	0.9471	-0.0052	0.9716	0.9022	0.9930	0.0567
14	0.714	0.9775	-0.0058	0.9529	1.0163	0.9985	0.0504
18	0.556	0.9882	-0.0064	0.9098	1.5193	0.9997	0.0467
20	0.5	0.9785	-0.0073	0.9423	1.8127	0.9992	0.0382
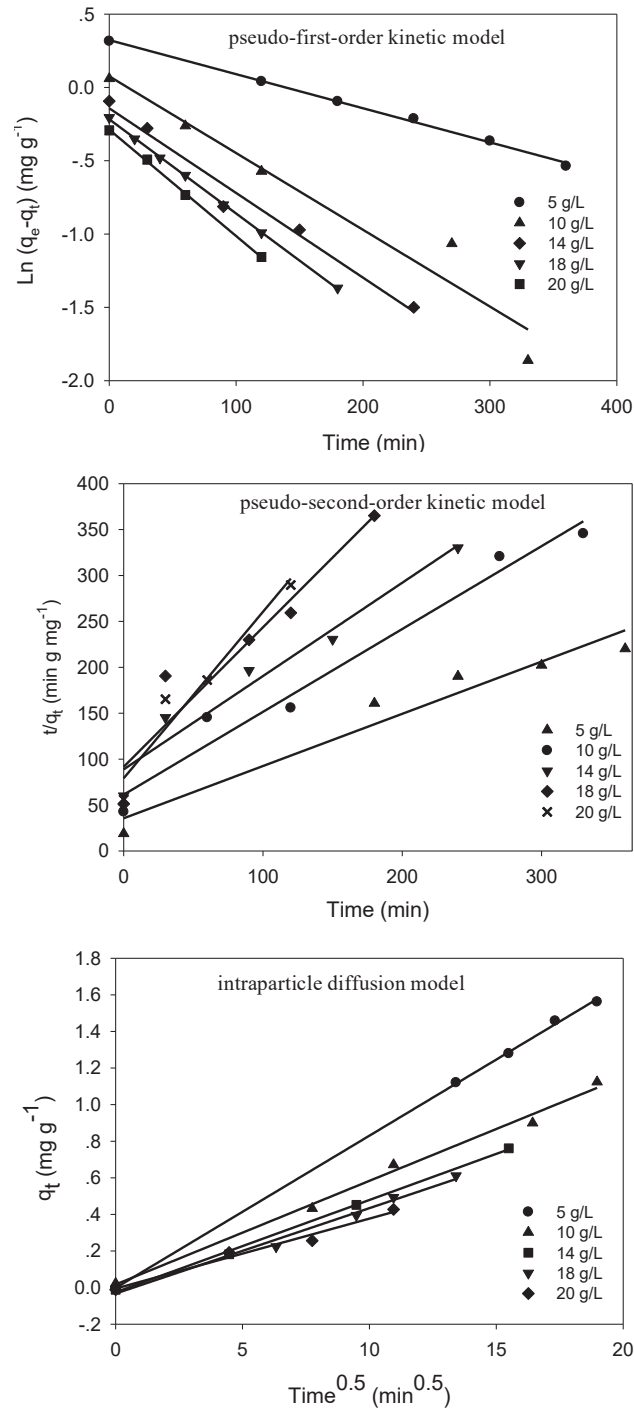
Fig. 7: Pseudo-first-order, pseudo-second-order plots and intraparticle diffusion model plots for X-3B adsorption on rice wine lees.

significantly higher than the correlation coefficient between the pseudo-first-order kinetics and the pseudo-second-order kinetics, which indicated that the intraparticle diffusion model was more suitable for describing the adsorption of X-3B by rice wine lees. Otherwise, we could see from Fig. 7 that the correlation line between q_t and $t^{1/2}$ did not pass through the origin.

CONCLUSION

In this paper, the effect of initial pH, initial concentration of X-3B and the different dosage of rice wine lees on the adsorption of X-3B by rice wine lees were investigated. The results showed that the effect of solution pH on adsorption performance was significant. As the pH value decreased, the adsorption performance enhanced, indicating that the removal rate of Reactive Brilliant Red X-3B became higher. At the same time, the removal rate of X-3B increased with the increase of the amount of rice wine lees and decreased with the increase of the initial concentration. By fitting the adsorption data, it was found that the adsorption reaction of rice wine lees to X-3B was consistent with the Langmuir isotherm adsorption model. The adsorption process accorded with intraparticle diffusion model, and the maximum adsorption capacity was 12.38 mg/g.

ACKNOWLEDGEMENTS

REFERENCES

Annadurai, G., Juang, R.S. and Lee, D. J. 2002. Use of cellulose-based wastes for adsorption of dyes from aqueous solutions. J. Hazard. Materi., 92(3): 263-274.

Arslan, I., Balcio lu, I.A. and Bahnemann, D.W. 2000. Advanced chemical oxidation of reactive dyes in simulated dyehouse effluents by Ferrioxalate-Fenton/UV-A and TiO₂/UV-A processes. Dyes Pigm., 47(3): 207-218.

Bechtold, T., Burtscher, E., Turcanu, A. and Bobleter, O. 2010. The reduction of vat dyes by indirect electrolysis. Coloration Technology, 110(1): 14-19.

Guo-Feng, Z. and He, Q. 2007. Ingredients and flavor analysis of yellow wine lees and study of its feasibility of making condiments. China Condiment., 4: 20-25.

Konstantinou, I. K. and Albanis, T. A. 2004. TiO₂-assisted photocatalytic degradation of azo dyes in aqueous solution: Kinetic and mechanistic investigations: A review. Appl. Catal. B., 49(1): 1-14.

Lu, X., Yang, B., Chen, J. and Sun, R. 2009. Treatment of wastewater containing azo dye reactive brilliant red X-3B using sequential ozonation and upflow biological aerated filter process. J. Hazard. Materi., 161(1): 241-245.

Peng, W., Qianyun, M., Dongying, H. and Lijuan, W. 2005. Adsorption of methylene blue by a low-cost biosorbent: Citric acid modified peanut shell. Desalination Water Treat., 57(22): 1-9.

Sivaraj, R., Namasivayam, C. and Kadirvelu, K. 2001. Orange peel as an adsorbent in the removal of Acid violet 17 (acid dye) from aqueous solutions. Waste Manag., 21(1): 105-110.

Sundrarajan, M., Vishnu, G. and Joseph, K. 2007. Ozonation of light-shaded exhausted reactive dye bath for reuse. Dyes Pigm., 75(2): 273-278.

Tantak, N. P. and Chaudhari S. 2006. Degradation of azo dyes by sequential Fenton oxidation and aerobic biological treatment. J. Hazard. Materi., 136(3): 698-705.

Wang, X. S., Zhou, Y. and Jiang, Y. 2008. Removal of methylene blue from aqueous solution by non-living biomass of marine algae and freshwater macrophyte. Adsorp. Sci. Technol., 26(10): 853-863.

Won, S. W., Choi, S. B., Chung, B. W., Park, D., Park, J. M. and Yun, Y. S. 2004. Biosorptive decolorization of reactive orange 16 using the waste biomass of *Corynebacterium glutamicum*. Ind. Eng. Chem. Res., 43(24): 7865-7869.

Wong, Y. C., Szeto, Y. S., Cheung, W. H. and McKay, G. 2004. Adsorption of acid dyes on chitosan-equilibrium isotherm analyses. Process Biochem., 39(6): 695-704.

Xiaolian, Z., Zihui, L., Xing, Y., Yisheng, S., Qingle, Z. and Liqing, Z. 2016. Adsorption mechanism of distillers' grain to conge red and malachite green. New Chemical Materials, 44(2): 207-213.

Yong, L. I., Song, L. V. and SuFang, Z. 2008. Experimental study on treatment of active red printing and dyeing wastewater with Fenton agent. Environ. Sci. & Technol., 31(3): 88-90.

Zheng, G and He, Q. 2007. Ingredients and flavor analysis of yellow wine lees and study of its feasibility of making condiments. China Condiment., 4: 20-25.

Zhu, X., Liu, Z., Yang, X., Sun, Y. and Zhang, Q. 2016. Adsorption mechanism of distillers' grain to conge red and malachite green. New Chemical Materials, 44(2): 207-213.

Original Research Paper

Open Access Journal

Impact of the COVID-19 Pandemic on the Air Quality in Delhi, India

Apurva Goel†
Department of Environmental Studies, H.V. Desai College, Pune, Maharashtra, India
†Corresponding author: Apurva Goel; apurva.goel@gmail.com

ABSTRACT

The COVID-19 pandemic is one of the biggest health calamities that the world has faced, which has infected millions of people and lead to hundreds of thousands of deaths all over the world. It has impacted the economic, social and health aspects of the countries to quite an extreme level. But an indirect positive impact can also be seen on the environment. In this paper, taking the example of Delhi, one of the most polluted cities of India, an analysis has been done to compare the levels of air pollutants (PM2.5, PM10, NOx and ozone) during the lockdown and the same period in the previous years. The study shows that the extent to which the industries, vehicles, power plants etc. release the air pollutants and severely impact the environment and human health. As during the lockdown when all such activities were either stopped or very much restricted, a reduction of almost 60% in the particulate matter pollution and up to 40% in the NOx pollution was observed while the ozone levels were reduced by 30-40% as compared to the same period during the previous two years. In the end, some suggestions have been made which can play some part to control air pollution once the lockdown is over.

INTRODUCTION

The year 2020 began with the world facing one of the most devastating health calamities of the century, i.e. COVID 19 pandemic, killing lakhs of people around the world. It has become the greatest challenge for the governments of all the countries including the giant nations like USA, UK, China, Russia, etc. to save their people from getting succumbed to this life-threatening virus. The reports of the spreading the Corona Virus Disease (COVID) among the human population first emerged from Wuhan in the Hubei Province of China in December 2019 (Huang et al. 2020). Soon within 2-3 months, the virus had spread to almost all parts of the world. Till date, millions of people have been infected by this virus causing hundreds of thousands of deaths. The countries which are most affected include the United States, Spain, Russia, United Kingdom, Italy, Brazil and many more.

The virus spreads when an infected person coughs or sneezes and droplets are thrown out in the air. These droplets can land on different surfaces which can be picked up by any person who touches that surface and then touches the nose, mouth or eyes (Rothan & Byrareddy 2020). As per the World Health Organization (WHO 2020), the most important thing to protect oneself from the virus is to keep the hands clean by washing them properly with soap at regular intervals or when exposed to anything from outside or any person. Social distancing is another way by which the community spread of the Coronavirus can be controlled (Lewnard & Lo 2020).

With these guidelines, the countries have taken various measures to protect their people from this pandemic. Some of the measures include the shutting down of the international and domestic travel; shutting down of schools, offices, industries; complete lockdown of people in their houses, shutting down the public transport, etc. These steps have helped in controlling the spread of the virus, but it has brought the entire world's economy under the threat of high inflation, loss in productivity, migration of labours, unemployment and excessive expenditure on the health care systems for the treatment of the COVID-19 victims.

In India, the Prime Minister of India had announced a strict Nationwide lockdown for its 1.3 billion population from 24th March 2020 as a preventive measure against the COVID 19 pandemic (Pulla 2020). All the institutions, industries, highways including the markets, shops public places were all closed, while only a few basic necessity shops like dairy, grocery, medical and fruits and vegetables were allowed to be open, but only for a certain period during the day. People were asked to stay at home and only come out for buying essentials during the allotted time slot maintaining social distancing (Lancet 2020). Though this step helped India to control the graph of the COVID-19 cases, there were many negative impacts also which people had to face, especially the below poverty class people and the labours whose only source of income is their daily wages. The government of India has taken all necessary measures to help the poor by

providing them with the basic goods of necessity and free food, but still, the help could not be reached to 100% of the needy people due to many limitations.

The COVID-19 pandemic has impacted not only the health aspect, but it has also impacted the social, economic and environmental aspects of all the countries (McKibbin & Fernando 2020, Chakraborty & Maity 2020). An indirect effect of the COVID-19 pandemic can also be seen on the environment, but this impact is a positive one (Zambrano-Monserrate et al. 2020). Due to the outbreak of the COVID-19, people are forced to stay at home due to the lockdown and has also resulted in the closure of all the industries, institutions and reduction in the vehicular movement. This has proved to be very beneficial for the environment. Due to the non-functioning of the industries, the waste emission, which is a major cause for the water and air pollution, has decreased to a very large extent. Again, as there are very restricted movements of the vehicles on road, the NOx, PM2.5 and greenhouse gases emissions have also reduced to a great extent (Sharma et al. 2020). People can breathe clean air and even experiencing clear sky, due to the absence of smog, for the first time in many years (Sinha & Saran 2020). As the tourists are not found on the beaches, hill stations and jungles, land pollution has also reduced in such places.

In this paper, the author has analysed the environmental impact on the air pollution levels in India during the lockdown period due to the COVID-19 pandemic. To determine the impact on the air pollution, Delhi was taken as the area of study and the air quality data for PM2.5, PM10, NOx and ozone levels from 5 monitoring stations were compared with the levels in the previous year. Some suggestions are also recommended which if implemented can play some role in controlling the air pollution once the lockdown of the nation is over.

MATERIALS AND METHODS

For the analysis of the air quality during the lockdown, Delhi has been taken as the study area. Delhi is the national capital of India located at 28.61° N 77.23° E. Delhi holds the second position in the list of the megacities of the world ((United Nations 2018). Delhi being one of the most polluted cities of the country and ranking (Hariharan 2019) on the global scale is an ideal area for the study. Five monitoring stations (Ashok Vihar-DPCC, DTU – CPCB, IGI Airport (T3)-IMD, Wazirpur and Najafgarh) were selected (Fig. 1) and the data reported from these stations were taken from the CPCB website (https://app.cpcbccr.com/ccr/#/caaqm-dashboard/caaqm-landing) for the year 2018, 2019, 2020 during February, March and April. The 24-hour average concentration of 4 major pollutants i.e., PM2.5, PM10, NOx and Ozone has been obtained and analysed. The February and March (up to 23rd) were the non-lockdown periods while April is the complete lockdown period. The current data were compared with the data of the same period in the previous years, i.e. 2018 and 2019, as the air quality largely depends on the seasonal conditions. The monitoring stations were selected on
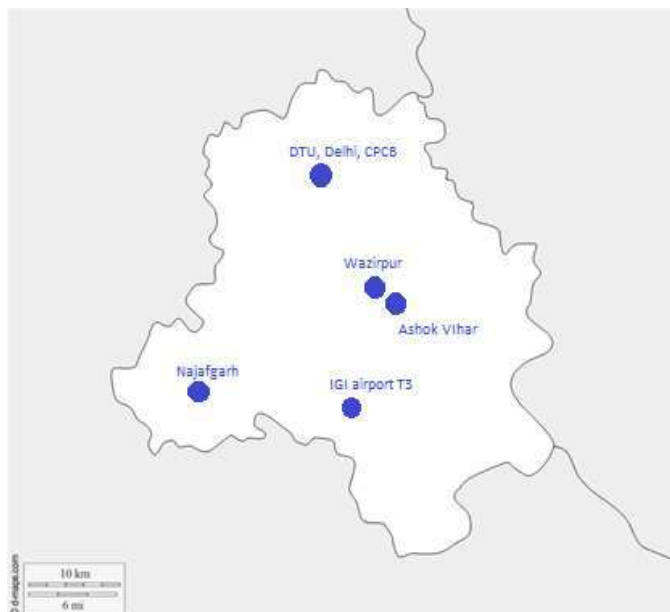
Fig. 1: Locations of the monitoring stations.

the basis on the data availability, level of pollution reported by them and cover the wider area of the city.

RESULTS

Particulate Matter

Particulate matter is a mixture of solid particles and liquid droplets in the air, some of which can be seen through the naked eye, while some are so small that they could only be detected through an electron microscope. These include the dust, dirt, soot, smoke and drops of liquids. Based on the size of the particles they are divided into PM2.5 and PM10.

Particulate matter poses a great risk to human health. PM10 can irritate the eyes, nose and throat. Particles that are very fine, i.e. PM2.5 are more dangerous as these can mix with the bloodstream and even go deep into the lungs. They are many times associated with lung cancer also.

Tables 1 and 2 show the average monthly values of the PM2.5 and PM10 respectively, for February, March and April in the year 2018, 2019 and 2020. It can be from the data that during the month of April 2020, i.e the lockdown period, the PM2.5 values are ranging between 40-50 μg/m^3, which is below the National Ambient Air Quality Standard (NAAQS) value of 60 μg/m^3, while the readings for all the other periods is way beyond the standard value. Similarly, the PM10 values are ranging between the 90-140 μg/m^3, which is just closer to the NAAQS standard value of 100 μg/m^3, while all the other readings are almost 2 or 3 times the standard value.

The values of the current year are compared with the previous two years and the per cent reduction in the values during the lockdown, i.e. for April was determined (Tables 3 & 4).

As can be seen from Table 5 and Fig. 2, there has been a substantial decrease in the PM2.5 pollutants in the air during April 2020 due to the lockdown. The maximum decrease of 50.95% was found at station DTU-CPCB. Similarly, from Table 4 and Fig. 3, a maximum decrease of 68.04% in the PM10 value was at the station Wazirpur.

NOx

Nitrogen oxides is a collective term used for the nitrogen monoxide (NO) and nitrogen dioxide (NO$_2$). These gases are emitted in the air mainly from the fuel combustion in vehicles, power plants and industries. Previous studies have reported that almost 80-90% for the NOx and CO pollutants are produced from the transport sector in the Delhi Region (Gurjar et al. 2004, Tyagi et al. 2016).

NOx react in the atmosphere to form smog and acid rain. Breathing air in such an environment can cause respiratory problems, damage the lung tissues and other breathing-related problems in humans. Acid rain is also very dangerous to both plants and human beings.

Tables 5 shows the average monthly values of the NOx, for February, March and April in the year 2018, 2019 and 2020. The values of the current year were compared with the previous two years and the per cent reduction in the values during the lockdown, i.e. for April was determined (Table 6).

It can be observed from Table 6 and Fig. 4, that a significant decrease in the NOx occurs during April. A maximum reduction of 70.75% was reported from the Ashok Vihar-DPCC

Table 1: PM2.5 monthly average values for the 5 monitoring stations in μg/m^3.

Year	Ashok Vihar-DPCC			DTU - CPCB			IGI Airport (T3) - IMD			Wazirpur - DPCC			Najafgarh - DPCC		
	Feb	March	Apr	Feb	March	Apr	Feb	March	Apr	Feb	March	Apr	Feb	March	Apr
2018	172.04	119.95	101.38	169.76	122.81	87.84	161.80	69.20	59.18	162.85	120.14	99.064	123.40	94.10	76.08
2019	141.68	92.43	95.33	118.77	92.81	84.62	168.20	72.43	69.23	166	98.355	101.44	110.17	83.86	68.17
2020	134.55	67.73	48.59	152.58	76.39	50.93	214.82	48.34	39.07	146.49	71.972	52.392	112.08	66.54	47.13

Table 2: PM10 monthly average values for the 5 monitoring stations in μg/m^3.

Year	Ashok Vihar-DPCC			DTU – CPCB			IGI Airport (T3) - IMD			Wazirpur - DPCC			Najafgarh - DPCC		
	Feb	March	Apr	Feb	March	Apr	Feb	March	Apr	Feb	March	Apr	Feb	March	Apr
2018	330.68	286.48	315.21	NA	385.35	299.36	241.80	143.30	175.87	365.42	287.82	371.52	212.95	216.16	269.90
2019	236.55	193.65	167.72	203.57	194.84	263.70	251.23	176.59	224.13	295.39	231.58	307.84	167.52	145.23	191.96
2020	230.35	121.84	95.15	285.28	154.61	123.80	343.10	116.33	88.02	272.28	170.07	108.57	175.57	133.68	143.72
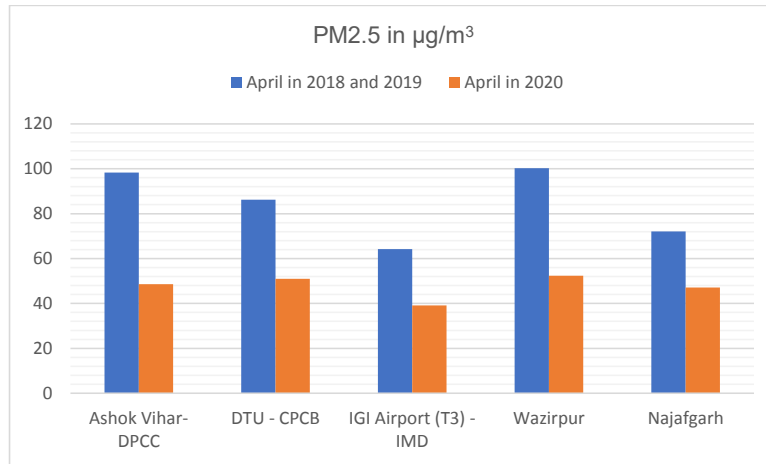
Fig. 2: The PM2.5 values in April 2020 compared to the average of 2018 and 2019 for the same period.
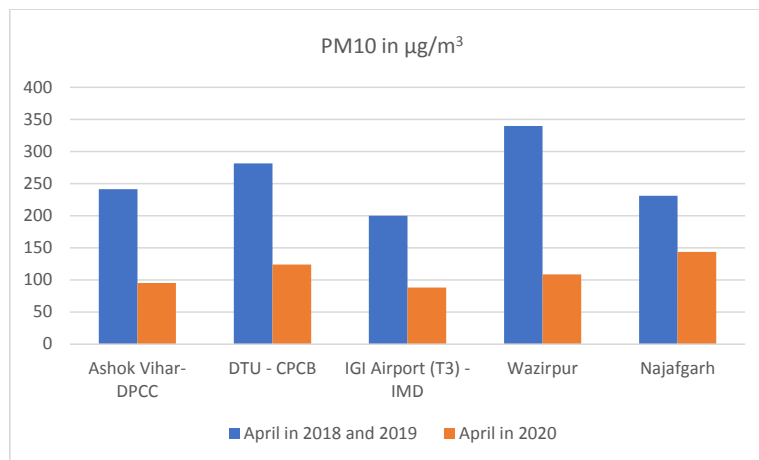
Fig. 3: The PM10 values in April 2020 compared to the average of 2018 and 2019 for the same period.
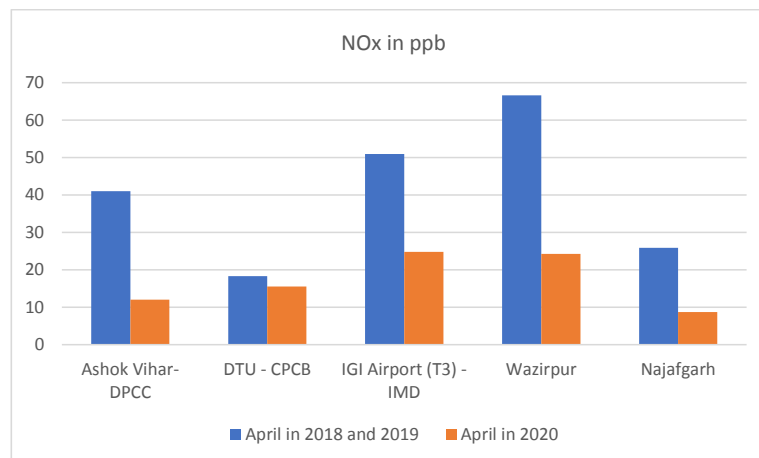
Fig. 4: The NOx values in April 2020 compared to the average of 2018 and 2019 for the same period.

Table 3: Per cent reduction in the PM2.5 in April in 2020 compared to the average of the 2018 and 2019 April values.

Stations	Average of the Year 2018 and 2019 for April ($\mu g/m^3$)	Value in April 2020 ($\mu g/m^3$)	%Reduction
Ashok Vihar-DPCC	98.35	48.59	50.59
DTU-CPCB	86.23	50.93	40.94
IGI Airport (T3)-IMD	64.21	39.07	39.15
Wazirpur	100.25	52.39	47.74
Najafgarh	72.13	47.13	34.66

Table 4: Per cent reduction in the PM10 in April in 2020 compared to the average of the 2018 and 2019 April values.

Stations	Average of the Year 2018 and 2019 ($\mu g/m^3$)	Value in April 2020 ($\mu g/m^3$)	%Reduction
Ashok Vihar-DPCC	241.45	95.15	60.59
DTU-CPCB	281.53	123.8	56.03
IGI Airport (T3)-IMD	200	88.02	55.99
Wazirpur	339.68	108.57	68.04
Najafgarh	230.93	143.72	37.76

Table 5: NOx monthly average for the 5 monitoring stations in ppb.

Year	Ashok Vihar-DPCC			DTU - CPCB			IGI Airport (T3) - IMD			Wazirpur			Najafgarh		
	Feb	March	Apr	Feb	March	Apr	Feb	March	Apr	Feb	March	Apr	Feb	March	Apr
2018	56.63	41.99	37.21	48.76	31.25	8.76	114.57	46.88	53.81	65.009	60.015	54.104	31.91	28.50	31.14
2019	57.18	50.88	44.71	41.74	27.86	27.79	164.89	78.44	48.03	92.537	72.173	79.074	32.87	24.82	20.60
2020	51.13	32.11	11.98	30.10	19.24	15.53	96.43	74.02	24.77	68.597	47.143	24.246	24.08	16.96	8.71

monitoring station. A satellite image (Fig. 5) showing the average concentration of nitrogen dioxide over India during the period of 1st January to 24th March and 25th March to 20th April for the year 2019 and 2020 also shows the reduction in the concentration of the NO_2 during the lockdown.

Ozone

Ozone found in the stratosphere is good ozone as it protects the earth from the harmful ultraviolet rays. But the ground-level ozone is bad for humans as it has a negative effect on human health. Ozone is not a primary pollutant as it is not directly emitted by the sources. It is a secondary pollutant formed due to the photochemical reactions of NOx and VOCs in the presence of sunlight.

Inhalation of ozone causes breathing problems, coughing, chest pain, throat irritation, damage of lung tissues and other health issues.

Table 7 shows the average monthly values of the ozone, for February, March and April in the year 2018, 2019 and 2020. The values of the current year were compared with the previous two years and the per cent reduction in the values

during the lockdown, i.e. for April was calculated (Table 8).

Table 8 and Fig. 6 shows that there has been a good reduction in the ozone concentration during the lockdown period in four out of five stations [an exception being the DTU-CPCB station which may be due to lesser reduction in the NOx levels (15%)]. Studies have shown that the reduction in VOCs is more effective in limiting ozone production as compared to the NOx (Jhun et al. 2015).

DISCUSSION

The lockdown has restricted the commercial activities, construction activities, vehicular movement and industrial activities which are the major contributor to the air pollutants. From the above analysis, we can see that there has been a significant decrease in the concentration of major pollutants like PM2.5, PM10, NOx and ozone in the air during the lockdown period due to the Covid-19. This result is consistent with a study by Sharma et al. (2020) who reported a maximum reduction of 49% in AQI in Delhi. The AQI in Delhi has always been under the 'very poor' to 'severe' category due to which the people are under constant threat of health

Table 6: Percentage reduction in the NOx in April in 2020 compared to the average of the 2018 and 2019 April values.

Stations	Average of the Year 2018 and 2019 (ppb)	Value in April 2020 (ppb)	% Reduction
Ashok Vihar-DPCC	40.96	11.98	70.75
DTU-CPCB	18.28	15.53	15.04
IGI Airport (T3)-IMD	50.92	24.77	51.36
Wazirpur	66.59	24.25	63.58
Najafgarh	25.87	8.71	66.33

Table 7: Ozone monthly average for the five monitoring stations in $\mu g/m^3$.

Year	Ashok Vihar-DPCC			DTU - CPCB			IGI Airport (T3) - IMD			Wazirpur			Najafgarh		
	Feb	March	Apr	Feb	March	Apr	Feb	March	Apr	Feb	March	Apr	Feb	March	Apr
2018	34.90	47.78	62.54	NA	0.02	9.21	101.50	31.54	36.14	26.012	33.988	46.134	50.05	60.07	79.13
2019	30.03	39.37	45.96	34.77	41.47	54.30	99.33	23.15	25.59	22.221	33.985	45.08	47.74	55.93	78.15
2020	27.95	27.81	36.42	47.32	52.62	78.77	113.08	13.57	25.92	11.424	4.8438	33.059	39.05	44.78	38.17

Table 8: Per cent reduction in the Ozone in April in 2020 compared to the average of the 2018 and 2019 April values.

Stations	Average of the Year 2018 and 2019 ($\mu g/m^3$)	Value in April 2020 ($\mu g/m^3$)	% Reduction
Ashok Vihar-DPCC	54.25	36.42	32.87
DTU-CPCB	31.76	78.77	-148.02
IGI Airport (T3)-IMD	30.87	25.92	16.03
Wazirpur	45.6	33.059	27.50
Najafgarh	78.64	38.17	51.46

issues. During the lockdown, the AQI in Delhi has reached to 'satisfactory' to 'moderate' category.

This shows the extent to which the anthropogenic activities are responsible for the increase in the concentration of pollutants in the air, due to which the air quality is becoming worst for human beings. There has been an increasing number of health issues which people are facing in the urban areas as they are continuously forced to breathe in polluted air (Pandey & Devotta 2005). These pollutants are also the reason for the major global issues like climate change and global warming (Alcamo et al. 2002).

Restricting the anthropogenic activities causing the release of pollutants in the air, can be an ideal solution to the control of air pollution, but slowing down the economy and growth of the country is not a kind of solution that would be feasible for any country. Various other measures can be taken to put a control on them which in turn will help in reducing the concentration of harmful pollutants in the environment.

1. During the lockdown, wherever possible, people are working from home as they cannot travel. Organizations which never allowed the work from home model earlier have now accepted this model and allowing the employees to work from home. The feedback received is that there has been no impact on work front especially for the IT industry and the ones whose majority of the work is on the computers (Mitta 2020). If this model is continued, and employees are asked to come to the office only when needed, there would be major drop vehicular movement. The companies can also opt for a 50% work from a home model, where 50% of their workforce is always working from home. As reported by CPCB, the vehicular contribution to the total urban air pollution in Delhi and Mumbai is about 76-90% for CO, 66-74% for NOx, 5-12% for SO_2 and 3-12% for PM (Gulia et al., 2015).

2. Majority of the offices, including the government offices are using the video conferencing for their meetings during the lockdown. If people start using it for their Meetings regularly, their travel will reduce which will bring down the number of vehicles on the road.

3. The industries cannot be stopped from their operations, but strict action can be taken on the control of its emissions. The government should imply stricter rules and impose stringent monitoring on the emissions emitted by the industries.

Fig. 5: Satellite image showing the average nitrogen dioxide over India. Source: ESA/Copernicus
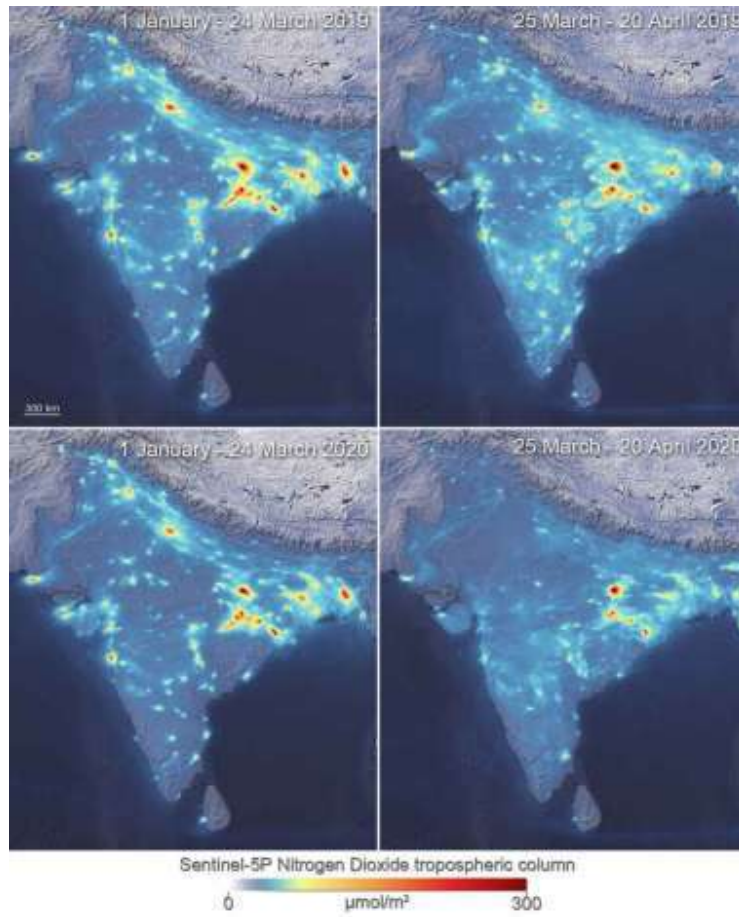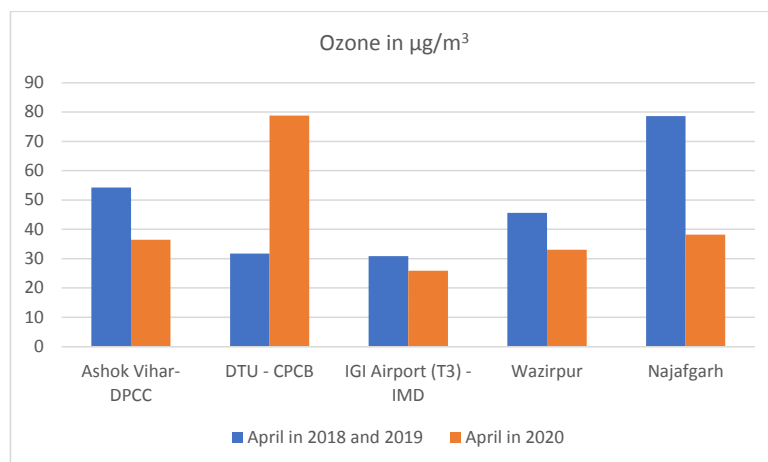

Fig. 6: The ozone values in April 2020 compared to the average of 2018 and 2019 for the same period.

4. During the lockdown, the government has imposed a model where people do not need to travel to places for necessities like groceries, fruits, vegetables and medicines but these necessities have been reached out to them at their places. If this model can continue even after lockdown, wherever feasible, it will surely contribute to lessening the air pollutants. More virtual online supermarkets should be introduced so that their services could reach more and more people. People should be given special discounts and perks to encourage them to use online markets instead of travelling and going to the markets.

5. Many service industries have started their online working model to continue to provide their services to customers. They should think of continuing this model even after the lockdown as this will decrease the travel of the people.

CONCLUSION

The Covid-19 pandemic has shaken the entire world with hundreds of thousands of deaths and millions of people affected due to this virus. It has impacted the economy, health care systems and the social life of people. Most of the countries have shut down the institutions, industries and transport and asked people to stay at home to control the spread of the virus.

The only positive side that be seen during this difficult time is the impact on the environment. With the reduced anthropogenic activities causing pollution, the environment is breathing easily during this period. Taking Delhi, as the study area, different parameters (PM2.5, PM10, NOx and ozone) of five monitoring stations were analysed and compared with the values in the previous year. The results show that there has been a considerable reduction in the concentration of air pollutants in the air. A reduction of almost up to 50% was found in the PM2.5 values, while the PM10 values showed a reduction of up to 68% and the NOx values showed a reduction of up to 70%.

Everyone knows that this is a temporary effect and pollution level will become regular after the lockdown is over. But it is time to give a thought to the level at which the environment is getting affected due to the uncontrolled human activities. If these activities cannot be stopped completely, they can definitely be reduced. The lockdown period has introduced many different models of working, education and business which require none or very less travel. People should seriously think on such models to continue which is going to reduce the vehicular movements and in turn reduce the emission of pollutants in the air. The regulatory bodies should also take this experience as a very good example and work on different plans to impose strict regulations on the emissions from the industries and power plants.

REFERENCES

Alcamo, J., Mayerhofer, P., Guardans, R., van Harmelen, T., van Minnen, J., Onigkeit, J., Posch, M. and de Vries, B. 2002. An integrated assessment of regional air pollution and climate change in Europe: Findings of the AIR-CLIM Project. Environmental Science & Policy, 5(4): 257-272.

Chakraborty, I. and Maity, P. 2020. COVID-19 outbreak: Migration, effects on society, global environment and prevention. Science of The Total Environment, 728: 138882.

Gulia, S., Nagendra, S.S., Khare, M. and Khanna, I. 2015. Urban air quality management-A review. Atmospheric Pollution Research, 6(2): 286-304.

Gurjar, B.R., Van Aardenne, J.A., Lelieveld, J. and Mohan, M. 2004. Emission estimates and trends (1990–2000) for megacity Delhi and implications. Atmospheric Environment, 38(33): 5663-5681.

Huang, C., Wang, Y., Li, X., Ren, L., Zhao, J., Hu, Y., Zhang, L., Fan, G., Xu, J., Gu, X. and Cheng, Z. 2020. Clinical features of patients infected with 2019 novel coronavirus in Wuhan, China. The lancet, 395(10223): 497-506.

Jayant Sinha & Samir Saran 2020. View: In the lockdown, a breath of fresh air View: In the lockdown, a breath of fresh air. The Economic Times, May 08, 2020. https://economictimes.indiatimes.com/news/politics-and-nation/view-in-the-lockdown-a-breath-of-fresh air/articleshow/75635142.cms?utm_source=contentofinterest&utm_medium=text&utm_campaign=cppst

Jhun, I., Coull, B.A., Zanobetti, A. and Koutrakis, P. 2015. The impact of nitrogen oxides concentration decreases on ozone trends in the USA. Air Quality, Atmosphere & Health, 8(3): 283-292.

Lancet, T. 2020. India under COVID-19 lockdown. Lancet (London, England), 395(10233): 1315.

Lewnard, J.A. and Lo, N.C. 2020. Scientific and ethical basis for social-distancing interventions against COVID-19. The Lancet. Infectious diseases, 20(6): 631.

McKibbin, W. and Fernando, R. 2020. The economic impact of COVID-19. Economics in the Time of COVID-19: 45.

Mitta, Sridhar 2020. Work from home has been 'successful' during Covid-19 lockdown. What next? https://economictimes.indiatimes.com/magazines/panache/work-from-home-has-been-successful-during-covid-19-lockdown-what-next/articleshow/75470580.cms?utm_source=contentofinterest&utm_medium=text&utm_campaign=cppst

Pandey, J.S., Kumar, R. and Devotta, S., 2005. Health risks of NO_2, SPM and SO_2 in Delhi (India). Atmospheric Environment, 39(36): 6868-6874.

Pulla, P. 2020. Covid-19: India imposes lockdown for 21 days and cases rise. BMJ, 368: m1251

Revathi Hariharan 2019. Delhi is the most polluted city in the world today, says air quality report. https://www.ndtv.com/india-news/delhi-is-the-most-polluted-city-in-the-world-today-says-air-quality-report-2124800

Rothan, H.A. and Byrareddy, S.N. 2020. The epidemiology and pathogenesis of coronavirus disease (COVID-19) outbreak. Journal of Autoimmunity, 102433.

Sharma, S., Zhang, M., Gao, J., Zhang, H. and Kota, S.H. 2020. Effect of restricted emissions during COVID-19 on air quality in India. Science of The Total Environment, 728: 138878.

Tyagi, S., Tiwari, S., Mishra, A., Hopke, P.K., Attri, S.D., Srivastava, A.K. and Bisht, D.S. 2016. Spatial variability of concentrations of gaseous pollutants across the National Capital Region of Delhi, India. Atmospheric Pollution Research, 7(5): 808-816.

United Nations Department of Economic and Social Affairs 2018. Revision of World Urbanization Prospects. United Nations Department of Economic and Social Affairs, New York.

WHO 2020. World Health Organization Clinical Management of Severe Acute Respiratory Infection When Novel Coronavirus (2019-nCoV) Infection Is Suspected: Interim Guidance (2020). World Health Organization, Geneva.

Zambrano-Monserrate, M.A., Ruano, M.A. and Sanchez-Alcalde, L. 2020. Indirect effects of COVID-19 on the environment. Science of The Total Environment, 728: 138813.

Original Research Paper   doi https://doi.org/10.46488/NEPT.2020.v19i03.021   **Open Access Journal**

Use of Crystalline Silica Waste for Enhancement of Engineering Properties of Black Cotton Soil

M. Selvaraj, M. Krithigaisrilatha, S. Syed Masoodhu and N. Natarajan†

Department of Civil Engineering, Dr. Mahalingam College of Engineering and Technology, Pollachi-642003, Tamil Nadu, India

†Corresponding author: N. Natarajan; itsrajan2002@yahoo.co.in

ABSTRACT

Construction of pavement layers on subgrade soil with excellent properties reduces the thickness of pavements and consequently reduces the initial cost of construction. However, construction of pavement on poor soil subgrade like black cotton soil is unavoidable due to several constraints. In such a situation, the enhancement of subgrade properties can be attained by the addition of foreign materials. The worldwide growing usage of cement has led to a larger collection of crystalline silica from the cement manufacturing plants. The disposal of the crystalline silica is extremely challenging and also causes an environmental impact. Hence this waste material can be used for enhancement of the strength of the weak soils. Chemical analysis has revealed that crystalline silica is rich in oxides such as silicon oxide, aluminium oxide and calcium oxide. In this study, the black cotton soil is blended with 8%, 12%, 16%, 18% and 20% crystalline silica by the weight of the dry soil. Laboratory tests, namely, standard proctor compaction test, California Bearing Ratio (CBR) test and Unconfined Compressive Strength (UCC) test were carried out to examine the performance of crystalline silica mixture in black cotton soil. The outcome suggests that a potential increase in crystalline silica content enhances the maximum dry density (MDD). The results also indicate there is a huge potential to use crystalline silica as an admixture to strengthen the black cotton soil. Moreover, the employment of crystalline silica might also benefit the environment and construction cost.

INTRODUCTION

Environmental pollution emanating from the industries is a serious cause of concern. Rapid industrialization and urbanization have increased the level of pollution significantly. Every year an enormous quantity of waste materials is being dumped on the valuable land resulting in degradation of the existing soil. Moreover, the developed nations tend to perceive the developing nations as a source of dump yards for the disposal of solid waste matter. Thus, solid waste management has become a serious issue for third world countries. Solid waste disposal is posing a threat for many countries in today's scenario and many investigations are being carried out to convert the industrial and domestic wastes into usable materials. One among them is to utilize the solid waste materials for the stabilization of the weak and expansive soils such as black cotton soil. The internal structure of the black cotton soil is provided in Fig. 1.

Expansive soil is a term that denotes any soil or rock that has a potential for shrinking and swelling under changing moisture conditions (Nelson & Miller 1992). Structures that are built on such soils are subjected to severe damages. Soil stabilization is a process of enhancing the soil material resulting in improved bearing capacity, soil strength, and durability under adverse moisture and stress conditions (Joel & Agbede 2011).

These solid wastes can be of various types, namely, industrial (fly ash, bottom ash, foundry ash, copper slag, blast furnace slag, etc.), agricultural (bagasse, groundnut shell, rice husk, coconut shells, etc.), mineral (quarry dust, marble dust, etc.) and domestic (waste tyres, incinerator ash, etc.) (Sabat & Pati 2014). The volume of industrial waste production surpasses the waste production from other sources such as domestic, agricultural and mineral wastes due to the rapid growth of industrialization in meeting the ever-demanding needs of the people. Hence, the focus of our study is the stabilization of the black cotton soil using crystalline silica, an industrial waste.

Fly ash has been added for the stabilization of various expansive soils. Among fly ash, there are many varieties like class-C, class-F, etc. Various researchers have explored the effect of class-F on expansive soils (Pandian et al. 2001, Ji-ru & Xing 2002, Phanikumar & Sharma 2004, Amu et al. 2005, Hakari & Puranik 2012, Maneli et al. 2013, Radhakrishnan et al. 2014). The effect of class-C on expansive
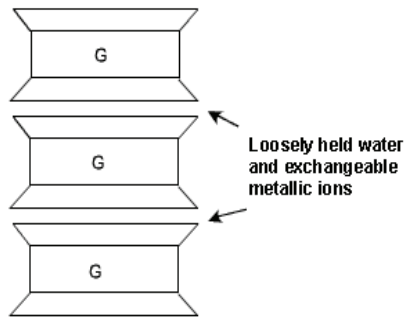
Fig.1: Internal structure of black cotton soil.

soils has been studied by Amu et al. (2005), Cokca (2001), Nalbantoglu (2004), Pandian & Krishna (2003), Misra et al. (2005). Cement kiln dust has been used for stabilization of expansive soils (Peethamparan & Olek 2008, Moses & Saminu 2012). The effect of the addition of silica fume on geotechnical properties of expansive soils was analysed by Kalkan & Akbulut (2004) and Negi et al. (2013). Havanagi et al. (2006) mixed copper slag with fly ash in expansive soils in different proportions and investigated their suitability in embankment, sub base and basements. Kalkan (2006) stabilized expansive clay with red mud (a waste material generated during the production of alumina) and cement red mud and found increment in the strength and decrement in the swelling percentage. Apart from these, various other industrial waste materials have been used in the past such as granulated blast furnace slag (Sharma & Sivapullaiah 2012, Celik & Nalbantoglu 2013), ceramic dust (Sabat 2012, Sabat & Bose 2014), brick dust (El-Aziz & Abo-Hashema 2013), and polyvinyl waste (Oyekan et al. 2013). Hotti et al. (2019) used plastic bottle granules as an additive for the stabilization of black cotton soil at Nargund taluk, Karnataka state. Fauzi et al. (2016) evaluated the engineering properties of black cotton soil stabilized with high density polyethylene (HDPE) and waste crushed glass as additives for subgrade improvement. Kumar & Singh (2017) analysed the stabilization of black cotton soil with cement kiln dust and reported that the optimum moisture content increases and the maximum dry density decreases with the cement kiln dust content. From

the above literature, it is evident that crystalline silica has not been used for the stabilization of the black cotton soil. In this study, an attempt has been made for the first time on the utilization of crystalline silica for the stabilization and enhancement of the strength of black cotton soil.

MATERIALS AND METHODS

Black cotton soil collected from a site in Erramanaickenpatti, Palani, Tamilnadu (Latitude 10°28'52'' N and Longitude 77°35'02'' E) has been used in this work. The soil sample was collected at a depth of 1m. The soil sample was prepared following IS-2720 Part 1. Crystalline silica sand of size less than 300 microns was collected from the ACC fly ash brick plant at Madukkarai in Coimbatore.

The chemical characterization of crystalline silica sand was found using Scanning Electron Microscopy (SEM) analysis. The results of the SEM test are given in Table 1.

From Table 1, it is evident that the element (O K) was found to be relatively high when compared with other elements.

Laboratory tests such as standard proctor compaction test, California Bearing Ratio (CBR) test and Unconfined Compressive Strength (UCC) test were carried out to examine the performance of crystalline silica mixture in black cotton soil.

RESULTS AND DISCUSSION

In Proctor compaction test, the compaction characteristics namely optimum moisture content and corresponding maximum dry density of the soil for a continuous increase in moisture content was determined as per IS 2720-7:1980. The variation of dry density with respect to water content is shown in Fig. 2.

With the addition of water to the black cotton soil, at low moisture content, it became easier for the soil particles to move over one another during the application of the compaction force. This caused the reduction of voids which subsequently increased dry density. As the water content

Table 1: Composition of crystalline silica.

S.No	Element	Concentration
1.	O K	36.15
2.	Al K	3.42
3.	Si K	6.37
4.	Ca K	17.35
5.	Fe K	1.11

increased, the soil particles were surrounded by larger water films around them. This increase in dry density continued until the stage where the water starts to occupy the space that could have been occupied by the soil grains. Thus the water at this stage impedes the closer packing of grains and reduces the dry unit weight. During compaction, removal of more void increases the density but it is impossible to remove all the air voids. So, practically the compaction curve cannot cross the zero air voids curve, therefore the void ratio is always greater than zero. From Fig. 2, it was also found that the optimum moisture content of the soil is 22% and the maximum dry density of the soil is 1.422g/cc.

In an unconfined compression test, we determined the unconfined compressive strength of the soil as per IS2720-10:1991 and the plot of the stress distribution is shown in Fig. 3. The plot also aids in the verification of the bulking of soil under various loading conditions.

California Bearing Ratio test was done for evaluating the bearing capacity of soil sample for the design of flexible pavement. Tests were carried out on natural or compacted soils under water-soaked and un-soaked conditions. The results obtained were compared with the curves of the standard test to have a conception of the strength of the underlying subgrade soil. While designing pavements, this CBR value governs the thickness of other layers, i.e. if CBR of soil is high, the layer thickness will be less.

Based on the standard formula and Fig. 4, the value of CBR of soil under un-soaked condition is 5.91%. The CBR test was performed on the soaked soil sample also. The sample was subjected to the soaking period of 96 hours before loading to ensure the worst field conditions.

Based on standard formula and Fig. 5, the value of CBR of soil in soaked condition is 1%. It is observed from the obtained values that the CBR value will generally be higher for the dry soil because the shear strength of dry soil is higher than the shear strength of wet soil. Moreover, since CBR is mostly associated with mechanical strength, the CBR (un-soaked value) will be higher than the CBR soaked value and a similar conclusion can be arrived here. Soaked CBR is used for the design of pavement as the earth beneath the pavement crust does not exactly remain dry throughout the year after the construction of the pavement. Some water does eventually reach the subgrade having percolated through interconnected voids, present either due to inadequate compaction, faulty mix design or potholes or by infiltration through the unpaved shoulders. The water affects the shear strength and bearing capacity

(CBR is the index of bearing capacity) of the subgrade, and weakens the subgrade, when moisture content exceeds the optimum moisture content (OMC). The various indexes and engineering properties of the soil are given in Table 2.

The compaction test was done with black cotton soil with the addition of crystalline silica to determine the optimum percentage of crystalline silica that would increase the dry density. With this optimum percentage, the unconfined compressive strength test and the California bearing ratio test were performed.

Effect of Crystalline Silica on Black Cotton Soil

The black cotton soil was added with 8%, 12%, 16% and 20% of crystalline silica and different percentages of water were added to determine the maximum dry density and the optimum moisture content.
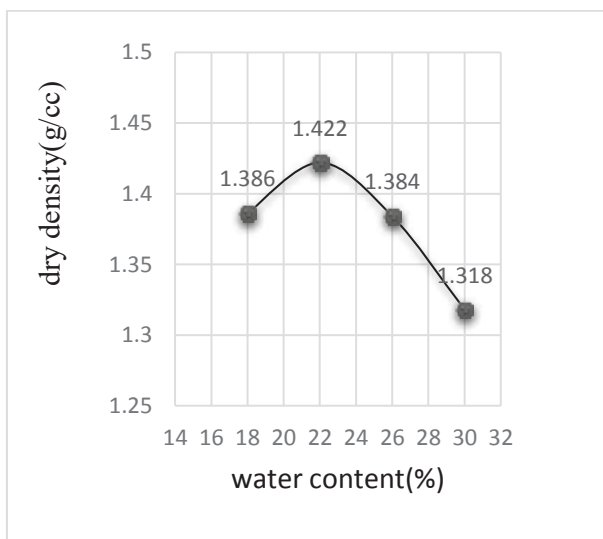
Fig. 2: Variation of dry density with water content.
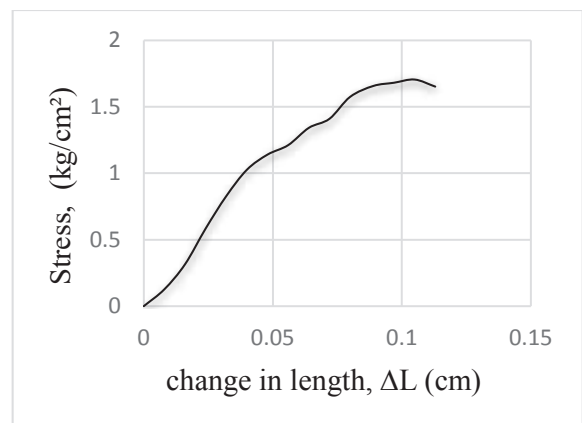
Fig. 3: Variation of stress with the change in length in UCC test for virgin soil.

Fig. 4: Variation of load with penetration in CBR test during the un-soaked condition.
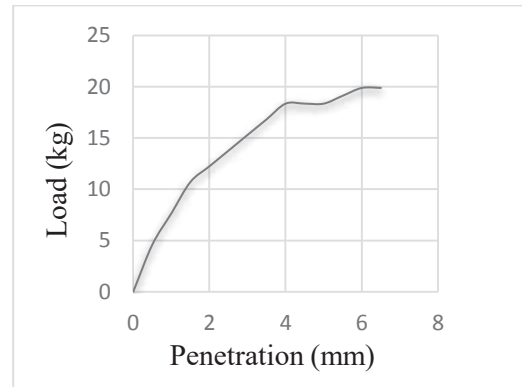
Fig. 5: Variation of load with penetration in CBR test during the soaked condition.

The unconfined compressive strength of the soil was carried out at an optimum percentage of 16% crystalline silica sand mixed with black cotton soil to determine the bulking characteristic of modified soil since the dry density is maximum at about 1.486 g/cc for the addition of 16% of silica sand when compared to others. A graph was plotted between stress and change in length for the addition of 16% of silica and the same has been illustrated in Fig. 6 to verify the bulking characteristics.

It can be inferred from Fig. 6 that the shear strength of the soil increases with the decrease in water content and an increase in dry density. Undisturbed soil can exist with either flocculent or dispersed structures depending upon mineralogy, the ion concentration of the pore fluid and the stress history. The structure is a principal factor of shear strength since a flocculent structure will tend to exhibit higher strength than a dispersed structure. The higher strength in the flocculent soil was probably because a greater number

Table 2: Obtained values for various properties of soil.

S. No	Test Conducted	Value
1.	Natural moisture content (Oven Drying Method)	33%
2.	Specific Gravity (Density Bottle Method)	2.07
3.	pH	8.9
4.	Organic content	16.66%
5.	Ash content	83.33%
6.	Differential free swell	40%
7.	Colour	Dark grey
8.	Atterberg's limits: Liquid Limit(W_L) Plastic Limit(W_P) Shrinkage Limit(W_S) Plasticity Index(I_P) Consistency Index(I_C) Shrinkage Ratio(R) From Plasticity chart (soil type)	68% 22.78% 15.23% 41.29% 0.85 1.48% MH type
9.	OMC MDD	22% 1.422g/cc
10.	Unconfined compressive strength	175.6 kN/m^2
11.	Fine-grained particles Coarse-grained particles	98.64% 1.36%
12.	CBR test: Unsoaked condition Soaked condition	5.91% 1%

of interparticle contacts would have disrupted during the shearing process. As the natural water content increases, which increases void ratio and degree of saturation, the shear strength of the black cotton soil decreases since the particles are forced apart, thereby decreasing the magnitude of the attractive forces. This indicates that the shear strength parameters, i.e., cohesion and angle of internal friction decrease with increasing water content.

With reference to shear strength, emphasis can be made on compacted samples. The states of particle arrangement (structure) that exist at various phases of compaction are shown in Fig.7. The changes in the arrangement of soil particles are explained as follows. At point A, the electrolyte concentration is very high due to the low water content and prevents the diffuse double layer of ions encompassing every particle from developing absolutely. The depression of the diffuse layer leads to low interparticle repulsion resulting in a tendency towards flocculation of the colloids. If the water content is increased to point B, the electrolyte concentration is reduced, resulting in an expansion of the double layer, increased repulsion between particles and a lower degree of agglomeration, which is an increased degree of particle orientation. Further increase in water content to an extent C, increases the sequel and ends up in a still higher increase in particle orientation. The mineralogical composition of the black cotton soil will determine the magnitude of variation of structure with moisture content. The above discussion explains the effect of moisture content and mineralogy on the shear strength of remoulded samples of the cohesive soil. The shear strength of the black cotton soil increases to a maximum and then decreases with increasing water content. The increase in strength at low water content indicates the need for some amount of water before the diffuse double layer is satisfied. Additional water added above optimum then reduces the electrolyte concentration, thereby,

allowing changes in particle orientation which decrease the shear strength.

The CBR value of the black cotton soil with the addition of the optimum percentage of crystalline silica in the unsoaked and soaked condition was determined, and the values are plotted in Fig. 8 and Fig. 9.

Based on the results obtained from the compaction test, unconfined compression test and California bearing ratio test, the following remarks could be proposed for stabilizing weak soil using crystalline silica. Addition of crystalline silica into the black cotton soil changed the proctor compaction parameters as given in Table 3. The maximum dry density increased with increase in crystalline silica content while the optimum moisture content decreased. From Fig. 10, it is noted that the inclusion of crystalline silica in the black cotton soil causes an improvement in maximum dry density up to 16%.

The variation of maximum dry density with varying optimum moisture content in the crystalline silica treated black cotton soil is shown in Fig.11

The variation of unconfined compressive strength in the black cotton soil before and after the addition of crystalline silica is shown in Fig.12. The unconfined compression strength has increased from 174 kN/m^2 (natural soil) to 341.9kN/m^2 (treated soil). The CBR values have increased for both soaked and unsoaked condition for the soil treated with silica content. (Table 4). Unsoaked CBR value has increased by more than 1.4 times when compared to the initial CBR value. Although the CBR value has increased for the soaked condition also, the change is not significant due to loss of cohesion and additional softening of soil due to soaking.

The variation of CBR value in the black cotton soil before and after the addition of crystalline silica are shown in Fig. 13 and Fig. 14.
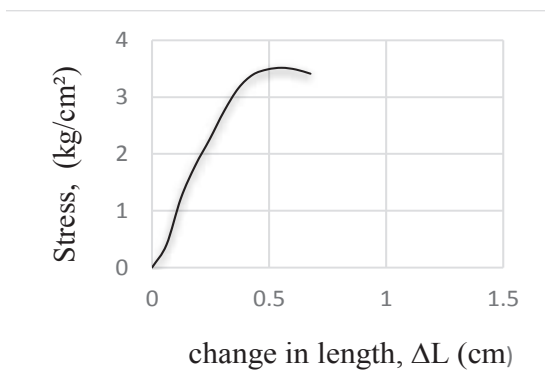
Fig. 6: Variation of stress with the change in length for the addition of 16% of silica.
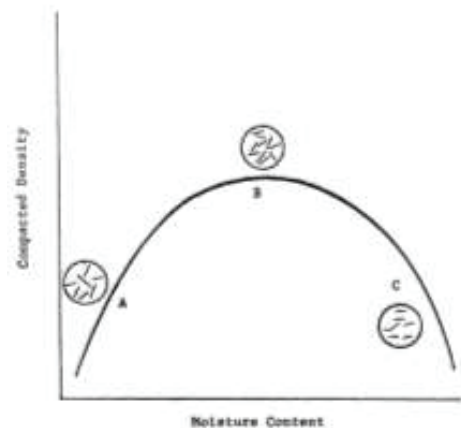
Fig. 7: Variation of compacted density with moisture content.
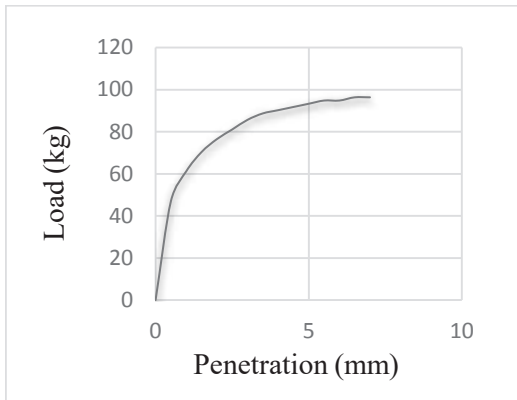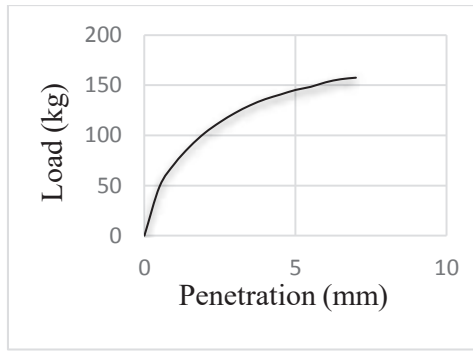
Fig. 8: Variation of load with penetration in CBR test during the un-
soaked condition for treated soil.
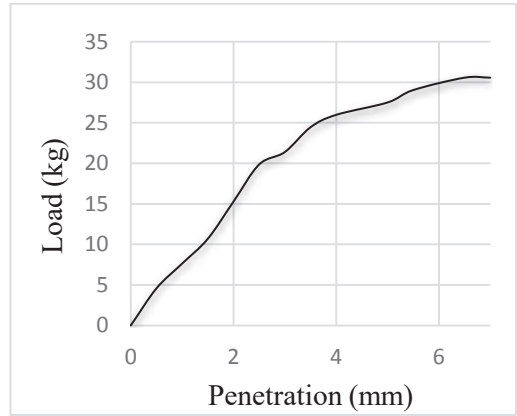
Fig. 9: Variation of load with penetration in CBR test during the soaked
condition for treated soil.

CONCLUSION

The optimum content of crystalline silica waste was found to be 16% as the mixture attained an increase in UCS value when compared with the virgin soil. CBR value also increased under both un-soaked as well as soaked condition for the silica treated soil. The results of this study confirm

Crystalline Silica Sand (CSS) as a potential stabilizer in improving engineering qualities of black cotton soil. Crystalline Silica, a waste material from the cement manufacturing plant is cost-effective, environmentally sustainable and can be gainfully used in pavement engineering construction. This application will enable the nation in achieving economic growth and industrialization if employed as part of the green growth development strategy.

Table 3: Variation of MDD and OMC of stabilized black cotton soil.

Soil Type	OMC	MDD (g/cc)
Black Cotton soil	22%	1.42
BC + 8% crystalline silica	22%	1.42
BC + 12% crystalline silica	20%	1.426
BC + 16% crystalline silica	18%	1.482
BC + 18% crystalline silica	14%	1.439
BC + 20% crystalline silica	14%	1.438

Table 4: CBR value.

Condition	Natural Soil	Treated Soil
Unsoaked	5.91%	8.3%
Soaked	1%	1.45%
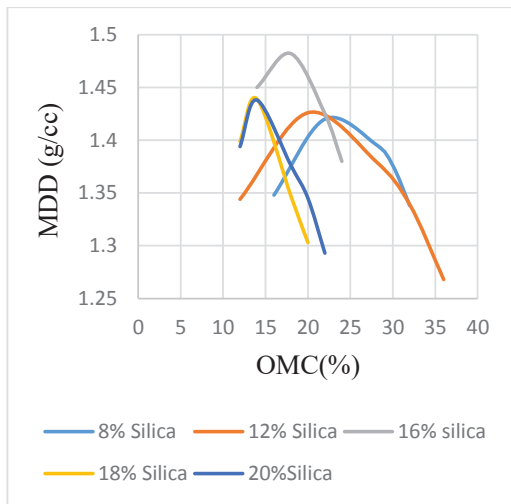
Fig. 10: Variation of OMC and MDD with various percentages
of silica content.
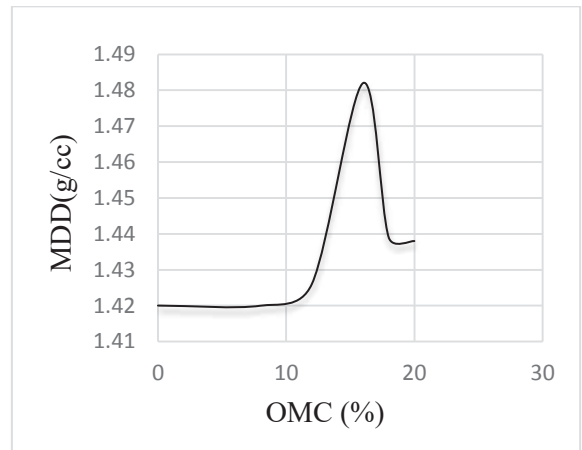
Fig.11: Variation of MDD and OMC of stabilized black cotton soil.
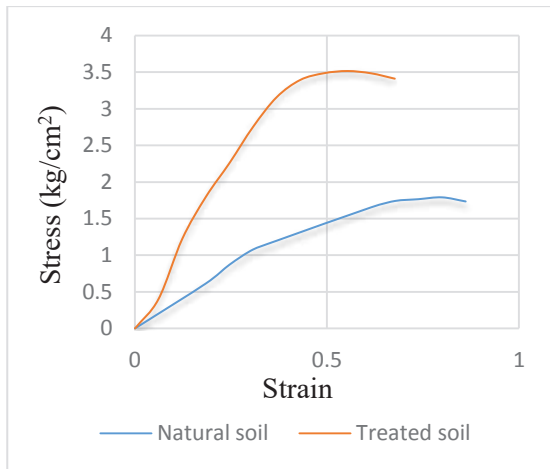
Fig.12: Variation of UCS with the addition of silica.
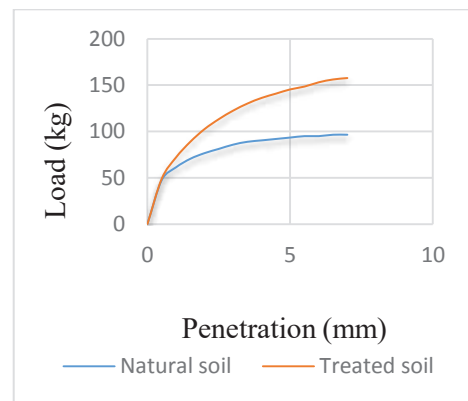
Fig.13: Variation of CBR with the addition of crystalline silica (un-soaked).
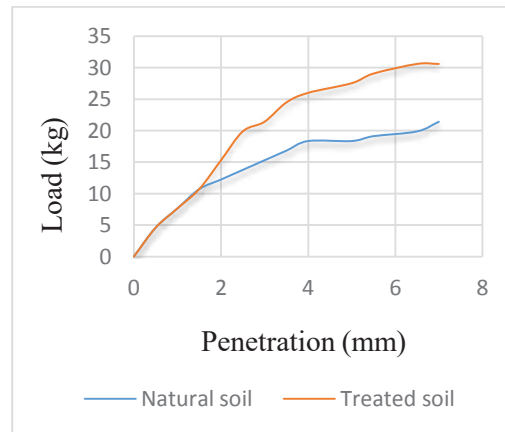
Fig. 14: Variation of CBR with the addition of crystalline silica (soaked).

REFERENCES

Amu, O. O., Fajobi, A.B. and Oke, B.O. 2005a. Effect of eggshell powder on the stabilizing potential of lime on an expansive clay soil. Research Journal of Agriculture and Biological Sciences, 1(1): 80-84.

Amu, O. O., Fajobi, A.B. and Afekhuai, S.O. 2005b. Stabilizing potential of cement and fly ash mixture on expansive clay soil. Journal of Applied Sciences, 5(9): 1669-1673.

Aziz, A. M. and Abo-Hashema, M. 2013. Measured effects on engineering properties of clayey subgrade using lime–Homra stabilizer. International Journal of Pavement Engineering, 14(4): 321-332.

Celik, E. and Nalbantoglu, Z. 2013. Effects of ground granulated blast furnace slag (GGBS) on the swelling properties of lime-stabilized sulfate-bearing soils. Engineering Geology, 163: 20-25.

Cokca, E. 2001. Use of class C fly ashes for the stabilisation of an expansive soil. Journal of Geotechnical and Geoenvironmental Engineering, 127 (7): 568-573.

Fauzi, A., Djauhari, Z. and Fauzi, U.J. 2016. Soil engineering properties improvement by utilization of cut waste plastic and crushed waste glass as additive. International Journal of Engineering and Technology, 8(1): 3059-3061.

Hakari, U.D. and Puranik, S.C. 2012. Stabilization of black cotton soil using fly ash, Hubbali-Dharwad municipal corporation area, Karnataka, India. Global Journal of Researches in Engineering- Civil and Structural Engineering, 12(2).

Havanagi, V.G., Prasad, P.S., Guruvittal, U.K. and Mathur, S. 2006. Feasibility of utilization of copper slag-fly ash-soil mixes for road construction. Highway Research Bulletin, 75: 59-67.

Hotti, B., Kabadi, S.A., Kuchabal, B., Koganur, K. and Padaganur, V. 2019. Stabilisation of black cotton soil using plastic bottle granules. International Journal of Technical Innovation in Modern Engineering Science, 5(6): 277-282.

Ji-ru, Z. and Xing, C. 2002. Stabilization of expansive soil by lime and fly ash. Journal of Wuhan University of Technology-Materials Science Edition, 17 (4): 73-77.

Joel, M. and Agbede, I.O. 2011. Mechanical-cement stabilization of laterite for use as flexible pavement material. Journal of Materials in Civil Engineering, 23(2): 146-152.

Kalkan, E. 2006. Utilization of red mud as a stabilization material for the preparation of clay liners. Engineering Geology, 87(3-4): 220-229.

Kalkan, E. and Akbulut, S. 2004. positive effects of silica fume on the permeability, swelling pressure and compressive strength of natural clay liners. Engineering Geology, 73: 145-156.

Kumar, A. and Singh, A.K. 2017. Stabilisation of soil using cement kiln dust. International Journal of Innovative Research in Science, Engineering and Technology, 6(6): 11631-11637.

Misra, A., Biswas, D. and Upadhyaya, S. 2005. Physico-mechanical behavior of self cementing Class C fly ash-clay mixtures. Fuel, 84(11): 1410-1422.

Maneli, A., Abiola, O.S., Kupolati, W.K. and Ndambuki, J. 2013. Evaluation of fly ash and ground granulated blast furnace slag on consistency limits of black cotton soil. OIDA International Journal of sustainable development, 6(10): 49-54.

Moses, G.K. and Saminu, A. 2012. Cement kiln dust stabilization of compacted black cotton soil. Electronic Journal of Geotechnical Engineering, 17: 825-836.

Nalbantoglu, Z. 2004. Effectiveness of Class C fly ash as an expansive soil stabilizer. Construction and Building Materials, 18: 377-381.

Negi, C., Yadav, R.K. and Singhai, A.K. 2013. Effect of silica fume on index properties of black cotton soil. International Journal of Scientific and Engineering Research, 4(8): 828-832.

Nelson, J.D. and Miller, D.J. 1992. Expansive Soils Problems and Practice in Foundation and Pavement Engineering. John Wiley and Sons, Inc.

Oyekan, G.L., Meshida, E.A. and Ogundalu, A.O. 2013. Effect of ground polyvinyl waste on the strength characteristics of black cotton clay soil. Journal of Engineering and Manufacturing Technology, 1: 1-10.

Pandian, N. S. and Krishna, K.C. 2003. The pozzolanic effect of fly ash on the California bearing ratio behavior of black cotton soil. Journal of Testing and Evaluation, 31(6): 1-7.

Pandian, N.S., Krishna, K.C. and Sridharan, A. 2001. California bearing ratio behavior of soil/fly ash mixtures. Journal of Testing and Evaluation, 29(2): 220-226.

Peethamparan, S. and Olek, J. 2008. Study of the effectiveness of cement kiln dusts in stabilizing Na-montmorillonite clay. Journal of Materials in Civil Engineering, 20(2): 137-146.

Phanikumar, B.R. and Sharma, R.S. 2004. Effect of fly ash on engineering properties of expansive soils. Journal of Geotechnical and Geoenvironmental. Engineering, 130 (7): 764-767.

Radhakrishnan, G., Anjan Kumar, M. and Prasad Raju, GVR. 2014. Swelling properties of expansive soils treated with chemicals and fly ash. American Journal of Engineering Research, 3(4): 245-250.

Sabat, A.K. and Bose, B. 2014. Strength, swelling and durability characteristics of fly ash-lime stabilized expansive soil-ceramic dust mixes. International Journal of Earth Sciences and Engineering, 7(3): 1210-1215.

Sabat, A.K. 2012. Stabilization of expansive soil using waste ceramic dust. Electronic Journal of Geotechnical Engineering, 17(2): 3915-3926.

Sabat, A.K. and Pati, S. 2014. A review of literature on stabilization of expansive soil using solid wastes. Electronic Journal of Geotechnical Engineering, 19: 6251-6267.

Sharma, A.K. and Sivapullaiah, P.V. 2012. Improvement of strength of expansive soil with waste granulated blast furnace slag. Proceedings of Geo Congress, 3920-3928.

Original Research Paper

Open Access Journal

Biogas Investment Intention of Large-Scale Pig Farmers Under the Emission Trading System

Wenjie Yao†

Zhejiang University of Water Resources and Electric Power, Hangzhou, 310018, China
†Corresponding author: rantom_821024@163.com

ABSTRACT

Based on the field research data of 424 large-scale pig farmers in Zhejiang Province, this paper takes the biogas fermentation as the main adoption behaviour of pollution treatment, and make the quantitative analysis on the biogas investment intention and its influencing factors on large-scale pig farmers under the emission trading system. The research shows that the emission trading system can encourage large-scale pig farmers to adopt biogas fermentation to deal with pollution and make environmental protection investment for waste resources utilization, which mainly depends on the pig breeding scale, the biogas digesters purchased or not, the benefit evaluation of biogas fermentation and the biogas fermentation technology service existed or not, rather than environmental awareness. Therefore, it is feasible to introduce the emission trading system into the agricultural non-point source pollution control with pig breeding pollution as the typical example. For the pig breeding industry, emission trading can be transformed from the traditional redistribution of environmental capacity to the redistribution of production scale.

INTRODUCTION

Because privatization of public resource property right is difficult to operate, it is generally considered unfeasible to implement an emission trading system in the field of agricultural non-point source pollution (Stiglitz 1989). In recent years, more and more scholars (Haiyu 2007, Zhiyong et al. 2012, Weijun et al. 2013, Guangyue et al. 2014, Min et al. 2017) have applied emission trading as an important economic means to control agricultural non-point source pollution, but they have not realized that environmental capacity is not easy to determine because different geographical, meteorological and hydrological conditions have a great impact on pollution migration and transformation. Therefore, the emission trading system in the field of agricultural non-point source pollution cannot be based on environmental capacity allocation, but can only be implemented based on production scale allocation, that is, to control pollution from the source of production. Under the production pattern of large-scale pig breeding, as the main source of agricultural non-point source pollution, the pollution of pig breeding is different from that of chemical fertilizers and pesticides. It can be isolated from the production process and has the special applicability of the emission trading system.

However, can the emission trading system encourage large-scale pig farmers to invest in environmental protection? In the field of industrial point source pollution, some

conclusions have been answered in the affirmative. This system enables enterprises to increase investment in environmental protection and invest excessively in pollution treatment technology under the expectation of higher emission trading price (Laffont et al. 1995, Yingde 2012). Moreover, it can encourage enterprises to carry out technological innovation and reduce the unit cost of pollution treatment (Carlson et al. 2000). Of course, some contrary findings should not be ignored. The new environmental protection technology will reduce the marginal cost of pollution treatment of enterprises, leading to a decline in the emission trading price, and reducing the innovation income of enterprises. Therefore, enterprises are not strongly willing to invest in environmental protection under this system (Villegas-Palacio et al. 2009). Especially compared with environmental taxes and fees, if enterprises are short-sighted, the system will not significantly improve their willingness to invest in environmental protection (Milliman et al. 1989, Requate 1995, Requate et al. 2001, Requate et al. 2003).

We are committed to seeking the environmental protection investment intention of large-scale pig farmers under the emission trading system. Based on the field research data of 424 large-scale pig farmers in Zhejiang Province, the biogas fermentation is taken as the main adoption behaviour of pollution treatment, and the quantitative analysis is made on the biogas investment intention and its influencing factors

of large-scale pig farmers under the emission trading system. We aim to provide a realistic basis and lay an empirical foundation for introducing the emission trading system into the agricultural non-point source pollution control with pig breeding pollution as the typical example, to explore the corresponding analysis framework of property rights trading.

MATERIALS AND METHODS

Theoretical Framework

Compared with industrial point source emission trading, emission trading in pig breeding pollution control is essentially a kind of scale right trading. There are three main reasons. First, pig waste comes from a single production form, and the quantity of pollution can be controlled by adjusting the production scale spontaneously. Second, cultivated land is the main carrier of pig waste consumption environment, which has the exclusivity of private use in spatial distribution. Third, the utilization of pig waste as resources has great potential, which can generate economic incentives for environmental protection. Therefore, for the pig breeding industry, emission trading can be transformed from the traditional redistribution of environmental capacity to the redistribution of production scale. This change makes the producers with low cost of emission reduction no longer sell emission rights, but buy scale rights to improve efficiency. Under this system, according to the established environmental capacity standard, namely "the carrying capacity of livestock per 0.067 ha of cultivated land", pig farmers with the ability to recycle wastes will buy scale rights and have strong willingness to invest in environmental protection, and pig farmers who cannot recycle wastes will sell scale rights and have a strong willingness to give up raising pigs when the average cost of production is higher than the average benefit of production.

We take biogas fermentation as the main way to recycle pig waste. The willingness to invest in biogas facilities reflects the extent to which the emission trading system can enable pig farmers to consciously adopt environmental protection. Based on relevant literature (Xinyu 2007, Hao et al. 2008, Bin 2009, Yi et al. 2012) and combined with field investigation, we assume that large-scale pig farmers adopt biogas fermentation behaviour to deal with pollution and have scale economy, or at least no diseconomy of scale, and they have a certain willingness to invest in biogas facilities and are influenced by the eight factors including "large-scale pig farmer from other place or not", "degree of education", "amount of cultivated land", "pig breeding scale", "average annual income of raising pigs", "biogas digesters purchased or not", "benefit evaluation of biogas fermentation" and "Biogas fermentation technology service existed or not".

Generally speaking, if the emission trading system is implemented, pig farmers may be willing to invest in biogas facilities for five reasons. First, due to the lack of cultivated land for pig farmers from other places or the shortage of supporting cultivated land for local pig farmers, a large amount of pig waste cannot be effectively returned to cultivated land. Under environmental regulations, the scale of breeding must be expanded by purchasing scale rights, so as to realize the scale economy effect of pollution treatment. Second, pig farmers with higher education and strong environmental awareness tend to actively respond to the implementation of the emission trading system. Third, pig farmers have higher income or even need to expand the scale of breeding, but diseconomy of scale exists in pollution treatment. Fourth, pig farmers have purchased and built biogas digesters and are encouraged by the scale economy of pollution treatment, or have a higher evaluation of the benefits of biogas fermentation, so they are more responsive to the implementation of emission trading system. Fifth, there are supporting services related to biogas fermentation technology around the pig farm, which can overcome the diseconomy of the scale of pollution treatment.

Model Building

Under the emission trading system, whether large-scale pig farmers are willing to invest in biogas facilities is a type 0-1 dichotomous dependent variable. Hence we used the binary Logit model to estimate the relevant influencing factors. For the dependent variable "biogas investment intention", a large-scale pig farmer who had been willing to invest in biogas facilities was assigned a value of 1, while a large-scale pig farmer who had been unwilling to invest in biogas facilities was assigned a value of 0. The specific form of the binary Logit model is as follows:

$$\log it\left(I_i\right) = \alpha_0 + \sum_{k=1}^{n} \alpha_k X_{ki} + \eta \qquad \ldots(1)$$

Here, I_i is the probability that the i-th large-scale pig farmer is willing to invest in biogas facilities; X_{ki} is the k-th influencing factor of the biogas investment intention of the i-th large-scale pig farmer; α_0 and α_k are the corresponding regression coefficients; η is the random error. We set eight independent variables (Table 1).

RESULTS AND DISCUSSION

We took large-scale pig farmers as the survey objects. According to the regulations of *China Animal Husbandry Yearbook*, we took 50 pigs raised at the end of every year as the lower statistical limit of large-scale pig breeding and used the Conditional Value Assessment Method to explore large-scale pig farmers' biogas investment intention under the

Table 1: Independent variables and their instructions.

Independent Variables	Symbol	Instructions
Large-scale pig farmer from another place or not	X1	No = 0, Yes = 1
Degree of education	X2	Years of academic education: Primary school = 6, Middle school = 9, High school = 12, Junior college = 15, Undergraduate = 16
Amount of cultivated land	X3	A unit of 0.067 hectares
Pig breeding scale	X4	The amount of pig raised at the end of every year
Average annual income of raising pigs	X5	Ten thousand Yuan
Biogas digesters purchased or not	X6	No = 0, Yes = 1
Benefit evaluation of biogas fermentation	X7	Not very good = -1, Almost flat = 0, Very good = 1
Biogas fermentation technology service existed or not	X8	No = 0, Yes = 1

emission trading system. During 2018-2019, we distributed 450 questionnaires to large-scale pig farmers in Hangzhou, Jiaxing, Ningbo, Quzhou and other areas in Zhejiang Province. After information screening and reliability assessment, 424 questionnaires were confirmed to be valid, accounting for 94.22%. The characteristics of survey data are shown in Table 2. The survey results show that: if the emission trading system is implemented, 94.81% (402 households) large-scale pig farmers are willing to invest in biogas facilities, while 5.19% (22 households) large-scale pig farmers are not; 3.54% (15) large-scale pig farmers are willing to give up raising pigs completely, while 96.46% (409) farmers are not; among the large-scale pig farmers (22 households) unwilling to invest in biogas facilities, 68.18% (15 households) are willing to give up raising pigs completely, while 31.82% (7 households) are not. Therefore, it is practical to adopt biogas fermentation as the main behaviour of pollution treatment for large-scale pig farmers under the emission trading system.

We used STATA 11 statistical software to estimate the parameters of the binary Logit model with the maximum likelihood estimation method, and further screened the independent variables of the model by the stepwise forward regression method (the standard of P-value of all variables selected was set at 0.100). The results show that the regression equations are well fitted (Table 3).

If the emission trading system is implemented, the larger the pig breeding scale, the biogas digesters are purchased, the lower the benefit evaluation of biogas fermentation, and the biogas fermentation technology service is existed, the stronger the biogas investment intention for large-scale pig farmers will be, and a large-scale pig farmer from other place or not, the amount of cultivated land, the average annual income of raising pigs and the degree of education have no significant impact on large-scale pig farmers' willingness to invest in biogas facilities. A large-scale pig farmer from other place or not, the amount of cultivated land and the average annual income of raising pigs are closely related to the pig breeding scale. With no cultivated land for the large-scale pig farmers from other places, insufficient supporting cultivated land for local farmers, and high average annual income of raising pigs, the expansion of pig breeding scale will be stimulated by purchasing scale rights under the of scale trading system. If the original pollution treatment behaviour exists diseconomy of scale, large-scale pig farmers will be willing to invest in biogas facilities. The biogas fermentation technology service existed is an important factor in the willingness to invest in biogas facilities for large-scale pig farmers and determines the extent to which they respond to the emission trading system. If large-scale pig farmers have already built biogas digesters, they may be motivated by the scale economy of pollution treatment and form behavioural inertia, thus actively responding to the implementation of the emission trading system, but this has nothing to do with the awareness of environmental protection determined by large-scale pig

Table 2: Characteristics of the survey data for large-scale pig farmers.

Independent Variables	X1	X2	X3	X4	X5	X6	X7	X8
Maximum	1	16	16	2800	60	1	1	1
Minimum	0	0	0	50	2	0	-1	0
Mean	0.202 8	7.438 7	4.346 5	288.563 7	7.110 5	0.681 6	-0.761 8	0.75
Standard Deviation	0.402 6	3.285 6	2.272 9	404.995 2	3.986 5	0.466 4	0.448 1	0.433 5

Table 3: Regression results of the binary Logit model for large-scale pig farmers' willingness of investment in biogas facilities under the emissions trading system.

Independent Variables		Coefficient	Standard Error	
X4		0.0042*	0.0022	
X6		1.5969***	0. 4879	
X7		-0.7579*	0. 4551	
X8		1.3955***	0. 4681	
Sample Size	424		Log likelihood	-70.607 8
LR chi2	31.81***		Pseudo R^2	0. 183 8

Note: ***, ** and * respectively indicate that the estimated results are significant at the levels of 1%, 5% and 10%. Pearson's test value of model regression is 139.15 (P value is 0.997 8), which doesn't reach the significance level of 5%.

farmers' own education level. Of course, some studies have highlighted the significance of environmental awareness. For example, Yi et al. (2012) believe that if pollution emission subsidy is implemented, pig farmers with higher education level are more likely to choose the disposal method of organic manure. Contrary to the theoretical expectation, it is not that the benefit evaluation of biogas fermentation is higher, large-scale pig farmers are willing to invest in biogas facilities under the emission trading system. The reason is likely to be that the scale economy of biogas fermentation as the main adoption behaviour of pollution treatment can only be achieved when the pig breeding scale is expanded to a certain extent. However, under the emission trading system, it not only needs to increase production input but also may have the risk of bidding for scale rights, which may not be able to be borne by many small-scale pig farmers. Here, it can also be verified from the fact that the larger the pig breeding scale, the stronger the biogas investment intention.

CONCLUSION

The emission trading system can encourage large-scale pig farmers to adopt biogas fermentation to deal with pollution and make environmental protection investment for waste resources utilization. In response to the implementation of the emission trading system, large-scale pig farmers are willing to invest in biogas facilities, mainly depending on the pig breeding scale, the biogas digesters purchased or not, the benefit evaluation of biogas fermentation and the biogas fermentation technology service existed or not, rather than environmental awareness. Therefore, it is feasible to introduce the emission trading system into the agricultural non-point source pollution control with pig breeding pollution as the typical example. For the pig breeding industry, emission trading can be transformed from the traditional redistribution of environmental capacity to the redistribution of production scale. However, it is still urgent to investigate and confirm

whether the adoption of biogas fermentation by large-scale pig farmers to deal with pollution does not exist diseconomy of scale. Only then can the system design be carried out from five aspects: environmental capacity standard, transaction operation mode, transaction price determination, public participation mode and supporting measures.

REFERENCES

Bin, L. 2009. Study on determinants of biogas engineering development in large-scale pig farms: The case from Fujian. Fujian Agriculture and Forestry University, Fuzhou, China.

Carlson, C., Burtraw, D., Cropper, M. and Palmer, K.L. 2000. Sulfur dioxide control by electric utilities: What are the gains from trade? Journal of Political Economy, 108(6): 1292-1326.

Guangyue, Z., Hong, Z. and Yiqian W. 2014. Study on emission trading system for agricultural source pollution in Weifang. Environmental Science and Management, 39(10): 24-28.

Haiyu, Z. 2007. Research on the application of tradable emissions to agricultural non-point source pollution. Ecological Economy, 4: 137-139.

Hao, H., Hui, Z. and Danping Y. 2008. An analysis of the determinants in option of biogas technology for swine farmers in Jiangsu Province. China Biogas, 26(5): 21-25.

Laffont, J. J. and Tirole, J. 1995. Pollution permits and environmental innovation. Journal of Public Economics, 62(1-2): 127-140.

Milliman, S. R. and Prince, R. 1989. Firm incentives to promote technological change in pollution control. Journal of Environmental Economics & Management, 17(3): 247-265.

Min, Q., Jianchun, Z. and Xiaotong, L. 2017. Design and innovation of agricultural non-point source pollution emission trading system. Journal of Northwest A&F University (Social Science Edition), 17(1): 155-160.

Requate, T. and Unold, W. 2001. On the incentives created by policy instruments to adopt advanced abatement technology if firms are asymmetric. Journal of Institutional & Theoretical Economics Jite, 157(4): 536-536.

Requate, T. and Unold, W. 2003. Environmental policy incentives to adopt advanced abatement technology: Will the true ranking please stand up? European Economic Review, 47(1): 125-146.

Requate, T. 1995. Incentives to adopt new technologies under different pollution-control policies. International Tax and Public Finance, 2(2): 295-317.

Stiglitz, J. E. 1989. Markets, market failures, and development. American Economic Review, 79(2): 197-203.

Villegas-Palacio, C. and Coria, J. 2009. Taxes, permits, and the adoption of abatement technology under imperfect compliance. Working Papers

in Economics, 368: 1-29.

Weijun, Y. and Junqing, H. 2013. Research on initial allocation of emission rights of agricultural non-point source pollution based on AHP method a case of the Ashe River basin. Science-Technology and Management, 15(1): 10-13.

Xinyu, P. 2007. Study on biogas technology adoption behaviour and green subsidy policy of livestock farming pollution prevention: Evidence from specialized pig breeding households. Chinese Academy of Agricultural Sciences, Beijing, China.

Yingde, H. 2012. Enterprise environmental protection behaviors under regulation of emission tradable policy based on the data of 223 enterprises from Zhejiang Province. Zhejiang University, Hangzhou, China.

Yi, Y., Hui, Z. and Hao H. 2012. Study on the factors affecting breeding farmers' environmental investment in the perspective of pollution subsidies: based on the survey of farmers from Shanghai, Jiangsu and Zhejiang. China Population, Resources and Environment, 22(2): 159-163.

Zhiyong, L., Tao, H. and Yan, W and Xin, H.Z.P.X. 2012. Research on emission trading to be applied to agricultural non-point source pollution control. Environment and Sustainable Development, 37(5): 37-41.

Effect of Seed Priming Treatment with Nitrate Salt on Phytotoxicity and Chlorophyll Content Under Short Term Moisture Stress in Maize (*Zea mays* L.)

Varinder Singh*, Anaytullah Siddique*†, Vijai Krishna** and Manpreet Singh*

*Department of Agronomy, School of Agriculture, Lovely Professional University, Phagwara-144411, Punjab, India,
**Department of Environmental Science, Rajiv Gandhi South Campus, Barkachha, BHU, Varanasi-221005, U.P. India
†Corresponding author: Anaytullah Siddique; anaytullahsiddique@gmail.com

ABSTRACT

An experiment was carried out to appraise the effect of seed priming treatment with $Mg(NO_3)_2$ against various levels of externally imposed moisture stress by polyethylene glycol-6000 on phytotoxicity in shoot and root and chlorophyll content in maize plant under laboratory conditions. The phytotoxicity of shoot and root was increased as the elevated levels of PEG-6000 towards T_1 to T_4 (i.e. 1.5 to 4.5 %, Set-I) as compared to control set (T_0, i.e. without treated set), while the least values of phytotoxicity were recorded in T_5 and onwards increased slowly up to T_8 (i.e. 1.5 to 4.5 % of PEG-6000 + primed seed, Set-II). The same trend of phytotoxicity was recorded for both the plant parts at both the times of observations, i.e. shoot and root 120 and 240 hours. The chlorophyll content of shoot was recorded in decreasing trend onwards from T_1 to T_4 in treatment set-I as compared to T_0, i.e. control. While the highest amount of chlorophyll content was recorded in T5 followed by T6 as compared to the rest of the treatments.

INTRODUCTION

Maize (*Zea mays* L.) is one of the valuable crops for human beings in respect to food, feed and as a raw material for many food industries. As the production of maize is concerned, it has the third rank after wheat and rice in the world (Tian et al. 2014). Rapid and uniform seed germination, emergence and healthy seedlings establishment are essential for keeping the good foundation for future vegetative as well as reproductive growth of maize crop to have optimum crop production. Drought is one of the very devastating conditions that reflect their presence very fast on every stage of growth. Due to the change of internal levels of water status, various physiological, biochemical and molecular changes appear within the plant especially seed germination, seedling growth, chlorophyll, sugar and proline content etc. Deviation in chlorophyll content leads to disturbing photosynthetic process results adversely in production of photosynthate (Chutia & Borah 2012, Wang et al. 2018). In general, plant losses their turgor pressure because of drought stress, but up to a certain extent, plant try to make a balance between soil and plant by accumulating solutes by producing osmoregulatory compounds like proline, glycine and betaine (Anaytullah et al. 2007, Siddique et al. 2018, Reddy et al. 2004). Seed priming technique is now one of the options that show positive results in the various crops to improve not only seed germination and early seedling emergence

but also for long term effect during plant life up to grain yield under various kinds of environmental stresses like heat stress, drought stress, salinity stress, etc. (Zhou et al. 2009, Tian et al. 2014, Yari et al. 2010). Priming treatment with nitrate salts like $Mg(NO_3)_2$, KNO_3 and $Ca(NO_3)_2$ are one of the most beneficial compounds that help to improve all the stages of growth especially beginning stage of the plant under normal as well as overcome the effect of temperature, heat, salinity and drought stress (Anaytullah & Bose 2007, Anaytullah et al. 2012, Siddique & Bose 2015, Srivastava et al. 2017, Mahmoudi et al. 2012).

MATERIALS AND METHODS

Genetically pure and fresh seeds of maize variety SUNNY-NMH-777 were collected and the effect of seed priming treatment with nitrate salt against externally imposed moisture stress under laboratory condition was appraised. The trial was split into two sets for better understanding, i.e. elevated concentrations of polyethylene glycol-6000 + without treated seed (Set-I) and elevated concentrations of polyethylene glycol-6000 + primed seed (Set-II). The experiment was conducted in CRD along with nine treatments and three replications. The various concentrations of externally imposed moisture stress were created by the use of polyethylene glycol-6000 (i.e. 1.5, 2.5, 3.5 and 4.5 %). The priming treatment was applied through $Mg(NO_3)_2$ @ 7.5mM up to

15 hours. After completion of priming duration, seeds were washed properly with distilled water and dried up to original weight under room temperature. Both the sets of treatment arranged systematically by transferring the fifty seeds in each Petri dish according to their sequence. The lab trial was conducted under growth chamber (Model No-NU-151) at 20±1°C temperature and 80 % RH. The phytotoxicity of shoot and root was derived from the formula given by Chou & Lin (1976) at both the times of observations, i.e. 120 and 240 hours intervals.

$$\text{Phytotoxicity (\%)} = \frac{\begin{array}{c}\text{Length of shoot or root (Control plant)} - \\ \text{Length of shoot or root (Treated plant)}\end{array}}{\text{Length of shoot or root (Control plant)}} \times 100$$

The extraction and determination of chlorophyll content in shoots of maize were made according to the formula given by (Witham et al. 1971). As per the protocol, one gram shoot sample was homogenized by pestle and mortar with 80% acetone. The resulting green liquid was transferred to a 100 mL volumetric flask and the final volume was made to 100 mL by adding 80% acetone. The O.D. of chlorophyll extract was recorded at 645 and 630 nm by a spectrophotometer. The amount of total chlorophyll was calculated by the formula given below.

$$\text{Total chlorophyll (mg/g)} = \{20.2 \ (D \ 645) + 8.02 \ (D \ 663)\} \times \frac{V}{1000 \times W}$$

Statistical Analysis

The data obtained from the present work were analyzed using SPSS software version 23 and compared the results by DMRT at ≤ 0.05.

RESULTS

Phytotoxicity to Shoot and Root

Data in Fig-1a and 1b show the effect of different concentrations of PEG-6000 and the overcome effect of seed priming treatment on phytotoxicity in shoot and root of 5 and 10 days old maize seedlings. Phytotoxicity in shoot and root was increased as the concentrations of PEG-6000 was increased from 1.5 % to 4.5% either alone or in combination with $Mg(NO_3)_2$ treated sets. But the level of phytotoxicity was increased maximum in PEG-6000 treated set in comparison to PEG-6000 + primed seed sets in both shoot and root. The observations were recorded at two different intervals, i.e. 120 hrs and 240 hrs for phytotoxicity of root and shoot. The minimum phytotoxicity in shoot and root was recorded in T_5 (1.5 % of PEG-6000 + primed seed) which was followed by T_6 and T_7 at both the time of observations (120 hrs and 240 hrs) in comparison to control set. Data in Figs. 1a and 1b show that T-5 and T_6 have a non-significant difference for each other but have a significant difference with rest of the treatments at both the times of intervals for phytotoxicity in shoot and root. Data also reveal that T_6 and T_7 overcome the effect of PEG-6000 induced moisture stress and recorded lower phytotoxicity of shoot and root in comparison to T_1 and T_2. It was realized from Figs. 1a and 1b that the phytotoxicity of shoot was greater than the phytotoxicity of root at both the times of observations including all the treatments.

Chlorophyll Content

Data presented in Fig. 2 reflect the effect of different concentrations of PEG-6000 and overcome the effect of primed seed treatment on chlorophyll content. Chlorophyll content
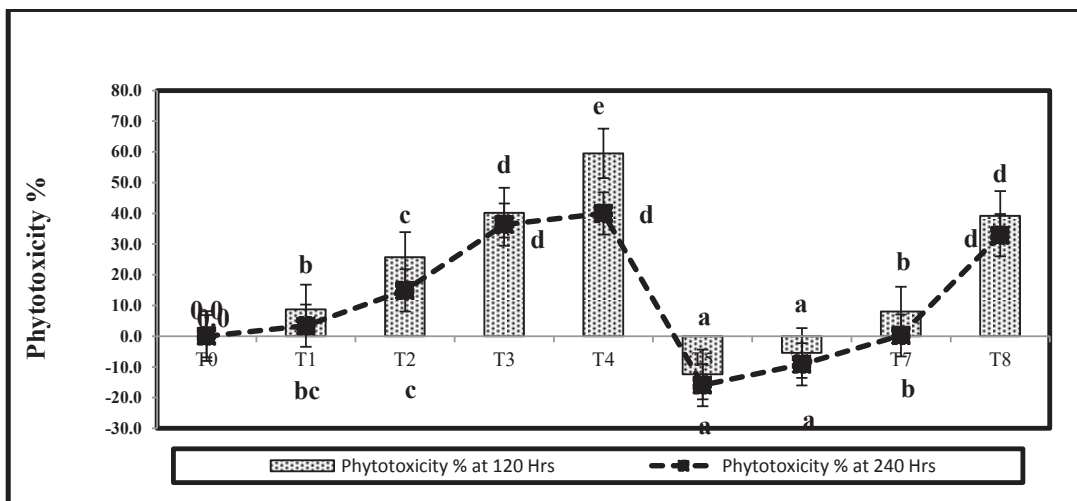
Fig. 1a: Effect of seed priming treatment with $Mg(NO_3)_2$ on phytotoxicity (%) in shoot under PEG-6000 induced moisture stress in maize.
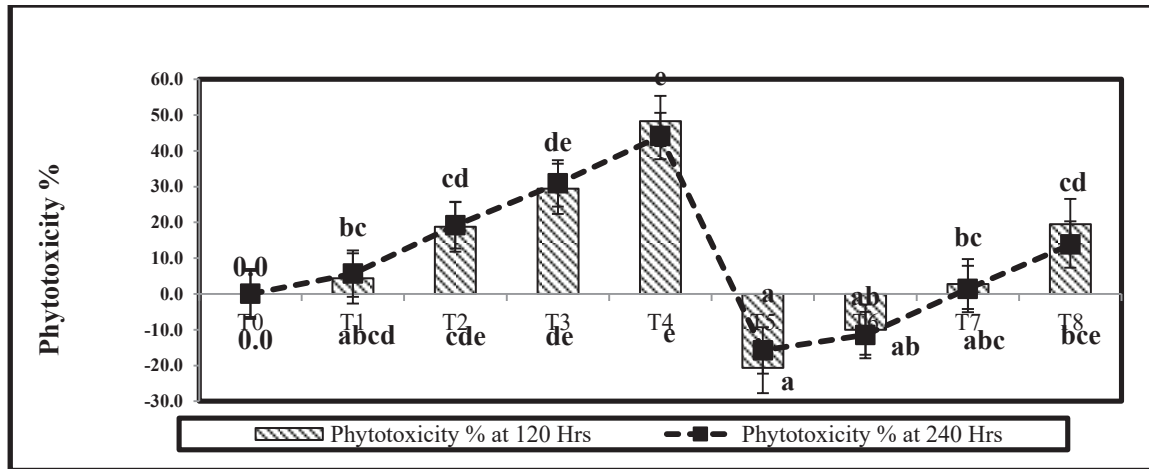
Fig. 1b: Effect of seed priming treatment with $Mg(NO_3)_2$ on phytotoxicity (%) in root under PEG-6000 induced moisture stress in maize.

was decreased as the concentration of PEG-6000 was increased from 1.5 % to 4.5% either alone or in combination with $Mg(NO_3)_2$ treatments. But the maximum reduction was recorded in PEG-6000 treated set in comparison to PEG-6000 + primed seed. Observations were recorded at two different intervals of 120 hrs and 240 hrs for chlorophyll content. Among the treatments (i.e. different concentrations of PEG-6000 alone and along with magnesium nitrate treated sets), the chlorophyll content was recorded better in PEG-6000 + primed seed in comparison to control. The maximum chlorophyll content was recorded in T_5 (1.5 % of PEG-6000 +

primed seed) followed by T6 in comparison to control, i.e. 0.201 and 0.591 $mg.g^{-1}$ at both the times of observations. Data presented in Fig. 2 show that T-5 and T-6 have non-significant differences between them but have a significant difference with most of the treatments at both the times of intervals. The least value of chlorophyll content was recorded by T_4 and T_3. When data were compared between 120 hrs and 240 hrs of intervals, it was found that chlorophyll content records greater values at 240 hrs intervals than 120 hrs of intervals including all the treatments.

The statistical analysis of chlorophyll content was carried

Fig. 2: Effect of seed priming treatment with $Mg(NO_3)_2$ on chlorophyll content ($mg.g^{-1}$) in soot under PEG-6000 induced moisture stress in maize.
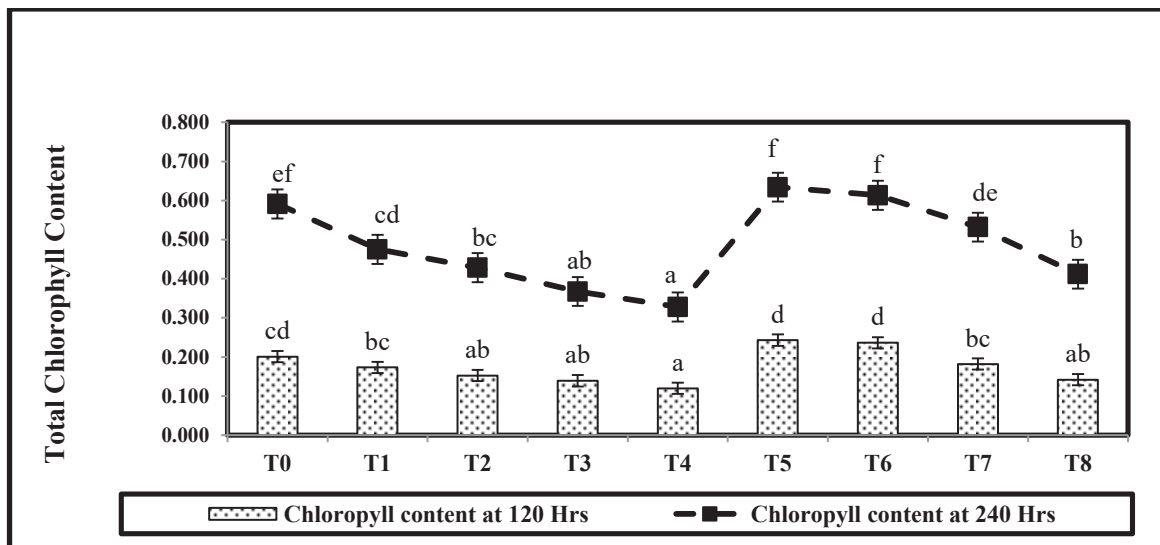
out through SPSS and found that the data is overall significant at p 0.05 % and have a significant difference between the treatments.

DISCUSSION

Elevated levels of PEG-6000 from lower to higher concentration, create the phytotoxicity in the seedlings by suppressing the water uptake as per the intensity of external moisture stress by the seed (Siddique & Dubey 2017, Anaytullah et al. 2007). Synthesis of photosynthetic pigment within seedling is very essential to become independent or maintaining continuous growth of seedlings or plants. In our study, it is observed that the reduction of photosynthetic pigment depends on the intensity of moisture stress or drought while the similar results were also reported by Mohammadkhani & Heidari (2007) and Rahbarian et al. (2011). It is well known that under such drought stress, the plant generates reactive oxygen species like O_2^- OH^* and H_2O_2 and every ROS act adversely on different molecules like singlet oxygen dominantly damage lipid and protein molecules while H_2O_2 react with cellular components (Das & Roychoudhury 2014, Yadav & Sharma 2016). These ROS groups of compounds are produced mainly in chloroplasts and mitochondria within the plant cells under different types of stresses, hence the probability is always very high to get damaged their skeleton due to increased levels of phytotoxicity, therefore, inhibiting or suppressing the biosynthesis of chlorophyll molecules in the chloroplast as per the severity of stress (Noctor et al. 2017, Aswani et al. 2019). The similar result in respect to overcoming the effect of moisture stress by various types of seed priming treatments was also reported by Pant & Bose (2016) and Murungu (2011).

REFERENCES

Anaytullah and Bose, B. 2007. Nitrate hardened seeds increase germination, amylase activity and proline content in wheat seedlings at low temperature. Physiology Molecular Biology of Plants, 13 (3&4): 199-207.

Anaytullah, Bose, B. and Yadav, R.S. 2007. PEG-induced moisture stress: Screening for drought tolerance in rice. Indian J. Plant Physiology, 12(1): 88-90.

Anaytullah, Srivastava, A.K. and Bose, B. 2012. Impact of seed hardening treatment with nitrate salts on nitrogen and anti-oxidant defense metabolisms in wheat (Triticum aestivum L.) under timely, late and very late sown conditions. Vegetos, 25(1): 292-299.

Aswani, V., Rajsheel, P., Bapatla, R.B., Sunil, B. and Raghavendra, A.S. 2019. Oxidative stress induced in chloroplasts or mitochondria promotes proline accumulation in leaves of pea (Pisum sativum): Another example of chloroplast-mitochondria interactions. Protoplasma, 256(2): 449-457.

Chou, C.H. and Lin, H.Z. 1976. Autointoxication mechanisms of Oryza sativa. I. Phytotoxic effects of decomposing rice residues in soil. J. Chemical Ecology, 2(3): 353-367.

Chutia, J. and Borah, S.P. 2012. Water stress effects on leaf growth and chlorophyll content but not the grain yield in traditional rice (Oryza sativa Linn.) genotypes of Assam, India II. Protein and proline status in seedlings under PEG induced water stress. American Journal of Plant Sciences, 3(7): 971-980.

Das, K. and Roychoudhury, A. 2014. Reactive oxygen species (ROS) and response of antioxidants as ROS-scavengers during environmental stress in plants. Frontiers in Environmental Science, 2: 1-13, https://doi.org/10.3389/fenvs.2014.00053.

Mahmoudi, H., Massoud, R.B., Baatour, O., Tarchoune, I., Salah, I.B., Nasri, N., Abidi, W., Kaddour, R., Hannoufa, A.A., Lachaal, M. and Ouerghi, Z. 2012. Influence of different priming methods for improving salt stress tolerance in lettuce plants. Journal of Plant Nutrition, 35(12): 1910-1922.

Mohammadkhani, N. and Heidari, R. 2007. Effects of water stress on respiration, photosynthetic pigments and water content in two maize cultivars. Pakistan Journal of Biological Science, 10(22): 4022-4028.

Murungu, F. S. 2011. Effect of seed priming and water potential on seed germination and emergence of wheat (Triticum aestivum L.) varieties in laboratory assay and in the field. African Journal of Biotechnology, 10(21): 4365-4371.

Noctor, G. Reichheld, J.P. and Foyer, C.H. (ed.) 2017. ROS-related redox regulation and signaling in plants. Seminar in Cell and Developmental Biology. Elsevier Ltd., 80, pp. 3-12.

Pant, B. and Bose, B. 2016. Mitigation of the influence of PEG-6000 imposed water stress on germination of halo primed rice seeds. International Journal of Agriculture, Environment and Biotechnology, 9(2): 275-281.

Rahbarian, R., Khavari-Nezad, R., Ganjeali, A., Bagheri, A. and Najafi, F. 2011. Drought stress effects on photosynthesis, chlorophyll fluorescence and water relations in tolerant and susceptible chickpea (Cicer arietinum L.) genotypes. Acta Biologica Cracoviensia Series Botanica, 53(1): 47-56.

Reddy, A.R., Chaitanya, K.V. and Vivekanandan, M. 2004. Drought induced responses of photosynthesis and antioxidant metabolism in higher plants. Journal of Plant Physiology, 161(11): 1189-1202.

Siddique, A. and Bose, B. 2015. Effect of seed invigoration with nitrate salts on morpho-physiological and growth parameters of wheat crop sown in different dates in its cropping season. Vegetos, 28(1): 76-85.

Siddique, A., Kandpal, G. and Kumar, P. 2018. Proline accumulation and its defensive role under diverse stress condition in plants: an overview. Journal of Pure and Applied Microbiology, 12(3): 1655-1659.

Siddique, A. and Kumar, P. 2018. Physiological and biochemical basis of pre-sowing soaking seed treatment-an overview. Plant Archives, 18 (2): 1933-1937.

Srivastava, A.K., Siddique, A., Sharma, M.K. and Bose, B. 2017. Seed priming with salts of nitrate enhances nitrogen use efficiency in rice. Vegetos, 30(4): 99-104.

Tian, Y., Guan, B., Zhou, D., Yu, J., Li, G. and Lou, Y. 2014. Responses of seed germination, seedling growth, and seed yield traits to seed pretreatment in maize (Zea mays L.). Scientific World Journal, 1-8.

Wang, Z., Li, G., Sun, H., Ma, L., Guo, Y., Zhao, Z., Gao, H. and Mei, L. 2018. Effects of drought stress on photosynthesis and photosynthetic electron transport chain in young apple tree leaves. Biol. Open., 7(11): 1-9.

Witham, F.M., Devid, F.B. and Roberts, M.D. (ed.) 1971. Experimental Plant Physiology. Van Nostrand Reinhold, New York, pp. 55-56.

Yadav, N. and Sharma, S. 2016. Reactive oxygen species, oxidative stress and ROS scavenging system in plants. Journal of Chemical and Pharmaceutical Research, 8(5): 595-604.

Yari, L., Aghaalikani, M. and Khazaei, F. 2010. Effect of seed priming duration and temperature on seed germination behavior of bread wheat (*Triticum aestivum* L.). ARPN Journal of Agricultural and Biological Science, 5(1): 1-6.

Zhou, Z.S., Guo, K., Abdelrahman, A.E. and Yang, Z.M. 2009. Salicylic acid alleviates mercury toxicity by preventing oxidative stress in roots of *Medicago sativa*. Environmental and Experimental Botany, 65(1): 27-34.

Microclimate Energy Considerations in Building Design for Arid Regions

A. A. Alaskary*, A. M. Hasson**†, M. J. Jweeg**and M. L. Al-Waily***

*Institute for Urban and Regional Planning, University of Baghdad, Baghdad, Iraq
**Technical Engineering, AlFarahidi University, Baghdad, Iraq
***Department of Mechanical Engineering, Faculty of Engineering, University of Kufa, Kufa, Iraq
†Corresponding author: A. M. Hasson; am.hasson2@gmail.com

ABSTRACT

Climate is one of the main parameters that can influence building designs in Iraq. Analysis and assessment of microclimatological data can aid urban architects and engineers to optimize human comfort through environmentally sustainable practices. The results indicated that the long-term measurements of total solar insolation and ambient temperatures have increased by 2.9% and 6.5% respectively. Albedo resulted in good correlation with heating coefficients and temperature of R^2 = 0.89 and 0.63 respectively. Annual cooling degree days and heating degree days have reduced, while annual mean ambient temperatures and annual solar radiation have increased.

INTRODUCTION

Climate change has become one of the central issues of international concern (Al-Maamary et al. 2017, Butera 2014). Its impact may lead to drought, dust storms, floods and other events that will have serious effects on the sustainability of communities and their development (Osman et al. 2014, Zakaria et al. 2013). Sustainable building designers must take into account climatic factors such as temperature, detrimental weather phenomena, weather forecast, relative humidity, wind direction and speed, rainfall, soil temperature and sunshine (Zareaian & Zadeh 2013). Sustainable design involves promoting environmental quality by minimising the adverse impact on the natural environment and buildings (Waro & Mwasha 2013). It involves complex interactions among environmental, economic and social parameters in which it must be analysed and treated by the various stakeholders involved (Nste et al. 2017). The majority of construction designs adopted in Iraq leaves the buildings exposed to solar radiation (Rashid 2014).

A large percentage of Iraqi households use cooling equipment and mechanical air-conditioning. However, the challenge arises with a lack of electrical power and the unaffordability of privately-owned electrical generators (Roaf & Bairstow 2008).

Hence, minimal mechanical air-conditioning is needed for sustainable building designs. Climate data play an important role in setting sustainable construction and building standards, especially regarding renewable energy input and potential. Based on the severe climate conditions found in Iraq, sustainable building is essential to face the challenge of climate change issues (Al-Waeli et al. 2017, Al-Waeely et al. 2014).

Renewable energies are important tools to support social and environmental energy sustainability (Langston & Ding 2001). Climatological information is required to understand how to construct sustainable buildings, and assess their energy efficiency, suitable for human comfort (Rashid 2014).

Hui & Cheung (1997) and Lam (1995) have indicated that technical innovation is needed to optimize building design for climate change, especially for severe hot summers. It is necessary to design sustainable buildings with less cooling systems and equipment, to overcome the heat flow from hot southern winds during summer months (Hasson et al. 2013). To assess the risk level of climate change and allow for its inherent properties and weather, data limitations must be understood and analysed (Jaramillo-Nieves & Del-Río 2010, Rashid 2014). Long-term data plays an important role in solar energy input annual assessments.

The main objective of this research is to investigate the influence of heat energy on building design in the Iraqi construction industry by analysing the environmental changes experienced over 16 years in the Baghdad region. This can

support designers in understanding the development of the local climate when designing sustainable buildings. Many factors such as wind direction and pattern, community population and distribution and social matters are not investigated in this study (Lam 1995).

MATERIALS AND METHODS

Data Collection

Microclimatological parameters, including total solar radiation (specifically incoming and outgoing radiation) and air temperatures, have been provided by the Iraqi Meteorological Service. In this study, the degree-day values in relation to the mean temperature of 26.9°C for the region are used for the last 10 years (2007-2017).

Albedo, cooling and heating degrees and correlation analysis are calculated based on the collected data of solar radiation and temperatures for the Baghdad region only (Al-Waeely et al. 2014, Huld et al. 2018). The relationship between roof albedo and the temperature is performed by analysing diurnal variant values of building roof albedo and roof temperature.

Study Area

Iraq is a country located in southwest Asia. It covers an area of 437,072 km^2 with a population of 38,988,704 million (Huld et al. 2018, USAID 2010). Iraq has three main climate regions: arid desert, semi-arid steppe and moist mountainous. The desert region is extremely arid and hot, with average diurnal temperatures in the summer season ranging from 25°C-43°C and falling to 4°C-17°C in the winter season (Hasson et al. 2017, Encyclopedia 2009). The steppe region is also hot, with average diurnal temperatures ranging from 26°C-46°C in the

summer season and falling to 5°C-18°C in the winter season (Hasson et al. 2013, Cofaigh et al. 1996). Finally, in the mountain region, the climate is considered to be cooler and wetter than the steppe region. The diurnal temperature at summer can range from 27°C-44°C while in winter it can range from 4°C-15°C (ESA 2017, Encyclopedia 2009, USAID 2010).

The Iraqi climate is characterized as arid region hot and dry most of the year (USAID 2010). In summer the highest temperatures occur in June, July and August, which can range between 43°C-53°C (Encyclopedia 2009, Fanack 2018), while in winter the temperature ranges from 1°C-8°C. The annual rainfall at the desert region can reach 200 mm, while it ranges between 200-400 mm within the steppe region from November to April to about 400-1000 mm or more in the mountain region (Omer 2011, King et al. 2003). The impact of the south/south-easterly Sharqi (Eastern) and the north/north-westerly Shamal (Northern) winds leads to extreme dust storms which occur in summer and autumn (Muir 2009, Al-Ansari et al. 2013).

RESULTS AND DISCUSSION

Based on the scientific research into the impact of climate change, there is a demand for data on the various microclimatic parameters such as air temperature, relative humidity, wind speed and direction, solar radiation, and orange dust, particularly for the Baghdad region, as information to support urban planners and engineers (King et al. 2003). This essential information enables designers to compare the design implications of these climatic relationships.

Results show a noticeable variation in each month and season at low solar elevations (solar altitude less than 30°C). Fig. 1 represents the global solar radiation to ambient temperature ratio during the year.
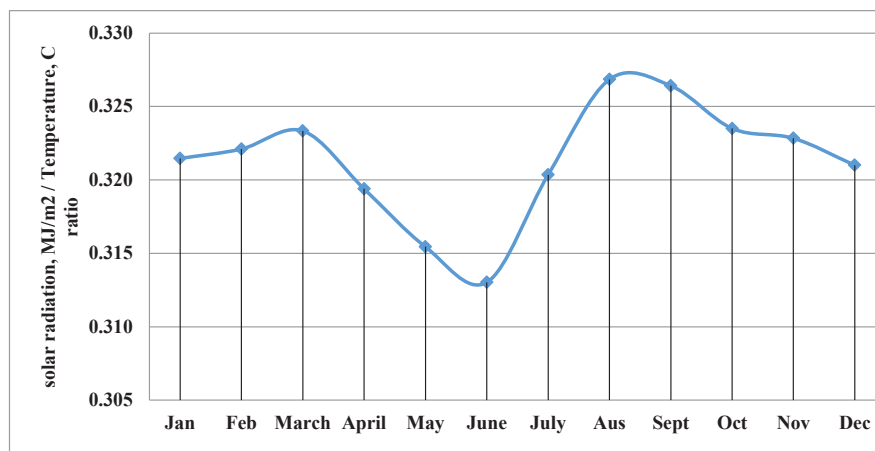
Fig. 1: Monthly average of daily ratios of global solar radiation and temperature.

The measured data of ambient temperature, AT and actual sunshine duration, ASD, total solar radiation, Rs and wind speed WS relationships are shown in Fig. 2. There is a linear relation between the values. The equations were formed with a good confidant of correction coefficient (Fig. 2a, b and c and Table 1).

Screening of Fig. 3 and Table 1 shows correlations in the slope of the regressions, suggesting that there will be outcomes as a result of these climatic factors. Thus, the influence that sunshine duration, solar radiation and wind speed have on ambient temperature can have consequences such as the presence of possible dust storms and overheat.

Fig. 3 shows that the annual average of daily ambient temperature means for the Baghdad region over the past 10 years was increased by a percentage of 7.9 while the level of degree-days was reduced by 10.7%.

Also, it has been found by analysing the annual heating and cooling degree-days over the study period (2008-2017) by taking into consideration a temperature of 26.6°C as a reference, that the Baghdad region has heated up as specified by the growth of cooling days and a lessening of heating days. This has important implications for urban climate and energy. The degree-day technique is used to estimate heat utilization in the early phase of thermal design (Yang & Lu 2004, Chen et al. 2001).

To assess the difference of the long-term value of temperatures in the Baghdad region, a degree-day set for the study period has been established, as shown in Fig. 3.

Albedo

Albedo is a ratio of the irradiance absorbed to the irradiance reflected of a surface (Al-Ansari et al. 2014). Albedo plays an important role when determining climate change and energy budgets (Al-Ansari 2013). Albedo values typically range from 10% to 50% (Bonafoni et al. 2017). It can be increased up to 60%, particularly on industrial and residential building roofs. For a given surface under the sun, albedo can be found in Fig. 5 and using the following equation (Schaaf et al. 2009, Bretz et al. 1998):

$$(1-\alpha)\ I = \varepsilon\ \sigma\ (T^4 s - T^4\ sky) + hc\ (Ts - Ta)$$

Surface temperature has a close relation with surface albedo (Akbari et al. 2009, Zhang et al. 2005). Previous studies indicate that surface temperature and albedo are intimately related in high-latitude regions (Li & Xiao 2007). However, few studies have focused on the quantification of surface temperature to surface albedo relationship.

Albedo plays an increasingly significant role in the summer season. This has happened in accordance with low solar altitude. Any change in solar angle combined with the influence of surface characteristics such as colour and type of the materials, can influence albedo values. High values of albedo denote a large amount of the incoming solar energy

Table 1: The expansion coefficient in AT = a₁ + bx equation the correlation coefficient (R^2).

Ambient temperatures	Intercept (a)	Slope (b)	R^2
Wind Speed, m/s	-5.94	37.70	0.67
Total solar radiation, MJm^{-2} Rs	2.71	-1.80	0.78
Actual sunshine duration, hr ASD	4.92	41.79	0.79
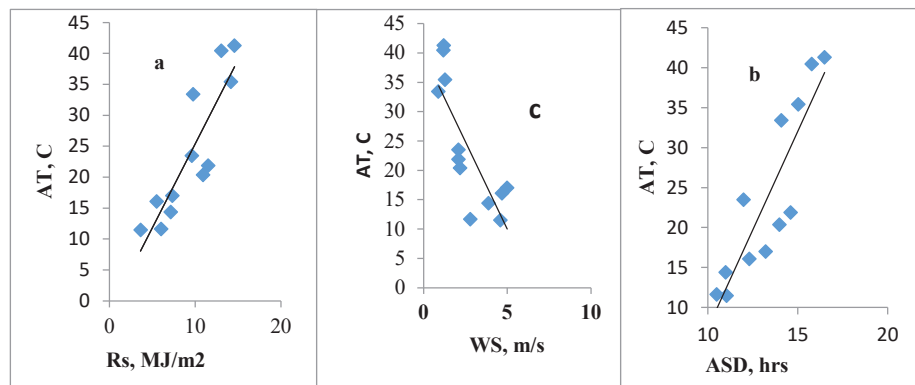
Fig. 2: Relationships between the annual average, monthly mean of ambient temperature and solar radiation (a), actual sunshine duration (b) and wind speed (c).

and solar radiation is being reflected by the surface.

Finally, when using the relationship of albedo to temperature (α/T), a noticeable diurnal variation in each month was found. However, during low solar elevations (solar altitude less than 30°) there is a strong correlation between temperature and albedo ($R^2 = 0.90$) as illustrated in Fig. 5.

Heating Coefficient (B)

The heating coefficient is shown between materials of the building surface and the atmosphere in Fig 6.

The statistical relationship between albedo and heating coefficient parameters has good correlation confidence listed in Fig. 7, with R^2 value of 0.63.

Night-Time Net Radiation, NTNR

NTNR is the energy radiation emitted during the night hours, which has a significant effect on the proportion of the day-time net radiation, DTNR.

At night time the longwave radiation values have varied between -0.37 and 1.73 MJ/m^2 which points out that the monthly variation in the value of nocturnal net radiation, NNR, was slightly different.

Fig. 8 shows the monthly average of long-wave net solar radiation. After sunset high values of negative net radiation occurred, they then decreased progressively, as the building roof ambient temperature decreased during the night hours, running to its minimal at sunrise. The roof (or the surface environment) was affecting long-wave net radiation.

Thus, the outward longwave radiation, which forms the factor NTNR, remains continuously throughout each month of the recorded period.

Construction materials are the crucial factor in meeting human comfort requirements while keeping sustainable economics to a maximum. Building design must consider climatic conditions, human comfort, expansion potential, environment and equipment maintainability.

	2007	2008	2009	2010	2011	2012	2013	2014	2015	2016	2017
Cooling	2000	2005	2000	2010	2015	2015	2022	2029	2033	2042	2044
Heating	316	315	315	310	310	305	311	312	310	305	302
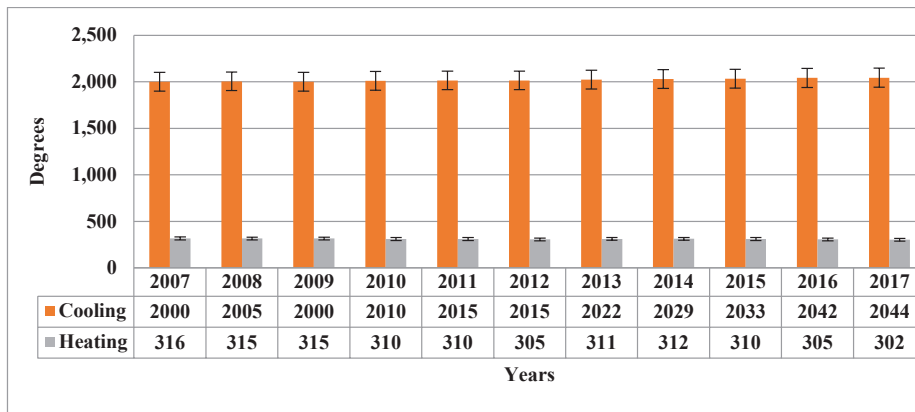
Fig. 3: Annual average of monthly heating and cooling degree-days.
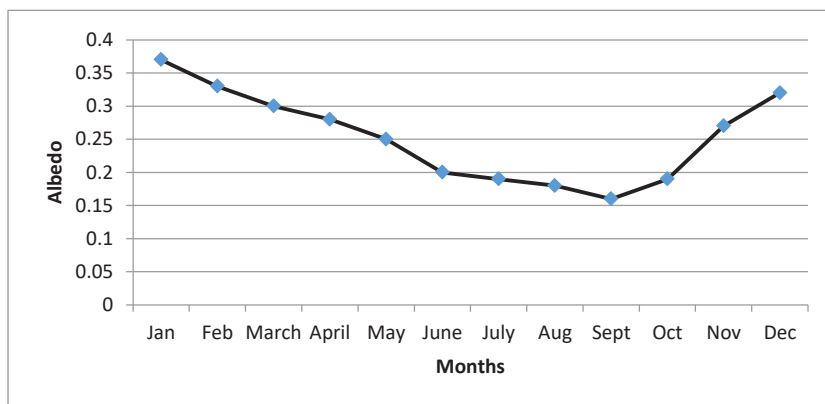
Fig. 4: Daily mean for monthly average albedo values.

Design Recommendation

Based on the potential influence of climatic factors on the building issues discussed, we recommend as follows: For architectural enhancement, fixtures such as external cladding, which can make the construction process more efficient while improving the visible impact of the project. The fundamental requirement for the design of sustainable buildings is that the buildings run at minimum cost and comply with a severe environment. Parameters such as building orientation, shading, and materials appropriate for the climatic conditions of Baghdad must be factored in (Pike 1994, Torrance 1991).

Due to power shortages for mechanical air conditioning, designers have the challenge to fit replacements for sustainable buildings based on the tenants' energy requirements and climatic conditions. A direct substitute is available plant materials. The plant colour is relevant to sunlight density and duration.

Ventilation

Based on the severe climate especially during summer months, standards for ventilation and thermal comfort for sustainable residential and commercial buildings are needed. Traditional designs forming the majority of urban residential housing and older commercial buildings in the Baghdad region have had long lives are useful for long-time measurements. When urban engineers design sustainable buildings that account for the possibility of future climatic conditions, this will not only protect the wellbeing of occupants but could also produce economic benefits in the form of green building and longer building lives (Chen et al. 2001, Prelgauskas 2003).

Fortunately, building designers are good at incorporating these natural forces into their style and finding out the likely design solutions that produce sensible conclusions (Chapin et al. 1966, Prelgauskas 2003, Cofaigh et al. 1996).
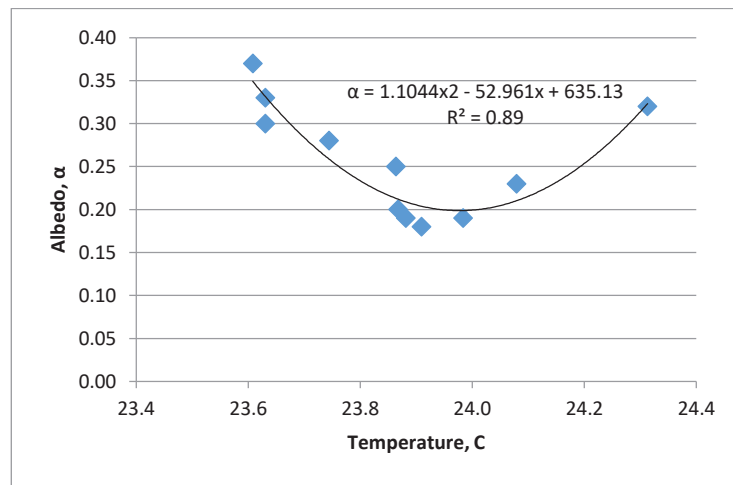
Fig. 5: Theoretical variation in temperature for values of albedo relationship at noon on the third day of the month.
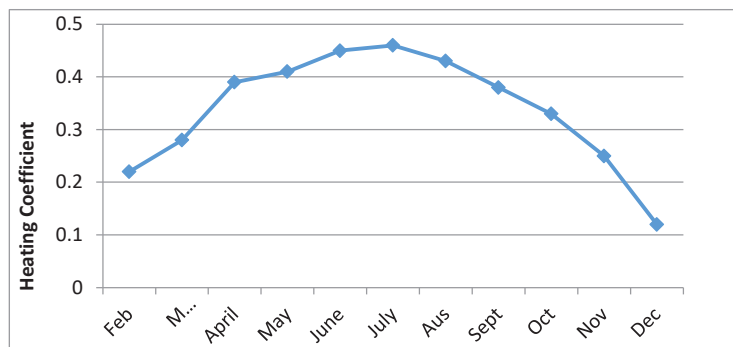
Fig. 6: Annual average of the monthly range of heating coefficients.
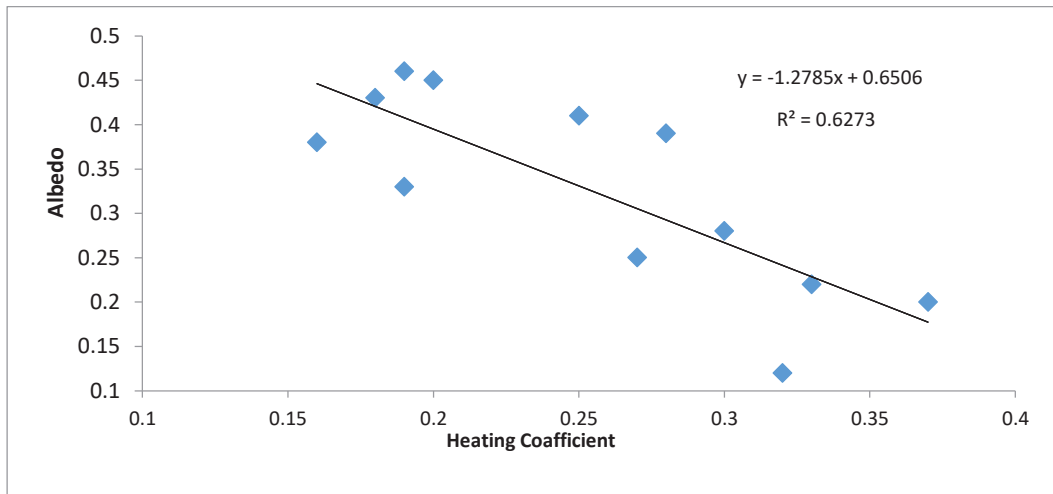
Fig. 7: Relationship between albedo and heating coefficient values.
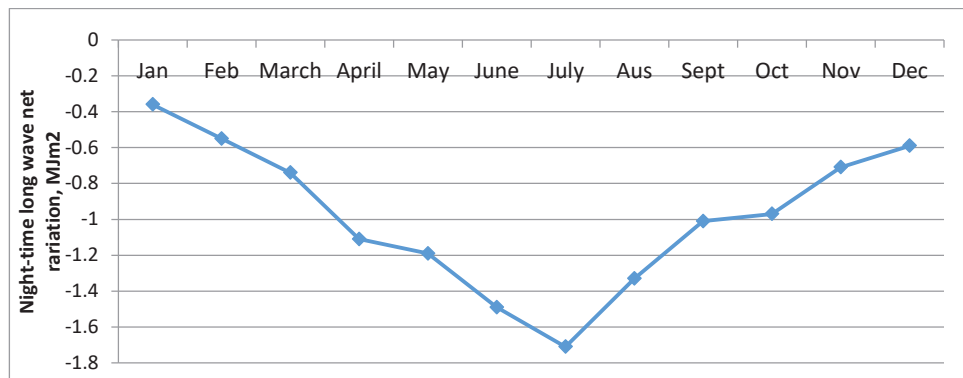
Fig. 8: Monthly mean night-time net longwave radiation.

CONCLUSIONS

Based on the outcomes of the analysis of historical climatic information in the Baghdad region for the study period, considerable alternations have taken place in Iraq. Annual CDD and HDD have reduced, while the annual mean of ambient temperature and annual solar radiation have increased.

Building surface materials, light colours and external cladding are the main factors affecting heat absorbance and transmittance. Consequently, air passing over the surface becomes cooler, especially at sunset. Since most buildings are exposed to solar radiation, it is, therefore, essential to design for human comfort based on the climatic context of a building. Sustainability in building and urban design strategies should be the focus of architects and engineers in arid climates. The relationship between local climatic conditions such as airflow and building position, orientation and shading must be considered in its connection to the consequent human comfort and integrity.

ACKNOWLEDGEMENTS

REFERENCES

Akbari, H., Menon, S. and Rosenfeld, A. 2009. Global cooling: Increasing worldwide urban albedos to offset CO_2. Climatic Change, 94: 275-286.
Al-Ansari, N. A., Ezz-Aldeen, M., Knutsson, S. and Zakaria, S. 2013. Water harvesting and reservoir optimization in selected areas of South Sinjar Mountain, Iraq. Journal of Hydrologic Engineering, 18: 1607-1616.
Al-Ansari, N. 2013. Management of water resources in Iraq: Perspectives and prognoses. Engineering, 5(8): 667-684.
Al-Ansari, N.A., Ali, A. and Knutsson, S. 2014. Present conditions and

future challenges of water resources problems in Iraq. Journal of Water Resource and Protection, 6: 1066-1098.

Al-Ansari, N. A., Abdellatiff, M., Zakaria, S., Mustafa, Y. T. and Knutsson, S. 2014. Future prospects for macro rainwater harvesting (RWH) technique in North East Iraq. Journal of Water Resource and Protection, 6: 403-420.

Al-Waeely, A. A., Salman, S. D., Abdol-Reza, W. K., Chaichan, M. T ., Kazem, H. A. and Al-Jibori, S. H. 2014. Evaluation of the spatial distribution of shared electrical generators and their environmental effects at Al-Sader City-Baghdad-Iraq. International Journal of Engineering & Technology IJET-IJENS, 14(2): 16-23.

Al-Maamary, H. M. S., Kazem, H. A. and Chaichan, M. T. 2017. Climate Change: the game changer in the GCC region. Renewable and Sustainable Energy Review, 76: 555-576.

Al-Waeli, A., Al-Asadi, K. and Fazleena, M. 2017. The impact of Iraq climate condition on the use of solar energy applications in Iraq: a review. International Journal of Science and Engineering Investigations, 6(68): 64-73.

Bretz, S., Akbari, H. and Rosenfeld, A. 1998. Practical issues for using solar-reflective materials to mitigate urban heat islands. Atmospheric Environment, 32(1): 95-101.

Butera, F. M. 2014. Sustainable building design for tropical climate principles and applications for Eastern Africa. United Nations Human Settlements Programme, (UN-Habitat).

Bonafoni, S., Baldinelli, G. and Rotili, A. 2017. Albedo and surface temperature relation in urban areas: analysis with different sensors. Urban Remote Sensing Event (JURSE). Joint, Dubai, United Arab Emirates.

Chapin, F. S., Sturm, M., Serreze, M. C., McFadden, J. P., Key, J. R., Lloyd, A. H., McGuire, A. D., Rupp, T. S., Stan, H., Hpfstede, G. and Kalma, J. D. 1966. Radiation balance of natural conditions. Q.J. R. Meteorological Soc., 92: 128-140.

Cofaigh, E. O., Johan, A. and Lewis, J. O. 1996. The Climate Dwelling: An Introduction To Climate Responsive Residential. James & James Ltd., 35-38.

Chen, Y. H., Li, X. B. and Xie, F. 2001. Study on surface albedo distribution over Northwest China using remote sensing technique (in Chinese). Scientia Geographica Sinica, 21(4): 327-333.

Encyclopedia Britannica 2009. Online.Tigris-Euphrates River System: Physical Features, available at: http://www.britannica.com/eb/article-9110543/Tigris-Euphrates-riversystem

ESA 2017. United 22Nations Department of Economic and Social Affairs.). Population Division. Retrieved 10 September, 2017.

Fanack, A. 2018. Chronicle of the Middle East & North Africa. accessed, March. https://fanack.com/iraq/geography/

Hui, S. C. and Cheung, K. P. 1997. Multi-year (MY) building simulation: Is it useful and practical? In: Proc. of the IBPSA Building Simulation Conference. Prague, Czech.

Hasson, A., Alaskari, A. and Jweeg, M. 2013. Energy balance on soil-tree canopy system through urban heat island mitigation. International Journal of Enhanced Research in Science and Technology, 2(1).

Hasson, A., Kubba, A. E., Kubba, A. I. and Hall, G. 2017. Heat balance and its effect on building types. journal of Civil Construction and Environmental Engineering, 2(1): 7-11.

Huld, T., Paietta, E., Zangheri, P. and Pascua, I. P. 2018. Assembling typical meteorological year data sets for building energy performance using reanalysis and satellite-based data. Atmosphere, 9(53): 1-22.

King, W. C., Eugene, J., West, P. P. N., Anderson, P. J., Cowher, D. D.,

Dalton, J. B., Gloede, J. S., Herl, B. K., Lahood, A., Lohman, A. D., Mangin, P. E., Malinowski, J. C., Palka, E. J., Pannell, R. P., Sampson, M. R. and Thompson, W. C. 2003. A Geography. Department of Geography & Environmental Engineering United States Military Academy Jon C Malinowski, USA.

Lam, J. C. 1995. Degree-day climate parameters for Hong Kong. International Journal of Ambient Energy, 16: 209-18.

Langston, G . and Ding, K. 2001. Sustainable Practices in the Built Environment. 1st ed., Routledge Publishing, UK.

Li, G. P. and Xiao, J. 2007. Diurnal variation of surface albedo and relationship between surface albedo and meteorological factors on the western Qinghai-Tibet Plateau. Scientia Geographica Sinica, 27(1): 63-67.

Muir, J. 2009. Iraq Marshes Face Grave New Threat. BBC News, 24 February, http://news.bbc.co.uk/2/hi/middle_east/7906512.stm .

Nste, N., Adhujari, R. S., Delpero, C., Leonforte, F. and Timis, I. 2017. Sustainable building design in Kenya. The 8th International Conference on Applied Energy-ICAE2016., Energy Procedia, 105: 2803-2810.

Omer, T. M. A. 2011. Eroding Soils and Expanding Deserts, Country Pasture/ Forage Resource Profile. FAO, Iraq.

Osman, Y., AL-Ansari, A., Abdellatif, M., Aljawad, S. and Knutsson, S. 2014. Expected future precipitation in central Iraq Using LARS-WG stochastic weather generator. Scientific Research Publishing Inc., 948-959.

Pike, P. 1994. Weather Data, Building Services Research and Information Association, Berkshire, England.

Prelgauskas, E. 2003. Arid climates and enhanced natural ventilation. Environment design guide, DES 20. Australian Institute of Architects, Melbourne.

Roaf, S. and Bairstow, A. 2008. The Oxford conference: a re-evaluation of education in architecture. WIT Press, Southampton., UK.

Rashid, H. A. 2014. Microclimatic Factors Effect on Productivity of Construction Industry. Open Journal of Civil Engineering, 173-180.

Rashid, H. A. 2014. Model tool for predicting of outdoor air temperatures on construction materials manufacture performance in Baghdad. ARPN Journal of Engineering and Applied Sciences, 9(7).

Schaaf, C. B., Cihlar, J., Belward, A ., Dutton, E. and Verstraete, M. 2009. Albedo and reflectance anisotropy in ECV-T8. GTOS Assessment of the Status of the Development of Standards for the Terrestrial Essential Climate Variables, 26-27, Rome, Italy.

Torrance, V. B. 1991. Buildings as climate modifiers. Energy and Buildings, 16 (3-4): 907-913.

USAID 2010. Climate Change Risk Profile: Iraq. United States Agency for International Development, USA.

Waro, H. and Mwasha, A. 2013. The impact of sustainable building envelope design on building sustainability using Integrated Performance Model. International Journal of Sustainable Built Environment, 2(2): 153-171.

Yang, H. and Lu, L. 2004. Study of typical meteorological years and their effect on building. American Society of Heating, Refrigerating and Air Conditioning Engineers. ASHRAE Transactions, 110(2): 424-431.

Zhang, C. C., Wang, X. Y. and Cui, Y. L. 2005. A study of the ground surface parameters in the Yellow River Delta using remote sensing data. Hydrology and Engineering Geology, 2: 71-75.

Zakaria, S., Al-Ansari, N. and Knutsson, S. 2013. Historical and future climatic change scenarios for temperature and rainfall for Iraq. Journal of Civil Engineering and Architecture, 7(12): 1574-1594.

Zareaian, S. and Zadeh, K. A. 2013. The role of climate factors on designing and constructing buildings (from urbanization architecture approach). Bulletin of Environment. Pharmacology and Life Sciences, 3: 197-200.

Diversity of Butterflies (Lepidoptera: Papilionoidea) in a Temperate Forest Ecosystem, Binsar Wildlife Sanctuary, Indian Himalayan Region

M. K. Arya†, A. Verma and P. Tamta

Insect Biodiversity Laboratory, Department of Zoology, D.S B. Campus, Kumaun University, Nainital-263002, Uttarakhand, India

†Corresponding author: M. K. Arya; dr.manojkumar19@rediffmail.com

ABSTRACT

Observational studies aiming to elucidate the differences in butterfly fauna along altitudinal gradients in Binsar Wildlife Sanctuary were carried out during 2014-2015. The study revealed a total of 2591 individuals belonging to 46 species and 35 genera under six families of butterflies. Four species under legal protection were also recorded. Family Nymphalidae was the most dominant with 22 species followed by Pieridae (12 species), Lycaenidae (4 species), Papilionidae, Riodinidae (3 species each) and Hesperiidae (2 species). Higher values of species richness, abundance and diversity were recorded for transects at the low altitudinal site. Species such as *Aglais caschmirensis* (Fruhstorfer), *Pieris canidia indica* Evans, *Pieris brassicae* Linnaeus and *Byasa polyeuctes letincius* (Fruhstorfer) were most abundant, while *Dodona ouida* Hewitson, *Udara dilectus* Moore, *Aulocera padama* Kollar, *Talicada nyseus* (Guérin-Méneville) and *Argynnis childreni* (Gray) accounting for 1.38% of the total individuals of butterflies, were least abundant species during the study period. Results of the study on diversity and distributions of butterflies are preliminary ones which would help in strengthening the biodiversity status of the Binsar Wildlife Sanctuary.

INTRODUCTION

The Indian Himalayan Region is a repository for rich biological diversity and to ensure its proper conservation, protected areas in the form of Biosphere Reserves, National Parks, Sanctuaries and Conservation Reserves have been established (Rodgers & Panwar 1988). Uttarakhand, the newest Himalayan state in India, stretching across 53,485 sq km, is blessed with ample natural resources and harbours a charismatic range of biodiversity. Almost 64.79% of its total geographical area is designated as forest area while forest cover is limited to 35% of the geographical area (FSI 2011). In recent decades, the state has witnessed a plethora of natural disasters aggravated by man-made factors which have affected the ecology of the region at a large scale (Tayal et al. 2015).

Despite the central role of nature reserves in global efforts for conservation of biodiversity, policies such as downgrading and downsizing of the protected areas have been contentiously adopted, especially in developing countries of the world (Mascia & Pailler 2010). Based on national priorities, the disparity in ranking the importance of protected areas underscore the need for resilient and robust conservation strategies which must be adopted in the present era with an unprecedented rate of biodiversity loss and extinction. The protected areas located in the Indian Himalayan Region especially those which are low profiled ones hold immense

potential to enhance the components of biological representativeness, integrity and human sustenance in the region (Rawal & Dhar 2001). Binsar Wildlife Sanctuary (hereafter referred as BWLS), which is a natural habitat for many species of flora and fauna has recently received the attention of the government and non-government organizations and is being developed as a hot tourist destination in the calm and pristine environment of the Kumaon Himalaya. From different *in situ* conservation sites of the Indian Himalayan Region, numerous scientific records regarding distribution and diversity of butterflies have been published by various workers (Arora 1994, Arora 1995, Uniyal & Mathur 1998, Joshi et al. 2004, Joshi 2007, Joshi & Arya 2007, Singh 2009, Joshi et al. 2008, Kumar 2008, Bhardwaj & Uniyal 2013, Pandey et al. 2013, Tewari & Rawat 2013, Qureshi et al. 2014, Arya 2015, Sondhi & Kunte 2016, Singh & Sondhi 2016, Arya & Dayakrishna 2017, Kumar et al. 2017). Till date, no comprehensive approaches have been made to understand butterfly diversity of the BWLS. Considering the importance of butterflies as efficient pollinators essential for continuity of the ecosystem services (Tiple et al. 2006), their ecological roles in the food web and as indicators (Kunte 2000, Hill et al. 2002), for promoting conservation programs (New 2011) and ecotourism as well (Arya et al. 2018), it is imperative to evaluate species composition, status and habitat preferences of butterflies from the present region. Moreover, butterflies, in

particular, are facing a threat of range contraction both across the latitudinal and altitudinal gradients due to global climate change. Thus steps of inventorizing biodiversity patterns along such gradients have strong conservation implications (Acharya & Vijayan 2015). Keeping this in view, the present study was primarily aimed at examining species composition and diversity of butterflies along altitudinal gradients in the BWLS for their future conservation in the protected area. The present study also aims to generate information for conservation authorities regarding the development and management of the sanctuary.

MATERIALS AND METHODS

Study Area

BWLS, with a total geographical area of 47.67 sq km is located in Almora and Bageshwar districts of the state Uttarakhand (Fig. 1). The sanctuary lies under geographical coordinates 29°39'-29°44'N and 79°41'-79°49'E and the altitude ranges between 1200 to 2500 m above sea level. BWLS represents one of the oldest protected landscapes in the Kumaon Himalayan region characterized by hilly terrains, ravines and ridges providing a wide array of microhabitats to diverse flora and fauna. Before India's independence in 1947, the study area was notified as the 'Protected Forest' in 1893 and later its status was revived as the 'Reserve Forest'

in 1897. After independence, the status was upgraded to 'Wildlife Sanctuary' by the Government of India in 1988. The region of BWLS is also renowned for its religious, historical, cultural and recreational values. The sanctuary is earmarked with two zones, core zone (4 sq km) and a buffer zone (43.67 sq km). Human activities are restricted in the core zone of the sanctuary which comprises biodiversity of strategic importance. The vegetation is represented by a characteristic moist temperate type of forest surrounded by villages and agricultural lands. The sanctuary is home to 40 species of trees, 26 shrubs, 50 herbs, 19 grasses and six ferns (Ilyas 1998) which are congenial for the survival of butterflies. The monthly mean temperature ranges from 2.2 to 15.5°C during winter and from 17.20 to 26.6°C during the summer season. The annual mean precipitation is about 1041.8 mm (Kala & Majila 2013).

Based on altitudinal variations, two distinct sites were selected for the sampling of butterflies. Two permanent transects with distinct habitat features each of length 800m on different altitudes were laid down at each study site. The characteristic features of each transect selected in the study site have been summarized in Table 1. Human activities such as agriculture practicing, livestock grazing and tourism are frequent at the lower altitudinal site, while the higher altitudinal site remained least disturbed during the observations made in the present study.
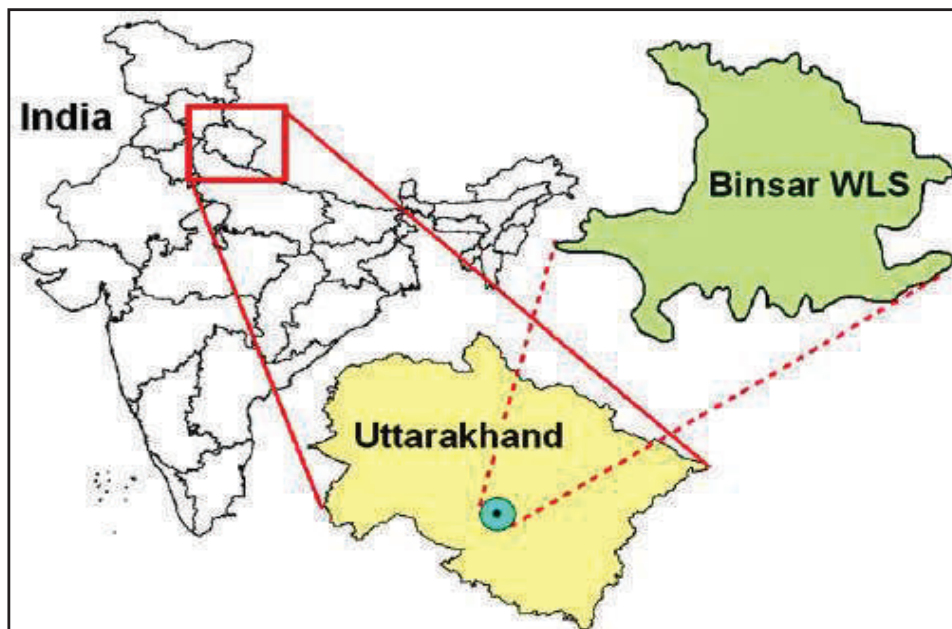
Fig. 1: Line drawing map showing the location of BWLS.

Sampling of Butterflies

Census on butterfly populations was undertaken in consecutive four days of each month at different sites of BWLS from July 2014 to June 2015. Both transects at lower altitudinal zone were walked with constant pace for one hour each between 08:30 hr to 11:30 hr and on the next day, between 12:00 hr to 15:00 hr for each sampling period. The same sampling method was followed for each transect at higher altitudinal zone from the next two consecutive days. 'Pollard Walk' method was adopted for the sampling of butterflies during cloudless days (Pollard 1979, Pollard & Yates 1993). The individuals of butterflies were counted up to 5m on both sides of each transect. Identification of butterflies was carried out in the field visually through photography and with the assistance of the field guides (Haribal 1992, Kehimkar 2014, Sondhi & Kunte 2018). Butterflies were neither killed nor collected during the present study. In the case, sight records where the identification was not possible, butterflies were captured by using the aerial net avoiding any harm and identified subsequently released at the same spot of capture. The climatic factors such as monthly temperature and relative humidity associated with each transect were also recorded using thermo-hygrometer.

Status of Butterflies

To determine the local status of the identified butterflies in the sanctuary, species were characterized into four groups based on the overall number of sightings in the study area, namely, fairly common (with more than 50 sightings), common (between 21-50 sightings), uncommon (between 11-20 sightings) and rare (with less than 10 sightings), respectively.

Similarity Index

The species composition between transects was measured using the formula of Magurran (1988): Similarity index (C) = 2c/a +b

Where, a is the number of species in area A; b is the number of species in area B; c is the number of shared species between the two areas.

Statistical Analysis

Data were pooled to compare the diversity of butterflies across different sites along altitudes. Various measures of diversity (Simpson, Shannon-Weiner, evenness, Margalef and Berger Parker) were computed by using the program PAST 3.4 (Hammer et al. 2014). Bray Curtis cluster and their similarity matrix of butterflies across different transects were analyzed with the help of ecological analysis software, BIODIVERSITY PRO VERSION 2 (Lambshead et al. 1997).

RESULTS AND DISCUSSION

During the study, a total number of 2591 individuals belonging to 46 species and 35 genera under six families of butterflies were counted from four permanent transects with 24 species common to all transects (Tables 2 and 3). Family Nymphalidae was the most dominant with 18 genera and 22 species followed by Pieridae (8 genera, 12 species), Lycaenidae (4 genera, 4 species), Papilionidae (2 genera, 3 species), Riodinidae (1 genus, 3 species) and Hesperiidae (2 genera, 2 species). Such variations at both generic and species levels, especially among butterfly communities, reflect the habitat complexity and range of larval host plants available in the

Table 1: Characteristic features of selected study sites in the BWLS.

Sampling Sites		Altitude (m a.s.l.)	Temp. Range (°C)	Relative Humidity (%)	Habitat characteristics and major vegetation
Low Altitude (1200-1700 m)	Transect 1 (Ayarpani)	1250	9-29	30-75	Pine dominant with large canopy gaps forest; *Pinus roxburghii, Pyrus pashia, Myrica esculenta, Quercus leucotrichophora, Cornus macrophylla, Berberis asiatica*
	Transect 2 (Binneshwar Mahadev)	1650	8.3-27	56-88	Oak forest with moderate canopy gaps; *Quercus semicarpifolia, Quercus leucotrichophora, Quercus floribunda, Aesculus indica, Juglans regia, Rubus ellipticus*
High Altitude (2100-2500 m)	Transect 3 (Jhandidhar)	2100	6-26	57-89	Oak-Deodar forest with dense canopy cover; *Quercus semicarpifolia, Quercus floribunda, Cedrus deodara, Daphne papyracea, Deutzia staminea*
	Transect 4 (Zero point)	2500	5.5-24	57.8-90	Hilltop grassland surrounded with *Quercus semicarpifolia, Rhododendron arboreum* and *Cedrus deodara*

Table 2: Butterfly species composition and their relative abundances at four transects in BWLS.

S.No.	Lepidoptera: Papilionoidea	Low Altitude Site			High Altitude Site			Relative Abundance (%)	Status
		T 1	T 2	Total	T 3	T 4	Total		
	Family: Nymphalidae								
1	*Aglais cashmirensis* (Fruhstorfer)	170	120	290	90	48	138	16.51	FC
2	*Argynnis childreni* (Gray)	6	3	9	-	-	-	0.34	R
3	*Argynnis hyperbius* Linnaeus	17	11	28	10	6	16	1.69	C
4	*Aulocera swaha* Kollar	35	16	51	15	4	19	2.70	FC
5	*Aulocera padma* Kollar	-	-	-	6	2	8	0.30	R
6	*Callerebia annada* (Moore)	17	16	33	12	5	17	1.92	C
7	*Callerebia scanda* (Kollar)	12	10	22	8	7	15	1.42	C
8	*Danaus chryssippus* (Linnaeus)	14	6	20	-	-	-	0.77	UC
9	*Euploea core* (Cramer)	35	16	51	-	-	-	1.96	FC
10	*Junonia iphita* Cramer	17	13	30	11	10	21	1.96	FC
11	*Kallima inachus* Boisduval	-	-	-	20	9	29	1.11	C
12	*Kaniska canace* (Linnaeus)	12	5	17	4	2	6	0.23	C
13	*Lasiommata schakra* (Kollar)	8	3	11	-	-	-	0.42	UC
14	*Lethe verma* Kollar	20	9	29	7	6	13	1.62	C
15	*Neptis sankara* (Kollar)	8	4	12	2	2	4	0.61	UC
16	*Neptis zaida* Westwood	20	-	20	10	5	15	1.35	C
17	*Peudergolis wedah* (Kollar)	12	6	18	-	-	-	0.69	UC
18	*Phalanta phalantha* (Drury)	28	14	42	-	-	-	1.62	C
19	*Sephisa dichroa* (Kollar)	6	2	8	3	2	5	0.50	UC
20	*Vanessa cardui* Linnaeus	25	11	36	10	7	17	2.04	FC
21	*Vanessa indica* Herbst	20	10	30	10	5	15	1.73	C
22	*Ypthima nareda nareda* (Kollar)	13	4	17	3	1	4	0.81	C
	Family: Pieridae								
23	*Belenois aurota* (Fabricius)	36	14	50	-	-	-	1.92	C
24	*Catopsilia pomona* Linnaeus	40	20	60	-	-	-	2.31	FC
25	*Colias fieldi* Menetries	17	8	25	8	7	15	1.54	C
26	*Eurema brigitta rubella* Wallace	12	6	18	9	5	14	1.23	C
27	*Eurema hecabe* Linnaeus	26	12	38	-	5	5	1.65	C
28	*Eurema laeta* Boisduval	16	7	23	10	6	16	1.50	C
29	*Gonepteryx rhamni nepalensis* Linnaeus	33	17	50	15	9	24	2.85	FC
30	*Aporia agathon agathon* (Gray)	-	10	10	10	2	12	0.84	C
31	*Aporia agathon phryxe* (Boisduval)	18	9	27	-	-	-	1.04	C
32	*Pieris brassicae* Linnaeus	65	50	115	42	38	80	7.52	FC
33	*Pieris canidia indica* Evans	100	96	196	82	38	120	12.19	FC
34	*Pontia daplidice* (Linnaeus)	-	-	-	12	3	15	0.57	UC
	Family: Lycaenidae								
35	*Heliophorus sena* Kollar	64	59	123	33	22	55	6.86	FC
36	*Lycaena panava* (Kollar)	31	16	47	-	10	10	2.04	FC

S.No.	Lepidoptera: Papilionoidea	Low Altitude Site			High Altitude Site			Relative Abundance (%)	Status
		T 1	T 2	Total	T 3	T 4	Total		
37	Talicada nyseus (Guérin-Méneville)	6	2	8	1	-	1	0.34	R
38	*Udara dilectus* Moore	-	-	-	5	-	5	0.19	R
	Family: Papilionidae								
39	*Byasa polyeuctes letincius* (Fruhstorfer)	37	30	67	10	7	17	3.24	FC
40	*Papilio bianor polyctor* Boisduval	23	20	43	15	7	22	2.50	FC
41	*Papilio polytes* Linnaeus	29	21	50	10	-	10	2.31	FC
	Family: Riodinidae								
42	*Dodona durga durga* (Kollar)	20	10	30	10	5	15	1.73	C
43	*Dodona eugenes* Bates	12	6	18	6	3	9	1.04	C
44	*Dodona ouida* Hewitson	5	-	5	-	-	-	0.19	R
	Family: Hesperiidae								
45	*Ochlodes brahma* Moore	10	6	16	-	-	-	0.61	UC
46	*Tagiades cohaerens cynthia* Evans	6	5	11	-	-	-	0.42	UC
	Total	1101	703	1804	499	288	787		

Abbreviations: T 1 = Transect 1; T 2 = Transect 2; T 3 = Transect 3; T 4 = Transect 4; FC = Fairly common; C = Common; UC = Uncommon and R = Rare

region (Chowdhury 2014). In terms of the total number of individuals reported, Nymphalidae was the most dominant family (43.07% of the total number of individuals), followed by Pieridae (35.24%), Lycaenidae (9.61%), Papilionidae (8.07%), Riodinidae (2.97%) and Hesperiidae (1.04%), respectively (Table 3). Such domination of Nymphalid butterflies might be due to the polyphagous nature of their larval forms and similar pattern with the predominance of family Nymphalidae have also been extensively registered from different protected areas of Uttarakhand (Joshi 2007, Joshi & Arya 2007, Joshi et al. 2008, Kumar 2008, Singh 2009, Bhardwaj & Uniyal 2013, Uniyal et al. 2013). As far as knowledge on butterfly diversity from BWLS is concerned, it is important to mention here that the present study is the first constituting systematic survey based on standardized methods. Due to differences in habitat and sampling time and efforts, it would be inappropriate to make quantitative comparisons in the diversity of butterflies from other protected areas of Uttarakhand. However, the richness of butterfly

fauna in BWLS was fairly higher when compared to the nearby protected area, Askot Wildlife Sanctuary, with known records of 32 species so far (Pandey et al. 2013). Similarly, Arya & Dayakrishna (2017) reported 36 species of butterflies from Nandhaur Wildlife Sanctuary located at foothills of the Kumaon Himalayan Region. Also, Smetacek (2012) reported 243 species of butterflies from Nainital district in the Kumaon region during 1951-2010, which is a long term survey compared to the short term survey conducted in the current research.

Based on the observations, *Aglais caschmirensis* Kollar was the most abundant and frequently sighted species in all transects constituting 16.51% of the total individuals of butterflies recorded in the present study. The other frequently observed butterflies in the sanctuary includes species such as *Aulocera swaha* Kollar, *Junonia iphita* Cramer, *Vanessa cardui* Linnaeus, *Gonepteryx rhamni nepalensis* Linnaeus, *Pieris brassicae* Linnaeus, *Pieris canidia indica* Evans, *Heliophorus sena* Kollar, *Byasa polyeuctes letincius*

Table 3: Number of genera, species and individuals of different families of butterflies recorded from BWLS.

S. No.	Family	Number		
		Genera	Species	Individuals
1	Nymphalidae	18	22	1116
2	Pieridae	8	12	913
3	Lycaenidae	4	4	249
4	Papilionidae	2	3	209
5	Riodinidae	1	3	77
6	Hesperiidae	2	2	27

(Fruhstorfer) and *Papilio bianor polyctor* Boisduval. These species exhibited a declining trend in their abundance across transects that were laid along increasing altitudes. On the other hand, five species were recorded as rare including *Dodona ouida* Hewiston, *Udara dilectus* Moore, *Aulocera padama* Kollar, *Talicada nyseus* (Guerin-Meneville) and *Argynnis childreni* (Gray), which altogether accounted for 1.38% of the total individuals of butterflies recorded during the study period. These species were reported rarely from one or two transects. Butterfly species composition of sites at a lower and higher elevation was rather similar (similarity index of 0.789) and this was true across all three dominant families with similarity indices of Nymphalidae 0.777, Pieridae 0.8 and Lycaenidae 0.857.

Transect 1 supported maximum numbers of species of butterflies (41 species), followed by Transect 2 (40 species), Transect 3 (32 species) and Transect 4 (31 species), respec-

tively. Twelve species of butterflies were recorded from transects at the lower altitudinal site (Transect 1 and 2) with the most frequently and commonly observed species among them being *Belenois aurota* (Fabricius), *Catopsilia pomona* Linnaeus, *Aporia agathon phryxe* (Boisduval), *Euploea core* (Cramer), *Phalanta phalantha* (Drury) while species such as *Lasiommata schakra* (Kollar), *Danaus chryssippus* (Linnaeus), *Pseudoergolis wedah* (Kollar), *Ochlodes brahma* Moore and *Tagiades cohaerens cynthia* Evans were recorded occasionally with 11 to 20 number of sightings. Four species of butterflies *Aulocera padama* Kollar, *Kallima inachus* Boisduval, *Pontia daplidice* (Linnaeus) and *Udara dilectus* Moore with varied degree of recorded relative abundance were restricted to the higher altitudinal site. In comparison with the findings of Hannyngton (1910-11), all recorded species have a wide distribution in the Kumaon Himalayan region. No endemism in the species was recorded. However,

Table 4: Various diversity indices calculated for the butterfly community across different transects in BWLS.

| Diversity indices	Transect 1	Transect 2	Transect 3	Transect 4	Low Altitude Site	High Altitude Site
Species number	41	40	32	31	42	34
Individuals	1101	703	499	288	1804	787
Simpson D	0.947	0.9293	0.9179	0.9205	0.9412	0.9204
Shannon- Wiener	3.339	3.138	2.959	2.942	3.283	2.993
Evenness	0.6872	0.5765	0.6026	0.6115	0.6345	0.5864
Margalef	5.711	5.949	4.99	5.298	5.468	4.949
Berger Parker	0.1544	0.1707	0.1804	0.1667	0.1608	0.1753
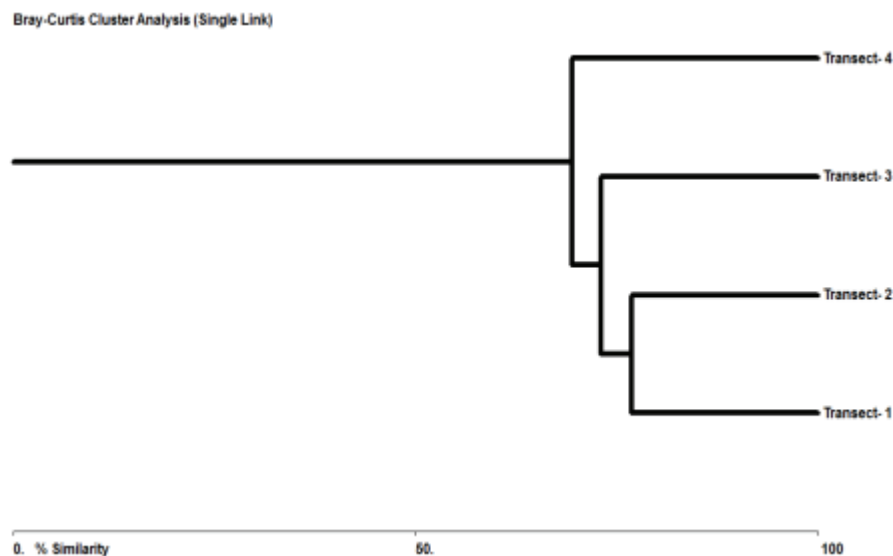
Fig. 2: Bray Curtis cluster analysis of quantitative data on butterflies.

five species are legally protected under the Indian Wildlife Protection Act of 1972 namely, *Neptis sankara* (Kollar) under Schedule I, *Aporia agathon agathon* (Gray), *Neptis zaida* Westwood and *Pontia daplidice* (Linnaeus) under Schedule II and *Euploea core* (Cramer) under Schedule V (Anonymous 2006).

It is a well-studied aspect of Lepidopteran ecology that habitats at the lower elevations yield more number of species than those at the higher elevations (Lien 2013). The significant differences in the values of the Shannon diversity index as a measure of alpha diversity along altitudes were observed during the study period (Table 4). The calculated diversity value was higher for Transect 1 (3.339), followed by Transect 2 (3.138), Transect 3 (2.959) and Transect 4 (2.942), respectively. The low dominance values indicate that species of butterflies were distributed more or less evenly across transects. Such values indicate a significant decrease in species richness and diversity of butterflies with the increase in altitude supporting the observations made by Lewis et al. (1998), Lien (2013) and Joshi & Arya (2007). The similarity of species composition among different transects has also been presented in Fig. 2. The similarity matrix from the quantitative data showed that taxonomic composition of butterflies was much similar in the mixed oak forests of transects that were laid at the lower altitudinal site, corresponding to the value of 76.82%, followed by Transect 2 and Transect 3 with a similarity index value of 73.04%. Transect 4 laid at high altitude in the hilltop grassland stood out clearly showing linkage at the similarity matrix value of 39.16%. The overall observations made in the present study suggest that habitat complexity, floral diversity and climatic variables such as temperature and relative humidity associated with each transect might act as major drivers and determinants of the altitudinal patterns of butterfly assemblages in the sanctuary.

Protected areas are critical for nature conservation and maintaining ecosystem services and thus inventorying biodiversity in such zones is of prime importance (Vina & Liu 2017). Owing to the diversified vegetation pattern along altitudes, the sanctuary provides sufficient natural resources required for survival of a good range of butterflies throughout the year. Despite the religious, cultural and biological significance of the BWLS, it remained a low profiled protected area of the state Uttarakhand. The unplanned and improper tourism management and tremendous pressure from factors such as slash and burn system, the prevalence of frequent forest fires especially in the pine forests during summers, overgrazing mainly close to the lower altitudinal zone of the sanctuary, pose potential threats of regional loss and extinction of biodiversity. Thus, our study suggests that the region must be monitored for other biological resources which would assist in managing and preserving endangered

flora and fauna as well as in strengthening the status of the sanctuary. The preliminary results on butterflies revealed in the present study are also expected to provide necessary information to the conservation planning authorities for proper management of the BWLS while also allowing scope and direction for future research and opportunities of ecotourism in the sanctuary.

ACKNOWLEDGMENTS

REFERENCES

Acharya, B.K. and Vijayan, L. 2015. Butterfly diversity along the elevation gradient of Eastern Himalaya, India. Ecological Research, 30: 909-919.

Anonymous 2006. The Wildlife (Protection) Act, 1972. Natraj Publishers, Dehradun, pp. 253.

Arora, G.S. 1995. Lepidoptera: Rhopalocera. In: Fauna of Nanda Devi Biosphere Reserve, Ecosystem Series. Zoological Survey of India, Calcutta, 1, pp. 61-73.

Arora, G.S. 1994. Lepidoptera: Butterflies. In: Fauna of Rajaji National Park, Fauna of Conservation Areas. Zoological Survey of India, Calcutta, 5, pp. 245-300.

Arya, M.K., Verma, A. and Neha 2018. Biodiversity assessment of butterflies in Kumaun Lesser Himalayan oak forest for promoting ecotourism at city Nainital. Journal of Himalayan Ecology and Sustainable Development, 13: 75-95.

Arya, M.K. 2015. Observations on trophic levels of different groups of insect population vis a vis insect pollinators in a protected forest ecosystem in the Western Himalayas. Journal of Experimental Zoology India, 18(1): 271-277.

Arya, M.K. and Dayakrishna 2017. Species richness and diversity of butterflies in the landscape of Nandhaur Wildlife Sanctuary, Nainital, Uttarakhand. Journal of Environment and Bio-Sciences, 31(2): 307-315.

Bhardwaj, M. and Uniyal, V.P. 2013. High-altitude butterfly fauna of Gangotri National Park, Uttarakhand: Patterns in species, abundance composition and similarity. Envis Bulletin: Arthropods and Their Conservation in India (Insects and Spiders), 14(1): 38-48.

Chowdhury, S. 2014. Butterflies of Sundarban Biosphere Reserve, West Bengal, Eastern India: A preliminary survey of their taxonomic diversity, ecology and their conservation. Journal of Threatened Taxa, 6(8): 6082-6093.

FSI 2011. State of Forest Reports, Forest Survey of India, Dehradun, India.

Hammer, O., Harper, D.A.T. and Ryan, P.D. 2014. PAST-PAlaeontological STatistics Version 3.04.

Hannyngton, F. 1910-11. Butterflies of Kumaun. Journal of Bombay Natural History Society, 20(3): 871-872.

Haribal, M. 1992. The Butterflies of Sikkim: Himalayas and their Natural History. Sikkim Nature Conservation Foundation, Gangtok, Sikkim, pp. 217.

Hill, J.K., Thomas, C.D., Fox, R., Telfer, M.G., Willis, S.G., Asher, J. and Huntley, B. 2002. Responses of butterflies to twentieth century climate warming: Implications for future ranges. Proceedings of Royal Society B, 269: 2163-2171.

Ilyas, O. 1998. People and Protected Area-The case of Binsar Wildlife Sanctuary. World Wide Fund for Nature-New Delhi, India, pp. 54.

Joshi, P.C. and Arya, M. 2007. Butterfly Communities along altitudinal gradients in a Protected Forest in the Western Himalayas, India. The Natural History Journal of Chulalongkorn University, 7(1): 1-9.

Joshi, P.C. 2007. Community structure and habitat selection of butterflies in Rajaji National Park, a moist deciduous forest in Uttaranchal, India. Tropical Ecology, 48(1): 119-123.

Joshi, P.C., Kothari, K., Badoni, V.P., Arya, M. and Agarwal, A. 2004. Species composition and density of entomofauna vis a vis altitudinal variations and disturbances in Nanda Devi Biosphere Reserve, Uttaranchal, India. Asian Journal of Microbiology, Biotechnology and Environmental Science, 6(2): 301-308.

Joshi, P.C., Kumar, K. and Arya, M. 2008. Assessment of insect diversity along an altitudinal gradient in Pindari forests of Western Himalaya, India. Journal of Asia-Pacific Entomology, 11: 5-11.

Kala, C.P. and Majila, B.S. 2013. Status of the forest and wildlife in the Binsar Wildlife Sanctuary. In: Kala, C.P., and Silori, C.S. (eds.), Biodiversity Communities and Climate Change. TERI Publication, New Delhi, India, pp. 25-35.

Kehimkar, I. 2014. The Book of Indian Butterflies. Bombay Natural History Society: Oxford University Press, pp. 497.

Kumar, K., Joshi, P.C. and Arya, M. 2017. Variation in population density and biomass of butterflies in Nanda Devi Biosphere Reserve (NDBR), West Himalaya, Uttarakhand. Journal of Environment & Bio-Sciences, 31(1): 9-16.

Kumar, P. 2008. Insecta: Lepidoptera (Rhopalocera). In: Fauna of Corbett Tiger Reserve, Conservation Area Series. Zoological Survey of India, Kolkata, 35, pp. 205-220.

Kunte, K. 2000. Butterflies of Peninsular India. Universities Press, Hyderabad.

Lambshead, P.J.D., Paterson, G.L. J. and Gage, J.D. 1997. Biodiversity Professional, Version 2.0. The Natural History Museum and The Scottish Association for Marine Science.

Lewis, O.T., Wilson, R.J. and Harper, M.C. 1998. Endemic butterflies on Grande Comore: Habitat preferences and conservation priorities. Biological Conservation, 85: 113-121.

Lien, V.V. 2013. The effect of habitat disturbance and altitudes on the diversity of butterflies (Lepidoptera: Rhopalocera) in a tropical forest of Vietnam: Results of a long-term and large scale study. Russian Entomological Journal, 22 (1): 51-65.

Magurran, A.E. 1988. Ecological Diversity and its Measurement. Princeton University Press, Princeton, New York.

Mascia, M.B. and Pailler, S. 2010. Protected area downgrading, downsizing and degazettement (PADDD) and its conservation implications. Conservation Letters, 00: 1-12.

New, T.R. 2011. Launching and steering flagship Lepidoptera for conservation benefit. Journal of Threatened Taxa, 3(6): 1805-1817.

Pandey, P., Joshi, P.C. and Kaushal, B.R. 2013. Role of insects in sustaining

a forest ecosystem in Western Himalaya, India. Journal of Applied Biosciences, 39(1): 1-22.

Pollard, E. 1979. A national scheme for monitoring the abundance of butterflies. The First Three Years British Entomological and Natural History Society. Proceedings and Transactions, 12: 77-99.

Pollard, E. and Yates, T.J. 1993. Monitoring butterflies for Ecology and Conservation. Chapman and Hall, London.

Qureshi, A.A., Bhagat, R.C. and Bhat, D.M. 2014. Diversity of butterflies (Lepidoptera: Papilionoidea and Hesperoidea) of Dachigam National Park, Jammu and Kashmir, India. Journal of Threatened Taxa, 6(1): 5389-5392.

Rawal, R.S. and Dhar, U. 2001. Protected area network in Indian Himalayan region: Need for recognizing values of low profile protected areas. Current Science, 81(2): 175-184.

Rodgers, W.A. and Panwar, H.S. 1988. Planning a Wildlife Protected Area Network in India. Vol. I. The Report, Wildlife Institute of India, Dehradun.

Singh, A.P. 2009. Butterflies of Kedarnath Musk Deer Reserve, Garhwal Himalaya, India. Journal of Threatened Taxa, 1(1): 37-48.

Singh, A.P. and Sondhi, S. 2016. Butterflies of Garhwal, Uttarakhand, Western Himalaya, India. Journal of Threatened Taxa, 8(4): 8666-8697.

Smetacek, P. 2012. Butterflies (Lepidoptera: Papilionoidea and Hesperoidea) and other protected fauna of Jones Estate, a dying watershed in the Kumaon Himalaya, Uttarakhand, India. Journal of Threatened Taxa, 4(9): 2857-2874.

Sondhi, S. and Kunte, K. 2016. Butterflies (Lepidoptera) of the Kameng protected area complex, Western Arunachal Pradesh, India. Journal of Threatened Taxa, 8 (8): 9053-9124.

Sondhi, S. and Kunte, K. 2018. Butterflies of Uttarakhand- A Field Guide. Bishen Singh Mahendra Pal Singh (Dehradun), Titli Trust (Dehradun) National Centre for Biological Sciences (Bengaluru), pp. 310.

Tayal, A., Nirwani, D. and Jabin, S. 2015. Disaster Management–Uttarakhand floods in India a case study. Journal of Energy Research and Environmental Technology, 2(2): 89-93.

Tewari, R. and Rawat, G.S. 2013. Butterfly fauna of Jhilmil Jheel Conservation Reserve, Haridwar, Uttarakhand, India. Biological Forum: An International Journal, 5(2): 22-26.

Tiple, A.D., Deshmukh, V.P. and Dennis, R.L.H. 2006. Factors influencing nectar plant resource visits by butterflies on a university campus: implications for conservation. Nota Lepidopteralogica, 28(3/4): 213-224.

Uniyal, V.P. and Mathur, P.K. 1998. Diversity of butterflies in the great Himalayan National Park, Western Himalaya. Indian Journal of Forestry, 21(2): 150-155.

Uniyal, V.P., Bhardwaj, M. and Sanyal, A.K. 2013. An Assessment of Entomofauna for Management and Conservation of Biodiversity in the Gangotri Landscape. Annual Progress Report, Wildlife Institute of India, Dehradun, pp. 237.

Vina, A. and Liu, J. 2017. Hidden roles of protected areas in the conservation of biodiversity and ecosystem services. Ecosphere, 8(6): 1-16.

Capital Enrichment, Innovation Capability and Environmental Pollution Effect: Evidence from China's Manufacturing Industry

Fengju Xu*, Lina Ma*, Xiaoying Li**† and Najaf Iqbal***

*Wuhan University of Technology, Hubei, Wuhan, 430070, China
**Changjiang Polytechnic, Hubei, Wuhan, 430070, China
***Hunan University of Arts and Science, Hunan, Changde, 415000, China
†Corresponding author: Xiaoying Li; 603700103@qq.com

ABSTRACT

In recent years, the issue of environmental pollution caused by the manufacturing industry has been widely criticized. To explore the relationship between capital enrichment and environmental pollution, the mediating effect model was constructed by using the panel data of 28 sub-sectors of China's manufacturing industry from 2011 to 2017. Results show that the phenomenon of capital enrichment is mainly concentrated in industries with high-profit margins, intensive technology, national policy support, and resource or national monopolistic positions. Both capital enrichment and innovation capability have a promotion effect on inhibiting environmental pollution, but with the decline of innovation capability, the effect of capital enrichment on pollution weakens. Innovation capability plays a mediating role, which leads to the mechanism of capital enrichment → innovation capability → environmental pollution. The impact of capital enrichment on environmental pollution under different levels of innovation capability is heterogeneous, and the effect is stronger in high-tech industries.

INTRODUCTION

Since the national reforms and opening-up policies of 1978, the demographic dividends and the low-cost advantages of primary production factors have resulted in the rapid development of China's manufacturing industry. The world-class manufacturing centres are formed in the regions of Bohai Rim, the Pearl River Delta, and the Yangtze River Delta in China. In a matter of three decades, China has been developed into the world's largest manufacturing factory, leading to the rapid growth of China's economy. However, for a long time, the development of China's manufacturing industry has relied heavily on the cheap labour, land and other natural resources, and a high tolerance for environmental pollution. It is an extensive growth pattern that relies heavily on inputs, cost-competitive strategies, high energy consumption resulting in serious environmental pollution issues and low resource-utilization. The innovation has remained far slower than the rate of environmental degradation resulting in the practical dilemma of high levels of pollution.

Given the background of constructing the spatial patterns of saving resources and protecting the environment, scholars have begun to pay attention to the relationship between capital enrichment and pollution caused by the manufacturing industry. However, the existing literature mainly focuses on the impact of FDI, human capital, and financial capital on the environment (Al-Mulali et al. 2015), without reaching any consistent conclusions. The systematic analysis of the internal interaction mechanism between capital enrichment and environmental pollution is far less addressed. Another interesting variable is innovation ability which is also under-discussed in the context of rising productivity levels, capital accumulation and pollution effects. Only on the premise of continuous improvement of innovation capability, it plays a role in environmental pollution (Schot et al. 2018), because capital is the material basis for technology innovation. When capital enrichment is at a high level, its support for innovation activities is strong, resulting in the spillover effects for green technologies. The phenomenon of green production can reduce and ultimately eliminate the negative effects on the environment and promote the manufacturing industry to realize the economic and ecological benefits of the resources.

Capital is the material guarantee for innovation capability largely, and innovation capability is the most important way to reduce environmental pollution (Zailani et al. 2015). However, ignoring this important nexus, existing studies focus on the single perspective of capital and pollution or innovation and pollution, and rarely integrate capital and innovation capability into one framework to analyze their impact on environmental pollution. The capital, innovation, and environmental pollution may form a complete framework, but

the existing research ignores the interaction between these variables and lacks the discussion on the mediating effect of innovation capability. This study builds the logical framework of capital enrichment → innovation capability → environmental pollution and analyzes the internal mechanism. It also investigates the pollution effects resulting from capital under different levels of innovation capability.

PAST STUDIES AND HYPOTHESIS DEVELOPMENT

On the relationship between capital and pollution, existing scholars mainly focus on the perspective of foreign capital and human capital. The foreign capital entering the Chinese market brought green production technology, scientific management experience and global unified environmental standards, resulting in the positive environmental effects. Industries with higher levels of foreign investment have fewer pollutant emissions. The above-mentioned studies can be described as the phenomenon of pollution halo. Liang (2014) also supported the conclusion that foreign capital could increase resource efficiency through technology diffusion and reducing sulfur dioxide emissions. The human capital perspective determines the ability of a country to absorb and diffuse technology (Xu et al. 2020), which is more likely to support enterprises to use new technologies for promoting the green environmental production.

The relationship between the development of manufacturing industry, resource consumption, and pollution emissions in China has recently gained the attention of eminent scholars. The environment has been incorporated into the economic growth model as a factor of production. Factor endowment, especially the material capital determines the comparative advantage of polluting industries. Rubashkina et al. (2014) found that the influence of manufacturing with different endowment advantages on environmental pollution is heterogeneous. Capital enrichment weakens the carbon emission intensity and causes a change from negative to positive environmental effects. With the development of China's financial market, companies can absorb more capitals (Frankel et al. 1999), and promote the inhibition of environmental pollution by using clean energy or technology. So, the following hypothesis is proposed.

Hypothesis 1: Capital Enrichment Reduces the Degree of Environmental Pollution

According to Schumpeter's augmentation model and the Neo-Classical growth model, innovation plays the essential impact on capital enrichment (Xu et al. 2020). Insufficient capital may reduce the probability of innovative projects and inhibit innovation output. In China's financial environment where the capital supply is not completely market-oriented, the innovation capability of enterprises is greatly constrained by this supply shortage. Relying solely on their internal resources will not be enough to meet the fast-growing market requirements where the cost of innovation is fairly high. With an increase in innovation capability and favourable national policies, more market potential is released and the support of capital resources for innovation is strengthened (Xiong et al. 2020). The source of the innovation capital gradually shifts to the diversified sources including the capital market, government agencies and its affiliates (Du et al. 2020). A high level of innovation capability encourages firms to invest more capital in innovation activities, producing cyclic effects. Rodrigo-Alarcón et al. (2017) also emphasized the role of social capital in promoting innovation capability.

There are a few studies available in the literature on the relationship between innovation capability and environmental pollution, and most of these present the perspective of technological progress. The positive and promotional effect is controversial (Fagerberg et al. 2013, Schmidt et al. 2019). As the emission and pollution reduction caused by the innovation is realized through stimulating the innovation compensation effect which is the core factor for improving market competitiveness. The innovation is the main reason for reducing the intensity of energy consumption and it shows a tendency of energy conservation. Zailani et al. (2015) took the automobile manufacturing industry as research samples and found that the innovation and application of green technology can significantly improve environmental performance. However, some believe that the inhibitory effect of innovation capability on environmental pollution is limited. Since the total amount of environmental pollution is increasing (Schmidt et al. 2019), the sustainable development of the whole society should be achieved through innovative transformation (Fagerberg et al. 2013, Schot et al. 2018).

From the practice of China's manufacturing industry, innovation-driven is the breakthrough for its sustainable development and also the key to moving it towards the high-end of the global value chain. It means that a large number of traditional workers may gradually be replaced by a small number of modern knowledge-based workers. With the improvement of capital in the manufacturing industry, the intensity of investment in innovation has been continuously rising. Enterprises have effectively reduced the emissions of environmental pollution by adopting advanced pollution control technologies, green production, and environmental management measures. Therefore, this study argues that the innovation capability of the manufacturing industry can cause a reduction in environmental pollution, and the innovation capability may play a mediating role between the relationship

of capital enrichment and environmental pollution. So the following hypothesis is proposed.

Hypothesis 2: Innovation Capability Plays a Mediating Role Between the Relationship of Capital Enrichment and Environmental Pollution

Methodology

Modelling: To investigate the impact of the manufacturing industry's capital enrichment on environmental pollution, the following basic model is constructed.

$$EP_{i,t} = \beta_0 + \beta_1 CE_{i,t} + Controls_{i,t} + \varepsilon_{i,t} \qquad ...(1)$$

Where $EP_{i,t}$ is the environmental pollution of the ith manufacturing industry at time t, CE is the capital enrichment, β is a constant term, and ε is the random error term. Adopted from Abbasi et al. (2016) and Li et al. (2020), the following variables are controlled: human capital intensity (Human), degree of openness (Open), R&D intensity (RD), fixed asset investment (Asset), and firm-scale (Size). To examine the hypothesis proposed above, innovation capability is first included in the equation then capital enrichment is introduced to construct a new equation. To examine the channel effect, the interactive item $CE^* IC$ is introduced and the centralization method is used to avoid multicollinearity issues possibly caused by introducing the interaction term (Dalal et al. 2012).

$$EP_{i,t} = \beta_0 + \beta_1 IC_{i,t} + Controls_{i,t} + \varepsilon_{i,t} \qquad ...(2)$$

$$EP_{i,t} = \beta_0 + \beta_1 CE_{i,t} + \beta_2 IC_{i,t} + \Sigma Control + \varepsilon_{i,t} \qquad ...(3)$$

$$EP_{i,t} = \beta_0 + \beta_1 CE_{i,t} + \beta_2 IC_{i,t} + \beta_3 CE_{i,t}^* IC_{i,t} + \Sigma Control + \varepsilon_{i,t} \qquad ...(4)$$

To test the mediating effect of innovation capability on the relationship between capital enrichment and RP, the following model is constructed by adopting from the mediating effect test method.

$$EP_{i,t} = \beta_0 + \beta_1 CE_{i,t} + \Sigma Control + \varepsilon_{i,t} \qquad ...(5)$$

$$IC_{i,t} = \gamma_0 + \gamma_1 CE_{i,t} + \Sigma Control + \varepsilon_{i,t} \qquad ...(6)$$

$$EP_{i,t} = \mu_0 + \mu_1 CE_{i,t} + \mu_2 IC_{i,t} + \Sigma Control + \varepsilon_{i,t} \qquad ...(7)$$

Where β_1 is the total effect of capital enrichment on environmental pollution, μ_1 is the direct effect of capital enrichment on environmental pollution, $\gamma_1\mu_2$ is the mediating effect and its relative value is the ratio of the mediating effect to the total effect.

Data sources: Consistent with the 2012 industry classification standard of the China Securities Regulatory Commission (CSRC), this study finally selects 28 manufacturing industry segments.

The sample period ranges from 2011 to 2017 and missing values are calculated (included) by linear interpolation. All data are from the National Bureau of Statistics, the China Statistical Yearbook, China Energy Statistical Yearbook, China Environmental Statistical Yearbook, and the China Science and Technology Statistical Yearbook.

Variables: *Capital Enrichment of manufacturing industry*: The capital enrichment results from a constant accumulation of the capital inflows. This study analyzes the capital distribution in China's manufacturing industry to determine whether there is an objective phenomenon of capital enrichment or not. The average annual capital distribution of 28 manufacturing segments from 2011 to 2017 is shown in Fig. 1.

As evident from Fig. 1, it shows that the total capital of certain industries exceeds the industry median irrespective of the benchmark chosen (total capital of the industry, the capital owned by a single enterprise/the capital occupied by the industrial added value of RMB 100 million). Therefore, the phenomenon of capital enrichment exists objectively, which is the result of excessive capital inflows to an industry.
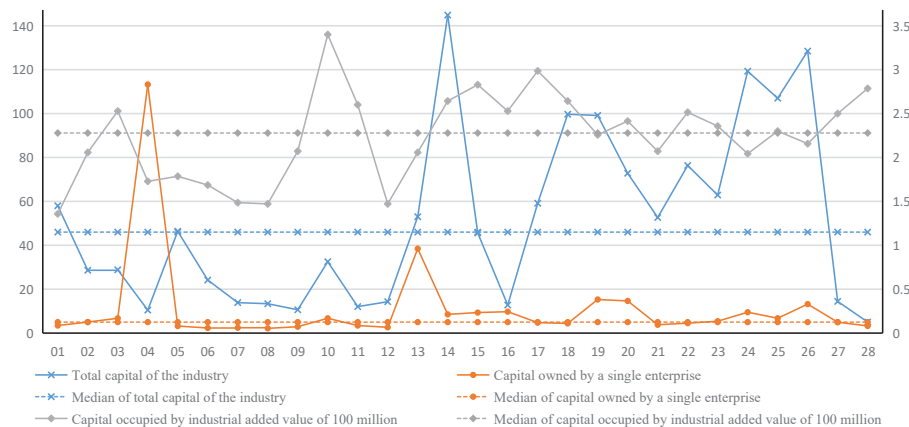

Fig. 1: Average capital distribution of 28 manufacturing industries in 2011-2017.

Note: The code means 28 sub-sectors of China's manufacturing industry.

It reflects the distribution of capital in different regions or industries and can create new value in the process of capital flow to achieve the continuous growth of capital enrichment. The most intuitive manifestation of capital enrichment is the increase in the total capital amount. According to the different sources of investment, i.e., the state, collective, corporate, individuals, Hong Kong, Macao, Taiwan, and foreign capital, this study defines the above total capital as capital enrichment.

Innovation capability of manufacturing industry: The formation of innovation capability is the result of the comprehensive contribution of many factors and the existing literature presents numerous related studies. Referring to Connie (2014) and Roper et al. (2015), the following comprehensive evaluation index system of innovation capability is constructed by combining with characteristics of the manufacturing industry and influencing factors of innovation capability, as given in Table 1. The entropy weight method is adopted to calculate the weight of each index.

Environmental pollution of manufacturing industry: As evident from the existing literature, there is no consistent standard for the measurement of environmental pollution. It is mainly measured by all or a single index of wastewater, waste gas, and solid wastes (Kolkis 2019, Li et al. 2019). Some scholars use the entropy weight method to combine the following indicators into the composite index of environmental pollution, i.e., wastewater, chemical oxygen demand, ammonia nitrogen, sulfur dioxide, and solid waste discharge. Since the National Bureau of Statistics no longer publishes the wastewater and waste gas wastes in different industries after 2012, this study uses solid waste discharge per unit of production value as the proxy variable for environmental pollution.

RESULTS AND DISCUSSION

Scatter Plot

To verify the hypothesis proposed in this study initially, the scatter plot method is used to examine the relationship between the main variables. Fig. 2 shows the scatter plot of capital enrichment and environmental pollution, and capital enrichment and innovation capability. The capital enrichment has a negative impact on environmental pollution, and a positive impact on innovation capability, which is consistent with the main idea of this study. However, the transmission

(a) Capital Enrichment and Environmental Pollution   (b) Capital Enrichment and Innovation Capability
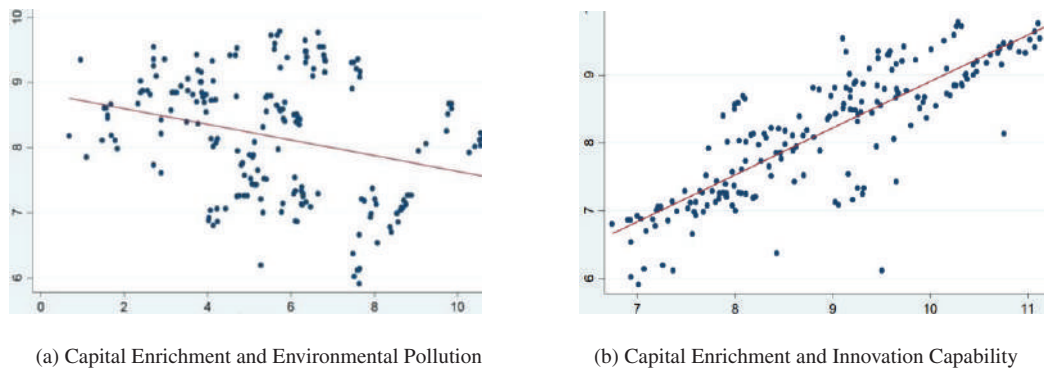
Fig. 2: Scatter plot between main variables.

Table 1: Evaluation index system of innovation capability in china's manufacturing industry.

First Class Index	Second Class Index	Third Class Index
Innovation resource input	Human resource input	Number of R&D personnel, R&D personnel full-time equivalent, and average number of employees
	Financial resource input	R&D expenditure, investment intensity of R&D expenditure, funding for new product development, and the ratio of fixed assets equipment
Innovation implementation capability	R&D capacity	Number of R&D institutions, R&D projects, and new products
	Production & marketing capacity	Marketing expense, expenditure on technology introduction, expenditure on digestion and absorption expenditure on purchasing domestic technology, and expenditure on technical renovation
Innovation output	Patent output	Number of patent applications, invention patent applications proportion of utility model patents, and patent applications / R&D personnel
	Non-patent output	Main operating revenue, revenue of new products, total exports of new products, and total profit

Table 2: Basic regression results of capital enrichment, innovation capability and environmental pollution.

Variable	Model (1)	Model (2)	Model (3)	Model (4)
CE	-3.601***(0.406)		-2.194***(0.392)	-2.001***(0.752)
IC		-1.595***(0.146)	-1.217***(0.151)	-1.062*(0.595)
CE*IC				-0.018**(0.070)
Human	-0.045(0.115)	-0.527***(0.131)	-0.519***(0.121)	0.518***(0.121)
Open	-3.169***(0.734)	-2.075***(0.716)	-1.251*(0.680)	-1.258*(0.702)
RD	-0.130**(0.061)	-0.112**(0.056)	-0.126**(0.052)	-0.132**(0.052)
Asset	4.952***(0.382)	2.841***(0.135)	4.568***(0.333)	4.533***(0.332)
Size	0.043(0.044)	-0.029*(0.041)	-0.010(0.038)	0.002(0.037)
Constant	-7.816***(1.045)	-2.865**(1.137)	-3.354***(1.060)	-4.617(5.144)
Obs	196	196	196	196
R²	0.788	0.816	0.842	0.842

Note: Robust standard errors in brackets; $^*p < 0.1$, $^{**}p < 0.05$, $^{***}p < 0.01$.

mechanism among capital enrichment, innovation capability and environmental pollution remains to be further tested.

Transmission Mechanism Analysis

It proposes that the capital enrichment of China's manufacturing industry not only directly affects environmental pollution but also indirectly through innovation capability. So, it explores the transmission mechanism among capital enrichment, innovation capability and environmental pollution by using a panel of China's manufacturing industry. The software used for the analysis is Stata15.0. The linear regression is initially performed on capital enrichment, innovation capability, and environmental pollution, and the interaction term between capital enrichment and innovation capability is also introduced. The centralized treatment method is used to reduce possible collinearity problems, and the results are shown in Table 2.

The model (1) in Table 2 shows the direct influence of capital enrichment on environmental pollution. The results show that capital enrichment and environmental pollution are

negatively correlated at 1%, with the coefficient of -3.601, indicating that manufacturing capital enrichment can bring down the pollution effect. The main reason may be that the higher level of capital enrichment encourages enterprises to invest additional capital in green technology innovation, adopt cleaner energy, advanced manufacturing technology, and effectively manage the experience to reduce pollutant emissions. The results support hypothesis 1 proposed above. The model (2) presents the impact of innovation capability on environmental pollution. There is a significant negative correlation between these two variables at 1%, indicating that the higher the level of innovation capability, the stronger the promotional effect on reducing pollution.

The transmission mechanism of capital enrichment affecting environmental pollution through innovation capability is analyzed. If it is right, in the regression model where environmental pollution is used as the explained variable, if innovation capability is removed, the effect of capital enrichment on environmental pollution should remain significant. After introducing innovation capability, the coefficients of

Table 3: Mediating effect of innovation capability.

Variable	Model (5)	Model (6)	Model (7)
	EP	IC	EP
CE	-3.601***(0.406)	1.156***(0.169)	-2.194***(0.392)
IC			-1.217***(0.151)
Controls	Yes	Yes	Yes
Obs	196	196	196
R²	0.788	0.986	0.842
Sobel	Z=5.215, the P-value is 0.000; Mediating Effect/Total Effect=39.07%		

Note: Robust standard errors in brackets; $^*p < 0.1$, $^{**}p < 0.05$, $^{***}p < 0.01$.

Fengju Xu et al.

capital enrichment decrease fairly but both capital enrichment and innovation capability are significant at 1%. By further introducing the interaction term *CE * IC*, its coefficient is -0.018, but the significance of innovation capability significantly decreased from 1% to 10%. It suggests that with the decline of innovation capability, the inhibitory effect of capital enrichment on environmental pollution becomes weak.

Mediating Effect Analysis

To further explore the role of innovation capability in the relationship between capital enrichment and environmental pollution, the empirical test is performed according to the mediating effect model. The results are shown in Table 3.

Results from the model (5) show that the coefficient of capital enrichment is -3.601 and significant at 1%, demonstrating that capital enrichment has a promotional effect on reducing environmental pollution. In the model (6), the coefficient of innovation capability is 1.156 and significant at 1%, showing that capital enrichment can improve the level of innovation capability. The main reason is that capital is the material basis for the implementation of innovation activities. The higher capital enrichment enables firms to have more capital for technical innovation, and then promote the spillover effect of technology. In the model (7), the coefficients of capital enrichment and innovation capability are both negative and significant at 1%, indicating that innovation capability indeed plays a mediating role. Additionally, the *Z* value in the Sobel test is 5.215 and significant at 1%, showing that the mediating effect of innovation capability is significant. Its proportion in the total effect is 39.07%, which proves the validity of hypothesis 2.

Robustness Test

Considering that the annual data may fluctuate greatly, this study processes it three times and re-estimates the relationship between capital enrichment, environmental pollution

and innovation capability. The results are shown in the Robust 1 in Table 4.

The capital enrichment of China's manufacturing industry has a negative effect on environmental pollution and a positive effect on innovation capability, both of which are significant. After adding capital enrichment and innovation capability at the same time, the coefficient of capital enrichment remains significant, but the negative effect on environmental pollution is decreased from -3.974 to -1.845. The Z-value in the Sobel test is 6.348 and significant at 1%, proving once again that innovation capability has the mediating effect.

Considering that the environmental pollution effect brought by capital enrichment may have hysteresis, this study re-estimates the model by using the one-period lagged values of the explained variable. The results are shown in the robust 2 in Table 4. Results reveal that innovation capability still plays a significant mediating role in the relationship between capital enrichment and environmental pollution, which proves the robustness of the above results.

Further Analysis

Due to a large number of China's manufacturing segments, the innovation capability and development priorities are different among sectors, which may reduce the practical significance of the results if they are not classified. Referring to OECD's classification criteria for the manufacturing industry, 28 segments are divided into the low-tech and high-tech industry by combining with their innovation capability. The results of the environmental pollution effect caused by capital enrichment under different innovation capability levels are shown in Table 5.

As revealed by the results, the impact of capital enrichment on environmental pollution in the low-tech industries is -2.357 at 1% significant level, and innovation capability plays a mediating effect on their relationship. By using the Sobel test method, it finds that the *Z* value in the Sobel test is

Table 4: Mediating effect of innovation capability after shifting mean values.

Variable		EP	IC	EP
Robust 1	CE	-3.974***(0.430)	1.129***(0.151)	-1.845***(0.369)
	IC			-1.886***(0.157)
	Sobel	Z=6.348, the P-value is 0.000; Mediating Effect/Total Effect=53.58%		
Robust 2	L.CE	-2.444***(0.410)	0.900***(0.161)	-1.388***(0.399)
	IC			-1.174***(0.179)
	Human	-0.245*(0.134)	0.547***(0.053)	0.398**(0.154)
	Sobel	Z=4.252, the P-value is 0.000; Mediating Effect/Total Effect=43.23%		

Note: Robust standard errors in brackets; *p < 0.1, **p < 0.05, ***p < 0.01.

Table 5: Environmental pollution caused by capital enrichment under different levels of innovation capability.

Variable	Low-tech industry			High-tech industry		
	EP	IC	EP	EP	IC	EP
CE	-2.357***(0.476)	0.624***(0.191)	-1.739***(0.455)	-6.479***(0.746)	1.679***(0.284)	-3.378***(0.730)
IC			-0.991***(0.195)			-1.847***(0.295)
Controls	yes	yes	yes	yes	yes	yes
R²	0.831	0.769	0.858	0.844	0.564	0.921
Sobel	Z=2.748, Mediating Effect/Total Effect=26.24%			Z=4.298, Mediating Effect/Total Effect=47.86%		

Note: Robust standard errors in brackets; *p < 0.1, **p < 0.05, ***p < 0.01.

2.748 and significant at 1%. The proportion of the mediating effect in the total effect is 26.24%. However, the regression coefficients between capital enrichment and environmental pollution, and capital enrichment and innovation capability in the high-tech industry are -6.479 and 1.679, respectively, both of which are significant at 1%. The Z value in the Sobel test is 4.298 and significant at 1%. Compared with the low-tech industries, the mediating effect in the high tech-industries is 47.86% of the total effect. This finding indicates that the mediating effect of innovation capability is more significant in high-tech industries.

CONCLUSIONS

Based on the panel data of 28 sub-sectors of China's manufacturing industry from 2011 to 2017, this study explores the nexus between capital enrichment, innovation capability and environmental pollution by using the basic regression model and the mediating effect model. The main conclusions are as follows:

Firstly, the industries with higher levels of capital enrichment generally possess one or more of the following characteristics: higher-profit margins, technology-intensive, national policy support, and resource-based national monopoly industry. There is a significant negative correlation between capital enrichment and environmental pollution, showing that an increase in capital enrichment can reduce environmental pollution. Secondly, capital enrichment has a positive impact on innovation capability, while innovation capability has a negative impact on environmental pollution. The interaction effect of innovation capability between capital enrichment and environmental pollution is significantly negative, indicating that with the decline of innovation capability, the inhibitory effect of capital enrichment on environmental pollution becomes weak. Thirdly, the relationship between capital enrichment and environmental pollution is affected by innovation capability which plays a significant mediating effect. Fourthly, in both low-tech industries and high-tech manufacturing industries, the innovation capability has the

mediating effect, and it is heterogeneity under different innovation capabilities.

ACKNOWLEDGEMENT

REFERENCES

Abbasi, F. and Riaz, K. 2016. CO_2 emissions and financial development in an emerging economy: An augmented VAR approach. Energy Policy, 90(3): 102-114.

Al-Mulali, U., Ozturk, I. and Lean, H.H. 2015. The influence of economic growth, urbanization, trade openness, financial development, and renewable energy on pollution in Europe. Natural Hazards, 79(1): 621.

Connie, Z. 2014. The inner circle of technology innovation: A case study of two Chinese firms. Technological Forecasting & Social Change, 82(2): 140-148.

Dalal, D.K. and Zickar, M.J. 2012. Some common myths about centering predictor variables in moderated multiple regression and polynomial regression. Organizational Research Methods, 15(47): 339-362.

Du, Y.C. and Wang, R.X. 2020. Impact of corporate governance ability on capital gains in mixed ownership enterprises. Transformations in Business & Economics, 19(2): 92-113.

Fagerberg, J., Martin, B.R. and Andersen, E.S. 2013. Innovation Studies: Evolution and Future Challenges. Oxford University Press, Oxford.

Frankel, J.A. and Romer, D. 1999. Does trade cause growth? American Economic Review, 89(3): 379-399.

Kolkis, S. 2019. Benchmarking the sustainability of urban energy, water and environment systems and envisioning a cross-sectoral scenario for the future. Renewable and Sustainable Energy Reviews, 103(7): 529-545.

Li, M. and Wang, Q. 2020. Does industrial relocation alleviate environmental pollution? A mathematical economics analysis. Sustainability, 22(14): 4673-4698.

Li, Z., Wang, X., Li, J., Zhang, W., Liu, R., Song, Z., Huang, G. and Meng, L. 2019. The economic-environmental impacts of China's action plan for soil pollution control. Sustainability, 11(8): 2322-2334.

Liang, F.H. 2014. Does foreign direct investment harm the host country's environment? Evidence from China. International Finance Journal, 15(12): 1-28.

Rodrigo-Alarcón, J., García-Villaverde, P.M. and Ruiz-Ortega, M.J. 2017. From social capital to entrepreneurial orientation: The mediating role of dynamic capabilities. European Management Journal, 32(2): 1-15.

Roper, S. and Hewitt-Dundas, N. 2015. Knowledge stocks, knowledge flows and innovation: Evidence from matched patents and innovation panel data. Research Policy, 44(7): 1327-1340.

Rubashkina, Y., Galeotti, M. and Verdolini, E. 2014. Environmental regulation and competitiveness: Empirical evidence on the Porter Hypothesis from European manufacturing sectors. Energy Policy, 61(2): 119-134.

Schmidt, T. and Sewerin, S. 2019. Measuring the temporal dynamics of policy mixes: An empirical analysis of renewable energy policy mixes' balance and design features in nine countries. Research Policy, 48(10): 1-13.

Schot, J. and Kanger, L. 2018. Deep transitions: Emergence, acceleration, stabilization and directionality. Research Policy, 47(6): 1045-1059.

Xiong, Z., Wang, P.J. and Zhao, Y. 2020. Re-innovation from failure, institutional environmental differences, and firm performance: Evidence from China. Amfiteatru Economic, 22(53): 197-219.

Xu, F.J., Ma, L.N. and Najaf, I. 2020. Interaction mechanism between sustainable innovation capability and capital stock: Based on PVAR model. Journal of Intelligent and Fuzzy Systems, 38(6): 7009-7025.

Zailani, S., Govindan, K. and Iranmanesh, M. 2015. Green innovation adoption in automotive supply chain: The Malaysian case. Journal of Cleaner Production, 108(19): 1115-1122.

Bioaccumulation of Vanadium in Selected Organs of the Freshwater Fish *Heteropneustes fossilis* (Bloch)

Ambili Ravindran* and M. V. Radhakrishnan**†

*Research & Development Centre, Bharathiar University, Coimbatore-641 046, Tamilnadu, India
**Department of Zoology, Chikkanna Government Arts College, Tirupur-641 602, Tamilnadu, India
†Corresponding author: M. V. Radhakrishnan; mvrkrishnan44@yahoo.com

ABSTRACT

Extensive industrialization and urbanization have introduced domestic as well as industrial wastes into aquatic ecosystems.Dueto lack of proper treatment and improper mode of disposal, the water bodies have become more polluted with toxic substancesand their adverse effects including mortality to aquatic organisms, are becoming more prominent.In recent years, much attention has been paid to the possible danger of metal poisoning in humans as a result of consumption of contaminated fishes. Vanadium is a rare elementfound combined with certain minerals and mainly from the production of certain alloys used in jet engines. Humans may be exposed to excessive vanadium and may develop adverse vascular effects.In the present investigation, efforts have been made to investigate the effect of sublethal concentration of vanadium (6.5 ppm; 10% of 96h LC_{50}) on the bioaccumulation in gill, liver and skin of the catfish *Heteropneustes fossilis* for 60 days. The pattern of bioaccumulation was in the order liver > gill > skin. Theresults suggest that the organ-specific variation is directly related to the structural and functional change, proximity to the toxicant and presence of ligands having high affinity to vanadium.

INTRODUCTION

In India, even though industrialization has not reached the level attained in the developed countries, pollution of aquatic habitats seems to be an inevitable problem. More toxic compounds are being increasingly detected in aquatic ecosystems. With the advent of the agricultural and industrial revolution, most of the water sources are becoming contaminated with diverse pollutants (Khare & Singh 2002). Industrial discharges containing toxic and hazardous substances, including heavy metals, contribute significantly to the pollution of aquatic ecosystems(Gbem et al. 2001,Woodling et al. 2001). According to Satyanarayanan et al.(1985), the presence of heavy metals on the east coast of India deserves special mention as it almost forms a repository for industrial effluents and city sewage. Among the various heavy metals, in general, vanadium is a biologically non-essential, non-biodegradable, persistent type of heavy metal and its compounds are known to have high toxic potentials. Further, continuous, low-level vanadium exposure may have a gross biological impact comparable to that of recurring exposures of much greater intensity. In freshwater fish, metal uptake is taking place mainly through three routes namely, gills, skin and also from food via the intestinal wall (Karlsson-Norrgran & Runn 1985). On the other hand, the metal retention

capacity of fishes is dependent on their metal assimilation and excretion capabilities (Rao & Patnaik 1999). According to Ferardet al.(1983),aquatic organisms take up heavy metals and concentrate them to amounts considerably higher than those found in the environment. Therefore, it is important to find the pathways of accumulation of heavy metals and their affinity to different tissues, especially in fishes. In this context, the present investigation has been designed to study the pattern of bioaccumulation of vanadium in the gills, liver and skin of the catfish *Heteropneustes fossilis*(Bloch.) exposed to sublethal concentrations of vanadium.

MATERIALS AND METHODS

Collection and maintenance of fish: The freshwater fish *Heteropneustes fossilis* (12 ± 2 cm length and 34 ± 2 g weight) were collected locally, brought to the laboratory and kept in a tank with size $60 \times 30 \times 30$ ($l \times b \times h$) cm, filled with tap water for acclimatization for about two weeks. During the acclimatization, the fish were fed with minced goat liver on every alternate day. Water in the tank was renewed, three or four times in a week and aerated to ensure sufficient oxygen supply. For the fish used in the experiment, feeding was stopped two days before the start of the experiment to reduce the quantum of excretory products in the tank.

Estimation of LC$_{50}$: Before the commencement of the experiment, 96h LC$_{50}$ value was determined using trimmed spearman Karber method (Hamilton et al. 1977)which was found to be 65 ppm after 95% trimming.

Experimental protocol: For the analysis of sublethal toxicity six groups of 10 fish each were exposed separately to vanadium (6.5ppm; 10% of 96 h LC$_{50}$) solution prepared in tap water. The experimental medium was prepared by dissolving vanadium (6.5ppm) in tap water having dissolved oxygen 6 ppm, pH 7.5, water hardness 40.44 mg/L and water temperature 28±2°C (APHA 2008). Each group was exposed to 50 L of the experimental medium. Parallel groups of 10 fish each were kept in separate aquaria containing 50 L tap water without the addition of vanadium as control. Feeding was allowed in the experimental as well as control groups every day for a period of 3 h before the renewal of the media throughout the tenure of the experiment. After the expiry of 5, 10, 20, 30, 40 and 60 days of exposure five fish each from the respective experimental as well as control groups were sacrificed and bioaccumulation of vanadium was found.

Estimation of vanadium: For the analyses, the gill, fragments of the liver and a part of the skin on the dorsal surface of each fish were dissected, washed with distilled water and weighed following FAO methods (2006). The separated organs were dried at 120°C in Petri dishes until reaching a constant weight. The separated organs were placed in digestion flasks and ultra-pure concentrated nitric acid and hydrogen peroxide(1:1 v/v) were added. The digestionflasks were then heated to 130°C until all the materials were dissolved. Digest was diluted with double distilledwater appropriately and vanadium was assayed. Atomic absorption spectrophotometer (Perkin Elmer) using element-specific hollow cathode lamp in default condition, by flame absorption mode was used to approximate the metal concentration (Kendall & Scanlon 1982). The metal standard recommended by Perkin Elmer was used for checking the sensitivity of the instrument and calibration.

The data obtained were subjected to standard statistical analysis each sampling time and their respective control groups in different groups. Duncan's multiple range test (Bruning & Kintz 1968) was performed to determine whether the parameters altered significantly by exposure periods.

RESULTS

Gill: Of all the tissues investigated, the rate of accumulation of vanadium was maximum ingills of the exposed fish.No detectable amount of vanadium was observed in the gills of the control fish. The gill registered 1. 92 ± 0.02, 0.98 ± 0.05, 0. 85 ± 0.01, 0.71 ± 0.02 and 1. 18 ± 0.01 ppm of vanadium

for 5, 10, 20, 30 and 60 days of exposure to sublethal concentration of vanadium solution (Fig. 1). After an initial surge, the metal concentration decreased gradually until the 30th day. However, the fag end of the experiment registered an increasing trend in the accumulation pattern.

Skin: Even though skin constitutes the single tissue having maximum surface area and direct contact with the toxicant medium, the rate of accumulation was less when compared to other tissues, such as gills and liver (Fig. 1).No vanadium was traceable in the skin of the control fish. The skin recorded 0.35 ± 0.01, 0. 48 ± 0.01, 0. 25 ± 0.01, 0. 18 ± 0.01and 0.15 ± 0.00 ppm of vanadium for 5, 10, 20, 30 and 60 days of exposure to sublethal concentration of vanadium solution (Fig. 1).In the case of the experimental fish, the rate of accumulation decreased during the later periods, leading to an overall decrease in the rate of bioaccumulation of vanadium in the skin tissue.

Liver: As with the case of gills, vanadium could not be traced in the liver of the control fish. In the case of the experimental groups, even though the quantity of accumulated vanadium was less in case of the liver when compared to gills, the pattern of accumulation showed a more or less continuous increasing trend at all the periods of exposure. The liver recorded 0.71 ± 0.02, 0. 84 ± 0.02, 0. 96 ± 0.01, 1.12 ± 0.01and 1.26 ± 0.02 ppm of vanadium for 5, 10, 20, 30 and 60 days of exposure to sublethal concentration of vanadium solution (Fig. 1).

DISCUSSION

The exposure of *H. fossilis* to sublethal concentration of vanadium caused significant accumulation in the organs and the accumulation was associated with the duration of exposure in different tissues. The rate of accumulation was in the order gill > liver > skin and it may be inferred that the pattern of accumulation of vanadium differs from tissue to tissue. The critical analysis revealed that the rate of accumulation in the various tissues in comparison to their respective controls is influenced by the duration of exposure. However, there occurred significant variations in the concentration of accumulated vanadium in the various tissues studied at different exposure periods when compared with the respective preceding exposure periods. This difference in accumulation may be attributed to the proximity of the tissue to the toxicant medium, the physiological state of the tissue, presence of ligands having an affinity to vanadium and/or to the role of the tissue in the detoxification process.

From the point of view of proximity to toxicant of the various tissues analysed, gills and skin are in direct contact with the toxic medium, whereas liver is exposed through
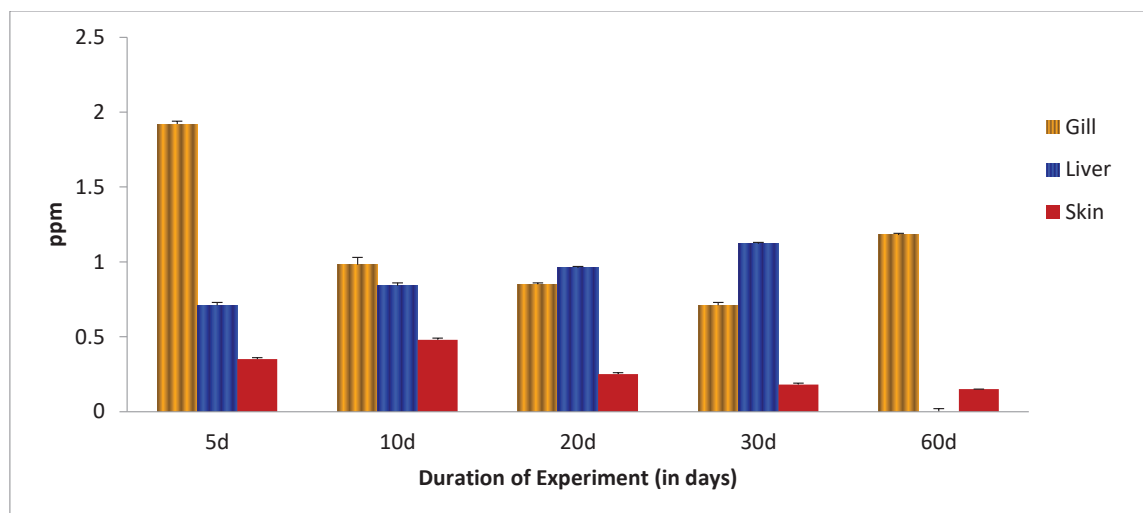
Fig. 1: Bioaccumulation of vanadium (ppm) in gill, liver and skin of *H. fossilis*in different experimental groups after 5, 10, 20, 30 and 60 days of sublethal exposure**.**

media effect. Even though the gills and skin come into direct contact with the ambient toxicant, the pattern of bioaccumulation showed considerable differences between them. While gill was the organ accumulating the maximum vanadium, skin accumulated a far lower amount. Even though reports indicate a correlation between bioaccumulation of metals and exposure concentration, along with exposure time (Giles 1988), such a correlation did not exactly seem to fit data from the present study, as both skin and gill are faced with the same concentration of the toxicant and the same exposure period. A probable reason for the observed difference in the metal accumulating capacity of gills and skin may be the physiological state of the tissue and/or structural and functional organization of these organs. In the case of fish and crustaceans, as well as molluscs, gills are one of the target organs to suffer instantaneously from ambient toxicants. One of the basic reasons for the gills to act as the primary site for cadmium accumulation, as observed in the present study, is its external position and its proximity to the ambient toxicants. In addition, the highly branched structural organization of the gill and the resultant highly increased surface area, along with the large volume of water passing through the gill surface and the highly vascular physiological state and the relatively small biomass when compared to their surface area (Mayer et al. 1991) make the gill a prime site for vanadium accumulation.

As far as the presence of various ligands in the tissues is concerned, being an oxyphilic and sulphophilic element, vanadium undergoes multiple bondings in the body (Moore &Ramamoorthy 1984), forming stable complexes with a variety of organic compounds. In the present study, the increased mucogenesis under the influence of toxicant, as also reported by Rajan& Banerjee (1991), might result in the formation of a mucous trap over the gills for the vanadium ions due to the preferential attraction of cadmium to the -SH groups present in the mucus. The cation binding capacity of the fish mucus is also reported by Ingerssolet al. (1990). However, according to Paul & Banerjee (1997), due to the constant and increased ventilatory movements of the operculum under the influence of the xenobiotics, the protective mucous plug inside the opercular chamber is quite often discharged into the medium. Such discharges of the mucous plug might make the gills a more vulnerable site for the accumulation of vanadium. All these structural and functional peculiarities of the gills, along with the high vascularization, might be responsible for the highest rate of accumulation of vanadium. On the contrary, the skin, which also comes under the direct contact stress of the toxicant, shows a far lesser rate of bioaccumulation. According to Rajan& Banerjee (1991) and Paul & Banerjee (1996), the mucogenic activity of the body skin epithelium in fish is very high when compared to gills (Hemalatha& Banerjee 1997). This increased mucogenesis may play a crucial role in preventing the vanadium ions from entering the body, as the coagulated mucus all over the body might be acting as a protective ion trap. Further, unlike gill, discharge of the body mucus into the medium is not an active process as there are no ventilatory movements in the skin epithelium, and the rejected epithelial cells, along with the proteinaceous contents of the other degenerating cells, form a protective

scab over the skin. Such a protective covering may act as an efficient trap for the metal ions and, at a later stage, when the cellular debris along with the mucous mass is released into the medium, the entire accumulated vanadium ions might be rejected into the medium itself and thereby greatly retard their entry into the body skin. Moreover, the regeneration of the exhausted and sloughed mucous cells is quite quick in the case of body skin when compared to the opercular epithelium (Paul & Banerjee 1996, 1997) and gills (Hemalatha& Banerjee 1997), leaving less time for the accumulation of vanadium on the body skin epithelium. The intermittent increases observed in the concentration of vanadium in skin and gill at various stages of exposure may be attributed, at least partially, to the temporary breakdown of the mucogenic barrier due to the exhaustion of the mucous cells after their hyperactivity.

Even though the liver did not come into direct contact with the medium, the vanadium accumulation pattern followed more or less the same pattern as that of gills. Many other workers have also reported the increased metal accumulation capacities in liver and gills of aquatic organisms (Protasowicki&Chodyniecki 1992, Narayanan et al. 1997). One of the main reasons attributed to the increased presence of heavy metals in these organs is their capacity to accumulate vanadium brought by blood from other parts of the body and induce the production of the metal-binding protein, metallothionein, which is believed to play a crucial role against the toxic effects of heavy metals by binding them (Bhattacharya et al. 1985). According to Klavercampet al. (1984), the gill and the liver are the main sites of metallothionein production and metal retention. This may be yet another main reason for the enhanced presence of vanadium in the gills, skin and liver. Also, all these tissues are rich in the metal binding-SH groups (Rema & Philip 1997) and therefore it is not surprising that the metal ions are complexed in these organs. According to Kent (1998), the liver is involved in the detoxification of toxic substances circulating in the bloodstream. Moreover, liver, being the major organ of metabolic activities including detoxification (Klavercampet al. 1984), vanadium might also be transported into this from other tissues, including gills and skin, for subsequent elimination. Such transportation might lead to higher rates of accumulation in the liver. The possibility of such detoxification related mobilization of accumulated vanadium may be one reason for the intermittent reduction in the quantity of accumulated vanadium in gills, as well as the skin at various stages of exposure.

CONCLUSION

The pattern of bioaccumulation in *Heteropneustes fossilis* after sublethal vanadium treatment clearly shows that heavy metals, whatever the concentration, are quite unbiological and caution should be exercised in allowing vanadium into the aquatic environment. By knowing the mechanism of the specific toxic action of poisons, it is possible to use various pharmacological compounds to reduce the toxic effect of pollutants. Further, the toxic effect of metals in organisms in contaminated water is an important aspect of environmental awareness, because it may affect all members of the food chain. Moreover, management of our water bodies is required if they are to be used for diverse purposes as domestic and industrial supply, crop irrigation, sports and commercial fisheries, power generation, etc.

REFERENCES

APHA 2008. Standard Methods for Examination of Water and Wastewater.19th ed. American Public Health Association, Washington DC.

Bhattacharya, T., Ray,A.K. and Bhattacharya, S. 1985. Response of *Channapunctatus* under short term and long term exposure to industrial pollutants: Induction of histopathology in the kidney. Z. Mikrosk. Anat. Forsch (Leipz), 899: 327-334.

Bruning, J.L. and Kintz, B.L. 1968. Computational Handbook of Statistics. Foresman and Company, Dallas, USA, p. 308.

FAO 2006. State of World Aquaculture 2006. FAO Fisheries Technical Paper, 500:134.

Ferard, J.F., Jouany,J.M.,Truhaut,R. andVasseur, P. 1983. Accumulation of cadmium in a freshwater food chain experimental model. Ecotoxicol. Environ. Safe., 7: 43-52.

Gbem, T.T., Balogun,J.K., Lawal,F.A. andAnnune, P.A. 2001. Trace metal accumulation in *Clariasgariepinus* exposed to sublethal levels of tannery effluent. Sci. Total. Environ., 271: 1-9.

Giles, M.A. 1988. Accumulation of cadmium by rainbow trout, *Salmogairdneri*, during extended exposure. Can. J. Fish. Acquat. Sci., 45: 1045-1053.

Hamilton, M.A., Russo, R.C. and Thurston, R.V. 1977. Trimmed Spearman Karber method for estimating median lethal concentrations in toxicity bioassays. Environ. Sci. Tech., 11: 714-719.

Hemalatha, S. and Banerjee, T.K. 1997. Histopathological analysis of acute toxicity of zinc chloride on the respiratory organs of air breathing catfish *Heteropneustes* (*Saccobranchus*) *fossilis* (Bloch.).Vet. Archiv.,67(1): 11-24.

Ingerssol, C.G., Saches,D.A., Meyer,J.S.,Gutley,D.D. andTietige, J.E. 1990. Epidermal response to pH, aluminium and cadmium exposure in brook trout (*Salveniusfontinales*) fry. Can. J. Fish. Aquat. Sci., 47: 1616-1622.

Karlsson-Norrgren, L. and Runn, P. 1985. Cadmium dynamics in fish: Pulse studies with ^{109}Cd in female Zebrafish, *Brachydaniorerio*. J. Fish. Biol., 27: 571-581.

Kendall, R.J. and Scanlon, P.F. 1982. A rapid method for analysis of tissues for heavy metals using atomic absorption spectrophotometer. Northwest Sci.,56: 265-267.

Kent, C. 1998. Basic Toxicology. John Wiley Sons.Inc, New York, pp. 402.

Khare, S. and Singh, S. 2002. Histopathological lesions induced by copper sulphate and lead nitrate in the gills of freshwater fish *Nandusnandus*. J. Ecotoxicol. Environ. Monit., 12: 105-111.

Klavercamp, J. E., MC Donald,W.A., Duncan,D.A. andWagenann, R. 1984. Metallothionein and acclimation to heavy metals in fish, a review. In: Contaminant Effects on Fisheries (Cairns, V. W., Hodson, P. V.,Nriagu, J. O. Eds.), Wiley, New York, pp. 99-113.

Mayer, W., Kretschmer,M., Hoffmann,A. and Harish, G. 1991. Biochemical and histochemical observations on effects of low level heavy metal load (lead, cadmium) in different organ systems of the freshwater crayfish,

Astacusastacus L. (Crustacea: Decapoda). Ecotoxicol. Environ. Safe., 21: 137-156.

Moore, J.W. and Ramamoorthy, S. 1984. Heavy Metals in Natural Waters: Applied Monitoring and Impact Assessment. Springer Verlag, Tokyo, 1-268.

Narayanan, K.R., Lyla,P. S. and Ajmal Khan, S. 1997. Pattern of accumulation of heavy metals (mercury, cadmium and zinc) in the mud crab *Scylla serrata.* J. Ecotoxicol. Environ. Monit., 7: 191-195.

Paul, V.I. and Banerjee, T.K. 1996. Analysis of ammonium sulphate toxicity in the catfish *Heteropneustesfossilis* using mucocyte indexing. Pol. Arch. Hydrobiol., 43: 111-125.

Paul, V.I. and Banerjee, T.K. 1997. Histopathological changes induced by ambient ammonia (ammonium sulphate) on the opercular linings of the live fish *Heteropneustesfossilis* (Bloch). Dis. Aquat. Org., 28: 15-161.

Protasowicki, M. andChodyneicki, A. 1992. Bioaccumulation of cadmium in some organs of carp, *Cyprinuscarpio* L. in case of per os administration. Arch. Pol. Fish., 1: 61-66.

Rajan, M.T. and Banerjee, T.K. 1991. Histopathological changes induced by acute toxicity of mercuric chloride on the epidermis of freshwater catfish *Heteropneustesfossilis* (Bloch). Ecotoxicol. Environ. Safe., 22: 139-152.

Rema, L.P. and Philip, B. 1997. Accumulation of an essential metal (zinc) and a non-essential metal (mercury) in different tissues of *Oreochromismossambicus* (Peters). Ind. J. Exp. Biol., 35: 67-69.

Satyanarayanan, D., Rao,I. M. andPrasada Reddy, B.R. 1985. Chemical oceanography of harbor and coastal environment of Visakhapatnam (Bay of Bengal). Part I: Trace metals in water and particulate matter. J. Mar. Sci., 14: 139-146.

Woodling, J. D., Brinkman,S. F. and Horn, B.J. 2001. Non uniform accumulation of cadmium and copper in kidneys of wild brown trout *Salmotrutta* populations. Arch. Environ. Contam. Toxicol., 40: 381-385.

Alginate Incorporated Multi-Walled Carbon Nanotubes as Dispersive Micro Solid Phase Extraction Sorbent for Selective and Efficient Separation of Acidic Drugs in Water Samples

N. Z. Othman, N. S. M. Hanapi†, W. N. W. Ibrahim and S. H. Saleh

Faculty of Applied Sciences, Universiti Teknologi MARA, 40450 Shah Alam, Selangor, Malaysia
†Corresponding author: N.S.M. Hanapi; norsuhaila979@uitm.edu.my

ABSTRACT

Innovative development of a simple and rapid dispersive micro solid phase extraction (D-µ-SPE) method combined with high performance liquid chromatography (HPLC) based on alginate incorporated with multi-walled carbon nanotubes (Alg-MWCNT) was developed for the analysis of five selected acidic drugs in the water sample. The effect of dispersive micro solid phase extraction parameters such as the mass of sorbent, sample pH, extraction time and desorption time on the peak area of analytes were optimized. Under the optimum extraction conditions, a linear response was achieved in the concentration range of 1 µg.L^{-1} to 500 µg.L^{-1} (R^2 ≥ 0.9959). The limits of detection for the method at a signal to noise ratio of 3 were between 0.03 µg.L^{-1} and 0.08 µg.L^{-1}. The proposed method was successfully applied for the determination of four acidic drugs in tap water samples with relative recoveries ranging from 75 % to 105 %. The proposed Alg-MWCNT sorbent showed high potential as an alternative sorbent for dispersive micro solid phase extraction of acidic drugs in aqueous matrices.

INTRODUCTION

In the last few decades, pharmaceuticals have played an increasingly important role in improving the quality of life. Tons of pharmaceutical substances are used in human medicine for diagnosis, treatment or prevention every year (Azzouz & Ballesteros 2012). The emission of this emerging contaminant as one of the environmental problems may require legislative intervention as they may cause acute effects on flora and fauna even at a low concentration level (Petrovic et al. 2008). The water resource issues in Malaysia have grown in magnitude as the organic contaminant, especially from the disposal of waste, industries and agriculture by-product, may flow and contaminate our water reservoirs (Osman et al. 2012).

Non-steroidal anti-inflammatory drugs (NSAIDs) are among the most frequently prescribed drugs in modern medicine. This group of pharmaceutical drugs provides analgesic (pain-killing) and anti-pyretic (fever-reducing) effect and in higher doses, this drug gives an anti-inflammatory effect (Meek et al. 2010). In this study, a method by using dispersive micro solid phase extraction (D-µ-SPE) for the extraction of these pharmaceutical drugs has been proposed. Model compounds were selected among the pharmaceuticals which are salicylic acid, naproxen, diclofenac, ibuprofen and mefenamic acid.

Pharmaceutical residues are usually present in environmental water samples in trace levels. There are several extraction techniques carried out by the researchers mainly for the isolation and preconcentration of NSAIDs in aqueous matrices such as Solid Phase Extraction (SPE) (Asghari et al. 2016), Solid Phase Microextraction (SPME) (Moeder et al. 2000), Hollow Fiber Liquid-Phase Microextraction (HF-LPME) (Sagristà et al. 2010), Stir Bar Sorptive Extraction (SBSE) (Tanwar et al. 2015), Magnetic Solid Phase Extraction (MSPE) (Wang et al. 2017), Dispersive Liquid-Liquid Microextraction (DLLME) (Park & Myung 2015) and Ultrasound-Assisted Emulsification Microextraction (UAEME) (Lee et al. 2014).

Operating costs, amount of organic solvent used, sample throughput and simplicity of operation frequently becomes the determining factor in choosing the right extraction technique (Saim et al. 1997). However, the most common sample isolation and pre-concentration technique for the extraction of pharmaceuticals in water samples is solid phase extraction (SPE). SPE has been claimed as effective sample preparation for removal of interfering compound and enrichment of analyte (Hennion et al. 1999). Researchers are devoted to developing new sorbents to enhance the extraction process. There were many successful works on the use of different kinds of sorbent materials used in SPE such as molecularly imprinted polymers (MIPs) and carbon nanotubes (CNTs).

The selection of a suitable SPE extraction sorbent depends on the mechanism of interaction between the sorbent and analyte of interest (Żwir-Ferenc & Biziuk 2006).

Carbon nanotubes have long been recognized as the stiffest and strongest man-made material (Spitalsky et al. 2010). It possesses advantages in adsorbent-adsorbate interactions but high production cost and non-biodegradable materials (Ren et al. 2011). However, due to its insolubility and creating a homogenous is difficult as it tends to agglomerate caused by strong inter-tube Van der Waals forces (Ibrahim et al. 2015). Besides, because of its nano size, the excellent properties of these structures can only be exploited if they are homogeneously embedded into polymers (Spitalsky et al. 2010). Several types of polymers based on natural products such as cellulose and starch have been proposed in analytical sample preparation due to their biodegradability, good physical and chemical properties and low cost (Hanapi et al. 2017). Many researchers have been working on the use of this sorbent incorporated with biopolymers such as alginate, agarose and chitosan as promising materials to overcome these drawbacks.

Alginate is a biomaterial that has numerous applications in biomedical science and engineering due to its favourable properties, including biocompatibility and ease of gelation (Lee & Mooney 2012). It offers excellent adsorption due to the presence of hydrophilic and reactive functional groups (Crini 2005). This biopolymer contains a high amount of D-mannuronic acid (M block) and L-guluronic acid (G-block) which can be cross-linked easily by using bivalent ions such as calcium ions to form hydrogels in gelation process (Vijayalakshmi et al. 2016). However, it is easily soluble in aqueous media which limits its application as an adsorbent.

Hence, this research was conducted to investigate the use of MWCNTs incorporated with alginate as a promising material to overcome the disadvantages of these two components with the aid of D-μ-SPE which is believed to be a simple, rapid and efficient method compared to the traditional SPE method.

MATERIALS AND METHODS

Chemicals and Materials

Ibuprofen, naproxen, diclofenac, mefenamic acid and salicylic acid were purchased from Sigma-Aldrich (purity assay in range of 98-101 %). Acetonitrile (ACN) and methanol (MeOH) of high performance liquid chromatography (HPLC) grade were purchased from Merck (Darmstadt, Germany). Calcium chloride ($CaCl_2$) was obtained from HmbG Chemicals (Germany). Methane sulfonic acid (MSA) was purchased from Sigma-Aldrich (St. Louis, USA). Ultrapure

water was produced from Barnstead Nanopure (Thermo Scientific). Sodium hydroxide and hydrochloric acid were obtained from Merck, Darmstadt, Germany and sodium alginate from Qrec (New Zealand). Multi-walled carbon nanotubes (MWCNTs) with specific surface area > 233 m^2/g, purity > 95 %, 8-15 nm outer diameter × 50 μm in length was purchased from Sun Nanotech (Jiangxi, China).

Preparation of Standard and Sample Solutions

The individual stock solution of ibuprofen, naproxen, diclofenac, mefenamic acid and salicylic acid were prepared separately in HPLC grade methanol at a final concentration of 1000 mg.L^{-1}. All standard solutions were stored in the amber glass bottle at 4°C when not in use. A series of working standard solutions were prepared in methanol by dilution before analysis to prevent from the decomposition of analytes. For calibration standards in the extraction procedure, spiked water samples were prepared by adding 1 mL of 10 mg.L^{-1} standard solutions into 9 mL of deionized water at a final concentration of 1 mg.L^{-1}.

The river and tap water samples were collected in bottles pre-cleaned with acetone and filtered through a nylon membrane filter to remove colloidal particles and stored in a freezer at 4°C until analysis. For accuracy and precision studies, the river and tap water samples (10 mL, pH 3) were spiked with the standard mixture of five pharmaceuticals NSAIDs to give a final concentration of 1 mg.L^{-1} for each analyte.

Preparation of Alg-MWCNT Composite Beads

The method used was adapted and modified from literature (Jeon et al. 2010, Sahasathian et al. 2010). The composite beads were prepared by the suspension method. Initially, 3 % (w/v) of sodium alginate solution was prepared by stirring it at 60°C. Meanwhile, 0.3 g of MWCNT was dispersed in 30 mL deionized water under sonication for 30 min. Then, the MWCNT solution was added into the sodium alginate solution and sonicated for another hour. The mixture solution was dripped through the injection needle into 1000 mL of 4% (w/v) of calcium chloride solution. The Alg-MWCNT beads were formed upon contact with calcium ions. After removal from calcium chloride bath, the beads were rinsed thoroughly with deionized water using an 11 μm filter paper and dried in the oven at 50°C for 24 hours.

Dispersive Solid Phase Extraction Procedure by Using Alg-MWCNT Sorbent

About 0.3 g of Alg-MWCNT powders were dispersed into the aqueous sample (10 mL, pH 3). To trap the analytes, the mixture was vigorously stirred with a magnetic stir bar for

30 minutes. Subsequently, the Alg-MWCNT powder was isolated from the solution by centrifugation (4000 r min^{-1}, for 10 min). The supernatant was discarded. About 2 mL of desorption solvent was added, and then the mixture was sonicated for 15 minutes to desorb the analytes. The mixture was then centrifuged at 4000 r min^{-1}, for 5 minutes. The solvent was collected and evaporated to dryness under a soft stream of nitrogen gas. Finally, 10 µL of the extract was injected into the HPLC system for analysis. A visual summary of this method is illustrated in Fig. 1. The Alg-MWCNT composite beads could be reused several times after washing with 2 mL of methanol and water, respectively. Several optimization parameters for D-µ-SPE were optimized by changing one factor at a time.

Chromatographic Conditions

All analyses were performed using an automated high performance liquid chromatography Dionex Ultimate 3000 (Sunnyvale, CA, USA) system, using an Acclaim Polar Advantage II (5 µm, 120 Å, 4.6×150 mm) (Dionex USA) as the analytical column. A gradient elution consisting of acetonitrile, 10 mM methane sulfonic acid (MSA) and ultrapure water was applied. The flow rate was programmed at 1 mL min^{-1}. For initialization of the LC analysis, the chromatographic system was cleaned and stabilized for an hour. The quantification of NSAIDs was performed by measuring the peak area of the chromatogram. NSAIDs were detected using a diode array detector at a selected wavelength of 230 nm.

Validation of the Analytical Method

The extraction method was assessed for linearity (R^2), limit of detection (LOD), limit of quantification (LOQ), precision (% RSD) and accuracy (% relative recovery) before sample analysis. Linearity was measured by plotting the calibration curve of five different concentration levels for the standard mixture of NSAIDs. The same calibration graph was used for the determination of LOD and LOQ. Method precision was measured using three different extractions of calibration standard at the lowest concentration.

RESULTS AND DISCUSSION

Preparation of Alg-MWCNT Composite Beads

In the present work, the alginate incorporated multi-walled carbon nanotubes were prepared by the suspension method. Fig. 2 illustrates a mechanism for the formation of alginate incorporated multi-walled carbon nanotubes (Alg-MWCNT). The formations of Alg-MWCNT composite beads start with the carboxylated MWCNTs which were physically combined with sodium alginate which be-came the backbone holding the MWCNTs together. The incorporated Alg-MWCNT structure would form hydrogels immediately after in touch with the calcium chloride solution. This formation occurs due to the active site in a long chain of alginate structure which provides the ability of cross-linked in the presence of divalent ions such as calcium, resulting in the rapid formation
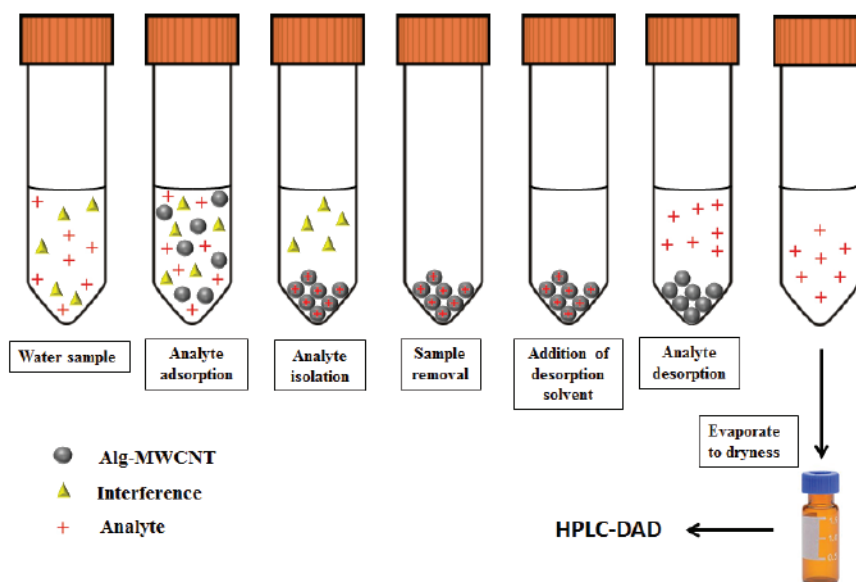

Fig. 1: Dispersive micro solid phase extraction (D-µ-SPE) procedure by using Alg-MWCNT as a sorbent.
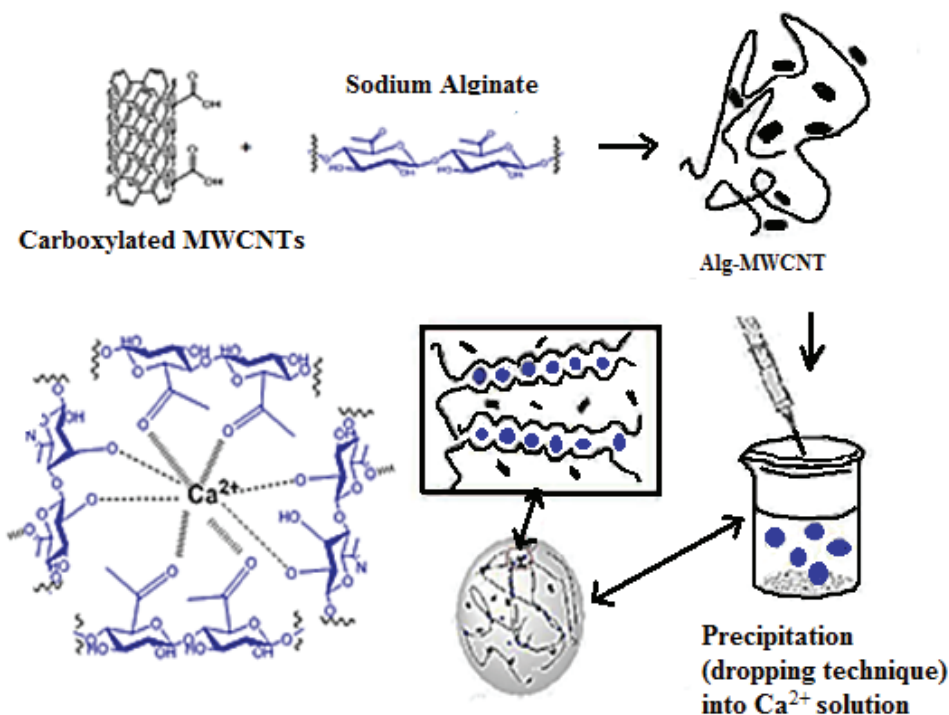
Fig. 2: Mechanism for the formation of Alg-MWCNT.

of hydrogels. The divalent cations preferentially bind toward the G-block rather than M-block (Braccini et al. 1999). The formation of this hydrogels is based on its gel-forming ability through cation binding which was a transition from water soluble sodium alginate into water insoluble calcium alginate (Fertah et al. 2017).

Optimization of Extraction Parameter

The salicylic acid (SAL), ibuprofen (IBU), naproxen (NAP), diclofenac sodium salt (DIC) and mefenamic acid (MEF) were selected as model analytes in this study as they are the most often used NSAIDs. To determine the optimum conditions for the extraction of NSAIDs from aqueous samples, many parameters that can affect the extraction efficiency were investigated namely extraction time, desorption time, the effect of pH and mass of sorbent. The optimization was carried out using one variable at a time while other parameters were kept constant. Optimization was carried out using deionized water samples spiked with each NSAID to give a concentration of 1 mg.L^{-1} in 10 mL of water samples. About 1 mL of acetonitrile was used as a desorption solvent. The triplicate extractions were carried out for each parameter optimized in this study.

Effect of Sample pH on Peak Area of Analytes

The experiment was carried out by varying the pH value in the range of pH 2 to pH 5 to determine the effect of sample pH on the extraction of NSAIDs. The sample pH is expected to significantly influence the efficiency of extraction. According to the pKa values of salicylic acid, naproxen, diclofenac, ibuprofen and mefenamic acid (pKa = 2.98, 4.15, 4.08, 4.91 and 4.2 respectively), at lower pH than the pKa value, these compounds would mostly exist in molecular form. While at higher pH than the pKa value, they are in an ionized form.

It was observed that the peak area slightly increased with increasing pH from pH 2 to pH 3 and highest at pH 3 (Fig. 3a). The peak area starts to decrease after pH 3. As the target compounds were acidic, the pH of the sample solution was adjusted in the proper acidic range since acidification of an aqueous solution is likely to reduce the dissociation of the weakly acidic analytes which can improve the extraction efficiency (Silva et al. 2008). The extraction was observed to be the best at pH 3, as the sample solution was sufficiently acidic to neutralize the analytes. It has been demonstrated that pH is a determining condition in the adsorption process of non-steroidal anti-inflammatory drugs onto the sorbent

and pH 3 is the most suitable condition for the analysis of NSAIDs. Therefore, pH 3 was selected as the best pH value and used in subsequent experiments.

Effect of Extraction Time on Peak Area of Analytes

For the optimization of extraction times, in the range of 10 to 50 minutes were employed. The effect of contact time between adsorbent and analytes is shown in Fig. 3b. It was observed that the adsorption capacity of NSAIDs was rapidly increased from 10 to 30 minutes of extraction time. The highest extraction efficiency was obtained at 30 minutes of extraction time. After 30 minutes, the peak area was slowly decreased. This could be due to a long duration of extraction time causes the back extraction of analytes from acceptor into the sample solution (Hernando et al. 2006). Therefore, 30 minutes was selected as the optimal extraction time and used in the subsequent experiments.

Effect of Desorption Time on Peak Area of Analytes

Ultrasonication method was used for the desorption solvent to desorb NSAIDs from the Alg-MWCNT sorbent as this technique was suitable to be applied for reversible adsorption (Loh et al. 2013). The effect of desorption time in the range of 5-25 minutes of sonication was investigated. It was found that maximum desorption time for the analytes was achieved within 15 minutes of sonication. Beyond 15 minutes of sonication, the peak area of analyte was decreased (Fig. 3c). This is probably due to the heat produced by the sonicator caused the degradation of analyte during the sonication step. Therefore, desorption time of 15 minutes prior to sonication was chosen for subsequent experiments.

Effect of Mass of Sorbent on Peak Area of Analytes

For the optimization of the mass of sorbent, about 0.1g to 0.5g of Alg-MWCNT powder was employed. The result showed that the lowest proposed mass of sorbent which is 0.1 g gave the lowest peak area (Fig. 3d). 0.3 g of sorbent gives the highest peak area of analytes. No significant increase in the peak area was observed with further increase in sorbent mass. The peak areas continue to decrease even with the increase in the mass of sorbent. This might be due to the saturated capacity of MWCNTs as a primary sorption site, thus the excessive amount of sorbent used (more than 0.3 g) resulted in more difficult desorption and required higher volume of desorption solvent (Dahane et al. 2013). Hence, sorbent mass of 0.3 g was applied for subsequent studies as the peak area for the analytes were at maximum.

Method Validation and Analytical Performance of D-μ-SPE

The optimization of dispersive solid phase extraction method was then validated for relative recoveries, sample calibration and LOD. Good linearity from the linearity range of 1-500 $\mu g.L^{-1}$ was obtained for the four analytes, where the coefficients of determination (R^2) were in the range of 0.9959-0.9996. The LODs and LOQs were calculated at a signal to noise ratio of 3 and the results were in the range of 0.03-0.08 $\mu g.L^{-1}$ for LODs. The precision of the method was measured by the relative standard deviation (RSD) and the results were between 2.6-7.5 for % RSD. Table 1 shows the validation data for D-μ-SPE of NSAIDs from water samples.

Application of D-μ-SPE on River and Tap Water Samples

The developed Alg-MWCNT-D-μ-SPE method was successfully applied to river and tap water samples. Relative recovery studies were conducted by spiking the water samples to give a final concentration of 100 $\mu g.L^{-1}$. The results were tabulated in Table 2. It showed that good relative recoveries were obtained in the range of 75 % to 105 %. Thus, dispersive micro

Table 1: Validation data of D-μ-SPE of NSAIDs in water samples.

Sample	Analytes	Linear range ($\mu g.L^{-1}$)	Coefficient of determination R^2	LOD ($\mu g.L^{-1}$)	Precision (RSD, %) ($n = 3$)
Tap water	Salicylic Acid	1-500	0.9989	0.054	3.2
	Naproxen	1-500	0.9975	0.063	5.1
	Diclofenac	1-500	0.9959	0.034	3.9
	Ibuprofen	1-500	0.9996	0.080	2.7
	Mefenamic Acid	1-500	0.9994	0.078	7.5
River water	Salicylic Acid	1-500	0.9985	0.061	4.1
	Naproxen	1-500	0.9992	0.068	7.1
	Diclofenac	1-500	0.9991	0.042	2.6
	Ibuprofen	1-500	0.9993	0.059	5.9
	Mefenamic Acid	1-500	0.9979	0.075	5.6

N.Z. Othman et al.

Table 2: Relative recoveries (%) and method precisions (RSD %, *n* = 3) of D-μ-SPE in tap water and river water samples.

Sample	Analyte	Relative recoveries (%)	RSD (%)
		Spiking level (*n* = 3) 100 μg.L^{-1}	
Tap water	Salicylic Acid	82.7	4.2
	Naproxen	90.1	5.9
	Diclofenac	102.5	6.6
	Ibuprofen	75.3	3.8
	Mefenamic Acid	89.1	4.1
River water	Salicylic Acid	77.4	2.3
	Naproxen	86.2	7.3
	Diclofenac	105.1	6.8
	Ibuprofen	83.0	2.0
	Mefenamic Acid	97.4	3.6

solid phase extraction proved to be an efficient technique for extracting drugs in aqueous matrices. Fig. 4 shows HPLC chromatogram of five NSAIDs which are salicylic acid (SAL), naproxen (NAP), diclofenac (DIC), ibuprofen (IBU) and mefenamic acid (MEF) in river and tap water samples.

CONCLUSION

In this study, we report the use of alginate incorporated with multi-walled carbon nanotubes for the extraction of acidic drugs using dispersive micro solid phase extraction combined with HPLC-UV. Several parameters were optimized in D-μ-SPE method. The optimum parameters were used in the analysis of real samples. The optimum conditions were as follows: pH of the solution at pH 3, 30 minutes for the extraction time, 15 minutes for the desorption time and 0.3 g for the mass of sorbent. All the five analytes which are salicylic acid, naproxen, diclofenac, ibuprofen and mefenamic
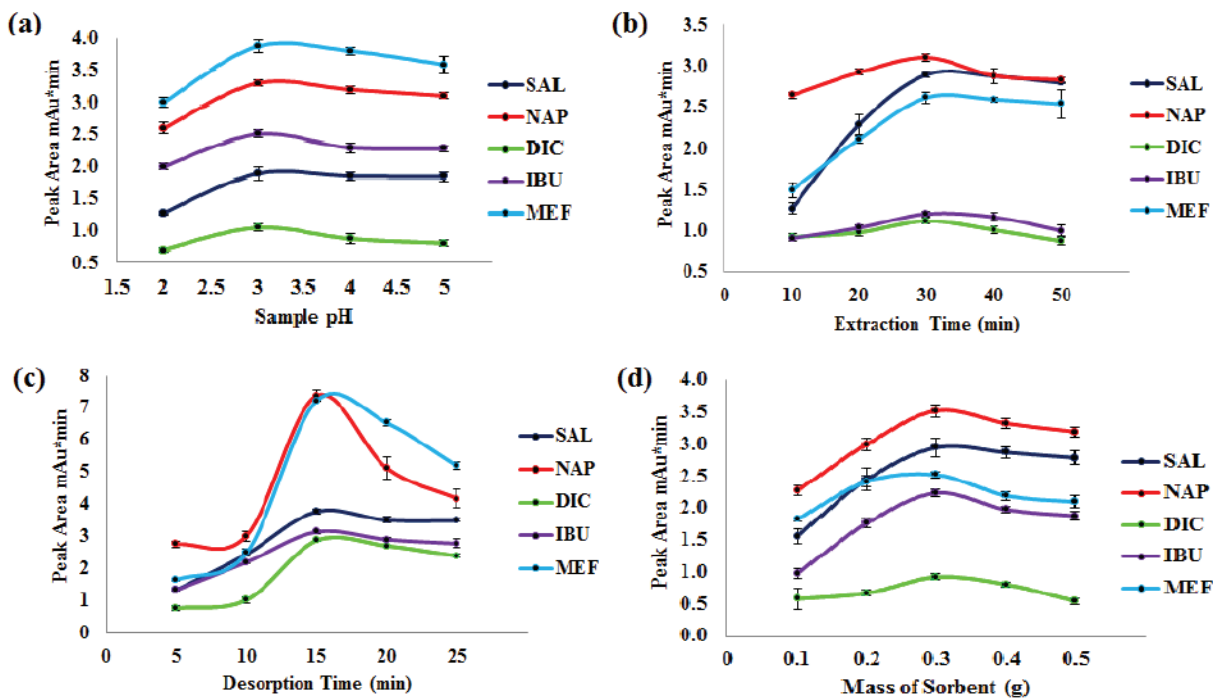

Fig. 3: Optimization for the extraction performance of Alg-MWCNT. (a) Effect of sample pH, (b) extraction time, (c) desorption time and (d) mass of sorbent on Alg-MWCNT-D-μ-SPE of NSAIDs in water samples. (Error bars represent standard deviations of results, n = 3).
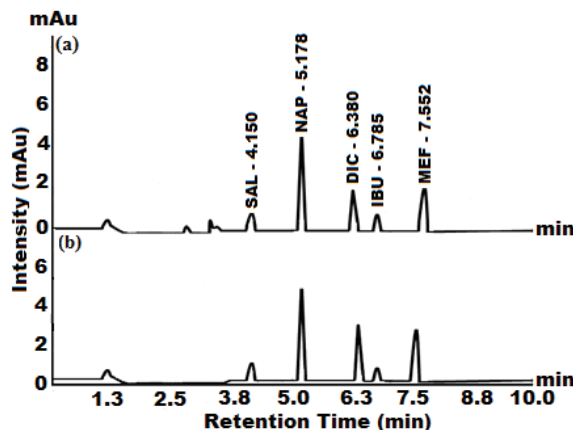
Fig. 4: HPLC chromatogram of five NSAIDs in (a) river water samples and (b) tap water samples.

acid were successfully extracted using the same conditions in D-μ-SPE. Good linearities were achieved for the analytes with coefficients of determination R^2, in the range of 0.9959-0.9996. The method was successfully applied to the analysis of river water and tap water samples, with good relative recoveries in the range of 75-105 %. Thus, the D-μ-SPE method proved to be a simple, sensitive, selective and green extraction method which could potentially be used in the chemical laboratory for routine analysis of water samples.

ACKNOWLEDGEMENT

REFERENCES

Asghari, A., Khanalipoor. F., Barfi, B. and Rajabi, M. 2016. Optimized miniaturized air-assisted liquid-liquid microextraction for determination of non-steroidal anti-inflammatory drugs in bio-fluid samples. RSC Adv., 6(111): 109473-109484.

Azzouz, A. and Ballesteros, E. 2012. Combined microwave-assisted extraction and continuous solid-phase extraction prior to gas chromatography–mass spectrometry determination of pharmaceuticals, personal care products and hormones in soils, sediments and sludge. Sci. Total Environ., 419: 208-215.

Braccini, I., Grasso, R.P. and Pérez, S. 1999. Conformational and configurational features of acidic polysaccharides and their interactions with calcium ions: A molecular modeling investigation. Carbohydrate Research, 317(1-4): 119-130.

Crini, G. 2005. Recent developments in polysaccharide-based materials used as adsorbents in wastewater treatment. Progress in Polymer Science, 30(1): 38-70.

Dahane, S., García, M.G., Bueno, M.M., Moreno, A.U., Galera, M.M. and Derdour, A. 2013. Determination of drugs in river and wastewaters using solid-phase extraction by packed multi-walled carbon nanotubes and liquid chromatography-quadrupole-linear ion trap-mass spectrometry. J. Chromatogr. A, 1297: 17-28.

Fertah, M., Belfkira, A., Taourirte, M. and Brouillette, F. 2017. Extraction and characterization of sodium alginate from Moroccan *Laminaria digitata* brown seaweed. Arabian Journal of Chemistry, 10: S3707-S3714.

Hanapi, N.S.M., Sanagi, M.M., Ismail, A.K., Ibrahim, W.A.W. and Ibrahim, W.N.W. 2017. Ionic liquid-impregnated agarose film two-phase micro-electrodriven membrane extraction (IL-AF-μ-EME) for the analysis of antidepressants in water samples. J. Chromatogr. B, 1046: 73-80.

Hennion, M.C. 1999. Solid-phase extraction: Method development, sorbents, and coupling with liquid chromatography. J. Chromatogr. A, 856(1-2): 3-54.

Hernando, M.D., Mezcua, M., Fernández-Alba, A.R. and Barceló, D. 2006. Environmental risk assessment of pharmaceutical residues in wastewater effluents, surface waters and sediments. Talanta, 69(2): 334-342.

Ibrahim, W.N.W., Sanagi, M.M., Hanapi, N.S.M. and Ibrahim, W.A.W. 2015. Preparation of chemically stable multi-wall carbon nanotubes reinforced blended agarose/chitosan composite film. Der Pharma Chemica, 7(6): 353-356.

Jeon, S., Yun, J., Lee, Y.S. and Kim, H.I. 2010. Removal of Cu(II) ions by alginate/carbon nanotube/maghemite composite magnetic beads. Carbon Letters, 11(2): 117-121.

Lee, C.H., Shin, Y., Nam, M.W., Jeong, K.M. and Lee, J. 2014. A new analytical method to determine non-steroidal anti-inflammatory drugs in surface water using in situ derivatization combined with ultrasound-assisted emulsification microextraction followed by gas chromatography-mass spectrometry. Talanta, 129: 552-559.

Lee, K.Y. and Mooney, D.J. 2012. Alginate: Properties and biomedical applications. Progress in Polymer Science, 37(1): 106-126.

Loh, S.H., Sanagi, M.M., Ibrahim, W.A.W. and Hasan, M.N. 2013. Multi-walled carbon nanotube-impregnated agarose film microextraction of polycyclic aromatic hydrocarbons in green tea beverage. Talanta, 106: 200-205.

Meek, I.L., Van de Laar, M.A. and Vonkeman, H. 2010. Non-steroidal anti-inflammatory drugs: an overview of cardiovascular risks. Pharmaceuticals, 3(7): 2146-2162.

Moeder, M., Schrader, S., Winkler, M. and Popp, P. 2000. Solid-phase microextraction–gas chromatography-mass spectrometry of biologically active substances in water samples. J. Chromatogr. A. 873(1): 95-106.

Osman, R., Saim, N., Juahir, H. and Abdullah, M.P. 2012. Chemometric application in identifying sources of organic contaminants in Langat river basin. Environ. Monit. Assess., 184(2): 1001-1014.

Park, S.Y. and Myung, S.W. 2015. Simultaneous determination of non-steroidal anti inflammatory drugs in aqueous samples using dispersive liquid-liquid microextraction and HPLC analysis. Bull. Korean Chem. Soc., 36(12): 2901-2906.

Petrovic, M., Radjenovic, J., Postigo, C., Kuster, M., Farre, M., De Alda, M.L. and Barceló, D. 2008. Emerging contaminants in wastewaters: Sources and occurrence. In: Emerging Contaminants from Industrial and Municipal Waste, pp. 1-35.

Ren, X., Chen, C., Nagatsu, M. and Wang, X. 2011. Carbon nanotubes as adsorbents in environmental pollution management: a review. Chemical Engineering Journal, 170(2-3): 395-410.

Sagristà, E., Larsson, E., Ezoddin, M., Hidalgo, M., Salvadó, V. and Jönsson, J.Å. 2010. Determination of non-steroidal anti-inflammatory drugs in sewage sludge by direct hollow fiber supported liquid membrane extraction and liquid chromatography-mass spectrometry. J. Chromatogr. A, 1217(40): 6153-6158.

Sahasathian, Teerawat, Praphairaksit, N. and Muangsin, N. 2010. Mucoadhesive and floating chitosan-coated alginate beads for the controlled gastric release of amoxicillin. Archives of Pharmacal Research, 33(6): 889-899.

Saim, N.A., Dean, J.R., Abdullah, M.P. and Zakaria, Z. 1997. Extraction of polycyclic aromatic hydrocarbons from contaminated soil using Soxhlet extraction, pressurised and atmospheric microwave-assisted extraction, supercritical fluid extraction and accelerated solvent extraction. J. Chromatogr. A, 791(1-2): 361-366.

Silva, A.R.M., Portugal, F.C. and Nogueira, J.M.F. 2008. Advances in stir bar sorptive extraction for the determination of acidic pharmaceuticals in environmental water matrices: comparison between polyurethane and polydimethylsiloxane polymeric phases. J. Chromatogr. A, 1209(1-2): 10-16.

Spitalsky, Z., Tasis, D., Papagelis, K. and Galiotis, C. 2010. Carbon nanotube-polymer composites: Chemistry, processing, mechanical and electrical properties. Progress in Polymer Science, 35(3): 357-401.

Tanwar, S., Di Carro, M. and Magi, E. 2015. Innovative sampling and extraction methods for the determination of nonsteroidal anti-inflammatory drugs in water. J. Pharm. Biomed. Anal., 106: 100-106.

Vijayalakshmi, K., Gomathi, T., Latha, S., Hajeeth, T. and Sudha, P.N. 2016. Removal of copper (II) from aqueous solution using nanochitosan/sodium alginate/microcrystalline cellulose beads. International Journal of Biological Macromolecules, 82: 440-452.

Wang, T., Liu, S., Gao, G., Zhao, P., Lu, N., Lun, X. and Hou, X. 2017. Magnetic solid phase extraction of non-steroidal anti-inflammatory drugs from water samples using a metal organic framework of type Fe_3O_4/MIL-101 (Cr), and their quantitation by UPLC-MS/MS. Microchim. Act., 184(8): 2981-2990.

Żwir-Ferenc, A. and Biziuk, M. 2006. Solid phase extraction technique-trends, opportunities and applications. Polish Journal of Environmental Studies, 15(5).

Concentration of Trace Metals in Blood and the Relationship with Reproductive Hormones (Estradiol and Progesterone) of Obese Females Living Around A Mining Area in Brits, South Africa

G. N. Lion†*, G. A. Ogunbanjo** and J.O. Olowoyo*

*Department of Biology, Sefako Makgatho Health Sciences University, Medunsa 0204, South Africa
**Department of Family Medicine & PHC, Sefako Makgatho Health Sciences University, Medunsa, 0204, South Africa
†Corresponding author: G. N. Lion; ntebo.lion@smu.ac.za

ABSTRACT

Obesity is a rapidly growing problem in South Africa, with 70% of women reported as being obese. Studies have reported that high levels of trace metals may impair the production of reproductive hormones, which may, in turn, interfere with normal oocyte development in females. This study investigated the concentrations of trace metals in blood samples of obese individuals living around a mining industry and examined the overall effect on reproductive hormones of these obese females. A mixed-method research approach consisting of qualitative and quantitative (cross-sectional descriptive survey) was used in the study. Only females with BMI ≥ 30 were allowed to participate in the study. Blood samples were collected in two 5 mL tubes from each of the participants. Concentrations of trace metals in the blood samples were determined by the use of ICP-MS. Hormonal level measurement was also carried out. The results showed that the trace metal concentrations in the blood samples of participants were in the order Mn > Cr > Co > As > Pb > Cd. The mean concentrations of Mn, Cr, Co and As were above the WHO standards. The hormonal analysis showed that there was a positive correlation between estradiol and progesterone levels with Mn concentration. Cr and As concentrations showed a negative correlation between estradiol and progesterone levels. Also, a negative correlation was established between estradiol levels with Pb and Cd concentrations. The study showed that exposure to trace metals as pollutants may have an impact on the general and reproductive health of obese females living around mining activities.

INTRODUCTION

Trace metals occur naturally in the environment and form essential components of humans, plants and animals. However, increasing levels of these metals in the environment can adversely affect the environment and living organisms (Jarup 2003). Various sources of these elements include soil erosion, natural weathering of the earth's crust, mining, industrial effluents, urban runoff, sewage discharge geogenic, agricultural, pharmaceutical, domestic effluents, vehicular emissions and atmospheric depositions among others (Wang et al. 2005, Wang et al. 2010, Morais et al. 2012).

Mining activities in South Africa have been implicated as one of the major contributors of trace metals in the environment (Lion et al. 2012, Olowoyo et al. 2013). It has been reported that these mining activities may increase the concentration of trace metals in soil and plants around its vicinity if unchecked or uncontrolled (Koz et al. 2012, Olowoyo et al. 2013).

Trace metals enter the surroundings by natural means and through human activities. These pollutants may then find their way into the human body through occupational exposure which includes mining dust, inhalation of dust, direct ingestion of soil and water, dermal contact of contaminated soil and water, and consumption of vegetables grown in agricultural land situated near mining activities (Olowoyo & Lion 2016). The most commonly found trace metals in wastewater include As, Cd, Cr, Cu, Pb, Ni, and Zn, all of which cause risks for human health and the environment (Lambert et al. 2000).

Various studies have been conducted to evaluate human health risks due to trace metal exposure through various exposure pathways, especially soil and food chain (MacIntosh et al. 1996, Albering et al. 1999, Hough et al. 2004, Baastrup et al. 2008, Mari et al. 2009, Man et al. 2010). Although these metals have crucial biological functions in living cells, often their chemical coordination and oxidation-reduction properties have given them an additional benefit so that they can escape control mechanisms such as homeostasis, transport, compartmentalization and binding to required cell constituents (Monisha et al. 2014). These metals bind with protein sites which are not made for them by displac-

ing original metals from their natural binding sites causing malfunctioning of cells and ultimately toxicity. Research has also revealed that oxidative deterioration of biological macromolecules is primarily due to binding of trace metals to the DNA and nuclear proteins (Flora et al. 2008). Metals sometimes act as a pseudo element of the body while at certain times they may even interfere with metabolic processes (Monisha et al. 2014).

It was recently reported that trace metals such as, Cd, Zn, Pb, Ni, and Hg may exhibit endocrine-disrupting activity (Georgescu et al. 2011). Divalent metals, including Pb and Hg, can initiate the estrogen receptor by interacting with amino acids at the receptor binding site (Zhang et al. 2008), and both metals exert estrogenic changes in experimental models (Choe et al. 2003). Stoica et al. (2000), also reported that Cd may obstruct the hormone-binding domain of the estrogen receptor- , thereby affecting subsequent transcriptional processes (Guével et al. 2000). A study by Georgescu et al. (2011), also revealed that the Zn atom from the Zn fingers of the estrogen receptor can be replaced by several trace metal molecules such as Co, Cu, Cd, and Ni, which then interferes with hormonal functions.

Denier et al. (2009), reported that Zn, Cu and Cd were able to potentiate the estradiol-induced response in a dose-dependent manner, thus indicating that Zn can act as a potential endocrine disrupter by modulating the estrogenic activity of endogenous hormones (xenoestrogen).

The World Health Organization (2015), reported that more than 10 % of females are severely affected by infertility. The reproductive health of females of childbearing age is currently a major worldwide public health problem. According to Mendola et al. (2007) and Bloom et al. (2011), environmental factors, such as exposure to trace metals, can cause reproductive dysfunction in females and affect their reproductive hormones. Toxic metals may induce hormonal changes affecting the menstrual cycle, ovulation, and female fertility (Sengupta 2015). Furthermore, hormones have been reported to have an affinity for trace metals. It has been reported that trace metals tend to bind to hormones at the receptors site and cause hormonal dysfunction (Georgescu et al. 2011). Metals, such as Pb, Cd, and As, are reproductive toxicants widely distributed in the environment (CDC 2005). Several epidemiological studies on menstruation have indicated that metals affect hormone levels (Mednola et al. 2007, Gallagher 2009, Krieg 2007, Nagata 2005, Guo 2011). Furthermore, Pb and Cd have been identified in human follicular fluid (Paksy 2001, Al Saleh 2007, Langley 2014) and As was shown to cause dose-related increases in ovarian tumours (Tokar 2011). Chang et al. (2006), indicated that females with blood Pb levels higher than 25 µg/L had

a 3-fold increased risk of infertility compared with females whose blood Pb levels were less than 25 µg/L.

This study addresses the devastating effect of trace metals in blood and the relationship on reproductive hormones (estradiol and progesterone) of obese females exposed to mining activities. This is due to the recent report that showed that 70% of females in South Africa have been reported as either overweight or obese. According to the survey conducted by the South African Medical Research Council (SAMRC), Statistics South Africa and the Department of Health (2015), females are more prone to extra weight/pounds than their male counterparts (De Ridder & Coetzee 2015). More devastating report for obese females is the fact that trace metals have recently been linked to health issues associated with obesity. Furthermore, significant relationships between metallic elements (including blood Zn, Cu, Mn, and Hg) with obesity, and a positive relationship with body mass index (BMI), low-density lipoprotein cholesterol (LDL - C), triglyceride, total cholesterol, and homeostatic model assessment of insulin resistant (HOMA - IR) has been demonstrated in the literature (Feldman et al. 2015, Fan et al. 2017).

However, studies relating to trace metals and their role on the reproductive hormones such as estradiol and progesterone especially in obese females exposed to mining activities have not been done in South Africa, to the best of our knowledge. Even though it has been highlighted that 70% of females are classified as either obese or overweight. Literature also indicates that increasing interest should also be directed towards interactions between different elements (Blazewicz et al. 2013) as a means of understanding the role of trace metals exposure to human health which includes reproduction.

The toxicity of trace metals disrupts the body's natural ability to balance blood sugar and metabolize cholesterol (Feldman et al. 2015). Obesity has also been associated with pregnancy complications and plays a role in increasing fertility problems, e.g. gestational diabetes, pre-eclampsia, sleep apnoea (Tasneem et al. 2008). It has also been reported that trace metals may impair the production of reproductive hormones, which may, in turn, interfere with normal oocyte development (Najeba & Mohamad 2013). Their toxicity impairs the production of estradiol and progesterone. Moreover, trace metals play a role in increasing fertility problems and affect the hypothalamic-pituitary-ovarian axis (Tasneem et al. 2008).

Toxicity by one trace element may cause a deficiency or disturb the bioavailability of another element (Cepeda-Lopez et al. 2011). High tissue copper aggravates obesity and tends to raise tissue sodium levels while lowering tissue potassium levels, subsequently resulting in water retention (Demer-

dash 2015, Fan et al. 2017). Higher prevalence of Iron (Fe) deficiency has been reported in obese children and females than in males (Ferrari et al. 2011). Hence the objective of the study was to investigate the concentrations of trace metals in blood samples of obese females living around a mining industry and to examine the overall effect on reproductive hormones of obese females.

MATERIALS AND METHODS

Study Design

A mixed research approach consisting of a qualitative and quantitative cross-sectional descriptive survey was carried out. For the analysis of blood samples collected, ICP-MS was used to determine the concentrations of trace metals in the blood of the obese individuals used in the study.

Study Setting

The study was carried out in a mining area situated in Brits/ North West, South Africa [25°44′46′ S; 28°11′17′ E]. An initial visit to the area showed 82 housing units. It was assumed from the study that each housing unit had either a young female or adult member living in them. According to the report provided by De Ridder & Coetzee (2015), 70% of women in South Africa are reported to be obese, hence it is envisaged to have about 57 obese females from the mining area who may qualify to participate in the study. However, a total of 40 obese females (aged 16-45 years) participated in the study.

Sample/Study Population

Female teenagers ($\geq$ 18 years) and adults aged 18-45 years with BMI $\geq$ 30 were identified and participated in the study. A written informed consent form was distributed to participants. Due to the sensitivity of the study, the identity of participants was protected. No unique identifier was used and the study was conducted with only willing participants.

Blood samples were collected from each female participant. Blood was drawn by vein puncture by a certified professional from participants under contamination controlled conditions. Blood samples were collected in two 5 mL BD Vacutainer sterile glass tubes certified for trace metals analysis and hormonal assay. An amount of 143 USP units of sodium heparin was put in each tube (only for trace metal analysis) as an anticoagulant. Tubes were enclosed with a royal blue coloured Hemogard enclosure then taken to National Institute for Occupational Health (NIOH) accredited lab for trace metal analysis. For hormonal determination, test tubes with a yellow coloured Hemogard closure were used. The samples were then taken to Dr. George Mukhari Academic Hospital National Health Laboratory Services (DGMAH NHLS) for analysis. All blood samples were stored at ambient temperatures until analysed for trace metals and hormonal levels (estradiol and progesterone) within twelve hours

Individuals with BMI $\geq$ 30 but taking mineral supplements and those diagnosed with diabetes were excluded from the study. Females on hormone replacement therapy

Table 1: Characteristics of obese female participants living around a mining area in Brits (n = 40).

Variables	Study population
Age (years)	
18-35	67.5%
36-45	32.5%
BMI (kg/m^2)	
= 30	57.5%
>30 <35	17.5%
>35	25%
Metals [µg/L; $\overline{x} \pm$ SD (Range)]	
Mn	12.97 ± 6.04 (6.79 - 33.99)
Cr	3.70 ± 4.11 (0.41 - 19.01)
Co	2.19 ± 4.43 (0.20 - 18.8)
As	0.84 ± 0.41 (0.27 - 2.20)
Cd	0.20 ± 0.20 (0.02 - 1.10)
Pb [µg/dL; $\overline{x} \pm$ SD (Range)]	0.67 ± 0.34 (0.50 - 1.84)
Hormones	
Estradiol [pmol/L; $\overline{x} \pm$ SD (Range)]	724.95 ± 2393.24 (37 - 15040.00)
Progesterone [nmol/L; $\overline{x} \pm$ SD (Range)]	6.79 ± 17.46 (0.3 - 93.50)

and those using contraceptives were also excluded from the study as this may affect the hormone balance.

RESULTS AND DISCUSSION

Table 1 shows the results of trace metal analysis and hormonal levels from blood samples collected from obese females living around a mining area in Brits. From the results, the mean concentrations of Mn, Cr, Co, As and Pb were higher than the permissible limit for human exposure (WHO 2000). However, the mean concentration of Cd was lower than the permissible limit.

The mean concentrations of estradiol and progesterone were within the acceptable hormonal range. However, progesterone level was lower than ≤15.90 nmol/L while estradiol was higher than 275 pmol/L which are levels indicating anovulation levels (Gaskins et al. 2009). A significant and strong positive correlation existed between the blood estradiol levels and progesterone levels (r=0.88; p<0.01), which shows that both hormones influence the increase or decrease of each other. The correlation was also determined among the levels of Mn, Cr, Co, As, Pb Cd and the reproductive hormones (estradiol and progesterone) in the blood of obese females living around a mining area (Table 3).

The concentration of Mn was higher than all the metals with a range of 6.79-33.99 µg/L, a mean of 12.97 µg/L and a standard deviation of 6.04 in obese females. The results also showed that there was a positive correlation between estradiol (r=0.08; p>0.05) and progesterone (r=0.12; p>0.05) levels with Mn concentration. The results showed that an increase in Mn concentrations increases progesterone and estradiol levels. Manganese was also positively correlated with Co (r=0.40; p<0.01), where a significant increase in one metal increased the other.

The high levels of Mn recorded in the participants' blood may be due to mining activities since the mine is situated opposite to the informal settlements, industrial activities in the area, vehicular emissions (from the main road next to the informal settlement) and fuel combustion (used for heat in winter and food preparation). The concentration of Mn in this study is similar to those reported by Fan et al. (2017) with a range 3.21-58.86 µg/L and mean 10.69 µg/L in obese individuals aged 6-19 years, in the United States, which demonstrated a significant relationship between metallic elements (including blood Zn, Cu, Mn, and Hg) with obesity, and a positive relationship with BMI, low-density lipoprotein cholesterol (LDL-C), triglyceride, total cholesterol, and homeostatic model assessment of insulin-resistant (HOMA-IR). Their findings showed that the relationship between obesity and metallic elements could be different in obese populations with elevated BMI or changes in other obesity biochemical parameters when compared to populations with lower BMI. The findings of this study also correlate with the findings of Stasys (2007) and Najeba & Mohamad (2013) which showed that high levels of Mn may affect female health and further impact fertility and fecundity (Gallagher et al. 2010).

The concentration of Cr ranged between 0.41-19.01 µg/L, a mean of 3.70 µg/L and a standard deviation of 4.11 in obese females. The results showed that there was a weak and negative correlation between Cr concentration with es-

Table 2: WHO standards/ permissible limits for human exposure to trace metals (µg/L).

Trace Metals	Mn	Cr	Co	As	Cd	*Pb
Levels	12.60	0.23	0.30	1.00	1.12	0.08

* (µg/dL)

Table 3: Correlations between trace metals and reproductive hormones in the blood of obese females living around a mining area in Brits (n = 40).

Variables	Mn	Cr	Co	As	Pb	Cd	Estradiol	Progesterone
Mn	1	0.143	0.404**	0.088	0.027	0.007	0.078	0.122
Cr	0.143	1	-0.074	0.053	0.032	0.332*	-0.138	-0.152
Co	0.404**	-0.074	1	-0.053	0.187	-0.156	0.043	-0.012
As	0.088	0.053	-0.053	1	-0.069	0.128	-0.045	-0.064
Pb	0.027	0.032	0.187	-0.069	1	0.178	-0.114	-0.038
Cd	0.007	0.332*	-0.156	0.128	0.178	1	-0.054	0.014
Estradiol	0.078	-0.138	0.043	-0.045	-0.114	-0.054	1	0.878**
Progesterone	0.122	-0.152	-0.012	-0.064	-0.038	0.014	0.878**	1

* (p< 0.05), ** (p< 0.01)

tradiol (r= -0.14; p>0.05) and progesterone (r= -0.15; p>0.05) levels. This means that higher Cr concentrations above the permissible limit lower the progesterone and estradiol levels (Table 3). The high levels of Cr in the blood of participants may be as a result of emissions from a chromium mine next to the informal settlement and several industries such granite cutting and tire manufacturing industries located within a 3 km radius from the informal settlement. Other sources of Cr may be due to the combustion of fossil fuels and cigarette smoking. Since the participants were not active smokers, the high levels of Cr in their blood may be as a result of smoke emission from the mine next to the residential area as well as the result of passive smoking as reported by Paakko et al. (1989) and Bernhard et al. (2015). Their findings show that concentrations of about 4.3 mg/kg (dry weight) are found in smokers compared to 1.3 mg/kg in non-smokers, increasing with age and smoking time.

According to Martin & Griswold (2009) and Tangahu et al. (2011), chromium is known as a carcinogen, which causes skin cancer, lung cancer and inflammation of the blood vesicles. High levels of Cr reported in a study by Ajayi et al. (2012), showed Cr levels of 45.16±1.16 μg/dL may disturb the production of reproductive hormones and interfere with normal oocyte development. Furthermore, it has been reported to cause spontaneous abortions and result in low birth weight (Bonde et al. 1992, Hjollund et al. 1995, Hertz-Picciotto 2000, Ajayi et al. 2012). Since decreasing progesterone levels were reported with high concentrations of Cr, we can deduce that our findings agree with those found in the literature (Hertz-Picciotto 2000, Ajayi et al. 2012), that spontaneous abortion can occur as a result of high Cr concentrations and low progesterone levels in the blood.

Cobalt concentrations in the blood of obese females ranged between 0.20-18.84 μg/L, with a mean of 2.19 μg/L and a standard deviation of 4.43 μg/L. The results showed that there was no correlation between Co concentrations with estradiol (r=0.04; p>0.05) and progesterone (r= -0.01; p>0.05) levels (Table 3). The results of this study show that high Co concentrations do not affect the levels of both hormones (estradiol and progesterone). However, in another study carried out by Philippe (1975), Co radiation at high doses has been shown to elicit pro-found decrements in reproductive ability in animal species. The study further shows that single doses of >100rad of Co radiation cause decreased fertility in exposed female mice. Their findings further show that continuous exposure of female mice to an average daily dose 8–16 rad/day causes a decreased number of offspring per litter and decreased reproductive performance, with 100% sterility occurring at 32 weeks of exposure at 8 rad/day. Pedigo & Vernon (1993), reported that cobalt dichloride (400 ppm in drinking water for 10 weeks) increases pre-implantation losses of pregnant female rats.

Sources of high levels of Co recoded from the participants may be as a result of the consumption of alcoholic beverages (beer) which participants were observed to highly indulge in. Other problems associated with high Co apart from the mining activities is the consumption of large quantities of alcoholic beverages (beer) which may contain foam stabilizers such as cobalt sulphate ($CoSO_4$) or cobalt chloride ($CoCl_2$). Reports show that individuals who consume a lot of beer with $CoSO_4$ have suffered from cardiomyopathy which is the weakening of the heart (Alexander 1972, Bonenfant et al. 1969, Morin & Daniel, 1967). Alcohol and heart conditions may have fatal consequences on obese individuals, especially when coupled with trace metal exposure from different sources of pollutants. Other sources contributing to high Co levels in the blood of participants include occupational exposure (cobalt-containing alloys and salts) and environmental contamination due to industrial activities in Brits. Cobalt has also been reported to be carcinogenic in humans. Exposure to Co may initiate an inflammatory process that infiltrates the T- lymphocytes (immune-mediated cells) and increase the body's hypersensitivity response. There are no studies on the reproductive or developmental effects of Co exposure in humans, to the best of our knowledge, however, studies have reported on stunted growth and decreased survival of newborn puppies [Agency for Toxic Substances and Disease Registry (ATSDR) 1992, California Environmental protection Agency (CalEPA) 1997)].

The mean concentration of As in the blood of obese female participants were below the permissible limit of 1.00 μg/L. The mean concentration was 0.84 ± 0.41 μg/L with a range of 0.27-2.20 μg/L (Table 1). However, 29.3% of the participants recorded, had As value higher than 1.00 μg/L. The results from Table 3 shows that there was a weak negative correlation between As and hormonal levels progesterone (r= -0.06; p>0.05) but there was no correlation with estradiol (r= -0.04; p>0.05). This shows that as the concentrations of As increases, there was a decrease in the levels of progesterone but no effect on estradiol levels.

Arsenic is carcinogenic, it causes cancer in soft organs, skin, lungs, liver and bladder (Martin & Griswold 2009, Tangahu et al. 2011). Sources of As in the environment include mining or industrial activates as well as lifestyle activities such as cigarettes smoking. Literature shows that no similar studies have been done on the effects of As on obese females and reproductive hormones. However, a study by Akram et al. (2010), examined the adverse effects of As exposure on uterine function and structure of female rats. The study findings show that there was a dose-dependent decrease observed in

mean uterine diameter, epithelial height, the thickness of the endometrium, myometrium, and in plasma levels of estradiol, progesterone, FSH and LH in all the treatment groups compared to control at 100 and 200 ppm of sodium arsenite in drinking water. The study concluded that arsenic is a major threat to female reproductive health, acting as a reproductive toxicant and as an endocrine disruptor. The study further showed that As restricted the function and structure of the uterus, by altering the gonadotropins and steroid levels, not only at high dose concentration but also at low (50 ppm) levels, when the rats become mature.

The concentration of Pb was also higher than the permissible limit of 0.08 μg/dL value with a mean of 0.67 ± 0.34 μg/dL and range of 0.50-1.86 μg/dL. A weak negative correlation existed between Pb concentration and levels of estradiol (r= -0.11; P>0.05) however no correlation was established between Pb concentration and progesterone (r= -0.04; p>0.05) levels. Therefore, higher levels of Pb above the permissible limit indicated a decrease in estradiol levels, while there was no effect on progesterone levels. Sources of Pb may be as a result of mining, paint, vehicular emissions and industrial activities.

When compared to the study by Ajayi et al. (2012), the mean concentration of lead was higher with a mean of 85.96 ± 1.09 μg/dL. However, their results showed that elevated serum levels of Pb may contribute to spontaneous abortion by lowering the progesterone levels. High levels of Pb have also been recorded in studies by Sekhar et al. (2009) and Patrick (2006), where it was reported that once Pb has been absorbed in the blood, it can decrease the number of red blood cells and lead to anaemia. According to Najeba & Mohamad (2013), Pb has also been detected in human follicular fluid (liquid composed primarily of hormones) which interferes with reproduction. In expectant females, prolonged exposure to high levels of Pb may lead to spontaneous abortions, premature delivery and low birth weights (UK Teratology Information Services 2010). This condition also has a direct effect of female fecundity especially when obesity is also a factor.

The lowest value of all the metals was recorded for Cd in the blood of obese female participants. Cd levels were below the permissible limit with a mean value of 0.20 ± 0.20 μg/L and a range of 0.02-1.10 μg/L. There was no correlation between Cd and progesterone (r=0.01) levels but a negative and weak correlation between Cd and estradiol (r= -0.05) levels was established. Correlations showed that as the concentrations of Cd increases, the level of progesterone were not affected, however, there was a decrease in the levels of estradiol.

Detected Cd levels in the blood of participants maybe as a result of household items such as detergent, paint, vehicular emissions and mining activities near the residential area. In a study by Ajayi et al. (2012), the mean concentration of lead was higher than the permissible limit set by WHO (2000), with a mean of 45.8 ± 0.77 μg/L. Their findings showed that high serum levels of Cd may contribute to spontaneous abortion due to its effect on progesterone levels.

However, even though lower levels have been recorded for As and Cd (Table 2), close monitoring is required as these metals may bioaccumulate and affect human health. The results show that there was a positive correlation between Mn levels and Co levels in the blood (r=0.40; p< 0.01). Blood Cr levels also showed a positive correlation with blood Cd levels (r=0.33; p<0.05). This observation showed that an increase in one metal had an impact on the increase of another metal.

Generally, from the results, obese participants with progesterone levels of < 0.3 nmol/L recorded high concentrations of Cr, Co and Pb. Moreover, an obese female participant with a high level of estradiol (3462 pmol/L) also had the highest Mn (33.99 μg/L) concentration in the blood. Several studies have suggested a link between trace metal exposure and hormonal variations (Gallagher et al. 2010, Pollack et al. 2011).

Furthermore, females with variations in reproductive hormone levels are considered at risk for cardiovascular diseases (Rossouw et al. 2002) breast cancer and ovarian cancer (Brinton et al. 1988). This study agrees with the findings of Aksel et al. (1976) and Lutoslawska et al. (2006) which showed that hormonal alterations may increase anovulation, with effects on fertility. Especially if these alterations are as a result of high levels of trace metals found in the blood. According to Tasneem et al. (2008), the prevalence of infertility in industrialized countries has increased from 8% to 15% over the past 2 decades. Ultimately these toxic metals may result in complications including fertility, fecundity and nulliparity (Najeba & Mohamad 2013). The association between metal toxicity and hormonal variations in obese females could have dire consequences for female reproductive health, which may lead to infertility.

CONCLUSION

The study showed that exposure to trace metals as pollutants may have an impact on the general and reproductive health of obese females living around mining activities. From the results, it can be concluded that mining activity may pose a high potential risk to these obese females' general health as well. However, the participants' exposure to trace metals found in the blood from the mining area may be as a result of multi pathways. The findings of this study cannot be generalizable due to the limitation of a small sample size. Furthermore, mechanisms on the impact of trace metals on reproductive

health are yet to be understood. More detailed and in-depth mechanisms on trace metals and reproductive health relationship are necessary for the future to examine whether adverse health outcomes occur, and provide decision-making support for pollution control in this metal-polluted area accordingly. Further research is underway with regards to understanding mechanisms on trace metals reproductive health of obese females exposed to mining activities.

ACKNOWLEDGEMENTS

REFERENCES

Ajayi, O.O., Charles-Davies, M.A. and Arinola O.G. 2012. Progesterone, selected heavy metals and micronutrients in pregnant Nigerian women with a history of recurrent spontaneous abortion. African Health Sciences, 12(2): 153-159.

Alexander, C.S. 1972. Cobalt-beer cardiomyopathy: A clinical and pathologic study of twenty-eight cases. The American Journal of Medicine, 53(4): 395-417.

Albering, H.J., van Leusen, S.M., Moonen, E.J.C., Hoogewerff, J.A. and Kleinjans, J.C.S. 1999. Human health risk assessment: A case study involving heavy metal soil contamination after the flooding of the river Meuse during the winter of 1993-1994. Environmental Health Perspective, 107: 37-43.

Akram, Z., Jalali, S. and Shami S.A. 2010. Adverse effects of arsenic exposure on uterine function and structure in female rat. Experimental Toxicology Pathology, 62: 451- 459.

Aksel S., Wiebe, R.H., Tyson, J.E. and Jones, G.S. 1976. Hormonal findings associated with a luteal cycle. Obstetrics and Gynecology, 48: 598-602.

[ATSDR] Agency for Toxic Substances and Disease Registry. 1992. Impact of lead contaminated soil on public health. Atlanta: U.S. Department of Health and Human Services.

Baastrup, R., Sørensen M, Balstrøm, T., Frederiksen, K. and Larsen, C.L. 2008. Arsenic in drinking-water and risk for cancer in Denmark. Environmental Health Perspective, 116(231).

Bernhard, D., Rossmann, A. and Wick, G. 2015. Metals in cigarette smoke. IUBMB Life, 57(12): 805-809.

Błażewicz, A., Klatka, M., Astel, A., Partyka, M. and Kocjan R. 2013. Differences in trace metal concentrations (Co, Cu, Fe, Mn, Zn, Cd and Ni) in whole blood, plasma, and urine of obese and nonobese children. Biological Trace Elements Research, 55(2): 190-200.

Bloom, M.S., Louis, G.M., Sundaram, R., Kostyniak, P.J. and Jain, J. 2011. Associations between blood metals and fecundity among women residing in New York State. Reproductive Toxicology, 31(2): 158-63.

Bonde, J.P.E., Olsen, J.H. and Hansen, K.S. 1992. Adverse pregnancy outcome and childhood malignancy with reference to paternal welding exposure. Scandinavian Journal of Work and Environmental Health, 18: 169-177.

Bonenfant, J.L., Auger, C., Miller, G., Chenard, J. and Roy, P.E. 1969. Quebec beer-drinkers' myocarditis: Pathological aspects. Annals of the New York Academy of Science, 156 (1): 577-582.

Brinton, L.A., Schairer, C., Hoover, R.N.F. and Fraumeni, J.F. 1988. Menstrual factors and risk of breast cancer. Cancer Investigation, 6: 245-254.

Choe, S.Y.K., So-Jung, K., Hae-Gyoung, L., Ji, C., Younghee, L. and Hun, K.Y. 2003. Evaluation of estrogenicity of major heavy metals.

The Science of the Total Environment, 15(21): 312 10.1016/S0048 -9697(03)00190-6.

CDC, Third National Report on Human Exposure to Environmental Chemicals. 2005. http://www.jhsph.edu/research/centers-and-institutes/center-for-excellence-in-environmental-health-tracking/Third_Report.pdf.

Chang, S.H., Cheng, B.H., Lee, S.L., Chuang, H.Y., Yang, C.Y. and Sung, F.C. 2006. Low blood lead concentration in association with infertility in women. Environmental Research, 101 (3): 380-386.

Cepeda-Lopez, A.C., Osendarp, S.J., Melse-Boonstra, A., Aeberli, I., Gonzalez-Salazar, F., Feskens, E., Villalpando, S. and Zimmermann, M.B. 2011. Sharply higher rates of iron deficiency in obese Mexican women and children are predicted by obesity-related inflammation rather than by differences in dietary iron intake. American Journal of Clinical Nutrition, 93: 975-983.

CalEPA/ DTSC. 1997. Selecting Inorganic Constituents as Chemicals of Potential Concern at Risk Assessment at Hazardous Waste Facilities. Final Policy. Human and Ecological Risk Division, DTSC.

Demerdash, H.M. 2015. Obesity and trace elements. Obesity Research Open Journal, 2(3): 98-100.

Denier, X. and Hill, E.M.2009. Estrogenic activity of cadmium, copper and zinc in the yeast estrogen screen. Toxicology in vitro, 23: 569-573.

De Ridder, J.H. and Coetzee, D. 2013. Childhood obesity in South Africa: Are we sitting on a time bomb? Global Journal of Health and Physical Education Pedagogy, 2: 239-249.

Flora, S.J.S., Mittal, M. and Mehta, A. 2008. Heavy metal induced oxidative stress & its possible reversal by chelation therapy. Indian Journal of Medical Research, 128: 501- 523.

Feldman, A., Aigner, E., Weghuber, D, and Paulmichl, K. 2015. The Potential role of iron and copper in pediatric obesity and nonalcoholic fatty liver disease. Biomedical Research International Article. https://doi.org/10.1155/2015/287401.

Fan, Y., Zhang, C. and Bu, J. 2017. Relationship between selected serum metallic elements and obesity in children and adolescent in the U.S. Nutrients, 9(2): 104.

Ferrari, P., Kulkarni, H., Dheda, S., Betti, S., Harrison, C., Timothy, G., Pierre, S.t. and Olynyk, J.K. 2011. Serum iron markers are inadequate for guiding iron repletion in chronic kidney disease. Clinical Journal of American Society of Nephrology, 6: 77-83.

Georgescu, B., Georgescu, Cărăban, S., Bouaru, A. and Paşcalău, S. 2011. Heavy Metals acting as endocrine disrupters. Animal Science and Biotechnologies, 44(2): 89.

Guével, R., Petit, F.G., Le Goff, P., Métivier, R., Valotaire, Y. and Pakdel, F. 2000. Inhibition of rainbow trout (Oncorhynchus mykiss) estrogen receptor activity by cadmium. Biology Reproduction, 63: 259-266.

Gallagher, C.M., Moonga, B.S. and Kovach, J.S. 2010. Cadmium, follicle-stimulating hormone, and effects on bone in women age 42-60 years, NHANES III. Environmental Research, 110(1): 105-11.

Guo, Z., Guo, H. and Xia, Y. 2011. Effects on endocrine system of female rats exposed to chronic arsenic. Journal of Hygiene Research, 40(2): 178-179.

Gaskins, A.J., Mumford, S.L., Zhang, C., Wactawski-Wende, J., Hovey, K.M., Whitcomb, B.W., Howards, P.P., Perkins, N.J., Yeung, E. and Schisterman, E.F. 2009. BioCycle Study Group. Effect of daily fiber intake on reproductive function: the BioCycle Study. American Journal of Clinical Nutrition, 90: 1061-1069.

Hjollund, N., Bonde, J.S. and Hansen, K. 1995. Male-mediated risk of spontaneous abortion with reference to stainless steel welding. Scandinavian Journal of Work, Environment & Health, 21(10): 5271/sjweh.37.

Hertz-Picciotto, I. 2000. The evidence that lead increases the risk for spontaneous abortion. American Journal of Industrial Medicine, 38: 300-309.

Hough, R.L., Breward, N., Young, S.D., Crout, N.M.J. and Tye, A.M. 2004. Assessing potential risk of heavy metal exposure from consumption of home-produced vegetables by urban populations. Environmental Health Perspective, 112(215).

Jarup, L. 2003. Hazards of heavy metal contamination. British Medical Bulletin, 68: 167-182.

Koz, B., Cevik, U. and Akbulut, S. 2012. Heavy metal analysis around Murgul (Artvin) copper mining area of Turkey using moss and soil. Ecological Indicators, 20: 17-23

Krieg, E.F. 2007. The relationships between blood lead levels and serum follicle stimulating hormone and luteinizing hormone in the Third National Health and Nutrition Examination Survey. Environmental Research, 104(3): 374-82.

Lambert, M., Leven, B.A. and Green, R.M. 2000. New methods of cleaning up heavy metal in soils and water. Environmental Science and Technology Briefs for Citizens; Manhattan, KS: Kansas State University.

Langley, S.A. 2014. Nutrition Screening Form for Female Infertility Patients. Canadian Journal of Dietetic Practice and Research, 75(4): 195-201.

Lion, G.N. and Olowoyo, J.O. 2012. Population health risk due to dietary intake of toxic heavy metals from *Spinacia oleracea* harvested from soils collected in and around Tshwane, South Africa. South African Journal of Botany, 88: 178-182.

Lutoslawska, G., Niedbalska, M., Skierska, E., Keska, A., Szpocinska-Byszewska, E. and Zolnowska, M. 2006. Plasma proinsulin, C-peptide and sex hormone concentrations in regularly menstruating premenopausal females with ovulatory and anovulatory menstrual cycles. Journal of Sports Medical and Physical Fitness, 46: 138-142.

MacIntosh, D.L., Kabiru, C., Scanlon, K.A. and Ryan, P.B. 2000. Longitudinal investigation of exposure to arsenic, cadmium, chromium and lead via beverage consumption. Journal of Exposure Analysis and Environmental Epidemiology, 10(2): 196-205.

Mari, M, Nadal, M., Schuhmacher, M. and Domingo, J.L. 2009. Exposure to heavy metals and PCDD/Fs by the population living in the vicinity of a hazardous waste landfill in Catalonia, Spain: Health risk assessment. Environment International, 35: 1034-1039.

Man, Y.B., Sun, X.L., Zhao, Y.G., Lopez, B.N. and Chung, S.S. 2010. Health risk assessment of abandoned agricultural soils based on heavy metal contents in Hong Kong, the world's most populated city. Environment International, 36: 570-576.

Monisha, J., Tenzin, T., Naresh, A., Blessy,B.M. and Krishnamurthy N.B. 2014. Toxicity, mechanism and health effects of some heavy metals. Interdisciplinary Toxicology, 7(2): 60-72.

Mendola, P., Messer, L.C. and Rappazzo, K. 2008. Science linking environmental contaminant exposures with fertility and reproductive health impacts in the adult female. Fertility Sterility., 89(2): 81-94

Martin, S. and Griswold, W. 2009. Human health effects of heavy metals. Environmental Science and Technology Briefs from Citizens, 15: 1-6.

Morais, S., Costa, F.G. and Pereira, M.L. 2012. Heavy metals and human health. In: Oosthuizen, J. (eds). Environmental Health-emerging Issues and Practice. 227-246.

Morin, Y. and Daniel, P. 1967. Quebec beer-drinkers' cardiomyopathy: Etiological considerations. Canadian Medical Association Journal, 97: 926-928.

Nagata, C., Nagao, Y., Shibuya, C., Kashiki, Y. and Shimizu, H. 2005. Urinary cadmium and serum levels of estrogens and androgens in postmenopausal Japanese women. Cancer Epidemiology Biomarkers and Prevention, 14(3): 705-708.

Najeba, S. and Mohamad J. 2013. Heavy metals in blood and urine impact on the woman fertility. Chemistry and Materials Research, 3(3): 2224-3224.

Olowoyo, J.O, Odiwe, A.L., Mkolo, N.M. and Macheka, L. 2013. Investigating the concentration of different elements in soil and plant composition from mining area. Polish Journal of Environmental Studies, 22: 1135-1141.

Olowoyo, J.O. and Lion, G.N. 2016. Urban farming as a possible source of trace metals in human diets. South African Journal of Science, 112(1/2): 2014 - 0444, 6.

Paakko, P., Kokkonen, P., Anttila, S. and Kalliomaki PL. 1989. Metals in cigarette smoke. Environmental Research, 49: 197-207.

Paksy, K., Gáti, I., Náray, M. and Rajczy, K. 2001. Lead accumulation in human ovarian follicular fluid, and in vitro effect of lead on progesterone production by cultured human ovarian granulosa cells. Journal of Toxicology and Environmental Health, Part A, 62(5): 359-366.

Patrick, L. 2006. Lead toxicity, part II: The role of free radical damage and the use of antioxidants in the pathology and treatment of lead toxicity. Alternative Medical Review, 11: 114-126.

Pedigo, N.G. and Vernon, M.W. 1993. Embryonic losses after 10-week administration of cobalt to male mice. Reproductive Toxicology, 7: 111-116.

Philippe, J.V. 1975. Fertility and irradiation: A preconceptional investigation in teratology. American Journal of Obstetrics and Gynecology, 123(7): 714-718.61.

Pollack, A.Z., Schisterman, E.F. and Goldman, L.R. 2011. Cadmium, lead, and mercury in relation to reproductive hormones and anovulation in premenopausal women. Environmental Health Perspective, 119(8): 1156 -1161.

Rossouw, J.E., Anderson, G.L., Prentice, R.L., Lacroix, A.Z., Kooperberg, C. and Stefanick, M.L. 2002. Risks and benefits of estrogen plus progestin in healthy postmenopausal women: principal results from the Women's Health Initiative randomized controlled trial. Journal of American Medical Association, 288: 321-333.

Saleh, I., Coskun, S., Mashhour, A., Shinwari, N., El-Doush, I. and Billedo, G. 2008. Exposure to heavy metals (lead, cadmium and mercury) and its effect on the outcome of in-vitro fertilization treatment. International Journal of Hygiene and Environmental Health, 211(5-6): 560-579.

Sekhar, K.C. 2009. Environmental risk assessment studies of heavy metal. contamination in the industrial area of Kattedan, India- a case study. UK Human and Ecological Risk Assessment: An International Journal, 12(2): 37-41 408-422.

Sengupta, P., Banerjee, R., Nath, S., Das, S. and Banerjee, S. 2015. Metals and female reproductive toxicity. Human Exposure Toxicology, 34(7): 679-97.

South African Medical Research Council (SAMRC). 2015. Statistics South Africa and the Department of Health. Annual Report.

Stasys, T. 2007. Investigation of distribution of heavy metals between blood plasma and blood cell Annali di Chimica. Società Chimica Italiana, 97: 1139.

Stoica, A. 2000. Activation of estrogen receptor- by the heavy metal cadmium. Molecular Endocrinology, 14: 10.1210/me.14.4.545.

Tasneem, G.K. 2008. Copper, chromium, manganese, iron, nickel, and zinc levels in biological samples of diabetes mellitus patients. Biological Trace Elements Research, 122: 1-18

Tangahu, B.V., Abdullah, S.R.S., Basri, H., Idris, M., Anuar, N. and Mukhlisin, M. 2011. A review on heavy metals (As, Pb, and Hg) uptake by plants through phytoremediation. International Journal of Chemistry and Engineering, 2011.

Tokar, E.J., Benbrahim-Tallaa, L. and Waalkes, M.P. 2011. Metal ions in human cancer development. Metal Ions in Life Science, 8: 375-401.

UK, Teratology Information Service Beta-adrenoceptor blocking drugs in pregnancy monograph. 2010. Retrieved from http://www.toxbase.org.

Wang, X., Sato, T., Xing, B. and Tao, S. 2005. Health risks of heavy metals to the general public in Tianjin, China via consumption of vegetables and fish. Science of the Total Environment, 350: 28-37.

Wang, X.Q., He, M.C., Xie, J., Xi, J.H. and Lu, X.F. 2010. Heavy metal pollution of the world largest antimony mine-affected agricultural soils in Hunan province (China). Journal of Soils Sediments, 10: 827-837.

World Health Organization 2015. Sexual and reproductive health: Infertility is a global public health issue.

WHO 2000. Air Quality Guidelines for Europe (2nd Edn.), World Health Organization Regional Publications European Series No.91.

Zhang, J.M., Konkle, A.T., Zup, S.L. and McCarthy, M.M. 2008. Impact of sex and hormones on new cells in the developing rat hippocampus: A novel source of sex dimorphism? Europian Journal of Neuroscience, 27(4): 791-800.

Treatment of Effluents Containing High Total Dissolved Solids By Multi-Effect Evaporator

Sareddy Ravi Sankara Reddy, Manoj Kumar Karnena, Bhavya Kavitha Dwarapureddi and Vara Saritha†

Department of Environmental Science, GITAM Institute of Sciences, GITAM (Deemed to be) University, Visakhapatnam, Andhra Pradesh, India

†Corresponding author: Vara Saritha; vsjr08@gmail.com

ABSTRACT

Pharmaceutical effluent disposal is a serious problem in the present times. The manufacturing process involves the use of both organic and inorganic compounds, which contribute to high chemical oxygen demand and dissolved solids. The common techniques used to extract available salts and to produce reusable waters are evaporation and cooling. Evaporators are equipment used for evaporation which is a kind of heat transfer system in which transfer mechanism is controlled by natural or forced convection. Multi-effect evaporators in many industries are used for volume reduction and cutting down the waste handling cost. This paper focusses on studying the efficiency of multi-effect evaporators in the pharmaceutical industry for the treatment of high total dissolved solids (HTDS) waste streams. The feed and condensate parameters were monitored for three years. Competence of the treatment process is presented in terms of reduction in TDS and COD. The current study evaluates the efficiency of MEE in terms of removal of total dissolved solids and chemical oxygen demand. Removal efficiencies are more than 98% for TDS and 50% for COD.

INTRODUCTION

Evaporation is understood as vaporization of liquid or solvent from a solution. The objective of evaporation is to concentrate solution. Evaporators are equipment used for evaporation which is kind of heat transfer systems in which transfer mechanism is controlled by natural or forced convection. The process of evaporation includes feeding of solution and heating with a heat source like steam leading to the conversion of water in the solution to vapour which is condensed while the solution that got concentrated is removed for further processing.

Use of single evaporator is called single effect evaporator system while the use of more than one evaporator is termed as the multiple-effect evaporator system (Hanamapure et al. 2016). Addition of each effect increases the steam economy of the system. Evaporation is the most energy-intensive process in an industrial operation, hence, many researchers have focussed on the processes to shrink consumption of energy to make the process cost-effective. Operating strategies employed include compression and bleeding of vapour, feed, condensate and product flashing, and feed and steam splitting.

Evaporators, precisely multi-effect evaporators, have become an integral part of many processes in wide industries including sugar, paper and pulp, dairy, desalination, food processing and pharmaceuticals, etc. (Shah & Bhagchandanc 2012, Sarma & Barma 2010, Kumar et al. 2013, Kumar et al. 2010, Zain & Kumar 1996, Danish & Sachin Pratap 2014, Bhargava et al. 2008). Multi-effect evaporators yield high value of the coefficient of performance in comparison to a single effect evaporator system. Fluctuations in load are controlled easily by controlling individual evaporator. Further, lesser space and initial cost are additional advantages of single compressor multi-evaporator systems.

Multi-effect evaporators in many industries are used for volume reduction and cutting down of waste handling cost (Bhargava et al. 2008). In distillery units, spent wash is subjected to volume reduction through multi-effect evaporator or reverse osmosis (Apte 2012). Black liquor is one of the voluminous and critical pollutant streams from paper and pulp industry processes which contains solids between 12 to 20%. The concentration of this stream to nearly 50% is carried out in multi-effect evaporator using low-pressure steam, where vapour from one evaporator is supplied as steam for the next evaporator resulting in a high steam economy (Deepak Kumar et al. 2010).

Application of evaporation in the pharmaceutical industry is two-fold. First, in the manufacturing process, evaporation is used to eliminate excess moisture from pharmaceutical products which improves the stability of the product enabling

its easy handling. Further, evaporation aids in preserving long-term activity and stabilization of enzymes. Second, evaporation of wastewaters from the manufacturing process of the pharmaceutical industry is carried out using multi-effect evaporators which will reduce the volume and separate solvents from the effluents. 99% reduction in total dissolved solids and 90% reduction in total organic carbon for various industrial wastewaters was achieved upon treatment with multi-effect evaporator. Highest removal of total organic carbon was seen in pharmaceutical wastewaters.

Leakages and scales are common problems associated with evaporators, overcoming these problems will result in enhancing the efficiency of multi-effect evaporators as reported by Salakki et al. (2014). Their evaluation presented 91.5% and 96% exclusion of chemical oxygen demand and total dissolved solids respectively. Further, the pharmaceutical industry has adopted multiple-effect (falling and forced circulation) evaporator towards achieving zero liquid discharge (Gupta et al. 2018). Studies on bulk drug industry showed that effluent treatment is carried out by multi-effect evaporators for waste streams containing high total dissolved solids followed by biological treatment (Vuppala et al. 2012). 98% reduction in COD and TDS was reported by Salakki et al. 2014 when pharmaceutical effluent was treated in the multi-effect evaporator.

This paper focusses on studying the efficiency of multi-effect evaporators in the pharmaceutical industry for the treatment of high total dissolved solids (HTDS) waste streams. Competence of the treatment process is presented in terms of reduction in TDS and COD.

MATERIALS AND METHODS

Flowchart of methodology for the treatment system for multiple-effect evaporation to remove dissolved solids from the pharmaceutical industry is shown in Fig. 1.

Study Area

The present study has been carried out at MSN Laboratories Private Limited, a research-based pharmaceutical company in Hyderabad, Andhra Pradesh, India.

Sample Collection

Water samples from MEE feed condensate and concentrate were collected every day with a temporal frequency of morning, afternoon and evening, and the composite sample was made from the three samples. Samples were collected in sterile plastic containers and transferred instantly to the laboratory in the premises of the industry. The analysis was taken up immediately and completed within 48 hours. Samples were stored at 4°C for analysis during the following days.

Physico-Chemical Analysis

Total of 24 physico-chemical parameters was analysed as per the standards methods (APHA 2012). All the parameters were analysed in triplicate to avoid errors.

RESULTS

Table 1 presents the treatment of process effluents using Multiple Evaporators represents focussing on three parameters pH, TDS and COD. Table 1 presents the ten-month
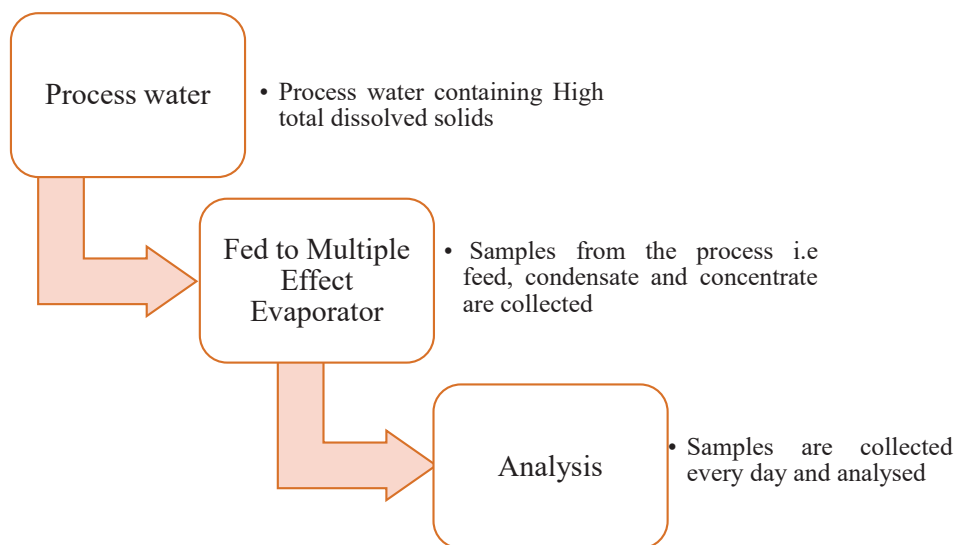

Fig. 1: Flowchart of methodology.

data of MEE treatment with details of feed, condensate and concentrates for the year 2018.

pH trend for MEE feed was found to be lowest and highest during January and August, i.e. 6.69 and 7.20. Lowest and highest values for TDS were 32867.74 mg/L and 41605.00 mg/L during January and June. Further, the lowest and highest values for COD were observed to be 47200.00 mg/L and 56506.67 mg/L in January and October.

With reference to MEE condensate pH trend was observed to be lowest (7.83) during January and highest of 8.55 in September. Lowest and highest values for TDS were 373.23 mg/L and 506.00 mg/L during January and October. Further, the lowest and highest values for COD were observed to be 19483.87mg/L and 23973.33mg/L in January and October.

pH variations for MEE concentrate were noted as 5.75 being lowest and 6.00 being highest reported during January and April respectively. Similarly, the lowest and highest values for TDS were recorded to be 191390.32 mg/L and 205580.00 mg/L in January and September. Regarding COD, 139933.55 mg/L and 172960.00 mg/L were the least and highest values obtained during January and October respectively.

Table 2 presents the percentage reduction in TDS and COD during the study after treatment with multiple effect evaporators. Maximum average percentage reduction of TDS was observed to be 98.77% and COD of 58.26%.

DISCUSSION

Term multi-effect evaporators originate from multiple ef-

Table 1: Treatment of process effluents using Multiple Effect Evaporators (MEE).

Months	Stripper / MEE Feed			MEE Condensate			MEE Concentrate/Atfd Feed		
	pH	TDS (mg/L)	COD (mg/L)	pH	TDS (mg/L)	COD (mg/L)	pH	TDS (mg/L)	COD (mg/L)
January	6.69	32867.74	47200.00	7.83	373.23	19483.87	5.75	191390.32	139933.55
February	7.03	33532.14	53142.86	8.18	420.71	22314.29	5.83	204089.29	145314.29
March	6.99	35393.55	50829.03	8.24	400.97	20903.23	5.88	197154.84	151696.77
April	7.03	38604.33	53306.67	8.23	422.00	22186.67	6.00	206376.67	159906.67
May	7.00	36743.33	51600.00	8.46	417.00	21293.33	5.90	203676.67	154293.33
June	6.77	41605.00	53013.33	7.99	461.67	21693.33	5.60	200906.67	164880.00
July	7.06	37219.35	54890.32	8.40	462.58	22941.94	5.63	202600.00	166916.13
August	7.20	35125.81	52670.97	8.34	455.16	22277.42	5.88	200680.65	165845.16
September	7.14	34580.00	54026.67	8.55	488.33	23053.33	5.83	205580.00	172746.67
October	7.08	34240.00	56506.67	8.50	506.00	23973.33	5.90	202833.33	172960.00

Table 2: TDS and COD removal in percentage (%).

Months	TDS	COD
January	98.86	58.72
February	98.75	58.01
March	98.87	58.88
April	98.91	58.38
May	98.87	58.73
June	98.89	59.08
July	98.76	58.20
August	98.70	57.70
September	98.59	57.33
October	98.52	57.57
November	-	-
December	-	-
Avg (%)	98.77	58.26

fective use of energy in performing the task of evaporation. Under this configuration, condensation of live steam takes in the first effect evaporator only, vapours produced are sent to condense in the next or second effect evaporator for further evaporation. This process is repeated until the last evaporator is reached where condensation of the produced vapours takes place in a condenser equipped with cooling water (Bremford & Muller-Steinhagen 1994, Konopa 1997). Foremost mention of the multiple-effect evaporator (MEE) was dated during 1840, regarding one of the oldest and widely adopted desalination process in the world (Al-Mutaz 2015).

Adopted widely for seawater desalination (El-Dessouky et al. 1999), MEE, with its applications, has also become an integral part of many industrial processes including dairy, petrochemicals, pulp and paper and food processing. Among others, one of the advantages of MEE is the reduction in the cost of handling waste by reducing the volume of the waste (Bhargava et al. 2008). Many workers have studied mathematical and nonlinear mathematical modelling approaches for MEE (El-Dessouky and Ettouney, 2002, Yılmaz & Söylemez 2012, Gautami & Khanam 2012, Druetta et al. 2013, El-Dessouky et al. 2000, Ettouney 2006) with regard to energy efficiency. EI-Dessouky et al. (2000), presented various models for MEE systems design for seawater desalination. However, the point to be noted is that these works were only regarding seawater desalination. Hence, it is understood that these studies have not made any consideration regarding the treatment of various industrial effluents to reduce the volume and other applications.

Treatment of pharmaceutical effluents using MEE in the present study has resulted in a significant reduction in total dissolved solids (99%) and chemical oxygen demand (88.32%). The study carried out by Srikanth et al. (2012) in a bulk drug industry reported that wastewater streams having HTDS were treated using MEE, where these wastewaters were initially sent through a steam stripper which was followed by MEE and then to agitated thin film drier (AFTD). The similar process has been adopted in the treatment of wastewaters in the present study. Chow et al. (2001) reported lesser steam requirement (3655 kg) for treating 25KL effluent in MEE after a detailed study on the operating conditions in treating pharmaceutical industry wastewaters. When wastewater with high TDS was treated in MEE, 99% recovery of water was stated by Matkar et al. (2017). The input quantity was 30 KLD while 27 KLD was recovered.

Salakki et al. (2014) evaluated the performance of MEE for treatment of pharmaceutical industry and stated that they obtained 91.5% reduction in chemical oxygen demand, while the reduction in total dissolved solids was 96%. Apte & Hivarekar (2014) have quoted technique of multi-effect evaporation to be an efficient alternative towards achieving volume reduction of up to 75% while studying the treatment options for distilleries. Further, they stated that if the condensate can be treated properly, it can be utilized as a source of raw water. Reduction of COD from 2000 mg/L to 60-240 mg/L was obtained when textile wastewaters were prone to treatment with evaporation followed by reverse osmosis.

From the above discussion of the previous studies regarding efficiency of MEE treatment, this process is considered to be highly attractive for its design and operating features making it both competitive and applicable for several industries and processes. Features that make MEE competitive as per the previous and present study are:

1. Process configuration of MEE permits simple alterations for routing and distributing wastewater streams among the effects of the system (El-Dessouky et al. 1998, El-Dessouky et al. 2000).

2. Capital investment of MEE is considered to be low in comparison to other processes owing to its lesser number of effects, partition walls and tube connections (Morin 1993, Wade 1993, Hamed et al. 2004, El-Dessouky et al. 2000).

3. Operation load stability of MEE is observed over a range of 30% to 120% of its design capacity (El-Dessouky et al. 1995, Darwish et al. 1996, Fritzmann et al. 2007, Greenlee et al. 2009, Al-Bastaki et al. 1999). This feature is attributed to less feed to product ratio permitting larger variation in the operating conditions of the system.

Rukade & Bhosale (2014) opined that if MEE and RO were to be incorporated in the treatment design as alternatives for the technology of volume reduction primarily, then such systems may be promising and provide a benchmark database reducing costs and area requirements. Further, these may add to the notion of zero discharge. Previous studies stated that one of the major aspects of zero liquid discharge plant is having multiple-effect evaporator as one of the treatment options which can save 50% of water per day, which is a large amount that can be utilized for other purposes (Hareesh 2017).

CONCLUSIONS

Results of physico-chemical characteristics of pharmaceutical wastewaters reveal thorough or higher degree treatment of high total dissolved solids stream which initially starts with feeding this stream to multiple-effect evaporator. The study on the efficiency of MEE is evaluated in terms of removal of total dissolved solids and chemical oxygen demand. Removal efficiencies are as follows:

- Reduction in total dissolved solids was more than 98 % during the entire study period, the maximum average percentage reduction of TDS was observed to be 98.77 %.

- Reduction in chemical oxygen demand was above 50 % during the study period, maximum average percentage reduction of COD was observed to be 58.26 %.

REFERENCES

Al-Bastaki, N.M. and Abbas, A. 1999. Modeling an industrial reverse osmosis unit. Desalination, 126(1-3): 33-39.

Al-Mutaz, I. S. and Wazeer, I. 2014. Comparative performance evaluation of conventional multi-effect evaporation desalination processes. Appl. Therm. Eng., 73(1): 1194-1203.

Apte, S. 2012. Anaerobic Filter for Distillery Condensate Treatment. Lap Lambert Academic Publ.

Bhargava, R., Khanam, S., Mohanty, B. and Ray, A.K. 2008. Simulation of flat falling film evaporator system for concentration of black liquor. Comput. Aided Chem. Eng., 32(12): 3213-3223.

Bremford, D. J. and Müller-Steinhagen, H. M. 1994. Multiple effect evaporator performance for black liquor. Part 1: Simulation of steady state operation for different evaporator arrangements. Appita J., 47(4): 320-326.

Chow, C., Anand, A.K., Ranasinghe, J. and Stats, D.A. 2001. U.S. Patent No. 6,170,263. Washington, DC: U.S. Patent and Trademark Office.

Danish, M. and Singh, S.P. 2014. A short note on the solution of a multi-effect evaporator system employed in pulp and paper industry. Appl. Math. Model., 38(15-16): 4157-4160.

Darwish, S., Riad, A.S. and Soliman, H.S. 1996. Electrical conductivity and the effect of temperature on photoconduction of n-ZnSe/p-Si rectifying heterojunction cells. Semicond. Sci. Tech., 11(1): 96.

Druetta, P., Aguirre, P. and Mussati, S. 2013. Optimization of multi-effect evaporation desalination plants. Desalination, 311: 1-15.

El-Dessouky, H.T. and Ettouney, H.M. 1999. Multiple-effect evaporation desalination systems. Thermal Analysis. Desalination, 125(1-3): 259-276.

El-Dessouky, H. T., Ettouney, H. M. and Al-Juwayhel, F. 2000. Multiple effect evaporation-Vapour compression desalination processes. Chem. Eng. Res. Des., 78(4): 662-676.

El-Dessouky, H.T. and Ettouney, H.M. 2002. Fundamentals of Salt Water Desalination. Elsevier.

Ettouney, H. 2006. Design of single-effect mechanical vapor compression. Desalination, 190(1-3): 1-15.

Fritzmann, C., Löwenberg, J., Wintgens, T. and Melin, T. 2007. State-of-the-art of reverse osmosis desalination. Desalination, 216(1-3): 1-76.

Gautami, G. and Khanam, S. 2012. Selection of optimum configuration for multiple effect evaporator system. Desalination, 288: 16-23.

Greenlee, L. F., Lawler, D. F., Freeman, B. D., Marrot, B. and Moulin, P. 2009. Reverse osmosis desalination: Water sources, technology, and today's challenges. Water Res., 43(9): 2317-2348.

Gupta, S. K., Shin, H., Han, D., Hur, H. G. and Unno, T. 2018. Metagenomic analysis reveals the prevalence and persistence of antibiotic-and heavy metal-resistance genes in wastewater treatment plant. J. Microbiol., 56(6): 408-415.

Hanamapure, N. S., Saini, D. R. and Pharande, M. S. A. 2016. Optimization of parameters of multi effect evaporator used in the design for the dye industry. Int. J. Sci., 2(10): 1056-1059.

Hareesh, G., Arun, S. and Shanmugam, D. P. 2017. Comparative analysis of multiple effect evaporators and anaerobic digester (UASB) for an effective management of RO reject from tannery. Int. J. Civ. Eng., 8(4): 809-815.

Konopa, J. P. 1997. Multiple effect evaporator throughput extension with unique chemistry. In: Tappi Pulping Conference, Tappi Press, (pp. 1041-1044).

Kumar, A., Badde, S., Kamble, R. and Pokharkar, V.B. 2010. Development and characterization of liposomal drug delivery system for nimesulide. Int. J. Pharm. Pharm. Sci., 2(4): 20-27.

Kumar, D., Kumar, V. and Singh, V. P. 2013. Modeling and dynamic simulation of mixed feed multi-effect evaporators in paper industry. Appl. Math. Model., 37(1-2): 384-397.

Matkar, A.D., Shelke, R.D. and Deshpande, H.N. 2017. Design and analysis of vertical evaporator refrigerator without freezer compartment. Int. J. Adv. Res. Dev., 2(10): 7-21.

Morin, O.J. 1993. Design and operating comparison of MSF and MED systems. Desalination, 93(1-3): 69-109.

Rukade, S. K. and Bhosale, S. M. 2015. Applicability of evaporation and reverse osmosis techniques for volume reduction of textile mill effluent. Int. J. Sci. Res., 4(11): 2123-2127.

Salakki, S., Raj, L.A., Patil, J.H. and Shetty, V. 2014. Improving the efficiency of multiple effect evaporator to treat effluent from a pharmaceutical industry. Int. J. Innov. Res. Sci. Eng. Technol., 3(7): 14727-14731.

Sarma, G. and Barma, S. D. 2010. Energy management in multiple–effect evaporator system: A Heat Balance Analysis Approach. Gen. Math Notes, 1(2): 84-88.

Shah, D. J. and Bhagchandani, C. G. 2012. Design, modelling and simulation of multiple effect evaporators. Int. J. Sci. Eng. Technol., 1(3): 1-5.

Vuppala, N. S., Suneetha, C. and Saritha, V. 2012. Study on treatment process of effluent in bulk drug industry. Int. J. Res. Pharm. Biomed. Sci., 3(3): 1095-1102.

Wade, N. M. 1993. Technical and economic evaluation of distillation and reverse osmosis desalination processes. Desalination, 93(1-3): 343-363.

Yılmaz, İ.H. and Söylemez, M.S. 2012. Design and computer simulation on multi-effect evaporation seawater desalination system using hybrid renewable energy sources in Turkey. Desalination, 291: 23-40.

Zain, O. S. and Kumar, S. 1996. Simulation of a multiple effect evaporator for concentrating caustic soda solution - computational aspects. J. Chem. Eng. Jpn., 29(5): 889-893.

University-Industry Knowledge Collaboration in Chinese Water Pollution Abatement Technology Innovation System

Guoxin Liu, Pengfei Zhang† and Feng Zhang

Wuhan University of Technology, Wuhan 430000, China

†Corresponding author: Pengfei Zhang; zpf.90@163.com

ABSTRACT

University-industry knowledge collaboration is one of the keys to overcoming the current development bottleneck in water pollution abatement technology in China. To explore university-industry knowledge collaboration in Chinese water pollution abatement technology innovation system, characteristics and dynamic evolution law of knowledge collaboration were analyzed by using patent data from China for the period 2000-2018. Results show that university-industry knowledge collaboration continues to increase and experiences three development phases in Chinese water pollution abatement technology innovation system. University-industry knowledge collaboration in each province (city) keeps growing and the difference between provinces (cities) is decreasing, but the difference remains significant. The scale, scope, and depth of inter-regional university-industry knowledge collaboration continue to increase, but they are still not large enough. Although the scale and linking efficiency of university-industry knowledge collaboration improve significantly, the subgroups are too many and the agglomeration degree of networks is low.

INTRODUCTION

Water Pollution Abatement (WPA) plays a major role in ensuring water security, preserving ecosystems, and supporting sustainable development. Thus, most countries pay great attention to the development of WPA technology, the patents of which account for approximately 1% of overall patents. As a country with high water stress and serious water pollution, China has been increasing investments in WPA technology innovation in the past two decades. Today, China has the third largest share in global WPA patented inventions. However, high-value WPA technologies from China account for only 3.7% (Proskuryakova et al. 2018). Hence, for China to address the increasing WPA stress, greater efforts must be made to innovation more high-value WPA technologies.

Aside from increasing investment in R&D, greater importance must be attached to the development of knowledge collaboration in Chinese WPA technology innovation system to overcome the innovation bottleneck. Knowledge collaboration refers to activities such as co-development, co-authorship, and collaborative R&D (McKelvey et al. 2003) and it is widely acknowledged as an important vehicle for technology diffusion and technology innovation in any innovation system (Ye et al. 2008, Dooley et al. 2016). Innovation system theory claims that technology innovation is essentially the result of collective knowledge development.

Firms and universities are two of the most important actors in national and industrial innovation systems. Triple helix theory highlights that industry, university, and government interact to enhance innovation (Etzkowitz et al. 1996). Knowledge collaboration among industry, university, and research institution not only leads to innovation benefits directly but also improves the marginal contribution of "division of knowledge" (Yu et al. 2017). In this sense, knowledge collaboration between university and industry (hereafter UI knowledge collaboration) is one of the keys to Chinese high-value WPA technology innovation.

Previous literature has analyzed WPA technology innovation in China. The patents on WPA technology in China have been increasing rapidly since 2007, and currently, China has become one of the top WPA inventor countries (Tan et al. 2019). Most of the applicants in Chinese WPA technology domain are from those more economically-developed regions such as Jiangsu, Beijing and so forth (Yang et al. 2016). In addition, amongst all the applicants, universities account for the largest share in China's overall WPA technology patents (Wang et al. 2013). At the same time, studies have been conducted on knowledge collaboration analysis in China (Ma et al. 2011, Lei et al. 2011) and in some technology domains such as ICT and new energy vehicles (Gao et al. 2016, Cao et al. 2019). However, little attention is given to knowledge collaboration in the WPA technology domain. This study analyzes the characteristics and evolution of UI

knowledge collaboration in Chinese WPA innovation system and contributes to WPA technology innovation literature as well as knowledge collaboration literature.

METHODOLOGY

Patent Statistics and Social Network Analysis

Patents contain rich information, such as technology field, applicant, and priority, which are easy to access. The statistics and analysis of patent data can yield numerous useful and relevant information or knowledge. Co-application for a patent between a university and a firm is a major form of UI knowledge collaboration. Hence, this study uses patent data and a series of patent indicators to analyze UI knowledge collaboration in Chinese WPA innovation system.

Social network analysis (SNA) is a visualization technique used to analyze networks that consist of a set of nodes and links. A node can be a person, an institute, or a region, whereas links represent relationships between two adjacent nodes. SNA can depict how nodes link with one other directly and indirectly in qualitative and quantitative

ways. This study constructs several UI knowledge collaboration networks and then analyzes their characteristics and evolution.

Data

This study uses a search strategy developed by OECD (Table 1) to search the patent database of the State Intellectual Property Office of China for WPA technology patents that are co-applied by Chinese universities and firms. Only patents for inventions are considered for their high level of innovation. The time horizon is set from 2000 to 2018, and the locations of applicants are limited to 31 Chinese provincial administrative regions, which consist of 27 provinces and 4 cities, excluding Hong Kong, Macao, and Chinese Taipei.

2,024 patents that meet the requirements are collected. Between 2000 and 2018, the scale of UI co-application for WPA technology patent in China keeps expanding year by year, and its growth rate is almost the same with that of the overall applications for WPA technology patents in China (Fig. 1).

Table 1: IPC Class/Code of WPA Technologies.

| IPC Class/Code	Description
B63B35/32	Vessels or like floating structures adapted for special purposes- for collecting pollution from open water
B63J4	Arrangements of installations for treating waste-water or sewage
C02F	Treatment of water, wastewater, sewage, or sludge
C05F7	Fertilizers from wastewater, sewage sludge, sea slime, ooze, or similar masses
C09K3/32	Materials for treating liquid pollutants, e.g. oil, gasoline or fat
E02B15/04-10	Devices for cleaning or keeping clear the surface of open water from oil or like floating materials by separating or removing these materials
E03C1/12	Plumbing installations for wastewater
E03F	Sewers–Cesspools
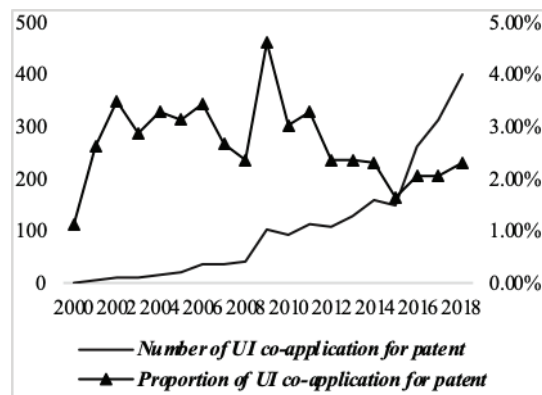
Fig. 1: Chinese UI Co-application for Patent in WPA Technology, 2000-2018.

RESULT ANALYSIS

Overall Trend in UI Knowledge Collaboration

In Chinese WPA technology innovation system, the scale of UI knowledge collaboration continues to expand in terms of actors, ties, and activities between 2000 and 2018, with a growth rate of approximately 30% (Fig. 2).

Furthermore, the development of UI knowledge collaboration in Chinese WPA technology innovation system is in three phases (Table 2). Phase I is the initial stage. In this phase, the scale of UI knowledge collaboration is small, whereas the growth rate is approximately 40%. At the end of Phase I, the scale of UI knowledge collaboration experienced a surge in 2009, and then began to grow slowly at a speed of approximately 8% until 2015, that is phase II. In phase II (2009-2015), the scale of UI knowledge collaboration is four times larger than that in phase I, but the growth rate is only about a fifth of that in phase I. After phase II, the scale of UI knowledge collaboration experienced a surge again in 2016, which is the beginning of phase III (2016-2018). In phase III, not only the scale is much higher than that in the two previous phases, but the growth rate is also higher.

The Geography of UI Knowledge Collaboration

Knowledge collaboration can be categorized as intra-regional or inter-regional according to whether actors are located in the same region. In Chinese WPA technology innovation system, intra-regional UI knowledge collaboration accounts for more than 70% of overall UI knowledge collaboration. This figure indicates that actors prefer to collaborate with partners who are close to them. First, as shown in Table 3, the top provinces (cities) account for more than 76% of overall intra-regional UI knowledge collaboration. These regions are basically the regions with high economic level and where several universities are located. Second, the commutative share of the top provinces (cities) in intra-regional UI knowledge collaboration has been declining from phase I to phase III. This trend indicates that UI knowledge collaboration is thriving in other regions. Third, the difference among the top provinces (cities) has been decreasing from phase I to phase III on the whole. Finally, from phase I to III, the ranks of Jiangsu, Guangdong, and Beijing have grown steadily, and they have become the top 3 in phase III. Shandong, Hunan, and Chongqing have enjoyed the most rapid growth in intra-regional UI knowledge collaboration, resulting in a great leap in their ranks. Shanghai, Zhejiang, and Tianjin are the three provinces (cities) whose ranks have been declining, indicating that their development in intra-regional UI knowledge collaboration is slow.

Despite a lower share in overall UI knowledge collaboration, inter-regional UI knowledge collaboration plays a critical role in facilitating technology diffusion in the whole innovation system. Inter-regional UI knowledge
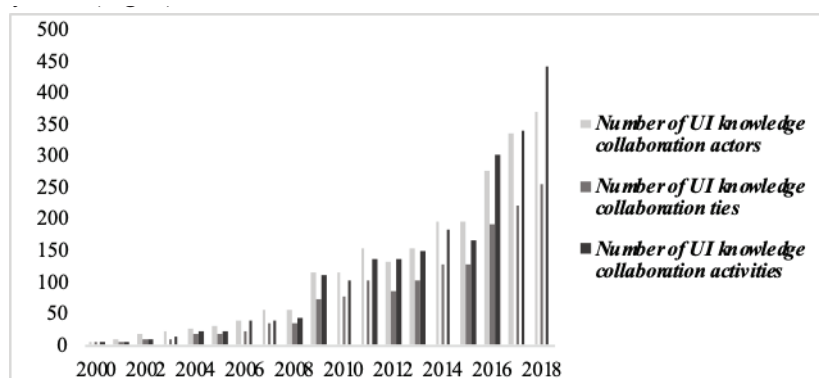

Fig. 2: UI knowledge collaboration in Chinese WPA technology innovation system, 2000-2018.

Table 2: Scale and growth rate of UI knowledge collaboration in each phrase.

Phases	Number of UI knowledge collaboration actors		Number of UI knowledge collaboration ties		Number of UI knowledge collaboration activities	
	Average	Growth rate	Average	Growth rate	Average	Growth rate
Phase I (2000–2008)	29	39.08%	18	43.01%	23	47.98%
Phase II (2009–2015)	153	9.16%	100	9.46%	141	7.21%
Phase III (2016–2018)	327	15.78%	223	15.70%	361	21.18%

Table 3: Top provinces/cities in intra-regional UI knowledge collaboration.

Phases	Regions	UI knowledge collaboration activities			UI knowledge collaboration ties		
		Number	Share	Commutative share	Number	Share	Commutative share
Phase I (2000–2008)	Shanghai	41	29.50%	29.50%	28	28.28%	28.28%
	Jiangsu	38	27.34%	56.83%	16	16.16%	44.44%
	Guangdong	12	8.63%	65.47%	12	12.12%	56.56%
	Zhejiang	11	7.91%	73.38%	8	8.08%	64.64%
	Beijing	10	7.19%	80.58%	10	10.10%	74.74%
	Hubei	5	3.60%	84.17%	5	5.05%	79.80%
	Tianjin	5	3.60%	87.77%	5	5.05%	84.85%
	Yunnan	4	2.88%	90.65%	3	3.03%	87.88%
	Anhui	2	1.44%	92.09%	2	2.02%	89.90%
	Guangxi	2	1.44%	93.53%	1	1.01%	90.91%
Phase II (2009–2015)	Jiangsu	150	21.55%	21.55%	78	20.05%	20.05%
	Shanghai	103	14.80%	36.35%	44	11.40%	31.51%
	Beijing	97	13.94%	50.29%	40	10.36%	41.93%
	Guangdong	75	10.78%	61.06%	46	11.92%	53.90%
	Zhejiang	45	6.47%	67.53%	29	7.51%	61.46%
	Shandong	34	4.89%	72.41%	15	3.89%	65.36%
	Hubei	26	3.74%	76.15%	20	5.18%	70.57%
	Tianjin	26	3.74%	79.88%	20	5.18%	75.52%
	Hunan	17	2.44%	82.33%	7	1.81%	77.34%
	Anhui	14	2.01%	84.34%	12	3.11%	80.47%
Phase III (2016–2018)	Jiangsu	160	19.88%	19.88%	78	18.06%	18.06%
	Guangdong	98	12.17%	32.05%	52	12.04%	30.10%
	Beijing	71	8.82%	40.87%	44	10.19%	40.28%
	Shandong	62	7.70%	48.58%	37	8.56%	48.85%
	Shanghai	56	6.96%	55.53%	29	6.71%	55.56%
	Hubei	55	6.83%	62.36%	30	6.94%	62.50%
	Hunan	37	4.60%	66.96%	26	6.02%	68.52%
	Chongqing	28	3.48%	70.44%	13	3.01%	71.53%
	Zhejiang	25	3.11%	73.54%	20	4.63%	76.16%
	Anhui	22	2.73%	76.28%	8	1.85%	78.01%

collaboration also enhances innovativeness due to greater cognitive diversity. Fig. 3 shows the geographic distribution of inter-regional UI knowledge collaboration. In phase I, the scale of inter-regional UI knowledge collaboration network is relatively small, with only 23 nodes and 46 links (weighted). Moreover, 82.61% of links (weighted) are focused on only four nodes, that is, Beijing, Shanghai, Jiangsu, and Tianjin. These four provinces (cities) are the centres in inter-regional UI knowledge collaboration in phase I. In phase II, the inter-regional UI knowledge collaboration network

consists of 27 nodes and 193 links (weighted). This result means that the scope, scale, and depth of inter-regional UI knowledge collaboration significantly increase in this phase. Additionally, more local hubs are found in the network, with 10 nodes whose degree values are above 7, indicating that more provinces (cities) have become centres of inter-regional UI knowledge collaboration. In phase III, inter-regional UI knowledge collaborations are distributed across more provinces (cities). Meanwhile, the links (weighted) are far more than that in phase II,

considering the time horizon. The number of nodes with degree values above 7 is still 10.

Evolution of UI Knowledge Collaboration Network

To demonstrate how universities and firms interact with each other, the UI knowledge collaboration network in each phase is constructed (Fig. 4). In UI knowledge collaboration network, a node represents a university or a firm engaged in knowledge collaboration, and a link represents knowledge collaboration ties between a university and a firm. The size of a node indicates its degree value, and the strength of a link indicates its weighted value.

It further uses SNA indicators, like scale, degree, K-core, and length to illustrate characteristics and evolution of UI knowledge collaboration networks in Chinese WPA technology innovation system (Table 4).

Firstly, as shown in Figure 4 and Table 4, the scale of UI knowledge collaboration keeps expanding from phase I to phase III. In phase I, nodes and links (weighted or unweighted) are comparatively few, and many links are isolated. Moreover, the nodes of the main component account for only 16% of all nodes. Hence, UI knowledge collaboration network in phase I is characterized by a small scale and low density. In phase II, the scale of the UI knowledge collaboration network increases significantly from phase I, and the nodes of its main component account for 40% of all nodes. In phase III, the scale of UI knowledge collaboration network and its main component further expand, and links among nodes become denser.

Secondly, the overall agglomeration degree of networks in each phase is relatively low. On one hand, the average degree of nodes is below 2, indicating that knowledge collaboration among actors is not wide. On the other hand, no significant change occurs in k-core, which means that knowledge collaboration among actors lacks diversity. According to network theory and social capital theory, networks with high agglomeration degree
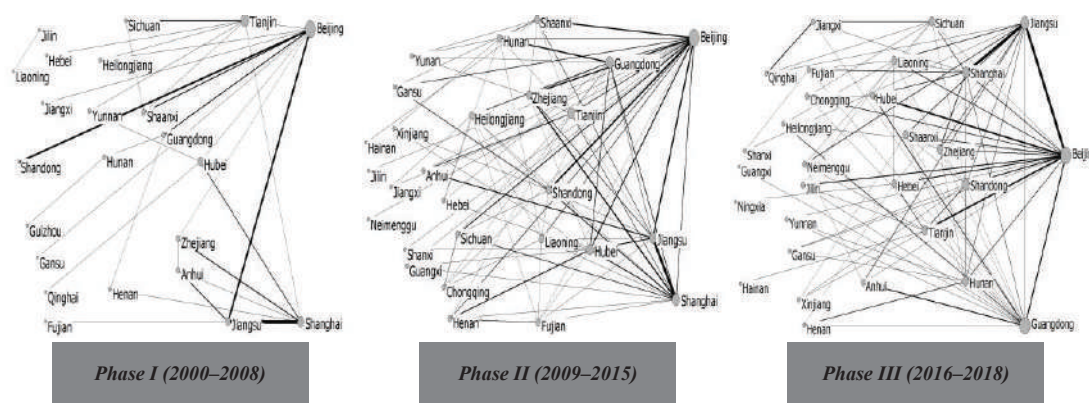

Fig. 3: Inter-regional UI knowledge collaboration network in each phase.

Table 4: Indicators of UI knowledge collaboration networks in each phase.

Indicators	Phase I	Phase II	Phase III
Number of nodes	195	695	786
Number of links	145	580	615
Number of links (weighted)	204	987	1,082
Average degree	1.49	1.67	1.56
K-core	2	2	2
Number of components	51	124	147
Scale of main component	32 (16.41%)	280 (40.29%)	362 (46.01%)
Diameter of main component	4	21	32

Phase I (2000–2008)　　　　*Phase II (2009–2015)*　　　　*Phase III (2016–2018)*
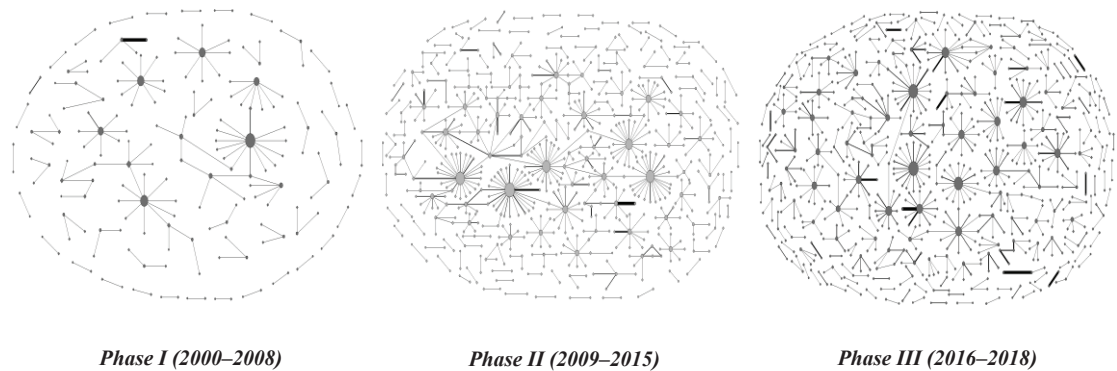
Fig. 4: UI Knowledge collaboration network in each phase.

and density perform better in knowledge exchange and knowledge creation.

Finally, the linking efficiency of the network continues to improve from phase I to phase III. The main component is the largest subgroup in the network, in which all nodes are linked either directly or indirectly. Thus, knowledge and information exchange among actors in the main component are most fluent and intensive. As seen in Table 4, the scale of the main component increases from 32 (16.41%) to 362 (46.01%) from phase I to phase III. The diameter of the main component is another indicator of the connectedness of nodes, and it increases from 4 to 32 from phase I to phase III. The improvement in linkage efficiency is expected to facilitate knowledge flow in UI knowledge collaboration network, thereby enhancing knowledge creation. A superior network is conducive to knowledge exchange in large scope and with high speed, thereby generating scale effect, complementary effect, and cross-fertilization effect of knowledge creation (Pyka 2002).

CONCLUSIONS

UI knowledge collaboration in Chinese WPA technology innovation system based on patent data was investigated and analyzed. The main conclusions are as follows:

Firstly, between 2000 and 2018, UI knowledge collaboration in Chinese WPA technology innovation system is in three phases. Phase I is characterized by a low level and high growth rate. Phase II is characterized by a moderate scale and low growth rate. Phase III is characterized by a high level and moderate growth rate.

Secondly, UI knowledge collaboration is mainly distributed in a few provinces (cities) that are characterized by high economy and several universities, whereas other provinces (cities) fall behind those top provinces (cities) in the development of UI knowledge collaboration. However, the difference between provinces (cities) decreases from phase I to III, indicating that UI knowledge collaboration is thriving in more regions. Also, the growth pace of provinces (cities) in UI knowledge collaboration varies. Among the top provinces (cities), the ranks of Jiangsu, Guangdong, and Beijing grow steadily, and they have become the top 3 in phase III. Shandong, Hunan, and Chongqing enjoy the most rapid growth in intra-regional UI knowledge collaboration, resulting in a great leap in their ranks. Shanghai, Zhejiang, and Tianjin are three provinces (cities) whose ranks are declining, indicating that their development in intra-regional UI knowledge collaboration is slow.

Thirdly, despite a low share in the overall UI knowledge collaboration, inter-regional UI knowledge collaboration keeps developing from phase I to III. The scale, scope, and depth of inter-regional knowledge collaboration increase significantly, and the geographic distribution becomes wider. Inter-regional UI knowledge collaboration plays a significant role in facilitating knowledge exchange in the whole innovation system.

Finally, from phase I to III, not only the scale keeps growing, but also the linking efficiency of UI knowledge collaboration network. This trend indicates that the UI knowledge collaboration network in Chinese WPA technology innovation system is developing and upgrading. However, the agglomeration degree and the connectedness of UI knowledge collaborative network are low, which limits knowledge diffusion and exchange among universities and firms.

ACKNOWLEDGEMENT

REFERENCES

Cao, X., Li, C.Y. and Lin, C.R. 2019. A research on the evolution of patent cooperation networks based on new energy vehicles. Science Research Management, 40(8): 179-187.

Dooley, L., Kenny, B. and Cronin, M. 2016. Interorganizational innovation across geographic and cognitive boundaries: does firm size matter? R&D Management, 46(1): 227-243.

Gao, X. and Chen, K.H. 2016. Analysis on the evolution of patterns and network structure for industry-university-research institute cooperation in the Chinese ICT industry based on SIPO patents. Science of Science and Management of Science and Technology, 37(11): 34-43.

Lei, T. and Chen, X.D. 2011. Network map analysis of university-firm's co-application for patents. Science Research Management, 32(2): 67-73.

Leydesdorff, L. and Etzkowitz, H. 1996. Emergence of a triple helix of university-industry-government relations. Science and Public Policy, 23: 279-286.

Ma, Y.Y., Liu, F.C. and Sun, Y.T. 2011. Research on Chinese university-enterprise cooperation networks of patent applications. Studies in Science of Science, 29(3): 390-395.

McKelvey, M., Alm, H. and Riccaboni, M. 2003. Does co-location matter for formal knowledge collaboration in the Swedish biotechnology-pharmaceutical sector? Research Policy, 32: 483-501.

Proskuryakova, L. N., Saritas, O. and Sivaev, S. 2018. Global water trends and future scenarios for sustainable development: The case of Russia. Journal of Cleaner Production, 170: 867-879.

Pyka, A. 2002. Innovation networks in economics: from the incentive-based to the knowledge-based approaches. European Journal of Innovation Management, 5(3): 152-163.

Tan, F.X., Hou, S.J., Wang, H.L. et al. 2019. Status analysis of sewage treatment patents and development trend. Environment Engineering, 37: 74-81.

Wang, S.M. and Lei, Y.D. 2013. Research on patent map in the field of sewage and wastewater treatment in China. Journal of Fudan University (Natural Science), 52(1): 99-103.

Yang, J., Feng, Y. and Qian, Y. 2016. Patent information study on biological sewage and wastewater treatment. Bulletin of Science and Technology, 32(9): 242-246.

Ye, Y.W., Yamamoto, Y. and Nakakoji, K. 2008. Expanding the knowing capability of software developers through knowledge collaboration. International Journal of Technology, Policy and Management, 8(1): 41-58.

Yu, W.X., Gu, X. and Xiong, W.M. 2017. Research on knowledge division and knowledge collaboration in industry-university-research institute collaborative innovation. Studies in Science of Science, 35(3): 737-745.

Variation in Concentrations of $PM_{2.5}$ and PM_{10} During the Four Seasons at the Port City of Visakhapatnam, Andhra Pradesh, India

Kavitha Chandu and Madhavaprasad Dasari†

Department of Electronics and Physics, GITAM Institute of Science, GITAM (Deemed to be) University, Visakhapatnam, 530045, Andhra Pradesh, India

†Corresponding author: Madhavaprasad Dasari; madhavaprasaddasari@gmail.com

ABSTRACT

This paper presents a summary of $PM_{2.5}$, PM_{10} and gaseous pollutant concentrations measured during each season of the year from March 1, 2018 to February 28, 2019 in Visakhapatnam city (17.6868°N, 83.2185°E) located on the east coast of India. The city is studded with 14 major industries and surrounded on three sides by mountains and the Bay of Bengal on the fourth side. The monthly variations of mass concentrations of $PM_{2.5}$, PM_{10} and gaseous pollutants SO_2, NO_2 and CO recorded revealed the impact of atmospheric pollutants originating from industry, urbanization and increased automobile traffic. The seasonal variability of PM concentrations, highest in winter and lowest in summer, is observed. The annual averages for 2018 in Visakhapatnam are 103.5 ± 55.1 μg/m³ and 111.5 ± 29.1 μg/m³ for $PM_{2.5}$ and PM_{10} respectively. To establish the causal relationship between $PM_{2.5}$, PM_{10} and the gaseous pollutants we used Pearson correlation and regression statistical methods. The Pearson correlation coefficients between PMs and gaseous pollutants were either high or moderate. Regression results further confirmed that NO_2 and SO_2 significantly impacted $PM_{2.5}$ and PM_{10} in Visakhapatnam city.

INTRODUCTION

Exposure to particulate matter $PM_{2.5}$ and PM_{10} with an aerodynamic diameter less than 2.5 and 10 μm respectively is a global concern due to their adverse health effects. Prolonged exposure to these particles affects healthy people and seriously impacts those with existing diseases. It causes breathing discomfort for people with asthma and heart diseases. According to WHO, an increase in total PM by 10 μg/m³ per year increases mortality by 6 per cent. Most cities in India have been experiencing severe air pollution due to fast-paced urbanization and rapid economic growth. SPM primarily originating from gaseous pollutants is posing a grave threat to human health. Gaseous pollutants CO, SO_2 and NO_2 are reported in several studies to be leading to high PM levels. Several studies considered the pollutant conditions in cities across the world and analysed the impact of these pollutants on human health (Samet 2000, Sarnat 2001, Katsouyanni 2001, Ito et al. 2007). However, studies on Visakhapatnam city are scanty and even those done refer to an earlier period.

The research presented here is an analysis of $PM_{2.5}$ and PM_{10} concentrations from the industrial zone of Visakhapatnam. The industrial development, initiated around 1950, triggered a population explosion in Visakhapatnam. The population of Visakhapatnam in the year 2018 as per estimated data was 4.056 Million (Population of India 2018). The city is

studded with major industries mainly Hindustan Zinc Limited (HZL), Coromandel Fertilizers Limited (CFL), Visakhapatnam Port Trust (VPT), Hindustan Petroleum Corporation Limited (HPCL), Bharat Heavy Plates and Vessels (BHPV), Hindustan Polymers Limited (HPL), Visakhapatnam Steel Plant (SP), Coastal Chemicals (CC), Andhra Cement Company (ACC) and Simhadri Thermal Power Corporation (STPC). About 200 ancillary industries were also established to supplement the main industries, which turned the central basin of Visakhapatnam into an "air-polluting chimney". The city was declared as one of the critical (NEERI 2005) and severely polluted areas (CEPI 2013) in the country.

The city with an area of about 680 km² is surrounded on three sides by mountains and the Bay of Bengal on the fourth. It is effectively shielded from winds, with only marine air moving into the basin. The major industries along with the Port are located within a distance of 13 km from the coast.

Combustion emits large quantities of chemicals from industries such as zinc, fertilizer, polymers, cement, steel production and petroleum. This situation is further aggravated by atmospheric aerosol content which is highest during the dry periods, resulting in a high ionic content due to precipitation scavenging. Marine aerosols also add to the industrial contribution. The emissions and aerosols are shielded from the wind by mountains on three sides, only allowing coastal

spray (marine aerosols) from the east. Visakhapatnam, thus, is subject to heavy air pollution, when compared to inland areas. Also, urbanization increased automobile traffic, and industrialization produces large emissions of SO_x and NO_x. The concentrations of air pollution vary from location to location as they depend on atmospheric conditions (Murthy 2004) like wind direction, speed, temperature and humidity.

In India, 99.9% of the country's population resides in areas that exceed the WHO Air Quality Guideline of 10 µg/m^3 (annual average), and half of the population resides in areas where the Indian National Ambient Air Quality Standard (NAAQS) for PM2.5 (40 µg/m^3) is exceeded (Greenstone et al. 2015, Srinivas 2013, Venkataraman et al. 2018). In another report, the annual averages for 2012 in Vishakhapatnam were 70.4±29.7, 18.9±14.4 and 15.6±6.3 for PM_{10}, SO_2, and NO_2 respectively (Guttikunda et al. 2015). Rao & Satish (2014) reported that the cause of air pollution in Visakhapatnam is not only due to the industries but also due to traffic.

Against this background, the present study focuses on analysing the mass concentrations of PM and gaseous pollutants. The objectives of the study are to examine the present levels of PM concentrations and their causative factors.

MATERIALS AND METHODS

The real time hourly mass concentrations of $PM_{2.5}$, PM_{10}, CO, NO_2 and SO_2 are recorded by National Air Quality Index of Central Pollution Control Board compiled for each city under the Ministry of Environment, Forests and Climate Change, India. The instruments measuring the mass concentrations are located in the central point of the city. The mass concentrations of $PM_{2.5}$ and PM_{10} are measured using beta attenuation method. The gas pollutants NO_2, SO_2 and CO are measured using the gas phase chemiluminescence method, ultraviolet fluorescence method and NDIR spectroscopy respectively. The data are publicly accessible and data used in this paper were obtained from the website (https://app.cpcbccr.com/).

The hourly mean variations of $PM_{2.5}$, PM_{10}, NO_2, SO_2 and CO in each season (Summer: March, April and May,

Rainy: June, July, August and September, Autumn: October and November, Winter: December, January and February) during March 2018 - February 2019 at the present location were measured.

RESULTS AND DISCUSSION

The annual mean $PM_{2.5,}$ PM_{10} and the gaseous pollutants NO_2, SO_2 and CO concentrations in Visakhapatnam are 103.514.4±3.0 ,49.3±8.6 ,29.1±111.5 ,55.1± and 35.57.8± µg/m^3, respectively for the year 2018-2019. Both $PM_{2.5}$ and PM_{10} levels have exceeded the annual mean limit, posing a high health risk (Balakrishnan et al. 2013, CPCB 2009). Based on the annual average values, the worse air quality may be attributable to some specific feature of local/regional emission sources mixed with meteorological influences. The mean values of concentrations of PMs and air pollutants for different seasons are listed in Table 1.

Seasonal Variations

The hourly data were used to examine diurnal variability of $PM_{2.5}$ and PM_{10} concentrations and major air pollutants in each season. The seasonal variability of $PM_{2.5}$ (Fig. 1) and PM_{10} (Fig. 2) is lowest in summer and highest in winter. The higher concentrations of $PM_{2.5}$ and PM_{10} were observed during winter (178.5, 150.7 µg/m^3 respectively) and autumn (111.05, 115.6 µg/m^3 respectively) than summer and rainy seasons (Latha & Badarinath 2005). The PM concentrations are high during daytime than night time. The peak value was observed at 11:00 a.m. and falls to lowest in afternoon hours at 1:00 p.m. It is evident from NO_2 (Fig. 3) observations, that the increase in PM after 4:00 p.m. and before 11:00 a.m. is because of vehicle emissions as a result of transportation in rush hours. The heavy-duty vehicle traffic is more during the morning and night hours. As traffic-related emissions are less from 12:00 p.m. to 3:00 p.m., there is a significant decrease in NO_2 and PM concentrations in all seasons. The emissions from heavy-duty vehicles are more than those of light weight vehicles. The decreasing boundary layer heights also contribute to an increase in PM concentrations after 4:00 p.m. In all the seasons during night time, the high $PM_{2.5}$ levels

Table 1: Mean values of PMs and gaseous pollutants for different seasons in Visakhapatnam.

	Summer	Rainy	Winter	Autumn	Annual Mean
$PM_{2.5}$	58.24±10	66.46±6.2	178.57±41.8	111.05±22.5	103.58±55.1
PM_{10}	84.74±10.8	95.10±5.8	150.77±37.8	115.68±20.9	111.57±29.1
NO_2	42.37±10.7	49.49±9.29	61.48±25.8	43.97±15.3	49.33±8.6
SO_2	16.74±8.19	12.96±2.07	17.23±6.2	10.78±2.5	14.43±3
CO	28.79±9.5	32.84±8.8	46.98±11.2	33.75±5.16	35.59±7.9

are due to accumulation of emissions from automobiles and secondary PM formation.

The variation pattern of SO$_2$ (Fig. 4) is similar in different seasons and exhibited unique high SO$_2$ levels in summer. During summer, the major contributing factors for SO$_2$ may be coal stocked in Port and used in thermal power plant and other industries and vehicle exhaust. It is well known that wind flows from south-west direction during summer and rainy seasons where all the industries are located while the airflow is from northeast direction during the remaining part of the year. The wind direction could be obstructing the pollutants to go into the atmosphere during winter.

The variations in CO concentrations (Fig. 5) peaks during morning and evening traffic hours and valley in afternoon shows a clear link to the boundary layer height evolution.

Pearson Correlation Coefficients

Correlation method is used to gauge the extent and nature of the relationship between each of the impacting (independent) variables considered in the present study and PM levels. The results are presented in Table 2. The Pearson correlation coefficients between PMs and NO$_2$ and SO$_2$, as observed (Table 2) were either high or moderate in different seasons (PM$_{2.5}$ with NO$_2$: r =0.89-0.59; PM$_{10}$ with NO$_2$: r = 0.89-0.79; PM$_{2.5}$ with SO$_2$: r = 0.85-0.47; PM$_{10}$ with SO$_2$: r = 0.39-0.79, PM$_{2.5}$ with CO: r =0.71-0.43; PM$_{10}$ with CO: r =0.70-0.33). The correlation between PM$_{2.5}$ and CO is higher than the correlation between PM$_{10}$ and CO.

It may be observed that all the three independent variables exhibited the theoretically expected positive relationship with PM levels indicating that NO$_2$, SO$_2$ and CO contribute
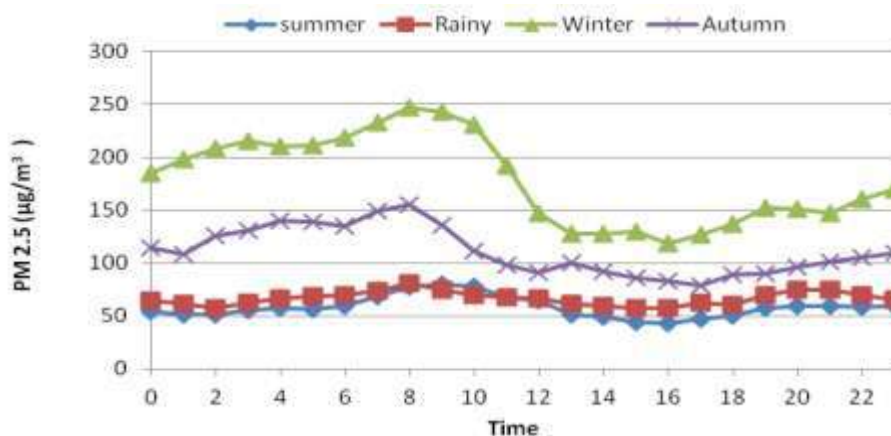

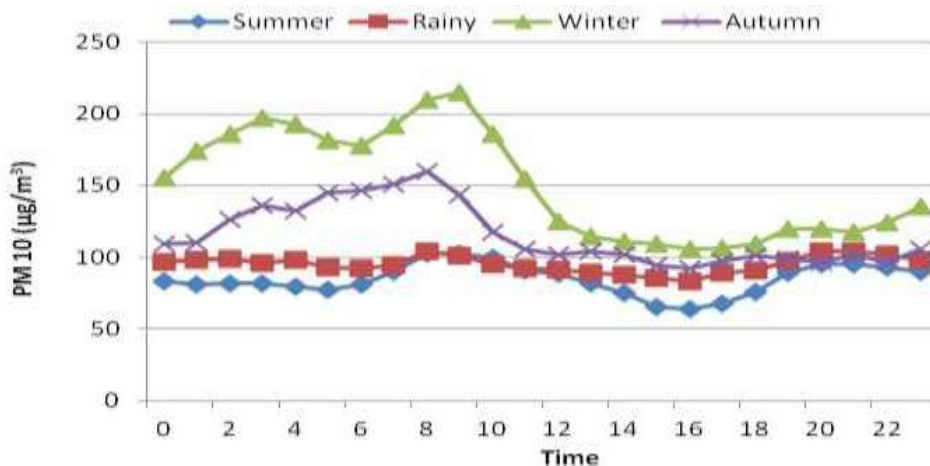Fig. 1: Diurnal variations of hourly PM$_{2.5}$ concentrations.

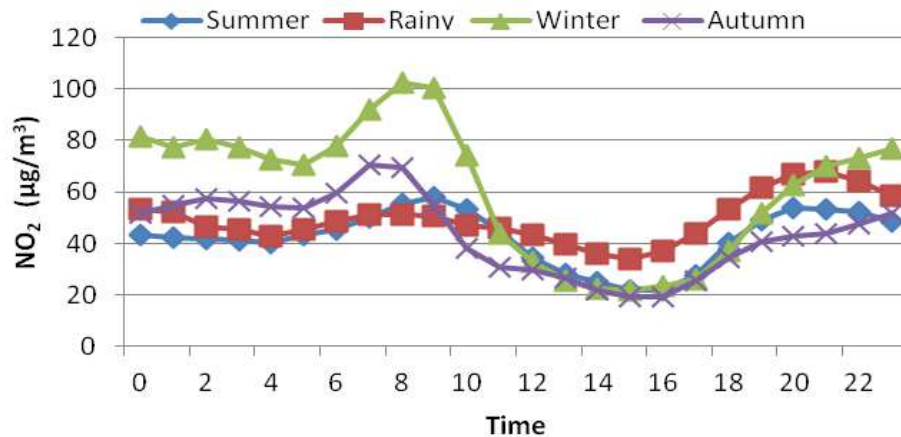Fig. 2: Diurnal variations of hourly PM$_{10}$ concentrations.

Fig. 3: Diurnal variations of hourly NO_2 concentrations.

to the pollution levels recorded in Visakhapatnam city. The positive impact is visible through all the four seasons of the year. It could be further observed that the magnitude of the correlation coefficients varies across variables and seasons. In the summer season, all the three variables recorded high correlation with $PM_{2.5}$ and PM_{10} levels excepting CO on $PM_{2.5}$ with moderate correlation. During rainy season NO_2 recorded high correlation while SO_2 and CO exhibited weak to moderate correlation. All the variables evinced a high correlation with $PM_{2.5}$ and PM_{10} levels in the winter season. In autumn NO_2 and SO_2 registered high correlation while CO recorded weak correlation with PM levels. All the coefficients are statistically significant across all the variables and seasons. It may be concluded that the three variables considered in the study are significantly correlated with PM levels with varied magnitude across seasons and even variables.

The exact magnitude of the impact of each of the independent variable on pollution levels could be further discerned through the following equation.

$$Y = a + bX_1 + cX_2 + dX_3 + U \qquad \ldots(1)$$

Where Y = $PM_{2.5}$ and PM_{10} levels taken independently,

X_1 = NO_2 mean levels, X_2 = SO_2 mean levels, X_3 = CO mean levels, U = error term and a, b and c are the estimated coefficients of the three independent variables.

The variables are theoretically expected to possess a linear relationship with PM levels and hence multiple linear regression method is adopted to estimate the coefficient values of the variables.

The regression results are presented in Tables 3-6 by season. It could be discerned (Table 3) that the considered variables explained 79 per cent of the variation in $PM_{2.5}$ level in summer season in Visakhapatnam city as observed from adjusted . Both NO_2 and SO_2 registered expected signs. The coefficients of both NO_2 and SO_2 are significant at 5 and 1 per cent respectively. Further, one unit change in NO_2 is likely to cause 0.43 unit change in $PM_{2.5}$. Similarly, a unit change in SO_2 may impact $PM_{2.5}$ by 0.74 units. It may, therefore, be inferred that NO_2 and SO_2 significantly impact $PM_{2.5}$ during the summer season in Visakhapatnam city.

It is evident from Table 3 that the influence of the considered variables on PM_{10} for the same season. The results show

Table 2: Pearson correlation coefficients between PMs and gaseous pollutants.

Pollutants	Seasons							
	Summer		Rainy		Winter		Autumn	
	r ($PM_{2.5}$)	r (PM_{10})	r ($PM_{2.5}$)	r (PM_{10})	r ($PM_{2.5}$)	r (PM_{10})	r ($PM_{2.5}$)	r (PM_{10})
NO_2	0.767	0.889	0.591	0.793	0.870	0.825	0.891	0.804
SO_2	0.855	0.750	0.475	0.396	0.771	0.719	0.752	0.789
CO	0.429	0.701	0.472	0.347	0.714	0.638	0.453	0.337

Table 3: Regression analysis results for the summer season.

Dependent variable	Intercept	Independent variable			$\bar{R}^2$
		NO$_2$	SO$_2$	CO	
PM$_{2.5}$	31.61	0.43** (2.94)	0.74* (4.78)	-0.15 (-1.10)	0.79
PM$_{10}$	48.10	0.55* (3.97)	0.40** (2.74)	0.21 (1.63)	0.83

Note: Figures in brackets are 't' values; *significant at 1% level, ** significant at 5% level

Table 4: Regression analysis results for the rainy season.

Dependent variable	Intercept	Independent variable			$\bar{R}^2$
		NO$_2$	SO$_2$	CO	
PM$_{2.5}$	42.27	0.31 (1.96)	0.64 (0.85)	0.01 (0.06)	0.29
PM$_{10}$	68.10	0.62 (5.92)	0.41 (0.83)	-0.27 (-2.09)	0.65

Note: Figures in brackets are 't' values

that adjusted is 0.83 explaining 83 per cent of the variation in PM$_{10}$ by the considered variables. All the coefficients bear expected signs, however, NO$_2$ and SO$_2$ turned out to be significantly determining PM$_{10}$ levels in the city. A unit change in NO$_2$ causes 0. 55 unit change in PM$_{10}$. In the case of SO$_2$, one unit change in SO$_2$ leads to 0.40 unit change in PM$_{10}$ level. Hence even in the case of PM$_{10}$ only NO$_2$ and SO$_2$ are significant factors contributing to PM$_{10}$ levels in summer in Visakhapatnam city.

Turning to the rainy season, as observed (Table 4), is low explaining 29 per cent of the variation in PM$_{2.5}$ level. Of the variables, none is significant as impacting PM$_{2.5}$. However, all the variables have only a tendency to determine PM$_{2.5}$ positively. When it comes to PM$_{10}$ the is high (0.65) and NO$_2$ and CO are significant causative factors. Unexpectedly, CO impacts PM$_{10}$ negatively albeit the magnitude of the variable is low (0.27). SO$_2$ is not a significant determinant of PM$_{10}$. Hence, NO$_2$ is the only factor contributing to PM$_{10}$ levels in rainy season in Visakhapatnam city.

For winter (Table 5), high for both PM$_{2.5}$ and PM$_{10}$

indicate that the considered variables could explain 94 per cent and 91 per cent of variation respectively in pollution levels. All the variables registered expected signs and significant at the 1 per cent level.

The magnitudes of coefficients of both NO$_2$ and SO$_2$ are high indicating that one unit change in them impact PM$_{2.5}$ and PM$_{10}$ by more than twice. However, CO is significantly contributing negatively to both PM$_{2.5}$ and PM$_{10}$. The negative sign could be due to a high correlation between NO$_2$ and CO resulting in the biased estimate of CO.

In autumn (Table 6), PM$_{2.5}$ is significantly impacted by all three variables. So is the case with PM$_{10}$. values are high. NO$_2$ and SO$_2$ are significant, so is CO but the sign is negative. It may be inferred that NO$_2$ and SO$_2$ are significant factors impacting both PM$_{2.5}$ and PM$_{10}$ levels.

CONCLUSIONS

It is observed that the annual averaged PMs exceeded the WHO standards (10μg/m^3) in all seasons. The PM concen-

Table 5: Regression analysis results for the winter season.

Dependent variable	Intercept	Independent variable			$\bar{R}^2$
		NO$_2$	SO$_2$	CO	
PM$_{2.5}$	139.21	2.40* (8.24)	2.20* (5.18)	-3.11 (-4.97)	0.94
PM$_{10}$	154.39	2.74* (8.88)	1.46** (3.23)	-4.20 (-6.33)	0.91

Note: Figures in brackets are 't' values; *significant at 1% level, ** significant at 5% level
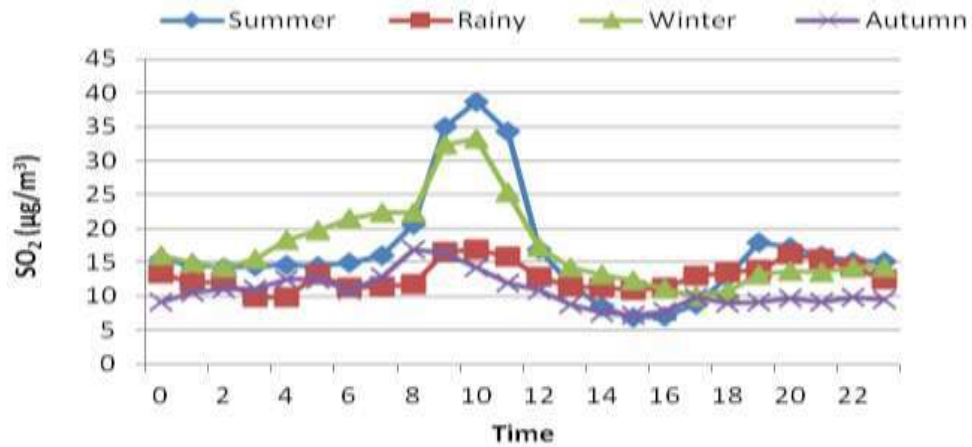
Fig. 4: Diurnal variations of hourly SO_2 concentrations.
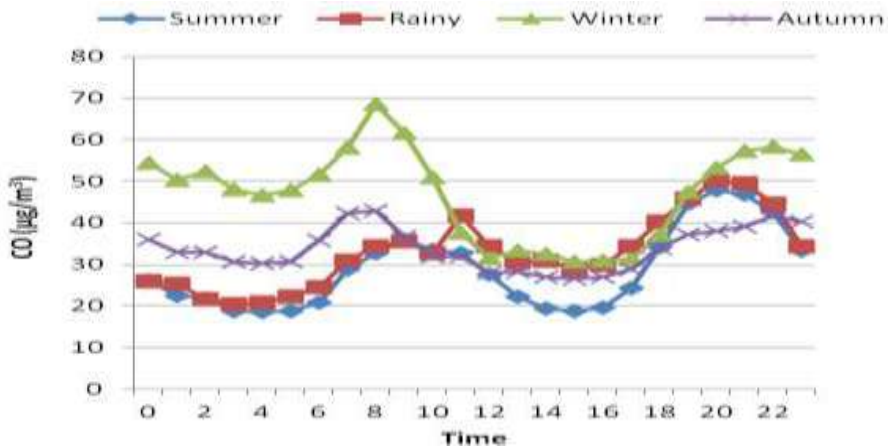

Fig. 5: Diurnal variations of hourly CO concentrations.

trations showed a remarkable seasonal variability, highest during winter and lowest during the summer. The winter maximum is due to temperature inversion and stagnant weather. The diurnal variations of PM concentrations and gaseous pollutants were analysed. The concentration of PM and air pollutants showed significant correlation. The major contributing factors are NO_2, a tracer for vehicle emissions and SO_2, a tracer for combustion. It is clear from the study that high health risk is evident associated with fine particulate matter pollutions to the people living in Visakhapatnam city.

Table 6: Regression analysis results for the autumn season.

Dependent variable	Intercept	Independent variable			$\bar{R}^2$
		NO_2	SO_2	CO	
PM $_{2.5}$	62.21	1.36* (7.66)	2.48** (2.95)	-1.33 (-3.02)	0.88
PM $_{10}$	82.77	1.11* (5.59)	3.53** (3.76)	-1.60 (-3.26)	0.83

Note: Figures in brackets are 't' values; *significant at 1% level, ** significant at 5% level

REFERENCES

Balakrishnan, K., Ganguli B. and Ghosh, S. 2013. A spatially disaggregated time-series analysis of the short-term effects of particulate matter exposure on mortality in Chennai, India. Air Qual. Atmos. Health, 6: 111-121.

CEPI 2013. Criteria for Comprehensive Environmental Assessment of Industrial Clusters, Central Pollution Control Board, New Delhi.

CPCB 2009. National Ambient Air Quality Standards. Notification B-21906/20/90/PCI-L. Central Pollution Control Board, New Delhi, India.

Greenstone, M., Nilekani, J., Pande, R., Ryan, N., Sudarshan, A. and Sugathan, A. 2015. Lower pollution, longer lives: Life expectancy gains if India reduced particulate matter pollution. Econ. Polit. Wkly., L 40-46.

Guttikunda, S.K., Goel, R., Mohan, D., Tiwari, G. and Gadepalli, R. 2015. Particulate and gaseous emissions in two coastal cities-Chennai and Vishakhapatnam, India. Air Quality, Atmosphere & Health, 8(6): 559-572.

Katsouyanni, K., Touloumi, G., Samoli, E., Gryparis, A., Le Tertre, A., Monopolis, Y., Rossi, G., Zmirou, D., Ballester, F., Boumghar, A., Anderson, H.R., Wojtyniak, B., Paldy, A., Braunstein, R., Pekkanen, J., Schindler, C. and Schwartz, J. 2001. Confounding and effect modification in the short-term effects of ambient particles on total mortality: Results from 29 European cities within the APHEA2 project. Epidemiology, 12: 521-531.

Ito, K., Thurston, G.D. and Silverman, R.A. 2007. Characterization of PM2.5, gaseous pollutants, and meteorological interactions in the context of time-series health effects models. Journal of Exposure Science and Environmental Epidemiology, 17: S45–S60.

Latha, K.M. and Badarinath, K.V. 2005. Seasonal variations of PM10 and PM2.5 particles loading over tropical urban environment. Int. J. Environ. Health Res., 15(1): 63-68.

Murty, B.P. 2004. Environmental Meteorology. IK International Pvt. Limited.

NEERI 2005. Ambient air quality survey and air quality management plan for Visakhapatnam Bowl Area. National Environmental Engineering Research Institute Nagpur.

Population of India 2018. Retrieved from https://indiapopulation2018.in/population-of-visakhapatnam-2018.html

Rao, V.L. and Satish, P. 2014. The study of an increment of air pollution over a coastal city. Int. J. Curr. Microbiol. App. Sci., 3(8): 910-924.

Samet, J.M., Dominici, F., Zeger, S., Schwartz, J. and Dockery, D.W. 2000. The National Morbidity, Mortality, and Air Pollution Study (NMAPS). Part I. Methods and methodological issues, Cambridge, MA: Health Effects Institute, 2000 (Report No. 94).

Sarnat, J.A., Schwartz, J., Catalano, P.J. and Suh, H.H. 2001. Gaseous pollutants in particulate matter epidemiology: Confounders or surrogates? Environ Health Perspect, 109: 1053-1061.

Srinivas J. and Purushotham A.V. 2013. Determination of air quality index status in industrial areas of Visakhapatnam, India. Res. J. of Engineering Sci., 2(6): 13-24.

Venkataraman, C., Brauer, M., Tibrewal, K., Sadavarte, P., Ma, Q., Cohen, A., Chaliyakunnel, S., Frostad, J., Klimont, Z., Martin, R.V., Millet, D.B., Phillip, S., Walker, K. and Wang, S. 2018. Source influence on emission pathways and ambient PM2.5 pollution over India (2015-2050). Atmos. Chem. Phys., 18: 8017-8039.

Influence of Expressway Construction on the Ecological Environment and the Corresponding Treatment Measures: A Case Study of Changyu (Changchun-Fuyu Lalin River) Expressway, China

Gao Jiayin*, Zhang Mingfei**, Hu Zhaoguang** and Shan Wei***†

*College of Engineering and Technology, Northeast Forestry University, Harbin 150040, China
**College of Civil Engineering and Architecture, Zhengzhou University of Aeronautics, Zhengzhou, 450046, China
***Institute of Cold Regions Science and Engineering, Northeast Forestry University, Harbin 150040, China.
†Corresponding author: Shan wei; shanwei456@163.com

ABSTRACT

With astounding advances, China expressway construction has caused inevitable environmental destruction around the construction projects. A series of expressway construction-induced environmental problems is caused by the noise pollution of machinery and equipment in expressway construction, atmospheric pollution caused by fuel consumption, soil contamination caused by abandoned waste materials and gases generated by asphalt mixture during road paving, and increasing traffic volume. In this study, the literature regarding expressway construction-induced environmental pollution was combined by taking Changyu (Changchun-Yulin Lalin River) Expressway as an example. The impacts of expressway construction on the ecological environment were analyzed, and feasible treatment measures were proposed. Results show that the expressway construction in various countries across the globe aggravates the regional ecosystem damage unavoidably to a certain extent; The environmental impacts caused by Changyu Expressway are manifested at five aspects, namely, water environmental pollution, vegetation deterioration, heavy metal pollution, water and soil losses, and induction of geological disasters; The environmental impacts of expressway construction can be mitigated by reasonable route selection, strengthening planning and environmental protection, preventing water and soil losses, reinforcing atmospheric pollution detection, reducing sewage discharge, enhancing vegetation recovery, and relieving the impact on animal habitats. The study results serve as an important reference for identifying the sources of expressway environmental risks and lowering the environmental pollution caused by expressway construction to an acceptable level.

INTRODUCTION

The expressway construction in China is developing at considerable speed. As shown in Fig. 1, the total mileage of China expressways has rapidly increased from 16,200 km in 2000 to 149,600 km in 2019, and the annual average growth rate has reached 43%. However, the rapid advancement of expressway construction has brought unavoidable environmental destruction around the construction projects. Under frequent human activities, the ecological environment experiences irreversible pollution and destruction and threatens human health and survival. Sustainable development is advocated within the global scope at present. As a livelihood project, expressway engineering must consider environmental benefits when creating economic benefits. The high-speed construction of expressway projects has caused serious environmental problems in the affected zones along the expressways. These environmental problems include biodiversity degradation and disordered biological clock of animals and plants, water and soil losses, motor vehicle exhaust emission and noise generated by road traffic vehicles along the expressways, ecological and natural environmental quality problems and socioeconomic environmental phenomenon, such as water environmental pollution, caused by transportation of dangerous chemicals. However, high filling and deep excavation are unavoidable during expressway construction, and bridging by tunnelling through mountains is common, resulting in environmental destruction.

Given that wide black bituminous pavements commonly used on expressways have strong heat absorptivity, along with increased coverage area of roadside desertification land, the surface temperature along the expressways is elevating, thereby accelerating permafrost thawing within the expressway region and leading to pavement drying and grassland degeneration. This condition accelerates the desertification progress within the expressway region and degrades its ecological environment. The linear cutting action of expressways
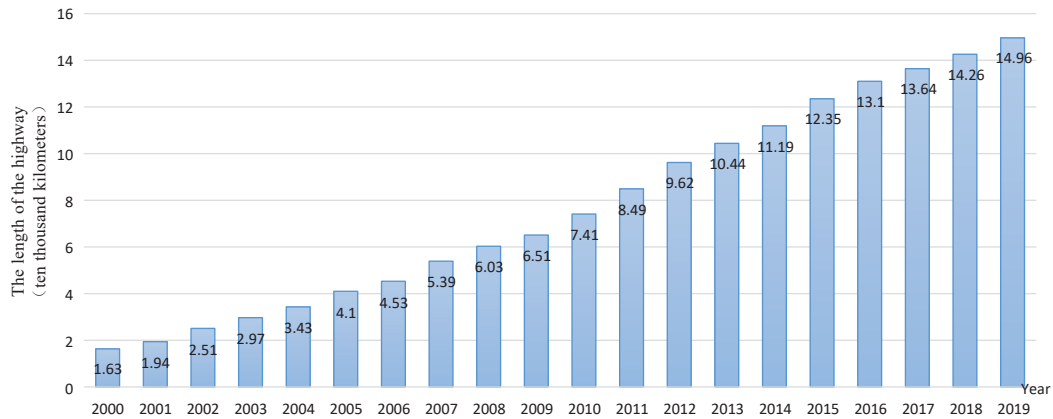
Fig. 1: Expressway mileages in China during 2000-2019.

aggravates the ecological environment deterioration. Therefore, field investigation must be first conducted to deeply analyze the possible adverse effects of various engineering construction links on the surrounding environment and evaluate the severity of such effects following the involved scope of influence to achieve expressway environmental protection. A practical and feasible protection scheme can be formulated. Environmental protection should be prioritized in actual expressway construction links, such as construction design and technological application. Improving environmental protection functions of highways can lengthen their service life and mitigate environmental destruction caused by engineering construction.

PAST STUDIES

An expressway is an important mark of modernization of a country and its transportation and major infrastructure in national economic and social development. Expressway construction plays an important role in promoting national economic development, reasonable productivity distribution, and interregional cooperation, improving the investment environment, raising the living standard, promoting the domestic demand, and stimulating the economic development and prosperity of regions nearby the expressways. However, expressway construction projects generate major and far-reaching influences on the wide-range ecological environment within a large region during the construction and operation periods. For the environmental impacts of expressways and their control measures, Foppen (1994) believed that road construction is a double-edged sword, where it accelerates economic development and transformation of transportation modes but causes immeasurable losses to the natural environment and results in environmental separation from landscapes. Reijnen et al. (1995) studied the influences

of motor traffic on bird breeding density in deciduous and coniferous forests and the importance of automobile noise and visibility as possible factors influencing the bird breeding density. Forman et al. (2000) thought that traditional transportation planning has an evident influence on eco flow and biodiversity. They estimated the influence positions and distances of nine processes by taking a suburban four-lane expressway with 24 km in length in Boston as an example. The study results indicated the impact of expressway traffic noise on bird communities and showed that the road extends outward for more than 100 m as the barrier disturbing the wildlife tourism aisle. Geneletti (2003) deemed that the road network is an important reason for the declining quantity and quality of natural habitats and proposed a road project BIA (Biodiversity Impact Assessment) method that can be used to directly analyze the expressway construction-induced direct ecosystem loss. Viard et al. (2004) monitored the heavy metal content in soil at the two sides of French A31 Expressway, and the results indicated that the maximum pollution ranges from 5 m to 20 m. Xu et al. (2006) elevated the expressway subgrade in permafrost region to mitigate the influence of freeze-thawing on the road stability of alpine steppe with low vegetation coverage. However, mostly sands and grits are found on the expressway slope, thereby improving the erosion potential of slope soil. Xia et al. (2007) found that vegetation destruction of the highway construction phase, linear road cutting, and automobile running limit the utilization of wildlife aisles. The influence of transportation development on Tibetan antelope habitat and migration is the present and future primary factor threatening Tibetan antelopes. Hjortenkrans et al. (2008) analyzed the heavy metal content in exposed soil along the two highways in Sweden and pointed out that the heavy metal content in 0-10 cm soil is remarkably higher than that in 10-30 cm soil. Given that road

is a linear source of pollution, the heavy metals in soil present highway-centred and two side-extended banding distribution laws. Bukowiecki et al. (2010) considered that non-exhaust emissions generated by highway operation generate a large load on the air environment in the road region. These emissions mainly include particles formed by the resuspension of sedimentary road dusts, which are caused by automobile braking wear, tyre wear, pavement wear, and vehicles. Yan et al. (2013) investigated the heavy metal contents in surface soil within the road region distant from villages, towns, and region of industrial and agricultural activities. They found that the heavy metal concentration in surface soil exponentially declines with lowered ecological risks with the increase in distance from the road boundary through field investigation and laboratory experiment. Karlson et al. (2014) believed that road construction exerts extensive impacts on terrestrial and aquatic ecosystems, and the road network is increasingly associated with biodiversity loss across the world (Karlson et al. 2014). Zhang et al. (2015) explored the heavy metal enrichment degree in soil along Tibetan expressways and found that the heavy metal content is the highest in soil on the alpine steppe, followed by those in alpine meadow and alpine desert. Zhang et al. (2017) investigated the heavy metal pollution and assessed the ecological risks along six roads of different land-use types in Sachsen State in Germany. The results showed that the surface load of Zn and Cu presents a declining trend from the city centre toward the urban fringe. Taking China as an individual case, Wu et al. (2019) discussed the governmentally perceived scope of environmental impacts and the transformation of concepts into management methods. The results showed that the government can effectively improve the environmental and ecological protection level by strengthening the environmental management of expressways. Existing literature shows that the expressway construction has entered a rapid development phase across the globe, and the expressway construction has unavoidably aggravated the regional ecosystem destruction to a certain extent, thereby deteriorating the ecological environment along expressways and impacting their environmental quality. The environmental impacts of expressway construction were analyzed, and control measures were proposed by taking Changyu Expressway as an example. The findings serve as a reference for enriching the evaluation system for the environmental impacts of expressways and mitigating the environmental pollution caused by expressway construction and operation.

BASIC INFORMATION OF CHANGYU EXPRESSWAY

Natural Environment

The Changyu Expressway project is located in Fuyu City, Jilin Province. The geographic position coordinates of the project are east longitude of 125°57'-126°05' and northern latitude of 44°56'-45°08'. This area belongs to a mid-temperate-zone continental monsoon climate with four distinctive seasons, which is dry and windy in spring and hot and rainy in summer with short autumn and long and cold winter. Changyu Expressway K1097+100–K1097+860 belongs to a soft soil foundation segment. A temperature monitoring equipment was buried at the right slope foot of K1097+200 section to perform sustainable long-time monitoring to understand the change in surface temperature in the study area. The surface temperature data are shown in Fig. 2. As shown in the surface temperature profile, the study area enters the frost period at the beginning of November, the seasonally frozen ground is unthawed until the end of April, the earth freeze-up time lasts for 5.5 months, and the maximum depth of seasonally frozen ground reaches 1.8 m. Thus, it belongs to a severe cold area.
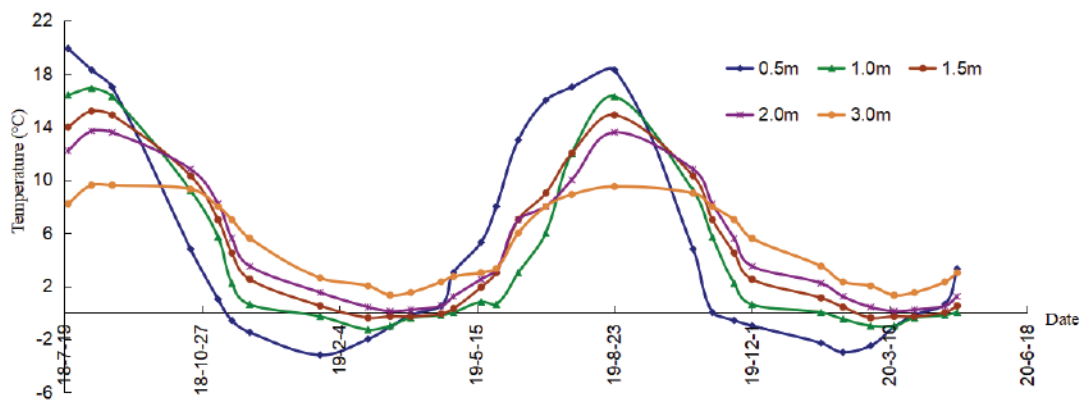

Fig. 2: Time-dependent change curves of surface temperature at the right slope foot of K1097+200.

Engineering Geological Conditions

The Changyu Expressway project belongs to the flood plain landform in the east of Songliao Plain. During the geological survey of this road segment, the drilling results show that the 0-15 m depth range is quaternary Holocene alluvium. The groundwater type within the range of surveying depth in this area is loose rock-type porewater. The groundwater level is shallow at the sand layer, ranging from 7.5 m to 8.5 m. The strata in this area are described from top to bottom as follows: (1) Silty clay: yellow, plastic, and slightly wet. The moisture content is within 12.8%-29.0%, and the burial depth of the roof is 0-3.2 m. (2) Mucky soil: grey, with thickness ranging from 3.5 m to 7.5 m, moist, soft plastic or fluid plastic, and paddy field segment. The moisture content is within 31.9%-43.6%, and the strata thickness is within 3.5 m-7.5 m. (3) Fine sand: grey, slightly dense, saturated, and the main components are quartz and feldspar. The burial depth of the roof is 3.2-7.8 m. In the drilling reconnaissance, a soil sampler was used to collect several groups of undisturbed soil samples at the silty clay and mucky soil layers. Physical and mechanical property laboratory experiment of the collected samples was performed following the geotechnical testing regulations, and the soil physical and mechanical test indexes of different strata were obtained, including moisture content, unit weight, natural density, void ratio, specific gravity, cohesion, and internal friction angle, as presented in Table 1. The moisture content in mucky soil is high in the study area with weak soil mass strength. Thus, it belongs to a soft soil layer.

ECOENVIRONMENTAL IMPACTS OF CHANGYU EXPRESSWAY CONSTRUCTION

Water Environmental Pollution

Changyu Expressway construction threatens drinking water safety in the water conservation areas and is closely related to people's health and social stability. Some drinking water and surface water conservation areas are rivers and conveyance canals with large drainage area and long flowing length. Expressway construction certainly passes through or spans in some drinking water and surface water conservation areas. During the construction period, the generated pollutants and water and soil losses will be diffused into water sources, thereby leading to water pollution. The construction materials, such as asphalt, oil, and chemicals, will cause water environmental pollution if improperly kept and washed by rainwater to enter the water body during the construction period. In the construction period of the riverside road segment, the soil will be washed by rainwater into the river during subgrade and pavement construction, thereby causing partially high content of suspended matter in the river. Production wastewater in the construction period, domestic wastewater of the construction camps, and sewage from toll station and curing area in the operation period will generate adverse effects on the surrounding water body.

Vegetation Damage

Changyu Expressway is located in a flat area. Intensely disturbed by human activities, natural vegetations are mainly drought-resistant, barren, and heliophilous herbs, along with some heliophilous undershrub, and the biomass is low. Different from plants, animals are mobile and can proactively avoid damage. Changyu Expressway project construction will not generate an extreme effect on the diversity or population quantity of bird and reptile-type wildlife species, especially on the degradation of bird diversity, and will not have any influence on wildlife habitats. The heaps of debris during the construction will induce rats, mosquitos, snakes, and frogs. However, these living organisms will seek habitats again after the construction is completed. The noise, light, waste gas, vibration, and pavement runoff pollutants in the operation period will pollute the living environment of animals, break their original life pace, reduce their living environmental quality, and force them to seek for other activity and living places. This expressway belongs to a closed project with a certain obstructing effect on animals. However, a certain quantity of bridges and culverts is reserved in the design phase for animals to pass through the expressway. The animals present two-side extended distribution along the expressway, which is taken as aisle. Thus, this expressway has a minor obstructing effect on normal animal communication and foraging.

Heavy Metal Pollution

The heavy metal pollution generated by expressway transportation mainly derives from fuel consumption, wear of automobile metal parts and tyres, and chemical substances

Table 1: The summary sheet of physical and mechanical indexes of foundation soil in the test segment.

Soil type	Moisture content	Unit weight γ_ω (kN/m^3)	Natural density (g/cm^3)	Void ratio	Specific gravity	Cohesion (kPa)	Internal friction angle (°)
Silty clay	20.1%	17.2	1.96	0.83	2.75	40.95	21.5
Mucky soil	35.3%	15.9	1.79	1.25	2.56	14.95	7.9

released by pavement materials and curing chemicals. The heavy metals are diffused in the particulate form together with atmospheric diffusion in tail gas form, pavement sputtering dust diffusion, and surface runoffs, and are accumulated in the soil at the two sides of the road. The generated polluting metallic elements come from fuels, engine oil, tyre wear, braking wear, and vehicle exhaust catalysts. The mass monitoring data manifest that the soil at the two sides of Changyu Expressway is polluted by toxic metallic elements to different degrees where the pollution caused by Pb and Cd is the most serious, followed by Zn and Cu.

Water and Soil Losses

During the main construction process of Changyu Expressway, the construction links, such as subgrade and mountain excavation, and construction of a large number of tunnels, bridges, and culverts generate many spoils and waste slags, resulting in farmland and vegetation damage and exposed surface and degradation of soil erosion durability. The surface soil should be first peeled off and stored and backfilled when soil is collected in the borrow area, easily causing water and soil losses because of rainfall or gale weather. The slope formed by piling of spoils and waste slags will easily undergo water erosion and serious man-made water and soil losses and will induce debris flow disaster if not protected with engineering measures or afforestation measures. Many construction roads will be built in the construction period, and numerous heavy trucks running on the road during the construction will damage the pavement and generate a large quantity of raised dust. Stock ground, mixing field, and precast yard stacked with soils, stones, and sands will also experience serious water and soil losses if they are untimely protected as requested.

Geological Disaster

The expressway construction-induced landslide mainly occurs during the construction process. For instance, mountain excavation reduces the supporting force of slope rock mass and triggers landslide. Taking earth at the slope foot may cause landslide at the fragile part of the slope. In the zone with unstable rock masses, engineering blasting activity will trigger landslides. In the mountainous area, a landslide triggered by expressway construction is the main geological disaster. Abandoning spoils and building structures at the trailing edge of ancient landslide enlarges the additional stress, and thrust load-type landslide is generated because of increasing gliding force. Excavating a large quantity of earthwork will intercept the shallow buried aquifer and destruct shallow groundwater system, making it impossible for underground water to flow toward lower reaches, causing outcrop of groundwater appearing at cutting slope or sub-grade bottom, degrading the stability of highway subgrade and slope, and causing a landslide. A geological disaster, which is a common existence in the expressway construction process with strong destructive effect, is debris flow. During the expressway construction process, the vegetations along the expressway will be damaged, the bare area of soil mass will be increased, and enormous spoils will be generated because of earth excavation, these conditions result in many loose matter sources for the occurrence of debris flow, and heavy rainfall highly induces debris flow.

ENVIRONMENTAL PROTECTION MEASURES IN CHANGYU EXPRESSWAY CONSTRUCTION

Reasonable Route Selection and Strengthened Planning

Reasonable route selection is the precondition for relieving the negative eco-environmental impacts of expressway construction. The route selection should evade areas with good forest cover or eco-environmentally sensitive areas with special functions and occupy less cultivated land, especially basic farmland. High-tech surveying methods and monitoring means, such as precise surveying and mapping and reconnaissance via 3S technology, should be adopted in reasonable route selection. The expressway should be kept away from segments with unstable geological conditions, such as fracture and karst cave, to prevent geological disasters in the construction process. The route selection scheme should be optimized to obtain a route selection scheme considering economic and ecological benefits. Environmental protection and ecological experts can be invited to participate in the entire expressway planning and design and evade some foreseeable problems. The experience and lessons should be summarized and problem causes should be analyzed following the planning and design based on the construction conditions of the already completed project and the ecological environmental status of the project to be constructed. The next stage of work should be concretely arranged after overall planning and coordination to ensure that ecological priority principle is conducted. The coordination with the surrounding environment should be realized as possible to promote the entire green expressway construction.

Strengthen Environmental Protection and Prevent Water and Soil Losses

The ecological environmental protection work must be timely tracked in the expressway construction process, including water and soil conservation and prevention of water and soil losses. Earth excavation and backfilling should not be conducted in the rainy season. The average precipitation is large in the south and small in the north of Jilin Province

where Changyu Expressway is located, and many mountains but few hills are found in this area. The precipitation is larger than those on plains and hills of the same latitude because of high altitude. The precipitation distribution is relatively nonuniform in Jilin Province in different seasons, and the rainy season in the south is different from that in the north. Therefore, the rainfall laws in different areas should be understood in Changyu Expressway construction, earth excavation and backfilling should be completed, and water and soil conservation work should be conducted to prevent secondary disasters, such as water and soil losses before the rainy season comes. Slope protection measures, including slope cutting or graded slope cutting, should be taken. During the subgrade excavation process, temporary settling pond should be set where surface runoffs meet to intercept sediments brought by the surface runoffs. After the subgrade is built, the settling pond should be timely bulldozed for plant plantation or land reclamation. Different water and soil conservation measures should be taken in different stages in accordance with the project features. The soil and water conservation measures in the construction period should centre on engineering measures, assisted by biological control measures. The site of the borrow area should be reasonably planned and original spoils should be scientifically utilized. In the operation phase, high importance should be attached to subgrade slope protection, and flexible slope protection-dominated biological environmental engineering technologies should be used under most circumstances. These conditions can improve landscapes and contribute to ecological self-recovery in the natural recovery period.

Enhance Atmospheric Pollution Detection and Reduce Sewage Discharge

Atmospheric pollution is mainly controlled during the operation period. Although the raised dust in the construction period will generate adverse effects on field constructors and periphery villagers, extremely good dust removal effect can be reached by watering on the construction site. The primary atmospheric pollution source in the expressway project is motor vehicle exhaust emission during the operation period. During the operation period, related departments should strictly conduct motor vehicle exhaust emission testing system and forbid vehicles with exhaust gas emission exceeding the limit to run on the road through spot check at toll stations. The quality of oil products should be strictly controlled at gas stations in service areas along the expressway to reduce pollutant discharge from the source. The sewage discharge should be reduced through optimization design. The sewage discharge system in the expressway area and domestic sewage treatment scheme for supporting facilities have great water environmental impacts in the expressway

project. Measures should be taken as early as the construction planning phase of Changyu Expressway. Surface drainage will be mixed with oil leaked by automobiles. Thus, pavement sewage should be discharged into a biological pond for oil removal, sedimentation, and purification or it may be discharged into the urban sewage treatment system together with domestic sewage generated by supporting facilities.

Reinforce Vegetation Recovery and Lessen Impacts on Animal Living Environment

The existing roads should be used to transport building materials or earth as possible. All types of vehicles should strictly run on the existing roads or the built construction roads and should not take shortcuts because this may grind crops and surface vegetations. Crops and vegetations around the construction site should not be destructed, temporary facilities and temporary projects should be reasonably planned and designed, and arbitrary construction should be forbidden. The construction areas involving forest land and fire risk should be monitored during the construction period to prevent fire disasters. The trees should be moved out for afforestation at other places when deforestation is essential for the main construction and temporary land use. Plants should be cultivated on the slope and new plant communities can be established to reach the goals of recovering the ecology and controlling water and soil losses. The afforestation project should highlight the characteristics of Anhui, centre on block plantation with prominent large colour lumps and large lines. Safety and environmental aesthetic effect should be considered, and attention should be paid to unification and coordination of road cultural and greenery landscapes. Wildlife aisle should be set below the main works to ensure normal foraging, reproduction, and interpopulation connections. The corresponding dedicated animal aisles should be set or the number of highway culverts should be increased and animal, deceleration, and no totting signs should be set at road segments where nationally protected wild animals come and go, including road segments where endangered species pass through. The forest region construction scheme should be optimized, the construction progress should be accelerated, the construction time in the forest region should be shortened, and blasting operation should be avoided to the greatest extent to avoid disturbing wild animals. The construction in the peak period of wild animal activities should be avoided, such as avoiding high-noise operations, such as blasting and piling in the morning, at dusk, and in the evening. Building materials, cement, oil products, and chemicals containing hazardous substances should not be stacked nearby water bodies, such as rivers and lakes, and wastes in the construction should not be locally poured or thrown into water bodies.

CONCLUSION

The ecological environmental impacts of expressway construction projects in China are mainly manifested by surface vegetation damage in areas along the expressways and land occupation and ecological problems and water and soil losses arising out of the expressway construction. Taking reliable and feasible control measures in the expressway construction period can reduce the destruction of the ecological environment on the two sides of the expressway to the minimum level. Taking Changyu Expressway in China as an example, the literature regarding environmental pollution caused by expressway construction were combined, and the ecological environmental impacts of expressway construction were analyzed in this study. The study results manifest that the expressway constructions around the world have unavoidably aggravated the destruction of regional ecosystems. Changyu Expressway has formed environmental impacts in five aspects, namely, water environmental pollution, vegetation deterioration, heavy metal pollution, water and soil losses, and geological disaster. The proposed measures include strengthening expressway construction planning, preventing water and soil losses, enhancing waste gas and sewage detection, and reinforcing vegetation and animal protection. Future in-depth studies, including continuing grading evaluation of ecological environmental impacts of expressway construction projects, perfecting environmental evaluation index system and ecological environmental influence model of expressway region, and improving the evaluation method of ecological risk and human health risk caused by expressways, should be conducted.

REFERENCES

Bukowiecki, N., Lienemann, P., Hill, M., Furger, M., Richard, A., Amato, F., Prévôt, A., Baltensperger, U., Buchmann, B. and Gehrig, R. 2010. PM_{10} emission factors for non-exhaust particles generated by road traffic in an urban street canyon and along a freeway in Switzerland. Atmospheric Environment, 44(19): 2330-2340.

Foppen, R. R. 1994. The effects of car traffic on breeding bird populations in woodland. i. evidence of reduced habitat quality for willow warblers (*Phylloscopus trochilus*) breeding close to a highway. Journal of Applied Ecology, 31(1): 85-94.

Forman, R. T. T. and Deblinger, R. D. 2000. The ecological road-effect zone of a Massachusetts (U.S.A.) Suburban Highway. Conservation Biology, 14(1): 36-46.

Geneletti, D. 2003. Biodiversity impact assessment of roads: An approach based on ecosystem rarity. Environmental Impact Assessment Review, 23(3): 343-365.

Hjortenkrans, D. S. T., Bergbäck, B. G. and Häggerud, A. V. 2008. Transversal immission patterns and leachability of heavy metals in road side soils. J. Environ. Monit., 10(6): 739-746.

Karlson, M., Moertberg, U. and Balfors, B. 2014. Road ecology in environmental impact assessment. Environmental Impact Assessment Review, 48: 10-19.

Reijnen, R., Foppen, R. and Thissen, B. J. 1995. The effects of car traffic on breeding bird populations in woodland. III. Reduction of density in relation to the proximity of main roads. Journal of Applied Ecology, 32(1): 187-202.

Viard, B., Pihan, F., Promeyrat, S. and Pihan, J. 2004. Integrated assessment of heavy metal (Pb, Zn, Cd) highway pollution: Bioaccumulation in soil, Graminaceae and land snails. Chemosphere, 55(10): 1349-1359.

Wu, L., Ye, K., Gong, P. and Xing, J. 2019. Perceptions of governments towards mitigating the environmental impacts of expressway construction projects: A case of China. Journal of Cleaner Production, 236: 117704.

Xia, L., Yang, Q., Chao, L., Wu, Y. and Feng, Z. 2007. The effect of the Qinghai-Tibet railway on the migration of Tibetan antelope *Pantholops hodgsonii* in Hoh-xil National Nature Reserve, China. Oryx, 41(3): 352-357.

Yan, X., Gao, D., Zhang, F., Zeng, C., Xiang, W. and Zhang, M. 2013. Relationships between heavy metal concentrations in roadside topsoil and distance to road edge based on field observations in the Qinghai-Tibet Plateau, China. International Journal of Environmental Research and Public Health, 10(3): 762-775.

Xu, X., Zhang, K., Kong, Y., Chen, J. and Yu, B. 2006. Effectiveness of erosion control measures along the Qinghai-Tibet highway, Tibetan plateau, China. Transportation Research Part D: Transport and Environment, 11(4): 302-309.

Zhang, H., Wang, Z., Zhang, Y., Ding, M. and Li, L. 2015. Identification of traffic-related metals and the effects of different environments on their enrichment in roadside soils along the Qinghai-Tibet highway. Science of the Total Environment, 521: 160-172.

Zhang, J., Hua, P. and Krebs, P. 2017. Influences of land use and antecedent dry-weather period on pollution level and ecological risk of heavy metals in road-deposited sediment. Environmental Pollution, 228: 158-168.

Original Research Paper | https://doi.org/10.46488/NEPT.2020.v19i03.034 | Open Access Journal

Assessment of Groundwater Pollution Due to Textile Industrial Activities in and Around Tirupur Region, Tamil Nadu, India

K. Arumugam*†, T. Karthika*, K. Elangovan** and A. Rajesh Kumar***
*Department of Civil Engineering, Kongu Engineering College, Perundurai-638 060, Tamil Nadu, India
**Department of Civil Engineering, PSG College of Technology, Coimbatore-641 004, Tamil Nadu, India
***GBH International Construction, Pvt. Ltd., Dubai
†Corresponding author: K. Arumugam; sixface@kongu.ac.in

ABSTRACT

Groundwater is the most important resource for human consumption and the support of habitat and for maintaining the feature of base flow to river courses, while its quality is necessary to ensure sustainable safe exploit of the resources for all purposes. The untreated or inappropriate industrial effluents discharge on the surface causes harsh groundwater pollution in the industrial area of the nation. Sixty groundwater samples have been collected from boreholes and water samples were analysed to examine the groundwater quality of Avinashi-Tirupur-Palladam region. The samples were examined for the physico-chemical parameters like pH, electrical conductivity (EC) and total dissolved solids (TDS), major cations like calcium (Ca^{2+}), magnesium (Mg^{2+}), sodium (Na^+), potassium (K^+) and major anions like bicarbonate (HCO_3^-), carbonate (CO_3^{2-}), chloride (Cl^-), nitrate (NO_3^-) and sulphate (SO_4^{2-}), along with fluoride. The abundance of major cations and anions was investigated. Spatial distribution map based on total dissolved solids indicates that the Noyyal and Nallar river basins, central regions of the study area, are more affected. The chemical parameter data of groundwater samples of the study area are plotted in Gibbs's diagram. Based on the Piper diagram, different water types were identified. Hydro-chemically, the quality of the groundwater for human consumption was determined. The ion concentration distribution indicates that most of the groundwater sample locations in the study area are not suitable for domestic use.

INTRODUCTION

Water is one of the most crucial factors determining the quality of life of the people. Change of climate and growing disruptions in the rainfall patterns, industrial activities and soil moisture directly affect the water availability and its quality for drinking and agriculture purposes. The latest patterns of climate changes and groundwater deficit reflected the depletion of water sources and deterioration of groundwater quality in many regions of the world (Raju et al. 2014, Toumi et al. 2015). Recently due to rapid industrialization severe environmental problems in most of the regions, due to improper discharge of effluents into river site by industries such as textile, dyeing, paper processing industries have been found (Hwang et al. 2017). Groundwater quality is being modified when it is in the course of movement during the hydrological cycle and various processes such as transpiration, evaporation, exchanges of cation/anion, dissociation of different minerals, mixing of local waters (Selvarani & Elangovan 2009). The disparity on the concentration of different hydro-geochemical constituents dissolved in groundwater resolves its usefulness for household, industrial and agricultural uses (Samson & Elangovan 2011). Study of

aquifer hydro-chemical characteristics of water is critical for management plan and study skims in the study area and chemical species of groundwater are regarded as valuable information on the geological account of the aquifers and the suitability of various usages (Elangovan & Rani 2017). Evaluation and management of groundwater possessions require an understanding of hydro-chemical and hydro-geological properties of the aquifer (Umar et al. 2001). Groundwater quality refers to the physico-chemical and natural characteristics of water (Santhosh & Revath 2014). Investigation on the geochemical processes to control groundwater chemical composition in and around the river path may lead to improved understanding of the hydro-chemical system in such areas. The studies contribute to effective management and utilization of the groundwater resources. Textile processing plants generally employ synthetic and cotton fibres, include an integrated operation system of printing and dyeing, applying a broad variety of organic dyes and full assortment stages of fabric processes such as starching, singeing and fire retarding (Achwal 1997). Each stage requires water which is finally eliminated as wastewater carrying chemicals used in each state with it (Villegas-Navarro et al. 2001). New tech-

nologies such as remote sensing and GIS have proved to be valuable for understanding the geological environment and geomorphologic conditions accompanied by conventional survey systems (Solomon & Quiel 2006). It is familiar that a contaminated environment has a detrimental effect on the health of people, life of animal and vegetation. During the last few years, there has been information about undesirable changes in the quality of groundwater by the people inhabiting the study area (Sujatha & Reddy 2003).

MATERIALS AND METHODS

The study area lies between latitudes 1100'10°" N-1130'12°" N and longitudes 7700'10°" E-7730'28°" E (Fig. 1) with a geographical area of 450 km^2. The study area accounts for 90% of India's cotton knitwear export value estimated as 3,500 crores. Tirupur is the prime garment exporter in India and it is referred to as the textile valley of India. The study area covers Tirupur taluk, parts of Avinashi and Palladam taluks which are characterized by undulating terrain with the height ranging between 290 and 320 meters above the mean sea level and slanting gradually from west to east direction. The Noyyal river runs all across the study area, almost dividing it into two halves. The various types of soils of the

study area are red calcareous, brown soil and non-calcareous soil. Geologically, the area is underlain by a broad range of high-grade metamorphic gneissic complex (Arumugam et al. 2015). The drainage pattern is the dendritic form (Fig. 2) and they have been found to continue from the Western Ghats. NE-SE trending lineaments are less in number and observed at wide intervals. The geomorphic units exposed from the study area are pediments, shallow pediments, duricrust and shallow buried pediments. The common rock type of the area is hornblende-biotite-gneisses (unclassified gneiss) pink granite, charnockite and complex gneiss along with alluvial rocks and limestones (Fig. 3).

For assessing the groundwater pollution, 62 groundwater samples from the boreholes have been collected and analysed for physico-chemical parameters such as pH, electrical conductivity (EC) and total dissolved solids (TDS), major cations viz., calcium (Ca^{2+}), magnesium (Mg^{2+}), sodium (Na^+), potassium (K^+) and major anions viz. bicarbonate (HCO_3^-), carbonate (CO_3^{2-}), chloride (Cl^-), nitrate (NO_3^-) and sulphate (SO_4^{2-}), in the laboratory by the standard methods given by the American Public Health Association (APHA 1995). The groundwater sample locations were selected for covering the entire study area and attention was given to the
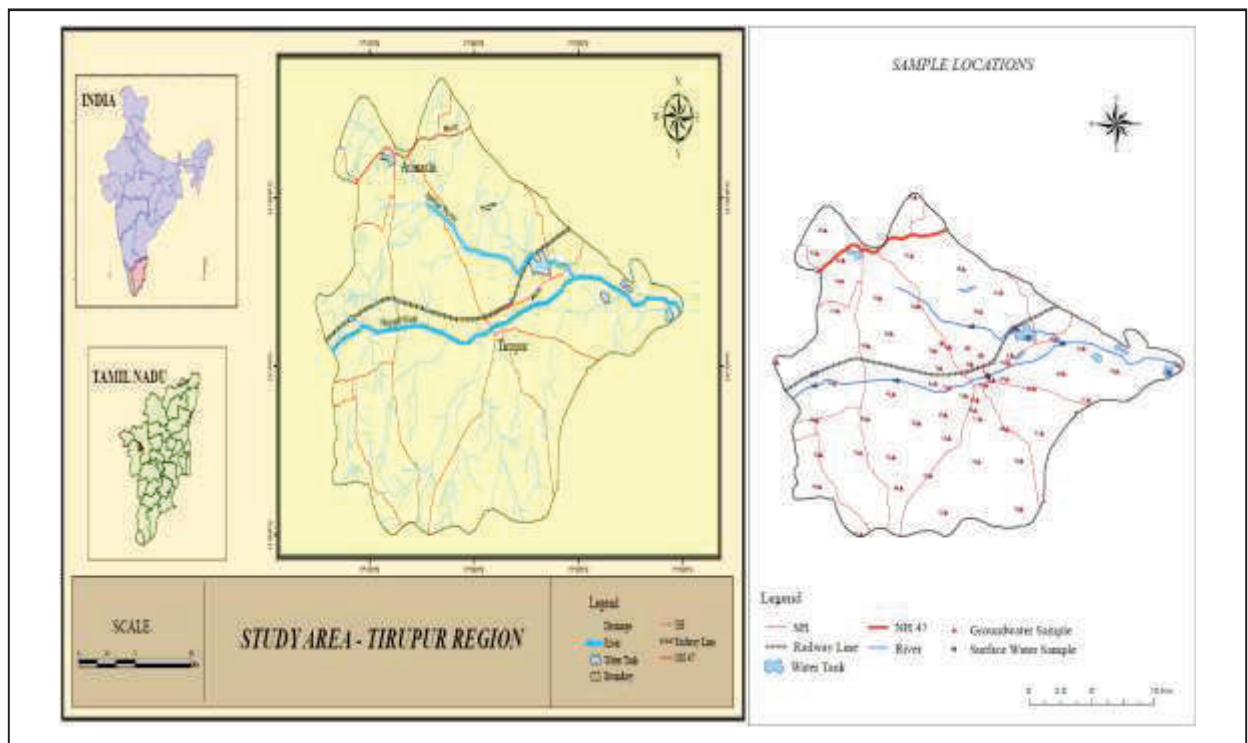

Fig. 1: Sample locations of the study area.

areas where toxic waste is expected**.** About one-third of the sampling stations are within the Tirupur city area and the remaining sampling stations are parts of Palladam and Avinasi taluks. Sampling was conceded using pre-cleaned polyethylene containers. The groundwater samples were evaluated following the drinking water quality standards given by the World Health Organization (WHO 1993) and Bureau of Indian Standards (ISI 2012). The solution of groundwater should be electrically neutral. However, they are rarely equal in practice. The variation increases as the ion concentration value increases (Raju 2006). The exactness of the chemical analysis was verified by calculating ion-balance errors where the errors are generally about 10% (Subramani et al. 2005).

RESULT AND DISCUSSION

To evaluate the quality of subsurface water to find its suitability for domestic purposes, groundwater samples were collected from the study area. The major issue which decides the quality of its groundwater in the study area is textile industrial units and their processes. The water quality may give information about the environment through which the water has disseminated. The results of the analytical data of the chemical parameters and the statistical parameters such as minimum, maximum, mean and median are given in Table 1. For understanding the distribution pattern of the different ion concentration of the parameters, contour maps were generated. Electrical conductivity (EC) values ranged from 847 µS/cm to 9,940 µS/cm with mean and median values of 2,738 µS/cm and 2,235 µS/cm respectively. The

large disparity in EC is mostly attributed to anthropogenic activities and the geochemical course prevailing the region. The values of pH ranged from 6.62 to 8.26 with an average value of 7.71. The values show that the samples of the groundwater of the study area are mostly alkaline. However, in all the sample locations, the pH of the groundwater is within the permissible limits.

To determine the appropriateness of groundwater for any purpose, it is essential to categorize the groundwater based on its hydro-chemical properties like TDS values (Davis & Dewiest 1996, Freeze & Cherry 1979). The total dissolved solids of the groundwater samples have ranged from 550 to 5,998 mg/L with the average and median values of 1,771 mg/L and 1,552 mg/L. This overall evaluation of mean and median values indicates that the water in the study area is unfit for drinking purpose. The spatial distribution map for the TDS prepared using GIS software is illustrated in Fig. 4. The study indicates that all the groundwater samples exceed the desirable limit of 500 mg/L. Moreover, Noyyal and Nallar river basins are highly affected by different anthropogenic activities.

The concentration of cations Ca^{2+}, Mg^{2+}, Na^+ and K^+ ions ranged from 2 to 915, 0 to 485, 25 to 1,123 and 7 to 271 mg/L with a mean of 168, 94, 226 and 69 mg/L respectively. The order of abundance of the cations is $Ca^{2+} > Mg^{2+} > Na^+ > K^+$. The anion concentrations, HCO_3^-, SO_4^{2-}, Cl^-, NO_3^- and CO_3^- range from 140 to 789, 0 to 1215, 36 to 3195, 0 to 572 and 0 to 282 mg/L with a mean of 413, 162, 548, 78 and 54 mg/L respectively. The order of dominance of anions is $Cl^- > HCO_3^- > SO_4^{2-} > NO_3^- > CO_3$. Hydro-geochemical
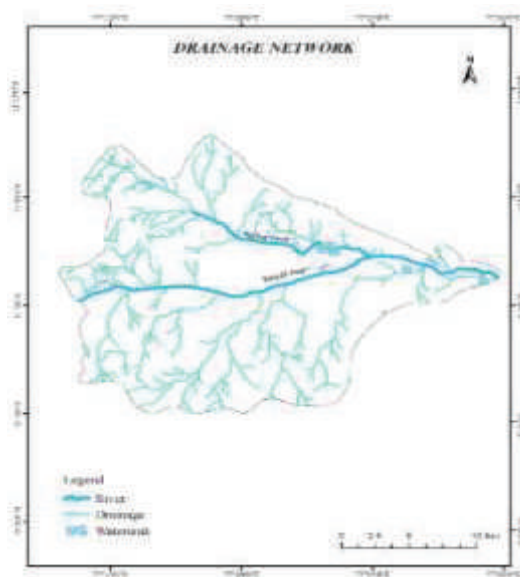

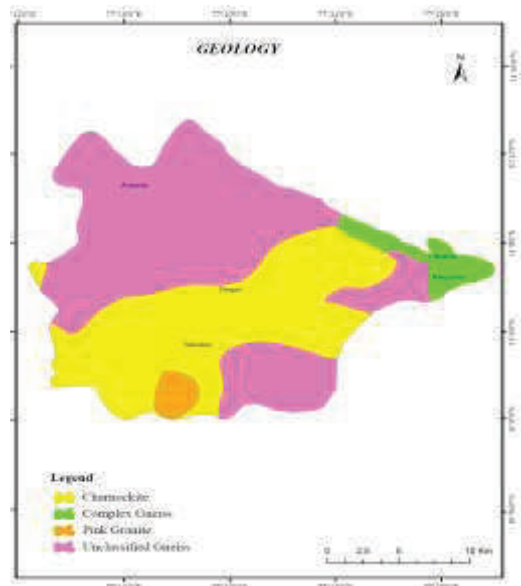
Fig. 2: Drainage network of the study area.

Fig. 3: Geology of the study area.

Table 1: Drinking water specifications given by ISI (2012) and WHO (1993), and summary statistics of groundwater parameters.

Water quality parameters	ISI (2012) Maximum permissible	WHO (1993) Maximum permissible	Minimum concentration	Maximum concentration	Mean	Median
EC (µS/cm)	-	-	847	9,940	2,738	2,235
pH	6.5-9.2	6.5-9.5	6.62	8.26	7.71	7.55
TDS (mg/L)	1,500	1,500	550	5,998	1,771	1,552
TH as $CaCO_3$ (mg/L)	600	500	214	3,610	788	627
Ca^{2+} (mg/L)	200	200	29	915	168	128
Mg^{2+} (mg/L)	100	150	0	485	94	75
Na^+ (mg/L)	-	200	25	1,123	226	159
K^+ (mg/L)	-	12	7	271	69	52
HCO_3^- (mg/L)	300	-	140	789	413	398
CO_3^{2-} (mg/L)	-	-	0	282	54	28
Cl^- (mg/L)	1,000	600	36	3,195	548	396
NO_3^- (mg/L)	-	45	0	572	78	61
T. Alk (mg/L)	600	-	211	734	435	429
SO_4^{2-} (mg/L)	400	400	0	1,215	162	99
F^- (mg/L)	1.2	1.5	0	2.11	0.71	0.61

processes such as ion exchange processes, precipitation, and the residence instance along the flow path control the chemical composition of the region (Nwankwoala & Udom 2011). Process of evaporation increases salinity by increasing sodium and chloride with the increase of TDS. Lack of good drainage setting, semi-arid climate conditions, gentle slope, and residence time of the groundwater also contribute to the quality of groundwater (Subba Rao 2006). According to Gibb's diagram the ratio of Na^+ : ($Na^+ + Ca^{2+}$) and Cl^- : ($Cl^- +$

HCO_3^-) is a function of TDS. It is extensively used to review the functional sources of dissolved chemical parameters such as evaporation-dominance, precipitation-dominance and rock-dominance (Gibbs 1970). The data of the groundwater samples of the study area are plotted in Gibbs's diagram. The distribution of the groundwater sample locations suggests that the chemical weathering of rock-forming minerals and evaporation control the quality of groundwater in the study region (Fig. 5).
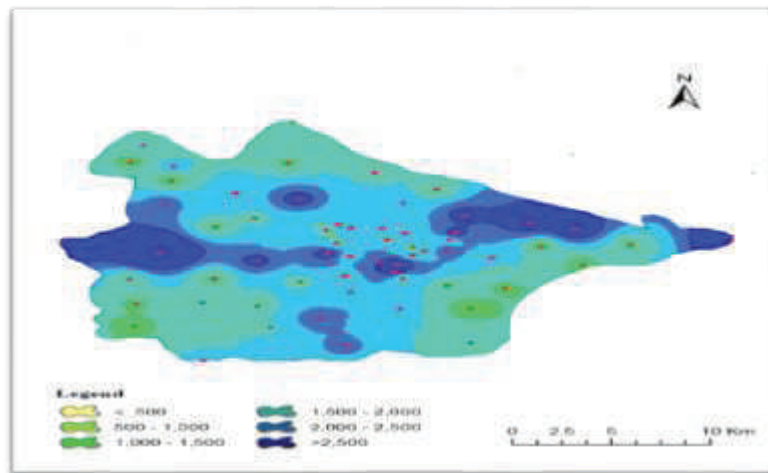

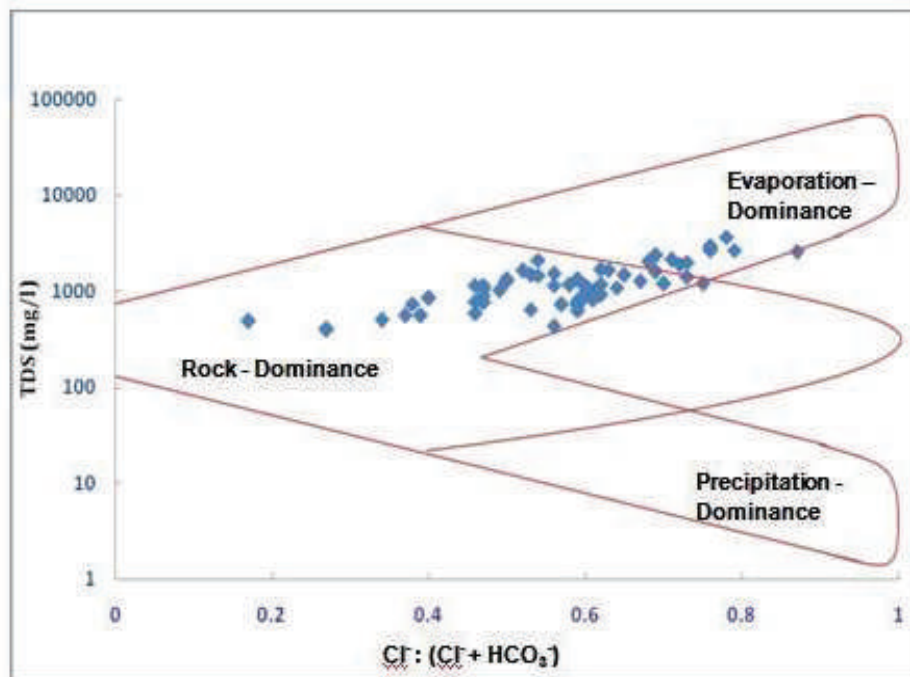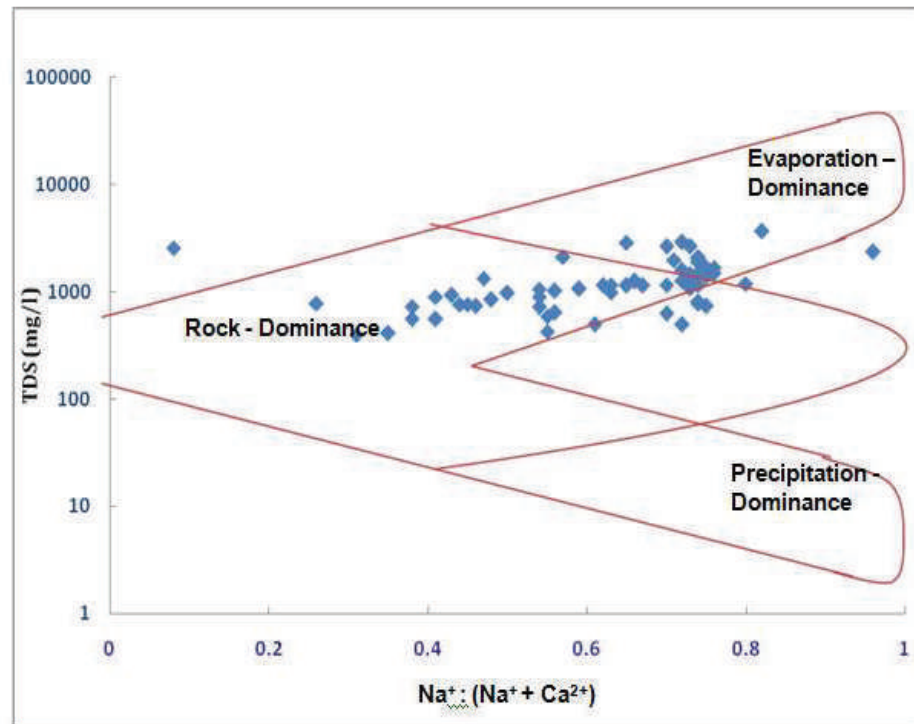Fig. 4: Spatial variation of total dissolved solids.

Fig. 5: Mechanism controlling of groundwater.

The concentration of major ions of the groundwater samples has been used to categorize groundwater into different types based on main cations and anions. The majority of the graphical methods have been intended to simultaneously represent the TDS concentrations and the relative extent of certain major ions. Piper diagram is generally used graphically to understand the problem concerning the geochemical assessment of groundwater. The diagram (Fig. 6) shows the different water types such as calcium-sodium-bicarbonate-chloride (Ca-Na-HCO_3-Cl), sodium-bicarbonate-chloride (Na-HCO_3-Cl), calcium-sodium-chloride (Ca-Na-Cl), calcium-bicarbonate-chloride (Ca-HCO_3-Cl), calcium-bicarbonate (Ca-HCO_3), calcium-sodium-bicarbonate (Ca-Na-HCO_3) and calcium-chloride (Ca-Cl). The abundance of the cations and anions based on dominance is given in Table 2. Substratum containing fluoride minerals is usually respon-

Table 2: Relative abundance of major cations and anions for groundwater samples.

Sl . No.	Cations	% of samples	Anions	% of samples
1.	Na > Ca > K > Mg	30.68	HCO_3 > Cl > SO_4 > NO_3	24.17
2.	Na > Ca > Mg K	24.19	HCO_3 > C l > NO_3 > SO_4	20.97
3.	Ca > Na > Mg > K	11.29	Cl > HCO_3 > SO_4 > NO_3	25.81
4.	Na > K > Ca > Mg	09.68	Cl > HCO_3 > NO_3 > SO_4	11.29
5.	Ca > Na > K > Mg	01.62	NO_3 > HCO_3 > Cl > SO_4	-
6.	Ca > Mg > Na > K	12.90	HCO_3 > NO_3 > Cl > SO_4	01.62
7.	Mg > Ca > Na > K	03.22	HCO_3 > SO_4 > Cl > NO_3	06.45
8.	Na > Mg > Ca > K	04.80	Cl > SO_4 > HCO_3 > NO_3	08.07
9	Mg > Na > K > Ca	01.62	SO_4 > Cl > NO_3 > HCO_3	01.62

Fig. 6: Piper diagram depicting hydrochemical facies of groundwater.

sible for a high concentration of the ion in groundwater and industrial contaminations of the atmosphere and vegetation by fluoride have been a severe problem. Small doses (0.5 to 1.00 mg/L) have a significant influence on the dental system, while in higher doses (> 1.5 mg/L), causes issues of dental fluorosis and gastrointestinal fluorosis (Sahu & Vaishnav 2006). The fluoride concentration of the groundwater samples ranges from 0 to 2.11 mg/L with the mean value of 0.71 mg/L.

CONCLUSION

The hydro-chemical parameter analysis of the investigation reveals that the study region is alkaline. Noyyal and Nallar river basins are more affected by anthropogenic activities. The order of abundance of the cations is $Ca^{2+} > Mg^{2+} > Na^+ > K^+$ and anions is $Cl^- > HCO_3^- > SO_4^{2-} > NO_3^- > CO_3$. Based on the Piper diagram, the alkalies (Na^+ and K^+) significantly exceed the alkaline earths (Ca^{2+} and Mg^{2+}), and strong acids (Cl^- and SO_4^{2-}) exceed the weak acids (HCO_3^- and CO_3). The distribution of the groundwater sample locations proves that the chemical weathering of the rock-forming minerals and evaporation process control the quality of groundwater in the study region. The investigation proves that most of the groundwater samples of the study area are not suitable for domestic use.

REFERENCES

Achwal, W.B. 1997. Problems during analysis of textile as per ecostandards and the customer articles ordinance (Part I), Colourage, 44: 29-31.

APHA 1995. Standard Methods for the Examination of Water and Wastewater, 17th edn., American Public Health Association, Washington, DC.

Arumugam, K., Rajesh Kumar, A. and Elangovan, K. 2015. Evolution of hydrochemical parameters and quality assessment of groundwater in Tirupur Region, Tamil Nadu, India. Int. J. Environ. Res., 9: 1023-1036.

Davis, S.N. and Dewiest, J. M. 1996. Hydrogeology, Wiley, New York, 463.

Elangovan, K. and Rani, R. 2017. Study on suitability of groundwater for irrigation purpose in Parambikulam Aliyar project area, India. Indian Journal of Geomarine Science, 46(5): 1052-1060.

Freeze, R.A. and Cherry. J. A. 1979. Groundwater. Prentice-Hall, New Jersey.

Gibbs, R.J. 1970. Mechanism controlling world water chemistry. Science, 17: 1088-1090.

Hwang, J.Y., Park, S., Kim, H.K., Kim, M.S., Jo, H.J., Kim, J.I., Lee, G.M.,

Shin, I.K. and Kim, T.S. 2017. Hydrochemistry for the assessment of groundwater quality in Korea. Journal of Agricultural Chemistry and Environment, 6(1): 1-29.

ISI 2012. Status of Surface and Groundwater Resources. Bureau of Indian Standards, New Delhi, 2012.

Nwankwoala, H.O. and Udom, GJ. 2011. Hydro-chemical facies and ionic ratios of groundwater in Port Harcourt, Southern Nigeria. Research Journal of Chemical Sciences, 1(3): 87-101.

Raju, N.J. 2007. Hydrogeochemical parameters for assessment of groundwater quality in the upper Gunjanaeru River basin, Cuddapah District, Andhra Pradesh, South India. Environmental Geology, 52(6): 1067-1074.

Raju, N.J., Ram, P. and Gossel, W. 2014. Evaluation of groundwater vulnerability in the lower Varuna catchment area, Uttar Pradesh, India using AVI concept. Journal of the Geological Society of India, 83: 273-278.

Sahu, A. and Vaishnav, M.M. 2006. Study of fluoride in ground water around the BALCO, Kobra Area (India). Journal of Environ. Science and Engg., 48: 65-68.

Samson, S. and Elangovan, K. 2011. Assessment of groundwater quality for drinking purpose in Namakkal district, Tamil Nadu. India. Poll Res., 30: 85-94.

Santhosh, P. and Revath, D. 2014. Geochemical studies on the quality of groundwater in Tirupur District, Tamilnadu, India. Journal of Chemical, Biological and Physical Sciences, 4: 1780-1786.

Selvarani, G. A. and Elangovan, K. 2009. Hydrogeochemistry analysis of groundwater in Noyyal river basin, Tamilnadu, India. International Journal of Applied Environmental Sciences, 4: 211-227.

Solomon, S. and Quiel, F. 2006. Groundwater study using remote sensing and geographic information systems (GIS) in the central highlands of Eritrea. Hydrogeology Journal, 14(6): 1029-1041.

Subba Rao, N. 2006. Seasonal variation of groundwater in parts of Guntur District, Andhra Pradesh, India. Environmental Geology, 49: 413-429.

Subramani, T., Elango, L. and Damodarasamy, S.R. 2005. Groundwater quality and its suitability for drinking and agricultural use in Chithar River Basin, Tamil Nadu, India. Environ. Geol., 47: 1099-1110.

Sujatha, D. and Reddy, B.R. 2003. Quality characterization of groundwater in the south-eastern part of the Ranga Reddy district, Andhra Pradesh, India. Environmental Geology, 44(5): 579-586.

Toumi, N., Hussein, B.H. and Rafrafi, S. 2015. Groundwater quality and hydrochemical properties of Al-Ula region, Saudi Arabia. Environmental Monitoring and Assessment, 187(3): 84.

Umar, A., Umar, R. and Ahmad, M.S., 2001. Hydrogeological and hydrochemical framework of regional aquifer system in Kali-Ganga sub-basin, India. Environmental Geology, 40(4-5): 602-611.

Villegas-Navarro, A., RammHrez-M, Y., Salvador-S, M.S. and Gallardo, J.M. 2001. Determination of wastewater LC_{50} of the different process stages of the textile industry. Ecotoxicology and Environmental Safety, 48: 55-61.

WHO 1993. Guidelines for Drinking Water Quality, Vo.1, Recommendations, 2nd Edn., World Health Organization, Geneva.

Exploring an Environmentally Friendly Microbially Induced Calcite Precipitation (MICP) Technology for Improving Engineering Properties of Cement-Stabilized Granite Residual Soil

Shuang Li*(**)(***), Yan-ning Wang*(**)(***), Dong Liu*(**)(***), Ankit Garg*(**)(***) and Peng Lin*(**)(***)†

*Department of Civil and Environmental Engineering, Shantou University, Shantou Guangdong 515063, China
**Guangdong Structural Safety and Monitoring Engineering Technology Research Centre, Shantou Guangdong 515063, China
***Intelligent Manufacturing Key Laboratory of Ministry of Education, Shantou University, Shantou, China
†Corresponding author: Peng Lin; cuglishuang@163.com

ABSTRACT

This study explored Microbially Induced Calcite Precipitation (MICP) technology to improve the engineering properties [i.e., unconfined compressive strength (UCS)] of granite residual cemented-soil through calcite precipitation. The influence of age and cement mixing ratio on strength, stiffness and the stress-strain relationship of MICP induced calcite precipitation in granite residual cemented-soil was investigated. Scanning electron microscope (SEM) was used to analyse the microstructure characteristics of the cemented-soil. Based on the results, the cemented granite residual soil reinforcement mechanism was proposed. The following conclusions were obtained: (1) MICP technology can significantly enhance and improve the engineering properties such as strength, stiffness and toughness of cemented-soil. Compared with the control group, the maximum growth rate of the test group was 87.5%, and the maximum growth rate of the elastic modulus was 141.18%; (2) Soil particles were cemented through MICP technology, making the cemented-soil surface denser; (3) The MICP technology makes the cemented-soil treatment method more sustainable for its use in improving the stability of geo-structures.

INTRODUCTION

The granite reserves in the southern region, including Hong Kong and Macao, are widely distributed, mainly in low hilly areas (Chen 2007). Granite residual soil is a special type of soil with a small gap in its mineral composition in different regions. In Guangdong, the content of kaolinite in granite residual soil is between 70% and 94%. Besides, the granite residual soil also has engineering properties such as water disintegration, and strong hydrophilicity. Lin et al. (2011) performed a series of studies on the properties of granite residual soil with reduced strength and softening under different water contents (Zhang 2009, Liang et al. 2015). This kind of property makes it a great safety hazard in the extreme climate, especially in the rainstorm season. At present, it is usually adding cement to improve the shear strength and resistance to disintegration ability. Liu et al. (2018) used fly ash to improve granite residual soil. The experimental results showed that adding a certain amount of fly ash to granite residual soil can significantly improve

its water stability. However, most of the chemical slurries synthesized with external admixtures are toxic, which also cause environmental pollution (Karol 2003).

Microbially Induced Calcite Precipitation (MICP) is a new technology that has evolved in recent years along with the continuous development of discipline-crossing on environmental sciences and civil engineering. It is a series of biochemical reactions in bacterial metabolism to produce a cementation process of calcium carbonate, which does not produce toxic substances, is environmentally friendly and efficient. MICP technology has been applied in many fields, such as sewage treatment, concrete material repair, anti-seepage repair, soil remediation of heavy metal pollution, soft foundation reinforcement and improvement. The solutions used in MICP technology (including bacterial solution and cement solution) have lower consistency than traditional chemical slurries and are more likely to penetrate the interior of rock and soil (Chu et al. 2012), which has obvious effects on deep cracks or deep rock soils (Ivanov & Chu 2008).

The application of *Bacillus* mixed nutrient solution and cement solution to degraded limestone can deposit calcium carbonate on the limestone surface and greatly reduce the water absorption coefficient of the limestone surface (Dick et al. 2006).

Whiffin et al. (2007) first proposed the use of microbial induced calcium carbonate to cement sand and proved that the method is effective. Van et al. (2010) used MICP technology to carry out a large-scale *in-situ* sand test of $100m^3$, successfully cementing nearly 1/2 of the sand together, and proved that the mechanical strength of the sand treated by MICP technology improved substantially. In addition to the research on the strength, a large number of scientific research results have been obtained in terms of stiffness (Lin et al. 2011), permeability (Fang et al. 2015, Jia et al. 2016), and durability (Huang et al. 2018, Peng et al. 2019).

At present, the use of MICP technology mainly focuses on the single use of the technology to reinforce the soil, while the MCP technology is less used in combination with other types of external additives such as cement, to strengthen the soil. Mukherjee et al. (2013) stirred bacteria and cement soil into cement bricks. The results showed that the water absorption and porosity of the cement bricks treated by MICP were significantly reduced, and the compressive strength was improved. Liang et al. (2019) investigated the effects of different calcium sources on the shear strength of granite residual soil. The results showed that the shear strength of granite residual soil treated by MICP technology was improved. When calcium acetate was used as a calcium source, the curing effect of MICP was improved better.

Based on the above results, this study researched the engineering characteristics of cement-soil treated by MICP technology. It is expected that the strength of cement-soil can meet the engineering needs in the shorter curing age and lower cement dosage.

MATERIALS AND METHODS

Materials

Soil preparation and physical and mechanical properties: The soil used in the test was granite residual soil and baked at 105°C for 24 h, crushed and passed through 2 mm sieve. The basic physical and mechanical indexes were determined according to the "Standard for Geotechnical Test Methods" (GB/T50123-1999), as given in Table 1. The kind of cement was P.O 42.5.

Preparation of bacterial solution and cement solution: The strain used in this experiment was *Sporosarcina pasteurii* (China General Microorganisms Collection and Management Center, No. CGMCC 1.3687). The culture medium was prepared according to the 0907 medium (Table 2) provided by CGMCC, and the pH was adjusted to 8.0. They were put then into the high-pressure steam sterilization pot, and later into the aseptic operating table and cooled. The activated bacteria were inoculated into 200 mL culture medium in a 250 mL Erlenmeyer flask in a constant temperature shaking incubator (30°C, 150 r/min), and after culturing for 24 to 36 hours, the OD600 = 0.8 was determined. The cement solution was 1 mol/L $CaCl_2$ and 1 mol/L urea.

Methods

We set two groups, one group was ordinary cement-soil, and the other group was microbial cement-soil. The moisture content of each group of cement soil was 25%. Table 3 gives the mixing ratio of cement-soil in the test group, and Table 4 the mixing ratio of cement-soil in the control group.

Table 1: Basic physical properties of granite residual soil.

Physical index	Value
Water content (%)	28.5
Density (g.cm^{-3})	1.93
Void ratio	0.78
Liquid limit (%)	34.2
Plasticity index	11.5

Table 3: Cemented-soil mix proportion of the test group.

Soil mass (g)	1800
Water content (%)	25
Cement ratio (%)	10, 15, 20
Cement mass (g)	180, 270, 360
Total mass of solution (g)	540, 585, 630
Bacterial fluid mass (g)	360, 390, 420
Urea mass (g)	90, 97.5, 105
CaCl$_2$ mass (g)	90, 97.5, 105

Table 2: 0907 *Sporosarcina pasteurii* medium.

Number	0907	
	Peptone	5.0 g
Content	Beef extract	3.0 g
	Urea	20.0 g
	Deionized water	1.0 L

Table 4: Cemented-soil mix proportion of the control group.

Soil mass/g	1800
Water content (%)	25
Cement ratio	10, 15, 20
Cement mass (g)	180, 270, 360
Water mass (g)	540, 585, 630

Three parallel samples were set for each group. The sample size was 3.91 cm in diameter and 8.0 cm in height. Knockout time was 24 hours, then they were sealed with plastic sealed bags, and placed in a standard curing room for further maintenance. The curing conditions were: temperature (25 ± 2) °C, relative humidity ≥ 95%, and the curing age 7d, 14d, 28d.

RESULTS

Result Analysis

Analysis of the UCS test: Taking average UCS values of three parallel samples as the intensity value, the results of the UCS test and analysis are given in Table 7. It can be seen from Fig. 1 that under the same age, the UCS value of

the microbial enhanced cement soil is greater than the UCS value of the ordinary cement-soil, and the growth rates were 51.85%, 87.5% and 47.37% at 7d; the growth rates were 19.77%, 50.3% and 23.26%, at 14d; and the growth rates were 22.81%, 64.46% and 41% at 28d.

It can be seen from Fig. 2 that under the same cement mixing ratio, the UCS values of the cement soils of the two groups increased with the increase of the curing age and the UCS value of the cement-soil of the experimental group is larger than that of the control group. When the cement ratio is 10%, the difference between the two groups is not large, and the difference increases with the increase of cement ratio. In the control group, when the cement ratio increased from 10% to 15%, the growth rates are significantly lower than that of the test group. From the overall view of Fig. 2, the
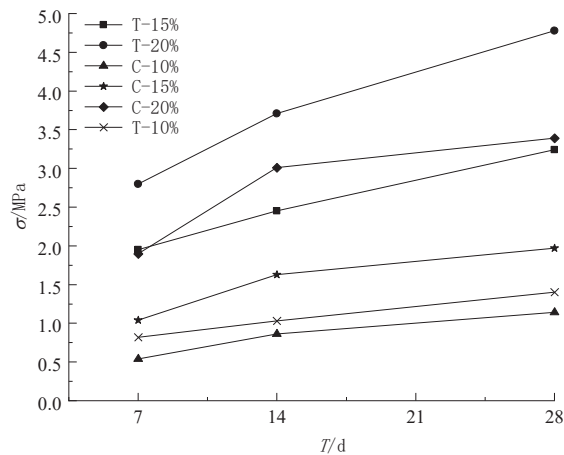
Fig. 1: Comparison of UCS between the test group and the control group with different cement incorporation ratios.
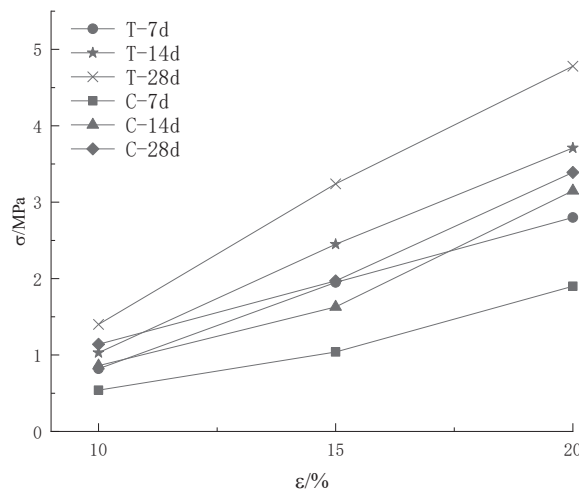
Fig. 2: Comparison of UCS between the test group and the control group for different curing ages.

Shuang Li et al.

UCS values of the test group were significantly larger than that of the control group when the curing age was 7 days, and the UCS values of the control group are similar to that of the control group at 14 days, indicating that the MICP technology can also play a significant role in reinforcing the granite residual soil.

The general formula (1) is obtained by linear fitting the curves of Fig. 1 and Fig. 2. The values of each parameter are given in Table 5 and Table 6. As provided in Table 5 and Table 6, the strength of cement-soil treated by MICP increases. The law of strength growth is more in line with the

linear relationship, and the fitting effect is more significant.

$$f = a + b \cdot x$$

Stress-strain curves and analysis: Fig. 3 is the stress-strain curve at the curing age of 28d. It can be seen from Fig. 3 (a) and (b) that the stress-strain curves of the cement-soils in both groups have undergone the compaction process in the initial stage, but the stress changes of the test group are smaller than that of the control group at the same strain; after the upper concave section, a section of the approximately straight line appears, and the deformation of the cement-soil conforms to the linear elastic relationship; after this stage,

Table 5: Fitting results of UCS of the test group and the control group (refer to Fig. 1).

Group	ε (%)	a	b	R^2
Test group	10	0.635	0.027	0.998
	15	1.555	0.061	0.993
	20	2.265	0.092	0.959
Control group	10	0.400	0.027	0.897
	15	0.870	0.041	0.772
	20	1.710	0.065	0.597

Table 6: Fitting results of the UCS of the test group and control group.

Group	T/d	a	b	R^2
Test group	7	-1.113	0.198	0.988
	14	-1.623	0.268	0.998
	28	-1.93	0.338	0.995
Control group	7	-0.880	0.136	0.954
	14	-1.555	0.229	0.931
	28	-1.208	0.225	0.955
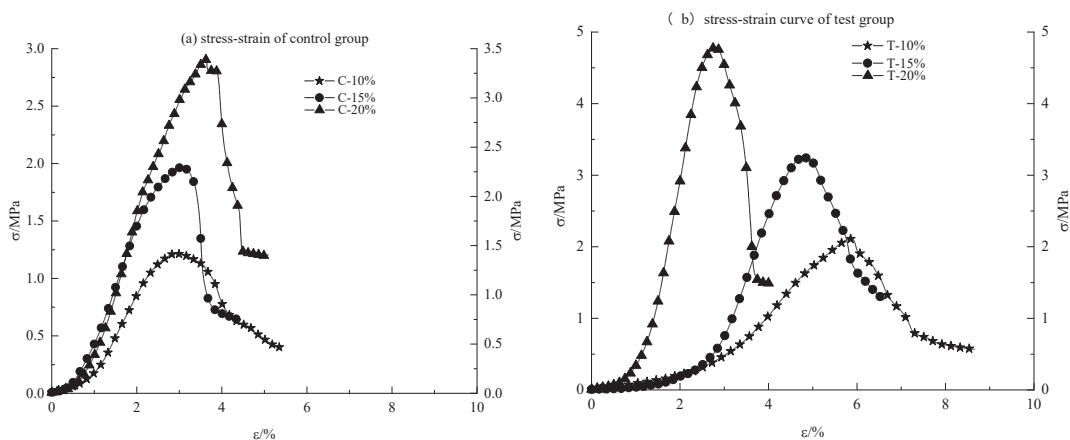
Fig. 3: Stress-strain curve of cement-soil corresponding to 28d age.

the curve becomes curved before the stress reaches the peak stress, accompanied by plastic deformation. When the stress peak is reached, the curve begins to fall and, the sample begins to break. From the comparison of (a) and (b), when the cement mixing ratio changes from small to large, the strain corresponding to the peak stress of the cement-soil of the control group tends to become larger. When the cement mixing ratios are 10%, 15% and 20%, the strains of ordinary cement-soils are 2.89%, 3.01% and 3.64%, respectively, while the strains corresponding to the peak stress of the cement-soil in the test group show a trend of decreasing, and the corresponding strains of cement-soil are 5.85%, 4.79%, 2.80%. It shows that the addition of cement can improve the toughness of the residual soil, and the MICP technology can further improve the toughness of the cement-soil in the condition that the cement content is not high.

Fig. 4 is the stress-strain curve of the two groups when the cement content is 15%. It can be seen from Fig. 4 (a) and (b) that the values of the UCS test of the two groups are related to the age of the curing. The strain corresponding to the peak stress of ordinary cement-soil in the control group is smaller than that in the test group, and the strains corresponding to the peak stress at the age of 7d, 14d and 28d are 3.13%, 3.16% and 3.07%, respectively. The strains corresponding to the peak stress of the test group were 4.06%, 3.77% and 4.79%, respectively. It shows that at the same curing age, MICP technology can improve the toughness of cement-soil. According to the strain values corresponding to the peak stress of the two groups, it can be found that the influence of curing age on the toughness of cement soil is smaller than the cement mixing ratio.

Deformation modulus: The stress-strain curve shows that the initial compaction phenomenon exists in the cement-soil samples, and stress-strain relationship increases approximately linearly. The elastic modulus (E) is an important parameter to reflect an object resisting the elastic deformation. It can be calculated according to the ratio of stress and strain in the elastic-strain curve of the stress-strain curve. The slope can be obtained through linear fitting the linear elastic stage of the stress-strain curve, which can be regarded as the elastic modulus. The calculation results are provided in Table 8.
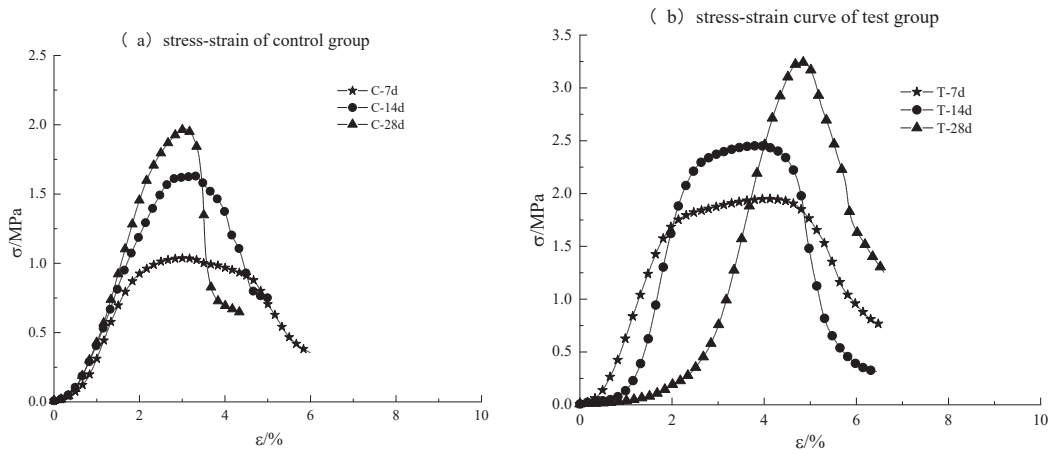
Fig. 4: Stress-strain curve of cemented-soil for cement mixing ratio of 15%.

Table 8: Elasticity modulus of cemented-soil samples.

			T/d		
			7	14	28
ε (%)	10	T-E/MPa	0.27	0.56	0.61
		C-E/MPa	0.21	0.48	0.55
	15	T-E/MPa	1.14	1.63	1.7
		C-E/MPa	0.69	0.75	0.99
	20	T-E/MPa	1.9	2.41	3.28
		C-E/MPa	0.84	1.1	1.37

Note: T-E represents elastic modulus of the test group, C-E represents elastic modulus of the control group

It can be seen from Fig. 5 that the elastic modulus (E) of the two groups increases with the increase of the curing age and the cement mixing ratio. The elastic modulus of the test group is significantly larger than that of the control group, and the samples are more likely to exhibit brittle fracture. It also can be seen from Fig. 5(a) and (b) that the difference between the elastic modulus becomes larger and larger with the cement mixing ratio increasing, while the effect in the control group is not obvious. When the cement mixing ratio is 15%, the elastic modulus of the test group is 3.22 times, 1.91 times, 1.79 times than the cement mixing ratio 10%, respectively. When the cement mixing ratio is 20%, the elastic modulus of the test group is 0.67 times, 0.48 times, 0.93 times than the cement mixing ratio 15%, respectively. When the cement mixing ratio is 15%, the elastic modulus of the control group is 2.29 times, 0.56 times, 0.8 times than that of the cement mixing ratio 10%, respectively. When the cement mixing ratio is 20%, the elastic modulus of the control group is 0.22 times, 0.47 times, 0.37 times than the cement mixing ratio 15%, respectively. According to the results in Table 7,

the elastic modulus of microbial enhanced cement soil is the largest compared with ordinary cement soil at 7d, while the overall growth rate at 14d is lower than that of the other two groups. The cement-soil with cement mixing ratio 20% has the largest elastic modulus (3.28MPa), which is 1.41 times than that of ordinary cement with the same mixing ratio.

CURING MECHANISM

Cement hydration process: The cement hydration is the coagulation and hardening of the cement. When the cement meets water, it produces gelling substances, which can cement the soil particles, thereby increasing the strength of the cement-soil. The addition of the microorganisms will affect the cement hardening process, and in general, it will develop in a direction that is conducive to increasing the strength of the cement soil.

Pozzolanic effect: The strong pozzolanic effect can increase the strength of the cement soil at various ages, and the free oxides in the granite residual soil such as SiO_2 and Al_2O_3

Table 7: Summary of measured UCS of the cemented-soil samples.

			T/d		
			7	14	28
ε (%)	10	T-UCS/MPa	0.82	1.03	1.4
		C-UCS/MPa	0.54	0.86	1.14
	15	T-UCS/MPa	1.95	2.45	3.24
		C-UCS/MPa	1.04	1.63	1.97
	20	T-UCS/MPa	2.8	3.71	4.78
		C-UCS/MPa	1.9	3.01	3.39

Note: T-UCS represents the values of UCS of the test group, C-UCS represents the values of UCS of the control group.
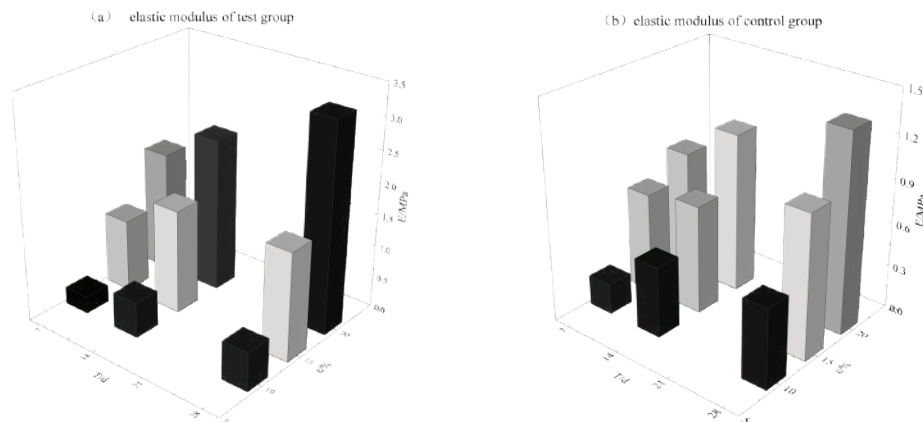
Fig. 5: Relationship between elastic modulus, age and cement mixing ratio for cemented-soil.
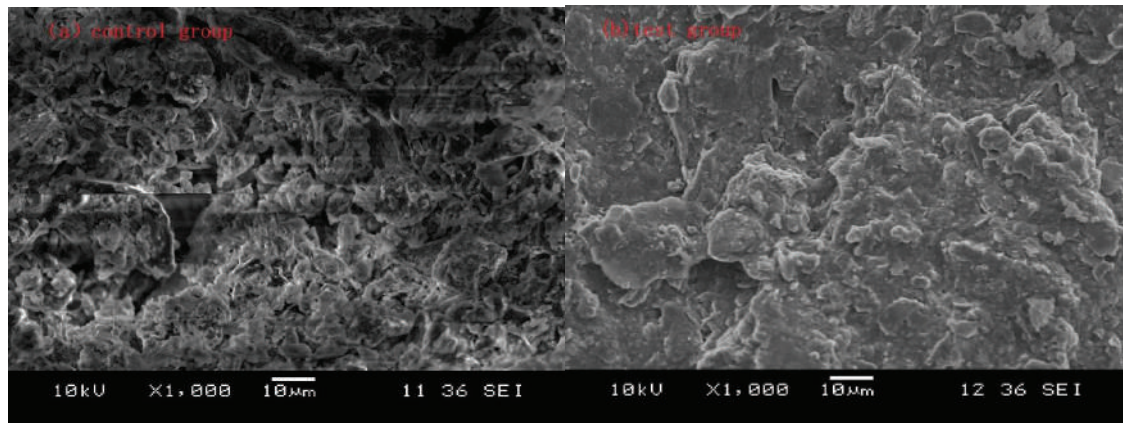
Fig. 6: SEM photographs of cemented-soil.

also have a pozzolanic effect, thereby further amplifying the reaction (Goldman & Bentur 1993, Hou et al. 2014).

Filling and cementation effect: Fig. 6 is a comparison of scanning electron microscopy (SEM) results between the test group and the control group when the cement mixing ratio is 15% and the curing age is 7 days. Comparing the figures (a) and (b), we can see that the surface of the cement-soil of the control group has many pores which are also large, while the surface of the cement-soil of the test group has very few pores at this magnification, and the surface is denser than the control group. (a) There are already gelatinous substances between the soil particles, however, some of the soil particles are not cemented, and the cement-soil is generally loose; (b) the soil particles are tightly cemented, and the cement-soil is generally denser. Calcium carbonate deposited by microorganisms has a cementation effect to further bond the soil particles, thereby increasing the strength of the cement soil.

CONCLUSION

MICP technology can effectively reinforce granite residual soil. Compared with ordinary cement-soil, the values of UCS of cement-soil with the added bacterial solution are greatly improved, and the maximum growth rate is 87.5%. Also, the UCS at the 14-day of the test group exceeded the unconfined compressive strength at the 28-day age of the control group.

The strain corresponding to the peak stress of the cement-soil treated by MICP is generally larger than that of ordinary cement-soil. The strain corresponding to the peak stress of the cement-soil decreases with the increase of the cement mixing ratio. However, the UCS of ordinary cement-soil increases with the increase of cement mixing ratio,

indicating that cement hydration will increase the toughness of residual soil, but microbes will change this direction of action. The experimental results of the two groups show that the effect of curing age on toughness is small.

The elastic modulus values of the two groups were obtained by fitting the line segments of the stress-strain curve. The results show that the MICP technology can increase the elastic modulus of the cement-soil compared with ordinary cement soil. The maximum growth rate is 141.18%.

The mechanism of MICP technology to treat cement soil is cement hardening, pozzolanic reaction and filling effect. Due to the fine soil of granite residual soil and small pores, it will limit the living space of microorganisms to a certain extent, so in the microbial-cement slurry-soil system, these effects interact and work together, so the curing mechanism is very complicated. The curing effect and mechanism of the fine-grained soil on the concentration of bacteria and water are to be further studied.

In this study, the MICP technology was successfully applied to the reinforcement of granite residual soil, which proved that the strength characteristics of cemented-soil treated by MICP technology were significantly enhanced. In the future, the effects of factors such as bacterial liquid concentration, calcium salt types and water content on the strength characteristics of cemented-soil will be studied.

ACKNOWLEDGEMENT

REFERENCES

Chen, Z. J. 2007. The engineering characteristics of granite residual soil and analysis of the cut slope stability in Shantou City. Geology and Mineral Resources of South China, 2.

Chu, J., Stabnikov, V. and Ivanov, V. 2012. Microbially induced calcium carbonate precipitation on surface or in the bulk of soil. Geomicrobiology Journal, 29(6): 544-549.

Dick, J., De Windt, W., De Graef, B., Saveyn, H., Van der Meeren, P., De Belie, N. and Verstraete, W. 2006. Bio-deposition of a calcium carbonate layer on degraded limestone by bacillus species. Biodegradation, 17(4): 357-367.

Fang, X.W., Shen, C.N., Chu, J., Wu, S.F. and Li, Y. S. 2015. An experimental study of coral sand enhanced through microbially-induced precipitation of calcium carbonate. Yantu Lixue/Rock and Soil Mechanics, 36(10): 2773-2779.

Goldman, A. and Bentur, A. 1993. The influence of microfillers on enhancement of concrete strength. Cement and Concrete Research, 23(4): 962-972.

Hou, P., Qian, J., Cheng, X. and Sha, S. P. 2014. Effects of the pozzolanic reactivity of nano SiO_2 on cement-based materials. Cement and Concrete Composites, 55.

Huang, M., Zhang, J., Jin, G., Jiang, Y., Qiu, J., Gong, H. and Guo, S. 2018. Magnetic resonance image experiments on the damage feature of microbial induced calcite precipitated residual soil during freezing-thawing cycles. MICP. Yanshilixue Yu Gongcheng Xuebao/Chinese Journal of Rock Mechanics and Engineering, 37(12): 2846-55.

Ivanov, V. and Chu, J. 2008. Applications of microorganisms to geotechnical engineering for bioclogging and biocementation of soil in situ. Reviews in Environmental Science & Biotechnology, 7(2): 139-153.

Jia, Q., Zhang, X. and Jiang, H. 2016. Experiment research on microbial induced clogging in soil by bacterially induced calcium carbonate deposition. Sichuan Building Science, 42(1): 93-95.

Karol, R.H. 2003. Chemical Grouting and Soil Stabilization, Revised and Expand. CRC Press, Boca Raton.

Liang, S. H., Fang, C. X., Niu, J. G. and Zeng, W. H. 2019. Research on effect of microbial induced calcite precipitation adopting different calcium sources on cement granite residual soil. Industrial Construction, 49(7): 102-107.

Liang, S. H., Zhou, S. Z., Zhang, L. and Wang, M. 2015. Statistical analysis of physical and mechanical indexes of granite residual soil in eastern Guangzhou. Journal of Guangdong University of Technology, 18(1): 29-33.

Lin, P., Chen, H. M. and Wang, Y. Q. 2011. Behavior of the unsaturated granite residual soil and its effects on earth dam project. Geotechnical Special Publications (GSP), 217: 68-75.

Liu, S., Chen, Z. B., Chen, W. W. and Wei, Y. 2018. Experience study on granite residual soil improved by fly ash. Journal of Fuzhou University (Natural Science Edition), 46(5): 115-120.

Mukherjee, A., Dhami, N. K., Reddy, B. V. V. and Sudhakara Reddy, M. 2013. Bacterial calcification for enhancing performance of low embodied energy soil-cement bricks. 3rd International Conference on Sustainable Construction Materials and Technologies, Kyoto, Japan.

Peng, J., Wen, Z.L., Liu, Z.M., Sun, Y.C., Feng, Q.P. and He, J. 2019. Experimental research on MICP-treated organic clay. Yantu Gongcheng Xuebao/Chinese Journal of Geotechnical Engineering, 41(4): 733-740.

Van, L. A., Ghose, R., Van-der-Linden, T.J.M. and Van-der-Star, W.R.L. 2010. Quantifying bio-mediated ground improvement by ureolysis:a large scale biogrout experiment. Journal of Geotechnical & Geoenvironmental Engineering, 136(12): 1721-1728.

Wang, W.J., Zhu, X.R. and Fang, P.F. 2005. Analysis on reinforcement mechanism of nanometer silica fume reinforced cemented clay. Zhejiang Daxue Xuebao (Gongxue Ban)/Journal of Zhejiang University (Engineering Science), 39(1): 148-153.

Whiffin, V. S., van Paassen, L. A. and Harkes, M.P. 2007. Microbial carbonate precipitation as a soil improvement technique. Geomicrobiology Journal, 24(5): 417-423.

Drinking Water Quality Assessment and Predictive Mapping: Impact of Kota Stone Mining in Ramganjmandi Tehsil, Rajasthan, India

Arushi Rana† and Rashmi Sharma

School of Earth Sciences, Banasthali Vidyapith, Niwai, Tonk, Rajasthan-304 022, India

†Corresponding author: Arushi Rana; aarushi.rana.1992@gmail.com

ABSTRACT

Rajasthan generates 1055 million litres per day as wastewater, out of which 27 million litres is treated and nearly 1028 million litres untreated wastewater is discharged in various water resources. The present study is based on the impact of Kota stone or limestone mining on water resources. Among those villages and census towns, experiencing mining activity, a total of 26 surface water and groundwater samples were tested and analysed. Mining waste often creates eutrophication, toxification, temporary hardness and sometimes permanent hardness. The mining belt was 17.54 km² in the year 2000 which further increased to 24.25 km² in the year 2018. The parameters analysed were pH, EC, TDS, alkalinity, total hardness, calcium and magnesium hardness, DO, COD, chloride, sodium and potassium. The predictive mapping for the mining belt was executed in Arc GIS software using Inverse Distance Weightage (IDW) method. The mean of pH was 9.13, TDS 457.12 mg/L, total hardness 593.52 mg/L, calcium hardness is 205.54 mg/L, magnesium hardness 387.53 mg/L, COD 442.2 mg/L, Na⁺ 139.9 mg/L, K⁺ 19.40 mg/L, Cl⁻ 318.29, DO 3.04mg/L and alkalinity 14.02 mg/L.

INTRODUCTION

Karr (1986) gave five principal factors which comprise the integrity of surface water. The factors are flow and hydrology focussing on land use, velocity, high and low extremes of flow, precipitation, groundwater recharge and discharge. The second factor is habitat and structure focussing on vegetation, siltation, sinuosity, current, instream cover, gradient, channel morphology and bank stability. The third factor is energy source including nutrients, sunlight, seasonal cycles, organic matter and productivity. The fourth factor is biotic parameters including disease predation, competition and parasitism. The last factor is chemical parameters like solubility, adsorption, alkalinity, temperature, dissolved oxygen, pH, turbidity, hardness, organics, nutrients and toxins (Novotny 2003). By 2025, it is expected that water withdrawals will increase by 50% in the developed countries and 18% in developing countries (UNEP 2013). Even if we study the past statistics, the same phenomenon can be seen, in the year 2001 a $4 million study of 175 scientists from around the globe sponsored by United Nations summarized few issues such as half of the world's wetlands have been drained destroying their habitats; except for Russia and Canada, all the industrial nations have cleared their natural forests; agricultural land nearly 40% has been degraded due to erosion, natural depletion and water stress (Novotny 2003). World water development report by the United Nations in the year 2019

states India in the category of the nations facing 25 to 70% physical water stress. Nearly 780000 deaths occurred due to inadequate water and sanitation services all over the world in the year 2018. The waterborne diseases remain a significant disease burden among vulnerable and disadvantaged group worldwide, especially among low-income economies, 4% of the population estimated about 25.5 million, suffered from diarrhoea in 2015, among which 60% were under the age of 5 years (UNESCO 2019).

Hydrochemical analysis is of great significance to the sustainable management of water resource utilization, protection of the ecological environment. Zhang et al. (2019) worked on the surface hydrochemistry of Syr Darya River in Kazakhstan at 39 locations and analysed regional hydrochemical characteristics and evaluated irrigational suitability of the regions. The cations studied were Na⁺, Ca²⁺, and Mg²⁺ and anions studied were SO₄²⁻ and Cl⁻. The main hydrochemical type was Ca-Mg-SO₄-Cl⁻.

The pH value of the study ranges from 7.95 to 9.31 and the mean value of dissolved oxygen is 8.96. the salinity of the surface water varied from 342 mg/L to 4014 mg/L. 94.87% of samples were above the limit of 500 mg/L (Zhang et al. 2019). Groundwater aquifers were studied in Regina, Canadian prairies. A total of 14 parameters were selected including eight trace metals: arsenic (As), calcium (Ca), magnesium (Mg), manganese (Mn), potassium (K), sodium (Na), and

uranium (U), as well as seven anionic species and groundwater parameters: bicarbonate (HCO_3^-), chloride (Cl^-), sulphate (SO_4^{2-}), total dissolved solids (TDS), total hardness (TH), pH and electrical conductivity (EC). A strong correlation is seen between sulphate and calcium, sodium and chloride, and sulphate and magnesium. Calcium and magnesium were also strongly correlated. 63.2 % of the samples fall in the doubtful to unsuitable and unsuitable according to Wilcox Diagram (Pan et al. 2019).

Soleimani et al. (2018) worked the groundwater quality for drinking and irrigational purpose in a rural area of Sarpol-e-Zahab city, Kermanshah province in Iran. Thirty samples were analysed for EC, TDS, TH, Na^+, Mg^{2+}, Ca^{2+}, Cl^- and SO_4^{2-} ionic constituents. Water quality has been assessed according to the United States Department for Agriculture.

Every 2-year monitoring says that the water quality for agriculture lies in the good or excellent category. Spearman's Correlation analysis and factor analysis displays a good correlation between physio-chemical parameters.

The greed to look good, live good and portray good, often leave the natural environment in a dilemma as if it is just for one particular species. Humans are both the polluters and sufferers of environmental damage. It is the relationship between human and environment, which when becomes imbalanced, affects not only humans but also innumerable species existing in the environment. Environmental monitoring helps decision making for both the government and non-governmental organisations.

Ramganjmandi is a tehsil of the district of Kota in the state of Rajasthan, in which lies the Ramganjmandi city (Fig. 1). It is known as a stone city and coriander city. It is 73 km away towards the south of Kota on the Delhi Mumbai broad gauge railway line. The major minerals mined here are limestone or building stone (52 units), sandstone (2 units), and masonry stone (9 units) and stone gravels (Department of Mines and Geology 2014).

The area of Ramganjmandi and the undergoing most important activity of Kota stone and sandstone mining needs specific attention. Monitoring any industrial activity is the first step before finding any solution. The sustainability of any activity should be the key focus before even executing them. The area which is now a dump of a scrap of limestone has not lived in a preferable environment. The heaps of scrap contributing to land degradation; the slurry on soil affecting the soil quality; the continuous grinding; extraction of mineral making the air polluted; the dumpage of waste in the surface water and long term impact on groundwater; health
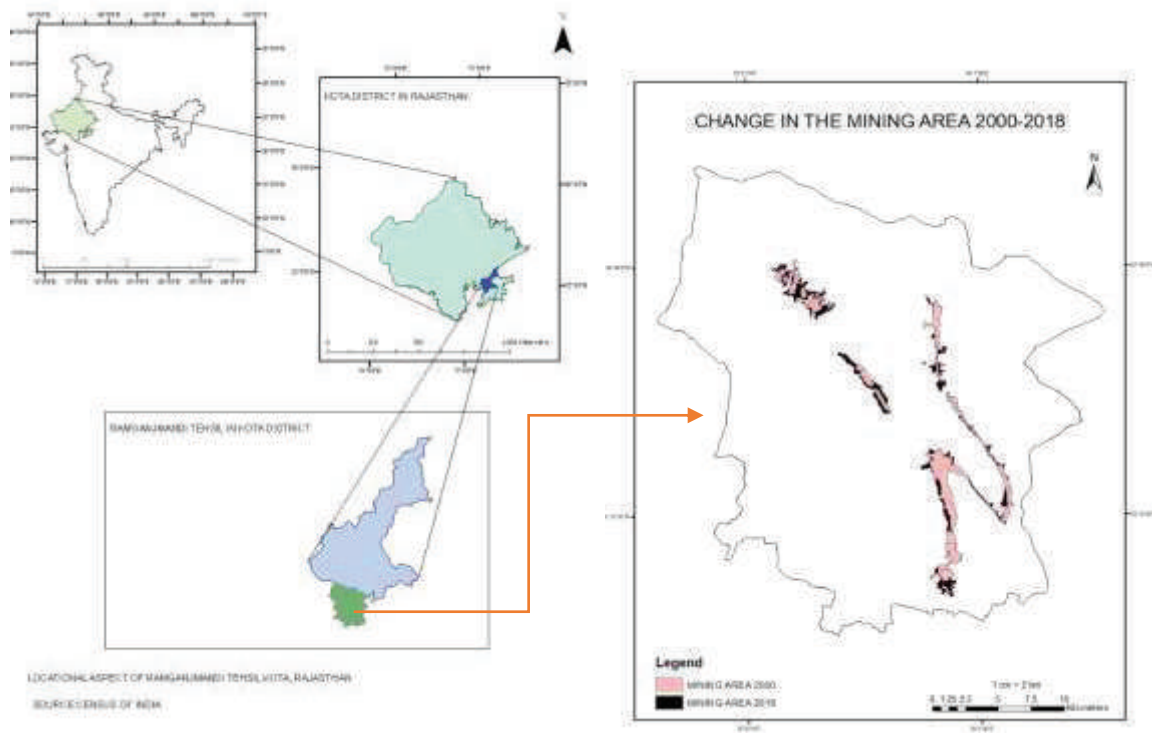
Fig. 1: Location of Ramganjmandi tehsil.

dilapidation because of the combined effect of ecosystem imbalance are sufficient reasons to make this research problem significant. Ramganjmandi once famous for coriander cultivation is now famous for mines, extraction, poor air quality, water unfit for drinking, loss of agricultural land, deforestation and massive solid waste disposal.

MATERIALS AND METHODS

Study Area

The latitudinal extension of Ramganjmandi is 24°08'00" N to 24°11'10" N and the longitudinal extension is 75°13'04" E to 76°01'57" E. Its location is shown in Fig.1. The town is situated on the southwestern portion of Hadoti plateau at an altitude of 357.43 meters above mean sea level. The slope is south to the south-east in direction. The soil is black with some deposits of limestone. The mining belt extended in Kumbhkot, Julmi, Suket, Khemaj, Udupura, Chechat and Kamalpura region. The mining region in the area was 17.548 km^2, which now extended to 24.205 km^2. The mining area expanded by 6.657 km^2.

Water Quality Assessment

Twenty six water samples (Fig. 2) have been taken from 24.250 km^2 area of the mining belt. GPS location was taken along with Juno Trimble. The samples were taken in dark coloured, distilled water-washed bottles. The dissolved oxygen was fixed onsite. pH, electrical conductivity, total dissolved solids and temperature were measured using multi-parameter PC5 TEST R 35 series kit. The sensor was thoroughly washed with distilled water before immersing in the sample. Dissolved oxygen was checked by azide modification Winkler's method. COD was determined with the help of COD reflux apparatus, wherein the wastewater was oxidized completely with potassium dichromate. Alkalinity was estimated by titrating with standard sulphuric acid. Sodium and potassium were determined with the help of flame photometer. Hardness was determined by titrating with standard EDTA reagent. Chloride was measured by Mohr titration method (APHA 1995).

Spatial Interpolation

Interpolation is the process of predicting unknown values for the non-sampled locations from the known values of sampled locations. Most attempts at spatial predictions are mathematical, based on the geometry and also some attention to the physical nature of the phenomenon (Webster & Oliver 2007). A static model for water quality has been created for the concerned region with the help of inverse distance weightage method. A shapefile of 26 sampled sites was created as point file in Arc
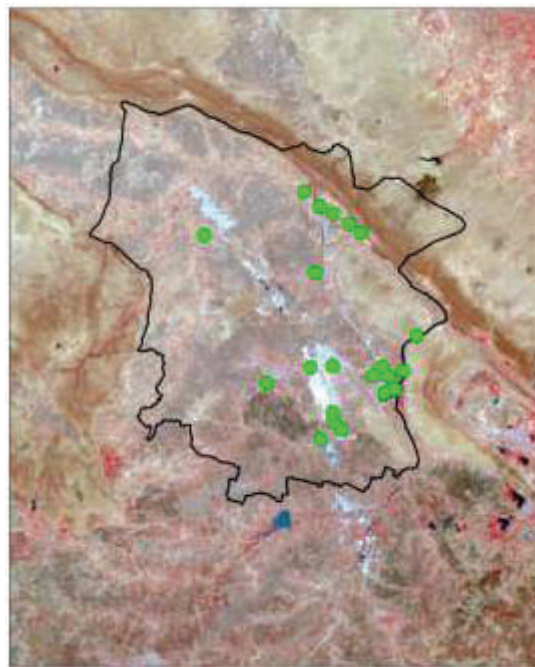
Fig. 2: Sample sites for water collection.

GIS. The attribute table was created for the 14 parameters. Inverse distance weightage method in Geostatistical Analyst tool was used for interpolation. The details are represented as a raster.

RESULTS AND DISCUSSION

The water quality with minimum and maximum values is given in Table 1. The correlational matrix as developed according to Karl Pearson's coefficient of correlation shows a high degree of positive correlation (Table 2) between TH-alkalinity (r=0.60), magnesium hardness and alkalinity (r=0.58), chloride-alkalinity (r=0.60), EC-TDS (r=0.88), COD-pH (r=0.55), TH-chloride (0.99), calcium hardness-TH

(r=0.78), magnesium hardness-chloride (0.98), magnesium hardness-calcium hardness (r=0.75) and calcium hardness and chloride (r=0.79).

The predictive mapping of water quality parameters-inverse distance weightage interpolation is shown in Figs. 3-14.

pH: The region shows pH values ranging from 6 to 10.9 (Fig. 3). Low pH values are depicted in the southern part of the tehsil in Suket and Kumbhkot regions. The pH values must range between 6.5 and 8.5 as per BIS standards (Soleimani et al. 2018). Beyond this, the water will affect the mucous membrane and water supply systems. WHO guideline for pH is 8.5.

Table 1: Water quality parameters and statistical representation.

Parameters	Minimum	Maximum	St. Deviation	Median	Mean
EC (μS)	367	939	140.1	692.3	675.29
TDS (mg/L)	261	666	87.212	450	457.12
Temperature (°C)	29	33.4	1.085	31.2	31.04
Total hardness (mg/L)	128	2740	755.46	275	593.52
Calcium hardness (mg/L)	58.8	588	148.54	187.5	205.54
Magnesium hardness (mg/L)	56	2183.5	619.23	143.6	387.53
COD (mg/L)	96	698	201.76	450	442.2
DO (mg/L)	1.8	5.8	0.865	3.7	3.04
Na (mg/L)	32.6	570	165.11	61	139.9
K (mg/L)	1.18	86.3	27.769	5.1	19.403
Chloride (mg/L)	57	1593.2	447.16	110	318.29
Alkalinity (mg/L)	8	20	3.35	14	14.02
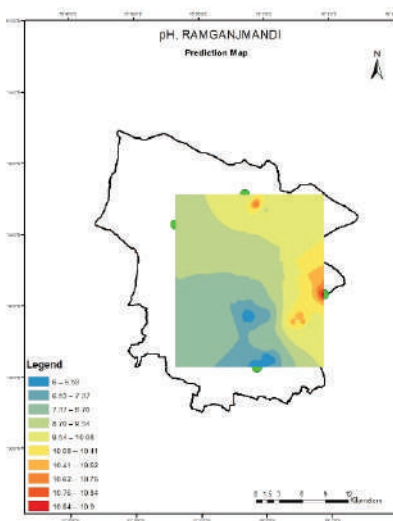
Fig. 3: pH
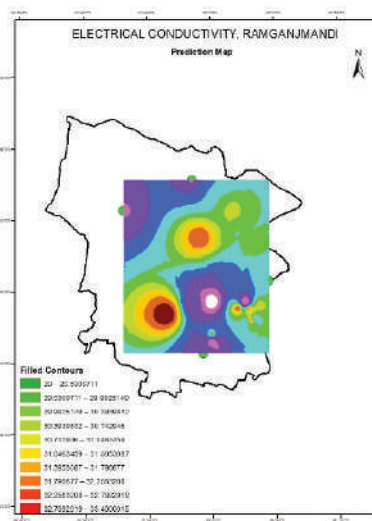
Fig. 4: Electrical Conductivity
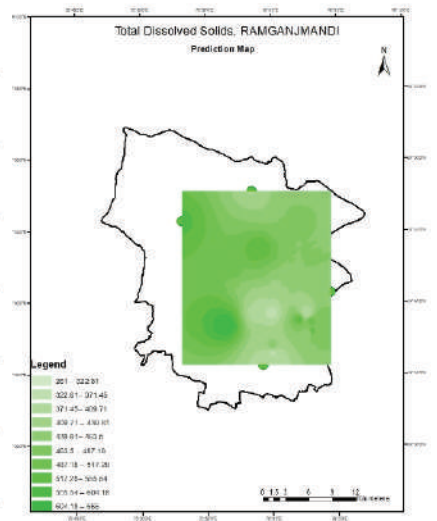
Fig. 5: Total disslved solids

Table 2: Correlational matrix of water quality parameters.

	Temp	pH	TDS	Alkalinity	TH	Mg hardness	Chloride	COD	EC	Ca hardness	DO
Temperature	1										
pH	0.49	1.00									
TDS	0.18	0.33	1.00								
Alkalinity	-0.32	-0.50	-0.41	1.00							
TH	-0.44	-0.84	-0.46	0.60	1						
Mg Hardness	-0.44	-0.82	-0.48	0.58	1.00	1					
Chloride	-0.48	-0.87	-0.48	0.60	0.99	0.98	1				
COD	0.20	0.55	0.29	-0.20	-0.44	-0.44	-0.48	1			
EC	0.24	0.35	0.88	-0.22	-0.43	-0.46	-0.45	0.44	1		
Ca Hardness	-0.25	-0.71	-0.19	0.51	0.78	0.75	0.79	-0.32	-0.05	1	
DO	0.35	0.43	-0.12	-0.08	-0.24	-0.21	-0.30	-0.05	-0.18	-0.37	1

Electrical conductivity: The values of EC range from 367 to 939 µS (Fig. 4). The mean value is 675.29 µS and standard variation is 140.1 µS depicting a high variability (Table 1). Most of the samples lie in the excellent, good and permissible category of agricultural suitability (Richards 1954). Wherein, 79.8 % of samples lie in the permissible category and rest lie under the good and excellent category.

Total dissolved solids: The values of TDS vary from 261 to 666 mg/L (Fig. 5). High TDS concentration lies in the southeastern region. The TDS values above 500 mg/L are unacceptable according to BIS standards, beyond this the palatability decreases and water may cause gastrointestinal irritation. 25% of the samples lie under the unsuitable category of drinking water. The mean value is 457.12 mg/L (Table 1). WHO reports on TDS and health in areas surveyed like Australia and the Soviet Union indicate that the high TDS causes inflammation of gallbladder and stones increased over a period of 5 years. High TDS level often results in scaling of water pipes, water heaters, boilers, household equipment like kettles as it increases the corrosive ability of the water.

COD: Chemical Oxygen demand is the amount of oxygen required for oxidation of most organic matter and oxidizable inorganic substances with the help of a strong chemical oxidant. The higher the COD, more is the water organically polluted. The COD content for the region varies from 96 to 698 mg/L. The mean value of COD is 442.2 mg/L (Table 1). The IDW interpolated sites show water with a high value of COD in the southeastern section, wherein River Aru flows
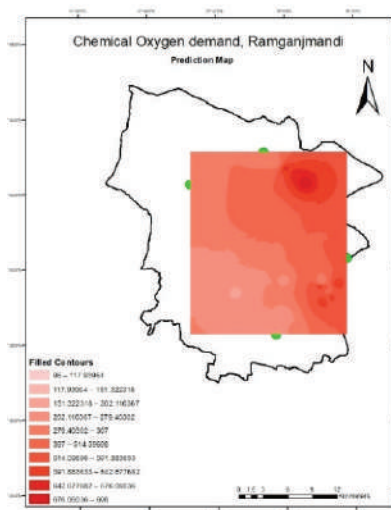
Fig. 6: Chemical Oxygen Demand
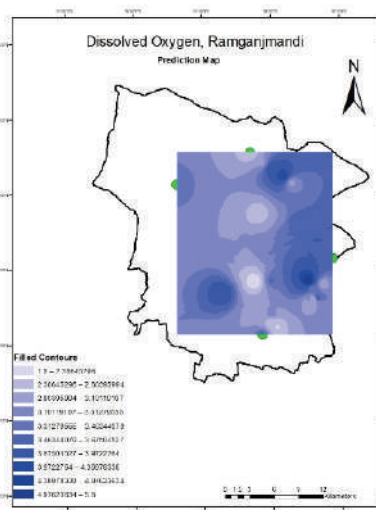
Fig. 7: Dissolved Oxygen
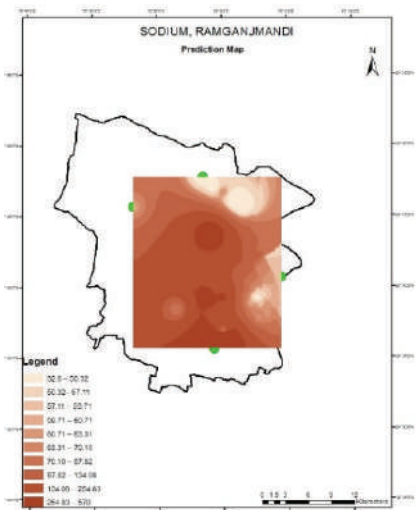
Fig. 8: Sodium

on the boundary of the Tehsil between Kota and Jhalawar districts of Rajasthan (Fig. 6). The river shows high COD content which is indicative of dumpage of inorganic waste from the mining industry.

Dissolved oxygen: The dissolved oxygen in the region varies from 1.8 to 5.8 mg/L and the mean value is 3.04 mg/L (Table 1). The standard deviation of DO is 0.865 showing less variability. For class A streams, 6 mg/L is required (CPCB 1979). A level of 5-8 mg/L is suitable for healthy fish growth. The DO concentration is minimum in the pre-monsoon period due to high temperature (Fig. 7).

Sodium: Sodium is ubiquitous in water. A taste threshold value of 30 to 60 mg/L is accepted by US EPA. BIS standards state 200 mg/L as sodium concentration limit. The sodium concentration in the Tehsil has a maximum value of 570 mg/L in the southern part and the minimum value of 36 mg/L (Table 1). The standard deviation is high as 165.11, showing a higher degree of variability in the sampled sites (Fig. 8). The river water shows appropriate sodium concentration throughout its flow. High Na in the water in the form of chloride and sulphate makes the water unfit for consumption. High Na concentration also leads to hypertension (Maiti 2011). Increased intake of sodium content is detrimental to people suffering from hypertension, heart diseases and kidney problems (Kundu & Nag 2018).

Potassium: The potassium concentration varies from 1.18 to 86.3 mg/L. The sampled sites show a higher degree of variability with a standard deviation of 27.76 (Table 1). The mean value is 19.40 mg/L (Fig. 9). The southern part shows a higher potassium concentration.

Total hardness: The water of the region turns out to be hard(-Fig. 10). The values range from 140 to 2740 mg/L (Table 1). BIS standards for TH is 200 mg/L and relaxation is till 600 mg/L in case of absence of an alternative source. Low hardness is seen in the upper course of the River Aru wherein it flows through the reserved forest. 92.3% of the samples are unfit for drinking as per BIS standards. Since the region has limestone-based geology, the hardness increases in such cases. All the samples lie in the hard to very hard category.

Calcium hardness: The calcium concentration should be 75 mg/L or may extend to 200 mg/L in case of absence of an alternative source. The calcium hardness in the region varies from 58.8 to 588 mg/L (Table 1). 92.3% of the samples are unfit for drinking purpose.

Magnesium hardness: The required limit for magnesium hardness is 30 mg/L and the tolerance limit is 100 mg/L. The region has a maximum of 2183.5 mg/L and a minimum of 56 mg/L (Table 1). The region shows high variability in the magnesium hardness. The southern part shows a higher magnesium concentration (Fig. 12).

Alkalinity: It is measured as the buffering capacity of bases to neutralize acids. It depicts the capability of water to resist change in pH. The alkalinity in the region varies from 8 to 20 mg/L (Fig. 13). Alkalinity in itself is not harmful to human beings but water supply with less than 100 mg/L is desirable. At higher levels, alkalinity imparts a bitter taste to the water.

Chloride: The chloride level should be less than 200 mg/L as per WHO standards. 30.76% of the sampled sites exceed this criterion. The maximum value of chloride is 1593.24 mg/L and the minimum value is 57 mg/L (Fig. 14).
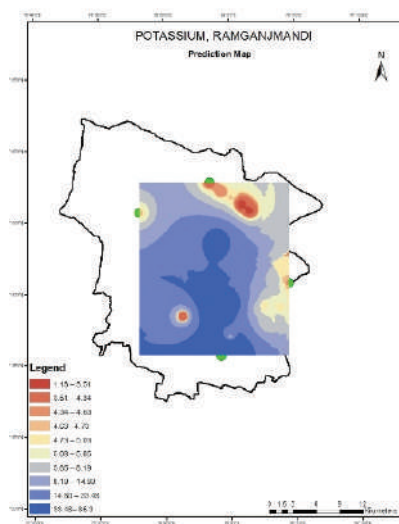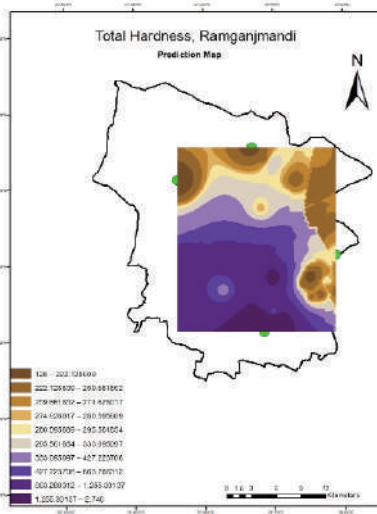

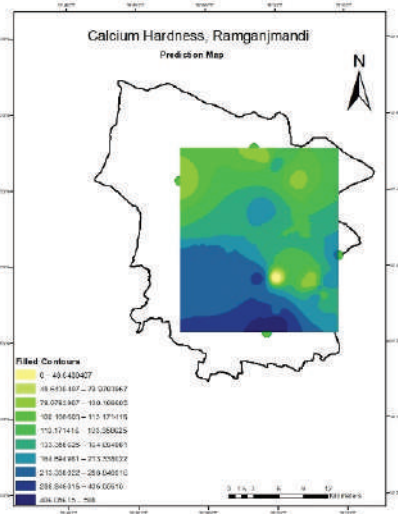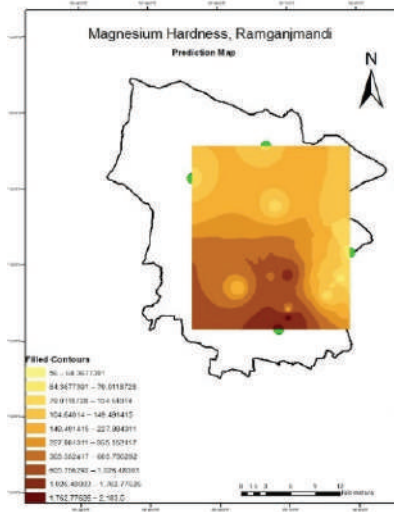Fig. 9: Potassium　　　　Fig. 10: Total Hardness　　　　Fig. 11: Calcium Hardness
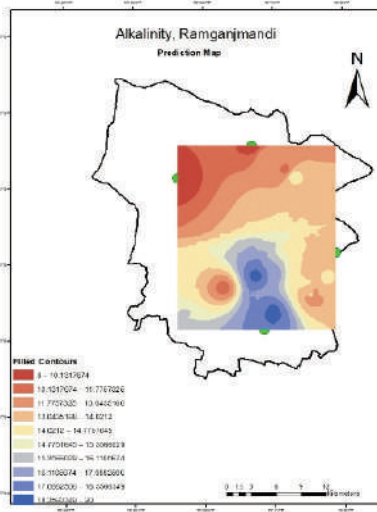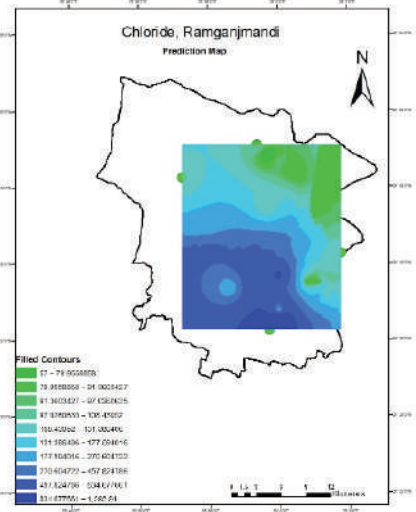
Fig. 12: Magesium Hardness

Fig. 13: Alkalinity

Fig: 14: Chloride

CONCLUSION

The study depicts a high degree of correlation between the TH-alkalinity, magnesium-alkalinity, chloride-alkalinity, EC-TDS, COD-pH, TH-chloride, calcium-TH, magnesium-chloride, magnesium-calcium and calcium-chloride. Such type of correlation can be attributed to limestone-based geology in case of groundwater and limestone mining in case of surface water. The alkalinity levels in the region seem to be under control. The chloride level is considerably high in the Kumbhkot region. In terms of hardness, most of the samples are unfit for drinking purpose. The level of dissolved oxygen is adequate among all the samples. Water seems to be alkaline as per the pH values of the samples. Sodium and potassium levels are under the prescribed limit, but in the southern part of the tehsil, it is as high as 560 mg/L. High COD levels are seen in the water samples of Aru river, indicating mining waste disposal in the river.

ACKNOWLEDGEMENT

REFERENCES

APHA 1995. Standard Methods For The Examination of Water and Wastewater. American Public Health Association, Washington DC.

CPCB 1979. Surface Water Quality Criteria for Different Uses. Central Pollution Control Board, New Delhi.

Department of Mines and Geology 2014. Minor minerals, production, income and number of labours. Ramganjmandi, Kota, Rajasthan.

Karr, J.R. 1986. Assessing Biological integrity in running waters a method and its rationale. Special Publication/Illinois Natural History Survey, USA, 5: 2-22.

Kundu, A. and Nag, S.K. 2018. Assessment of ground water quality in Kashipur block, Purulia District, West Bengal. Applied Water Sciences, 40(1): 33-51.

Maiti, S.K. 2011. Handbook of Methods in Environmental Studies: Air, Noise, Soil and Overburden Analysis. Oxford Book Company, Jaipur.

Novotny, V. 2003. Water Quality: Diffuse Pollution and Watershed Management. John Wiley & Sons, New Jersey.

Oliver, M.A. and Webster, R. 2007. Geostatistics For Environmental Scientists. John Wiley & Sons, West Sussex, England.

Pan, C., Ng, K.T.W. and Richter, A. 2019. An integrated multivariate statistical approach for the evaluation of spatial variations in groundwater quality near an unlined landfill. Environmental Science and Pollution Research, 26(6): 5724-5737.

Richards, L. 1954. Diagnosis and Improvement of Saline and Alkali Soils. Agriculture Handbook. United States Salinity Laboratory, USDA, Washington.

Soleimani, H., Abbasnia, A., Yousefi, M., Mohammadi, A.A. and Khorasgani, F.C. 2018. Data on assessment of groundwater quality for drinking and irrigation in rural area Sarpol-E Zahab City, Kermanshah Province Iran. Data in Brief,17(1): 148-156. doi:10.1016/j.dib.2017.12.061

UNEP 2013. A Snapshot on World Water Quality Towards A Global Assessment. Nairobi, Kenya.

UNESCO 2019. United Nations World Water Development Report Leaving No One Behind. Paris, France.

Webster, R. and Oliver, M.A. 2007. Geostatistics for Environmental Scientists. John Wiley & Sons.

Zhang, W., Ma, L., Abuduwaili, J., Ge, Y., Issanova, G. and Saparov, G. 2019. Hydrochemical Characteristics and irrigational suitability of surface water in the Syr Darya river Kazakhstan. Environ. Monit. Assess.,191(9): 572.

Efficient Adsorptive Performance of Medical Stone Decorated by Carbon Dots

Baolong Zhao*, Leilei Hu*, Hengjia Kang* and Zhihong Zheng*(**)†

*School of Environmental and Municipal Engineering, North China University of Water Resources and Electric Power, Zhengzhou 450011, China

**Henan Vocational College of Water Conservancy and Environment, Zhengzhou 450008, China

†Corresponding author: Zhihong Zheng; zzh@ncwu.edu.cn

ABSTRACT

Carbon dots could significantly change the property of a normal material and have received wide attention in the recent decade. In this research, glucose as a carbon source, carbon dots decorated medical stone (CD-MS) was successfully synthesized for efficient adsorptive removal of organic pollutants. Pyrolytic temperature and glucose concentration for the adsorbent preparation were proved to have a significant impact on the adsorptive performance. The optimal pyrolytic temperature and glucose concentration were found to be 300°C and 0.5 M, yielding the optimized adsorbent 0.5CD-MS-300 superior to other carbon dots decorated MS. Surface morphology analysis demonstrated that the carbon dots were successfully immobilized on the surface of MS while the atomic ratio of C increased from 2.6% of the raw MS to 11.25% of the 0.5CD-MS-300. Three organic pollutants including p-nitrophenol, orange II and methylene blue with different charge properties were employed to explore the adsorptive performance of the 0.5CD-MS-300. The results indicated that the surface of 0.5CD-MS-300 was negatively charged while carbon dots had significantly improved the adsorption capability of the raw MS. As such, the resulting adsorbent 0.5CD-MS-300 can be considered as a powerful adsorbent for the removal of some organic contaminants from wastewater.

INTRODUCTION

With the development of industry and agriculture, a large number of organic contaminants, such as dyes, endocrine-disruptors, and pharmaceutical and personal care products, have come into the natural environment along with the discharge of effluents (Westerhoff et al. 2005, Crini 2006). These organic pollutants existing in wastewater can cause a severe hazard to human and animal health due to the delivery of the food chain. To date, there are many treatment technologies, including coagulation, sonocatalytic degradation, photocatalytic degradation and adsorption, to be applied to the removal of the organic pollutants (Polubesova et al. 2006, Li et al. 2014, Mahata et al. 2007, Zhang et al. 2006). Among these technologies, the adsorption process is considered as a promising and reliable method due to its ease of operation, low energy consumption, low cost and high efficiency (Qu 2008).

Medical stone (MS) is one kind of natural silicate mineral without toxicity. Its main mineral components include $Na(AlSi_3O_8)$, $Na(AlO_2)(SiO_2)_3$, $K(AlSi_3O_8)$, $K(AlO_2)(SiO_2)_3$, $Ca(Al_2Si_2O_8)$ and $Mg(Al_2Si_2O_8)$ (Gao et al. 2011). MS has a tetrahedron structure of $[SiO_4]^{2-}$ bonding to metal ions (such as K, Na, Ca, Mg, Cu and Al, etc.), contributing to the formation of a large internal surface area (Gao et al. 2012). Therefore, a series of excellent performances for MS

are expected, such as biological activity, the ability of dissolving and adsorbing and adjusting pH capacity. Meanwhile, it is widely used for food preservation, water purification and medical care. In recent years, MS had been studied as an adsorbent material, which achieved remarkable advances on the adsorption of heavy metals in wastewater (Gao et al. 2011, Zhou et al. 2015). Even though, to our best knowledge, there have been few reports about the adsorption removal of organic contaminants.

Carbon dots are novel carbon-based nanomaterial. They contain abundant oxygen-containing functional groups (-OH, -COOH and -C=O) on the surfaces, with good solubilities and optical properties. As such, carbon dots are widely implemented for bioimaging, chemical sensors, and photovoltaic devices, etc. (Ding et al. 2014, Shen et al. 2012). In recent years, CDs have been considered an ideal candidate material for organic or inorganic pollutants removal due to their rich functional groups, ease of preparation and low toxicity (Hsu & Chang 2012). However, some significant disadvantages of CDs based adsorbent focused on the dissolution of CDs as well as difficulties of separation and regeneration (Liu et al. 2017). Consequently, it is a necessity of combining CDs with other constituents to synthesize CDs-functionalized adsorbents.

In this research, we prepared the carbon-dots decorated medical stone (CD-MS) for the efficient adsorption of organic pollutants. Glucose, with numerous hydroxy groups and formyl groups, was chosen as the precursor of CDs and can provide more active adsorption sites on the surfaces of the MS (Hsu & Chang 2012). The effects of pyrolytic temperature and glucose concentration for the adsorbent preparation were emphatically studied. At the same time, p-nitrophenol (PNP), orange II (ORII) and methylene blue (MB) with different charge properties in a neutral aqueous solution were selected as target organic pollutants to investigate the adsorptive performance and adsorption capacity of the CD-MS.

MATERIALS AND METHODS

Chemicals: Orange II (ORII) (mass fraction > 95%) was purchased from Beijing Chemical Reagents Company. Methylene blue (MB) (mass fraction > 98.5%, chemical pure) was purchased from Tianjin Chemical Reagent Research Institute. P-nitrophenol (PNP) used was of analytical grade

and provided by Tianjin Guangfu Fine Chemical Research Institute, China. Other chemicals were of analytical grade and used without further purification. Deionized (DI) water was used throughout the research. The molecular structures of ORII, MB and PNP are shown in Fig. 1.

Adsorbent preparation: The natural medical stone (MS) was obtained from the Hunan Province of China. It was shattered with a multi-function pulveriser and subsequently sieved to a particle size between those of 80-mesh screens and 100-mesh screens. Firstly, 10 g of the powdered MS was immersed to 200 mL of 0.5 M or 0.05 M glucose solution and the mixture was shaken at a speed of 120 rpm for 12 h. Then, the resulting samples were rinsed with DI water for five times and oven-dried overnight at 80°C. The prepared carbon dots decorated medical stone (CD-MS) are denoted as 0.5CD-MS and 0.05CD-MS in the following studies.

Desired amounts of MS, 0.5CD-MS and 0.05CD-MS were tightly placed in a ceramic crucible with a lid and pyrolyzed in a muffle furnace under oxygen-limited conditions. The pyrolysis temperature was raised to the desired
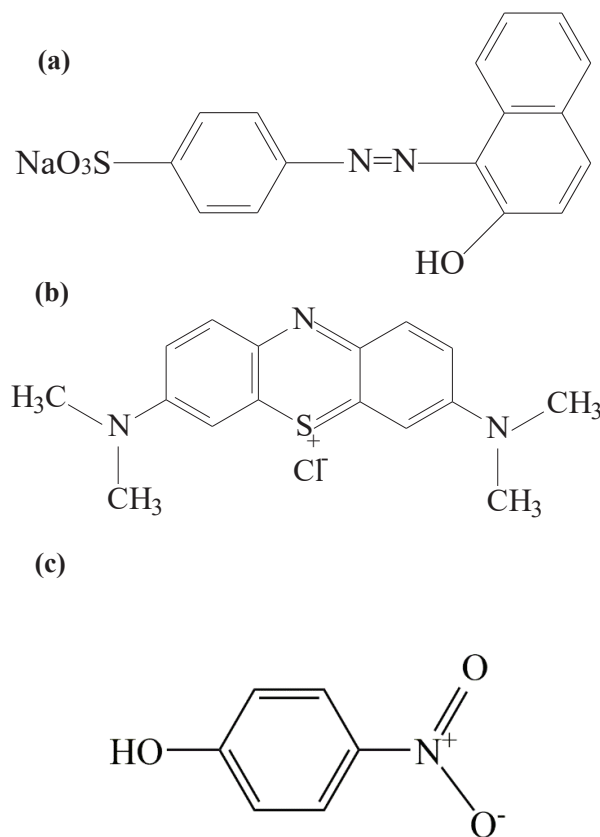
(a)

(b)

(c)

Fig. 1: The molecular structures of ORII (a), MB (b), and PNP (c).

values of 200°C, 300°C and 400°C at a heating rate of 10°C min^{-1} and held constant for 2 h. After pyrolyzation, the samples were allowed to cool down to room temperature in the furnace. These pyrolyzed 0.05CD-MS were denoted as 0.05CD-MS-200, 0.05CD-MS-300 and 0.05CD-MS-400, respectively, while the pyrolyzed 0.5CD-MS are denoted as 0.5CD-MS-200, 0.5CD-MS-300 and 0.5CD-MS-400, respectively. Similarly, the adsorbent MS-200, MS-300 and MS-400 were also prepared.

Batch adsorption studies: Batch experiments were conducted in a series of 250-mL conical flasks. In the flasks, 20 mg of the adsorbent was added to 100 mL solution with an initial PNP, ORII or MB concentration of 20 mg/L. Then, the flasks were sealed and shaken at 298 K at a speed of 120 rpm for 24 h to achieve equilibrium. Solution pH was maintained at neutral unless otherwise stated. To examine the effect of glucose concentration, 5 mg adsorbent (0.5CD-MS or 0.05CD-MS) was used to adsorb PNP with an initial concentration of 5 mg/L.

Characterization: The morphology and superficial element compositions of MS and 0.5CD-MS-300 were characterized by a Hitachi S-4800 field scanning electron microscope (FESEM) coupled with an energy dispersive spectrometer (EDS).

Analysis methods: All the samples were collected and filtered by microporous membranes (0.45μm) before analysis. The concentration of PNP, ORII and MB was measured using UVmini-1240 spectrophotometer (Shimadzu, Japan) at the wavelength of maximum adsorption of 317 nm, 483 nm, and 664 nm, respectively (Cheng et al. 2019, Mi et al.

2016). The adsorption capacity was calculated using the following equation:

$$q_e=(C_0-C_e)V/M \qquad …(1)$$

Where, q_e (mg/g) is the adsorption capacity at equilibrium; C_0 and C_e (mg/L) are the initial and equilibrium concentrations of PNP, ORII, and MB, respectively; V (L) is the solution volume, and M (g) is the weight of adsorbents.

RESULTS AND DISCUSSION

Effect of Pyrolytic Temperature and Glucose Concentration on PNP Adsorption

Both the pyrolytic temperature and glucose concentration were important for adsorbent preparation. It was observed from Fig. 2 that the CD-MS pyrolyzed at 300°C had a comparatively higher adsorption capacity for PNP removal. The concentration of glucose for the adsorbent preparation was expected to have a significant impact on the uptake of contaminants as well. As illustrated, it was noted that the adsorption capacity of PNP by 0.5CD-MS was higher than that by 0.05CD-MS under the same pyrolytic temperature. Further, at the pyrolytic temperature of 300°C, the adsorption capacities by the 0.5CD-MS and 0.05CD-MS were 4.16 mg/g and 1.88 mg/g, respectively. This might be attributed to the increasing bonding sites on the CD-MS surfaces resulted from the increase of glucose concentration. Similar experimental results were also observed by Xue et al. (2013). As such, 0.5CD-MS-300 was used for the following experiments.

On the other hand, as the structure of pore canals and surface area of internal pores of CD-MS varied as a conse-
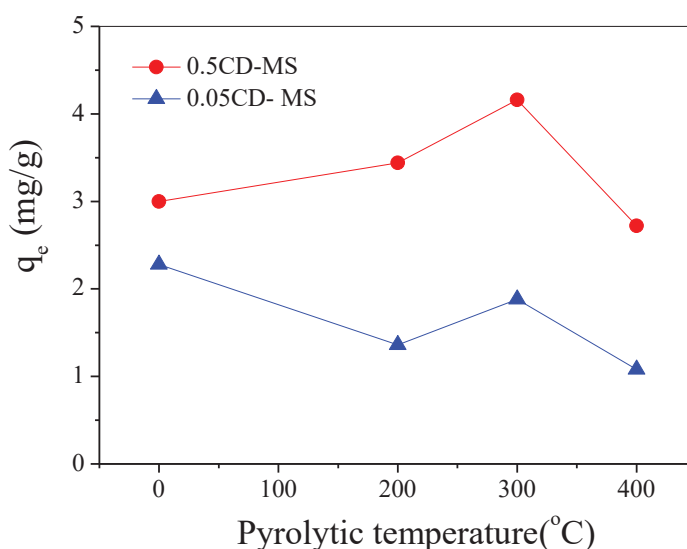

Fig. 2: Effect of glucose concentration and pyrolytic temperature on adsorption of PNP. PNP 5.0 mg/L, neutral solution pH.

quence of the different pyrolytic temperatures, the adsorption capacity of PNP by the resulting adsorbents was expected to vary accordingly. The relationship between pyrolytic temperature and adsorption capacity of PNP is presented in Fig. 2. It shows that the adsorption capacity of PNP by 0.5CD-MS-300 reached the maximum of 4.16 mg/g, which might be attributed to the removal of crystal water in the pore canals and the increase of the surface area of internal pores as the pyrolytic temperatures rose. However, continuous increase of pyrolytic temperature was not helpful for the uptake of PNP and the adsorption capacity declined, which might be attributed to the collapse of pore canals.

Characterization of the Carbon Dots Decorated Medical Stone

As stated above, the 0.5CD-MS-300 demonstrated the highest adsorption capacity for PNP in comparison to other adsorbents. The surface morphology of the 0.5CD-MS-300 and the raw MS was characterized by SEM and presented herein. From Fig. 3a and c, it was observed that the raw MS presented a natural crystal structure, although it was difficult to find some pore canals from the MS surfaces. Differently, the surface structure of the 0.5CD-MS-300 became loose after pyrolysis, and some sponge pores were scattered onto

the surfaces of the adsorbent, which might facilitate the adsorption of contaminants (Yu et al. 2013). This demonstrated pyrolysis treatment can change the surface structure of MS. From Fig. 3b and d, many fine particles aggregated on the surfaces of MS, which were deduced to be carbon dots immobilized on the surfaces of MS.

To further explore whether carbon dots had decorated on the surfaces of MS, EDS analysis was conducted. As illustrated in Fig. 4a and b, comparing to the atomic ratio of C increased from 2.6% of the raw MS to 11.25% of the 0.5CD-MS-300, which was reasonably attributed to the introduction of CDs on the surfaces of MS. Accordingly, the atomic ratio of O decreased from 57.97 % of the raw MS to 53.70% of the 0.5CD-MS-300. Pyrolysis under different temperatures and immobilization of carbon dots had significantly altered the surface properties of the raw MS.

Effect of Adsorbent Dosage on PNP Adsorption

The effect of adsorbent (0.5CD-MS-300) dosage from 100 mg/L to 800 mg/L was investigated and presented in Fig. 5. The plot showed that uptake of PNP decreased gradually with an increase of adsorbent dosage. One reason was that the unsaturated adsorption sites increased with increasing adsorbent dosage at a fixed concentration and volume of
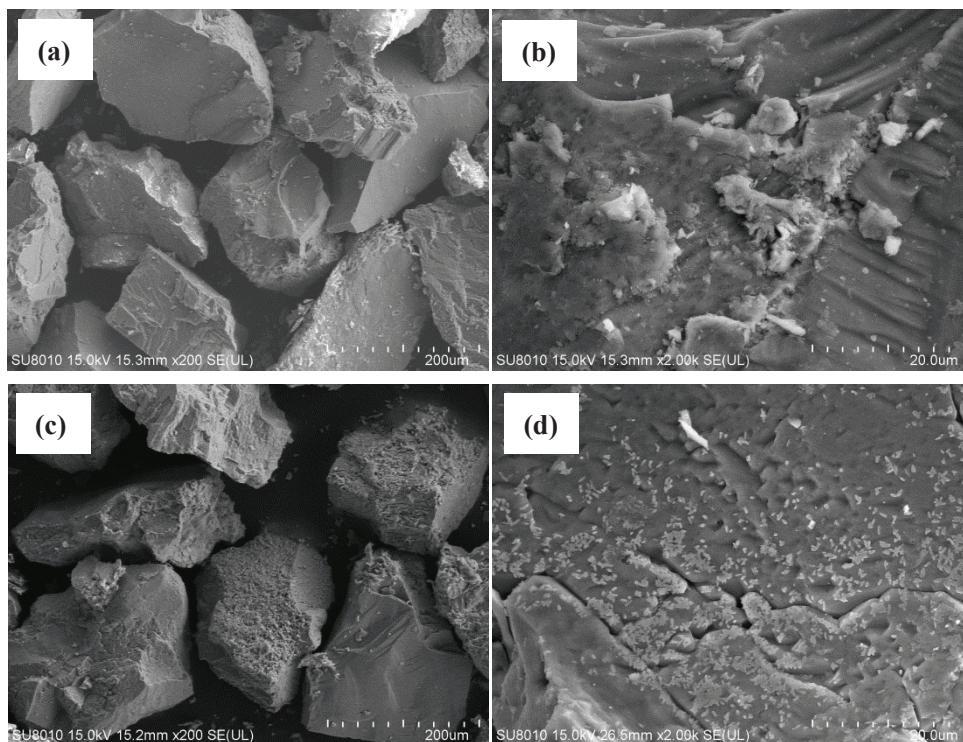

Fig. 3: SEM images of the raw MS (a, b) and the 0.5CD-MS-300 (c, d).

PNP. The other was attributed to the decrease of surface area and the increase of diffusion path length of adsorbent due to the particle aggregation (Shirmardi et al. 2016, Kumar et al. 2010).

Adsorptive Performance of Carbon Dots Decorated Medical Stone

The surface charge property of an adsorbent always plays an important role during the adsorptive removal of organic contaminants. Three organic pollutants with different charge properties including PNP, ORII and MB were selected to explore the adsorptive performance of the 0.5CD-MS-300. The initial concentration of the three contaminants was fixed at 20 mg/L. As illustrated in Fig. 6, it was noted that the adsorption capacity of PNP and MB by 0.5CD-MS-300 was much higher than that of ORII. The adsorption capacity of PNP, MB, and ORII was 27.87 mg/g, 15.37 mg/g, and 0 mg/g, respectively. This indicated that the 0.5CD-MS-MS had a high adsorption selectivity for organic pollutants with different charge properties.

To our knowledge, PNP ($pK_a = 7.15$) in water solution exists in two species of molecule and anion, and molecular
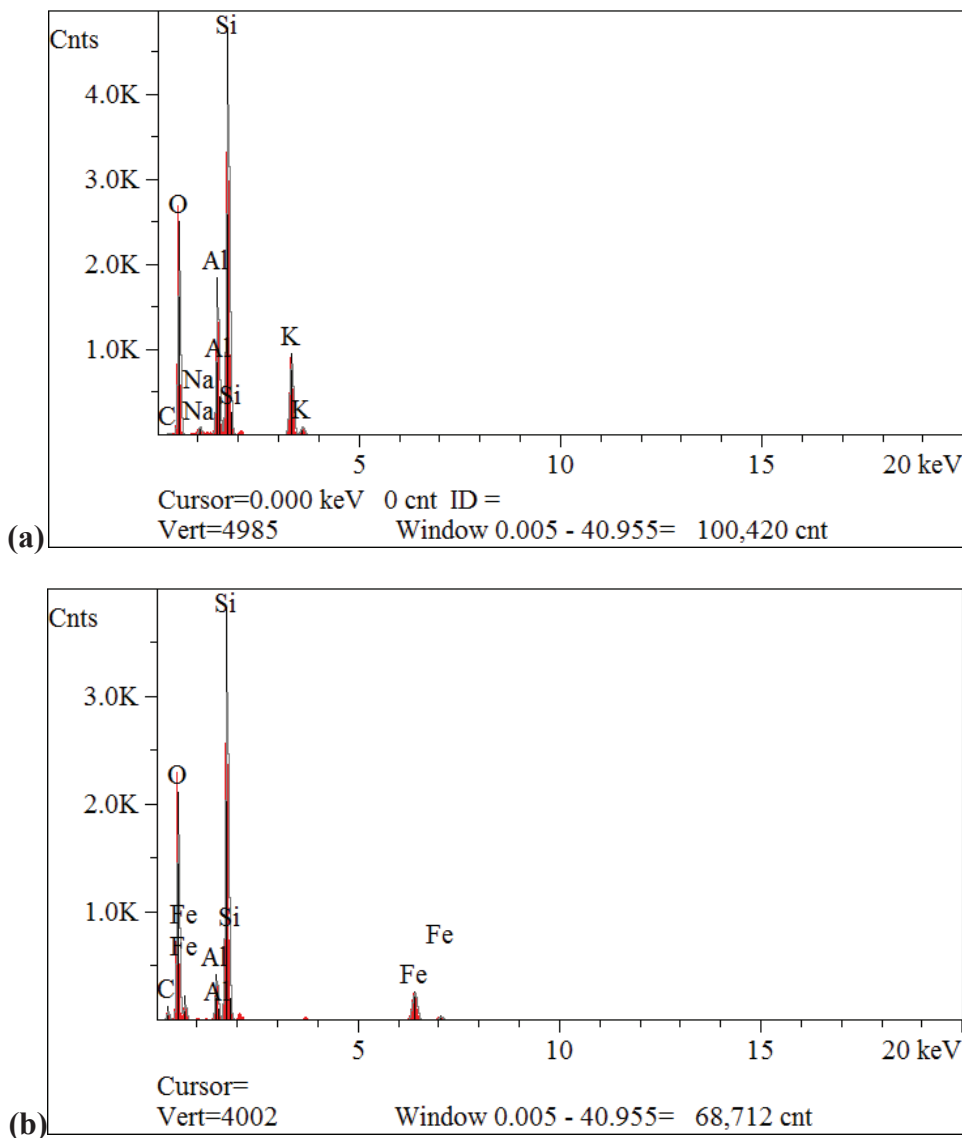
Fig. 4: EDS analysis results of the raw MS(a) and the 0.5CD-MS-300 (b).
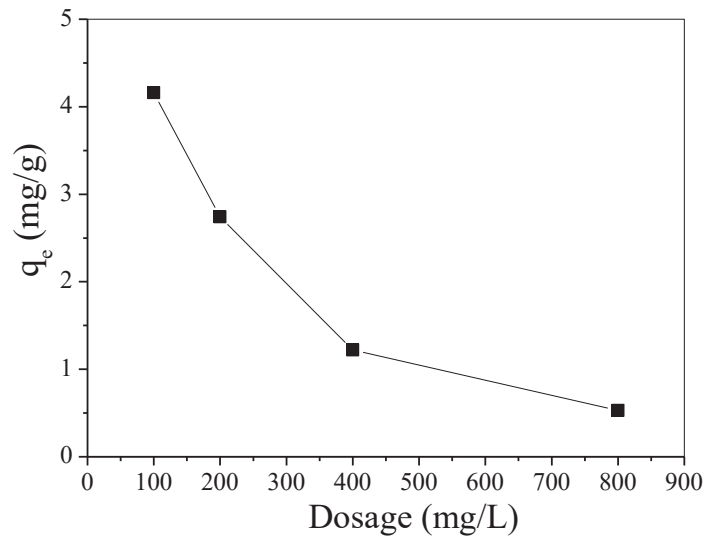
Fig. 5: Effect of adsorbent dosage on PNP adsorption. PNP 5.0 mg/L, neutral solution pH.
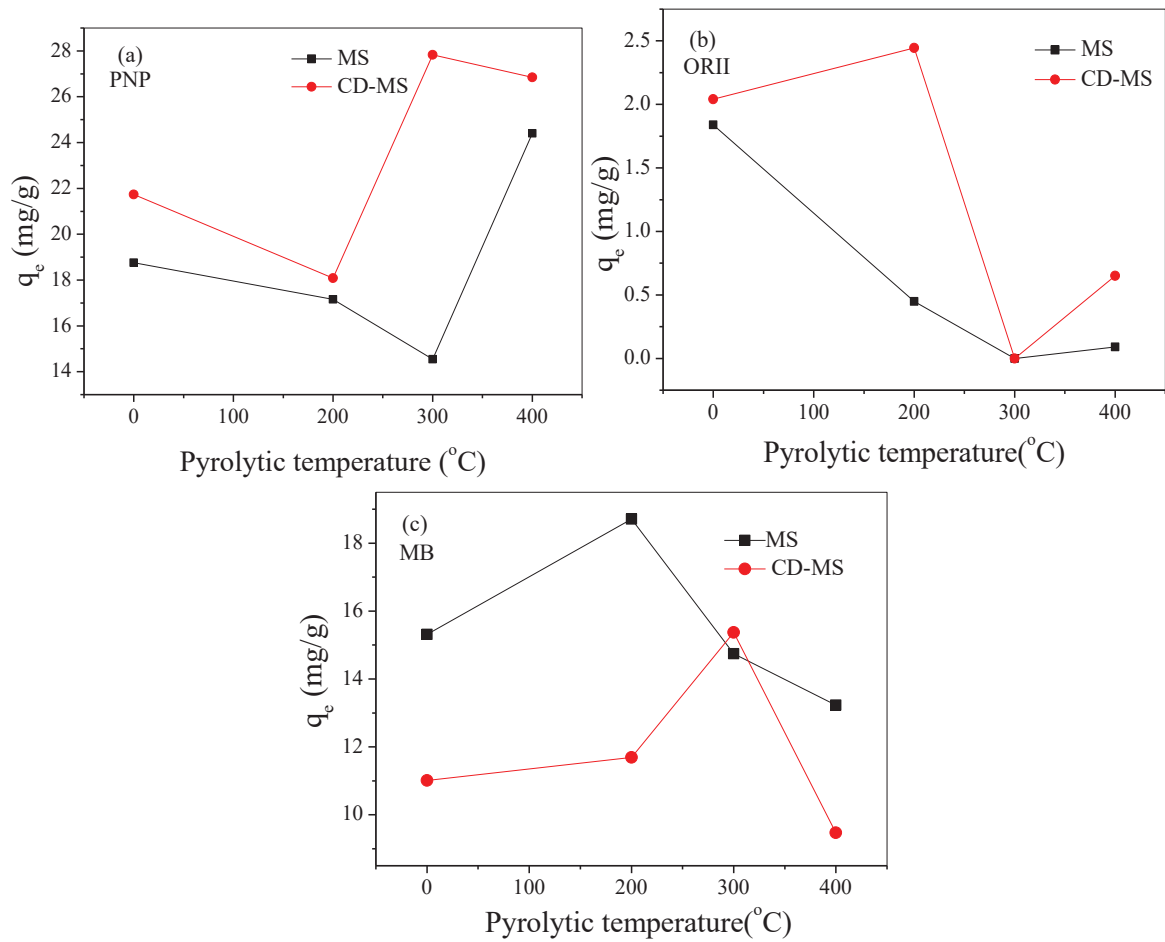
Fig. 6: Adsorption of PNP (a), ORII (b) and MB (c) onto the raw MS and the 0.5CD-MS-300.
Contaminant concentration 20.0 mg/L, neutral solution pH.

PNP can convert to anions at pH > 7.15 due to dissociation (Sarkar et al. 2010). Meanwhile, MB is moderately alkaline in water and produces cation (C^+ or CH^+) (Gobi et al. 2011). By contrast, ORII (pK_a = 10.6 and pK_a = 1) has three different forms depending on the pH of the aqueous solution, noted H_2L which is doubly protonated and dominant at pH < 1, HL^- which is mono protonated and dominant at pH 1-10.6, L^{2-} which is non-protonated and dominant at pH > 10.6 (Abramian & El-Rassy 2009). Therefore, the three pollutants have different electrical characteristics in a neutral aqueous solution and the predominant species of PNP, MB and ORII are molecule, cation (C^+ or CH^+), and anion (HL^-), respectively. Accordingly, from the results mentioned above, it could be deduced that the surface of 0.5CD-MS-300 was negatively charged, which was beneficial to MB adsorption due to an electrostatic attraction. Meanwhile, the results indicated that electrostatic attraction/repulsion was an important adsorption mechanism for 0.5CD-MS-300, which also facilitated the high adsorption selectivity for these organic pollutants. However, an interesting phenomenon was that the adsorption capacity of PNP is excellent. As mentioned, most of PNP exists as molecules in a neutral solution, which indicated that the effect of electrostatic force was not dominant. Therefore, considering the abundant O-containing functional groups of carbon dots on the 0.5CD-MS-300, the higher adsorption capacity of PNP might be attributed to H-bond interaction between PNP molecules and the surface functional groups of the adsorbent, π-π interaction, and π-stacking forces (Zheng et al. 2017).

In addition, the 0.5CD-MS-300 demonstrated a higher adsorption capacity towards PNP and ORII than the raw MS in general, indicating that the introduction of carbon dots was beneficial to the adsorption capability for PNP and ORII. By contrast, the introduction of carbon dots declined the adsorption of MB. Therefore, the surface of the 0.5CD-MS-300 was predominantly negatively charged.

CONCLUSION

Carbon dots decorated medical stone (CD-MS) was creatively prepared by immobilizing carbon dots on the surfaces of medical stone (MS). Compared to the raw MS, the 0.5CD-MS-300 demonstrated an excellent adsorption capability for PNP. Bach experiments for the adsorption of the three pollutants including PNP, ORII and MB with different charge properties, indicated that the surface of 0.5CD-MS-300 was negatively charged. Furthermore, 0.5CD-MS-300 had a high adsorption selectivity for different organic pollutants, which was attributed to the electrostatic attraction/repulsion as one of the fundamental adsorption mechanisms. In a word, carbon dots had successfully decorated the raw medical stone and

the resulting adsorbent 0.5CD-MS-300 can be considered as a powerful adsorbent for the removal of organic pollutants from wastewater.

REFERENCES

Abramian, L. and El-Rassy, H. 2009. Adsorption kinetics and thermodynamics of azo-dye Orange II onto highly porous titania aerogel. Chem. Eng. J., 150: 403-410.

Cheng, M., Jiang, J.H., Wang, J.J. and Fan, J. 2019. Highly salt resistant polymer supported ionic liquid adsorbent for ultrahigh capacity removal of p-nitrophenol from water. ACS Sustain. Chem. Eng., 7: 8195-8205.

Crini, G. 2006. Non-conventional low-cost adsorbents for dye removal: A review. Bioresour. Technol., 97: 1061-1085.

Ding, C.Q., Zhu, A.W. and Tian, Y. 2014. Functional surface engineering of C-dots for fluorescent biosensing and in vivo bioimaging. Acc. Chem. Res., 47(1): 20-30.

Gao, G.H., Lei, Y.H., Dong, L.H., Liu, W.C., Wang, X.F., Chang, X.T., Liu, T., Yin, Y.S. and Ajayan, P.M. 2012. Synthesis of nanocomposites of silver nanoparticles with medical stone and carbon nanotubes for their antibacterial applications. Mater. Express, 2(2): 2185-5849.

Gao, T.P., Wang, W.B. and Wang, A.Q. 2011. A pH-sensitive composite hydrogel based on sodium alginate and medical stone: Synthesis, swelling, and heavy metal ions adsorption properties. Macromol. Res., 19(7): 739-748.

Gobi, K., Mashitah, M.D. and Vadivelu, V.M. 2011. Adsorptive removal of methylene blue using novel adsorbent from palm oil mill effluent waste activated sludge: Equilibrium, thermodynamics and kinetic studies. Chem. Eng. J., 171: 1246-1252.

Hsu, P.C. and Chang, H.T. 2012. Synthesis of high-quality carbon nanodots from hydrophilic compounds: Role of functional groups. Chem. Commun. (Camb), 48: 3984-3986.

Kumar, P.S., Ramalingam, S., Senthamarai, C., Niranjanaa, M., Vijayalakshmi, P. and Sivanesan, S. 2010. Adsorption of dye from aqueous solution by cashew nut shell: Studies on equilibrium isotherm, kinetics and thermodynamics of interactions. Desalination, 261: 52-60.

Li, G.T., Zhao, W.G., Wang, B.B., Gu, Q.Y. and Zhang, X.W. 2014. Synergetic degradation of Acid Orange 7 by fly ash under ultrasonic irradiation. Desalin. Water Treat., 57(5): 1-8.

Liu, F.B., Zhang, W.T., Chen, W.J., Wang, J., Yang, Q.F., Zhu, W.X. and Wang, J.L. 2017. One-pot synthesis of $NiFe_2O_4$ integrated with EDTA-derived carbon dots for enhanced removal of tetracycline. Chem. Eng. J., 310: 187-196.

Mahata, P., Aarthi, T., Madras, G. and Natarajan, S. 2007. Photocatalytic degradation of dyes and organics with nanosized $GdCoO_3$. J. Phys. Chem. C, 111: 1665-1674.

Mi, X., Li, G.T., Zhu, W.Y. and Liu, L.L. 2016. Enhanced adsorption of Orange II using cationic surfactant modified biochar pyrolyzed from cornstalk. Journal of Chemistry, 2016, 1-7.

Polubesova, T., Zadaka, D., Groisman, L. and Nir, S. 2006. Water remediation by micelle-clay system: Case study for tetracycline and sulfonamide antibiotics. Water Res., 40: 2369-2374.

Qu, J.H. 2008. Research progress of novel adsorption processes in water purification: A review. J. Environ. Sci., 20: 1-13.

Sarkar, B., Xi, Y.F., Megharaj, M., Krishnamurti, G.S. and Naidu, R. 2010. Synthesis and characterisation of novel organopalygorskites for removal of p-nitrophenol from aqueous solution: isothermal studies. J. Colloid Inter. Sci., 350(1): 295-304.

Shen, J.H., Zhu, Y.H., Yang, X.L. and Li, C.Z. 2012. Graphene quantum dots: Emergent nanolights for bioimaging, sensors, catalysis and photovoltaic devices. Chem. Commun. (Camb), 48: 3686-3699.

Shirmardi, M., Alavi, N., Lima, E.C., Takdastan, A., Mahvi, A.H. and Babaei, A.A. 2016. Removal of atrazine as an organic micro-pollutant from aqueous solutions: A comparative study. Process Saf. Environ., 103: 23-35.

Westerhoff, P., Yeomin, Y., Snyder, S. and Wert, E. 2005. Fate of endocrine-disruptor, pharmaceutical, and personal care product chemicals during simulated drinking water treatment processes. Environ. Sci. Technol., 39: 6649-6663.

Xue, G.H., Gao, M.L., Gu, Z., Luo Z.X. and Hu, Z.C. 2013. The removal of p-nitrophenol from aqueous solutions by adsorption using gemini surfactants modified montmorillonites. Chem. Eng. J., 218: 223-231.

Yu, Q.J., Cui, C.Y., Zhang, Q., Chen, J., Li, Y., Sun, J.P., Li, C.Y., Cui, Q.K., Yang, C.H. and Shan, H.H. 2013. Hierarchical ZSM-11 with intergrowth structures: Synthesis, characterization and catalytic properties. J. Energy Chem., 22: 761-768.

Zhang, X., Li, A.M., Jiang, Z.M. and Zhang, Q.X. 2006. Adsorption of dyes and phenol from water on resin adsorbents: Effect of adsorbate size and pore size distribution. J. Hazard Mater., 137: 1115-1122.

Zheng, H.S., Guo, W.Q., Li, S., Chen, Y.D., Wu, Q.L., Feng, X.C., Yin, R.L., Ho, S.H., Ren, N.Q. and Chang, J.S. 2017. Adsorption of p-nitrophenols (PNP) on microalgal biochar: Analysis of high adsorption capacity and mechanism. Bioresource Technol., 244: 1456-1464.

Zhou, W.X., Guan, D.G., Sun, Y., Sun, C.M., Xu, G.L., Chen, T., Yu, Z.S., Xu, Y. and Yan, H. 2015. Removal of Nickel (II) ion from wastewater by modified maifanite. Mater. Sci. Forum, 814: 371-375.

Riparian Zones and Pollination Service: A Case Study from Coffee-Agrosystem Along River Cauvery, South India

N. Deepthi*†, B.C. Nagaraja* and M. Paramesha

*Department of Environmental Science, Bangalore University, Jnanabharathi Campus, Bangalore-560 056, India
**St. Joseph's College (Autonomous), 36, Langford Road, Langford Gardens, Bangalore-560 027, India
†Corresponding author: N. Deepthi; deepthi.padma@gmail.com

ABSTRACT

The study aims to understand the influence of pollinator visitation rate to coffee plantations located along the riparian zones of river Cauvery in Karnataka, using distance as a criterion. Plots were fixed at 10 m, 30 m and 60 m points from the edge of riparian zone towards the coffee plantations. In each of these three points, five plants were selected. In each plant, four branches with approximately six inflorescences per branch were observed for 15 minutes and the visitation rate of selected floral visitors to *Coffea canephora* was recorded. To understand if a riparian zone was a suitable pollinator habitat, bee colonies in the riparian zone were identified through a transect of approximately 500 m adjacent to the study plot. The total number of bee visits for *Apis dorsata*, *Apis cerana*, *Tetragonula iridipennis* and *Apis florea* was 18,100 for an observation time of 9540 minutes. *A. dorsata* and *A. cerana* were the main contributors to the total number of visits. The visitation rate of pollinators, *A. cerana* and *A. dorsata* decreased with increase in distance from the riparian zone. Additionally, colonies of *A. cerana* and *A. dorsata* were found in the riparian zones indicating riparian zones as potential pollinator habitats. A negative relationship has been observed between total species visits and distance indicating a reduction in species visits with increased distance from the riparian zone. Conservation of riparian zones increases pollination service to adjacent coffee plantations along with a multitude of other ecosystem services.

INTRODUCTION

Riparian zones are interfaces between terrestrial and aquatic ecosystems. They cannot be delineated easily (Gregory et al. 1991) and the width varies up to several metres. They are ecotones with high biodiversity and productivity in contrast to the larger landscape (Naiman et al. 1998). Moreover, they are high energy systems, which are favoured by humans for food, water, dwelling sites, recreation and other uses (Johnson & Haight 1984). Further, they provide multiple ecosystem services such as water purification, nutrient removal, riverbank stabilization, act as corridors, habitat provider, fodder, fuelwood and others (Jose 2009, Naiman et al. 2010). This diverse ecosystem is under threat and is one of the major areas where biodiversity is being lost (Sparovek et al. 2002), which in turn affects the delivery of ecosystem services. Riparian zones are threatened by agricultural land expansion (Sunil et al. 2010), extraction of water, grazing, waste dumping and expanding human habitations (Naiman et al. 2010).

Food production is an ecosystem service which depends on water, soil formation, pollination and others. Changes in pollination service will affect food production and impact human well-being (Millennium Ecosystem Assessment 2005, Potts et al. 2016). There is a global decline in managed and wild pollinators in agricultural landscapes (Roubik et al. 2018) even though animal pollinators contribute 15-30% of global food production and bees (*Apis*) being one of the important pollinators of most crops (Roubik 1995, Potts et al. 2010). Agricultural crop productivity depends at least partially on unmanaged or wild pollinators from semi-natural habitats (Kremen et al. 2002, Kremen et al. 2004). Natural landscapes like riparian zones could be potential sources of pollinators to nearby agricultural land. But studies considering riparian zones as exclusively pollinator sources are limited probably because of the complex nature of riparian zones such as varying width, habitats, flowering pattern, accessibility and others. Most studies tend to combine other natural habitats like forests along with riparian zone to study pollination. For instance, in California pollination services to hybrid sunflower (*Helianthus annuus*), almond (*Prunus dulcis*) and muskmelon (*Cucumis melo*) was higher when the farmland was located close to natural habitats, such as riparian, oak woodland, chaparral and mixed oak (Greenleaf &

Kremen 2006, Ricketts et al. 2008). Similarly, in Costa Rica pollinator visits from riparian zones and forest fragments to coffee farms reduced with increasing distance (Ricketts 2004), while in Portugal, riparian scrubland and riparian forest supported higher pollination services in comparison to other land uses such as agricultural land, mixed forest, coniferous forest and eucalyptus forest (Santos et al. 2018).

In India, there are no specific studies on assessment of riparian ecosystem services but fewer studies restricted to the biodiversity of the riparian zone (Sunil et al. 2016). Besides, there are no specific guidelines/policies governing riparian zones in India (Sunil et al. 2011). Studies on the riparian zone as a potential pollination services provider to adjacent agricultural systems are limited in India and hence an attempt is being made to study the same along the riparian zones of river Cauvery in Kodagu district, Karnataka. With this background, the study addresses the research question; does the proximity of riparian zone influence visitation rate of pollinators to *Coffea canephora*?

MATERIALS AND METHODS

Study Area

Cauvery is one of the major rivers of peninsular India and supports huge populations in Karnataka and Tamil Nadu for

domestic, irrigation, industries and hydropower generation. It originates (12°25' N, 75°34' E, 1341 m) in the Western Ghats in Karnataka and flows through the state of Tamil Nadu before entering the Bay of Bengal (GOI 2014). It flows for about 320 km in Karnataka, while its total length is approximately 800 km. Its basin (81,155 km^2) is spread across Tamil Nadu and Pondicherry (54%), Karnataka (42%) and Kerala (4%) (Jayaram 2000). The upstream of the river in Karnataka flows through the district of Kodagu well-known for its coffee plantations. Area of Kodagu district is approximately 4,102 km^2 and 33% of it is under coffee-agroforestry (Garcia et al. 2010). Two popular varieties of coffee, *Coffea arabica* and *Coffea canephora* are cultivated, with the latter having the highest area under cultivation (56,000 ha) according to Coffee Board of India. Rest of the land area in the district is under paddy cultivation and protected areas either as sacred grooves, reserve forest, wildlife sanctuaries and national park. In coffee-agroforestry system, coffee is cultivated under the shade of native or exotic tree species, additionally, pepper vines are grown on shade trees as a supplementary crop.

Methods

The study was carried out during March 2017 in coffee-agrosystems located along river Cauvery, Kodagu district, India. Suitable coffee-agroforests were selected at every 8 km
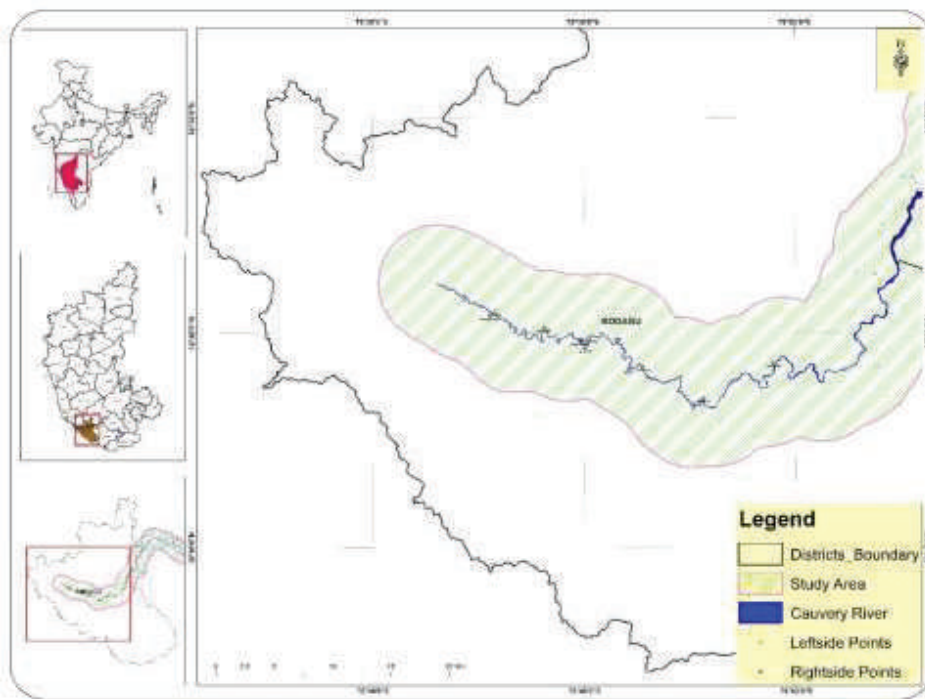

Fig. 1: The study area.

interval (n=11) along the riparian zone which was spread on both left (n=6) and right (n=5) bank of the river (Fig. 1). The study used distance as a criterion to understand pollination service to crops (Ricketts 2004, Winfree & Kremen 2009). In each sampling plot, from the edge of riparian zone 10, 30 and 60 m points were fixed to understand the pollinator visitation to *Coffea canephora* inflorescence. In each of these three points, five plants (each at 20 m interval) were marked (Fig. 2). In each plant, four branches with approximately six inflorescences per branch were observed for 15 minutes (Boreux et al. 2013).

During the observation period, the visitation rate of selected floral visitors to *Coffea canephora* was recorded. A bee visit meant a bee visiting a flower for more than one second duration (Kremen et al. 2004) which could be for either collecting resources or pollination (Ricketts 2004). The number of visits was very low before 07:00 and after 13:00 hrs, hence the sampling time was standardised to 07:00 to 13:00 hrs. These observational plots are suitable for studying pollinator abundance and richness in a specified area (Westphal et al. 2008).

The entire study was carried out only in irrigated coffee plantations because during mass flowering no bee visits were observed in almost half of the plantations studied by Boreux et al. (2013) in Kodagu. Plots beyond 60 m were not chosen as blooming was not observed on the day of the study, because of the variation in irrigation patterns. Also, with increasing distance, there could be chances of bees visiting from the nearby forest fragments which could hamper the objective of the study. Furthermore, these coffee-agroforests did not have any bee boxes in the surroundings that could hamper the objective of the study.

The pollination service rendered by riparian forest along river Cauvery was studied by using indicator species, coffee plants (*Coffee canephora*) and bees. *Coffee canephora*, an evergreen shrub or small tree is cultivated extensively in Kodagu district. It is locally known as Robusta coffee and can grow up to 10 m with a shallow root system. It requires an average rainfall of 1800 mm/year, temperature between 24°C and 30°C and well-drained, loamy, slightly acidic and rich in humus soil. It begins yielding 2-3 years after planting. It requires about 4-8 weeks of a dry period, which builds water stress and helps in initiating flowering (Nair 2010).

In Kodagu district, flowering is initiated due to summer rains in February and March. If rains are delayed, irrigation is adopted to initiate flowering. One to three inflorescences are borne on each leaf axil, with each inflorescence consisting of three to six flowers, stalkless to stalked, with stalks up to 7 mm. The blooming attracts many pollinators such as bees, butterflies and other insects. It is a wind-pollinated crop but entomophilous pollination enhances fruit set and increases yield (Roubik 2002).

Previous studies by Ricketts (2004) and Krishnan et al. (2012) found *Apis* species to be the highest visitor to Coffee. Hence, *Apis cerana* (Asiatic honey bee), *Apis dorsata* (Giant honey bee), *Apis florea* (Dwarf honey bee) and *Tetragonula iridipennis* (Stingless bee) were selected for the study. To understand if the riparian zone was a suitable pollinator habitat, bee colonies in the riparian zone were identified through a transect of 500 m adjacent to the study plot. Transect method shows species richness as well as composition (Westphal et al. 2008). The data related to coffee pollinators, location of bee colonies, yield, etc., were also collected from coffee farmers and workers through informal interviews to
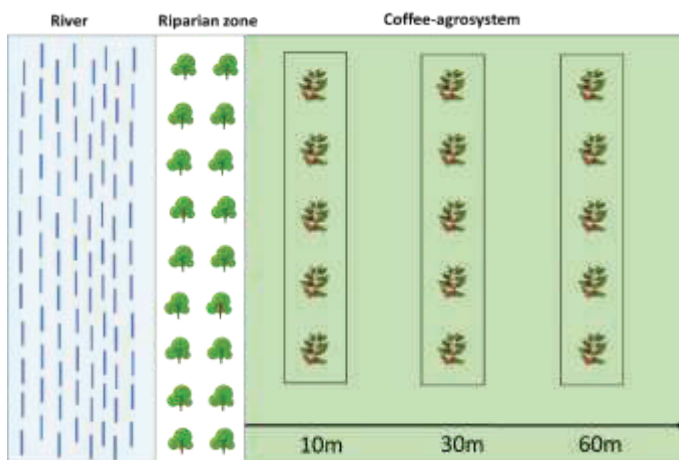

Fig. 2: Sampling design for pollination study in the coffee-agrosystem landscape of River Cauvery.

understand community perception towards bee pollination and its habitat.

RESULTS AND DISCUSSION

The total number of bee visits for the four selected species was 18,100 for an observation time of 9,540 minutes. Klein et al. (2003) recorded 2269 individuals with an observation time of 1125 minutes and the trend is almost similar to the present study. Species abundance based on bee visits was in the following order: *Apis dorsata*, *Apis cerana*, *Tetragonula iridipennis and Apis florea* (Table 1). *Apis dorsata* and *Apis cerana* were the main contributors to the total number of visits. It was also observed that apart from *Apis* species, lepidopterans and dipterans also visited coffee inflorescence but their numbers were very low. Krishnan et al. (2012) observed 58% of *Apis dorsata* visits to *Coffea canephora* in Kodagu.

The distance of coffee plants from the riparian zone had a significant impact on the pollinator abundance for two species *A. cerana* and *A. dorsata*. The average number of visits for 15 min per branch for *A. cerana* decreased with increasing distance (10 m to 60 m) from the riparian zone. *A. dorsata* showed consistent visits for 10 m and 30 m, while for 60 m there was a decrease in visits. However, *T. iridipennis* exhibited increasing visits with increase in distance. At 10 m distance, the visits were nil, while at 30 m and 60 m the visits were just one. *A. florea* exhibited low visitation rate (≤1 visit) at all the three distances. Thus, *A. cerana* and *A. dorsata* species abundance was higher closer to the edge of the riparian zone (Fig. 3). Total species visits were log-transformed to reduce the space between units. A negative relationship has been observed between total species visits and distance indicating a reduction in species visits with increased distance from the riparian zone. A similar observation was recorded in Costa Rica, bee species richness in coffee farms reduced as the distance from the riparian forest increased (Ricketts 2004).

In the colony count study, for a total of 5500 m transect in the riparian zone, colonies of *A. dorsata, A. cerana* and *A. florea* were observed (Table 2). *T. iridipennis* was absent in the transect studied. Higher number of colonies have been observed for *A. dorsata*, while *A. florea* least. Colonies of

Table 1: Species wise bee visits to *Coffea canephora* inflorescence.

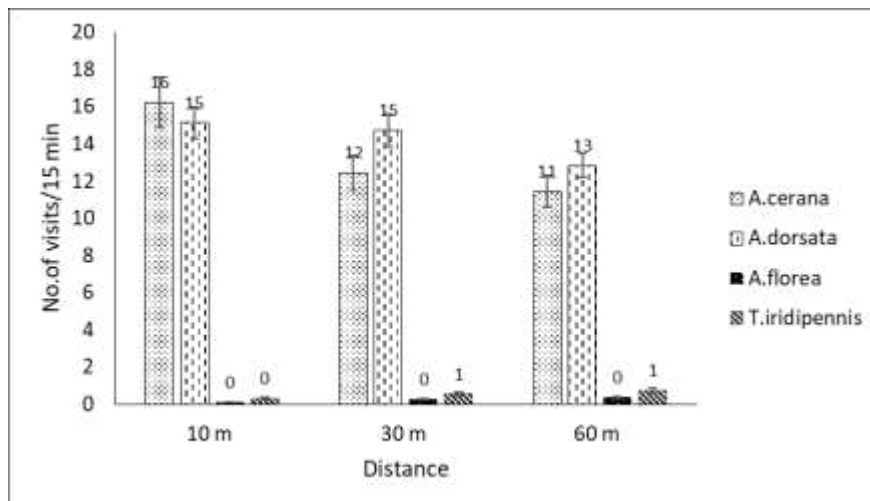| Bee species	No. of visits	(%)
Apis cerana Fabricius	8543	47
Apis dorsata Fabricius	9070	50
Apis florea Fabricius	158	1
Tetragonula iridipennis Smith	329	2
Total	18100	

Fig. 3: Proximity-wise mean bee visits/15 minutes to *Coffee canephora* at increasing distance from the edge of the riparian zone.

Table 2: Bee colonies found in the riparian zone adjacent to study plots.

Study species	No. of colonies	Nesting site in the riparian zone
Apis cerana	4	Tree cavities, fallen logs and lateral caving in the river bank
Apis dorsata	8	Branches of tall trees and bridges.
Apis florea	2	Branches of shrubs

A. dorsata were found on branches of tall trees and under the bridges. Paar et al. (2000) also recorded *A. dorsata* colonies were restricted to forests due to their habit of nesting at greater heights such as tall trees. Thus, riparian zones are found to be suitable nesting habitat for *A. dorsata* species.

Qualitative interviews with coffee farmers and workers revealed *A. dorsata* built colonies in riparian zones during summers which were the flowering season for coffee. A mixed response was obtained towards the presence of colonies during rains, some mentioned that the colonies moved towards forests, while some were not aware of it. Majority of the respondents strongly agreed coffee fruit set was enhanced by bee pollination particularly *A. dorsata*. Awareness among communities on pollinators and their habitats will increase their income from coffee as well as promote pollinator habitat conservation in the riparian landscape.

Unlike other coffee-agroforests in the region, the ones that are adjacent to the river have multiple advantages in terms of water availability as well as pollinators. Hence, promoting riparian habitat heterogeneity such as increasing floral and nesting resources, wildflower margins and hedgerows increases pollinator (Santos et al. 2018) richness and abundance, further increasing crop productivity. Further studies could compare the crop productivity to the number of bee visits in the riparian landscape.

CONCLUSION

Natural habitats and agricultural landscapes are ecologically interconnected as pollinator diversity is essential for entomophilous crops (Kremen et al. 2002). Among other factors such as species of natural pollinators, foraging range, attractive flowers, etc., farmland distance to the natural habitat of wild pollinators plays a significant role in pollination success. The study concludes (i) Coffee-agrosystems adjacent to riparian zones observed higher *A. dorsata* visits, a significant pollinator of *Coffea canephora*, (ii) Riparian zones are important habitat for pollinators mainly *A. dorsata* and *A. cerana*, apart from other forest fragments present across Kodagu district. Thus, the conservation of riparian zones can increase pollination service to the coffee farms, enhance crop productivity and increase economic gains.

REFERENCES

Boreux, V., Krishnan, S., Cheppudira, K. G. and Ghazoul, J. 2013. Impact of forest fragments on bee visits and fruit set in rain-fed and irrigated coffee agro-forests. Agriculture, Ecosystems & Environment, 172: 42-48.

Garcia, C. A., Bhagwat, S. A., Ghazoul, J., Nath, C. D., Nanaya, K. M., Kushalappa, C. G., Raghuramulu, Y., Nasi, R. and Vaast, P. 2010. Biodiversity conservation in agricultural landscapes: challenges and opportunities of coffee agroforests in the Western Ghats, India. Conservation Biology, 24(2): 479-488.

Government of India 2014. Cauvery basin. Ministry of Water Resources, Government of India (GOI). Retrieved from www.india-wris.nrsc.gov.in, on 1st November, 2015.

Greenleaf, S. S. and Kremen, C. 2006. Wild bees enhance honey bees' pollination of hybrid sunflower. Proceedings of the National Academy of Sciences, 103(37): 13890-13895.

Gregory, S.V., Swanson, F.J., McKee, W.A. and Cummins, K.W. 1991. An ecosystem perspective of riparian zones. BioScience, 41(8): 540-551.

Jayaram, K.C. 2000. Kaveri Riverine System: An Environmental Study. The Madras Science Foundation, Chennai.

Johnson, R.R. and Haight, L.T. 1984. Riparian problems and initiatives in the American Southwest: A regional perspective. In: Warner, R.E., & Hendrix, K.M (eds). California Riparian Systems: Ecology, Conservation and Productive Management. University of California Press, Berkley.

Jose, S. 2009. Agroforestry for ecosystem services and environmental benefits: An overview. Agroforestry Systems, 76(1): 1-10.

Klein, A. M., Steffan Dewenter, I. and Tscharntke, T. 2003. Bee pollination and fruit set of *Coffea arabica* and *C. canephora* (Rubiaceae). American Journal of Botany, 90(1): 153-157.

Kremen, C., Williams, N. M. and Thorp, R. W. 2002. Crop pollination from native bees at risk from agricultural intensification. Proceedings of the National Academy of Sciences, 99(26): 16812-16816.

Kremen, C., Williams, N.M., Bugg, R.L., Fay, J.P. and Thorp, R.W. 2004. The area requirements of an ecosystem service: Crop pollination by native bee communities in California. Ecology Letters, 7(11): 1109-1119.

Krishnan, S., Kushalappa, C.G., Shaanker, R.U. and Ghazoul, J. 2012. Status of pollinators and their efficiency in coffee fruit set in a fragmented landscape mosaic in South India. Basic and Applied Ecology, 13(3), 277-285.

Millennium Ecosystem Assessment 2005. Ecosystems and Human Well-being: Synthesis. Island Press, Washington, DC.

Naiman, R.J., Decamps, H. and McClain, M.E. 2010. Riparia: Ecology, Conservation, and Management of Streamside Communities. Elsevier, USA.

Naiman, R.J., Fetherston, K.L., McKay, S.J. and Chen, J. 1998. Riparian forests. In: Naiman, R.J., and Bilby, R.E. (eds) River Ecology and Management: Lessons from the Pacific Coastal Ecoregion, Springer-Verlag, New York.

Nair, K.P. 2010. The Agronomy and Economy of Important Tree Crops of the Developing World. Elsevier, USA.

Paar, J., Oldroyd, B.P. and Kastberger, G. 2000. Entomology: Giant honeybees return to their nest sites. Nature, 406(6795): 475.

Potts, S.G., Biesmeijer, J.C., Kremen, C., Neumann, P., Schweiger, O. and Kunin, W. E. 2010. Global pollinator declines: Trends, impacts and drivers. Trends in Ecology & Evolution, 25(6): 345-353.

Potts, S.G., Ngo, H.T., Biesmeijer, J.C., Breeze, T.D., Dicks, L.V., Garibaldi, L.A., Hill, R., Settele, J. and Vanbergen, A. 2016. The assessment report of the Intergovernmental Science-Policy Platform on Biodiversity and Ecosystem Services on Pollinators, Pollination And Food Production. The Intergovernmental Science-Policy Platform on Biodiversity and Ecosystem Services.

Ricketts, T.H. 2004. Tropical forest fragments enhance pollinator activity in nearby coffee crops. Conservation Biology, 18(5): 1262-1271.

Ricketts, T.H., Regetz, J., Steffan Dewenter, I., Cunningham, S. A., Kremen, C., Bogdanski, A., Gemmill-Herren, B., Greenleaf, S.S., Klein, A. M., Mayfield, M. M. and Morandin, L.A. 2008. Landscape effects on crop pollination services: Are there general patterns? Ecology Letters, 11(5): 499-515.

Roubik, D.W. 1995. Pollination of cultivated plants in the tropics (No. 118). Food & Agriculture Organisation of the United Nations, Rome.

Roubik, D.W. 2002. Tropical agriculture: The value of bees to the coffee harvest. Nature, 417(6890): 708.

Roubik, D.W., Sihag, R.C., Kevan, P.G., Garibaldi, L.A., Cunningham, S.A., Aizen, M.A., Packer, L., Harder, L.D., Krell, R., Biddinger, D.J. and Rajotte, E.G. 2018. The pollination of cultivated plants: A compendium for practitioners. Vol 1. Food and Agriculture Organization of the United Nations, Rome.

Santos, A., Fernandes, M.R., Aguiar, F.C., Branco, M.R. and Ferreira, M.T. 2018. Effects of riverine landscape changes on pollination services: A case study on the River Minho, Portugal. Ecological Indicators, 89: 656-666.

Sparovek, G., Ranieri S. B. L., Gassner, A., De Maria, I.C., Schnug, E., dos Santos, R.F. and Joubert, A. 2002. A conceptual framework for the definition of the optimal width of riparian forests. Agriculture, Ecosystems & Environment, 90(2): 169-175.

Sunil, C., Somashekar, R. K. and Nagaraja, B. C. 2010. Riparian vegetation assessment of Cauvery River basin of South India. Environmental Monitoring and Assessment 170(1-4): 545-553.

Sunil, C., Somashekar, R.K. and Nagaraja, B.C. 2011. Impact of anthropogenic disturbances on riparian forest ecology and ecosystem services in Southern India. International Journal of Biodiversity Science, Ecosystem Services & Management, 7(4): 273-282.

Sunil, C., Somashekar, R.K. and Nagaraja, B.C. 2016. Diversity and composition of riparian vegetation across forest and agroecosystem landscapes of river Cauvery, southern India. Tropical Ecology, 57(2): 343-354.

Westphal, C., Bommarco, R., Carre, G., Lamborn, E., Morison, N., Petanidou, T., Potts, S. G., Roberts, S.P., Szentgyorgyi, H., Tscheulin, T. and Vaissiere, B.E. 2008. Measuring bee diversity in different European habitats and biogeographical regions. Ecological Monographs, 78(4): 653-671.

Winfree, R. and Kremen, C. 2009. Are ecosystem services stabilized by differences among species? A test using crop pollination. Proceedings of the Royal Society B: Biological Sciences, 276(1655): 229-237.

Original Research Paper

Open Access Journal

Experimental Study on the Permeability and Microstructure of Remoulded Silty Clay Corroded by Landfill Leachate

Chaofeng Wang*, Haijun Lu*(**)†, Dinggang Li* and Jixiang Li*

* School of Civil Engineering and Architecture, Wuhan Polytechnic University, Wuhan 430023, China
** State Key Laboratory of Geomechanics and Geotechnical Engineering, Institute of Rock and Soil Mechanics, Chinese Academy of Sciences, Wuhan 430071, China
†Corresponding authors: Haijun Lu; lhj@whpu.edu.cn

ABSTRACT

This paper explores the macroscopic permeability characteristics, pore distribution, mineral composition, and microstructure changes in remoulded silty clay under different concentrations and different back pressures through flexible-wall triaxial permeability tests, nuclear magnetic resonance tests, X-ray diffraction tests, and scanning electron microscope tests. The results of the flexible-wall triaxial permeability tests indicate that the hydraulic conductivity of the landfill leachate with different concentrations increases to the peak value in 108-132 h period and then decreases to a stable value in 252–264 h period under the action of different back pressures. The nuclear magnetic resonance tests show that the pore distribution of the remoulded silty clay is macropore after it is corroded by the leachate. Increasing the concentration of landfill leachate and reducing the back pressures can reduce the overall development effect of pores. The X-ray diffraction tests show that the weakly acidic corrosive environment provided by remoulded silty clay and landfill leachate reduce respectively the contents of montmorillonite, muscovite, and illite by 33.52 %, 23.57 % and 63.51 %, while kaolinite and albite increase by 283.40 % and 188.64 %. Finally, scanning electron microscope tests show that the corrosion of landfill leachate and the plugging of organic pollutants in the infiltration process reduce the apparent pore ratio of the microstructure of remoulded silty clay and the hydraulic conductivity gradually decreases.

INTRODUCTION

Currently, compacted clay is widely used as an impervious material for landfills in China. Its permeability is key, and it must comply with the requirements of the Chinese code which states that the hydraulic conductivity should not be greater than 1.0×10^{-7} cm/s (CJJ176-2012). The leachate produced by the landfill site has complex components, high dissolved concentrations of heavy metal ions and various other ions, and it contains aromatic hydrocarbons and other industrial organic compounds (Kjeldsen et al. 2002). When leakage occurs, the leachate corrodes the impermeable layer at the bottom of the landfill site, changes the microstructure of the clay layer at the bottom, destroys the stability of the impermeable layer, and can lead to serious pollution of surface water and groundwater.

In recent years, there have been numerous experimental explorations and theoretical results on the macroscopic characteristics and microstructure of clay. Some scholars explored the changes in the conventional parameters of pollutants and the relationship between the mechanical properties and the

microstructure of compacted clay after the landfill leachate eroded, which can help evaluate the applicability of liner materials. The possibility of high concentration leachate blocking compacted clay was simulated. Combined with SEM photos, it is shown that the compacted clay has hydraulic blockage under leachate erosion (Li et al. 2013, Zhao et al. 2016, Met & Akgün 2015, Zhan et al. 2017, Razakamanantsoa & Djeran-Maigre 2016, Safari & Valizadeh 2017). Researchers have investigated the effects of bentonite, lime, zeolite, and other materials as well as ion concentration and valence on clay permeability (Dontsova & Norton 2015, Roth & Pavan 1991, Zhou et al. 2015, Varank et al. 2011, Li et al. 2008). The permeability characteristics of original clay, recomposed clay and improved clay are explored, and a more suitable calculation expression for consolidation hydraulic conductivity of remoulded clay is calculated, which has important guiding significance for practical engineering (Gu et al. 2003). Although there have been many research works on the erosion of compacted clay using the landfill leachate, there are few studies on the relationship between the mineral composition, pore distribution, microstructure

changes, and macroscopic permeability characteristics of the remoulded silty clay by landfill leachate corrosion; therefore, the correlation needs to be further explored.

To study the relationship between the macro permeability and microstructure of remoulded silty clay corroded by landfill leachate, this paper analyses the change of hydraulic conductivity curve of remoulded silty clay through flexible-wall triaxial permeability tests. Then, through nuclear magnetic resonance (NMR) tests, X-ray diffraction (XRD) tests, and scanning electron microscope (SEM) tests, pore distribution, mineral composition, and microstructure changes in the remoulded silty clay were respectively studied. Finally, the macro permeability characteristics and microstructure changes in remoulded silty clay corroded by landfill leachate were analysed to illustrate the relationship between them.

MATERIALS AND METHODS

Materials

The buried depth of the soil used for the test is about 2 m, which is taken from a construction site in Huangpi District, Wuhan, China, and it is utilized for independent sealed storage. Its basic physical characteristics are provided in Table 1, and its basic chemical and mineral composition are listed in Table 2. Fresh landfill leachate used in the test was obtained from the Chenjiachong Landfill Site in Xinzhou District of Wuhan City, with a concentration of 100 %. Its basic physical and chemical characteristics are summarized in Table 3. 1 L and 5 L distilled water was added to each litre of fresh landfill leachate to prepare 50 % and 16.7 % landfill leachate for the tests.

Methods

Flexible-wall triaxial permeability tests: These tests are carried out according to the standard ASTM D5084-2010. The instrument adopts the PN3230M environmental geotechnical flexible wall permeameter (triple type) manufactured by GEOEQUIP. It adopts the cell pressure of 350 kPa, and back pressures of 100, 200, and 300 kPa. The cylindrical soil sample with a diameter of 50 mm and a height of 100 mm is corroded by landfill leachate with concentrations of 100 %, 50 %, and 16.7 %, and the variation rule of the hydraulic conductivity of each layer is observed and obtained. According to the standards (ASTM D5084-2010, SL237-1999), the hydraulic conductivity is calculated by:

$$K = \frac{QL\rho}{10At \cdot \Delta P} \qquad \ldots(1)$$

Where, k is the hydraulic conductivity, cm/s; Q is the amount of water seepage in penetration time t, ml; L is the

Table 1: Basic physical characteristics of remoulded silty clay used in the tests.

Optimum water content (%)	Maximum dry density (g·cm^{-3})	Liquid limit (%)	Plastic limit (%)	Plasticity index	Porosity ratio	Specific gravity (g·cm^{-3})
18.5	1.71	34.4	18.8	15.6	0.36	2.65

Table 2: Basic chemical and mineral composition of remoulded silty clay used in the tests.

pH	Soluble salt (%)	Organic matter (%)	Mineral composition (%)					
			Quartz	Montmorillonite	Kaolinite	Albite	Muscovite	Illite
5.5	0.6	1.8	23.41	20.94	4.76	6.69	21.09	23.10

Table 3: Basic chemical characteristics of landfill leachate.

Contaminants	Parameter values (mg·L^{-1})	Determination method	Contaminants	Parameter values (mg·L^{-1})	Determination method
pH	6.1	GB/T 6920-86	COD	4107	HJ/T 399-2007
DO	3.7	GB/T 7489-87	TOC	692.5	HJ 501-2009
N-NO$_3$	16.57	HJ/T 346-2007	SO$_4^{2-}$	5.8	GB/T 13196-91
N-NO$_2$	0.50	HJ/T 197-2005	Cl$^-$	2022.9	GB/T 11896-89
N-NH^{4+}	2779.9	HJ 666-2013	Na$^+$	1855.6	GB/T 11903.89
P-PO$_4$	21.2	HJ 669-2013	Zn	276	GB 7472-1987
TP	25.5	HJ 671-2013	Cu	891	HJ 485-2009
BOD$_5$	1457.1	HJ 505-2009	Ni	370	GB 11912-1989

height of the sample, cm; ρ is the solution density, g/cm^3; A is the cross-sectional area of the sample, cm^2; and ΔP is the backpressure, kPa.

Nuclear magnetic resonance (NMR) tests: The NMR apparatus model was PQ-001 Mini NMR (Shanghai Niumai Electronic Technology Co. Ltd.). The magnetic field strength was 0.5±0.08 T and the operational test area was 60 mm × 60 mm. To generate a stable and uniform magnetic field, the temperature of the magnet unit was set to $32 \pm 0.01°C$, and a polytetrafluoroethylene ring cutter that has a diameter of 45 mm and a height of 20 mm was used for sample preparation. First, three layers of cylindrical soil samples were cut from the bottom to the top at 0-20 mm, 40-60 mm, and 80-100 mm, respectively, after the flexible-wall triaxial permeability tests. Then, the central soil samples of each layer were collected by polytetrafluoroethylene ring cutters for NMR tests. Finally, the transverse relaxation time T_2 is provided by the Carr–Purcell-Meiboom-Gill (CPMG) sequence and the pore distribution of the remoulded silty clay is obtained.

T_2 can be expressed by the T_2 surface relaxivity ρ_2, S/V that is the ratio of the pore surface area S to the pore water volume V and pore radius R as:

$$\frac{1}{T_2} \approx \rho_2 \left(\frac{S}{V}\right)_{pore} = \rho_2 \frac{2}{R} \qquad …(2)$$

Further, Eq. (2) is simplified as:

$$T_2 = a \cdot R \qquad …(3)$$

In the formula, the value of a is a constant, which is 2.25 ms/μm. According to Eq. (3), pore distribution can be set up according to the T_2 distribution curves (Tian et al. 2013, Li et al. 2008).

X-ray diffraction (XRD) tests: According to the Chinese code (SY/T 5163-2010), under the condition of 50°C, the lower soil samples (0-20 mm) with various concentrations of corrosion are dried to constant quality and then ground into powder by mortar. After passing through a 200-mesh sieve, the samples are diffracted by an X-ray diffractometer with the model of EMPYREAN at a speed of 4°/min (2θ) and a diffraction angle of 5-85° (2θ).

Scanning electron microscopy (SEM) tests: In the tests, an SEM model S-3000 N was used. First, the lower soil samples (0-20 mm) with various concentrations of corrosion are placed at 105°C and dried until the quality is constant to prevent the moisture in the soil samples from affecting the display of scanning images. Then, the soil with a size of about 1 cm × 1 cm × 1 cm is selected and placed in the vacuum. Finally, the magnification of the SEM is adjusted to 2,000 times. Scanning photographs are taken and images analysis is performed.

RESULTS AND DISCUSSION

Permeability characteristics: The hydraulic conductivity curves of different concentrations of leachate corrosion remoulded silty clay under different back pressures are shown in Figs. 1-3, all of which meet the requirements of the Chinese code that it should not be more than 1.0×10^{-7} cm/s (CJJ176-2012). With different landfill leachate concentrations and different back pressures, the hydraulic conductivity curve shows the phenomenon of first increasing to the peak value and then decreasing to a stable value with time. For the same concentration of the leachate, the larger the back pressure at the same time, the greater is the hydraulic con-
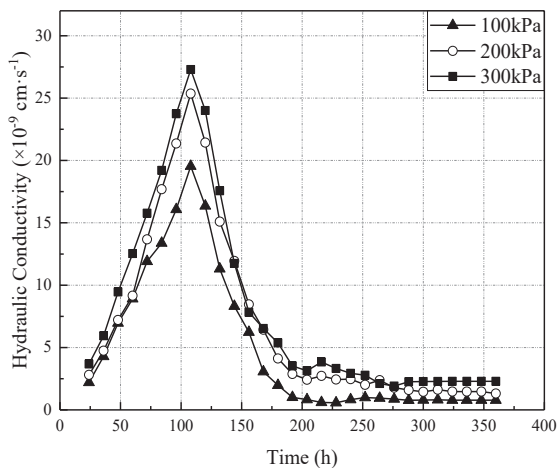

Fig. 1: Hydraulic conductivity curves of 100% landfill leachate corrode remoulded silty clay under different back pressures.
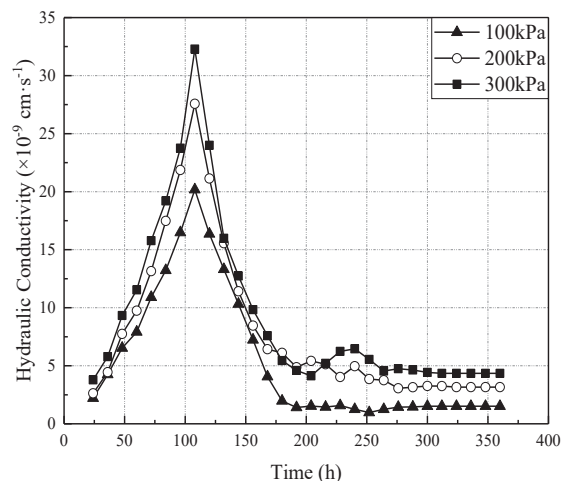

Fig. 2: Hydraulic conductivity curves of 50% landfill leachate corrode remoulded silty clay under different back pressures.
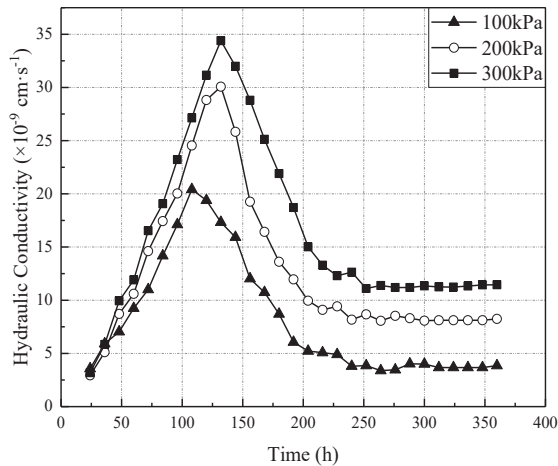
Fig. 3: Hydraulic conductivity curves of 16.7% landfill leachate corrode
remoulded silty clay under different back pressures.

Fig. 4: Pore distribution curve of remoulded silty clay corroded by
100% landfill leachate under 100 kPa back pressure.

ductivity. The leachate concentration is different; however, the time for the hydraulic conductivity to reach the peak value is between 108 and 132 h, and the time for reaching the stable value is between 252 and 264 h. With the same back pressure at different concentrations, the more dilute the concentration, the longer is the increase in the time of hydraulic conductivity and shorter is the time to reach the stable value; the peak value and stable value are also higher.

When the concentration is 100 %, 50 % and 16.7 %, the peak value and stable value of hydraulic conductivity are respectively in the range of 19.54-20.42×10^{-9} cm/s and 0.78-3.67×10^{-9} cm/s under the action of 100 kPa back pressure; under the action of 200 kPa back pressure, the peak value and stable value of hydraulic conductivity are in the range of 25.36-30.07×10^{-9} cm/s and 1.47-8.11×10^{-9} cm/s, respectively; under 300 kPa back pressure, the peak value and stable value of hydraulic conductivity is respectively in the range of 27.14-32.29×10^{-9} cm/s and 2.29-11.29×10^{-9} cm/s.

The hydraulic conductivity curves show an upward trend at first, which may be explained by the fact that the sample is not completely saturated when the vacuum saturation procedure is adopted, and the hydraulic conductivity is related to the saturation. When the test is started, the bubble and the soil particles move relatively slowly, and the liquid flows around the soil particles through the bubble (Liang & Liu 2012). Therefore, when the soil column is initially pressurized, the leachate can quickly pass through the soil sample, and the hydraulic conductivity curves show an up-ward tendency. After 100 h, there is almost no air in the soil column, and it is almost completely saturated. The applied cell pressure consolidates the soil column. Simultaneously, the effective pores of the soil column are gradually reduced
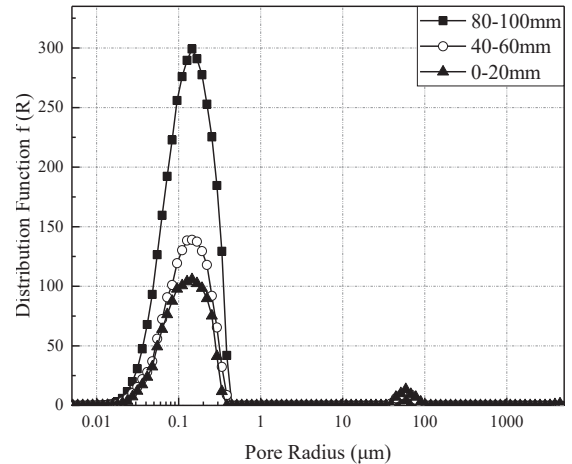
by the leachate. Anaerobic microorganisms metabolize inside the soil sample to form biofilms and inorganic precipitates. Thus, this increases the permeability difficulty and decreases the hydraulic conductivity curve (Zhang et al. 2012).

Pore distribution: The pore distribution of the remoulded silty clay can be obtained according to the T_2 distribution curve of the saturated soil samples. As showing in Figs. 4-6, under the different back pressures, the pore distribution curves of each layer of remoulded silty clay after being cor-roded by the leachate of different concentrations have two peaks, according to International Union of Pure and Applied Chemistry (IUPAC) standard, which are mainly distributed in the range of 0.01-1.03 μm (peak 1) and 14.55-89.30 μm (peak 2). This indicates that the pore distribution characteristics of each layer of remoulded silty clay are macropores. Under the 100 kPa back pressure, the total pore volume distribution of remoulded silty clay corroded by 100 % leachate is 24.48 % less than that of 50 % leachate corrosion, and the total pore volume distribution of 50 % leachate and 100 kPa back pressure is 34.65 % less than that of 16.7 % leachate and 300 kPa back pressure. This shows that increasing the landfill leachate concentration and reducing back pressure can reduce the overall pore volume distribution and the development effect of the overall pore structure.

Under the same back pressure, the pore volume of the bound water corresponding to peak 1 increases gradually and the pore volume of the free water corresponding to peak 2 decreases gradually in the remoulded silty clay layer from the bottom to the top with the same concentration. Under 100 kPa back pressure, when the landfill leachate concentration is 100 % and 50 %, the pore volume distribution of the bound water in the remoulded silty clay from the bottom to the top

increases by 220.92 % and 107.60 %, respectively, and the pore volume distribution of the free water decreases by 68.90 % and 71.46 %, respectively.

When the landfill leachate concentration is 16.7 %, the pore volume distribution of bound water increases by 85.00 % and that of free water decreases by 80.21 % under 300 kPa back pressure. Therefore, the volume distribution of bound water pores in the lower soil sample is less than that in the upper layer, and the volume distribution of free water pores is more than that in the upper layer. This is due to the infiltration process of the landfill leachate from the bottom to the top. On the one hand, the lower soil sample first passes through the landfill leachate, and the corrosion effect of internal pores in the lower layer is more serious than that in the upper layer, resulting in more free water pores in the lower layer than that in the upper layer. On the other hand, the activities of organic pollutants and anaerobic microorganisms in landfill leachate will first block the bound water pores in the lower layer, resulting in a decrease in the bound water pores in the lower layer, which also explains the phenomenon that the hydraulic conductivity curve increases first and then decreases from the microscopic pore distribution.

Mineral composition and microstructure: To explore the difference in the mineral composition and microstructure of remoulded silty clay after being corroded by the leachate of different concentrations, the NMR test results show that the pore changes in the lower layer of the remoulded silty clay are the most obvious under the corrosion of landfill leachate. Therefore, it is considered to select a representative lower layer remoulded silty clay for XRD and SEM tests, and the XRD curves obtained

are shown in Fig. 7; the mineral composition changes are illustrated in Fig. 8; and the SEM scanning images of 2000 times are shown in Fig. 9.

The main mineral composition of the lower remoulded silty clay corroded by the leachate of different concentrations is similar, which comprises quartz, montmorillonite, kaolinite, albite, muscovite and illite. Before and after the leachate of different concentrations was corroded, the content of quartz did not change, which accounts for 23.41-23.97 %. When the leachate concentration is 100 %, the content of each mineral component decreases or increases most obviously. The contents of montmorillonite, muscovite, and illite decrease by 33.52 %, 23.57 %, and 63.51 %, respectively, while those of kaolinite and albite increase by 283.40 % and 188.64 %, respectively. This is because the soil sample comes from the near-surface soil, and the montmorillonite is formed in an alkaline environment, with strong adsorption capacity and cation exchange capacity. When the pH value of the remoulded silty clay is 5.5 and the pH value of landfill leachate is 6.1, the permeability test is in a weak acidic environment, the montmorillonite content is reduced, and illite also releases K^+ ions into the solution resulting in a decrease in content (Tucker 1964); aluminosilicate gradually converts into kaolinite in an acidic environment. The K^+ migration generated by the dissolution of aluminosilicates such as feldspar is faster than that generated by dissolution, and it cannot reach the K^+ concentration value required to generate illite. The acidic solution provided by flexible-wall triaxial permeability tests is more favourable for the dissolution of associated kaolinite by aluminosilicates, and kaolinite has a relatively weak adhesion. The migration will occur during the infiltration process to block the channels connected be-
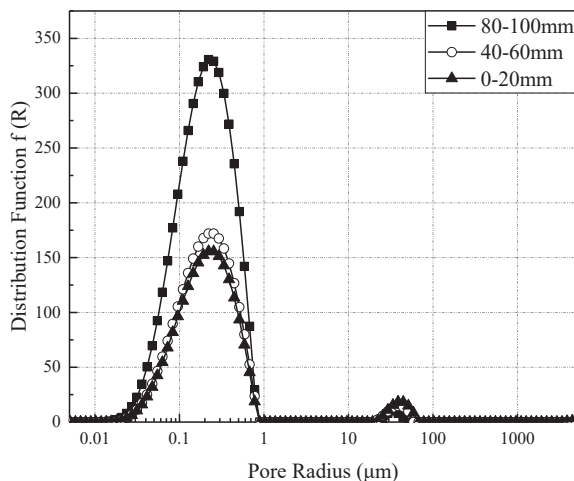

Fig. 5: Pore distribution curve of remoulded silty clay corroded by 50% landfill leachate under 100 kPa back pressure.
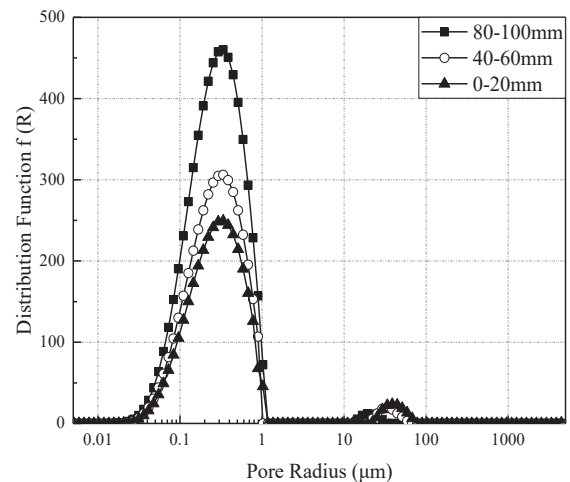

Fig. 6: Pore distribution curve of remoulded silty clay corroded by 16.7% landfill leachate under 300 kPa back pressure.
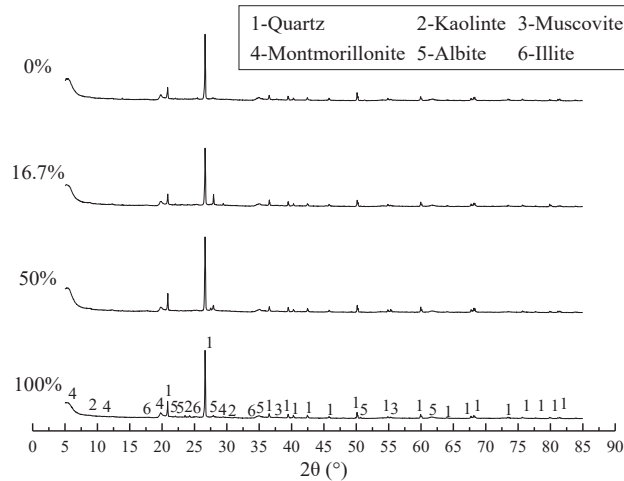
Fig. 7: XRD curves of lower remoulded silty clay corroded by different concentrations of landfill leachate.
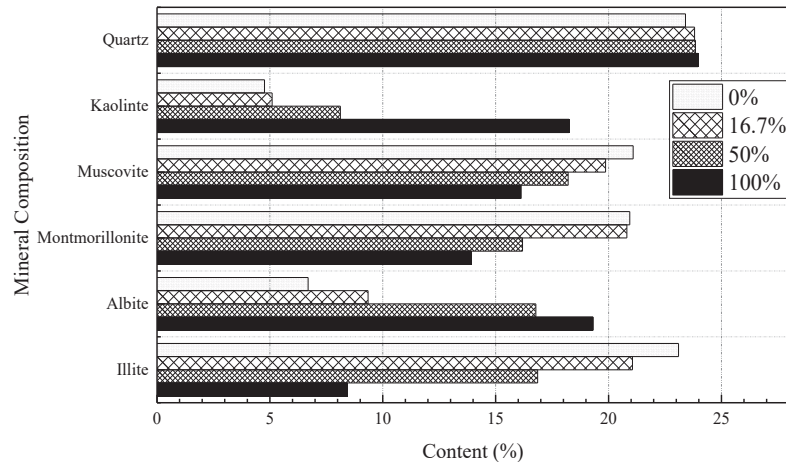

Fig. 8: Mineral composition changes in lower remoulded silty clay corroded by landfill leachate of different concentrations.

tween pores, which will lead to a decrease in the hydraulic conductivity (Jin et al. 2018).

Lower remoulded silty clay originally had irregular lamellar structure after being corroded by the landfill leachate of different concentrations. It showed irregular honeycomb and structural aggregates. According to XRD and SEM test results, the formation of aggregates in the SEM images is a product of the cementation of organic pollutants in the landfill leachate and soil particles, in the form of edge-to-face combination. With an increase in the infiltration time, the macropores in remoulded silty clay gradually change into micropores and the apparent void ratio gradually decreases, which can well explain the phenomenon that the hydraulic conductivity curve shows a gradual decreasing trend. The higher the concentration of landfill leachate, the

more intense is the corrosion of the remoulded silty clay. The phenomenon of cementation and agglomeration is obvious. The soil particles aggregate tightly, and the number of loose micro-particles reduces. The irregular honeycomb is obvious in SEM images, and the hydraulic conductivity decreases.

CONCLUSIONS

To study the permeability characteristics and microstructure changes of remoulded silty clay caused by landfill leachate corrosion, this paper analysed the permeability characteristics of remoulded silty clay based on flexible-wall triaxial permeability tests. Based on NMR, XRD, and SEM tests, pore distribution, mineral composition, and microstructure changes of remoulded silty clay were studied, and the following conclusions were drawn:

(a) 0 %
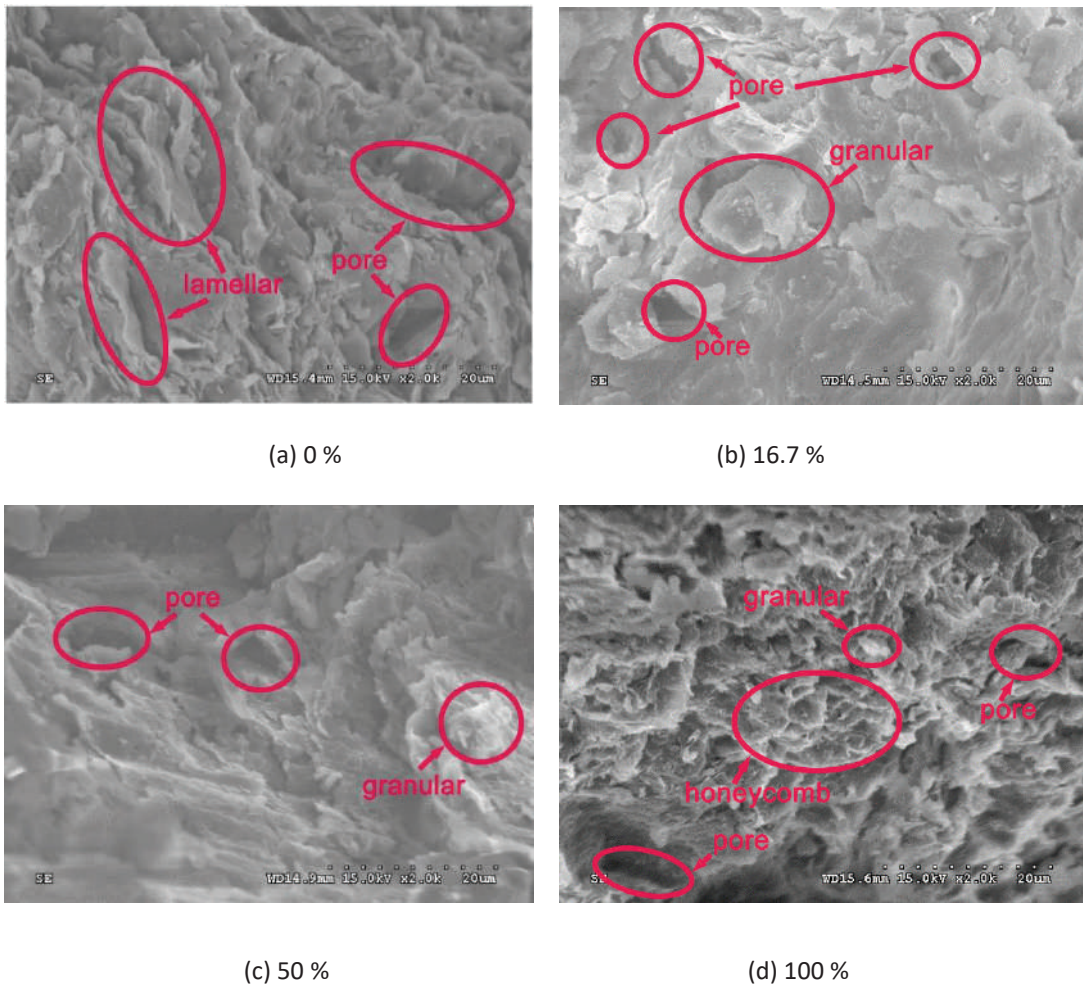

(b) 16.7 %

(c) 50 %

(d) 100 %

Fig. 9: SEM images (magnified 2000 times) of lower remoulded silty clay corroded by different concentrations of landfill leachate.

1. The saturated hydraulic conductivity of remolded silty clay measured by flexible-wall triaxial permeability tests is not more than 1.0×10^{-7} cm/s, which shows the phenomenon of increasing the peak value and then decreasing it to a stable value. The value of the hydraulic conductivity is related to the back pressure and the concentration of the landfill leachate. The larger the back pressure and the smaller the concentration, the larger is the value of hydraulic conductivity.

2. The pore size of the remoulded silty clay corroded by the leachate is distributed in the range of 0.01-1.03 μm and 14.55-89.30 μm. The pore distribution is macropores, and the pore volume of the bound water in the remoulded silty clay increases gradually from the bottom to the top, while the pore volume of the free water decreases slightly. The concentration of the landfill leachate increases and the back pressure reduces, and the overall pore volume distribution decreases.

3. The main mineral composition of the lower remoulded silty clay after the leachate of different concentrations is basically unchanged, with quartz accounting for the largest percentage, and the content remains unchanged before and after corrosion. When the leachate concentration is 100 %, the change of each mineral composition is the most obvious, with the contents of montmorillonite, muscovite, and illite decreasing while kaolinite and albite increasing. During the process that the landfill leachate corrodes the remoulded silty clay, while the mineral composition changes, the soil particles will be cemented into irregular aggregates, the leachate concentration increases, the aggregates become more compact, and the hydraulic conductivity gradually decreases.

ACKNOWLEDGEMENTS

REFERENCES

ASTM D5084 (American Society for Testing and materials) 2010. Standard test methods for measurement of hydraulic conductivity of saturated porous materials using a flexible wall permeameter. Annual Book of ASTM Standards.

CJJ176 2012. Ministry of Building and Construction, P.R. China 2012. Technical code for geotechnical engineering of municipal solid waste sanitary landfill (CJJ176-2012), Beijing, (in Chinese).

Dontsova, K.M. and Norton, L.D. 2015. Clay dispersion, infiltration, and erosion as influenced by exchangeable Ca and Mg. Soil Science, 167(3): 184-193.

Gu, Z.W., Sun, B.N. and Dong, Y.N. 2003. Testing study of permeability of the original clay, recomposed clay and improved clay with stabilizer zdyt-1. Chinese Journal of Rock Mechanics and Engineering, 22(3): 505-508.

Jin, P.P., Ou, C.H., Ma, Z.G., Li, D. Ren, Y.J. and Zhao, Y.F. 2018. Evolution of montmorillonite and its related clay minerals and their effects on shale gas development. Geophysical Prospecting for Petroleum, 57(3): 344-355.

Kjeldsen, P., Barlaz, M.A., Rooker, A.P., Baun, A., Ledin, A. and Christensen, T.H. 2002. Present and long-term composition of MSW landfill leachate: a review. Critical Reviews in Environmental Science and Technology, 32(4): 297-336.

Li, H.B., Zhu, J.Y. and Guo, H.K. 2008. Methods for calculating pore radius distribution in rock from NMR T2 spectra. Chinese Journal of Magnetic Resonance, 25(2): 273-280.

Li, J.S., Xue, Q., Wang, P. and Liu, L. 2013. Influence of leachate pollution on mechanical properties of compacted clay: A case study on behaviors and mechanisms. Engineering Geology, 167: 128-133.

Liang, A.M. and Liu, X. 2012. Testing study on permeability characteristics of unsaturated soil. Journal of Jinggangshan University (Natural Science), 33(2): 76-79, 87.

Met, İ. and Akgün, H. 2015. Geotechnical evaluation of Ankara clay as a compacted clay liner. Environmental Earth Sciences, 74(4): 2991-3006.

Razakamanantsoa, A. R. and Djeran-Maigre, I. 2016. Long term chemo-hydro-mechanical behavior of compacted soil bentonite polymer complex submitted to synthetic leachate. Waste Management, 53: 92-104.

Roth, C. H. and Pavan, M. A. 1991. Effects of lime and gypsum on clay dispersion and infiltration in samples of a Brazilian Oxisol. Geoderma, 48(3-4): 351-361.

Safari, E. and Valizadeh, R. 2017. Analysis of biological clogging potential in a simulated compacted clay liner subjected to high-strength leachate infiltration. International Journal of Environmental Science and Technology, 15(5): 1029-1038.

SL237 1999. Ministry of Water Resources, P.R. China 1999. Specification of soil test (SL237-1999), Beijing, (in Chinese).

SY/T 5163-2010. National Energy Administration, P.R. China 2010. Analysis method for clay minerals and ordinary non-clay minerals in sedimentary rocks by the X-ray diffraction (SY/T 5163-2010), Beijing, (in Chinese).

Tian, H., Wei, C., Wei, H., Yan, R. and Chen, P. 2013. An NMR-based analysis of soil-water characteristics. Applied Magnetic Resonance, 45(1): 49-61.

Tucker, BM. 1964. The solubility of potassium from soil illites. I. the dependence of solubility on pH. Soil Research, 2(1): 56-66.

Varank, G., Demir, A., Top, S., Sekman, E., Akkaya, E., Yetilmezsoy, K. and Bilgili, M. S. 2011. Migration behavior of landfill leachate contaminants through alternative composite liners. Science of the Total Environment, 409(17): 3183-3196.

Zhan, L.T., Xu, H., Chen, Y.M., Lü, F., Lan, J.W., Shao, L.M., Lin, W.A. and He, P.J. 2017. Biochemical, hydrological and mechanical behaviors of high food waste content MSW landfill: preliminary findings from a large-scale experiment. Waste Management, 63: 27-40.

Zhang, H.Y., Yang, B., Gao, Q.Q. and Zhang, G.W. 2012. Permeability and heavy metal retardation of sewage sludge barrier. Rock and Soil Mechanics, 33(10): 2910-2916.

Zhao, Y., Xue, Q., Huang, F., Hu, X. and Li, J. 2016. Experimental study on the microstructure and mechanical behaviors of leachate-polluted compacted clay. Environmental Earth Sciences, 75(12): 1006.

Zhou, C., Fan, X., Ning, Z., Li, P., Liu, C., Yang, P., Liu, Y., Shi, Z. and Li, Y. 2015. Reducing riverbed infiltration using mixtures of sodium bentonite and clay. Environmental Earth Sciences, 74(4): 3089-3098.

Analysis of Air Quality Characteristics Based on Information Diffusion Technology in Beijing, China

He ji*, Chen Haitao*†, Duan Chunqing**, Chen Xiaonan*** and Wang Wenchuan*

*School of Water Resources, North China University of Water Resources and Electric Power, Zhengzhou City Henan Province, 450045, PR China
**Beijing Water Affairs Center for Suburbs, Haidian District Beijing, 100073, PR China
***Construction and Administration Bureau of South-to-North Water Diversion Middle Route Project, Haidian District Beijing, 100038, PR China
†Corresponding Author: Chen Haitao; zzchenhaitao@126.com

ABSTRACT

To study the characteristics of air quality and the relationship between air quality and weather factors, based on daily meteorological data from 2016 to 2019 in Beijing using information diffusion technology, the probability distribution of air quality index in different seasons and the development trend of air quality have been studied, and the relationship between weather factors and air quality discussed. The results show that: 1) According to the air quality, the order of the four seasons is summer, spring, autumn and winter. In summer, the frequency of moderate air pollution and above is about 2.54%, and the frequency of serious air pollution is about 0%. In winter, the frequency of moderate air pollution and above is 17.83%, and the frequency of serious air pollution is 2.93%. 2) The air quality of Beijing has been improving in recent years, which shows that with the strengthening of air pollution control efforts, certain results have been achieved. 3) Quantitative analysis of the relationship between winter air quality index and temperature and wind in Beijing shows that the degree of air pollution in winter increases with the increase of temperature and decreases with the increase of wind force. The frequency of mild air pollution and above is about 8.91% when the daily maximum temperature is below 0°C and 48.78% when the daily maximum temperature is above 9°C. The frequency of mild air pollution and above is about 45.17% when the daily maximum wind force is level 0, and 20.89% when the daily maximum wind force is level 3 and above. Examples show that the information diffusion technology can make full use of the location information of the sample points by transforming the traditional sample data points into fuzzy sets, and achieves good results in frequency statistics and trend fitting. The model established in this paper has the value of popularization and application.

INTRODUCTION

People all over the world have suffered or are suffering from the haze, including China, the United States, Germany, Japan and so on. Haze pollution has become an important threat to the global environment. Along with the rapid development of economy in China, air pollution problems arise and lead to frequent haze in different degrees, which not only affects people's lives and health but also makes the environmental problems more and more serious in the future.

Air pollution and haze weather do great harm to human beings. Air pollution directly leads to a significant increase in the incidence of respiratory diseases, affecting physical and mental health. Haze pollution leads to reduced visibility, increased traffic accidents, affecting daily activities such as travel. Haze causes serious losses to agricultural production, aquaculture production and tourism development, and affects ecosystems.

In the autumn and winter of 2016, China's air pollution became more serious. The haze pollution problem extended from some areas to all parts of the country, covering 25 provinces. More than 100 large and medium-sized cities had haze weather of varying degrees, which not only affected the sea, land and air traffic conditions but also caused direct harm to people's physical and mental health. As the capital of China, Beijing is the political, cultural and economic centre of the whole country. However, in recent years, haze weather has occurred frequently. It is necessary to analyse the characteristics of air quality in-depth, which can provide a decision-making basis for the prediction and prevention of haze pollution weather.

The London smog event in Britain and the Los Angeles photochemical smog event in the United States appeared earlier than the haze weather in China and were the first to suffer from haze pollution. The results show that sulphur oxides and dust produced by coal combustion in the process

of industrial development were the direct causes of London smog events, and the accumulation of air pollutants with time due to the existence of inversion layer was the indirect cause (Davis et al. 2002). Primary pollutants from motor vehicles and chemical plants and secondary pollutants from photochemistry caused photochemical smog in Los Angeles, USA (Hinton et al. 2006). Minguillon (2012) used a positive definite matrix to analyse the main components and formation factors of PM2.5 in Switzerland. Through a comparative study of PM10 in residential and industrial areas in Calcutta, India, Chalouolakou et al. (2003) found that soot and motor vehicle emissions had the greatest impact on haze pollution in the region. With the continuous occurrence of haze weather in China, many Chinese scholars have conducted in-depth studies on the weather characteristics during the occurrence of haze. Wang (2011) found that the sharp increase of PM2.5 concentration in Beijing in 2008 was due to the slow movement of atmospheric clouds, which made the air unable to circulate rapidly, and the accumulation of atmospheric pollutants caused haze pollution. Wang (2002) studied the distribution and evolution of visibility in Beijing under haze pollution. Jiang et al. (2017) studied the meteorological factors of haze weather with the worst visibility in Zhengzhou City. The results showed that the meteorological conditions during haze pollution were low-level wind, relatively stable atmospheric structure and low-level inversion layer. Qian et al. (2006) analysed the time distribution characteristics of fog and haze weather in Guangdong Province, and found that the visibility of fog and haze weather is different from seasonal variation.

There are also many studies on haze prediction. Jian et al. (2012) used the autoregressive integral moving average model to predict the PM10 concentration in heavy traffic areas of Hangzhou, China. Dong et al. (2009) proposed a hidden Markov model to predict high PM2.5 concentration in haze-polluted weather. Li (2017) predicted PM2.5 concentration by multivariate statistical methods. Su et al. (2008) established a haze prediction model based on the Chi-square test and BP neural network. Mishra et al. (2015) combined with neural network and fuzzy logic regression to predict PM2.5 concentration in haze weather in India.

For a long time, many scholars have done many studies on the causes, hazards and control of haze, and have achieved rich results. At present, there are many characteristic analysis models of haze, such as regression, statistics and neural networks and so on. When there are contradictory samples or small samples in data processing, the effect of traditional methods is unsatisfactory. Information diffusion technology is a data processing method rising in recent years. By transforming data points into fuzzy sets, the location information of samples can be fully utilized, especially for data analysis

under incomplete conditions of samples (Huang 2018, Chen 2012). Regional air quality data are usually short in length and not abundant in quantity. The non-linear relationship regression and stable probability distribution among factors can be well realized by using information diffusion technology.

Taking Beijing as a typical research area and air quality index as research index, this paper uses information diffusion technology to analyse the evolution characteristics of air quality in different seasons in Beijing, calculates the probability distribution of haze occurrence in different seasons, and studies the evolution trend of air quality and air quality in recent years. To provide a scientific basis for prevention, early warning and control of local air pollution, the relationship between air pollution and temperature, wind force factors is discussed.

DATA AND METHODS

Survey of Research Area

Beijing is the capital of China, located in the northwest end of the North China Plain, adjacent to Tianjin in the east, surrounded by Hebei Province in the west, south and north. The total area of the city is about 16410 km^2, of which the mountainous area accounts for about 60% and the plain area accounts for about 40%. Beijing has 16 districts under its jurisdiction, of which 6 are in the urban area, namely Dongcheng District, Xicheng District, Haidian District, Fengtai District, Chaoyang District and Shijingshan District. There are 10 suburban districts, including Yanqing District, Huairou District, Miyun District, Changping District, Shunyi District, Pinggu District, Mentougou District, Tongzhou District, Fangshan District and Daxing District (Fig. 1). The climate in Beijing is a typical warm temperate humid continental monsoon climate. The seasonal variation of precipitation is great. The precipitation is mostly concentrated in summer and the annual average precipitation is about 585 mm.

Beijing is the political, economic and cultural centre in China, which attracts worldwide attention. However, in recent years, haze weather has frequently appeared. In January 2013, Beijing experienced the most haze intrusion in 59 years. It experienced four haze attacks for 25 days. The maximum PM2.5 index reached 755. According to the air pollution index published by relevant departments, the pollution situation has reached the "serious pollution" level. Since the beginning of winter in 2015, the haze has appeared frequently, lasting for up to two weeks. In December, the "red" warning of fog was issued. Haze has become a common weather condition in Beijing, causing huge adverse effects on the citizens. Although all parties have made great efforts to control the haze, no significant effect has been achieved.

Fig. 1: Sketch of administrative divisions in Beijing.

Data Sources

The assessment of air quality grade is based on the technical regulations of the Environmental Air Quality Index (AQI) (HJ633-2012) in China. Air pollution index is divided into six grades: 0-50, 51-100, 101-150, 151-200, 201-300 and more than 300. The bigger the index and the higher the level, the more serious the pollution is, and the more obvious the impact on human health is.

When the air pollution index belongs to the interval (0, 50], the air quality level is 1, and the air quality is excellent. There is no air pollution. All kinds of people can move normally.

When the air pollution index belongs to the interval (50, 100], the air quality level is 2, and air quality is good. Air quality is acceptable, but some pollutants may have a weak impact on the health of a very small number of abnormally sensitive people. It is suggested that abnormally sensitive people should reduce outdoor activities.

When the air pollution index belongs to the interval (100, 150], the air quality level is 3, and the air quality condition belongs to mild pollution. The symptoms of susceptible people are slightly aggravated, and the irritation symptoms are found in healthy people. It is suggested that children, the elderly people and patients with heart and respiratory diseases should reduce intensive outdoor exercise.

When the air pollution index belongs to the interval (150, 200], the air quality level is 4, and the air quality condition belongs to moderate pollution. The haze will further aggravate the symptoms of susceptible people and may affect the heart and respiratory system of healthy people. It is suggested that patients with diseases should avoid high-intensity outdoor exercise and that the general population should reduce outdoor exercise.

When the air pollution index belongs to the interval (200, 300], the air quality level is 5, and the air quality condition belongs to heavy pollution. The symptoms of patients with heart disease and pulmonary disease are significantly aggravated, exercise tolerance is reduced, and symptoms are common in healthy people. It is suggested that children, the elderly and patients with heart disease and pulmonary disease should stay indoors, stop outdoor exercise, and the general population should reduce outdoor exercise.

When the air pollution index is more than 300, the air quality level is 6, and the air quality is seriously polluted. It is suggested that children, the elderly and patients should stay indoors to avoid physical exhaustion and the general population should avoid outdoor activities.

ANALYSIS MODEL OF AIR QUALITY CHARACTERISTICS BASED ON INFORMATION DIFFUSION TECHNOLOGY

Air Quality Index Frequency Distribution Based on Information Diffusion

Information diffusion is a new way to study function approximation by using the method of fuzzy sets. The advantage of this method is that its estimation accuracy is higher than that of the traditional histogram. In particular, when the overall hypothesis of a given sample is not guaranteed to be correct

and the sample size is small, this new method is very useful to avoid the artificial destruction of the data structure and make full use of the information carried by each knowledge sample point.

Suppose that the discourse domain is U. A single observed sample point can diffuse the information it carries to all the points in the universe according to the following formula:

$$f_i(u_j) = \frac{1}{h\sqrt{2\pi}} \exp\left[-\frac{(x_i - u_j)^2}{2h^2}\right] \qquad \dots(1)$$

Where, h is the information diffusion coefficient, which can be calculated by the maximum value a and minimum value b in the sample and the number of sample points n.

$$h = \begin{cases} 0.8146(b-a), & n = 5; \\ 0.5690(b-a), & n = 6; \\ 0.4560(b-a), & n = 7; \\ 0.3860(b-a), & n = 8; \\ 0.3362(b-a), & n = 9; \\ 0.2986(b-a), & n = 10; \\ 2.6851(b-a)/(n-1), & n \geq 11 \end{cases} \qquad \dots(2)$$

Set,

$$C_i = \sum_{j=1}^{m} f_i(u_j) \qquad \dots(3)$$

The membership function of the corresponding fuzzy subset is:

$$\mu_{x_i}(u_j) = \frac{f_i(u_j)}{C_i} \qquad \dots(4)$$

Where $\mu_{x_i}(u_j)$ is called normalized information diffusion of sample point x_i.

Let,

$$q(u_j) = \sum_{i=1}^{n} \mu_{x_i}(u_j) \qquad \dots(5)$$

$$Q = \sum_{j=1}^{m} q(u_j) \qquad \dots(6)$$

the frequency value of the sample point at u_j is

$$p(u_j) = \frac{q(u_j)}{Q} \qquad \dots(7)$$

Where, $p(u_j)$ is the exceeding probability of u_j.

According to the air quality index data in spring (March to May), summer (June to August), autumn (September to November) and winter (December to January of the following year), the probability distribution of air quality index in each season can be analysed by using the above information diffusion method.

Trend Analysis of Air Quality Based on Information Diffusion Approximate Reasoning

Regression analysis based on information diffusion technology is not only easy to calculate, but also can better reflect the overall trend of the data changes. Without grouping data artificially, it can automatically fit local trend changes and finally get a smooth, fluctuating regression curve.

Approximate reasoning based on information diffusion is a non-linear regression model between two variables. The main steps are as follows:

(1) Suppose that there are L samples $\{(x_1,y_1),(x_2,y_2),\dots,(x_l,y_l)\}$. According to the distribution of sample values, the discrete domains of input variable x and output variable y can be determined respectively $U=\{u_1,u_2\dots,u_s\}$, $V=\{v_1,v_2,\dots,v_r\}$. (x_i,y_i) can be transformed into a fuzzy set according to the following formula:

$$A_i : \mu_{x_i}(u) = \exp\left[-\frac{(u-x_i)^2}{2h_x^2}\right], \quad u \in U \qquad \dots(8)$$

$$B_i : \mu_{y_i}(v) = \exp\left[-\frac{(v-y_i)^2}{2h_y^2}\right], \quad v \in V \qquad \dots(9)$$

Where, h_x and h_y are information diffusion coefficients of input and output samples respectively, calculated according to equation (2).

Table 1: Probability distribution of air quality in each season.

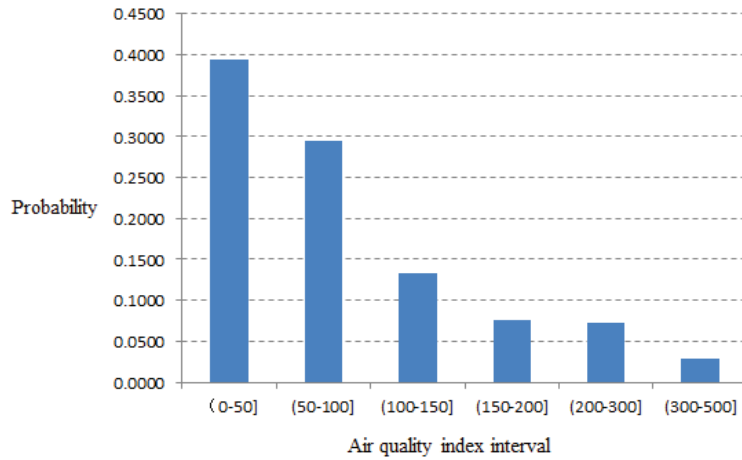| Index interval	Winter	Spring	Summer	Autumn
(0, 50]	0.3933	0.1882	0.2752	0.3669
(50, 100]	0.2952	0.4135	0.5184	0.3171
(100, 150]	0.1332	0.2333	0.1811	0.1901
(150, 200]	0.0757	0.0999	0.0254	0.0637
(200, 300]	0.0733	0.0470	0.0000	0.0586
(300, 500]	0.0293	0.0181	0.0000	0.0037

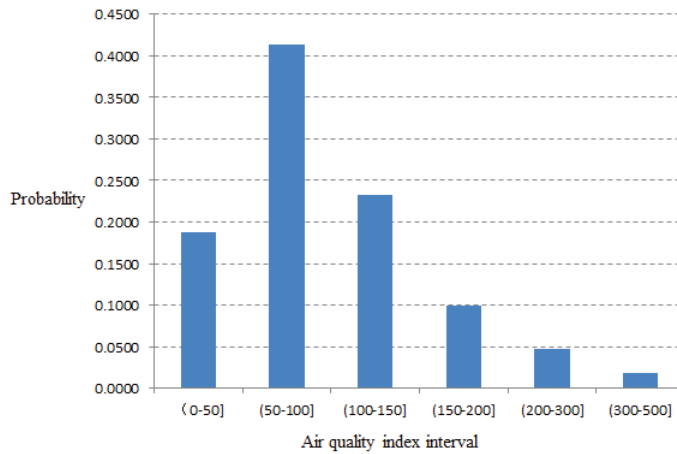Fig. 2: Probability distribution of air quality in winter.

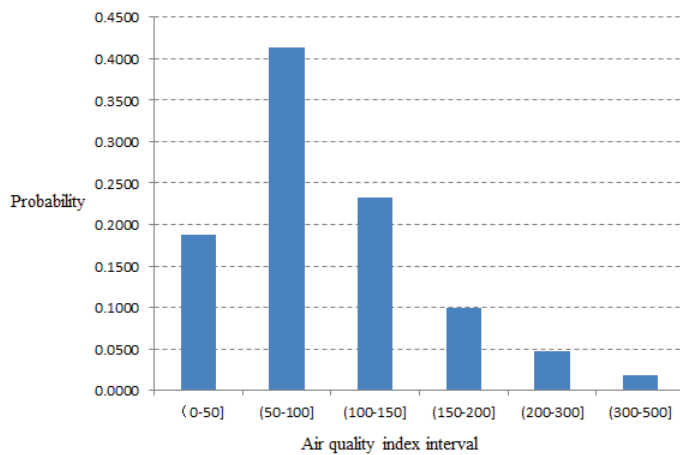Fig. 3: Probability distribution of air quality in spring

Fig. 4: Probability distribution of air quality in summer.

(2) According to the fuzzy set A_i and B_i transformed from the sample point (x_i, y_i), the fuzzy relations R_i can be obtained, which is calculated by the following formula:

$$\mu_{R_i}(u,v) = \mu_{A_i}(u)\mu_{B_i}(v) \qquad \ldots(10)$$

(3) For input data x_0, the estimated value of output y_0 is deduced. Converting x_0 to a fuzzy set according to the following equation:

$$\mu_{x_0}(u_j) = \begin{cases} 1 - |x_0 - u_j|/d, & |x_0 - u_j| \leqslant d \\ 0, & |x_0 - u_j| > d \end{cases} \qquad \ldots(11)$$

Where, $d = |u_1 - u_2|$.

(4) According to the fuzzy relation R_i and the transformed fuzzy set from x_0, fuzzy reasoning is carried out as follows:

$$\mu_{y_0} = \sum_u \mu_{x_0}(u)\mu_{R_i}(u,v) \qquad \ldots(12)$$

Let v' satisfy the following function relation:

$$\mu_{y_0}(v') = \max_{v \in V}\{\mu_{y_0}(v)\} \qquad \ldots(13)$$

v' is called an estimated value of y_0, and the membership of v' is taken as the weight w_i.

(5) According to the above method, l estimated values of y_0 and corresponding weights are obtained for each group of samples. The final y_0 estimate is calculated by weighted average:

$$\bar{y}_0 = \left(\sum_{i=1}^{l} w_i \hat{y}_i\right) \Big/ \left(\sum_{i=1}^{l} w_i\right) \qquad \ldots(14)$$

The nonlinear regression relationship between air quality index and time is established by the information diffusion approximate reasoning method to describe the changing trend of air condition.

ANALYSIS OF AIR QUALITY CHARACTERISTICS IN BEIJING

Analysis of Air Quality Index Distribution in Different Seasons

According to the daily air quality data in different seasons, the air quality distribution in each season is analysed by information diffusion technology. The probability distribution of air quality grades in each season is shown in Table 1 and Figs. 2-6.

According to the calculation results, the air quality is the best in summer and the worst in winter. The air quality index in summer is less than 200, and there is no heavy pollution or serious pollution. The frequency of moderate pollution is about 2.54% in summer. In winter, the frequency of serious pollution is 2.93%, and the frequency of moderate air pollution and above is 17.83%.

Analysis of Change Trend of Air Quality in Winter

Air quality is the worst in winter. The trend of winter air quality in Beijing was studied by information diffusion technology. After fitting the daily air quality data in winter, the trend of air quality was obtained.

After processing the original data by information diffusion technology, it can better reflect the changing trend of air quality. From the overall trend, the air quality index shows a decreasing trend, that is to say, air quality has improved to a certain extent.

Correlation Analysis Between Air Quality Index and Meteorological Factors

Based on the winter air quality data in Beijing, the relationship between air quality index and daily maximum tempera-
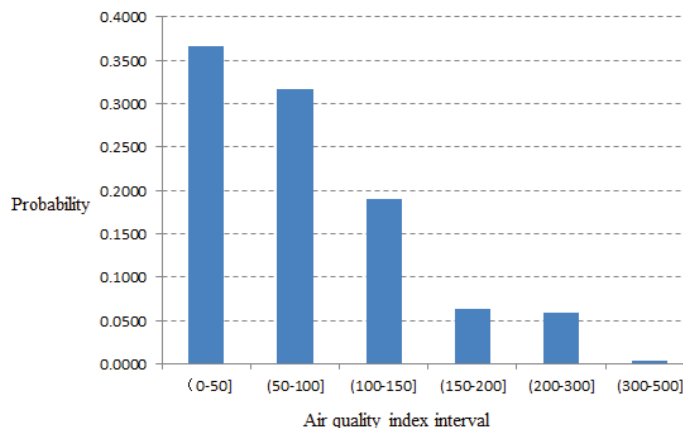

Fig. 5: Probability distribution of air quality in autumn.

Table 2: Probability distribution of air quality in different daily maximum temperature levels.

Air quality level	Temperature level 1	Temperature level 2	Temperature level 3	Temperature level 4
(0, 50]	0.6656	0.4188	0.2879	0.2350
(50, 100]	0.2453	0.3476	0.2853	0.2770
(100, 50]	0.0324	0.1086	0.1578	0.2752
(150,200]	0.0562	0.0410	0.1037	0.1035
(200, 00]	0.0005	0.0596	0.1135	0.0930
(300, 00]	0.0000	0.0244	0.0518	0.0161

ture and daily maximum wind power was analysed by using information diffusion technology. Because of the uncertainty of the correlation, this paper studies the correlation through probability analysis. Firstly, meteorological factors are graded. The daily maximum temperature is divided into 1~4 grades according to the distribution range of the measured data, and the daily maximum wind force is divided into 0~5 grades according to the relevant meteorological classification standards. The higher the grade value of meteorological factors is, the greater the corresponding value is. Then, the probability distribution of air quality corresponding to different meteorological factor levels is calculated, and the uncertainty relationship between air quality and meteorological factors is analysed from the perspective of probability. According to the calculation, the distribution of winter air quality index in Beijing at different temperature levels is shown in Table 2:

As can be seen from the data in the table above, the higher the winter temperature is, the worse the air quality is. When the air temperature belongs to grade 1 (0°C or below), the distribution of the air quality index is mainly excellent and good. No heavy pollution or serious pollution has occurred. The frequency of mild air pollution or above is about 8.91%.

When the air temperature belongs to grade 4 (9°C or above), the frequency of mild air pollution or above is 48.78%, and heavy pollution and serious pollution occur more frequently, reaching 11%.

The distribution of winter air quality index in Beijing at different wind force levels is shown in Fig. 7:

As can be seen from the data in Fig. 7 that the higher the winter wind force is, the better the air quality is. The frequency of mild air pollution and above is about 45.17% when the daily maximum wind force is level 0, and 20.89% when the daily maximum wind force is level 3 and above.

CONCLUSIONS

Information diffusion technology was applied to the study of air quality characteristics. The example shows that the information diffusion technology can make full use of the position information of the data by fuzzing the sample data and obtaining a good result of probability calculation and regression analysis. Based on the analysis of air quality in Beijing by information diffusion model, the following characteristics are found: The probability of air pollution is
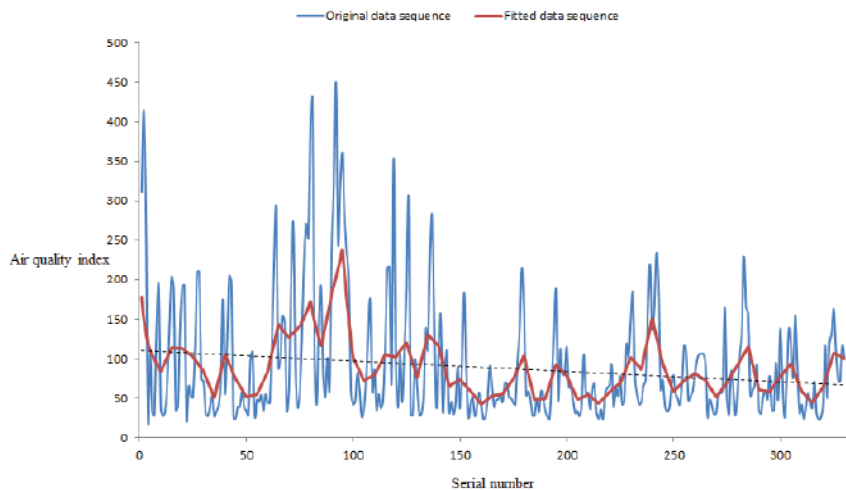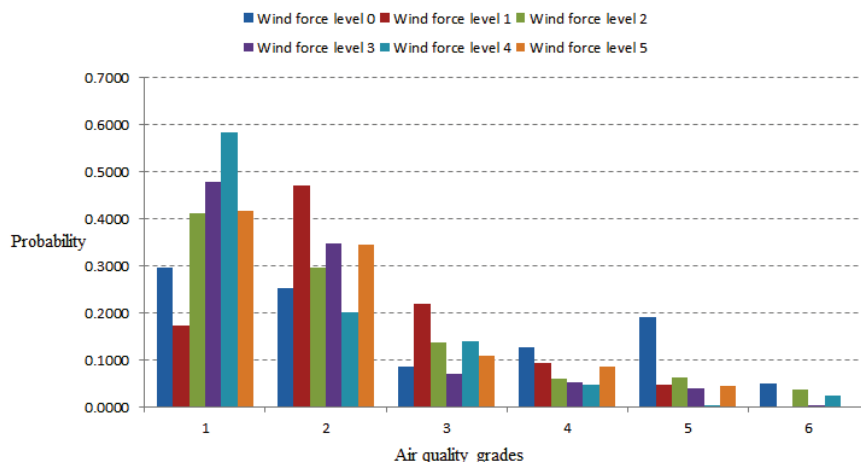

Fig. 6: Trend of air quality in winter.

Fig. 7: Probability distribution of air quality under different wind force levels.

Fig. 7: Probability distribution of air quality under different wind force levels.

the highest in winter. In recent years, air quality has been improving to some extent. The air quality of Beijing in winter has a certain relationship with meteorological factors such as air temperature and wind force. The higher the air temperature is, the smaller the wind force is, the greater the probability of air pollution.

ACKNOWLEDGEMENT

REFERENCES

Chaloulakou, A., Kassomenos, P., Spyrellis, N., Demokritou, P. and Koutrakis, P. 2003. Measurements of PM 10, and PM 2.5, particle concentrations in Athens, Greece. Atmospheric Environment, 37(5): 649-660.

Chen, X.N., Jia, Q., Gao, Y., Liu, S. and Duan, C.Q. 2012. Analysis on wheat drought risk based on information diffusion technology in Xi'an city. Journal of North China Institute of Water Conservancy and Hydroelectric Power, 33(3): 20-22.

Davis, D.L., Bell, M.L. and Fletcher, T. 2002. A look back at the London smog of 1952 and the half century since. Environmental Health Perspectives, 110(12): 374-375.

Dong, M., Kuang, Y. and Kuang, Y. 2009. PM2.5 concentration prediction using hidden semi-Markov model based times series data mining. Expert Systems with Applications, 36(5): 9046-9055.

Hinton, G.E. and Salakhutdinov, R.R. 2006. Reducing the dimensionality of data with neural networks. Science, 313(5786): 504-507.

Huang, C.F. 2018. Improving estimation of typhoon risk by using information diffusion model. Systems Engineering - Theory & Practice, 38(9): 2315-2325.

Jian, L., Zhao, Y., Zhu, Y.P., Zhang, M.B. and Bertolatti, D. 2012. An application of ARIMA model to predict submicron particle concentrations from meteorological factors at a busy roadside in Hangzhou, China. Science of the Total Environment, 426(2): 336-245.

Jiang, Q.J., Li, H., Wang, S.P. and Fu, C.L. 2017. Study on causes and countermeasures of haze in Zhengzhou. Guangzhou Chemical Industry, 45(16): 136-137.

Li, H.M. 2017. Prediction of haze weather based on cubic exponential smoothing model. Journal of the Environmental Management College of China-EMCC, 27(3): 52-55.

Minguillón, M.C., Querol, X., Baltensperger, U. and Prévôt, A.S.H. 2012. Fine and coarse PM composition and sources in rural and urban sites in Switzerland: local or regional pollution. Science of the Total Environment, 428(12): 191-202.

Mishra, D., Goyal, P. and Upadhyay, A. 2015. Artificial intelligence based approach to forecast PM 2.5, during haze episodes: A case study of Delhi, India. Atmospheric Environment, 102(2): 239-248.

Qian, J.P., Huang, F., Du, J., Wang, G., Jin, A. and Peng, L. 2006. Spatial-temporal characteristic of meteorological visibility under fog and haze condition in Guangdong Province. Ecology and Environment, 15(6): 1324-1330.

Wang, B.B. 2011. The analysis of the pollution characteristics and influence factors of PM2.5 in Beijing during the Olympic games. Shangdong Normal University, pp. 82-90.

Wang, J.Z., Xu, X.D. and Yang, Y.Q. 2002. A study of characteristics of urban visibility and fog in Beijing and the surrounding area. Journal of Applied Meteorological Science, 13(Suppl.): 160-169.

Original Research Paper   **Open Access Journal**

Optimization of Protease Production by *Bacillus isronensis* Strain KD3 Isolated from Dairy Industry Effluent

N. S. Patil* and J. V. Kurhekar*†

*Department of Microbiology, Bharati Vidyapeeth's, Dr. Patangrao Kadam Mahavidyalaya, Sangli, Maharashtra, India
†Corresponding author: J. V. Kurhekar; jaya_kurhekar@rediffmail.com

ABSTRACT

Proteases have a broad range of applications in pharmaceuticals, detergents and food processing industries. Protease producing strains are used profusely in industrial applications and the bioremediation process of wastewaters. In the present research work, efficient protease producing strain was isolated from dairy industry effluent. Screening of protease activity by isolates was checked by growing them on milk agar (skimmed) by spot inoculation method and further estimation was performed using quantitative protease assay. The efficient protease producing strain was identified based on morphological as well as biochemical characteristics as per standard keys of Bergey's Manual of Determinative Bacteriology, later confirmed by 16s rRNA sequencing and BLAST analysis as *Bacillus isronensis* strain KD3. The maximum protease was produced at 42°C; pH 7-8; 200 rpm; and 7% inoculum concentration after 48h of the incubation period.

INTRODUCTION

Enzymes are the biocatalysts, which catalyse multiple biochemical reactions within a short time. Proteases are hydrolases (E.C.3.4.21.14) which breakdown the peptide bonds of amino acids of a protein (Sathyavrathan & Kavitha 2013). Proteases have wide applications in pharmaceutical, detergent and food processing industries (Gupta et al. 2005, Verma et al. 2011). Proteases can be defined as enzymes degrading substrate, catalysing complete hydrolysis of proteins (Baroudi et al. 2000). Casein is a major protein occupying 80% of total milk protein. It is a phosphoprotein and different forms of casein depend on the number of phosphate groups attached (Caprita 2008). There are different sources found in nature for protease production like market waste, dairy industrial waste and sewage wastewater (Vasantha & Subramanian 2012). Kolhe & Pawar (2011) reported that the dairy industry effluent has a large amount of protein (especially casein), which may be a good source for isolation of proteolytic bacteria. Patil & Kurhekar (2018a) has reported that bacterial protease has more significance in the industry as compared to animal and fungal proteases. Appleby (1955) isolated proteolytic bacteria from rumen of sheep. Kamoun et al. (2008) have reported some protease producing bacterial strains namely *Bacillus subtilis, Bacillus alcalo, Bacillus licheniformis, Bacillus thuringiensis, Bacillus firmus* and fungal strains such as *Aspergillus miller, Penicillium griseofulvin, Aspergillus flavus* and *Aspergillus*

niger. Patil & Kurhekar (2018b) screened caseinase producing bacteria from dairy industry effluent and further studied them quantitatively.

Commercially available proteases are stable at variable pH and are highly active (Maurer 2004). Mostly produced by different *Bacillus* species, especially alkaline proteases have wide substrate specificity and purification cost is very low (Haddar et al. 2010). Protease producing strains have a large range of applications in food, detergent, textile, tanning, leather and pharmaceutical industries (Prakasham et al. 2005). To check the effect of physiological parameters on production of protease, various factors like medium pH, temperature, agitation speed, inoculum concentration, incubation time and nutrient supplements like sources of carbon as well as nitrogen were taken into the consideration (Badhe et al. 2016). The present investigation aimed to screen strain producing protease from dairy industry effluent and to optimize protease production for different cultural conditions.

MATERIALS AND METHODS

Dairy Industry Effluent

The dairy industrial effluent was obtained from the Effluent Treatment Plant (ETP) of a dairy industry located in Pune district, Maharashtra, India. The effluent samples for analysis were collected and kept in clean and sterile glass containers,

stored in an icebox at low temperature and immediately transported to the laboratory, for further analysis. Before use, the effluent samples were maintained at low temperature, i.e. 4°C in a refrigerator to avoid any physicochemical change (APHA 2005, Trivedy & Goel 1984).

Isolation and Screening of Protease Producing Bacteria

The protease producing bacteria were isolated from dairy industry effluent by the enrichment method. It was performed in a 250 mL of Erlenmeyer flask with 100 mL sterile nutrient broth, inoculated with 10 mL of effluent sample. The flasks were placed overnight on a rotary shaker at 150 rpm at 37°C. A loop full of enriched culture streaked on sterile nutrient agar plates was incubated at 37°C for 24 h. Morphologically different isolated colonies were streaked on nutrient agar plates, for obtaining pure cultures. Cultural characteristics of isolates were studied. Nutrient agar slants were used for maintaining pure cultures at 4°C. The screening was done to find out the most potential bacterial isolate with proteolytic activity. For this study, colonies with different morphologies were marked for future study. Protease activity was qualitative detected using Skimmed Milk Agar (Skimmed Milk Powder - 10 %, Peptone - 0.5 %, Agar Agar - 2.5%, pH - 7.2). The halo casein hydrolysis zone was seen on the plate after the incubation at 30°C for 24 and 48 h. The zone diameter for each isolate was measured after 24 hours of the incubation period. The strain with maximum protease activity (qualitatively) was used for further study.

Protease Assay

The protease enzyme assay was performed with some modifications in the protocol suggested by Tsuchida et al. (1986) involving casein as substrate. The bacterial isolate was grown in Nutrient Broth with 1% casein as a substrate and then incubated for 24 h at 30°C. Cell-free supernatant was subjected to enzyme assay. Enzyme solution, i.e. supernatant (100 µL) was added to 900 µL substrate (2 mg/mL (w/v) solution of casein in Tris-HCl buffer (10 mM) with pH 8.0. Incubation of the mixture was carried out for 30 min at 45°C. The reaction was stopped with the addition of chilled trichloroacetic acid 10 (w/v) in equal volume and kept for 15 min, which allowed the insoluble proteins to precipitate. By centrifugation for 10 min, at 10000 rpm at 4°C, neutralization of supernatant was carried out with 5 mL 0.5 M Na_2CO_3 solution (0.5 M). With the addition of 3-fold diluted Folin-Ciocalteu reagent, optical density was measured at 600 nm in triplicate. One protease unit can be defined as the enzyme amount that produces 1 µg tyrosine per mL per min, under standard assay conditions (Lowry et al. 1951).

Identification of Protease Producing Isolate

Bacterial isolate exhibiting highest zone of protein hydrolysis was used further for study. The efficient protease producing strain was identified based on morphological as well as biochemical characteristics as per standard keys of Bergey's Manual of Determinative Bacteriology (Bergey et al. 1974), and later confirmed by 16s rRNA sequencing and BLAST analysis.

Optimization of Protease Production for Different Cultural Conditions

For optimization of protease production at different pH, the bacterial isolate was grown separately in Nutrient Broth supplemented with 1% casein and pH of 4, 5, 6, 7, 8, 9, 10 and 11 at 37°C. To optimize the temperature conditions, the temperatures were set as 20, 25, 30, 37, 42 and 50°C. The highest caseinase production was recorded in a quantitative mode and the same was continued for further study. To investigate the impact of different speeds of agitation, the efficient bacterial isolates were allowed to grow separately in Nutrient Broth supplemented with 1% casein at variable shaking conditions of 100, 150, 200, 250, 300 and 350 rpm at optimum pH and temperature value recorded earlier. Inoculum concentration of 1% to 10% was tested separately in Nutrient Broth medium having 1% casein with optimum conditions as per the earlier study. To observe the impact of incubation time, the isolate was tested separately in Nutrient Broth medium supplemented with 1% casein with all the optimum conditions and tubes were incubated separately for the period of 8, 16, 24, 32, 40, 48, 56, 64 and 72 h. Further, the suitable incubation time was recorded based on protease assay and continued for further study. Carbon sources were tested as 1%, i.e. maltose, glucose, starch and sucrose separately. Different nitrogen sources were screened for 1% ammonium sulphate, tryptone, beef extract and malt extract. The physicochemical parameters were selected as per the earlier study. The production of protease was determined by quantitative assay.

Statistical Analysis

The experimental data were analysed using Bonferroni's multiple comparison test.

RESULTS AND DISCUSSION

Isolation and Screening of Protease Producing Bacteria

Thirty morphologically distinct bacterial colonies were isolated on Nutrient Agar medium from selective enrichment of dairy industry effluent samples. To screen protease producing

strains; individual culture of each isolate was spot inoculated in centre of Milk Agar plates. Positive strains were evaluated by observation of clear hydrolysis zone surrounding the colony. In all, twelve bacterial strains namely KD1, KD2, KD3, KD4, KD5, KD6, KD7, KD8, KD9, KD10, KD11 and KD12 (Assigned names for laboratory use only) were identified as protease producers due to their clear zone of casein hydrolysis around the colony. The casein hydrolysis zone was measured for each isolate and results are given in Table 1. As per qualitative test results isolate KD3 showed high protease activity as compared to remaining isolates (Fig. 1). So, isolate KD3 was used for further study.

Phylogenetic Identification of Selected Bacterial Strain

The selected bacterial strain with higher protease activity was identified as *Bacillus isronensis* strain *KD3* based on morphological as well as biochemical characteristics as per standard keys of Bergey's Manual of Determinative Bacteriology (Bergey et al. 1974) and by molecular characterization (16s rRNA sequencing) (Fig. 2). The 16s rRNA sequence of *Bacillus isronensis* strain *KD3* was compared with NCBI-BLAST data bank and then deposited in NCBI data bank (Accession No. LC260011) for the phylogenetic analysis. DND file obtained from CLUSTAL alignment was employed for phylogram built up by using the MEGA5 software. The built phylogram was documented with close homology of the bacteria isolated with the best matched bacterial sequence and highlighted by marking in a phylogram (Fig. 3).

Optimization of Protease Production for Different Cultural Conditions

Effect of pH on the production of protease: pH strongly affects ion transport and nutrients across the cellular membrane. It also plays an important role in multiple enzymatic

Table 1: Diameter of clear hydrolysis zone surrounding the bacterial isolates on Milk Agar plates for 24 hours at 30°C.

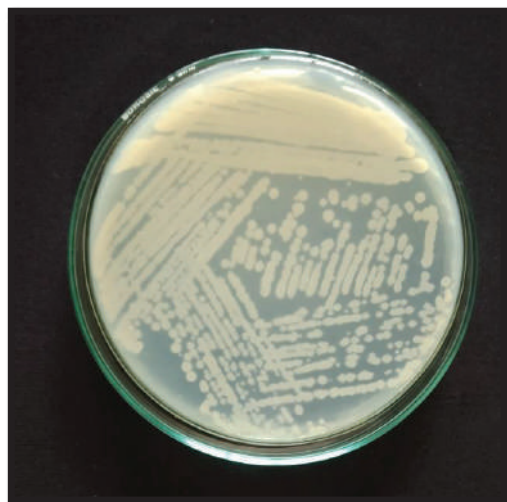| Bacterial isolates	Diameter of zone surrounding the colony (mm)	Protease activity (U/mL)
KD1	7	50
KD2	10	81.5
KD3	18	120.4
KD4	12	94.5
KD5	13	96.8
KD6	8	54.2
KD7	7	50
KD8	14	101
KD9	15	107
KD10	12	95
KD11	11	85
KD12	10	81.5

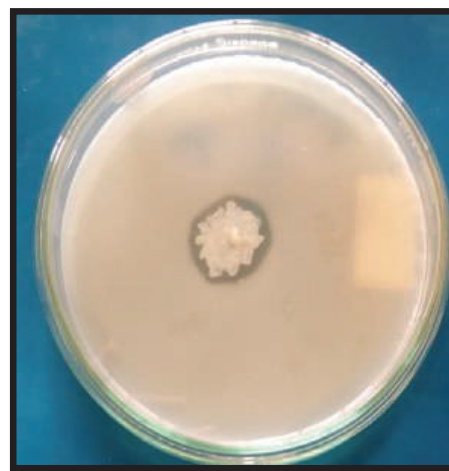Fig. 1: *Bacillus isronensis* strain *KD3* on the nutrient agar plate.

Fig. 2: *Bacillus isronensis* strain *KD3* on milk agar showing zone of proteolysis.

processes (Moon & Parulekar 1991). In the present study, production of protease was observed as negligible in isolate, set at pH 4, 5, 10 and 11 while best protease production was noted at pH 7 and pH 8 (Fig. 4). *Bacillus isronensis* strain *KD3* was preferred as it produced higher protease (P<0.0001) at alkaline pH with 41±0.51 U/mL. The production was observed to prefer neutral to mildly alkaline conditions for protease production. In a related study, Kembhavin et al. (1993) reported that thermostable alkaline protease, isolated from *Bacillus subtilis* NCIM No. 64, was capable of growing in a medium set at varying pH of 5-11 and in all these conditions it was able to produce protease successfully. According to Nascimento et al. (2004), thermophile *Bacillus* sp. was able to produce optimum protease activity at pH 8 and it was reduced when pH was set at 5.5 and 9, after incubating crude

enzyme for 24 h. In another report, alkalophilic *Bacillus* sp. JB 99 was able to produce protease activity at pH 11 with the temperature set at 70°C and confirmed to be serine alkaline protease in feature (Johnvesly & Naik 2001).

Effect of temperature on production of protease: Induction of protease production in the medium inoculated with isolate was allowed to manifest by providing incubation at different temperatures ranging 20, 25, 30, 37, 42 and 50°C sets. *Bacillus isronensis strain KD3* was reported with maximum production at temperature 42°C with 59± 0.81 U/mL value and later on with further increase or decrease in temperature, a sharp fall in activity was recorded (Fig. 5). According to Nascimento et al. (2004) protease activity in a thermophilic *Bacillus subtilis* grown in liquid medium
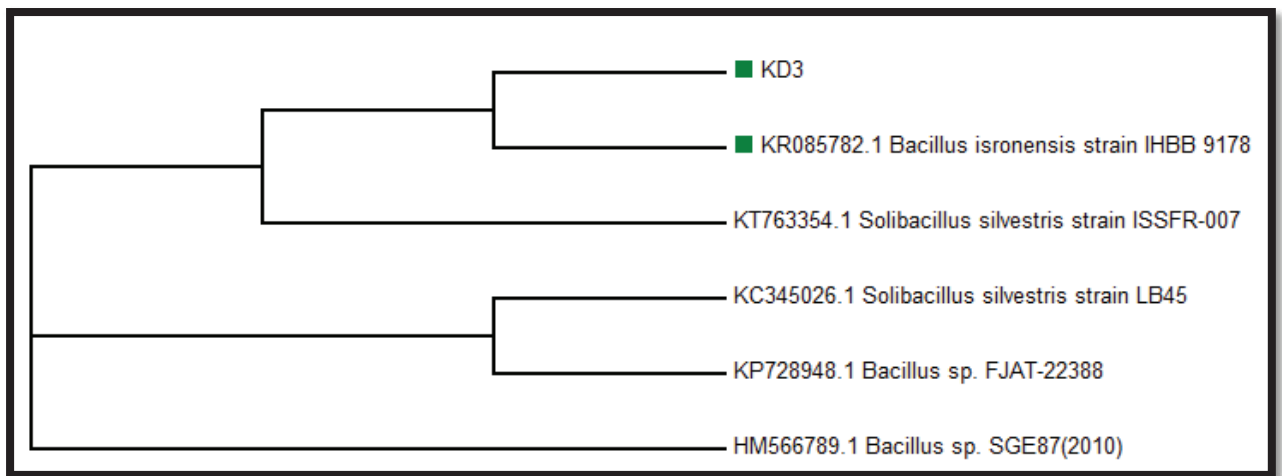

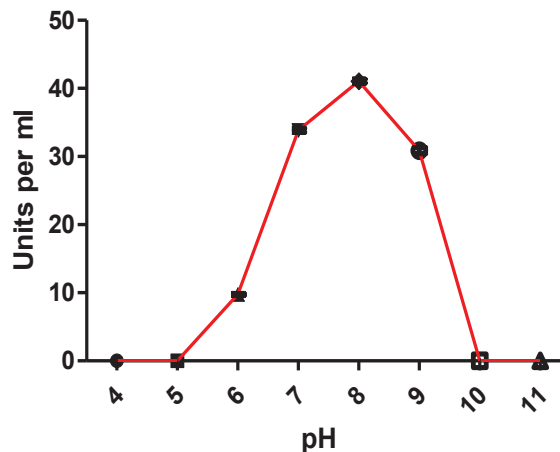Fig. 3: Phylogram of *Bacillus isronensis* strain *KD3*.

Fig. 4: Effect of pH on the production of protease.

supplemented with trisodium citrate was able to produce optimum protease at 60°C since the bacterium was a thermophile. In the case of our study, we deduced that protease production remained at its best with the temperature of 37°C-42°C considering that our isolates are mesophilic. In a similar study and report, which was very close to our findings, Kanekar et al. (2002) showed that isolates of genera *Bacillus, Staphylococcus, Micrococcus, Pseudomonas* and *Arthrobacter* exhibit optimum protease activity when the medium was maintained at 30°C under shaking conditions. Kumar (1999) reported the production of protease by *Bacillus* species was 84.09 U/mL at 45°C.

Effect of speed of agitation on the production of protease: In the present investigation, protease production was shown to be affected by agitation speeds applied to the medium. Agitation speed was set at 100-350 rpm, recorded that between 150 and 250 rpm it was able to produce better protease in all media (Fig. 6). *Bacillus isronensis* strain *KD3* showed maximum protease production at 200 rpm with 49±0.058 U/mL and second best was shown at 150 rpm (26±0.32 U/mL). As the revolution increased, activity lowered down speedily and reached to the minimum of 8.8±0.26 U/mL at 350 rpm. As per the results, agitation speed set at 150-200 rpm was most optimum for protease production in the study. As per Escobar & Barnett (1993) enzyme production remained in direct proportion to shaker speed when they investigated the recovery of mould acid protease from *Mucor miehei CBS 370.65*. Genckal & Tari (2006) reported while studying *Bacillus* sp. strain *I18, L18,* and *L21* that better protease and growth could be achieved when conditions were set at 30°C (strain I18) and 37°C for *L18* and *L21* strains. Similarly, agitation speed was 100 rpm for I18 and 180 rpm for L18

and L21. This study is similar to our finding, where the use of 150-200 rpm is the normal range reported.

Effect of inoculum concentrations on production of protease: Optimization of protease production was carried out for different inoculum concentration set as 1% to 10%. *Bacillus isronensis* strain *KD3* reported better production with 6% with 39±0.68 U/mL and showed improved activity for 7% inoculum concentration which gives 42±0.3 U/mL of activity (Fig. 7). Later on, a decrease in the value was recorded. A significant difference from 1% to 10% bacterial inoculation of protease production showed better activity with 7% inoculation significantly ($p<0.05$). In the present investigation, the effect of concentration of inoculum on the production of protease has been put forth. It was noted that inoculum in the range of 5-7% improved caseinase production at its best as compared to 1-3% and 8-10% concentration.

Impact of time of incubation on the production of protease: *Bacillus isronensis* strain *KD3* was reported to be better protease producer at 48 h (42±0.56 U/mL) (Fig. 8). It was negligible during the first 16 h and decreased beyond 56 h till 80 h. That was the incubation time last recorded. As observed, the highest production of protease was obtained at 48-56 h of incubation by the isolates. In a similar study, Beg et al. (2003) reported that in a shake flask culture *Bacillus mojavensis* was able to produce protease within 24 h with an activity of 558 U/mL and it was further reduced down in a bioreactor to 10-12 h. In a similar study, production of alkaline protease in *Bacillus* species was investigated in the fermentation of solid-state type and increased protease activity was reported at 24 h when lentil husk and wheat bran were used as substrate (Uyar & Baysal 2004).
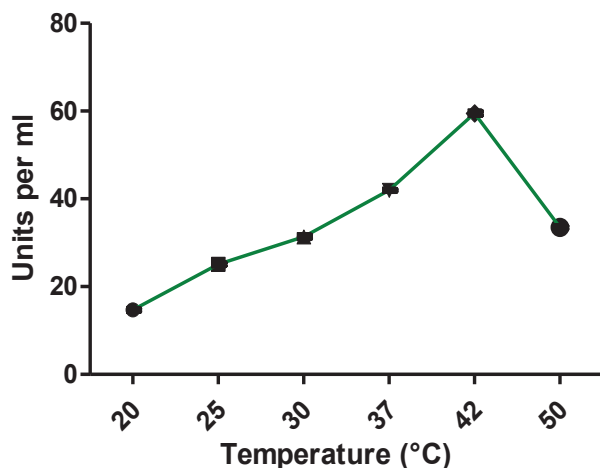

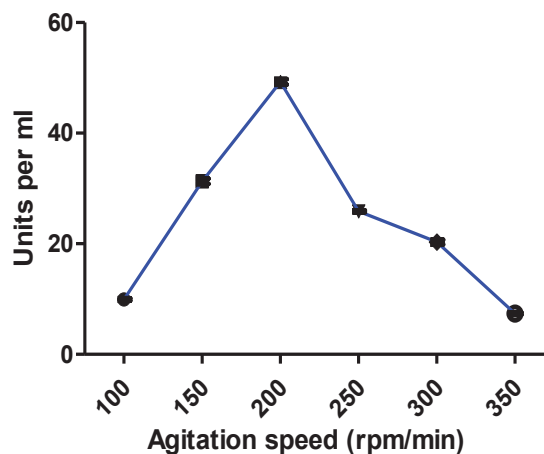Fig. 5: Effect of temperature on the production of protease.

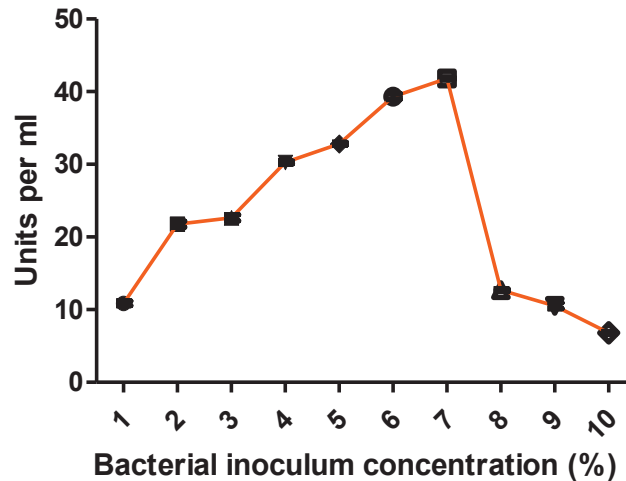Fig. 6: Effect of speeds of agitation on the production of protease.

Fig. 7: Effect of inoculum concentration on the production of protease.

Effect of various sources of nitrogen on the production of protease: Among the all nitrogen sources (1%) tested, production of protease was observed to get affected by the supplement such as ammonium sulphate, tryptone, beef extract and malt extract (Fig. 9). As compared to control, *Bacillus isronensis* strain *KD3* not get induced by any nitrogen source and value of protease production was reported to be either low or constant to control. This indicated a neutral effect of source of nitrogen on protease production. Use of ammonium sulphate was found improving protease production as reported by Varela et al. (1996) working with *Bacillus subtilis*. Rahman et al. (2005) also strongly supported the finding that strain *K* of *Pseudomonas aeruginosa* was able to produce stable protease when nitrogen source as tryptone, soybean and yeast extract was provided.

Effect of various sources of carbon on the production of protease: During the carbon source optimization study, *Bacillus isronensis* strain *KD3* was not affected by the carbon source addition as no stable increase in protease was observed in any set of carbon source (Fig. 10). In the present study, carbon source glucose was reported better for protease activity. In a similar study, glucose with a concentration of 2 mg/mL was reported as the optimum concentration for production of protease in *Bacillus mojavensis* when studied in 14 L bioreactor, as predicted by the statistical model. It was also reported that >2 mg/mL level of glucose turned out to be responsible for catabolic repression in protease production (Beg et al. 2003). Kole et al. (1988) advocated for simultaneous control of ammonium and glucose concentrations in *Bacillus subtilis* in fermentation conditions for better protease
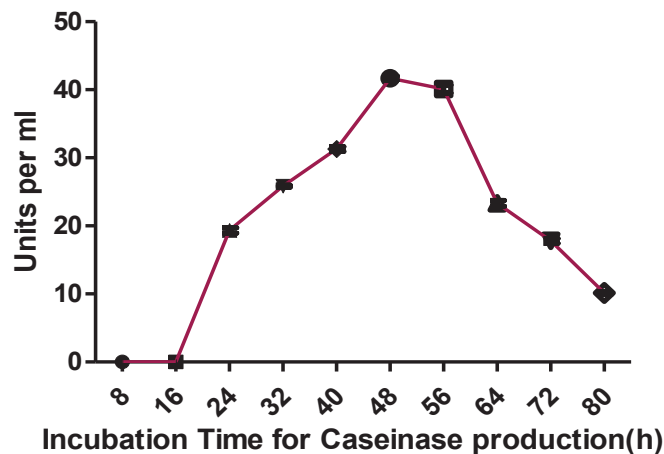

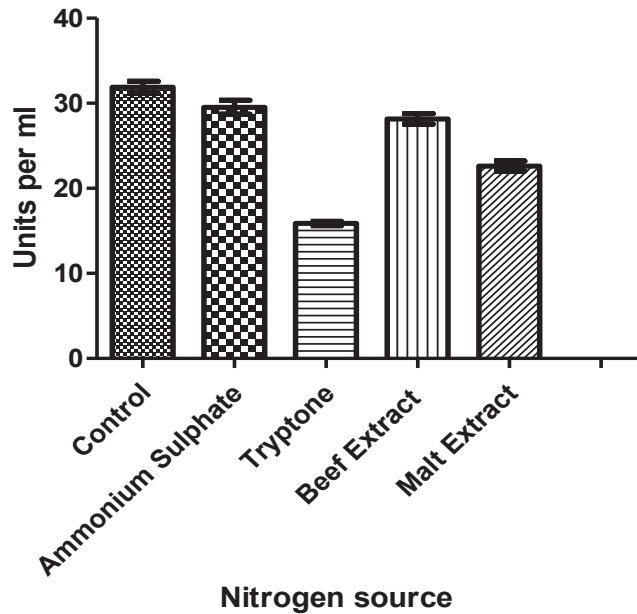Fig. 8: Impact of incubation time on the production of protease.

Fig. 9: Effect of sources of nitrogen on the production of protease.

production. In a report, glucose supplemented in a medium with a pH range of 9.5-11.5 and temperature 65°C, was able to induce protease production in Microbacterium sp. isolated and identified from Ethiopian alkaline soda lake. This study also supports our finding that glucose acts as a promoter for better protease activity (Gessesse & Gashe 1997). Similarly, starch has been reported positive for better protease production as reported by Naidu & Devi (2005), Reddy et al. (2008) and Feng et al. (2001) while investigating the *Bacillus* sp.; *Bacillus* sp. RKY3 and *Bacillus pumilus* strain respectively.

REFERENCES

APHA-AWWA-WPCP 2005. Standard Method for Examination of Water and Wastewater. (21st ed.), American Public Health Association, Washington.

Appleby, C.J. 1955. The isolation and classification of proteolytic bacteria from the rumen of the sheep. J. Gen. Microbiol., 12: 526-533.

Badhe, P., Joshi, M. and Adivarekar, R. 2016. Optimized production of extracellular proteases by *Bacillus subtilis* from degraded abattoir waste. J. Bio. Sci. Biotechnol., 5: 29-36.

Bayoudh, A. Gharsallah, N. Chamkha, M. Dhouib, A. Ammar, S. and Nasri, M. 2000. Purification and characterization of an alkaline protease
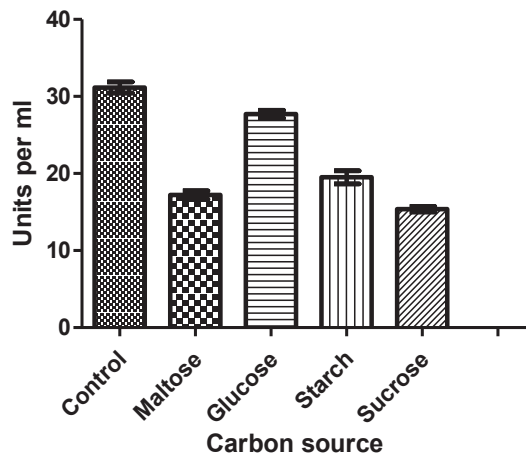

Fig. 10: Effect of various sources of carbon on the production of protease.

from *Pseudomonas aeruginosa* MN1. Ind. Microbiol. Biotechnol., 24: 291-295.

Beg, Q., Sahai, V. and Gupta, R. 2003. Statistical media optimization and alkaline protease production from *Bacillus mojavensis* in a bioreactor. Process Biochemistry, 39(2): 203-209.

Bergey, D., Buchanan, R. and Gibbons, N. 1974. Bergey's Manual of Determinative Bacteriology. (8th ed.), The Williams and Wilkins Co., Baltimore, USA, pp. 15-36.

Caprita, R. and Caprita, A. 2008. Comparative study on milk casein assay methods. Lucrari Stiintifice Zootechnie si Biotechnologii, 41(1): 758-762.

Escobar, J. and Barnett, S. 1993. Effect of agitation speed on the synthesis of *Mucor miehei* acid protease. Enzyme and Microbial Technology, 15(12): 1009-1013.

Feng, Y., Yang, W., Ong, S., Hu, J. and Ng, W. 2001. Fermentation of starch for enhanced alkaline protease production by constructing an alkalophilic *Bacillus pumilus* strain. Applied Microbiology and Biotechnology, 57(2): 153-160.

Genckal, H. and Tari, C. 2006. Alkaline protease production from alkalophilic *Bacillus* sp. isolated from natural habitats. Enzyme and Microbial Technology, 39(4): 703-710.

Gessesse, A. and Gashe, B. 1997. Production of alkaline protease by an alkaliphilic bacteria isolated from an alkaline soda lake. Biotechnology Letters, 19(5): 479.

Gupta, A., Roy, I., Patel, R., Singh, S., Khare, S. and Gupta, M. 2005. One step purification and characterization of an alkaline protease from halo alkaliphilic *Bacillus* sp. J. Chromatography A., 1075: 103-108.

Haddar, A., Fakhfakh, Z., Noomen, H., Fakher, F., Moncef, N. and Alya Sellami, K. 2010. Low-cost fermentation medium for alkaline protease production by *Bacillus mojavensis A21* using hulled grain of wheat and sardinella peptone. Journal of Bioscience and Bioengineering, 110(3): 288-294.

Johnvesly, B. and Naik, G. 2001. Studies on production of thermostable alkaline protease from thermophilic and alkaliphilic *Bacillus* sp. *JB-99* in a chemically defined medium. Process Biochemistry, 37(2): 139-144.

Kamoun, A., Haddar, A., Ali, N., Basma, F., Kanoun, S. and Nasri, M. 2008. Stability of thermostable alkaline protease from *Bacillus licheniformis* RP1 in commercial solid laundry detergent formulations. Microbiological Research, 163(3): 299-306.

Kanekar, P., Nilegaonkar, S., Sarnaik, S. and Kelkar, A. 2002. Optimization of protease activity of alkaliphilic bacteria isolated from an alkaline lake in India. Bioresource Technology, 85(1): 87-93.

Kembhavi, A., Kulkarni, A. and Pant, A. 1993. Salt-tolerant and thermostable alkaline protease from *Bacillus subtilis NCIM No. 64*. Applied Biochemistry and Biotechnology, 38(1-2): 83-92.

Kole, M., Draper, I. and Gerson, D. 1988. Production of protease by *Bacillus subtilis* using simultaneous control of glucose and ammonium concentrations. Journal of Chemical Technology & Biotechnology, 41(3): 197-206.

Kolhe, A. and Pawar, V. 2011. Physico-chemical analysis of effluents from dairy industry. Recent Research in Science and Technology, 3(5): 29-32.

Kumar, C., Tiwari, M. and Jany, K. 1999. Novel alkaline serine proteases from alkalophilic *Bacillus* species: Purification and some properties. Process Biochemistry, 34(5): 441-449.

Lowry, O., Rosebrough, N., Farr, A. and Randall, R. 1951. Protein measurement with Folin phenol reagent. J. Bio. Chem., 193(1): 265-275.

Maurer, K. 2004. Detergent proteases. Curr. Op. Biotechnol., 15(4): 330-334.

Moon, S. and Parulekar, S. 1991. A parametric study of protease production in batch and fed-batch cultures of *Bacillus firmus*. Biotechnol. Bioeng., 37: 467-83.

Naidu, B. and Devi, K. 2005. Optimization of thermostable alkaline protease production from species of *Bacillus* using rice bran. African Journal of Biotechnology, 4(7): 724-726.

Nascimento, D. and Martins, L. 2004. Production and properties of an extracellular protease from thermophilic *Bacillus* sp. Brazilian Journal of Microbiology, 35(1-2): 91-96.

Patil, N. and Kurhekar, J. 2018a. Development of microbial consortia for biodegradation of dairy industry effluent. International Journal of Research and Analytical Reviews, 5(4): 47-50.

Patil, N. and Kurhekar, J. 2018b. Potential applications of *Aeromonas hydrophila* in biodegradation of dairy industry effluent. International Journal of Advanced and Innovative Research, 5(3): 85-91.

Prakasham, S., Rao, S. and Sarma, P. 2005. Green gram husk- an inexpensive substrate for alkaline protease production by *Bacillus* sp. in solid state fermentation. Bioresource Technol., 97(13): 1449-1454.

Rahman, A., Geok, L., Basri, M. and Salleh, A. 2005. An organic solvent-tolerant protease from *Pseudomonas aeruginosa* strain *K*: Nutritional factors affecting protease production. Enzyme and Microbial Technology, 36(5-6): 749-757.

Reddy, A., Wee, J., Yun, S. and Ryu, W. 2008. Optimization of alkaline protease production by batch culture of *Bacillus* sp. *RKY3* through Plackett-Burman and response surface methodological approaches. Bioresource Technology, 99(7): 2242-2249.

Sathyavrathan, P. and Kavitha, M. 2013. Production of alkaline protease from *Bacillus licheniformis* (NCIM 2044) and media optimization for enhanced enzyme production. International Journal of Chem. Tech. Research, 5(1): 550-553.

Trivedy, R.K. and Goel, P.K. 1984. Chemical and Biological Methods for Water Pollution Studies. Environmental Publications, Karad, pp. 1-251.

Tsuchida, O., Yamagota, Y., Ishizuka, J., Arai, J., Yamada, J., Takeuchi, M. and Ichishima, E. 1986. An alkaline protease of an Alkalophilic *Bacillus* sp., Current Microbiology, 14(1): 7-12.

Uyar, F. and Baysal, Z. 2004. Production and optimization of process parameters for alkaline protease production by a newly isolated *Bacillus* sp. under solid state fermentation. Process Biochemistry, 39(12): 1893-1898.

Varela, H., Ferrari, M. D., Belobrajdic, L., Weyrauch, R. and Loperena, L. 1996. Effect of medium composition on the production by a new *Bacillus subtilis* isolate of protease with promising unhairing activity. World Journal of Microbiology and Biotechnology, 12(6): 643-645.

Vasantha, S. and Subramanian, A. 2012. Optimization of cultural conditions for the production of extracellular protease by *Pseudomonas* species. International Current Pharmaceutical Journal, 2(1): 1-6.

Verma, O., Kumari, P., Shukla, S. and Singh, A. 2011. Production of alkaline protease by *Bacillus subtilis* (MTCC 7312) using submerged fermentation and optimization of process parameters. Euro. J. Exp. Bio., 1: 124-129.

Simulation of Nitrogen Pollution in the Shanxi Reservoir Watershed Based on SWAT Model

A-long Li*, Chen Haitao*, Liu Yuanyuan**, Lin Qiu* and Wang Wenchuan*†

*School of Water Conservancy, North China University of Water Resources and Electric Power, Zhengzhou City, Henan Province, 450045, PR China

**Henan Huarun Engineering Design Co., Ltd., Zhengzhou City Henan Province, 450045, PR China

†Corresponding Author: Wang Wenchuan; liuyuan_hs@sina.com

ABSTRACT

This study applied the Soil and Water Assessment Tool (SWAT) to the Shanxi Reservoir watershed, a drinking water source in Zhejiang Province, China. The important sources of non-point source pollution (NPS) in Shanxi reservoir watershed are agricultural fertilizer application, domestic sewage and livestock breeding, this brings new challenges to water source management. The simulated runoff and water quality parameters total nitrogen (TN) were compared to those of the observed values in the watershed. The Nash-Suttcliffe efficiency (*NSE*) was 0.94 for monthly runoff during the calibration period 2007-2010, and 0.84 during the validation period 2011-2012. The model can well satisfy the simulation of runoff. For monthly TN of Sancha water quality monitoring station, the *NSE* is 0.7 in the calibration period of March 2009 to April 2011, and 0.75 in the verification period of May 2011 to December 2012. For the Jiujiang water quality monitoring station, the model index parameters are slightly lower than Sancha, but it is also very good for water quality simulation. The four parameters of total nitrogen, organic nitrogen (ORGN), nitrate-nitrogen (NO$_3$-N) and ammonia nitrogen (NH$_4$-N) were used to analyse the nitrogen pollution of Shanxi Reservoir watershed. The multi-year monthly average results of nitrogen pollutant loadings show significant differences, with large fluctuations every month. ORGN and NH$_4$-N showed a consistent trend, showing a steady growth trend from January to June, peaking in August and continuing to decline in other months, and NO$_3$-N peaked in March. The pollution load of TN in Shanxi reservoir watershed ranged from 142.27 kg/km^2 to 725.31 kg/km^2, showing a large spatial difference. The pollution load of the tributary basin is weaker than that of the main stream, which generally shows an increasing trend from upstream to downstream. Overall, the pollutant load is consistent with land use and agricultural production and living conditions, showing typical characteristics of non-point source pollution. Through the establishment of regional nitrogen pollution model and the study of pollutant distribution characteristics, this study puts forward some suggestions for controlling the nitrogen pollution load of the Shanxi Reservoir watershed, optimizes the agricultural planting mode, and intercepts the pollution sources that are not directly discharged into the water body.

INTRODUCTION

For a long time, as an important source of water pollution in river basins, non-point source pollution (NPS) has received more and more attention. Due to the effects of excessive fertilization and pesticide abuse in agricultural production activities, in the absence of management measures, pollutants such as nitrogen and phosphorus will be eutrophicated with runoff into the water bodies of the basin, resulting in environmental hazards such as blooms (Brezonik et al. 1999). In the surface water of Europe, nitrogen and phosphorus pollutants account for more than 50% of the water entering the basin with agricultural production (Gao & Zhang 1999). As the key to NPS, nitrogen pollution is more prominent in the management of reservoir water source. In China, more

than 15 million tons of nitrogen is lost each year outside the farmland. There are eutrophication problems in 85% of lakes in China, and the important source of water deterioration is also NPS (Hu et al. 2002). Because NPS has the characteristics of strong randomness, extensiveness, and long latency period, the difficulty of governance is greatly increased (He et al. 1998).

Water quality models play an important role in NPS research. The mechanistic model can better simulate the basic situation of the basin, such as the case of land surface hydrology, agricultural production (Wang & Jin 2016). But there are difficulties in calibration parameters. As a large NPS model, SWAT model has a good effect on NPS simulation and has built-in a variety of scenario management measures.

It is an effective tool for determining the best management measures (BMPs) in the basin (Wang et al. 2003).

The important sources of NPS in drinking water in Shanxi reservoir watershed are agricultural fertilizer application, domestic sewage and livestock breeding, this brings new challenges to water source management. As a primary water source protection site, although the water quality of the main stream in the reservoir area of Shanxi is Class II is according to Chinese Water Quality Standard (GB3838-2002), the water quality of some of the tributaries is not optimistic. The main objective of this study was to: 1) Establishing SWAT model of Shanxi reservoir watershed; 2) Simulation of runoff and nitrogen pollution in the basin; 3) Analyse nitrogen pollution to clarify its temporal and spatial characteristics.

MATERIALS AND METHODS

Study Area

The Shanxi Reservoir watershed is located in the south of Zhejiang Province, China, where the dam was completed in 2000 and began to impound. The reservoir as a drinking water source in Wenzhou City, providing drinking water for 7 million people. There are several tributaries within the basin, the tributaries are steep and steep flow, belonging to mountainous rivers, with a total watershed area of 1529 km^2. JN, WC, TS three counties are located in the basin. The multi-year average precipitation and temperature are 1876.9 mm and 19.6 , respectively. The rainfall is concentrated in April and September, accounting for 74.7% of the whole year. The average number of years of precipitation is 149 days, the minimum year is only 80 days. Between July and September, under the control of the subtropical high ridge, prevailing southerly winds, hot weather, frequent typhoon activities, more thunderstorms and typhoons, causing greater floods. The land use in the catchment area is mainly forest land, grassland, agricultural land and residential land (Mei et al. 2016). Study area location is shown in Fig. 1.

Application of SWAT, Calibration and Validation

The SWAT (Soil and Water Assessment Tool) model is a distributed, mechanistic hydrological water quality model based on GIS developed by the US Department of Agriculture (USDA). The model can simulate runoff, sediment, nutrients, pesticides, etc.

Arc SWAT 2012 was used as a tool for this study. The collected data was applied to complete SWAT modelling following the principle of first runoff and then pollution loads, and construct, calibration and validation of the SWAT model of Shanxi reservoir watershed. This study uses SWAT-CUP software as a model calibration tool.

SWAT water quality model is established following the order of the first hydrological re-water quality. First, we constructed the monthly scale hydrological model, from 2004 to 2006 as a model warm-up period, data from 2007 to 2010 were used for calibration and data from 2011 to 2012
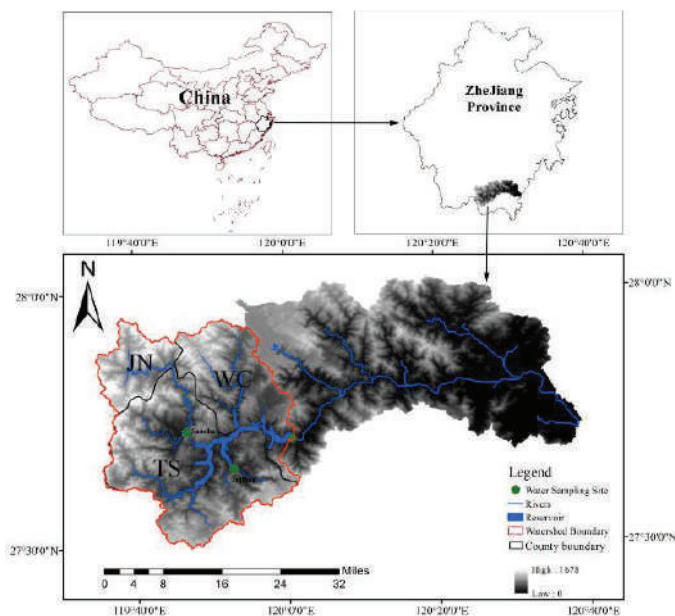

Fig.1: Geographic location and water quality monitoring site of the study area.

were used for validation. After the runoff simulation meets the accuracy requirements, calibration and verification of the monthly scale water quality model were performed on the data of the two water quality sites in the basin.

In China, often monitored water quality indicators do not include organic nitrogen and nitrate nitrogen. However, we believe that when the runoff calibration is accurate and the water quality is calibrated with TN as a water quality indicator, the key parameters for the model mechanism and process are accurate. Due to the lack of organic nitrogen and nitrate nitrogen measured data, while the two indicators for the importance of surface water quality assessment, we use accurate SWAT model to output the value of these indicators.

Data Sources

The DEM data is the 30 m × 30 m precision data obtained from the Geospatial Data Cloud (http://www.gscloud.cn/). Land use data are based on Landsat TM 30 M remote sensing images in accordance with the national land use classification method of interpretation, the use of ArcGis10.2 reclassified as SWAT land use database. The soil data were derived from the FAO's HWSD Soil Database, converted by the SPAW software to the SWAT required soil database.

There are four rainfall stations in the basin, one hydrological station and two water quality stations as shown in Fig. 1. The daily precipitation data from 1956 to 2012 were provided by the local meteorological department for the construction of the model. The daily flow data for 2007-2012 were provided by the local water conservancy department. Water quality monitoring frequency was once a month, two stations from 2009 to 2012 TN data provided by the local Environmental Protection Agency. Fertilization data were calculated based on the "Statistical Yearbook of Wenzhou" and the field survey, livestock excrement data according to previous studies.

RESULTS AND DISCUSSION

Calibration and Verification of Runoff and Nitrogen Pollution Simulations

This study uses the three statistical parameters, Nash-

Sutcliffe efficiency *(NSE)*, the coefficient of determination (R^2) and Relative error (Re) to indicate the accuracy of the SWAT model simulation results [Eqs. (1), (2) and (3)]. The closer *NSE* and R^2 values are to 1, the more accurate the model is, and the smaller the absolute value of the Re is, the more accurate the model is (Narsimlu et al. 2015).

$$NSE = \frac{\sum_{i=1}^{n}(Obs_i - \overline{Obs})^2 - \sum_{i=1}^{n}(Sim_i - \overline{Sim})^2}{\sum_{i=1}^{n}(Obs_i - \overline{Obs})^2} \qquad \ldots (1)$$

$$R^2 = \frac{[\sum_{i=1}^{n}(Obs_i - \overline{Obs})\sum_{i=1}^{n}(Sim_i - \overline{Sim})]^2}{\sum_{i=1}^{n}(Obs_i - \overline{Obs})^2 \sum_{i=1}^{n}(Sim_i - \overline{Sim})^2} \qquad \ldots (2)$$

$$Re = \frac{\sum_{i=1}^{n} Sim_i - \sum_{i=1}^{n} Obs_i}{\sum_{i=1}^{n} Obs_i} \qquad \ldots (3)$$

Where Obs_i is the ith observed value, $\overline{Obs}$ is the average observed value over the length of the simulation sequence, Sim_i is the ith simulated value, $\overline{Sim}$ is the average simulated value over the length of the simulation sequence.

Runoff Calibration and Verification

The hydrological model was calibrated and validated using continuous runoff data for 2007-2012. The data for the four years from 2007 to 2010 were used as the calibration period, and the verification period was from 2011 to 2012.

The fit of the measured and simulated values of runoff in the calibrator and verification period is shown in Fig. 2. The model evaluation results are shown in Table 1. It can be seen that the R^2 and *NSE* of the runoff are both above 0.94 during the calibration period, and the verification period value is slightly lower than the calibration period but also above 0.84. As can be seen from Fig. 2, the simulation of runoff peaks and valleys is very good. The fit between these two simulated values and the measured values is satisfactory, which indicates that the model can well simulate the runoff, which lays a good foundation for the next stage of water quality simulation.

TN Calibration and Verification

After the calibration and verification of the runoff met the model requirements, we began to calibrate and verify the TN. This study calibrated and validated TN data for two

Table 1: The statistical goodness-of-fit indicators during model evaluation.

Type	Calibration			Verification		
	NSE	R^2	Re(%)	*NSE*	R^2	Re(%)
Runoff	0.94	0.95	-0.07	0.84	0.85	1.85
TN(Sancha)	0.7	0.73	-13	0.75	0.86	-31.3
TN(Jujiang)	0.57	0.73	-18	0.88	0.73	-1.9

water quality monitoring stations, Sancha and Jiujiang, from 2009 to

2012. The period from March 2009 to April 2011 was selected as the calibration period, and the period from May 2011 to December 2012 was the verification period.

The results of the model evaluation are given in Table 1. It can be seen from the table that the calibration and verification of TN Sancha are better than that of Jiujiang, and both R^2 and *NSE* are close to greater than 0.7, which is perfect in water quality simulations. It can be seen that the SWAT model of this study can be used to simulate TN of the Shanxi Reservoir watershed.

The fitting of the observed and simulated values of the Jiujiang watershed is shown in Fig. 3. As can be seen from the figure, similar to the results of the runoff simulation, the model has a very high simulation fit for the peak and estimate of the TN. Most studies have shown that the SWAT model is better than the dry season in the simulation of water quality during the simulation of water quality, which is also reflected in this study. Although the dry season observations and the

simulated values are not as good as the wet season, it can be seen that the model we built is still a very good simulation of TN in terms of trends, and these deviations are within the acceptable range.

Temporal Distribution of Nitrogen Pollution Load

This study simulates the monthly average loads of nitrogen pollution in Shanxi Reservoir watershed from 2007 to 2012. The annual variation of the monthly average load of various nitrogen pollutants is shown in Fig. 4. It can be seen that the load of nitrogen pollutants varies greatly and shows obvious changes during the year.

The annual variation trend of organic nitrogen and ammonia nitrogen is very consistent. From January to June, there was a constant growth trend, with a slight decline in July and then peaking in August. Other months continue to decline, which may be because the application of pesticides and fertilizers in the first six months is an accumulation process in the basin. By August, the study area is affected by extreme weather such as heavy rain and even typhoon, which
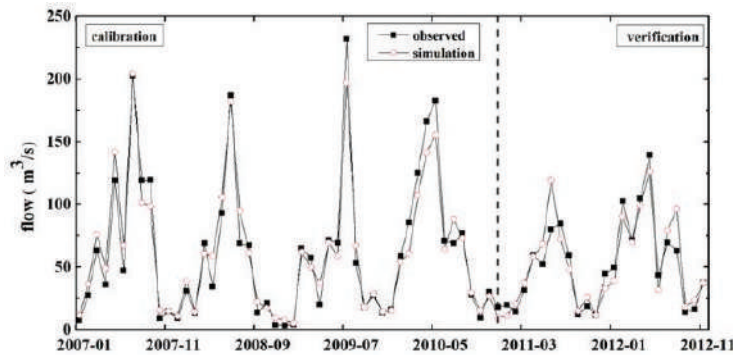

Fig. 2: Observed and simulated values of runoff during the calibration period and verification period 2007-2012.
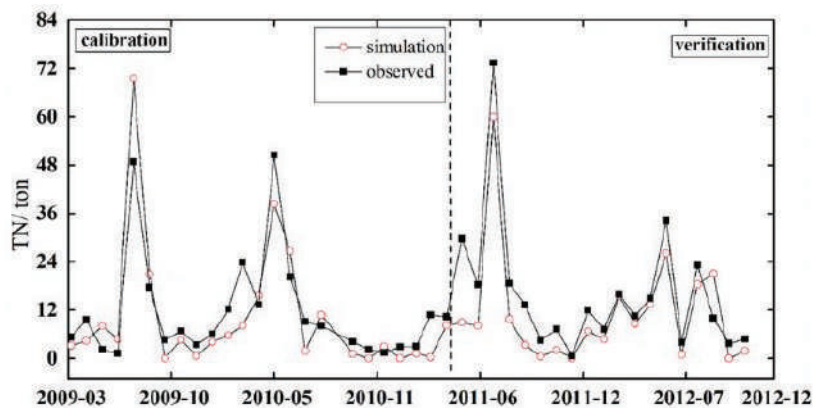

Fig. 3: Observed and simulated values of TN during the calibration period and verification period 2009-2012.

indicates that the pollutant load and runoff are closely related. In the dry season, due to the decrease of precipitation, the runoff is reduced, which greatly reduces the amount of loss (Joongdae et al. 2012). However, the load of the two has a huge difference, which may have a major relationship with the type of land use in the basin.

Unlike the peaks of organic nitrogen and ammonia nitrogen in August, the nitrate-nitrogen load reached a peak in March, which may be related to the agricultural farming method in the basin. During this period, rice cultivation began to be planted in the basin, and the application of nitrogen fertilizer may bring huge nitrate-nitrogen loads.

Spatial Distribution of Nitrogen Pollution Load

Table 2 lists the annual average area loss of nitrogen pollutants from 2007 to 2012. It can be seen that the main contribution of total nitrogen in the Shanxi Reservoir watershed is organic nitrogen, followed by nitrate nitrogen and ammonia nitrogen. The spatial distribution of nitrogen pollutants in each sub-basin of Shanxi Reservoir watershed is shown in Fig. 5.

As can be seen from Fig. 5, the areas with serious nitrogen pollutants are mainly concentrated in the two counties of TS and WC, while the pollutant load in JN is much smaller. This is mainly because the two counties in TS and WC have more human activities and busy agricultural production, while in JN many mountainous forests, human activities are relatively small, and the local agricultural production is not particularly developed.

The average annual total nitrogen loss in the Shanxi Reservoir basin is 438 tons, and the loss per unit area of each sub-basin is from 142.27 to 725.31 kg/km^2. The areas with the most serious total nitrogen pollution load per unit area are sub-basins of 10, 29 and 12, and the annual total nitrogen loss is 725.3 kg/km^2, 636.4 kg/km^2 and 588.2 kg/km^2, respectively. It can be seen from Fig. 5 that the spatial distribution of organic nitrogen and total nitrogen is consistent. Sub-basin 10 is dominated by livestock and poultry farming, and the discharge of animal manure and domestic sewage is the main reason for the large organic nitrogen content in the region. Sub-basin 29 is the seat of the county government of TS County, and the intense human activities have brought about a large loss of organic nitrogen. The sub-basin 12 is the same as the sub-basin 10.

The area with the highest nitrate-nitrogen load is located in sub-basin 25, reaching 6.3 kg/km^2. This sub-basin is located in the agricultural planting area of TS. The land-use type and unreasonable agricultural planting methods are the main reasons for the high nitrate content in this area. The ammonia nitrogen load in the 17 and 18 sub-basins is the largest, reaching 9.26 kg/km^2, 9.21 kg/km^2, respectively. The two sub-basins are located near the exit of the basin. The town of Shanxi is located in it. The intense human activities may be the main reason for the large ammonia nitrogen load in this area.

It can also be seen from the figure that the pollution load of the tributary basin is weaker than that of the main stream, and at the same time it generally shows an increasing trend from the upstream to the downstream. Overall, pollutant loading is consistent with land use and agricultural production and living conditions, presenting typical characteristics of NPS (Chen et al. 2016).

CONCLUSIONS

In the Shanxi Reservoir watershed, this study established a SWAT-based NPS model. The model shows a very good simulation of nitrogen pollution by calibration and verification of runoff and TN. The study also found that the pollution load of
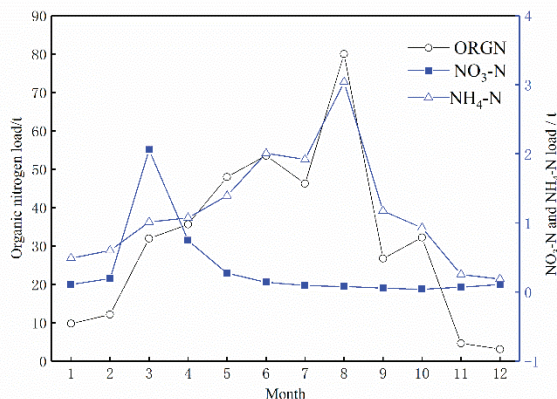

Fig. 4: Monthly average change in nitrogen pollution load.

Table 2: Annual average nitrogen pollutant loss in each sub-basin.

| Sub-basin	ORGN (kg/km²)	NO₃-N (kg/km²)	NH₄-N (kg/km²)	TN (kg/km²)
1	145.15	0.99	0.69	146.83
2	247.97	1.34	0.51	249.83
3	320.49	2.04	0.11	322.65
4	272.85	1.68	2.49	277.02
5	184.01	0.63	0.49	185.13
6	139.58	0.97	1.71	142.27
7	235.82	1.73	2.81	240.37
8	508.21	0.98	1.64	510.84
9	231.99	1.74	2.86	236.58
10	723.37	0.44	1.49	725.31
11	270.21	1.12	0.60	271.94
12	584.83	0.68	2.74	588.23
13	228.34	3.94	4.17	236.44
14	249.06	2.77	8.21	260.08
15	282.03	1.50	1.10	284.63
16	235.98	2.74	1.64	240.35
17	247.76	2.66	9.26	259.73
18	251.02	2.59	9.21	262.87
19	260.01	2.48	7.07	269.56
20	182.36	0.96	2.17	185.50
21	213.06	2.98	1.84	217.86
22	357.48	0.50	3.08	361.06
23	254.01	2.99	2.73	259.75
24	240.72	2.76	5.49	248.99
25	258.11	6.30	0.51	264.90
26	413.43	1.28	7.25	421.95
27	522.05	1.66	2.51	526.24
28	343.82	0.86	0.56	345.24
29	633.34	2.52	0.52	636.38
30	542.62	0.63	3.79	547.05
31	278.35	2.44	5.70	286.50
32	350.52	2.02	3.36	355.90
33	541.91	1.63	2.35	545.86
34	348.47	1.83	0.78	351.05
35	340.28	1.74	1.55	343.58
36	309.23	1.15	0.75	311.13
37	473.01	2.51	3.81	479.35
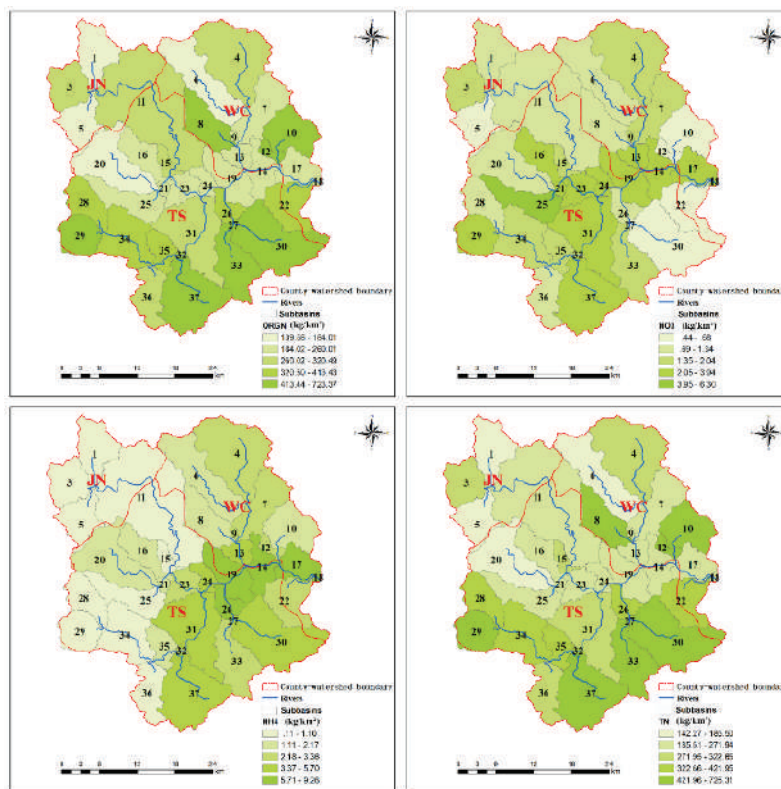
Fig. 5: The spatial distribution of nitrogen pollutants in each sub-basin.

organic nitrogen and ammonia nitrogen in the study area is closely related to precipitation runoff. The nitrate-nitrogen pollution load is related to the agricultural planting method. The study of the spatial distribution of pollutant load found that the nitrogen pollution in the region showed typical non-point source pollution characteristics. The areas with heavy organic nitrogen and ammonia nitrogen load are mainly located in areas where human activities are intense, while the areas with heavy nitrate-nitrogen load are mainly located in agricultural planting areas. The pollutant load in the tributary area is less than the main steam. Through the establishment of regional nitrogen pollution model and the study of pollutant distribution characteristics, this study puts forward some suggestions for controlling the nitrogen pollution load of the Shanxi Reservoir watershed, optimizes the agricultural planting mode, and intercepts the pollution sources that are not directly discharged into the water body.

In the next phase of the study, SWAT's built-in scenario management module can be applied to set up different management measures for heavily polluted areas, study the reduction of pollutants, and provide decision-making basis for local management departments.

ACKNOWLEDGEMENTS

REFERENCES

Brezonik, P.L. Easter, K. W. Hatch, L. Mulla, D. and Perry, J. 1999. Management of diffuse pollution in agricultural watersheds: Lessons from the Minnesota River basin. J. Water Science & Technology, 39(12): 323-330.

Chen, L., Wang, G., Zhong, Y. C. and Shen, Z. Y. 2016. Evaluating the impacts of soil data on hydrological and nonpoint source pollution prediction. J. Science of the Total Environment, 563-564: 19-28.

Gao, C. and Zhang, T. L. 1999. Management measures for controlling agricultural nutrient polluted water environment in European countries. J. Journal of Ecology and Rural Environment, 15(2): 50-53.

He, C. S., Fu, B.J. and Chen, L. X. 1998. Management and control of non-point source pollution. J. Environmental Science, (5): 87-91.

Hu, X. T., Chen, J. N. and Zhang, T. Z. 2002. A study on non-point source pollution models. J. Chinese Journal of Environmental Science, 23(3): 124.

Joongdae, C., Minhwan, S., Jiseong, Y. and Jeongryeol, J. 2012. Effect of rice straw mulch on runoff and NPS pollution discharges from a vegetable field. J. Soil & Water Engineering International Conference of Agricultural Engineering-cigr-ageng: Agriculture & Engineering for A Healthier Life, 2012.

Mei, K., Shang, X., Wang, Z. F., Huang, S. H., Dong, X. and Huang, H. 2016. Study on the influence of land use on nitrogen memory effect in watershed. J. Journal of Environmental Science, 36(10): 3856-3863.

Narsimlu, B., Gosain, A. K., Chahar, B. R., Singh, S. K. and Srivastava, P. K. 2015. SWAT model calibration and uncertainty analysis for streamflow prediction in the Kunwari River Basin, India, using sequential uncertainty fitting. J. Environmental Processes, 2(1): 79-95.

Wang, X. C. and Jin, M. J. 2016. Progress in the application of distributed hydrological model SWAT in non-point source pollution research. J. Journal of Agricultural Science Yanbian University, 38(3): 271-276.

Wang, Z. G. and Liu, C. M. 2003. The theory of SWAT model and its application in Heihe Basin. J. Progress in Geography, 22(1).

Adsorption of Pb(II) in Aqueous Solution by the Modified Biochar Derived from Corn Straw with Magnesium Chloride

Keyuan Huang, Yuanyuan Cai, Yaowei Du, Jun Song, Huan Mao, Yany Xiao, Yue Wang, Ningcan Yang, Hai Wang and Li Han†

School of Life Science, Shaoxing University, Shaoxing, 312000, P.R. China

†Corresponding author: Li Han; 51778067@qq.com

ABSTRACT

Lead wastewater not only causes deterioration of water quality but also further enters the human body through the food chain and is harmful to human health. Therefore, there is an urgent need to find an economical, simple and efficient water treatment technology to treat lead-contaminated wastewater in waterbodies. In this paper, the modified biochar derived from corn straw by magnesium chloride is prepared. Adsorption experiments of Pb(II) in solution by the modified biochar are carried out. Experiment results show that the modified biochar mainly contains C and O elements, and a large number of functional groups. The adsorption amount of Pb(II) by modified biochar reaches 5.15 mg/g under 0.2 g of modified biochar, 25 mg/L initial concentration of Pb(II) ion, reaction time of 480 min, temperature 25°C and at a speed of 200 rpm. The adsorption process of Pb(II) ions in solution by the modified biochar fits on the Freundlich isotherm model. Pseudo-second order kinetic model can better describe the adsorption process of Pb(II) ion in solution by the modified biochar. The process of adsorbing Pb(II) ions in solution by modified biochar is dominated by multi-layer adsorption process and chemical adsorption process.

INTRODUCTION

With the widespread application of lead products and lead compounds, lead pollution in the environment has become increasingly serious (Fan et al. 2008, Zhu et al. 2014, Chen et al. 2018). Lead wastewater not only causes deterioration of water quality but also further enters the human body through the food chain and is harmful to human health (Shen et al. 2015, Ho et al. 2017, Shen et al. 2019). Therefore, there is an urgent need to find an economical, simple and efficient water treatment technology to treat lead-contaminated wastewater (Hang et al. 2017, Kwak et al. 2019). At present, the methods for removing Pb(II) ions in solution mainly include chemical precipitation, physical filtration separation, bio-concentration, physical adsorption, and chemical removal (Xiong et al. 2017, Zhang et al. 2019). Among these methods, the adsorption method has become one of the priority methods in practice because of its low cost, high efficiency, and easy operation. It is considered to be one of the most interesting treatment methods in current research (Mohan et al. 2014, Shi et al. 2019). Some adsorbents, such as activated carbon, activated zeolite, resin adsorbent, etc., have the disadvantages of high cost, difficulty in separation, and easy secondary pollution (Shen et al. 2017). Therefore, the development of new, cheap and effective adsorption material has attracted

much attention by some researchers (Liu & Zhang 2009, Zhou et al. 2013, Zhou et al. 2017).

Biochar is mainly composed of carbon, hydrogen and oxygen. It is a light carbon material with high carbon content and high aromatization properties (Yahya et al. 2016, Wan et al. 2018, Hang et al. 2019). Therefore, it has a certain adsorption capacity for heavy metals, such as Pb(II) ions, Cu(II) ions, Cr(VI), etc., which affects the distribution, migration and bioavailability of these heavy metals in the environment (Devi & Saroha 2014). However, the adsorption capacity of single biochar for heavy metals is far less than that of a composite modified with other materials (Huang et al. 2015, Huang et al. 2018, Mostafa et al. 2018). The modified biochar by the composite material has the characteristics of low preparation cost, excellent physical and chemical properties, simple operation, good environmental compatibility, etc., and is widely used for the adsorption treatment of heavy metals wastewater (Zhou et al. 2018). The biochar produced by the anoxic pyrolysis of agricultural and forestry waste is a material with developed pore structure, large specific surface area, rich oxygen-containing functional groups and excellent adsorption performance (Mallampati et al. 2012, Mandu et al. 2012, Wang et al. 2015). The yield of the corn stalk

in China is huge, which is a common raw material for the preparation of biochar (Yuan et al. 2011).

In this study, the corn straw is chosen as the biomass raw material, which is pyrolyzed under anaerobic conditions to prepare the modified biochar derived from corn straw. Then biochar is modified by the magnesium chloride. The modified biochar by magnesium chloride is obtained. Adsorption experiments of Pb(II) in solution by the modified biochar are carried out in the laboratory. Adsorption kinetics and adsorption isotherms have been discussed in detail.

MATERIALS AND METHODS

Preparation of biochar: The corn straw from the farmland in the suburbs of Jinan city was washed several times with distilled water and dried at 105°C to constant weight. It was then pulverized and passed through a 40 mesh sieve. 20 g of 40-mesh corn straw was pyrolyzed in a muffle furnace at 250°C for 2 hours. The entire operational process was carried out under N_2 gas condition. It was cooled to room temperature, smashed and sieved into 100 mesh to obtain the biochar.

Preparation of the modified biochar by magnesium chloride: 2 g of biochar was taken in a 250 mL Erlenmeyer flask containing 100 mL of 0.01 mol/L magnesium chloride solution and stirred on a magnetic stirrer for 6 hours. It was washed 3 times with distilled water and dried at 105°C to constant weight to obtain the modified biochar by magnesium

chloride. The characteristics of biochar were determined by SEM, EDS and FT-IR.

Adsorption experiment: 0.2 g of biochar or 0.2 g of modified biochar was taken in a 250 mL Erlenmeyer flask containing 100 mL of 25 mg/L $Pb(NO_3)_2$ solution. It was shaken for 480 minutes in a constant temperature shaking box at 25°C and a speed of 200 rpm. The sample was filtered through a 0.45 μm filter and determined by atomic absorption spectrometry. Each adsorption test was repeated three times.

Data analysis: The amount of adsorption was calculated by the following formula:

$$q_e = \frac{(C_0 - C_e) \times V}{m} \qquad \ldots(1)$$

Where, q_e (mg/g) is the amount of adsorption per unit mass of adsorbent at the end of adsorption. C_0 (mg/L) and C_e (mg/L) are the initial concentration of the adsorbate in the solution and the concentration at the equilibrium of adsorption. V (mL) is the volume of solution and m (g) is the dosage of the modified biochar.

RESULTS AND DISCUSSION

The characteristics of modified biochar: The SEM image of modified biochar is shown in Fig.1. The surface of the modified biochar is very smooth and some fragments are present. The specific surface area of modified biochar is relatively large, which is favourable for adsorption.
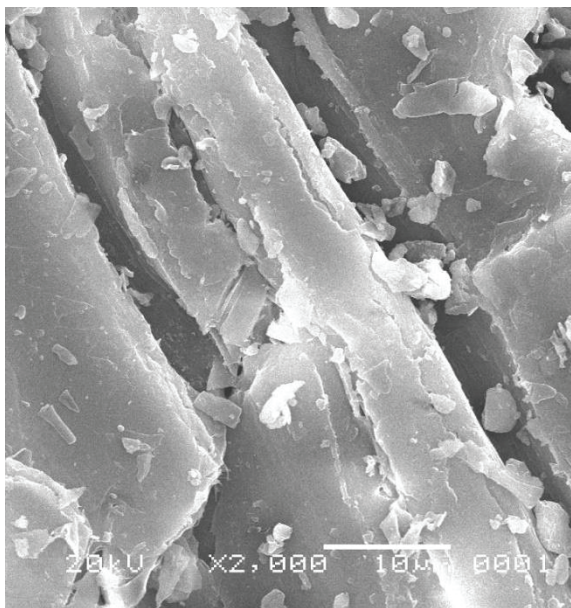

Fig.1: SEM image of modified biochar.

Fig. 2 shows the EDS analysis of biochar. As shown in Fig.2, it implies that modified biochar mainly contains C and O elements, and their contents are 68.85% and 26.68% respectively. This can be thought that the modified biochar is hydrophilic and polar. A small amount of element, such as Mg, Si, S, Cl, K and Ca, is also present on the surface of the modified biochar.

The FT-IR spectra of modified biochar are shown in Fig. 3. It can be concluded that the surface of the modified biochar contains a large number of functional groups. The peak shape is wider between 3100 cm^{-1} and 3600 cm^{-1}, which is -OH stretching vibration (Wang et al. 2008). The peak at 1695 cm^{-1} is the stretching vibration peak of C=O in -COOH functional group. The absorption peak at 1440 cm^{-1} is a C=O stretching vibration (Zhang et al. 2018). The absorption peak at 1228 cm^{-1} is a C-O stretching vibration peak. The peak between 515 cm^{-1} and 735 cm^{-1} is C-H stretching vibration peak (Li et al. 2019). The presence of these functional groups will facilitate the adsorption of pollutant by the modified biochar (Günay et al. 2007).

Adsorption capacity experiment: It can be seen from Fig. 4 that the adsorption capacity of Pb(II) ions in aqueous solution by the modified biochar is significantly enhanced. The adsorption capacity of Pb(II) ions by the modified biochar is more than twice than the unmodified biochar. The adsorption amount of Pb(II) by modified biochar reaches 5.15 mg/g under 0.2 g of modified biochar, 25 mg/L initial concentration of Pb(II) ion, react time of 480 min, temperature 25°C and at a speed of 200 rpm.

Adsorption kinetic: The process of describing the adsorption of solids to liquids is often described by Pseudo-first order kinetic equations and Pseudo-second order kinetic
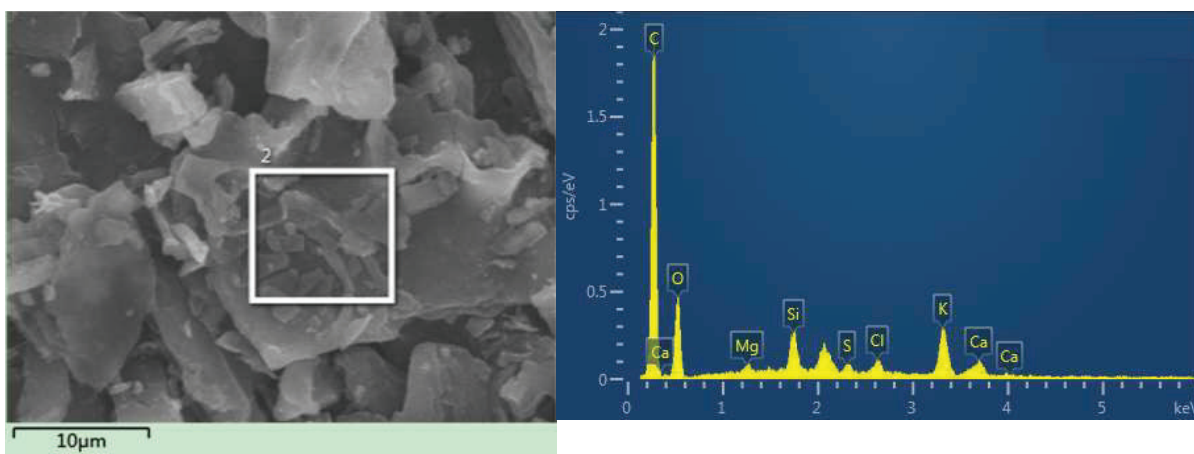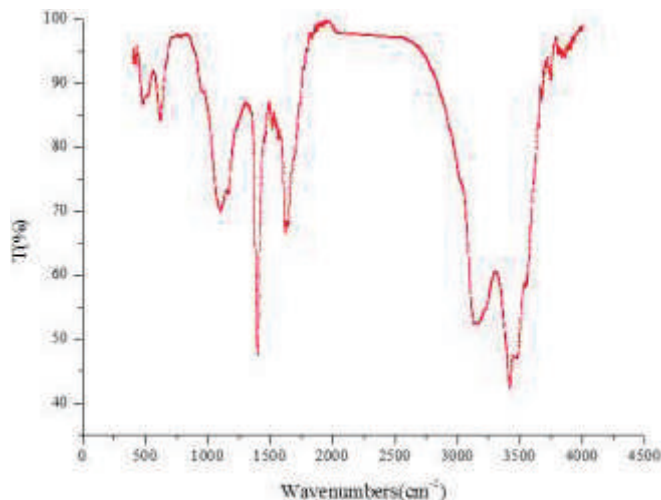

Fig. 2: EDS analysis of modified biochar.

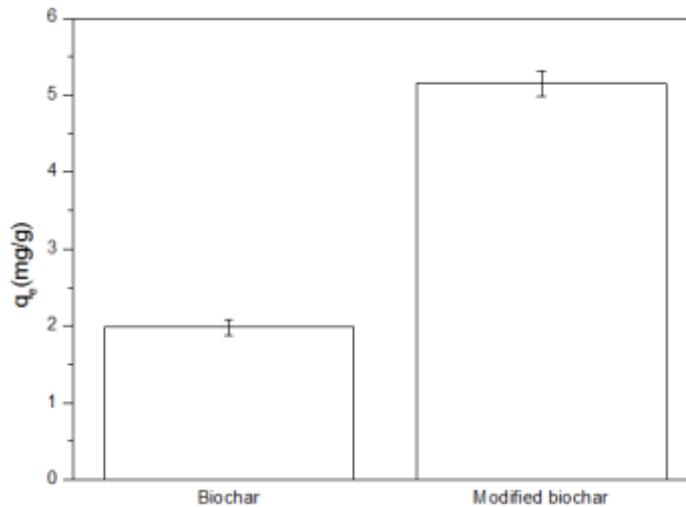Fig. 3: FT-IR spectra of modified biochar.

Fig. 4: Adsorption amount of Pb(II) ions in solution by biochar and modified biochar.

equations. Its expression is Eq. 2 and Eq. 3 (Giles et al. 1960).

$$q_t = q_e(1 - e^{-K_1 t}) \qquad \dots(2)$$

$$\frac{t}{q_t} = \frac{1}{K_2 q_e^2} + \frac{t}{q_e} \qquad \dots(3)$$

Where q_t (mg/g) and q_e (mg/g) are adsorption amount of the adsorbent to the adsorbate at the adsorption time t (min) and the adsorption equilibrium respectively. K_1 (min^{-1}) and K_2 (min^{-1}) are constants.

The adsorption experiments of the contact time influence were carried out according to the following experimental procedure. 0.2 g of modified biochar was taken in a 250 mL Erlenmeyer flask containing 100 mL of 25 mg/L Pb(NO$_3$)$_2$ solution. The contents were shaken for a serial contact time (5, 10, 15, 30, 45, 60, 120, 240, 360 and 480 min) in a constant temperature at 25°C and a speed of 200 rpm. According to the test results, the fitting equation was performed according to Eq. 2 and Eq. 3. The adsorption kinetic parameters of modified biochar on Pb(II) ions in solution are given in Table 1. According to the value of R^2, the pseudo-second order kinetic model can better describe the adsorption process of modified biochar on Pb(II) ion in solution. Therefore, it can be concluded that the process of adsorbing Pb(II) ions in solution by modified biochar is mainly chemical adsorption.

Adsorption isotherms: In this study, Langmuir isotherm model and Freundlich isotherm model were chosen to describe the adsorption isotherm. Their equations are as below (Liu & Liu 2008, Foroughi-dahr et al. 2015):

$$q_e = \frac{K_L q_{max}}{1 + K_L C_e} \times C_e \qquad \dots(4)$$

$$\ln q_e = \ln K_F + \frac{1}{n} \ln C_e \qquad \dots(5)$$

Where, C_e (mg/L) is the equilibrium concentration in the solution, q_e (mg/g) is the adsorbate adsorbed at equilibrium, q_{max} (mg/g) is the maximum adsorption capacity, n is the Freundlich constant related to adsorption intensity, K_L (L/mg) and K_F ((mg/g)$^{1/n}$) are the adsorption constants for Langmuir and Freundlich models respectively.

The adsorption experiments of the Pb(II) ions concentration influence were carried out. 0.2 g of modified biochar was taken in a 250 mL Erlenmeyer flask containing 100 mL of a serial of Pb(II) ions concentration (20, 40, 60, 80 and 100 mg/L). They were shaken for 480 minutes in a constant temperature shaking box at 25°C and a speed of 200 rpm. According to the results of the adsorption experiments and Eq. 4 and Eq. 5, parameters of Langmuir isotherm model and Freundlich isotherm model for the description of Pb(II)

Table 1: Kinetics parameters of Pb(II) ions in solution by modified biochar.

Pseudo-first order kinetic model			Pseudo-second order kinetic model		
K_1(min^{-1})	q_e(mg/g)	R^2	K_2(min^{-1})	q_e(mg/g)	R^2
0.03	5.31	0.942	0.09	5.68	0.986

Table 2: Parameters of the Langmuir isotherm model and Freundlich isotherm model for the description of Pb(II) ions in solution adsorption onto modified biochar.

Langmuir			Freundlich		
q_{max}(mg/g)	K_L(L/mg)	R^2	K_F((mg/g)$^{1/n}$)	n	R^2
6.12	0.03	0.747	2.24	0.18	0.982

ions in solution adsorption onto modified biochar are given in Table 2.

From Table 2, Freundlich isotherm model can better describe the adsorption isothermal process of modified biochar on Pb(II) ions in solution according to the value of R^2. The adsorption process is monolayer adsorption process. Therefore, it can be concluded that the process of adsorbing Pb(II) ions in solution by modified biochar is dominated by multi-layer adsorption.

CONCLUSIONS

Based on the above experimental results, the following conclusions can be drawn.

(1) The adsorption ability of Pb(II) ions in solution by the modified biochar is better than that of the unmodified biochar. The surface of the modified biochar is very smooth structure and some fragments are present. It contains a large number of functional groups, such as C=O, C-H, -OH, etc.

(2) The adsorption amount of Pb(II) by modified biochar reaches 5.15 mg/g under 0.2 g of modified biochar, 25 mg/L initial concentration of Pb(II) ion, react time of 480 min, temperature 25°C and a speed of 200 rpm.

(3) Pseudo-second order kinetic model can better describe the adsorption process of modified biochar on Pb(II) ion in solution. The process of modified biochar on Pb(II) ions in solution fits the Freundlich isotherm model.

(4) The process of adsorbing Pb(II) ions in solution by modified biochar is dominated by multi-layer adsorption and chemical adsorption process.

ACKNOWLEDGEMENTS

REFERENCES

Chen, Y.F., Ho, S.H., Wang, D.W., Wei, Z.S., Chang, J.S. and Ren, N.Q. 2018. Lead removal by a magnetic biochar derived from persulfate-ZVI treated sludge together with one-pot pyrolysis. Bioresource Tech., 247: 463-470.

Devi, P. and Saroha, A.K. 2014. Synthesis of the magnetic biochar composites for use as an adsorbent for the removal of pentachlorophenol from the effluent. Bioresource Tech., 169: 525-531.

Fan, T., Liu, Y., Feng, B., Zeng, G., Yang, C., Zhou, M., Zhou, H., Tan, Z. and Wang, X. 2008. Biosorption of cadmium(II), zinc(II) and lead(II) by *Penicillium simplicissimum*: isotherms, kinetics and thermodynamics. J. Hazard. Mater., 160: 655-661.

Foroughi-dahr, M., Abolghasemi, H., Esmaieli, M., Nazari, G. and Rasem, B. 2015. Experimental study on the adsorptive behavior of Congo red in cationic surfactant-modified tea waste. Process Saf. Environ., 95: 226-236.

Giles, C.H., MacEwan, T., Nakhwa, S. and Smith, D. 1960. Studies in adsorption. Part XI. A system of classification of solution adsorption isotherms, and its use in diagnosis of adsorption mechanisms and in measurement of specific surface areas of solids. J. Chem. Soc., 6: 3973-3993.

Günay, A., Arslankaya, E. and Tosun, I. 2007. Lead removal from aqueous solution by natural and pretreated clinoptilolite: Adsorption equilibrium and kinetics. J. Hazard. Mater, 146: 362-371.

Hang, Y., Si, Y., Zhou, Q., Yin, H.B., Wang, A.L. and Cao, A.M. 2019. Morphology-controlled synthesis of calcium titanate particles and adsorption kinetics, isotherms, and thermodynamics of Cd(II), Pb(II), and Cu(II) cations. J. Hazard. Mater., 380: 120789-120798.

Hang, Y., Yin, H., Ji, Y., Liu, Y., Lu, Z., Wang, A., Shen, L. and Yin, H.X. 2017. Adsorption performances of naked and 3-aminopropyl triethoxysilane-modified mesoporous TiO_2 hollow nanospheres for Cu^{2+}, Cd^{2+}, Pb^{2+}, and Cr(VI) ions. J. Nanosci. Nanotechnol., 17: 5539-5549.

Ho, S.H., Chen, Y.D., Yang, Z.K., Nagarajan, D., Chang, J.S. and Ren, N.Q. 2017. High-efficiency removal of lead from wastewater by biochar derived from anaerobic digestion sludge. Bioresource Tech., 246: 142-149.

Huang, D.L., Deng, R., Wan, J., Zeng, G.M., Xue, W.J., Wen, X.F., Zhou, C.Y., Hu, L., Liu, X.G., Xu, P., Guo, X.Y. and Ren, X.Y. 2018. Remediation of lead-contaminated sediment by biochar-supported nano-chlorapatite: Accompanied with the change of available phosphorus and organic matters. J. Hazard. Mater., 348: 109-116.

Huang, X., Liu, Y., Liu, S., Tan, X., Ding, Y., Zeng, G., Zhou, Y., Zhang, M., Wang, S. and Zheng, B. 2015. Effective removal of Cr(VI) using -cyclodextrin-chitosan modified biochars with adsorption/reduction bifunctional roles. RSC Adv., 6: 94-104.

Kwak, J.H., Islam, M.S., Wang, S.Y., Selamawit, A.M., Naeth, M.A., Mohamed, G.E. and Scott X.C. 2019. Biochar properties and lead(II) adsorption capacity depend on feedstock type, pyrolysis temperature, and steam activation. Chemosphere, 231: 393-404.

Li, J.H., Zheng, L.R., Wang, S.L., Wu, Z.P., Wu, W.D., Nabeel, K.N., Sabry, M.S., Jörg, R., Bolan, N., Yong, S. and Wang, H.L. 2019. Sorption mechanisms of lead on silicon-rich biochar in aqueous solution: Spectroscopic investigation. Sci. Total Environ., 672: 572-582.

Liu, Y. and Liu, Y.J. 2008. Biosorption isotherms, kinetics and thermodynamics. Sep. Purif. Tech., 61: 229-242.

Liu, Z.G. and Zhang, F.S. 2009. Removal of lead from water using biochars prepared from hydrothermal liquefaction of biomass. J. Hazard. Mater., 167 (1-3): 933-939.

Mallampati, S.R., Mitoma, Y., Okuda, T., Sakita, S. and Kakeda, M. 2012. Enhanced heavy metal immobilization in soil by grinding with addition of nanometallic Ca/CaO dispersion mixture. Chemosphere, 89: 717-723.

Mandu, I., Gao, B., Yao, Y., Xue, Y.W., Zimmerman, A., Pratap, P. and Cao, X.D. 2012. Removal of heavy metals from aqueous solution by biochars derived from anaerobically digested biomass. Bioresource Tech., 110: 50-56.

Mohan, D., Kumar, H., Sarswat, A. and Alexandre, F.M. 2014. Cadmium and lead remediation using magnetic oak wood and oak bark fast pyrolysis biochars. Chem. Eng. J., 236: 513-528.

Mostafa, F.E., Ahmed, M., Gao, B., Yin, X.Q., Zahoor, A. and Wang, H.Y. 2018. Sorption of lead ions onto oxidized bagasse-biochar mitigates Pb-induced oxidative stress on hydroponically grown chicory: Experimental observations and mechanisms. Chemosphere, 208: 887-898.

Shen, Z.T., Hou, D.Y., Jin, F., Shi, J.X., Fan, X.L., Tsang, C.W. and Aless, D.S. 2019. Effect of production temperature on lead removal mechanisms by rice straw biochars. Sci. Total Environ., 655: 751-758.

Shen, Z.T., Jin, F., Wang, F., McMillan, O. and Al-Tabbaa, A. 2015. Sorption of lead by Salisbury biochar produced from British broadleaf hardwood. Bioresource Tech., 193: 553-556.

Shen, Z.T., Zhang, Y.Y., Jin, F., McMillan, O. and Al-Tabbaa, A. 2017. Qualitative and quantitative characterisation of adsorption mechanisms of lead on four biochars. Sci. Total Environ., 609: 1401-1410.

Shi, J.X., Fan, X.L., C.W.T, Wang, D., Shen, F., Hou, Z.T. and Alessi, S.D. 2019. Removal of lead by rice husk biochars produced at different temperatures and implications for their environmental utilizations. Chemosphere, 235: 825-831.

Wan, S.L., Wu, J.Y., Zhou, S.S., Wang, R., Gao, B. and He, F. 2018. Enhanced lead and cadmium removal using biochar-supported hydrated manganese oxide (HMO) nanoparticles: Behavior and mechanism. Sci. Total Environ., 616-617: 1298-1306.

Wang, S., Gao, B., Li, Y., Mosa, A., Zimmerman, A.R., Ma, L.Q., Harris, W.G. and Migliaccio, K.W. 2015. Manganese oxide-modified biochars: Preparation, characterization, and sorption of arsenate and lead. Bioresource Tech., 181: 13-17.

Wang, X.S., Tang, Y.P. and Tao, S.R. 2008. Removal of Cr(VI) from aqueous solutions by the nonliving biomass of Alligator weed: Kinetics and equilibrium. Adsorption J. Int. Adsorption Soc., 14: 823-830.

Xiong, W., Jing, T., Yang, Z., Zeng, G., Zhou, Y., Wang, D., Song, P., Rui, X., Chen, Z. and Min, C. 2017. Adsorption of phosphate from aqueous solution using iron-zirconium modified activated carbon nanofiber: performance and mechanism. J. Colloid Interf. Sci, 493: 17-23.

Yahya, N.Y., Ngadi, N., Jusoh, M. and Halim, N.A.A., 2016. Characterization and parametric study of mesoporous calcium titanate catalyst for transesterification of waste cooking oil into biodiesel. Energy Convers. Manage, 129: 275-283.

Yuan, J.H., Xu, R.K. and Zhang, H. 2011. The forms of alkalis in the biochar produced from crop residues at different temperatures. Bioresource Tech., 102: 3488-3497.

Zhang, J.Q., Hu, X.L., Zhang, K.J. and Xue, Y.W. 2019. Desorption of calcium-rich crayfish shell biochar for the removal of lead from aqueous solutions. J. Colloid Interf. Sci., 554: 417-423.

Zhang, S.Q., Yang, X., Liu, L., Ju, M.T. and Zheng, K. 2018. Adsorption behavior of selective recognition functionalized biochar to Cd(II) in wastewater. Materials, 11: 299-305.

Zhu, X., Liu, Y., Feng, Q., Chao, Z., Zhang, S. and Chen, J. 2014. Preparation of magnetic porous carbon from waste hydrochar by simultaneous activation and magnetization for tetracycline removal. Bioresource Tech., 154(2): 209-214.

Zhou, X.H., Liu, Y.C., Zhou, J.J., Guo, J., Ren, J.L. and Zhou, F. 2018. Efficient removal of lead from aqueous solution by urea-functionalized magnetic biochar: Preparation, characterization and mechanism study. J. Taiwan Inst. Chem. Eng., 91: 457-467.

Zhou, Y.M., Gao, B., Zimmerman, R.A., Fang, J., Sun, Y.N. and Cao, X.D. 2013. Sorption of heavy metals on chitosan-modified biochars and its biological effects. Chem. Eng. J., 231: 512-518.

Zhou, Y.Y., Liu, X.C., Xiang, Y.J., Wang, P., Zhang, J.C., Zhang, F.F., Wei, J.H., Luo, L., Lei, M. and Tang, L. 2017. Modification of biochar derived from sawdust and its application in removal of tetracycline and copper from aqueous solution: Adsorption mechanism and modeling. Bioresource Tech., 245: 266-273.

Adaptations to Climate Variability and Agrarian Crisis in Kolar District, Karnataka, India

B.N. Krishnakanth and B.C. Nagaraja†

Department of Environmental Science, Bangalore University, Bangalore-560 056, Karnataka, India

†Corresponding author: B.C. Nagaraja; nagenvi@gmail.com

ABSTRACT

The dynamics in climatic variability is prominently affecting the agriculture system, particularly the small and marginal land holding farmers in arid and semi-arid regions which are highly vulnerable. The present study in Kolar district assessed the variability scale and dynamics of rainfall over the decades, it revealed the current day's agrarian crisis, resulting in impacts on farmers and adaptations by farmers to changing situations. The study also reveals that over the decades there has been a considerable variation in rainfall pattern in the study area but there was no significant average rainfall variation till the last decade, after which there was a significant seasonal variation that directly affects the sowing pattern and associated agricultural practices. The exploitation of groundwater for water-intensive commercial crops has increased rapidly from the past decade that resulted in the critically depleted groundwater table. To meet the livelihood demands some farmers were observed to have shifted to non-agricultural occupations. It is a serious threat at this point of time as the agriculture output has to be fed to the larger portion of the society and decreased output from agriculture eventually leads to inflation. So, it is very crucial to adapt all possible measures to retain farmers in agriculture practice. Hence, understanding and scientific assessment of the risks associated with the changing climate and its variables is the need of the hour, particularly in arid and semi-arid regions which are going to be highly vulnerable. Studies like this will help in policy-making and management planning to cope up with the dynamic climatic factors.

INTRODUCTION

Climate change is one of the most harmful global problems and considered a bottle-neck for sustainable development (Lema & Majule 2009). Climate is an important factor for agricultural productivity and any variation in these factors is bound to result in a larger impact on crop yield (Ashalatha et al. 2012). Climate variability has proved and continues to be the prime cause of imbalance in global food production in the developing world, particularly in arid and semi-arid tropical countries. Agricultural productivity in tropical Asia is dependent not only on temperature variations but also to varying monsoon patterns (Sivakumar et al. 2005).

Agriculture in India accounts for a major share in GDP (16%) and even shares major portion (49%) of employment and also has the potential to act as a hindrance to development (Hari et al. 2018). In Karnataka, more than 70% of the geographical area is classified as an arid or semi-arid region which constitutes about 18% of land under this category in India (Nautiyal et al. 2018).

About 700 million (60%) people in India are dependent on agriculture and associated occupations in one or the other

way (Kuruvilla 2013). Failing to adapt to climate change by the farmers will result in the reduction of agricultural production by 12% average and by up to 18% in rain-fed areas by the end of this century (Hari et al. 2018). The current study was thus aimed at understanding the historical rainfall behaviour and the farmers' perception of climate variability, impacts and adaptation strategies in the agricultural sector in Kolar district.

STUDY AREA AND METHODOLOGY

Kolar is an administrative district in the South Indian state of Karnataka (Fig. 1). It is the headquarter of Kolar District and is historically known for gold mining. Administratively, the district is divided into 6 taluks, viz. Bangarpet, Kolar, Mulbagal, Malur, KGF & Srinivasapur, 27 Hoblies and 156 Gram Panchayats. Among the taluks in the district, Srinivasapura is the biggest (860 sq.km) and Malur is the smallest taluk (645sq.km). Kolar is also called the land of silk, milk and gold. Farmers are known for horticulture, floriculture, sericulture and growing vegetable crops. The district lies almost in the central part of peninsular India, which has an immense bearing on its geo-climatic conditions. The district
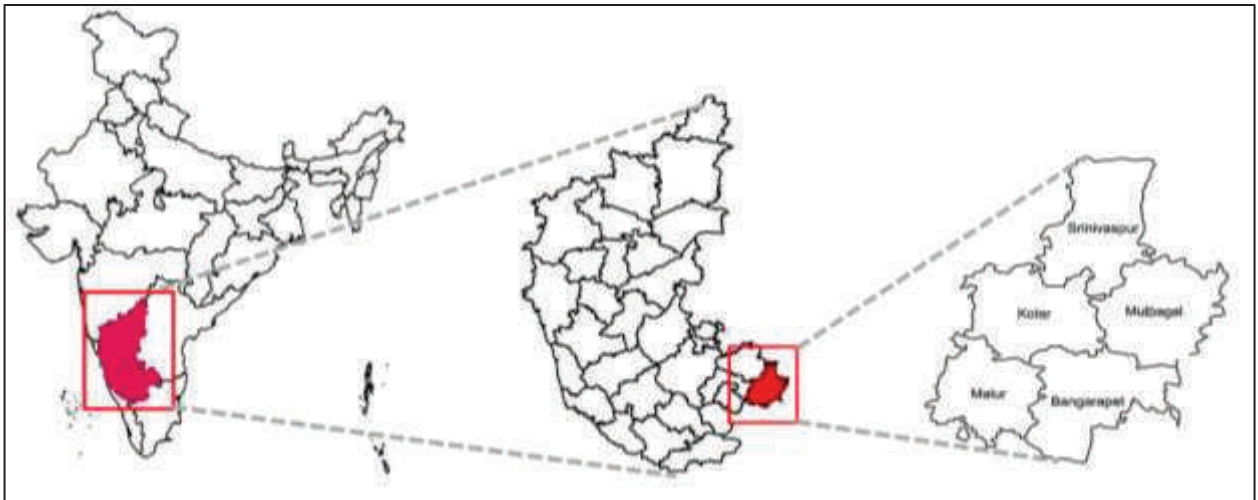
Fig. 1: The study area.

has about 29936 bore wells which are also highest in the state and is the main source of irrigation.

The primary objective of this study was aimed at understanding the farmers' perception of climate and variability, impacts and adaptation strategies in the agricultural sector. Both secondary and primary data were used. A mixed-method approach (combination of quantitative and qualitative methods), along with tools from both social and environmental sciences were used for primary data collection. Tools such as Participatory Rural Appraisal (PRA) and Focus Group Discussions (FGD) (Uddin & Anjuman 2013) were adopted to understand the historical agriculture in the region. A total of 61 households in villages from Bangarpet, KGF, Kolar, Malur, Mulbagal and Srinivaspura taluks were interviewed. The combined use of qualitative and quantitative techniques, particularly in assessing the adaption and impacts in agriculture can give us the confidence about what information is being gathered, observed, measured and analysed to arrive at the findings (Place et al. 2007).

RESULTS AND DISCUSSION

Rainfall Trend Analysis

Rainfall is an important climatic factor that plays a vital role in agriculture, particularly in the arid and semi-arid regions, where the availability of surface and groundwater is very less. Agriculture productivity is the key contributor to the country's economy and declined agriculture production due to altering climatic factors will result in various socio-economic crisis.

To understand the historical behaviour of rainfall, day-wise rainfall data of the study area was acquired from Karnataka State Natural Disaster Management Centre from 1971 to 2017 and analysed. The five decadal rainfall trend analysis (Fig. 2) revealed that Mulbagal taluk received consistent rainfall compared to other taluks of the study area with a mean rainfall of 812 mm. During 1981-1985, it received the lowest average rainfall of 630 mm and the highest annual average rainfall of 924 mm was recorded during 1996-2000. Kolar taluk stands second with a mean rainfall of 807 mm, highest annual average of 926 mm during 1996-2000 and lowest of 632 mm during 1981-1985. Malur, Bangarpet and Srinivaspur taluks showed that there is a moderate amount of variation in rainfall over the decades. The mean rainfall during the last 4.5 decades among the 5 taluks ranged from 770-812 mm, which reveals that Kolar district historically received consistent annual rainfall without any considerable variation in rainfall.

The monthly average rainfall data of the last decade were analysed to understand climate variability in Kolar district (Fig. 3). The results revealed that December, January, February and March received a negligible amount of rainfall except March received 75 mm in 2008 and December received 81 mm in 2016, April received mean rainfall of 45 mm with the highest monthly average of 105 mm during 2015 and lowest of 3 mm in 2016. Whereas May received more rainfall compared to June and July months with a mean rainfall of 109 mm, highest of 163 mm and lowest of 70 mm. May has behaved more consistently in rainfall throughout the decade. June and July months which are beginning of monsoon in Karnataka exhibits similar behaviour in the entire decade with the lowest rainfall of 23 mm in 2008 and highest of 176 mm in 2016. June, July and August months showed a considerable amount of variation in rainfall throughout the decade, it indicates that it influences
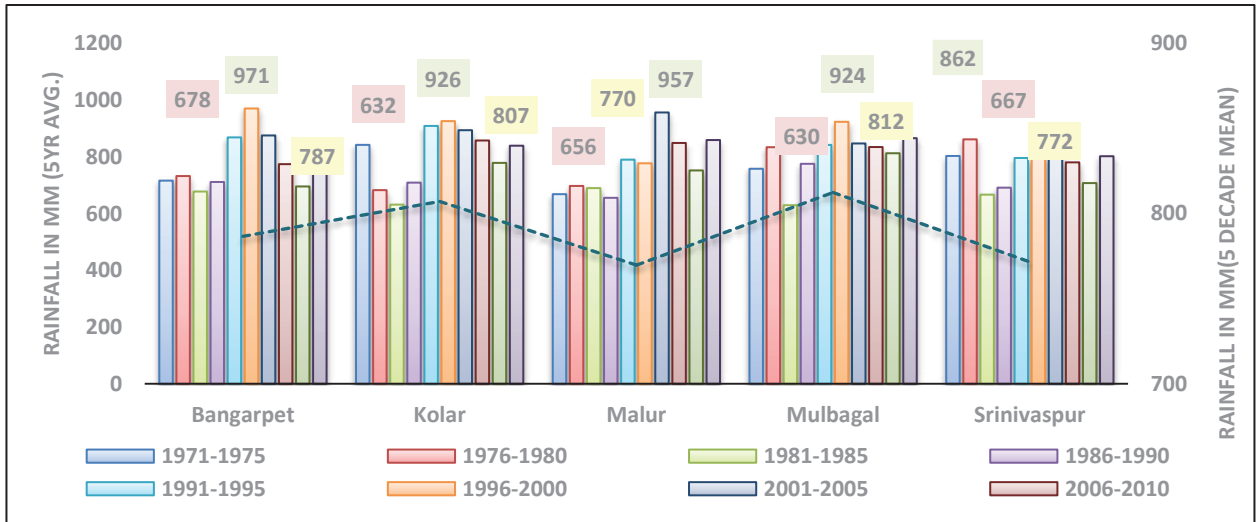
Fig. 2: Five-year average rainfall trend in the last four and half decades of Kolar District.

rain-fed cropping in the region. September which falls in the latter part of monsoon received maximum rainfall in a year for the entire decade with a mean rainfall of 131 mm, highest of 268 mm in 2009 and lowest of 31 mm in 2012. October and November fall in post-monsoon season, of which October received maximum rainfall with a mean rainfall of 122 mm and highest of 310 mm during 2017, but November 2015 recorded highest average rainfall of 349 mm.

To understand the inter-seasonal variation in rainfall, season-wise average rainfall analysis (Fig. 4) was conducted for last one decade, March and May months were categorized as pre-monsoon, June to September as monsoon and October to December as post-monsoon seasons. The results revealed that pre-monsoon received a mean rainfall of 173 mm, the highest rainfall of 228 mm in 2015 and lowest of 121 mm during 2014. Result also revealed that average pre-monsoon
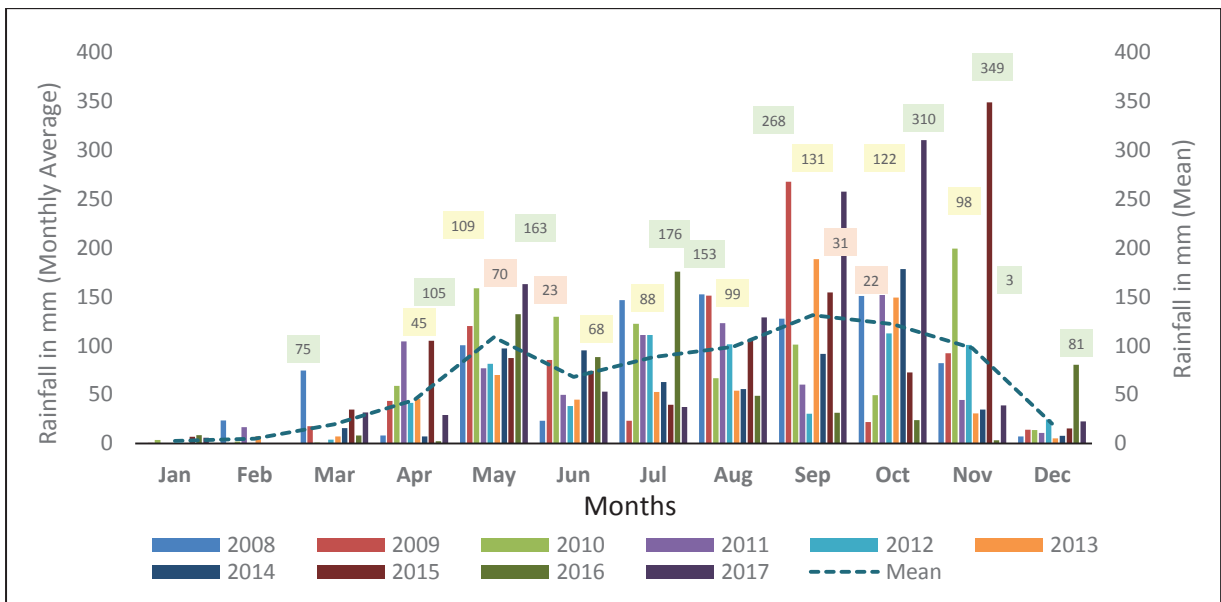

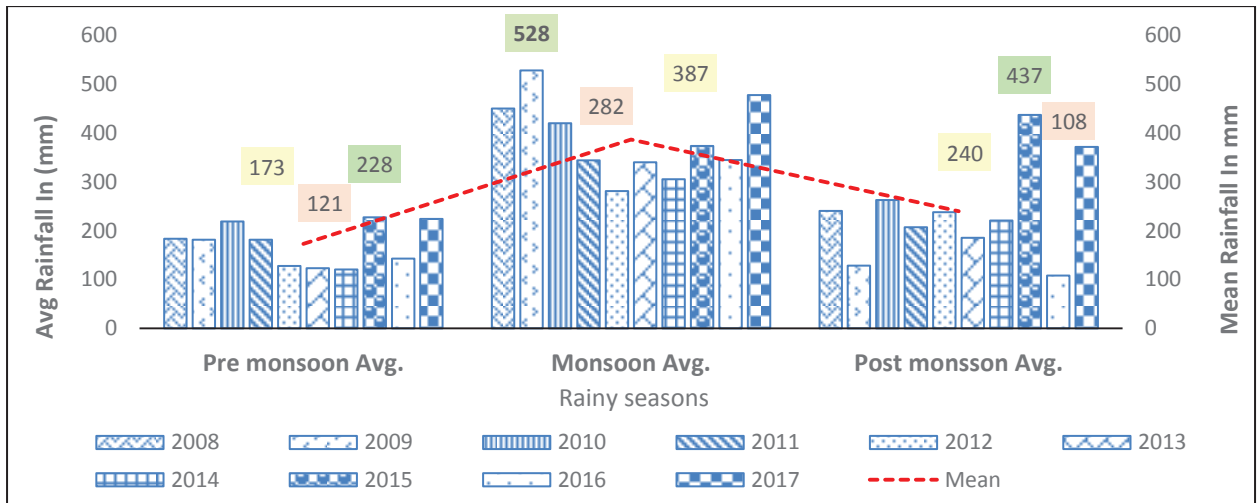Fig. 3: Decadal monthly average rainfall trends in Kolar district.

Fig. 4: Season-wise decadal rainfall trends in Kolar district.

rainfall showed downtrend from 2010 to 2014. Monsoon season received mean rainfall of 387 mm, highest of 528 mm in 2009 and showed downtrend till 2012, lowest was 282 mm in 2012 and from 2013 the rainfall showed an increasing trend. Post monsoon has irregularly behaved throughout the decade with the highest rainfall of 437 mm in 2015 to lowest of 108 mm in 2016 with a mean rainfall of 240 mm.

Agrarian Crisis

The information on farmer's perception, climate variability and adaptations to the agrarian crisis was collected from selected households in villages falling in the study area. Study reveals that all the respondents opined that they are experiencing irregular monsoon in the last one decade.

About 72% of respondents opined that irregular monsoon attributes for drought scenario, 12% respondents expressed groundwater depletion while 9 % expressed dependency on water-intensive crops, and 6 % opined unscientific agriculture practices and 1% respondents expressed that all the above factors attribute for drought (Fig. 5). About 42% of the respondents opined overexploitation of groundwater, 36% opined lack of rainfall, 14 % opined eucalyptus plantation while 8% expressed lack of rainwater harvesting measures as the reasons for bore-well failure in the region (Fig. 6). Regarding fallow land, 70% opined water shortage as the prime cause, while 25 & 20% respondents expressed lack of capital and labour shortage respectively as the reasons accounting for fallow land (Fig. 7).
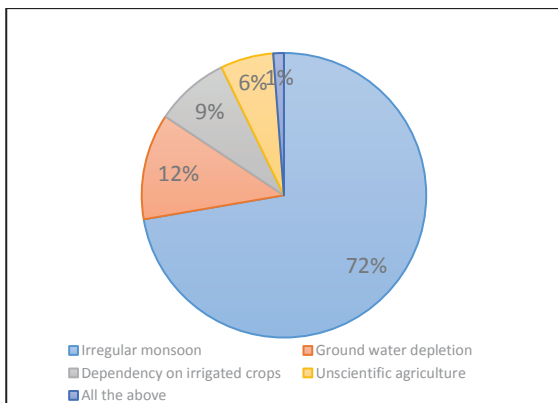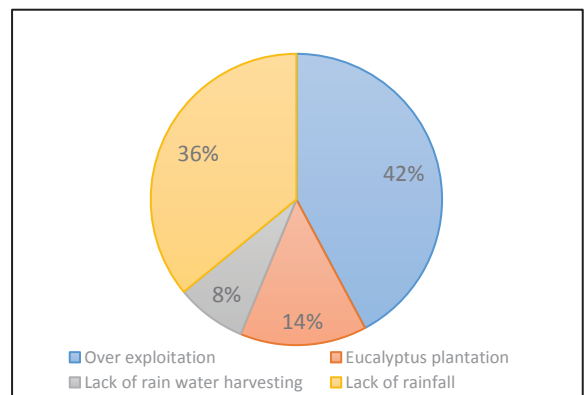

Fig. 5: Farmer's perception on Drought.

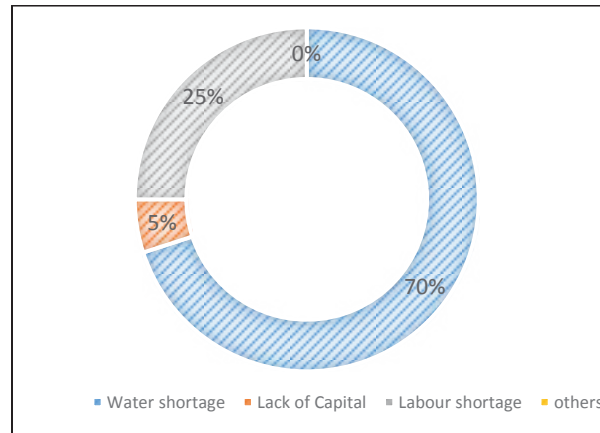Fig. 6: Farmer's perception on bore-well failure.\

Fig. 7: Farmer's perception on fallow land.

Table 1: The tree population in Kolar district, Karnataka.

| Sl. No.	Tree Species	No. of individuals
1	*Santalum album* L.	850
2	*Mangifera indica* L.	709
3	*Tectona grandis* L. f.	366
4	*Eucalyptus globulus* Labill.	341
5	*Pongamia pinnata* (L.) Pierre	224
6	*Azadirachta indica* A. Juss.	217
7	*Tamarindus indica* L.	191
8	*Melia dubia* Cav	160
9	*Grevillea robusta* A. Cunn. ex R. Br.	150
10	*Anacardium occidentale* L.	150
11	*Syzygium cumini* var. cumini	19
12	*Moringa oleifera* Lam.	4
13	*Cinnamomum camphora* (L.) J. Presl	4
14	*Aegle marmelos* (L.) Correa	3
15	*Artocarpus heterophyllus* Lam.	1
16	*Ficus benghalensis* L. var. *krishnae* (C. DC.) Corner	1
17	*Murraya koenigii* (L.) Spreng.	1
18	*Manilkara zapota* (L.) P.Royen	1
	Total	3392
1	*Cocos nucifera* L.	719
2	*Musa paradisiaca* L.	30
3	*Carica papaya* L.	17
	Grand Total	4158
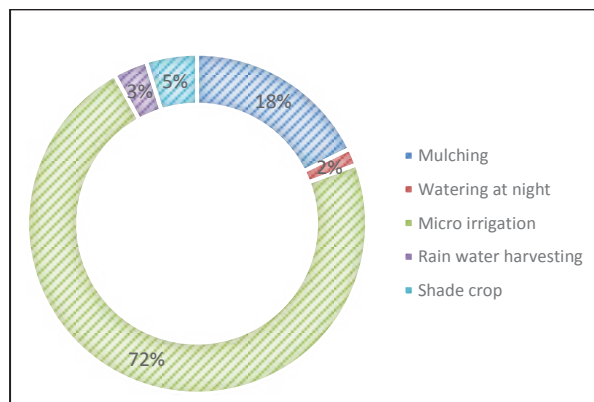
Fig. 8: Agricultural best practices.
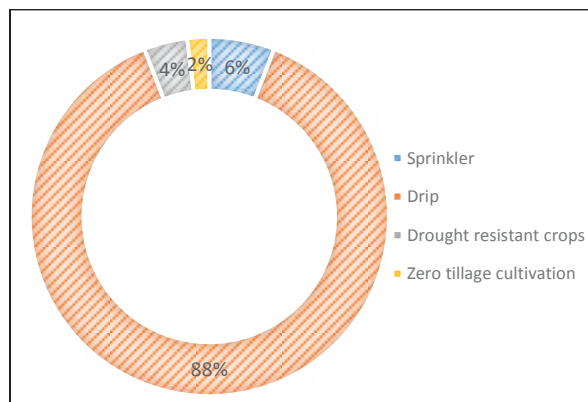
Fig. 9: Irrigation Measures to conserve water.

Adaptations

Agroforestry practice is essentially important to overcome the impacts of prolonged droughts and crop failure resulting from monsoon shifts. Farmers can rely on agroforestry as an alternate source of income during drought, it also plays a vital role in integrated soil nutrient management, providing a sustainable source of fodder and timber. Results of the household survey revealed that 85% of the respondents practiced agroforestry that includes 18 tree species, predominantly *Santalum album* and *Mangifera indica* (Table 1).

The present study revealed that 72% farmers practiced micro-irrigation system and 18 % used mulching techniques, 2% adopted night-time irrigation, 5% used shade crops to avoid evaporation after irrigation and 3% practiced rainwater harvesting (Fig. 8). Further, 88% farmers incorporated drip irrigation, 6% used sprinkler system, 2% practiced zero tillage method to preserve soil moisture and 4 % shifted to drought resistant crop varieties to cope with water scarcity (Fig. 9).

Survey also revealed that some farmers have shifted to other occupations to feed the livelihood demands, 15% farmers have shifted to other occupations to overcome drought impacts, about 23 % respondents expressed low yield in agriculture as the reason for the shift, 23% opined low rainfall, 23% expressed non-availability of the marketplace, 14% opined labour shortage, 4% expressed middle man interference while 9% opined as other reasons.

About 48% of farmers expressed that there is support from the Government to mitigate Agrarian crisis with adequate financial resources and 52% expressed that there is no support. Programs such as farm pond, crop insurance and distribution of free seeds and fertilizers were found to be most effective as 34, 35 and 28% farmers opined

respectively, while only 3% expressed crop appreciation pay as benefiting.

CONCLUSION

Over decades there was a considerable variation in rainfall pattern in the study area, but there was no significant average rainfall variation till the last decade. This significant seasonal variation directly affects the sowing pattern and associated agricultural practices. Increase in the exploitation of groundwater for water-intensive commercial crops has increased rapidly from the past one decade resulting in the critically depleted groundwater table. Adding to this, there are no effective rainwater harvesting and recharge mechanisms in the region. Farmers are fighting repeated droughts and irregular monsoon, resulting in shifting of farmers from agriculture to other occupations which eventually leads to inflation. Hence, it is very crucial to adapt all the possible measures to retain the farmers in agriculture practice. Even though the government have taken up several programs, it was observed that there are still significant gaps in effective implementation and percolation of benefits to the end users. More importance should be given on precise farming practices, promoting sustainable agriculture and irrigation practices, soil nutrient management, watershed development, dairying and animal husbandry to improve the livelihood of the farmers.

REFERENCES

Ashalatha, K.V., Munisamy, G. and Bhat, A.R.S. 2012. Impact of climate change on rainfed agriculture in India: A case study of Dharwad. International Journal of Environmental Science and Development, 3(4): 368-371.

Hari, S. Khare, P. and Subramanian, A. 2018. Climate change and Indian agriculture. Article retrieved from https://voxdev.org/topic/agriculture/climate-change-and-indian-agriculture.

Kuruvilla, B. 2013. Report on the agrarian crisis in India and Climate Change. Roxa Luxemburg Stiftung, South Asia.

Lema, M.A. and Majule, A.E. 2009. Impacts of climate change, variability and adaptation strategies on agriculture in semi arid areas of Tanzania: The case of Manyoni District in Singida Region, Tanzania. African Journal of Environmental Science and Technology, 3(8): 206-218.

Nautiyal, S. Bhaskar, K. and Khan, I. Y. D. 2018. Biodiversity conservation in semi-arid landscape. Central and North Eastern dry zones of Karnataka. Policy brief-17. Institute for Social and Economic Change. Retrieved from http://www.isec.ac.in/Policy%20Brief%2017_Biodiversity_conservation_in_semi_arid_landscape_of_Karnataka_final.pdf

Place, F. Adato, M. and Hebinck, P. 2007. Understanding rural poverty and investment in agriculture: An assessment of integrated quantitative and qualitative research in Western Kenya. World Development, 35(2): 312-325.

Sivakumar, M.V.K. Das, H.P. and Brunini, O. 2005. Impacts of present and future climate variability and change on agriculture and forestry in the arid and semi-arid tropics. In increasing climate variability and change. Springer, Dordrecht., pp. 31-72

Uddin, M.N. and Anjuman, N. 2013. Participatory rural appraisal approaches: An overview and an exemplary application of focus group discussion in climate change adaptation and mitigation strategies. International Journal of Agricultural Research, Innovation and Technology, 3(2): 72-78.

Phosphorus in the Sediments of Yangzong Lake, China

Yuxi Zhang*(**), Bing Zhou*(**)† and Jiansheng Shi*
*The Institute of Hydrogeology and Environmental Geology, C.A.G.S., Shijiazhuang, China
**China University of Geosciences, Beijing, China
†Corresponding author: Bing Zhou; winnerg0126@sina.com

ABSTRACT

Total 150 sediments samples were collected from the Yangzong Lake, and the total phosphorus, pH, redox potential and organic carbon were analysed to quantitatively study the dispersal and sources of phosphorus and its influential factors. The results indicated that the total phosphorus content in sediments was 318-3931 mg/kg, which decreased slightly with depth. In the sediments at the depths of 0-2cm, 2-4cm, 4-6cm, 6-8cm and 8-10cm, the phosphorus contents were 1151mg/kg, 1126mg/kg, 1138mg/kg, 1057mg/kg and 893mg/kg respectively. The contents of phosphorus in the sediments were high on both north and south banks and reduced gradually towards the centre of the lake. Before the 1980s, the phosphorus distribution in the sediments was mainly influenced by natural factors such as pH value, redox potential and organic matter. But after the 1980s, the phosphorus distribution was mainly affected by the position of sewage discharge. Sources of phosphorus in the sediments have changed from the local source to the multiple sources, and from the point source to surface source. Currently, soil erosion and agricultural non-point source pollution are the main sources of phosphorus in Yangzong Lake.

INTRODUCTION

As one of the main nutrients in a lake ecosystem, phosphorus has a very important effect on the lake eutrophication (Liu et al. 2012, Luo et al. 2017, Lü et al. 2018). As one of the nine plateau lakes in Yunnan Province, Yangzong Lake is the freshwater lake for local residents (Zhang et al. 2010). With the rapid development of industry and agriculture around the Yangzong Lake and continuous input of exogenous nutrients, the eutrophication problem of the Yangzong Lake has become increasingly prominent. The sudden "water bloom" incidents occur from time to time (Zhang et al. 2013). In recent years, the water body itself is usually taken as the object in the eutrophication study of the Yangzong Lake. However, the study on the distribution of phosphorus in the sediment is seldom reported. The phosphorus stored in the sediments is a potential source of endogenous pollution for the overlying water. It can be released from sediments into the water under appropriate conditions.

Through the high-density stratified sampling for the sediments in the Yangzong Lake, the distribution characteristics of phosphorus in the sediments and its influence factors were investigated. The source and pollution history of phosphorus were discussed. The work provides a scientific basis for the accurate evaluation and improvement of the environmental quality and also for the pollution control and protection of Yangzong Lake.

MATERIALS AND METHODS

Study Area

Yangzong Lake (E102°59′-103°02′, N24°51′-24°58′) belongs to Nanpan River system of the Pearl River Basin. The lake surface is in fusiform shape, with the width of 2.5km from west to east and the length of 12.7km from north to south. The shoreline is 32.3km long. The lake has the drainage area of 286km^2 and the lake surface area of 31.9km^2 (at the water level of 1770m). The maximum depth is 29.1m, and the water storage capacity is 0.604 billion m^3. The water exchange cycle is 13a (Zhang et al. 2012). The recharge water sources are mainly natural rainfall, the catchment of the Yangzong Lake and the Qixing Lake, the artificial recharge from Baiyi River, and groundwater. The lake water empties into the Nanpan River through the only water outlet, Tangchi River.

Sampling and Analysis

The sediments of the Yangzong Lake were systematically sampled, as shown in Fig. 1. To obtain the distribution characteristics of phosphorus in the sediments from the Yangzong Lake, seven cross-sections were arranged from south to north at the interval of about 1.5km. The sampling points were set up on the eastern and western banks of each cross-section and at the centre of the lake. The sampling points were more

densely arranged in the water areas near the industrial and mining enterprises around the lake. A total of 30 sampling points were set and numbered N01-N30. The collection and stratification of samples were performed using the "LENZ sediment sampler" manufactured by HYDRO-BIOS (Germany). The sampling was done at every 2cm from top to bottom for each sampling point. There were five layers in total. Finally, a total of 150 samples were obtained. The samples were put into polyethylene bags and the bags were sealed.

The sediment samples were air-dried in the laboratory. After the removal of plant and animal residues and stones, the samples were ground and passed through the nylon screen (200 mesh). After the bottling, the samples were sent to the Geochemical Exploration Supervision and Testing Center of the Ministry of Land and Resources. The testing indicators included total phosphorus, pH value, redox potential and total organic carbon. The analytical methods included plasma spectroscopy (ICP-OES) and potential method. The soil reference materials conforming to the national standard (GSF-2, GSF-3, GSF-4) and repeated samples were added

for quality control in the analysis process. The qualification rates of the reference materials and repeated samples were all 100%. The result of the experiment was reliable. The data were analysed by Microsoft Excel 2003 and SPSS18. 0. The diagram was drawn using Mapgis6.7. The isoline was interpolated by Universal Kriging method.

RESULTS AND DISCUSSION

Phosphorus Content

The contents of phosphorus in the sediments from the Yangzong Lake were mostly above the lower limit of concentration (600mg/kg) that could cause ecological toxicity in the guideline issued by the Ontario Ministry of Energy, Canada (1992) (Sieliechi et al. 2014). This indicates the potential ecological risk.

The content of phosphorus in the sediments of the surface layer (0-2cm) was in the range of 836-1910mg/kg. The average value was 1151mg/kg. The contents of phosphorus in the sediments on the north and south banks were high and
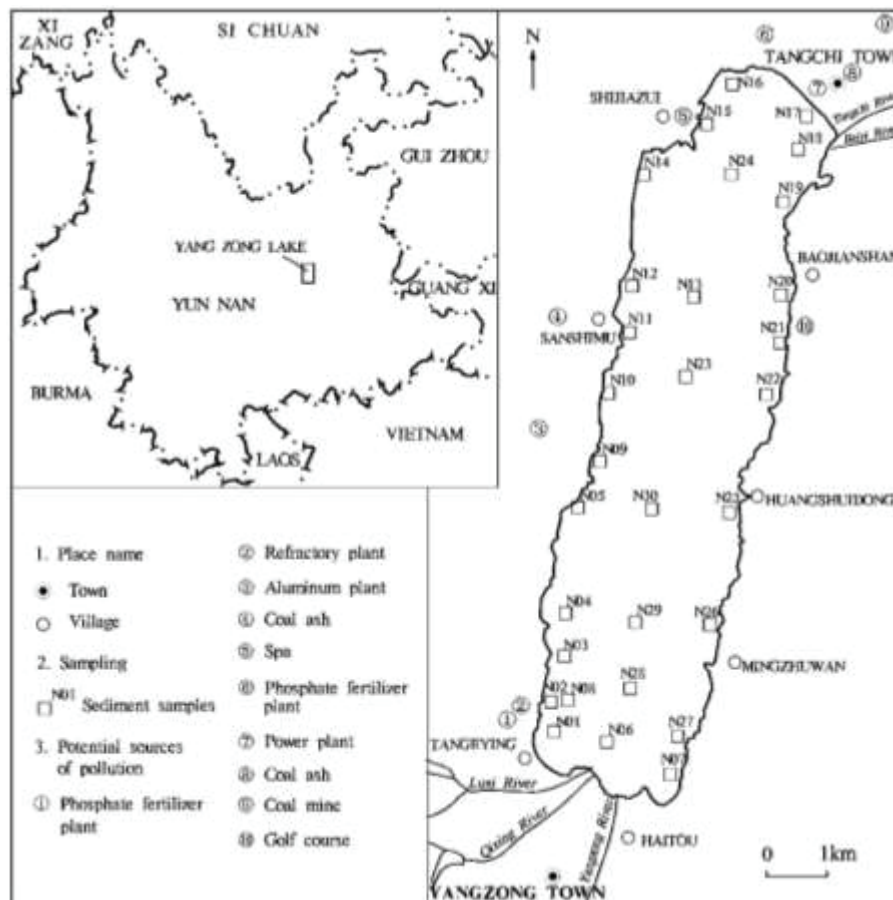

Fig. 1: Sampling sites in Yangzong Lake.

generally above 1400mg/kg. The point N16 on the north bank had the highest value. The contents of phosphorus in the middle of the lake were relatively low. Most of them were below 1000mg/kg, with the minimum value occurring at the point N30.

The content of phosphorus from the depth of 2-4cm was 685-2346mg/kg. The average value was 1126mg/kg. The regional distribution of phosphorus at this depth showed more significant variation than that of the surface layer. The contents of phosphorus on the north bank and the southeast corner were high. They were generally above 1400 mg/kg. The point N27 at the southeast corner had the maximum value. The contents of phosphorus in the middle of the lake area were low. The contents in part of the western lake were less than 800mg/kg. The point N10 on the west bank had the minimum value.

The contents of phosphorus in the sediments from the thickness of 4-6cm were in the range of 547-3931mg/kg. The average was 1138mg/kg. The variation in regional distribution of phosphorus was more significant. The areas with high contents of phosphorus were the north bank and southeast corner. The contents of phosphorus on the north bank changed little compared with that in the upper layer. However, the phosphorus content in the southeast corner significantly increased compared with that in the upper layer. The point N27 had the highest value, which was also the maximum content of phosphorus in the sediments of the entire Yangzong Lake. The contents of phosphorus in the middle of the lake were still low. Larger areas near the

west and east banks had the contents of phosphorus less than 800mg/kg compared with the upper layer.

The contents of phosphorus in the sediments from the depth of 6-8cm ranged from 475 to 2460mg/kg. The average was 1057mg/kg. The areas with a high content of phosphorus were on the north and south banks. The content of phosphorus in the north bank was higher compared with that in the upper layer. The content in the southeast corner significantly decreased compared with that in the upper layer. The point N27 still had the maximum value. The content of phosphorus in the middle of the lake decreased, and those in part of west and east banks were less than 600mg/kg. The point N21 on the east bank had the minimum value. The content of phosphorus in the sediments from the depth of 8-10cm was 318-1734mg/kg. The average was 893mg/kg.

The contents of phosphorus in the whole lake area decreased significantly. The areas with phosphorus content larger than 1400mg/kg were shrunken sharply on the north bank. They disappeared on the south bank. The content of phosphorus was above 1000mg/kg only in part of the southeast corner. The point N17 on the north bank had the maximum value. There was an enlargement of the area with the phosphorus content less than 600mg/kg in the middle of the lake. The contents of phosphorus in part of the east bank were less than 400mg/kg. The point N20 on the east bank had the minimum value.

The spatial distribution of phosphorus in different layers of sediments is shown in Fig. 2. The general distribution pattern was that the contents of phosphorus are high on the

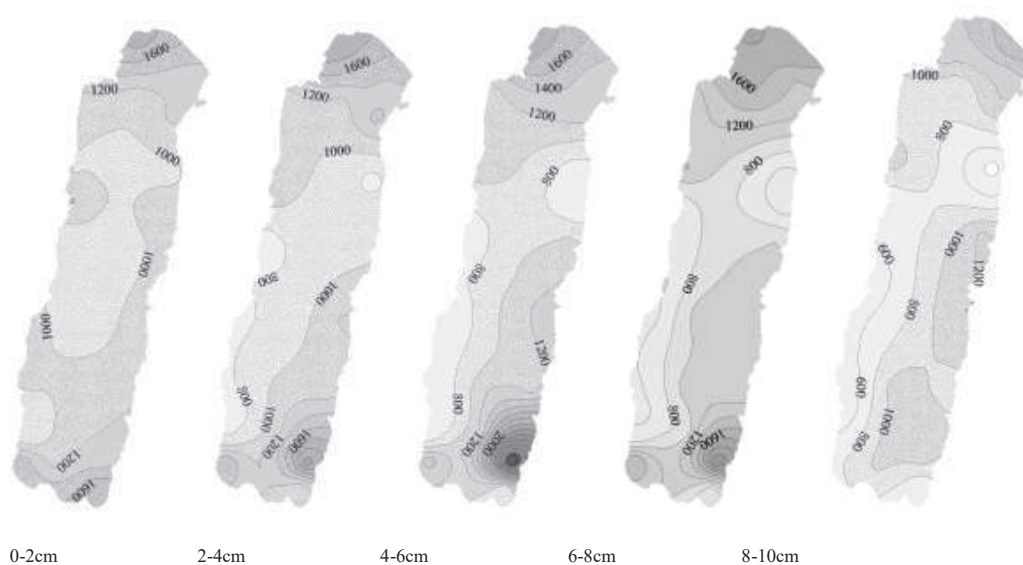| 0-2cm | 2-4cm | 4-6cm | 6-8cm | 8-10cm |

Fig. 2: Spatial distribution of phosphorus in sediments of Yangzonghai Lake (mg/kg).

north and south banks. The content of phosphorus decreased gradually towards the centre of the lake. There were three regions with high contents of phosphorus, near Tangchi on the north bank, in the south of the Pearl Bay in the southeast corner, and near Tangeying in the southwest corner. The low phosphorus contents were mainly found in two areas, along the shore from Tangeying on the west bank to Sanshimu and the near Baojianshan District on the east bank.

Vertically, the contents of phosphorus in the sediments presented a decreasing trend from top to bottom layers of the sediments, as shown in Fig. 3. The contents of phosphorus in the sediments from the depth of 0-6cm decreased slowly, and those below 6cm decreased significantly. The contents of phosphorus were high on the north and south banks. The contents of phosphorus in the sediments increased first and then decreased from top to bottom. The content of phosphorus in the sediments from the depth of 4-6cm was the maximum in the south of the Pearl Bay. The phosphorus content in the sediments from the depth of 6-8cm was the highest near Tangchi Town on the north bank.

Analysis of Influencing Factors on Phosphorus

The sediment adsorption on phosphorus is affected by many factors. The correlation analysis was performed for the four factors, i.e. phosphorus content in the sediments of each layer, pH value, redox potential and organic carbon (Table 1). The results indicated that the contents of phosphorus in the sediments of the upper layers (0-4cm) were not related to any of these indices. However, the contents for the lower layers (4-10cm) had a significant correlation with all indices. The sedimentation rate of the Yangzong Lake is about 1.55mm/a. The sediments from the depth of 0-10cm reflect the sedimen-
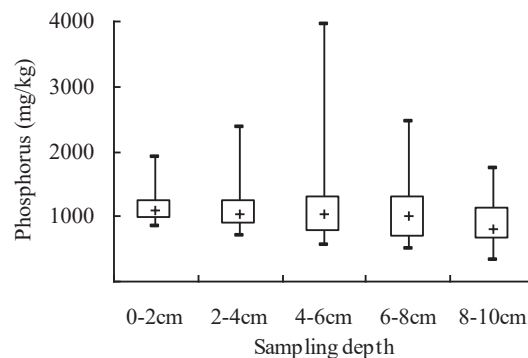

Fig. 3: Phosphorus content in sediments.

Table 1: Correlation between phosphorus content and pH, ORP, OC in sediment by various layers.

Sampling layers	Regression Equation	R^2	P
	$[P]=2.2365[pH]+1133.6$	1×10^{-7}	0.988
0-2 cm	$[P]=-0.0378[ORP]+1149.1$	1×10^{-7}	0.998
	$[P]=150.34[OC]+619.48$	0.130	0.050
	$[P]=-1958.3[pH]+16329$	0.066	0.155
2-4 cm	$[P]=33.102[ORP]+2749.8$	0.064	0.146
	$[P]=191.97[OC]+632.96$	0.211	0.015
	$[P]=-5845.4[pH]+46277$	0.376	0.000
4-6 cm	$[P]=98.807[ORP]+5743.3$	0.374	0.000
	$[P]=163.8[OC]+779.27$	0.108	0.074
	$[P]=-3594.5[pH]+28781$	0.240	0.005
6-8 cm	$[P]=60.624[ORP]+3852.3$	0.238	0.006
	$[P]=190.19[OC]+653.27$	0.325	0.001
	$[P]=-2362[pH]+19082$	0.288	0.003
8-10 cm	$[P]=39.925[ORP]+2703.8$	0.279	0.002
	$[P]=136.9[OC]+631.03$	0.433	0.000

tary environment since the 1960s. The contents of phosphorus in the sediments from the Yangzong Lake were generally low in the 1960s. There were very few human interventions at that time. The distribution was mainly affected by natural factors, such as pH value, redox potential and organic matter. Over time, human activities have been increased. In the last 20 years, with the rise of the agriculture, fisheries, mining and tourist industries near the Yangzong Lake, the pollutant emissions have been rising. The control effects of natural factors on the phosphorus distribution are masked by large, concentrated inputs. The position of pollutant emissions has gradually become the dominant factor for the phosphorous distribution in the sediments. The correlation of phosphorus in the sediments from the bottom to the top layers (from old to new) with each index decreased gradually. The area with a high content of phosphorus coincided with the area of intensive human activities.

pH: The pH value is the key factor that affects the sediment adsorption on phosphorus. Both high and low pH values can promote the release of phosphorus in sediments to the water body of the upper layer (Zhu & Yang 2018). The sediment adsorption on phosphorus could be characterized with a " - shaped" curve with the increase of pH value. The study shows that the sediment adsorption on phosphorus is relatively low in the strongly acidic environment with pH < 2. The adsorption quantity presents an increasing trend with the increase of pH value. The adsorption reaches the maximum near the neutral pH value. The sediment adsorption on phosphorus decreases with the increase of pH value in the alkaline environment with pH> 7 (Zhu et al. 2012). This is because when the pH value is low, the concentration of H^+ in water is high. It is easy for H^+ to bind to the phosphorous ion charged negatively in water, which results in the great reduction of the sediment adsorption on phosphorus. When

the pH value is high, there are more OH^- ions in water. They will compete for the adsorption points on the surface of sediments with the phosphorous ions in water. Therefore, the sediment adsorption on phosphorus will reduce. Only when the pH value is close to neutrality, the surface of sediments carrying positive charge will have an ability to compete for the phosphorous ions with the H^+ of low concentration. Meanwhile, the concentration of OH^- is not too high. The phosphorus can compete with OH^- to be adsorbed on the sediment surface. Therefore, the adsorption quantity of phosphorus will be higher (Li et al. 2010).

The pH values of the sediments in the Yangzong Lake ranged from 7.53 to 7.94. The average pH values for each layer from top to bottom were 7.75, 7.72, 7.76, 7.71 and 7.70, respectively. The pH values of sediments in each layer showed a small variation. The sediments were all weakly alkaline. The pH values of sediments from the depth of 4-10cm had a very significant negative correlation with phosphorus content (Fig. 4), that is, the contents of phosphorus decreased with the increase of pH value.

ORP: Redox potential is one of the important parameters showing the adsorption of phosphorus onto the surface of oxides of Fe (hydrate), etc. (Koskiaho et al. 2015). When the sediments are in the oxidative environment, Fe^{3+} ions will bind to phosphorous ions and deposits in the sediments in the form of iron phosphate or the soluble phosphorus in water is adsorbed by ferric hydroxide, and gradually deposits. Meanwhile, the sediments have strong adsorption action on phosphorus. There will be no release of phosphorus. When the sedimentary environment is in the reducing state, the Fe^{3+} ions are reduced to Fe^{2+}. The insoluble ferric hydroxide is changed into soluble ferrous hydroxide, which results in the release of phosphorus from the sediments into the water. The phosphorus concentration of the water body will
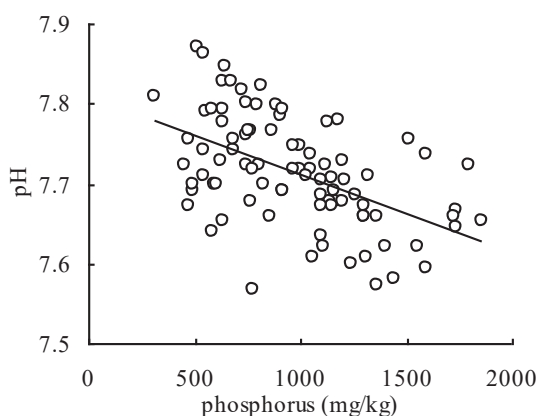

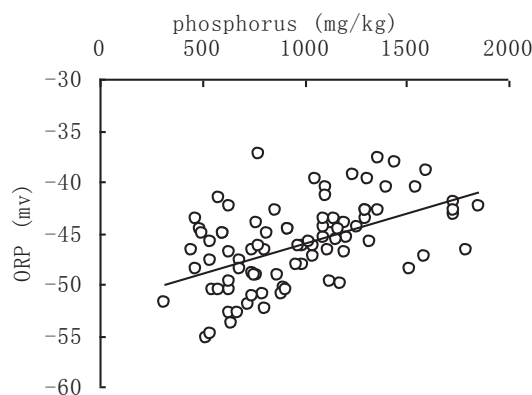Fig. 4: Concentration of phosphorus as a function of pH in 4-10 cm sediments.

Fig. 5: Concentration of phosphorus as a function of ORP in 4-10 cm sediments.
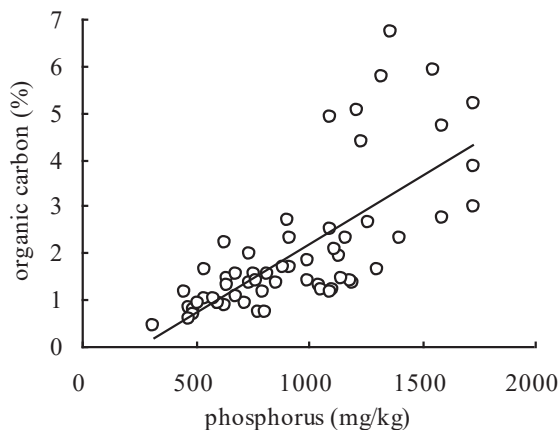
Fig. 6: Concentration of phosphorus as a function of OC in 6-10 cm sediments.

rise as a result. It was found through the continuous flow release system by Peng & Chen (1987) that the release rate of phosphorus from the lacustrine sediments under reducing conditions was more than ten times larger than that under oxidizing conditions.

The redox potential of sediments in the Yangzong Lake ranged from -59 to -35. The redox potentials of sediments in each layer showed a small variation. The sediments were all in the micro reducing environment. In this study, the redox potential of sediments from the depth of 4-10cm had a significant positive correlation with total phosphorus in the sediments (Fig. 5). The content of phosphorus increased with the rise of redox potential.

Organic matter: Organic matter can promote the sediment adsorption on phosphorus as well as its deposition (Liu et al. 2016). The small molecule substances produced by the decomposition of organic matter can increase the adsorption capacity of phosphorus. The saccharides can enhance the adsorption energy of phosphorus (Chen et al. 2015). The amino acids can increase the maximum adsorption capacity of phosphorus. The organic matter and its degradation products can promote the adsorption capacity of sediments on phosphorus in various ways. The content of organic matter was not determined in this study. Considering the relationship between the organic carbon and organic matter, the organic carbon was used in place of organic matter for the analysis in this article. The contents of organic carbon in the sediments from Yangzong Lake were in the range of 0.41%-6.72%. The average content of each layer from top to bottom was 3.53%, 2.63%, 2.21%, 2.12% and 1.91%, respectively. With the increase of depth, the organic carbon decreased gradually. It decreased most significantly at the depth of 0-6cm and the decrease of amplitude was slowed down below 6cm. For the

sediments from the depth of 6-10cm, there was a significant positive correlation between the organic carbon and phosphorus contents (Fig. 6), that is, the content of phosphorus increased with the increase of organic matter.

Human activity: In the sediments from the depth of 0-10cm, human activity has been a constant factor that affects the phosphorus distribution. The influence degree increases gradually with the enhancement of human activities. The content of phosphorus in the sediments and the variation of spatial distribution both indicated the change of the phosphorous sources (Parsons et al. 2017).

Before the 1980s, the agricultural non-point source pollution and urban sewage discharge were the major sources of phosphorus. Tangchi Town on the north bank and Yangzong Town on the south bank were the areas of intensive human activities and also the main distribution areas of farmland. The phosphorus fertilizer enters the lake with the farmland drainage and storm runoff. The domestic sewage was discharged into the lake through the Baiyi River on the north bank and the Yangzong Lake on the south bank. Therefore, in the sediments from the depth of 6-10cm, the contents of phosphorus in the area along the shore of Tangchi Town and Yangzong Town were relatively high.

After the 1980s, the industry, mining, tourism and fishery surrounding the Yangzong Lake have emerged. Industrial and domestic sewage discharge has increased. The motor vessels in the lake district increased. The factors such as the cage fish culture in each town along the shore have resulted in an increase of phosphorus discharge into the lake. The water quality of the lake is deteriorating.

The monitoring data in the 1990s showed that the total phosphorus discharged into the lake was about 139.46 tons

per year. The phosphorus by the cage fish culture was about 72 tons per year, accounting for 52% of the total amount discharged into the lake. The second largest was the fish culture in pools, and the phosphorus discharged into the lake was about 45 tons per year, accounting for 32% of the total amount. The third was the industrial wastewater and domestic sewage, with the amounts of phosphorus discharged into the lake being about 6.75 tons per year and 4.38 tons per year, respectively. The amount of phosphorus discharged for non-point source was 11.33 tons per year. The point source pollution is the main form of phosphorus input. The cage fish culture was once distributed along the shore near Tangchi Town and Yangzong Town. Therefore, the phosphorus contents in the sediments from the depth of 2-6cm were still high. The phosphorus pollution on the south bank was more serious than that on the north bank. It was because there was a large number of fish culture in pools along the shore to the east of the mouth of Yangzong Lake. The blue-green algae bloomed in the Yangzong Lake for 3 consecutive years from 1997 to 1999. The water quality decreased to class IV. After that, a series of pollution prevention measures were implemented, such as the banning of cage fish culture and motor fishing vessels in the Tangchi Town on the north bank. One year later, the same measures were also adopted for Yangzong Town on the south bank. The phosphorus content declined significantly after these measures. The water quality gradually recovered to class III. The contents of phosphorus in the sediments on the north and south banks first increased and then decreased from bottom to top (from old to new). This demonstrated that the phosphorus pollution in the Yangzong Lake experienced the transition from light pollution to heavy pollution and then back to light. The decline rate of phosphorus contents in the sediments on the south bank was less than that on the north bank, due to the delayed implementation of the control measures. Besides, the organic carbon in the sediments from the depth of 2-4cm had a "significant" correlation with the content of phosphorus. However, the pH value and ORP for the same layer both had an "insignificant" correlation with the content of phosphorus. We believe that the correlations of natural factors such as pH value and ORP with phosphorus are weakened due to human interventions (Bertolet et al. 2018). However, the human factor in this period is mainly aquaculture. While the phosphorus is discharged into the lake by the fish farming, a large number of residual feeds producing organic matters and fish excrements are also discharged. Therefore, in the sediments of this layer, the organic carbon had a significant correlation with the phosphorus content.

After 2000, with the increase of the exploitation and development around Yangzong Lake, the soil and water loss arising from land development has become an impor-tant source of phosphorus. The monitoring data in 2005 (Boulion 2018, Welch et al. 2017) showed that the content of phosphorus amounted to 204.4 tons due to the soil and water loss in the Yangzong Lake, accounting for 67.8% of the total phosphorus discharged into the lake. The second largest pollution is agricultural non-point source pollution. The loss of fertilizer phosphorus was about 51.5 tons, accounting for about 17.1% of total phosphorus. Point source pollution, such as the industrial wastewater, domestic sewage and aquaculture, also makes a significant contribution. The discharge of phosphorus along with the industrial wastewater was about 40.44 tons; the discharge by the tourism wastewater was 1.11 tons, and that with the urban sewage was 0.224 tons. The aquaculture industry discharged 3.746 tons of phosphorus into the lake. Although the content of phosphorus in the sediments in the local area declined compared with that in the lower layer, the content of phosphorus still showed an increasing trend in the whole lake area. At this time, besides the large number of enterprises rising in the areas along the shores of Tangchi Town and Yangzong Town (such as hot spring resorts, phosphate fertilizer plants and refractory factories), the enterprises such as aluminium factories and golf courses have also developed in Sanshimu and Baojianshan District (Chen et al. 2016, Feng et al. 2019). The phosphorus in the sediments near these areas all presented significant increases.

Since the 1960s, the main source of phosphorus in the Yangzong Lake has changed with time, from the agricultural non-point source to the cage fish farming, and then to soil and water loss. The type of pollution source has changed from the non-point source to point source, and to non-point source pollution. The number of pollution sources is also increasing constantly.

CONCLUSION

The contents of phosphorus in the sediments from the Yangzong Lake were in the range of 318-3931mg/kg. The average contents of arsenic in the sediments at the depth of 0-2, 2-4, 4-6, 6-8 and 8-10cm were 1151, 1126, 1138, 1057 and 893mg/kg, respectively. Vertically, the content of phosphorus increased gradually from bottom to top. On the planar view, the contents of phosphorus were high on the north and south banks and they decreased towards the centre of the lake. The distribution of phosphorus in the sediments was affected by both the natural factors and human factors. Before the 1980s, the distribution of phosphorus in the sediments was mainly influenced by the natural factors such as the pH value, redox potential and organic matter. After the 1980s, the distribution of phosphorus was mainly affected by the position of pollution discharge. The phosphorus source in the Yangzong Lake is increasing in number and the pollution type changes

from the point source to the non-point source pollution. At present, the main sources of phosphorus are soil and water loss and agricultural non-point source pollution. The control of soil and water loss and the loss of chemical fertilizers are crucial for controlling the eutrophication of Yangzong Lake.

ACKNOWLEDGEMENT

REFERENCES

Bertolet, B.L., Corman, J.R., Casson, N.J., Sebestyen, S.D., Kolka, R.K. and Stanley, E.H. 2018. Influence of soil temperature and moisture on the dissolved carbon, nitrogen, and phosphorus in organic matter entering lake ecosystems. Biogeochemistry, 139(3): 293-305.

Boulion, V.V. 2018. Phosphorus budget of Lake Baikal and the Angara cascade water reservoirs: Modeling, reconstruction, and prognosis. Dokl. Biol. Sci., 480(1): 90-92.

Chen, C.Y., Deng, W.M., Xu, X.M., He, J., Wang, S.R., Jiao, L.X. and Zhang, Y. 2015. Phosphorus adsorption and release characteristics of surface sediments in Dianchi Lake, China. Environ. Earth Sci., 74(5): 3689-3700.

Chen, X., Li, H., Hou, J., Cao, X.Y., Song, C.L. and Zhou, Y.Y. 2016. Sediment-water interaction in phosphorus cycling as affected by trophic states in a Chinese shallow lake (Lake Donghu). Hydrobiologia, 776(1): 19-33.

Feng, W.Y., Li, C.C., Zhang, C., Liu, S.S., Song, F.H., Guo, W.J., He, Z.Q., Li, T.T. and Chen, H.Y. 2019. Characterization of phosphorus in algae from a eutrophic lake by solution 31P nuclear magnetic resonance spectroscopy, Limnology, 20(2): 163-171.

Koskiaho, J., Tattari, S. and Röman, E. 2015. Erratum to: Suspended solids and total phosphorus loads and their spatial differences in a lake-rich river basin as determined by automatic monitoring network. Environ. Monit. Assess., 187: 286.

Li, X.L., Eckhard, G. and Horst, M. 2010. Phosphorus depletion and pH decrease at the root-soil and hyphae–soil interfaces of VA mycorrhizal white clover fertilized with ammonium. New Phytol., 119: 397-404.

Liu, J.Z., Luo, X.X., Zhang, N.M. and Wu, Y.H. 2016. Phosphorus released from sediment of Dianchi Lake and its effect on growth of *Microcystis aeruginosa*. Environ. Sci. Pollut. Res., 23(16): 16321-16328.

Liu, E.F., Shen, J., Yang, X.D. and Zhang E.L. 2012, Spatial distribution and human contamination quantification of trace metals and phosphorus in the sediments of Chaohu Lake, a eutrophic shallow lake, China. Environ. Monit. Assess., 184(4): 2105-2118.

Luo, Y.H., Nie, X.Q., Li, X.L., Dai, Z.L., Xu T. and Huang, Y.P. 2017. Distribution and emission flux estimation of phosphorus in the sediment and interstitial water of Xiangxi River. Environ. Sci., 38: 2345-2354. (in Chinese)

Lü, C., He, J. and Wang, B. 2018. Spatial and historical distribution of organic phosphorus driven by environment conditions in lake sediments. J. Environ. Sci., 64: 32-41.

Parsons, C.T., Rezanezhad. F., O'Connell. D.W. and Cappellen, P.V. 2017. Sediment phosphorus speciation and mobility under dynamic redox conditions. Biogeosciences, 14: 1-36.

Peng, J. X. and Chen, H. J. 1987. Eutrophication and Prevention of Water. China Environmental Science Press, pp. 77.

Sieliechi, J.M., Dangwang Dikdim, J.M. and Noumi, G.B. 2014. Speciation of phosphorus in the sediments of Lake Bini (Ngaoundere-Cameroon). Environ. Technol., 35: 1831-1839.

Welch, E.B., Gibbons, H.L., Brattebo, S.K. and Corson-Rikert, H.A. 2017. Distribution of aluminium and phosphorus fractions following alum treatments in a large shallow lake. Lake Reserv. Manage., 33(2): 1-7.

Zhang, Y.X., Liu, J.T. and Wang, J.C. 2013. Distribution of phosphorus in the sediments of Yangzonghai Lake and its influencing factors. Saf. Environ. Eng., 20: 43-48. (in Chinese)

Zhang, Y.X., Sun, J.C., Xiang. X.P., Jing J.H, Liu J.T, Huang G.X., Wang J.C, Chen, Xi and Cui, H.W. 2010. A survey of heavy metals in sediments of Yangzonghai Lake in Yunnan Province: Their source and distribution. Environ. Sci. Technol., 33: 171-175. (in Chinese)

Zhang, Y.X., Xiang, X.P., Zhang, Y., Chen, X., Liu, J.T., Wang, J.C., Zhang, Y.J. and Sun, J.C. 2012. Distribution and sources of arsenic in Yangzonghai Lake, China. Environ. Sci., 33: 3768-3777. (in Chinese)

Zhu, B., Wang, Z.H. and Zhang, X.B. 2012. Phosphorus fractions and release potential of ditch sediments from different land uses in a small catchment of the upper Yangtze River. J. Soil Sediment, 12: 278-290.

Zhu, G.R. and Yang, Y. 2018. Variation laws and release characteristics of phosphorus on surface sediment of Dongting Lake. Environ. Sci. Pollut. R., 25: 12342-12351.

Quality Assessment of Groundwater from the Coal Bearing Aquifer in the Xinji Coalfield, Anhui Province, China

S.B. Feng* and L.H. Sun**

*School of Resources and Civil Engineering, Suzhou University, Anhui 234000, China
**Key Laboratory of Mine Water Resource Utilization of Anhui Higher Education Institute, Suzhou University, Anhui 234000, China
†Corresponding author: L.H. Sun; sunlinh@126.com

ABSTRACT

In this study, a total of 50 groundwater samples from the coal-bearing aquifer in the Xinji coalfield (one sub-coalfield of the Huainan coalfield) have been collected, and their major ion concentrations have been measured for the evaluation of its suitability for drinking and irrigation, and then the mechanism controlling the water chemistry have been analysed. The results indicate that the groundwater samples are slightly alkaline with TDS higher than the freshwater (<1000 mg/L), and most of them are classified to be Cl^- and HCO_3^- types. The groundwater samples have WQI range from 5.63 to 179 (mean = 64.9), suggesting that these samples are good for drinking. However, the results of sodium adsorption ratio and residual sodium carbonate indicate that only a few of the samples can meet the requirement of irrigation, but must be treated before application. Gibbs diagram and the relationships between major ions, as well as the factor analysis, imply that water-rock interaction is the main process controlling the groundwater chemistry, including the dissolution of evaporate minerals and the weathering of silicate minerals.

INTRODUCTION

Water is the most important resource in the world, not only because it is essential for life, but also its role played in human activities including the agriculture and industry. Among all of the water resources, the groundwater makes up about 20% of the world's freshwater supply (Lvovitch 1970), and the global groundwater storage is equal to the total amount of freshwater stored in the snow and ice pack of the earth.

To be one of the most important agricultural bases of China, the North China Plain has played a fundamental role during the evolutionary history of China. However, because of the lacking of the surface water resource, the groundwater has played an important role in the development of the area (Chen et al. 2005). Near 56% of the water supply for more than 100 million people is provided by groundwater and most of the area use groundwater for irrigation. In some of the cities (Beijing, Shijiazhuang, Handan), the groundwater accounts for more than 70% of the water supply in recent years (Zhang et al. 2000).

Meanwhile, the North China Plain is an important energy base of China, because of its high reserves of coal and petroleum. There are many large coalfields (e.g. Lianghuai coalfield) and oilfields (e.g. Dagang, Shengli, Huabei &

Zhongyuan) distributed in the plain. Similar to other areas, these oil and coal fields are also lacking water. However, paradoxically, during the production of coal, a large quantity of water from the underground need to be discharged for the safety of coal mining, because water is considered to be the most dangerous one among the five typical disasters in coal mines (including water, fire, gas, dust, roof), as water inrush has brought to human with the highest loss (Gui & Chen 2007). And therefore, how to control the water hazard with the utilization of the water resource simultaneously has become an important issue concerned by the governments and the scientists.

There are two main coalfields in the northern Anhui province, China, which are located north and south to the Huai River, namely the Wanbei coalfield and the Huainan coalfield. During the last ten years, the groundwater in the Wanbei coalfield has been systematically studied (Sun & Gui 2013, Lin 2016, Sun 2018), whereas the groundwater in the Huainan coalfield, especially the quality aspect has not been well considered yet. Therefore, in this study, a total of 50 groundwater samples from the coal-bearing aquifers in four coal mines in the Xinji coalfield (one sub-coalfield of the Huainan coalfield) have been collected, and their major ion concentrations have been measured for the evaluation of its

quality for drinking and irrigation, and then the mechanism controlling the water chemistry has been studied. The reason for choosing this aquifer is because it is a direct threat to the safety of coal mining and the main source of water discharged during coal mining.

MATERIALS AND METHODS

Hydro-Geological Background

Xinji coalfield is located in the middle-north of the Anhui province, China. There are five coal mines in the area: the Banji coalmine, Xinji coalmine, Yangcun coalmine, Kouzi coalmine and Liuzhuang coalmine, which are located west to the Fengtai County and north to the Yinshang County, with a total area of 425 km² (Fig. 1). The designed production of coal in the field is more than 30 million tons per year. Water resources in the area are rich because the Huai River and its tributaries flow through the area. The climate of the area is mild and belongs to marine-continental climate with an annual average temperature of 15.1°C. The average annual rainfall is 884 mm, and most of them concentrated in June to August. However, the groundwater is the main water source for the industry and domestic use in the coal mine areas, because they are located far away from the rivers.

Previous investigations revealed that there are five main aquifer systems in the coalfield from shallow to deep; the loose layer aquifer system, the Permian coal-bearing sandstone aquifer system, the Carboniferous limestone aquifer system, the Ordovician limestone aquifer system and the Cambrian nappe aquifer system. Among these five aquifer systems, the groundwater in the Permian coal-bearing sandstone aquifer system is the direct threat for the safety of coal mining, similar to the Huaibei coalfields (Sun 2018).

Methods

A total of 50 groundwater samples were collected from the coal-bearing aquifers in the four coal mines of the coalfield: 10, 10, 15 and 15 from the Banji, Kouzi, Liuzhuang and Xinji coalmines (Table 1). Water pH and total dissolved solids (TDS) were measured in the field with a portable pH-meter
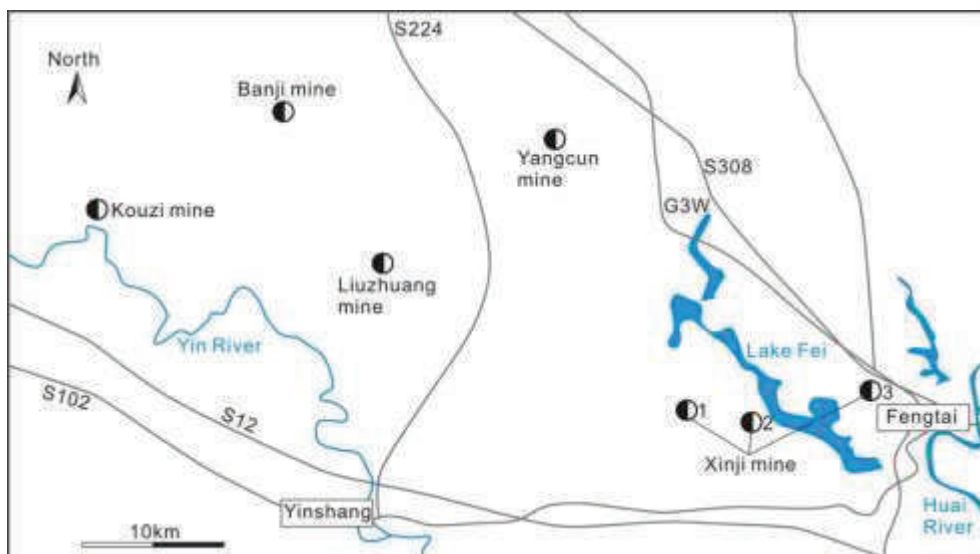

Fig. 1: Locations of the coal mines related to this study.

Table 1: Mean major ion concentrations (mg/L) of the groundwater samples.

Location	Number	pH	Na^+	Ca^{2+}	Mg^{2+}	Cl^-	SO_4^{2-}	HCO_3^-	CO_3^{2-}	TDS
Banji	10	8.23	465	20	10	485	48	392	25	1249
Kouzi	10	8.19	932	10	6	409	162	1137	159	2246
Liuzhuang	15	8.06	788	18	14	658	135	691	55	2014
Xinji	15	8.34	627	31	23	636	77	460	63	1686

and TDS-meter. Water samples were filtered through 0.45 µm pore size membranes and collected into 2-L polyethylene bottles that had been cleaned in the laboratory. Then, the samples were sent to the laboratory for analyses of major ions. Na^+, Ca^{2+}, Mg^{2+}, Cl^- and SO_4^{2-} were measured by ion chromatography, whereas alkaline (including HCO_3^- and CO_3^{2-}) was analysed by acid-base titration. The quality control was carried out by standard sample (the correlation coefficient between actual concentration and measured concentration was higher than 0.99). All the analysis was conducted in the Engineering Research Centre of Coal Mine Exploration, Anhui province, China.

RESULTS AND DISCUSSION

Major Ion Concentrations

The analytical results of the major ion concentrations are given in Table 1. As can be seen from the table, all the groundwater samples have Na^+ concentration much higher than Ca^{2+} and Mg^{2+} for the cations, whereas Cl^- and HCO_3^- are the dominant anions. However, although all the groundwater samples were collected from similar aquifers in four coal mines, their major ion concentrations are different from each other. Detailed information about the major ion concentrations is as follows.

The mean concentrations of Na^+, Ca^{2+}, Mg^{2+}, Cl^-, SO_4^{2-}, HCO_3^- and CO_3^{2-} for the groundwater samples from the Banji coalmine are 465, 20, 10, 485, 48, 392 and 25 mg/L, respectively. The decreasing order of mean concentrations of major ions is $Cl^- > Na^+ > HCO_3^- > SO_4^{2-} > CO_3^{2-} > Ca^{2+} > Mg^{2+}$. This order is consistent with those of the groundwater from the Xinji coalmine (Table 1), the mean concentrations of Na^+, Ca^{2+}, Mg^{2+}, Cl^-, SO_4^{2-}, HCO_3^- and CO_3^{2-} for the groundwater samples from it are 627, 31, 23, 636, 77, 460 and 63 mg/L, respectively. Comparatively, the groundwater samples from the Kouzi and Liuzhuang coalmines have higher mean Na^+ and HCO_3^- but lower mean Ca^{2+} and Mg^{2+} concentrations relative to the Banji and Xinji coalmines, and the concentration orders are also different. Such a phenomenon suggests that the hydrological conditions of all the coalmines are overall consistent with each other, but there are still some differences (e.g. the water-rock interactions).

The mean total dissolved solids (TDS) of the groundwater samples from the four coalmines varied from 1249 to 2246 mg/L, and all the samples have TDS higher than the freshwater (<1000 mg/L) (Davis & Dewiest 1966). The mean pH values of the samples range from 8.06 to 8.34, implying that the groundwater samples are slightly alkaline.

Hydrochemical Types

Classification of hydrochemical types for groundwater is important because of the dominant anion species of water change systematically from HCO_3^-, SO_4^{2-} to Cl^- as groundwater flows from the recharge zone to the discharge zone (Toth 1999, Jalali 2005). And therefore, the classification of the hydrochemical types in this study can provide information for the understanding of the hydrological evolution of the studied aquifers. Classification of water in this study is based on the concentrations of cations and anions by using the software Aquachem and Piper diagram, and the result is shown in Fig. 2.

The result indicates that all the groundwater samples from the four coalmines are mainly classified to be of two
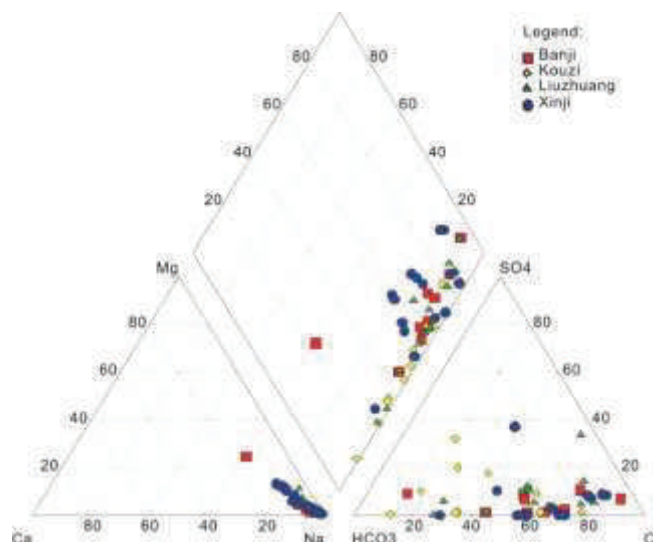

Fig. 2: Piper diagram.

types (Cl⁻ and HCO₃⁻ types). For the groundwater samples from the Banji, Liuzhuang and Xinji coalmines, most of the samples are classified to be Na-Cl type (80% of the samples, respectively), whereas the groundwater samples from the Kouzi coalmine are mainly classified to be the Na-HCO₃ type (70%). Such results suggest that the hydrological condition of these four coalmines are different from each other. The groundwater from the former three coalmines might have been affected by more serious of the evaporation (e.g. located in the discharge zone) or dissolution of the evaporate minerals (e.g. halite or gypsum), whereas the groundwater from the Kouzi coalmine might have been influenced by the weathering of silicate minerals (Sun 2018).

Quality Evaluation for Drinking

There are several methods been applied for the water quality evaluation, and the most popular applied ones include the comparison with the quality standard (e.g. World Health Organization) (WHO 2008) and the water quality index (WQI) (Varol & Davraz 2015). The latter was calculated for evaluating the quality for drinking based on several key parameters of water chemistry according to their different importances in the overall quality of water for drinking purposes (Vasanthavigar et al. 2010). The assigned weight ranges from 1 to 5. The maximum weight of 5 has been assigned for TDS, Cl⁻ and SO₄²⁻, 4 for Na⁺, and 3 for Ca²⁺ and Mg²⁺. The detailed process is as follows:

First step: weight calculation with equation $Wi = wi / \sum_{i=1}^{n} wi$, where Wi is the relative weight, wi is the weight of each parameter, n is the number of parameters.

Second step: quality rating with equation Qi = 100×Ci/Si, where Qi is the quality rating, Ci is the concentration of each chemical parameter (mg/L), and Si is the World Health Organization standard (Na⁺ 200 mg/L, Ca²⁺ 300 mg/L, Mg²⁺ 30 mg/L, Cl⁻ 250 mg/L, SO₄²⁻ 250 mg/L, TDS 1500 mg/L) (WHO 2008).

Third step: water quality index calculation with equation $WQI = \sum_{i=1}^{n} Wi \times Qi$.

Based on the results, the quality of the water for drinking can be classified to be in five classes (excellent < 50, good 50-100, poor 100-200, very poor 200-300 and unsuitable >300) (Vasanthavigar et al. 2010). The groundwater samples in this study have WQI range from 5.63 to 179 (mean = 64.9), and only one sample has WQI higher than 100, suggesting that these samples are good for drinking when considering about only their major ion concentrations.

Quality Evaluation for Irrigation

Parameters applied for the suitability evaluation of the groundwater for irrigation include the sodium adsorption ratio (SAR), percentage sodium (% Na), permeability index (PI), residual sodium carbonate (RSC), Kelly's ratio and magnesium ratio (Todd 1995, Michael 2008). In this study, the most popular applied parameters (SAR & RSC) have been chosen.

SAR expresses the relative activity of sodium ions in the exchange reactions with the soil (Todd 1995). This ratio measures the relative concentration of sodium to the calcium and magnesium. SAR is an important parameter for determining the suitability of groundwater for irrigation. Excess sodium concentration can reduce the soil permeability and soil structure, and irrigation using water with high sodium adsorption ratio may require soil amendments to prevent long-term damage to the soil. SAR is a measure estimated by Na⁺/SQRT((Ca²⁺ + Mg²⁺)/2) (in meq/L). The calculated values of SAR for the groundwater samples in this study were 2.84-195 (mean = 39.4). According to the criterion for irrigation (SAR < 10, excellent; 10-18, good; 18-26, doubtful;
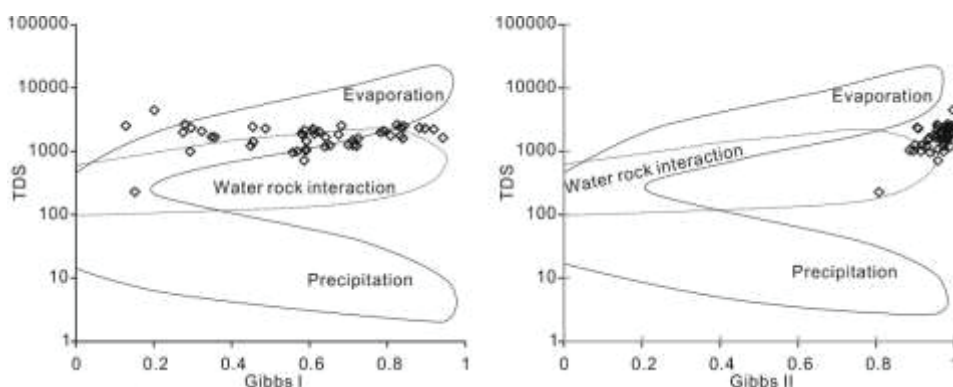

Fig. 3: Gibbs diagram.

>26, unsuitable) (Richards 1954), 2, 8 and 10 samples were classified to be excellent, good and doubtful, respectively. Such results indicate that these groundwater samples must be treated before the irrigation application.

RSC exists in irrigation water when the carbonate (CO_3) plus bicarbonate (HCO_3) content exceeds the calcium (Ca^{2+}) plus magnesium (Mg^{2+}) content of the water. An excess value of RSC in water leads to an increase in the adsorption of sodium in soil (Michael 2008). The results of this include direct toxicity to crops, excess soil salinity (EC) and associated poor plant performance, and where appreciable clay or silt is present in the soil, loss of soil structure and associated decrease in soil permeability. RSC is a measure employed by calculating $(CO_3^{2-} + HCO_3^-)-(Ca^{2+}+ Mg^{2+})$. RSC values < 1.25 meq/L indicate good water quality. If the value of RSC is between 1.25 and 2.5 meq/L, the water is slightly suitable while at a value >2.5 the water is considered as unsuitable for irrigation. RSC values of the groundwater samples in this study are from -4.54 to 64.6 (mean = 11.0). Based on the criterion for irrigation, only 8 samples (16%) can be used for irrigation directly.

Mechanism Controlling Water Chemistry

The Gibbs diagram proposed by Gibbs (1970) can be used for understanding the relationship of the chemical components of groundwater from their respective aquifer lithology. Three factors controlling groundwater chemistry can be classified by the diagram: precipitation, evaporation and water-rock interaction dominance. As to the groundwater, these factors are recharge, evaporation (or dissolution of evaporates) and water-rock interaction.

The calculation functions of Gibbs ratios are Gibbs ratio I = $Cl^-/(Cl^-+HCO_3^-)$ and Gibbs ratio II = $(Na^++K^+)/(Na^++K^++Ca^{2+})$ (in meq/L). In this study, the Gibbs ratio I and II values for the groundwater samples are 0.13-0.94 (mean = 0.60) and 0.81-1.00 (mean = 0.96), respectively. From the Fig. 3, it can be seen that most of the samples in this study are plotted into the water-rock interaction and evaporation areas, indicating that the water-rock interaction and the evaporation (or discharge of the groundwater and dissolution of evaporate minerals) in the aquifer systems play an important role for controlling the groundwater chemistry.

Moreover, it can be seen from Fig. 4 that the groundwater samples in this study have Ca^{2+}/Na^+ ratios ranging from 0 to 0.24 (mean = 0.04), and Mg^{2+}/Na^+ ratios range from 0 to 0.41 (mean = 0.05), which suggest that weathering of silicate minerals and dissolution of evaporate minerals are the main types of water-rock interaction in the aquifer system. It is also supported by the correlation between Ca^{2+}/Na^+ and HCO_3^-/Na^+ (Fig. 4) that the samples have HCO_3^-/Na^+ range between 0.05 and 1.22 (mean = 0.37). Some other information can also be achieved from the relationships between Na^+ and Cl^- that all the samples have higher Na^+ relative to Cl^-, which indicates the contribution of Na^+ from the weather-
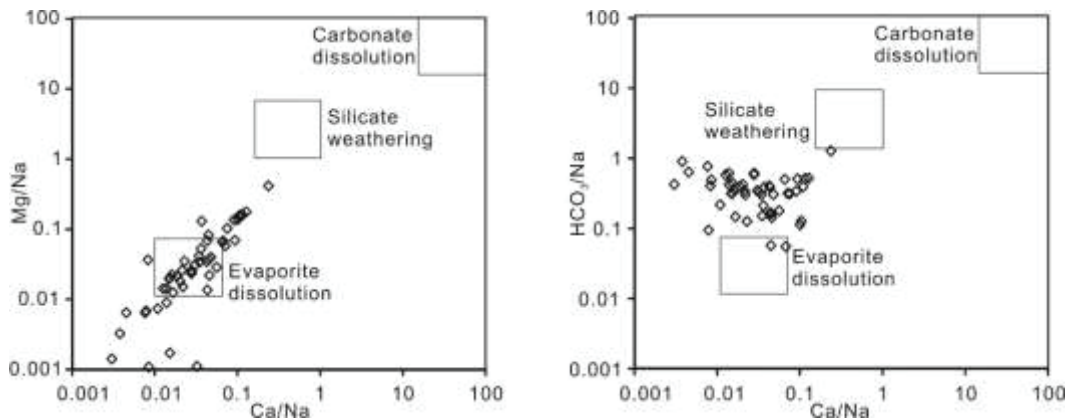

Fig. 4: Ca/Na-Mg/Na and Ca/Na-HCO₃/Na diagrams.

Table 2: Result of factor analysis.

Species	Na^+	Ca^{2+}	Mg^{2+}	Cl^-	SO_4^{2-}	HCO_3^-	Eigenvalue	Explained
Factor 1	-0.129	0.929	0.876	0.789	0.141	-0.632	2.690	44.8%
Factor 2	0.945	-0.098	-0.059	0.326	0.721	0.540	1.823	30.4%

ing of silicate minerals except for the dissolution of halite, such consideration is further confirmed by the relationship between (Ca^{2+}+Mg^{2+}) and (HCO_3^-+SO_4^{2-}) that most of the samples (47 in 50) have higher (HCO_3^-+SO_4^{2-}) relative to (Ca^{2+}+Mg^{2+}). During the weathering of silicate minerals, Na^+ and HCO_3^- can be released into the water simultaneously.

Factor Analysis

As one of the most popular applied mathematical methods, factor analysis has long been used for environmental studies for tracing the source of pollutants (Liu et al. 2003, Almasoud et al. 2015) and also, applied for understanding the source of chemical constitutes in the groundwater (Sun 2018).

In this study, two factors have been extracted based on the factor analysis with an eigenvalue higher than one after varimax rotation (Table 2). As can be seen from the table, the first factor, which accounts for 44.8% of the total variance explanation, has high positive loadings of Ca^{2+}, Mg^{2+} and Cl^-, whereas the second factor with 30.4% of the total variance explanation, has high positive loadings of Na^+ and SO_4^{2-}, and then HCO_3^-. According to previous studies (Sun & Gui 2015), these two factors can be explained to be the dissolution of chloride minerals (Factor 1) and the dissolution of sulphate minerals and weathering of silicate minerals (Factor 2). This consideration is consistent with the results obtained by the above analysis (including the Gibbs diagram and the relationships between major ions) that the dissolution of evaporate minerals (including the chloride and sulphate) and the weathering of silicate minerals played an important role for controlling the groundwater chemistry therein.

CONCLUSIONS

Based on the analysis of the major ion concentrations of the groundwater from the coal-bearing aquifer in four coal mines in the Xinji coalfield, the following conclusions have been made:

(1) The groundwater samples are slightly alkaline with TDS higher than the freshwater (< 1000 mg/L), and most of them are classified to be Cl^- and HCO_3^- types.

(2) The groundwater samples have WQI range from 5.63 to 179 (mean = 64.9), only one sample has WQI higher than 100, suggesting that these samples are good for drinking. Comparatively, according to the results of sodium adsorption ratio and residual sodium carbonate, only a few of the samples can meet the requirement of irrigation but must be treated before application.

(3) Gibbs diagram and the relationships between major ions, as well as the factor analysis, implies that water-rock interaction is the main process controlling the

groundwater chemistry, including the dissolution of the evaporate minerals (including the chloride and sulphate) and the weathering of silicate minerals.

REFERENCES

Almasoud, F.I., Usman, A.R. and Al-Farraj, A.S. 2015. Heavy metals in the soils of the Arabian Gulf coast affected by industrial activities: Analysis and assessment using enrichment factor and multivariate analysis. Arabian Journal of Geosciences, 8(3): 1691-1703.

Chen, Z., Zhen, L.N., Zhao, J.Z., Qi, J. and Nan, Y. 2005. Isotopes and sustainability of ground water resources. North China Plain, Ground Water, 43(4): 485-493.

Davis, S.N. and Dewiest, R.J.M. 1966. Hydrogeology. Wiley, New York.

Gibbs, J. R. 1970. Mechanisms controlling world water chemistry. Science, 170: 1088-1090.

Gui, H.R. and Chen L.W. 2007. Hydrogeochemistric Evolution and Discrimination of Groundwater in Mining District. Geological Publishing House, Beijing.

Jalali, M. 2005. Major ion chemistry in the Bahar area, Hamadan, western Iran. Environmental Geology, 47: 763-772.

Lin, M.L., Peng, W.H. and Gui, H.R. 2016. Heavy metals in deep groundwater within the coal mining area, northern Anhui Province, China: Concentration, relationship, and source apportionment. Arabian Journal of Geosciences, 9(4): 319.

Liu, C.W., Lin, K.H. and Kuo, Y.M. 2003. Application of factor analysis in the assessment of groundwater quality in a blackfoot disease area in Taiwan. Science of the Total Environment, 313(1): 77-89.

Lvovitch, M.I. 1970. World Water Balance (general report). World Water Balance: Proceedings of the Reading Symposium.

Michael, A.M. 2008. Irrigation Theory and Practice. Vikas Publishing House Pvt. Ltd., New Delhi.

Richards, L.A. 1954. Diagnosis and Improvement of Saline Alkali Soils: Agriculture (Vol. 160). US Department of Agriculture, Washington.

Sun, L.H. 2018. Application of hydrochemistry for inrush water source identification in coal mine: Approach based on statistical analysis. Mining Science, 25: 115-124.

Sun, L.H. and Gui, H.R. 2013. Groundwater from deep limestone aquifer in Linhuan coalfield, northern Anhui Province, China: Quality and controlling factor analysis. International Journal of Applied Environmental Sciences, 8(2): 167-176.

Sun, L.H. and Gui H.R. 2015. Hydro-chemical evolution of groundwater and mixing between aquifers: A statistical approach based on major ions. Applied Water Science, 5(1): 97-104.

Todd D. K. 1995. Groundwater Hydrology. John Wiley and Sons Publications, 3rd Ed, New York.

Toth, J. 1999. Ground-water as a geologic agent: An overview of the cause, processes and manifestations. Hydrogeology Journal, 7: 1-14.

Varol, S. and Davraz, A. 2015. Evaluation of the groundwater quality with WQI (Water Quality Index) and multivariate analysis: a case study of the Tefenni plain (Burdur/Turkey). Environmental Earth Sciences, 73(4): 1725-1744.

Vasanthavigar, M., Srinivasamoorthy, K., Vijayaragavan, K., Rajivganthi, R., Chidambaram, S., Anandhan, P., Manivannan, R. and Vasudevan, S. 2010. Application of water quality for groundwater quality assessment: Thirumanimuttar Sub basin, Tamil Nadu, India. Environmental Monitoring and Assessment, 171(1-4): 595-609.

WHO 2008. Guidelines for Drinking Water Quality. World Health Organization, Geneva.

Zhang, Z.H., Shen, Z.L., Xue, Y.Q., Ren, F.H., Shi, D.H., Yin, Z.Z. and Sun, X.H. 2000. Evolution of Groundwater Environment in North China Plain. Geological Publishing House, Beijing.

Risk Perception, Choice of Source and Treatment Decision: Exploring Water Consumption Behaviour in Darjeeling, India

Pravesh Tamang*† and Sebak Jana**

*Department of Economics, Presidency University, Kolkata, India
**Department of Economics, Vidyasagar University, Midnapore, India
†Corresponding author: Pravesh Tamang; singarpravesh@gmail.com

ABSTRACT

Using a unique dataset of 524 households from an urban hill town of Darjeeling in India, this study addresses two key issues of (a) determining the drivers of risk perception from water use, and (b) understanding whether water treatment decisions and choice of water sources are jointly made by the households. The results from probit model show that the age of the head, perception of the aesthetic qualities of water (odour and colour), education level of the head, the volume of improved water used, water treatment decision and expenditure on the water are the significant drivers of risk perception. The results of a rare investigation on the likelihood of the joint decision of treating water and choice of water source show that these decisions are indeed jointly made in the study area. Households decision to treat water from an unimproved source and the choice of improved water can be seen as substitutes.

INTRODUCTION

Water and sanitation are very crucial to the survival of people and the planet, and hence at the core of sustainable development. There have been advances in the use of 'improved sanitation facilities' (from 59% in 2000 to 68% in 2015) and 'improved water sources' (from 82% in 2000 to 91% in 2015) at the global level (United Nations 2016). However, in developing countries, not all 'improved sources' used are safe, and in 2012, an estimated 1.8 billion people were exposed to drinking water source contamination. In addition, the figures which pertain to the number of people having access to safe water seem to be overestimated as recent studies have shown that having access to 'improved sources' does not necessarily mean access to 'safe water' (Bain et al. 2014, Onda et al. 2012). Lack of safe water, sanitation, and hygiene in most of the developing countries led to 88% of deaths from diarrheal diseases, with a majority of them being children under the age of 5 (UNICEF 2008). In India, an estimated 38% of all deaths are attributable to diarrhoea (Walker et al. 2012).

The risks from water contamination, which emerge from sources around watersheds, raw sewage and industrial waste, are more visible in a developing country like India. Making water consumption decisions in such a situation demands reliance on sensory data or perceptions, such as the sight of a dead cow or the smell of rancid water (Crampton & Ragusa 2016). In those cases where contamination cannot be directly observed or perceived, individuals may have to rely on municipal reports on water quality. However, such information has not been easily available or updated, and also not easily understood by an average consumer (Crampton 2014).

Therefore, it becomes important that individuals rely on the personal judgement of water attributes to determine potential risks. Such attributes may include colour (how the water looks), taste, and smell of water (Crampton & Ragusa 2016). An alternative to this would be to 'trust' that the water providing agency is providing water that adequately addresses all the risks, and thus influences all the stakeholders (Serveiss 2002, Sterling et al. 2014) which is very likely to happen in the municipalities of India, and in Darjeeling (our study area) in particular. This could be so because citizens, who form a vital component of stakeholders, have little or no public discourse on the water quality. Such lack of public discourse is evident in developed nations like Australia and New Zealand too (Crampton & Ragusa 2016).

Studies which identify factors that affect risk perception related to water perception are still scarce and their findings being not conclusive (Onjala et al. 2014). Some related studies have found that perceived odour and taste of water (Jardine et al. 1999, Nauges & Berg 2009), the perceived taste of water and its related source (Levallois et al. 1999), age, income, and distance to the water treatment facility (Turgeon at al. 2004) to be the major drivers of risk perception.

Darjeeling is an urban hill town and a very popular tourist destination in north-eastern India and faces many issues in water services provided by the Darjeeling municipality. Lack of safe drinking water and sanitation services has added woes to the public health which often become more acute during the summer tourist season (Mell & Sturzaker 2014). The major sources of water contamination in the region are the unsafe biological matter and runoff of solid wastes (Rai 2011). Exposure to such untreated water leads to various water-related diseases such as stomach infection and typhoid. Typhoid was the third most reported disease in Darjeeling in the year 2003, and in the same year, less than 50% had access to safe water and sanitation (Sharma et al. 2009). The Darjeeling municipality was established in 1850 (considered to be one of the oldest municipalities in India) and the comprehensive water infrastructure laid during 1910-1930 for a population of 10,000. About 95% of the existing pipeline and valves were laid in 1930, and the infrastructure is in great need for renovation and restructuring. Out of 21,782 households in 32 wards of the town, only 2689 households (i.e. 12%) have municipal water connections and pay INR 500.00 annually as water bill to the municipality (Tamang & Jana 2017b).

The number of studies related to the perception of risk related to water consumption by households in developing countries is not much as per our knowledge. And in case of Darjeeling, this is the first effort to understand the issues of risk perception from water use and treatment decisions associated with the source of water that the households use. This study shall fill this gap and contribute to the literature by providing answers to the following questions; (a) what are the various drivers of risk perception from water use? (b) are the choice of water source (improved or unimproved source in this case) and a decision to treat water jointly made?

MATERIALS AND METHODS

Data

The data for the study come from a primary survey of households in Darjeeling town conducted in the year 2014. A pilot survey followed by a group discussion and focus group interviews with the local members selected at random were conducted before drafting the final questionnaire. From this preliminary analysis, we could get more insights on the various sources of water predominantly used in the neighbourhood, some of the water-related diseases that affected in the recent past, and their water treatment behaviour. The field investigators, who were the students from Darjeeling Government College, were trained by giving classes, conducting mock interviews and group discussions. This was an advantage because they could speak the local language and thus were in a better and comfortable position in conducting the survey. The random sample consisted of 524 households from the 32 wards of the town.

The questionnaire was divided into four sections. The first section consisted of questions on the socio-economic and demographic characteristics such as household ID, name of the respondent, relationship with the head, gender, age, education level, marital status, etc. The second section had questions about household characteristics such as type of residence, ownership, number of rooms, etc. The third section consisted of questions on health and hygiene. Questions were mainly based on the incidence of water-related diseases (diarrhoea, gastroenteritis, eye diseases, cholera, vomiting, blood in mucus or faeces, typhoid, and malaria), different kinds of toilet facilities used, hygiene behaviour, etc. The fourth and final section had questions about the different sources of water currently used by the households, the volume of water collected, perceived water quality (taste, odour and colour), expenditure on water, water treatment behaviour, etc.

Risk Perception

The first objective of the study is to determine the different drivers of risk perception related to water consumption. A probit model is used for this analysis. The response variable is an indicator of perceived health risk from water consumption from various water sources. Initially, the respondents answered whether they perceived no risk (=1), low risk (=2), or high risk (=3) from the water they consume from various sources. Risk perception is defined as an individual's intuitive risk judgement (based on aesthetic and non-aesthetic qualities) about drinking water (Anadu & Harding 2000). Therefore, the study also considered the aesthetic qualities (taste, colour, and odour) of water as the elements, and the nature of risk described to the respondents was about the various water-related diseases (included in the third section of the questionnaire and mentioned earlier) that could affect the households.

However, it was found that no risk (=1) responses were only 7 out of 524. Therefore, this was merged with the low risk (=2) option. This led us to code this response variable as a binary (0 = low risk, 1 = high risk) contrary to the ordinal specification in the questionnaire. The explanatory variables, which influence health risk perception, and are used in the analysis include the perception of water (taste, colour, and odour), age of the head of the household, education level of the head (primary, secondary, and graduate and above), water treatment behaviour (treat or do not treat), monthly expenditure on water (on all kinds of water sources), and water source (improved or unimproved source).

Based on the classification of water sources by the Joint Monitoring Programme, WHO and UNCF, piped water into dwelling, piped water in the yard, public standpipe and rainwater have been grouped under improved water sources; and unprotected spring, and water truck and private vendor are grouped under unimproved water sources (United Nations Children Fund & World Health Organisation 2017). According to the Joint Monitoring Programme, WHO and UNCF - "An improved drinking-water source is defined as one that, by nature of its construction or through active intervention, is protected from outside contamination, in particular from contamination with the faecal matter" (WHO & UNICEF 2012).

Following Wooldridge (2012), the econometric model specification of risk perception is given as follows;

$$y^* = \beta_0 + x\beta + e, \qquad y = \begin{cases} 1, if \ y^* > 0 \\ 0, if \ y^* \leq 0 \end{cases} \qquad ...(1)$$

where, $e \sim N(0, 1)$, y^* is the unobserved latent variable, y indicates the level of risk (low risk = 0, and high risk = 1), x denotes the vector of explanatory variables described earlier.

Household's Decision to Treat Water

The second objective of this paper is to see if a higher perceived risk leads to a higher probability to treat water before drinking it. Drinking water has different sources and the decision to treat or not to treat water before drinking is likely not to be independent of the choice of the water source (Onjala et al. 2014). With this assumption of simultaneous nature of the decision about water source and water treatment, and following Nauges & Berg (2009), a bivariate probit model with the following specification is derived;

$$s^* = z_1'\gamma_1 + e_1; s = 1 \ if \ s^* > 0, s = 0, otherwise$$

$$t^* = z_2'\gamma_2 + e_2; y = 1 \ if \ t^* > 0, t = 0, otherwise \qquad ...(2)$$

Here, e_1 and $e_2 \sim$ Bivariate Normal (BVN), s is the choice of using an improved water source, t is the decision to treat water before drinking, s^* and t^* are the two latent variables, z_1 and z_2 are the vectors of explanatory variables. In equation (2), the two latent variables s^* and t^* are not observed, but the variables s and t, which indicates the choice of the water source by a household and their decision to treat or not to treat before drinking it are observed. Therefore, the variable s indicates whether the household used an improved or unimproved source of water. Thus, equation (2) considers the joint probability that households choose water either from an improved or an unimproved source (s), and treat water before drinking it (t).

It is assumed, following Nauges & Berg (2009), that the explanatory factors are the same in both equations, i.e. $z_1 = z_2$. It is also important to see that if the error terms e_1 and e_2 are correlated (i.e. $\rho \neq 0$). The likelihood ratio test is used

to test the null hypothesis that $\rho = 0$. This statistic is used to test for the absence of correlation between the two sets of probit equations. Under the null hypothesis that $\square = 0$, the model consists of independent probit equations, which can be estimated separately (Greene 2012).

The variable s (the choice of water source) takes the values 0 if the source is unimproved and 1 if it is an improved source. Similarly, t takes the values 1 and 0 if a household treats and does not treat water respectively. The other explanatory variables used in the model are the age of the head, whether the head is female, education level of the head (primary, secondary, graduate and above), income category (below INR 10000, INR 10000 to 50000, and above 50000), employment status of the head, and the number of children below the age of 5. The employment status of the head variable had five levels (Table 1), however, because of the low number of observations in the casual, informal and unemployed levels, they were grouped under 'informal' employment. Hence, the employment status variable used in the bivariate model consists of three levels; informal, government employee and retired.

RESULTS

The description and descriptive statistics of the variables used in the analysis are presented in Table 1. It can be seen that the median age of the head of the sample households is 47 years with above-average higher educational attainments (in fact, there were no illiterate heads in the sample), and about 60% of the households used unimproved water source. As mentioned earlier, the households were asked whether they perceived "no risk", "low risk" or "high risk" from the water that they consume. The number of responses for "no risk" was only seven, so this option was merged with the "low risk" option. Therefore, from Table 1 it can be seen that all the households perceived risk from the water consumption, but the level of risk (low risk = 47.9%, high risk = 52.1%) seemed to be almost equally weighted. In terms of the aesthetic qualities of water in terms of odour, colour and taste, the households had varied responses.

A majority of the households (92%) perceive water to have a good odour, but at the same time, about 86% seem to be not satisfied with the colour of the water. However, in terms of perceived taste of water, the households are almost equally weighted. In the study, "bad colour" implied that water was turbid with suspended particles like mud sediments and waste particles. The turbidity of water could possibly be because of the illegal tapping along the distribution line which exposes the pipelines to sediments from the soil and other waste particles when the pipelines pass through roads and drains. Another reason could be because 60% of the

Table 1: Description and descriptive statistics of the variables used (Sample = 524).
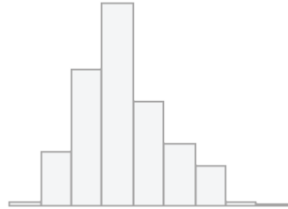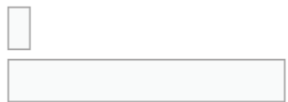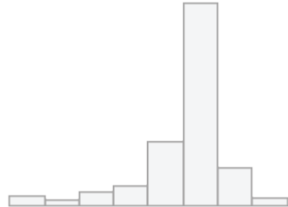
No	Variable	Stats / Values	Freqs (%)	Graph
1	**water_source** [source of water]	0. unimproved 1. improved	315 (60.1% 209 (39.9%)	
2	**riskpercep** [whether the household perceived low risk or high risk from the use of water for drinking]	0. low risk 1. high risk	251 (47.9%) 273 (52.1%)	
3	**age_head** [age of the head]	Mean (sd) : 48.2 (13.7) min < med < max: 16 < 47 < 95 IQR (CV) : 18 (0.3)		
4	**edu_head** [education level of the head of the family]	1. Graduate & above 2. Higher Secondary 3. Primary	199 (38.0%) 187 (35.7%) 138 (26.3%)	
5	**water_odour** [perceived odour of water]	0. bad 1. good	38 (7.2%) 486 (92.8%)	
6	**water_col** [perceived colour of water]	0. bad 1. good	452 (86.3%) 72 (13.7%)	
7	**water_taste** [perceived taste of water]	0. bad 1. good	254 (48.5%) 270 (51.5%)	
8	**treat_water** [whether the households treated water before drinking]	0. do not treat 1. treat	69 (13.2%) 455 (86.8%)	
9	**log_exp_water** [log of expenditure on water in INR per month]	Mean (sd) : 2.6 (0.7) min < med < max: 0 < 2.7 < 3.8 IQR (CV) : 0.5 (0.3)		

Table cont....

...Cont. Table

10	**vol** [volume of water collected in litres per day]	Mean (sd) : 537 (917) min < med < max: 0 < 175 < 8000 IQR (CV) : 520 (1.7)		
11	**femalehead** [whether the head was female]	0. no 1. yes	446 (85.1%) 78 (14.9%)	
12	**income** [monthly income of the family]	1. Below 10,000 2. 10,000 – 50,000 3. Above 50,000	270 (51.5%) 163 (31.1%) 91 (17.4%)	
13	**disease** [whether any family member had any episode of water related disease in the last six months]	0. no 1. yes	447 (85.3%) 77 (14.7%)	
14	**emp_head** [employment status of the head of the family]	1. Casual Employee 2. Govt Employee 3. Informal 4. Retired 5. Unemployed	76 (14.5%) 122 (23.3%) 65 (12.4%) 197 (37.6%) 64 (12.2%)	
15	**child** [number of children below the age of 5 in the family]	Mean (sd): 0.1 (0.4) min < med < max: 0 < 0 < 3 IQR (CV): 0 (3.2)	0 : 472 (90.1%) 1 : 43 (8.2%) 2 : 8 (1.5%) 3 : 1 (0.2%)	

Source: Author's computation from survey data.

sample households collect water from unimproved sources and there is a high chance that they end up with bad aesthetics in water.

The median volume of water collected from improved sources (piped water into dwelling, piped water in the yard, public standpipe, and rainwater) is 175 litres per month, and irrespective of the source of water, about 87% of the households treat water (i.e. either boil, filter, add chlorine or stain) before drinking. This means that for an average household of 5 members, the water availability is a meagre 8.75 litres per capita per day, which is far below the recommended per capita water availability of 200 litres per day for municipal households in India and the per capita availability of 20 litres per capita per day reported in a water and waste disposal study commissioned by Darjeeling Municipality in 2002. An important aspect of water scarcity could be attributed to the burgeoning population of the town.

The majority of the sample households (51%) had incomes below INR 10,000. Most of the heads were retired personnel (about 38% and a majority of them had retired from the Indian Army, Gorkha Regiment) and others working as government employees (23.3%) and the rest working in the informal sector (shops, vendors, etc.) and casual employees (mostly being casual teachers in schools and colleges). There were a very small number of families with children below the age of 5 (90% of the families had no child below the age of 5), and only 15% of the households report the prevalence of water-related diseases (like diarrhoea, gastroenteritis, eye diseases, vomiting, typhoid, etc.) is among the family members during the last six months.

Table 2 reports the results from the probit regression model with perceived health risk as to the dependent variable. The results find that the significant drivers of risk perception are the age of the head, education level of the head, perception of the aesthetic qualities of water, the volume of improved water used, water treatment decision, and expenditure on water. All the coefficients of the variables have expected signs and are statistically significant at 1%, 5% and 10% levels of significance.

It can be inferred that the older heads in the sample are more likely to report higher risks from water that they use. Heads of the households with primary and secondary levels of education are less likely to report higher risk as compared to the graduates or those having even higher educational attainment, and this probability increases for lower levels of education (secondary -16% to primary -19%). The households having a "good" perception about the aesthetic qualities of water (odour and colour) are less likely to report "high risk" from water use. These results are similar to the findings of (Jardine et al. 1999, Levallois et al. 1999, Nauges & Berg 2009).

If the households collect water from an unimproved source, they are more likely to report higher risks. However, if they collect water from an improved source, they are less likely to report high risks, but this probability is very low (0.01%). And also, households with higher expenditure on water (per month) are more likely to report higher risks, as the higher volumes of water collected are usually procured from water vendors (sold in trucks and carts) which are unimproved sources.

Table 2: Results of the probit model with dependent variable = risk perception.

	Estimate		Marginal Effects	
age_head	0.007552 (0.004303)	*	0.003005 (0.00171)	*
Education of the head (base = Graduate)				
edu_headPrimary	-0.4848 (0.1369)	***	-0.191539 (0.053060)	***
edu_headSecondary	-0.4054 (0.1506)	***	-0.160586 (0.058708)	***
Perception about water quality				
water_odorgood	-1.931 (0.3759)	***	-0.495754 (0.037973)	***
water_colgood	-0.5136 (0.2346)	**	-0.201384 (0.088055)	**
water_tastegood	-0.1297 (0.1182)		-0.0515712 (0.046901)	
treat_watertreat	-0.2569 (0.1741)		-0.1007971 (0.06687608)	
log_exp_water	0.2266 (0.09118)	**	0.0901565 (0.03628202)	**
water_sourceunimproved	0.2287 (0.12)	*	0.0906404 (0.04725925)	*
vol	-0.0002686 (0.00007776)	***	-0.000102 (0.000030968)	***
(Intercept)	1.607 (0.5175)	***		

* p < 0.1, ** p < 0.05, *** p < 0.01

It is also important to understand that since only 2,689 out of 21,872 (12%) of the households have a municipal connection, the issue of multiple illegal tapping of water pipes along the course of the path has become rampant in the town (Tamang & Jana 2017b). This implies that more than 2,689 households (and more than 39.9% of the sample households in this study) draw upon municipal water, albeit through unauthorised means. This would explain the perception of water quality as being good and the low prevalence of water-related diseases.

The second objective of the paper is to understand whether the decision to treat water and the choice of water source are jointly made. Table 3 summarizes the results from a bivariate probit regression. The coefficients for improved water source and the decision to treat water along with the marginal effects of the joint probability that the households choose improved water source and also treat water are reported in the table. The likelihood ratio test which is used to test the null hypothesis that $\rho = 0$ is rejected (see Table 3), and we can conclude that there is a negative association ($\rho = -0.2$) among the choice of water source and treatment decision. This means that households would treat water from an unimproved source and do not treat those from an improved source. Therefore, treating water from unimproved

sources and the choice of the improved water source can be seen as substitutes (Onjala et al. 2014).

From the marginal effects reported in Table 3, we can infer that households with female heads are less likely to treat water or chose an improved source as their main source of drinking water. Higher educational attainment of the head is also a positive and an important factor in the joint decision of water treatment and choice of the improved water source as compared to the lower levels (base = primary). However, this cannot be confirmed at the graduate and higher level of educational attainment as the estimate is not statistically significant but the direction of change is still positive. Similarly, households having a history of water-related diseases during the past six months and those who perceive water to be of high risk, increase the likelihood of having an improved water source and treating water by 9% and 4% respectively. This is also seen to be true with those households who have children of age less than 5.

DISCUSSION

Using a unique dataset of 524 households from an urban hill town of Darjeeling in India, this study addresses two key issues of (a) determining the drivers of risk perception from water use, and (b) understanding whether water treatment

Table 3: Bivariate probit model for the joint decision of treating water and choice of the water source.

	Improved water source		Water is treated		Marginal Effects	
agehead	-0.001863 (0.0043146)		0.0025882 (0.0055865)		0.0003007 (0.0005341)	
femalehead	0.2917604 (0.175605)	*	-0.7947914 (0.280762)	***	-0.0810337 (0.0264772)	**
Education of the head (base = Primary)						
secondary	-0.1358546 (0.1524655)		0.3498633 (0.2077779)	*	0.0359699 (0.0198315)	*
graduate_and_above	-0.2870002 (0.1590904)	*	0.1946223 (0.2150053)		0.0285324 (0.0204698)	
Income level of the household (base = Below 10,000)						
10,000 to 50,000	0.1995249 (0.1378145)		-0.2205172 (0.1865709)		-0.027263 (0.0178276)	
above 50,000	0.0115453 (0.167218)		0.2933057 (0.2104085)		0.0250984 (0.0203028)	
disease_yes	-0.6650379 (0.1630546)	***	0.748401 (0.1865748)	***	0.092038 (0.0203936)	***
risk_perception	-0.364791 (0.116668)	***	0.3066869 (0.1561886)	*	0.0414356 (0.015255)	**
log_exp_water	0.0288407 (0.0843193)		0.1849516 (0.1186379)		0.0149573 (0.0112087)	
Employment status of the head (base = Informal)						
Retired	0.2113224 (0.1380626)		0.2542488 (0.1768716)		0.0136409 (0.0171066)	
Govt. employee	0.0961065 (0.1593869)		0.2328213 (0.2011365)		0.0164179 (0.0192891)	
child	-0.2118614 (0.1445517)		0.3030059 (0.1784118)	*	0.0349499 (0.0174268)	**
_cons	0.5760646 (0.3292189)	*	-2.346801 (0.4689399)	***		
/athrho	-0.2066754 (0.0989003)					
rho	-0.2037821 (0.0947932)					

Likelihood-ratio test of rho=0: chi2(1) = 4.41739 Prob > chi2 = 0.0356

decisions and choice of water sources are jointly made by the households. The results from probit model show that the age of the head, perception of the aesthetic qualities of water (odour and colour), education level of the head, the volume of improved water used, water treatment decision and expenditure on the water are the significant drivers of risk perception. The results of a rare investigation on the likelihood of the joint decision of treating water and choice of water source show that these decisions are indeed jointly made in the study area. Households decision to treat water from an unimproved source and the choice of improved water can be seen as substitutes.

An important implication of the study is that improving the aesthetics of water (odour and colour) is certainly going to change the risk perception of people. At present, there is just one sand and gravel filtration plant in Darjeeling (located in Jorebunglow at a distance of 8 km from the town), that filters the water before it is supplied to the town. However, during the course of the path, there are many illegal tappings, pipes passing through garbage dumping areas, which increase the chances of the deterioration of the aesthetics of water even after it is filtered (Tamang & Jana 2017a). Increasing the number of filtration plants would indeed help improve the aesthetics of water. Also, the Darjeeling municipality should share water quality test reports and necessary information with the public at regular intervals.

The households in the region have a high willingness to pay (WTP) for improved water services (Tamang & Jana 2017b), and we also see that treating water and choosing improved water are substitutes, which implies that policies should be aimed at increasing the number of piped connections which is at a low of 12%.

REFERENCES

Anadu, E. and Harding, A. 2000. Risk perception and bottle water use. Journal of the American Water Works Association, 92(11): 82-92.

Bain, R., Cronk, R., Wright, J., Yang, H. and Slaymaker, T. 2014. Fecal contamination of drinking-water in Low- and Middle-Income Countries: A systematic review and meta-analysis. PLoS Med, 11(5), p.e1001644.

Crampton, A. 2014. Water, an essential resource and potential health risk! rural perceptions, awareness and knowledge of health risks. Retrieved from https://researchoutput.csu.edu.au/en/publications/water-an-essential-resource-and-potential-health-risk-rural-perce

Crampton, A. and Ragusa, A. 2016. Exploring perceptions and behaviors about drinking water in Australia and New Zealand: Is it risky to drink water, when and why? Hydrology, 3(1): 8.

Greene, W. H. 2012. Econometric Analysis (Seventh). New York University.

Jardine, C. G., Gibson, N. and Hrudey, S. E. 1999. Detection of odour and health risk perception of drinking water. Water Science and Technology, 40(6): 91-98.

Levallois, P., Grondin, J. and Gingras, S. 1999. Evaluation of consumer attitudes on taste and tap water alternatives in Québec. Water Science and Technology, 40(6): 135-139.

Mell, I. and Sturzaker, J. 2014. Sustainable urban development in tightly constrained areas: A case study of Darjeeling, India. International Journal of Urban Sustainable Development, 6(1): 65-88.

Nauges, C. and Berg, C. Van Den. 2009. Perception of health risk and averting behaviour: An analysis of household water consumption in Southwest Sri Lanka. Toulouse School of Economics, 1-33.

Onda, K., LoBuglio, J. and Bartram, J. 2012. Global access to safe water: Accounting for water quality and the resulting impact on MDG progress. Int. J. Environ. Res. Public Health, 9: 880-894.

Onjala, J., Ndiritu, S. W. and Stage, J. 2014. Environment for development risk perception, choice of drinking water, and water treatment evidence from Kenyan Towns. J. Water Sanitation and Hygiene for Development, 4(2): 268-280.

Rai, P. 2011. Solid waste management in Darjeeling Municipality. In: M. Desai & S. Mitra (eds.), Cloud Stone and the Mind: The People and Environment of Darjeeling Hill Area. New Delhi: K. P. Bagchi & Company.

Serveiss, B. 2002. Applying ecological risk principles to watershed assessment and management. Environmental Management, 29(2): 145-154.

Sharma, P., Ramakrishnan, R., Hutin, Y., Manickam, P. and Gupte, M. 2009. Risk factors for typhoid in Darjeeling, West Bengal, India: Evidence for practical action. Tropical Medicine and International Health, 14(6): 696-702.

Sterling, S. M., Garroway, K., Guan, Y., Ambrose, S. M., Horne, P. and Kennedy, G. W. 2014. A new watershed assessment framework for Nova Scotia: A high-level, integrated approach for regions without a dense network of monitoring stations. Journal of Hydrology, 519: 2596-2612.

Tamang, P. and Jana, S. K. 2017a. Water scarcity in the hill town of Darjeeling: Effects on women's health. Intercontinental Journal of Human Resource Research Review, 5(7): 113-120.

Tamang, P. and Jana, S. K. 2017b. Willingness to pay for improved water services: A case of Darjeeling, India. Asian Journal of Water, Environment and Pollution, 14(2): 51-59.

Turgeon, S., Rodriguez, M. J., Thériault, M. and Levallois, P. 2004. Perception of drinking water in the Quebec City region (Canada): The influence of water quality and consumer location in the distribution system. Journal of Environmental Management, 70(4): 363-373.

UNICEF 2008. Why improved sanitation is important for children. Retrieved from http://www.unwater.org/wwd08/docs/kids-sanitation.pdf

United Nations 2016. Progress towards the sustainable development goals: Report of the Secretary General (Vol. 28564). https://doi.org/10.1017/S0020818300006640

United Nations Children Fund and World Health Organisation. 2017. Progress on drinking water, sanitation and hygiene - Joint Monitoring Programme 2017 Update and SDG Baselines. In: World Health Organisation. https://doi.org/10.1111 / tmi.12329

Walker, C., Perin, J., Aryee, M., Boschi-Pinto, C. and Black, R. 2012. Diarrhea incidence in low-and middle-income countries in 1990 and 2010: a systematic review. BMC Public Health, 12(220).

WHO and UNICEF 2012. WHO/UNICEF Joint Monitoring Programme (JMP) for Water Supply and Sanitation. Retrieved from https://web.archive.org/web/20120606072534/http://www.wssinfo.org/definitions-methods/introduction/

Wooldridge, J. 2012. Introductory Econometrics: A Modern Approach. South-Western Educational Publishing.

The Influence of Atrazine on the Growth, Development and Oxygen Consumption of *Pelophylax nigromaculatus* Tadpoles

Minyi Huang*†, Qiang Zhao*, Yaqi Zhang*, Yuxiang Lin* and Yinhua Ma*

*College of Agriculture and Biotechnology, Hunan University of Humanities, Science and Technology, Loudi, Hunan, 417000, China

†Corresponding author: Minyi Huang; huang.m.y@163.com

ABSTRACT

Amphibians grow and reproduce in water, and are sensitive to water pollution. Atrazine is one of the widely distributed herbicides that can damage the amphibians. To study the influence of atrazine on the growth, development and oxygen consumption of *Pelophylax nigromaculata* larvae, 26 stages of tadpoles were raised in water containing different concentrations of atrazine (0, 8, 16, 32 and 64 μg/L). After treatments at different times (10, 15, 20, 25 d), the snout vent length (SVL), total length, body width and the bodyweight of tadpoles were measured, and oxygen consumption of tadpoles was checked with an aquatic biorespirometer. The results showed that with the increase of treatment time, the SVL, whole length, body width and the bodyweight of *P. nigromaculatus* tadpoles of each concentration group increased. At the same treatment time, the SVL, whole length, body width and the bodyweight of *P. nigromaculatus* tadpoles gradually decreased with the increase of concentration. Compared with the control group, the oxygen consumption in the treatment groups increased in the short-term treatment (10 d), had no difference in the medium-term treatment (15 d) and decreased in the long-term treatment (20 and 25 d).

INTRODUCTION

Atrazine is a kind of ubiquitously used pesticide herbicide in farmland ecosystems for its low cost and good weeding effect (Solomon et al. 2008, Figueira et al. 2017). Atrazine is highly polar and soluble in water. It has a long residual period in the environment and has highly toxic bio-accumulation. Atrazine is dissolved in the waters around farmlands after extensive use, which has harmful effects on the ecological environment and animal survival.

Atrazine can have harmful effects on fish, amphibians and aquatic reptiles, which can be accumulated in organisms and easily absorbed by skin, respiratory tract and digestive tract (Solomon et al. 2008). Atrazine can produce neurotoxicity mainly including oxidative stress injury, neurotransmitter disorder and neurocyte injury (Jin et al. 2014). At the same time, it can affect the synthesis, release, transmission and sensitivity of neurotransmitters, inhibit the transmission speed of excitation, lead to changes in the morphology of the central nervous system, and damage neurons and glial cells (Figueira et al. 2017). Atrazine can also induce oxidative stress, lipid peroxidation and enzyme activity, leading to neurological disorders, affecting the balance between activation and inhibition of synaptic transmission (Schmidel et al. 2014). Atrazine can

significantly affect estrogen receptors by interacting with them (Albanito et al. 2015).

Amphibians are extremely sensitive to the changes in waters and their surrounding environments. In recent years, the number of amphibian population has been decreasing rapidly. Atrazine in water is one of the main reasons for the decrease in amphibians. Studies have been done on the effects of atrazine on fish, reptiles, birds and mammals, however, studies on the effects of atrazine on amphibians mainly focus on embryonic development, tissue damage, oxidative stress, and so on (Mitchkash et al. 2014, Brodkin et al. 2007, Orton et al. 2006, Tavera-Mendoza et al. 2002). For example, atrazine can affect an individual's survival, development and motor retardation of *Limnodynastes peronii* (Mitchkash et al. 2014). Atrazine can reduce the number of white cells in *Rana pipiens* and affected the activity of phagocytes (Brodkin et al. 2007). Atrazine can change the ratio of male to female, resulting in a reduction of sperm cells in the testis of *R. pipiens* (Orton et al. 2006). Tadpoles of *Xenopus laevis*, exposed to atrazine (21 μg/L) for 48 hours, can cause a 57% reduction in testicular volume and a 7% reduction in the number of germ cells (Tavera-Mendoza et al. 2002).

Different species have different sensitivities to atrazine, especially in embryonic and metamorphic individuals, which are more sensitive to atrazine (Allran & Karasov 2010).

Respiration is an activity of gas exchange between animals and the outside medium, which plays an important role in the survival of animals. Most of the studies on oxygen consumption are focused on the invertebrates, fish or mammals (Lee et al. 2003, Lamarre et al. 2016), but less on amphibian tadpoles, especially on the effects of atrazine on the respiratory capacity of tadpoles.

Pelophylax nigromaculatus is a widely distributed species in farmland in China, which is greatly affected by environmental pollution. In this study, *P. nigromaculatus* tadpoles were exposed to water containing different concentrations of atrazine, and the effects of different treatment time and concentration of atrazine on the growth, development and oxygen consumption of *P. nigromaculatus* tadpoles were studied.

MATERIALS AND METHODS

Sexually matured individuals of *P. nigromaculatus* were collected in the field and mated in the laboratory. Fertilized eggs were hatched after frogs spawning, until 26 stages. Healthy and similar size tadpoles were selected for the experiment. The atrazine with a purity of 38% used was procured from Bonong Chemical Technology Co., Ltd. of China. The mother liquor of 1g/L atrazine was prepared with pure water.

When the tadpoles reached stage 26, four treatment groups and one control group were set up. The treatments of atrazine were of 8, 16, 32 and 64 µg/L respectively, and three corresponding parallel groups were set up in each treatment. Each group contained 20 similar and healthy tadpoles, which were fed in 4 L water which was aerated for more than 3 days. During the experiment, soybean milk residue was fed at 8 a.m. every day. After 2 hours of feeding, the water was changed. During the experiment, the water temperature was 21-23°C, the dissolved oxygen was 6.8-7.5 mg.L^{-1}, the relative humidity in the air was 65%-73%, and the dark:light period in the laboratory was 12 h:12 h. The experiment was supported by the local government, and the breeding and use of experimental animals followed the committee principles.

After different times of treatments (10, 15, 20 and 25 d), the snout vent length (SVL), total length, body width and the bodyweight of tadpoles were measured respectively by the digital Vernier calliper, and oxygen consumption of tadpoles was assessed with an aquatic biorespirometer (Q-Box AQUA Aquatic Respirometry, Qubit Systems Inc. Kingston, Ontario, Canada). The system uses a cylindrical breathing chamber (3.7 cm diameter, 15 cm long) which is installed in an improved insulated cooler used as an experimental chamber. During the whole experiment, the oxygen consumption measurement was recorded every 5 minutes.

The Statistic software was used for statistical analysis of data, and one-way ANOVA analysis was conducted among groups, $P < 0.05$ was considered as a significant difference.

RESULTS

Compared with the low concentration group (8 µg/L) and the control group, the high concentration groups (16, 32 and 64 µg/L) had a smaller size and slower movement under the same treatment time (Fig. 1). In the high concentration groups (16, 32 and 64 µg/L) treated for 25 days, some individuals
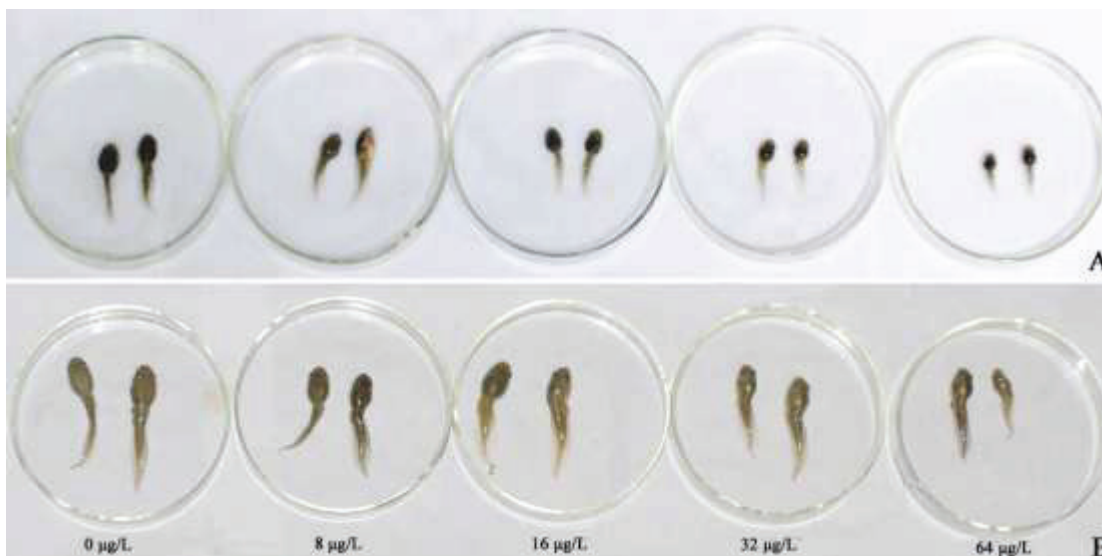

Fig. 1: The morphological size in *P. nigromaculata* under the different atrazine concentrations (0, 8, 16, 32 and 64 µg/L) and different test times (A 10 days, B 25 days).

were observed to have body bending, abnormal eyes and other deformities (Fig. 1).

With the increase of treatment time, the SVL, whole length and body width of each concentration group increased (Figs. 2, 3, 4). At the same treatment time, the SVL, whole length and body width gradually decreased with the increase of concentration (Figs. 2, 3, 4).

After 10 and 15 days of treatment, there was no significant difference in the SVL, whole length and body width between the high concentration groups (32 and 64 µg/L),
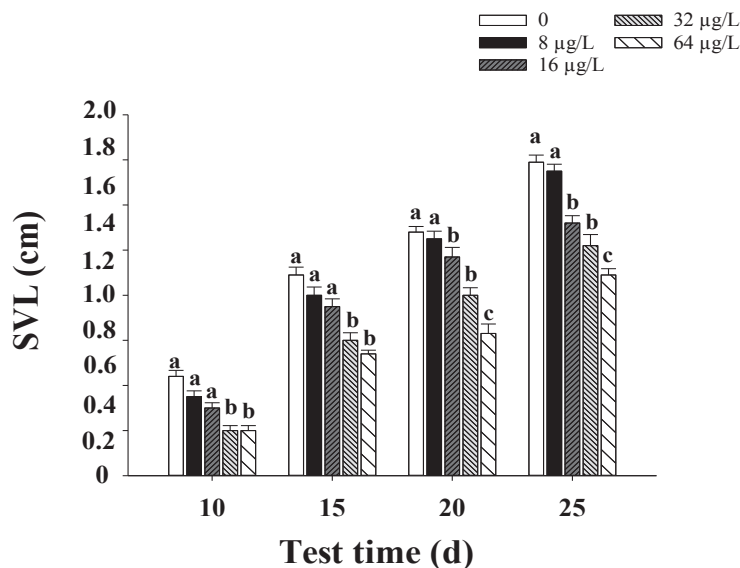

Fig. 2: The snout vent length (SVL) in *P. nigromaculata* under the different atrazine concentrations (0, 8, 16, 32 and 64 µg/L) and different test times (10, 15, 20 and 25 d). Values represent the mean ± SE. Treatments with different letters differ significantly (Tukey's test, a = 0.05, a > b > c).

Fig. 3: The whole length in *P. nigromaculata* under the different atrazine concentrations (0, 8, 16, 32 and 64 µg/L) and different test times (10, 15, 20 and 25 d). Values represent the mean ± SE. Treatments with different letters differ significantly (Tukey's test, a = 0.05, a > b > c).

Fig. 4: The body width in *P. nigromaculata* under the different atrazine concentrations (0, 8, 16, 32 and 64 µg/L) and different test times (10, 15, 20 and 25 d). Values represent the mean ± SE. Treatments with different letters differ significantly (Tukey's test, a = 0.05, a > b > c).
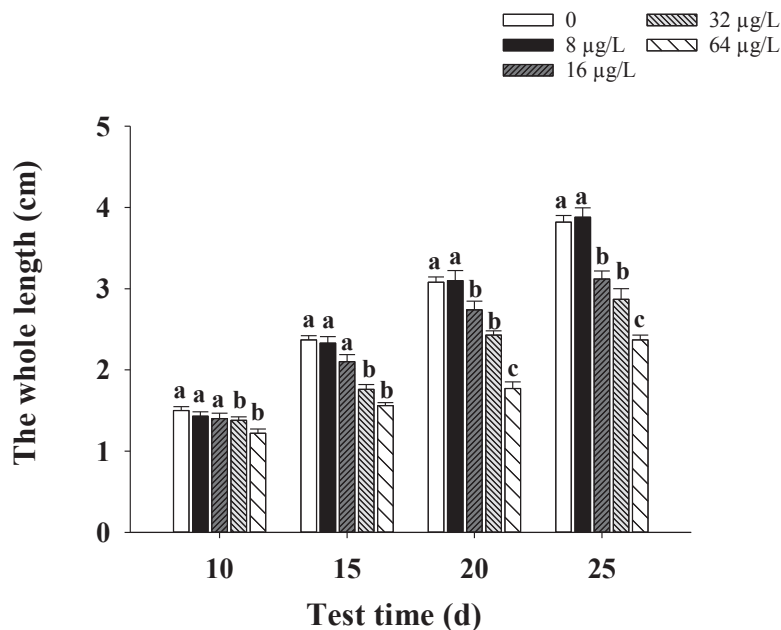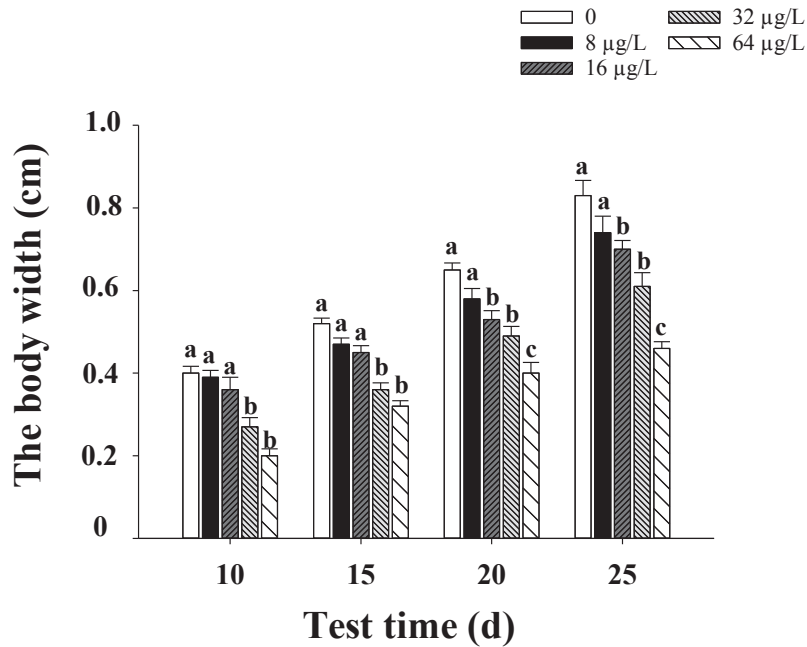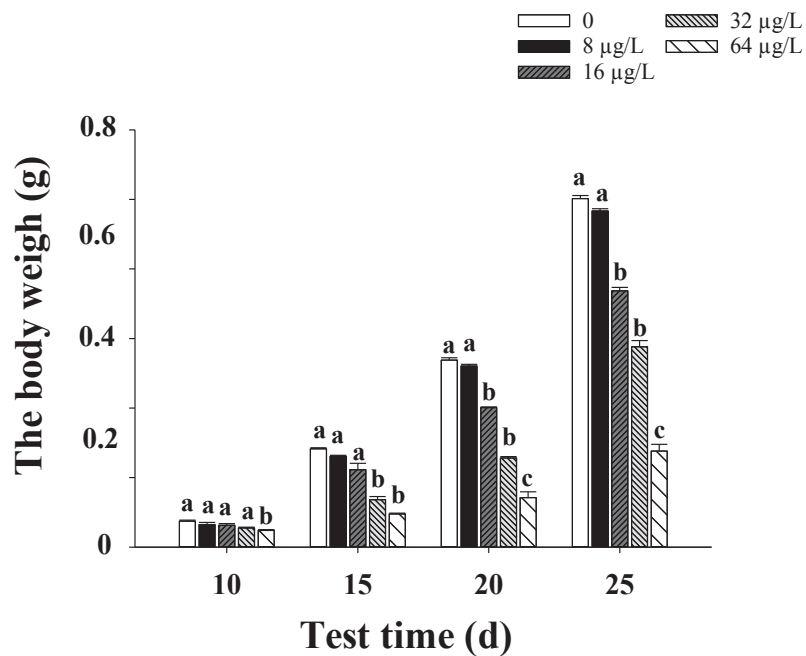

Fig. 5: The body weight in *P. nigromaculata* under the different atrazine concentrations (0, 8, 16, 32 and 64 µg/L) and different test times (10, 15, 20 and 25 d). Values represent the mean ± SE. Treatments with different letters differ significantly (Tukey's test, a = 0.05, a > b > c).

but they were significantly lower than other treatments ($P < 0.05$) (Figs. 2, 3, 4). After 20 and 25 days of treatment, the SVL, whole length and body width in 64 µg/L treatment group were the lowest, significantly lower than those of other treatment groups ($P < 0.05$). There was no significant difference in the SVL, whole length and body width in the 16 and 32 µg/L treatment groups ($P > 0.05$), but they were significantly lower than those of 8 µg/L treatment group and control group ($P < 0.05$) (Figs. 2, 3, 4).

With the increase of treatment time, the body weight of each concentration group increased (Fig. 5). At the same treatment time, the body weight gradually decreased with the increase of concentration (Fig. 5).

After 10 days of treatment, the high concentration group (64 µg/L) was significantly lower than other treatments ($P < 0.05$), and there was no significant difference among other treatments (0, 8, 16 and 32 µg/L) ($P > 0.05$) (Fig. 5). After 15 days of treatment, there was no significant difference between the 64 and 32 µg/L treatment groups ($P > 0.05$), but they were significantly lower than other treatment groups ($P < 0.05$) (Fig. 5). After 20 days and 25 days, the changes of body weight were similar. The 64 µg/L treatment group was the lowest, significantly lower than other treatment groups

($P < 0.05$). There was no significant difference between the 16 and 32 µg/L treatment groups ($P > 0.05$), but they were significantly lower than the 8 µg/L treatment group and the control group ($P < 0.05$) (Fig. 5).

Oxygen consumptions of *P. nigromaculatus* tadpoles in different concentrations at 10, 15, 20 and 25 days treatment were measured by a respirometry system (Fig. 6). There was no significant difference between body weight and oxygen consumption in tadpole ($P > 0.05$). With the extension of treatment time, the oxygen consumption of each concentration group increased. But under the same treatment time, with the increase of treatment concentration, the oxygen consumption showed a variety of changes (Fig. 6).

After treatment for 10 days, oxygen consumption increased with the increase of treatment concentration. Compared with the control group, the oxygen consumption of the treatment group was significantly higher than that of the control group ($P < 0.05$). High concentration treatment groups (32 and 64 µg/L) were significantly higher than other treatments ($P < 0.05$), and there was no significant difference among other treatments (0, 8 and 16 µg/L) ($P > 0.05$) (Fig. 6). After 15 days of treatment, with the increase of treatment concentration, oxygen consumption showed a waveform

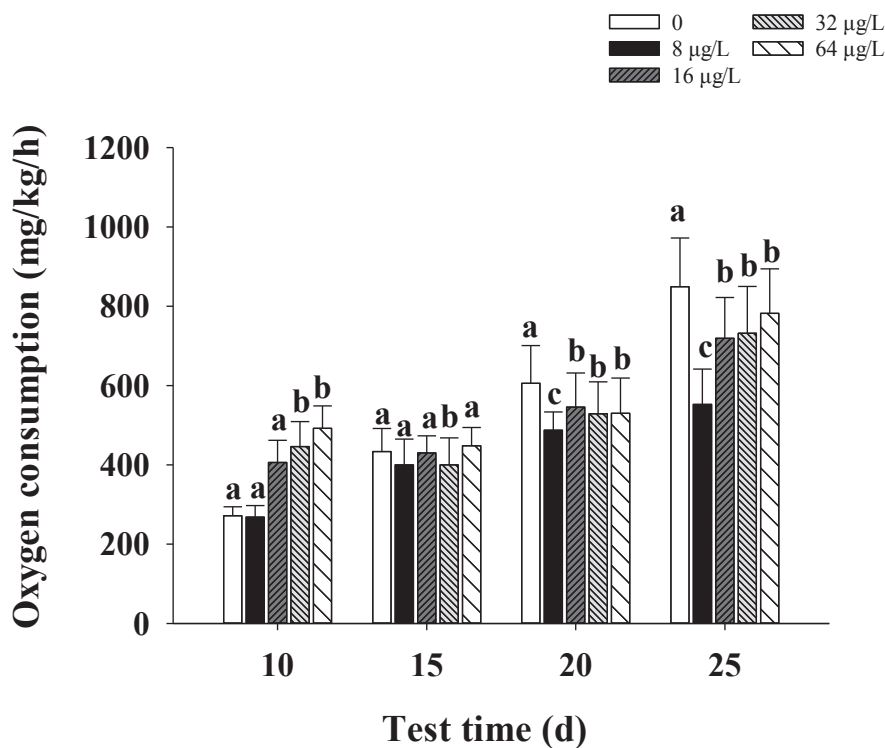Fig. 6: The oxygen consumption of tadpoles in *P. nigromaculata* under the different atrazine concentrations (0, 8, 16, 32 and 64 µg/L) and different test times (10, 15, 20 and 25 d). Values represent the mean ± SE. Treatments with different letters differ significantly (Tukey's test, a = 0.05, a > b > c).

change. On the whole, there was no significant difference between the treatment group and the control group ($P > 0.05$). After 20 and 25 days of treatment, oxygen consumption showed waveform change. Compared with the control group, the oxygen consumption of the treatment group showed a downward trend. Among them, 8 µg/L treatment group was the lowest ($P < 0.05$) (Fig. 6).

DISCUSSION

Because tadpoles live in water, they are more sensitive to pollutants where they live. With the prolongation of exposure time, their snout vent length (SVL), whole length, body width and body weight increased, however, with the increasing of concentration, relative to the control, the growth of tadpoles decreased obviously. This indicated that certain concentrations of atrazine influence the growth and development of tadpole in a certain period, which is similar to other studies (Freeman et al. 2005, Mitchkash et al. 2014, Mendonça et al. 2016). Mendonça et al. (2016) documented that atrazine exposure can lead to a slower rate of metamorphosis in *Podocnemis expansa*, resulting in decreased swimming and leaping ability of individuals. Mitchkash et al. (2014) also found that atrazine could affect individual survival, development and motor retardation in *Limnodynastes peronii*. The growth retardation of tadpoles by atrazine may be due to the influence of atrazine on the thyroid in *Bufo americanus* tadpoles (Freeman et al. 2005).

The respiratory system can quickly respond to the changes in the external environment, so it is an important indicator of the body's functional state. Amphibian larvae live in water and breathe by gills. Moreover, the skin of tadpole has good permeability. Therefore, tadpoles' respiratory system is susceptible to the influence of their living water. It was reported that atrazine can induce respiratory difficulty in adult *R. pipiens* by increasing buccal and thoracic ventilation (Allran & Karasov 2010). The acute exposure of atrazine (8.1 mg/L) can alter routine oxygen consumption in *Tilapia sparrmanii*, especially reflecting a drastic decrease within 3 hours (Grobler et al. 1989).

There is a certain correlation between oxygen consumption and treatment time. Our findings confirm that atrazine affected oxygen consumption of tadpoles in *P. nigromaculata*. Compared with the control group, the oxygen consumption in the treatment groups increased in the short-term treatment (10 d), had no difference in the medium-term treatment (15 d) and decreased in the long-term treatment (20 d and 25 d). Other studies have similar findings. For example, atrazine (150 µg/L) can induce respiratory oxygen consumption increasing in 2-day postfertilization fathead minnow (*Pimephales promelas*) eggs after using the self-referencing

micro-optrode technique after 2 h exposures to atrazine (Sanchez et al. 2008). The long-term atrazine treatment can lead to changes in morphological damage of the respiratory tract, which induce a decrease in oxygen consumption. Previous studies have shown that herbicides can cause significant changes in skin morphology, cell and epithelial cell proliferation or hypertrophy and chromatid breakdown, and affect the physiology of respiratory tract morphology in bullfrog tadpoles (Rissoli et al. 2016). High concentration atrazine can cause blood composition and oxygen consumption change in *Tilapia mossambica*, which induce respiratory distress in fish (Prasad et al. 1991).

REFERENCES

Albanito, L., Lappano, R., Madeo, A., Chimento, A., Prossnitz, E.R., Cappello, A.R., Dolce, V., Abonante, S., Pezzi, V. and Maggiolini, M. 2015. Effects of atrazine on estrogen receptor α- and G protein-coupled receptor 30-mediated signalling and proliferation in cancer cells and cancer-associated fibroblasts. Environ. Health. Perspect., 123: 493-499.

Allran, J.W. and Karasov, W.H. 2010. Effects of atrazine on embryos, larvae, and adults of anuran amphibians. Environ. Toxicol. Chem., 20(4): 769-775.

Brodkin, M.A., Madhoun, H., Rameswaran, M. and Vatnick, I. 2007. Atrazine is an immune disruptor in adult northern leopard frogs (*Rana pipiens*). Environ. Toxicol. Chem., 26: 80-84.

Figueira, F.H., de Quadros Oliveira, N., de Aguiar, L.M., Escarrone, A.L., Primel, E.G., Barros, D.M. and da Rosa, C.E. 2017. Exposure to atrazine alters behaviour and disrupts the dopaminergic system in *Drosophila melanogaster*. Comp. Biochem. Physiol. C Toxicol. Pharmacol., 202: 94-102.

Freeman, J.L., Beccue, N. and Rayburn, A.L. 2005. Differential metamorphosis alters the endocrine response in anuran larvae exposed to T₃ and atrazine. Aquat. Toxicol., 75(3): 263-276.

Grobler, E., Vuren, J. H.J.V. and Preez, H.H.D. 1989. Routine oxygen consumption of *Tilapia sparrmanii* (cichlidae) following acute exposure to atrazine. Comp. Biochem. Physiol. C Toxicol. Pharmacol., 93(1): 37-42.

Jin, Y., Wang, L., Chen, G., Lin, X., Miao, W. and Fu, Z. 2014. Exposure of mice to atrazine and its metabolite diaminochlorotriazine elicits oxidative stress and endocrine disruption. Environ. Toxicol. Pharmacol., 37(2): 782-90.

Lamarre, S.G., Maccormack, T.J., Sykes, A.V., Hall, J.R. Speers-Roesch, B., Callaghan, N.I. and Driedzic, W.R. 2016. Metabolic rate and rates of protein turnover in food deprived cuttlefish, *Sepia officinalis* (Linnaeus 1758). Am. J Physiol. Regul. Integr. Comp. Physiol., 310(11): 1160-1168.

Lee, C. G., Farrell, A. P., Lotto, A., MacNutt, M.J., Hinch, S.G. and Healey, M.C. 2003. The effect of temperature on swimming performance and oxygen consumption in adult sockeye (*Oncorhynchus nerka*) and coho (*O. kisutch*) salmon stocks. J. Exp. Biol., 206(18): 3239-3251.

Mendonça, J. S., Vieira, L.G., Valdes, S.A., Vilca, F.Z., Tornisielo, V.L. and Santos, A.L. 2016. Effects of the exposure to atrazine on bone development of *Podocnemis expansa* (Testudines, Podocnemididae). Ecotoxicology, 25: 594-600.

Mitchkash, M.G., McPeek, T. and Boone, M.D. 2014. The effects of 24-h exposure to carbaryl or atrazine on the locomotor performance and overwinter growth and survival of juvenile spotted salamanders (*Ambystoma maculatum*). Environ. Toxicol. Chem., 33: 548-552.

Orton, F., Carr, J.A. and Handy, R.D. 2006. Effects of nitrate and atrazine on larval development and sexual differentiation in the northern leopard frog *Rana pipiens*. Environ. Toxicol. Chem., 25: 65-71.

Prasad, T.A., Srinivas, T., Rafi, G.M. and Reddy, D.C. 1991. Effect in vivo of atrazine on haematology and O_2 consumption in fish, *Tilapia mossambica*. Biochem. Int., 23(1): 157.

Rissoli, R.Z., Abdalla, F.C., Costa, M.J., Rantin, F., McKenzie, D.J. and Kalinin, A.L. 2016. Effects of glyphosate and the glyphosate based herbicides *Roundup Original* and *Roundup Transorb* on respiratory morpho physiology of bullfrog tadpoles. Chemosphere, 156: 37-44.

Sanchez, B.C., Ochoaacuña, H., Porterfield, D.M. and Sepúlveda, M.S. 2008. Oxygen flux as an indicator of physiological stress in fathead minnow (*Pimephales promelas*) embryos: A real-time biomonitoring system of water quality. Environ. Sci. Technol., 42(18): 7010-7017.

Schmidel, A.J., Assmann, K.L., Werlang, C.C., Bertoncello, K.T., Francescon, F., Rambo, C.L., Beltrame, G.M., Calegari, D., Batista, C.B., Blaser, R.E., Roman Júnior, W.A., Conterato, G.M., Piato, A.L., Zanatta, L., Magro, J.D. and Rosemberg, D.B. 2014. Subchronic atrazine exposure changes defensive behaviour profile and disrupts brain acetyl-cholinesterase activity of zebrafish. Neurotoxicol. Teratol., 44: 62- 69.

Solomon, K.R., Carr, J.A., Du Preez, L.H., Giesy, J.P., Kendall, R.J., Smith, E.E. and Van Der Kraak, G.J. 2008. Effects of atrazine on fish, amphibians, and aquatic reptiles: A critical review. Crit. Rev. Toxicol., 38(9):721-772.

Tavera-Mendoza, L., Ruby, S., Brousseau, P., Fournier, M., Cyr, D. and Marcogliese, D. 2002. Response of the amphibian tadpole (*Xenopus laevis*) to atrazine during sexual differentiation of the testis. Environ. Toxicol. Chem., 21: 527-531.

Net Anthropogenic Nitrogen Input (NANI) Evolution and Total Nitrogen (TN) Concentration Response in Zhaoshandu Water Source

A-long Li*, Hai-tao Chen*, Yuan-yuan Liu**, Lin Qiu* and Wen-chuan Wang*†

*School of Water Conservancy, North China University of Water Resources and Electric Power, Zhengzhou City Henan Province, 450045, PR China
**Henan Huarun Engineering Design Co., Ltd., Zhengzhou City, Henan Province, 450045, PR China
†Corresponding Author: Wen-chuan Wang; liuyuan_hs@sina.com

ABSTRACT

The nitrogen concentration/flux of water is very sensitive to the response of Net Anthropogenic Nitrogen Inputs (NANI), but the research on the dynamic response of nitrogen concentration to NANI is still rarely reported. In this study, the source of Zhaoshandu water source in Zhejiang Province, China, was used as the research object. The dynamic response of total nitrogen (TN) concentration to NANI in the basin was quantitatively analysed from 2005 to 2014. The results show that the NANI of the water source has a growing trend. It has increased by 6.73% in ten years. The average annual average of NANI is 85.76 kg ($hm^2 \cdot a^{-1}$), which is 1.7 times the national average of 2009. The average contribution rate of atmospheric nitrogen, chemical fertilizer nitrogen, food and feed nitrogen and crop fixed nitrogen is 40.98%, 34.06%, 20.25% and 4.7% respectively. The spatial difference of NANI is large, showing an increasing trend from the upstream mountainous area along the downstream. The sub-basin 2 is the key source of nitrogen pollution in this water source. NANI is the only independent variable of the TN concentration regression model with a variance interpretation rate of 55.4%. In the future, it is necessary to reduce the nitrogen input intensity of nitrogen, food and feed for chemical fertilizers as the main target, and to achieve the goal of water quality improvement by reducing the NANI intensity in the basin.

INTRODUCTION

The increase of nitrogen concentration/flux in rivers not only endangers the ecosystem health of the water itself but also is one of the main causes of eutrophication of water bodies such as lake banks, estuaries and coasts (Chen et al. 2014, Zhang & Chen 2014). How to effectively control nitrogen pollution in water has become one of the important scientific issues in the world. In the past two decades, the water body nitrogen pollution control strategy has experienced the development process from the end treatment, source control, process emission reduction, water ecological restoration to the comprehensive application of various control methods (Gao et al. 2016). However, in many regions/basins, despite the adoption of measures such as reducing fertilization and land-use conversion, the effectiveness of nitrogen pollution control is not optimistic (Stålnacke et al. 2003). One of the important reasons is that the response of river nitrogen pollution to human activities in the basin cannot be clarified. It can be seen that only by clarifying the dynamic response of water body nitrogen concentration/flux to human activities in the basin can provide a scientific basis for formulating an effective watershed nitrogen management strategy.

The existing methods rely mainly on the watershed model (SWAT, AGNPS, etc.) around the dynamic response of the nitrogen concentration/flux of the flowing water to the human activities in the basin. However, the watershed model is complex in structure, high in data requirements, difficult to calibrate and verify, and in application and promotion are greatly limited (Wang et al. 2016, Yang et al. 2007). In 1996, Howarth et al. (1996) pioneered the net anthropogenic nitrogen input (Net Anthropogenic Nitrogen Input, NANI) algorithm, which provides a new and effective means for assessing human input of reactive nitrogen. The NANI algorithm belongs to the quasi-material balance method, which mainly calculates the net anthropogenic nitrogen input of the region/basin based on conventional economic and social statistics. In general, net anthropogenic nitrogen inputs in a region include four inputs for fertilizer application of nitrogen, human food and animal feed nitrogen, crop fixed nitrogen and atmospheric sedimentation nitrogen, and NANI is the sum of these four inputs. Numerous studies have found that water nitrogen concentration/flux is very sensitive to the response of watershed NANI, and the quantitative relationship between the two can be expressed as linear or exponential (Chen et al. 2016, Han et al. 2009, Howarth et al. 2012).

In summary, NANI has become an effective method to express the comprehensive impact of human activities on the nitrogen cycle process, providing a new way to study the response of water nitrogen concentration/flux to human activities. However, studies on the dynamic response of nitrogen concentration in water sources to NANI are still rarely reported in China (Zhang & Chen 2014). Therefore, it is of great practical significance to study the dynamic response of nitrogen concentration in the water source to NANI. In this study, the Zhaoshandu water source in Zhejiang Province, China, was used as the research object. From 2005 to 2014, the regression model of TN concentration on NANI and main natural factors was established to promote nitrogen management and promote water nitrogen control in the basin.

MATERIALS AND METHODS

Study Area

The study area is located in the upper reaches of Feiyun River in Zhejiang Province, China. The river originates from the mountainous area of southwest Zhejiang, with a total length of 203 km and a drainage area of 3252 km^2. The main water conservancy project in the water source of Zhaoshandu includes a multi-year regulation reservoir and a water diversion project. It has functions of water supply, power generation and flood control, and is one of the important drinking water sources in southern Zhejiang (Fig. 1). The normal water storage level of the upstream multi-year regulation reservoir is 142m, with a total storage capacity of 1.824 billion m^3. The entire water source basin area is 2280 km^2, and the upper control basin area above the upstream reservoir dam site is 1529 km^2 (Fig. 1). Affected by the subtropical monsoon climate, the average annual precipitation is 1876mm, and the average annual precipitation is 149 days. The precipitation is unevenly distributed during the year, and the rainfall is concentrated from April to September, accounting for 75% of the whole year. The average elevation of the whole basin

is 573m, the soil is mainly red soil, and the rest are yellow soil, purple soil, coarse soil and paddy soil. The land-use type is mainly forest land, accounting for 71% of the total area, followed by cultivated land, accounting for about 20%.

Data Source

In this study, a hydrological water quality monitoring station was set up in the water diversion project (before the anti-regulation reservoir dam), and seven rainfall observation stations were set up in the basin. There are multiple water quality monitoring stations in the basin, and the frequency of water quality monitoring is once a month. The monthly TN concentration data from 2005 to 2014 is provided by the local environmental protection department. The daily flow and water level data for the same period are provided by the local water conservancy department. The SWAT model is used to divide the basin boundaries above the counter-regulation reservoir. The basin boundary covers the large area of two county-level administrative regions and a small area of two county-level administrative regions (Fig. 1). The main data source for calculating NANI is the calendar yearbook of the four county-level administrative regions. After calculating the NANI of the county-level administrative region, the watershed boundary and the administrative boundary are superimposed and analysed using ArcGIS 10.2.

NANI Calculation

Referring to previous studies, NANI was obtained by summing up atmospheric precipitation nitrogen, nitrogen fertilizer, crop fixed nitrogen, and food and feed nitrogen (Chen et al. 2016, Gao et al. 2016). The calculation formula is expressed as follows:

NANI = Atmospheric N+ Fertilizer N+ Crop fixed N+ Food & feed N

Where,
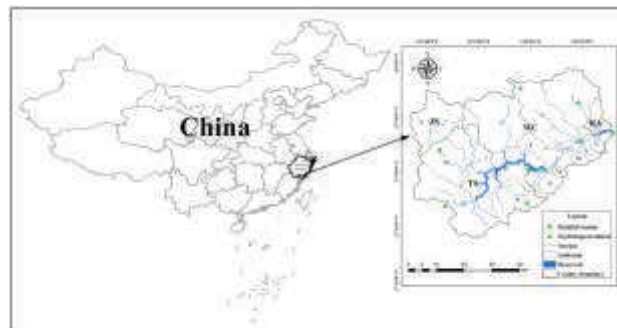
1. Atmospheric N. The main forms of atmospheric

Fig.1: Geographic location of the study area.

precipitation nitrogen are NH_y, NO_y and organic nitrogen. In the NANI model, only atmospheric precipitation nitrogen in the form of NO_y is considered, including dry deposition and wet deposition (Smedberg et al. 2012). Atmospheric nitrogen refers to the research results of (Liu et al. 2013) on the southeastern region of China and (Wang et al. 2015) on the research results of the Taihu Lake Basin in China. The values of different years are calculated using the average of two studies.

2. Fertilizer application of nitrogen. The statistics of nitrogen fertilizer in the statistical yearbook are divided into pure nitrogen fertilizer and nitrogen fertilizer in compound fertilizer. According to the application amount, the nitrogen content is reduced by the content and molecular weight, and the specific nitrogen content is 46% of urea, 35% of ammonium nitrate, and 12.8% of compound fertilizer. The amount of nitrogen fertilizer applied is obtained by adding the nitrogen content of each type of fertilizer.

3. Fixed nitrogen for crops. The fixed nitrogen of crops is calculated from the crop planting area and the ability of nitrogen fixation rate per unit area of crops. In this study, the planting area of nitrogen-fixing crops was obtained from the statistical yearbook. According to the characteristics of Zhaoshandu water source and the research results of the Taihu Lake Basin, the nitrogen fixation rate of crops was as follows: green fertilizer was $150 \, kg \cdot (hm^2 \cdot a)^{-1}$, for legume crop was $64 \, kg \cdot (hm^2 \cdot a)^{-1}$; $45 \, kg \cdot (hm^2 \cdot a)^{-1}$ for paddy fields and $15 \, kg \cdot (hm^2 \cdot a)^{-1}$ for other dry land and gardens (Ti et al. 2012, Yan et al. 2011).

4. Food and feed nitrogen. Food and feed nitrogen is the amount of nitrogen consumed by human food and animal feed minus the amount of nitrogen in animal products for human consumption and the amount of nitrogen harvested by crops. Nitrogen in human food is calculated by multiplying the per capita consumption of nitrogen by the population. The nitrogen content of the animal's consumption of food is obtained by multiplying the amount of nitrogen consumed by the individual of the livestock during the year. The nitrogen content of animal products is obtained by multiplying the amount of livestock in the year by the nitrogen content of the animal product, and food that cannot be ingested due to deterioration and other reasons is calculated at 10% of the total production. The nitrogen consumption of human and livestock and the nitrogen content of animal products refer to the research results of Han et al. (2011), as given in Table 1. Taking into account the number of years of stocking and the number of livestock in the statistical yearbook, the amount of livestock in the year is used to calculate the amount of livestock. The calculation method refers to Smedberg et al. (2012).

The amount of nitrogen harvested by the crop is obtained by multiplying the yield of the various crops in the statistical yearbook by the nitrogen content of the crop. The nitrogen content of various crops is taken from the Chinese Food Ingredients Table (Wang 2002). The nitrogen content of various crops calculated in this study is given in Table 2. The vegetables are calculated according to the nitrogen content of the main ingredient cabbage. Food that cannot be ingested due to deterioration and other reasons is calculated at 10% of total production.

RESULTS AND DISCUSSION

Temporal Change of NANI

According to the calculation, the average NANI of Zhaoshandu water source was $85.76 \, kg \cdot (hm^2 \cdot a)^{-1}$ from 2005 to 2014, and the average contribution rates of atmospheric nitrogen, fertilizer nitrogen, food and feed nitrogen and crop-fixed nitrogen, were 40.98%, 34.06%, 20.25%, and 4.7%, respectively. Atmospheric sedimentation nitrogen and fertilizer nitrogen are the main inputs of NANI in this water source, with a total contribution rate of 75.04%, which is similar to the calculation results in China such as Jiaojiang River Basin (Chen et al. 2014), Haihe River Basin (Chen et al. 2016) and Poyang Lake Basin (Gao et al. 2016). According

Table 1: Nitrogen consumption and excretion of human or individual animals.

Species	Consumption of nitrogen (kg.a^{-1})	Excretion of nitrogen (kg.a^{-1})	Animal product nitrogen content (kg.a^{-1})
Pig	16.68	11.51	5.17
Cattle	54.82	48.78	6.03
Sheep	6.85	5.75	1.1
Chicken	0.57	0.37	0.2
Duck	0.63	0.41	0.22
Human	4.39	4.39	0.00

Table 2: Nitrogen content of major agricultural products.

Agricultural products	Nitrogen content (kg.kg^{-1})
Cereals	0.01184
Wheat	0.0192
Soybean	0.0562
Broad bean	0.0406
Sweet potato	0.0018
Rapeseed	0.0456
Vegetables	0.0032
Tangerine	0.0014

to the results of (Han et al. 2014), the average NANI in China in 2009 was 50.13 kg·(hm^2·a)$^{-1}$, and the average NANI in Zhaoshandu water source from 2005 to 2014 was 1.7 times the national average, for a water source. In other words, the NANI intensity is at a high level. During the period from 2005 to 2014, NANI has a growing trend, increasing from 81.98 kg·(hm^2·a)$^{-1}$ in 2005 to 87.50 kg·(hm^2·a)$^{-1}$ in 2014 and an increase of 6.73% in ten years (Fig. 2).

It can be seen from Fig. 2 that the dynamic trends of different inputs of NANI in Zhaoshandu water source are different. Atmospheric sedimentation nitrogen has a linear increasing trend, which is based on the research results of southeastern China (Han et al. 2014) and Taihu Lake Basin (Wang et al. 2015), and also assumes that the atmospheric sedimentation nitrogen of the water source has a linear increase year by year. Nitrogen application by chemical fertilizers also has an increasing trend, especially after 2009, due to the increase in the intensity of local agricultural production activities. Food and feed nitrogen was relatively

stable before 2010 and has declined year after year since 2010. Since 2009, the local management department has carried out water and soil conservation and ecological clean small watershed construction projects in water sources, which has achieved remarkable results. Crop fixed nitrogen remained stable during the study period because the area under which nitrogen-fixed crops were grown did not change much during the 10 years. Since fertilizer application of nitrogen and atmospheric subsidence nitrogen account for most of NANI, the trend of these two inputs determines the trend of NANI.

Spatial Change of NANI

In this study, the NANI of the water source basin was calculated at the county-level administrative regional scale. However, the spatial scale of the county-level administrative district was too large. This study uses the spatial analysis function of Arcgis10.2 to distribute NANI and its components to each sub-basin according to the area weighting method. The spatial distribution of the NANI and its multi-year averages in the 17 sub-basins of the Zhaoshandu water source is shown in Fig. 3. It can be seen from Fig. 3a that the spatial difference of NANI intensity in each sub-basin is larger, showing a trend of increasing from the upstream mountainous area to downstream. The areas with the largest and smallest NANI intensity were sub-basins 2 and 11 with 135.26 kg·(hm^2·a)$^{-1}$ and 72.4 kg·(hm^2·a)$^{-1}$, respectively. The sub-basin 2 is located at the exit of the water source, mainly in the RA. The NANI intensity was 1.87 times of sub-basin 11. The fertilizer nitrogen, food and feed nitrogen are 3.21 times and 2.17 times respectively of sub-basin 11. For atmospheric deposition of nitrogen, this study assumes
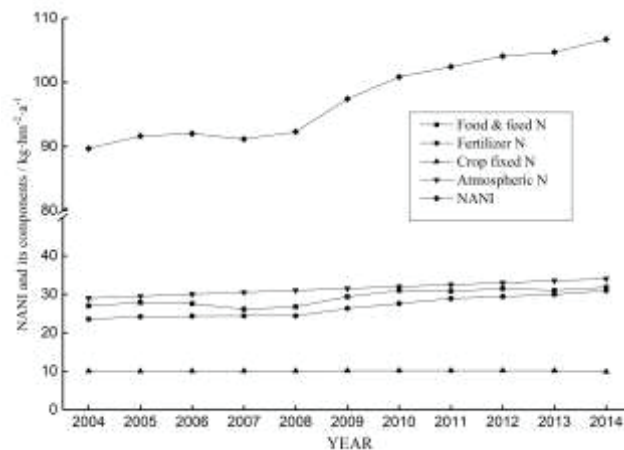

Fig. 2: Dynamic changes of NANI and its inputs from 2005 to 2014.

that the spatial distribution throughout the water source is uniform and the intensity of each administrative area is the same (Fig. 3e). The fixed nitrogen of crops mainly depends on the planting area of nitrogen-fixing crops. The application of nitrogen in fertilizers mainly depends on the planting area of crops and the fertilization intensity. The food and feed nitrogen mainly depend on the population density and the scale of livestock and poultry breeding, so there is a certain spatial difference. In general, there are some differences in the level of economic and social development of different administrative units. After spatial analysis, the nitrogen input values of each sub-basin were obtained, which results in the spatial heterogeneity of NANI. The occurrence of non-point source pollutants (NPS) is affected by many factors such as soil, topography, climate, hydrology, land use and management. The spatial difference is very significant. The pollutants output by a few landscape units often account for the majority of the pollution load of the entire basin and thus become a key source of NPS. Since 2012, while continuing to promote the comprehensive improvement of livestock and poultry breeding, the local government has vigorously promoted the transformation of rural water sources and cross-regional pooling, minimizing the population of primary and secondary water source protection areas, and minimizing the pollution of storage, thereby achieving the purpose of reducing the total amount of pollutants entering the reservoir. On this basis, spatial identification of key source areas of NPS is significant for the control and management of NPS in the basin. For the water source, sub-basin 2 is not only strong in NANI, but also 2.71 times of the national average $(50.13 \text{ kg} \cdot (\text{hm}^2 \cdot \text{a})^{-1})$, and it is at the water intake, which has the greatest potential risk to water quality. Therefore, it is a key source of nitrogen pollution in the water source, and it is necessary to take targeted source control measures.

Net Anthropogenic Nitrogen Input and TN Concentration Response

It is important to identify the dynamic changes of water quality time series and reveal the dynamic response of water quality to pollution sources, which has important practical significance for water quality protection (Zhang & Chen 2014). According to the long-term nitrogen input data and water nitrogen concentration, the response relationship between water nitrogen concentration and watershed NANI is constructed by multiple linear regression model, which can identify the driving and contribution of human activities to the change of water nitrogen concentration (Gao et al. 2016). To reveal the quantitative relationship between TN concentration in Zhaoshandu water source and NANI and related hydrological and meteorological factors, this study used the annual average TN concentration of the diversion project during 2005-2014 as the dependent variable, with the whole basin NANI. The annual average precipitation of the whole basin, the annual average temperature of the whole basin and the annual average water level of the diversion project are independent variables, and a multiple linear regression model was established. After stepwise regression analysis, the variables with significant influence are retained, and the variables with insignificant influence are eliminated. The final model expression is as follows:

$$[TN] = 0.04 \times [NANI] - 2.888 \qquad \dots(1)$$
$$(R^2 = 0.554, p = 0.014)$$

Where, [TN] is the annual average TN concentration of water $(\text{mg} \cdot \text{L}^{-1})$, and [NANI] is the annual average NANI intensity of the whole basin $(\text{kg} \cdot (\text{hm}^2 \cdot \text{a})^{-1})$.

For the TN concentration model of the Zhaoshandu water source, the only independent variable is NANI, which is
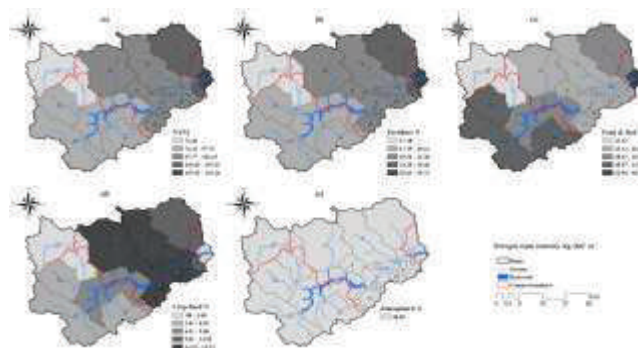

Fig. 3: Spatial distribution of NANI.

consistent with Gao et al. (2016) for the regression model of Poyang Lake TN concentration to NANI. In general, factors affecting the nitrogen concentration of water bodies may be affected by factors such as hydrometeorology in addition to the intensity of NANI. However, NANI's time scale is years, and many basins lack long-term water quality data, resulting in a small sample size of the regression model, which may not be able to identify the impact of hydrological and meteorological factors. The coefficient of determination of the regression model of the Zhaoshandu water source reached 0.554 (p=0.014), indicating that the TN concentration of the water source responded strongly to NANI. In recent years, with the continuous advancement of the "five-water joint governance" in Zhejiang Province, the local government has fully implemented the "five major" projects for water source protection, including domestic sewage treatment, domestic garbage treatment, livestock and poultry pollution control, and major tributary ecological protection. "Five major" project construction of water source protection include such as repair, automatic online monitoring of water quality and early warning system. The interpretation rate of the variance of NANI to TN concentration reached 55.4%, indicating that human activities are the main driving force for the change of nitrogen concentration in the water source of Zhaoshandu watershed, and also pointed out the direction for future nitrogen management of water source. The atmospheric nitrogen input intensity is large, and it is difficult to control. It is difficult to avoid nitrogen fixation in crops, but the input intensity is not large. In the future management of watershed nitrogen, it is necessary to reduce the input of food and feed nitrogen and fertilizers nitrogen as the main target. By reducing the NANI intensity in the basin, it is expected to achieve the goal of water quality improvement.

CONCLUSIONS

1) During the period from 2005 to 2014, the average NANI of the Zhaoshandu water source was 84.80 kg·(hm^2·a)$^{-1}$, which is 1.7 times the national average in China. The atmospheric nitrogen, fertilizer application of nitrogen, food and feed nitrogen and the average contribution rates of fixed nitrogen in crops were 40.98%, 34.06%, 20.25% and 4.7%, respectively. The water source NANI has a growing trend, increasing by 6.73% in ten years.

2) The spatial difference of NANI in each sub-basin is large, showing a trend of increasing from the upstream mountainous area along the downstream. The strength of NANI in sub-basin 2 is up to 2.71 times the national average in China, and it is at the water intake, which has the greatest potential risk to water quality. It is the key source of nitrogen pollution in

this water source and needs to adopt targeted source control measures.

3) The main influencing factor of the annual average concentration of TN in Zhaoshandu water source area is NANI, and the interpretation rate of the variance of TN concentration reaches 55.4%. In future watershed nitrogen management work, nitrogen, food and feed nitrogen input should be reduced. Strength is the main goal, and the goal of water quality improvement is achieved by reducing the NANI intensity of the basin.

ACKNOWLEDGEMENTS

REFERENCES

Chen, D. J., Huang, H., Hu, M. P. and Dahlgren, R. A. 2014. Influence of lag effect, soil release, and climate change on watershed anthropogenic nitrogen inputs and riverine export dynamics. J. Environmental Science & Technology, 48(10): 5683-90.

Chen, Y., Gao, W., Wang, D., Liu, Y., Wu, Y. Y. and Guo, H. C. 2016. Net nitrogen input and river response characteristics of human activities in water-deficient areas: taking the Haihe River Basin as an example. J. Journal of Environmental Science, 36(10): 3600-3606.

Gao, W., Gao, B., Yan, C. A. and Liu, Y. 2016. Anthropogenic nitrogen and phosphorus input evolution and lake water environment response in Poyang Lake Basin. J. Journal of Environmental Science, 36(9): 3137-3145.

Han, H., Allan, J. D. and Donald, S. 2009. Influence of climate and human activities on the relationship between watershed nitrogen input and river export. J. Environmental Science & Technology, 43(6): 1916.

Han, Y. G., Fan, Y. T., Yang, P. L., Wang, X. X., Wang, Y., Tian, J., Lei, X. and Wang, C. 2014. Net anthropogenic nitrogen inputs (NANI) index application in Mainland China. J. Geofisica International, 213(1): 87-94.

Han, Y. G., Li, X. Y., Nan, Z. and Li, B. 2011. Study on nitrogen accumulation of human activities in Beijing area from 2003 to 2007. J. Environmental Science, 32(6): 1537-1545.

Howarth, R., Swaney, D., Billen, G., Garnier, J., Hong, B., Humborg, C., Johnes, P., Mörth, C. M. and Marino, R. 2012. Nitrogen fluxes from the landscape are controlled by net anthropogenic nitrogen inputs and by climate. J. Frontiers in Ecology & the Environment, 10(1): 37-43.

Howarth, R. W., Billen, G., Swaney, D., Townsend, A., Jaworski, N., Lajtha, K., Downing, J. A., Elmgren, R., Caraco, N. and Jordan, T. 1996. Regional nitrogen budgets and riverine N & P fluxes for the drainages to the North Atlantic Ocean: Natural and human influences. J. Biogeochemistry, 35(1): 75-139.

Liu, X. J., Zhang, Y., Han, W. X., Tang, A., Shen, J. L., Cui, Z. L., Vitousek, P., Erisman, J. W., Keith, G. and Peter, C. 2013. Enhanced nitrogen deposition over China. J. Nature, 494(7438): 459-462.

Smedberg, E., Eriksson, H. H., Swaney, D. P., Howarth, R. W., Mirth, C. M., Humborg, C., Hong, B. and Bouraoui, F. 2012. Evaluating regional variation of net anthropogenic nitrogen and phosphorus inputs (NANI/NAPI), major drivers, nutrient retention pattern and management implications in the multinational areas of Baltic Sea basin. J. Ecological Modelling, 227: 117-135.

Stålnacke, P., Grimvall, A., Libiseller, C., Laznik, M. and Kokorite, L. 2003. Trends in nutrient concentrations in Latvian rivers and the response to

the dramatic change in agriculture. J. Journal of Hydrology, 283(1): 184-205.

Ti, C. P., Pan, J. J., Xia, Y. Q. and Yan, X. Y. 2012. A nitrogen budget of mainland China with spatial and temporal variation. J. Biogeochemistry, 108(1/3): 381-394.

Wang, G. Y. 2002. Chinese Food Ingredient List 2002.

Wang, X. C. Jin, M. J. and Feng, H. D. 2016. Progress in the application of distributed hydrological model SWAT in non-point source pollution research. J. Journal of Agricultural Science Yanbian University, 38(3): 271-276.

Wang, Y., Liu, N. K. and Wang, J. F. 2015. Study on atmospheric deposition of nitrogen and phosphorus in Taihu Lake Basin. J. Environmental Science

and Management, 40(5): 103-105.

Yan, X. Y., Cai, Z. C., Rong, Y., Ti, C. P., Xia, Y. Q., Li, F. Y., Wang, J. Q. and Ma, A. J. 2011. Nitrogen budget and riverine nitrogen output in a rice paddy dominated agricultural watershed in eastern China. J. Biogeochemistry, 106(3): 489-501.

Yang, J., Reichert, P., Karim, C. and Yang, H. 2007. Hydrological modelling of the Chaohe Basin in China: Statistical model formulation and Bayesian inference. J. Journal of Hydrology, 340(3): 167-182.

Zhang, B. F. and Chen, D. J. 2014. Dynamic response of nitrate flux in a typical river in Zhejiang Province to net human nitrogen input from 1980 to 2010. J. Environmental Science, (8): 2911-2919.

Study of Antimicrobial Resistance Pattern of *Escherichia coli* and *Klebsiella* Strains and Multivariate Analysis for Water Quality Assessment of Tigris River, Baghdad, Iraq

Ban O. Abdulsattar*, Jwan O. Abdulsattar**, Khetam H. Rasool*, Abdul-Rahman A. Abdulhussein* and Mohammad H. Abbas*

*Department of Biology, College of Science, Mustansisiyah University, Baghdad, Iraq
**Department of Chemistry, College of Science, Mustansisiyah University, Baghdad, Iraq
†Corresponding author: Jwan O. Abdulsattar; abdulsattarjwan@yahoo.com

ABSTRACT

The present study aims to assess the pollutant impact from everyday untreated or partially treated industrial wastes, wastewater treatment plants and Baghdad Medical City wastewater discharge into Tigris River, Baghdad, Iraq. Water samples were collected from seven locations of the Tigris River near Baghdad Medical City in November 2018. Morphological characteristics and biochemical methods were used to characterize *Escherichia coli* and *Klebsiella* isolates revealing that the Tigris River accumulate different amounts of antibiotic-resistant *E. coli and Klebsiella sp.* isolates and that pattern of resistance is different in each site. *E. coli* was the predominant bacterial contaminant at site 1 which is near sewage of several hospitals in Baghdad Medical City. The influence of different water quality parameters (total dissolved solids, electric conductivity, alkalinity, turbidity, total hardness, calcium, magnesium, sodium, potassium, phosphate ion, nitrate, sulphate, chloride) and heavy metals (Cd, Zn, Co, Cu, and Ni) were investigated at bacterial contaminated site 1. Besides, physiological parameters (pH value and temperature) were applied. The results revealed that these parameters were within Iraqi standards levels with a slight increase in pH and temperature at site 1.

INTRODUCTION

Historically, the Tigris and the Euphrates are the two most significant rivers in Iraq. The Tigris River gains great importance as it is considered the main source of water for Baghdad city, which enters the capital city of Baghdad from the north and exit from the south dividing Baghdad city into the right (Karkh) and left (Rusafa) sections (Alobaidy et al. 2010). For several years the Iraqi rivers were facing problems such as the huge number of dams built in the upstream by Turkey and Iran (Al-Ansari 2013), the floods caused by rains and the discharge of wastewater from the residential and commercial establishments along Tigris River. A little knowledge is currently available on to what extent the biological and chemical pollution affects the Tigris River ecosystems in Baghdad city. Due to the anthropogenic activities, the ecosystems for plants and living organisms are threatened by toxic pollutants, which are passed directly from factories and hospitals into the river without any real treatments (Gadza\la-Kopciuch 2004).

One of the major pollutants is antibiotics and antibiotic-resistant bacteria. The heavy use and abuse of antibiotics have resulted in multi-resistant bacteria (Icgen & Yilmaz

2014, Lv et al. 2015, Xu et al. 2017). Although a complete picture of the ecology of the antibiotic-resistant bacteria is still missing, the growing use of antibiotics for medical treatments and in animal production as growth promoters has increased a selective pressure in bacterial populations and the development of antibiotic-resistant bacteria (Titilawo et al. 2015, Zarfel et al. 2013, Zhang et al. 2015). There is a continuous release of antibiotics into the environment from different human activities such as wastewater treatment plants and hospitals effluents, combined sewer overflows, processing plant effluents and agricultural waste (Davies & Davies 2010, Michael et al. 2013). The presence of antibiotics in the Tigris River draws the attention of the researchers due to the risk of spreading antibiotic resistance determinants through microbial communities. The wastewater carries antibiotics and their metabolites, which is excreted with urine and faeces (Harnisz 2013, Le Corre et al. 2012, Leung et al. 2012). In addition, there is a direct inflow of resistant bacteria to the wastewater, especially from the hospital wastewater (Chagas et al. 2011, Korzeniewska 2011). These two major sources of contaminant are released into rivers and lakes directly or from treated sewage. Also, several factories and

hospitals drain their wastewater into the river. As a result, there are many direct and indirect sources which are responsible for the contamination of the Tigris River in Baghdad city (Ibrahim & Asmaa 2017).

Water quality tests stand as an informatics platform to provide valuable data that lead to maintaining a healthy aquatic ecosystem. Some aquatic ecosystems can resist large and different changes in water quality without any detectable effects on the ecosystem, however other ecosystems are more sensitive to small changes in the physical and chemical parameters which can lead to degradation of the ecosystem and affect biological diversity. The changes of physical and chemical water quality are a result of human influences and usually gradual and undetectable due to the invisible adaptations of aquatic ecosystems unless a dramatic shift in ecosystem condition occurs (Stark Jr et al. 2000). The physical and chemical characteristics of a water sample are compared with the World Health Organization (WHO) guidelines or standards to determine water quality. One of the problems is the lack of expert study and regular monitoring of the water quality of most rivers (Robertson et al. 2006, Wickham et al. 2005). It is important to perform river water quality assessment to evaluate the water quality and to detect pollution sources (Sin et al. 2001, Yuan et al. 2011). The rapid population growth and intensive domestic activities, in addition to expanding industrial and agricultural production, which has resulted in the release of large quantities of toxic chemicals, especially heavy metals into rivers worldwide (Srebotnjak et al. 2012, Su et al. 2013). However, toxic metals are not considered in many studies like the major ion chemistry of rivers. Heavy metals may undergo many changes in their speciation due to dissolution, precipitation, sorption, and complexation phenomena during their transport in rivers (Abdel-Ghani & Elchaghaby 2007, Akcay et al. 2003) and this will affect their behaviour and bioavailability (Nicolau et al. 2006, Nouri et al. 2011). A study suggested that the downstream of Tigris River is more seriously polluted by heavy metals than the upstream and midstream sites in Baghdad city (Obaidy 2014). While another study reported that some heavy metals (Cu, Hg, Pb, and Zn) were within the normal limit except Cd ion, which was slightly elevated in Tigris River water samples in Baghdad city (Ibrahim & Asmaa 2017). This work aims to study the profile and prevalence of antibiotic-resistant bacteria in the environment of Tigris River in Baghdad city near Baghdad Medical City and also measures the physical and chemical parameters in Tigris River to understand their effect on the aquatic ecosystem and biological diversity and to investigate whether Tigris River water has been contaminated with heavy metals or not.

MATERIALS AND METHODS

Study sites and collection of water samples: Total 7 river water samples were collected from different locations of the Tigris River in Baghdad city, Iraq in November 2018. Samples were collected from 50 cm below the surface of the Tigris River in 100 mL sterile bottles and 1 m from the edge. All samples were immediately placed on ice and transported back to the laboratory on the same day of collection for further processing.

Physicochemical parameters: Physicochemical parameters including temperature (°C) and pH were determined for each Tigris River sample site and recorded using standard methods. This was done with three replication per sample.

Isolation and characterization of bacteria: After the removal of larger particulates by centrifugation at 5000 rpm for 10 minutes, 100 µL and 50 µL from each supernatant were spread on a selective media (MacConkey agar and EMB agar) plates. After 24 hours of incubation at 37°C, the bacterial colonies with distinct colony morphology were selected and analysed for morphological and biochemical characteristics by IMVIC analysis test.

Antimicrobial susceptibility testing: The antibiotic susceptibility test was done by disc diffusion method. All isolates were cultured on MacConkey agar and incubated for 18 hours at 37°C. In the next day, two to three colonies of these organisms were emulsified with normal saline to adjust the inoculum density equal to that of 0.5 MacFarland turbidity standards. Using a cotton swab, each bacterial isolate was spread on Mueller-Hinton agar and left for 10 min at room temperature, and 8 different antibiotics (Amikacin (AK-30 µg), gentamicin (GM-10 µg), Ciprofloxacin (CIP-10 µg), trimethoprim (TMP-10 µg), Amoxicillin (Ax-25 µg), imipenem (IPM-10 µg), Cefotaxime (CTX-30 µg), Azithromycin (AZM-15 µg) discs were placed on the top of the agar and all plates were incubated at 37°C for 24 hrs. After the incubation period, the inhibition zone diameters around the discs were measured using a ruler and then classified according to the standardized table supplied by CLSI guidelines (Wayne 2014).

Chemical analysis: Chemical analysis including the total dissolved solids (TDS), electric conductivity (E.C.), alkalinity (ALK), turbidity (tur) and total hardness (TH), and the major ions (Ca^{2+}), magnesium (Mg^{2+}), sodium (Na^+), potassium, (K^+), phosphate ion (PO_4^{-3}), nitrate (NO_3^-), sulphate (SO_4^{2-}) and chloride (Cl^-) were measured using different methods as listed in Table 1.

Heavy metals analysis: Heavy metals including cobalt, zinc, copper, cadmium, and nickel were determined by

Table 1: Methods used for measuring chemical parameters.

Test	Method
Total Dissolved Solids (TDS)	Gravimetric method (Drying at 103-105 °C)
Electric conductivity (E.C)	Electric conductivity meter
Alkalinity (ALK)	pH meter
Turbidity (tur)	Nephelometer
Total hardness (TH)	EDTA titration method
Ca^{2+}	Atomic absorption spectrophotometer
Mg^{2+}	Atomic absorption spectrophotometer
Na^+	Atomic absorption spectrophotometer
K^+	Atomic absorption spectrophotometer
PO_4^{-3}	Spectrophotometer
NO_3^-	Spectrophotometer
SO_4^{2-}	Turbidity metric method
Cl^-	Spectrophotometer

atomic absorption spectrophotometer for water sample in triplicate per sample.

RESULTS AND DISCUSSION

Description of the Study Area

Water samples were taken from 7 sites from Tigris River near the Medical city; Baghdad, Iraq. The total sites distance was 1.975 meters; site 1 was the municipal sewage of Baghdad Medical city and samples were taken from both side of Tigris River as can be seen from Fig 1.

Isolation of *E. coli* and *Klebsiella*

The occurrence of *E. coli* and *Klebsiella* in river water samples varied in different sites. The highest number of bacteria was located at site 1, which indicated that the river water

Fig. 1: Description of the study sites. S1: Baghdad Medical city municipal sewage, S2: Medical city hospitals, S3: Medical city hospitals, S4: Residential area, S5: Qishla building, S6: Qishla hour, and S7: Mosque Wazzar.

was severely polluted and suitable for the rapid growth of bacteria (Fig. 2).

The number of *E. coli* and *Klebsiella* at site 1 was significantly higher than the average level of all sampling sites. One possible explanation for this high bacteria abundance was that the water sample at site 1 was collected from the sewage of several hospitals. Site 7 showed a lower number of bacterial isolates. Therefore, it could be speculated that we can see low numbers of bacterial isolates as we go far from sources for river water pollutions.

Profile of Multi-Drug Resistant *E. coli* and *Klebsiella* Isolates from Tigris River

A total of 9 confirmed *E. coli* and *Klebsiella* isolates were profiled for their probable phenotypic resistance to 8 different antimicrobials. All *E. coli* isolates showed a high level

of resistance against amoxicillin as shown in Fig. 3. Varied resistances for other antibiotics were recorded as follows: high levels of resistance equally observed against Gentamicin and Azithromycin. The *E. coli* isolate at S1 was more resistant to different antibiotics than *E. coli* isolate at S7. Conversely, all the *E. coli* isolates were susceptible to Ciprofloxacin and Imipenem. Although wastewater treatment processes reduced bacterial numbers in the sewage and attributed to a partial reduction of microorganism number due to the dilution of treated sewage in river water. The bacterial isolates showed resistance to different antibiotics, which indicates high contamination in the S1 site with antibiotic-resistant bacteria discharged from the sewage of Baghdad medical city hospitals. The pollution of river water is influenced by population density and economic activities, especially sewage effluent. Even with the presence of several water treatment
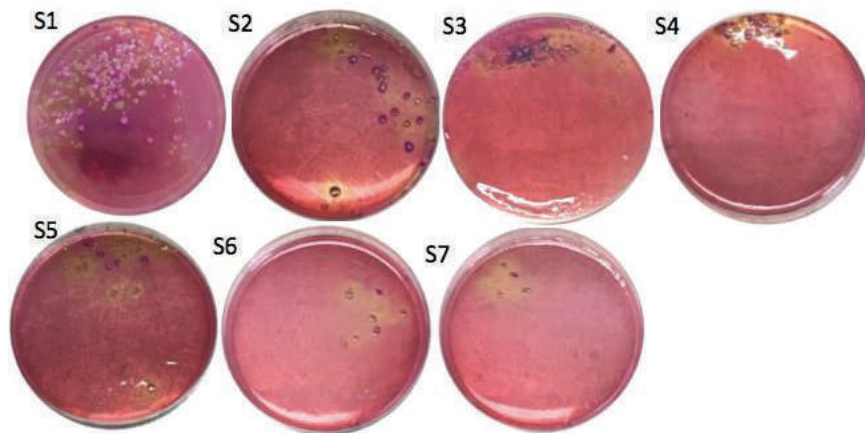

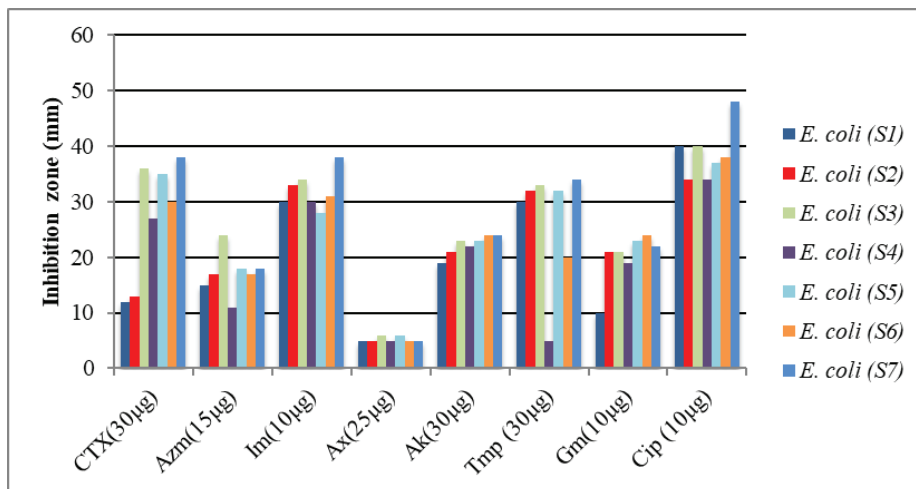Fig. 2: Heterogenic diversity of the bacteria from Tigris River water samples.

Fig. 3: Antimicrobial resistance of *E. coli* isolated from a river sample.

plants located within Baghdad city, water samples from these plants were contaminated with faecal coliform (Hassan & Mahmood 2018). The presence of coliforms in drinking water is an indicator of water contamination with bacteria or viruses that occur in a faecal matter (Bain et al. 2014). A study showed that upstream of the Tigris River in Baghdad city has the highest total coliform presence (AL-Dulaimi & Younes 2017). The large population, extensive industrial activities and sewage of several hospitals may attribute for contamination of Tigris River with coliform and especially *E. coli*. The comparison between *Klebsiella* isolates was not considered since *Klebsiella* isolates were detected only in two sites from total of seven sites.

The comparison between *E. coli* and *Klebsiella* isolates in S1 and S7 cited in Fig. 4 revealed that *E. coli* and *Klebsiella* isolates at both sites were resistant to amoxicillin and *E. coli* isolates at S1 and S7 were more resistant to different antibiotics than *Klebsiella* isolates which were sensitive to ciprofloxacin, gentamicin, and trimethoprim. This result may be attributed to the *E. coli* resistance characteristics, which indicates that multilateral exchange of genetic material between bacteria of both anthropogenic and en-vironmental origins is currently occurring and presents a phenomenon of growing importance or river water sample collected near S1 site carried faecal coliforms bacteria from untreated hospital sewage coming from all units of the hospitals, including laboratories, rehabilitation, dialy-sis, hospitalization, and surgery units, clinics, maternity, laundry, and the cafeteria.

The difference between *E. coli* and *Klebsiella* isolates from S1 showed that *E. coli* are more resistant to selected antibiotics than *Klebsiella*. The obtained result indicates that *E. coli* heavily contaminates the Tigris River. The discharged sewage may also contain antibiotics used as a treatment for patients in these hospitals. A study by Mahmood et al. (2019) confirmed the contamination of water samples in Baghdad city with different antibiotics including fluoroquinolones and B-lactams. The highest antibiotic concentration recorded was ciprofloxacin in the Al-Wihda plant, while amoxicillin was not detected in the same site. Despite the treatment of the municipal sewage, river water may be a good reservoir for antibiotic-resistant microorganisms and plasmid-mediated antibiotic resistance genes. This may pose a public health risk, which needs future evaluation and control.

Table 2: Temperature and pH parameters of the studied area.

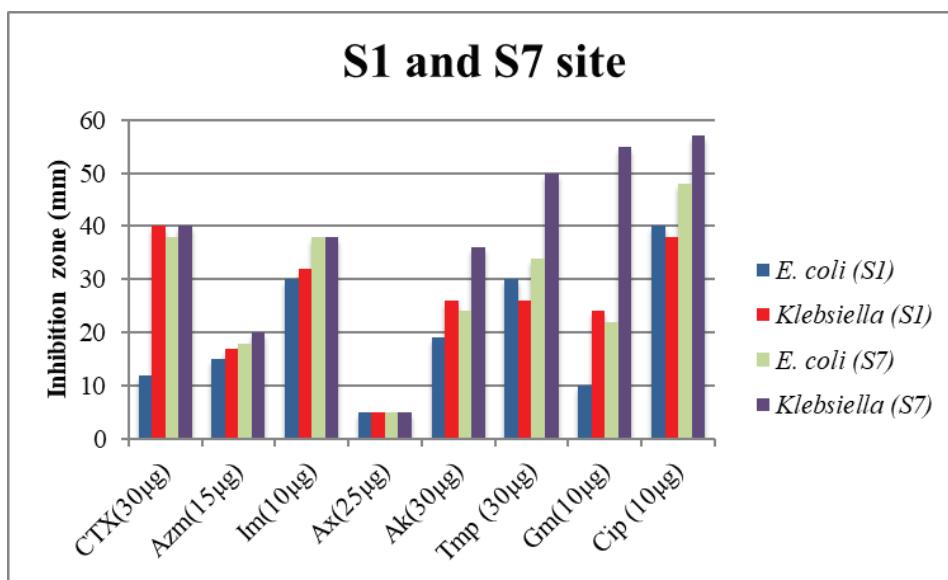| Site	S1	S2	S3	S4	S5	S6	S7
Temperature	22	18.1	18.3	18	18.3	18	18.5
pH	8	7	7	7.5	7	7	7

Fig. 4: Antimicrobial resistance of *E. coli* and *Klebsiella* isolated from S1 and S7 river sample.
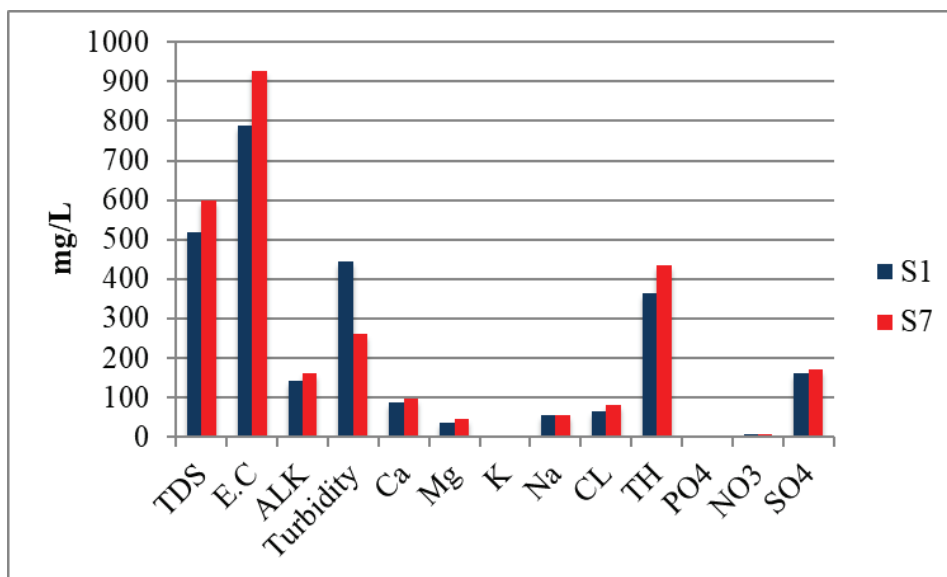
Fig. 5: The concentration of major ions and some environmental parameters in the Tigris Rivers, Baghdad city at site 1 and 7.

Physicochemical Characteristics

The water temperature is an important factor in water quality and the distribution of organisms in an aquatic ecosystem in addition to its role in many metabolisms and other transformations in a water body (Smith 2004). The physicochemical parameters of river water samples are presented in Table 2. The temperature ranged from 18-18.5°C from site 2 to site 7. The highest temperature was noticed at site 1 (22°C), which is near Medical City hospitals. Minor differences in pH were observed between sampling sites. The pH values ranged from 7 to 8, indicating that the Tigris River in Baghdad city is alkaline (pH >7). The highest pH was also recorded at site 1. There are no significant differences in temperature and pH between sampling sites. The Iraqi rivers are characterized by high buffer capacity which explains high pH (Hassan 2004, Abbas 2017).

Environmental Parameters and Metal Concentration

The results in Fig. 5 show different environmental parameters and metal concentrations in water samples of the Tigris River that revealed the difference in turbidity only while there was no significant variation for the other parameters between site 1 and site 7 in this study.

Anthropogenic activity has a great impact on the Tigris River ecosystem. A recent study revealed that middle of Tigris River in Baghdad city (Al-Sarrafia Bridge and Al-Shuhada Bridge) is heavily polluted than upstream of Tigris River (Al-Ani et al. 2019). This study recorded data from February

2017 to February 2018, which agree with our obtained data in November 2018. Due to the increase in rainfall proportion and high water levels in winter in addition to domestic wastes, the turbidity levels increases in river water (Gangwar et al. 2012, Al-Obaidi 2009). In the aquatic ecosystems, electrical conductivity is considered as a good indicator to evaluate total dissolved solids in river water and water purity. The obtained data showed that conductivity in site 1 and site 7 is less than (1500 μS/cm) which is the Iraqi permissible limits for electrical conductivity (Hassan & Mahmood 2018).

The concentration for each heavy metal was measured and Co, Zn, Cu, Cd and Ni were Nil, 0.007, 0.011, Nil and 0.059 ppm, respectively which indicates that site 1 was not contaminated with heavy metals. The result of heavy metal concentrations in site 1 gives an insight view of Tigris River sample safety at site 1. A study suggested that the site, which is located at the downstream of Tigris River is more seriously polluted by heavy metals than the upstream and midstream sites in Baghdad city (Obaidy et al. 2014).

CONCLUSION

The contamination of the Tigris River in Baghdad city with antibiotic-resistant bacteria is a threat to human health and the river ecosystem. The cause of resistance, or mode of transmission of the antibiotic-resistant gene between pathogenic and environmental bacteria, is unknown. This study indicates that Tigris River in Baghdad city near Baghdad Medical City is a major source of antibiotic-resistant *E. coli*. A vast

quantity of antibiotic-resistant bacteria is discharged to the aquatic ecosystem with hospital sewage. Urgent measures are needed to minimize the effects of releasing wastewaters into water resources. One of the solutions that could minimize the spreading of antibiotic-resistant bacteria to the environment is the preliminary disinfection of hospital sewage before its inflow into the sewage system or Tigris River. This study can provide a platform for defying the currently most popular antibiotic options for human therapy by studying the resistance characteristics of the isolates described in this study. It also appears that drug-resistant *E. coli* is widely distributed in all the rivers sampling sites. Monitoring physiological and chemical parameters in the Tigris River is needed for proper management. Determination of the water quality is essential and comparing the physical and chemical characteristics of a water sample with water quality guidelines. These parameters should be usually at acceptable levels either to humans or aquatic organisms. This study also confers that site 1 is not contaminated with heavy metals.

ACKNOWLEDGEMENTS

REFERENCES

Abbas, A.A.A. and Hassan, F.M. 2017. Water quality assessment of Euphrates river in Qadisiyah province (Diwaniyah river), Iraq. Iraqi J. Agric. Sci., 48(6).

Abdel-Ghani, N.T. and Elchaghaby, G.A. 2007. Influence of operating conditions on the removal of Cu, Zn, Cd and Pb ions from wastewater by adsorption. International Journal of Environmental Science & Technology, 4: 451-456.

Akcay, H., Oguz, A. and Karapire, C. 2003. Study of heavy metal pollution and speciation in Buyak Menderes and Gediz river sediments. Water Res., 37: 813-22.

Al-Ani, R.R., Al Obaidy, A.M.J. and Hassan, F.M. 2019. Multivariate analysis for evaluation of the water quality of Tigris River within Baghdad city in Iraq. Iraqi J. Agric. Sci., 50: 331-42.

Al-Ansari, N. 2013. Management of water resources in Iraq: Perspectives and prognoses. Engineering, 5: 667-84.

Al-Dulaimi, G. A. and Younes, M. K. 2017. Assessment of potable water quality in Baghdad City, Iraq. Air, Soil and Water Research, 10: 1178622117733441.

Al-Obaidi, A.H. 2009. Evaluation of Tigris river quality in Baghdad for the period between (November 2005-October 2006). Engineering and Technology Journal, 27(9): 1736-1745.

Alobaidy, A.H.M.J., Maulood, B.K. and Kadhem, A.J. 2010. Evaluating raw and treated water quality of Tigris River within Baghdad by index analysis. J. Water Resour. Prot., 2: 629.

Bain, R., Cronk, R., Wright, J., Yang, H., Slaymaker, T. and Bartra, M, J. 2014. Fecal contamination of drinking-water in low- and middle-income countries: a systematic review and meta-analysis. PLoS Med, 11: e1001644.

Chagas, T.P., Seki, L.M., Cury, J.C., Oliveira, J.A., Davila, A.M., Silva, D.M. and Asensi, M.D. 2011. Multi resistance, beta-lactamase-encoding genes and bacterial diversity in hospital wastewater in Rio de Janeiro, Brazil. J. Appl. Microbiol., 111: 572-81.

Davies, J. and Davies, D. 2010. Origins and evolution of antibiotic resistance. Microbiol. Mol. Biol. Rev., 74: 417-33.

Gadza\La-Kopciuch, R.B.B., Bartoszewicz, J. and Buszewski, B. 2004. Some considerations about bioindicators in environmental monitoring. Pol. J. Environ. Stud., 13: 453-62.

Gangwar, R.K.K.P., Singh, J. and Singh, A.P. 2012. Assessment of physico-chemical properties of water: River Ramganga at Bareilly, UP. J. Chem. Pharm. Res., 4: 4231-4.

Harnisz, M. 2013. Total resistance of native bacteria as an indicator of changes in the water environment. Environ. Pollut., 174: 85-92.

Hassan, F.M. and Mahmood, A.R. 2018. Evaluate the efficiency of drinking water treatment plants in Baghdad City-Iraq. J. Appl. Env. Microbiol., 6: 1-9.

Hassan, F.M., 2004. Limnological features Diwanyia River, Iraq. Baghdad Science Journal, 1(1): 119-124.

Ibrahim, I.A. and Asmaa, S.A.K. 2017. The relation between bacterial and heavy metal water pollution and blood micronuclei as biomarkers in the Tigris river fish. Baghdad Sci. J., 14: 126-134.

Icgen, B. and Yilmaz, F. 2014. Co-occurrence of antibiotic and heavy metal resistance in Kizilirmak River isolates. Bull. Environ. Contam. Toxicol., 93: 735-43.

Korzeniewska, E. 2011. Emission of bacteria and fungi in the air from wastewater treatment plants - A review. Front Biosci. (Schol Ed.), 3: 393-407.

Le Corre, K.S., Ort, C., Kateley, D., Allen, B., Escher, B.I. and Keller, J. 2012. Consumption-based approach for assessing the contribution of hospitals towards the load of pharmaceutical residues in municipal wastewater. Environ. Int., 45: 99-111.

Leung, H. W., Minh, T. B., Murphy, M. B., Lam, J. C., So, M. K., Martin, M., Lam, P. K. and Richardson, B.J. 2012. Distribution, fate and risk assessment of antibiotics in sewage treatment plants in Hong Kong, South China. Environ. Int., 42: 1-9.

Lv, L., Yu, X., Xu, Q. and Ye, C. 2015. Induction of bacterial antibiotic resistance by mutagenic halogenated nitrogenous disinfection byproducts. Environ. Pollut., 205: 291-298.

Mahmood, A. R., Al-Haideri, H. H. and Hassan, F. M. 2019. Detection of antibiotics in drinking water treatment plants in Baghdad City, Iraq. Advances in Public Health, 2019: 10.

Michael, I., Rizzo, L., Mcardell, C. S., Manaia, C. M., Merlin, C., Schwartz, T., Dagot, C. and Fatta-Kassinos, D. 2013. Urban wastewater treatment plants as hotspots for the release of antibiotics in the environment: a review. Water Res., 47: 957-95.

Nicolau, R., Galera-Cunha, A. and Lucas, Y. 2006. Transfer of nutrients and labile metals from the continent to the sea by a small Mediterranean river. Chemosphere, 63: 469-76.

Nouri, J., Lorestani, B., Yousefi, N., Khorasani, N., Hasani, A.H., Seif, F. and Cheraghi, M. 2011. Phytoremediation potential of native plants grown in the vicinity of Ahangaran lead-zinc mine (Hamedan, Iran). Environ Earth Sci., 1(62): 639-644.

Obaidy, A.M.J., Talib, A.H. and Zaki, S.R. 2014. Environmental assessment of heavy metal distribution in sediments of Tigris River within Baghdad City. International Journal of Advanced Research, 2(8): 947-952.

Robertson, D. M., Saad, D. A. and Heisey, D. M. 2006. A regional classification scheme for estimating reference water quality in streams using land-use-adjusted spatial regression-tree analysis. Environ. Manage., 37: 209-29.

Sin, S. N., Chua, H., Lo, W. and Ng, L. M. 2001. Assessment of heavy metal cations in sediments of Shing Mun River, Hong Kong. Environ. Int., 26: 297-301.

Smith, R. 2004. Current Methods in Aquatic Science. University of Waterloo, Canada.

Srebotnjak, T., Carr, G., Sherbinin, A. D. and Rickwood, C. 2012. A global water quality index and hot-deck imputation of missing data. Ecological Indicators, 17: 108-119.

Stark Jr, H.P., Goldstein, R.M., Fallon, J.D., Fong, Al, Lee Ke, Et Al. [Internet]. Reston, Va: U.S. Geological Survey. 2000. Water quality in upper Mississippi River basin, Minnesota, Wisconsin, South Dakota, Iowa, and North Dakota, 1995-98 [Online]. Available: http://pubs.er.usgs.gov/publication/cir1211.

Su, S.X.R., Mi, X., Xu, X., Zhang, Z. and Wu, J. 2013. Spatial determinants of hazardous chemicals in surface water of Qiantang River, China. Ecol Indic, 1: 375-81.

Titilawo, Y., Obi, L. and Okoh, A. 2015. Antimicrobial resistance determinants of *Escherichia coli* isolates recovered from some rivers in Osun State, South-Western Nigeria: Implications for public health. Sci. Total Environ., 523: 82-94.

Wayne, P., 2014. Clinical and Laboratory Standards Institute: Performance standards for antimicrobial susceptibility testing: Twenty-fourth informational supplement, M100-S24. Clinical and Laboratory Standards Institute (CLSI), 34(1).

Wickham, J.D., R.K., Wade, T.G. and Jones, K.B. 2005. Evaluating the relative roles of ecological regions and land-cover composition for guiding establishment of nutrient criteria. Landsc. Ecol., 1(20): 791-798.

Xu, Y.B., Hou, M.Y., Li, Y.F., Huang, L., Ruan, J.J., Zheng, L., Qiao, Q.X. and Du, Q.P. 2017. Distribution of tetracycline resistance genes and AmpC beta-lactamase genes in representative non-urban sewage plants and correlations with treatment processes and heavy metals. Chemosphere, 170: 274-281.

Yuan, G.L., Liu, C., Chen, L. and Yang, Z. 2011. Inputting history of heavy metals into the inland lake recorded in sediment profiles: Poyang Lake in China. J. Hazard Mater., 185: 336-45.

Zarfel, G., Galler, H., Feierl, G., Haas, D., Kittinger, C., Leitner, E., Grisold, A. J., Mascher, F., Posch, J., Pertschy, B., Marth, E. and Reinthaler, F.F. 2013. Comparison of extended-spectrum-beta-lactamase (ESBL) carrying Escherichia coli from sewage sludge and human urinary tract infection. Environ. Pollut., 173: 192-9.

Zhang, S., Han, B., Gu, J., Wang, C., Wang, P., Ma, Y., Cao, J. and He, Z. 2015. Fate of antibiotic resistant cultivable heterotrophic bacteria and antibiotic resistance genes in wastewater treatment processes. Chemosphere, 135: 138-45.

An Empirical Study on the Environmental Effects of Industrial Spatial Agglomeration Since the Reform and Opening-up

S.R. Yan*, H. L. Huang*, W. H. Li*, L.N. Wang*, M.W. Tian* and H.P. Yan**†

*College of Accounting and Finance, Jiangxi University of Engineering, Xinyu 338000, China
**School of Marxism, Hainan University, Haikou 570228, China
†Corresponding author: H.P. Yan; glx682@163.com

ABSTRACT

In the past 40 years after China adopted the reform and open-up policy, China's expediting industries spatial agglomeration has resulted in severe damage to the environment. In China, the one whether the pollution haven hypothesis (PHH) is true or not is the hot issue under the research of academic circles. By establishing the mechanism model of industries spatial agglomeration and environmental pollution in this paper, we discovered upon our empirical study that China's industrial spatial agglomeration process had apparent threshold characteristics for environmental pollution, those direct investment and scientific innovation of foreign merchants apparently improved environmental pollution, so PHH is not true in China and such conclusion provides empirical support for China's industrial agglomeration and environmental policymaking. At the end of the paper, the policy proposals for improving environmental pollution in future are made, which have important significance for China's high-quality economic development.

INTRODUCTION

Since China adopted the reform and open-up policy 40 years ago, China's expediting industries spatial agglomeration and extensive economy growth caused severe damage to the environment. In China, whether the pollution haven hypothesis (PHH) is true or not is the hot issue under the research of academic circles. Facing a series of severe environmental pollution problems, the Chinese government at all levels have promulgated a series of environmental protection policies in succession, but the environmental pollution problems are still serious (Yamashita et al. 2014). In recent years, the emission of all kinds of pollutants in China has been increasing. However, emission of all kinds of pollutants is reducing in certain regions as the regional industrial agglomeration level improves, which is rightly different from those at the national levels (Shao et al. 2017). Logically, pollutant emission is the inevitable product of industrial development, and industrial agglomeration development is certainly correlated with environmental pollution; both of different phenomena aforesaid provide a better research perspective, namely the one whether the industrial agglomeration intensifies or improves environmental pollution. Based on this question, a research was made in this paper and the theoretical model for the impact of industrial agglomeration on environmental pollution was further discussed, which provides a theoretical support for recognizing correctly the relationship between industrial

agglomeration and environmental pollution. Meanwhile, the data of 30 provinces and municipalities (autonomous regions) of China from 2009 to 2016 were used to analyse the impact of industrial agglomeration on environmental pollution, such objective evaluation on the function of industrial agglomeration on environmental pollution will benefit to realize the national objective of energy conservation and emission reduction, and provide a new perspective and thinking for the systematic engineering of improving the environmental pollution of China (Ning et al. 2016).

Previous researches were conducted based on the complicated relationship between industrial agglomeration and environmental pollution, and uncertain external effect of industrial agglomeration for the environment (Almulali et al. 2015). There was a lack of support of the theoretical model for the relationship between industrial agglomeration and environmental pollution, and previous researches were made based on the linear models (Baek et al. 2009). Based on which, the research in this paper was made from the following three aspects. Firstly on the theoretical level, the Copeland-Taylor model was borrowed in this paper to construct a theoretical model for the impact of industrial agglomeration on environmental pollution, and thereby the relationship between industrial agglomeration and environmental pollution was further analysed (Ottaviano et al. 2002); secondly on the perspective level, the threshold effect

of industrial agglomeration on environmental pollution was investigated and the existence and range of threshold effect was analysed from the perspective of industrial agglomeration threshold (Zeng & Zhao 2009); lastly on the level of methodology, the threshold panel model was adopted in this paper to make analysis, which is rightly different from the previous and non-linear approaches adopted by previous researches, such as the cross term regression (Virkanen, 1998, Frank 2001). Moreover in the paper, a further and more objectively analysis on the impact of China's industrial agglomeration on environmental pollution was made by adopting the threshold panel model and by comparing with the linear approaches (Walter & Ugelow 1979, Stiebale 2011, Venables 1996).

THEORETICAL MODEL

By borrowing the Copeland-Taylor model in this paper, a theoretical model for the impact of industrial agglomeration on environmental pollution was established.

Production Function

Hypothesizing that a community produces two kinds of products, namely the cleaning product Y and the capital-intensive pollution product X, where the production of pollution product X produces the environmental pollutant Z, which causes not only the negative external effect but also produces social cost. In view of the clearly defined property right, enterprises must pay the corresponding cost for the emission of pollutants; in reality, the corresponding cost is represented by the environment tax, pollutant charge or pollutant discharging license fee. Enterprise aims at pursuing the maximized profit; where the one that enterprise discharges pollutant randomly is not the best optimal choice; instead, a portion of production factors are used for reducing pollutant emission. Hypothesizing that the percentage of the production factor used by enterprises for governing pollution to the total production factors is γ, where $0 \leq \gamma \leq 1$. When $\gamma = 0$, it means the one that enterprise does not govern pollution; at this moment, the yield of enterprise is the potential yield F of the enterprise; when $0 < \gamma < 1$, it means the one that enterprise uses the production factors at the percentage of γ to govern pollutants; at this moment, the actual yield of enterprise is $(1 - \gamma)F$ and meanwhile the pollutant Z will generate, so:

$$X = (1 - \gamma)F \qquad \qquad …(1)$$

$$Z = \phi(\gamma)F \qquad \qquad …(2)$$

$$\phi(\gamma) = \frac{1}{A}(1 - \gamma)^{\frac{1}{a}} \qquad \qquad …(3)$$

Here $\phi(\gamma)$ is the pollution discharge function for γ, and is the decreasing function of γ; A is the production technology, and the parameter $a \in (0, 1)$.

Hypothesizing the production factor is the capital K and the labour L, so the production function is expressed respectively in the one as follows:

$$X = (1 - \gamma)F(k_X, L_X) \qquad \qquad …(4)$$

$$Y = H(K_Y, L_Y) \qquad \qquad …(5)$$

$$Z = \phi(\gamma)F(K_X, L_X) \qquad \qquad …(6)$$

Hence,

$$Z = \frac{1}{A}(1 - \gamma)^{\frac{1}{a}} F(K_X, L_X) \qquad \qquad …(7)$$

$$X = (AZ)^a [F(K_X, L_X)]^{1-a} \qquad \qquad …(8)$$

Production Decision

Hypothesizing the one that enterprise produces X and wants maximized profit, the decision at this moment can be made by two independent processes (Lee 2007). On one hand, in the circumstances that the given capital cost is r and the labour pay is w, the enterprise will select an optimal capital-labour ratio to realize the minimized production cost C_F of unit potential output. On the other hand, in the circumstances that the given unit potential production cost is C_F and the pollution discharge cost is γ, the optimal combination of the potential output F and the pollution discharge Z will be selected to realize the minimized production cost C_X required by the realization of unit product X, so:

$$C_F(r, w) = \min\{ra_{KF} + wa_{LF}, F(a_{KF}, a_{LF}) = 1\} \qquad …(9)$$

$$C_X(\lambda, C_F) = \min\{\lambda AZ + C_F F, (AZ)^a F^{1-a} = 1\} \qquad …(10)$$

By solving the Equations (9) and (10) on the optimal level, we can obtain:

$$TRS_{KL} = \frac{\partial F}{\partial K_X} \cdot \frac{\partial F}{\partial L_X} = \frac{r}{w} \qquad \qquad …(11)$$

$$\frac{(1 - a)AZ}{aF} = \frac{C_F}{\lambda} \qquad \qquad …(12)$$

Decision on Pollution Discharge

Hypothesizing the price of product X is P_X and there is perfect competition market, the profit of enterprise will be zero, so:

$$P_X X = c_F F + \lambda(AF) \qquad \qquad …(13)$$

Based on the Equations (12) and (13), so:

$$Z = \frac{aP_X X}{\lambda A} \qquad \qquad …(14)$$

Thereby the equation aforesaid can be re-written as:

$$Z = (P_X X + P_Y Y)\frac{a}{\lambda A}\frac{P_X X}{(P_X X + P_Y Y)} \quad \ldots(15)$$

So:

$$Z = S\frac{a}{\lambda A}\mu_X \quad \ldots(16)$$

Where $S = P_X X + P_Y Y$ stands for the scale factor;

$\mu_X = \dfrac{P_X X}{(P_X X + P_Y Y)}$ stands for the percentage of product X to the total value of output, namely the structural factor.

Take the logarithm for both sides of the Equation (16), so:

$$\ln Z = \ln S + \ln a + \ln\mu_X - \ln A - \ln\lambda \quad \ldots(17)$$

Industrial agglomeration will affect the industrial scale and will affect technological advancement through inter-industry overflow effect, and will further affect the regional economic structure. If so, the impact of industrial agglomeration on industrial scale, technological advancement and economic structure can be expressed in the one as follows:

$$S = S'(aggl) \quad \ldots(18)$$

$$A = A'(aggl) \quad \ldots(19)$$

$$\mu_X = \mu_X'(aggl) \quad \ldots(20)$$

Industrial agglomeration (aggl) impacts emission degree of pollutant through three levels, i.e., S, A and μ_X (in the Equation 17), so the model can be further re-written as the one as follows:

$$\ln Z = \ln S'(aggl) + \ln\alpha + \ln\mu_X'(aggl) - \ln A'(aggl) - \ln\lambda \quad \ldots(21)$$

In view of the Equation (21), we can find that there is a complicated relationship between industrial agglomeration (aggl) and environmental pollution, and its influential effect size depends on the size of its impact on S, A and μ_X, and its function is nonlinear.

MEASUREMENT MODEL, VARIABLE AND DATA

Setting and Method of Measurement Model

The analysis in this paper will be conducted based on the threshold panel model of Hansen; the threshold value and quantity of the model will depend completely on the sample data.

The basic form of Hansen threshold is $y_i = \beta_1 x + e_i, q_i \leq \gamma$ and $y_i = \beta_2 x + e_i, q_i > \gamma$.

Where, q_i is the threshold variable, it can be one regression element of explaining variable X, or one independent threshold variable; γ is the special threshold value.

In order to obtain the estimated value of the parameter, every observed value will be subtracted from the interclass average value to eliminate the individual effect, so the model can be changed into the one as follows: $y_i^* = \beta x^*(\gamma) + e_i^*$; $y_i^* = y_i - \bar{y}_i, x_i^* = x_i - \bar{x}_i, e_i^* = e_i - \bar{e}_{i^\circ}$.

By piling up all observed values, it can be further changed into the matrix form, i.e.: $Y_I^* = X^*(\gamma)\ \beta + e^*$.

By using the conditional least square method and by calculating the minimum residual sum of squares S (γ), the estimated value of threshold value $\hat{\gamma}$ can be obtained:

$\hat{\gamma} = \arg\min\limits_{\gamma} S(\gamma)$.

Through the further calculation, the parameter estimate, residual vector and corresponding residual sum of squares can be obtained.

After obtaining the parameter estimate, the focus process will be the one to conduct the significance test on the threshold effect and threshold estimate. The original hypothesis of threshold effect significance test is $H_0 : \beta_1 = \beta_2$, the test statistics is $F_1 = [S_0 - S(\hat{\gamma})]/\hat{\sigma}^2$, S_0 is the residual sum of squares obtained from the original hypothesis H_0. There is no way to identify the threshold value γ in the original hypothesis H_0. If so, the distribution of F_1 statistics is non-standard. To acquire its asymptotic distribution, Hansen (1999) proposed to use the "self-sampling method" and further establish its P value; the original hypothesis of threshold estimate significance test is $H_0 : \hat{\gamma} = \gamma_0$, so the corresponding likelihood ratio test statistic is $LR_1 = [\ S(\gamma) - S(\hat{\gamma})]/\hat{\sigma}^2$, and its distribution is non-standard. Therefore, Hansen (1999) proposed to establish a confidence interval for γ, and provide a simple formula $LR_1(\gamma_0) \leq c(a)$, wherein the equation of $c(a) = -2\ln(1 - \sqrt{1-a})$, a is the significance level.

The parameter estimates and significance test aforesaid focused on the single threshold model. If there are two or more threshold values in the model, there is a need to extend the model. In accordance with the threshold model of Hansen, the model is hypothesized in the paper as follows:

$\ln P_{it} = a_i + \beta_1 aggl_{it} \cdot I(thre_{it} \leq \gamma) + \beta_2 aggl_{it}(thre_{it} > \gamma) + \beta_n X + \varepsilon_{it}$.

Where, P is the pollutant discharge, aggl is the industrial agglomeration, X is a group of other control variables affecting environmental pollution, especially the direct investment of foreign merchant, environmental regulation, energy con-

sumption and technological innovation; the subscripts i and t stand respectively for the region and year, and there is the threshold variable, γ is the threshold value, and $I(\cdot)$ is the indicator function.

Variable Selection and Data Description

Pollutant discharge (P): In reality, pollutant discharge includes mainly atmospheric pollution, water pollution, waste pollution and noise pollution. In view of the existing research, the one how to establish a comprehensive pollution index is used to reflect the one that there is no awareness consensus for the overall pollution of a region; therefore, more researches use the specific pollution indicators. Currently, China is the country in which the sulphur dioxide is discharged maximally, which is the main component of atmospheric pollutant, and the data has higher reliability. In this paper, the total discharge of industrial sulphur dioxide is used as the measuring indicator of pollution discharge.

Industrial agglomeration level (aggl): The measurement index of industrial agglomeration includes Hoover index, E-G index, Gini coefficient, location quotient, etc.; all of these indexes have certain merits and demerits. However, since the location quotient can reflect the spatial distribution of geographic elements authentically and relieve the regional scale error factor, it is used by most of the scholars at home and abroad. The calculation formula of the location quotient aggl of the industry r in the region i is detailed as follows:

$$aggl = (\frac{e_{ir}}{\sum_i e_{it}}) / (\frac{\sum_r e_{ir}}{\sum_i \sum_r e_{ir}}).$$

Where, e_{ir} is the total output value of the industry r in the region i. In this paper, the total industrial output value of various regions was used to calculate the location quotient to measure the industrial agglomeration level of every region.

Other control variables: *Direct investment of foreign merchant (fdi):* From the perspectives of domestic and overseas researchers, the direct investment of foreign merchant impacts the environmental quality of host country via scale effect, structure effect and technological progress effect. However, certain scholars thought that the direct investment of foreign merchant intensified the environmental pollution of China; but meanwhile, some other scholars thought that the direct investment of foreign merchant improved the environmental pollution of China. Based on which, the influence of the direct investment of foreign merchant on the environment will be investigated in the paper, where the direct investment amount of foreign merchant used by each region in the past years will be used to measure, and these investment amounts will be adjusted into the RMB price

according to the intermediary price of foreign exchange in the past years.

Environmental regulation (pr): As the social concern on environmental quality becomes more and more and the weight of environment in governmental appraisal increases, the government will increase the input of environmental governance and protection, whereas the environmental regulation will become severer and severer and enterprise's pollution discharge cost will increase too; if so, the enterprise will be pushed to make technological innovation and which will benefit to reduce environmental pollution. In this paper, the impact of environmental regulation factors on environmental pollution will be investigated by using the total investment amount of every region for the governance of industrial pollution.

Energy consumption (ener): As China's urbanization and industrialization process expedites, China's energy consumption is continuously increasing; moreover, the coal takes up a great proportion in the energy consumption structure of China; meanwhile, the main features of China's industrial development is the high energy consumption and the high emission; therefore, the increasing energy consumption will cause huger stress on the environmental pollution of China. In this paper, the total energy consumption of various regions is adopted to make the measurement.

Technological innovation (sr): Technological innovation will promote technological progress, and technological progress will facilitate enterprise to change production style and optimize structure; thereby enterprise may reduce pollution discharge and improve regional environmental pollution. In this paper, the total R&D expenditure of industrial enterprises above designated size in every region will be used to make the measurement.

Due to the availability of data, the data of 30 provinces and municipalities of China other than Tibet during the period from 2009 to 2016 were used in this paper to make the analysis. The data required were originated from the Environmental Statistics Yearbook of China, Industrial Economic Statistics Yearbook of China, Statistics Yearbook of China and Statistical Yearbook of other provinces and municipalities in the past calendar years.

EMPIRICAL ANALYSIS

Threshold Effect Test

Before determining the form of the model, there is a need to determine the number of thresholds. In view of the practice of Hansen, the industrial agglomeration level (aggl) can be used as the threshold variable, and 1, 2 and 3 threshold values are hypothesized to exist, where the corresponding value F and

P are detailed in Table 1. The result showed that the value F of the single threshold is highly significant, and its corresponding value P is 0.016; whereas the corresponding value F of the dual and triple threshold is not significant, and their corresponding value P is higher than 0.10. Thich means the one using the industrial agglomeration level as the threshold variable refuses the original hypothesis of a linear relationship and there is a single threshold effect, which means the one that the relationship between industrial agglomeration and environmental pollution is non-linear.

Furthermore, the threshold value can be obtained; the confidence interval with the threshold estimate of 0.529% is [0.528, 0.625], see Table 2 for the details. To understand the estimate of the threshold value and the construction process of the confidence interval, the likelihood ratio graph can be used, namely the likelihood ratio function sequence LR (γ) serves as the tendency chart of threshold parameter; when the likelihood ratio LR (γ) is 0, the estimated threshold value γ will be equal to 0.529.

Threshold Model Estimates

The column II of Table 3 shows the threshold estimate of industrial agglomeration and environmental pollution. From this, it can be seen that the impact of industrial agglomeration on environmental pollution has a remarkable threshold feature. When the industrial agglomeration level is less than 0.529, the impact of industrial agglomeration on environmental pollution is positive and its coefficient is 0.2805; when the industrial agglomeration level is higher than 0.529, the impact of industrial agglomeration on environmental pollution gets substantive change and it turns into a negative value, -0.5016; it signifies that there is a turning point between industrial agglomeration and environmental pollution. Such a turning point is rightly the threshold value. The relationship between industrial agglomeration and environmental pollution is not a simple linear relationship, and it is rightly different from most of the previous research

conclusions. When the industrial agglomeration level is lower than the threshold value, the industrial agglomeration will intensify environmental pollution; the major reason causing this phenomenon is the one that industrial agglomeration scale effect takes up the leading function and it results in the capacity expansion, whereas the technology spillover effect of industrial agglomeration is not remarkable and which results in the one that resource consumption rate exceeds resource regeneration rate and environment's bearing capacity, and finally causes environmental pollution increase. When the industrial agglomeration level exceeds the threshold valve, the industrial agglomeration will turn to improve environmental pollution, which signifies that industrial agglomeration will cause positive external effect on environment; the major reasons causing such a phenomenon are: (1) when industrial agglomeration level improves to a certain extent, industrial agglomeration effect will be higher than crowding effect, which will promote market scale expansion and benefit to enhance scale economy effect and promote industrial production efficiency and management level to improve, and thereby make the pollution discharge of unit output reduce; (2) improvement of industrial agglomeration level will promote regional economic development and improve regional per capita income level; in accordance with the Environment Kuznets Curve, the economic development, when it breaks through specific turn point, will be beneficial to improve environmental pollution; (3) improvement of industrial agglomeration level to a given extent will make the technology spillover effect become remarkable, and technology spill over effect will benefit to push intra-industry enterprise technology advancement, where technology advancement will reduce the pollution discharge of unit output through direct effect and indirect effect, and thereby improve environmental pollution.

In other control variables, the regression coefficient of foreign merchant's direct investment for environmental pollution is negatively significant, which signifies that the

Table 1: Threshold effect test.

Item	F-statistics	P-value	BS Number	1% Critical value	5% Critical value	10% Critical value
Single threshold	15.372**	0.016	400	15.208	10.501	7.502
Double threshold	3.564	0.214	400	20.086	9.076	5.683
Triple threshold	5.419	0.108	400	12.714	8.064	5.804

Note: ** indicates significant at 5% level.

Table 2: Results of threshold estimation value.

Item	Threshold Estimation value	95% confidence interval
Single threshold model	0.529	[0.528, 0.625]

direct investment of foreign merchant benefits to promote the improvement of environmental pollution of China to some extent, so the "pollution haven hypothesis (PHH)" is not true in China; this conclusion is rightly in conformity with the research conclusions of most of the scholars. The impact coefficient of environmental regulation on environmental pollution is positively significant, it signifies that environmental regulation does not improve China's environmental pollution and which differs from the theoretical analysis expectation. How to understand such a result? In the appraisal of local government, the percentage of environmental factor is increasing gradually, and local government attaches more importance to environmental pollution and therefore increases more investment on the region where it suffers from severe environmental pollution. So, more investment of local government on environmental pollution governance is rightly the representation of the aggravated environmental pollution. To some extent, the more the investment on pollution governance is, the severer the environmental pollution under governance is. The possible reason causing this phenomenon is the one that China's subsidy for environmental pollution governance and China's loan for environmental

pollution governance focus only on pollutant governance and control, but both of them have limited incentive for enterprise and thereby the efficiency of investment on environmental pollution governance is not at a high level. The regression coefficient of energy consumption is positive, but it fails to pass the significance test; it signifies that energy consumption has a limited function on environmental pollution and it is not the main factor intensifying environmental pollution. Technological innovation can efficiently improve China's environmental pollution, it signifies technological innovation will promote the research, development and use of new environmental protection technology, which will benefit to improve traditional industry and develop emerging industry, and thereby improve environmental quality.

To make a comparison, the linear model estimate was made for the relationship between industrial agglomeration and environmental pollution in the paper, where the linear model estimate was respectively made by using the fixed effect and the system generalized method of moments (see Row 3-4 of Table 3 for specific results). From the estimated results, it can be seen that industrial agglomeration will result in environmental pollution and the coefficient is higher

Table 3: Estimated results of threshold and linear model.

Explanatory Variable	Threshold estimation	Linear estimation (FE)	Linear estimation (SYS-GMM)
aggl. I (q ≦ γ)	0.2805*** (2.94)	-	-
aggl. I (q>γ)	-0.5016** (-2.27)	-	-
aggl	-	0.3641** (2.43)	0.4796*** (9.84)
lnfdi	-0.0061*** (-4.34)	-0.0203** (-2.07)	-0.0389**** (-3.46)
lnpr	0.1075*** (5.37)	0.1203*** (5.61)	0.0206*** (5.04)
lnener	0.0408 (0.64)	0.0405 (0.61)	0.0397** (2.05)
lnsr	-0.0587*** (-2.65)	-0.0802*** (-2.79)	-0.0407*** (-5.73)
cons	2.764*** (7.48)	3.0304*** (7.61)	0.6802*** (4.87)
Abond test For AR (1)	-	-	-2.894 [0.007]
Abond test For AR (2)	-	-	0.0365 [0.865]
Sargan test	-	-	23.972 [0.504]

Note: Z-statistics are shown in parentheses in the table, and square brackets are P-values; ***, **, and * indicate significant at 1%, 5%, and 10%, respectively; the system generalized moment regression model is two-step.

than the threshold estimate, which is rightly caused by the one that linear model does not consider the difference in the high or low industrial agglomeration level, and different industrial agglomeration level results in the different spillover effect and agglomeration effect, and thereby causes the different functions for environmental pollution. Therefore, the relationship between industrial agglomeration and environmental pollution is the non-linear. If the estimate is made only based on the linear model, it is very much possible to miss important explanation.

CONCLUSION

In this paper, the Copeland-Taylor model was used to deduce a theoretical model to represent the influencing mechanism of industrial agglomeration for environmental pollution. Based on this, the panel data of 30 provinces and municipalities (autonomous regions) of China during the period from 2009 to 2016, as well as the threshold regression method were used to make empirical analysis on the relationship between industrial agglomeration and environmental pollution. According to the research findings, the relationship between industrial agglomeration and environmental pollution is not a simple linear relationship, but the impact of industrial agglomeration on environmental pollution has remarkable threshold features. When industrial agglomeration level is lower than the threshold value, the industrial agglomeration will intensify environmental pollution; when industrial agglomeration level is higher than the threshold value, the industrial agglomeration will benefit to improve environmental pollution. Additionally, foreign merchant's direct investment and technological innovation will improve environmental pollution to some extent, and PHH (pollution haven hypothesis) is not true in China; the environmental regulation does not improve China's environmental pollution, and the energy consumption is not the major factor intensifying environmental pollution.

The research conclusions of the paper provide the following policy enlightenments: (1) Manage the relationship between industrial agglomeration and environmental pollution in a dynamic manner. Since a low industrial agglomeration level will intensify environmental pollution, efficient measures should be taken to improve industrial agglomeration level to the threshold valve; once it reaches to the threshold value, environmental pollution can be improved through the threshold effect of industrial agglomeration; therefore, improving the industrial agglomeration level is the major way of improving China's environmental pollution. (2) Treating the function of industrial agglomeration on environmental pollution objectively; in the development course of industrial agglomeration level, the differentiated policy should be made

for the different regions. In the region with low industrial agglomeration level, all appropriate measures can be taken to improve industrial agglomeration level and the direct investment of foreign merchant and severe environmental regulation can be used to improve environmental pollution and avoid from "pollution firstly and pollution governance secondly". In the region with high industrial agglomeration level, all appropriate measures, such as encouraging industrial technology innovation, optimizing industrial agglomeration direction, leading industrial agglomeration to develop toward high value-added industry (including high-end R&D and design) should be taken. (3) Encouraging to introduce foreign capital, formulate differentiated policy based on regional environmental pollution and industrial development level, lead foreign capital to transfer to clean industry, pay attention to attract foreign-owned enterprise having environmental technology advantages, use overseas advanced technology and environmental protection standard to achieve the dual objectives of capital attraction and environmental protection, and push China's economy to get high-quality development.

ACKNOWLEDGEMENTS

REFERENCES

Almulali, U., Ozturk, I. and Lean, H. H. 2015. The influence of economic growth, urbanization, trade openness, financial development, and renewable energy on pollution in Europe. Nat. Hazards., 79(1): 621-644.

Baek, J., Cho, Y. and Koo, W. W. 2009. The environmental consequences of globalization: A country-specific time-series analysis. Ecol. Econ., 68(8): 2255-2264.

Frank, A. 2001. Urban air quality in larger conurbations in the European Union. Environ. Modell. Softw., 16(4): 399-414.

Lee, L. 2007. Gmm and 2SLS estimation of mixed regressive, spatial autoregressive models. J. Econom., 137(2): 489-514.

Ning, L. T., Wang, F. and Li, J. 2016. Urban innovation, regional externalities of foreign direct investment and industrial agglomeration: Evidence from Chinese cities. Res. Policy, 45(4): 830-843.

Ottaviano, G. I. P., Tabuchi, T. and Thisse, J. F. 2002. Agglomeration and trade revisited. Int. Econ. Rev., (43): 409-436.

Shao, S., Tian, Z. and Yang, L. 2017. High speed rail and urban service industry agglomeration: evidence from China's Yangtze River Delta region. J. Transp. Geogr., (64): 174-183.

Stiebale, J. 2011. Do financial constraints matter for foreign market entry? A firm-level examination. The World Economy, 34(1): 123-153.

Venables, A. J. 1996. Equilibrium location of vertically linked industries. Int. Econ. Rev., 37: 341-359.

Virkanen, J. 1998. Effect of urbanization on metal deposition in the bay of Toolonlahti, southern of Finland. Mar. Pollut. Bull., 36(9): 729-738.

Walter, I. and Ugelow, J. L. 1979. Environmental policies in developing countries. Ambio., 8(2/3): 102-109.

Yamashita, N., Matsuura, T. and Nakajima, K. 2014. Agglomeration effects of inter-firm backward and forward linkages: Evidence from Japanese manufacturing investment in China. J. Jpn. Inst. Econ., 2014(34): 24-41.

Zeng, D. and Zhao, L. Pollution havens and industrial agglomeration. J. Environ. Econ. Manage., 58(2): 141-153.

... Continued from inner front cover

- The text of the manuscript should run into **Abstract, Introduction, Materials & Methods, Results, Discussion, Acknowledgement** (if any) and **References** or other suitable headings in case of reviews and theoretically oriented papers. However, short communication can be submitted in running with **Abstract and References.** The references should be in full with the title of the paper.

- The figures should preferably be made on a computer with high resolution and should be capable of withstanding a reasonable reduction with the legends provided separately outside the figures. Photographs may be black and white or colour.

- Tables should be typed separately bearing a short title, preferably in vertical form. They should be of a size, which could easily be accommodated in the page of the Journal.

- References in the text should be cited by the authors' surname and year. In case of more than one reference of the same author in the same year, add suffix a,b,c,.... to the year. For example: (Thomas 1969, Mass 1973a, 1973b, Madony et al. 1990, Abasi & Soni 1991).

List of References

The references cited in the text should be arranged alphabetically by authors' surname in the following manner: (Note: The titles of the papers should be in running 'sentence case', while the titles of the books, reports, theses, journals, etc. should be in 'title case' with all words starting with CAPITAL letter.)

Dutta, A. and Chaudhury, M. 1991. Removal of arsenic from groundwater by lime softening with powdered coal additive. J. Water Supply Res. Techno. Aqua., 40(1) : 25-29.

Hammer, D.A. (ed.) 1989. Constructed Wetlands for Wastewater Treatment-Municipal, Industrial and Agricultural. Lewis Publishers Inc., pp. 831.

Haynes, R. J. 1986. Surface mining and wetland reclamation. In: Harper, J. and Plass, B. (eds.) New Horizons for Mined Land Reclamation. Proceedings of a National Meeting of the American Society for Surface Reclamation, Princeton, W.V.

Submission of Papers

- The paper can be submitted by e-mail as an attachment in a single WORD file at **contact@neptjournal.com**
- The paper can also be submitted online in a single WORD file through the journal's website: **www.neptjournal.com**

Attention

1. Any change in the authors' affiliation may please be notified at the earliest.
2. Please make all the correspondence by e-mail, and authors should always quote the manuscript number.

Note: In order to speed up the publication, authors are requested to send the publication charges as soon as they get the 'initial acceptance' letter, and also correct the galley proof immediately after receipt. The galley proof must be checked with utmost care, as publishers owe no responsibility for mistakes. The papers will be put on priority for publication only after receiving the processing and publication charges.

Nature Environment and Pollution Technology

(Abbreviation: Nat. Env. Poll. Tech.)
(An International Quarterly Scientific Journal)

Published by

Technoscience Publications
A-504, Bliss Avenue, Opp. SKP Campus
Balewadi, Pune-411 045, Maharashtra, India

In association with
Technoscience Knowledge Communications
Mira Road, Mumbai, India

For further details of the Journal please visit the website. All the papers published on a particular subject/topic or by any particular author in the journal can be searched and accessed by typing a keyword or name of the author in the 'Search' option on the Home page of the website. All the papers containing that keyword or author will be shown on the home page from where they can be directly downloaded.

www.neptjournal.com